# Magnetic Materials and their Applications

by

Dr-Ing. Carl Heck
*Standard Elektrik Lorenz AG*
*(German associate of ITT)*

*Translated from the German by*
*Stuart S. Hill, M.Eng.*

London
Butterworths

THE BUTTERWORTH GROUP

ENGLAND
Butterworth Co. (Publishers) Ltd
London: 88 Kingsway, WC2B 6AB

AUSTRALIA
Butterworths Pty Ltd
Sydney: 586 Pacific Highway Chatswood, NSW 2067
Melbourne: 343 Little Collins Street, 3000
Brisbane: 240 Queen Street, 4000

CANADA
Butterworth & Co. (Canada) Ltd
Toronto: 14 Curity Avenue, 374

NEW ZEALAND
Butterworths of New Zealand Ltd
Wellington: 26–28 Waring Taylor Street, 1

SOUTH AFRICA
Butterworth & Co. (South Africa) (Pty) Ltd
Durban: 152–154 Gale Street

English translation
© Butterworth & Co. (Publishers) Ltd, 1974

English edition first published 1974

This is an updated English version of
*Magnetische Werkstoffe und ihre technische Anwendung*, originally published in Heidelberg
by Dr Alfred Hüthig Verlag GmbH in 1967

ISBN 0 408 70399 7

Printed in Hungary

# Preface

The preparation of the English translation of my book has provided the opportunity to revise and update the material. Since the German publication substantial progress has been made: new materials have been developed and come on the market; designs have been improved to meet the requirements of miniaturisation in electronics; and the properties of various magnetic materials have been modified and adapted to new applications. In addition, completely new branches of research and development have opened up. For example, it became necessary to extend the chapter on permanent-magnet materials to include the new family of cobalt–rare earth magnets ($SmCo_5$), and to introduce the internationally standardised RM cores used in transmission and other electronic equipment. New storage possibilities based on orthoferrites have also arisen and are dealt with in Chapter 15.

Progress in Standards specifications, especially of the International Electrotechnical Commission (IEC), have been respected in the text. However, as DIN specifications are available in Britain and cannot be directly correlated with BSI specifications, no attempt has been made to convert these. The lists of suppliers and trade names have also been updated, and the magnetic-materials products of such countries as Italy, Japan, and India are now quoted.

As a result of all these additions, the list of references for each chapter has been extended, with only a very few obsolete titles deleted to save space. For the same reason, some less important tables have been omitted. Thus I trust that this improved and updated English version will be of value and service to all concerned with the development and use of magnetic materials.

Fischbach bei Nürnberg C. H.

# 1

# Introduction

The text which follows seeks to close a gap in the technical literature of which the user of magnetic materials is particularly conscious. There is no lack of good authoritative books dealing with magnetism and with the properties of magnetic materials, but the classical approach, founded on metallurgical physics, often makes it unnecessarily hard for the user to discover and understand the definitive properties of the available materials which are adapted to his own special problems.

Historically, the development of magnetic materials for technical applications was bound up with the development of metallurgy and the general study of metals, but a now situation has been created by the rapid introduction into technology of the ceramic oxides (ferrites). However, ferrimagnetic materials can no longer be treated as pure extensions of the more traditional substances; instead, a joint consideration of the two groups of materials seemed necessary. Thus, in this book, substances are not divided according to metallurgical considerations, as was formerly customary, but rather from the standpoint of the user. The increasing refinement of technology suggests a similar approach, in that the familiar language of magnetism is no longer adequate—one need only think of the properties of materials used in magnetic storage or in microwave techniques, where hysteresis phenomena, for example, have faded into the background.

Any discussion of the technical properties of magnetisable materials must be preceded by certain observations on magnetism itself and its manifold phenomena. In this connection it would certainly be beyond the scope of this book to develop basic magnetic theory in detail, but an attempt is made to sketch-in the theoretical groundwork of magnetism as far as is absolutely necessary to connect it with the behaviour of magnetic materials. Fundamental studies are to be found in Anderson[1], Bates[3], Bozorth[4], Kneller[9], Koch and Jellinghaus[11], Pawlek[15], Rado and Suhl[16], Snoek[21], Van Vleck[23], and Wonsowski[25].

By working from the requirements of the various technically important fields, this text proceeds to an exposition of magnetic materials and guides the reader, in the simplest manner possible, in the problems of particular material applications. Thus the book is intended primarily for practical use. It seeks to connect past experience with modern understanding, to offer a glimpse into the theoretical foundations and, above all, to examine the

properties essential to particular applications of magnetic materials and to help the engineer to choose his materials properly.

Substances which, in spite of historical or theoretical importance, have not succeeded (or only to a limited degree) in winning a place in technology are on the whole dealt with only briefly.

An integral part of this text is the definition of magnetic characteristics and factors and an examination of their foundations. The hysteresis loop in all its different forms is discussed in terms of domain theory, whose vividness helps to elucidate magnetic mechanisms. Further, the effect of external conditions on the behaviour of magnetic materials and on the course of the underlying magnetic processes is discussed.

An exhaustive review of present-day knowledge of magnetic materials is quite out of the question because of the enormous expansion of this field in recent years. Even in specialised fields, knowledge has increased to such an extent that there are innumerable books dealing with particular problems, such as permanent magnets[6, 8, 10, 18], magnetic materials for the communications industry[17], ferrites[12, 19, 20], microwave ferrites[2, 5, 13], thin films[14], magnetic domains[22], and magnetic stores[7, 24]. Obviously a fundamental study of magnetic materials would need a small library, and the present review can be only partially balanced by the comprehensive list of references given at the end of each chapter. By preference, those works have been quoted which themselves quote further sources so that a reader may be encouraged to follow up any given theme. A particular selection of technical literature may well omit much valuable material and, on the other hand, some work may have been included which could have been dispensed with. It is hoped that the critical reader will forgive this and other inadequacies.

## REFERENCES

1. ANDERSON, J. C.: Magnetism and Magnetic Materials. Chapman & Hall, London (1968)
2. AULOCK, W. H. VON: Handbook of Microwave Ferrite Materials. Academic Press, New York/London (1965)
3. BATES, L. F.: Modern Magnetism. University Press, Cambridge (1951)
4. BOZORTH, R. M.: Ferromagnetism. Van Nostrand Co. Inc., Toronto/New York/London (1951)
5. CLARRICOATS, P. J. B.: Microwave Ferrites. Chapman & Hall, London (1961)
6. FISCHER, J.: Abriss der Dauermagnetkunde. Springer, Berlin/Göttingen/Heidelberg (1949)
7. HICKMAN, R. E. B.: Magnetic Recording Handbook. G. Newnes Ltd, London (1962)
8. IRELAND, J. R.: Ceramic Permanent Magnet Motors. McGraw-Hill Book Co., New York (1968)
9. KNELLER, E. Ferromagnetismus. Springer, Berlin/Göttingen/Heidelberg (1962)
10. KOCH, J. and RUSCHMEYER, K.: Permanentmagnete I–III. Valvo GmbH, Hamburg (1967–1970)
11. KOCH, K. H. and JELLINGHAUS, W.: Einführung in die Physik der magnetischen Werkstoffe. F. Deuticke, Vienna (1957)
12. LANGER, E. and SCHMITT, R.: Rechteckferrite. Siemens AG, Berlin/Munich (1967)
13. LAX, B. and BUTTON, K. J.: Microwave Ferrites and Ferrimagnetics. McGraw-Hill Book Co. Inc., New York/San Francisco/Toronto/London (1962)

14. NEUGEBAUER, C. A., NEWKIRK, J. B. and VEMILYEA, D. A.: Structure and Properties of Thin Films. Chapman & Hall, London (1959)
15. PAWLEK, F.: Magnetische Werkstoffe. Springer, Berlin/Göttingen/Heidelberg (1952)
16. RADO, G. T. and SUHL, H.: Magnetism I–III. Academic Press, New York (1963–1966)
17. RICHARDS, C. E. and LYNCH, A. C. (eds): Soft Magnetic Materials for Telecommunications. Pergamon Press Ltd, London (1953)
18. SCHÜLER, K. and BRINKMANN, K.: Dauermagnete. Springer, Berlin/Heidelberg/New York (1970)
19. SMIT, J. and WIJN, H. P. J.: Ferrite. Deutsche Philips GmbH, Hamburg (1962)
20. SNELLING, E. C. Soft Ferrites, Properties and Applications. Iliffe, London (1969)
21. SNOEK, J. L.: New Developments in Ferromagnetic Materials. Elsevier Publ. Co. Inc., New York/London/Amsterdam/Brussels (1949)
22. STEWART, K. H.: Ferromagnetic Domains. University Press, Cambridge (1954)
23. VAN VLECK, J. H.: The Theory of Electric and Magnetic Susceptibilities. University Press, Oxford (1952)
24. WINCKEL, F. (ed.): Technik der Magnetspeicher. Springer, Berlin/Göttingen/Heidelberg (1960)
25. WONSOWSKI, S. W.: Moderne Lehre vom Magnetismus. Deutscher Verlag der Wissenschaften, Berlin (1956)

# 2

# Review of magnetic effects

## 2.1 PRELIMINARY REMARKS

The magnetic material longest known to man is lodestone or magnetite, which has, basically, the chemical constitution $Fe_3O_4$ or $FeO \cdot Fe_2O_3$, i. e. ferroferrite. It was known to the ancients that this mysterious substance attracted other bodies of like nature.

The development of ferromagnetic theory and the improvement of magnetisable materials are not based on this well-known ore but rather on metallic iron, nickel, cobalt, and their alloys. From earliest times there was keen desire both to understand the magnetisation of iron oxide and to follow out its consequences. The beginnings of the development of magnetics are related to the development of metallurgy which started some 100–150 years ago. This yielded hypotheses concerning a variety of magnetic effects which today are mostly named after their discoverers.

Frequently it was particular theoretical views as to the nature of matter and a study of the phenomenon of magnetism that led to particular 'Questions put to Nature' and stimulated further new experiments. The results not only furthered actual knowledge but initiated hypotheses leading to modifications of the materials themselves. The advance of electrical technology and its growing importance in our own century was made possible by the development of new magnetic materials. Many modern applications go back to long-known effects which were worked out with no practical aims in mind. It would seem reasonable, therefore, to use these observations as an historical framework and at the same time to clarify, through them, the problems of magnetism.

## 2.2 THE MOST IMPORTANT EFFECTS

### 2.2.1 The Joule effect

In 1842 J. P. Joule (1818–1889) reported the following effect: when a piece of iron becomes magnetised, it elongates in the direction of magnetisation and contracts transversely[12]. Later, this behaviour was named magnetostriction. It occurs with all magnetic materials, is of either sign, and varies in value with the field strength.

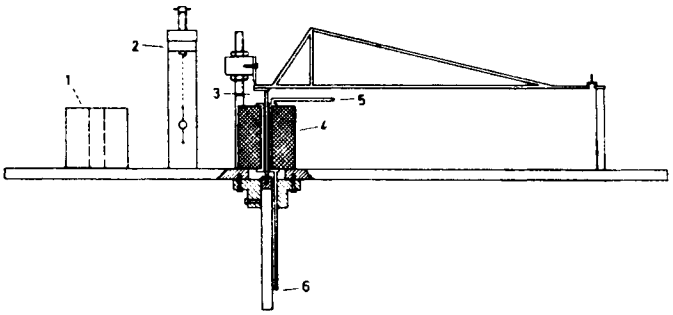



*Figure 2.1. Experimental arrangement for measuring the Joule effect: 1, compensation coil; 2, magnetometer; 3, iron bar; 4, magnetising coil; 5 and 6, water cooling*[27]

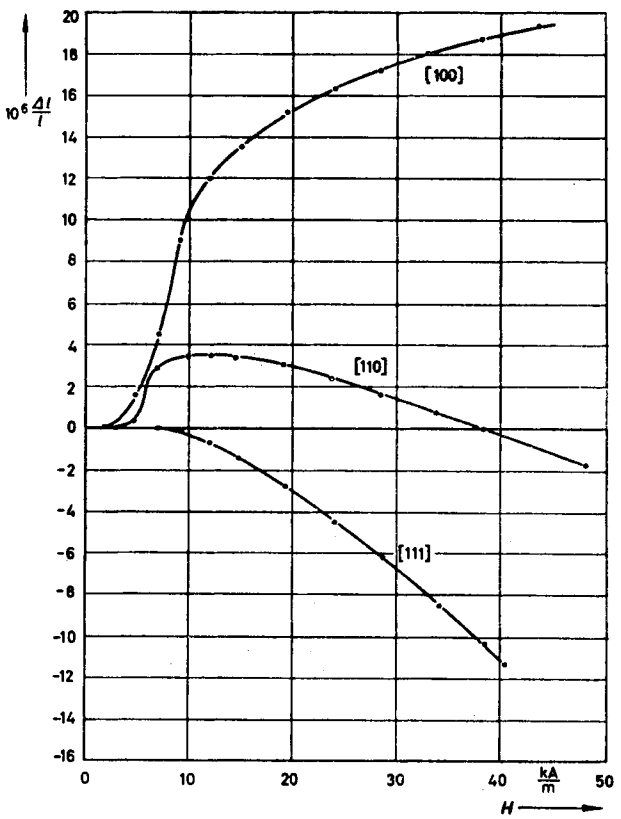



*Figure 2.2. Magnetostriction of a single iron crystal*[27]

In 1925 Webster[27] carried out the first systematic measurements on single crystals. The experimental arrangement used by him is shown in Figure 2.1. It comprises a combination of mechanical levers and optical mirrors whose function is greatly to amplify a small change of length. A brass rod is soldered onto the measuring piece which is connected, through a 17 cm stiff lever-arm, to a glass plate. The short arm of this lever is 0·5 cm long and presses against a brass knife-edge. At the end of the longer arm there is a small tilting galvanometer mirror, whose inclination is observed through a fixed telescope at a distance of 3 m. Webster was able to measure changes of length of 2 nm with this device. The curves of Figure 2.2 are an example of a measurement undertaken to determine the dependence of magnetostriction on crystal orientation and on field strength.

### 2.2.2 The Faraday effect

Like the Cotton–Mouton effect (see page 9) this well-known effect, named after Faraday (1791–1867), is important both in optics and in microwave techniques. However, the Faraday effect is non-reciprocal, whereas optical rotation in doubly refracting crystals, as in the Cotton–Mouton effect, is reciprocal; that is to say, if the plane of polarisation is turned through an angle $\alpha$ by directing a polarised beam of light onto the surface of a doubly refracting crystal, and if the beam is reflected from the rear face of this crystal, the rotation of the beam on re-emergence from the crystal is reversed. By contrast, in the Faraday effect, the angle of rotation is doubled if the polarised beam re-emerges from the medium after reflection.

By the 'Faraday optical effect' is to be understood the rotation of the plane of polarisation of a linearly polarised electromagnetic wave when passing through a suitable medium in the presence of a magnetic field[7]. The sense of the rotation is determined by that of the applied magnetic field parallel to the direction of the beam. Both positive and negative rotations are found in optics. The angle of rotation $\alpha$ is proportional to the length $l$ traversed in the given substance and to the field strength $H$, i.e.

$$\alpha = WlH$$

The constant $W$, when $l$ is measured in centimetres, $\alpha$ in minutes of arc, and $H$ in oersteds, is called the Verdet constant, after M. E. Verdet (1824–1866)[24], who conducted comprehensive investigations into the Faraday effect. For glass, for example, $W = 3{\cdot}5'$/cm Oe. The angle $\alpha$ is a function of frequency.

In 1884 A. Kundt (1838–1894)[16] investigated the Faraday effect in ferromagnetic substances and found that thin transparent laminae of iron, only some 50 nm thick, gave a rotation 30 000 times greater than glass of the same thickness, i.e. 280 000°/cm. The rotating power of cobalt was found to be of about the same order, whereas nickel showed only half the effect. König[15], using extremely thin sheets of iron, was even able to observe rotations corresponding to 765 000°/cm.

In recent times the microwave Faraday effect has achieved great technical prominence[9]. Here, rotation of the plane of polarisation of a linearly polarised wave in a waveguide is utilised by passing it through a ferrimagnetic material magnetised in the direction of wave propagation.

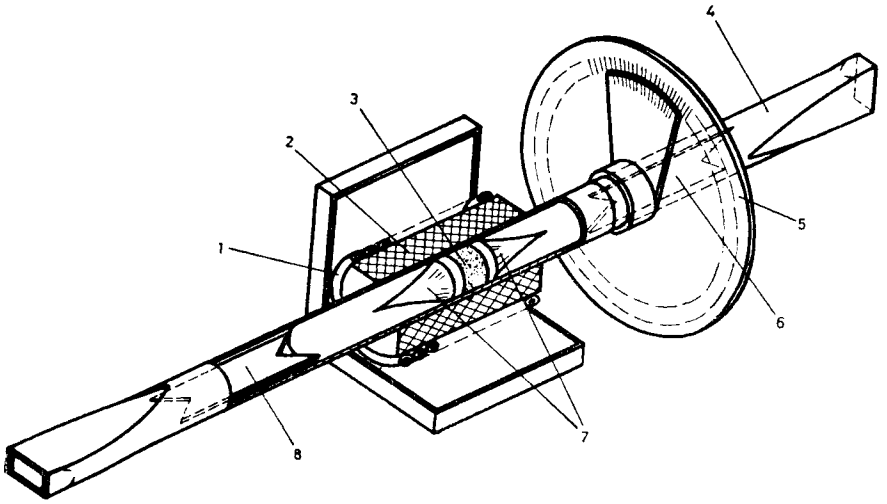



*Figure 2.3. Arrangement for measuring the Faraday rotation; 1, cooling coil; 2, winding; 3, ferrite; 4, rotatable element; 5, fixed protractor; 6, strip for absorbing vertically polarised waves; 7, terminations for avoiding reflections; 8, strip for absorbing horizontally polarised waves*[9]

Figure 2.3 shows a set-up whereby the rotation of a polarised wave in a rectangular waveguide may be determined[9]. Inserted in the rectangular waveguide is a section of cylindrical guide containing the measuring piece, a slice of ferrite. The magnetic field is produced by a coil wound around the tube. The angle of Faraday rotation can be measured by twisting the output plane of the waveguide, suitably provided with an indicator of angular displacement. For ferrites, angles of some 50–200°/cm have been measured.

### 2.2.3 The Matteucci effect

The Matteucci effect has been known since 1847[17]. If a ferromagnetic rod lying lengthwise in a magnetic field is twisted, then its magnetisation changes. Further, Matteucci stated that, if a galvanometer be connected between the two ends of the iron cylinder, then twisting and untwisting the cylinder causes induced currents to be observed in the galvanometer circuit. If the iron cylinder were twisted and untwisted only during a first magnetising, and then remagnetised, a sudden pulse of current appeared at that moment in the circuit associated with the cylinder. Matteucci investigated cylinders of iron and steel and established that, independently of the direction of the mechanical torsion of the cylinder, the magnetisation first increased with the torsion and then fell.

As Sir William Thomson found in later experiments[6], the sequence of responses shows hysteresis effects for cyclical torsions (Figure 2.4). Thomson explained the effect by supposing that, as a consequence of magnetostriction, helical magnetisation was produced: a circular component was superposed on the initial longitudinal effect.

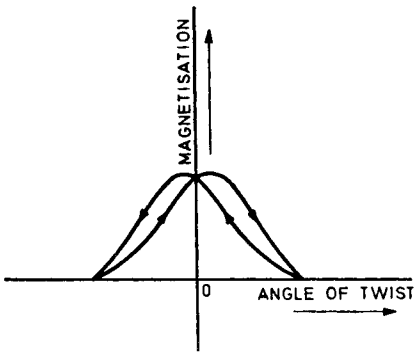



*Figure 2.4. Magnetic changes produced by twisting an iron cylinder*[6]

Against this 'positive' Matteucci effect, v. Schmoller[19] later discovered a 'negative' Matteucci effect characterised by the appearance, for magnetisation in one sense, of electromotive forces in the opposite sense.

### 2.2.4 The Wiedemann effect

G. Wiedemann (1826–1899) described the effect named after him in three parts[29]:

1. If an iron wire is twisted while a galvanic current is passing through it, or after the current has passed, the wire becomes magnetised.
2. If a galvanic current flows through a magnet in the direction of its axis, the magnet will twist.
3. If, through an iron wire lying along the axis of a magnetic solenoid a direct current is passed and, afterwards, a weak current passed through the solenoid, the wire will twist in the same direction as if the two currents had been passed in reverse order. This twist increases with increasing intensity of the magnetising current up to a certain maximum. With still stronger magnetising currents, the wire untwists.

The results of this investigation were taken by Wiedemann as proof of the correctness of the hypothesis of rotatable molecular magnets. Today, over 100 years later, they form the basis of a magnetic storage principle (see page 640).

### 2.2.5 The Villari effect

According to E. Villari[25], an elastic elongation of a ferromagnetic material produces a permeability change in the direction of the applied tension. Materials which lengthen with magnetisation, i.e. show positive magnetostriction, increase their permeability under tensile stress. Materials with negative magnetostriction reduce their permeability under the influence of tensile stress.

Villari discovered by his researches that an iron bar lengthens when magnetised by a weak field but contracts when a particular field strength is exceeded. This result is called the Villari effect. It determines the change of sign of the magnetostriction effect in iron (see Figure 2.2).

### 2.2.6 The Kerr effect

The Kerr effect in magneto-optics goes back to an observation made in 1876 by J. Kerr (1824–1907)[13]: if polarised light falls on, and is reflected by, the polished end-face of a magnet, then the plane of polarisation of the reflected beam is rotated. In general, the term 'Kerr effect' is used to indicate change of amplitude and phase when a polarised light-beam is reflected from a ferromagnetic mirror surface. By means of this effect, the magnetic condition of metallic or ceramic (ferritic) surfaces may be studied. The effect is used in, for example, the direct observation of magnetic domains.

Corresponding to the magneto-optical Kerr effect there is also an electro-optical effect. (Consider the artificial birefringence of nitrobenzene, known under the name 'Kerr cell'.)

### 2.2.7 The Hopkinson effect

If the permeability of a ferromagnetic object is measured at very small field strengths as a function of temperature, a definite maximum can be established before the Curie temperature is reached[10], as is shown, for example, in Figure 2.5 for a Mn–Zn ferrite. This maximum is not found at higher field strengths. Its presence is termed the Hopkinson effect and can be explained by the observation that crystal anisotropy approaches zero at a lower temperature than does spontaneous magnetisation. Döring[4] was able to offer a qualitative explanation, in the special case of nickel, in terms of wave-spin theory.

### 2.2.8 The Cotton–Mouton effect

The 'artificial' or forced birefringence of all transparent substances under the influence of a magnetic field perpendicular to the direction of incident light is called the 'optical Cotton–Mouton effect'. Cotton and Mouton[3] named the effect 'magnetic birefringence'. If $l$ is the length of the transparent object, $H$ the magnetic field strength, and $C_m$ the Cotton–Mouton constant, then the path difference between the two beams

$$k = C_m l H^2 \text{ wavelengths}$$

For the sodium D line in nitrobenzene at 20°C

$$C_m = 2{\cdot}41 \times 10^{-12}$$

Ferrites are transparent at microwave frequencies and therefore show a

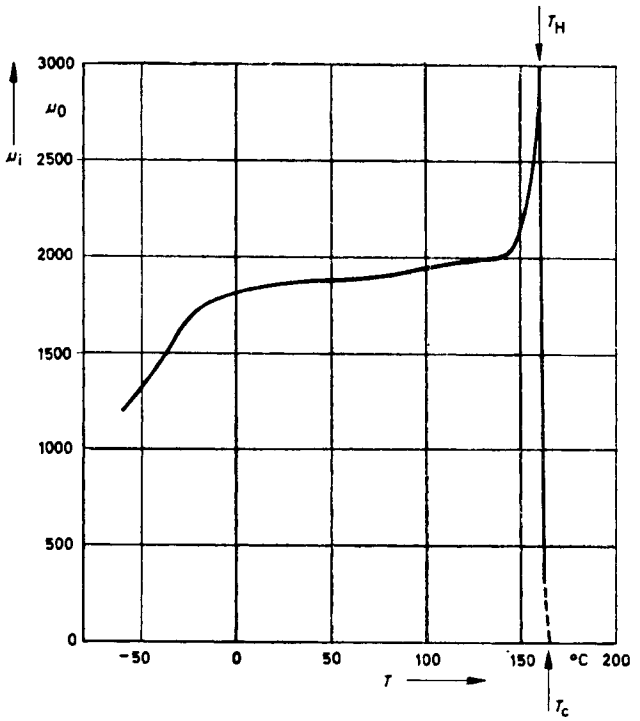



*Figure 2.5. Initial permeability of a* Mn–Zn *ferrite as a function of temperature*

'microwave Cotton–Mouton effect' over a few gigahertz on application of a direct magnetic field[18].

The magnetic field of the normal beam runs parallel to the applied direct magnetic field, and that of the other (non-normal) beam is perpendicular to it. There is a phase difference between the two beams. The Cotton–Mouton effect, in contrast with the Faraday effect, is reciprocal.

### 2.2.9 The Barnett effect

The Barnett effect is one of the magnetomechanical effects. It arose out of the investigations of S. J. Barnett in the years 1909–1914, in which he explored the relation between magnetisation and the rotation of magnetised rods and bars[2].

Using the experimental arrangement sketched in Figure 2.6, Barnett demonstrated that a magnetic moment arises when magnetisable material is rotated. In his experiment, he set up two roughly equal horizontal rods A and B and arranged similar coils around their central portions. These coils were connected in series with each other and with a fluxmeter. One of the rods remained stationary while the other could be set in rotary motion in alternate directions or brought to rest. The resulting changes of flux were determined

by the fluxmeter and the changes in flux density per revolution per second calculated.

Barnett was looking particularly for analogies applicable to terrestrial magnetism. His experiments enable the relation between mechanical torque $I$ and magnetic moment $M$ to be found, and this can be used to determine the gyromagnetic ratio $\gamma = M/I$ (see Section 2.2.10).

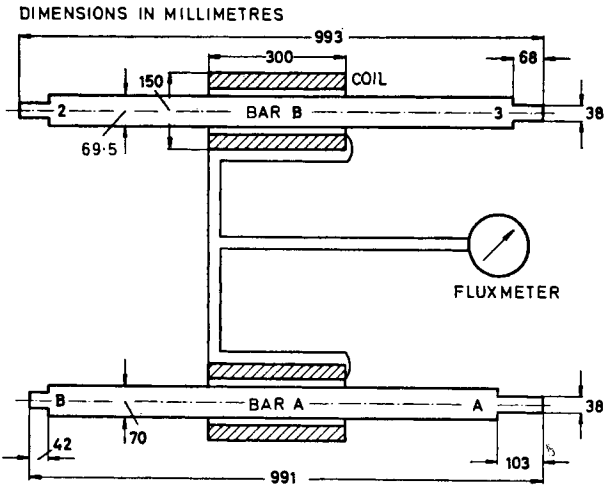



*Figure 2.6. Experimental arrangement for studying the Barnet effect*[2]

### 2.2.10 The Einstein–de-Haas effect

A. Einstein (1879–1955) and W. de Haas sought to prove that the magnetic moment of an atom of iron arose from orbiting electrons via the so-called molecular current ('molecular' in Ampère's original sense of 'elementary'). The possibility of testing this experimentally stems from the theory that each orbiting electron can be assigned a mechanical angular momentum and a magnetic moment. The magnetic atom behaves mechanically like a spinning top whose axis coincides with the magnetic axis. A change of magnetisation in a sample must, therefore, be connected with a change of angular momentum[5].

While in the Barnett effect (see above) magnetisation is produced by rotation, the reverse is true for the Einstein–de-Haas effect: here, a torque corresponds to a change of magnetisation. In the actual experiment (Figure 2.7) a small iron rod, 7 mm long, was placed in the alternating field of two similar coils $A_1$ and $A_2$. The rod was suspended by a glass fibre G of about 0·2 mm thickness fixed at the upper end to a brass tube E, whose effective length could be changed by inserting another tube C into the mouth of tube E at D. Tube C carried a clamp B, whose jaws were pressed together by a spring F, giving an accurately defined length of suspension. To the rod S in the gap between coils $A_1$ and $A_2$ were attached two small mirrors allowing the turning angle to be read off. The two coils were connected together and

produced an alternating field of some 4 kA/m. The relation (for soft iron)

$$\frac{2m}{e} = 1{\cdot}11\times10^{-8}\,\text{g/A s}$$

was deduced from the moment of inertia of the rod and the resonance frequency of the oscillation. This is in good agreement with the theoretically expected result ($1{\cdot}13\times10^{-8}$ g/A s).

The Barnett effect and the Einstein–de-Haas effect come under the heading of 'magnetomechanical or gyromagnetic effects' since both are involved in the determination of the gyromagnetic ratio $\Delta M/\Delta I$ ($I$ = torque and $M$ = magnetic moment).

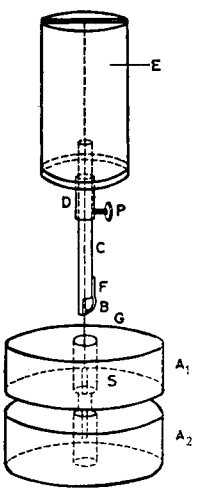



*Figure 2.7. Experimental arrangement for studying the Einstein–de-Haas effect*[5]

The gyromagnetic ratio $\gamma = \Delta M/\Delta I$ is of great importance in magnetic theory since its magnitude indicates whether electron spin or orbital spin dominates the magnetic process and it can also be used to determine the ratio $e/m$. If $e$ is the charge of the electron and $m$ its mass, and if, further, $g$ is the Landé factor and $\mu_0$ the absolute permeability of free space, then

$$\gamma = \frac{g}{2}\,\mu_0\frac{e}{m}$$

If we assume $g = 2$ for ferromagnetic materials, then, taking $\mu_0 = 4\pi\times10^{-7}$ V s/A m and $e/m = 1{\cdot}76\times10^{8}$ A s/g, we have

$$\gamma = 0{\cdot}22\ \text{MHz m/A}$$

If, on the other hand, $\gamma$ is known, the Landé factor $g$ can be calculated.

Another method of determining $g$ involves resonance measurements in the microwave range. This generally leads to somewhat higher values than magnetomechanical methods. A few examples are set out in Table 2.1[14].

**Table 2.1** MEASURED VALUES OF $g$ FOR SOME MAGNETIC MATERIALS: (a) DETERMINED BY THE RESONANCE METHOD; (b) DETERMINED BY THE MAGNETOMECHANICAL METHOD

| *Material* | (*a*) | (*b*) |
|---|---|---|
| Iron | 2·12–2·17 | 1·93 |
| Cobalt | 2·22 | 1·87 |
| Nickel | 2·19–2·42 | 1·92 |
| Magnetite | 2·20 | 1·93 |
| Heusler alloy | 2·01 | 2·00 |
| Permalloy | 2·07–2·14 | 1·91 |
| Supermalloy | 2·12–2·23 | — |

The most reliable method of finding $\gamma$ is by means of the Einstein–de-Haas principle, which has been used in the last few years to achieve very accurate results for numerous magnetic materials[20, 21].

### 2.2.11 The Barkhausen effect

In 1917, Barkhausen (1881–1956)[1] found that iron produced a noise when magnetised or demagnetised. Figure 2.8 shows the experimental arrangement which led to the discovery. Barkhausen inserted an iron rod R into a small coil C of 25 mm diameter and having 300 turns. He connected a telephone T to this coil via an amplifier A having an amplification factor of 10 000; also a heavily damped mirror galvanometer G. He changed the field strength by advancing or withdrawing a 10 cm horseshoe magnet, the sense of the field being changed by turning the magnet through 180°. He stated

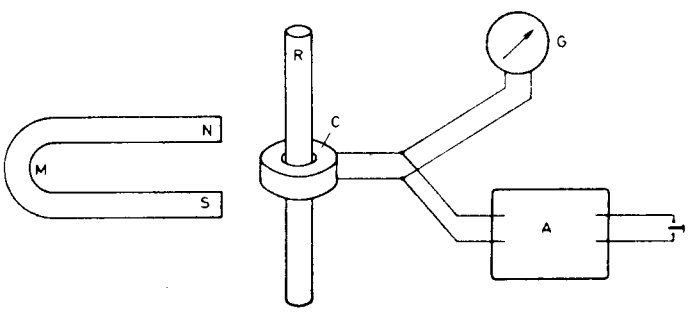



*Figure 2.8. Experimental arrangement for studying the Barkhausen effect*[1]

that: a gradual and uniform change of magnetomotive force causes the molecular magnets to jump suddenly into their new positions, so inducing non-uniform pulses in the surrounding coil which can be heard as noise in the telephone earpiece. The molecular magnets form themselves into larger or smaller groups having greater or less stability. An audible sound corresponds only to the formation or disruption of relatively large groups.

It is now known that the groups which Barkhausen referred to vary in size in different materials. According to a recent research it was found that, for example, for iron $0{\cdot}74\times10^{13}$ atoms and for nickel $2{\cdot}6\times10^{13}$ atoms are involved and these, therefore, occupy a volume of $0{\cdot}87\times10^{-10}$ cm$^3$ and $3{\cdot}1\times10^{-10}$ cm$^3$ respectively[22].

The relevant induced voltages are known, as is, also, the effect of grain size, but not much is known of the detailed process. Investigations into the Barkhausen effect are therefore still continuing[8, 23, 26]: up to the present more than 350 papers dealing with the effect are known[16a, 21a, 21b].

### 2.2.12 The magnetothermal effect (or magnetocaloric effect)

In 1918 P. Weiss (1865–1940) and A. Piccard[28] observed that the temperature of a ferromagnetic material rose if there was a sudden increase in field strength. For nickel the maximum temperature rise reaches about 1°C and for iron about 2°C. In modern scientific technique the reverse effect is used to reach very low temperatures—below 1 K.

### 2.2.13 The Hughes effect

In 1935 E. Hughes noticed that, in thin laminated cores of Mumetal or of Permalloy C, asymmetrical a.c. hysteresis occurred[11]. This asymmetry was especially marked if the maximum field strength lay in the region of maximum d.c. permeability. The effect was traced to polarisation within the substance of the laminae. The effect can be made to disappear by applying a very high magnetising force and then gradually reducing it.

## REFERENCES

1. BARKHAUSEN, H.: Geräusche beim Ummagnetisieren von Eisen (Phys. Z. **20** (1919) 401–402)
2. BARNETT, S. J.: Magnetization by rotation (Phys. Rev. (II) **6** (Oct. 1915) 239–270)
3. COTTON, A. and MOUTON, H.: Nouvelle propriété optique (birefrigence magnétique) de certains liquides organiques non colloidaux (C. R. **145** (1907) 229–230)
4. DÖRING, W.: Die Temperaturabhängigkeit der Anfangssuszeptibilität von Nickel unter Zug (Z. Phys. **124** (1948) 501–513)
5. EINSTEIN, A. and DE HAAS, W. I.: Experimenteller Nachweis Ampèrescher Molekularströme (Verh. D. Phys. Ges. **17** (1915) 152–170)
6. EWING, J. A.: Magnetische Induktion in Eisen und verwandten Metallen. Berlin/München (1892)
7. FARADAY, M.: On the magnetic affection of light, and on the distinction between the ferromagnetic and diamagnetic conditions of matter (Phil. Mag. (3) **29** (Sept. 1846) 153–156)

8. FORD, N. C. and PUGH, E. W.: Barkhausen effect in nickel–iron films (J. A. P. **30** (4) (Apr. 1959) 270 S–271 S)
9. HOGAN, C. L.: The ferromagnetic Faraday effect at microwave frequencies and its applications (Bell Syst. Tech. J. **31** (Jan. 1952) 1–31)
10. HOPKINSON, J.: Magnetic properties of alloys of nickel and iron (Proc. Roy. Soc. **48** (1890) 1–13)
11. HUGHES, E.: Magnetic characteristics of nickel–iron alloys with alternating magnetization forces (J. IEE **79** (1936) 213–223)
12. JOULE, J. P.: On a new class of magnetic forces (Ann. Electr. Magn. Chem. **8** (1842) 219–224)
13. KERR, J.: On rotation of the plane of polarization by reflection from the pole of a magnet (Rep. Brit. Ass. (1876) 40–41; Phil. Mag. (5) **3** (1877) 321–343; (1878) 161)
14. KITTEL, C.: On the gyromagnetic ratio and spectroscopic splitting factor of ferromagnetic substances (Phys. Rev. **76** (6) (Sept. 1949) 743–748)
15. KÖNIG, H.: Die kleinsten ferromagnetischen Elementarbereiche des Eisens (Naturwiss. **33** (1946) 71–75)
16. KUNDT, A.: Die electromagnetische Drehung der Polarisationsebene des Lichts durch Eisen, Cobalt und Nickel (Ann. Phys. Chem. **23** (1884) 228–252)
16a LAMBECK, M. Barkhausen-Effekt und Nachwirkung in Ferromagnetica. Walter de Gruyter & Co., Berlin (1971)
17. MATTEUCCI, CH.: Mémoire sur le magnétisme développé par le courrant électrique (C. R. **24** (1847) 301–302); Recherches expérimentales sur les phénomènes électromagnetiques développés par la tension (Ann. Chim. Phys. (III) **53** (1858) 385–417)
18. DU PRÉ, F. K.: On the microwave Cotton–Mouton effect in ferroxcube (Phil. Res. Rep. **10** (1955) 1–10)
19. V. SCHMOLLER, F.: Untersuchungen über den Matteucci-Effekt (Z. Phys. **93** (1935) 35–51)
20. SCOTT, G. G.: Magnetomechanical determination of gyromagnetic ratios (J. Phys. Soc. Japan **17** (B-1) (1962) 372–375)
21. SCOTT, G. G.: Gyromagnetic ratios of the iron–nickel alloys (Phys. Rev. **103** (1956) 561–563)
21a STIERSTADT, K.: Der magnetische Barkhausen-Effekt (Springer Tracts in Mod. Phys. **40** (1966))
21b STIERSTADT, K. and PFRENGER, E.: Die Temperaturabhängigkeit des magnetischen Barkhauseneffekts (Z. Phys. **179** (1964) 182–194)
22. STONER, E. C.: The analysis of magnetization curves (Rev. Mod. Phys. **25** (1) (Jan. 1953) 8)
23. TEBBLE, R. S.: The Barkhausen effect (Proc. Phys. Soc. **68** (1955) 1017–1032)
24. VERDET, E.: Sur les propriétés optiques développées dans les corps transparents par l'action du magnétisme (Ann. Chim. Phys. **41** (1854) 370–412
25. VILLARI, E.: Über die Änderungen des magnetischen Moments, welche der Zug und das Hindurchleiten eines galvanischen Stromes in einem Stabe von Eisen oder Stahl hervorbringen (Ann. Phys. Chem. (5) **6** (1865) 87–122)
26. WARREN, K. G.: Barkhausen noise in transformer cores (Electron. Techn. **38** (1961) 89–94)
27. WEBSTER, W. L.: Magneto-striction in iron crystals (Proc. Roy. Soc. (A) **109** (Dec. 1925) 570–584)
28. WEISS, P. and PICCARD, A.: On a new magnetocaloric phenomenon (C. R. **116** (1918) 352–354)
29. WIEDEMANN, G.: Magnetische Untersuchungen (Ann. Phys. Chem. **117** (1862) 193–217)

# 3

# Magnetic parameters of Materials

## 3.1 TYPES OF MAGNETIC MATERIALS

Strictly speaking all substances are magnetic, but only ferromagnetic and ferrimagnetic substances, the so-called 'magnetic materials' of technology, are capable of being magnetised by relatively weak fields.

The greater proportion of materials—solids, liquids, and gases—are paramagnetic or diamagnetic. Diamagnetic substances differ from paramagnetic substances as to the sign of their susceptibility (see page 20). The susceptibility is very small in the case of diamagnetic and paramagnetic substances and independent of field strength. Ferromagnetic and ferrimagnetic substances have, by contrast, high susceptibilities which vary with field strength.

### 3.1.1 Paramagnetic materials

These have positive susceptibilities $\varkappa$ lying between $10^{-3}$ and $10^{-6}$ (Table 3.1)[34, 74]. To this class belong most gases, many salts in the iron group, the

**Table 3.1** SUSCEPTIBILITIES OF SOME PARAMAGNETIC ELEMENTS AND COMPOUNDS AT 20°C

| *Material* | | $10^6 \varkappa$ | *Material* | | $10^6 \varkappa$ | |
|---|---|---|---|---|---|---|
| Al | Aluminium | 7·7 | U | Uranium | 33 | |
| Ba | Barium | 1·9 | W | Tungsten | 3·5 | |
| Ca | Calcium | 13·8 | | | | |
| Cr | Chromium | 38·7 | | | | |
| K | Potassium | 6·9 | | | | |
| Li | Lithium | 44 | | | | |
| Mg | Magnesium | 10 | | | | |
| Mn | Manganese | 121 | | | | |
| Na | Sodium | 8·6 | | | | |
| Os | Osmium | 0·069 | | | | |
| Pt | Platinum | 12 | | | | |
| Ta | Tantalum | 1·1 | | | | |
| | | | | CoO | 750 | |
| | | | | $Cr_2O_3$ | 380 | |
| | | | | CuO | 38 | |
| | | | | HCl | 9 500 | |
| | | | | $Fe_3C$ | 37 | at 1000°C |
| | | | | α-Fe | 116 | at 1000°C |
| | | | | γ-Fe | 24·9 | at 1000°C |

alkali metals, and also ferromagnetic and ferrimagnetic materials at temperatures above the Curie temperature. The fall-off of parametric susceptibility is inversely proportional to the rise of absolute temperature (the Curie law). For certain paramagnetic metals, the temperature law fails or the dependence is minimal; in some cases (titanium, uranium) the relation is anomalous.

A subdivision of paramagnetism is the phenomenon called *super-paramagnetism*. Super-paramagnetism is met in ferromagnetic or ferrimagnetic substances which are very finely divided, as when they appear as colloids or precipitates in non-magnetisable matrices. Disappearance of hysteresis and the collapse of the magnetising curves of an anisotropic substance, when plotted against $H/T$, are typical effects, among others, of super-paramagnetism[5a].

### 3.1.2 Diamagnetic materials

These have negative susceptibilities of the order of $10^{-6}$ which, for practical purposes, are independent of temperature. Examples of diamagnetic substances are the inert (noble) gases, hydrogen, many metals, most non-metals,

**Table 3.2** SUSCEPTIBILITIES OF SOME DIAMAGNETIC ELEMENTS AND COMPOUNDS

| *Material* | | $10^6 \varkappa$ | *Material* | | $10^6 \varkappa$ |
|---|---|---|---|---|---|
| Ag | Silver | − 2·4 | S | Rhombic sulphur | − 6·1 |
| Ar | Argon | − 6·1 | Sb | Antimony | −10·6 |
| Au | Gold | − 1·9 | Se | Selenium | − 4·0 |
| B | Boron | − 7·8 | Si | Silicon | − 1·2 |
| Be | Beryllium | −13·0 | Tl | Thallium | − 3·0 |
| Bi | Bismuth | −16·0 | Zn | Zinc | − 1·9 |
| C | Diamond | − 6·2 | | | |
| | Graphite | − 0·63 | | | |
| Cd | Cadmium | −23·9 | | $Al_2O_3$ | − 3·5 |
| Cu | Copper | − 1·08 | | $CaCO_3$ | − 4·4 |
| Ge | Germanium | − 1·5 | | $CO_2$ | − 6·0 |
| H | Hydrogen | −25·0 | | $Cu_2O$ | − 2·4 |
| He | Helium | − 5·9 | | Water | − 9·05 |
| Hg | Mercury | − 2·2 | | $H_2SO_4$ | − 5·0 |
| N | Nitrogen | − 5·4 | | $SO_2$ | − 3·0 |
| Pb | Lead | − 1·4 | | Ethyl alcohol | − 9·3 |
| | | | | Benzene | − 8·9 |

and many organic compounds (Table 3.2)[34]. On the other hand, there is a whole series of diamagnetic substances giving anomalous values: their susceptibilities are substantially higher and are dependent on temperature. To this list of substances belong antimony, bismuth, gallium, graphite, and thallium.

### 3.1.3 Ferromagnetic materials

The main characteristics of ferromagnetic and ferrimagnetic materials are the following: the susceptibility depends on the field strength; the relation between magnetisation and field strength is not single valued (being characterised by hysteresis); and in material below the Curie temperature there exist elementary regions of magnetisation, known as the Weiss 'domains'. Ferromagnetism and ferrimagnetism are, moreover, associated with particular crystal lattice formations; thus there can be no ferromagnetism in gases or liquids.

The metals iron, cobalt, and nickel and many of their alloys are ferromagnetic. Again, certain alloys of manganese with copper and aluminium (the Heusler alloys) and some rare earths (erbium, dysprosium, gadolinium) and several of their alloys are also ferromagnetic, as are certain intermetallic compounds even when they do not contain any ferromagnetic components[30a], for example $Au_4V$, $Sc_3In$, and $ZrZn_2$.

### 3.1.4 Ferrimagnetic materials

These include, for example, most ferrites with the general formula $MO \cdot Fe_2O_3$ where M stands for some bivalent metallic ion (iron, nickel, manganese, copper, magnesium). These oxides usually have a spinel-type crystal lattice. Only 'inverse' spinels are ferrimagnetic (see Section 7.1.5).

Associated with the 'cubic' ferrites are those with a hexagonal structure conforming to the pattern $MO \cdot 6Fe_2O_3$ where M stands for barium, strontium, or lead. There are, moreover, mixture compounds of cubic and hexagonal ferrites which are also ferrimagnetic.

Fairly recently a further group of ferrimagnetic materials has become known, namely compounds of iron oxide with oxides of the rare earths[117] having the general formula $5Fe_2O_3 \cdot 3M_2O_3$. Here M stands for yttrium or one of the trivalent elements such as gadolinium, terbium, dysprosium, holmium, erbium, thulium, ytterbium, or lutetium. These compounds crystallise like garnet (for example, $Fe_3Al_2Si_3O_{12}$) and are therefore called garnets or iron garnets. The most thoroughly explored of these compounds to date is yttrium–iron garnet.

### 3.1.5 Antiferromagnetic materials

These, like the ferromagnetic materials, are a particular subgroup of paramagnetic substances. Their susceptibilities are of the order of $10^{-3}$, but they increase with heating, up to a critical temperature, and then fall off again. The temperature at which antiferromagnetism disappears is called the Néel temperature. Many compounds are antiferromagnetic, for example manganese monoxide (MnO), iron oxide (FeO), nickel oxide (NiO), iron chloride ($FeCl_2$), and manganese selenide (MnSe)—to name just a few.

As will be further explained later, ferrimagnetism is a special form of antiferromagnetism, namely 'uncompensated' antiferromagnetism.

### 3.1.6 Metamagnetic materials

Certain substances can be either ferromagnetic or antiferromagnetic. Which of the two characteristics obtains depends on the magnetic field strength and the temperature. The substances are called metamagnetic, following Néel[144]. For MnAs a ferromagnetic condition is followed, at high temperature, by an antiferromagnetic condition. As may be seen from Figure 3.1, the magnetic polarisation $J$ falls very steeply at around 320°C. The expected Curie temperature is substantially higher, as shown by extrapolation of the curve $J_s^2 = f(T)$. Spontaneous magnetisation disappears round about 320°C.

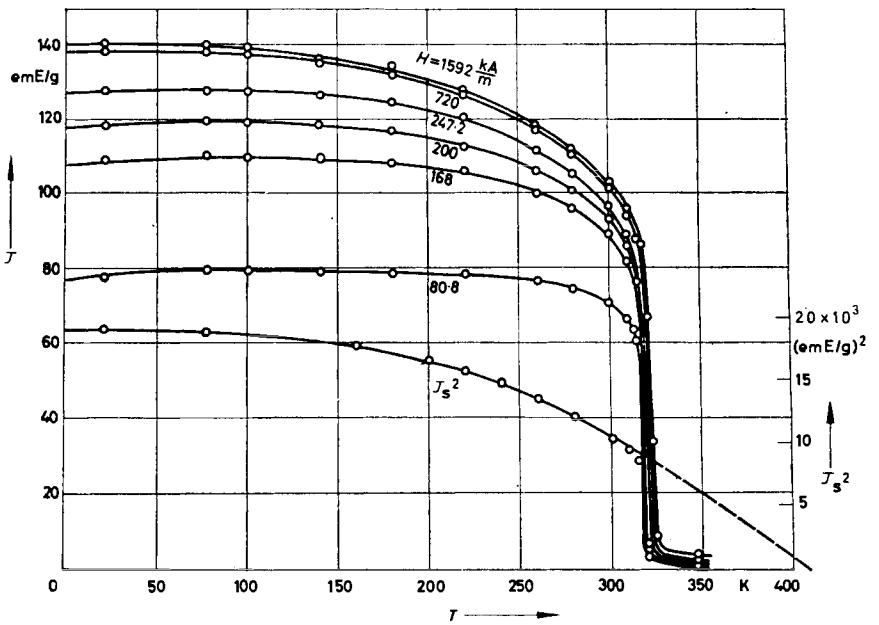



*Figure 3.1. Magnetisation curves for* MnAs[144]

MnBi shows a similar behaviour, as do holmium and terbium. Additional metamagnetic substances are dysprosium, erbium, and $MnAu_2$. These pass from an antiferromagnetic to a ferromagnetic condition at a critical field strength. The threshold value of the critical field strength increases with rising temperature[144].

## 3.2 THE PRINCIPAL CONCEPTS AND DEFINITIONS

The most important concepts for the description of the magnetic properties of materials are briefly explained. The designations and definitions of DIN 1325[33a] (German Standard 1325) will be followed for this purpose. In general, the definitions and symbols adopted follow the recommendation of IEC Publication 125[72a].

### 3.2.1 Susceptibility

Susceptibility $\varkappa$ is defined as the proportionality factor relating the field strength (magnetising force) $H$ to the magnetic polarisation $J$; both are, in general, vectors. Only when their directions coincide can they be treated as scalars. This is a common case and is presumed in the following equation:

$$\frac{J}{\mu_0 H} = \varkappa \tag{3.1}$$

Here, $\mu_0$ is the absolute permeability of free space, sometimes called the 'magnetic field constant' or the 'magnetic induction constant'; $\mu_0 = 4\pi \times 10^{-7}$ V s/A m $= 4\pi \times 10^{-7}$ H/m. For paramagnetic or diamagnetic materials, therefore, $\varkappa$ gives the rate of change of polarisation with respect to field strength (Figure 3.2).

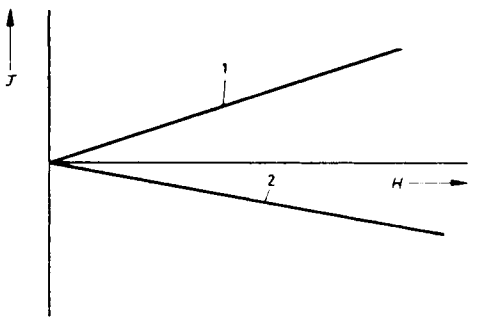



*Figure 3.2. Magnetising characteristics of paramagnetic and diamagnetic materials: 1 paramagnetic; 2, diamagnetic*

The saturation polarisation $J_s$ can be calculated from the number of magnetons per molecule. The Bohr magneton is the unit used for expressing the electron's magnetic moment: $J_s = n_B \mu_B N/M$ where $n_B$ is the number of Bohr magnetons, $\mu_B$ is one Bohr magneton $= 1{\cdot}1654 \times 10^{-29}$ V s m, $N$ is the Loschmidt number ($6{\cdot}025 \times 10^{23}$ molecules/mol), and $M$ is the gramme molecular weight. Since polarisation is generally quoted in terms of volume, rather than mass, the expression has to be multiplied by the density (see Table 13.20).

In practical technology, only the magnetism of ferromagnetic and ferrimagnetic substances is of functional importance; instead of polarisation $J$, it is convenient to use magnetic flux density (or magnetic induction) $B$, and to use permeability $\mu$ in place of susceptibility $\varkappa$.

### 3.2.2 Magnetic flux density

This is related to the magnetic polarisation $J$ by the equation

$$J = B - \mu_0 H \tag{3.2}$$

Also,

$$B = \frac{\Phi}{A} \tag{3.3}$$

where $A$ represents the area through which the induced flux $\Phi$ passes.

In what follows, the units used for $B$ and $H$ will conform to the international SI units (metre, kilogramme, second, ampere) (see DIN 1339)[33b]. Flux density will be quoted in V s/m$^2$ or tesla*, field strength in A/m, and magnetic flux in V s or weber†. The following relations will serve to convert to the earlier units, gauss‡ and oersted§.

$$1\ \text{G} = 10^{-4}\ \text{V s/m}^2 = 10^{-4}\ \text{Wb/m}^2 = 10^{-4}\ \text{T} = 0{\cdot}1\ \text{mT} \tag{3.4}$$

$$10^3\ \text{G} = 1\ \text{kG} = 1\ \text{mV s/dm}^2 = 0{\cdot}1\ \text{V s/m}^2 = 100\ \text{mT} \tag{3.5}$$

$$1\ \text{Oe} = \frac{10\text{A}}{4\pi\ \text{cm}} = \frac{1000}{4\pi}\ \text{A/m} = 79{\cdot}577\ \text{A/m} \tag{3.6}$$

$$1\ \text{G Oe} = 7{\cdot}96\ \text{mW s/m}^3 = 0{\cdot}0796\ \text{erg/cm}^3 \tag{3.7}$$

$$10^6\ \text{G Oe} = 7{\cdot}96\ \text{mW s/cm}^3 \tag{3.8}$$

Very small field strengths, for example the earth's field, are measured in $\gamma$ ($7{\cdot}9577 \times 10^{-4}$ A/m).

In ferromagnetic and ferrimagnetic substances, the flux density $B$ depends on the field strength. The relation $B = \text{f}(H)$ is determined by the structure and chemical nature of the substance. On the other hand, the saturation density $B_s$ is of magnitude independent of structure. At absolute zero, the saturation density $B_s$ is a maximum, and it falls to zero at the Curie temperature.

The saturation density of ferromagnetic metals and several ferrites (at room temperature) are displayed in Table 3.3. The influence of composition on the value of $B_s$ is shown in Figure 13.6 for the Fe–Ni alloys and in Figure 10.37 for the Fe–Co alloys.

If the normalised saturation polarisation is plotted against the normalised Curie temperature, a very similar picture is obtained for nearly all magnetisable substances. This is illustrated in Figure 3.3 for iron, cobalt, and nickel, relative saturation polarisation being plotted against Curie temperature (on the absolute scale)[159]. Barium ferrite gives a somewhat different shape of curve (see Figure 9.41).

* Named after N. Tesla (1856–1943).
† Named after W. E. Weber (1804–1891).
‡ Named after C. F. Gauss (1777–1855).
§ Named after H. C. Oersted (1777–1851).

**Table 3.3** SATURATION FLUX DENSITY $B_s$ AND CURIE TEMPERATURE $T_c$ FOR SOME FERROMAGNETIC AND FERRIMAGNETIC SUBSTANCES

| *Material* | $B_s$ (V s/m²) | $T_c$ (°C) | *Reference* |
|---|---|---|---|
| Iron | 2·158 | 770 | 29a |
| Cobalt | 1·900 | 1 121 | 46a |
| Nickel | 0·608 | 358 | 15 |
| Gadolinium | 1·363 | 16 | 15 |
| Dysprosium | — | −186 | |
| Erbium | — | −253 | 35a |
| $Fe_3Al$ | — | 500 | 15 |
| $Fe_3C$ | 1·24 | 215 | 15 |
| $Fe_3P$ | — | 420 | 15 |
| MnBi | 0·78 | 350 | 57 |
| $MnO \cdot Fe_2O_3$ | 0·52 | 295–303 | 55, 58, 116 |
| $xMnO(1-x)ZnO \cdot Fe_2O_3$ | See Figure 3.33 | | 58 |
| $FeO \cdot Fe_2O_3$ | 0·60 | 563–590 | 55, 64, 84, 116, 122 |
| $NiO \cdot Fe_2O_3$ | 0·34 | 575–597 | 55, 64, 116, 130 |
| $MgO \cdot Fe_2O_3$ | 0·14 | 325–440 | 55, 64 |
| $CuO \cdot Fe_2O_3$ | 0·17 | 410–490 | 55, 64, 85, 130 |
| $CoO \cdot Fe_2O_3$ | 0·50 | 495–520 | 55, 58, 64, 114, 116 |
| $Co_{0·5}Fe_{0·5} \cdot Fe_2O_3$ | — | 515 | 58 |
| $xCoO(1-x)ZnO \cdot Fe_2O_3$ | See Figure 3.33 | | 58 |
| $Li_2O \cdot Fe_2O_3$ | — | 632 | 71 |
| $LiO \cdot Fe_2O_3 \cdot Fe_3O_4$ | 0·39 | 590–670 | 55, 64 |
| $NiAl \cdot FeO_4$ | — | 350 | 85 |
| $NiCr \cdot FeO_4$ | — | 325 | 85 |
| $MgCr \cdot FeO_4$ | — | 50 | 85 |
| $BaO \cdot 6Fe_2O_3$ | 0·41 | 450 | 147 |

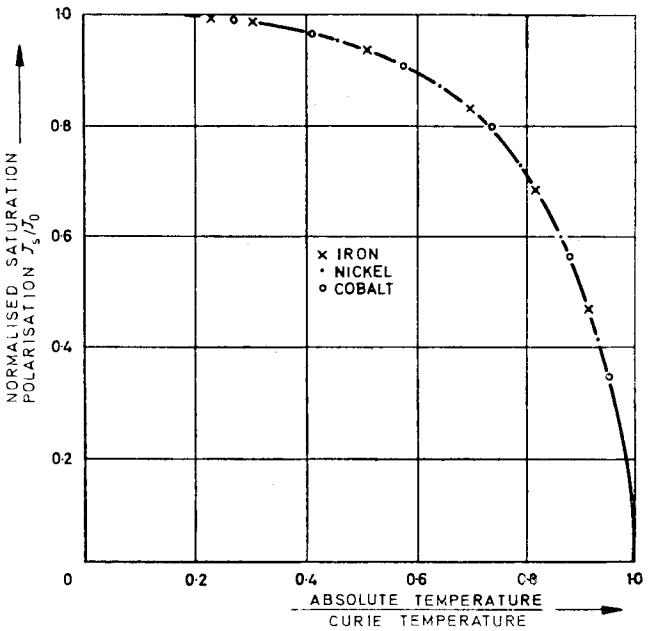



*Figure 3.3. Relation between normalised saturation polarisation and normalised Curie temperature*[159]

### 3.2.3 Magnetisation

By magnetisation $M$ is meant the polarisation $J$ referred to $\mu_0$:

$$M = \frac{J}{\mu_0} = \frac{B}{\mu_0} - H \tag{3.9}$$

### 3.2.4 The various permeabilities

#### 3.2.4.1 Absolute permeability

Absolute permeability is defined by

$$\mu = \frac{B}{H} \tag{3.10}$$

i.e. as the 'chord-gradient' of flux density against field strength. In empty space $\mu = \mu_0$. If the flux density and the magnetic field strength are vectors, the permeability is a tensor (see page 529).

### 3.2.4.2 Relative permeability

Relative permeability is a pure number

$$\mu_r = \frac{\mu}{\mu_0} \tag{3.11}$$

and is, therefore, called the 'permeability number'. Thus from equation 3.10

$$B = \mu H = \mu_r \mu_0 H \tag{3.12}$$

It follows, further, from equations 3.1 and 3.2, that

$$\varkappa = \mu_r - 1 \tag{3.13}$$

Where one is concerned with the permeability of a substance, one generally means the relative permeability $\mu_r$. Instead of writing

$$\mu_r = 100$$

it is also quite usual to write

$$\mu = 100\ \mu_0$$

which practice will generally be followed here. Then $\mu_0$ becomes one of the basic units like ampere or metre. The symbol $\mu$ often appears in the literature with a subscript which usually indicates the field strength at which the value of $\mu$ was measured. Thus in electrotechnology symbols such as $\mu_5$, $\mu_{20}$, and $\mu_{100}$ denote permeabilities at field strengths of 5 mOe, 20 mOe, and 100 mOe, i.e. $5/4\pi$ A/m, $20/4\pi$ A/m, and $100/4\pi$ A/m respectively (DIN 41 301 and IEC publication 125).

This would suggest that $\mu_0$ was the permeability at zero field strength. Indeed, in non-German journals one often sees $\mu_0$ used in the sense of 'initial permeability'. Nevertheless, it is now more customary to write $\mu_i$ for the initial permeability.

### 3.2.4.3 Initial permeability

The initial permeability $\mu_i$ cannot be measured directly. It is found by extrapolating to zero, measurements made at finite field strengths. Only if the measuring field is extremely low, in the range of a few A/m, will linear extrapolation lead to a correct value. Exact comparative measurements[112] confirm that, in this case, linear extrapolation is permissible. The defining equation for relative initial permeability is

$$\mu_i = \frac{1}{\mu_0} \lim_{H \to 0} \frac{B}{H} \tag{3.14}$$

Peak values of $B$ and $H$ must be inserted for a.c. measurements.

### 3.2.4.4 Maximum permeability

The maximum value attained when permeability is measured as a function of field strength is denoted by $\mu_m$. In Figure 3.4 the relation between field strength and permeability is plotted for a high-permeability Mn–Zn ferrite at 20°C and 70°C. As can easily be appreciated, $\mu_i$ and $\mu_m$ both depend on

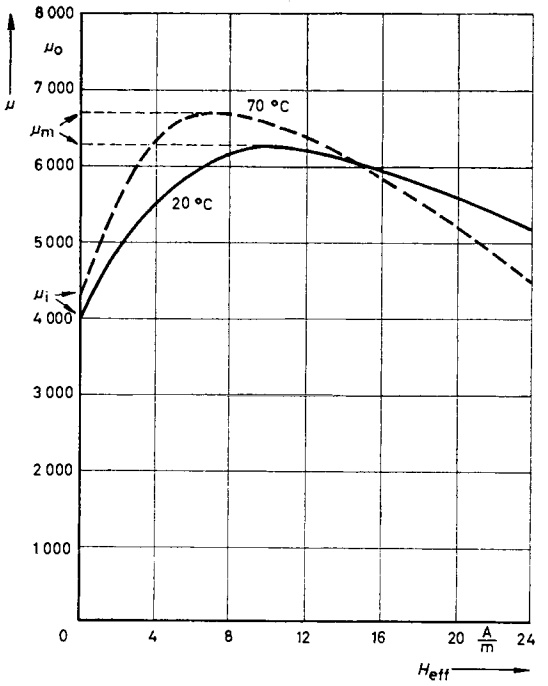



*Figure 3.4. Permeability of a* Mn–Zn *ferrite as a function of field strength at 20°C and 70°C*

temperature[65]; in fact, as the temperature increases, the permeability value increases and the maximum occurs at lower field strengths, which implies a drop in coercivity. Maximum permeability means maximum amplitude-permeability (see below).

### 3.2.4.5 Relative amplitude-permeability

Relative amplitude-permeability is defined as the permeability at a particular field strength (or a particular flux density) with a periodic change in $H$, there being no static field, thus

$$\mu_{amp} = \frac{1}{\mu_0}\frac{B}{H} \tag{3.15}$$

### 3.2.4.6 Superposed permeability

By superposed permeability is understood the permeability in an alternating field with a steady field superposed on it:

$$\mu_{\Delta} = \frac{1}{\mu_0} \frac{\Delta B}{\Delta H} \tag{3.16}$$

where $\Delta B$ and $\Delta H$ are peak-to-peak values as shown in Figure 3.5. The superposition, or minor, loop is always so located that the tip lies on the hysteresis loop and is enclosed by it. The superposition, or minor, loop, therefore, always lies within the hysteresis loop, i.e. on the rising branch it lies to the left and on the falling branch to the right.

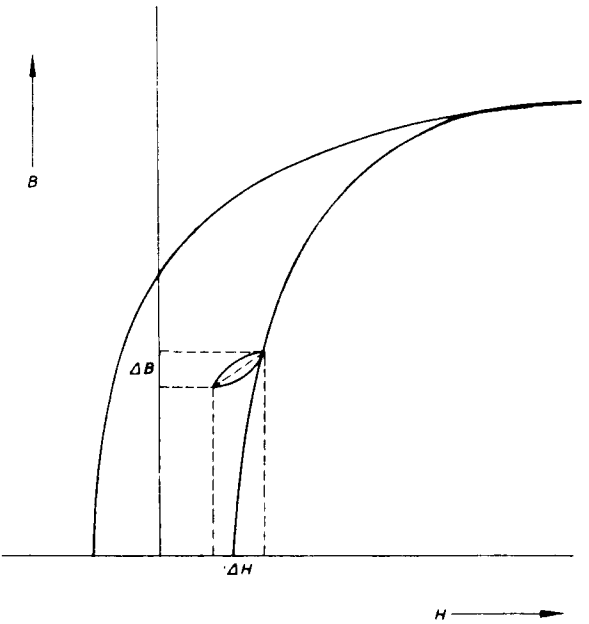



*Figure 3.5. Superposed permeability*

The dependence of superposed permeability on field strength is shown in Figure 3.7 for an Fe–Ni alloy with 45% Ni. The curve[15] shows the value of $\mu_{\Delta}$ for amplitudes $\Delta H$ of 0·8 A/m and 4 A/m.

### 3.2.4.7 Permanent permeability

Permanent permeability is a special case of superposed permeability which plays an important part in the technology of permanent magnets: $\mu_p$ represents the mean slope $\Delta B/\Delta H$ of a retrograde magnetisation loop which

starts, as a rule, on the demagnetisation curve appropriate to the particular permanent-magnet material (Figure 3.6). The relative permanent permeability is then

$$\mu_p = \frac{1}{\mu_0}\frac{\Delta B}{\Delta H} \tag{3.17}$$

Secondary effects can cause the foot, or starting point, F to shift to F′ without influencing the nominal value of $\mu_p$.

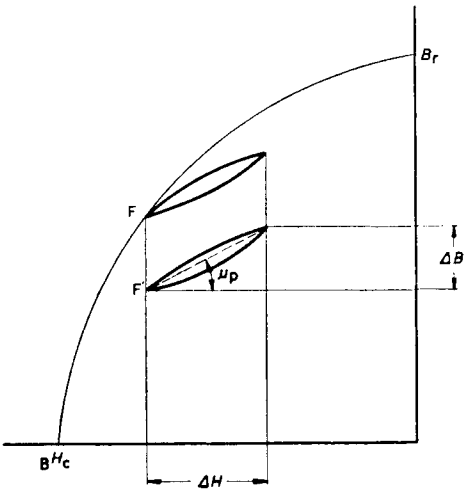



*Figure 3.6. Permanent permeability $\mu_p$*

### 3.2.4.8 Reversible permeability

Reversible permeability is a special case of superposed permeability for very small alternating fields:

$$\mu_{rev} = \lim_{H \to 0} \mu_\Delta \tag{3.18}$$

Figure 3.7 shows the field strength dependence of $\mu_\Delta$ along the initial magnetisation curve for the alloy 55% Fe–45% Ni. The value of $\mu_\Delta$ for $H = 0$ is identical to the initial permeability $\mu_i$. Gans[50] was able to show that the reversible susceptibility is a simple function of polarisation, independent of the previous history of the material.

The equation, in parametric form, is

$$\frac{\varkappa_{rev}}{\varkappa_i} = 3\left(\frac{1}{x^2} - \frac{1}{\sinh^2 x}\right)$$

$$\frac{J}{J_s} = \coth x - \frac{1}{x}$$

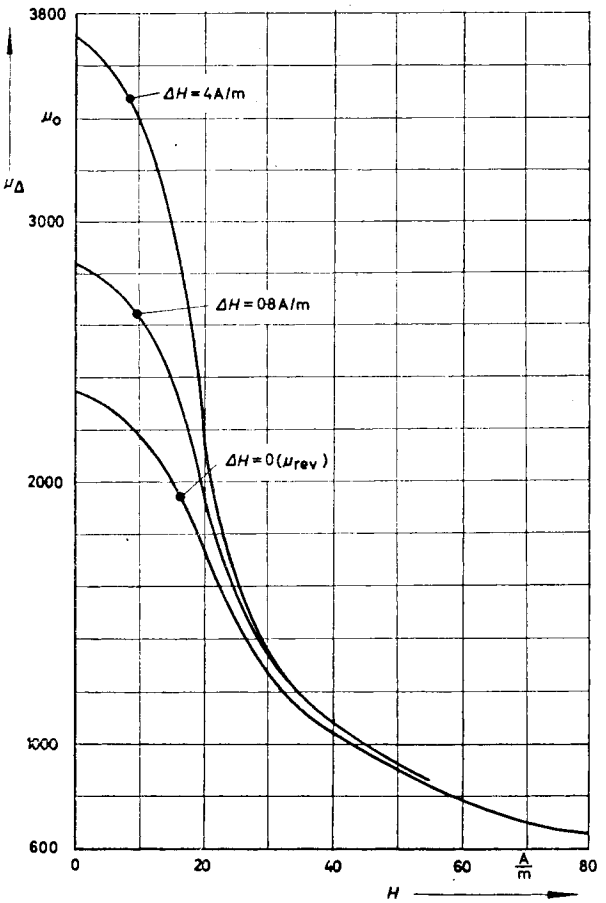



*Figure 3.7. Superposed permeabilities in relation to direct field strength for an alloy of 55% Fe and 45% Ni; the curve for $\Delta H = 0$ is, equally, the curve of reversible permeability $\mu_{rev}$*[15]

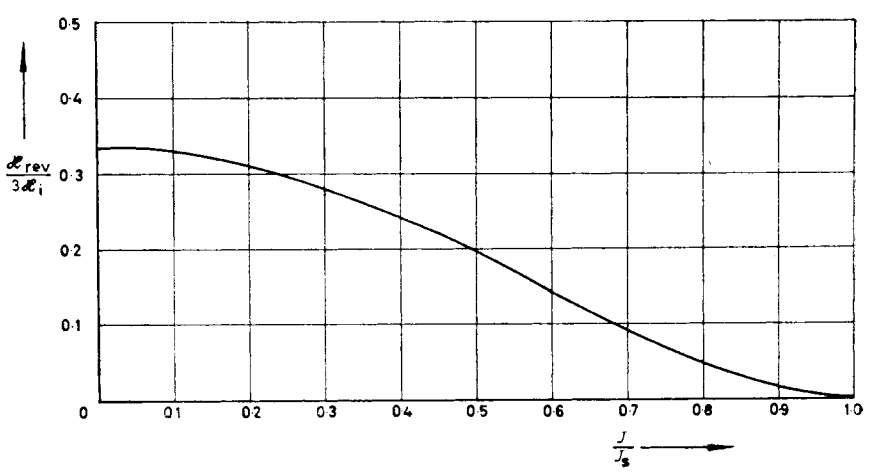



*Figure 3.8. Curve of reversible susceptibility, after Gans*[50]

If, therefore, $\varkappa_{rev}/\varkappa_i$ (the reversible susceptibility in comparison with the initial susceptibility) is plotted against $J/J_s$ (the polarisation in comparison with the saturation polarisation), the resulting curve is that shown in Figure 3.8.

If $\varkappa_{rev}$ or $\mu_{rev}$ is plotted against field strength for both branches of the curve, a butterfly-shaped curve[54] results. Figures 13.19 and 13.30 will serve as examples of this. However, plotting against flux density yields single-value curves (see, for example, Figure 12.11).

Reversible permeability plays an important part in a series of applications of magnetic materials, for example in transducers (Chapter 11), in many transformers used in communication work (Chapter 13), and in magnetic variometers [147a, 153].

### 3.2.4.9 Differential permeability

Differential permeability $\mu_{dif}$ characterises the change of flux density with magnetic field strength. It is also equal to the slope of the tangent at a point of the ($BH$) curve. At point Q (Figure 3.9) the differential permeability $\mu_{dif}$ is less than $\mu$. The relative differential permeability is

$$\mu_{dif} = \frac{1}{\mu_0} \frac{dB}{dH} \tag{3.19}$$

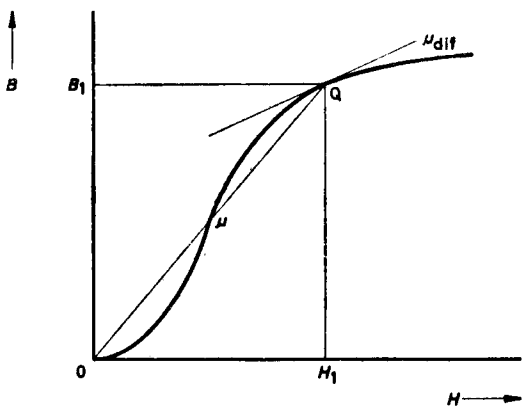



*Figure 3.9. Absolute permeability $\mu$ and differential permeability, $\mu_{dif}$ at point Q of the magnetising characteristic*

### 3.2.4.10 Permeability of toroids

To obtain genuine values for the characteristics of magnetisable bodies, avoiding as far as possible the influence of shape or of leakage, one is led to inductance measurements using toroidal cores. Laminated cores or ferrite cores are completely free from air-gaps, whereas in strip-wound cores (see Figure 5.2) the flux must jump a gap between individual turns that are not—at least not in general—negligibly small[1].

Let $L'$ be the inductance of a coil having $z$ turns but no core and $L$ the inductance of the same coil with core inserted; further, let $l_m$ be the length of the magnetic path, measured along the axis of the ring, and $A_m$ the cross-sectional area of the core. Then the relative toroidal permeability $\mu_{tor}$ is given by:

$$\mu_{tor} = 1 + \frac{1}{\mu_0} \frac{L - L'}{z^2} \frac{l_m}{A_m} \tag{3.20}$$

If $L \gg L'$ and $\mu \gg 1$, then we have approximately

$$\mu_{tor} = \frac{1}{\mu_0} \frac{L}{z^2} \frac{l_m}{A_m} = \frac{L}{z^2 K} \tag{3.21}$$

and

$$K = \mu_0 \frac{A_m}{l_m}$$

The magnetic field strength within the current-carrying coil is given by

$$H = \frac{iz}{l_m} \tag{3.22}$$

where $i$ is the current.

Strictly speaking, equations 3.20–3.22 hold only if the geometric axis of the toroid coincides with the magnetic axis. This, however, happens only when the ratio of the outer radius $r_o$ to the inner radius $r_i$ does not depart much from unity

$$\frac{r_o}{r_i} \to 1$$

In all other cases[108, 110, 158], especially for small rings with thick walls, $l_m$ must be replaced by $l'_m$, where

$$l'_m = \frac{2\pi(r_o - r_i)}{\ln (r_o/r_i)} \tag{3.23}$$

Substituting in equation 3.21,

$$\mu_{tor} = \frac{1}{\mu_0} \frac{L}{z^2} \frac{2\pi}{h \ln (r_o/r_i)} \tag{3.21a}$$

where $h$ is the height of the toroid. If, for example, we take $r_o/r_i = 2{\cdot}4$, then by equation 3.21 we obtain a value for $\mu_{tor}$ about 6% higher than by using the more accurate equation 3.21a.

A further source of error arises from the uneven distribution of flux density over the cross-section of the core: $B$ is always smaller near the outer surface than at the inner surface. The spread of permeabilities differs more especially at low flux densities. The true distribution of $\mu$ and $B$ over the core section should, ideally, be determined point by point. The differences

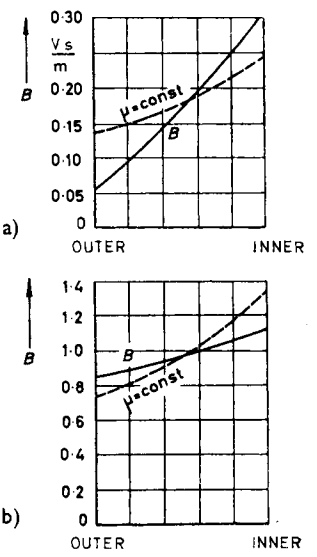



*Figure 3.10 Fall of B with increasing diameter for an iron toroid: (a) mean value of* $B = 0{\cdot}9908$ V s/m²; *(b) mean value of* $B = 0{\cdot}1734$ V s/m²

are less at high flux densities. Figure 3.10 reproduces an example taken from Niethammer[109].

For a toroidal core of wrought iron, of $r_o = 14{\cdot}1$ cm and $r_i = 7{\cdot}75$ cm, the curves show the distribution of flux density $B$ and permeability $\mu$ for two mean flux densities—$B = 0{\cdot}1734$ V s/m² and $B = 0{\cdot}9908$ V s/m².

### 3.2.4.11 Apparent permeability

The apparent relative permeability is defined as the ratio of the inductance $L$ of a coil with core, to the inductance $L'$ of the coil without core:

$$\mu_{app} = \frac{L}{L'}$$

$\mu_{app}$ has a unique value only for toroidal cores. In other cases the value depends on the shape of the coil and the core, and also on the particular placing of the coil on the core. Therefore, it is only for toroidal cores that the apparent permeability $\mu_{app}$ equals the effective permeability $\mu_e$; in this case the core has hardly any effect on the flux path.

### 3.2.4.12 Effective permeability

If a core is constructed of non-uniform material, an effective permeability, or an effective relative permeability, is defined by:

$$\mu_e = \frac{1}{\mu_0} \frac{L}{z^2} \sum \frac{l}{A} \tag{3.24}$$

or

$$\mu_e = \frac{\sum(l/A)}{\sum(l/\mu A)} \tag{3.25}$$

in which the ratios $l/A$ and $l/\mu A$ are formed for each element and summed over the total flux path; $l$ is the path length of each elementary section and $A$ the corresponding cross-sectional area. Calculations of cored coils with air-gaps rely particularly on equations 3.24 and 3.25.

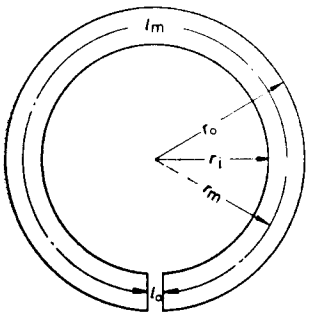



*Figure 3.11. Toroid with air-gap, shown diagramatically*

The procedure is as follows (see Figure 3.11). From equation 3.22,

$$B = \frac{iz}{l_m}\mu \tag{3.26}$$

and thence

$$\Phi = iz\mu\frac{A_m}{l_m} = \frac{iz}{l_m/\mu A_m} \tag{3.27}$$

In a thin toroidal core, the mean magnetic path length $l_m = 2\pi r_m = \pi(r_o + r_i)$ and the magnetic cross-section is $A = h(r_o - r_i)$.

If there occurs in the path of the mean flux $\Phi$ an air-gap whose length $l_a$ is small in comparison with the path length $l_m$ in the ferromagnetic core material (of permeability $\mu$), then equation 3.27 may be written

$$\Phi = \frac{iz}{(l_m/\mu A_m)+(l_a/\mu_a A_a)} \tag{3.28}$$

where $l_m \gg l_a$ and $l_m + l_a = l$. The permeability $\mu$ of the material should not be too small so that the leakage around the air-gap can be ignored. The air-gap permeability $\mu_a$ can be taken as unity. Equation 3.28 may now be written in the form

$$\Phi = \frac{iz\mu A}{l_m + \mu l_a} = \frac{izA}{l}\mu_e \tag{3.29}$$

where

$$\mu_e = \frac{\mu}{1+\mu(l_a/l_m)} \tag{3.30}$$

The effective permeability thus depends on that of the magnetic material ($\mu$) and on the gap ratio $l_a/l_m$. As an example, Figure 3.12 shows the relation $\mu_e = f(\mu)$.

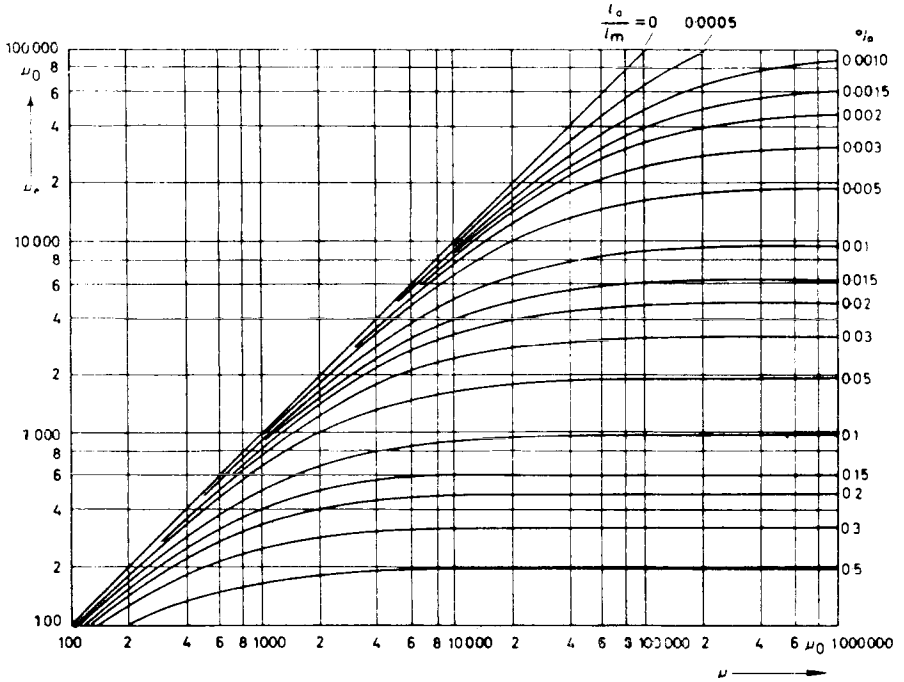



*Figure 3.12. Effective permeability $\mu_e$ as a function of material permeability $\mu$ and of gap ratio $l_a/l_m$*

### 3.2.4.13 Complex permeability

A dissipative ('lossy') coil can be regarded as a resistance and an inductance connected in series, so, just as the apparent resistance is given by a complex expression, so is the permeability, which can be written in the complex form:

$$\bar{\mu} = \mu_{LS} - j\mu_{RS} \tag{3.31}$$

Here $\mu_{LS}$ stands for the 'real' inductive permeability in the series circuit and $\mu_{RS}$ for the 'imaginary' resistive permeability;

$$j = \sqrt{(-1)}$$

Equation 3.31 can be written, among other ways, in the form

$$\bar{\mu} = \mu_s' - j\mu_s'' \tag{3.31a}$$

If, as is often convenient, a parallel connection of resistance and inductance is assumed, then the reciprocal of the complex permeability is given by

$$\frac{1}{\bar{\mu}} = \frac{1}{\mu_{LP}} + j\frac{1}{\mu_{RP}} \tag{3.32}$$

Another way of writing equation 3.32 is

$$\frac{1}{\bar{\mu}} = \frac{1}{\mu_p'} - \frac{1}{j\mu_p''} \tag{3.32a}$$

Here, $\mu_{LP}$ is the real inductive permeability for parallel connection and $\mu_{RP}$ the corresponding imaginary resistive permeability[140]. The reciprocal of permeability is called reluctivity. It should be noted that the values of $\mu_{LS}$ and $\mu_{LP}$ are different. The notion of complex permeability is often useful:

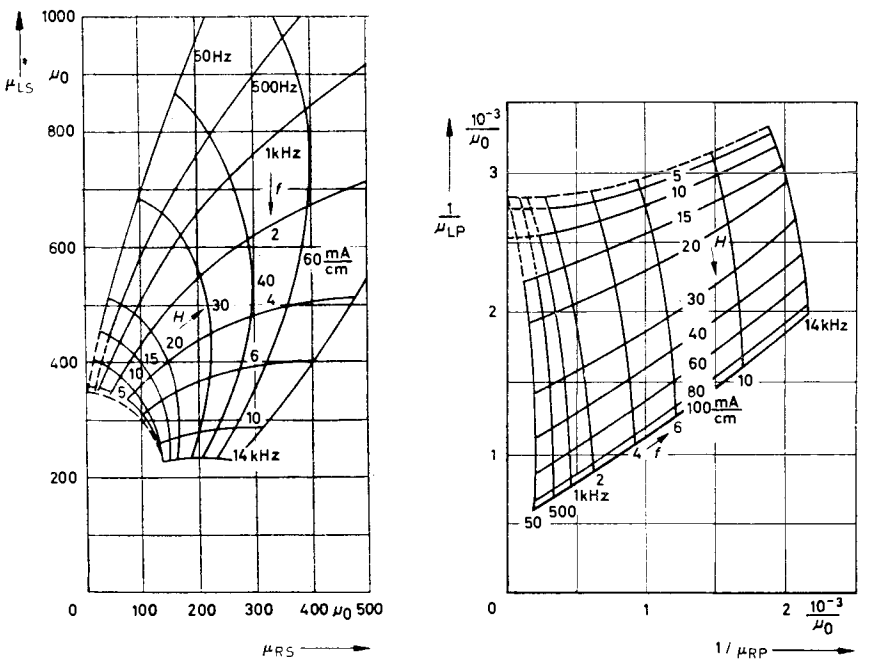



*Figure 3.13. Locus of complex permeability for an* Fe–Si *alloy (sheet thickness 0·3* mm*)*[41]

the magnetic properties of a substance, as functions of frequency and field strength, can often be displayed as a family of its loci. Loss components (hysteresis, eddy currents, and after-effects) can be found from the form of such a family (Figure 3.13)[41].

### 3.2.4.14 Inductivity factor

The inductivity factor $A_L$ is of magnitude proportional to the effective permeability. It is defined by

$$A_L = \frac{L}{z^2}$$

so equation 3.21 can be put in the form

$$\mu = \frac{A_L}{K}$$

The inductivity factor of a ferrimagnetic core, therefore, may be thought of as the inductance produced by a single turn; $A_L$ is generally quoted in nanohenries (nH). For ferrite pot cores, $A_L$ lies between 40 nH and 7000 nH or so, according to material, core size, length of air-gap, and winding. The $A_L$ value can be converted to the $\mu_e$ value for certain known types of core. For pot cores to DIN 41 293, Table 3.4 gives the result of such a conversion[33d].

**Table 3.4** RELATION BETWEEN THE $A_L$ VALUE AND THE RELATIVE EFFECTIVE PERMEABILITY $\mu_e$ FOR POT CORES TO DIN 41 293

| $A_L$ (nH) | $\mu_e$ | | | | | | |
|---|---|---|---|---|---|---|---|
| | 11 | 14 | 18 | 22 | 26 | 30 | 36 |
| 40 | 31 | 25 | | | | | |
| 63 | 48 | 40 | 30 | 25 | | | |
| 100 | 76 | 63 | 48 | 40 | 32 | | |
| 160 | 122 | 101 | 76 | 63 | 51 | | |
| 250 | 190 | 157 | 119 | 99 | 80 | 66 | 53 |
| 315 | 240 | 198 | 150 | 125 | 100 | 83 | 66 |
| 400 | 305 | 252 | 191 | 158 | 128 | 105 | 84 |
| 630 | (478) | (396) | 300 | 249 | 202 | 166 | 132 |
| 1 000 | (760) | (630) | (475) | (400) | 320 | 263 | 210 |
| 1 600 | (1 220) | (1 000) | (760) | (635) | (510) | (420) | 337 |
| 2 200 | | (1 390) | (1 050) | (870) | (700) | (576) | (462) |
| 3 600 | | | (1 720) | (1 430) | (1 140) | (945) | (755) |
| 4 600 | | | | (1 820) | (1 460) | (1 210) | (970) |
| 6 000 | | | | | (1 910) | (1 570) | (1 260) |
| 7 400 | | | | | | (1 930) | (1 560) |

### 3.2.5 Magnetic losses

#### 3.2.5.1 Jordan loss coefficients ($e$, $r$, $h$)

If a coil with a magnetic core is measured at low field strengths and at various frequencies $f$, a relation such as shown in Figure 3.14 is obtained. The resistance $R_{d.c.}$ for $f = 0$ is the ohmic resistance of the coil. If this is subtracted, the remainder $R_l$ of the total resistance is the a.c. component:

$$R_l = R - R_{d.c.} \tag{3.33}$$

If the dielectric loss is kept low, $R_l$ is that part of the resistance caused by losses in the core; $R_l$ increases more or less as the square of the frequency.

Thus a good approximation to a straight-line graph can be obtained by plotting the quotient $R_l/f$ or $R_l/fL$ against frequency. Measurements at varying field strengths yield a family of parallel straight lines (Figure 3.15a).

Extrapolating from this family to $H = 0$, it is found that the line does not, as one might expect, pass through the origin, but through a positive

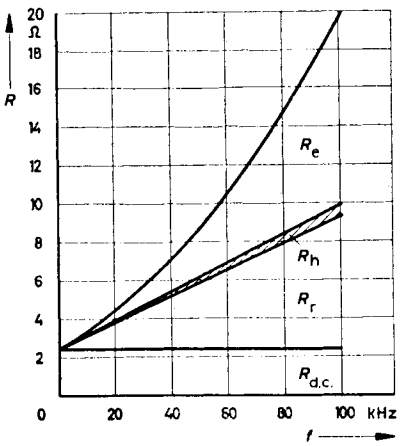



*Figure 3.14. Partition of loss in a dust core ($\mu = 50\ \mu_0$, $L = 10$ mH, $r = 7\%$, $e = 0{\cdot}1$ μs, $h = 45$ cm/kA)*

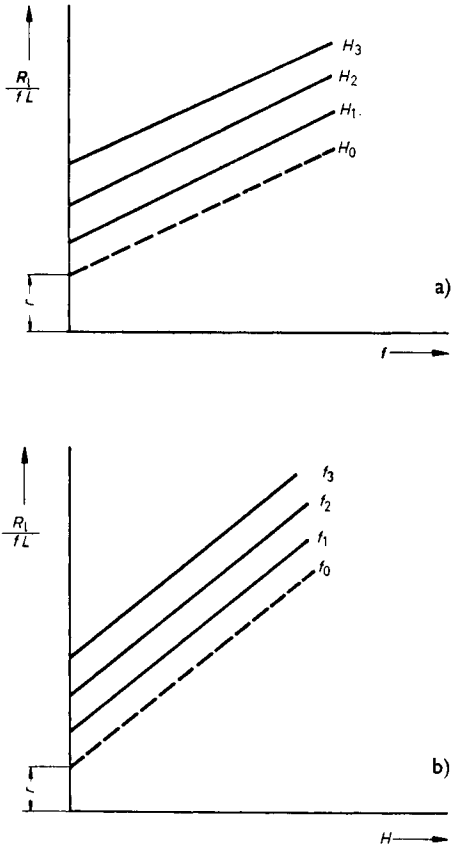



*Figure 3.15. (a) $R_l/fL$ as a function of frequency with H as parameter; (b) $R_l/fL$ as a function of field strength with f as parameter*

ordinate. It follows from the relation $R_l/fL$ as a function of $f$ that the loss resistance $R_l$ comprises three components, which lead, as shown by plotting $R_l/fL$ against $f$ or $H$, to three coefficients:

1. one component $R_r$ depends on the frequency but not on the field strength.
2. one component $R_e$ rises as the square of the frequency and is independent of field strength.
3. one component $R_h$ is a function of both frequency and field strength.

Then

$$R_l = R_r + R_e + R_h \tag{3.34}$$

or

$$R_l = rfL + ef^2L + hH_{\text{eff}}fL \tag{3.35}$$

from which can be derived

$$\frac{R_l}{fL} = r + ef + hH_{\text{eff}} \tag{3.36}$$

The coefficient $r$ is called the coefficient of magnetic viscosity or, alternatively, the residual-effect coefficient; $e$ is the eddy-current coefficient, and $h$ is the hysteresis coefficient.

The residual coefficient $r$ can easily be read off the graph of $R_l/fL$ against $H$ or $f$ (Figure 3.15). The gradient of the plot against frequency is a measure of the eddy-current factor $e$; the gradient of the plot against field strength yields the hysteresis factor $h$. In Figure 3.15a, the spacing of the lines is a measure of the eddy-current coefficient. A single graph thus suffices to determine $r$, $e$, and $h$.

The coefficient $r$ can be calculated from measurements at two frequencies $f_1$ and $f_2$, using the linear relationship between $R_l/fL$ and the frequencies $f$:

$$r = \frac{\left(\frac{R_l}{fL}\right)_2 - \left(\frac{R_l}{fL}\right)_1}{f_2 - f_1} \tag{3.37}$$

The factor $h$ can be computed from a two-point measurement of $H$ by means of the formula

$$h = \frac{\left(\frac{R_l}{fL}\right)_2 - \left(\frac{R_l}{fL}\right)_1}{H_2 - H_1} \tag{3.38}$$

The units in which the loss values are expressed can be derived from the defining equation 3.35. If the resistances $R_r$, $R_e$, and $R_h$ are measured in ohms, the frequency $f$ in kilohertz ($10^3\ \text{s}^{-1}$), the inductance $L$ in henries (equal to ohm seconds), and the field strength $H$ in A/cm, then:

$$r = \frac{R_r}{fL}\ \frac{\Omega\,\text{s}}{10^3\,\Omega\,\text{s}} = \frac{R_r}{fL}\ ‰ \tag{3.39a}$$

$$e = \frac{R_e}{f^2L}\ \frac{\Omega\,\text{s}^2}{10^6\,\Omega\,\text{s}} = \frac{R_e}{f^2L}\ \mu\text{s} \tag{3.39b}$$

$$h = \frac{R_h}{fLH}\ \frac{\Omega\,\text{s cm}}{10^3\,\text{A}\,\Omega\,\text{s}} = \frac{R_h}{fLH}\ \text{cm/kA} \tag{3.39c}$$

The quantities $r$, $e$, and $h$ are called the Jordan coefficients because they arose out of a proposal made by Jordan in 1924[75].

Today, however, there is a variant on the original Jordan proposal in that it is now usual to take $f = 1$ kHz as reference frequency where Jordan chose $f = 0{\cdot}8$ kHz.

### 3.2.5.2 The loss factor

In electrotechnology, the 'circular frequency' $\omega = 2\pi f$ is used, in many cases, instead of the frequency $f$. Tan $\delta$, the loss factor (i.e. the tangent of the loss angle $\delta$), replaces $R/2\pi fL$, and the above equations then become

$$\frac{R_l}{\omega L} = \frac{R_r}{\omega L} + \frac{R_e}{\omega L} + \frac{R_h}{\omega L} \tag{3.40}$$

which divides the loss factor of the core material into three components, namely

$$\tan \delta_c = \tan \delta_r + \tan \delta_e + \tan \delta_h \tag{3.41}$$

Further, equation 3.41 can be written in the form:

$$\tan \delta_c = \frac{R_l}{2\pi fL} = \frac{1}{2\pi}(r + ef + hH) \tag{3.42}$$

The reciprocal of the loss factor is $Q$, the quality factor (or sharpness factor):

$$Q = \frac{1}{\tan \delta_c} = \frac{2\pi fL}{R_l} \tag{3.43}$$

The loss factor, tan $\delta$, is a function of frequency and field strength. It alters, moreover, if the magnetic flux, for example in a transformer or choke, crosses an air-gap. However, the loss factor measured at zero frequency, divided by the initial permeability, $(\tan \delta)/\mu_i$, is a material constant, independent of gapping, which enables comparisons between different materials to be made (see, for example, Figure 13.88). This 'referred' loss factor must be multiplied by the effective permeability $\mu_e$ to obtain the loss factor of the core.

For an actual coil, tan $\delta_c$ of the core constitutes only one part of the total loss factor. One must include the loss factor of the winding which—leaving aside the loss angle due to winding capacities—can be split into two factors, tan $\delta_0$ and tan $\delta_{ew}$[66, 136]. Tan $\delta_0$ is a measure of d.c. current loss, so

$$\tan \delta_0 = \frac{R_{d.c.}}{\omega L} \tag{3.42a}$$

and tan $\delta_{ew}$ is a measure of eddy-current losses in the windings:

$$\tan \delta_{ew} = \frac{f^2 d^4 z^3 l_t}{\omega L \varrho l_f^2} \tag{3.42b}$$

where $\varrho$ is the specific electrical resistance of the conductor material, $l_t$ is the mean length of turn, and $l_f$ is the mean length of flux path.

Plotted against frequency, tan $\delta_0$ falls as the frequency rises, whereas tan $\delta_{ew}$ rises, and tan $\delta_c$ rises slowly at first and then more rapidly at the

higher frequencies. Each of these components, therefore, has its frequency characteristic, as reflected in Figure 3.16. If the three components are combined, a family of curves results, each member curve having a minimum whose location depends on the core and the winding data. A few examples are shown in Figure 3.17. The maxima are shifted according to the inductance $L$ and the winding space-factor (i.e. a number $K$ referring to the number of sections in the bobbin). Thus:

| | | |
|---|---|---|
| Curve 1 | $L = 2500$ mH | $K = 1$ |
| Curve 2 | $L = 60$ mH | $K = 1$ |
| Curve 3 | $L = 4$ mH | $K = 1$ |
| Curve 4 | $L = 4$ mH | $K = 3$ |
| Curve 5 | $L = 1$ mH | $K = 3$ |

The broken curve 6 is the limiting curve for the least possible factors on the assumption that the natural frequency $f = 1/2\pi\sqrt{(LC)} \geqslant (10\times$the driving frequency).

Using the permeability relation given in complex form in equations 3.31 and 3.31a, we get for the loss factor

$$\tan \delta_{cs} = \frac{\mu_s''}{\mu_s'} \quad \text{or} \quad \tan \delta_{cs} = \frac{\mu_{RS}}{\mu_{LS}} \tag{3.44}$$

for series connection, and, for parallel connection,

$$\tan \delta_{cp} = \frac{\mu_p'}{\mu_p''} \quad \text{or} \quad \tan \delta_{cp} = \frac{\mu_{LP}}{\mu_{RP}} \tag{3.45}$$

### 3.2.5.3 The Legg coefficients

In English publications, instead of the Jordan coefficients, one often meets a similar set derived from Legg[92]. The defining equation takes the form

$$\frac{R_l}{\mu f L} = aB_m + c + bf \tag{3.46}$$

In this equation, $B_m$ refers to the peak density (which Jordan measures in gauss). The equation thus introduces the permeability, which is absent in the Jordan formulation.

The coefficient $a$ corresponds to the hysteresis coefficient $h$; $c$ to the residual coefficient $r$; and $b$ to the eddy-current coefficient $e$. For converting the Legg coefficients into the Jordan coefficients, the following relations are needed:

$$\left.\begin{aligned} h &= a\mu^2\ 1770\ \text{cm/kA} \\ r &= c\mu\ 1000\ ‰ \\ e &= b\mu\ 1000^2\ \mu\text{s} \end{aligned}\right\} \tag{3.47}$$

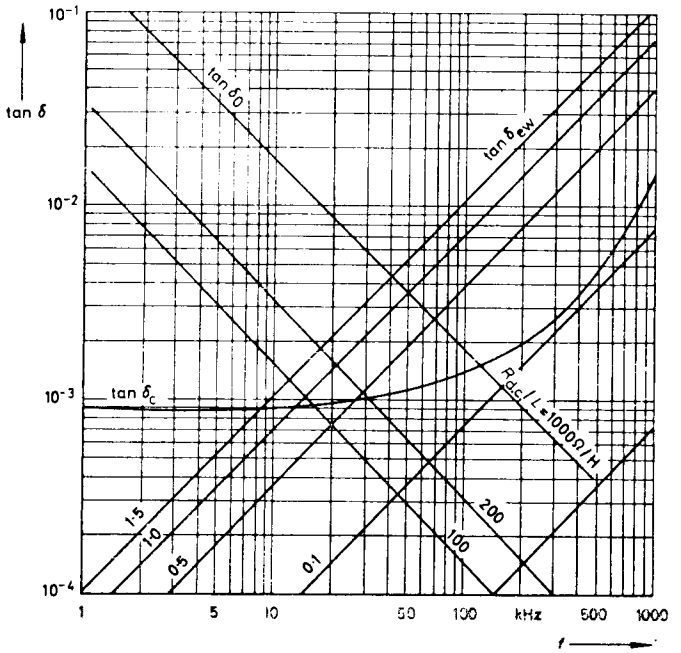



*Figure 3.16. Components of the loss factor tan δ for a coil having a pot core of ferrite*

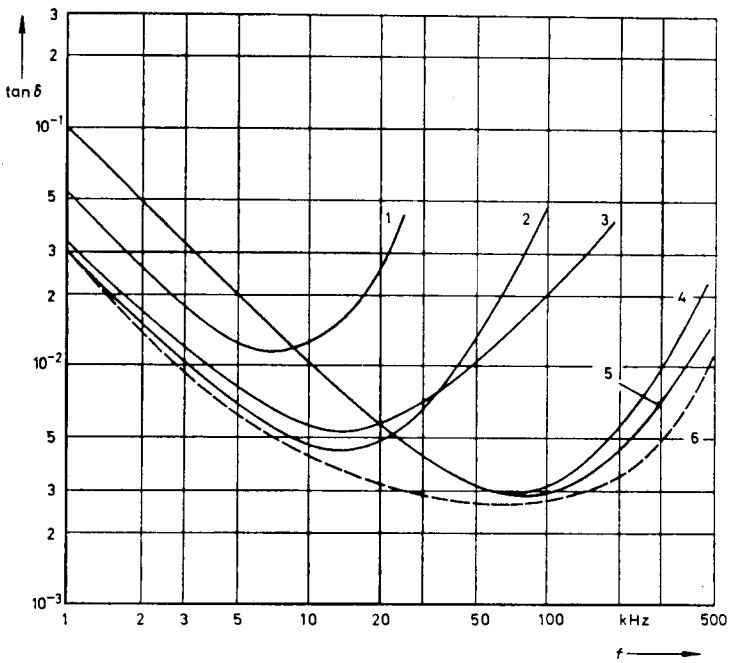



*Figure 3.17. Loss factor tan δ of a coil with pot core of ferrite as a function of frequency (for an explanation of designations 1–6 see text)*

The $\mu$-referred characteristics $h/\mu^2$, $r/\mu$, and $e/\mu$ are thus very similar to the Legg definitions and are, in fact, the same except for a numerical factor. Legg coefficients and the $\mu$-referred Jordan coefficients have the great advantage in practical use that they hold for magnetic bodies with or without air-gaps and permit a better comparison between materials than do the pure coefficients $e$, $r$, and $h$.

### 3.2.5.4 Examples of loss partition

To give a practical idea of the magnitudes of the various losses involved two examples will be given: one for a dust core and one for a ferrite core. Figure 3.14 shows the frequency dependence of total loss for a dust core of carbonyl iron.

The characteristics for the dust-core coil are: $R = 2{\cdot}5\ \Omega$, $L = 10$ mH, $H = 10$ A/cm, initial permeability $\mu_i = 50\mu_0$. Analysing the losses into their elements gave $r = 7‰$, $e = 0{\cdot}1$ μs, and $h = 45$ cm/kA. Up to about 80 kHz, the residual loss is the most important quantity; at higher frequencies the rising eddy-current losses are dominant.

In cores for high-frequency use, a lowering of the eddy-current loss is possible by the use of more finely divided powder. The eddy-current coefficient $e$, in fact, rises as the square of the grain cross-section and is also higher the greater the specific electrical conductance $\sigma$ and the permeability of the material[89]:

$$e \triangleq d^2\sigma\mu \tag{3.48}$$

As a rule, the eddy-current coefficient $e$ is quoted in microseconds (μs). We then have

$$\frac{e}{\mu\text{s}} \approx 1{\cdot}25 \times \frac{\mu}{\mu_0} \frac{\sigma}{(\Omega\,\text{cm})^{-1}} \frac{d^2}{\text{cm}^2} \tag{3.49}$$

The conductivity of ferrites is less than that of iron by several orders of magnitude, so a vanishingly small eddy-current loss is to be expected. However, if the value of $R_1/fL$ is plotted against frequency for a high-permeability ferrite core, then the usual chord-gradient of $R_1/fL$ associated with dust cores can be interpreted—though in a purely formal sense—as an eddy-current coefficient $e$ (Figure 3.18a), even though it really derives from a frequency-dependent residual effect[86].

The example shown in Figure 3.18a for a toroidal core of Mn–Zn ferrite demonstrates that the straight lines plotted are not parallel but get steeper as the measuring intensity increases. Thus the eddy-current coefficient is seen to depend on the field intensity. The dependence of $e$ on frequency, shown in the graph, can be evaluated from a study of the four lines shown. The value of $e$ extrapolated to $H = 0$ is designated $e_0$ (Figure 3.18b).

It is also clear from the graph that the hysteresis value $h$ is likewise frequency dependent. Figure 3.19a, for example, shows the growth rates of loss against field strength at 10 kHz, 50 kHz, and 100 kHz. Each gradient leads to a different value of $h$ (Figure 3.19b). Extrapolating to zero frequency gives

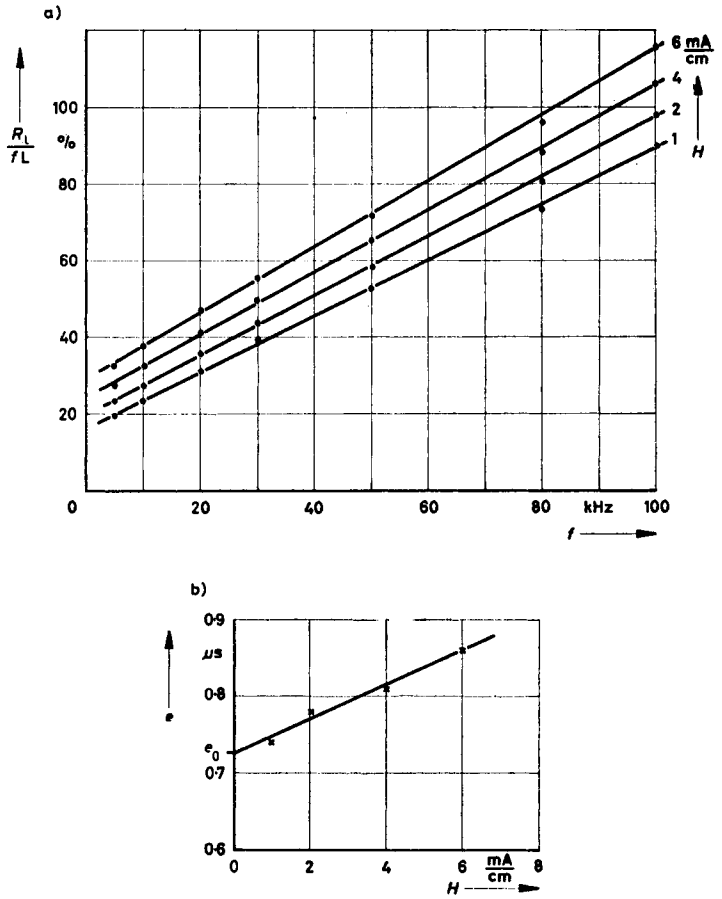



*Figure 3.18. (a) Measured values of $R_1/fL$ for a* Mn–Zn *ferrite as a function of frequency; (b) determination of eddy-current coefficient $e_0$*

$h_0 = 2700$ cm/kA. In this example, the dependence both of $e$ on field strength and of $h$ on frequency are more or less linear, but there are cases where this rule does not apply.

It sometimes happens, however, that departures are no more than apparent, especially where measuring ferrites of low coercive force or of low Curie temperature. Temperature and field strength have to be kept rigidly invariant during the measurement[11]. Indeed, Feldtkeller and Hettich[44] have demonstrated that, in attempts to evaluate Jordan factors, simplifications may creep in which could lead to false results. These errors can be avoided by evaluating the loss coefficients by means of measurements of the complex permeability. Figure 3.20 shows the complex permeability obtained in this way for a dust core of permeability $52\mu_0$. Using this method, the frequency relation of the residual loss may be readily obtained and distinguished from the eddy-current loss.

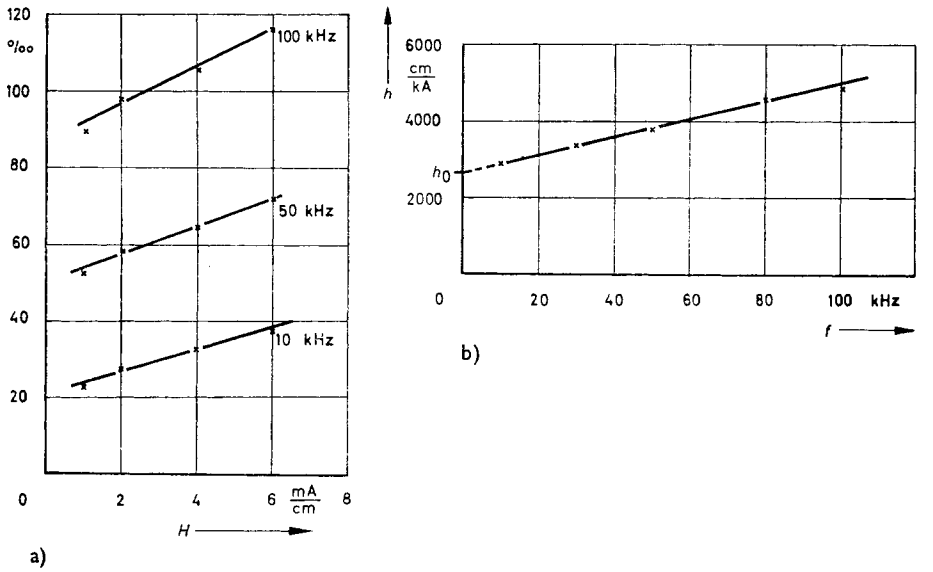



*Figure 3.19. (a) Measured values of $R_1/fL$ for a* Mn–Zn *ferrite as a function of field strength; (b) determination of hysteresis coefficient $h_0$*

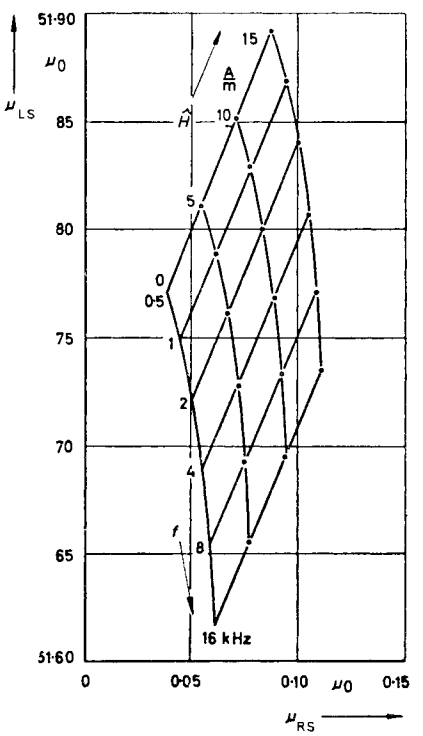



*Figure 3.20. Complex permeability of a dust core*[44]

**Table 3.5** LOSS COEFFICIENTS AND $\mu_i$-REFERRED LOSS COEFFICIENTS OF CORES OF INDUCTANCE COILS

| | *Tape cores to DIN 41 301 D1* | *Dust cores* | *Ferrite cores* |
|---|---|---|---|
| $\mu_i$ ($\mu_0$) | 2 000 | 50 | 3 950 |
| $e$ (μs) | — | 0·1 | 0·81 |
| $r$ (‰) | — | 7 | 14 |
| $h$ (cm/kA) | 6 000 | 45 | 1 800 |
| $e/\mu_i$ ($10^{-3}$ μs/$\mu_0$) | — | 2·0 | 0·20 |
| $r/\mu_i$ ($10^{-6}/\mu_0$) | — | 140 | 3·6 |
| $h/\mu_i^2$($10^{-6}$ cm/kA $\mu_0^2$) | 1·5 | 18 000 | 115 |
| $h/\sqrt{\mu_i}$ (cm/$\sqrt{\mu_0}$) | 130 | 6·5 | 29 |

The magnetic residual effect can occur in many forms and may be investigated in numerous materials by a variety of methods. Among the more important expositions only the following are quoted here: Feldtkeller[41, 43], Goldschmidt[54], Herrmann[69], Néel[102], Richter[123], Schulze[127], Snoek[133], Wijn[149], and Wilde[152]. Table 3.5 gives measured results for a dust core compared with a ferrite core.

The absolute values of $e$, $r$, and $h$ are higher for the ferrite core. Since, however, the initial permeability is significantly higher, the loss coefficients referred to $\mu_i$ are notably more favourable for ferrite than for iron dust cores.

### 3.2.5.5 Permeability rise factor

Hysteresis of magnetic materials causes undesired flux excursions which lead to harmonic distortion. Hysteresis must be as small as possible if these are to be kept low. Instead of measuring $h$ by means of resistance change, it is often both simpler and more useful to measure the rate of growth of the permeability of a coil with field strength and to consider this as the effective criterion.

The permeability rise factor will be called $\delta$. It is unlikely that this will lead to confusion with the loss angle $\delta$, because the gradient $\delta$ will always be used with an appropriate suffix, such as $\delta_{100}$ and $\delta_5$ (see DIN 41 301)[33c].

Originally the growth of permeability with field strength was defined as the permeability rise factor between 5 mOe and 10 mOe, and between 20 mOe and 100 mOe respectively. Thus:

$$\delta_5 = 66{\cdot}7\,\frac{\mu_{20}-\mu_5}{\mu_{20}}\ ‰ \tag{3.50}$$

$$\delta_{100} = 12{\cdot}5\,\frac{\mu_{100}-\mu_{20}}{\mu_{20}}\ ‰ \tag{3.51}$$

The $\delta$ values therefore indicate by how many ‰ the permeability changes for an increase in field strength of 1 mOe (0·0796 A/m). Since the introduction of SI units, equations 3.50 and 3.51 remain formally valid but now refer to the quantities $\mu_0 H_m = \mu_0 H/2$. This corresponds, therefore, to

$$20 \text{ mOe} = \frac{20}{4\pi} \text{ A/m} = 20 \times 10^{-7} \text{ V s/m}^2$$

The permeability rise factor is defined as the differential coefficient referred to the permeability $\mu_{20}$:

$$\delta = \frac{\Delta\mu}{\mu_0 \, \Delta H_m} \frac{1}{\mu_{20}} \tag{3.52}$$

The increment is given in units of $10^4$ m²/V s and indicates by how many ‰ the permeability changes for a change of $\mu_0 H_m$ of $10^{-7}$ V s/m².

In order not to have to alter the old figure for $\delta$, a certain complication of units has to be accepted in SI units. If equations 3.50 and 3.51 are used, a linear increment of $\mu$ is assumed.

### 3.2.5.6 Permeability rise factor and hysteresis coefficient

As can be seen from the Rayleigh loop[33] (see page 129), the hysteresis coefficient $h$ is related to the permeability rise factor $\delta$, in the low-field range in the following way:

$$h = \frac{8}{3} \frac{\mu_2 - \mu_1}{\mu_1 (H_2 - H_1)} \tag{3.53}$$

From this follows

$$h = \frac{2{\cdot}67 \Delta\mu}{\mu_1 \, \Delta H} = 2670 \, \delta \text{ cm/kA} \tag{3.54}$$

This relation holds only approximately since $\delta$ should really be referred to the initial permeability, whilst the definitions 3.50 and 3.51 are tailored to practical needs. Nevertheless, equation 3.54 serves well enough for assessment purposes. This will be shown for the Mn–Zn ferrite example mentioned above.

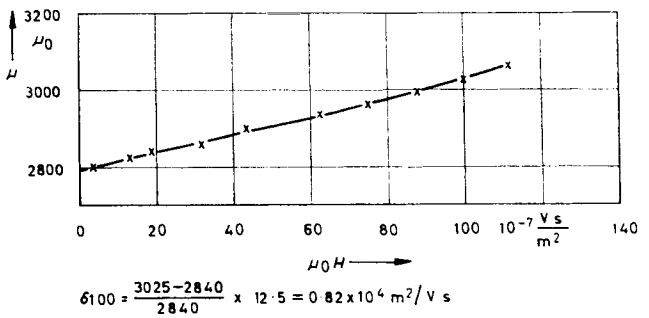



*Figure 3.21. Permeability against field strength: calculation of $\delta_{100}$ ($f = 5$ kHz, $T = 21$°C)*

Figure 3.21 shows the measured permeability rise factor plotted against field strength. It is not strictly linear, being slightly curved, but if the slight inaccuracy involved is neglected (as is justified for this kind of assessment) then, from equation 3.51,

$$\delta_{100} = \frac{3025-2840}{2840} \times 12{\cdot}5 = 0{\cdot}82‰$$

It then follows from equation 3.54 that

$$h = 2200 \text{ cm/kA}$$

Use of Figure 3.19b would give, for a measuring frequency of 5 kHz, $h = 2800$ cm/kA.

### 3.2.5.7 Hysteresis factor and hysteresis constant

In the Heaviside–Pupin loading coil technique, hysteresis effects are mostly expressed in terms of a hysteresis constant. This can be deduced from the hysteresis coefficient as follows.

From equations 3.34 and 3.35,

$$R_h = hHfL$$

and, from equation 3.22,

$$H = \frac{iz}{l}$$

If $A = V/l$ (where $V$ denotes volume) is substituted in equation 3.21, then

$$L = \frac{\mu z^2 V}{l^2}$$

which gives for $R_h$

$$R_h = \frac{h}{\sqrt{(\mu V)}} fiL^{3/2} \tag{3.55}$$

To get $R_h$ in ohms, $h$ must be expressed in cm/kA, $f$ in kilohertz, $i$ in amperes, $L$ in henries, $\mu$ in $\mu_0$, and $V$ in cm$^3$.

From equation 3.55, the hysteresis factor $F_h$ is defined as

$$F_h = \frac{R_h}{fi} = \frac{h}{\sqrt{(\mu V)}} L^{3/2} = KL^{3/2} \tag{3.56}$$

The hysteresis constant $K$ is thus a coil factor compounded from the hysteresis coefficient $h$, the permeability, and the volume of the core. The core material of the coil is represented by a magnitude $h/\sqrt{\mu}$. The constant $K$ is not

obtainable by direct measurement, so the alternative hysteresis constant $C$ is often used to characterise a coil:

$$C = \frac{\Delta R}{\Delta i f L^{3/2}} \tag{3.57}$$

This constant $C$ gives the change in resistance which results when the winding current is altered by 1 mA at a particular frequency $f$.

3.2.5.8 Hysteresis coefficient and the non-linear distortion factor

The distortion factor $k$ of a coil with ferromagnetic core is defined by the ratio of the e.m.f. of the third harmonic ($E_3$) to the change in the fundamental current, $i\omega L$:

$$k = \frac{E_3}{\Delta i \omega L} \tag{3.58}$$

If the loss factor $R/\omega L$ is much less than unity, then

$$\begin{aligned} k &= \frac{3}{5}\,\frac{R_h}{\omega L} \\ &= \frac{3}{5}\,K\frac{f i L^{3/2}}{2\pi f L} \\ &= 0{\cdot}955 \times 10^{-4}\, Ki\sqrt{L} \end{aligned} \tag{3.59}$$

The hysteresis constant $K$ thus limits both the hysteresis resistance $R_h$ and the non-linear distortion factor $k$ of a coil.

These relations offer the possibility of determining the hysteresis coefficient $h$ from a measurement of the $k$ factor. Thus

$$h = \frac{10\pi}{3}\,\frac{k}{H} = \frac{10{\cdot}45\,k}{H} \tag{3.60}$$

From the Rayleigh–Jordan relation[75], at low field intensities, $k$ may be written as equal to $3R_h/5\omega L$, and therefore

$$k = \frac{64}{10^{10}\mu_0}\,\frac{B_r}{B_m} = 0{\cdot}51\,\frac{B_r}{B_m} \simeq \frac{B_r}{2B_m} \tag{3.61}$$

From this expression it can be deduced[81] that a given peak value of the $k$ factor limits the permissible departure of the remanence $B_r$ from a linear function $B(H)$ relative to the peak induction flux $B_m$.

The frequency dependence of the non-linear distortion factor for coils with laminated cores was investigated by Kämmerer[76, 77].

3.2.5.9 Hysteresis material constant

This material constant $\eta_B$ is defined by the formula

$$\eta_B = \frac{R_h}{\omega L} \frac{1}{\mu_e B_m} = \frac{\tan \delta_h}{\mu_e B_m}$$

or as the ratio of the hysteresis loss factor $\tan \delta_h$ (equation 3.41) to the peak value of the flux density $B_m$, referred to the effective permeability $\mu_e$ [see IEC Publication 125, Amendment No. 1 (1965), Clause B3.2]. We can therefore write

$$\eta_B = \frac{hH}{2\pi\mu_e B_m}$$

From this we can arrive at conversion factors: $\eta_B = 1{\cdot}13h/\mu^2$ and $\eta_B = 1590a$.

3.2.5.10 Hysteresis core constant

This constant $\eta_i$ is defined somewhat after the manner of $\eta_B$, namely

$$\eta_i = \frac{R_h}{\omega L} \frac{1}{i_m \sqrt{L}} = \frac{\tan \delta_h}{i_m \sqrt{L}}$$

or

$$\eta_i = \frac{R_h}{i_m \omega L^{3/2}}$$

Comparing this definition with equation 3.57, the relation between hysteresis constant $C$ and hysteresis core constant $\eta_i$ is seen to be

$$C = 2\pi\eta_i \sqrt{2} = 8{\cdot}89\,\eta_i$$

The following relation between $\eta_B$ and $\eta_i$ may also be derived from these formulae:

$$\eta_i = \eta_B \sqrt{\frac{\mu_e^3}{V}}$$

3.2.5.11 Heavy-current losses

The losses involved in a magnetic cycle are due to the conversion of useful electromagnetic energy into a debased form, namely heat. Losses could therefore be determined with considerable accuracy by calorimetric measurements[70, 84a]. The method, however, is not very common in modern technology. Generally, a wattmeter method or a Ferrometer is employed. Loss of energy in the cores of transformers and machines used in heavy-current

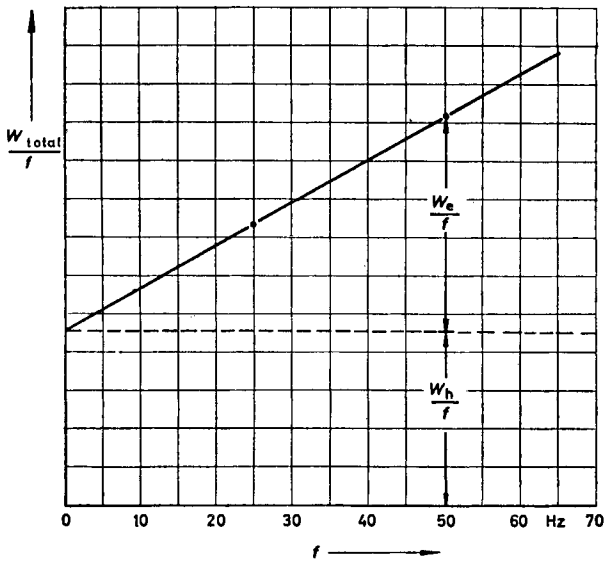



*Figure 3.22. Schematic diagram for determination of eddy-current loss in electrosheet;* $W_{total} = W_h + W_e$

engineering are compounded of a part that is independent of frequency (the hysteresis loss) and the eddy-current loss. The two types of loss may be separated in the following way: the total loss $W_{total}$ is measured at various frequencies and is divided by the measuring frequency $f$, and the result is plotted against frequency, as in Figure 3.22. A straight line is drawn through the measured points. The loss value corresponding (by extrapolation) to $f = 0$ is the hysteresis portion of the total loss.

*Numerical determination of loss partition*

The hysteresis loss $W_h$ can be numerically determined from the area of the hysteresis loop. The energy $A$ involved in a single magnetising cycle will appear in erg/cm$^3$ or mW s/cm$^3$. The relevant conversion relation is

$$1 \text{ erg/cm}^3 = 10^{-4} \text{ mW s/cm}^3 \tag{3.62}$$

In heavy-current work it is usual to relate power loss to mass rather than to volume. If $f$ is the frequency, or the number of magnetising cycles, and $d$ the density, then, for the said power loss,

$$W_h = \frac{Af}{d} \tag{3.63}$$

The proportion $W_e$ due to eddy-currents can also be calculated under certain restricted conditions—or at least approximated: the flux must be uniformly distributed throughout the individual laminae and must be sinusoidal in form—conditions not always fulfilled.

The flux is approximately sinusoidal if the ohmic resistance of the flux-measuring circuit is small compared with its inductive reactance. Then

$$W'_{\mathrm{w}} = \frac{(\pi D f B_{\mathrm{m}})^2}{6\varrho}$$

$$= \frac{1{\cdot}64}{\varrho}(DfB_{\mathrm{m}})^2\ 10^{-7}\mathrm{mW/cm^3}$$

and

$$W_{\mathrm{e}} = \frac{1{\cdot}64}{\varrho d}(DfB_{\mathrm{m}})^2\ 10^{-7}\ \mathrm{W/kg} \tag{3.64}$$

In equation 3.64, $D$ is the lamina thickness in millimetres, $f$ the frequency in hertz, $B_{\mathrm{m}}$ the peak induction flux in V s/m$^2$, $\varrho$ the specific electrical resistance in $\Omega$ cm, and $d$ the sheet density in g/cm$^3$. For example, if $D = 0{\cdot}5$ mm, $B_{\mathrm{m}} = 1$ V s/m$^2$, $f = 50$ Hz, $\varrho = 55\times10^{-6}\ \Omega$ cm, and $d = 7{\cdot}6$ g/cm$^3$, then

$$W_{\mathrm{e}} = \frac{1{\cdot}64\times0{\cdot}5^2\times1^2\times50^2}{55\times10^{-6}\times7{\cdot}6}\times10^{-7} = 0{\cdot}25\ \mathrm{W/kg}$$

Czerlinsky[31], measuring hot-rolled dynamo sheet, found a satisfactory agreement between calculated and measured results for eddy-current losses. Observed discrepancies can often be traced back to the non-fulfilment of the basic conditions required for calculation. Brailsford[23] has shown that, as the thickness of the sheet is increased, the penetration of the flux diminishes. The relative amplitudes at 50 Hz are shown in Figure 3.23 for normal dynamo sheets 0·4 mm, 0·8 mm, 1·6 mm, and 3·2 mm thick. In only the thinnest sheet does the flux occupy nearly the whole cross-section.

Even when the mean flux is sinusoidal there can be local departures. As the flux penetrates into the sheet from the surface, not only do amplitude and

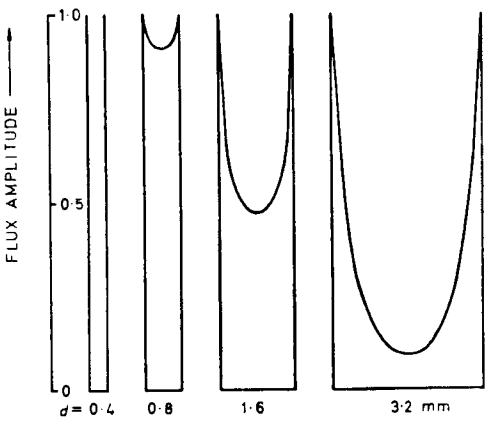



*Figure 3.23. Calculated amplitude of the alternating field in dynamo sheet of thickness 0·4* mm, *0·8* mm, *1·6* mm, *and 3·2* mm *at* $f = 50$ Hz[23]

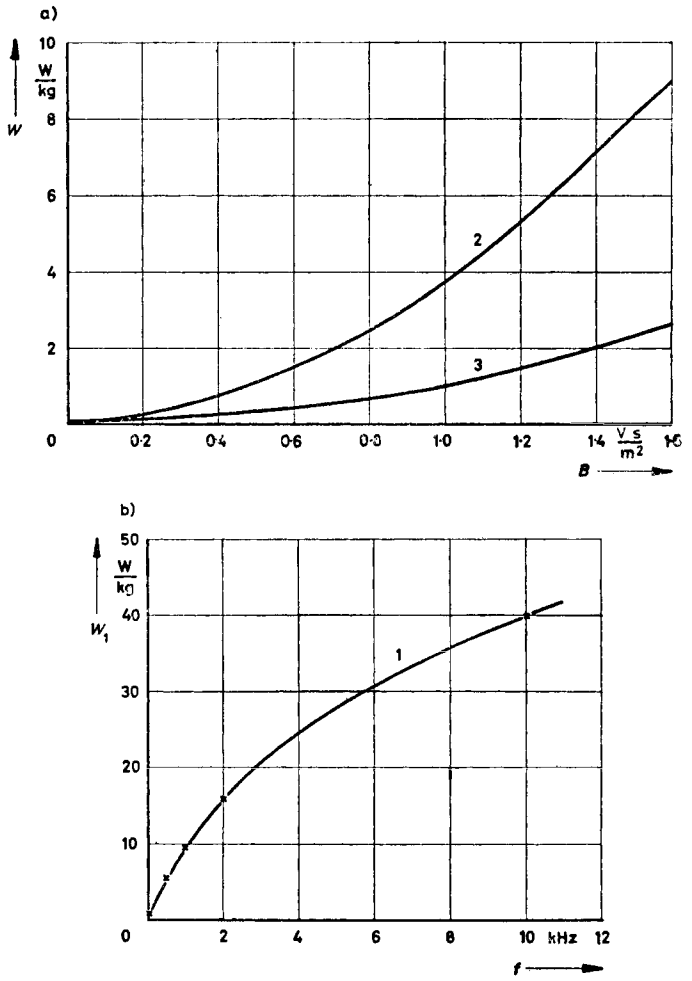



*Figure 3.24. (a) Power loss as a function of flux density; (b) power loss $W_1$ as a function of frequency; 1, dynamo sheet IV, 0·05* mm*; 2, unalloyed sheet, 0·75* mm*; 3, highly alloyed sheet, 0·35* mm

phase change but even the waveform itself. The same holds for the eddy-current waveform. These effects stem from the fact that equation 3.64 is only conditionally correct.

The heavy-current engineer is not so much interested in the individual losses $W_h$ and $W_e$ as in the total losses in the cores of transformers and generators. Hysteresis and eddy-current losses are additive:

$$W = W_h + W_e$$
$$= \left[\frac{Af}{d} + \frac{16{\cdot}4}{\varrho d}(DfB_m)^2\right] \times 10^{-8} \text{ W/kg} \qquad (3.65)$$

For a given type of lamination ($d$, $\varrho$, and $D$ constant) the total losses increase approximately as the square of the maximum flux density and of the frequency.

Figure 3.24a shows the dependence of total laminae loss on flux density $B$ for two different types of laminae, namely an unalloyed sheet of 0·75 mm and an alloyed lamina of 0·35 mm.

In practice, the relationship between watts loss and flux density $B$ is clarified by using the $B$ value at which measurements were carried out as a subscript. Measurement values are generally limited to 1·0 V s/m$^2$ and 1·5 V s/m$^2$, and then one may write $W_1$ and $W_{1,5}$ (at one time $W_{10}$ and $W_{15}$ were used, referring to 10 kG and 15 kG).

In Figure 3.24b the $W_1$ values for a 0·05 mm high-alloy sheet to DIN 46 400 are plotted against frequency up to 10 kHz. In general, frequencies in heavy-current engineering do not exceed 100 Hz and in the UK and most European countries 50 Hz is usual.

Types of sheet are often known by their losses in watts; thus a 'one-watt sheet material' indicates a quality of sheet such that the $W_1$ value at 50 Hz and 0·35 mm sheet thickness amounts to 1 W/kg.

### *Anomalous eddy-current losses*

More exact measurements have shown that the graph of Figure 3.22 is often not valid at medium and high flux densities: Figure 3.25 sets out measurements obtained by Stewart[138] for dynamo sheet at $B_m = 1$ V s/m$^2$. Total losses were plotted against frequency (curve 1). Curve 2 displays the calculated eddy-current losses, and curve 3 shows the difference between the former two curves. This difference curve 3 shows the additional or anomalous loss. The shape of the curve clearly shows that this loss rises rapidly, at first, with frequency and then more slowly.

Further investigation reveals that anomalous eddy-current loss increases rapidly with flux density. It can be deduced from Figure 3.26 that it increases approximately as the 1·8th power of $B$ between 0·5 V s/m$^2$ and 1·2 V s/m$^2$ (curve 4). The general experience that all losses increase as powers of $B$ between 1·6 and 2·0 cannot, however, be deduced from the mechanism of the

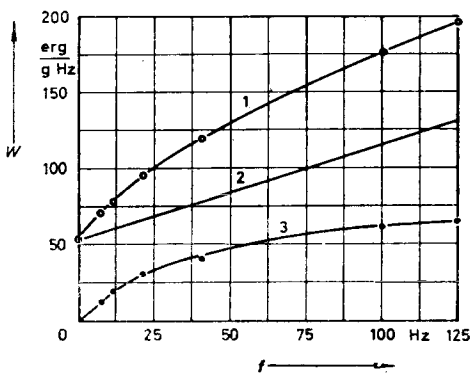



*Figure 3.25. Frequency dependence of losses in a low-loss sheet material at $B_m = 1$ V s/m$^2$: 1, total loss; 2, hysteresis loss plus calculated eddy-current loss; 3, 'extra loss' (1 − 2)*[138]

dependence of anomalous loss on flux density. Moreover, Stewart[138] found that the added losses were influenced by neither sheet thickness nor temperature. They must depend, therefore, on some special process. Stewart suggested an internal friction effect connected with a shift of the Bloch walls (which separate magnetic domains) during the magnetic cycling, and Williams, Shockley, and Kittel[155] ascribed the increased eddy-current loss to inhomogeneous distribution of permeability.

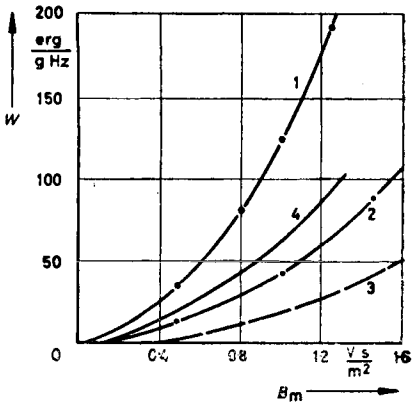



*Figure 3.26. Relation of losses to maximum flux density $B_m$ for specimens of low-loss sheet material ($f = 40$ Hz): 1, total loss; 2, hysteresis loss; 3, calculated eddy-current loss; 4, 'extra loss' (1 − 2 − 3)*[138]

Blake[9] has put forward a theory based on the fact (often observed experimentally) that Barkhausen 'jumps' occur with finite velocities. Large grains within the material and low speeds of movement of the domain walls are to be held responsible for the increased cycling losses. Nagashima[101], using extremely pure iron (99·99% Fe) was able definitely to observe that during magnetic cycling the walls of the larger domains moved more slowly than those of the smaller ones.

The results of Brailsford's researches[24] also indicate the influence of wall shifts. According to these experiments, the effect is not observable with rotating fields. If, then, the rotational process takes the place of the back and forth movement of the Bloch walls, the waveform phenomena disappear. Again, the observed fact that the effect shows more clearly for high-quality sheet tells in favour of the wall-shift effect. Brailsford[25], in fact, found that anomalous loss comprised about 8% of the total for 4% hot-rolled Fe–Si but was as much as 25% for high-quality cold-rolled Fe–Si sheet with 3·25% Si.

The problem of eddy-current anomaly is a focus of interest even today, as may be seen by the numerous research investigations recently devoted to it[2, 5, 29, 72, 107, 125, 137, 145]. All these investigations look for the cause of added loss in the construction of the Bloch wall and its dynamic behaviour under cyclic magnetisation. A model of the domain structure suggested by Pry and Bean[119] can be applied within a limited frequency range. However, no comprehensive theory of anomalous eddy-current loss has emerged up to the present.

*Hysteresis loss in a rotating field*

Hysteresis losses quoted for sheet material are usually derived from measurements in oscillating magnetic fields. However, materials are often used in fields which rotate (a.c. generators, induction motors).

The first experimental investigations were carried out by Ferraris[45] in 1888. He discovered that a laminated iron core could be made to turn in a rotating field by reason of its hysteresis. In 1892 Ewing[37] stated that: the atomic theory makes it probable that the work which is done in cyclic magnetisation is less, if the magnetised body rotates in a constant field, than if the magnetising force be taken through zero and up to the corresponding reversed value.

Quantitative measurements were made by Baily[4] a few years later. He stated—and this was verified many times later[26, 49, 126]—that, in weak rotating fields, the hysteresis losses are many times greater than in reciprocating fields, but at high field strengths, the rotational losses fall again and disappear when saturation is reached. The maximum corresponds to the knee of the hysteresis loop. Alternating-field hysteresis loss, on the other hand, increases all the way. There is thus a point where the two curves intersect.

Figure 3.27 shows three curves for a grain-oriented Fe–Si sheet with 3·1% Si: the rotating-field hysteresis loss $W_r$ and the alternating-field hysteresis loss $W_h$ are taken parallel to and perpendicular to the principal direction[22]. The ratio $W_r/W_h$ for equal magnetisation and increasing flux density falls continuously. In Figure 3.28 $W_r/W_h$ is plotted against $(B-\mu_0 H)/B_s$ following measurements by Brailsford[22]. The initial value is around 2·3, but $W_r/W_h$ becomes unity for $(B-\mu_0 H)/B_s = 0{\cdot}6$–$0{\cdot}7$.

Investigations by Zehler[161] have shown that the same connection between $W_r/W_h$ and flux density also holds in a rotating field with permanent-magnet materials (Alnico and chrome steel). Another relation, on the other hand, has been brought to light for materials having 'exchange anisotropy'[97] (see Figure 3.29). Here the rotational hysteresis does not vanish at high flux densities. These observations have also been noted in strips and thin films of Fe–Ni alloys[79].

The magnitude of the rotational hysteresis loss is determined by the chemical composition and the physical structure of the material. Baily[4] achieved a maximum of some 15 000 erg/cm$^3$ per cycle in magnetically soft charcoal iron, and for steel the maximum loss was about $W_r = 43\,000$ erg/cm$^3$ per cycle. According to Brailsford[23], hysteresis losses in rotational fields for dynamo sheet with 0·13% Si are about twice as high as for transformer steel with 3·72% Si.

Cold forming, bending, stretching, rolling, and mechanical working increase the rotational losses. In Figure 3.30 the $W_r$ losses are plotted[23] for an Fe–Si sheet with 4% Si. Loss curve 1 shows the original 0·65 mm laminant, and the significantly higher curve 2 shows this material after it has been cold worked, in a series of operations, down to 0·3 mm. Even a relatively mild annealing of 2 h at 630°C significantly reduces the loss value (curve 3). Annealing for 4 h at 1100°C lowers the hysteresis loss almost to the initial value (curve 4).

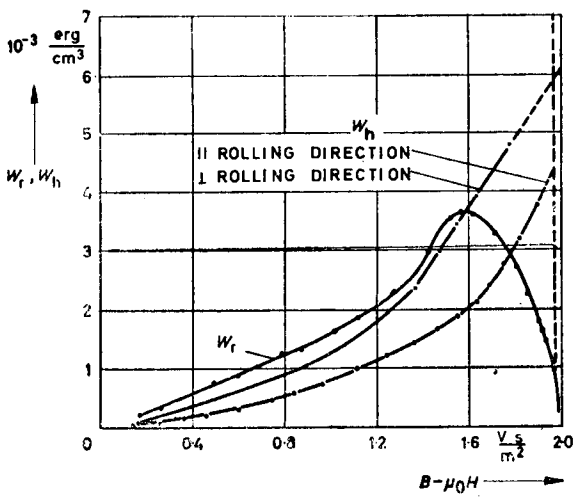



*Figure 3.27. Alternating hysteresis loss $W_h$ and rotational hysteresis loss $W_r$ in grain-oriented* Fe–Si *sheet*[22]

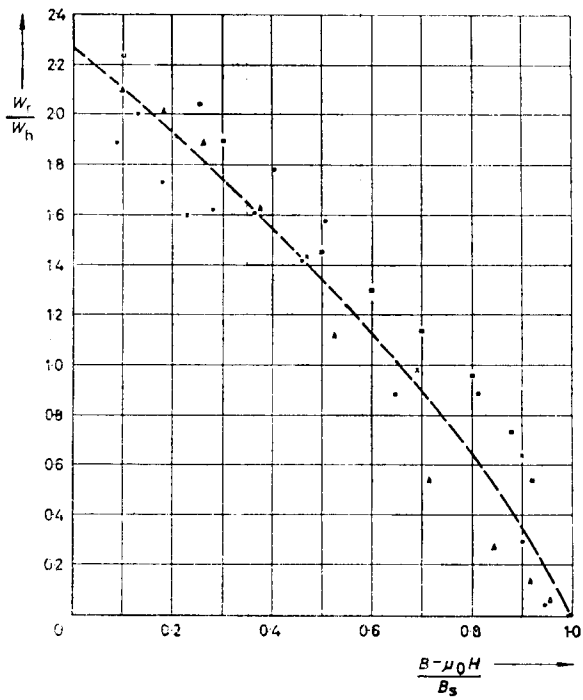



*Figure 3.28. Ratio of rotational to alternating hysteresis loss for various materials*[22]

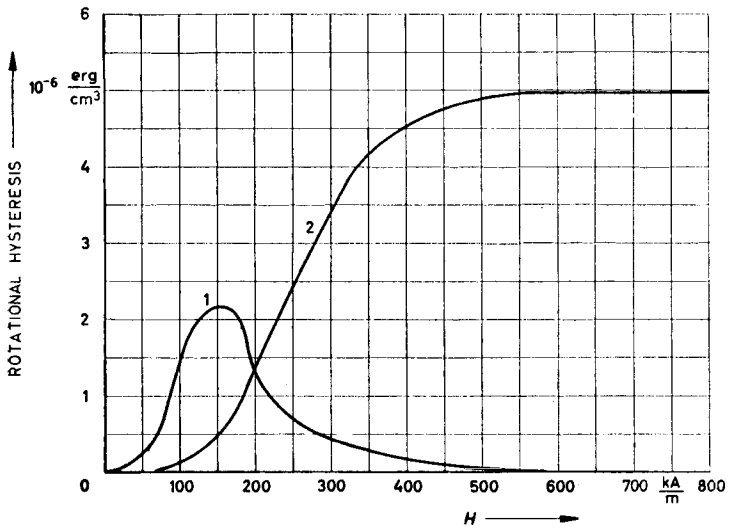



*Figure 3.29. Rotational hysteresis: 1, for a conventional material; 2, for a material exhibiting exchange anisotropy*[97]

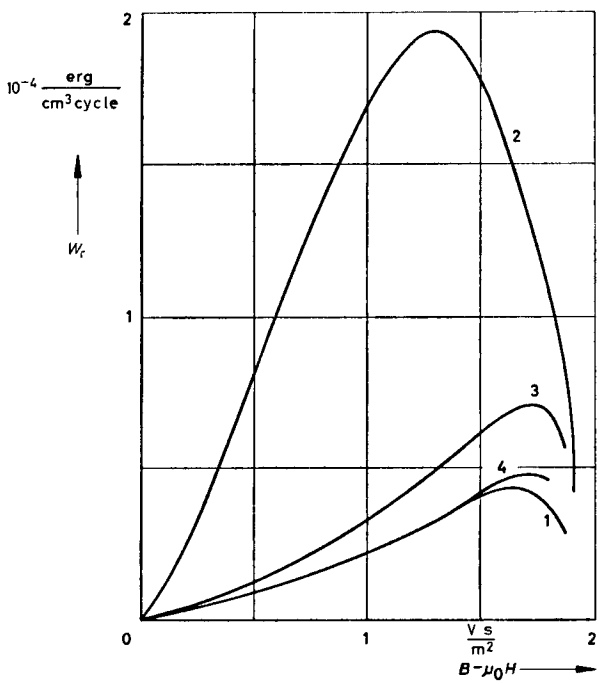



*Figure 3.30. Effect of cold working on the losses of* Fe–Si *with 4%* Si: *1, basic material 0·65* mm *thick; 2, cold-rolled down to 0·3* mm*; 3, annealed for 2* h *at 630*°C; *4, annealed for 4* h *at 1100*°C[23]

Seiwatz[128] maintains that at low frequencies (5–55 Hz) and up to field strengths of 880 kA/m, the rotational hysteresis loss is independent of frequency. Baily[4] also, in his researches, was not able to establish any influence of angular speed on the hysteresis losses.

Kornetzki and Lucas[88] have investigated rotational hysteresis theoretically and have reached the conclusion that, at low field strengths, movements of Bloch walls in accordance with Rayleigh's law are perceptible. For an isotropic polycrystalline material at very low field intensities, $W_r/W_h = 2{\cdot}36$ —in good agreement with the experimental result (see Figure 3.28). At high field intensity, $W_r$ vanishes because the domain walls also disappear, and the magnetic rotation with respect to crystal anisotropy occurs without hysteresis.

### 3.2.6 Permeability as a function of temperature

Since the ambient temperature of a magnetic body can vary, and since losses in a material lead to heating which causes a temperature rise in the core, the question arises as to how magnetic properties alter with changing temperature. The temperature dependence can best be indicated by a temperature coefficient or a temperature factor.

#### 3.2.6.1 Temperature coefficient and temperature factor

If one looks at a curve such as that shown in Figure 3.31, in which the permeability of a toroidal ferrite core is plotted over a wide temperature range, it will be seen that the temperature coefficient $\alpha$ between two temperatures $T_1$ and $T_2$, at which the initial permeabilities $\mu_1$ and $\mu_2$ were measured, i.e.

$$\alpha = \frac{\mu_2 - \mu_1}{(T_2 - T_1)\mu_1} \tag{3.66}$$

cannot be represented by a single figure. Even if $T_1$ and $T_2$ are taken as the limits of the working range, uncertainties arise in that, for many materials, the sign of the $\mu$ increment may change in the interval.

Specifying a temperature coefficient, therefore, is not always a sufficient indication of the shape of the temperature curve. In certain circumstances, it is essential to give several temperature coefficients with their effective ranges. It is usual, nowadays, to take 10°C and 60°C as end-points of the temperature ranges.

The coefficient can also be applied to the inductance values, for which equation 3.21 holds:

$$\alpha_L = \frac{L_2 - L_1}{(T_2 - T_1)L_1} \tag{3.67}$$

For the specification of materials, it is desirable to use a temperature coefficient based on $\mu_i$; this is the 'temperature factor'. If this factor is

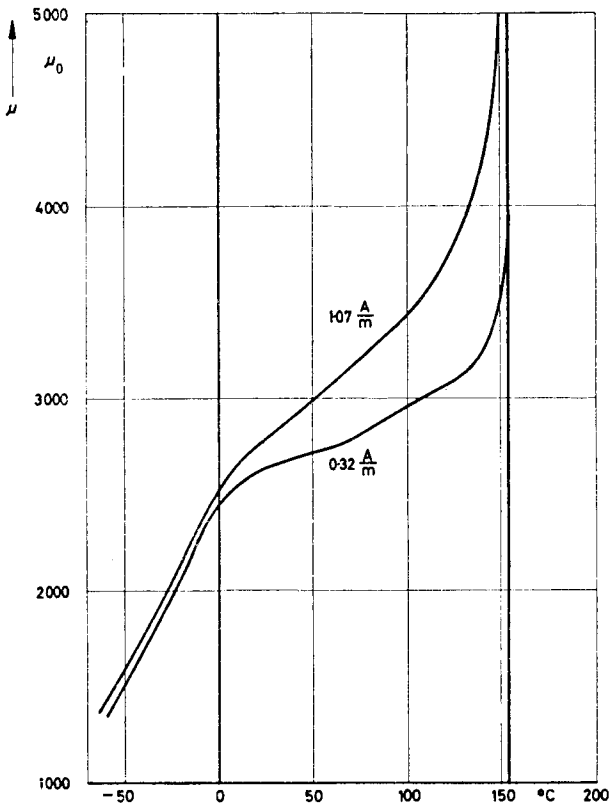



*Figure 3.31. Permeability of a* Mn–Zn *ferrite as a function of temperature and field strength*

multiplied by the effective permeability $\mu_e$, the temperature coefficient may easily be found. The temperature factor of permeability is thus

$$\frac{\alpha}{\mu_i} = \frac{\mu_2 - \mu_1}{(T_2 - T_1)\mu_1^2} \tag{3.68}$$

It is a material constant valid for cores with or without air-gaps. The temperature coefficient, on the other hand, only holds for a particular core. The initial permeability $\mu_i$ is usually taken for a temperature of 20°–23°C. If $\alpha/\mu$ is the temperature factor of a continuous toroidal core and $\alpha'/\mu_e$ the temperature factor of the same core with air-gap, then the relation

$$\frac{\alpha}{\mu} = \frac{\alpha'}{\mu_e} \tag{3.69}$$

holds, or

$$\frac{\alpha}{\alpha'} = \frac{\mu}{\mu_e} = G \tag{3.70}$$

$G$ is called the gapping factor.

For example, given, for 20°C, that $\mu_1 = \mu_i = 2500$, $\mu_e = 125$, and $\alpha' = 100\times10^{-6}$, what is the magnitude of $\mu_2$ at 70°C, what is $\alpha$, and what is the air-gap length $l_a$?

From equation 3.69,

$$\alpha = 2500\,\frac{100\times10^{-6}}{125} = 2\times10^{-3}$$

and $G = 20$. It further follows from equation 3.66 that

$$\mu_2-\mu_1 = 2\times10^{-3}\times2500\,(70-20) = 250$$

and

$$\mu_2 = 2750$$

Also, from equation 3.30,

$$G = 1+\mu\,\frac{l_a}{l_m}$$

Therefore

$$\frac{l_a}{l_m} = \frac{G-1}{\mu} = \frac{19}{2500} \doteq \frac{1}{132}$$

If, for example, $l_a+l_m = 75$ mm, then $l_a = 75/133 = 0{\cdot}56$ mm.

In this example, the effect of thermal expansion is neglected. The temperature factor attributable to thermal expansion is, for ferrites, about 20 ppm/K.

In tables the $\alpha/\mu$ values are mostly referred to the initial permeability $\mu_i$. Of course, by suitable connections, coils of greater effectiveness can be achieved, associated with higher $\mu$ values. Figure 3.31 serves as a useful reference to show how permeability in relation to temperature, and hence the temperature factor, may change with field strength.

### 3.2.6.2 Curie temperature

The Curie temperature is that temperature at which the spontaneous magnetisation of a ferromagnetic or ferrimagnetic material vanishes. Since measurements are not too easy to carry out at saturation, the Curie temperature is often defined as the temperature for which the relative permeability $\mu_r = 1$. The rapid falling off of permeability from the Hopkinson temperature is generally confined to a small arc of the curve and approaches the value $\mu = 1$ at a somewhat higher temperature. This implies that there is no unique Curie temperature, but a temperature range over which the Weiss domains disappear[47]. However, the transition from ferromagnetism to paramagnetism is sharper the more homogeneous the ferromagnetic body concerned.

In the steep drop in initial permeability as the Curie temperature is approached Fraunberger[48] found a second maximum which shows up when a direct field is superposed on a high-frequency measuring field. The relevant maximum is shifted towards a somewhat higher temperature and remains above the Curie temperature. Kussmann and Schulze[90] have clearly demonstrated that definitions of the Curie temperature based on non-magnetic

changes in the properties of iron, such as specific heat, the thermomagnetic effect, or the specific electrical resistance, are inadmissible.

The Curie temperature of a material must be known if, for example, it is necessary to lay down working limits for temperature; or if a magnetic heat treatment is to be carried out which, at the same time, involves the application of direct or alternating fields as the falling temperature passes through the Curie temperature; or if it becomes necessary to heat a material above its Curie temperature to remove remanence and to restore it to its virgin condition. It is only under particular conditions that demagnetisation can be fully

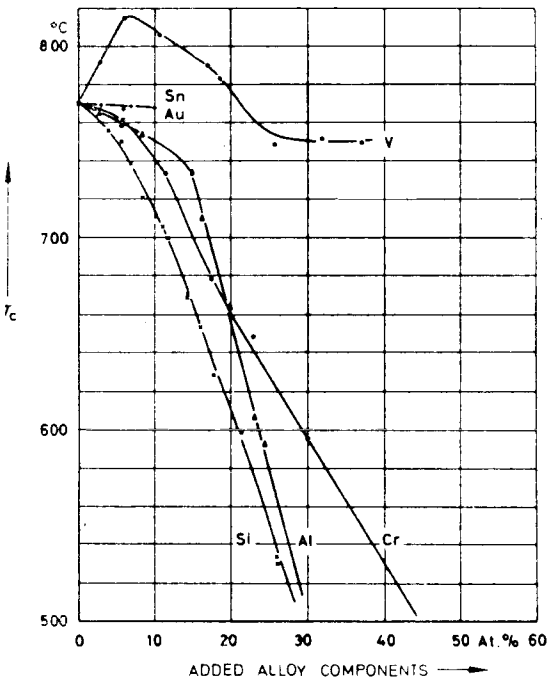



*Figure 3.32. Curie temperatures of iron variously alloyed* [40]

accomplished by applying a gradually diminishing alternating magnetic field. In these cases one may speak of 'conditioning' or cyclic demagnetisation[53, 114a].

Table 3.3 gives some insight into the values of the Curie temperature for various metals, alloys, and ceramics. The Curie temperatures of Fe–Ni alloys are shown in Figure 7.4[63]; similarly for the Fe–Ni–Cr alloys in Figure 18.4; also the Fe–Si alloys, the Fe–Al alloys, and the Fe–Au, Fe–Sn, and Fe–V alloys in Figure 3.32[40]. The Curie temperatures for a few mixed ferrites are set out in Figure 3.33[58]. The Curie temperatures of the technically important Mn–Zn ferrites and the Ni–Zn ferrites are to be found in Figures 13.72, 13.73, 13.95, and 13.97.

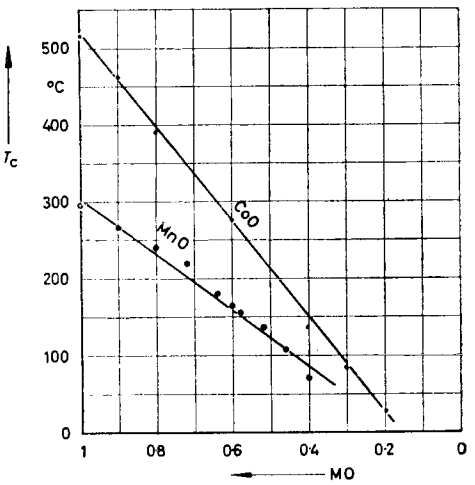



*Figure 3.33. Curie temperatures of the mixed ferrites* $Fe_2O_3 \cdot xCoO \cdot (1-x)ZnO$ *and* $Fe_2O_3 \cdot xMnO \cdot (1-x)ZnO$[58]

### 3.2.7 Losses as a function of temperature

Like initial permeability, magnetic losses change their value with temperature. Figure 3.34, based on work by Kampczyk[78], shows the temperature relations of the initial permeability, of the referred loss factor $(\tan\delta)/\mu_i$, and of the referred hysteresis coefficient $h/\mu_i^2$ for a Mn–Zn ferrite with a Curie

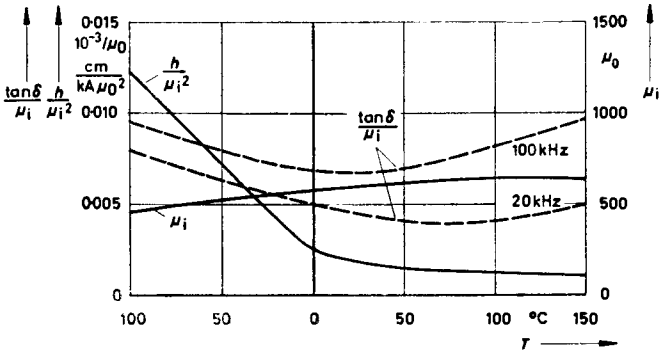



*Figure 3.34. Temperature dependence of the initial permeability, of the referred loss factor* $(\tan\delta)/\mu_i$, *and of the referred hysteresis coefficient* $h/\mu^2$ *for a* Mn–Zn *ferrite*[78]

temperature $T_c = 250°C$. The value of $(\tan\delta)/\mu_i^2$ passes through a minimum whose position is influenced by the measuring frequency: it moves towards higher values and lower temperatures at higher frequencies. The value of $h/\mu_i^2$ increases with falling temperature[78, 93].

According to measurements by Lescroël[93], the eddy-current coefficient increases more or less exponentially with temperature (Figure 3.35). At low temperatures the specific electrical resistance of ferrites is high, and for this

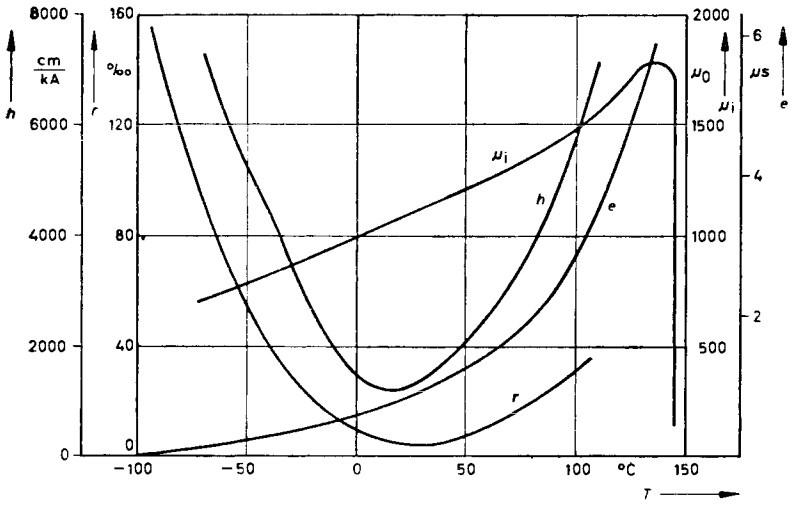



*Figure 3.35. Dependence of the loss coefficients e, r, and h of a* Mn–Zn *ferrite on temperature*[93]

reason eddy-current losses are of minor importance. Like the hysteresis coefficient $h$, the residual loss coefficient $r$ rises at low temperatures with falling temperature. It also rises with rising temperature above room temperature.

### 3.2.8 Drop in permeability with time

Directly after demagnetisation, either by raising the material above the Curie temperature, by cycling with continuously falling field intensity, by mechanical shock, or by radioactive irradiation, a very significant rise in initial permeability (Accommodation) is observed. The various methods detailed above, however, are by no means equivalent. Thus, for example, pure large-grain iron after being subjected to thermal shock shows a hysteresis loop which differs from that following cyclic demagnetisation[101]. For high-permeability alloys, the initial permeability after cyclic demagnetisation is higher than after demagnetisation by thermal shock[73].

Sommerkorn made similar observations[136a] for single crystals of Fe–Si with 3·5% Si. The value of permeability obtained by mechanical shock or vibration lies between the other two values. Boll[13a] noticed that, particularly in Fe–Ni alloys of pronounced cubic crystalline structure, the permeability following thermal demagnetisation was appreciably higher than if an a.c. routine had been used, and that the differences were smaller for materials with a less marked cubic structure. It will be perceived that the two methods yield different numbers of Bloch walls. Sommerkorn[136a] was able to detect a distinct connection between the domain structure of the above mentioned Fe–Si single crystals and the demagnetisation results.

**Table 3.6** INFLUENCE OF SILICON CONTENT ON DISACCOMMODATION FOR AN Fe–Si ALLOY[15]

| | *Silicon content* | | | |
|---|---|---|---|---|
| | 1·0% | 2·75% | 3·5% | 4·5% |
| $\mu_i$ | 486·6 | 614 | 710 | 1 105 |
| $\mu_i$ after 1 h | 478 | 588 | 681 | 993 |
| $\mu_i$ after 24 h | 473 | 573 | 660 | 835 |
| Drop in 24 h (%) | 2·8 | 6·7 | 7·0 | 24·4 |
| Percentage of 24 h drop in 1 h | 63·2 | 63·4 | 58 | 41·5 |

The permeability falls, in time, to its old value. Figure 3.36 shows that the fall in permeability of a Mn–Zn ferrite approximates to an exponential law. Very often, however, the function $\mu = f(t)$ is less simple[36]. The effect is called disaccommodation. It is especially marked for steels[3, 14, 27, 38, 120, 151], for Fe–Si[115, 131, 132] and many ferrites[20, 21, 36, 67, 72b, 94, 95, 113, 114a], and above all for the Mn–Zn ferrites.

According to an investigation by Patterson[115], the fall of permeability with time is greater, the larger the silicon content. The addition of silicon does indeed satisfactorily increase the initial permeability of iron and decreases the losses, but causes the percentage 24 h drop in permeability to increase notably (see Table 3.6).

Again, Smolinski and Zbikowski[132] were able to demonstrate a high value of disaccommodation for heavily alloyed transformer steel. The effect, however, could be made practically to disappear, by annealing at 1250°C in a hydrogen atmosphere: the permeability increase caused by the excitation completely disappears in a few minutes. Disaccommodation in the Mn–Zn ferrites depends to a large extent on the constituent balance (stoichiometry). If there is no excess of iron oxide, the disaccommodation is low. It rises,

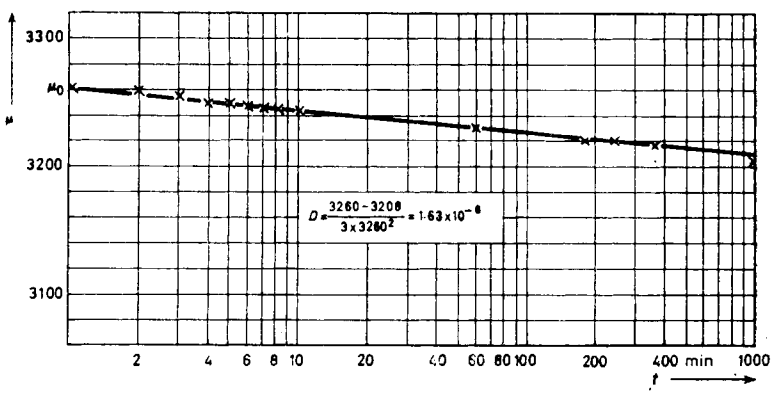



*Figure 3.36. Determination of the disaccommodation factor of a high-permeability* Mn–Zn *ferrite (H = 3* A/m, *T =* 30°C*)*

however, almost linearly with iron oxide content[94], but is also affected by the manganese oxide content. Lescroël and Pierrot[94] and also Ohta and Yamadaya[113] found that imbalance of the components in Mn–Zn ferrites led to an increase in disaccommodation which was significantly higher if the material was sintered in air than if sintered in nitrogen (Figure 3.37).

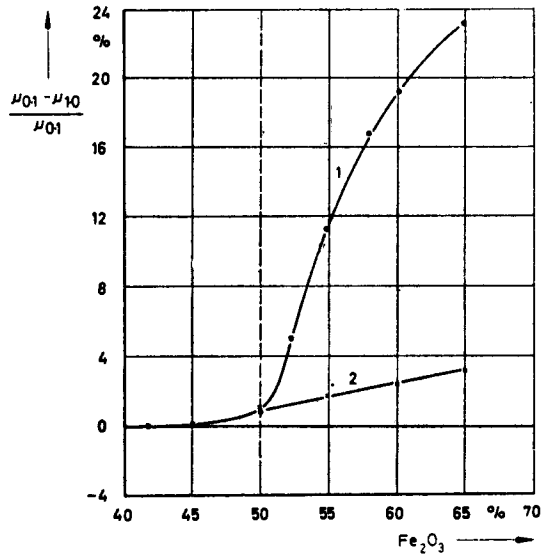



*Figure 3.37. Disaccommodation of a* Mn–Zn *ferrite as a function of* $Fe_2O_3$ *content: 1, sintered in air; 2, annealed in nitrogen*[113]

In order to avoid disaccommodation, an increase in loss has generally to be accepted, as it is not easy reliably to prepare iron-oxide-free Mn–Zn ferrites with low losses while maintaining, as far as possible, a specified temperature coefficient.

The internal features which lead to the phenomenon of disaccommodation are not yet clear. It is suspected that the unfilled cation sites in the crystal lattice play a critical role. According to this hypothesis, the drop in permeability is linked to the number of these 'holes' and to their diffusion.

Iida and Inoue[72b] were able to show that, for a high-permeability Mn–Zn ferrite ($\mu_i = 5300\mu_0$), accurate control of the dislocation density led to a fall of permeability after demagnetisation of only about 0·02% in 1000 s. This corresponds, according to equation 3.71 below, to a disaccommodation factor of

$$D = 1{\cdot}25 \times 10^{-8}$$

Disaccommodation $d$ is defined as the fall in $\mu$ per time-decade referred to the value at the start of the decade:

$$d = \frac{\mu_1 - \mu_{10}}{\mu_1 \log (t_2/t_1)}$$

It is usually quoted as a percentage. The value referred to $\mu_i$ is called the disaccommodation factor $D$ and is a constant of the material

$$D = \frac{\mu_1 - \mu_{10}}{\mu_1^2 \log (t_2/t_1)} \tag{3.71}$$

If, in the example of Figure 3.36, the duration of the observations be averaged over three decades, then

$$D = \frac{3260 - 3208}{3 \times 3260^2} = 1{\cdot}63 \times 10^{-6}$$

This may be considered a very suitable value for technical purposes since it represents a change of core permeability appreciably less than the drift of

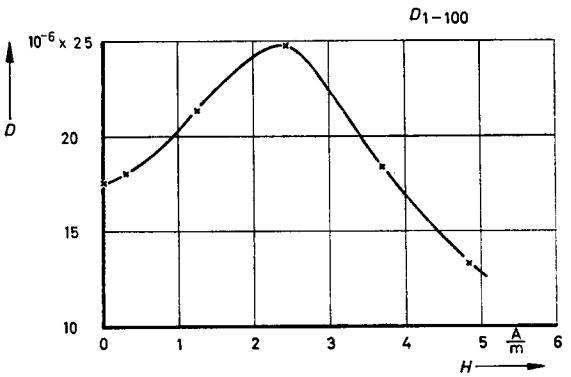



*Figure 3.38. Disaccommodation factor of a* Mn–Zn *ferrite at room temperature as a function of field strength*

other properties of the coil (manufacturing tolerances, adjustment uncertainties, temperature effects).

The disaccommodation of a coil may be derived from the disaccommodation factor $D$ by multiplying it by the effective permeability of the (gapped) core. Disaccommodation depends on both temperature and field strength, so every measured value must be considered on its merits. Figure 3.38 shows the variation of disaccommodation factor with field strength for a strongly disaccommodating Mn–Zn ferrite. The core was cyclicly demagnetised (or conditioned) by means of an alternating field whose amplitude was steadily reduced from eight times the coercivity to zero. The measurement gave a strongly marked maximum at a field strength of 2·5 A/m.

Disaccommodation retains a finite value in the neighbourhood of the initial permeability. The lowest field strength used in the measurement was 0·025 A/m. No disaccommodation could be detected at some 10 A/m, so it is principally a phenomenon of low field strength. In filter coils disaccommodation must be kept particularly low since every change of temperature and every vibration can induce the effect.

The location of the disaccommodation maximum can alter from one time-decade to another in various materials. In the example of Figure 3.38 the plotted points are averaged values for the two decades 1–10 min and 10–100 min after demagnetisation. The functional relation between disaccommodation and measuring temperature yields, between 30°C and 140°C, a curve of similar shape to that for measuring-amplitude. Figure 3.39 gives two measurements for a Mn–Zn ferrite of relatively small disaccommodation at various field strengths: at 0·29 A/m, $D$ reaches a maximum around 80°C.

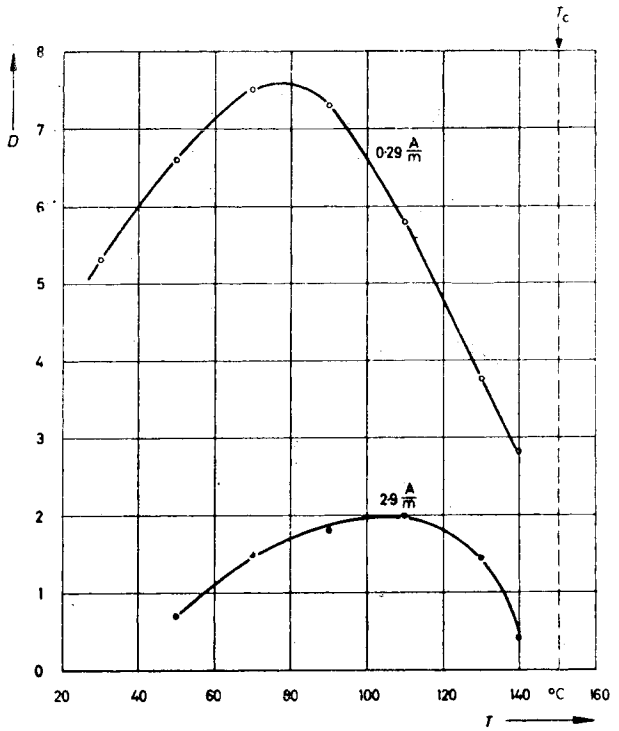



*Figure 3.39. Disaccommodation factor of a* Mn–Zn *ferrite as a function of temperature at two field strengths*

At higher intensities, the maximum value is lower and its location is shifted in the direction of higher temperature. The position of the maximum depends on the composition of the ferrite. Braginski, Marais, and Merceron[21] have stated that Mn–Zn ferrites can show two maxima, one at high and the other at very low temperature. Ni–Zn ferrites can show three maxima[20, 95]. In all these cases the height of the maximum increases with the oxygen content of the sintering atmosphere and shifts towards lower measuring temperatures for increasing sintering temperature.

Disaccommodation should not be confused with ageing. By *ageing* of magnetic material, which may also involve a time-fall of permeability, is to be understood an irreversible process like that of biological ageing[134]. The

disaccommodation process, on the other hand, is repeatable at will: but it would be illogical to speak of 'reversible ageing'.

Ageing is usually connected with a structural change of the material and occurs especially for precipitation alloys (see pages 251 and 383). Where ageing and disaccommodation occur in one and the same material, they may easily be distinguished: the drop in permeability is measured after demagnetising. After several hours, or days, further demagnetising cycles are applied. If the measured points coincide with those of the previous test, disaccommodation is involved but not ageing. If the second curve lies more or less parallel to the first but is lower in value, the shift indicates ageing. Also, small

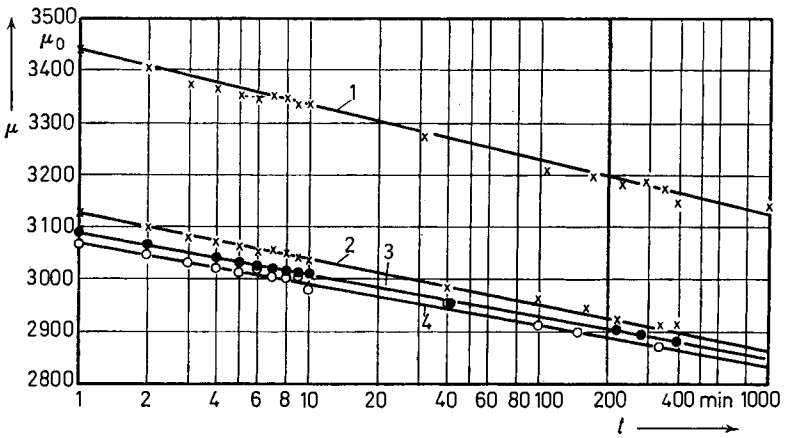



*Figure 3.40. Time-fall of permeability for a* Mn–Zn *ferrite: 1, initial measurement; 2, 110 days later; 3, 200 days later; 4, 830 days later*

amounts of ageing can be detected if the disaccommodation measurements are repeated after a long interval.

Sometimes Mn–Zn ferrites, directly after their preparation, show a high initial permeability. Thus, for example, the upper curve of Figure 3.40 is measured after demagnetisation; if the measurement be repeated 110 days later, a curve is obtained that is shifted towards lower $\mu$ values. For even bigger time-intervals, further curves are obtained; these show a reduction in this tendency, which ultimately disappears as ageing fades out. Disaccommodation remains roughly constant throughout the total interval.

### 3.2.9 Permeability as a function of frequency

If the permeability of a ferromagnetic or ferrimagnetic material be measured, then the following holds for laminated cores, dust cores, and ferrites: at low frequencies, $\mu$ is almost independent of frequency. However, for each type of material, there is a critical frequency above which the permeability falls. This critical frequency is reached at a lower value for high-permeability materials than for materials of lower permeability. Again, among sheets of various thicknesses, the thicker the sheet, the earlier the fall-off.

For sheet and strip, the initial permeability falls off, above the critical frequency, as $1/\sqrt{f}$. Figure 3.41 shows the shape of a typical permeability–frequency curve, according to a calculation by Kornetzki[87], for various kinds of sheets whose initial permeability lies between $300\mu_0$ and $100\,000\mu_0$.

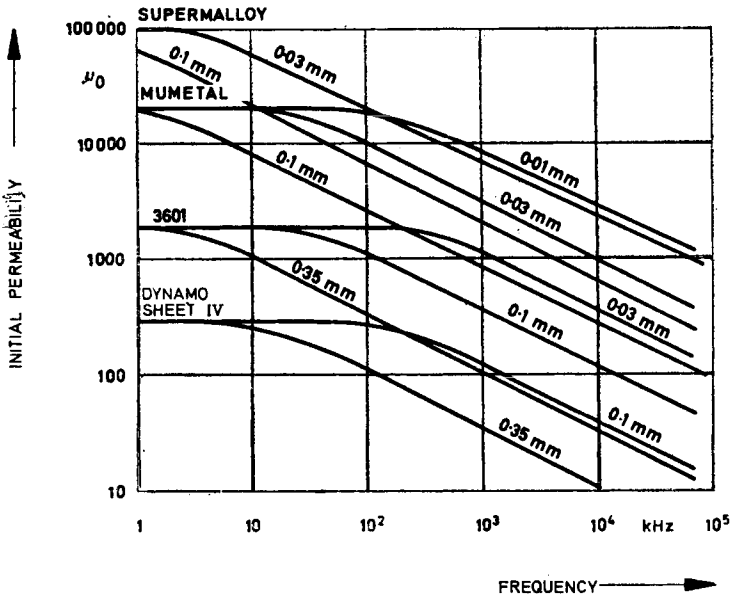



*Figure 3.41. Initial permeability of laminated cores as a function of frequency*[87]

The critical frequency $f_{cr}$ is almost wholly determined by eddy-current losses; it can be calculated from the formula

$$f_{cr} = \frac{4\varrho}{\pi\mu_i D^2} \tag{3.72}$$

in which $\varrho$ stands for the specific electrical resistance of the sheet, $D$ its thickness, and $\mu_i$ the initial permeability. Actually the drop is, in general, steeper than that shown in the figure; there are several reasons for this, such as the absence of insulation between individual laminae, inhomogeneity of the material, and relaxation effects. There are basically two ways of raising the critical frequency: either the specific electrical resistance $\varrho$ must be increased, or the sheet thickness $D$ must be reduced.

Now it has already been mentioned that ferrites have a specific electrical resistance greater than that of metallic materials by several orders of magnitude. One might therefore expect that their permeability would remain constant up to an arbitrarily high frequency, but this is not so. As Figure 3.42, taken from the same investigation by Kornetzki, shows, these materials also exhibit limiting frequencies above which the permeability falls. As for sheet material, the permeability remains constant up to higher frequencies the smaller the value of $\mu$. Above the critical frequency, $\mu$ falls as $1/f$.

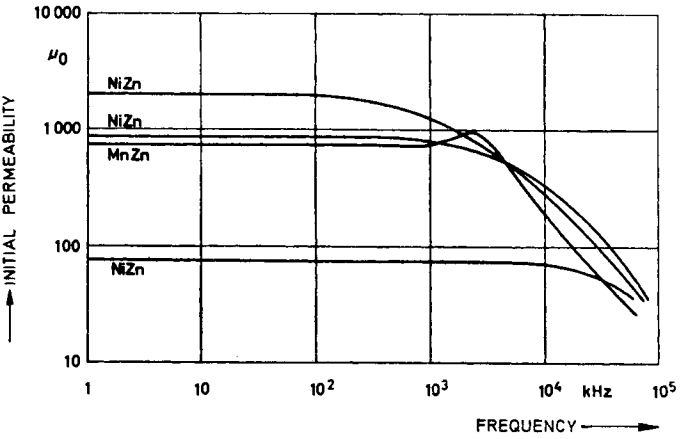



*Figure 3.42. Initial permeability of a few ferrites as a function of frequency*[87]

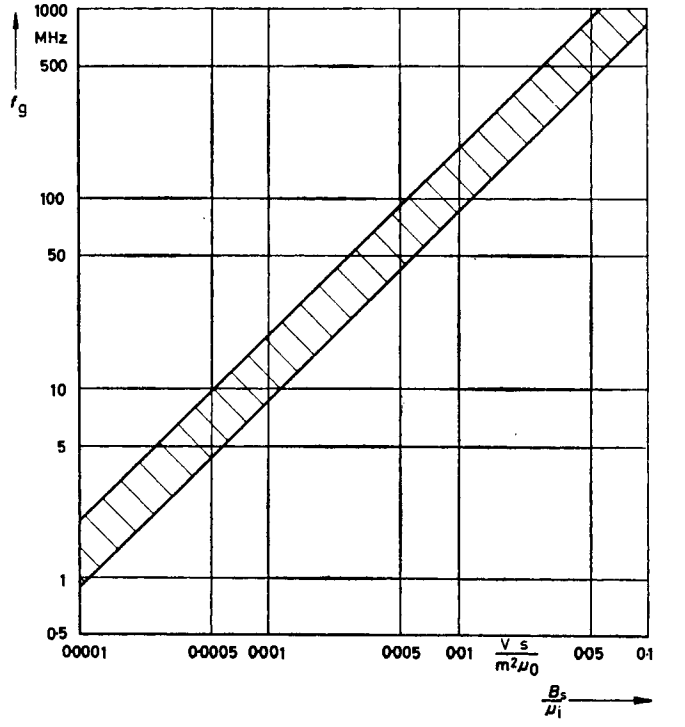



*Figure 3.43. Gyromagnetic limiting frequency* $f_g$[12]

In ferrites, as Snoek[135] was able to show, the critical frequency is connected with magnetic spin effects, so one speaks of a gyromagnetic critical frequency $f_g$. For this,

$$f_g = \frac{0{\cdot}1\gamma B_s}{\mu_i} \tag{3.73}$$

where $B_s$ is the saturation flux density, $\mu_i$ the initial permeability, and $\gamma = 0{\cdot}22$ MHz m/A is the gyromagnetic ratio for an electron, i.e. the ratio of magnetic moment and torque (see page 12). In contrast with $f_{cr}$, $f_g$ is independent of the thickness of the specimen.

Boll[12, 13] was able to show that the gyromagnetic critical frequency $f_g$ —which he called the spin-relaxation frequency—also applied to magnetic alloys. However, for normal sheet thicknesses, this effect was swamped by eddy-current effects. Only in strip thicknesses $D$ less than 5 μm was the effect detectable. In fact, equation 3.73 holds for all materials.

If $f_g$ is plotted against $B_s/\mu_i$, a curve like that of Figure 3.43 results[12]. Because of the magnetising process (wall movement, rotation, etc.), a numerical factor is involved and $f_g$ is subject to a range of variation shown in the figure by hatching. It can be seen from Figure 3.42 that, for Ni–Zn ferrites and Mn–Zn ferrites with $\mu_i = 1000\mu_0$, the critical frequency $f_g$ lies around 5 MHz. This figure may also be deduced approximately if $B_s = 0{\cdot}3$ V s/m$^2$ is inserted in equation 3.73.

Another effect besides the resonance effect defined by equation 3.73 is known to apply to Mn–Zn ferrites. It comes into play by reason of the high dielectric constant of these ferrites and is influenced by core dimensions. What is involved, therefore, is a volume-resonance effect. If $\varepsilon_i$ is the dielectric constant and $D$ the thickness, then

$$f_r = \frac{k}{D\sqrt{(\mu_i\varepsilon_i)}} \tag{3.74}$$

The constant $k = 2\times10^8$ m/s. If, for example, $D = 1$ cm, $\varepsilon_i = 50\,000\varepsilon_0$, and $\mu_i = 1000\mu_0$, then $f_r = 3$ MHz.

### 3.2.10 Losses as a function of frequency

As the loss factor tan $\delta$ in equation 3.42 comprises a frequency-dependent component, it is to be expected that the referred loss factor (tan $\delta$)/$\mu$ will rise with frequency. The detail of the rise is determined by the chemical composition and the structural properties of the material. A few examples are given: in Figure 3.44 (tan $\delta$)/$\mu$ is plotted against frequency from 10 kHz to 50 MHz, for two Fe–Ni alloys, neglecting hysteresis loss[12]. One of the alloys is Permenorm 3601 with 36% Ni and the other is Ultraperm 10 with 79% Ni and 5% Mo; the remainder, of course, is iron. Strips of each material of 3 μm, 6 μm, 10 μm, and 30 μm thickness were measured. The thicker strips show higher loss factors on account of eddy-current effects. For the thinnest strips, the loss increases by reason of spin relaxation and is accompanied by a fall in permeability (see page 68).

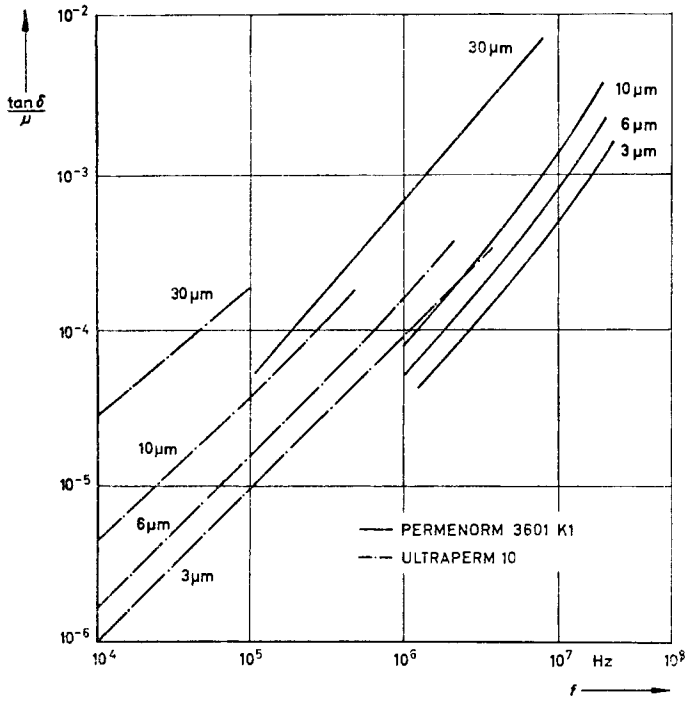



*Figure 3.44. Referred loss factor of thin strips as a function of frequency*[12]

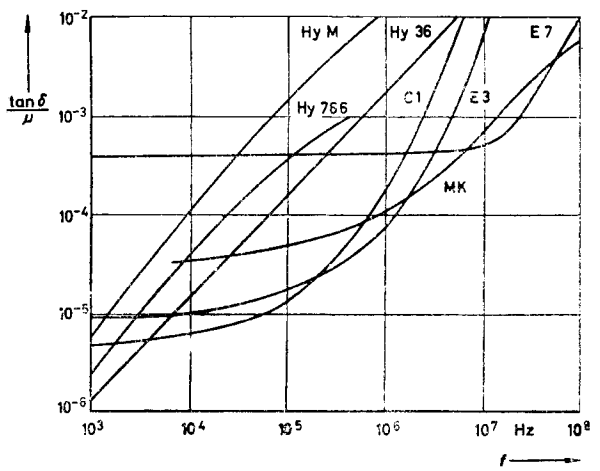



*Figure 3.45. Frequency characteristic of referred loss factor for* Fe–Ni *alloys, ferrites, and dust cores: Hy M = Hyperm maximum (79% Ni); Hy 36 = Hyperm 36 (36% Ni); Hy 766 = Hyperm 766 (76% Ni); MK = dust core of carbonyl iron EN; C1 =* Mn–Zn *ferrite; E3 and E7 =* Ni–Zn *ferrites*[68]

For strips 50 μm thick of the Fe–Ni alloys Hyperm Maximum (79% Ni), Hyperm 766 (76% Ni), and Hyperm 36 (36% Ni), a similar relation between loss factor and frequency holds, as shown in Figure 3.45[68]. For comparison, the $(\tan \delta)/\mu$ curves for a moulded MK core of carbonyl dust EN and for three different ferrites (C1, E3, and E7) are plotted in the same figure. The comparison demonstrates that above 10 MHz the advantage lies with the dust cores and the ferrites rather than the laminated cores because of their lower eddy-current coefficients. At lower frequencies, the residual loss makes itself felt unfavourably, particularly for the low-permeability ferrites, so, in this range, laminated cores are more advantageous than many ferrites. However, there are various ferrites on the market today that are superior to laminated cores even at low frequencies—see, for example, Figures 13.88 and 19.2. Above 100 MHz the dust core is the core with the lowest losses.

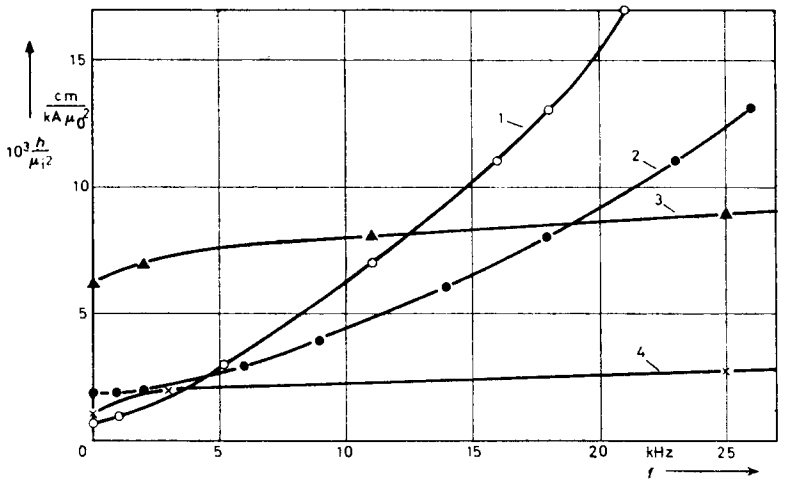



*Figure 3.46. Frequency characteristic of $h/\mu_i^2$ for* Fe–Ni *alloys and ferrites: 1, Hyperm 766; 2, Hyperm 36; 3, Hyperox E1 (*Ni–Zn *ferrite); 4, Hyperox C1 (*Mn–Zn *ferrite)*[68]

Hysteresis losses are also seen to depend on frequency. Figure 3.46 shows the referred hysteresis coefficient $h/\mu_i^2$ for two Fe–Ni alloys, one a Mn–Zn and the other a Ni–Zn ferrite[68].

The hysteresis coefficient rises much more steeply with frequency for laminated cores than for ferrites, so, particularly at high frequencies, the use of ferrites is advantageous. The frequency–loss relations for heavy-current laminae are reported in Section 10.3.4.

### 3.2.11 Magnetostriction

By magnetostriction is to be understood those relative elastic changes in length produced by the influence of a magnetic field (Joule effect). Longitudinal, transverse, and volumetric magnetostrictions are distinguished according as the change in length takes place along or perpendicular to the direction

of the field, or is observed as a volume change. Magnetostriction may have a positive or a negative sign: it is dependent on field strength and in some circumstances, as in iron (Figure 2.2), may change sign with increasing intensity. Magnetostriction $\lambda$ occurring at saturation in a polycrystalline substance will be designated saturation magnetostriction $\lambda_s$.

In single crystals, different magnetostrictive behaviour is observed in different directions. This has already been shown for single iron crystals in Figure 2.2, displaying results obtained by Webster. Along the diagonal of the cube [111] $\lambda$ is negative, along an edge [100] it is positive, and along the face diagonal [110] the sign passes at high intensities from positive to negative.

The longitudinal magnetostriction of single nickel crystals is negative in all directions, as shown in Figure 3.47 taken from investigations by Masiyama[96]. The absolute value of the contraction is greatest in the [100]

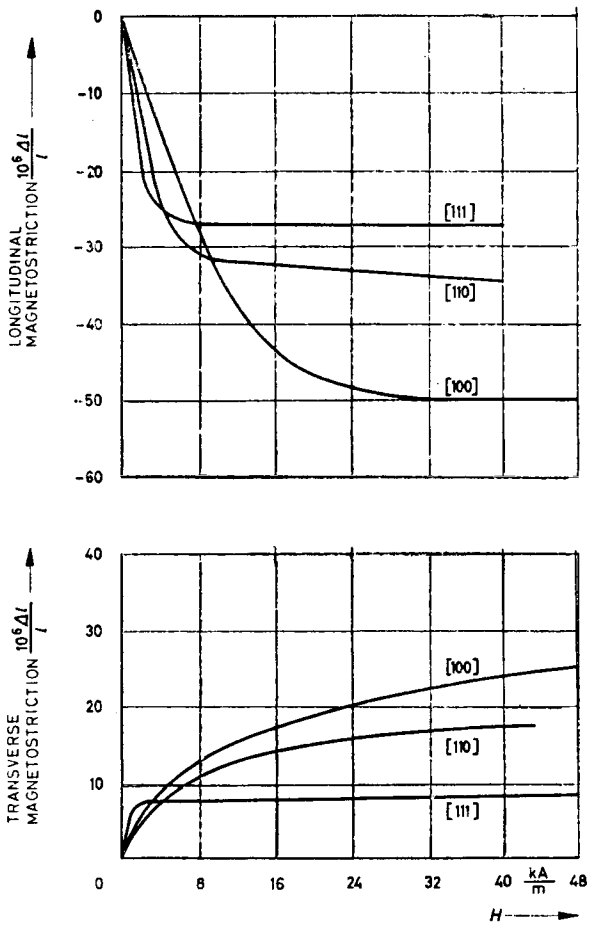



*Figure 3.47. Magnetostriction of a single crystal of nickel in the (110) plane*[96]

direction and least in the [111] direction. Transverse magnetostriction is positive in all crystal directions.

Magnetostriction constants for Fe–Ni alloys with more than 30% Ni are shown in Figure 13.8[19]. As can be inferred from this figure, the $\lambda_{111}$ magnetostriction, in the direction of easy magnetisation, for an Fe–Ni alloy having about 80% Ni is zero.

For single cobalt crystals, the longitudinal magnetostriction along the principal axis, direction [0001], is very slightly negative (Figure 3.48). It is more strongly negative at right angles to the principal axis and, according to measurements by Nishiyama[111], there is negligible difference in behaviour in the directions [10$\bar{1}$0] and [11$\bar{2}$1].

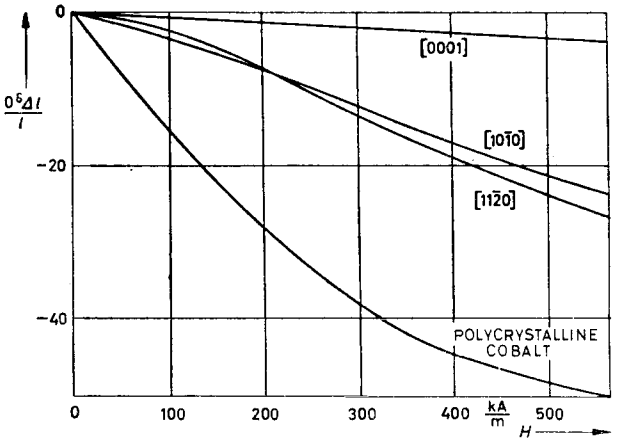



*Figure 3.48. Magnetostriction of a single crystal of cobalt: longitudinal effect of a rod*[111]

Nishiyama[111] observed a higher negative value of magnetostriction for polycrystalline cobalt than in any of the principal directions of the single crystal. He was able to elucidate this surprising result by means of measurements taken in the (10$\bar{1}$0) plane of a disc: it appeared that the transverse effect in the [0001] direction introduces a slight shortening whose magnitude is comparable with the longitudinal effect. On the other hand, a pronounced expansion was observed in the [10$\bar{1}$0] direction and in intermediate directions. The maximum elongation does not occur in either the [0001] or the [10$\bar{1}$0] directions, but in some intermediate direction.

Transverse magnetostriction can be positive or negative. It is notably strongly positive if the measuring field in the (10$\bar{1}$0) plane forms an angle of 67·5° with the principal axis (Figure 3.49). Magnetostriction values measured in polycrystalline materials for permanent magnets are of great theoretical importance since, in many cases, they determine the coercive force[105].

The highest value of magnetostriction so far known occurs in cobalt ferrite ($Co_{0.8}Fe_{2.1}O_4$). In the [100] direction, $\lambda$ has been measured[18] as $-540\times10^{-6}$, and, in the direction at right angles to this, as $+220\times10^{-6}$. Extremely high field intensities are needed to achieve saturation magnetostriction (Figure 3.50)[18]. All known ferrites have negative magnetostrictions,

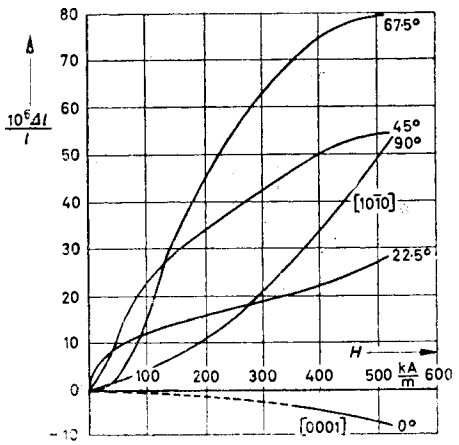



*Figure 3.49. Magnetostriction of a single crystal of cobalt; transverse effect of a circular disc (10$\bar{1}$0)*[111]

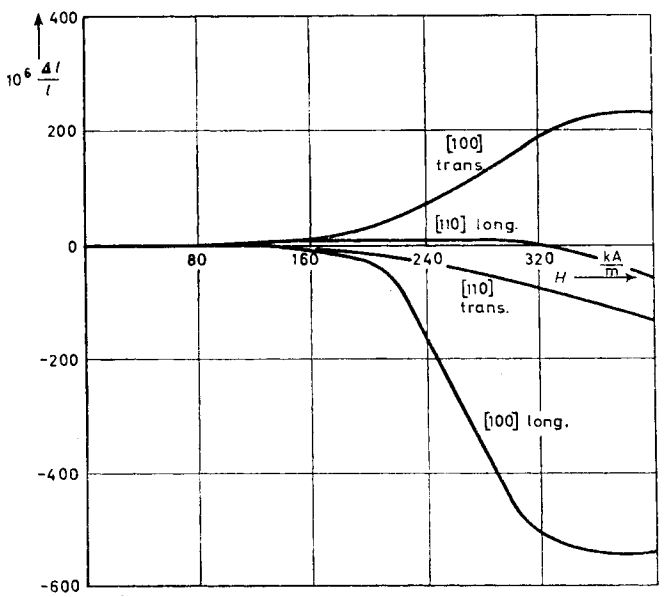



*Figure 3.50. Magnetostriction of a cobalt ferrite*[18]

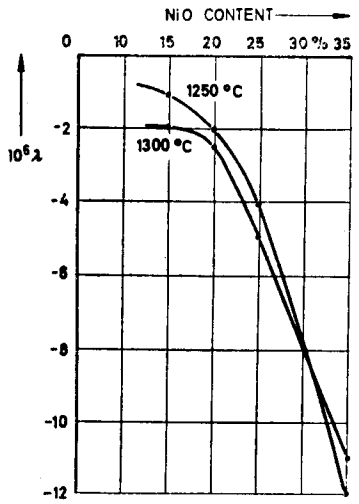



*Figure 3.51. Magnetostriction of* Ni–Zn *ferrites as a function of* NiO *content for various sintering temperatures*[59]

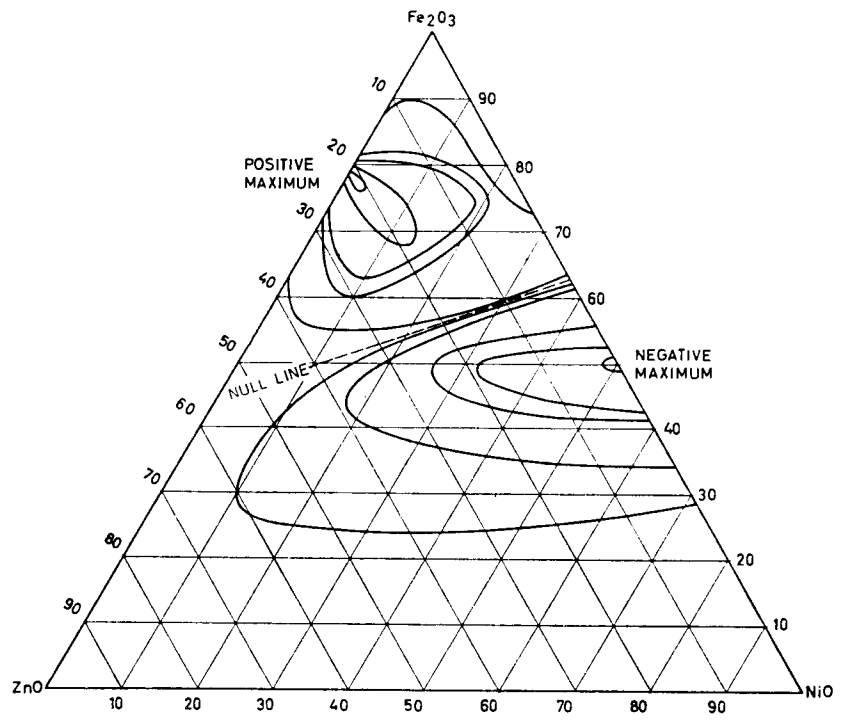



*Figure 3.52. Equal magnetostriction curves for* Ni–Zn *ferrites sintered in air at 1400°C*[64]

with the exception of magnetite, whose magnetostriction is positive. This is of great practical importance, as will be shown later.

Magnetostriction changes not only with magnetic field strength but also with temperature and is, moreover, affected by the previous history of the sample. Again, a 'form effect' has been observed. In Figure 3.51 values of magnetostriction are shown for Ni–Zn ferrites heat-treated at 1250°C and 1300°C[59]. Contours of equal magnetostriction for the three-component system $NiO–Fe_2O_3–ZnO$ are given in Figure 3.52[64]. The magnetostrictive properties of crystals can be specified either by a two-constant or by a five-constant system[15]. The two-constant system usually suffices to describe longitudinal magnetostriction, $\lambda_{100}$ and $\lambda_{111}$ being in the respective directions [100] and [111].

By introducing direction cosines $\alpha$ and $\beta$ for the angle between the direction of magnetisation and the respective crystal axes, the saturation magnetostriction $\lambda_s$ in a cubic crystal can be calculated from the following formula:

$$\lambda_s = \tfrac{3}{2}\lambda_{100}(\alpha_1^2\beta_1^2+\alpha_2^2\beta_2^2+\alpha_3^2\beta_3^2-\tfrac{1}{3})+3\,\lambda_{111}(\alpha_1\alpha_2\beta_1\beta_2+\alpha_2\alpha_3\beta_2\beta_3+\alpha_3\beta_3\alpha_1\beta_1) \tag{3.75}$$

A similar relation may be built up using five terms together with the five constants $h_1$, $h_2$, $h_3$, $h_4$, and $h_5$:

$$\begin{aligned}\lambda_s = {} & h_1(\alpha_1^2\beta_1^2+\alpha_2^2\beta_2^2+\alpha_3^2\beta_3^2-\tfrac{1}{3})+ \\ & +2h_2(\alpha_1\alpha_2\beta_1\beta_2+\alpha_2\alpha_3\beta_2\beta_3+\alpha_3\alpha_1\beta_3\beta_1)+ \\ & +h_4(\alpha_1^4\beta_1^2+\alpha_2^4\beta_2^2+\alpha_3^4\beta_3^2+2s/3-\tfrac{1}{3})+ \\ & +2h_5(\alpha_1\alpha_2\alpha_3^2\beta_1\beta_2+\alpha_2\alpha_3\alpha_1^2\beta_2\beta_3+\alpha_3\alpha_1\alpha_2^2\beta_3\beta_1)+ \\ & +h_3\,(s-\tfrac{1}{3})\text{ (for nickel)}+h_3 s\text{ (for iron)}\end{aligned} \tag{3.76}$$

in which

$$s = \alpha_1^2\alpha_2^2+\alpha_2^2\alpha_3^2+\alpha_3^2\alpha_1^2$$

If $h_3 = h_4 = h_5 = 0$, then the relations

$$\lambda_{100} = \tfrac{2}{3}h_1$$

and

$$\lambda_{111} = \tfrac{2}{3}h_2$$

are valid. If $h_4 = h_5 = 0$, then the following formula may be used and will be found to have considerable practical value:

$$\lambda_s = \frac{2\lambda_{100}+3\lambda_{111}}{5} \tag{3.77}$$

In Table 3.7, values for both systems of constants are given for iron and nickel. Further values for $\lambda_{100}$ and $\lambda_{111}$ are given in Tables 3.8 and 3.9. Various authors quote figures that often differ among themselves. These differences may well reflect differences of form and structure and in the previous history of the specimens.

**Table 3.7** COEFFICIENTS OF MAGNETOSTRICTION (AT ROOM TEMPERATURE UNLESS OTHERWISE STATED)

| *Material* | $10^6\lambda_{100}$ | $10^6\lambda_{110}$ | $10^6\lambda_{111}$ | $10^6\lambda_s$ | $10^6h_1$ | $10^6h_2$ | $10^6h_3$ | $10^6h_4$ | $10^6h_5$ | *Reference* |
|---|---|---|---|---|---|---|---|---|---|---|
| Iron | 22·2 | 11·3 | −20·7 | −3·5 | 32·9 | −35·2 | 3·4 | 0 | 7 | 119a |
| | 20 | — | −12 | — | — | — | — | — | — | 146 |
| Iron+3% Si | 24 | — | − 2·3 | — | — | — | — | — | — | 15 |
| Iron+4·4% Si (0°C) | 18·0 | 20·0 | − 3·0 | — | 40·5 | 10·1 | 38·6 | −13·5 | −44·0 | 143a |
| Iron+4·4% Si (82°C) | 23·0 | 22·0 | − 5·0 | — | 30·6 | 11·7 | 45·0 | 4·5 | −57·5 | 143a |
| Iron+78% Ni | | | | | | | | | | |
| quenched | — | — | — | — | 13·7 | 2·6 | −0·3 | 1·1 | − 0·1 | 16a |
| slowly cooled | — | — | — | — | 20·9 | 2·8 | 1·7 | − 1·4 | − 0·2 | 16a |
| Nickel | −46 | — | −25 | −34 | −24 | −47 | — | −51 | +52 | 15 |
| | | | | | −68·8 | −36·5 | −2·8 | − 7·5 | 7·7 | 16a |
| Cobalt | — | — | — | −50 | — | — | — | — | — | 111 |
| $Fe_3O_4$ (natural) | −16·7 | 65·4 | 90·6 | — | −15·3 | 142·4 | −9·43 | −9·70 | −50·5 | 6a |
| $Fe_3O_4$ (synthetic) | −19·5 | 57·1 | 77·6 | — | −24·5 | 123·3 | −0·40 | −4·76 | −20·1 | 6a |
| $Fe_3O_4$ | −19 | — | 81 | 41 | — | — | — | — | — | 17 |
| $Fe_3O_4$ (124 K) | −23 | — | 55 | 24 | — | — | — | — | — | 17 |
| $CoFe_2O_4$ | — | 45 | — | — | — | — | — | — | — | 10 |
| $Co_{1·1}Fe_{1·9}O_4$ | −250 | — | | | | | | | | |
| $Co_{0·8}Fe_{2·2}O_4$ | −590 | — | 120 | −210 | — | — | — | — | — | 17 |
| $Co_{0·3}Zn_{0·2}Fe_{2·2}O_4$ | −210 | — | 110 | − 18 | — | — | — | — | — | 17 |
| $Co_{0·3}Mn_{0·4}Fe_2O_4$ | −200 | — | 65 | − 40 | — | — | — | — | — | 17 |
| $Ni_{0·8}Fe_{2·2}O_4$ | − 36 | — | − 4 | − 17 | — | — | — | — | — | 17 |
| $Mn_{0·98}Fe_{1·86}O_4$ | − 35 | — | − 1 | − 15 | — | — | — | — | — | 17 |
| $Mn_{0·6}Zn_{0·1}Fe_{2·1}O_3$ | − 14 | — | 14 | 3 | — | — | — | — | — | 17 |

**Table 3.8** ANISOTROPIC CONSTANTS $K_1$ AND SATURATION MAGNETOSTRICTION $\lambda_{100}$ AND $\lambda_{111}$ FOR VARIOUS SINGLE CRYSTALS[62]

| *Composition by weight (remainder iron)* | $K_1$ ($10^3$ erg/cm$^3$) | $10^6\lambda_{100}$ | $10^6\lambda_{111}$ |
|---|---|---|---|
| $Fe_3O_4$ | −140 | −15·1 | 54·7 |
| 44·7% Ni, 25·4% Co | − 11 | 22·8 | 10·4 |
| 1·96% Mo, 80·6% Ni | − 3 | 2·8 | − 0·7 |
| 4·75% Mo, 79·2% Ni | − 1·5 | 4·8 | 1·3 |
| 3% Mo, 15·4% Al | − 29 | 21·0 | 11·8 |

**Table 3.9** ANISOTROPIC CONSTANT $K_1$ AND SATURATION MAGNETOSTRICTION $\lambda_{100}$ AND $\lambda_{111}$ FOR SINGLE CRYSTALS OF IRON AND NICKEL AND CERTAIN Fe–Ni AND Fe–Si ALLOYS: (a) INDICATES AN APPROXIMATELY RANDOM CONDITION, AND (b) A MORE OR LESS ORDERED CONDITION[62]

| *Composition by weight (remainder iron)* | $K_1$ ($10^3$ erg/cm$^3$) | | $10^6\lambda_{100}$ | | $10^{-6}\lambda_{111}$ | |
|---|---|---|---|---|---|---|
| | *(a)* | *(b)* | *(a)* | *(b)* | *(a)* | *(b)* |
| 100% Ni | −56 | — | −58·3 | — | −24·3 | — |
| 80·4% Ni | −10 | −13 | 7·9 | 8·2 | — | 2·1 |
| 75·4% Ni | − 7 | −30 | 16·2 | 12·0 | 6·1 | 9·2 |
| 70·1% Ni | − 1 | − 9·5 | 22·7 | 20·9 | — | 10·8 |
| 59·9% Ni | 1 | − 3·5 | 21·9 | 21·1 | — | 20·2 |
| 49·4% Ni | 5 | 3 | 6·4 | 7·4 | — | 27·5 |
| 39·8% Ni | 5 | 5 | − 9·5 | −10·7 | — | 27·4 |
| 100% Fe | 460 | — | 20·0 | — | −15·7 | — |
| 1·45% Si | 425 | — | 22·5 | — | − 9·7 | — |
| 3·06% Si | 365 | — | 23·0 | — | − 4·1 | — |
| 4·48% Si | 300 | 300 | 18·7 | 17·1 | 0·2 | −0·1 |
| 5·38% Si | 240 | 230 | 14·0 | 9·1 | 1·5 | 0·9 |
| 6·37% Si | 220 | 225 | − 1·3 | − 0·4 | 2·0 | 1·5 |

### 3.2.12 The hysteresis loop

The most outstanding characteristic of a magnetic material is its hysteresis loop, called also the (*BH*) curve or, not very happily, 'the characteristic'. The genesis of the loop, the various types of loops, and the influences bearing on them are matters to be discussed in detail in the next section. Here, only brief references to the relevant definitions and the commonest types will be offered: the term 'hysteresis' (Greek *hystereo* = delay) goes back to Ewing[39].

In the most general sense, hysteresis exists between two quantities $M$ and $N$ if a cyclical change in $N$ leads to cyclical variations of $M$ whereby the changes in $M$ lag behind changes in $N$. The value of $M$ at any particular

point of the cycle, therefore, depends not only on the instantaneous value of $N$ but also on prior changes—particularly on immediately previous changes. The notion of hysteresis is a very general one. There are many processes in Nature for which this is an underlying principle and which show no simple univalued relation. One has only to remember that even magnetostriction shows hysteresis effects as instanced, for example, by the Matteucci effect (Figure 2.4, page 8).

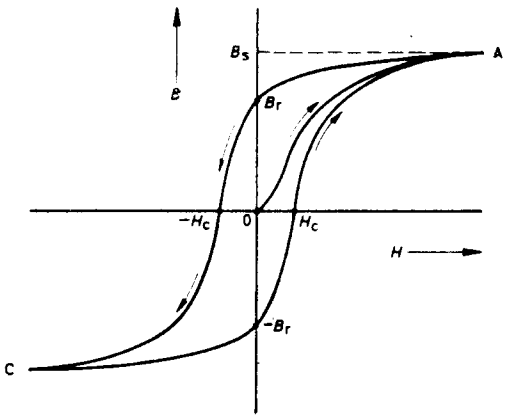



*Figure 3.53. Diagrammatic hysteresis loop*

The genesis of a hysteresis loop may be described, broadly, in the following way (Figure 3.53). Consider a toroidal core with two windings: in one of them flows the magnetising current which creates the magnetic force within the specimen; the other is connected to a measuring instrument from which the resulting flux density may be read (Figure 3.54). Starting from O,

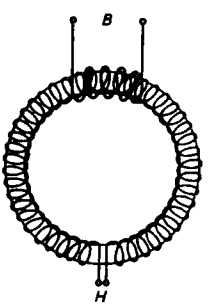



*Figure 3.54. Measurement of toroidal cores*

representing a general unmagnetised condition, the field strength $H$, is gradually increased; $B$ rises slowly at first, but then more steeply until, at higher intensities, only small increases in $B$ can be achieved. If the polarisation $B-\mu_0 H$ remains constant with increasing $H$, saturation has been reached. If, now, the magnetising current and, with it, the magnetising field are reduced to zero, the flux density $B$ does not return to zero but attains a positive value $B_r$ called its *remanence* value.

To make $B$ vanish, a negative field strength $H_c$ must be produced by the magnetising winding. This is called the *coercivity*. If the intensity is further increased in the negative sense, a reversed saturation density $-B_s$ is ultimately achieved. Now let the field strength increase once more in the positive sense, and the curve will rise again to the positive saturation density $B_s$ by a route through $-B_r$ and $+H_c$: the path is closed.

The $(BH)$ hysteresis curve comprises three branches:

1. The initial magnetisation curve OA which runs in the direction of the arrow—but only from the unmagnetised condition, i.e. at the first measurement.
2. The demagnetisation curve, A $B_r(-H_c)$ C.
3. The magnetisation curve, C $(-B_r)$ $H_c$A.

In the literature the initial magnetisation curve or virgin curve is often called simply the 'magnetisation curve'. The enclosed area is called the hysteresis area (or loop area). Its magnitude is a measure of the energy $W_h$ converted into heat at each cycle (see page 48).

Thus the work per cubic centimetre of core due to magnetisation is expressed by the formula

$$W_h = \int H \, dJ \triangleq \int H \, dB \tag{3.78}$$

Any $(BH)$ curve can be redrawn as a $(JH)$ curve by reference to the previously quoted equation 3.2. This means that there are two different coercivities, namely ${}_BH_c$ and ${}_JH_c$. The force ${}_JH_c$ can be appreciably higher than ${}_BH_c$, particularly for highly coercive permanent magnets, whereas for low-coercivity materials—the so-called 'soft' materials—the difference is negligibly small.

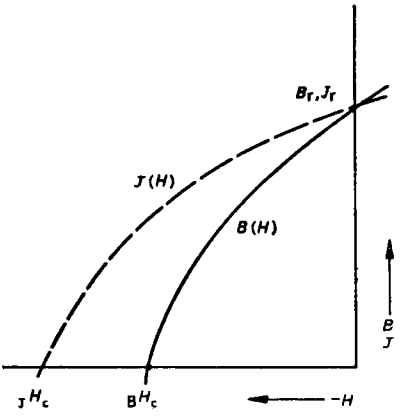



*Figure 3.55. Characteristics of flux density and polarisation in the second quadrant*

It is particularly the second quadrant in the $(BH)$ or $(JH)$ plane that is important for permanent magnets. At $H = 0$ both remanence values $B_r$ and $J_r$ coincide (Figure 3.55). The $B$ curve reaches the zero point, with falling intensity, before the $J$ curve since, from equation 3.2, $B$ is always less than $J$ for negative values of $H$. Just how significant the difference between $B_r$ and $J_r$ can be for permanent magnets is brought out by the example of Ag–Al–Mn, for which ${}_BH_c = 43$ kA/m whereas ${}_JH_c = 480$ kA/m.

### 3.2.13 The demagnetising factor

A toroidal core is particularly useful for determining the magnetic properties of a material since, especially in the region of low field intensity, the magnetic field is wholly confined to the material, i.e. magnetic lines of force do not leave the core (Figure 3.54).

Measuring samples are not always in ring form, however. It is often necessary, for example, to study a bar or strip. Specimens may be studied in this form by, for example, winding a coil for the determination of flux density $B$ and disposing it centrally with respect to a cylindrical magnetising

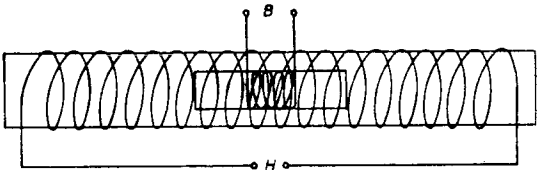



*Figure 3.56. Measurement of bars*

coil (Figure 3.56). It is then important to know the field strength within the solenoid coil: if $l$ is the length of the uniformly wound coil, $r$ its radius, and $z$ the number of turns, and if, further, $a$ is the distance from one end of the coil and $i$ the current which flows through it, then the field strength, according to Kohlrausch[83] is given by

$$H = \frac{iz}{2l}\left\{\frac{a}{\sqrt{(r^2+a^2)}}+\frac{1-a}{\sqrt{[r^2+(l-a)^2]}}\right\} \tag{3.79}$$

or

$$H = \frac{iz}{l}f$$

where $f \leqslant 1$. In the centre of the exciting coil ($a = \frac{1}{2}l$),

$$H = \frac{iz}{\sqrt{(4r^2+l^2)}} \tag{3.80}$$

If the coil radius is small compared with the length, this reduces to

$$H = \frac{iz}{l} \tag{3.81}$$

a relation already given by equation 3.22. At the ends of the coil,

$$H = \frac{iz}{2l}$$

which is thus half the central value.

The smaller the ratio $r/l$, the more homogeneous the field in the radial direction. Figure 3.57 displays, following Würschmidt[157], the value of the

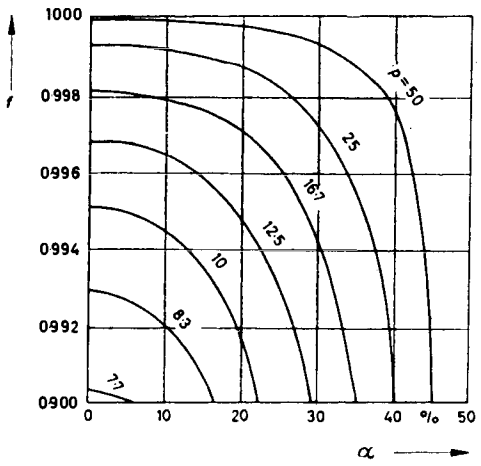



*Figure 3.57. Form factor f as a function of coil location α and the dimensional ratio p of the cylindrical coil*[157]

factor $f$ as a function of $\alpha = (l-a)/l$ for various cross-sectional ratios $p = l/2r$, within a range where the error does not exceed 1%. If this ratio $p = l/2r$ be given for a particular coil, the graph shows how long a measuring specimen should be, in relation to the length of the coil, if the non-uniformity of the field is to be kept within 1%.

The measuring specimen becomes a magnet in the magnetising field, with poles forming at its ends. Figure 3.58b shows schematically the uniform field in the middle of the coil. For comparison, Figure 3.58a shows the actual sample magnetised by the given field; this sample must be located in the centre of the coil. The magnetising flux entering the specimen produces a south pole, while the flux leaving it produces a north pole. The poles set up a field which opposes the original magnetising field. The result is spoken of as 'demagnetisation'.

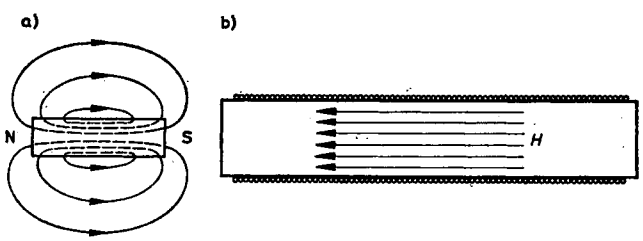



*Figure 3.58. (a) Field of a magnetised specimen; (b) field in the middle of a cylindrical coil*

If $M$ is the magnetisation of the test specimen, the field strength $H$ of the coil is reduced by an amount proportional to the magnetisation. The effective field strength $H'$ is therefore

$$H' = H - NM \tag{3.82}$$

where $N$ is called the demagnetising factor. The magnitude of $N$ depends on the shape of the specimen, i.e. on the ratio between length and cross-section. Strictly, $N$ is only calculable for an ellipsoid of revolution since only in this case is the flux density the same at all points.

If $p$ is the dimensional ratio, then

$$N = \frac{1}{p^2-1}\left\{\frac{p}{\sqrt{(p^2-1)}} \ln\left[p+\sqrt{(p^2-1)}\right]-1\right\} \tag{3.83}$$

The formula may be simplified for very elongated ellipsoids to

$$N = \frac{1}{p^2}(\ln 2p-1) \tag{3.84}$$

For a rod of infinite length ($p = \infty$), $N = 0$. If $p = 1$, i.e. if the ellipsoid becomes a sphere, then $N$ becomes $\frac{1}{3}$.

For permanent magnets, the demagnetising factor $N$ determines the ratio of the magnet length $l_m$ to the magnet cross-sectional area $A_m$ provided by the supplier in conformity with the following equation

$$N = \frac{A_m}{l_m}\frac{l_a}{A_a\sigma} = \frac{\mu_0 H}{\sigma B} \tag{3.85}$$

where $A_a$ and $l_a$ are the cross-sectional area and length of the air-gap, and $\sigma$ is the leakage factor of the gap.

Table 3.10 gives the demagnetising factor $N$ for the various dimensional ratios $p$ of an ellipsoid of revolution[61]. For cylindrical rods, or those of

**Table 3.10** DEMAGNETISING FACTORS[61]

| *Dimensional ratio, p* | $10^6$ $N$ | |
|---|---|---|
| | *Ellipsoid of revolution* | *Cylinder* |
| 5 | 55 818 | 54 107 |
| 10 | 20 283 | 20 290 |
| 15 | 10 742 | 11 140 |
| 20 | 6 747 | 7 146 |
| 25 | 4 671 | 4 997 |
| 30 | 3 437 | 3 660 |
| 40 | 2 117 | 2 180 |
| 50 | 1 440 | 1 456 |
| 60 | 1 050 | 1 042 |
| 70 | 804 | 788 |
| 80 | 637 | 621 |
| 90 | 527 | 502 |
| 100 | 430 | 414 |
| 150 | 207 | 198 |
| 200 | 127 | 119 |
| 300 | 64 | 64 |

rectangular cross-section, the calculation is difficult because the magnetisation of the specimen is non-uniform and so $N$ is also a function of $M$. Experimentally determined values of $N$ for cylinders of varying length are given in Table 3.10 for comparison with the ellipsoids. Only for $p$ greater than 300 is the difference negligibly small[61].

The true permeability $\mu$ of an ellipsoid can be calculated from the demagnetising factor $N$ and the measured apparent permeability $\mu'$. In fact, from equation 3.82,

$$\frac{1}{\mu} = \frac{1}{\mu'} - N$$

if $1/\mu$ is small compared with unity. This may be written as

$$\mu = \frac{\mu'}{1-\mu' N} = \frac{\mu' (1/N)}{(1/N)-\mu'} \tag{3.86}$$

It has to be remembered that $N$ depends on the permeability. Thus, for example, the demagnetising factor rises for a cylinder of circular cross-section and dimensional ratio $p = 50$ from $N = 0{\cdot}0025$ to $N = 0{\cdot}0150$ as the susceptibility increases from zero to infinity. Figure 3.59, following

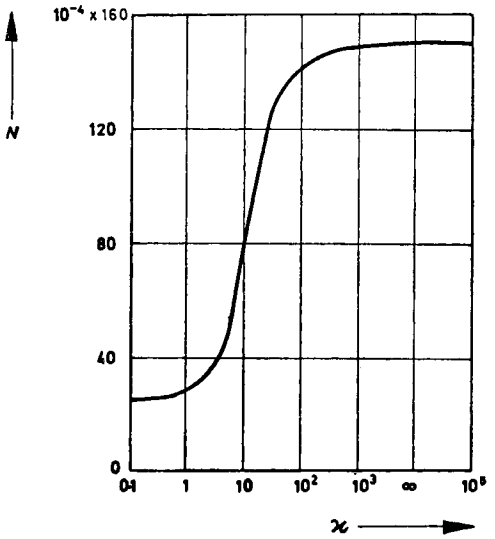



*Figure 3.59. Demagnetising factor N for a round-section cylinder (p = 50) as a function of the suspectibility χ*[157]

Würschmidt[157], shows the general form of the relation. For susceptibilities between 1000 and infinity, $N$ is practically constant, but, between $\varkappa = 1$ and $\varkappa = 100$, the value of $N$ changes very rapidly. The value for $\varkappa = 0$ corresponds to the demagnetising factor for a uniformly magnetised cylinder. Again, it can be seen from equation 3.82 that, when a hysteresis loop of a body having free poles is measured, $H$ must be corrected for each value

of $B$ (or of $M$). In the case where $N$ is independent of field strength, i.e. for an ellipsoid, the correction can be obtained from a linear function: for some arbitrary $M$ value, for example, the quantity $NM$ is determined and the point so found is joined to the origin (Figure 3.60). The straight line drawn in this way is the correction line (this may be called the shearing line because the nature of the correction is, mathematically, a transformation in shear).

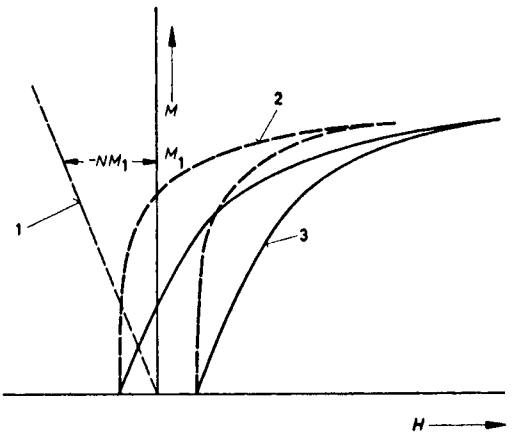



*Figure 3.60. Hysteresis loop displaced in shear: 1, shearing line; 2, corrected curve; 3, curve as measured*

The distance of any point thereon from the ordinate is the amount to be subtracted from the relevant curve to find the true hysteresis curve. The corrected curve differs, in particular, from the measured curve by reason of its increased steepness, i.e. its higher remanence. The enclosed area is the same in both cases. Also, the coercive force remains unaltered. For cylindrical specimens, a non-linear correction curve must be substituted for the straight line, and this can be determined ballistically or magnetometrically[156].

### 3.2.14 Magnetic anisotropies

#### 3.2.14.1 Magnetocrystalline anisotropy

Since the ferromagnetic and ferrimagnetic properties of a crystal lattice are connected, it is easily understood that the magnetic properties of crystals depend on direction within the structure, i.e. that a magnetic anisotropy is inevitable. We have already, in Figure 2.2, come across a case of magnetocrystalline anisotropy in a single crystal. The magnetic characteristics of the most important single crystals in relation to crystal direction are set out in detail in Chapter 4.

Crystal anisotropy is intimately connected with crystal energy. This is the energy needed to turn the magnetisation vector from the easy into the difficult direction. Crystal energy will be represented by the two constants

$K_1$ and $K_2$. For single-axis crystals (for example, cobalt) a sinusoidal series can usefully be written:

$$E_k = K_0 + K_1 \sin^2 \Phi + K_2 \sin^4 \Phi + \ldots \quad (3.87)$$

Higher-order terms are mostly not necessary; $\Phi$ is the angle between the direction of magnetisation and the hexagonal axis, and $K_0$ is the energy required for magnetisation in the [0001] axis. Similar formulae hold for cubic crystals somewhat in the following fashion:

$$A_k = K_0 + K_1(\alpha_1^2\alpha_2^2 + \alpha_2^2\alpha_3^2 + \alpha_3^2\alpha_1^2) + K_2\alpha_1^2\alpha_2^2\alpha_3^2 + \ldots \quad (3.88)$$

Here, $\alpha_1$ and $\alpha_2$ are the direction cosines appropriate to the magnetising direction and the crystal axes[5]. It is most generally useful to quote values for $K_1$. A few examples of the values taken by $K_1$ and $K_2$ are collected together in Table 3.11 following published results by Bickford[6], Birks[7], Bozorth[15], Gorter[55], Guillaud[57, 60], Nesbitt and Heidenreich[106], and Rathenau, Smit, and Stuijts[121].

**Table 3.11** CONSTANTS OF CRYSTAL ANISOTROPY AT ROOM TEMPERATURE

| *Material* | $K_1$ ($10^3$ erg/cm$^3$) | $K_2$ ($10^3$ erg/cm$^3$) | *Reference* |
|---|---|---|---|
| Iron | 400 to 525 | −170 to 290 | 15 |
| Nickel | −5 | −2 | 89a |
| Cobalt | 3 980 | 1 980 | 15 |
| Fe–Pd | 26 000 | — | 90a |
| Mn–Bi | 11 600 | — | 57 |
| Barium ferrite | 3 000 | — | 121 |
| Alnico 5 | 960 | — | 106 |
| Magnetite | −110 to −130 | −28 | 6, 8, 10 |
| $MnO \cdot Fe_2O_3$ | −2 to −3 | — | 10, 55 |
| $CoO \cdot Fe_2O_3$ | 3 800 | — | 55 |
| $NiO \cdot Fe_2O_3$ | −62 to −62·7 | — | 10, 55, 160 |
| Ni–Zn ferrite | 32 | — | 8, 160 |
| Mn–Zn ferrite | 15 | — | 160 |

Crystal anisotropies of reversible Fe–Ni alloys are plotted in Figure 4.26 (see also Table 4.3). Gengnagel and Wagner[52] measured $K_1$ for Fe–Si alloys with up to 14% Si. The results are shown in Figure 3.61.

The anisotropic constants set out in Tables 3.8 and 3.9 for magnetite and for various iron alloys come from Hall[62].

High crystal anisotropy may be one of the prerequisites for a high coercivity in permanent-magnet materials. For a suitably oriented spherical particle, the following relation holds, according to Kittel[82]

$$_JH_c = \frac{2K}{J_s} \quad (3.89)$$

where $_JH_c$ is the coercivity and $J_s$ is the saturated polarisation.

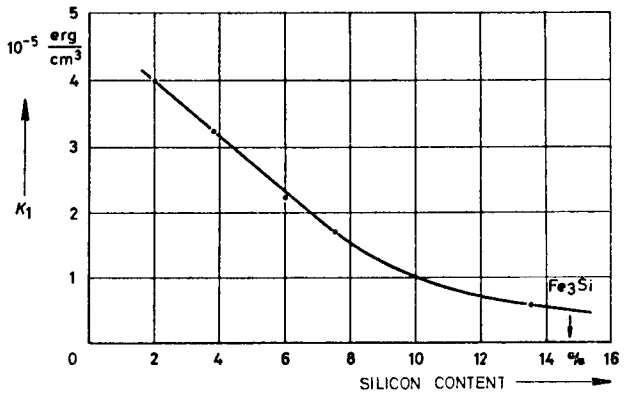



*Figure 3.61. $K_1$ for* Fe–Si *alloys as a function of silicon content, measured in the (001) plane*[52]

The values of anisotropic constants $K$ can be experimentally determined by four methods:

1. Single-crystal magnetisation curves are drawn for the various axial directions, and the area enclosed by the curves appropriate to the preferred and most difficult directions is measured (see, for example, Figure 4.22), from which the energy can be calculated.
2. By means of resonances in the centimetre-wave range[7].
3. By means of a magnetic-moment curve[16, 32, 143, 154].
4. From the initial permeability $\mu_i$ and the saturated polarisation $J_s$ according to the formula[148]

$$\mu_i - 1 = \frac{kJ_s^2}{K_1} \tag{3.90}$$

although this relation yields reliable values only in certain conditions[8].

To carry out magnetic-moment measurements, disc-shaped slices are cut from the specimen under investigation and arranged to move easily between the poles of a magnet, as sketched in simplified form in Figure 3.62[15]. No turning moment acts in any position if these small slices are isotropic. However, if for an anisotropic specimen the magnetic field makes an angle with the preferred direction, the field tries to rotate the specimen, with a measurable force, into the zero-angle position. Figure 10.20 shows examples of the measurement of a turning moment for a single crystal and for a textured laminated sheet. Six, Snoek, and Burgers[129] describe a simple measuring arrangement, while Byrnes and Crawford[28] and also Penoyer[118] describe an automatic balance method.

Cole and Honeycutt[30] describe a very rapid and, at the same time, automatic instrument in which the experimental sample rotates in a magnetic field at 1800 rev/min. An oscillograph traces the moment curve. Disc-shaped laminae of technical materials can be measured in a simple way using a measuring frame described by Ruess[124]. In the principal crystal

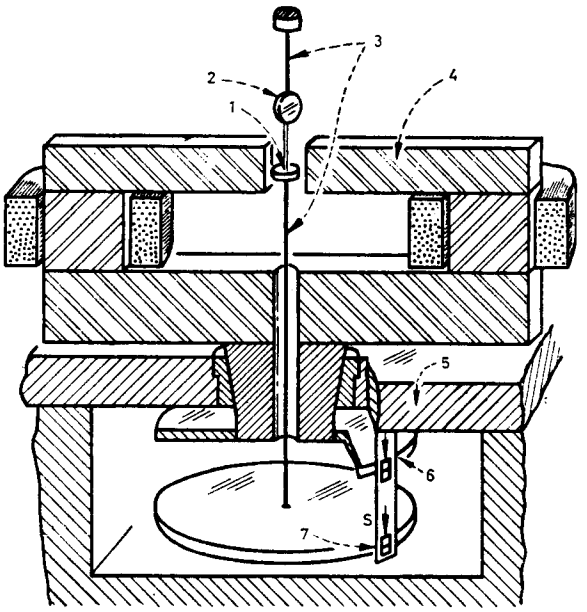



*Figure 3.62. Arrangements for measuring the magnetic turning moment or torque of thin magnetic discs: 1, specimen; 2, mirror; 3, torsion fibre of phosphor bronze; 4, electromagnet with bearing; 5, bench; 6, electromagnet scale; 7, torsion scale S*[15]

planes (100), (110), and (111), the moments for iron, for example are:

$$M_{100} = -K_1 (\sin 4\Phi)/2$$

$$M_{110} = -K_1 (2 \sin 2\Phi + 3 \sin 4\Phi)/8 - K_2 (\sin 2\Phi + 4 \sin 4\Phi - 3 \sin 6\Phi)/64$$

$$M_{111} = -K_2 (\sin 6\Phi)/18$$

where $\Phi$ is measured in the [001] direction for planes (100) and (110), and in the [110] direction for the (111) plane.

The measured values quoted in Table 3.11 are valid at room temperature. Crystal anisotropy, however, is a function of temperature. Figure 3.63 shows the temperature dependence of $K_1$ and $K_2$ for crystals of magnetite, following Bickford, Brownlow, and Penoyer[6], and Figure 3.64 shows the variation of $K_1$ for a nickel ferrite with temperature, according to Elbinger[35]. The anisotropic constants for an Fe–Si alloy with 3·1% Si were measured at low temperatures by Graham[56], and the results are given in Table 3.12.

Since magnetic components are usually designed to have only one operating direction, it is clearly desirable, in developing the relevant material, to improve the magnetic performance in this direction. For this reason the production, improvement, and exploitation of materials having a preferred direction is characteristic of much modern research. Crystalline anisotropy is only partly in evidence in the widely used polycrystalline materials because magnetic directions change from crystal to crystal. If one ensures, however,

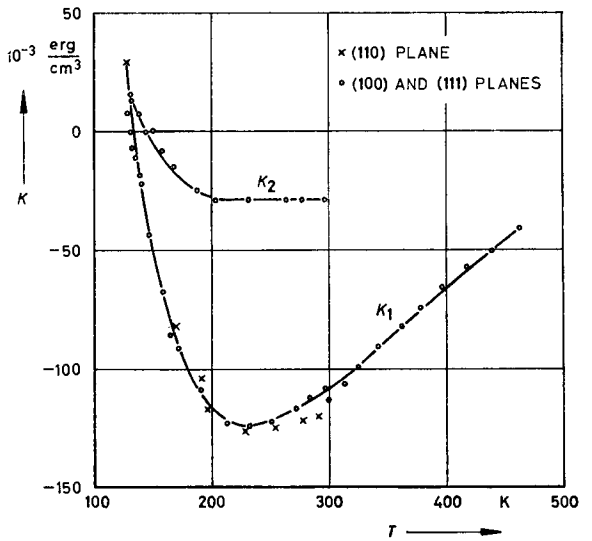



*Figure 3.63. Temperature characteristic of $K_1$ and $K_2$ for a single crystal of magnetite*[6]

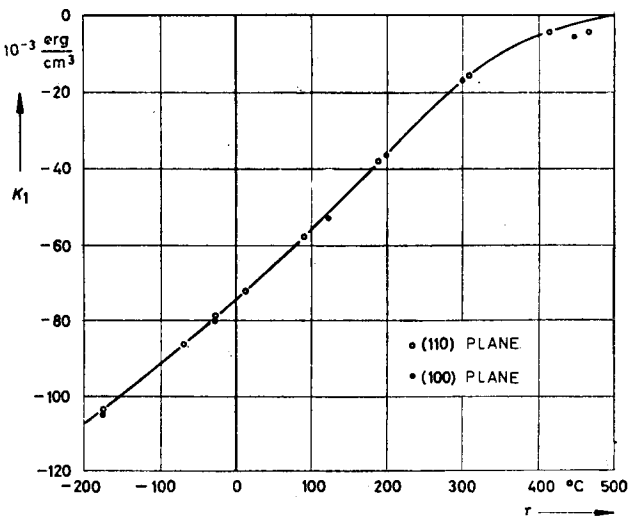



*Figure 3.64. Temperature characteristic of $K_1$ for a nickel ferrite*[35]

**Table 3.12**
ANISOTROPIC CONSTANTS FOR Fe–Si WITH 3·1% Si[56]

| *Temperature* (K) | $K_1$ ($10^3$ erg/cm$^3$) |
|---|---|
| 77 | 425 ± 10 |
| 195 | 405 ± 10 |
| 300 | 365 ± 10 |

that all crystals in a polycrystalline sample are similarly aligned, so that their preferred directions lie parallel throughout, then the properties are similar to those of single crystals. This mode of action brings about significant improvements in laminae and in permanent-magnet materials.

### 3.2.14.2 Form anisotropy

In the earlier review of demagnetising factors it was clearly brought out that the shape of a specimen is important. The dimensions of magnetic particles, for example of particles precipitated in a matrix, can lead to 'form anisotropy' or anisotropy of shape. For an elongated particle having the shape of an ellipsoid of revolution with axes $a$ and $b$, the demagnetising factors in these axial directions are designated $N_a$ and $N_b$.

If such a particle contains no Bloch walls, so constituting a single domain, then according to Stoner and Wohlfarth[139] the coercivity $H_c$ is given by

$$_JH_c = \frac{(N_b - N_a)J_s}{\mu_i} \tag{3.91}$$

Where the major axis coincides with the direction of the field and where it is long compared with the minor axis $b$, then

$$N_b - N_a = \tfrac{1}{2}$$

from which

$$_JH_c = \frac{J_s}{2\mu_i} \tag{3.92}$$

Coercivity of permanent magnets produced with the aid of form anisotropy plays an important practical role, since then $H_c$ is proportional to polarisation[100].

### 3.2.14.3 Stress anisotropy

The attention of scientists was aroused more than a century ago by the fact that stresses, in tension or compression, are capable of influencing magnetisation (Joule effect). In the history of ferromagnetics as later developed,

many investigations were devoted to stress anisotropy. The occurrence of stress anisotropy was of special importance in the production of martensitic steels and its avoidance is, to this day, an important requirement in the preparation of high-permeability materials.

Films of 100–300 nm thickness evaporated onto a glass slip acquire a stress which is measurable and, according to Finegan and Hoffman[46], amounts to about $10^{10}$ dyn/cm$^2$ or $10^9$ N/m$^2$. This stress is usually isotropic; if, however, it is evaporated obliquely onto a substrate, then anisotropic stresses are produced. For materials having dominant stress anisotropy and negligible crystal anisotropy, according to Kersten[80]

$$_{\sigma}H_c = \frac{s\lambda_s\sigma}{J_s} \tag{3.93}$$

where $s$ is a constant which can lie between 0 and 1·5, $\lambda_s$ is the saturated magnetostriction, and $\sigma$ is the mean internal stress.

### 3.2.14.4 Induced uniaxial anisotropy

In a group of magnetic materials, a magnetic anisotropy can be produced by applying a magnetic field to the randomly ordered polycrystalline sample as it cools through the Curie temperature. One speaks, in this case, of an induced uniaxial anisotropy. Generally, such thermomagnetic processing is only practicable if the Curie temperature is sufficiently high to allow ion or hole diffusion to occur.

The anisotropy comes about by reason of a 'direction ordering' of similar atoms in neighbouring lattice sites. The oriented superstructure so formed[103] has nothing to do with the known crystallographic superstructure. Oriented superstructures have been observed in Fe–Ni, Fe–Si, Fe–Co and Fe–Ni–Co alloys. Oriented superstructures can be produced not only by magnetic field routines but by mechanical manipulation at sufficiently high temperatures. Formation of anisotropy in textured Isoperms (see page 425) for example, will involve reference to this phenomenon[104].

Again, uniaxial anisotropy has been induced on evaporated or cathode-sputtered films of ferromagnetic material by the simultaneous application of magnetic fields[51, 91, 141]. Tanaguchi[142] has traced the appearance of induced anisotropy in cobalt-containing ferrites to anisotropic partitition of cations and vacant cation sites. Dislocations and impurities may also lead to magnetic anisotropy[141].

Heat treatment is used to promote anisotropy in Perminvar alloys, in ferrites with Perminvar characteristics, and in Fe–Co and Fe–Ni alloys, as well as in many materials for permanent magnets (Fe–Al–Ni–Co alloys). Induced uniaxial anisotropy can be measured in the same way as crystalline anisotropy[150].

### 3.2.14.5 Exchange anisotropy

To the four named anisotropies there has recently been added a fifth: exchange anisotropy. As the name implies, this anisotropy turns on a process of interchange and, in particular, interchange between a ferromagnetic substrate such as iron or cobalt and an antiferromagnetic oxide grown on its surface[99].

The effect can sometimes produce asymmetrical shifts of the hysteresis loop (Figure 3.65). If a sample formed of cobalt particles, covered by a skin of cobalt oxide, is cooled to −200°C, the symmetrical hysteresis loop 2 is obtained and will have a coercivity ${}_{B}H_{c}$ of 96 kA/m. If a magnetic field of, for example, 800 kA/m is applied during the refrigeration of the specimen, loop 1 is obtained for which $+{}_{B}H_{c} = 40$ kA/m and $-{}_{B}H_{c} = 300$ kA/m. It is possible that this kind of anisotropy may turn out one day to be useful, particularly for permanent-magnet work (see page 294).

Two other properties of this kind of material are worth mentioning since they may have future consequences: the magnetic anisotropy occurs only in one direction (in constrast to this, axial anisotropy has two stable conditions, alignment and anti-alignment); rotational hysteresis is also anomalous. The rotational hysteresis loss does not fall from a maximum to zero when cycled, as does that of normal materials (see page 55), but rises to a high value and then stays more or less constant[97] (see Figure 3.29). Meiklejohn[98] gives a review of such systems as have been investigated so far.

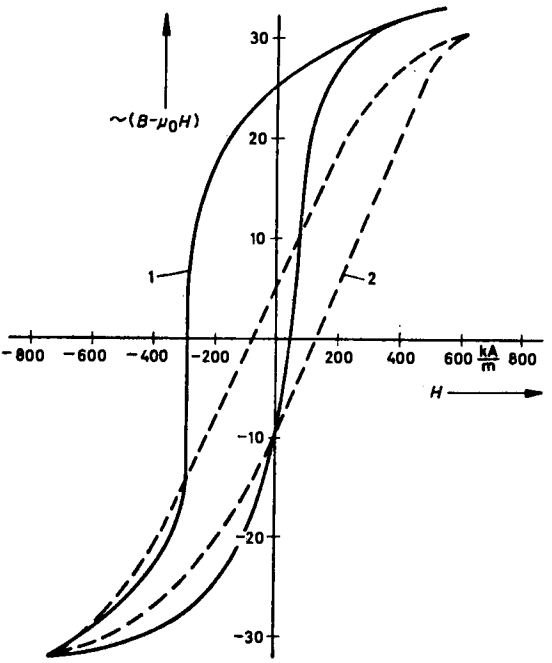



*Figure 3.65. Hysteresis loops of cobalt dust with oxidised skin: 1, cooled in a magnetic field to −196°C[99]; 2, without magnetic field during cooling*

## REFERENCES


1. ACKERMANN, F. W.: Trennfugen in weichmagnetischen Kreisen geringer Induktionsbelastung (T. Mitt. Krupp **14** (1956) 18–23)
2. ANDRÄ, W., GREINER, C. and SCHWAB, W.: Beobachtung der magnetischen Bereichsstruktur bei Wechselfeldmagnetisierung zur Prüfung der Theorie der Ummagnetisierungsverluste (Monatsber. Akad. Wiss., Berlin **2** (9) (1960) 539–544)
3. ATORF, H.: Die zeitliche Desakkommodation kleiner symmetrischer und unsymmetrischer Hystereseschleifen (Z. Phys. **76** (1932) 513–526)
4. BAILY, F. G.: The hysteresis of iron and steel in a rotating magnetic field (Trans. Roy. Soc. (A) **187** (1897) 715–746)
5. DE BARR, A. E.: Magnetic anisotropy in cold-reduced electrical sheet steel (Proc. IEE (II) **96** (Oct. 1949) 719–728)

5a BEAN, C. P. and LIVINGSTON, J. D.: Superparamagnetism (J. A. P. **30** (Apr. 1959) 120 S–129 S)

6. BICKFORD, L. R., BROWNLOW, J. M. and PENOYER, R. F.: Magnetocrystalline anisotropy in cobalt-substituted magnetite single crystals (Proc. IEE (B) **104** (1957) 238–244)

6a BICKFORD, L. R., PAPPIS, J. and STULL, J. L.: Magnetostriction and permeability of magnetite and cobalt-substituted magnetite (Phys. Rev. **99** (4) (Aug. 1955) 1210–1214)

7. BIRKS, J. B.: The properties of ferromagnetic compounds at centimetre wavelengths (Proc. Phys. Soc. (B) **63** (2) (Feb. 1950) 65–74)
8. BIRKS, J. B., First-order magnetic anisotropy constants of ferrites (Phys. Rev. **99** (1955) 1821)
9. BLAKE, L. R.: The eddy current anomaly in ferromagnetic laminae at high rates of change of flux (Proc. IEE (II) **96** (1949) 705–718)
10. BLOEMBERGER, N.: Magnetic resonance in ferrites (Proc. IRE **44** (Oct. 1956) 1259–1269)
11. BOCHIROL, L.: Séparation de pertes dans les noyaux de ferrites (J. Phys. Rad. **11** (1950) 49 S–50 S)
12. BOLL, R.: Dünne Bänder aus weichmagnetischen Werkstoffen und ihre Anwendungsformen (Elektronik **10** (1961) 293–298)
13. BOLL, R.: Wirbelströme und Spinrelaxation in dünnen Bändern aus weichmagnetischen Legierungen. Dissertation, Stuttgart (1959)

13a BOLL, R.: Ortskurven der komplexen Permeabilität dünner Bänder (Frequenz **14** (7) (1960) 227–238)

14. BOSMAN, A. J., BROMMER, P. E., VAN DAAL, H. J. and RATHENAU, G. W.: Time decrease of permeability in iron (Physica **23** (1957) 989–1000)
15. BOZORTH, R. M.: Ferromagnetism. Van Nostrand Co. Inc., Toronto/New York/London (1951)
16. BOZORTH, R. M.: Determination of ferromagnetic anisotropy in single crystals and in polycrystalline sheets (Phys. Rev. **50** (1936) 1076)

16a BOZORTH, R. M. and HAMMING, R. W.: Measurement of magnetostriction in single crystals (Phys. Rev. **89** (Feb. 1953) 865–869)

17. BOZORTH, R. M., TILDEN, E. F. and WILLIAMS, A. J.: Anisotropy and magnetostriction of some ferrites (Phys. Rev. **99** (1953) 1788–1798)
18. BOZORTH, R. M. and WALKER, J. G.: Magnetostriction of single crystals of cobalt and nickel ferrites (Phys. Rev. (2) **88** (5) (Dec. 1952) 1209)
19. BOZORTH, R. M. and WALKER, J. G.: Magnetic crystal anisotropy and magnetostriction of iron–nickel alloys (Phys. Rev. **89** (1953) 624–628)
20. BRAGINSKI, A., MARAIS, A. and MERCERON, T.: Trainage magnétique dans les solutions solides de ferrites de manganèse et de ferrites de nickel avec la magnétite (J. Phys. Soc. Japan **17** (B-1) (Mar. 1962) 300–303)
21. BRAGINSKI, A., MARAIS, A. and MERCERON, T.: Quelques résultats experimentaux sur les phénomènes de relaxation des ferrites de Mn–Zn (C. R. **253** (1961) 239–241)

22. BRAILSFORD, F.: Alternating hysteresis loss in electrolytic sheet steel (J. IEE **84** (1939) 399–407)
23. BRAILSFORD, F.: Magnetic Materials. Methuen & Co. Ltd, London/John Wiley & Sons Inc., New York (1951)
24. BRAILSFORD, F.: Investigation on the eddy-current anomaly in electrical sheet steels (J. IEE (II) **95** (Feb. 1948) 38–48)
25. BRAILSFORD, F.: (Proc. IEE (II) **97** (Apr. 1950) 130)
26. BRAILSFORD, F.: Rotational hysteresis loss in electrical sheet steel (J. IEE **83** (1938) 566–575)
27. BRISSONNEAU, P.: Amplitude de trainage de diffusion en fonction de la concentration des solutions solides fercarbone (Coll. Int. Magnétisme Grenoble (1958) CNRS, Paris (1959) 180–182)
28. BYRNES, W. S. and CRAWFORD, R. C.: Improved torque magnetometer (J. A. P. **29** (1958) 493–495)
29. CARR, W. J.: Energy loss resulting from domain wall motion (J. A. P. **30** (Apr. 1959) 90 S–91 S)
29a CLEAVES, H. E. and HIEGEL, J. M.: Properties of high purity iron (J. Res. Nat. Bur. Stds, **28** (1942) 643–667)
30. COLE, R. W. and HONEYCUTT, C. R.: Flux instrument for rapid comparison of crystal anisotropies (J. A. P. **30** (4) (Apr. 1959) 250 S–251 S)
30a CREVELING, L., LUO, H. L. and KNAPP, G. S.: Ferromagnetism in $Au_4V$. (Phys. Rev. Letters **18** (20) (1967) 851–852)
31. CZERLINSKY, E.: Die Eigenschaften handelsüblicher warmgewalzter Dynamobleche (Arch. Eisenhüttenw. **27** (1956) 35–40)
32. DAHL, O. and PFAFFENBERGER, J.: Anisotropie in magnetischen Werkstoffen (Z. Phys. **71** (1931) 93–105)
33. DEUTSCHMANN, W.: Über Massekerne (El. Nach. T. **9** (1932) 421–433)
33a DIN 1325, Magnetisches Feld Begriffe (Jan. 1972)
33b DIN 1339, Einheiten magnetischer Grössen (Sept. 1968)
33c DIN 41 301, Magnetic Materials for Transformers (July 1967)
33d DIN 41 293, Weichmagnetische Ferrit-Schalenkerne (1971)
33e DIN 46 400, Kalt- und warmgewalztes Elektrobleche und -band (1971)
34. EBERT, H.: Physikalisches Taschenbuch. Braunschweig (1951) 389
35. ELBINGER, G.: Temperaturabhängigkeit der magnetischen Kristallanisotropie von Nickelferrit (Naturw. **46** (1959) 140)
35a ELLIOTT, J. F., LEGVOLD, S. and SPEDDING, F. H.: Magnetic properties of erbium metal (Phys. Rev. **100** (6) (Dec. 1955) 1595–1596)
36. ENZ, U.: Relation between disaccommodation and magnetic properties of manganese-ferrous ferrites (Physica **24** (1958) 609–624)
37. EWING, J. A.: Magnetische Induktion. Berlin/München (1892) 302
38. EWING, J. A.: Time lag in the magnetization of iron (Proc. Roy. Soc. **46** (1889) 269–286)
39. EWING, J. A.: Experimental researches in magnetism (Phil. Trans. Roy. Soc. (II) **176** (1886) 523–640)
39a FAHLENBRACH, H. and SIXTUS, K.: Untersuchungen an verschiedenen pauschal unmagnetischen Zuständen (Z. Metallkde **40** (1949) 187–193)
40. FALLOT, M.: Ferromagnétisme des alliages de fer (Ann. Phys. **11** (6) (1936) 305–387)
41. FELDTKELLER, R.: Magnetische Nachwirkung in Spulenblechkernen bei schwachen Wechselfeldern (F. T. Z. **4** (1950) 112–117)
43. FELDTKELLER, R.: Die Formänderung der Hystereseschleife von Transformatorenblech bei magnetischen Kriechen (Z. ang. Phys. **4** (1952) 281–284)
44. FELDTKELLER, R. and HETTICH, H.: Der Frequenzgang der magnetischen Nachwirkung bei Massekernen (Z. ang. Phys. **2** (1950) 494–499)
45. FERRARIS, G.: Rotazioni elettrodinamiche prodotte per mezzo di correnti alternate (Atti R. Acc. Sci., Torino **23** (1887/88) 360–375)

46. FINEGAN, J. D. and HOFFMAN, R. W.: Stress anisotropy in evaporated iron films (J. A. P. **30** (4) (1959) 597–598)
46a FRASER, L. W., EVANS, D. J. I. and MACKIW, V. N.: Herstellung und Eigenschaften von duktilen Kobalt-Band (Kobalt **23** (June 1964) 62–69)
47. FRAUNBERGER, F.: Über einen neuen Nachweis der spontanen Magnetisierung oberhalb der Curietemperatur (Ann. Phys. **6** (2) (1948) 178–182)
48. FRAUNBERGER, F.: Eine neue Methode zur Bestimmung der Curietemperatur (Phys. Verh. **13** (1962) 88)
49. GANS, R. and LOYARTE, R. G.: Über drehende Hysterese (Arch. Elektrot. **3** (1915) 139–150)
50. GANS, R.: Die Gleichung der Kurve der reversiblen Suszeptibilität (Phys. Z. **12** (1911) 1053–1054)
51. GÄRTNER, H.: Einachsige magnetische Anisotropie dünner Nickel- und Eisenschichten aus der Kathodenzerstäubung (Z. Naturf. **16a** (1961) 841)
52. GENGNAGEL, H. and WAGNER, H.: Magnetfeldinduzierte Anisotropie an FeAl- und FeSi-Einkristallen (Z. ang. Phys. **13** (1961) 174–177)
53. GERLACH, W.: Die Abhängigkeit der ferromagnetischen Eigenschaften von der Temperatur als Grundlage für metall-physikalische Forschungen (Metallf. **2** (1947) 275–280)
54. GOLDSCHMIDT, R.: Über einige Eigenschaften magnetischer Materialien bei schwachen Feldern (VDE-Fachber. (1929) 108–110)
55. GORTER, E. W.: Some properties of ferrites in connection with their chemistry (Proc. IRE **43** (Dec. 1955) 1945–1973)
56. GRAHAM, C. D.: Magnetocrystalline anisotropy constant of 3·1% Si–Fe at room temperature and below (J. A. P. **30** (1959) 391–392)
57. GUILLAUD, C.: Ferromagnétisme des alliages binaires de manganèse. Thesis, Strasburg (1943)
58. GUILLAUD, C. and CREVEAUX, H.: Propriétés ferromagnétiques des ferrites mixtes de cobalt et de zinc et de manganèse et de zinc (C. R. **230** (1950) 1458–1460)
59. GUILLAUD, C., VILLERS, G., MARAIS, A. and PAULUS, M.: Propriétés des ferrites mixtes de nickel–zinc; in Solid State Physics, Vol. 3 (ed. Désirant and Michiels). Academic Press, New York (1960)
60. GUILLAUD, C. and ROUX, M.: Quelques propriétés ferromagnétiques des ferrites mixtes de nickel et de zinc (C. R. **228** (1949) 1133–1135)
61. GUMLICH, E.: Magnetische Messungen. Friedr. Vieweg & Sohn, Braunschweig (1918)
62. HALL, R. C.: Single crystal anisotropy and magnetostriction constants of several ferromagnetic materials including alloys of NiFe, SiFe, AlFe, CoFe and CoNi (J. A. P. **30** (6) (June 1959) 816–819)
63. HANSEN, M.: Der Aufbau der Zweistoffiegierungen. Berlin (1936)
64. HARVEY, R. L., HEGYI, I. J. and LEVERENZ, H. W.: Ferromagnetic spinels for radio frequencies (RCA Rev. **11** (Sept. 1950) 321–363)
65. HECK, C.: Ferrite (Radio Mentor **9** (1959) 707)
66. HECK, C.: Beiträge der Ferrite zur Miniaturisierung (VDE-Fachber. **19** (1956) II/157-II/161; SEG-Nachr. **5** (1957) 147–151)
67. HEISTER, W.: Temperaturgang und Desakkommodation der Anfangspermeabilität im System MnO–ZnO–$Fe_2O_3$ (T. Mitt. Krupp **17** (2) (1959) 82–89)
68. HEISTER, W.: Magnetische Werkstoffe für d. Nachrichten- und Hochfrequenztechnik (T. Mitt. Krupp **12** (1954) 161–174)
69. HERRMANN, P. K.: Über magnetische Nachwirkung (Z. Phys. **84** (1933) 565–570)
70. HERPER, D. J.: Direct method of measurement of losses in small samples of soft magnetic materials (J. Sci. Instr. **39** (1962) 13–15)
71. HILPERT, R. S., HOFFMANN, A. and HUCK, F. H.: Untersuchungen über die Natrium-, Lithium- und Kupferferrite und ihre Überführung in Nitride (Ber. D. Chem. Ges. **72** (1939) 848–853)

72. HU, H. and WIENER, G.: Correlation of energy losses with perfection of crystal orientation and domain structure (J. A. P. **30** (Apr. 1959) 86 S–87 S)
72a IEC Publication 125: General classifications of ferromagnetic oxide materials and definition of terms
72b IIDA, S. and INOUE, T.: Theoretical and experimental study of the induced anisotropy in iron–cobalt ferrites and disaccommodation phenomena in ferrites (J. Phys. Soc. Japan **17** (B-1) (Mar. 1962) 281–287)
73. JACKSON, R. C., LEE, E. W. and TROUGHTON, A. G. H.: The influence of the method of demagnetization on the reversible permeability of a high-permeability nickel–iron alloy (Brit. J. A. P. **9** (1958) 495–497)
74. JELLINGHAUS, W.: Suszeptibilitätsmessungen an Eisen-Kohlenstoff-Legierungen im Austenitgebiet (Z. ang. Phys. **15** (1963) 235–236)
75. JORDAN, H.: Die ferromagnetischen Konstanten für schwache Wechselfelder (El. Nach. T. **1** (1924) 7–29)
76. KÄMMERER, H.: Die Frequenzabhängigkeit des Klirrfaktors von Spulen mit Eisenblechkernen (A. E. Ü. **3** (1949) 249–256)
77. KÄMMERER, H.: Die Frequenzabhängigkeit des Spannungsklirrfaktors bei Spulen mit handelsüblichen Eisenblechkernen (F. T. Z. **2** (1949) 201–206)
78. KAMPCZYK, W.: Einige Eigenschaften und Anwendungen hochpermeabler Ferrite (Siemens-Z. **34** (2) (1960) 90–96)
79. KELLY, J. M.: Rotational losses in 4-79 molybdenum permalloy at low frequencies (Phys. Rev. **103** (1956) 499–500).
80. KERSTEN, M.: Grundlagen einer Theorie der ferromagnetischen Hysterese und der Koerzitivkraft. Hirzel, Leipzig (1944).
81. KERSTEN, M. and HESSE, H.: Hysteresearme Massekernspulen für das Trägerfrequenz-Fernsprechen (El. Nach. T. **14** (1937) 66–74).
82. KITTEL, C.: Domain theory and the dependence of the coercive force of fine ferromagnetic powders on particle size (Phys. Rev. **73** (1948) 810–811).
83. KOHLRAUSCH, F.: Praktische Physik, Vol. 2. Teubner, Leipzig (1955) 92.
84. KOPP, W.: Der thermische Verlauf des Paramagnetismus bei Magnetit, Platin und Palladium. Dissertation, St. Gallen (1919).
84a KOPPELMANN, F. and UNGER, G.: Kalorimetrische Messung der Ummagnetisierungsverluste von Ringkernen (ETZ-A **80** (22) (Nov. 1959) 773–777).
85. KORDES, E. and RÖTTIG, E.: Neue Mischoxyde mit Spinellstruktur (Z. anorg. allg. Chem. **264** (1951) 34–47).
86. KORNETZKI, M.: Ferritkerne für Hochfrequenzspulen (Siemens-Z. **2** (1951) 94–100).
87. KORNETZKI, M.: Messergebnisse an hochpermeablen Ferritkernen (Z. ang. Phys. **3** (1) (1951) 5–9).
88. KORNETZKI, M. and LUCAS, I.: Zur Theorie der Hystereseverluste im magnetischen Drehfeld (Z. Phys. **142** (1955) 70–82).
89. KORNETZKI, M. and WEIS, A.: Die Wirbelstromverluste im Massekern (Wiss. Ver. Siemens-Werke **18** (1936) 95–111).
89a KRAUSE, D. and PATZ, U.: Ermittlung der Konstanten $K_1$ und $K_2$ der Kristall-Anisotropieenergie von Nickel aus der Magnetisierungskurve (Z. ang. Phys. **21** (4) (1966) 342–345).
90. KUSSMANN, A. and SCHULZE, A.: Zur Definition des Curiepunktes (Phys. Z. **38** (1937) 42–47).
90a KUSSMANN, A. and MÜLLER, K.: Magnetische Eigenschaften der geordneten Phase FePd im homogenen und heterogenen Bereich (Z. ang. Phys. **17** (7) (1964) 509–511).
91. LAURIENTE, M. and BAGROWSKI, J.: Anisotropy sources for electrodeposited permalloy films (J. A. P. **36** (Mar. 1962) 1109–1110).
92. LEGG, V. E.: Magnetic measurements at low flux densities using the alternating current bridge (Bell Syst. Tech. J. **16** (1936) 39–62).
93. LESCRÖEL, Y.: Ferrites ferromagnétiques (Cables & Transm. **7** (4) (1953) 273–292).

94. LESCRÖEL, Y. and PIERROT, A.: Ferrites a faibles pertes utilisés dans les techniques de l'électronique et des télécommunications (Cables & Transm. **14** (3) (1960). 220–244)
95. MARAIS, A. and MERCERON, T.: Quelques résultats expérimentaux dans les phénomènes de relaxation des ferrites de Ni–Zn (C. R. **252** (1961) 3553–3555).
96. MASIYAMA, Y.: On the magnetostriction of a single crystal of nickel (Sci. Rep. Tohoku Imp. Univ. **17** (1928) 945–961).
97. MEIKLEJOHN, W. H.: Eine neue Art von magnetischen Werkstoffen (Phys. Bl. **14** (1958) 311–313).
98. MEIKLEJOHN, W. H.: Exchange anisotropy—A review (J. A. P. **33** (3) (1962) 1328–1335).
99. MEIKLEJOHN, W. H. and BEAN, C. P.: New magnetic anisotropy (Phys. Rev. **102** (1956) 1413–1414; **105** (1957) 904–913).
100. MENDELSOHN, L. I., LUBORSKY, F. E. and PAINE, T. O.: Permanent-magnet properties of elongated single-domain iron particles (J. A. P. **26** (10) (Oct. 1955) 1274–1280).
101. NAGASHIMA, T.: Magnetische Eigenschaften von sehr reinem Eisen (Ber. Arbg. Ferrom. (1959). Düsseldorf (1960) 148–154).
102. NÉEL, L.: Theorie du trainage magnétique des substances massives dans le domaine de Rayleigh (J. Phys. Rad. **11** (1950) 49–61).
103. NÉEL, L.: Les surstructures d'orientation (C. R. **237** (1953) 1613–1616).
104. NÉEL, L.: Surstructures d'orientation dues aux déformations mécaniques (C. R. **238** (1954) 305–308).
105. NESBITT, E. A.: The magnetostriction of permanent magnet alloys (J. A. P. **21** (Sept. 1950) 879–888).
106. NESBITT, E. A. and HEIDENREICH, R. D.: Physical structure and magnetic anisotropy of Alnico 5 (J. A. P. **23** (3) (Mar. 1952) 366–371).
107. NEURATH, P. W.: Hysteresis and eddy losses in silicon iron as a function of sheet thickness (J. A. P. **30** (Apr. 1959) 88 S–89 S).
108. NIETHAMMER, F.: Die ungleichmässige Feld- und Induktionsverteilung in ringförmigen Probestücken (Elektrot. u. Maschb. **34** (1916) 161–164).
109. NIETHAMMER, F.: Magnetismus. Enke, Stuttgart (1901) 10.
110. NIETHAMMER, F.: Einige experimentelle Untersuchungen über magnetische Hysterese (Wied. Ann. N. F. **66** (1898) 33).
111. NISHIYAMA, Z.: On the magnetostriction of single crystals of cobalt (Sci. Rep. Tohoku Imp. Univ. **18** (1929) 341–357).
112. NONNENMACHER, W. and SCHWEIZER, L.: Die Bestimmung der Permeabilität ferromagnetischer Stoffe aus der thermischen Rauschspannung von Spulen (Z. ang. Phys. **9** (5) (1957) 239–245).
113. OHTA, K. and YAMADAYA, T.: Magnetic anisotropy and disaccommodation of manganese–zinc ferrites (J. Phys. Soc. Japan **17** (B-1) (Mar. 1962) 291–295).
114. OKAMURA, T., TORIZUKA, Y. and KOJIMA, Y.: Ferromagnetic resonance in cobalt ferrite at high temperature (Phys. Rev. **84** (1951) 372).
114a OLSEN, E.: Reproduzierbarkeit von Variabilitätsmessungen an Ferroxcube-Schalenkernen (Valvo-Ber. **9** (4) (1964) 115–126).
115. PATTERSON, G. R.: Drift of magnetic permeability at low inductions after demagnetization (J. A. P. **9** (Oct. 1938) 646–653).
116. PAUTHENET, R.: Variation thermique d'aimantation spontanée des ferrites de nickel, cobalt, fer et manganèse (C. R. **230** (1950) 1842–1843).
117. PAUTHENET, R.: Les propriétés magnétiques des ferrites d'yttrium et de terres rares de formel 5 $Fe_2O_3 \cdot 3\, M_2O_3$ (Ann. Phys. **3** (1958) 424–462).
118. PENOYER, R. F.: Automatic torque balance for magnetic anisotropy measurements (Rev. Sci. Instr. **30** (8) (Aug. 1959) 711–714).
119. PRY, R. H. and BEAN, C. P.: Calculation of the energy loss in magnetic sheet materials using a domain model (J. A. P. **29** (1958) 532–533).
119a RADELOFF, C.: Bestimmung der sechs Magnetostriktionskonstanten des Eisens (Z. ang. Phys. **17** (1964) 247–253).

120. RATHENAU, G. W.: Time decrease of permeability in iron (J. A. P. **29** (3) (1958) 239–242).
121. RATHENAU, G. W., SMIT, J. and STUIJTS, A. L.: Ferromagnetic properties of hexagonal iron-oxide compounds with and without a preferred orientation (Z. Phys. **133** (1952) 250–260).
122. RENGER, K.: Die anfängliche Suszeptibilität von Eisen und Magnetit in Abhängigkeit von der Temperatur. Dissertation, Zürich (1913).
123. RICHTER, G.: Über magnetische und mechanische Nachwirkung; in Probleme der technischen Magnetisierungskurve (Becker). Berlin (1938) 93–113.
124. RUESS, L.: Über die Richtungsabhängigkeit magnetischer Eigenschaften von Elektroblechen und ihre Messung (ETZ-A **80** (1959) 588–593).
125. RUSBÜLDT, V.: Die Wirbelstromanomalie bei kornorientierten Blechkernen (EZT-A **78** (1957) 337–342).
126. SCHENKEL, M.: Beitrag zur Kenntnis des Verhaltens der rotierenden Hysterese (ETZ-A **23** (1902) 429–430).
127. SCHULZE, H.: Versuche zur magnetischen Nachwirkung bei Wechselstrom; in Probleme der technischen Magnetisierungskurve (Becker). Berlin (1938) 114–128.
128. SEIWATZ, H.: Low frequency rotational hysteresis losses in ferrites (J. A. P. **29** (June 1958) 994–995).
129. SIX, W., SNOEK, J. L. and BURGERS, W. G.: Een nieu magnetisch materiaal voor de kernen van pupinspoelen (Ingenieur, den Haag **49** (1934) E 199).
130. SMOLENSKI, G. A.: Ferrite zweiwertiger Metalle (Dokl. Akad. Nauk, SSSR **78** (5) (1951) 921–924).
131. SMOLINSKI, A. K., KASZKOWSKI, Z. and ZBIKOWSKI, M.: Influence of plastic deformation on the time decrease of permeability in transformer steel (J. A. P. **30** (4) (1959) 195 S–199 S).
132. SMOLINSKI, A. K. and ZBIKOWSKI, M.: The time decrease of permeability in transformer steel (Proc. IEE (6) **106** (1959) 23–26).
133. SNOEK, J. L.: New Developments in Ferromagnetic Materials. Elsevier Publ. Co. Inc., New York/London/Amsterdam/Brussels (1949).
134. SNOEK, J. L.: Time effects in magnetization (Physica **5** (8) (1938) 663–688).
135. SNOEK, J. L.: Gyromagnetic resonance in ferrites (Nature **160** (July 1947) 90).
136. SOMMER, J.: Spulen hoher Güte aus HF-Massenkernen für das Frequenzgebeit 100 Hz–100 kHz (Funk u. Ton **9** (1950) 458–468).
136a SOMMERKORN, G.: Elementarbereichsstrukturen verschiedener pauschal unmagnetischer Zustände (T. Mitt. Krupp **13** (1955) 71–83).
137. SORGER, G.: Die Wirbelstromanomalie in Blechkernen (Frequenz **8** (1954) 83–91).
138. STEWART, K. H.: Losses in electrical sheet steel (Proc. IEE (II) **97** (Apr. 1950) 121–125).
139. STONER, E. C. and WOHLFARTH, E. P.: A mechanism of magnetic hysteresis in heterogeneous alloys (Phil. Trans. Roy. Soc. **240** (1948) 599–642).
140. VAN SUCHTELEN, H.: A remark on the complex value of permeability (Phil. Matr. **17** (July 1960) 335–337).
141. TAKAHASHI, M.: Induced magnetic anisotropy of evaporated films, formed in a magnetic field (J. A. P. **33** (Mar. 1962) 1101–1106).
142. TANAGUCHI, S.: A theory of the uniaxial anisotropy induced by magnetic annealing in ferrites (Sci. Rep. Res. Inst. Tohoku Univ. **A9** (1957) 196–214).
143. TARASOV, L. P. and BITTNER, F.: Precise magnetic torque measurements on single crystals of iron (Phys. Rev. **52** (1937) 353).
143a VAN KEMPEN, H., KOHLHASS, R. and LANGE, H.: Über die Sättigungsmagnetostriktion von Eisen-Silizium-Einkristallen mit, 4·4 Gew. Proz. Si zwischen Raumtemperatur und Curie-Punkt (Z. Naturf. **21a** (9) (1966) 1512–1513).
144. VOGT, E.: Metamagnetismus (Z. ang. Phys. **14** (4) (1962) 177–182).
145. WALTER, J. L., HIBBARD, W. R., FIEDLER, H. C., GRENOBLE, H. E., PRY, R. H. and FRISCH-

MANN, P. G.: Magnetic properties of cube textured silicon-iron magnetic sheet (J. A. P. **29** (1958) 363–365).

146. WEBSTER, W. L.: Magneto-striction in iron crystals (Proc. Roy. Soc. (A) **109** (Dec. 1925) 570–584.
147. WENT, J. J., RATHENAU, G. W., GORTER, E. W. and VAN OOSTERHOUT, G. W.: Ferroxdure, eine Gruppe neuer Werkstoffe für Dauermagnete. (Phil. T. Rdsch. **13** (1952) 361–376).
147a WEIS, A.: Das Magnetvariometer (Funk u. Ton **4** (1950) 508–518, 559–568).
148. WEISZ, R. S.: Magnetic anisotropy constants of ferromagnetic spinels (Phys. Rev. **96** (1954) 800–801).
149. WIJN, H. P. J.: Magnetic relaxation and resonance phenomena in ferrites. Dissertation, Leiden (1953).
150. WIJN, H. P. J., VAN DER HELDE, H. and FAST, J. F.: Ordering in cobalt-ferrous ferrites (Proc. IEE **104 B** (1957) 412–417).
151. WILD, G. and PERRIER, A.: Methode d'étude et lois du vieillissement et du rajeunissement magnétiques de fers employés dans la technique téléphonique (T. Mitt. Schweiz. Tel. u. Tel. Verw. **3** (1925) 189–196).
152. WILDE, H.: Untersuchung der magnetischen Nachwirkung an handelsüblichen Silizium- und Nickel-Eisenblechen (Frequenz **3** (11) (1949) 309–319, 348–353).
153. WILDE, H.: Messungen über die reversible Permeabilität und ihre theoretische Deutung (Z. ang. Phys. **7** (11) (1955) 509–513).
154. WILLIAMS, H. J.: Some uses of the torque magnetometer (Rev. Sci. Instr. (Feb. 1937) 56).
155. WILLIAMS, H. J., SHOCKLEY, W. and KITTEL, C.: Studies of the propagation velocity of a ferromagnetic domain boundary (Phys. Rev. **80** (Dec. 1950) 1090–1094).
156. WÜRSCHMIDT, J.: Die Entmagnetisierungsfaktoren kreiszylindrischer Stäbe (Z. Phys. **19** (1923) 388–397).
157. WÜRSCHMIDT, J.: Theorie des Entmagnetisierungsfaktors und der Scherung von Magnetisierungskurven. Vieweg (1925).
158. VELANDER, E.: Über die Korrektionen bei magnetischen Messungen an ringförmigen Probestücken (Elektrot. u. Maschb. **34** (1916) 5–8).
159. VAN VLECK, J. H.: Fundamental theory of ferro- and ferri-magnetism (Proc. IRE **44** (10) (Oct. 1956) 1248–1258).
160. YAGER, W. A., GALT, J. K., MERRITT, F. R. and WOOD, E. A.: Ferromagnetic resonance in nickel ferrite (Phys. Rev. **80** (4) (Nov. 1950) 744–748).
161. ZEHLER, V.: Untersuchungen zur Rotationshysterese (Z. ang. Phys. **13** (1961) 139–141).

# 4

# The magnetising process and the basis of the hysteresis loop

## 4.1 THE ORIGIN OF MAGNETISM

All materials, i.e. the atoms of all known chemical elements, have the same basic construction: the atomic masses are, in principle, formed from the atomic nucleus; the electrical, chemical, and magnetic properties are determined by the electronic shells which surround the nucleus.

The smallest atom is that of hydrogen. It possesses an electron shell having one electron. In the series of atoms of increasing weight, set out in the Periodic Table, the number of electrons rises in discrete steps, as shown in Table 4.1.

The individual shells are at definite distances from the nucleus. Most of them are divided into subshells and may contain different numbers of electrons. The innermost shell is filled when it has only 2 electrons, whereas the next can hold 8, and the one beyond 18. It is customary to label these shells, from the centre outwards, with the letters K, L, M, N, and so forth, and to use s, p, d, and f to distinguish the subdivisions. As the number of electrons in the shells increases, the mass and the charge of the nucleus also increase. The following important fact, among others, emerges from Table 4.1, namely that electrons may appear in certain outer shells before all the inner shells are complete. This is the case for elements 19–28, for example, for which the 3d shell is incomplete although electrons exist in the 4s shell.

This is the first important feature of elements 26, 27, and 28, i.e. the ferromagnetic substances (iron, cobalt, and nickel). This, however, is not a sufficient criterion on which to found ferromagnetism. There is a further point to consider.

It is well known that the electrons in the shells of the various atoms are capable of two types of movement: they orbit around the nucleus, and they spin on their own axes. Both movements give rise to magnetic moments which are the respective causes of diamagnetism and paramagnetism.

Rotation about the axis is called spin. Spin may be either positive or negative. In filled shells, the number of positive and negative spins is the same, so the spin moments cancel each other out. It is just here that iron, cobalt, and nickel show this second peculiarity: the spin moments in the 3d shells of those elements are not compensated.

**Table 4.1** ELECTRON SHELLS OF ATOMS 1–36

| *Z* | *Element* | K | L | | M | | | N | | | |
|---|---|---|---|---|---|---|---|---|---|---|---|
| | | 1s | 2s | 2p | 3s | 3p | 3d | 4s | 4p | 4d | 4f |
| 1 | H | 1 | | | | | | | | | |
| 2 | He | 2 | | | | | | | | | |
| 3 | Li | 2 | 1 | | | | | | | | |
| 4 | Be | 2 | 2 | | | | | | | | |
| 5 | B | 2 | 2 | 1 | | | | | | | |
| 6 | C | 2 | 2 | 2 | | | | | | | |
| 7 | N | 2 | 2 | 3 | | | | | | | |
| 8 | O | 2 | 2 | 4 | | | | | | | |
| 9 | F | 2 | 2 | 5 | | | | | | | |
| 10 | Ne | 2 | 2 | 6 | | | | | | | |
| 11 | Na | 2 | 2 | 6 | 1 | | | | | | |
| 12 | Mg | 2 | 2 | 6 | 2 | | | | | | |
| 13 | Al | 2 | 2 | 6 | 2 | 1 | | | | | |
| 14 | Si | 2 | 2 | 6 | 2 | 2 | | | | | |
| 15 | P | 2 | 2 | 6 | 2 | 3 | | | | | |
| 16 | S | 2 | 2 | 6 | 2 | 4 | | | | | |
| 17 | Cl | 2 | 2 | 6 | 2 | 5 | | | | | |
| 18 | Ar | 2 | 2 | 6 | 2 | 6 | | | | | |
| 19 | K | 2 | 2 | 6 | 2 | 6 | | 1 | | | |
| 20 | Ca | 2 | 2 | 6 | 2 | 6 | | 2 | | | |
| 21 | Sc | 2 | 2 | 6 | 2 | 6 | 1 | 2 | | | |
| 22 | Ti | 2 | 2 | 6 | 2 | 6 | 2 | 2 | | | |
| 23 | V | 2 | 2 | 6 | 2 | 6 | 3 | 2 | | | |
| 24 | Cr | 2 | 2 | 6 | 2 | 6 | 5 | 1 | | | |
| 25 | Mn | 2 | 2 | 6 | 2 | 6 | 5 | 2 | | | |
| 26 | Fe | 2 | 2 | 6 | 2 | 6 | 6 | 2 | | | |
| 27 | Co | 2 | 2 | 6 | 2 | 6 | 7 | 2 | | | |
| 28 | Ni | 2 | 2 | 6 | 2 | 6 | 8 | 2 | | | |
| 29 | Cu | 2 | 2 | 6 | 2 | 6 | 10 | 1 | | | |
| 30 | Zn | 2 | 2 | 6 | 2 | 6 | 10 | 2 | | | |
| 31 | Ca | 2 | 2 | 6 | 2 | 6 | 10 | 2 | 1 | | |
| 32 | Ge | 2 | 2 | 6 | 2 | 6 | 10 | 2 | 2 | | |
| 33 | As | 2 | 2 | 6 | 2 | 6 | 10 | 2 | 3 | | |
| 34 | Se | 2 | 2 | 6 | 2 | 6 | 10 | 2 | 4 | | |
| 35 | Br | 2 | 2 | 6 | 2 | 6 | 10 | 2 | 5 | | |
| 36 | Kr | 2 | 2 | 6 | 2 | 6 | 10 | 2 | 6 | | |

To this feature of elements 26, 27, and 28 must be added a third: ferromagnetism can normally appear only in solid crystallised substances. In solid bodies the spin moment dominates. The outer electrons are more or less free and can—in metals, for example—act as conduction electrons (electronic carriers). In crystals there is an interaction between the atoms, or the ions, of the crystal lattice, which can lead to parallel alignment of the electrons. There, is however, a condition for the occurrence of this alignment, namely

that the ratio of the crystal spacing to the radius of the unfilled 3d shell must exceed a minimum value: it must be greater than 3.

Table 4.2, which sets out the characteristic values for elements 25–28, shows that this is uniquely true of the three known ferromagnetic materials. The table is completed by the inclusion of a so-called Heusler's alloy of copper and manganese: manganese by itself does not satisfy the conditions for ferromagnetism. A ferromagnetic alloy results only from the addition of a particular bound component.

**Table 4.2** RATIO OF ATOMIC SEPARATION $D$ TO RADIUS $r$ OF THE UNFILLED 3d SHELL FOR ELEMENTS 25–28, TOGETHER WITH THE CURIE TEMPERATURE[4]

| *Material* | $D$ (nm) | $r$ (nm) | $D/r$ | $T_c$ (°C) |
|---|---|---|---|---|
| Element 25, Mn | 0·252 | 0·0855 | 2·95 | — |
| Element 26, Fe | 0·250 | 0·0790 | 3·26 | 770 |
| Element 27, Co | 0·251 | 0·0690 | 3·64 | 1 120 |
| Element 28, Ni | 0·250 | 0·0635 | 3·94 | 358 |
| Cu–Mn | 0·258 | 0·0720 | 3·58 | 325 |

The forces which align the spins are electrostatic in nature and are known as 'exchange forces'. With rising temperature, thermal agitation works against the ordering effects of the exchange forces, so ferromagnetism disappears above a certain critical temperature. Above this limiting value, the Curie temperature, ferromagnetic materials become paramagnetic. The same holds for ferrimagnetic materials. The third peculiarity of magnetic materials is, therefore, a particular crystal structure.

Thus, for *ferromagnetism* to appear, the following three conditions must be met simultaneously:

1. There must be an unfilled inner electron shell within the atom.
2. There must be uncompensated electronic spins in this unfilled inner shell.
3. The ions of the atoms must form a crystal lattice having a lattice constant at least three times the radius of the unfilled electron shell.

From energy considerations it appears that not all the spins of a ferromagnetic body are spontaneously aligned as a whole but that the alignment spreads over a limited number of spins. Such mutually aligned spin groups are called 'elementary domains', 'Weiss domains', or, simply, 'domains'. Within a domain, the material is magnetised to saturation 'spontaneously', i.e. of itself, without external field (Figure 4.1a). Spontaneous magnetisation is a basic assumption of domain theory.

In a polycrystalline magnetic body the domains are, in general, randomly oriented, so, *in toto*, all lines of flux are (locally) closed and no field is detectable externally. Only by applying a magnetic field are the elementary magnets, which are inclined to the direction of the field, brought into parallel-

ism so as to be capable of forming poles at the free ends of a rod-like specimen.

The magnetism of magnetic oxide materials, *ferrimagnetism*, is also a crystal phenomenon. It occurs for crystals of 'spinel' structure, for example, whose lattice comprises sublattices A and B. The two sublattices are magnetically antiparallel and show markedly different magnetic moments. One may therefore also speak of a non-compensated antiferromagnetism (see Figures 4.1b and 4.1c).

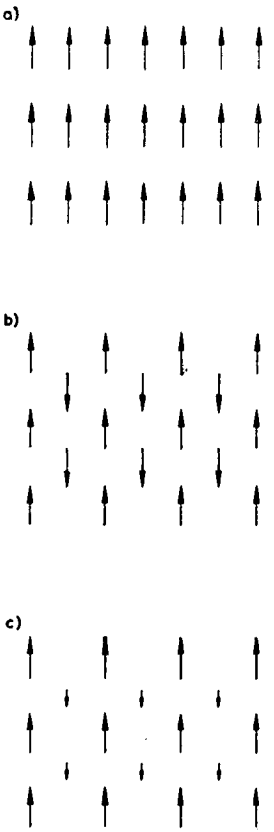



*Figure 4.1. Schematic representation of spin: (a) ferromagnetism; (b) antiferromagnetism; (c) ferrimagnetism*

As with ferromagnetic, so with ferrimagnetic materials there are elementary domains of spontaneous magnetisation and a critical temperature above which the material exhibits paramagnetic properties. Strictly speaking, there is no fundamental difference, from the user's point of view, between ferromagnetic and ferrimagnetic behaviour in, say, a wound core. The differing classifications of metallic and oxide (ceramic) materials relates rather to the cause of the magnetisation and, very importantly, to the different electrical conductivity; also to production techniques and mechanical properties. Both materials behave very similarly under the influence of a magnetic field.

Recent investigations have revealed that amorphous materials, also, may be ferromagnetic; for example, the amorphous alloy $Fe_7Pd_{73}Si_{20}$ is ferro-

magnetic below 28 K[13a]. Preliminary investigation of the magnetic susceptibility of solutions of rare-earth metals in mercury, of gallium and indium in the liquid phase, and also of binary alloys has led to the discovery of ferromagnetism in the eutectic liquid Au–Co[6a].

## 4.2 MAGNETIC DOMAINS

Domain theory enables one to attempt a description of hysteresis and the magnetic processes that determine it. It has been of great service in the development of new magnetic materials. A noteworthy advantage of this theory is that it is both simple and directly demonstrable. References to it in later discussions will be frequent, so its basic points will now be examined.

As already explained in the last section, it is supposed that a magnetic body below its Curie temperature comprises a large number of small domains each spontaneously magnetised to saturation. In general, the magnetic orientations are distributed at random, depending on the microstructure of its crystals. No overall external magnetic effect is discernible in any direction.

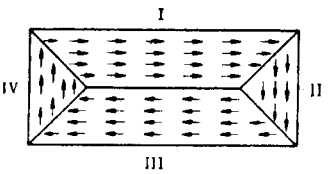



*Figure 4.2. Schematic representation of four contiguous elementary domains*

Each domain consists of a number of atoms whose resultant magnetic moments are mutually parallel. Figure 4.2 shows, schematically, the domains of a ferromagnetic body and their separating boundaries, their spins being so arranged that, overall, the flux paths are closed. In such an arrangement the magnetic energy is at a minimum. According to Williams[38], it is not difficult to trace the basic mechanism.

If it be assumed that the specimen consists of a single domain, then the external flux paths must be closed (Figure 4.3b). If $V$ is the volume of the domain, $J_s$ the saturation polarisation, and $N$ the demagnetising factor, then the magnetostatic energy $E_m$ of the domain takes the value

$$E_{m1} = \tfrac{1}{2}NJ_s^2V \tag{4.1}$$

The amount is significantly reduced if the domain is divided into two opposed magnetic domains (Figure 4.3c) in that $N$ and $V$ thereby become smaller. This leads to the notion of a boundary energy $E_w$ proportional to the boundary area $A$, namely

$$E_w \doteq e_wA \tag{4.2}$$

where $e_w$ is the energy of a unit element of boundary surface and is about 1 erg/cm$^2$.

The energy relations are even more favourable if, as in Figure 4.3d, the outer parts of the body are so shaped as to make it unnecessary for flux

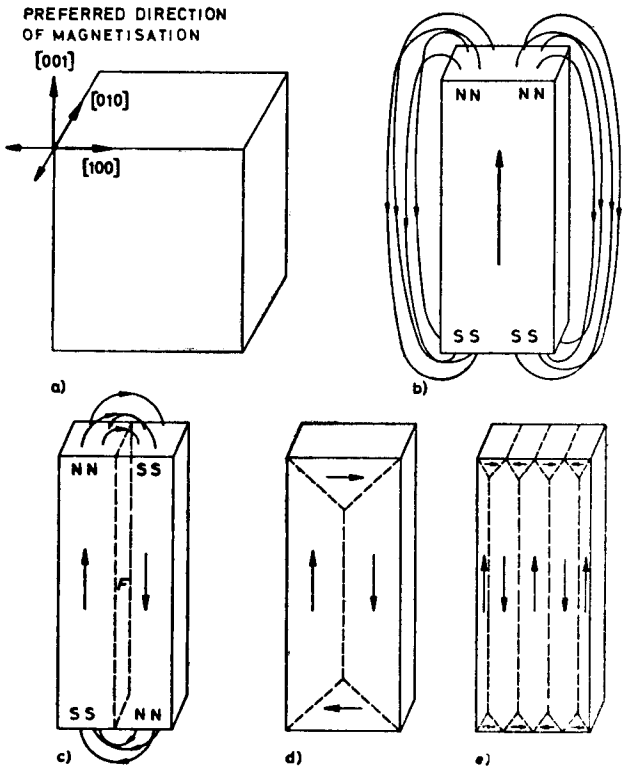



*Figure 4.3. Magnetostatic energy: (a) directions of easiest magnetisability (preferred directions) in a single crystal of* Fe–Si*; (b) creation of poles N and S when overall magnetisation has a unique direction; (c) for two domains the magnetostatic energy is reduced in comparison with (b); (d) closure or transverse domains eliminate the magnetic poles and the magnetostatic energy; (e) with a larger number of domains the total volume of the closure domains is reduced*[38]

to emerge. A still further division into domains increases the energy. Thus, from energy considerations, it can be appreciated that there will be a best configuration in which $E_m = E_w$. The size of the closed domains depends on the crystal energy $K$. In materials with a very large $K$, they are very small and may be entirely absent.

Néel[29] has investigated the possible theoretical partition into domains of a cubic crystal of iron. The result is illustrated in Figure 4.4, taken from his work. A thin and very long strip of rectangular section, and of width $L$, is cut from a single crystal parallel to the cube face (direction [100]). The larger interfaces are labelled S and S′ and the smaller T and T′. The face diagonal [011] lies along the length of the strip, as does the direction of the field $H$. In the single crystal of iron, the three edge directions [100], [010], and [001] are of equal status: [100] lies in the direction perpendicular to the face of the strip, while directions [010] and [001] make an angle of $\pm 45°$ with the length of the specimen. The domains form in such a way that their partitions lie

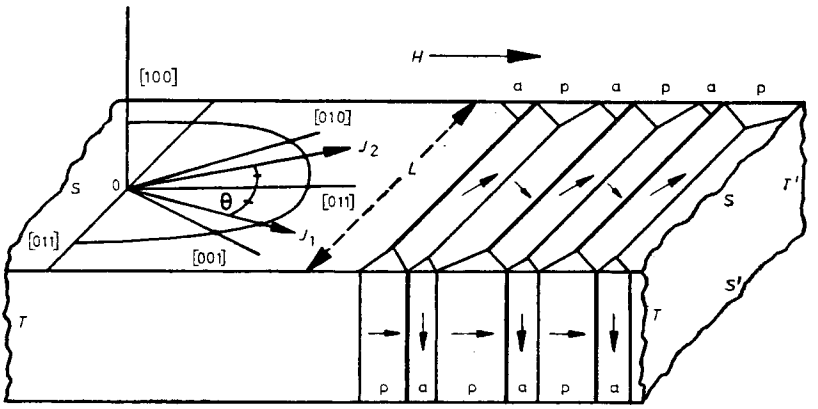



*Figure 4.4. Partition of a single crystal into elementary domains*[29]

perpendicular to the [011] direction and the flux, by and large, can follow the easiest path. There are 'closure domains' at the boundaries T and T'.

If the preferred direction lies slightly inclined to the surface of the specimen, the closure domains may be directly observed and form the so-called fir-tree structure (Figure 4.5—see plate section). In the lower half of the figure, the direction of magnetisation of individual domains is indicated. The figure is taken from a publication by Guillaud[13].

Associated with the closure domains are 'Néel's spikes'. They occur when a domain boundary moves across a dislocation or other crystal irregularity as a result of a change of magnetisation, i.e. when it crosses a hole or a foreign occlusion. It is by means of these peaked transition domains that leakage is avoided. Figure 4.6 shows an example drawn from the observations of

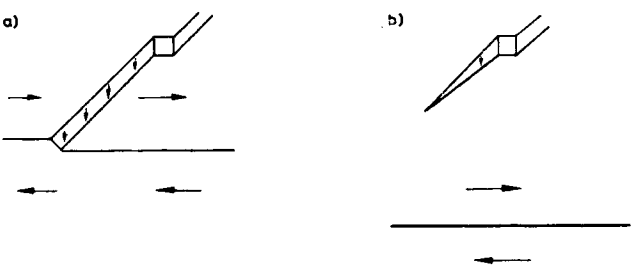



*Figure 4.6. Néel spikes*

Williams[38]. A Bloch wall, or domain boundary, moves from the top downwards across the dislocation and takes with it a transient tubular domain. Beyond a certain distance, the tube disappears but leaves a spike behind.

### 4.2.1 Making the domains visible

The domain boundaries can be rendered visible if a colloidal suspension of finely divided magnetic powder be washed over the polished surface of the sample and the resulting configuration be examined under a microscope. The

dust particles become magnetised by the stray field of the boundaries and collect in the region of this stray field (the 'Bitter process')[7]. The stray fields can also be pin-pointed by the use of a very tiny probe[27].

There are, besides this, two other ways to make the domains visible. One of them uses the magneto-optical Kerr effect. If plane-polarised light falls, normally, on a crystal plane which is perpendicular to the preferred magnetic direction, then the reflected ray is turned through about a quarter of a degree (see page 9). The direction of rotation is positive or negative according to the direction of magnetisation at the surface. In general, the domains show up bright, in a compensator, if the direction of magnetisation penetrates into the surface, or dark if it issues from it[24, 25, 41].

By means of the Kerr effect it is possible to investigate certain rapid reactions and also the behaviour of materials at higher temperatures, which cannot readily be done by the previously mentioned procedures. By suitable heat treatment of the carefully polished face, the Kerr effect can be so enhanced that a flawless picture of the domains can be achieved[24]. This is especially valuable for materials of low crystal anisotropy, where the low stray field of the domain boundaries is hardly sufficient to give a Bitter pattern.

The last method involves viewing in an electron microscope with a defocused objective. Here the walls appear light or dark according to the sense of the magnetic field penetrating the film. The method is particularly suitable for investigating thin layers[11].

The latest electron-miscroscope research has shown that the Weiss domains have underlying substructures, though these will not be discussed here[1].

### 4.2.2 Size and shape of domains

The size and shape of an elementary domain depend on many circumstances. In the first place, the properties of the material such as crystal energy and magnetostriction play an important part and, for the rest, such matters as the previous history of the specimen and its internal structure are significant.

When a sample is being magnetised, it can be effectively considered as a single domain if distortions due to crystal imperfections, occlusions, etc., can be avoided. One cannot actually speak of an upper limit of domain size. In a polycrystalline ferromagnet in its ordinary state, the diameter of a domain is, in practice, appreciably less than 1 mm. This is brought out by Figure 4.5 (see plate section), for example.

Whether a minimum domain size exists is not yet entirely certain. Hoffman[15], studying thin iron films down to less than 3 nm, could find no falling off in magnetisation compared with the bulk material, so long as the films were protected against oxidation.

As can be seen from the various pictures and figures, the domain boundaries are mostly straight and rarely curved, a fact that can be deduced from energy considerations. However, there are also occasional exceptions to this rule. Thus, Williams and Goertz[42] established the existence of circular domain boundaries in ring samples of Perminvar (43% Ni, 34% Fe, 23% Co) and noted that these were distributed concentrically throughout the sample.

'Spiral domains' appear in thin films under particular conditions of preparation. They can be found at the tapering end of a Permalloy film if a direct field be superposed during a cyclic magnetising process[12]. Figure 4.7 (see plate section) shows, at the left, a photomicroscopic picture of a sample and, at the right, in schematic form, the corresponding distribution of magnetisation directions.

### 4.2.3 The Bloch wall

What do the boundaries between individual domains look like? They are not to be confused with those grain boundaries which have become familiar through the micrographs of the metallurgists. Two contiguous domains may belong (though not of necessity) to the same crystallographic particle. What distinguishes them is simply the direction of magnetisation. The partition is nevertheless no mathematical fiction but a physical reality, a 'wall' of finite thickness. These walls have become known as Bloch walls, after Bloch who was deeply concerned with domain theory. Bloch was able to prove, in 1932, that magnetisation directions could not pass discontinuously from one domain to the next[3].

Bloch walls appear in single crystals and in polycrystalline bodies; they can run right through the crystal and in certain circumstances cross the grain boundaries. A 'Bloch wall' is the space between neighbouring domains in which the magnetic vectors pass smoothly from the direction appropriate to one domain to that of another. Figure 4.8 indicates in schematic form a so-called 180° wall. The limiting domains to left and right of the indicated Bloch

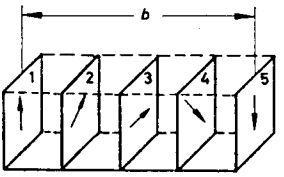



*Figure 4.8. Diagram of a 180° Bloch wall*

wall are magnetised upwards and downwards (1, 5). The Bloch wall between 1 and 5 comprises some 1 000 atoms; in the diagram an arrow represents the direction of magnetisation of each 250th atom. The absolute thickness of a 180° wall is about 200 nm for iron. A 90° wall such as that separating domains I and II and II and III in Figure 4.2 is about half as thick. The wall thickness is not the same for all substances; it depends on crystal structure, crystal anisotropy, stress distribution, chemical purity, and the temperature of the material in question.

In Figure 4.8 seen from end 1, the angular change of the spin is anticlockwise. In principle, it might equally be clockwise. If a particular sense of rotation predominates in the wall there is usually a uniaxial anisotropy. In single crystals with uniaxial anisotropy, cases are known where the rotational direction of the spin changes periodically[33]. In this way Bloch walls are divided into regions separated from each other by 'Bloch lines'. This division minimises the magnetostatic energy in the same way as, for example, the energy of the stray field in thin sheets is reduced by Bloch walls.

## 4.3 THE MAGNETISING PROCESS

### 4.3.1 Bloch-wall displacement

An important property of the Bloch wall is its mobility, which is a measure of magnetisability. The shift of the walls proceeds somewhat as follows. A direct magnetic field $H$ acts parallel to the surface of the wall, as drawn in Figure 4.9. The position of the Bloch wall for $H = 0$ is shown, above, over a breadth $b$, and, underneath, the wall is seen shifted to the left under an $H > 0$.

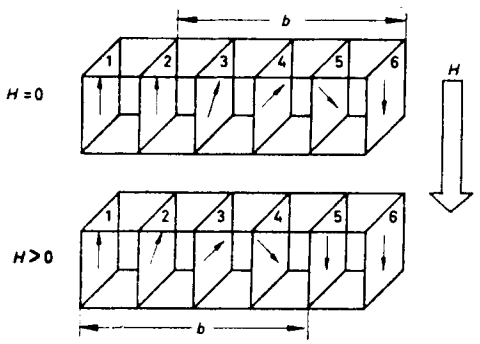



*Figure 4.9. Diagram of Bloch wall drift under the influence of a field H*

Suppose that an external field $H$, acting in the same sense as 6, is just strong enough to turn the vector 5 into the same direction as 6. The moments of 5's left-hand neighbours are then changed in direction by the same amount: 3 exhibits the same direction as did 4, and 2 the same as 3. Thus, *in toto*, the Bloch wall is shifted to the left by a quarter of its width.

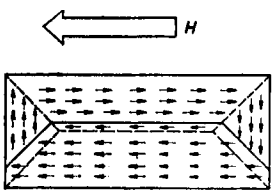



*Figure 4.10. Multidomain drift of Bloch walls*

Reference to Figure 4.2 shows that magnetisation acts on the Bloch walls in much the same way as indicated by Figure 4.10: the initial position is shown dotted and the later position indicated by full lines. Domain 1 was initially magnetised in the direction of the applied external field and increased in size under its influence at the expense of neighbouring domains. Application of a weak alternating field causes the walls to oscillate back and forth, from the positions shown, at the impressed frequency.

In what position, then, does a wall settle if the field is withdrawn: does the wall stay in the place where it finds itself or does it shift back to the starting position? Investigation has shown that both cases occur. For very weak

alternating fields, the walls swing reversibly about a stable position. But should the a.c. amplitude be large, then the Bloch walls pass into the next favourable energy configuration when the impressed force is removed.

### 4.3.2 Bloch-wall energy

The reversible and irreversible movements strongly suggest a comparison on the following lines (Figure 4.11). Imagine a ball rolled along an uneven base. Apart from the gravitational pull, only horizontal forces are assumed to act on it. If the ball is moved from the rest position by only a small amount,

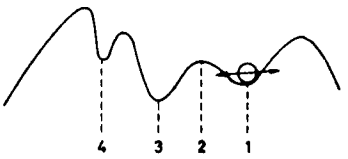



*Figure 4.11. Diagram of energy configuration (explanation in text)*

then on the removal of the disturbing force it falls back into the starting position, which can be designated position 1. If, now, the movement takes it beyond 2, it will find at 3 a new minimum of potential energy. With a still greater disturbance it might find a further point of stability at 4. The peak values of energy or 'energy bumps' of this illustration are, actually, always present in real crystals and can take various forms according to the distribution of impurities, foreign occlusions, dislocations, or mechanical stresses. As the Bloch-wall energy $e_w$ is proportional to the extent of its surface, the wall will always tend to stay in those positions which permit a reduction of this surface. The general order of magnitude of Bloch-wall energy is, say, 1 erg/cm$^2$. Néel[30] has given a basis for its calculation. Nagashima[28] estimates $e_w = 1{\cdot}8$ erg/cm$^2$ as a mean value for anisotropic iron, and $e_w = 0{\cdot}24$ erg/cm$^2$ for an alloy of 50% Fe and 50% Ni. For iron with 3% Si, $e_w$ amounts to 1·52 erg/cm$^2$.

### 4.3.3 The reversible rotation process

Figure 4.10 represents a considerable simplification in that the external field is taken parallel to one of the domains (domain I). Let us now examine this domain under the assumption that the external field acts obliquely with respect to the internal field. If the effect of the boundary domains be left out of account, then, assuming a sufficiently strong field $H$, conditions must be those shown in Figure 4.12. As the field $H$ is withdrawn, the vectors turn once more to the original preferred direction.

### 4.3.4 The irreversible rotation process

If the external field $H$ shown in Figure 4.12 is oppositely directed and if it is sufficiently strong, then the magnetisation vectors must turn through approximately 180°. These vectors will no longer snap back to the old position with

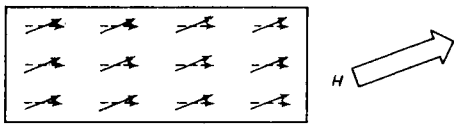



*Figure 4.12. Reversible rotational processes*

the withdrawal of the field since they would have to overcome a higher energy barrier. It is more favourable, from the energy standpoint, for them to settle in the direction opposite to the original position, especially when, as for iron, both directions are equally to be reckoned preferred directions of magnetisation.

A 'flip-flop' process can also take place, as shown by the following schema (Figure 4.13). If the external field is so directed that it has a component opposite to the magnetisation of a domain, then, at a particular field strength

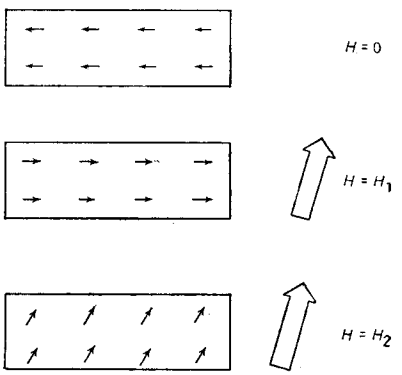



*Figure 4.13. Irreversible rotational processes*

$H$, the magnetisation vectors flip over by about 180°. If the field strength now increases from $H_1$ to $H_2$, the vectors gradually turn to line themselves up with the field direction. The magnetising process thus consists of an irreversible jump and a reversible rotation. Following the removal of the field, the vectors will take the direction opposite to the original. It is these irreversible processes which are responsible for the phenomenon of remanence about which more will be said in Section 4.4.

## 4.4 MAGNETISING PROCESSES AND THE HYSTERESIS LOOP FOR POLYCRYSTALLINE MATERIALS

### 4.4.1 The initial magnetising curve

As the crystals in a polycrystalline material are usually randomly directed, very different forces act on the individual domains as the field activity increases, so the aligning mechanisms dictating the relations of the domains and the external fields, expounded in the previous section, more or less overlap. The sum of all effects produced by the repeated magnetisation and

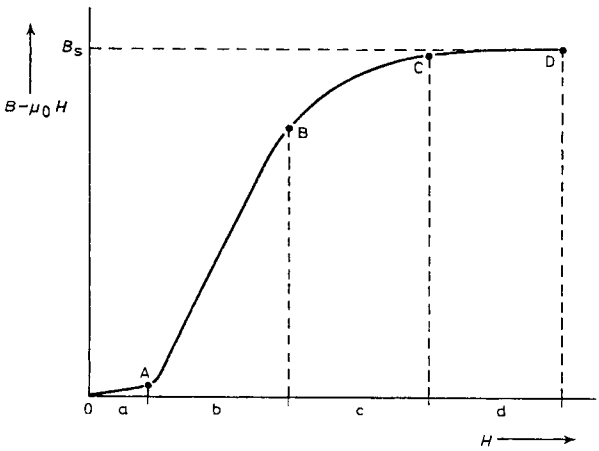



*Figure 4.14. Magnetising curve (virgin curve) (explanation in text)*

demagnetisation of a specimen are brought out in the hysteresis loop. Various regions of the loop may be distinguished.

Starting with field strength $H = 0$, we have $B = 0$. As $H$ increases, $B$ rises slowly at first, passes through a steeper region, and then grows more slowly with rising $H$, finally remaining stationary as the field strength $H$ rises further. If measured values are plotted after the manner of Figure 4.14, i.e. $B-\mu_0 H$ against $H$, then the curve becomes parallel to the $H$ axis at high field strengths i.e. the material is saturated. The following regions of the curve may thus be picked out:

a. Slow increase of flux density from O to A.
b. Steep rise of flux density between A and B.
c. Falling steepness between B and C.
d. Saturation region between C and D.

The four regions of the characteristic can be related to the following basic magnetic processes:

a. Reversible shifts of the Bloch walls.
b. Irreversible shifts of the Bloch walls and irreversible rotation processes.
c. Reversible rotation processes.
d. Saturation.

The transition from one region to another is smooth as long as the number of magnetised domains is large. If, however, the specimen comprises only a few domains, the curve will rise by discrete steps.

These steps can be very easily demonstrated if the hysteresis loop is displayed on an oscillograph and the integrating circuits of the device are switched out, i.e. if the curve displayed is the derivative of the hysteresis loop.

Instead of the continuous curve of Figure 4.15a, one branch of the curve may look like Figure 4.15b, for example.

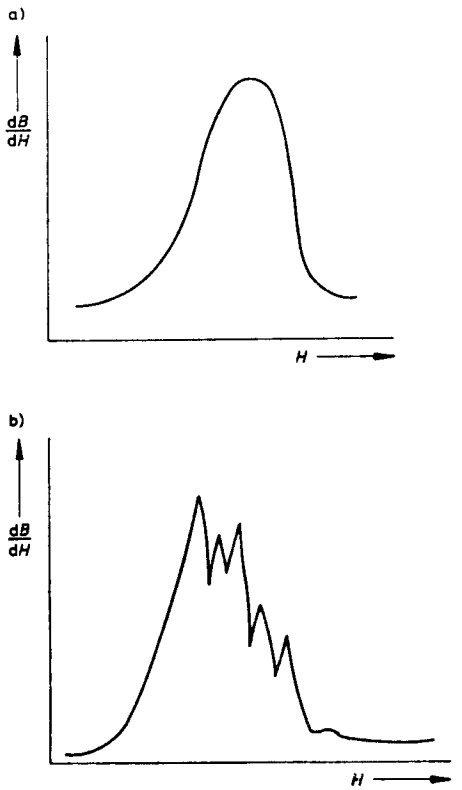



*Figure 4.15. Branch of a hysteresis loop differentiated: (a) in a specimen comprising many domains; (b) in a specimen having few domains (schematic presentation)*

### 4.4.2 The limiting loop

If, from the saturated condition of the specimen, one proceeds to reduce the magnetising field to vanishing point, then the $B$ value falls not along the initial magnetisation curve but much more slowly. For $H = 0$, $B$ still retains a positive value, namely the remanence (Figure 4.16).

If the negative field strength is increased to saturation, the negative flux density reaches saturation. The curve closes on itself if $H$ is again brought to zero and then raised to the positive saturation value. At each further repetition of this cycle, the curve always follows the same path. It is only possible to get back to the initial magnetisation curve if the specimen is demagnetised —as by heating it above the Curie temperature.

In the limiting loop, also named the major loop, only regions b, c, and d of the magnetisation curve are found. The 'a' region does not appear. The reversible low-field-strength wall shifts thus fail to appear under these conditions.

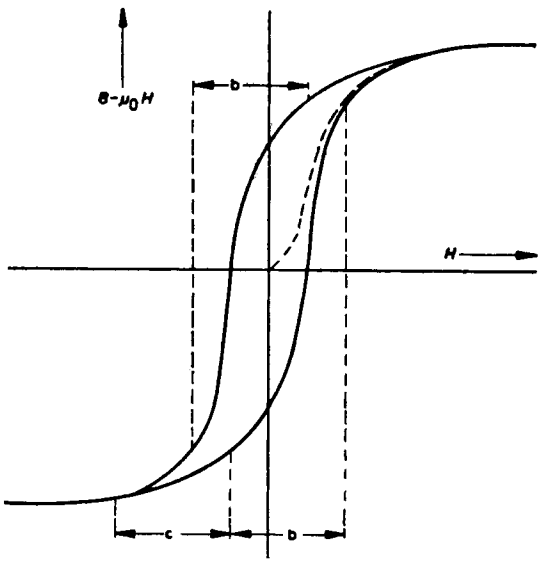



*Figure 4.16. Limiting (or major) hysteresis loop*

### 4.4.3 The hysteresis family

Apart from the major loop, an infinitely large number of inner, or minor, loops exist. If a sample is taken along the magnetising curve to any chosen $H$–$B$ value and the field then reduced so as to start a new magnetising cycle from this point as peak, a smaller hysteresis loop is obtained more or less similar to the limiting loop. The curves depart more and more from the usual S shape the lower the peak $H_m$. The set of loops derived from various peak points on the magnetisation curve is referred to as the hysteresis family (see Figures 4.17–4.19).

The characteristic values belonging to the inner loops which correspond to the remanence and coercivity of the extreme loop are called 'apparent remanence' and 'apparent coercivity'.

### 4.4.4 The ideal magnetising curve

For the exposition of basic magnetic processes it is convenient to use, in many cases, a hysteresis-free curve called, following Steinhaus and Gumlich[34], the 'ideal magnetising curve'.

The ideal curve can be obtained by superposing on the static field an alternating component which, to begin with, is greater than the static field but subsequently falls continuously to zero. Each value of the static field yields one point on the ideal curve.

Figure 4.20 shows, besides the hysteresis loop and the magnetisation curve, the ideal magnetisation curve (shown broken) for a soft steel with 0·6% C.

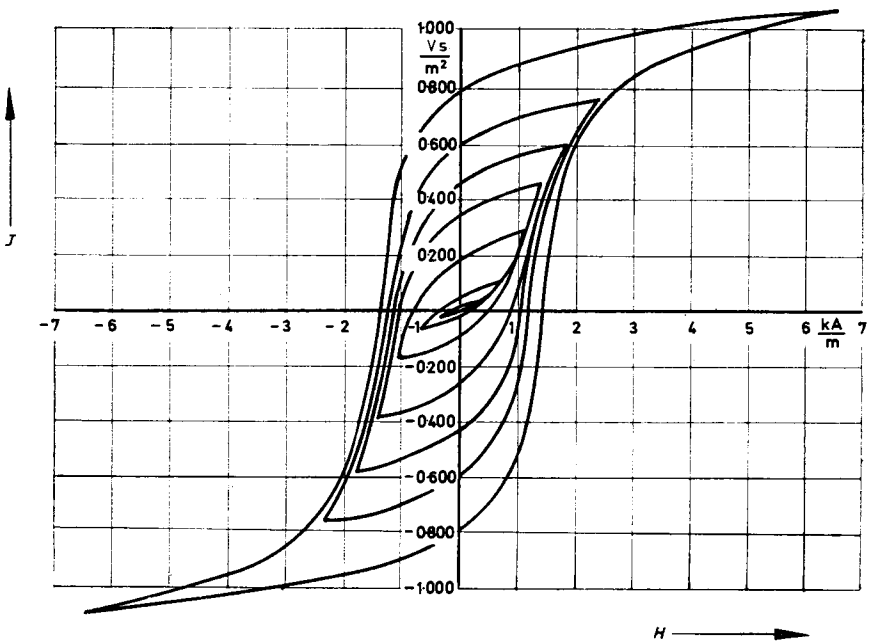



*Figure 4.17. Family of hysteresis loops for piano wire*[8]

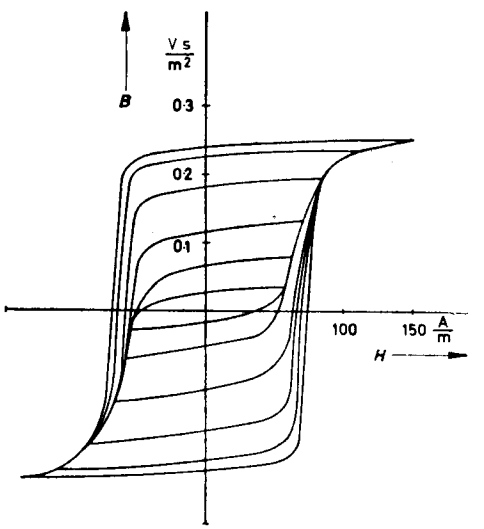



*Figure 4.18. Family of hysteresis loops for a* Mn–Mg *rectangular ferrite*[14]

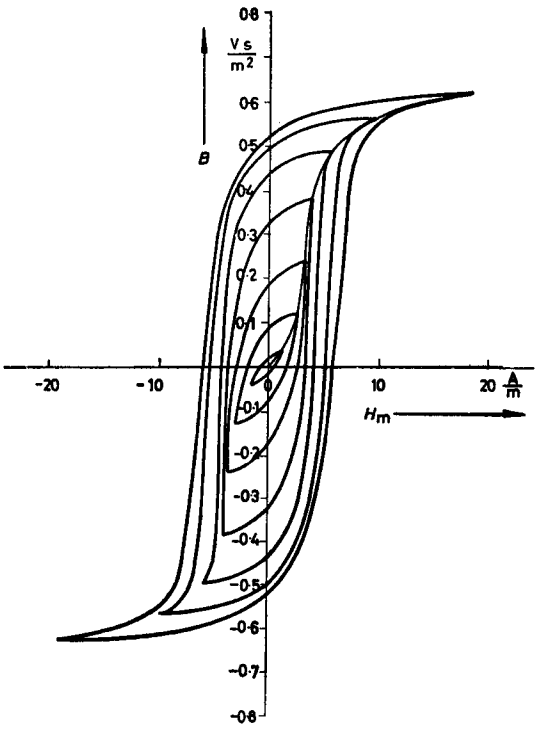



*Figure 4.19. Family of hysteresis loops for 4-79 Permalloy at 60* Hz[20]

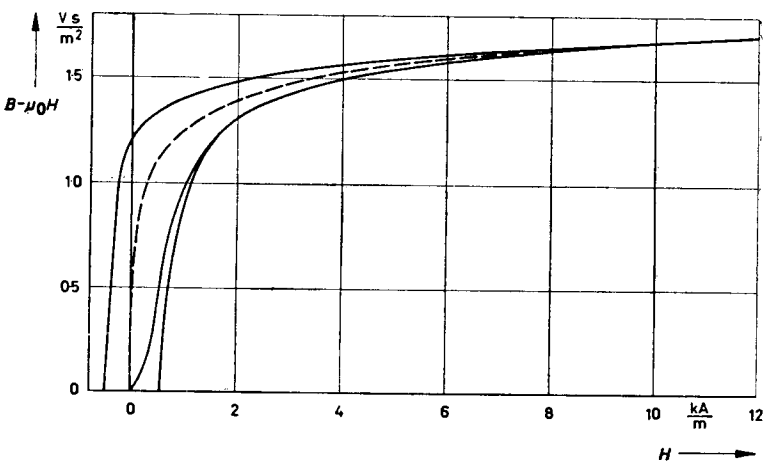



*Figure 4.20. Hysteresis loop and magnetising curve (solid line) together with the ideal magnetising curve (broken line) for a soft steel having 0·6%* C[34]

It is characteristic of the ideal curve that it lies above the magnetising curve and, more particularly, that it rises very steeply from the origin; further that the 'ideal' initial permeability is very high. Kornetzki and Röss[22, 23] were able to show, however, that it is not infinite.

The ideal curve is further differentiated from the magnetisation curve in that it can be traversed in both directions without hysteresis delay, whereas the magnetisation curve is only obtained with rising field strength.

## 4.5 MAGNETISING PROCESSES IN SINGLE CRYSTALS

The ordinary hysteresis loop is met with only in polycrystalline materials. Measurements performed on single crystals present another picture.

Necessary, as it obviously was, to investigate single crystals, this could only be carried out when it became possible to grow sufficiently large and sufficiently perfect crystals. Only in 1924 did it become feasible to grow iron crystals, for example, although nickel and cobalt crystals are easier to produce and were thus investigated earlier. Natural single magnetite crystals, already known at the turn of the century, were the subject of many investigations; but iron is the most important technical element magnetically, and so results obtained from the study of this substance were of the greatest significance for further development. It was knowledge gained about the directionality of magnetic properties in a single crystal that made it possible to manipulate polycrystalline materials towards a more monocrystalline type of performance.

Two ways of studying magnetic mechanisms in single crystals are known. Small rod-shaped fragments may be cut from the crystal in the desired direction. Dimensions are chosen which enable a good estimate of the demagnetising factor to be made; for this purpose, ellipsoidal or spherical samples are more suitable than cylindrical ones, but such measurements are somewhat uncertain, particularly at low field intensities.

An elegant method, which avoids the demagnetising factor, was devised by Williams[39]. He cut 'picture frames' from large crystals, their sides lying in the required principal directions (Figure 4.21). The influence of direction of magnetisation in various types of crystals can be studied accurately by measuring the ideal magnetising curve for these tiny frames.

### 4.5.1 The iron single crystal

If the ideal magnetisation curve is measured for iron, it is found that the [100], the [010], or the [001] direction is the easiest and the cube diagonal [111] the hardest to magnetise. This was shown in 1925 by Honda and Kaya[16] when investigating ellipsoids at field strengths up to 80 kA/m (Figure 4.22). The order of easy magnetisation [100], [110], [111] holds up to about 32 kA/m. Above this intensity, [111] is easier to magnetise than [110]. This reversal of order is allied to the change in sign of magnetostriction in the [110] direction (see Figure 2.2).

The crystal energy can be calculated from consideration of the closed

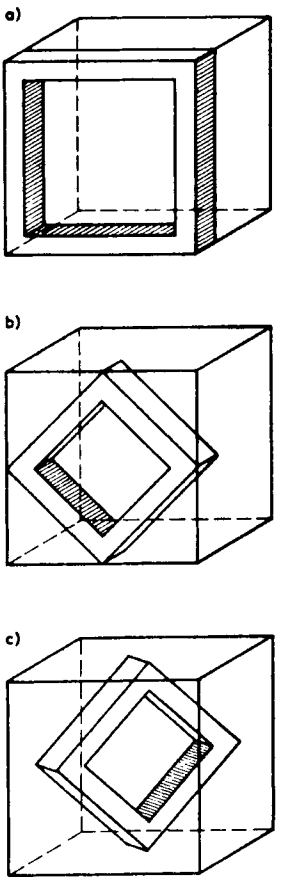



*Figure 4.21. Picture-frame cut from a cubic crystal: (a) sides parallel to [100]; (b) sides parallel to [110]; (c) sides parallel to [111]*

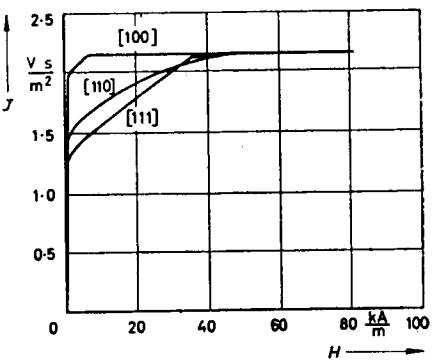



*Figure 4.22. Magnetising curves for a single crystal of iron measured in the (110) plane*[16]

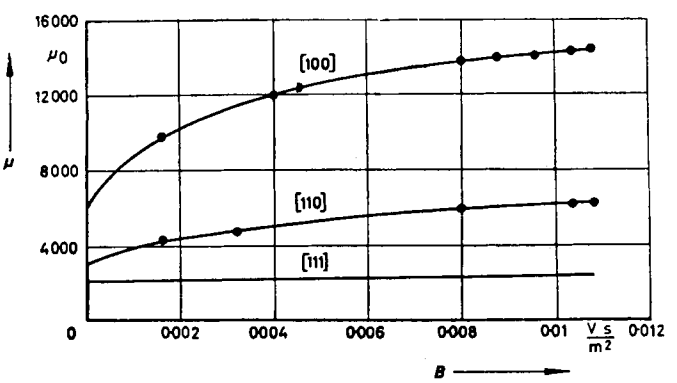



*Figure 4.23. Permeability of a single crystal of* Fe–Si *having 3·85%* Si *as a function of the direction of magnetisation*[39]

surfaces determined by the magnetisation characteristics appropriate to various measuring directions (see page 88).

For single crystals of iron containing silicon the directionality remains practically the same. Williams' picture-frame measurements[39] for single-crystals of iron containing 3·85% Si clearly show the relation between initial permeability and direction of measurement and also between rate of rise of permeability with flux density (Figure 4.23). The initial permeabilities, as might be expected on theoretical grounds, are in the ratios 6 : 3 : 2.

It follows from the anisotropy of the initial permeability that the Weiss domains in an iron crystal are not randomly oriented but tend towards a preferred direction parallel to the crystal edge.

### 4.5.2 The nickel single crystal

Single crystals of nickel also show different magnetisability in the three principal directions, but, as against iron, the sequence is reversed: the crystal can be most easily magnetised along the cube diagonal [111] and least easily in the edge direction [100] (Figure 4.24)[19]. This involves a change of the sign of crystal anisotropy. A value of $-5\times10^4$ erg/cm³ is usually taken for $K_1$ and a value of $+5\times10^4$ erg/cm³ for $K_2$ (see also Table 3.11).

Investigations of permeability as a function of flux density $B$ show that a similar relation holds as for iron. There is, however, no anisotropy of initial permeability (Figure 4.25), as it only makes its appearance at high field intensities[4].

The most technically important of the Ni–Fe alloys are those with more than 30% Ni. Among these 'reversible' alloys (see Section 13.4.6) those with 70–80% Ni are outstanding by reason of their unusually high permeability values. This is the region, as Figure 4.26 demonstrates, where a change of sign occurs in crystal anisotropy and in magnetostriction[5]. The exact location

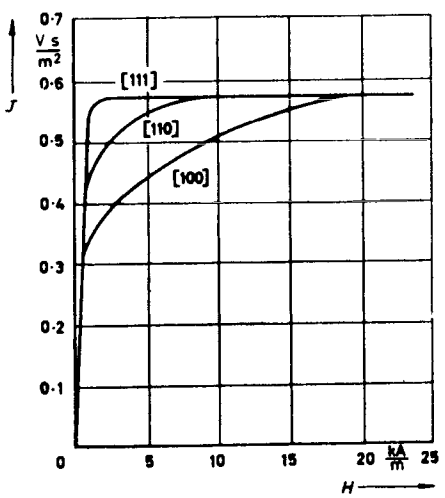



*Figure 4.24. Magnetisation curve for a single crystal of nickel in the (110) plane*[19]

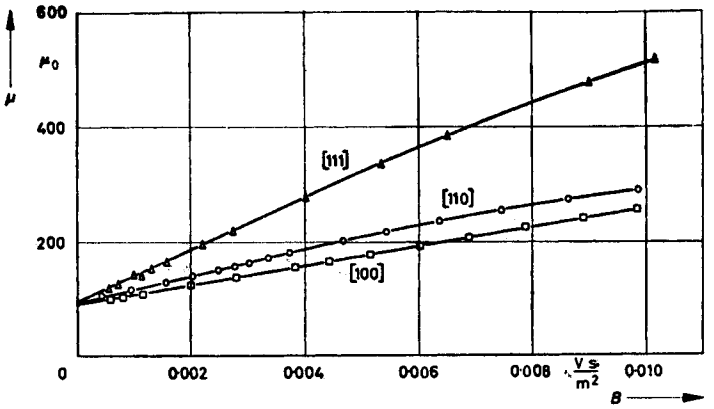



*Figure 4.25. Permeability of a single crystal of nickel*[4]

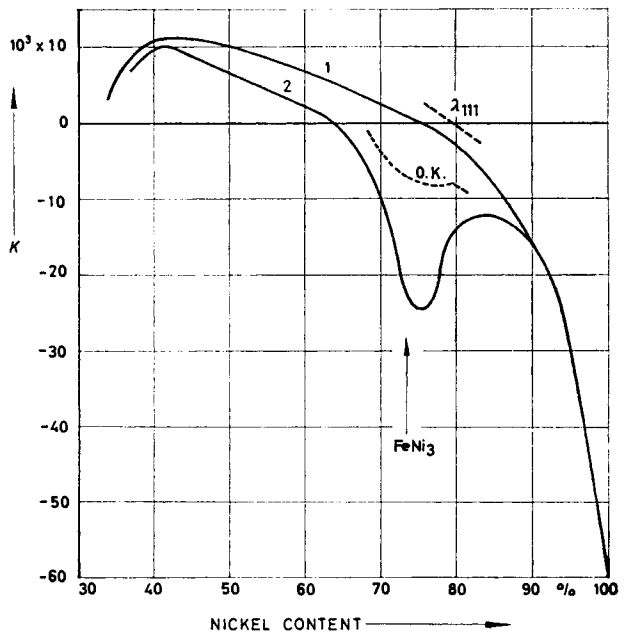



*Figure 4.26. Constants of magnetic anisotropy for reversible* Fe–Ni *alloys: 1, quenched; 2, cooled slowly (aligned); cooling rates in the range 600°–300°C were about* $10^5$ K/h *and* 2·5 K/h *respectively;* $\lambda_{111}$ *shows the composition for which this quantity passes through zero; curve O.K. sets out the results obtained at* 55 K/h[5]

**Table 4.3** ANISOTROPIC CONSTANTS $K_1$ AND $K_2$ OF SOME Fe–Ni ALLOYS AT VARIOUS TEMPERATURES[21]

| *Nickel content* (%) | *Temperature* (°C) | $K_1$ (erg/cm³) | $K_2$ (erg/cm³) |
|---|---|---|---|
| 50 | 14 | 33 200 | −183 000 |
| | 150 | 27 600 | −108 000 |
| | 300 | 18 400 | − 68 000 |
| 65 | 14 | 14 400 | − 70 000 |
| | 150 | 12 800 | − 48 000 |
| | 298 | 9 600 | − 32 000 |
| | 490 | 4 800 | − 11 000 |
| 70 | 14 | 6 800 | − 15 000 |
| | 150 | 2 400 | − 5 000 |
| | 300 | 0 | 0 |
| | 454 | 0 | 0 |
| 90 | 14 | −7 200 | − 24 000 |
| | 150 | −3 200 | − 12 000 |
| | 300 | 0 | − 8 000 |

of the zero crossing depends on the internal ordering of the alloy, which is affected by heat treatment[40].

According to investigations by Kleis[21], a change of ferromagnetic anisotropy occurs at an iron content of some 24%; with less iron the order of magnetisability 'easy, harder, hardest', is, as with nickel, [111], [110], [100], but with higher iron content becomes [100], [111], [110]. According to Bozorth[4a], Permalloy with 78·5% Ni is most easily magnetised in the [111] direction and an alloy with 45% Ni has its preferred direction parallel to the cube edge [100]. Table 4.3 gives the anisotropic constants $K_1$ and $K_2$ as functions of temperature for various Fe–Ni alloys.

### 4.5.3 The cobalt single crystal

The principal axis of the hexagonal cobalt crystal [0001] is, at the same time, the direction of easiest magnetisability, while magnetisation is harder in the perpendicular axis (Figure 4.27). It is also appreciably harder than the hardest direction for iron and nickel: saturation is reached as early as 20 kA/m, in nickel; in iron the saturation field strength is about 64 kA/m; but in cobalt it is 800 kA/m.

The enclosed area of the two curves for [0001] and [10$\bar{1}$0] is correspondingly large, giving the following pair of values for the anisotropy:

$$K_1 = 3{\cdot}98 \times 10^6 \text{ erg/cm}^3$$

$$K_2 = 1{\cdot}98 \times 10^6 \text{ erg/cm}^3$$

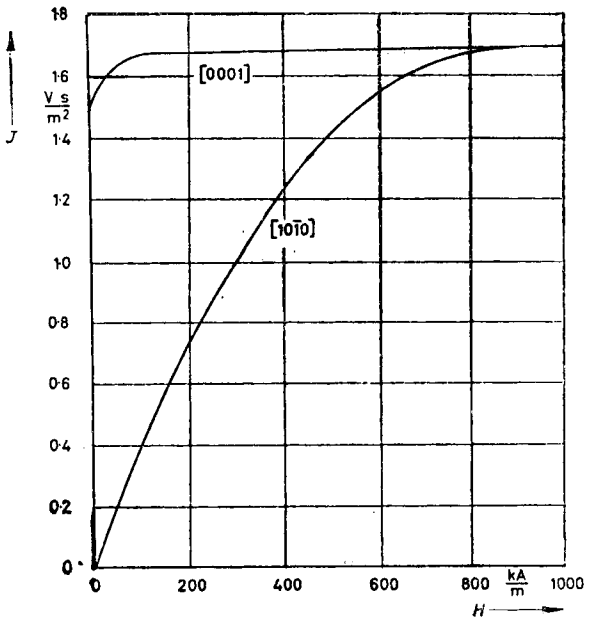



*Figure 4.27. Magnetisation curve for a crystal of cobalt*[2]

The elementary magnets of the cobalt crystal are almost wholly oriented along the principal axis. Rotational processes are involved in magnetisation in the direction normal to this and, when the field is switched off, there is an almost completely reversible return to the starting configuration. The remanence is therefore very little above zero[20]. The initial permeability of polycrystalline cobalt amounts to about $12\mu_0$ and the maximum permeability to about $20\mu_0$[8a].

### 4.5.4 Ferrite single crystals

The anisotropic constant $K_1$ is negative for most cubic ferrites, while $K_2$ plays a subordinate role, so the cubic diagonal is the direction of easiest magnetisability. Cobalt ferrite is exceptional to this extent, in that $K_1$ is positive and exceeds the value for other ferrites by an order of magnitude. Because of positive $K_1$ values, a preferred magnetic direction occurs along [100].

For magnetite ($FeO \cdot Fe_2O_3$), the direction of easiest magnetisability depends on the temperature: $K_1$ is positive at $-143°C$; between $-143°C$ and $-160°C$ magnetite behaves like iron, i.e. [100] is the preferred direction. As the temperature falls still further, the anisotropic constant $K_1$ increases once more in the positive direction. The permeability passes through a maximum at $-143°C$[2]. If a few percent of cobalt is added to the magnetite crystal during its preparation, the transition temperature is shifted towards higher values. By the addition of some 5% Co to manganese ferrite crystal, one can cause the anisotropy practically to vanish[36].

## 4.6 MICROMAGNETICS

At the beginning of this chapter the magnetic properties of individual atoms were considered. The exposition then passed to Weiss domains, which involve a great number of atoms.

The intermediate region involving just a few atoms was, in the first instance, passed over. However, in recent times this range has become much more important by reason of the introduction of thin films and finer powders. Different laws apply to magnetic bodies which, in one or more coordinates, have sizes comparable with the wall thickness from those applying to the larger samples hitherto examined almost exclusively. Brown[6] has coined the expression micromagnetics for the range of ultrafine particles; this notion has already proved valuable, and certain definite concepts have emerged from it. In particular, this way of looking at the problem has been very successful in the theory of permanent magnets.

Micromagnetics is concerned with magnetic particles whose dimensions lie in the same order of magnitude as the thickness of the Bloch walls. Classical energy considerations[10] are, without exception, based on the hypothesis that a condition of minimum energy is assumed by any magnetised body. The latest views are, however, refinements of this in two respects: in the first place an attempt is made to explore all circumstances in which local energy minima exist, and in the second place to define the conditions in which energies may enter higher levels and to find what determines when they will not. The problem thus consists in exploring all possibilities of small departures from uniform magnetisation.

A comparison with mechanical elasticity may serve to clarify what kind of processes are involved. In Figure 4.28 at the upper left (1a) a straight bar

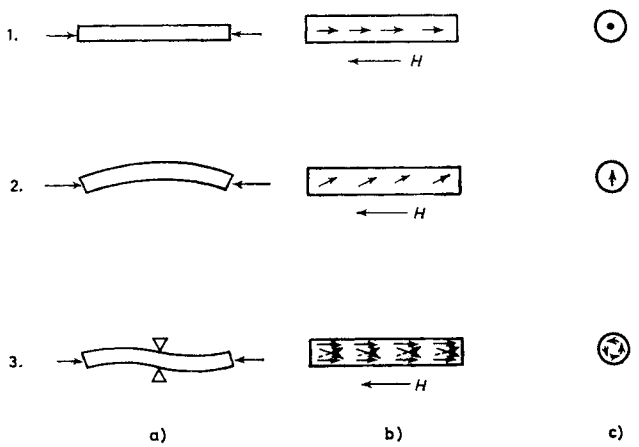



*Figure 4.28. (a) Characteristic values of the compressive force and corresponding transverse deflection, in the theory of the elastic stability of a strut; (b) characteristic values of the applied field, and corresponding transverse deviations from uniform magnetisation, in the theory of magnetic stability of a cylinder; (c) transverse component of magnetisation shown in an end-on view. From top to bottom: no deviation; rotation in unison; magnetic curling*[6]

is shown corresponding to a single domain that is to be magnetised in the axial direction (1b). No magnetic component acts at right angles to the axis of the bar, as indicated in the end-view (1c). If now the bar be compressed in the axial direction, then it will bend in various ways as soon as a certain critical stress is exceeded.

In the magnetic case the opposing external field corresponds to the compressional stress. Under its influence the magnetising vectors are turned, as a whole, so that a transverse component is introduced relative to the direction of rotation (case 2).

In this coherent rotation no work is done against the exchange forces of neighbouring atoms but only against the crystal energy and the demagnetising field. The characteristic field for this type of magnetisation does not depend on the size of the sample. The sample under pressure, however, can also bend in the manner illustrated in 3a. Translating this case into its magnetic analogue gives a circuital component of magnetisation, so one speaks of 'curling' magnetisation. The vectors of the elementary magnets form a closed flux running spirally round the surface of the diminutive bar without the possibility of any poles arising from the transverse component. Thus, no work needs to be expended against the demagnetising field. However, the external field has to overcome the exchange forces of nearby atoms and, also, the anisotropic forces. The intensity needed falls with increasing cross-section of the bar. Therefore, curling magnetisation will tend to dominate in large samples and coherent rotation in small ones. Research has shown, nevertheless, that coherent rotation cannot always take place in the very smallest particles: smaller coercive forces have usually been measured than would be expected from the theory.

In elongated particles there is a possible type of magnetisation which corresponds more closely to arching of the bar shown in Figure 4.28 (3b): this is called buckling[9]. In an infinitely long thin bar, the direction of the magnetisation vectors alternates sinusoidally along the length of the bar (Figure 4.29a).

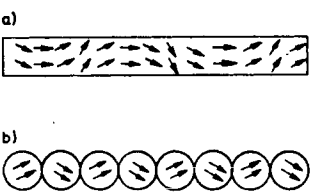



*Figure 4.29. Model of magnetisation reversal: (a) buckling magnetisation; (b) fan magnetisation*[18]

Even earlier, Jacobs and Bean[18] had proposed a different model which sought to explain why, in general, the coercivity in fine powders was found, experimentally, to be less than would be expected from the notion of coherent rotation: they discussed the chain of spheres model. According to this, the magnetising vectors become fanned out (Figure 4.29b) causing a lowering of coercivity. Thus, for cyclic magnetisation of very small particles there are four possible mechanisms to discuss:

1. Coherent rotation of the magnetisation vectors.
2. Curling magnetisation.

3. Buckling magnetisation.
4. Fanning out.

Which of these mechanisms operates at any given time depends on the anisotropic properties and on the dimensions of the particle. The details of these theories and the appropriate limiting conditions will not be further developed here, especially as the matter is still in a state of flux.

## 4.7 MAGNETISATION OF THIN FILMS

By 'thin films' is to be understood solid layers mostly less than 200 nm in thickness. They can be deposited by evaporation *in vacuo* onto a suitable substrate, precipitated electrolytically, or sputtered, and they may be formed from pure metals or, equally, from alloys. Films can be made uniform by taking the necessary care, and they offer excellent opportunities for observing elementary domains and their interfaces. They have a practical part to play in the making of magnetic stores (see page 623).

### 4.7.1 The Néel wall

Imagine that a magnetic sample is so thin that the Weiss domains penetrate the whole cross-section (Figure 4.30). The same holds true of the Bloch wall, which introduces a polarisation on the surface of the strip. In the Bloch wall it is known that the magnetisation vectors rotate in the plane of the wall (Figure 4.8).

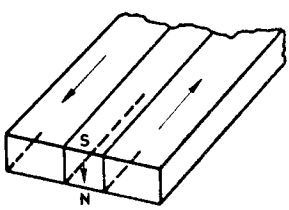



*Figure 4.30. Schematic representation of magnetisation in a thin sheet*

This kind of interface, however, is not optimum, from an energy standpoint, in extremely thin films. Néel[31] was able to prove by calculation that, as the thickness of the film falls, the Bloch-wall energy rises and the wall thickness lessens. The wall energy per square centimeter thus tends to a maximum. At a certain critical wall thickness another kind of wall forms whereby the spin directions rotate in the plane of the film. These are called Néel walls. Permalloy films having a composition 80% Ni–20% Fe and subjected to heat treatment in a magnetic field, or vacuum evaporated in a direct field, develop uniaxial anisotropy, i.e. a preferred magnetic direction parallel and antiparallel to the applied field. They behave like single crystals with only one anisotropic axis. In thin films of this high-permeability alloy, the formation of a 180° Bloch wall would be more unfavourable, with regard to energy, than the rotation of the spin vectors in the plane of the film. In this case,

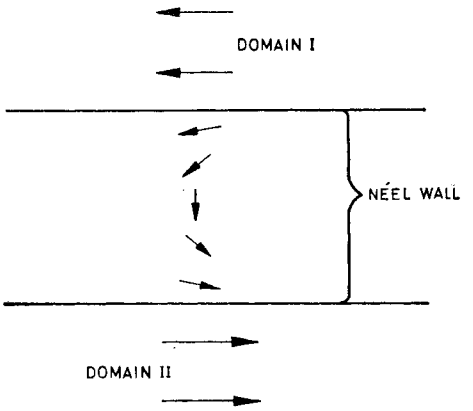



*Figure 4.31. Schematic representation of a Néel wall*

therefore, the free poles of the wall do not lie in the surface but within the material. Figure 4.31 shows, schematically, a 180° Néel wall on the surface of a Permalloy film.

Néel walls, like Bloch walls, can be rendered visible by means of a colloidal suspension of magnetic particles. They act as closure domains over the walls and are, therefore, held fast by them.

### 4.7.2 Crosstie walls

In the thickness range 20–100 nm for lightly anisotropic films, a peculiar wall configuration can arise, as was discovered in 1958[17]. Such configurations were called barbed-wire patterns and are characterised by short crosstie walls giving to interfaces their typical appearance. Figure 4.32 (see plate section) shows a typical photograph of this phenomenon for a Ni–Fe film 80 nm thick, following Methfessel, Middelhoek, and Thomas[26].

In order to elucidate how this comes about, Figure 4.33 shows, schematically, the directions of magnetisation within a 180° wall and in its immediate neighbourhood. Figure 4.33a illustrates how the wall between domains I and II must be polarised to achieve minimum energy. Flux lines which alternately leave and penetrate the plane of the film are called Bloch lines. Those lines of flux which turn, perpendicularly to the Bloch lines, in the plane of the sheet also alternate in direction. In those domains of Figure 4.33a shown dashed there exists in this way a high energy density. Figure 4.33b shows a more favourable configuration of energy such as in fact occurs in Nature: in a region where the lines of flux are highly curved, crosstie walls are formed.

The occurrence of a crosstie wall, therefore, always indicates the presence of a Bloch line which is normal to the plane of the film and which joins up with a neighbouring Bloch line in the intervening space.

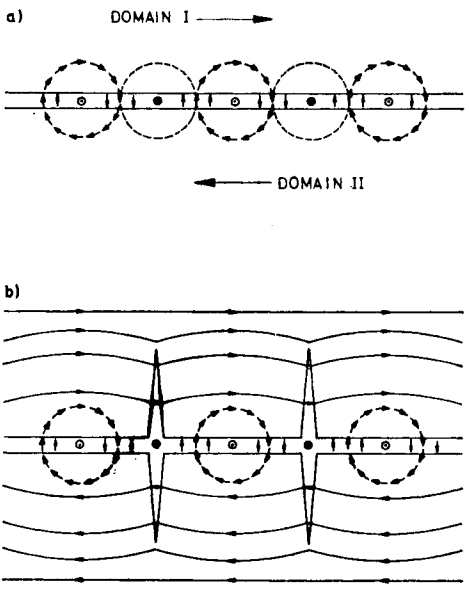



*Figure 4.33. Schematic diagram showing the production of barbed-wire configurations: ⊙ Bloch lines emerging normally to the plane of the film; ⊕ Bloch lines directed into the plane of the film*[17]

### 4.7.3 Intermediate walls

For the sake of completeness it should be noted that, in addition to Bloch walls and Néel walls, there exists also an intermediate type. This intermediate state is characterised by the direction of the stray field, which is neither normal to (Bloch wall) nor parallel to (Néel wall) the film surface, but lies somewhere between the two[31a, 32a]. De Blois was able to demonstrate the coexistence of Bloch, Néel, and crosstie walls[6b].

## 4.8 THE RAYLEIGH LOOP

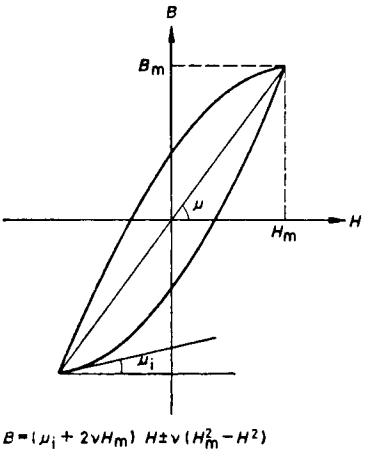
Those *B–H* loops of a hysteresis family which lie near the origin of coordinates are distinguished from loops which lie further afield in a remarkable way: In 1887 Lord Rayleigh (1842–1919)[32], discovered, by magnetic measurements in the low-intensity range, certain blade-shaped loops whose component curves were nearly parabolic. Figure 4.34 shows such a 'Rayleigh loop' schematically.

It has the advantage over all other hysteresis loops that it can be described by a mathematical equation. This equation takes the form:

$$B = (\mu_i + 2v\,H_m)\,H \pm v(H_m^2 - H^2) \qquad (4.3)$$

where $B$ is the flux density, $H$ the magnetic field strength, $H_m$ its peak value, $\mu_i$ the initial permeability, and $v$ the Rayleigh constant. The plus sign of the

*Figure 4.34. The Rayleigh loop*




second term applies to the rising branch and the minus sign to the falling branch of the curve.

If equation 4.3 is applied to the peaks of the parabolic branches for which $H = H_m$, it becomes:

$$B = \mu_i H + 2\nu H^2 \tag{4.4}$$

or

$$\frac{B}{H} = \mu = \mu_i + 2\nu H \tag{4.5}$$

Equation 4.5, known as the Rayleigh law, states that the permeability rises linearly with the field at low intensities. The Rayleigh constant $\nu$ expresses the rate of growth of the permeability.

The range of validity of the Rayleigh law extends to various values of intensity according to the type of material but lies, in general, below the coercivity. It can be artificially extended by introducing an air-gap into the magnetic circuit. The dust core is a typical example.

Hysteresis losses in the Rayleigh region are obtained by integrating the Rayleigh loop. For 1 cm$^3$ and for one cycle of a repetitive magnetising process[37]

$$W_h = \int H \, dB = \tfrac{8}{3} \nu H_m^3 \text{ erg} \tag{4.6}$$

For volume $V$ and frequency $f$, therefore,

$$W_h = \tfrac{8}{3} \nu f V H_m^3 \text{ erg/cm}^3 \tag{4.7}$$

In practical applications, the hysteresis coefficient $h$ usually replaces $\nu$. The two quantities are connected by the relation

$$h = \frac{9500\,\nu}{\mu_i} \tag{4.8}$$

Then $h$ is the hysteresis loss per ampere-turn per centimetre for 1 H at 1 kHz.

### 4.9 THE STEINMETZ LAW

Equation 4.6 of the previous section may also be written in the following form:

$$W_h = \frac{8}{3} \frac{vB_m^3}{\mu^3} \tag{4.9}$$

If the hysteresis loss, given by the area of the hysteresis loop, is plotted against the peak flux density, then, within the Rayleigh range, a third-order parabola is obtained so long as the change in $\mu$ can be neglected. If account is taken of the change in $\mu$, then it is found empirically in many cases that the relation between energy loss and flux density is roughly quadratic. The relation ceases to hold at higher flux densities.

Steinmetz[35] found that the following law held, especially for iron at flux densities between 0·2 V s/m² and 1·5 V s/m²:

$$W_h = 0{\cdot}002\, B^{1{\cdot}6} \tag{4.10}$$

What is surprising about this relation is that it does not contain $\mu$ and thus that the knee of the hysteresis curve has no particular significance.

If equation 4.10 is generalised to

$$W_h = \eta B^a \tag{4.11}$$

one arrives at the Steinmetz law in which $\eta$ is a constant of the material and $a$ is called the Steinmetz coefficient. Thus equation 4.10 in which $\eta = 0{\cdot}002$ and $a = 1{\cdot}6$ must be regarded as a special case.

Numerous investigations undertaken to test the validity of the Steinmetz law have shown that, the higher the coercivity of a material, the higher the value of $\eta$; thus $\eta$ is really a structural constant and can be reduced by, for example, heat treating the test sample. The value of $\eta$ can lie between $0{\cdot}05 \times 10^{-3}$ and $4 \times 10^{-3}$ for iron; it can be about 0·06 for permanent-magnet chrome steel, and around 0·6 for high-coercivity Alnico 5. The coefficient $a$ does not vary as widely as $\eta$ and in most alloys so far investigated has a value not far from 1·6.

The Steinmetz law holds also for ferrites. Even for rectangular ferrites, such as are used for information storage, $a$ may be taken as 1·6 from 0·025 V s/m² to 0·15 V s/m² (Figure 4.35). Above 0·15 V s/m², $a$ becomes 1·4 and in this case $\eta = 9{\cdot}4 \times 10^{-3}$. If this relatively hard ferrite is compared with a high-permeability Mn–Zn ferrite ($\mu_i = 2500\mu_0$), whose hysteresis loop is characterised by low remanence, then it is seen that $\eta$ is reduced to $0{\cdot}31 \times 10^{-3}$ and $a$ assumes the 1·6 value only for flux densities over 0·3 V s/m². Below this value of flux density, the cyclic losses increase proportionally to $B^3$ and thus follow the Rayleigh law. Investigation of the relation $W_h = f(B_m)$ can, therefore, lead to valuable conclusions and can easily show, for example, up to what values Rayleigh's law is valid. In rectangular ferrite, as one might expect, Figure 4.35 shows no trace of the $B^3$ law above 0·025 V s/m².

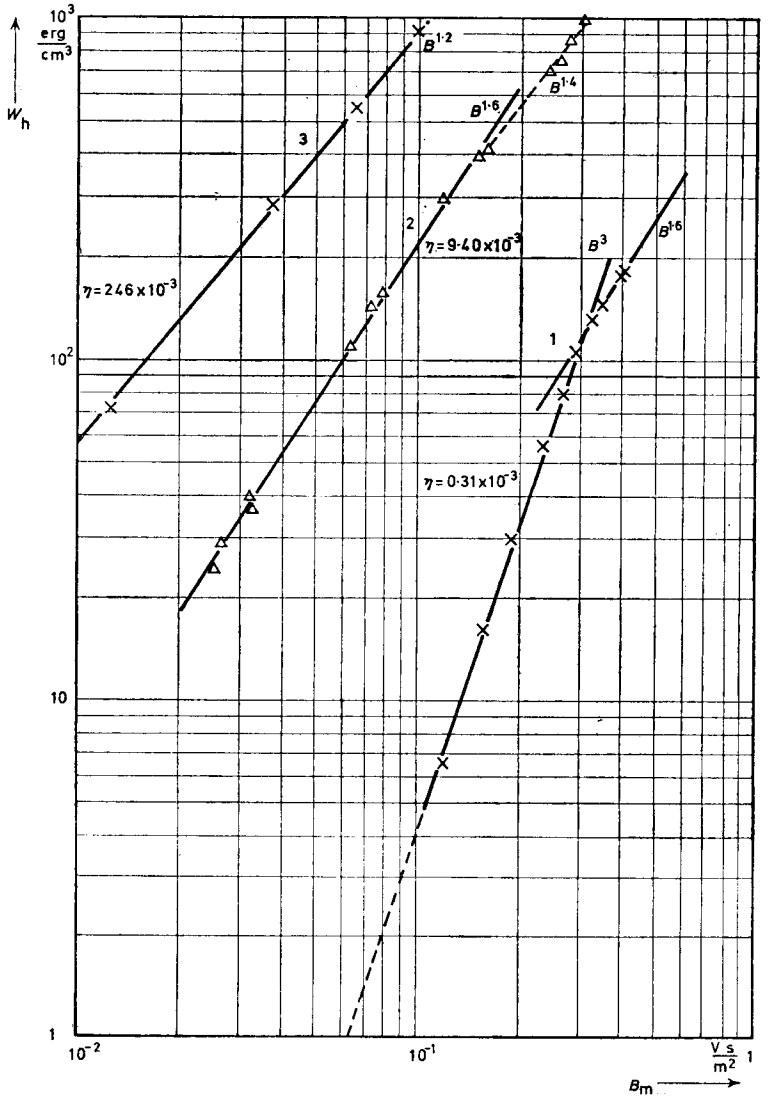



*Figure 4.35. Hysteresis loss $W_h$ as a function of flux density $B_m$: 1,* Mn–Zn *ferrite ($\mu_1$ = = 2500 $\mu_0$); 2, memory core of rectangular ferrite; 3, Perminvar ferrite*

## 4.10 THE VARIOUS SEGMENTS OF THE HYSTERESIS LOOP AND THEIR PRACTICAL APPLICATION

When a body is magnetised, various processes come into play according to the strength of the applied field. In use, then, it is of critical importance, because of the various losses, to know how far reversible or irreversible processes are involved. So it comes about that, in various technical fields, quite different hysteresis loops are desirable and that, in certain circumstances, only particular portions of the loop are of importance. This is clearly shown in the schematic presentation of Figure 4.36:

1. Coils used in communications, in filters, or for the inductive loading of cables are used at low field strengths of a few A/m so that they work in the Rayleigh region, where losses are low and initial permeability high. Stability and the temperature coefficient are, of course, important as well as permeability and loss coefficients.
2. Radiofrequency and high-frequency transformers as well as power transformers operate in an inner loop which is larger than the Rayleigh loop and involves some irreversible processes. The loop is used up to the knee or a little beyond. High permeability over the flux excursion

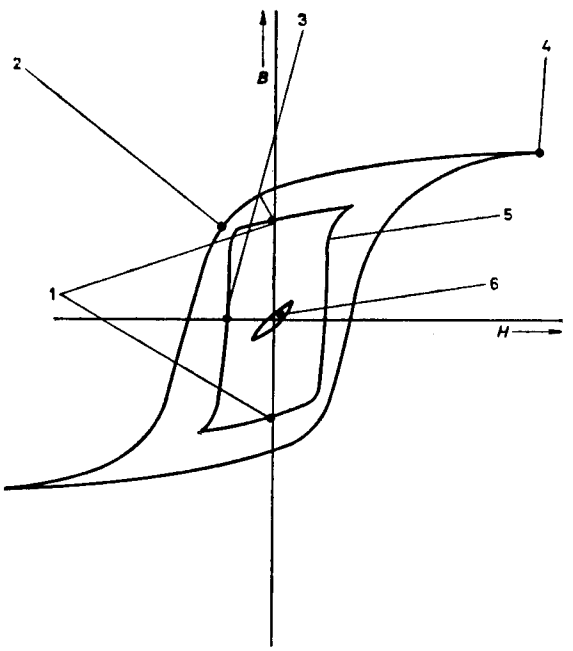



*Figure 4.36. Diagram showing the various regions of a hysteresis loop and their significance in practice: 1, memory store; 2, permanent magnets; 3, relays; 4, microwaves; 5, power transformers; 6, coils in communication engineering*

employed, together with low hysteresis and eddy-current losses are the principal requirements.

3. Again, cores used in magnetic switches and memories are mostly designed to use an inner loop. Memory cores are not magnetically cycled, but brief current pulses are used to establish one or other of the two remanence points. Only when this condition is upset—writing in or reading out—is a branch of the loop curve traversed. A specially shaped hysteresis loop is an important prerequisite for such applications.
4. Materials used in relay construction work on a 'sheared' hysteresis loop. Apparent remanence and coercivity are important: $H_c$ should be as small as possible, and the saturation density high. In order to meet the same specified tolerances over a wide manufacturing range, standard reproducible values are essential.
5. Permanent magnets are, in general, used at a 'working point' in the second quadrant of the hysteresis loop. As it is impossible to hold this working point stable if it lies on the major loop, it has to be brought onto an inner loop which should approximate to the limiting loop as far as possible. As a rule, the working point is so chosen, i.e. the magnetic circuit is so dimensioned, that the product $BH$ is as great as possible.
6. Many applications of ferrites in microwave technique involve the excitation of resonances, and these are produced by the simultaneous application of a very high frequency and a static field in a bar or strip of ferrite. In this procedure, the ferrite is brought nearly to saturation.

There are optimum design strategies for each of these six main fields of application. There are also, of course, in many cases, special requirements to be met such as working frequency and temperature ranges, influence of shock and vibration, and other specified mechanical conditions, together with bulk and weight considerations and secular changes, and, last but not least, price plays a not unimportant role.

## REFERENCES


1. BHIDE, V. G. and SHENOY, G. K.: Structure of subdivided Bloch walls (J. A. P. **34** (6) (June 1963) 1778–1785).
2. BICKFORD, L. R.: Ferromagnetic resonance absorption in magnetite single crystals (Phys. Rev. **78** (2) (1950) 449–457).
3. BLOCH, F.: Zur Theorie des Austauschproblems und der Remanenzerscheinung der Ferromagnetika (Z. Phys. **74** (1932) 295–335).
4. BOZORTH, R. M.: Ferromagnetism. Van Nostrand Co. Inc., Toronto/New York/London (1951).

4a BOZORTH, R. M.: The Permalloy problem (Rev. Mod. Phys. **25** (1953) 42–48).

5. BOZORTH, R. M. and WALKER, J. G.: Magnetic crystal anisotropy and magnetostriction of iron–nickel alloys (Phys. Rev. **89** (1953) 624–628).
6. BROWN, W. F.: Micromagnetics: domain walls (J. A. P. **30** (4) (Apr. 1959) 62 S–69 S).

6a BUSCH, G.: On the existence of ferromagnetism in liquid alloys (IEEE Trans. **Mag-5** (1969) 495).

6b DE BLOIS, R. W.: Ferromagnetic domain studies in highly perfect metal platelets (Report AFCRL-68-0414 (Sept. 1968)).

7. ELMORE, W. C.: Ferromagnetic colloid for studying magnetic structures (Phys. Rev. **54** (1938) 309–310).
8. EWING, J. A.: Experimental researches in magnetism (Phil. Trans. Roy. Soc. **176** (1885) 523–640).
8a FRASER, R. W., EVANS, D. J. I. and MACKIW, V. N.: Herstellung und Eigenschaften von duktilem Kobalt-Band (Kobalt **23** (June 1964) 62–69).
9. FREI, E. H., SHTRIKMAN, S. and TREVES, D.: Critical size and nucleation field of ideal ferromagnetic particles (Phys. Rev. **106** (1957) 446–455).
10. FRENKEL, J. and DORFMAN, J.: Spontaneous and induced magnetization in ferromagnetic bodies (Nature **126** (Aug. 1930) 274–275).
11. FUCHS, E.: Elektronenmikroskopische Beobachtungen zur Domänenentstehung (Z. ang. Phys. **13** (3) (1961) 157–160).
12. FULLER, H. W., RUBINSTEIN, H. and SULLIVAN, D. L.: Spiral walls in thin magnetic films (J. A. P. **32** (3) (Mar. 1961) 286 S–287 S).
13. GUILLAUD, C. and VAUTIER, R.: Les domaines élémentaires (Coll. Nat. Magnétisme, Strasbourg (1957). CNRS, Paris (1958).
13a HASEGAWA, R.: Magnetic properties of amorphous PdSi Alloys containing iron (J. A. P. **41** (10) (Sept. 1970) 4096–4100).
14. HECK, C.: Zur Phänomenologie der Ummagnetisierung von Speicherferriten (ETZ-A **80** (1959) 161–168).
15. HOFFMANN, H.: Die magnetischen Eigenschaften dünnster Eisenaufdampfschichten im Vakuum und ihre Änderung beim Luftzutritt (Z. ang. Phys. **13** (3) (1961) 149–151).
16. HONDA, K. and KAYA, S.: On the magnetization of single crystals of iron (Sci. Rep. Tohoku Imp. Univ. (1) **15** (6) (Dec. 1926) 721–753).
17. HUBER, E. E., SMITH, D. O. and GOODENOUGH, J. B.: Domain wall structure in permalloy films (J. A. P. **29** (3) (Mar. 1958) 294–295).
18. JACOBS, I. S. and BEAN, C. P.: An approach to elongated fine particle magnets (Phys. Rev. **100** (4) (Nov. 1955) 1060–1067).
19. KAYA, S.: On the magnetization of single crystals of nickel (Sci. Rep. Tohoku Imp. Univ. **17** (1928) 639–663).
20. KAYA, S.: On the magnetization of single crystals of cobalt (Sci. Rep. Tohoku Imp. Univ. **17** (1928) 1157–1177).
21. KLEIS, J. D.: Ferromagnetic anisotropy of nickel–iron crystals at various temperatures (Phys. Rev. **50** (1936) 1178–1181).
22. KORNETZKI, M.: Die Remanenz der idealen Magnetisierung (Z. ang. Phys. **14** (1962) 164–168).
23. KORNETZKI, M. and RÖSS, E.: Die ideale Magnetisierungskurve von Ferriten mit unterschiedlicher Magnetisierungsschleife (Z. ang. Phys. **13** (1961) 28–31).
24. KRANZ, J. and HUBERT, A.: Die Möglichkeiten der Kerr-Technik zur Beobachtung magnetischer Bereiche (Z. ang. Phys. **15** (3) (1963) 220–232).
25. LEE, E. W., CALLABY, D. R. and LYNCH, A. C.: The use of the Kerr effect for studying the magnetization of a reflecting surface (Proc. Phys. Soc. **72** (1958) 233–243).
26. METHFESSEL, S., MIDDELHOEK, S. and THOMAS H.: Domain walls in thin Ni–Fe films (IBM-J. Res.-Dev. **4** (2) (Apr. 1960) 96–106).
27. MURRMANN, H. and SCHWINK, CH.: Ausmessen des Streufeldes über Blochwänden (Phys. Verh. **3** (1962) 369).
28. NAGASHIMA, T.: Magnetische Eigenschaften von sehr reinem Eisen (Ber. Arb. Ferrom. (1959). Düsseldorf (1960) 148–154).
29. NÉEL, L.: Les lois de l'aimantation et de la subdivision en domaines élémentaires d'un monocristal de fer (J. Phys. Rad. (8) **5** (12) (Dec. 1944) 265–276).
30. NÉEL, L.: Quelques propriétés des parois des domaines élémentaires ferromagnétiques (Cahiers de Phys. **25** (1944) 1–20; C. R. **254** (1962) 2891).
31. NÉEL, L.: Energie des parois de Bloch dans les couches minces (C. R. **241** (1955) 533–537).

31a OREDSON, H. N. and TOROK, E. J.: One-dimensional walls (IEEE Trans. **Mag-4** (1) (1968) 44–47).
32. LORD RAYLEIGH: On the behaviour of iron and steel under the operation of feeble magnetic forces (Phil. Mag. (5) **23** (1887) 225–245).
32a RICKER, T.: Investigation of domain walls in thin films by low-angle electron deflection (IEEE Trans. **Mag-5** (1969) 179).
33. SHTRIKMAN, S. and TREVES, D.: Internal structure of Bloch walls (J. A. P. **31** (5) (May 1960) 147 S–148 S).
34. STEINHAUS, W. and GUMLICH, E.: Ideale d.h. hysteresefreie Magnetisierung (Verh. D. Phys. Ges. **17** (1915) 369–384).
35. STEINMETZ, C.: Note on the law of hysteresis (Electrician **26** (Jan. 1891) 261–262).
36. TANNENWALD, P. E. and SEAVEY, M. H.: Anisotropy of cobalt-substituted Mn ferrite single crystals (Proc. IRE **44** (Oct. 1956) 1343–1344).
37. WALLOT, J.: Theorie der Schwachstromtechnik. Springer, Berlin (1944).
38. WILLIAMS, H. J.: Ferromagnetic domains (El. Engng. **69** (Sept. 1950) 817–822).
39. WILLIAMS, H. J.: Variations of initial permeability with direction in single crystals of silicon iron (Phys. Rev. **52** (1937) 1004–1005).
40. WILLIAMS, H. J. and BOZORTH R. M.: Magnetic anisotropy of iron–nickel and copper–nickel alloys (Phys. Rev. **55** (1939) 673).
41. WILLIAMS, H. J., FOSTER, F. G. and WOOD, E. A.: Observation of magnetic domains by the Kerr effect (Phys. Rev. **82** (1) (Apr. 1951) 179–180).
42. WILLIAMS, H. J. and GOERTZ, M.: Domain structure of perminvar with rectangular hysteresis loop (J. A. P. **23** (3) (Mar. 1952) 316–323).

# 5

# The various shapes of hysteresis loops and their physical causes

The hysteresis loops observed during the measurement of magnetic materials may be classified into four main types:

Normal loops
Rectangular loops
Perminvar loops
Isoperm loops

In what follows, the fundamental difference criteria, their derivation, and their characteristic peculiarities will be discussed. The technical impact and application of these peculiarities will be deferred.

## 5.1 THE NORMAL HYSTERESIS LOOP

The ordinary hysteresis loop is S-shaped and is characterised by having a remanence value some 50–75% of saturation. This case occurs for materials composed of a great many crystals mutually oriented at random and where stress anisotropy dominates the influence of crystal anisotropy. There are then two preferred directions of magnetisation which, for negative magnetostriction, for example, lie parallel to the direction of greatest compressive stress or minimum tensional stress. If the magnetising field is removed after magnetisation, the magnetic vectors snap into the nearest acceptable direction of easy magnetisation and then take up an angle of $2\pi$ radians. Thus $B_r/B_s$ is about 0·5.

A normal loop is shown in Figure 4.16, for example. It is typical of polycrystalline isotropic materials, i.e. sheets, strips, or cast or sintered parts, for which no overall preferred direction is distinguishable. This type of loop is also encountered in hot-rolled transformer laminations, in ferrites of moderate permeability, or in permanent-magnet steels of low energy density.

Until a few years ago, the 'normal' hysteresis loop was, in fact, almost universally characteristic of magnetisation processes in engineering materials whether cores for light-current or heavy-current engineering were in question, or permanent magnets.

The latest technical developments in this field, however, create the impression that rectangular loops are destined to come more and more to the fore: anisotropic effects are gaining increasing importance.

## 5.2 THE RECTANGULAR LOOP (OR 'SQUARE' LOOP)

The term 'rectangular' loop usually implies a hysteresis loop having a remanence ratio $B_r/B_s$ between 0·8 and 1·0 (see Figure 4.18). Rectangular loops may occur for a variety of reasons. It is usually a question of some structurally determined anisotropy. For single crystals it is the crystal lattice which determines the anisotropy. A very high remanence value is always found in the direction of easiest magnetisability (see Figures 4.22 and 4.27).

In polycrystalline materials a spontaneous squaring of the hysteresis loop can occur: neglecting other influences such as magnetostriction, Gans[15] calculated remanence ratios for polycrystalline iron and nickel between 0·83 and 0·87. These values can be measured in any chosen direction within the material. Thus, from a macroscopic viewpoint, the material is isotropic. The 'squaring' of the hysteresis comes about through the crystal anisotropy of individual crystals. As a general rule this anisotropy cannot appear in genuinely polycrystalline samples of iron or nickel since, as a consequence of magnetostriction introduced by impurities or lattice defects, stresses are produced which greatly diminish the value of the remanence ratio. Examples are known, however, where rectangular hysteresis is observable in very pure samples.

Thus, Nagashima[33] found rectangular loops in very pure iron. Although $B_r/B_s$ was 0·6, there was nevertheless a spontaneous squaring of the hysteresis loop. The same material in a coarsely crystalline form was isotropic. The same result was observed for nickel[33]. Pfeifer[37] produced a 'rectification' of the hysteresis loop of Permalloy by annealing at 400°–600°C. This applied, in particular, to strips 25–300 μm thick.

The high apparent remanence observed in many ferrites and connected with loop squaring can also be related to excessive crystal anisotropy.

Spontaneous rectangularity differs from induced rectangularity or from that produced by texture or directional stress in that it can be measured in all directions of the sample and it does not appear at saturation but, as a rule, only in particular ranges. Two different causes for the occurrence of spontaneous rectangularity are suggested: either the effective domain anisotropy, compounded of crystal anisotropy and magnetostriction effects, is nearly zero[5], or the magnetostriction by itself is nearly zero[44]. Materials exist which support each of these hypotheses.

Rectangular loops can likewise be produced by applying suitably directed external stresses. Finally, there is the case of 'thermomagnetic treatment' which plays a part in many technical applications and by means of which rectangular loops can be induced.

### 5.2.1 Rectangular loops in metals

Rectangular loops can be produced in metals, for example, by applying extreme tensional stresses, as the investigations of Preisach[38] into Fe–Ni wires have demonstrated. Sharp-cornered loops can be achieved in this way having a remanence ratio scarcely distinguishable from unity. Again, the twisting of nickel and Fe–Ni wires shows a similar though somewhat less pronounced effect. After the removal of the tension, the original condition is re-established.

A permanent modification of the hysteresis loop, together with an enhancement of the remanence value, can be achieved by cold rolling of a suitable metallic alloy. This treatment leads to internal stresses within the material supplemented by alignment of the individual crystals, i.e. by a so-called texture effect. Krüger[29] found that, in rolling carbon steel to produce rectangular loops, the roll diameter was of critical importance. Those cases are of the greatest practical importance in which a crystallographic texture is obtained by a recrystallisation annealing associated with a rolling sequence.

Carefully controlled working conditions must be maintained to produce this result. A complete alignment is often to be obtained only with pure materials and exact control of optimum rolling conditions and heat treatment. One of the famous examples of textured sheet is the cubic structure of Fe–Ni alloy with 50% Fe and 50% Ni. To achieve the prerequisite conditions for the production of the cubic layer, the alloy must be heavily deformed—95% at least. A sheet of, for example, 5 mm thickness must be rolled down to 0·25 mm without intermediate annealing. The thickness reduction referred to the initial thickness of a strip, expressed in percent is called the degree of deformation $\eta$. A similar definition applies to wire, the diameter being the significant dimension. Therefore,

$$\eta = \frac{D_i - D_f}{D_i} 100\% \tag{5.1}$$

where $D_i$ and $D_f$ are the initial and final diameters. The rolling operation must be followed by a recrystallisation annealing at high temperature (for example, 1 h at 1100°C) to build up the required texture[36].

The cubic layer is characterised by a crystallographic alignment of the crystallites: the elementary cubes of the lattice lie with one face (100) in the plane of the sheet, and with an edge direction [001] along or perpendicular to the ribbon; this texture is represented by the symbol (100) [001] (see Figure 5.1a).

Since, for alloys of 50% Ni and 50% Fe, the cube edge is the direction of easiest magnetisation, the strip direction and the transverse direction are both preferred magnetic directions. All angles between these principal directions lead to less rectangularity of the hysteresis loop.

To take advantage of the preferred magnetic directions in applications involving laminae and strips of cubic grain texture, care must be taken to ensure that the magnetic flux in the elementary 'dice' is not inclined to the direction of easiest magnetisability. Since in laminated cores, such as shown in Figure 5.2a, the magnetisation directions change and since it is

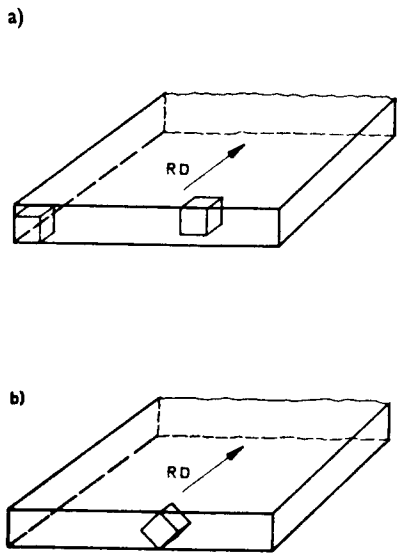



*Figure 5.1. Schematic diagram showing the disposition of elementary cubes in a thin strip (RD = rolling direction): (a) cubic texture; (b) Goss texture*

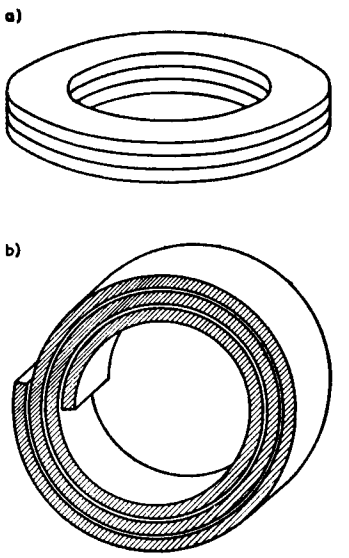



*Figure 5.2. Toroid shown diagrammatically: (a) sheet or laminated core; (b) strip-wound core*

not possible to avoid small air-gaps altogether, a better rectangularity of the hysteresis curve is obtained by the use of strip-wound cores (Figure 5.2b). To minimise the air-gaps in laminated cores, industry has developed optimum sections which are, generally speaking, suitable for texturing; however, a certain loss of remanence must be accepted even in the best commercial solutions.

Figure 5.3[2] shows a hysteresis family for an Fe–Ni sheet with cubic texturing, measured at 60 Hz. The hysteresis loops for $f = 0$ and $f = 400$ Hz are displayed in Figure 11.5.

The cube edge is also the preferred magnetic direction in single crystals of the technically very important iron alloy containing 1–3% Si. There has, therefore, been no lack of attempts to achieve a cubic texture in polycrystalline Fe–Si which, like that of the 50% Fe–Ni alloy, is characterised by two crystallographic and magnetic preferred directions in the plane of the sheet.

So far it has only been possible to achieve a partial orientation with the Fe–Si alloy, which became known as Goss texture and which has played an important technical role since 1935[6, 17]. Its characteristic is that a preferred direction has, indeed, been achieved in the rolling or strip direction but not in the perpendicular—i.e. transverse—direction. The magnetisation curve, therefore, in samples measured transversely to the rolling direction, lies below that appropriate to the actual rolling direction. This is shown in Figure 5.4[3] for 0·3 mm strips from an iron alloy having 3% Si, measured at 50 Hz. The difference between the two curves stems from the fact that, while a cube edge [100] does indeed lie in the strip direction, the cube face (100) is

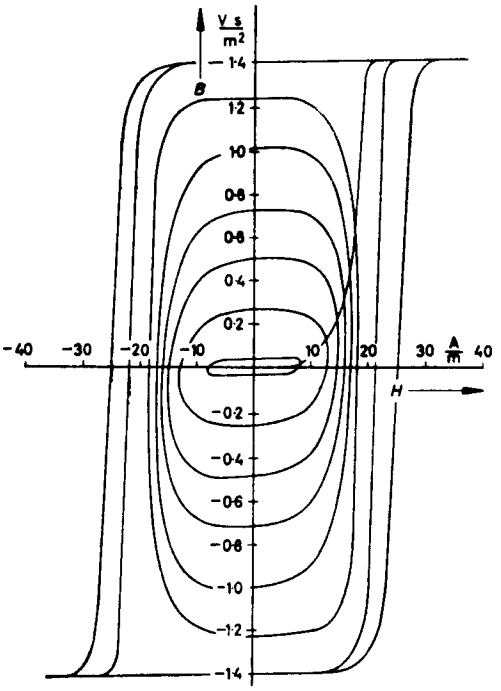



*Figure 5.3. Hysteresis family of an* Fe–Ni *sheet having cubic texture (Deltamax) measured at 60* Hz [2]

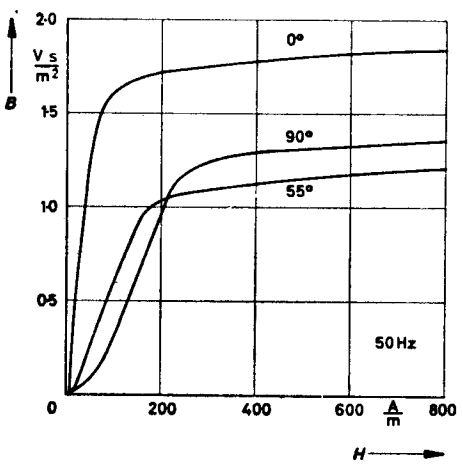



*Figure 5.4. Magnetising curves of* Fe–Si *with* 3% Si *(Goss texture)* [3]

inclined to the surface of the strip (Figure 5.1b). Goss texture is denoted by the symbol (110) [100].

In the course of further development over a period of 20 years, it was found possible (in the first instance for thin strips) by taking special precautions to introduce a second recrystallisation which increased the number of the (relatively few) crystallites having the desired grain orientation after the primary recrystallisation. They grow during the heat treatment until practically all unfavourably oriented crystallites have disappeared and the cubic layer is spread throughout the sheet[4].

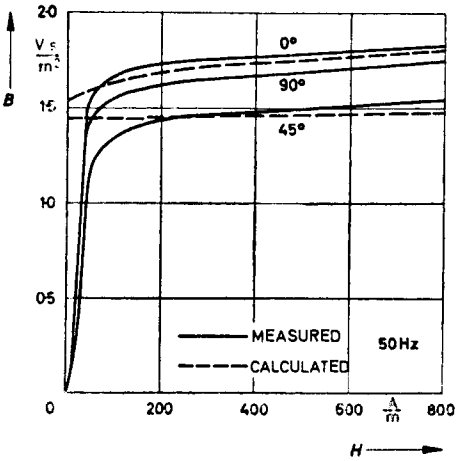



*Figure 5.5. Magnetising curves of* Fe–Si *having cubic texture*[3]

The consequence of this, magnetically, is that the transverse direction now becomes comparable to the longitudinal direction, as brought out in Figure 5.5 for a 0·04 mm sheet treated in this way[3]. As Möbius and Pawlek[32] have shown, it is also possible to achieve cubic grain texture in sheets up to 0·4 mm thick. These authors found, further, that the formation of texture was favoured by a silicon content of 1·8–2·2% and that optimal degrees of deformation had to be imposed to achieve a good cubic texture.

Walter *et al.*[43] established cubic texture in 97% Fe–3% Si sheets and strips, up to a thickness of 2·5 mm. According to Kohler[25], the presence in the atmosphere of particular additives (for example, $H_2S$) is decisive for the formation of cubic texture.

The third route to the production of rectangular loops in metallic alloys, by the use of a thermomagnetic treatment, leads to a consideration of the Perminvars, which will be discussed later. The best-known materials with rectangular hysteresis loops are displayed in Table 5.1.

**Table 5.1** MATERIALS WITH RECTANGULAR HYSTERESIS LOOPS

| *Material* | $H_c$ (A/m) | $B_s$ (V s/m²) | $B_r$ (V s/m²) | $B_r/B_s$ | *Reference* | *Remarks* |
|---|---|---|---|---|---|---|
| *Metals and alloys* | | | | | | |
| Iron (99·99% Fe) | 3 | — | 1·2 | 0·6 | 33 | Spontaneous |
| Nickel | — | — | — | — | 33 | Spontaneous |
| Nickel under tension | — | — | — | ~1 | 38 | Electrical stress |
| 55% Fe, 45% Ni | 24 | 1·6 | 0·5 | 0·5 | 31 | |
| 50% Fe, 50% Ni | 12·8 | 1·55 | 1·50 | 0·97 | 31, 36 | Cubic texture |
| 35% Fe, 65% Ni | 0·8 | 1·35 | 1·30 | 0·96 | 8, 31 | Magnetic field treatment |
| 21·5% Fe, 78·5% Ni | — | — | — | — | 37 | Spontaneous |
| 17% Fe, 79% Ni, 4% Mo | 4 | 0·87 | 0·50 | 0·58 | 31 | |
| 16% Fe, 79% Ni, 5% Mo | 1·2 | — | — | 0·90 | 37 | |
| 33% Fe, 65% Ni, 2% Mo | 0·48 | 1·264 | 1·202 | 0·95 | 31 | Magnetic field treatment |
| 49% Fe, 49% Co, 2% V | 20·8 | 2·40 | 2·15 | 0·88 | 18 | Spontaneous |
| 97% Fe, 3% Si | 9·6 | 2·0 | 1·54 | 0·77 | 3, 31 | Texture |
| 97% Fe, 3% Si | 5·6 | — | 1·22 | — | 43 | |
| *Ferrites* | | | | | | |
| Mg–Mn ferrites | 6·4 | 2·0 | 1·8 | 0·9 | 1 | Spontaneous |
| $Mg_{1-x}Cu_xFe_2O_4$ | — | — | — | 0·9 | 19 | Spontaneous |
| $(MgO)_{0·27}(FeO)_{0·73}Fe_2O_3$ | — | — | — | 0·95 | 22 | Magnetic field treatment |
| $Fe_{1-x}Co_xFe_2O_4$ ($x = 0·1$-$0·8$) | — | — | — | — | 26 | Magnetic field treatment |
| $(Ni_{0·4}Zn_{0·6})_{1·03-x}Co_xFe_{1·97}O_4$ ($x < 0·04$) | | — | — | — | 26 | Magnetic field treatment |
| $Mn_{1·45}Co_{0·05}Fe_{1·5}O_4$ | — | — | — | — | 26 | Magnetic field treatment |
| $(Ni_{0·4}Zn_{0·6})_{0·976}Co_{0·024}Fe_{1·92}O_4$ | — | — | — | — | 42 | Magnetic field treatment |

### 5.2.2 Rectangular loops in ferrites

#### 5.2.2.1 Spontaneous rectangular loops

There exist ferrites showing rectangular hysteresis loops although there is no texture and no orientation of the crystallites. Also in these cases there is no stress anisotropy, so the effect can only be assigned to the excess of crystal anisotropy. This situation applies especially to Mn–Mg ferrites whose composition is indicated along the sides of the triangle in Figure 5.6. The two parallel lines at 40% and 45% $Fe_2O_3$ serve to display the most favourable compositions. Albers-Schoenberg[1] first demonstrated these ferrites which show rectangular loops from the start, i.e. spontaneously.

Innumerable other compositions of similar behaviour are quoted in the literature (see Table 5.1). Examples are: Mn–Cu ferrite[44], Mn–Mg–Ni ferrite[44], Mn–Cd ferrite[11, 11a], and Mg–Cu ferrite[19]. In many cases three or four oxide constituents do not suffice and improved hysteresis loops require the addition of calcium oxide or chromium oxide[10].

The concept of rectangularity ratio is important in applications of materials with these loops to problems of magnetic storage of information. Figure

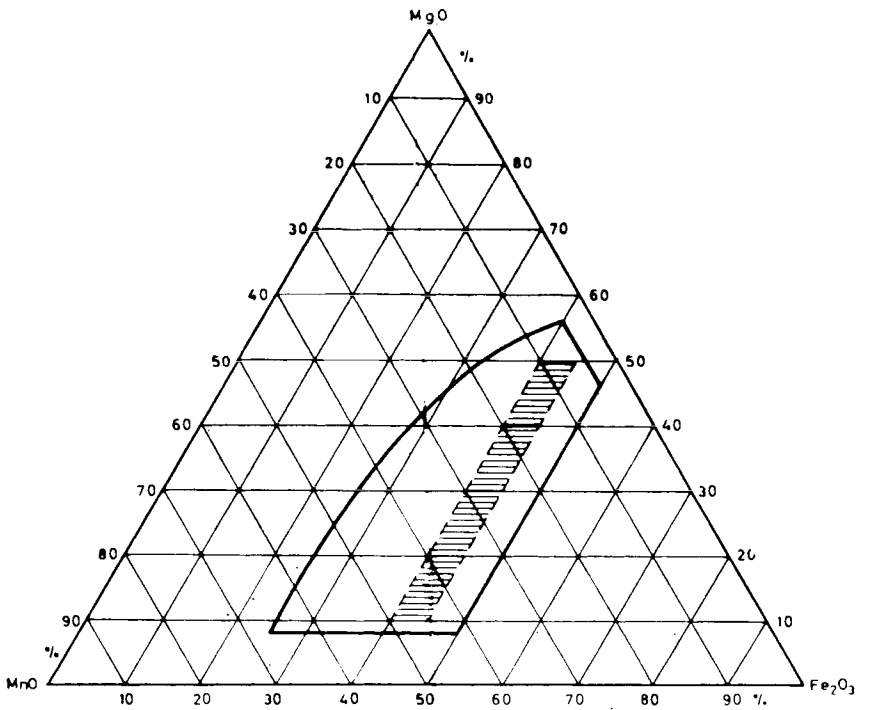



*Figure 5.6. Three-component diagram for* MnO–MgO–$Fe_2O_3$; *the enclosed portion comprises ferrites with rectangular hysteresis loops (which are particularly well marked within the shaded area)*

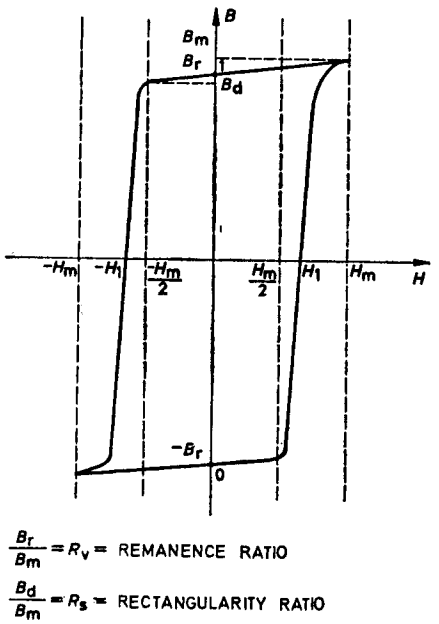



*Figure 5.7. Diagram of a rectangular hysteresis loop*

5.7 defines this ratio as $R_s = B_d/B_m$. The underlying theory is given on page 595. If the ratio $R_s$ is plotted against the peak field strength $H_m$ for various values of $H_m$, it becomes apparent that there is a relatively narrow region in which $R_s$ assumes a maximum value. The curve falls off steeply on both sides (Figure 5.8). In the example quoted here, a ratio $R_s > 0{\cdot}8$ is reached in the interval 35–75 A/m. The drop in the remanence ratio $R_v = B_r/B_m$ is not observed within the measurement range shown: it occurs only at higher intensities. Peak values $B_m$ of flux density rise appreciably, while the apparent coercivity $H_1$ rises only slightly. In the most useful range of application of this material, around 50 A/m, $H_1 \triangleq 0{\cdot}5\ H_m$[21].

Because it is possible to produce ferrites with a variety of coercivity values, one is free to specify the range of field strengths in which rectangularity is to be exhibited (see, for example, Figure 15.13, page 597).

### 5.2.2.2 Induced rectangularity in ferrites

Besides the materials exhibiting spontaneous rectangularity of their hysteresis loops, there exists, also, another class of ferrites where no rectangular loops appear initially but where these can be produced by other means.

For example, in all ferrites it is possible to force up the remanence value by applying mechanical stress. This was achieved in an investigation by Wijn and his colleagues by shrinking onto a toroidal core of negatively magnetostrictive ferrite, at an elevated temperature, a closely fitting mantle of a special glass[44]. On cooling, the glass sought to shrink faster than the ferrite and produced, in this way, compressive stress. This procedure raised the remanence, squaring the hysteresis loop.

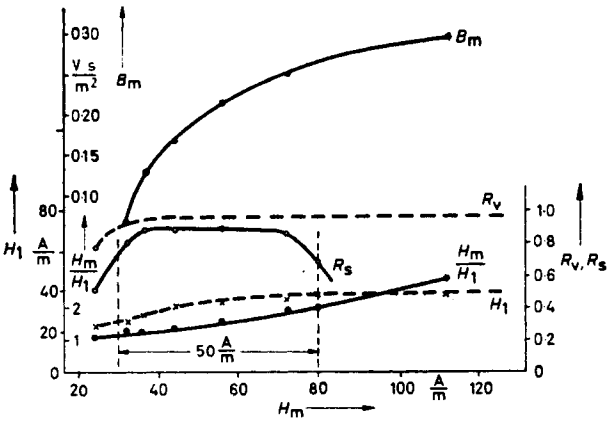



*Figure 5.8. Peak flux density $B_m$, remanence ratio $R_v$, rectangularity ratio $R_s$, and apparent coercivity $H_1$ for a spontaneous rectangular ferrite, expressed as function of field intensity*[21]

Again, stresses can be induced in a normal ferrite, with negative magnetostriction, by shrinking onto it a suitable plastic, and this will produce rectangular loops[46]. For ferrites exhibiting positive magnetostriction, one might expect a corresponding effect by applying tensile stress. A practical device of this sort, however, is not yet known.

There exists yet another kind of ferrite in which rectangular loops can be achieved by a suitable magnetic treatment—namely Perminvar materials. Before this method of loop control is discussed, something must be said about Perminvars themselves.

## 5.3 PERMINVAR LOOPS

Elmen[12] in 1921 discovered certain unusual shapes in the hysteresis loops of a group of Fe–Ni–Co alloys. Their shape could be varied widely by heat treatment or by changes in the composition. All these materials exhibited constant permeability at low field strengths, together with low hysteresis losses. Compared with usual compacted cores, those in which Perminvar

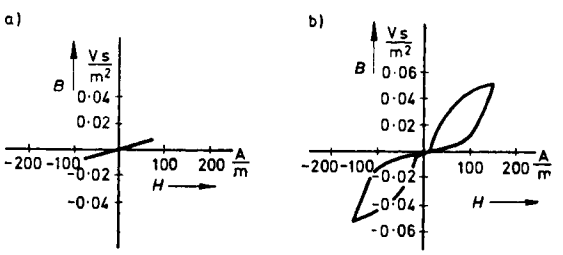



*Figure 5.9. Perminvar loop of a* Mg–Fe–Co *ferrite: (a) $H_m$ less than starting field strength; (b) $H_m$ greater than starting field strength*

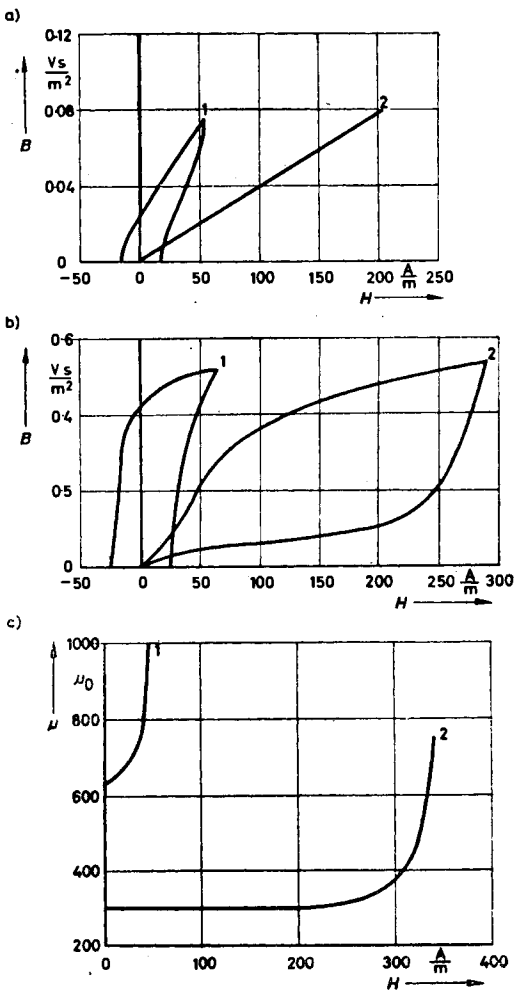



*Figure 5.10. Perminvar (30% Fe; 25% Co, 45% Ni): 1, sample quenched; 2, sample slowly cooled; (a) $H_m$ = 200 A/m; (b) $H_m$ = 290 A/m; (c) permeability*[13]

was used showed high values of permeability (50–100 $\mu_0$). By reason of the constant permeability at low flux densities, the combination term *Perminvar* was coined (*perm*eability *invar*iant).

A typical Perminvar loop is displayed in Figure 5.9. At a field strength less than the critical starting field strength (see diagram), the loop is practically closed. It opens only above this intensity, and then only at the ends. In the mid-region it remains constricted. With rising field strength, this constricting becomes less and disappears altogether at high intensities.

### 5.3.1 Perminvar loops in metals and alloys

Figure 5.10 shows certain further characteristic properties of a Perminvar composed of 30% Fe, 25% Co, and 45% Ni[13]. Those features of the graphs labelled 1 relate to samples that were quenched, i.e. cooled rapidly. The curves labelled 2 were taken after slower cooling (baking at 425°C). In the more slowly cooled sample, the hysteresis loop remains closed up to 200 A/m (Figure 5.10a) and opens at higher field strengths to a shape resembling a butterfly's wing (Figure 5.10b). Thus, the permeability of a slowly cooled sample remains constant over a wide range of field intensities and then rises steeply (Figure 5.10c).

The curve 2 of Figure 5.10b is typical of all Perminvars, though it is often less constricted than in this case. In many materials intermediate stages occur on the route to rectangularity as, for example, in the series displayed in Figure 5.11. This was taken from the detailed investigations of Kühlewein[30] into the properties of Perminvars. Not only the effect of iron content, but also the influence of heat treatment, can be seen here clearly. In the upper series the hysteresis loops corresponding to four compositions are indicated, all annealed at 900°C, and in the lower series the same materials are represented after annealing at 1000°C.

In the three-constituent diagram of Figure 5.12 (Fe–Co–Ni) the limits of the Perminvar range are plotted according to Elmen[13] and the four test-

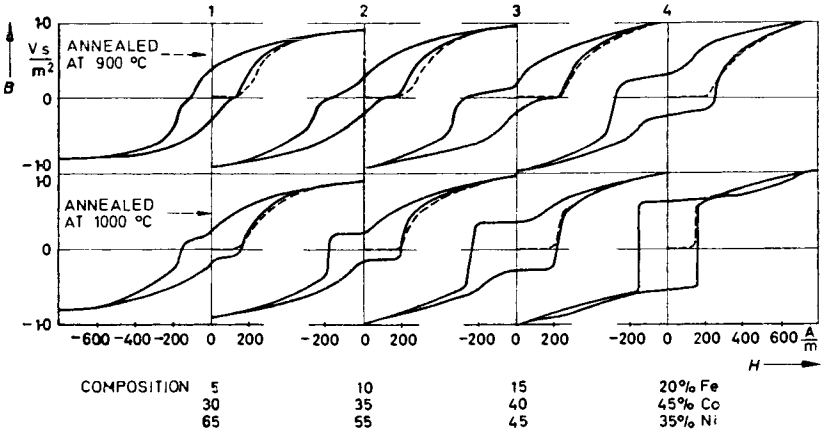



*Figure 5.11. Effect of heat treatment on the hysteresis loop of four different Perminvars*[30]

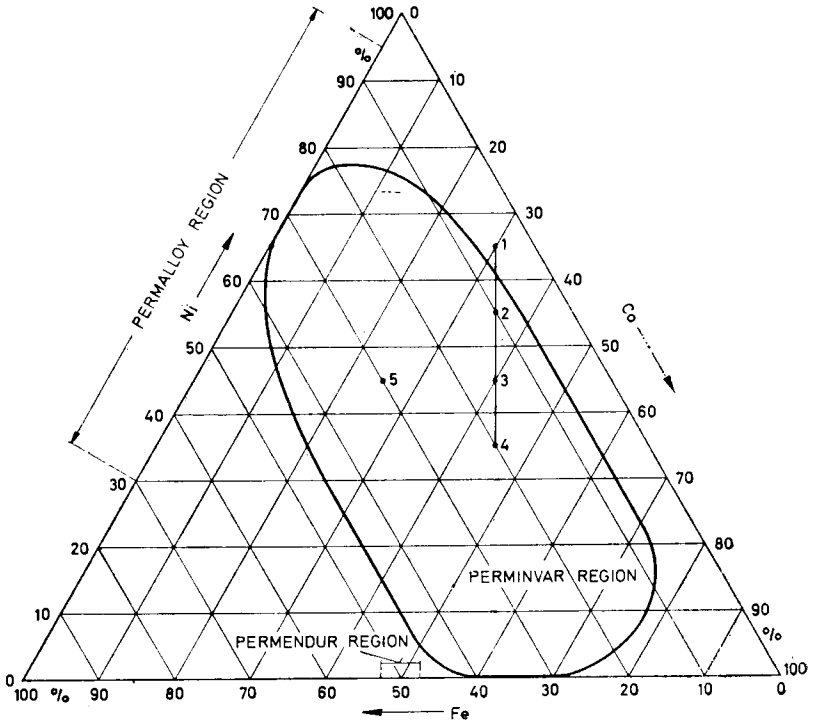



*Figure 5.12. Three-component diagram* Fe–Co–Ni[14]

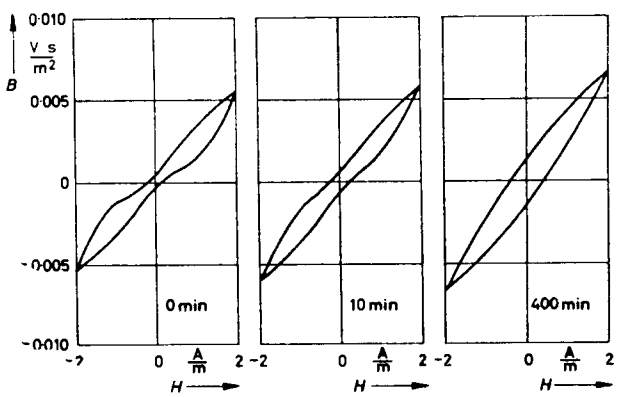



*Figure 5.13. Perminvar loops for* Fe–Si *after conditioning*[14]

samples mentioned above are labelled 1–4. The Perminvar of Figure 5.10 is designated 5 in Figure 5.12.

Köster and v. Kienlin[28] likewise found Perminvar properties in commercial Fe–Cr alloys with 17·9% and 24·7% Cr, as well as in a very pure alloy having 26·4% Cr in a temperature range from 350°C to 600°C. In general, the constriction of the hysteresis loop occurs only over a particular temperature range and a particular range of field strength. The Perminvar condition is often unstable but, depending on external factors, goes over, sooner or later, to a stable condition. In particular circumstances, constricted hysteresis loops, similar to those of Perminvar, may be observed also in the Rayleigh region. Thus, Feldkeller[14] found constricted hysteresis loops in Fe–Si sheet immediately after demagnetisation (Figure 5.13). This constriction fully disappeared during the observations which lasted from 1 h to 2 h. The effect could be explained as residual effect (viscosity) following diffusion of carbon.

### 5.3.2 Perminvar loops in ferrites

Hysteresis loops of the same or similar shape as those of the Perminvars can occur also in ferrites. The term 'Perminvar ferrites' is therefore used. Figure 5.14, for example, shows a family of hysteresis loops which were measured in a Mg–Fe ferrite with a small cobalt additive (65·9% Fe, 3·11% Mg, 0·11% Mn, 0·013% Co).

According to investigations published up to the present, the Perminvar effect occurs more particularly in iron-rich ferrite compositions. It is favoured by enrichment with cobalt[9]. Excess of oxygen also seems to have similar tendencies. In cases where the perminvar effect is observed in Mn–Zn and Ni–Zn ferrites of low iron content (stoichiometrically unbalanced), it only occurs at low temperatures (below $-80$°C)[26].

Perminvar properties have been established for a wide range of mixtures in magnetite with cobalt additive[24, 45]. As with metallic Perminvars, the rate of cooling of a sample heated to above the Curie temperature determines the appearance or otherwise of constricted loops. Here, too, it is only slow cooling that produces the Perminvar loops.

Figure 5.15 shows the hysteresis loops for the above-mentioned Mg–Fe ferrite: in Figure 5.15a the sample was cooled from 650°C to room temperature in 16 h; in Figure 5.15b the sample was quenched after it had been removed from the oven at 650°C and exposed to air at room temperature for some 3 min.

The range of temperature and of field strength over which constricted loops can be observed varies greatly with composition. What, then, are the causes of the Perminvar effect? As may be deduced from the temperature dependence of Perminvar properties, a relaxation process is involved which is conditioned by the internal structure. A stable condition is arrived at (a) through ion diffusion (as demonstrated in the case of carbon diffusion in iron); or (b) through electron diffusion, as seems to be the case for many ferrites; or (c) through diffusion of dislocations or holes (empty sites). Some-

times several diffusion processes occur together (ions, electrons, dislocations, or lattice energy).

It can well be imagined that, in materials with constricted hysteresis loops, the Bloch walls lie in deep energy troughs and are so oriented that 'binding'

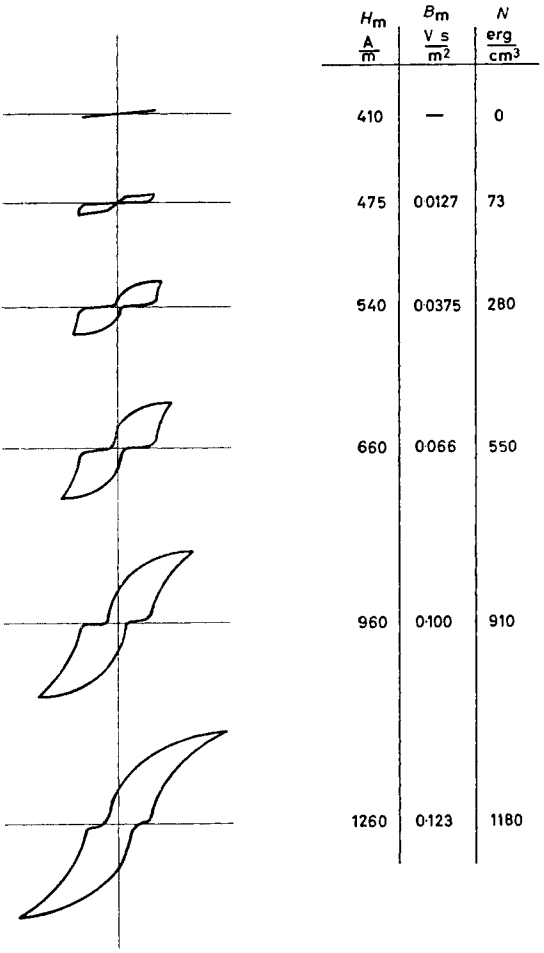



*Figure 5.14. Perminvar loops for* Mg–Fe *ferrite*

through uniaxial anisotropy is very great. At low intensities of the measuring field, therefore, there exist only a few reversible processes and almost no irreversible ones. The permeability is thus constant and relatively low over a wide intensity range. Only when the threshold intensity has been passed do irreversible processes, of a predominantly rotational nature, set in.

According to Nesbit and Heidenreich[35], the appearance of constricted loops in metals and ferrites is connected with a slight oxidation process which can occur, for example, during slow cooling.

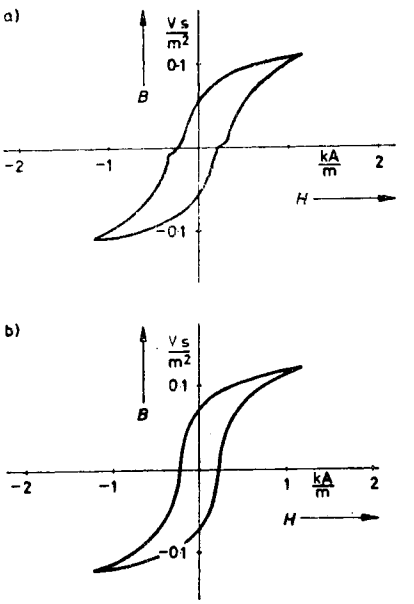



*Figure 5.15.* Mg–Fe *ferrite: (a) after slow cooling from 650°C (b) after rapid cooling from 650°C*

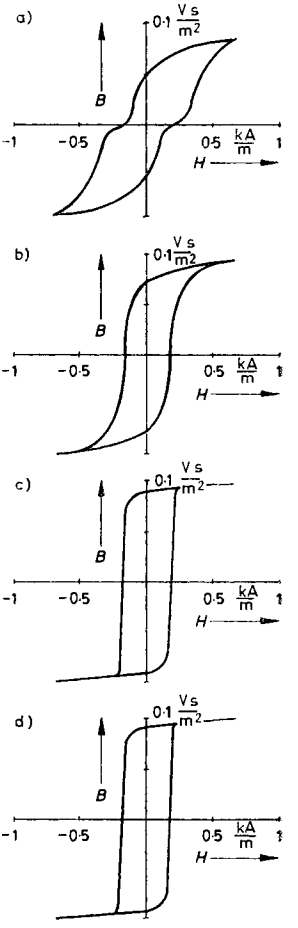



*Figure 5.16. Time changes of the loop of a* Mg–Fe *ferrite at 95°C under the influence of a measuring field and* $H_m = 680$ A/m *throughout*[22]*: (a)* $t = 0$, $B_m = 0{\cdot}086$ V s/m²; *(b)* $t = 21$ min, $B_m = 0{\cdot}091$ V s/m²; *(c)* $t = 305$ min, $B_m = 0{\cdot}094$ V s/m²; *(d)* $t = 1040$ min, $B_m = 0{\cdot}096$ V s/m²

### 5.3.3 Transformation of Perminvar loops to rectangular shape

As in the above-mentioned experiment by Feldtkeller, a situation is known also for ferrites in which the constriction effect occurs only at particular temperatures. Thus Sixtus[42] found a spontaneous rectangular loop at room temperatures for a ferrite whose formula is $(Ni_{0{\cdot}4}\,Zn_{0{\cdot}6})_{0{\cdot}976}\,Co_{0{\cdot}024}\,Fe_{1{\cdot}92}O_4$. When he switched on the measuring field at $-41°C$, he observed, at first, a constricted loop which changed after a minute to a normal shape, and finally to a rectangular shape.

Figure 5.16 shows the change of loop shape with time of another ferrite, in fact the already mentioned Mg–Fe ferrite, at 95°C. It is seen that the constricted loop passes into the normal type after a short time and then gradually assumes the rectangular shape[22]. The progress of this change of loop shape is associated with a stepwise increase of flux density $B_m$. At higher

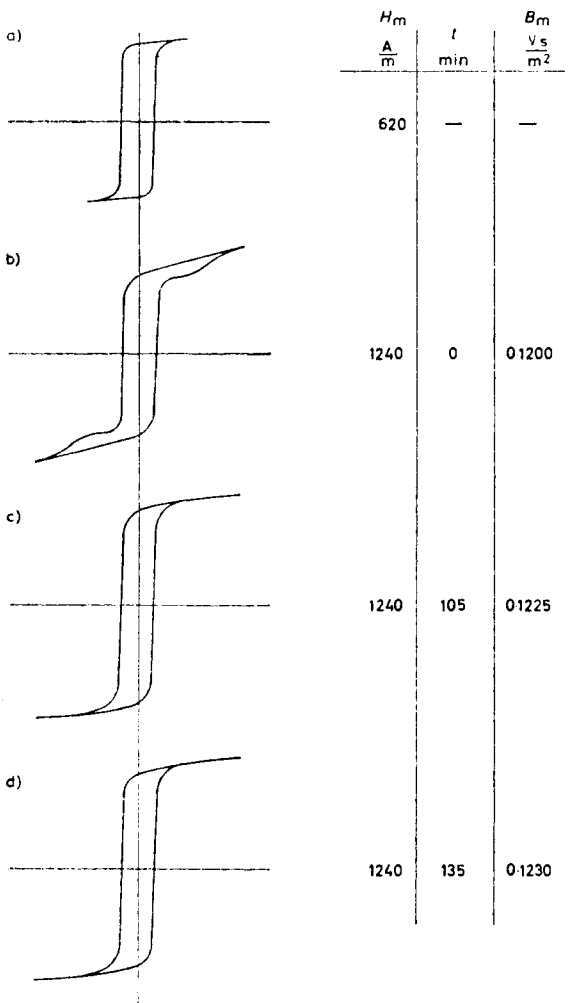



*Figure 5.17. Effect of field strength increase for an induced rectangular ferrite: $T = 95°C$ throughout*[22]

temperatures the transformation occupies a smaller time, while at lower temperatures it takes longer. The activation energy of the internal re-ordering can be calculated from this temperature dependence. It amounts to 1·4 eV (electron-volts). In the experimental example examined here, the 50 Hz measuring field was applied during the transformation process. A direct field also acts in the same way. The thermomagnetic treatment needed to produce rectangular loops in Perminvar generally consists of slowly cooling the sample from a higher temperature (i.e. 500°C) in the presence of a magnetic field. The rectangular loop produced at high temperature under the influence of a direct or alternating field remains stable at low temperature.

The temperature at which the loop changes shape over an observable time varies, depending on the individual ferrite considered.

Again, the field strength plays an important part. If, for example, a ferrite having no impressed rectangularity at low intensity is subjected to a high field strength, a loop is obtained whose flux density rises again beyond the old $B_m$ value (Figure5.17). This peak value only disappears after a further period of time; the remanence rises almost to the new value of $B_m$.This must

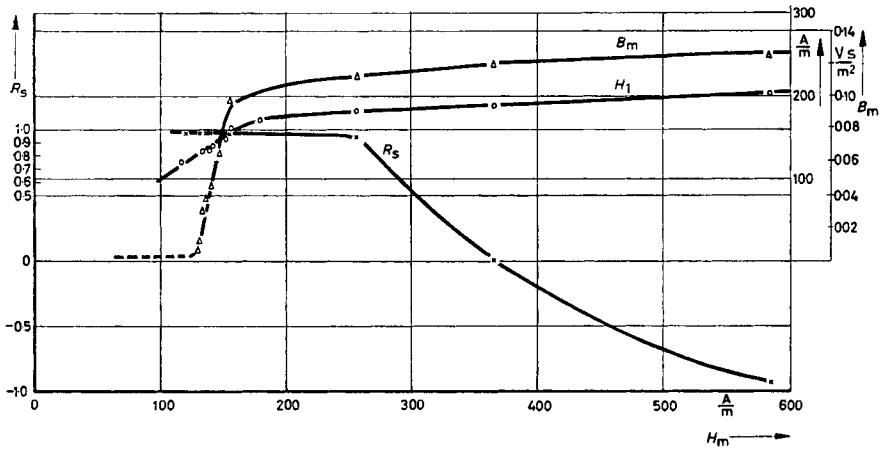



*Figure 5.18. Dependence on field strength of the most important characteristics for a rectangular ferrite of induced rectangularity*[22]

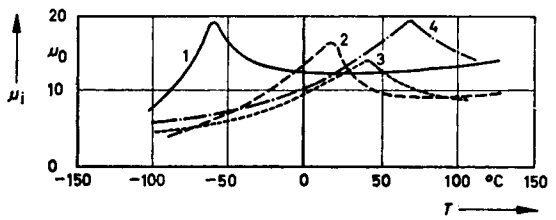



*Figure 5.19. Dependence of initial permeability on temperature for the composition* $(Mg_{0.6}Ni_{0.4})_{1-\delta}\,Co_\delta\,Fe_2O_4$*: 1,* $\delta=0.01$*; 2,* $\delta=0.02$*; 3,* $\delta=0.025$*; 4,* $\delta=0.03$[16]

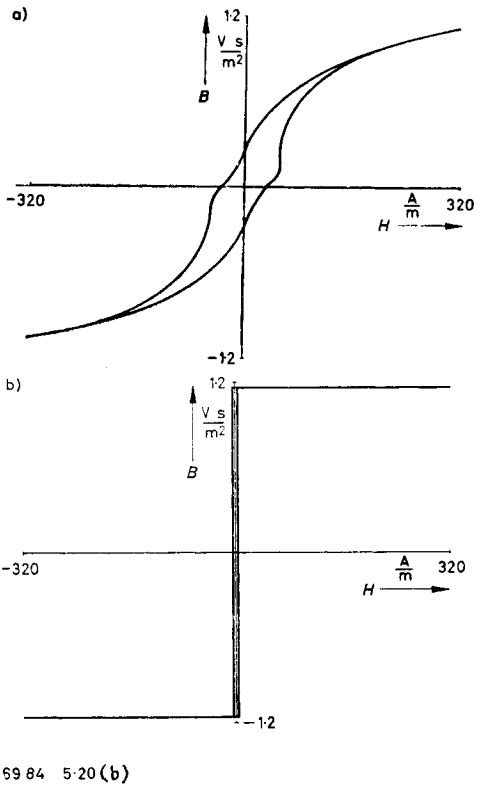
mean, therefore, that at the higher intensity domains are activated which remained unaffected at the lower. After some time, re-ordering processes supervene which lead to a large rectangular loop.

The rectangularity ratio is higher for a ferrite produced by modifying a Perminvar-type ferrite (Figure 5.18) than for a type having spontaneous rectangularity (Figure 5.8). It does not differ much from unity in the former case, as is manifested by the appreciably steeper rise of $B_m$ with field strength. In known ferrite cores with 'induced' rectangularity, the coercivity is mostly higher than in the spontaneous types, in particular if the cobalt constituent is relativity high[16].

Another effect of cobalt enrichment is the shift of maximum permeability with temperature. It is seen in Figure 5.19 that the highest value of initial

permeability of a ferrite series $(Mg_{0\cdot6}Ni_{0\cdot4})_{1-\delta}Co_\delta Fe_2O_4$, cooled in a magnetic field, occurs at $-60°C$ if $\delta = 0{\cdot}01$ (curve 1), but this becomes 20°C, 40°C, or 70°C if $\delta$ is 0·02, 0·025, and 0·03 respectively (curves 2–4).

In a similar way an alignment of the magnetisation vectors into the field direction can be obtained in metallic Perminvars by the operation of an 'ordering' magnetic field. This property of Fe–Ni Perminvar has been




69 84 5·20(b)

*Figure 5.20. Effect of thermomagnetic treatment on loop shape for an* Fe–Ni *alloy having 65%* Ni *(slow cooling from 1000°C): (a) with no magnetic field; (b) in a field of 800* A/m[8]

known since 1935. Dillinger and Bozorth[8] slowly cooled an Fe–Ni alloy with 65% Ni from 1000°C. They obtained the Perminvar loops shown in Figure 5.20a. If a field of 800 A/m was applied throughout the cooling, the rectangular loop of Figure 5.20b was obtained. The cooling rate was found to have less influence than the presence of the field and the use of a high annealing temperature. The applied magnetic field is highly effective for mixtures having Curie temperatures over 500°C especially with a preliminary heat treatment at an elevated temperature, for example 18 h annealing at 1400°C in a hydrogen atmosphere. According to the researches of Heidenreich, Nesbitt, and Burbank[23], it is the presence of oxygen as a contaminant which is the cause of the effect.

## 5.4 ISOPERM LOOPS

If an Fe–Ni sheet with cubic texturing is further rolled after recrystallisation, then a surprising alteration in magnetic properties takes place without substantial reorientation of the crystals. The rectangular shape persists in the transverse direction, but a flat narrow loop with very low remanence develops in the direction of rolling. This loop is generally called an Isoperm loop. *Isoperm* means much the same as Perminvar (*iso*, the same; *perm*, a contracted form of 'permeability'). Here, too, the permeability changes very little with increasing field strength, though, indeed, for different physical reasons from Perminvar, as will later appear. As a rule one speaks of Isoperm loops if the remanence ratio $B_r/B_m$ is appreciably below 0·5 and if the loop is smooth, i.e. without constriction.

### 5.4.1 Isoperm loops in metals and alloys

In 1933 loops of the type shown in Figure 5.21 were discovered by Dahl and Pfaffenberger[7] in the course of investigations into Fe–Ni–Cu and Fe–Ni–Al alloys (the precipitation Isoperms), and similar loops were later found in iron alloys, free of additives, composed of 60% Fe and 40% Ni (the textured Isoperms)[41] (see also Section 13.4.10).

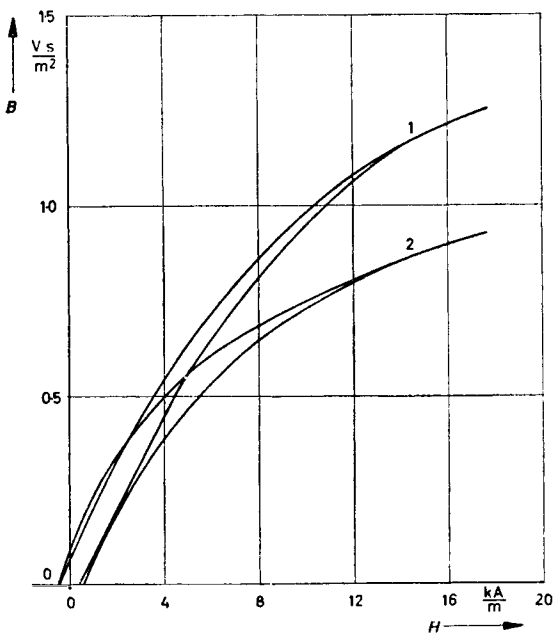



*Figure 5.21. Isoperm loops: 1, for an* Fe–Ni–Al *precipitation Isoperm*[7]*; 2, for a textured Isoperm 60% Fe–40% Ni*[41]

According to the investigations of Schweizerhof[40], Isoperm loops can also be produced by plating materials having different coefficients of expansion. Such combinations, for example, are an Fe–Ni alloy with 50% Ni, and a Ni–Cr steel having 18% Cr and 8% Ni.

The discoverers explained the Isoperm effect as an anisotropic effect in which the direction of easiest magnetisability is perpendicular to the measuring direction. The term 'precipitation Isoperms' implies anisotropy associated with internal stress produced by means of a precipitation phase. In textured Isoperms, lattice stresses are thought to act in conjunction with a filamentary structure superposed on the cubic texture. Dahl and Pfaffenberger confirmed experimentally that the two sorts of Isoperms have different stress configurations. For textured Isoperms, a tensional stress operating in the magnetisation and strip direction causes a drop in flux density, whereas, for the precipitation Isoperms, the effect is a steepening of the flux density curve and thus a worsening of the Isoperm properties. Another explanation of the anisotropy of textured Isoperm and of anisotropy produced by magnetic treatment procedures is, according to Néel[34], an atomic arrangement designated 'orientation superstructure'.

If the direction of the measuring field is normal to that in which Isoperm loops are observed, then rectangular loops are obtained. In the same way a very flat Isoperm loop can be established in Fe–Ni–Co alloys with induced rectangular loops perpendicular to the direction of easiest magnetisability. This was shown by an experiment using a tube of 60 cm length, 4·8 mm

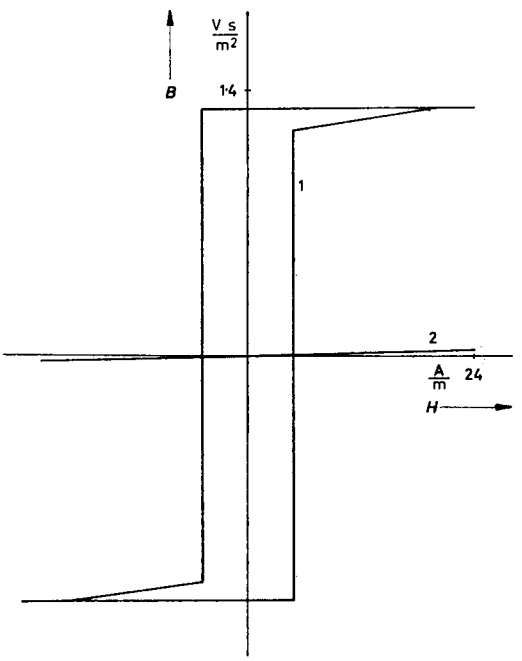



*Figure 5.22. Effect of field direction in the thermomagnetic treatment of the isoperm 30% Fe–25% Co–45% Ni: 1, parallel to the measuring field; 2, perpendicular to the measuring field*[8]

inner diameter, and 0·25 mm wall thickness, composed of an alloy of 30% Fe, 25% Co, and 45% Ni. It was annealed in hydrogen at 1000°C, and then again at 650°C and with a simultaneously applied field parallel to the axis of the tube. The tube was wound like a toroid with a measuring winding. Curve 2 of Figure 5.22 shows the hysteresis loop obtained in this way[8].

The sample was magnetised by a magnetic routine in which a current, flowing in an insulated conductor, passed along the axis of the tube so that a circumferential field was established. Measurement then disclosed a rectangular loop (curve 1). In the first measurement, in which the direction of the applied field was perpendicular to the measuring field, a value of $\mu_m = 1250\mu_0$ was obtained and in the other case, with both fields parallel to each other, $\mu_m$ amounted to 190 000 $\mu_0$.

### 5.4.2 Isoperm loops in ferrites

If the hysteresis loop of a high-permeability Mn–Zn ferrite is recorded, Isoperm loops result in many cases. Figure 5.23 reproduces the hysteresis loop of a Mn–Zn ferrite having $\mu_i = 2700\ \mu_0$, measured at 50 Hz.

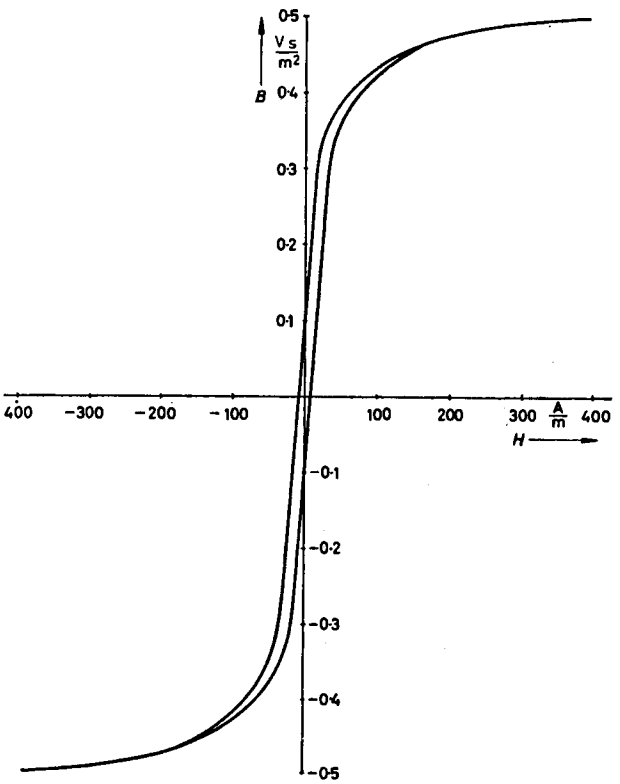



*Figure 5.23. Hysteresis loop of a high-permeability* Mn–Zn *ferrite*[20]

Guillaud and Barbezat[20] had already, in 1950, noted the strikingly narrow lance-like loops of a manganese ferrite whose remanence amounted to about 10% of the peak flux density. The inclination of the loop to the $B$-axis, and with it the permeability, remained constant over a wide range of field intensity.

A high value of initial permeability is characteristic of Isoperm ferrites, especially the Mn–Zn ferrite series. Values up to 2500 $\mu_0$ and more can today be achieved without difficulty. In this they differ from the metallic Isoperms whose $\mu_i$ scarcely exceeds 100 $\mu_0$[7]. Furthermore, these Isoperm ferrites are isotropic, while for metals having Isoperm loops there is generally some anisotropy which manifests itself in measurements in the transverse direction by, for example, the occurrence of rectangular loops. Again, an Isoperm loop can be obtained in ferrites having induced rectangular loops if the measurement is made perpendicular to the direction of easiest magnetisability[39]. Ferrite Perminvars, therefore, fully match metallic Perminvars in this respect.

When examining the losses in high-permeability Mn–Zn ferrites, we have already established that $W_h$ increases as $B^3$ up to a $B$ value of 0·3 V s/m², i.e. grows according to the Rayleigh relation, and only above this value of flux density does it obey the Steinmetz law. Thus, an Isoperm ferrite is characterised by an extended Rayleigh region (see Figure 4.35).

Like Perminvar loops, the Isoperm loops of high-permeability Mn–Zn ferrites are to be found within a particular temperature range (Figure 5.24).

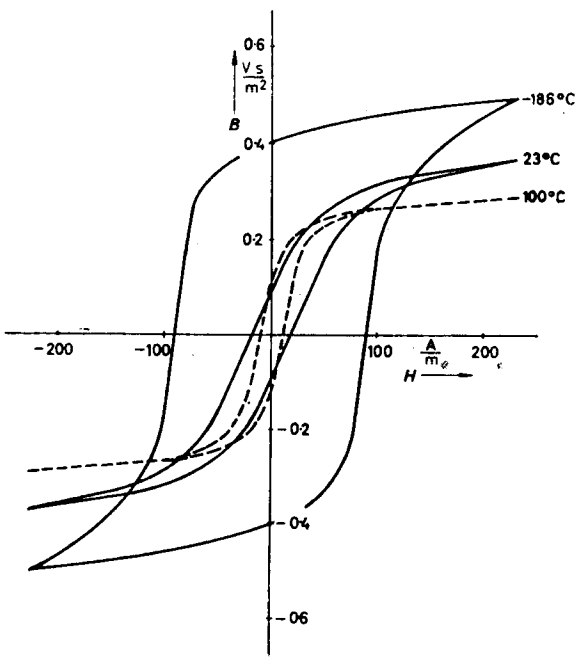



*Figure 5.24. Hysteresis loop of a commercial* Mn–Zn *ferrite which exhibits an Isoperm loop at 23°C (50* Hz*)*

At higher or lower temperatures they pass over into normal loops or into rectangular loops. In contrast to this, Figure 5.25 shows the hysteresis loops of a magnetic-memory or storage ferrite; these retain their shape over a wide temperature range.

The high permeability of spontaneous Isoperm loops suggests that the high constancy of permeability against field strength must stem from different physical causes from those responsible for the permeability of the Perminvars. The Bloch walls of Perminvar ferrites lie in deep narrow energy troughs produced by uniaxial anisotropy. The walls can, therefore, move but little in the 'reversible' regime.

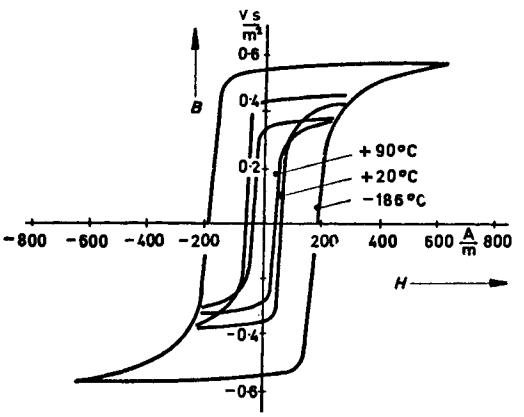



*Figure 5.25. Hysteresis loops of a rectangular ferrite at different temperatures and the same measuring field (50* Hz*)*

In contrast, in high-permeability Mn–Zn ferrites having Isoperm loops, the mobility of the domain walls is very high. Since, however, this could also be the case for a rectangular loop, there must be a further factor: i.e. either there are very many walls or, if fewer, they are very wide. Again, the presence of large closure domains makes the low values of remanence intelligible.

Other influences which likewise produce oblique hysteresis loops, such as magnetisation procedures giving rise to reversible rotation processes or the existence of gaps due to pores or inclusions, are, according to the researches of Kornetzki, Moser, and Röss[27], hardly relevant to the understanding of Isoperm loops in the Mn–Zn ferrites. In a later investigation Röss[39a] was led to assume that the low remanence is caused by internal demagnetisation at the grain boundaries, corresponding to a gap width of about 1 nm.

## REFERENCES

1. ALBERS-SCHOENBERG, E.: Square hysteresis loop ferrites in the system MgO–MnO–$Fe_2O_3$ (Ceram. Bull **35** (7) (1956) 276–279).
2. ARNOLD ENGNG. CO., MARENGO: Properties of Deltamax (Technical Bulletin TC-101 A (1960)).

3. ASSMUS, F., BOLL, R., GANZ, D. and PFEIFER, F.: Über Eisen-Silizium mit Würfeltextur. Magnetische Untersuchungen (Z. Metallkde. **48** (6) (1957) 341–343).
4. ASSMUS, F., DETERT, K. and IBE, G.: Über Eisen-Silizium mit Würfeltexturen. Ausbildung der Textur (Z. Metallkde. **48** (6) (1957) 344–349).
5. BALTZER, P. K.: Magnetostriction in ferrites possessing a square hysteresis loop (Proc. Conf. Magnetism and Magn. Mat. (1955). AIEE-T, **78** 247–252).
6. DE BARR, A. E.: Magnetic anisotropy in cold-reduced electrical sheet steel (Proc. IEE (II) **96** (Oct. 1949) 719–728).
7. DAHL, O. and PFAFFENBERGER, J.: Magnetisches Sonderverhalten kaltgewalzter Eisen-Nickel-Legierungen (Entwicklg. d. Isoperme) (Metallwirtsch. **14** (2) (Jan. 1935) 25–28).
8. DILLINGER, J. F. and BOZORTH, R. M.: Heat treatment of magnetic materials in a magnetic field (Physics **6** (9) (Sept. 1935) 279–284).
9. ECKERT, O.: Ferrites with constricted loops and thermal magnetic treatment (Proc. IEE **104B** (1957) 428–432).
10. EICHBAUM, B. R.: Development of high speed coincident current memory (J. A. P **31** (5) (May 1950) 117 S–118 S).
11. EICHBAUM, B. R.: New ferrites boost computer speeds (Mat. Des. Engng. (May 1959) 136).
11a EICHBAUM, B. R.: Evaluation of new high speed magnetic ferrite system for use in computer components (J. A. P. **30** (4) (Apr. 1959) 49 S–52 S).
12. ELMEN, G. W.: Magnetic properties of perminvar (J. Franklin Inst. **206** (1928) 317–338).
13. ELMEN, G. W.: Magnetic alloys of iron, nickel and cobalt (El. Engng. **54** (12) (Dec. 1935) 1292–1299; (1936) 887–889).
14. FELDTKELLER, R.: Die Formänderung der Hystereseschleife von Transformatorenblech beim magnetischen Kriechen (Z. ang. Phys. **4** (1952) 281–284).
15. GANS, R.: Über das magnetische Verhalten isotroper Ferromagnetika (Ann. Phys. (5) **15** (1932) 28–44).
16. GORTER, E. W. and ESVELDT, C. J.: Square loop ferrites obtained by magnetic annealing of new compositions (Proc. IEE **104 B** (1957) 419–421).
17. GOSS, N. P.: New development in electrolytic strip steels characterized by fine grain structure approaching properties of a single crystal (Trans. Am. Soc. Met. **23** (1935) 311–344).
18. GOULD, H. L. B. and WENNY, D. H.: Supermendur (El. Engng. **76** (Mar. 1957) 208–211).
19. GREIFER, A. P. and CROFT, W. J.: Some crystallographic and magnetic properties of square loop materials in ferrite systems containing copper (J. A. P. **30** (4) (Apr. 1959) 34 S–35 S).
20. GUILLAUD, C. and BARBEZAT, A.: Propriétés magnétiques d'un ferrite de manganèse dans les champ faibles (J. Rech. CNRS **11** (1950) 83–100).
21. HECK, C. and REINER, H.: Rechteckferrite und die Prüfung ihrer Speichereigenschaften (NTZ **11** (1958) 360–369; SEL-Nachr. **6** (1958) 199–208).
22. HECK, C. and VACCARI, G.: Beobachtungen an einem kobalthaltigen Magnesium-Eisenferrit mit Perminvareigenschaften (Z. ang. Phys. **17** (1964) 92–98).
23. HEIDENREICH, R. D., NESBITT, E. A. and BURBANK, R. D.: Magnetic annealing in perminvar, I. Structural origin (J. A. P. **30** (1959) 995–999).
24. V. KIENLIN, A.: Magnetische Werkstoffe mit Perminvareffekt (Z. ang. Phys. **9** (12) (1957) 631–640).
25. KOHLER, D.: Promotion of cubic grain growth in 3% silicon iron by control of annealing atmosphere composition (J. A. P. **31** (5) (May 1960) 408 S–409 S).
26. KORNETZKI, M.: Perminvarferrite (ETZ-A **80** (17) (Sept. 1959) 605–609).
27. KORNETZKI, M.: MOSER, E. and RÖSS, E.: Mangan-Zink-Ferrite mit verschiedenartigen Magnetisierungsschleifen (Z. ang. Phys. **13** (1) (1961) 31–36).

28. KÖSTER, W. and V. KIENLIN, A.: Temperaturabhängigkeit der Suszeptibilität von Eisen-Chrom-Legierungen (Arch. Eisenhüttenw. **27** (Dec. 1956) 787–792).
29. KRÜGER, G.: Das Auftreten von Rechteckschleifen bei Kohlenstoffstahl (Ber. Arbg. Ferrom. (1959); Düsseldorf (1960) 155–167).
30. KÜHLEWEIN, H.: Über die magnetischen Eigenschaften der Perminvare (Wiss. Ver. Siemens-Konzern **10** (2) (1931) 72–88).
31. LEGG, V. E.: Survey of square-loop magnetic materials (IEE Trans. **CP-4** (Dec. 1957) 106–109).
32. MÖBIUS, H. E. and PAWLEK, F.: Die Würfellage als Rekristallisationstextur bei Eisen-Silizium-Legierungen (Arch. Eisenhüttenw. **29** (7) (July 1958) 423–432).
33. NAGASHIMA, T.: Magnetische Eigenschaften von sehr reinem Eisen (Ber. Arbg. Ferrom. (1959). Düsseldorf (1960) 148–154).
34. NÉEL, L.: Les surstructures d'orientation (C. R. **237** (1953) 1613–1616).
35. NESBITT, E. A. and HEIDENREICH, R. D.: Magnetic annealing in perminvar, II. Magnetic properties (J. A. P. **30** (1959) 1000–1003).
36. PAWLEK, F.: Magnetische Werkstoffe. Springer, Berlin/Göttingen/Heidelberg (1952).
37. PFEIFER, F.: Möglichkeiten zur Beeinflussung der magnetischen Eigenschaften von Permalloylegierungen (ETZ-A **81** (1960) 945–949).
38. PREISACH, F.: Untersuchungen über den Barkhausen-Effekt (Ann. Phys. (5) **5** (6) (1929) 737–799).
39. RABL, H.: Ein Resonanzphönomen bei magnetfeldgetemperten Perminvarferriten (Z. ang. Phys. **11** (2) (1959) 57–63).
39a RÖSS, E.: Der Einfluss einer inneren Entmagnetisierung auf die Remanenz bei Mangan-Zink-Ferriten (Z. ang. Phys. **18** (5/6) (1965) 553–556).
40. SCHWEIZERHOF, S.: Ein neuer mehrschichtiger Werkstoff mit geradliniger Magnetisierungskurve (Z. Metallkde. **33** (1941) 175–185).
41. SIX, W., SNOEK, J. L. and BURGERS, W. G.: Een nieu magnetisch materiaal voor de kernen van pupinspoelen (Ingenieur, den Haag, **49** (1934) E 199).
42. SIXTUS, K.: Magnetische Eigenschaften und Nachwirkung bei Nickelzinkferrit mit Kobaltzusatz (Solid-State Physics in Electronics & Telecommunications **3** (1960) 91–103).
43. WALTER, J. L., HIBBARD, W. R., FIEDLER, H. C., GRENOBLE, H. E., PRY, R. H. and FRISCHMANN, P. G.: Magnetic properties of cube textured silicon-iron magnetic sheet (J. A. P. **29** (1958) 363–365).
44. WIJN, H. P. J., GORTER, E. W., ESVELDT, C. J. and GELDERMANS, P.: Bedingungen für eine rechteckige Hystereseschleife bei Ferriten (Phil. T. Rdsch. **16** (1954) 124–134).
45. WIJN, H. P. J., VAN DER HEIDE, H. and FAST, J. F.: Ordering in cobaltferrous ferrites (Proc. IEE **104B** (1957) 412–417).
46. WILLIAMS, H. J., SHERWOOD, R. C., GOERTZ, M. and SCHNETTLER, F. J.: Stressed ferrites having rectangular hysteresis loops (Comm. & Electronics (1953) 531–537).

# 6

# Factors influencing magnetic behaviour

Many technically important properties such as permeability and the loss factor of soft (easily magnetisable) substances or the maximum energy density of permanent magnets are influenced not only by the chemical constitution of the materials in question but also by their structure. Material structure, however, can be modified in a variety of ways. Only the most important of these will be considered here:

1. Impurities and small occlusions in the basic material.
2. The manner in which the end-product is formed.
3. The way the material is worked.

Moreover, the structure of the basic material used and the way it is produced play an important part, as do also the machine operations and other technological processes brought to bear in its preparation. Nevertheless, these are matters which will be disregarded in the following exposition.

The often very important effect of temperature, and of the conditions of measurement, on the values of the magnetic characteristics will be discussed later in connection with the specific properties of the various materials.

## 6.1 THE INFLUENCE OF IMPURITIES AND LOW-LEVEL ADDITIVES

It will have been noted during the review of Perminvar ferrites how tiny additions of cobalt or a slight excess of oxygen can alter the hysteresis loops of particular ferrites.

### 6.1.1 Metallic materials

Elements, small traces of which affect the purity of ribbons and sheets of various materials, are, in the main, the non-metals carbon, sulphur, nitrogen, and oxygen. On the other hand, phosphorus, often a natural contaminant of iron, is largely ineffective magnetically. Carbon, which reaches iron during the smelting process, affects the magnetic properties of alloys more than any other substance.

A substantial fraction of the impurities can be eliminated from iron by means of a suitable heat treatment. This is generally achieved by annealing in an atmosphere of pure hydrogen. This reduction of impurity chiefly affects the maximum permeability. The investigations of Cioffi[14] into annealing at temperatures up to 1475°C will serve as examples. The increase in maximum permeability in relation to a reduction in the content of carbon, oxygen, sulphur, and nitrogen, observed in such an investigation, is set out in Table 6.1[8]: the maximum permeability $\mu_m$ could be raised from 7000 $\mu_0$ to 227 000 $\mu_0$ by an 18 h annealing in hydrogen.

**Table. 6.1** MAXIMUM PERMEABILITY OF ARMCO IRON HEAT-TREATED IN PURE HYDROGEN AT 1475°C AND HAVING VARIOUS DEGREES OF PURITY

| *Duration of annealing* (h) | *Composition* (%) | | | | | | $\mu_m$ ($\mu_0$) |
|---|---|---|---|---|---|---|---|
| | C | S | O | N | Mn | P | |
| 0 | 0·012 | 0·018 | 0·030 | 0·0018 | 0·030 | 0·004 | 7 000 |
| 1 | 0·005 | 0·010 | 0·003 | 0·004 | — | — | 16 000 |
| 3 | 0·005 | 0·006 | 0·003 | 0·003 | — | — | 30 000 |
| 7 | 0·003 | | 0·003 | 0·001 | — | — | 70 000 |
| 18 | 0·005 | 0·003 | 0·003 | 0·001 | 0·028 | 0·004 | 227 000 |

Another structure-sensitive magnitude which, indeed, hardly falls short of permeability in this respect is coercivity. For an ordinary commercial grade of soft iron having about 0·2% impurity, $H_c$ is roughly 80 A/m. This value can be reduced to something like 1 A/m by annealing in hydrogen at 1480°C.

One means of purifying metallic materials much used today is vacuum melting—sometimes followed by a second melting. This procedure eliminates gaseous impurities. Even so, however, other impurities—though possibly only in minute quantities—may enter the melt from the crucible material. In recent times zone refining, developed for the treatment of small samples, has become important. A sample of iron can show an $H_c$, after a second melting, which is similar to that obtainable by the above-mentioned hydrogen annealing. Mager and Hillmann[36] achieved an $H_c$ of 1·6 A/m after a single zone melting.

Those elements whose presence strongly depresses the permeability act so unfavourably because they are almost insoluble in iron. Substances which are soluble only in another material at high temperature but not at room temperature separate-out on cooling; they produce stresses in the crystal lattice and thereby induce hardening. There are many cases in technology where hardening is desired; one need only think of steel or of Duralumin. Because the first permanent magnets were produced by means of mechanical hardening, permanent magnets are even today, often referred to as hard materials in contradistinction to magnetically soft materials. It is well known today that permanent magnets can be made out of mechanically soft materials and that many mechanically hard materials possess 'soft' magnetic

properties. All hardening constituents must be avoided or removed from iron which is to have high permeability and low coercive force. At high temperatures such additives may separate-out from the iron and reach the surface of the sample. The purification process then consists of bathing the sample in hydrogen so that it can combine with the impurities, which can then be removed. Moist hydrogen removes carbon impurities better than dry hydrogen. The so-called intrusion elements are not magnetically deleterious when dissolved in iron. The approximate upper limits of solubility are given in Table 6.2. As long as these limits are not exceeded, the degradation of the material characteristics is not too serious.

**Table 6.2** APPROXIMATE UPPER LIMITS OF SOLUBILITY IN IRON

| *Element* | % |
|---|---|
| Carbon | 0·007 |
| Oxygen | 0·01 |
| Sulphur | 0·02 |
| Nitrogen | 0·001 |
| Phosphorus | 1·0 |

Metallic impurities are less critical than non-metallic impurities on account of their greater solubility in iron. This is shown by the example of copper in iron. Copper is soluble in iron up to about 1%, the exact value of solubility depending on the presence of other constitutents, in particular carbon[24]. Solubility is less in iron containing 4% Si. Figure 6.1 demonstrates

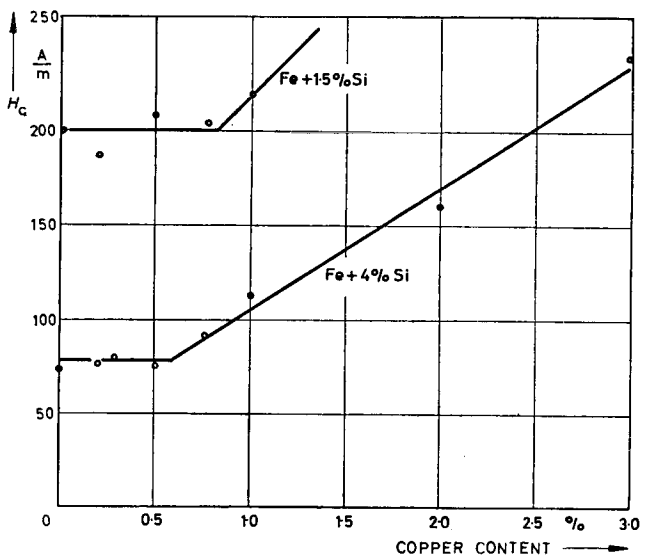



*Figure 6.1. Dependence of coercivity on copper content for a silicon iron*[33]

that the coercivity remains constant until the solubility limit is reached and thereafter rises steeply as more copper is added to the original material[33]. Beyond the solubility limit, metallic intrusions have the same deleterious effect on the structure of the iron as non-metallic intrusions.

Impurities do not necessarily bring about a deterioration of the material. What counts is the nature and the concentration of the contaminants. Sometimes low-level foreign constituents bring useful technical improvement. This is the case, for example, for silicon and aluminium additives in iron or for molybdenum in Fe–Ni alloys. An added element is often advantageous from the standpoint of improved mechanical workability or corrosion resistance. Thus, manganese in iron alloys facilitates rolling and copper increases the corrosion resistance. Natural iron ores always contain some additional substances which may remain after smelting.

Further elements may also enter the metal through the reworking of scrap iron. Whether refining is undertaken or not is an economic question. It is often the only way, for high-quality material, to achieve the desired figures. Pure iron strip can also be made by rolling powder which has received a previous treatment in hydrogen so as largely to remove the carbon[39].

A type of refined iron which is almost free from sulphur, phosphorus, copper, manganese, cobalt, chrome, zinc, and silicon, is carbonyl iron (see page 436). It serves as the base for the manufacture of dust cores, for instance. Apart from this, it is also used with advantage as the starting point either of unalloyed iron or of iron alloys of high purity[44].

Metals may also be purified by electrolytic deposition. Thus electrolytic iron, electrolytic nickel, and electrolytic manganese play an important part in the production of magnetic materials.

### 6.1.2 Oxide materials (ceramics)

The purity of the basic ingredients used in the production of ferrites is likewise of importance when it is a question of achieving high permeability and low loss. Guillaud[21] has shown that for high-quality ferrites it is essential not to exceed a total impurity of 0·02% by weight: for ferrites, also, the various impurities act in different ways.

Let $\mu_t$ be the permeability of an uncontaminated (or substantially uncontaminated) comparison sample and $\mu$ the permeability of a sample 'doped' with additives, then $\mu_t/\mu$ increases with increasing content $\tau$ of foreign substances. Figure 6.2 shows this relation for a Mn–Zn ferrite composed of 52·5% $Fe_2O_3$, 19% ZnO, and 28·5% MnO into which various amounts of potassium were introduced[22]. The two curves are the limit curves for the set of observations.

Guillaud also obtained similar curves for other added elements. All showed the same typical shape: an initially steep linear rise followed by a flat section leading to a limiting or saturation value. The position of the knee of the curve can thus be taken as a criterion for the effect of an additive. For potassium, $\tau$ lies between 0·20% and 0·28%, as may be seen from Figure 6.2.

The alkaline-earth metals are particularly unfavourable to high perme-

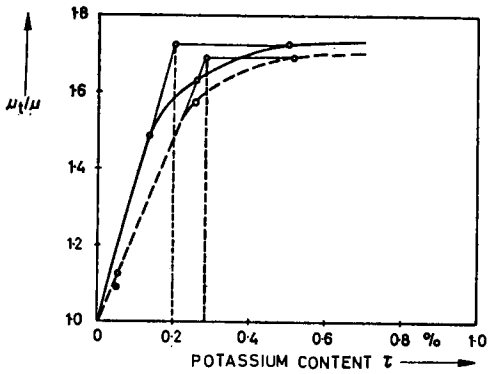



*Figure 6.2. Effect of potassium content τ on the permeability μ of a* Mn–Zn *ferrite ($\mu_t$ = permeability of the potassium-free comparison sample)*[22]

ability values for the technically important Mn–Zn ferrites. The greater the radius of the added ions, the greater the drop in permeability. Figure 6.3 shows the increase in the expression $(\mu_t/\mu)-1$ with ionic radius, according to the investigations of Guillaud[22], for the elements magnesium, calcium, strontium, and barium. It is clear from the curve how much more the large barium ion lowers the permeability than, for example, the smaller ion of magnesium.

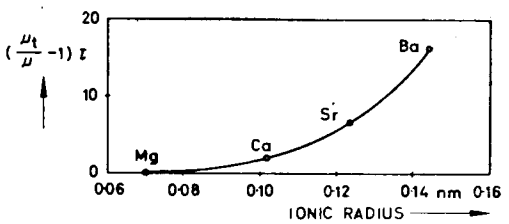



*Figure 6.3. Effect of the ionic radius of additives on the permeability of a* Mn–Zn *ferrite*[22]

The lowering of permeability by intrusions can be explained by supposing that the foreign ions introduce strains into the crystal lattice which increase with increasing diameter of the foreign ion. The drop in permeability is usually associated with an increase in the losses.

Calcium in Mn–Zn ferrites is an exception. For this ferrite a small addition of say 0·2% Ca raises the figure of merit $\mu Q = \mu/\tan\delta$ from about 150 000 to 550 000[23]. Guillaud traces this improvement to the fact that eddy-current losses are reduced by a factor of 10 : 1. Paulus and Guillaud[40], with the help of radioactive calcium ($Ca^{45}$) were able to prove that the calcium accumulated largely at the grain boundaries of the Mn–Zn ferrite, so insulating the individual grains from each other. There is thus no lack of cases where additives act beneficially. The action of lithium, which has a small ionic radius ($r$ = 0·078 nm), may be cited as a case in point. The addition of 0·3 at. % of lithium doubles the permeability of Ni–Zn ferrite.

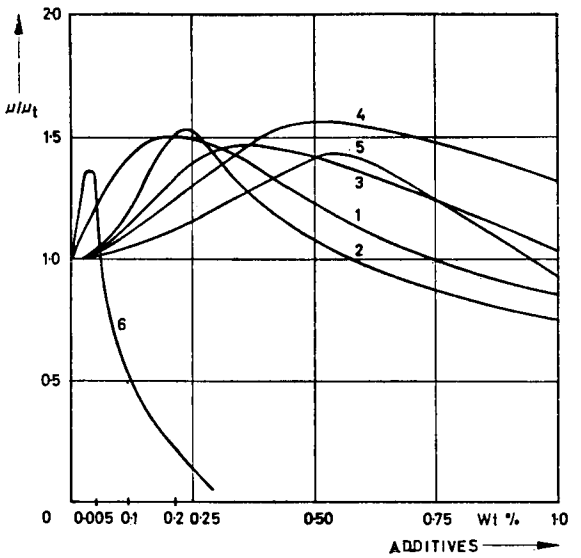



*Figure 6.4. Effect of small additions on the initial permeability of a* Mn–Zn *ferrite; the additives are: 1,* $MoO_3$*; 2,* CuO*; 3,* CdO*; 4, carbon; 5,* $Al_2O_3$*; 6,* $La_2O_3$[34]

Similarly, trifling additions of molybdenum oxide, copper oxide, cadmium oxide, carbon, aluminium oxide, and lanthanum oxide (in carefully controlled proportions) can increase the initial permeability of a pure ferrite by about 50%. Figure 6.4 gives curves of relative permeability $\mu/\mu_t$ against the proportion of additives; this is relative to the initial permeability $\mu_t$, for the pure material, of about $2600\mu_0$. Additives which exceed a critical value reduce the permeability[34]. By introducing a very small amount of trivalent aluminium or chromium, which takes the place of an equivalent amount of trivalent iron, the dependence of permeability on temperature can be improved over a wide temperature range. This is a most useful property of ferrites in many

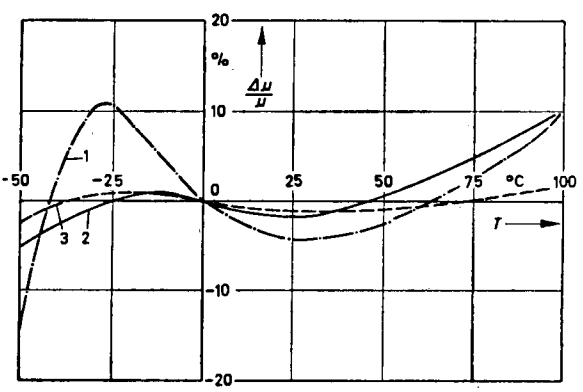



*Figure 6.5. Changes of relative permeability with temperature for a* Mn–Zn *ferrite: 1, without* $Al_2O_3$ *additive; 2, with 5%* $Al_2O_3$*; 3, with 10%* $Al_2O_3$[34]

applications. Figure 6.5 shows the effect of 5% and 10% $Al_2O_3$ for a temperature range of $-50°C$ to $+100°C$, according to the previously mentioned investigations of Lescroël and Pierrot[34]. The permeability maximum observed for the aluminium-free sample (curve 1) at $-25°C$ can be made almost to disappear by such additions; likewise the permeability minimum at $+25°C$ (curve 2 for 5% and curve 3 for 10% $Al_2O_3$).

## 6.2 EFFECT OF THE MANUFACTURING PROCESS

The magnetic characteristics of a magnetic material can be affected by the composition and by the degree of purity of the basic material; also by the way it is prepared. The type of rolling—whether hot or cold, whether with a high or a low deformation factor—and also the particular heat treatment applied have a considerable effect on the magnetic properties of sheet and strip.

The difficulty is that different magnetic properties are affected in different ways. For example, if the alloy known as Mumetal[42] is cold worked and then undergoes a heat treatment, the same initial permeability always results as long as the deformation factor remains less than 60%. But for higher deformation factors, $\mu_i$ becomes less and may reach only 75% of its original value. In contrast, the maximum permeability increases, even at low deformations, reaches a maximum at around 63%, and then falls for higher deformations. Figure 6.6[42] shows this effect.

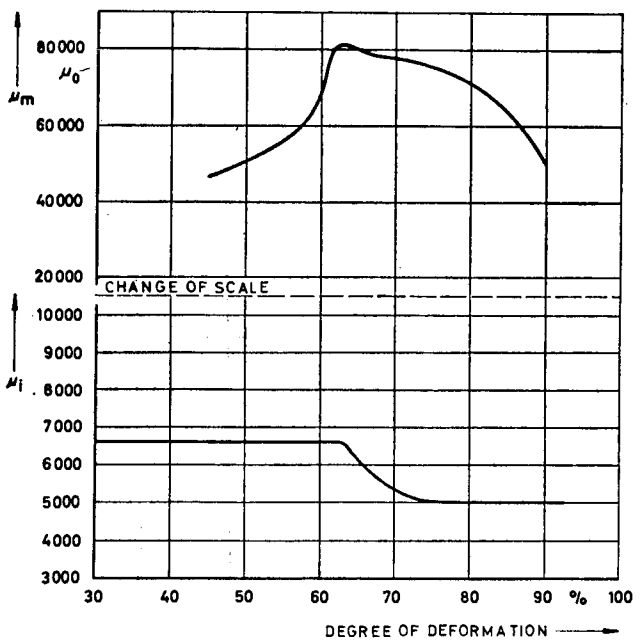



*Figure 6.6. Effect on Mumetal of degree of deformation before heat treatment*[42]

Heat treatment sometimes plays an essential role in permanent-magnet materials. Many magnetic bodies are not produced by melting but by the sintering of powders. The result is determined by the way the sintering process is carried out, i.e. by the temperature and duration of the sinter and by the gaseous atmosphere in which the whole operation takes place.

### 6.2.1 Effect of rolling temperature for sheet and strip

It was stated during the earlier discussion of sheet with cubic texture that the desired cubic structure can be achieved only if the recrystallisation annealing follows a preliminary rolling. The normal dynamo and transformer lamina, an iron alloy of 0·5–4% Si, has for the last 50 years been brought to the required thickness by means of hot rolling. For one thing, hot metals are more easily deformed than cold since they involve less internal friction and since there is less precipitation of substances which are insoluble at room temperature. A sheet material which has been deformed at high temperature is more or less isotropic in its properties.

It is, however, unavoidable that some cooling of the material should take place in the course of rolling, so cold forming occurs to a greater or lesser extent. This can be the cause of anisotropy in the sheet. If a magnetic anisotropy is found in Fe–Si sheet, the direction of easiest magnetisability in general lies along the direction of rolling though in many cases it can make a 45° angle with the rolling (or strip) direction. Where it is desired to take advantage of this preferred direction, the anisotropic directions of each sheet must be determined individually and the sheets classified accordingly.

The texture of cold-rolled recrystallised sheet is clear and strongly marked. Since the cold working of sheet material is more difficult than hot working

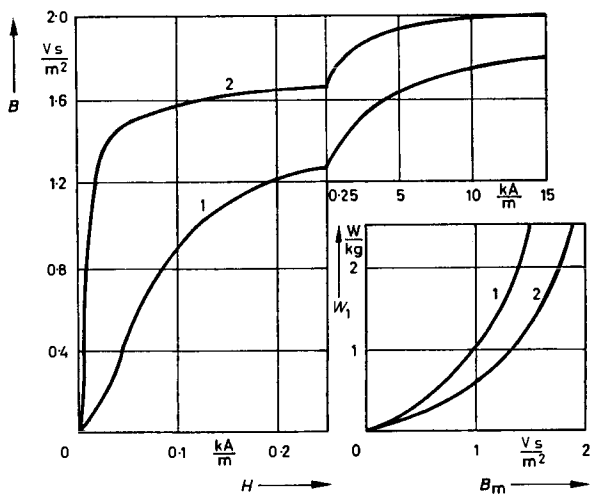



*Figure 6.7. Magnetising and loss curves for* Fe–Si *(sheet thickness, 0·35* mm*; measuring frequency 50* Hz*): 1, English hot-rolled transformer sheet with 4·5%* Si*; 2, American cold-rolled sheet with 3·25%* Si[9]

and demands a purer basic material, a difference in price is only to be expected. Nevertheless, it offers certain advantages: transformer cores made from 'directional' material can often be made smaller in size than those made from isotropic material, so there is a saving in both iron and copper, quite apart from the fact that smaller size is often of value in its own right.

Figure 6.7 shows the comparative effects of cold and hot rolling on an Fe–Si sheet, according to publications by Brailsford *et al.*[9]. Magnetisation curve 1 relates to an English transformer sheet with 4·5% Si, and curve 2 to an American cold-rolled sheet with 3·25% Si. The curve of total losses for 0·35 mm laminae at 50 Hz shows that at 1 V s/m² the losses $W_1$ of the hot-rolled sheet are twice as high as for the cold-rolled material. This is associated with the higher flux density for a given field strength shown by the cold-formed sheet. At 100 A/m it is almost twice as high as for hot-rolled material.

### 6.2.2 Effect of heat treatment on high-permeability materials

Heat treatment has many consequences for rolled metals and alloys: at temperatures from 250°C to 350°C the material recovers from the stresses induced by deformation, a recrystallisation takes place in the middle temperature range (800°–1000°C), and then the formation of grains begins. These stages pass more quickly at high temperatures (1100°–1400°C) and are more complete. If the preliminary degree of deformation was of the correct order, texturing occurs. By reason of the rapid diffusion of substances which occurs at temperatures above 1100°C, impurities may be expelled from the crystal lattices or the grain boundaries and sometimes diffuse to the actual surface of the body, so they are less damaging magnetically. The purification process is most effective for metals near the melting point; thus, operating temperatures between 1400°C and 1480°C have been successfully used for iron, whose melting point is 1528°C.

Figure 6.8 shows the characteristic curve for iron, according to investigations by Wonsowski[53], before and after various annealing routines. The flat

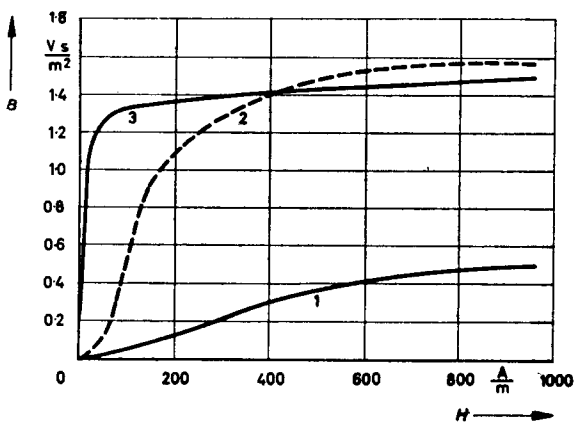



*Figure 6.8. Magnetising curve (or characteristic) of iron: 1, without annealing; 2, annealed at 900°C; 3, after annealing at 1400°C in hydrogen*[53]

curve 1 for iron after rolling is steepened to curve 2 by annealing at 900°C. The flux density at 0·2 kA/m rises from about 0·1 V s/m² to 1·1 V s/m², and after annealing in hydrogen at 1400°C (curve 3) the flux density at the same field strength rises to almost 1·4 V s/m². After annealing, sheet and strip of Fe–Si alloys must be cooled slowly to ambient temperature. Rapid cooling would worsen the permeability.

It is just the other way round for Fe–Ni alloys with 40–90% Ni. For a material so constituted, the highest value of initial permeability is obtained, if the sample is cooled rapidly. Two characteristic curves are shown in Figure 13.7, giving the initial permeability in relation to nickel content. The curves are well separated in the range 40–90% Ni in iron, but come into coincidence in the remaining ranges. Curve 1 gives measured values for a slowly cooled alloy and curve 2 for one which has undergone the 'permalloy routine' (see Section 13.4.6). A rate of cooling of 1500°C/min is best for obtaining a high initial permeability. A $\mu_i$ value of 12 000$\mu_0$ can be achieved in Permalloy with 78% Ni. The maximum permeability is also greatest for this composition and may attain some 100 000$\mu_0$, or even 120 000$\mu_0$ with very rapid cooling (5000°C/min). The coercivity is lower for a quenched sample than for one which is oven cooled, and reaches a minimum of $H_c$ = 4 A/m for an alloy having 78% Ni.

Randall[42] was able to show that not only the annealing temperature but also the rate it was arrived at was important for achieving high permeability and that the heat treatment which was best for achieving a high value of initial permeability might not be so for obtaining the highest value of the maximum permeability.

Heat treatment, however, does not only affect permeability values but may, for example in alloys of the Permalloy type, control the temperature dependence of permeability, the hysteresis coefficient, or the shape of the hysteresis loop[41].

### 6.2.3 Effect of heat treatment on permanent magnets

Permanent-magnet materials, which sometimes show high coercivity produced by precipitation hardening, for example Cu–Ni–Fe alloys, can be treated by the following routine: quenching from high temperatures (1000°–1100°C) to room temperature, and a subsequent heating (tempering) to a medium temperature (500°–600°C). According to the duration of this heat treatment, the coercive force first increases, reaches a maximum, and then falls.

This procedure is exemplified by the alloy consisting of 65% Cu, 20% Ni, and 15% Fe, as is shown in Figure 9.11: the $H_c$ value measured at room temperature attains a maximum if the tempering time lasts 50 h at a temperature of 600°C[5].

Alloys consisting of Cu–Ni–Co, Fe–Al–Ni–Co, Ag–Mn–Al, Fe–Co–Mo, or Ni–Au may be treated in much the same way as this Cu–Ni–Fe alloy. Tempering serves in each case to produce permanent-magnet properties. While heating lowers the coercive force for Fe–Ni and Fe–Si alloys, it increases it for precipitation-hardened magnetic alloys.

A certain type of permanent magnet is improved by an additional annealing in a magnetic field: anisotropy ensues which confers particularly good permanent-magnet qualities in the direction of easiest magnetisability. Following Bozorth[8], Figure 9.28 shows the relation between demagnetising characteristics and direction for an Fe–Al–Ni–Co alloy having 24% Co, 13·5% Ni, 8% Al, 3% Cu and 51·5% Fe.

The material was baked at 1300°C and cooled to room temperature in a magnetic field of 80–240 kA/m. It was tempered at 625°C for several hours to produce the necessary precipitation. The upper curve of Figure 9.28 is measured parallel to the direction of the field, i.e. in the preferred direction. The $(BH)_{max}$ value amounts to 41·6 mW s/cm$^3$. At right angles to this direction, the value is only 5·6 mW s/cm$^3$. Annealing without the presence of the field yields an energy density of 17·6 mW s/cm$^3$ in all directions.

A rise in coercivity can be achieved for barium ferrite powder by heat treatment. Heimke[28] was able to show that the coercivity of a presintered material could be significantly increased if tempering for half an hour at a temperature of 1000°C followed presintering at a temperature between 1160°C and 1370°C. Further heat treatments are discussed in Chapter 9.

### 6.2.4 Effect of sintering on metallic dusts

A special type of heat treatment is that known as sintering. As the name suggests, the object of this heat treatment is to sinter, or fuse together, the granular constituents of a compacted body. High temperatures are desirable for this as for all other diffusion processes.

For materials which are to have high permeability, the permeability value achieved depends on the temperature and duration of the sintering process. The density which the sintered elements attain is crucial. Steinitz[49] was able to show, using toroidal cores of chemically reduced compressed iron dust, that the maximum permeability was raised from $730\mu_0$ to $1500\mu_0$ by an increase in density of from, say, 75% to 93% (1 h sintering at 1150°C). If the sintering was continued for 24 h at 1250°C, then the maximum permeability attained a value of almost $3000\mu_0$.

In general, the coercivity falls as the maximum permeability rises. This drop in coercivity $H_c$ can be seen in Table 6.3, taken from the same work by Steinitz. In the table, $B_r$ stands for the remanence and $B_{3\cdot2}$ for the flux density at 3·2 kA/m.

Dietrich[17], by sintering a sponge iron dust with a particle size of $<40$ μm, achieved a mechanical density of 7·2 g/cm$^3$, an initial permeability of around $300\mu_0$, and a maximum permeability of up to $2200\mu_0$ at $B_r = 1{\cdot}1$ V s/m$^2$ and $H_c = 150$–$170$ A/m. Better magnetic values were mostly obtained for unalloyed iron which had been prepared by the usual processes, namely casting and rolling.

The form and size of the raw powder and its method of production have an effect on the results for the same sintering conditions. These determine the form and disposition of the pores in the sintered body.

There are powders that lend themselves well to sintering—and are then termed 'active' powders—and there are others less suitable. Sometimes the

**Table 6.3** MAGNETIC PROPERTIES OF SINTERED TOROIDAL CORES OF COMPRESSED IRON DUST[49]

| *Sintering* | *Density* (%) | $\mu_m$ ($\mu_0$) | $H_c$ (A/m) | $B_{3\cdot2}$ (V s/m²) | $B_r$ (V s/m²) |
|---|---|---|---|---|---|
| 1 h | 93 | 1 590 | 280 | 1·43 | 1·19 |
| 1 150°C | 89 | 1 600 | 280 | 1·34 | 1·16 |
| | 81 | 700 | 360 | 0·98 | 0·70 |
| | 78 | 700 | 340 | 0·88 | 0·64 |
| | 75 | 730 | 360 | 0·82 | 0·65 |
| 24 h | 90 | 2 500 | 152 | 1·28 | 1·02 |
| 1 250°C | 88·5 | 3 100 | 144 | 1·38 | 1·14 |
| | 83·5 | 2 100 | 160 | 1·13 | 0·93 |
| | 80·5 | 1 900 | 168 | 1·06 | 0·83 |
| | 79 | 2 100 | 160 | 1·02 | 0·85 |
| 24 h | 92 | 3 000 | 112 | 1·35 | 1·08 |
| 1 350°C | 82 | 2 000 | 144 | 1·10 | 0·92 |
| | 77 | 1 800 | 144 | 0·94 | 0·73 |

**Table 6.4** MAGNETIC PROPERTIES OF SINTERED CARBONYL IRON[18]

| | |
|---|---|
| $H_c$(A/m) | 6·4 |
| $\mu_i$ ($\mu_0$) | 3 000 |
| $\mu_m$ ($\mu_0$) | 20 000 |
| $B_r$ (V s/m²) | 0·6 |
| $B_s$ (V s/m²) | 2·2 |

**Table 6.5** MAGNETIC PROPERTIES OF SINTERED CARBONYL Fe–Ni ALLOYS[18]

| | *Slowly cooled* | | *Quenched from 600°C* |
|---|---|---|---|
| | 42% Ni 58% Fe | 50% Ni 50% Fe | 78% Ni 22% Fe |
| $\mu_5$ ($\mu_0$) | 9 500 | 8 200 | 14 700 |
| $\mu_m$ ($\mu_0$) | 33 200 | 56 200 | 85 900 |
| $H_m$ (A/m) | 6·24 | 4·48 | 2·32 |
| $H_c$ (A/m) | 3·04 | 2·96 | 1·68 |

'sintering activity' can be influenced by preliminary treatment of the powder. As a rule, good sintering powders show a greater shrinkage, on pressing, than do the inferior powders. Duftschmid, Schlecht, and Schubardt[18] obtained the magnetic values given in Table 6.4 for sintered carbonyl iron after a sintering and refining treatment in a hydrogen atmosphere. These results show how, by a combination of pure raw materials and a suitable heat treatment, the material constants can be improved. Alloys, also, can be prepared by sintering routines[20, 43]. Duftschmid, Schlecht, and Schubardt[18] obtained the values displayed in Table 6.5 in samples made from carbonyl iron and carbonyl nickel combined in various proportions, after a 4 h baking at 1100°C.

Brossa, Ferro, and Venturello[13] compared vacuum-melted Fe–Ni–Cu alloys, of Permalloy type, to which molybdenum and chromium had been added, with sintered alloys and found that the sintered samples showed improved magnetic properties, in particular an increase in initial permeability. The following example is taken from these investigations. The 'melted' alloy, having a composition of 77% Ni, 14% Fe, 5% Cu, and 4% Mo, had an initial permeability of 12 000$\mu_0$ and a maximum permeability of 185 000$\mu_0$. The sintered alloy of the same composition gave the values $\mu_i = 63\,000\mu_0$ and $\mu_m = 200\,000\mu_0$. The maximum permeability of the sintered alloy appeared at lower field strength than that of the normal commercial product.

The sintering routine has also been successfully followed in the preparation of Fe–Co and Fe–Si alloys. The sintering process offers the following advantages: the composition of an alloy can be determined with great accuracy; many impurities can be avoided, for example the influx of matter from the melting crucible; and the conversion of laboratory methods to those of mass production presents fewer difficulties than with smelted material.

For permanent magnets there are often commercial grounds for preferring a sintering to a casting process, especially for small magnets produced in large numbers. Sintering temperatures of 1300°C and over must be employed in order to achieve high energy densities. An example for Fe–Ni–Al alloys is given in Table 6.6[31].

**Table 6.6** EFFECT OF SINTERING TIME ON THE $(BH)_{max}$ VALUE OF Fe–Ni–Al ALLOYS[31]

| *Sintering time* (h) | $B_r$ (V s/m²) | $H_c$ (kA/m) | $(BH)_{max}$ (mW s/cm³) |
|---|---|---|---|
| 5 | 0·425 | 16 | 2·4 |
| 10 | 0·340 | 24 | 3·0 |
| 15 | 0·375 | 28·8 | 3·6 |
| 20 | 0·375 | 32·8 | 5·8 |

Composition: 25% Ni, 10% Al, 2% $TiH_2$, remainder Fe.
Moulding pressure: 1600 N/mm².
Sintering temperature: 1200°C.
Sintering atmosphere: hydrogen.

The sintering time can be reduced if the sintering temperature is increased. There is, however, a limit to this raising of temperature since, above a certain temperature, changes in composition may occur or the appearance of bubbles which may lead to uneven shrinkage. Thus care must always be taken to find the optimum sintering conditions.

### 6.2.5 Effect of sintering conditions on the preparation of ferrites

Ferrites are usually made by sintering. It is at the sintering temperature that the reactions take place between the carefully mixed raw materials—mostly oxides or carbonates—which lead to ferrite formation.

Heat treatment of ferrites must be examined from a different viewpoint compared with the metals, since oxygen exchange between the ferrite and the furnace atmosphere affects its magnetic, electrical, and mechanical properties.

#### 6.2.5.1 Effect of cooling speed

For most ferrites the speed of cooling is of importance only in so far as interaction with the furnace atmosphere during cooling can be minimised by rapid cooling. It goes without saying that the stresses introduced by rapid cooling will have some effect but these are of secondary importance. There are of course exceptions. Thus there are the peculiarities of the Perminvar ferrites to reckon with and also those cases where the lattice structure is highly temperature dependent.

The effect of cooling speed on the shape of the hysteresis loop of Perminvar ferrites was discussed on page 149. Magnesium ferrites are among those whose lattice structure is determined by the temperature. As the distribution of cations is different at high and at low temperatures—the spinel of formula $MgO \cdot Fe_2O_3$ is only partially inverted—different magnetic values are obtained by cooling from various temperatures. Figure 6.9, following an investigation by Economos[19], shows the steep rise of initial permeability, flux density, and remanence with an increase in the temperature from which the test piece was cooled. The samples were first heated rapidly to 1300°C and cooled to a lower temperature in steps before being quenched in oil at room temperature. The coercive force shows the opposite tendency to the other two parameters: it falls with increasing quenching temperature. This is seen even more clearly in the hysteresis loops shown in Figure 6.10 for the two extreme cases, 600°C and 1200°C.

#### 6.2.5.2 Effect of furnace atmosphere

The various types of ferrites do not behave identically in respect of oven atmosphere: nickel or cobalt ferrites, and ferrites made from the alkaline-earth metals (and mixtures of these with zinc ferrite) are very stable. In contrast, ferrites containing manganese are highly sensitive. This is connected

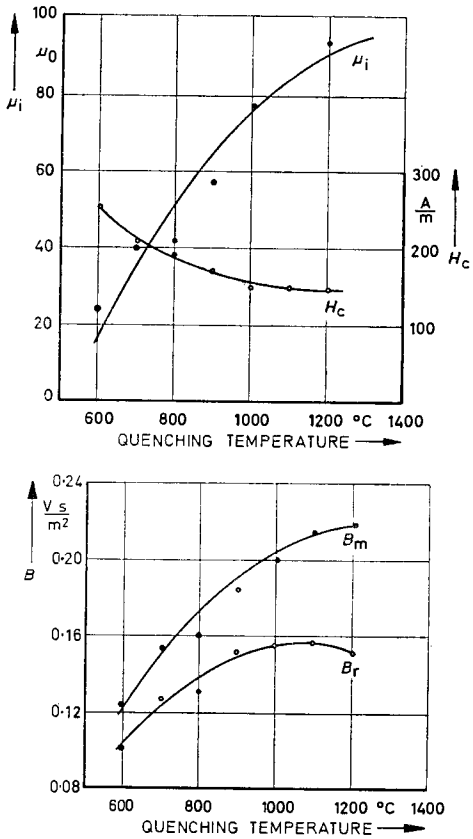



*Figure 6.9. Initial permeability $\mu_i$, coercivity $H_c$, remanence $B_r$, and peak flux density $B_m$ of a magnesium ferrite as a function of quenching temperature*[19]

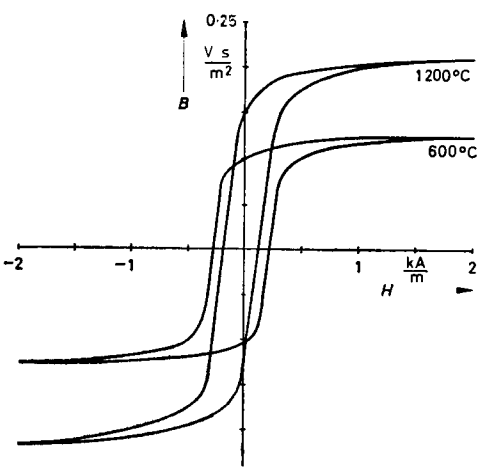



*Figure 6.10. Hysteresis loops of a magnesium ferrite after quenching from 600°C and 1200°C*[19]

with the fact that the manganese ion can assume different valencies, i.e. it may be bivalent, trivalent, or multivalent.

Manganese ferrites have considerable technical importance but are liable to certain manufacturing difficulties: a high sintering temperature should be employed since this leads (if pure raw materials are used) to a dense homogeneous ferrite structure. The difficulty, however, is that high temperatures mean increased interaction with the ambient atmosphere and involve a poor commercial utilisation of the furnace.

Above 600°C manganese oxide gives off oxygen so that, in conjunction with iron oxide, manganese ferrite is formed according to the chemical formula:

$$Mn_2O_3 + 2Fe_2O_3 \rightleftarrows 2Mn\,Fe_2O_3 + O$$

The oxygen yield is, in fact, desirable. However, as the reaction can go in either direction, a re-oxidation takes place on cooling and trivalent manganese is once more formed.

Krüll[32] and also Moore, Ellis, and Selwood[38] carried out fundamental investigations into the presence of the various manganese oxides, $MnO_2$, $Mn_2O_3$, and $Mn_3O_4$, and the conditions of equilibrium for various temperatures. It became clear that the equilibrium established depended, among other things, on the route followed in the preparation of the particular manganese oxide.

Provision of a neutral atmosphere, for example the introduction of pure nitrogen into the oven to secure an oxygen-free atmosphere, was not enough to prevent re-oxidation during the making of the ferrite: this was liable to promote the dissociation of the other oxide components—the iron oxide $Fe_2O_3$ and the zinc oxide ZnO—which is certainly undesirable.

A further circumstance has to be reckoned with: manganese (II) oxide and manganese (III) oxide are fairly soluble in iron oxide. Therefore, $Mn_2O_3$ may be precipitated out of the spinel phase owing to a lowering of the partial pressure of the oxygen[37]. It is thus understandable, that, by reason of these facts, the development of Mn–Zn ferrites was at first most difficult to reproduce consistently, a fact which Snoek[48] had already traced to the re-oxidation of the manganese during cooling. Repurified nitrogen, with 0·01–0·1% $O_2$ was used as atmosphere in the investigations of Toropow *et al.*[50] The oven temperature, however, was only taken to 1250°C so that no initial permeability higher than $1000\mu_0$ was attainable. Scholts and Piskarew[46] had by then reached values of $2000\mu_0$.

Heck and Weber[26, 27] were able to show that values of initial permeability of over $4000\mu_0$ could be reached for a ferrite of composition 51·8% $Fe_2O_3$, 24% MnO, and 24·2% ZnO after annealing at 1370°C. The values fell below this if either higher or lower temperatures were used. The example of a series of measurements plotted in Figure 6.11 demonstrates the connection between sintering temperature and permeability. The permeability maximum coincides more or less with the position of optimum loss factor $(\tan\delta)/\mu_i$.

Heister[30] derived a similar relation for the ferrites which he investigated: maximum permeability occurs at around 1360°C and the minimum loss factor around 1270°C. The position of the optima for permeability and loss and the best obtainable values depend to a large extent, apart from composi-

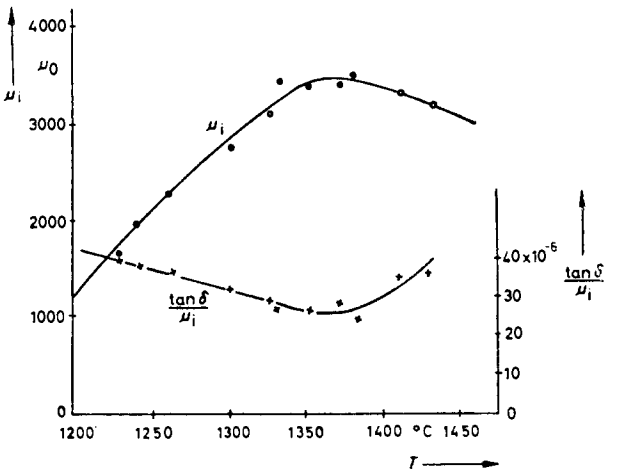



*Figure 6.11. Dependence on sintering temperature of initial permeability $\mu_i$ and referred loss factor $(\tan\delta)/\mu_i$, for a* Mn–Zn *ferrite*[27]

tion and annealing temperature, on the annealing time and on the particular oven conditions.

Three stages are to be recognised in the sintering of ferrites:

1. The green pressing is heated to the sintering temperature; during this heating the substances added to facilitate pressing, also gases and moisture, are driven off and the solid-state reactions begin.
2. The reaction and crystallisation processes of true sintering take place.
3. The piece is cooled to room temperature.

The oven atmosphere must be correct for each of these stages. However, the greatest effect is that due to the oxygen content during cooling. This may be illustrated by a few examples: Figure 6.12 shows the course of the temperature changes during the sintering of a Mn–Zn ferrite having 51·8% $Fe_2O_3$, 24% MnO, and 24·2% ZnO.

Curve 1 displays the optimum annealing conditions, namely heating during 5 h to 1380°C; baking at this temperature for 6 h in air; 'rinsing' with nitrogen just before switching off the furnace; and then maintaining a nitrogen flow during the whole of the cooling period—it lasted in this case for 14 h. The measured value of initial permeability was then found to be $\mu_i = 4470\mu_0$. The quantity of nitrogen used, namely 50 l/h, was adjusted to suit the volume of the oven used. This quantity is very critical: if the nitrogen 'rinse' after the air-baking (which in this case was somewhat prolonged) is reduced to half (curve 2), then the initial permeability of the test piece is only about one half as great, namely $\mu_i = 2700\mu_0$. Finally, curve 3 shows again the same temperature excursions as curve 1 but with a somewhat later (and then reduced) flushing with nitrogen. This further worsened the result: $\mu_i$ amounted now to only 1850 $\mu_0$.

The cooling conditions, then, must be carefully controlled if a high value of permeability is to be obtained. Cooling rate and oxygen concentration

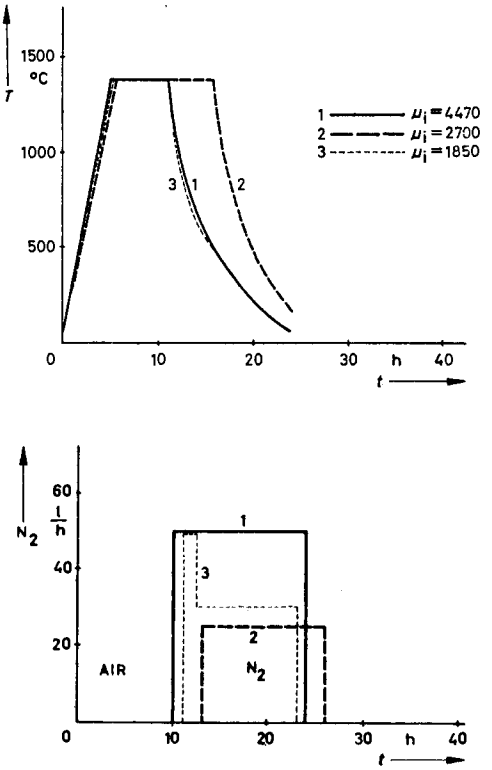



*Figure 6.12. Sintering of a* Mn–Zn *ferrite showing temperature changes and flow of nitrogen*[27]

in the atmosphere must be adapted to the composition of the ferrite and the particulars of the furnace, i.e. to the internal volume and to the mass of ferrite being treated. The effect of the annealing atmosphere depends on the mechanical state of the ferrite; very porous samples are significantly more sensitive than the more densely compacted. To achieve high density, samples must be annealed at high temperature or treated with suitable fluxes (the so-called mineralisers). Silicon oxide and boron oxide have proved useful mineralisers. If, for example, an ordinary Mn–Zn ferrite is heated in air for 1 h at 400°C, the permeability will fall to 10% of its original value. For a ferrite with 1% $SiO_2$ no fall in permeability is found as a result of this treatment (Figure 6.13); it sets in only above 450°C[34].

Another proposal for reducing the effect of the ambient atmosphere during cooling is to produce an enamel-like layer on the surface of the ferrite so as to inhibit gas interchange during cooling[47].

To obtain very low hysteresis and eddy-current losses, Lescroël and Pierrot[34] heat treated their Mn–Zn ferrites in the following way: heating in a nitrogen atmosphere for 4 h up to 1250°C; baking for 4 h at this temperature in a mixture of nitrogen and oxygen; and finally cooling in nitrogen. Prolonging the baking time increases both saturation and permeability values;

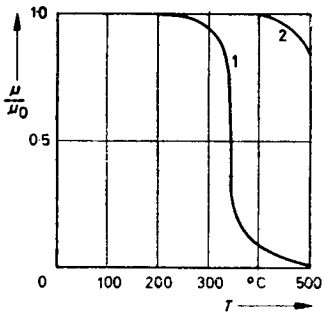



*Figure 6.13. Permeability changes in a specimen after heating for 1* h *at various temperatures: 1,* Mn–Zn *ferrite; 2,* Mn–Zn *ferrite with 1%* $SiO_2$[34]

chemical reaction is more complete and disaccommodation could be lowered if there were an excess of $Fe_2O_3$ in the mixture.

It is clear that the sintering conditions are of first importance, and very critical if the sample has a large superficial area. Absorption of oxygen through the surface has, in this case, a greater importance than for cores whose volume is large in relation to the surface. By abrading in successive steps the surface of a toroidal core of size 30 mm×18 mm×6 mm, made out of Mn–Zn ferrite and slowly cooled in nitrogen with a 2% addition of oxygen, one can perceive (Figure 6.14) the change of permeability with the

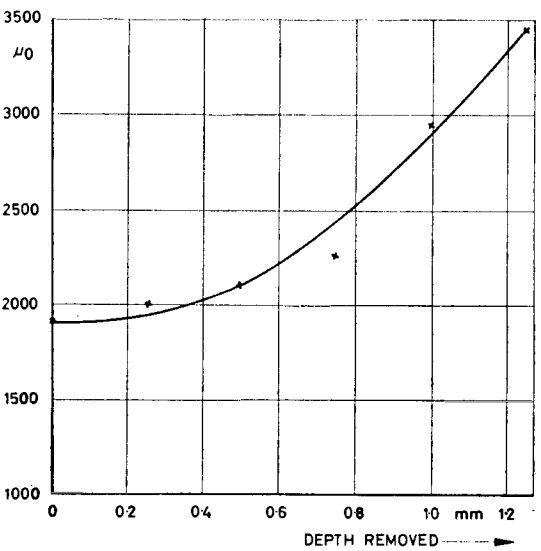



*Figure 6.14. Surface effect of annealing on the initial permeability of a* Mn–Zn *ferrite cooled in an atmosphere containing oxygen*[27]

corresponding re-oxidation of the core. In this experiment the outer layers had only a low permeability since the permeability of the core before removal of the outer skin (produced by heat treatment) was $\mu_i = 1900\mu_0$ while, for the body of the core after the abrasion, the permeability amounted to $\mu_i = 3450\mu_0$.

The manufacture of very small ferrite cores such as those used for magnetic storage demands much greater care than the making of larger cores.

### 6.2.6 Shape effects

The measured magnetic values of a sample can be determined by its form and structure and by its dimensions.

#### 6.2.6.1 Effect of sheet thickness

A marked connection between the thickness of a sheet or strip and its magnetic properties can often be observed, as a result of the way it has been made. This is particularly true of high-permeability materials. Thus Randall[42] found that for ordinary commercial Mumetal the initial permeability was maximum for a thickness of about 0·3 mm. Figure 6.15 shows the relation between permeability and thickness of sheet. The measuring frequency was 50 Hz.

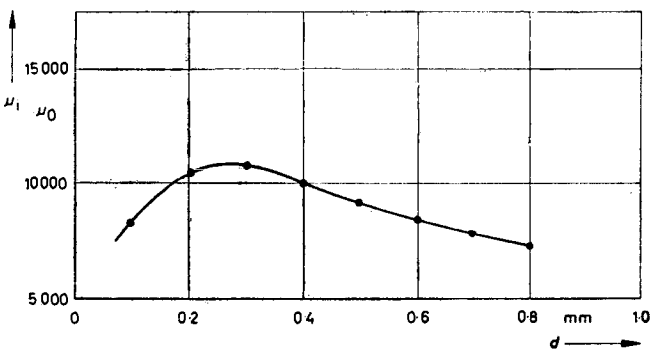



*Figure 6.15. Relation between initial permeability and sheet thickness for Mumetal*[42]

**Table 6.7** PROPERTIES OF EXTREMELY THIN STRIP WITH RECTANGULAR-TYPE LOOPS[6]

| | 50% Fe–50% Ni | | | | | *Permalloy* | | | | |
|---|---|---|---|---|---|---|---|---|---|---|
| Strip thickness (μm) | 30 | 15 | 10 | 6 | 3 | 30 | 15 | 10 | 6 | 3 |
| Coercivity (A/m) | 8 | 16 | 20 | 24 | 32 | 1·6 | 2·0 | 2·4 | 3·2 | 5·6 |
| Remanence ratio | 0·97 | 0·96 | 0·95 | 0·95 | 0·90 | 0·92 | 0·90 | 0·90 | 0·92 | 0·94 |
| Saturation flux density ($V\ s/m^2$) | 1·46 | | | | | 0·8 | | | | |
| Curie temperature (°C) | 470 | | | | | 410 | | | | |
| Specific electrical resistance (μΩ cm) | 45 | | | | | 60 | | | | |

High permeabilities are, therefore, not to be expected for just any thickness one might choose. Again, coercivity and remanence ratios depend on thickness, especially for very thin strip. Table 6.7 taken from an investigation by Boll[6], shows that for strip made of Fe–Ni or of Permalloy-type alloy, having rectangular hysteresis loops, the (static) coercivity increases with falling thickness.

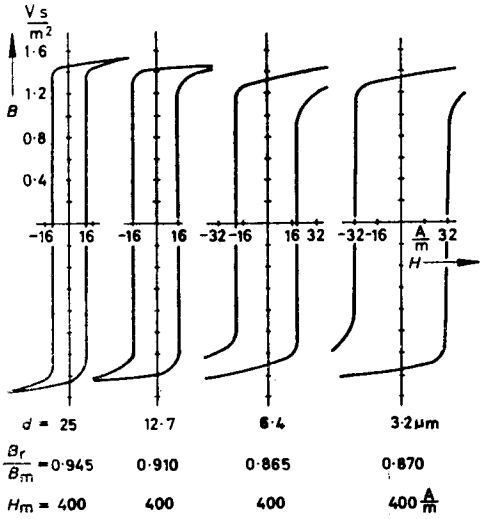



*Figure 6.16. Static hysteresis loops of grain-oriented* Fe–Ni *with 48%* Ni[35]

The observed fall in remanence and rise in coercivity which accompany reduced sheet thickness can also be deduced from the experiments of Littmann[35] on grain-oriented 52% Fe–48% Ni. This is shown in Figure 6.16. He found an even clearer relation between thickness and coercivity for a grain-oriented Fe–Si strip with 3% Si than for his Fe–Ni alloy.

### 6.2.6.2 Effect of core dimensions

If strip-wound cores are made up from strip having optimum magnetic properties, it may well be found that not all core sizes yield identical results.

The results depend largely on the cross-sectional ratio of the cores. Field intensities in toroidal cores fall from the inside outwards according to a hyperbolic function, but this applies to flux densities only in particular conditions. The distribution of permeability in a thick-walled core is, therefore, inhomogeneous[2]. Thick-walled toroidal cores thus show a measured mean of permeability, particularly below the maximum, greater than for thin-walled cores. The difference disappears above the maximum. The dimensional ratio, however, does not affect the watt-loss[2]. To keep the variation small, it is advisable to choose a ratio of outer diameter to inner diameter not greater than 1·5. This ratio must be kept less than 1·4 for materials which show rectangular hysteresis loops[2], otherwise unacceptably large

distortions of loop shape may occur. It must also be borne in mind that air-gaps occur even in strip-wound cores and the magnetising field and the induced flux must bridge these gaps[1]. Because of this, the flux distribution throughout the material may become non-uniform. On the other hand, an air-gap in a magnetic circuit becomes more effective the shorter the path in the ferromagnetic substance compared with the gap length. Thus, identical gap lengths behave quite differently in small and in large cores, whether they are strip-wound or laminated.

A few figures taken from some work by Boll[6] may serve to make this clear. Suppose laminated cores to EE 20 of DIN 41 302 are made from a material having a toroidal permeability $\mu_5 = 50\,000\mu_0$; then the permeability will fall to around $\mu_5' = 12\,000\mu_0$, i.e. to about a quarter. In the even smaller cores to EE 10 of the same standard, $\mu_5'$ is only $7000\mu_0$ (Figure 6.17). The

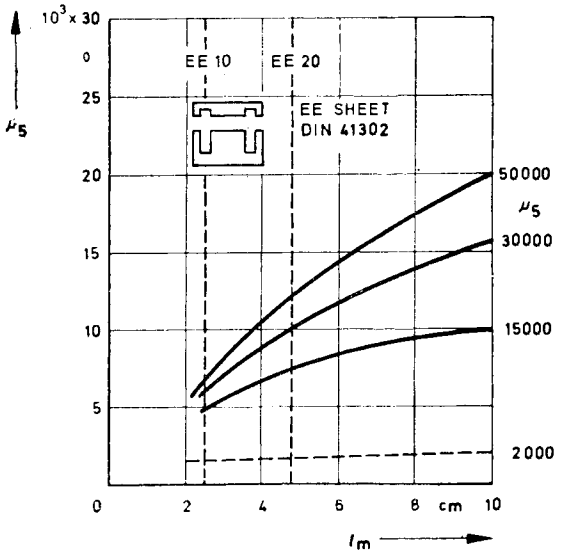



*Figure 6.17. Dependence of effective permeability on length of iron path for EE cores of various types of sheet*[6]

falling-off in $\mu$ with reduction in core dimensions is less steep for lower-permeability materials, but then the gapped permeability always remains higher for the high-permeability than for the low-permeability material. Brenner and Pfeifer[11, 12] have carried out studies and made calculations on the effect of the shape of laminations on the initial permeability, using various shapes specified in DIN 41 302, as well as some non-standard ones. Figure 6.18 shows some examples taken from these investigations. The gapped permeability $\mu_e$ is plotted against the magnetic path length $l_m$; measurements were at low field strength. The original material had a sheet thickness of 0·35 mm and an initial permeability of $30\,000\mu_0$. The thickness of the non-magnetic layer between the laminations amounted to $l_1 = 20$ nm. The laminations used (EE, EI, and E of the Standard) are drawn at the side of the graph.

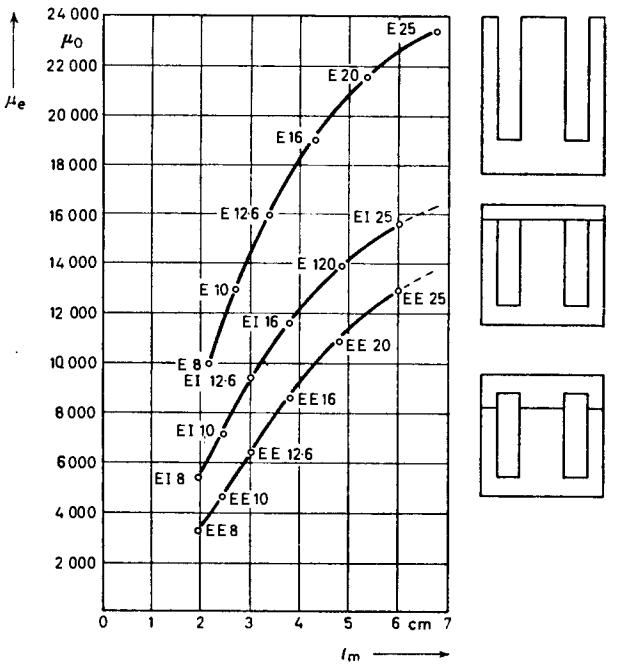



*Figure 6.18. Effective permeability $\mu_e$ of iron as a function of path length for various shapes of stampings ($\mu_i$ for the material, 30 000$\mu_0$; sheet thickness, 0·35* mm; *non-magnetic surface layer $l_1$ = 20* nm*)*[11]

The performance of a coil whose volume has been fixed by the designer can be influenced by the core shape. In the struggle to miniaturise components, even relatively small improvements sometimes assume considerable importance. Thus, for example[25], for materials having the same permeability, a pot core scores over an EE core (see Figure 13.59, page 463).

It is well known that the figures normally quoted in manufacturers' catalogues do not hold for very small or for very large magnets. The German Standard DIN 17 410[17a] allows for this in that specified values are limited to test pieces between 2 cm³ and 200 cm³ and no dimension of the magnet should be less than 8 mm. These limitations are introduced in acknowledgement of present-day manufacturing difficulties, but they also take account of the difficulties associated with the magnetic measurement of small samples.

## 6.3 EFFECTS DUE TO MECHANICAL WORKING

Magnetic materials must be brought, either by the supplier or by the user, into the shapes directly usable in the final product—coil, transformer, transducer, or magnet system—and so they are presented as stampings, pressings, punchings, etc. Strip cores are wound, laminated cores stacked, and suitable windings provided; they may be moulded, mounted, or impregnated. As all these processes may not be without effect on the behaviour of the material,

they must be so carried out as to introduce the least possible change. Where such changes (mostly deleterious) are unavoidable, their effects must be allowed for in the design of the relevant component.

### 6.3.1 Effect of winding strip cores

In the manufacture of strip-wound cores, a strip, cropped to the desired width, is wound-off from a larger roll to form small toroids. This operation introduces elastic—and sometimes plastic—deformation, with a consequent drop in permeability. The extent of this drop depends on the relative diameters of roll and toroid, the thickness of the strip, and the previous treatment of the material.

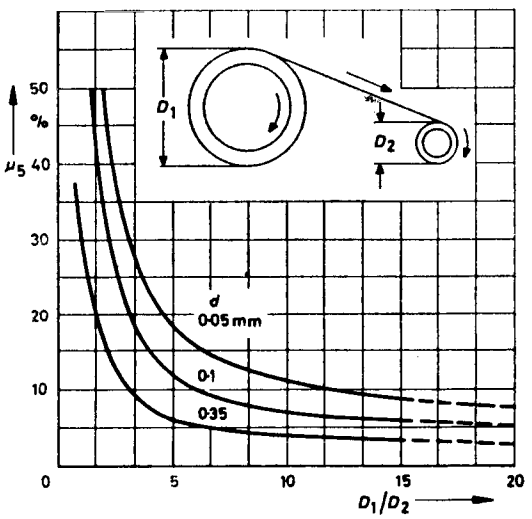



*Figure 6.19. Permeability $\mu_5$ of strip-wound cores of various strip thicknesses d; effect of respooling*

For example, strips of Permalloy C of thickness 0·05 mm, 0·1 mm, and 0·35 mm were wound-off from an original coil of diameter $D_1$ ($\doteq$230 mm) and formed into toroids of small diameter $D_2$[51]. Figure 6.19 shows the relative drop in permeability with increasing value of the ratio $D_1/D_2$. Even when the strips were wound to half the original diameter, $\mu_5$ fell for the 0·05 mm strip to one-half its value; for the 0·1 mm strip it fell to one-third; and for the 0·35 mm strip it fell to one-sixth of the initial value. If $D_1/D_2$ is 10, the corresponding figures are 11%, 7%, and 4% of the initial value.

### 6.3.2 Effect of stacking

Most 'sheet cores' in the electrical industry, whether in heavy-current or light-current engineering, consist of stacks of laminations. They may take the form of laminae of U, E, or I shapes following DIN 41 302 or may have

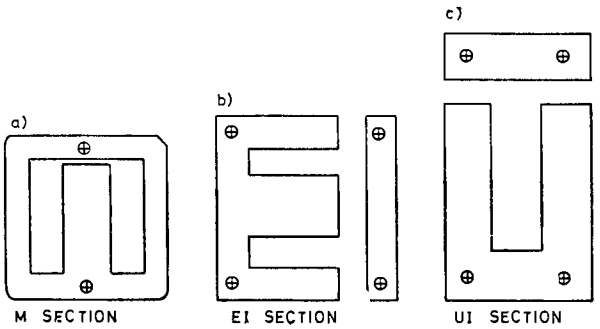



*Figure 6.20. Standardised shapes of laminations from DIN 41 302*

special shapes and sizes. Much use is made in light-current engineering of the so-called M shape (Figure 6.20). While U, E, and I sections can generally be stacked without harm, difficulties sometimes arise with M types, especially with lightly annealed relatively thick sheet. The middle tongue of the lamination has to be bent to thread it into the coil and must subsequently take up its original position.

Assmus[4] conducted an investigation into the drop in permeability for a particular stack of M laminations. Figure 6.21, taken from this investigation, provides the following information. In laminae of 42 mm edge (M42-type) made of Mumetal (77% Ni, 5% Cu, 2% Cr, and 16% Fe), the fall of the permeability $\mu_5$ with increase in the tongue deflection $a$ is greater the thicker the base material. For 9 mm deflection, the permeability of the 0·1 mm sheet was scarcely altered (upper curve), whereas it fell almost to half its value for the 0·35 mm material. The height of the stack was constant for laminations up to 0·21 mm and bending less than 9 mm (bottom broken curve). Thicker

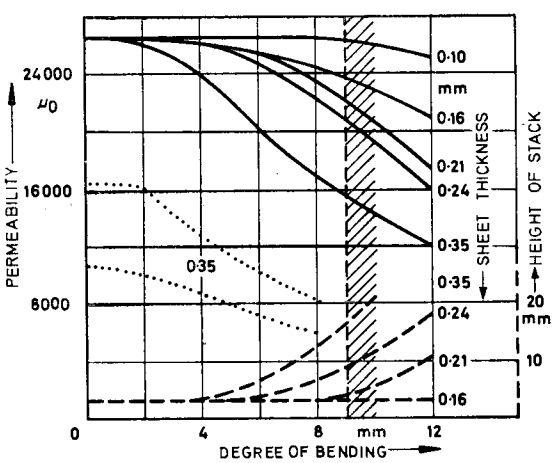



*Figure 6.21. Effect of tongue flexibility on permeability (solid curve) and on height of stack (broken curve) for M42-type Mumetal cores of various sheet thicknesses; dotted curves show the fall of permeability for 0·35* mm *laminations of lower initial permeability*[4]

laminations were plastically deformed by this amount of bending and would not return to the undeflected position. The (uncompressed) height of the stack had increased to twice its value for 0·24 mm sheet. The 9 mm deflection necessitated by the stacking of M42 cores is indicated by hatching. It appears from this experiment that M42 cores cannot be made from laminations of greater thickness than 0·16 mm without loss of quality.

Two dotted curves are drawn in the middle portion of Figure 6.21: they display the permeability drop for 0·35 mm laminations made from lower-permeability material. If the original permeability of the 0·35 mm laminations be taken as unity for each of the three curves, then these curves can almost be superposed.

Assmus found, quite generally, that the relation between the permissible deflection (for no plastic deformation) $a$, the core length $l$, and the thickness of lamination $d$, conformed to the equation

$$a = pl^2/d$$

The proportionality factor $p = 8\text{–}9 \times 10^{-4}$ is constant for laminations in the M series. Upper limits of thickness recommended for the various sizes of M laminations are shown in Table 6.8.

**Table 6.8** HIGHEST PERMISSIBLE THICKNESS OF LAMINATIONS FOR THE M SERIES OF STAMPINGS TO DIN 41 302[4]

| *Shape* | *Lamination thickness* (mm) |
|---|---|
| M20 | 0·08 |
| M30 | 0·10 |
| M42 | 0·15 |
| M55 | 0·20 |
| M65 | 0·25 |
| M74 | 0·30 |
| M85 | 0·35 |
| M102 | 0·35 |

The permeability of a stack is not only sensitive to plastic deformation; strains which remain in the elastic range can also prejudice the value. Elastic strains must, however, occur when the laminations are finally compressed into a tight stack. In particular, stampings of hot-rolled dynamo sheet, always somewhat wavy, may show increased losses under pressure. According to measurements made by Czerlinsky[16], $W_1$ rises with specific pressure $P$ in the following way:

$P = 0$ N/cm$^2$ $\quad W_1 = 2{\cdot}97$ W/kg
$P = 50$ N/cm$^2$ $\quad W_1 = 3{\cdot}06$ W/kg
$P = 100$ N/cm$^2$ $\quad W_1 = 3{\cdot}14$ W/kg
$P = 150$ N/cm$^2$ $\quad W_1 = 3{\cdot}21$ W/kg

Even if the individual laminations are flat, so that bending moments are eliminated, an unfavourable action takes place. For example, it has been observed that applying a specific loading of 40 N/mm² to Mumetal laminations, normal to the surface, lowers the initial permeability to half[51] (Figure 6.22). Stacks should therefore not be compressed more than is absolutely necessary.

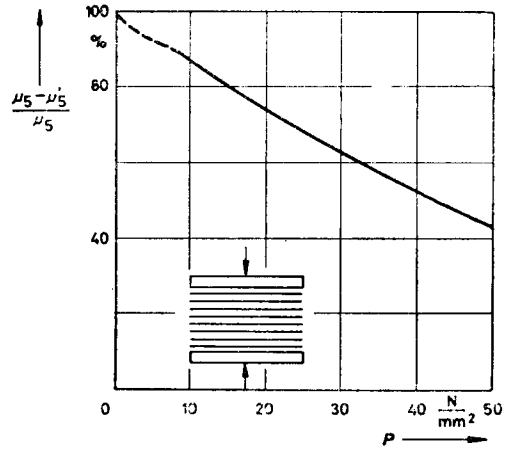



*Figure 6.22. Effect on permeability of stacking pressure for plane, parallel Mumetal sheets*[51]

Losses in strips of grain-oriented Fe–Si due to elastic bending increase, as does also the coercivity, as the bending radius is decreased. At the same time maximum permeability and remanence are reduced. The hysteresis loop thus becomes less rectangular. This was established by Cole[15] by measurements made on 'Epstein-strip' in the direction of rolling. Table 6.9 is taken from these investigations.

**Table 6.9** DEPENDENCE OF MAGNETIC PROPERTIES ON THE DEGREE OF BENDING OF GRAIN-ORIENTED Fe–Si SHEET[15]

| *Radius* (cm) | $\mu_m$ ($\mu_0$) | $H_c$ (A/m) | $B_r$ (V s/m²) | $W_{1\cdot5}$ (W/kg) |
|---|---|---|---|---|
| ∞ | 104 000 | 5·3 | 1·39 | 0·84 |
| 325 | 85 000 | 6·2 | 1·30 | 0·96 |
| 170 | 62 000 | 7·7 | 1·11 | 1·09 |
| 110 | 47 000 | 8·6 | 0·96 | 1·16 |
| 37·5 | 24 000 | 9·9 | 0·58 | — |
| 20 | 18 000 | 10·2 | 5·1 | — |

A further harmful effect often occurs in the assembly of transformer cores: in order to tighten the stack, screw-holes are often provided through which suitable bolts can be threaded. This, however, involves a reduction in the effective cross-section of the core.

Bolt-holes and the harmful effect of overtight clamping may be avoided if the laminations are stuck together with adhesive. Good results are obtained in this way, particularly for small and medium-sized transformers. The losses in transformers up to 5000 kV A can be reduced by 20% and more by this technique[10].

### 6.3.3 Effect of resin encapsulation

In many cases it has become normal practice to embed components, or groups of components, in resin in order to shield them from environmental chemical influences. Such encapsulation can have a considerable effect on the permeability of magnetic materials if the resin, in setting, induces compressive stress in the material. Resins which shrink greatly on setting or which harden unevenly should be avoided if possible. It is particularly important to prevent the resin penetrating the space between laminations. Where a material is required to have a hysteresis loop of predetermined shape, for example rectangular, the effects caused by inappropriate encapsulation techniques are easily detected. Figure 6.23 shows the hysteresis loop of a laminated core having a high remanence ratio (curve 1). After impregnation in a plastic resin, the remanence falls off steeply—the more steeply the more the core has been cooled. Curve 2 is the characteristic obtained at 60°C, and curve 3 at 25°C.

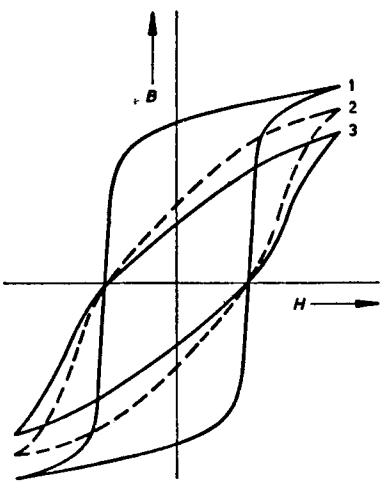



*Figure 6.23. Effect of encapsulation on a laminated core having a rectangular hysteresis loop: 1, before encapsulation; 2, encapsulated in plastic material and measured at 60°C; 3, encapsulated in plastic material measured at 25°C*

The loop will become steeper under the influence of external pressure if the material shows negative magnetostriction (see page 137). Figure 6.24 shows the effect produced, according to Williams *et al.*[52], by a strongly contracting resin called 'Selectron 5003' for a Ni–Zn ferrite of composition roughly $Ni_{0·3}Zn_{0·7}Fe_2O_4$. From Figure 6.25 one can appreciate the significant rise in

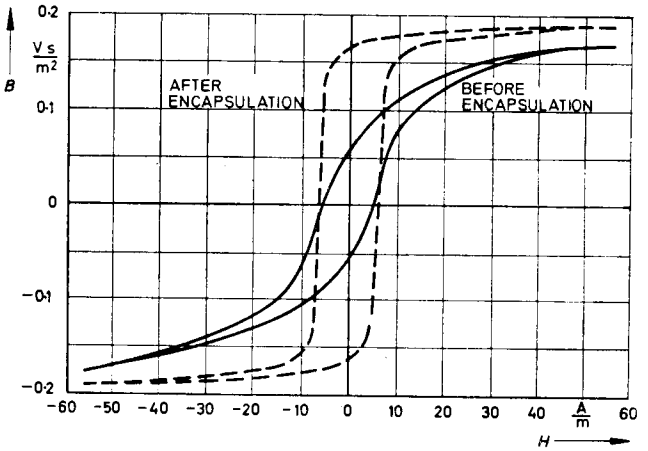



*Figure 6.24. Effect on a* Ni–Zn *ferrite of encapsulation in the plastic Selectron*[52]

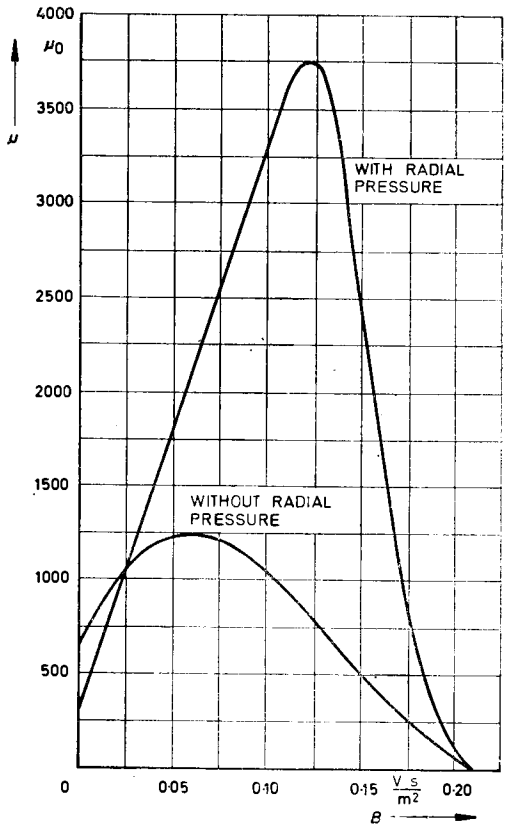



*Figure 6.25. Dependence of flux density on radial pressure for a* Ni–Zn *ferrite core*[52]

maximum permeability produced by radial pressure in the same material[52]. On the other hand, this type of stress reduces the initial permeability.

The particular resin mentioned, Selectron, was deliberately chosen in this case because of its high shrinkage (about 8%) in order to achieve a hysteresis loop of the greatest possible rectangularity. In general, however, the practical engineer will want to avoid shrinkage effects[7].

These can be minimised by using resins to which have been added inorganic substances such as silicon dioxide, powdered quartz, or glass fibre. Another possibility is to interpose, between core spool and encapsulating substance, a layer of material such as foam plastic or rubber, capable of absorbing the shrinkage stress. It is also possible to avoid shrinkage pressure altogether by, for example, using a compensating heating process to offset the setting process[29].

Another point in connection with the encapsulation of magnetic materials which should not be overlooked is that the process is often associated with a temperature rise in the material. A 'heat shock', however, can often promote disaccommodation in many substances, such as Mn–Zn ferrite, so some time must elapse after encapsulation before the component is used.

### 6.4 AMBIENT EFFECTS

Unprotected magnetic materials are exposed to a number of influences from their surroundings: moisture, fumes, or atmospheric oxygen, for example. Magnetic cores can sometimes be largely protected from these effects, by impregnating the wound component with a suitable plastic substance. It is, therefore, not necessary to lay much stress on these matters when developing magnetic materials. In addition, the corrosion resistance of many alloys can easily be enhanced by suitable additives—for iron, for example, copper may be added.

Coils and transformers can be protected from external stray fields which might affect their performance. Thus screens or shields made of copper, aluminium, or a high-permeability alloy may be provided (see page 674).

On the other hand it is appreciably harder to shield a component against high temperatures. Certain investigations applicable to permanent magnets are at present in hand. As far as present knowledge goes, Fe–Al–Ni–Co alloys are the best able to withstand a wide range of temperatures (see Section 9.7).

Among the soft materials, the Fe–Si alloys are, according to the investigations of Adams[3], the most resistant to external influences.

The latest technical development has brought a new problem with it: what effect do the various types of radiation have on the behaviour of magnetic materials? This leads to the need to develop materials which are not sensitive to radiation.

According to a fact-finding review by Schmelzer[45], neutron bombardment of soft magnetic materials raises the coercivity, lowers the maximum permeability, and somewhat reduces the saturation density. High-grade materials such as Permalloy or Mo-Permalloy are more radiation sensitive than lower-permeability materials.

Permanent-magnet materials scarcely alter their properties with a radiation dosage up to $10^{18}$ (integrated) fast neutrons. Alnico magnets are more stable

than the barium ferrites but, like all substances containing cobalt, they become radioactive when irradiated. Grain-oriented substances can suffer disorientation. Bombardment with protons or with alpha and beta particles produces the same results as neutron irradiation but is much rarer.

Those radiations most harmful to magnetic materials are regenerative, the regeneration depending both on time and on temperature.

An alloy having improved radiation resistance in respect of neutron bombardment is iron with 3% Si and 1% Al. Following irradiation at the rate of $2{\cdot}2\times10^{18}$ fast neutrons per square centimetre, the hysteresis loop of this material was but little affected, as is shown in Figure 6.26[3].

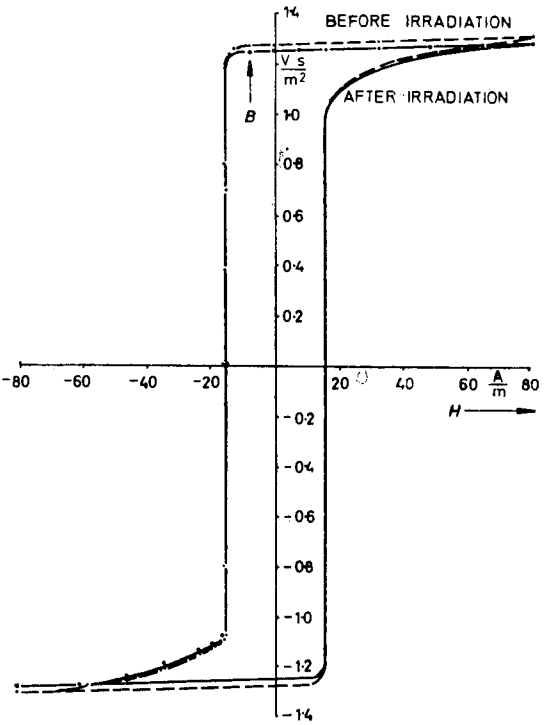



*Figure 6.26. Stability of an iron alloy having 3% Si and 1% Al under irradiation of $2{\cdot}2\times10^{18}$ fast neutrons per square centimetre*[3]

Table 6.10, taken from Schmelzer's review[45], gives the radiation sensitivity of a few substances in qualitative terms.

Gordon and Sery[20a] were able to show that irradiation by fast electrons can change the properties of Ni–Fe alloys. Supermalloy (80% Ni, 15% Fe, 5% Mo) was treated with a 2 MeV electron beam which produced a total integrated flux of $1{\cdot}1\times10^{17}$ electrons per square centimetre within 100 min. The temperature of the sample lay between 70°C and 135°C, and the applied magnetic field had a strength of 16 A/m. A rectangular hysteresis loop was obtained. In contrast to thermomagnetic treatment, the authors called this process 'radiomagnetic treatment'.

**Table 6.10** QUALITATIVE STABILITY OF MAGNETIC MATERIALS UNDER REACTOR-IRRADIATION AT $10^{16}$ INTEGRATED FAST NEUTRONS[45]

| *Material type* | *Designation* | *Stability at room temperature* | *Apparent stability at 500°C* |
|---|---|---|---|
| Fe–Si | Isotropic | vg | vg |
| | Anisotropic | vg | g |
| Fe–Co | 2V-Permendur | vg, r | g, r |
| | Supermendur | r | p, r |
| Fe–Al | 12 Alfenol | — | p |
| | 16 Alfenol | vg | u |
| | 3 Mo-Thermenol | — | u |
| Fe–Ni | 4-79 Mo-Permalloy | u | u |
| | Supermalloy | u | u |
| | Mumetal | u | u |
| | 50% Ni–50% Fe | p | u |
| Ferrites | Nickel Ferrite | vg | u |
| Dust cores | — | vg | u |
| Alnico | II | vg, r | g, r |
| | V | vg, r | vg, r |
| | XII | vg, r | u, r |
| Chrome steel | — | vg | u |
| Cunico | — | vg, r | u, r |
| Cunife | — | vg | u |
| Barium ferrite | — | vg | u |

vg = very good; g = good; p = poor; u = unsuitable;
r = becomes radioactive.

**Table 6.11** SOFT MAGNETIC FERRITES TO DIN 41 280[17b]

| *Type of ferrite* | $\mu_i$ *(nominal value)* $(\mu_0)$ | $10^6 \frac{\tan \delta}{\mu_i}$ *(max. value)* | $f$ (MHz) | $0{\cdot}8/\mu_i$ *at* $f$ MHz *(min. value)* | $10^3\ h/\mu_i^2$ *(max. value)* (cm/kA) | $10^6\alpha/\mu_i$ *at* 23°–70°C | $10^6\ D$ *at* 40°C *(max. value)* | $T_c$ *(min. value)* (°C) | $\varrho$ *(order of magnitude)* (Ω cm) |
|---|---|---|---|---|---|---|---|---|---|
| B 1 | 4 to 10 | 500<br>1 000 | 50<br>100 | 250 | — | 0 to 100 | — | 500 | $10^7$ |
| C 1 | 10 to 25 | 80<br>200 | 10<br>50 | 300 | 10 | 20 to 90 | — | 400 | $10^7$ |
| C 2 | | 250<br>900 | 10<br>50 | 150 | — | 0 to 20 | — | 400 | $10^5$ |
| C 3 | | 500<br>2 600 | 10<br>50 | 100 | — | 0 to 20 | — | 500 | $10^6$ |
| D 1 | 25 to 63 | 380<br>4 000 | 10<br>50 | 80 | — | 0 to 17 | — | 400 | $10^5$ |
| E 1 | 63 to 160 | 40<br>130 | 1<br>10 | 50 | 50 | 1 to 6 | — | 350 | $10^6$ |
| E 2 | | 100<br>250 | 1<br>10 | 50 | — | 0 to 12 | — | 350 | $10^5$ |
| F 1 | 160 to 400 | 50<br>300 | 0·2<br>5 | 8 | 20 | 0 to 8 | — | 250 | $10^4$ |

| | | | | | | | | | |
|---|---|---|---|---|---|---|---|---|---|
| G 1 | 400 to 1 000 | 15<br>50 | 0·05<br>1 | 2 | 8 | 0 to 8 | — | 200 | $10^4$ |
| G 2 | | 13<br>30 | 0·05<br>1 | 4 | 2·5 | 0 to 3 | 18 | 150 | $10^2$ |
| H 1 | 1 000 to 1 600 | 7<br>60 | 0·01<br>0·2 | 1·5 | 7 | 0 to 4 | — | 115 | $10^4$ |
| H 2 | | 2·5<br>25 | 0·01<br>0·2 | 2·0 | 2 | 0·8 to 2 | 8 | 145 | $10^2$ |
| H 3 | | 8<br>60 | 0·01<br>0·2 | 1·5 | 8 | 0 to 2 | — | 140 | $10^2$ |
| I 1 | 1 600 to 2 500 | 1·5<br>10 | 0·01<br>0·1 | — | 1·5 | −0·5 to +0·5 | 8 | 150 | $10^2$ |
| I 2 | | 1·5<br>10 | 0·01<br>0·1 | — | 1·5 | 0·5 to 1·5 | 8 | 150 | $10^2$ |
| I 3 | | 4<br>30 | 0·01<br>0·1 | — | 3 | 0·5 to 3 | — | 150 | $10^2$ |
| K 1 | 2 500 to 4 000 | 2<br>10 | 0·01<br>0·1 | — | 1·5 | −1 to +2 | — | 180 | $10^2$ |
| K 2 | | 5<br>20 | 0·01<br>0·1 | — | 3 | 0 to 4 | — | 125 | $10^2$ |
| L | ≥ 4 000 | — | — | — | — | — | — | — | — |

## REFERENCES


1. ACKERMANN, F. W.: Trennfugen in weichmagnetischen Kreisen geringer Induktionsbelastung (T. Mitt. Krupp **14** (1956) 18–23).
2. ACKERMANN, F. W.: Der Einfluss der Ringkerndimensionen auf die magnetischen Eigenschaften von Bandringkernen (T. Mitt. Krupp **15** (1957) 8–12).
3. ADAMS, E.: Recent developments in soft magnetic alloys (J. A. P. **33** (4) (1962) 1214–1220).
4. ASSMUS, F.: Verbiegungseinfluss bei Kernblechen aus Mu-Metall (Frequenz **4** (1950) 193–195).
5. BIEDERMANN, E. and KNELLER, E.: Gefüge und magnetische Eigenschaften von Dauermagnetlegierungen während der isothermen Ausscheidungshärtung (Z. Metallkde. **47** (1956) 760–774).
6. BOLL, R.: Metallische Magnetwerkstoffe und Kernformen in der Nachrichtentechnik (ETZ-A **80** (1959) 582–588).
7. BOLL, R.: Einbettung weichmagnetischer Werkstoffe in Kunststoffe (ETZ-A **77** (1956) 483–487).
8. BOZORTH, R. M.: Ferromagnetism. Van Nostrand Co. Inc. Toronto/New York/London (1951).
9. BRAILSFORD, F., OLIVER, D. A., HADFIELD, D. and POLGREEN, G. R.: Magnetic materials (J. IEE (I) **95** (96) (Dec. 1948) 522–543).
10. BRECHNA, H.: Properties of bonded cores of electrical machines and transformers (CIGRE-Ber. (1960) 118; ETZ-A **82** (1961) 25–26).
11. BRENNER, R. and PFEIFER, F.: Die Scherung der Anfangspermeabilität bei wechselseitig geschichteten Blechkernen (Frequenz **14** (1960) 167–181).
12. BRENNER, R. and PFEIFER, F.: Blechgeometrie und Permeabilität von Stanzteilkernen (Vacuumschmelze AG., Technical Informationsheet. M 13)
13. BROSSA, G., FERRO, A. and VENTURELLO, G.: Sulla preparazione dei leghe magnetiche a base ferro-nichel ad alta permeabilità per fusione sotto vuoto e per sinterizzazione (Met. Italiana **1** (1961) 17–23).
14. CIOFFI, P. P.: Hydrogenized iron (Phys. Rev. **39** (1932) 363–367).
15. COLE, R. W.: Effect of elastic bending on magnetic properties of oriented silicon iron (J. A. P. **29** (3) (Mar. 1958) 370–371).
16. CZERLINSKY, E.: Die Eigenschaften handelsüblicher warmgewalzter Dynamobleche (Arch. Eisenhüttenw. **27** (1956) 35–40).
17. DIETRICH, H.: Magnetische Eigenschaften von Sintereisen (Z. Metallkde. **52** (1961) 232–235).

17a DIN 17 410, Permanent Magnet Materials (Jan. 1963).

17b DIN 41 280, Weichmagnetische Ferritkerne (Mar. 1965).

18. DUFTSCHMID, F., SCHLECHT, L. and SCHUBARDT, W.: Die technische Verarbeitung von pulverförmigem Carbonyleisen nach dem Sinterverfahren (Stahl u. Eisen **52** (1932) 845–849).
19. ECONOMOS, G.: Effects of fabrication techniques on magnetic properties of magnesium ferrite (J. Am. Cer. Soc. **38** (9) (Sept. 1955) 335–340).
20. EVANS, H., GORDON SMITH, C. and WORN, D. K.: The use of powder metallurgy in the production of soft magnetic materials (Conf. Magnetism and Magnetic Mat., Pittsburgh (1955). AIEE (1955) 134–137).

20a GORDON, D. I. and SERY, R. S.: Uniaxial anisotropy by 'radiomagnetic' treatment; controlling factors in a new process (IEEE Trans. **Mag-1** (4) (Dec. 1965) 277–280).

21. GUILLAUD, C.: Propriétés magnétiques des ferrites (J. Phys. Rad. **12** (1951) 239–248).
22. GUILLAUD, C.: The properties of manganese–zinc ferrites and the physical processes governing them (Proc. IEE **104 B** (1957) 165–178).

23. GUILLAUD, C., PAULUS, M. and VAUTIER, R.: La diminuation des pertes par courant de Foucault dans les ferrites de manganèse-zinc par addition de calcium (C. R. **242** (June 1956) 2712–2715).
24. HANSEN, M.: Der Aufbau der Zweistofflegierungen. Berlin (1936).
25. HECK, C.: Beitrage der Ferrite zur Miniaturisierung (VDE-Fachber. **19** (1956) II/157–II/161; SEG-Nachr. **5** (1957) 147–151.
26. HECK, C.: SAF-Ferrite. (SEG-Nachr. **3** (1) (1955) 43–44).
27. HECK, C. and WEBER, J.: Einfluss der Glühgase auf die magnetischen Eigenschaften der Ferrite (Arch. Eisenhüttenw. **29** (8) (Aug. 1958) 495–504).
28. HEIMKE, G.: Die Koerzitivfeldstärke von Bariumferritpulvern (Z. ang. Phys. **15** (3) (1963) 271–272).
29. HEINRICH, A. and DRECHSLER, J.: Verfahren zum spannungsfreien Einbetten magnetisch weicher Werkstoffe in härtbare Giessharze (DBP 1059–173).
30. HEISTER, W.: Einfluss der Sintertemperatur auf die magnetischen Eigenschaften und das Kristallgefüge von Mn-Zn-Ferriten (Ber. D. Ker. Ges. **35** (1958) 249–258).
31. KIEFFER, R. and HOTOP, W.: Sintereisen und Sinterstahl. (Springer (1948) 486).
32. KRÜLL, F.: Über die Synthese und einige Eigenschaften von Polianit, Braunit, und Hausmannit (Chem. Erde **7** (1932) 473–482).
33. KUSSMAN, A., SCHARNOW, B. and MESSKIN, W. S.: Gekupferter Stahl für Dynamo- und Transformatorenbleche (Stahl u. Eisen **50** (1930) 1194–1197).
34. LESCROËL, Y. and PIERROT, A.: Ferrites a faibles pertes utilisés dans les techniques de l'éctronique et des télécommunications (Cables & Transm. **14** (3) (1960) 220–224).
35. LITTMANN, M. F.: Ultrathin magnetic alloy tapes with rectangular hysteresis loop (El. Engng. **71** (Sept. 1952) 792–794).
36. MAGER, A. and HILLMANN, H.: Über die Koerzitivkraft von zonengeschmolzenem Eisen (Z. ang. Phys. **13** (4) (1961) 171–172).
37. MASON, B.: Mineralogical aspects of the system $FeO$–$Fe_2O_3$–$MnO$–$Mn_2O_3$ (Geol. För. **65** (1943) 97–180).
38. MOORE, T. E., ELLIS, M. and SELWOOD, P. W.: Solid oxides and hydroxides of manganese (J. Am. Chem. Soc. **72** (Feb. 1950) 856–866).
39. NAESER, G. and ZIRM, F.: Walzen von Bändern aus Eisenpulver (Stahl u. Eisen **70** (1950) 995–1004).
40. PAULUS, M. and GUILLAUD, C.: Structure granulaire et propriétés des ferrites (J. Phys. Soc., Japan **17** (B-I) (1962) 632–640).
41. PFEIFER, F.: Möglichkeiten zur Beeinflussung der magnetischen Eigenschaften von Permalloylegierungen (ETZ-A **81** (1960) 945–949).
42. RANDALL, W. F.: Nickel-iron alloys of high permeability, with special reference to mumetal (J. IEE **80** (1937) 647–667).
43. RICHARDS, C. E., WALKER, E. V. and LYNCH, A. C.: Powder metallurgy for research into ferromagnetic materials (Conf. Magnetism and Magnetic Mat.. Pittsburgh (1955). AIEE (1955) 131–133).
44. SCHLECHT, L., SCHUBARDT, W. and DUFTSCHMID, F.: Über die Verfestigung von pulverförmigem Cabonyleisen durch Wärme- und Druckbehandlung (Z. Elektrochem. **37** (8/9) (1931) 485–492).
45. SCHMELZER, G.: Einfluss energiereicher Strahlung auf magnetische Werkstoffe (DEW-Techn.-Ber. **3** (3) (1963) 103–118).
46. SCHOLTS, N. B. and PISKAREW, K. A.: Vergleich der elektromagnetischen Eigenschaften ferromagnetischer Oxyde und anderer typischer magnetischer Stoffe (Is. Akad. Nauk USSR Phys. **16** (1952) 739–747).
47. SIXTUS, K.: Magnetisch hochwertiger Sinterkörper und Verfahren zu seiner Herstellung (DBP 868 421).
48. SNOEK, J. L.: New Developments in Ferromagnetic Materials. Elsevier Publ. Co. Inc., New York/London/Amsterdam/Brussels (1949).

49. STEINITZ, R.: Magnetic properties of iron compacts in relation to sintering temperature (J. A. P. **20** (July 1949) 712–714).
50. TOROPOW, N. A., RABKIN, L. T., FREIDENFELD, E. S. and EPSTEIN, B. S.: Phasenzusammensetzung und einige ferromagnetische Eigenschaften von Mangan–Zink-Ferriten (J. prikl. Chim. **26** (1953) 982–990).
51. Vacuumschmelze GmbH, Hanau: Handbuch Weichmagnetische Werkstoffe (1967).
52. WILLIAMS, H. J., SHERWOOD, R. C., GOERTZ, M. and SCHNETTLER, F. J.: Stressed ferrites having rectangular hysteresis loops (Comm. & Electronics (1953) 531–537).
53. WONSOWSKI, S. W.: Moderne Lehre vom Magnetismus. Deutscher Verlag der Wissenschaften, Berlin (1956).

# 7

# Mechanical properties

In Chapters 2–6 the most important theoretical aspects of magnetism were expounded. Now the mechanical, electrical, and, above all, the magnetic properties of the most important magnetisable materials will be discussed.

It was made clear in discussing the relation between crystal structure and direction of magnetisation that mechanical properties must also be borne in mind if the behaviour of magnetic materials is to be understood. Further, it is important for the designer to know the internal structure of his materials, their mechanical workability, rigidity, thermal conductivity, density, and coefficient of expansion; it seems desirable, therefore, to devote a few lines to these qualities.

## 7.1 CRYSTAL STRUCTURE

The majority of technically important magnetisable materials crystallise in cubic crystals and only a few in the hexagonal system.

For cubic crystals the [100], [110] and [111] directions are of paramount importance. Thomson[26] named these the principal axes of magnetic flux density. As can be seen from Figure 7.1, [100] indicates the edge-direction lying in the $x$-axis. The $y$ and $z$ directions (which have equal status for a cube) are designated [010] and [001]. Direction [110] is the face diagonal in the $xy$ plane and [111] represents the cube diagonal.

To indicate these directions, the above-defined numbers, known as the 'Miller index' numbers, will be enclosed in square brackets, while for the faces round brackets will be used. Thus, in Figure 7.1 two of the planes are labelled (001) and (010). The (001) face is perpendicular to the [001] direction, while the (100) face is perpendicular to the [100] direction, i.e. the $x$-axis.

Four figures are necessary to designate the directions (edges) and faces of a hexagonal crystal lattice: [0001] the direction of the principal axis ($z$ direction); [10$\bar{1}$0] the line of intersection between the (0001) and the (10$\bar{1}$0) planes; and [11$\bar{2}$0] the intersection of the (0001) plane and the (11$\bar{2}$0) plane (see Figure 7.2).

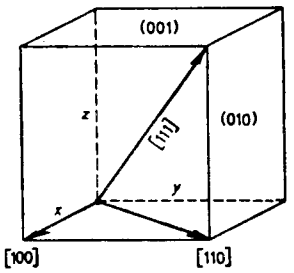



*Figure 7.1. Planes and line directions in a cube*

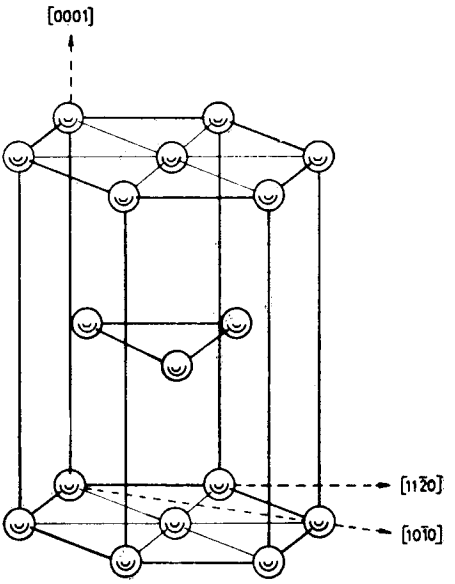



*Figure 7.2. Hexagonal crystal lattice*

### 7.1.1 Iron

Iron, the most important of all magnetic substances, crystallises with a cubic lattice. The $\alpha$-phase, stable at room temperature, is body-centred cubic (Figure 7.3a), that is, the atoms are so arranged in the lattice that there are eight atoms sited at the eight corners of the elementary cube and one atom is to be found at the point of diagonal intersection. Thus to each elementary cell belong $\frac{8}{8}+1 = 2$ atoms. The lattice constant has a value of 0·28606 nm at room temperature. Above 910°C the body-centred configuration passes over to the face-centred cube of $\gamma$-iron (Figure 7.3b). The elementary cell now has six atoms sited at the face-centres in addition to the eight corner atoms. Thus the face-centred cube holds twice as many atoms as the body-

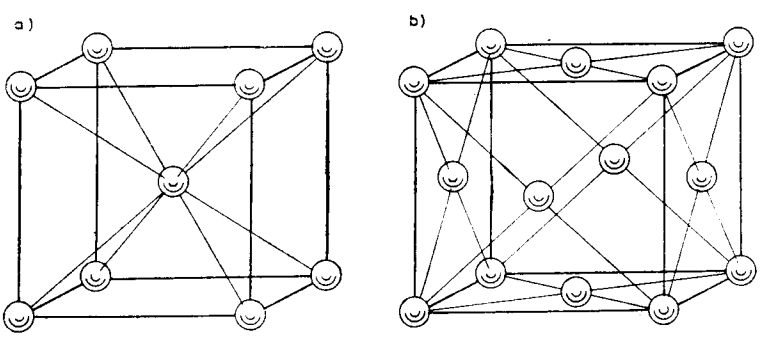



*Figure 7.3. Cubic lattice: (a) body-centred; (b) face-centred*

centred cube, namely $\frac{8}{8} + \frac{6}{2} = 4$. The density is not doubled, however, since the lattice constant increases at the same time. For $\gamma$-iron it amounts to $a = 0{\cdot}363$ nm.

Generally, $\gamma$-iron plays no part in magnetics since it is formed only above the Curie temperature. Pure iron and iron alloys doped with the usual small amounts of silicon, aluminium, and carbon crystallise below the Curie temperature with an $\alpha$-lattice.

### 7.1.2 Nickel

Nickel crystallises in the face-centred cubic lattice (Figure 7.3b). This is maintained at all temperatures. The lattice constant of nickel at room temperature is $a = 0{\cdot}35168$ nm.

### 7.1.3 Fe–Ni alloys

Fe–Ni alloys having more than 30% Ni crystallise in the face-centred cubic configuration. They are designated 'reversible' Fe–Ni alloys, since their Curie temperature is the same for heating and for cooling. This is not the case in the 0–30% range (Figure 7.4). Alloys in this range of composition

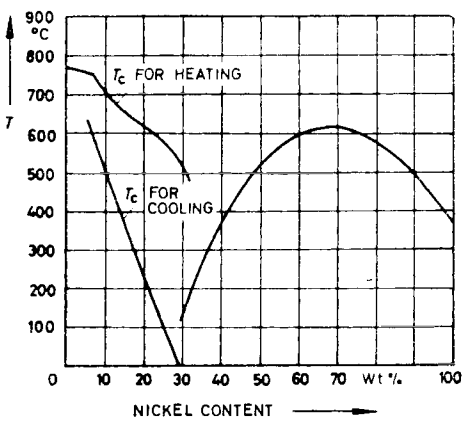



*Figure 7.4. Curie temperatures for* Fe–Ni *alloys*[12]

are therefore called 'irreversible' alloys. Up to a proportion of 20% Ni, the body-centred lattice configuration of $\alpha$-iron prevails; within the range 20–30% Ni both phases occur together[12]. This intermediate region is of technical interest because alloys having compositions within this range find application as temperature compensators (see section 18.2.1).

### 7.1.4 Cobalt

The crystal lattice of cobalt at room temperature is hexagonal (the hexagonal configuration of densely packed spheres) (see Figure 7.2). It remains unchanged up to (417±7)°C and then, above this temperature, passes over into the face-centred cubic form. The lattice constants of α-cobalt (hexagonal) are $a = 0{\cdot}25074$ nm and $c = 0{\cdot}40699$ nm. The lattice constant of cubic β-cobalt is $a = 0{\cdot}3561$ nm.

Fe–Co alloys with some 27–50% Co are of technical interest since they yield maximum permeability and saturation density (see Figure 10.37) [4,28]. The lattice of α-iron is retained up to a cobalt content of 78%.

### 7.1.5 Cubic ferrites

Most ferrites have the cubic lattice of a spinel. Spinel is a natural semi-precious stone having the chemical composition $MgO \cdot Al_2O_3$ (small naturally occurring contaminants are here neglected). The crystal lattice yields a unit cell of eight molecules, namely 32 tightly packed oxygen atoms, 8 magnesium ions, and 16 aluminium ions. The ions of magnesium and aluminium are to be found in the interstices[27].

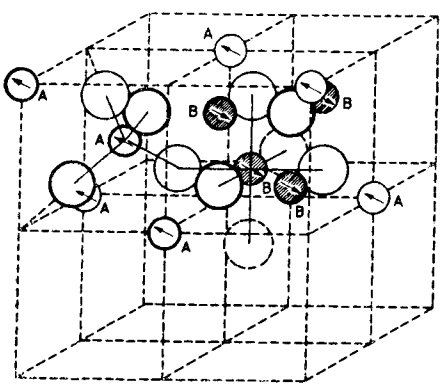



*Figure 7.5. Elementary cell of cubic ferrites: A, tetrahedral sites; B, octahedral sites*[7]

Figure 7.5 shows the elementary cell in schematic form. The whole cube, shown dashed is divided into eight 'sub-dice' in two of which are shown both possible ion arrangements; the large circles represent oxygen ions; the smaller metallic ions are labelled A and B. A and B ions differ in two ways: in the first place by the differing directions of the magnetic moments as shown by arrows in Figure 7.5 and, furthermore, by their positions in relation to the neighbouring oxygen ions. The A ions have four oxygen ions for neighbours and the B ions six. One speaks, therefore, of tetrahedral A sites and octahedral B sites[7].

Of the 96 internal sites in the elementary cell, 64 are tetrahedral and 32 octahedral—which, however, are only partially occupied. Figure 7.6 shows,

somewhat schematically, both the tetrahedral and the octahedral configurations.

In ordinary spinel the bivalent magnesium ion occupies a tetrahedral site and the trivalent aluminium ion an octahedral site. Contrasting with normal spinel, a type is known having an 'inverse' lattice in which the eight tetrahedral sites are not occupied by the bivalent but by the trivalent ions. Of 16 octahedral sites, half are occupied by bivalent and half are occupied by the trivalent ions.

In ferrites, the aluminium is replaced by trivalent iron, and in place of the

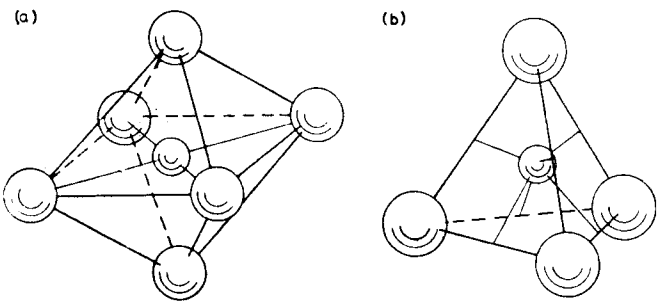



*Figure 7.6. Sublattice of ferrites: (a) octahedra; (b) tetrahedra (large circles, oxygen ions; small circles, metal ions)*

magnesium there is sometimes a bivalent metallic ion. The general formula for a ferrite therefore takes the form $M^{II}O \cdot Fe_2O_3$, where $M^{II}$ stands for the bivalent ion.

Both normal and inverse spinels occur among the ferrites; the normal type is not ferrimagnetic (zinc and cadmium ferrites). Only inverse spinels and mixtures of the two classes show ferrimagnetic properties. In the formula $M^{II}O \cdot Fe_2O_3$ the $M^{II}$ site can be occupied by ions of copper, manganese, iron, nickel, magnesium, etc. Furthermore, two or more of these ions can exist in the lattice at the same time. One may then speak of mixed ferrites; specially important among these are ferrites with zinc ions. The best known of these zinc mixture ferrites are Mn–Zn and Ni–Zn ferrites.

The transition from normal to inverse spinel is continuous in the zinc mixture ferrites; the lattice constant changes linearly. Figure 7.7, for example, shows this for a Ni–Zn ferrite according to an investigation by Sage and Guillaud[23]. The lattice constants of the other cubic ferrites are of the same order of magnitude, i.e. around 0·84 nm (see Table 7.1).

The values quoted in the literature are often not consistent with each other since the origin and method of preparation of the measured test piece affect the structure. Holgersson[16] carried out a systematic x-ray investigation into the fine structure of these materials.

The preparation of solid solutions of various ferrites can greatly affect their magnetic properties. An important role, here, is to be assigned to the radii of the bivalent substitution ions. High-grade soft magnetic ferrites can be obtained only if the radius of the $M^{II}$ ion is of the same order of magni-

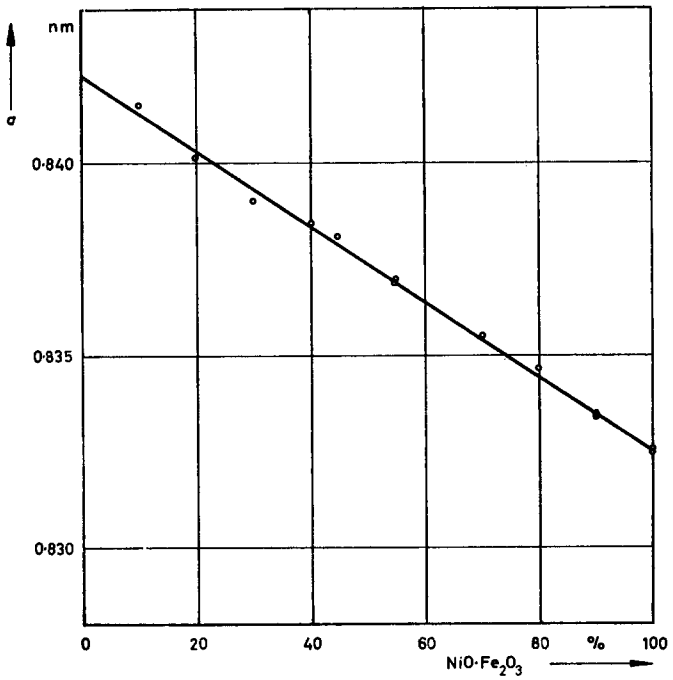



*Figure 7.7. Lattice constants of* Ni–Zn *ferrites*[23]

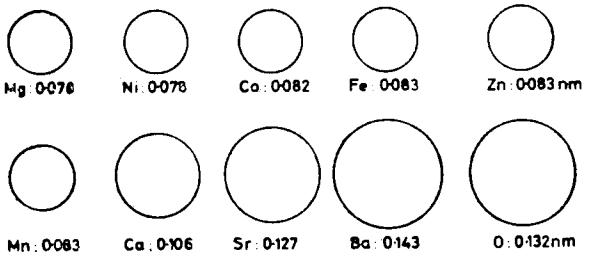



*Figure 7.8. Radii of bivalent ions*

**Table 7.1** LATTICE CONSTANTS AND X-RAY DENSITIES OF CERTAIN FERRITES

| | *Ferrite* | *a* (nm) | *c* (nm) | *d* (g/cm³) | *Reference* |
|---|---|---|---|---|---|
| Normal spinel | $ZnO \cdot Fe_2O_3$ | 0·8403 | — | 5·40 | 16 |
| | | 0·842 | — | — | 13 |
| | $CdO \cdot Fe_2O_3$ | 0·8731 | — | 5·76 | 16 |
| | | 0·869 | — | — | 13 |
| Inverse spinel | $CuO \cdot Fe_2O_3$ | 0·8445 | — | 5·28 | 16 |
| | | 0·837 | — | — | 13 |
| | $CoO \cdot Fe_2O_3$ | 0·836 | — | — | 13 |
| | | 0·8395 | — | 5·27 | 16 |
| | $FeO \cdot Fe_2O_3$ | 0·8417 | — | — | 16 |
| | | 0·839 | — | — | 13 |
| | $\gamma$-$Fe_2O_3$ | 0·832 | — | — | 13 |
| | $LiFe_5O_8$ | 0·831 | — | — | 13 |
| | $MgO \cdot Fe_2O_3$ | 0·836 | — | — | 13 |
| | | 0·8342 | — | 4·53 | 16 |
| | $MnO \cdot Fe_2O_3$ | 0·8572 | — | 4·87 | 16 |
| | $NiO \cdot Fe_2O_3$ | 0·8414 | — | 5·24 | 16 |
| | | 0·836 | — | — | 13 |
| Hexagonal ferrites | $BaO \cdot 6\,Fe_2O_3$ | 0·5876 | 2·317 | 5·3 | 1 |
| | | 0·59 | 2·32 | — | 5 |
| | $SrO \cdot 6\,Fe_2O_3$ | 0·5864 | 2·303 | 5·12 | 1 |
| | $PbO \cdot 6\,Fe_2O_3$ | 0·5877 | 2·302 | 5·62 | 1 |
| | W: $BaMe_2Fe_{16}O_{27}$ | 0·588 | 3·2845 | — | 5 |
| | X: $Ba_2Fe_2^{II}Fe_{28}^{III}O_{46}$ | 0·588 | 8·411 | — | 5 |
| | Y: $Ba_2Me_2Fe_{12}O_{22}$ | 0·5876 | 4·3558 | — | 5 |
| | Z: $Ba_3Me_2Fe_{24}O_{41}$ | 0·5885 | 5·230 | — | 5 |

tude as the iron ions, i.e. something under 0·1 nm. The relatively large sizes of the ions of the alkaline-earth metals, calcium, strontium, and barium are clearly shown, in schematic form, in Figure 7.8. The cubic ferrites of these alkaline-earth metals have very low permeability and high losses, so they are technically of little interest.

### 7.1.6 Hexagonal ferrites

Certain ferrites with a high iron content and containing ions of barium, strontium or lead have a hexagonal lattice, the so-called magnetoplumbite structure. The composition corresponds more or less to the formula $M^{II}O \cdot 6Fe_2O_3$. One half of the elementary cell is shown schematically in Figure 7.9 following an exposition by Adelsköld[1]. The other half can be obtained by mirror-reflection either from above or from below. In the case of $BaO \cdot 6Fe_2O_3$ the large barium ions bind together the two halves of the lattice.

The two lattice constants, defined by the dimensions of the elementary cell, are for $BaO \cdot 6Fe_2O_3$ $a = 0{\cdot}5876$ nm and $c = 2{\cdot}317$ nm. The axis ratio

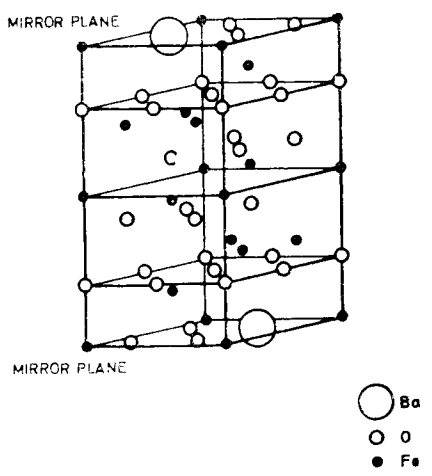



*Figure 7.9. Magnetoplumbite lattice of* $BaO \cdot 6Fe_2O_3$[1]

$c/a = 3{\cdot}94$ is thus very large and for this reason the crystal shows a large degree of magnetic anisotropy.

The hexagonal structure still holds very largely if a cubic ferrite is mixed with the basic substance $M^{II}O \cdot 6Fe_2O_3$. A wide range of materials with good high-frequency characteristics results from such combinations[17] (see Section 13.6.4.3). The lattice constants of the most important substances of the series (W, Y, and Z), are given in Table 7.1.

## 7.2 DENSITY

The density of a substance can be calculated from the atomic weight, the lattice constants, and the number of atoms in the elementary lattice. As the lattice constants can be found by means of fine-structure x-ray studies, one speaks of x-ray densities in contrast to mechanically determined densities (i.e. by weight). The two values do not coincide if there are inclusions of foreign substances, or pores or lattice faults. The x-ray density of metals is nearly the same as that determined mechanically, but for ferrites the mechanical density is almost always less than the x-ray density. The difference may amount to 10% or more.

The density $d$ of the metals iron, nickel, and cobalt and also of their technically useful alloys are set out in Table 8.1. According to McKeehan[22], the densities for crystals of pure iron and nickel differ somewhat from the figures quoted in the table, namely $d = 7{\cdot}775$ g/cm$^3$ for iron and $d = 8{\cdot}953$ g/cm$^3$ for nickel. These values are related to lattice constants $a_{Fe} = 0{\cdot}2872$ nm and $a_{Ni} = 0{\cdot}3510$ nm.

Chevenard[6] determined the densities of Fe–Ni–Cr alloys having up to 15% Cr. Figure 7.10 shows the reduction, with aluminium content, of the density of Fe–Al alloys, taken from x-ray investigations by Sykes and Bampfylde[25]. The densities of Fe–Si alloys can be deduced from equation 10.4 and are given in Figure 10.8 (see also Table 10.4). The densities of Fe–Co alloys are to be found in Table 7.2, following investigations by Weiss

**Table 7.2** DENSITIES OF Fe–Co ALLOYS (ADDITIVES 0·06% FOR IRON AND 0·26% FOR COBALT)[28]

| Co (%) | $d$ (g/cm³) | Co (%) | $d$ (g/cm³) |
|---|---|---|---|
| 0 | 7·86 | 59·8 | 9·29 |
| 19·2 | 7·93 | 69·0 | 8·41 |
| 28·2 | 8·01 | 79·1 | 8·55 |
| 38·1 | 8·09 | 89·3 | 8·70 |
| 48·2 | 8·18 | 100 | 8·87 |

**Table 7.3** EFFECTIVE PERMEABILITY AND DENSITIES OF DUST CORES

| *Magnetic material* | *Vol. %* | $\mu_e$ ($\mu_0$) | $d$ (g/cm³) | *Reference* |
|---|---|---|---|---|
| Iron dust | 95 | 60 | 7·4 | 19 |
| | 60 | 13 | $<5$ | 19 |
| Permalloy | | 80 | 7·8–8·3 | 24 |
| Mo-Permalloy | 97·5 | 125 | 7·8 | 20 |

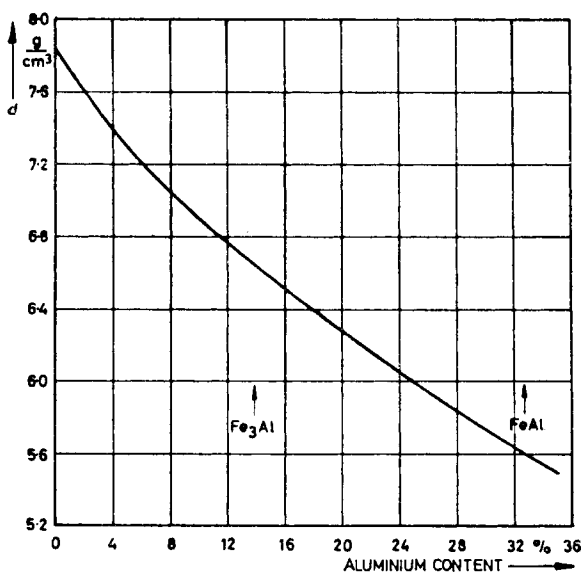



*Figure 7.10. Densities of* Fe–Al *alloys determined by x-ray measurements*[25]

and Forrer[28] carried out on a series of alloys made from electrolytically produced metals. The x-ray densities of the most important ferrites can be read from Table 7.1, and the density of various dust cores are given in Table 7.3.

## 7.3 MELTING POINT

The melting points of a few metals are quoted in Table 8.1. Van Arkel, Verwey, and Van Bruggen[2] determined the melting points of a number of ferrites, by measuring with a pyrometer the temperature at which ferrite bars formed droplets in an oxyhydrogen flame. The accuracy of the values set out in Table 7.4 is about $\pm 10°C$. It is not easy to obtain more exact figures for the melting points of oxide compounds since atmospheric conditions have an effect on the composition, and may thus falsify the measurements.

**Table 7.4** MELTING POINTS OF CERTAIN FERRITES[2]

| *Ferrite* | *Melting point* (°C) | *Ferrite* | *Melting point* (°C) |
|---|---|---|---|
| $BaO \cdot Fe_2O_3$ | 1 390 | $MgO \cdot Fe_2O_3$ | 1 760 |
| $CdO \cdot Fe_2O_3$ | 1 540 | $MnO \cdot Fe_2O_3$ | 1 570 |
| $CoO \cdot Fe_2O_3$ | 1 570 | $NiO \cdot Fe_2O_3$ | 1 660 |
| $CuO \cdot Fe_2O_3$ | 1 560 | $PbO \cdot Fe_2O_3$ | 1 530 |
| | | $ZnO \cdot Fe_2O_3$ | 1 590 |

A knowledge of at least the approximate melting point of the ferrites is important in that a ferrite can be sintered at a lower temperature if it has a lower melting point.

## 7.4 SPECIAL MECHANICAL PROPERTIES

In Table 7.5 will be found the elastic modulus and stability values for iron, cobalt, and nickel, as well as their specific heats, thermal conductivities, and linear coefficients of expansion. Hardness and the possibility of deep-drawing are important, for example, for relay stampings. These properties are set out in Table 7.6 for the magnetic materials most used in relay construction.

In the majority of applications, flexibility and weldability are required of magnetic sheet and strip. These qualities can be improved for brittle Fe–Si with over 3·5% Si by heating (see Figure 10.10).

For magnetically anisotropic materials the mechanical properties are also often directional. Thus, for example, the elastic modulus (Young's modulus) of grain-oriented electrosheet is lowest in the rolling direction and greatest at 55° to the rolling direction (see Table 7.7)[3].

**Table 7.5** MECHANICAL CONSTANTS AT ROOM TEMPERATURE

| | *Iron* | *Cobalt* | *Nickel* |
|---|---|---|---|
| Modulus of elasticity ($10^{11}$ N/m$^2$) | 2·13 | 2·05 | 1·99 |
| Tensional rigidity at 20°C ($10^{11}$ N/m$^2$) | 2·0–2·5 | — | 3·8–8·0 |
| Specific heat at 20°–100°C (cal/g K) | 0·108 | 0·091 | 0·107 |
| Thermal conductivity at 20°–100°C (kcal/K m h) | 63 | 58 | 51 |
| Linear coefficient of expansion at 25°–100°C (ppm/K) | 12·3 | 12·7 | 13·3 |

**Table 7.6** HARDNESS AND DRAWING QUALITY OF MAGNETIC SHEETS

| *Material* | *Density* (g/cm$^3$) | *Hardness* (HV) | *Drawing depth of 1 mm sheet* |
|---|---|---|---|
| Unalloyed iron | 7·8 | 80–135 | 9–11 |
| Fe–Si with 2·5–4% Si | 7·5–7·6 | 300–350 | Cannot be drawn |
| Fe–Ni with 36–76% Ni (+Cu, Cr, Mo) | 8·2–8·7 | 160–200 | 8–11 |

**Table 7.7** YOUNG'S MODULUS FOR ANISOTROPIC ELECTROSHEET[3]

| *Angle to rolling direction* | *E* ($10^{11}$ N/m$^2$) |
|---|---|
| 0° | 1·33 |
| 20° | 1·72 |
| 45° | 2·21 |
| 55° | 2·25 |
| 90° | 1·95 |

**Table 7.8** MECHANICAL CONSTANTS OF FERRITES AT ROOM TEMPERATURE (FOR GENERAL GUIDANCE)

| | |
|---|---|
| Modulus of elasticity ($10^{11}$ N/m$^2$) | ~ 1·5 |
| Rigidity in tension ($10^8$ N/m$^2$) | 18 |
| Rigidity in compression ($10^8$ N/m$^2$) | ~ 1–7 |
| Specific heat (cal/gK) | ~ 0·17 |
| Thermal conductivity (kcal/K m h) | 3·6–5·4 |
| Coefficient of linear expansion (ppm/K) | 6–10 |
| Hardness (mohs) | ~ 6 |

The mechanical properties of the ferrites have been less thoroughly investigated than those of iron or alloys. Table 7.8 may suffice to give a few reference data, the figures being taken from a variety of publications.

A further mechanical quality is frequently of interest for the practical application of magnetic materials, namely workability. Easily worked materials lend themselves to rolling, drawing, stamping, drilling, or other deformations under stress. Those which are hard to work can, as a rule, only accept surface treatment such as grinding. There are easily worked and unworkable materials to be found among both magnetically soft and magnetically hard alloys and compounds.

High-grade Fe–Al–Ni–Co alloys are hard and brittle, as are the ferrites. In addition, ferrites are often porous. Surface treatment is often limited to wet grinding with carborundum or diamond abrasive. Drilling and forming or drawing can be achieved by ultrasonic techniques. For example, Figure 7.11 (see plate section) shows a transfluxor core, produced ultrasonically from a plaquette of ferrite, together with the rest of the original plate.

A pressing made from powder shrinks on sintering. The shrinkage is greater or less according to the composition, grain size, density, and sintering conditions. Using pressures between $3\times10^8$ N/m$^2$ and $8\times10^8$ N/m$^2$, which according to Kieffer and Hotop[18] is sufficient for the production of satisfactory magnets, the shrinkage amounts to some 11·2–6·3%, but at $10^9$ N/m$^2$ it amounts to only 4·9%. For ferrites, a shrinkage of 1–22% must be reckoned with, leading to a size tolerance of between 2% and 3% for unworked ferrite. The surface of a sintered unworked ferrite shows a structure similar to that seen in micrographs of metal alloys. Figure 7.12 (see plate section) shows the surface of a Mg–Mn ferrite with 38% MnO[14]. The shape and size of the grains are dependent on the annealing atmosphere. Figure 7.12a shows the ferrite after cooling in air from 1400°C down to room temperature, while in Figure 7.12b cooling has taken place in a neutral atmosphere.

Heister[15] and others have studied the fracture surface of a Mn–Zn ferrite under the electron microscope. It appears that the structure is similar in its graininess to that of the normal surface. However, the appearance of the structure can be clearly altered by minute additions of, say, calcium, as experiments by Guillaud, Paulus, and Vautier have demonstrated[8, 9].

Levesque and Gerlach[21] have reported suitable techniques for the preparation of photomicrographs for the study of microstructure. Hanke and Burger[10, 11] investigated the chemical action of various etching acids on the surface of single crystals of manganese ferrite and also on polycrystalline Mn–Zn ferrites and garnets.

## REFERENCES

1. ADELSKÖLD, V.: X-Ray studies on magneto-plumbite $PbO\cdot6Fe_2O_3$ and other substances resembling 'beta-aluminia' $Na_2O\cdot11\ Al_2O_3$ (Ark. Kemi. Min. Geol. **12 A** (29) (1938) 1–9).
2. VAN ARKEL, A. E., VERWEY, E. J. W. and VAN BRUGGEN, M. G.: Ferrites I (Rev. trav. chim. **55** (1936) 331–339).

3. ARMCO STEEL CORP., MIDDLETOWN: Oriented electrical steels (1961).
4. BOZORTH, R. M.: Ferromagnetism. Van Nostrand Co. Inc., Toronto/New York/London (1951).
5. BRAUN, P. B.: The crystal structures of a new group of ferromagnetic compounds (Phil. Res. Rep. **12** (1957) 491–548).
6. CHEVENARD, P.: Les alliages á hautes teneurs en nickel et en chrome (Rev. Metallurg. **25** (1928) 14–34).
7. GORTER, E. W.: Some properties of ferrites in connection with their chemistry (Proc. IRE **43** (Dec. 1955) 1945–1973).
8. GUILLAUD, C. and PAULUS, M.: Perméabilité initiale et grosseur des grains dans les ferrites de manganèse–zinc (C. R. **242** (21) (1956) 2525–2528).
9. GUILLAUD, C., PAULUS, M. and VAUTIER, R.: La diminution des pertes par courant de Foucault dans les ferrites de manganèse–zinc par addition de calcium (C. R. **242** (23) (1956) 2712–2715).
10. HANKE, I. and BURGER, H.: Versetzungen in Mangan-Ferrit-Einkristallen (Z. ang. Phys. **14** (1962) 168–174, 301–306).
11. HANKE, I. and BURGER, H.: Die Ätzmethode, ein Hilfsmittel bei der Entwicklung von magnetischen Ferriten (Siemens-Z. **36** (Aug. 1962) 619–625).
12. HANSEN, M.: Der Aufbau der Zweistofflegierungen. Berlin (1936).
13. HARVEY, R. L., HEGYI, I. J. and LEVERENZ, H. W.: Ferromagnetic spinels for radio frequencies (RCA Rev. **11** (Sept. 1950) 321–363).
14. HECK, C. and WEBER, J.: Einfluss der Glühgase auf die magnetischen Eigenschaften der Ferrite (Arch. Eisenhüttenw. **29** (8) (Aug. 1958) 495–504).
15. HEISTER, W.: Mangan-Zink-Ferrite mit hoher Permeabilität und geringen Verlusten (T. Mitt. Krupp **15** (6) (1957) 130–144).
16. HOLGERSSON, S.: Röntgenographische Untersuchungen der Mineralien der Spinellgruppe und von synthetisch dargestellten Substanzen von Spinelltypus (Lunds Univers. Arsskr. (2) **23** (9) (1927) 1–112).
17. JONKER, G. H., WIJN, H. P. J. and BRAUN, P. B.: A new class of oxidic ferromagnetic materials with hexagonal crystal structures (Proc. IEE **104 B** (1957) 249–254).
18. KIEFFER R. and HOTOP, W.: Sintereisen und Sinterstahl. Springer (1948) 482.
19. KIESSLING, G. and LUDL, O.: Neuere Erkenntnisse aus der Massekerntechnik (ETZ **63** (1942) 413–416).
20. LEGG, V. E. and GIVEN, F. J.: Compressed powdered molybdenum permalloy for high quality inductance coils (Bell Syst. Techn. J. **19** (1940) 385–406).
21. LEVESQUE, P. and GERLACH, L.: The metallography of ferrites (J. Am. Cer. Soc. Cer. Abstr. **39** (3) (Mar. 1956) 119–120).
22. MCKEEHAN, L. W.: The crystal structure of iron–nickel alloys (Phys. Rev. **21** (1923) 402–407).
23. SAGE, M. and GUILLAUD, C.: Relation entre la structure cristalline et les propriétés magnétiques des ferrites mixtes de nickel et de zinc (C. R. **230** (20) (May 1950) 1751–1753).
24. SHACKELTON, W. J. and BARBER, I. G.: Compressed powdered permalloy (Trans. AIEE **47** (1928) 429–437).
25. SYKES, C. and BAMPFYLDE, J. W.: Physical properties of Fe–Al alloys (J. Iron Steel Inst. **130** (1934) 389–418).
26. THOMSON, W.: On the theory of magnetic induction in crystalline substances (Rep. 20th Meeting Brit. Ass. Sci., London (1851) 23).
27. VERWEY, E. J. W., HAAYMANN, P. W. and HEILMAN, E. L.: Über die Kristallstruktur der Ferrite und analoger Metalloxyde (Phil. T. Rdsch. **9** (1947/48) 186–192).
28. WEISS, P. and FORRER, R.: La saturation absolue des ferromagnétiques et les lois d'approche en fonction du champ et de la température (Ann. Phys. **12** (1929) 279–372).

# 8

# Electrical properties of magnetic materials

The electrical properties of magnetisable substances play an important part in many electrotechnical applications: electrical conductivity promotes eddy currents and prevents high-frequency fields penetrating appreciably below the surface (skin effect). The dielectric constant and the corresponding loss angle affect the applicability of ferrites to microwave techniques.

## 8.1 SPECIFIC ELECTRICAL RESISTANCE

Instantaneous application of direct fields or the continuous action of alternating fields produces eddy currents in ferromagnetic materials which increase—generally in an undesirable way—the a. c. resistance of the associated electrical circuit. According to equation 3.48, these eddy currents increase with electrical conductivity $\sigma = 1/\varrho$.

### 8.1.1 The electrical resistance of metals and alloys

The specific electrical resistance of pure metals is of the order of magnitude a few $\mu\Omega$ cm (see Table 8.1). Alloys have a higher resistance and are therefore superior to metals where it is desired to avoid eddy currents.

Figure 8.1 shows the rise in resistance for various iron alloys caused by the addition of a small percentage by weight of another metal. Copper, cobalt, and nickel change the resistance of iron only slightly. On the other hand, aluminium and silicon additives are appreciably more effective[8]. Thus, for example, the introduction into pure iron of 4·5% Si increases the specific electrical resistance $\varrho$ sixfold. Figure 8.1 shows the specific electrical resistance of Fe–Si alloys having a silicon content up to 6·3%.

According to Yensen[44] the curve between 0·35% and 6% Si can be represented by the equation

$$\varrho = 9{\cdot}6 + 18{\cdot}4\, p_{Si}\,(p_{Si} - 0{\cdot}35)\ \mu\Omega\ \text{cm} \tag{8.1}$$

where $p_{Si}$ indicates the silicon content in percent. An equation proposed by Gumlich[15], namely

$$\varrho = (9{\cdot}9 + 12 p_{Si})\ \mu\Omega\ \text{cm} \tag{8.2}$$

**Table 8.1** CHEMICAL COMPOSITION, DENSITY $d$, AND SPECIFIC ELECTRICAL RESISTANCE $\varrho$ OF MAGNETIC METALS AND ALLOYS AT ROOM TEMPERATURE, AND THEIR APPROXIMATE MELTING POINTS $T_M$

| *Material* | *Approximate composition* | $d$ (g/cm³) | $\varrho$ (μΩ cm) | $T_M$ | *Reference* |
|---|---|---|---|---|---|
| Iron | 100% Fe | — | 9·6 | — | 44 |
| | 99·9% Fe | 7·874 | 9·71 | 1 539 | 10a |
| | 99·8% Fe | 7·88 | 9·9 | 1 539 | 15 |
| Armco iron | 99·9% Fe | — | 10·7 | 1 532 | 1 |
| Fe–Si | 4% Si, remainder Fe | 7·65 | 60 | 1 450 | |
| Sendust | 9·5% Si, 5·5% Al, remainder Fe | 8·8 | 81 | — | 29 |
| Nickel | 99·6% Ni | 8·89 | 8·7 | 1 445 | |
| Cobalt | 99% Co | 8·84 | 9 | 1 495 | |
| | 99·95% Co | 8·85 | 6·3 | — | 13a |
| Permalloy A | 78·5 Ni, remainder Fe | 8·6 | 16 | 1 440 | |
| Permalloy B | 45% Ni, remainder Fe | 8·3 | 55 | — | 28 |
| Permalloy C | 77% Ni, 4% Mo, remainder Fe | 8·8 | 60 | — | 28 |
| Permalloy D | 36% Ni, remainder Fe | 8·15 | 90 | — | 28 |
| Permalloy F | 65% Ni, remainder Fe | 8·4 | 26 | — | 28 |
| 4-79 Mo-Permalloy | 78·5% Ni, 4% Mo, remainder Fe | 8·74 | 55 | — | 2 |
| Cr-Permalloy | 78·5% Ni, 3·8% Cr, remainder Fe | | 65 | — | 12 |
| M 1 040 | 72% Ni, 3% Mo, 14% Cu, remainder Fe | 8·7 | 60 | — | 38a |
| Mumetal | 75% Ni, 4% Mo, 5% Cu, remainder Fe | 8·6 | 55 | — | 38a |
| Supermalloy | 79% Ni, 5% Mo, remainder Fe | 8·77 | 65 | — | 2, 6 |
| Isoperm | 50% Ni, remainder Fe | 8·25 | 40 | 1 440 | |
| Deltamax | 50% Ni, remainder Fe | 8·25 | 45 | — | 2 |
| Permenorm 5 000 Z | 50% Ni, remainder Fe | 8·25 | 45 | — | 36 |
| Hipernic V | 50% Ni, remainder Fe | 8·25 | 45 | 1 450 | 43 |
| Permendur | 50% Co, remainder Fe | 8·3 | 6–7 | 1 470 | 12 |
| V-Permendur | 49% Co, 2% V, remainder Fe | 8·2 | 26 | — | 28 |
| Supermendur | 49% Co, 2% V, remainder Fe | 8·2 | 26 | 1 480 | 41 |
| Vicalloy | 52% Co, 10% V, remainder Fe | 8·2 | 60–67 | — | 42 |
| Hiperco 35 | 35% Co, 0·5% Cr, remainder Fe | 8·05 | 22–34 | 1 500 | 41 |
| Hiperco 27 | 27% Co, 0·56% Cr, remainder Fe | 7·95 | 19 | 1 500 | 41 |
| Magnetoflex 35 | 52% Co, 13% V, 35% Fe | 8·1 | 70–100 | — | 37 |
| Magnetoflex 40 | 52% Co, 8% V, 40% Fe | 8·1 | 60–90 | — | 37 |

**Table 8.1** *(cont.)*

| *Material* | *Approximate composition* | *d* (g/cm³) | *ϱ* (μΩ cm) | $T_M$ | *Reference* |
|---|---|---|---|---|---|
| H. C. R. Alloy | 50% Ni, remainder Fe | 8·25 | 40 | — | 28a |
| 45-25 Perminvar | 25% Co, 45% Ni, remainder Fe | — | 18 | — | 12 |
| 7-45-25 Mo-Perminvar | 7% Mo, 45% Ni, 25% Co, remainder Fe | — | 80 | — | 12 |
| Rhometal | 40–45% Ni, 5% Cr, 3% Si, remainder Fe | — | 90 | — | 3 |
| Resistopermalloy | — | — | 107 | — | 3 |
| Radiometal | 45% Ni, 0·6% Mn, remainder Fe | 8·3 | 55 | — | 9a |
| Radiometal 36 | 36% Ni, remainder Fe | 8·1 | 80 | — | 28b |
| Vacodur 16 | 16% Al, remainder Fe | 6·5 | 145 | — | 38 |
| Vacoperm 100 | 70–80% Ni, Cu, Mo, remainder Fe | 8·7 | 60 | — | 38a |

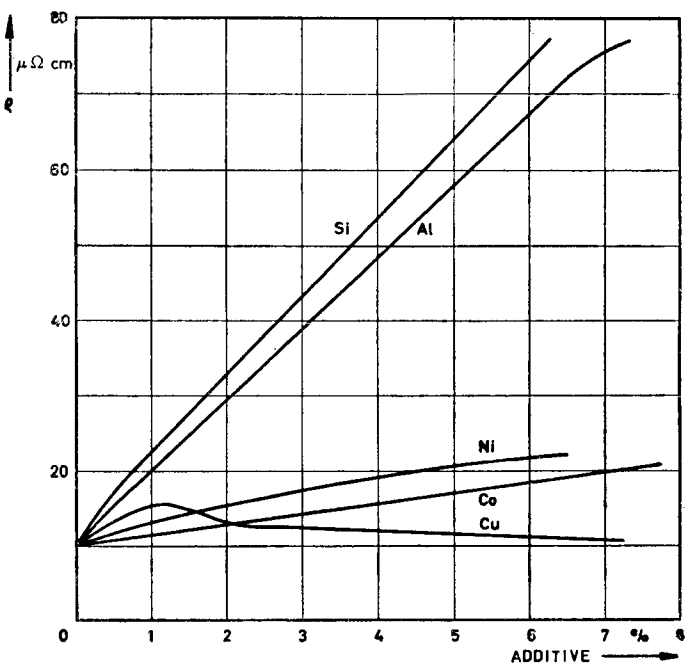



*Figure 8.1. Influence of additives on the electrical resistance of iron*[8]

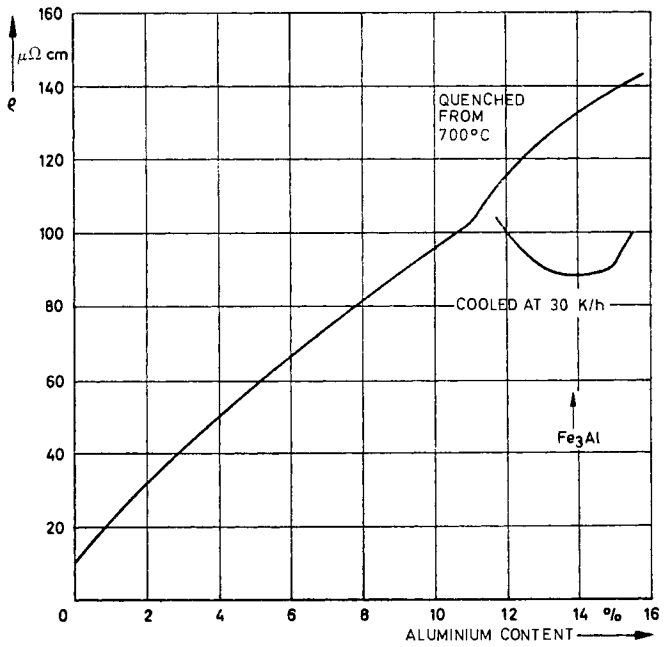



*Figure 8.2. Specific electrical resistance of* Fe–Al *alloys cooled slowly (30* K/h*) and quickly*[20]

looks, indeed, somewhat different but yields almost identical results. For higher values of silicon content, the curve of Figure 8.1 lies somewhat below that corresponding to this formula. Further values taken from the latest measurements are given in Table 10.4 (page 317).

The formula proposed by Gumlich[15] for Fe–Al alloys reads rather like that for Fe–Si alloys, namely

$$\varrho = (9{\cdot}9 + 11 p_{\mathrm{Al}})\ \mu\Omega\ \mathrm{cm} \tag{8.3}$$

and holds for 20°C and up to 4% Al. The temperature coefficient of the resistance falls with increasing aluminium content, and at 10% Al amounts to only 350 ppm/K.

In the range of composition of $Fe_3Al$ for example, at 12–14% Al a 'superstructure phase' takes place: the electrical and magnetic properties depend on the conditions of cooling. Samples quenched at 700°C, for example, have higher resistance than those which are slowly cooled (30 K/h). This is shown in Figure 8.2 based on investigations by Masumoto and Saito[20]. The specific electrical resistance attains a value of 167 μΩ cm if the aluminium content is 17%. Thermenol (16% Al, 3·3% Mo, remainder Fe) exhibits a specific electrical resistance almost as high, namely $\varrho = 162\ \mu\Omega$ cm (see page 342). The specific electrical resistance of a few Fe–Si–Al alloys is given in Table 10.12.

According to the investigations of Yensen[44] already mentioned, the specific electrical resistance of Fe–Mn alloys increases with increasing manganese

content $p_{Mn}$ in accordance with the equation

$$\varrho = (9{\cdot}6+7p_{Mn})\ \mu\Omega\ \text{cm}. \tag{8.4}$$

The sulphur content $p_S$ increases the specific electrical resistance in accordance with the equation

$$\varrho = (9{\cdot}6+12p_S)\ \mu\Omega\ \text{cm} \tag{8.5}$$

The addition of $p_P\%$ phosphorus raises the resistance according to the following law, if the proportion of phosphorus lies between 0·015% and 0·12%:

$$\varrho = 9{\cdot}6+60p_P+3{\cdot}5(p_P-0{\cdot}015)\ \mu\Omega\ \text{cm} \tag{8.6}$$

If iron contains between 0·02% (in solution) and 0·85% (in the form of $Fe_3C$ and pearlite), then $\varrho$ is to be calculated from

$$\varrho = [9{\cdot}6+82{\cdot}5p_C+4{\cdot}5(p_C-0{\cdot}02)]\ \mu\Omega\ \text{cm} \tag{8.7}$$

If an iron alloy contains up to 1% Mn, 0·1% S, 0·015% P, and 0·02% C, the relevant equation is

$$\varrho = (9{\cdot}6+7p_{Mn}+12p_S+60p_P+82{\cdot}5p_C)\ \mu\Omega\ \text{cm} \tag{8.8}$$

For example, if there is 0·01% of each of these elements present in the iron, the specific electrical resistance will be

$$\varrho = 9{\cdot}6+0{\cdot}07+0{\cdot}12+0{\cdot}60+0{\cdot}83 = 11{\cdot}22\ \mu\Omega\ \text{cm}$$

All Fe–Ni alloys exhibit higher specific electrical resistances than either iron or nickel alone. The maximum occurs at about 30% Ni. Figure 13.5 shows the relation according to an investigation by Elmen[12]. The resistance of

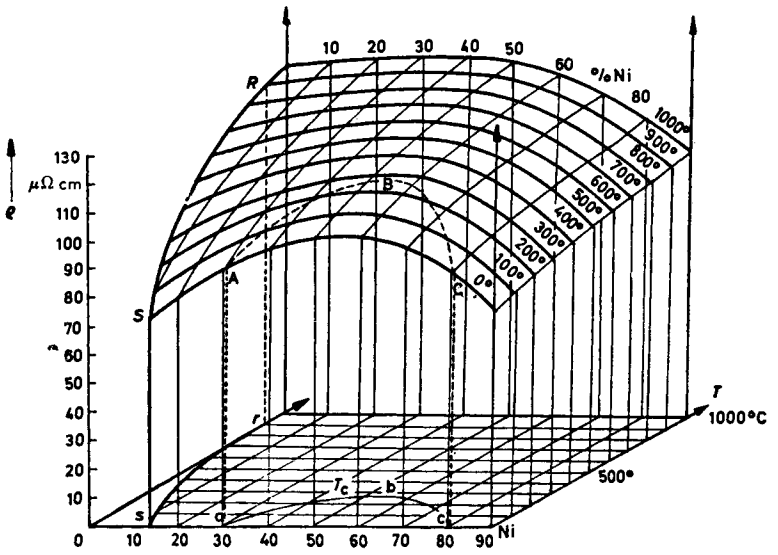



*Figure 8.3. Specific electrical resistance of* Fe–Ni–Cr *alloys having 10%* Cr[10]

Fe–Ni alloys can be raised still further by adding a third constituent: molybdenum and chrome are suitable (see Figure 13.12). Chevenard[10] carried out extensive investigations into the specific electrical resistance of the Fe–Ni–Cr alloys and its variation with temperature (see Figures 8.3).

The effect of molybdenum and chromium additives in raising the resistance is displayed in Table 8.1. That these also improve the magnetic properties is a point to be taken up later. A further example is Mumetal, a Permalloy whose resistance can be raised to 62 $\mu\Omega$ cm by alloying it with copper and chromium.

The resistance of ferromagnetic substances cannot be increased much above the round figure of 100 $\mu\Omega$ cm by the use of metallic additives; in no case can it be increased by several powers of 10. This only becomes possible if the material is reduced to a fine powder, each particle of which is insulated from its neighbours by a non-metallic impregnant. This is, in fact, the case with dust cores. Blechschmidt[4] found a specific electrical resistance for iron dust cores of $10^6$ $\Omega$ cm. Heavily compressed cores of Permalloy dust yielded 1–20 $\Omega$ cm[27].

### 8.1.2 Specific electrical resistance as a function of temperature

The specific electrical resistance of metals and their alloys rises with rising temperature, so at room temperature the temperature coefficient of the electrical resistance is positive. The numerical values for the three basic metals are:

| | |
|---|---|
| Iron | $\alpha_\varrho = 5{\cdot}6 \times 10^{-3}/\mathrm{K}$ |
| Cobalt | $\alpha_\varrho = 6{\cdot}5 \times 10^{-3}/\mathrm{K}$ |
| Nickel | $\alpha_\varrho = 6{\cdot}9 \times 10^{-3}/\mathrm{K}$ |

For commercially pure iron, nickel, and cobalt, the temperature relation up to 800°C is given in Table 8.2[1].

**Table 8.2** SPECIFIC ELECTRICAL RESISTANCE OF COMMERCIALLY PURE IRON, NICKEL, AND COBALT IN RELATION TO TEMPERATURE[1]

| *Temperature* (°C) | $\varrho$ ($\mu\Omega$ cm) | | |
|---|---|---|---|
| | *Iron* | *Nickel* | *Cobalt* |
| 0 | 9·6 | 8·7 | 5·68 |
| 100 | 15·0 | 12·2 | 9·30 |
| 200 | 22·6 | 17·3 | 13·88 |
| 300 | 31·4 | 23·0 | 19·78 |
| 400 | 43·1 | 28·0 | 26·56 |
| 500 | 55·3 | 31·2 | 32·20 |
| 600 | 69·8 | 33·2 | 40·20 |
| 700 | 87·0 | 35·5 | 49·20 |
| 800 | 105·5 | — | 58·60 |

### 8.1.3 The electrical resistance of ferrites

Ferrites have higher resistances than metals by several orders of magnitude. Even ferroferrite (magnetite), the least resistive of all the ferrites, has a resistance of some 5 mΩ cm, which is several orders of magnitude greater than the best values obtained for ferromagnetic metals. However, values up

**Table 8.3** SPECIFIC ELECTRICAL D. C. RESISTANCE $\varrho$ OF FERRITES AT 100°C[5]

| *Ferrite* | $\varrho$ (kΩ cm) | |
|---|---|---|
| | *Slowly cooled* | *Quenched* |
| $CuO \cdot Fe_2O_3$ | 500 | 4 |
| $CoO \cdot Fe_2O_3$ | 1 000 | — |
| $MgO \cdot Fe_2O_3$ | 1 000 | 0·7 |
| $NiO \cdot Fe_2O_3$ | 800 | 2 |
| $ZnO \cdot Fe_2O_3$ | 450 | 8 |

to $10^5$ MΩ cm are now known for ferrites. For a nickel ferrite of homogeneous stoichiometric composition, values as high as $\varrho = 10^6$ MΩ cm can be attained, according to Van Uitert[32].

#### 8.1.3.1 Electrical resistance as a function of temperature

Ferrites are classified as semiconductors, i.e. their electrical resistance drops with rising temperature; in fact the law is exponential, having more or less the form $\varrho = a \exp. (-b/T)$.

For various ferrites up to about 400°C, Bochirol[5] obtained a straight line, when he plotted log $\varrho$ against $1/T$. This law ceases to hold at higher temperatures. The curve then becomes concave, as seen from below. Figure 8.4 shows this relation for magnesium ferrite: of the two curves the upper one holds for slowly cooled samples, i. e. for 80°C/h drop from 700°C to 100°C, while the lower curve is for quenched samples. The influence already mentioned (Figure 6.9) of rate of cooling on the magnetic values shows itself, also, in the specific electrical resistance of magnesium ferrites. The same effect may be observed in certain other ferrites (see Table 8.3).

Bradburn and Rigby[7] confirmed the exponential law for $MgO \cdot Fe_2O_3$ in the range 610°–830°C (Figure 8.5). Both above and below this temperature range, the excitation energy is different: the conductivity does not change so quickly with temperature as the expected law would prescribe.

Magnesium ferrite is an electron conductor whose activation energy in the linear range 610°–830°C has a value of 1·16 eV. Guillaud and Bertrand[14] have measured high electrical resistances for pure magnesium ferrite: at

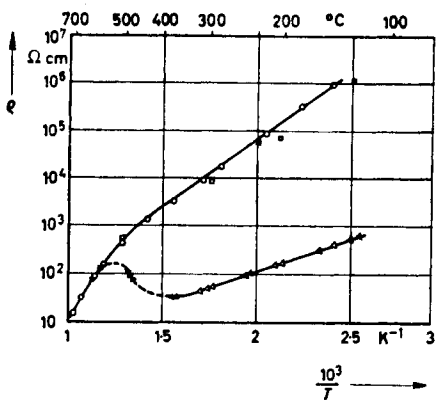



*Figure 8.4. Dependence of resistance on temperature for magnesium ferrite*[5]

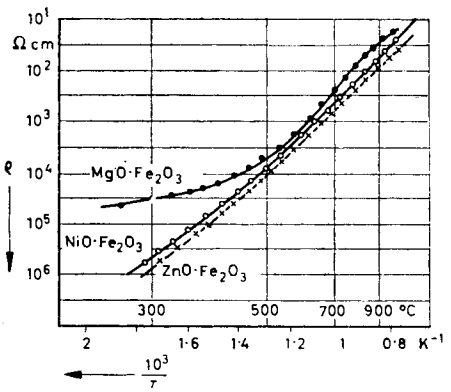



*Figure 8.5. Specific electrical resistance of magnesium ferrite, nickel ferrite, and zinc ferrite between 300°C and 1000°C*[7]

room temperature they found $\varrho = 63$ MΩ cm and at $-100$°C something over $10^5$ MΩ cm. This type of ferrite is, therefore, suitable as a basis for the development of ferrites usable at the highest frequencies.

Resistance characteristics $\varrho = f(T)$ mostly exhibit a rather flat kink[7], which lies around 500°C for the nickel ferrite $NiO \cdot Fe_2O_3$ and for the zinc ferrite $ZnO \cdot Fe_2O_3$ (see Figure 8.5). The activation energy of $NiO \cdot Fe_2O_3$ is 0·77 eV below the kink and 1·01 eV above it, while for $ZnO \cdot Fe_2O_3$ the corresponding values are 0·83 eV and 0·96 eV (see Figure 8.5). This inflexion is also found in many other ferrites. Komar and Kljuschin[18] were the first to note that the kinks occur in the neighbourhood of the Curie temperature. They were accounted for as re-ordering processes connected with slight structural changes or as changes in the dominant conduction mechanism.

The temperature dependence of electrical resistance is displayed in Figure 8.6[33] for the nickel ferrite $NiO \cdot Fe_{1.9}O_3$ and in Figure 8.7[40] for the barium ferrite $BaO \cdot 6Fe_2O_3$. The ferrite with the lowest specific electrical resistance is, as mentioned before, the ferroferrite $FeO \cdot Fe_2O_3$. At room temperature this resistance amounts to only 5 mΩ cm[34]. This is connected with the fact that bivalent and trivalent ions can enter the octahedral sites, and exchange

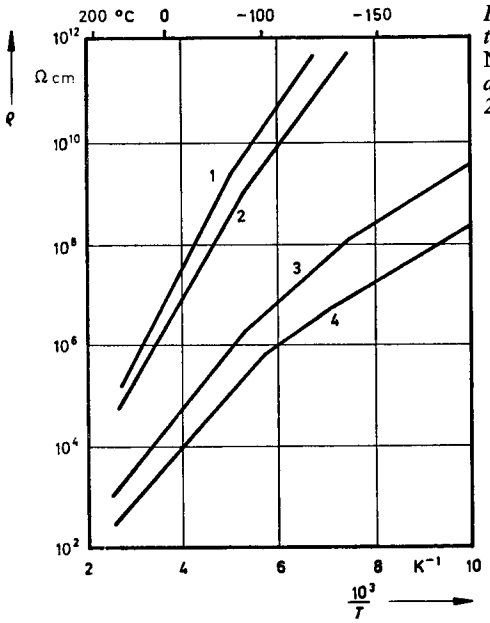



*Figure 8.6. Dependence of specific electrical resistance on temperature for* $NiO \cdot Fe_{1.9}O_3$ *which was sintered for 10* h *at the following temperatures: 1, 1200°C; 2, 1250°C; 3, 1300°C; 4, 1400°C*[33]

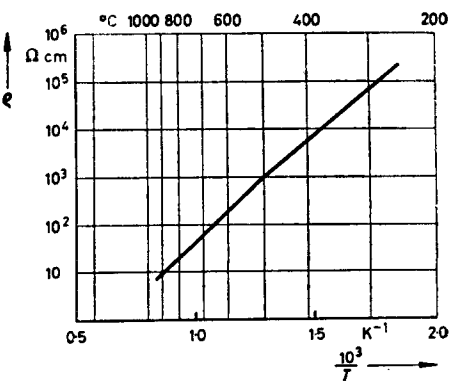



*Figure 8.7. Specific electrical resistance of barium ferrite* $BaO \cdot 6Fe_2O_3$ *as a function of temperature*[40]

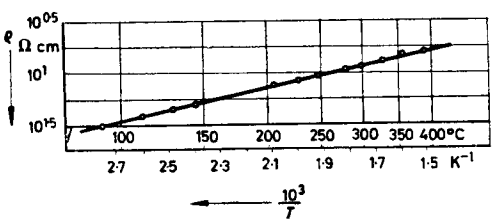



*Figure 8.8. Specific electrical resistance of magnetite*[7]

of electrons then becomes easily possible. The activation energy amounts to 0·1 eV, and the resistance gradient with falling temperature is thus very flat (Figure 8.8)[7].

### 8.1.3.2 Effect of additives

Many ferrites are required to exhibit high density as well as high electrical resistance, apart from purely magnetic properties. In general, however, high densities are obtainable only if the ferrite is sintered at high temperature.

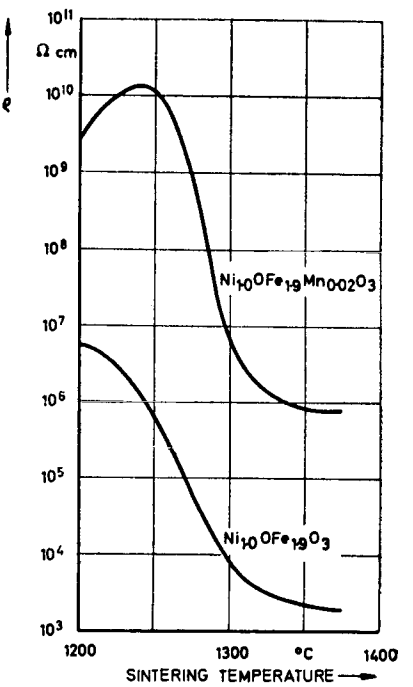



*Figure 8.9. Effect of sintering temperature on the specific electrical resistance of a nickel ferrite with and without a manganese additive*[33]

But the higher the sintering temperature, the lower the specific electrical resistance. As Figure 8.9 makes clear for a pure nickel ferrite to formula $Ni_{1\cdot0}Fe_{1\cdot9}O_4$, the resistance $\varrho$ falls by three orders of magnitude if the sintering temperature is raised from 1200°C to 1375°C[33]. Many types of ferrites behave in a similar manner.

Investigations into means of increasing the electrical resistance have been undertaken, in particular by Van Uitert. He found that the behaviour of mixed ferrites with suitable additives varied: Ni–Zn ferrite with critical additions of manganese and cobalt enabled significant increases of resistance to be achieved. The resistance $\varrho$ increased by several orders of magnitude by addition of only 0·02% Mn (Figure 8.9).

According to Guillaud and Bertrand[14], working with magnesium ferrite, the electrical resistance was lowered by the addition of zinc ferrite. However,

if part of the iron in a magnesium ferrite was replaced by aluminium, the specific electrical resistance, originally 10 kΩ cm, was increased by several orders of magnitude. For $MgAl_{0.4}Fe_{1.6}O_4$, for example, it could attain a value of $10^9\Omega$ cm if the sample were sintered at 1350°C in oxygen[34].

If about 10% of the magnesium is replaced by copper, whose oxide has a lower melting point (1230°C), then, according to Van Uitert[35], a Mg–Mn–Al–Cu ferrite can be prepared which unites high resistance with high

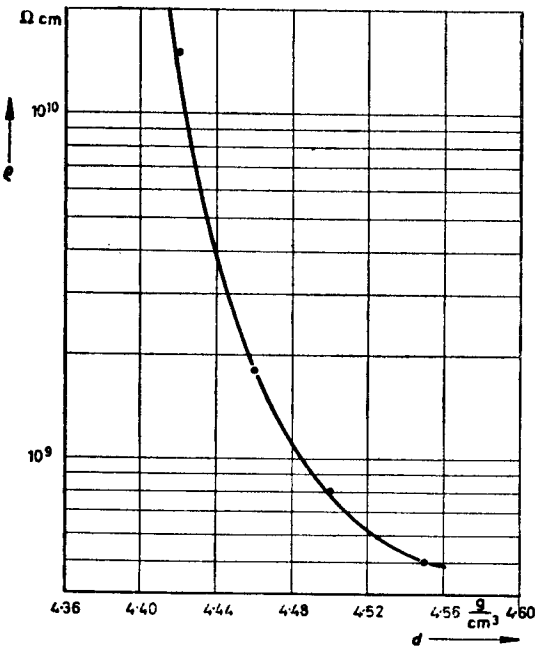



*Figure 8.10. Specific electrical resistance of the mixed ferrite* $Mg_{0.9}Cu_{0.1}Fe_{1.75}Mn_{0.04}O_{4\pm\varepsilon}$ *as a function of density*[35]

density. From Figure 8.10 it can be seen that for the ferrite $Mg_{0.9}Cu_{0.1}Fe_{1.75}Mn_{0.04}O_{4\pm\varepsilon}$ sintered at 1200°–1250°C there is, again, a falling off in resistance with increasing density.

Van Uitert[31], working with magnesium ferrite aluminates to the formula $Mg_{1.0}Al_xFe_{2-x}O_4$ and a constant addition of a certain amount of manganese, was able to achieve a specific electrical resistance of $10^4$ MΩ cm (see also page 560). Almost the same figure can be achieved with nickel ferrite to which copper and manganese have been added to give the approximate formulation $Ni_{0.9}Cu_{0.1}Fe_{1.9}Mn_{0.02}O_4$[32]. The resistance falls by several orders of magnitude if, in the composition, two copper atoms replace one of nickel. For the optimum composition, the relative density attained a value of 98% although the material was sintered at the relatively low temperature of 1100°C.

### 8.1.3.3 Effect of sintering conditions

To achieve high resistance values, special sintering conditions must be presupposed as well as a suitable composition. The importance of sintering temperature was mentioned in the section above (Figure 8.9). It may be appreciated, also, by looking at Figure 8.11, where, for the mixed ferrite

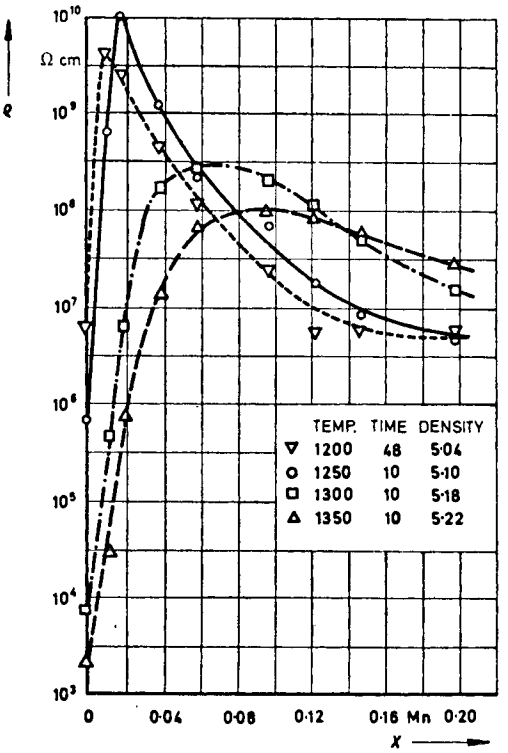



*Figure 8.11. Dependence of the resistance of* $Ni_{1\cdot0}\ Fe_{1\cdot8}\ Mn_x\ O_4$ *on the proportion of manganese and the effect of sintering temperature*[33]

$Ni_{1\cdot0}Fe_{1\cdot9}Mn_xO_4$, the dependence of resistance on various amounts of added manganese at various temperatures is plotted, following Van Uitert[33]. The highest resistance figure, namely $\varrho = 10^{10}\ \Omega$cm, was achieved for $x = 0{\cdot}02\%$ if sintering took place at 1250°C. At higher sintering temperatures the resistance of the sample fell. Higher manganese fractions might then give better results and would also lead to higher density.

Koops[19] was able to show experimentally how important the annealing atmosphere is and how strongly it can affect the electrical resistance of Ni–Zn ferrites: if a Ni–Zn ferrite of composition $Ni_{0\cdot4}Zn_{0\cdot6}Fe_2O_4$ is sintered at 1300°C, then entirely different figures are obtained for resistance by varying the oven atmosphere and the rate of cooling, the resistance being

measured at room temperature; Koops relates these variations to the proportion of iron oxide FeO determined by chemical analysis. After sintering in air and rapid cooling in air, the resistance measured at 1 kHz was 1·08 kΩ cm and the FeO content of the sample was 0·42%. If the same sample was cooled slowly in air, the FeO content was only 0·07% and the electrical resistance was more than 100 times higher, namely 136 kΩ cm.

Following an annealing in oxygen and rapid cooling in air, the figures were much the same as for annealing in air, namely 0·38% FeO and $\varrho = 1{\cdot}28$ kΩ cm. Annealing in oxygen and slow cooling in oxygen brought about the following pair of values: 0·10% FeO and $\varrho = 540$ kΩ cm. The d.c. resistance of a sample annealed in air at 1280°C and slowly cooled in air was 2·02 MΩ cm. This figure is of the same order of magnitude as the values given in Table 8.3.

The various values of resistance quoted in the literature for ferrites of the same type depend, in part, on the differing conditions under which they were prepared. Thus, the resistance values quoted by Harvey, Hegyi, and Leverenz[16] for the three-component system NiO–ZnO–$Fe_2O_3$ are relatively low because the test pieces were sintered in air at a high temperature (1400°C). The authors, however, were well aware that by sintering—or crystallisation, as they called it—at lower temperatures, resistances up to several MΩ cm could be achieved.

Sintering temperature in conjunction with a suitable furnace atmosphere thus largely determines the electrical resistance of ferrites. But not only the room temperature value of the resistance, but also its temperature variation is determined by the sintering conditions. Figure 8.6 shows curves for a nickel ferrite $Ni_{1{\cdot}0}Fe_{1{\cdot}9}O_4$ that was sintered for 10 h at the temperatures quoted[33]. The curves are built up from a series of straight-line sections which become flatter as the selected sintering temperature is increased.

### 8.1.3.4 The mechanism of conductivity

Koops[19] has shown that the bivalent ferrous ion, when associated in a spinel lattice with the trivalent ion, can substantially lower the resistance. This is to be attributed to the fact that in the spinel lattice an interchange of electrons can take place very readily between the $Fe^{2+}$ and $Fe^{3+}$ ions. Ferrites, therefore, which are to have high electrical resistance must be free from magnetite.

As with other semiconductors, such as germanium and silicon, two conduction mechanisms are to be dinstinguished, namely electron conduction and hole conduction—also called n-type and p-type conduction. If in a high-resistance material one cation is replaced by another that seeks a lower valency level, then, in general, p-conduction results; if, on the other hand, the added cation tends towards a condition of higher valency, this leads to n-conduction. Therefore, if there is an iron excess in a particular ferrite, $Fe^{2+}$ will form and a high electron conduction results.

Van Uitert[34] demonstrated the transition from p-type to n-type conduction in the ferrite $Ni_{0{\cdot}3}Zn_{0{\cdot}7}Fe_xO_{4\pm\varepsilon}$: for $x < 2$ the resistance of the stoichiometrically under-matched ferrite is greater than $10^9\Omega$ cm. When $x > 2$, it

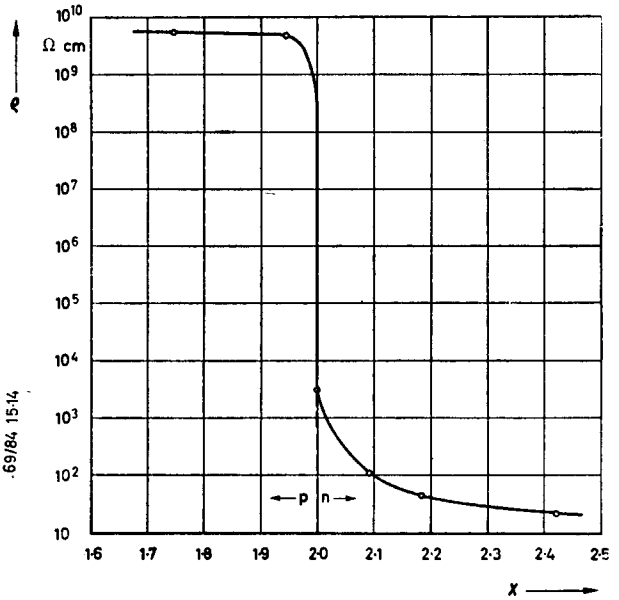



*Figure 8.12. Electrical resistance of* $Ni_{0\cdot3}\ Zn_{0\cdot7}\ Fe_x\ O_{4\pm e}$

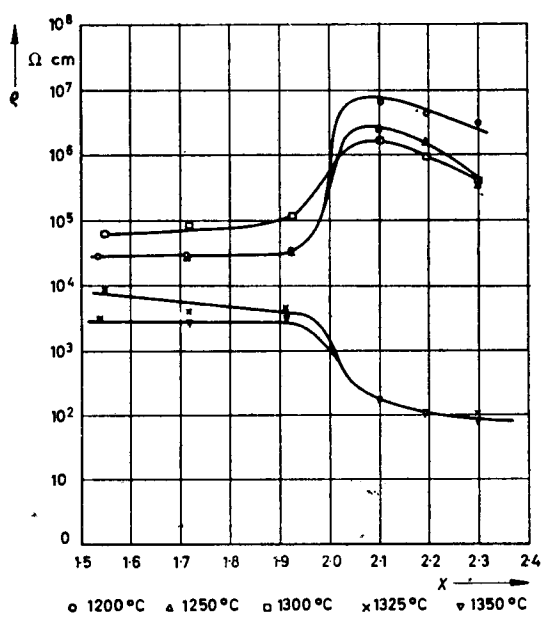



*Figure 8.13. Effect of sintering temperature on the electrical resistance of* $NiO{\cdot}Fe_xO_3$[30]

falls by five or six orders of magnitude (see Figure 8.12). Working with a nickel ferrite sintered at 1200°–1300°C, Van Uitert[30] established the existence of the opposite kind of curve, as one passes from a lack of iron to an excess, the resistance rises from 100 kΩ cm to 10 MΩ cm. Figure 8.13 displays the effect of sintering temperature on $NiO \cdot Fe_xO_3$. At sintering temperatures over 1300°C and for $x > 2$, there is a bias toward n-conduction.

### 8.1.3.5 Frequency dependence (dispersion)

The measured values of specific electrical resistance of ferrites depend, finally, not only on chemical composition, constituent balance, and sintering conditions, but also on the measuring frequency.

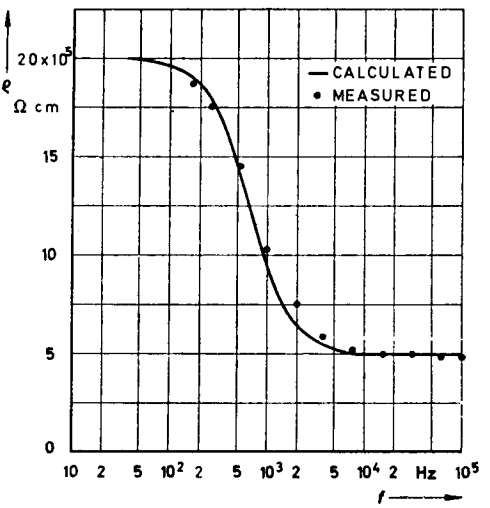



*Figure 8.14. Relation between resistance and frequency for the ferrite* $Ni_{0.4}Zn_{0.6}Fe_2O_4$[19]

The electrical resistance at 100 kHz of the ferrite $Ni_{0.4}Zn_{0.6}Fe_2O_4$, annealed in air at 1280°C and slowly air-cooled, is only one-quarter of the d.c. resistance. This is shown in Figure 8.14 and Table 8.4, following work already referred to by Koops[19]. This resistance drop, which—as will be shown later—is associated with a similar fall in dielectric constant, has led to a proposed ferrite model: ferrite particles are supposed to be individually conducting, relatively speaking, but separated by layers of lower-conductivity material.

This view is supported by the experiments of Rupprecht and Heck[26] concerned with electrical measurements on anisotropic permanent-magnet ferrites (Figure 8.15). They found, moreover, that for barium ferrite $BaO \cdot 6Fe_2O_3$ and lead ferrite $PbO \cdot 4Fe_2O_3$ the 'parallel' resistance $\varrho_P$ measured at 30 MHz, was dependent on direction. The electrical resistance in the direction of easiest magnetisation was greater than in the direction normal to it (Table 8.5). That the directionality was less obvious for the lead ferrite was due to

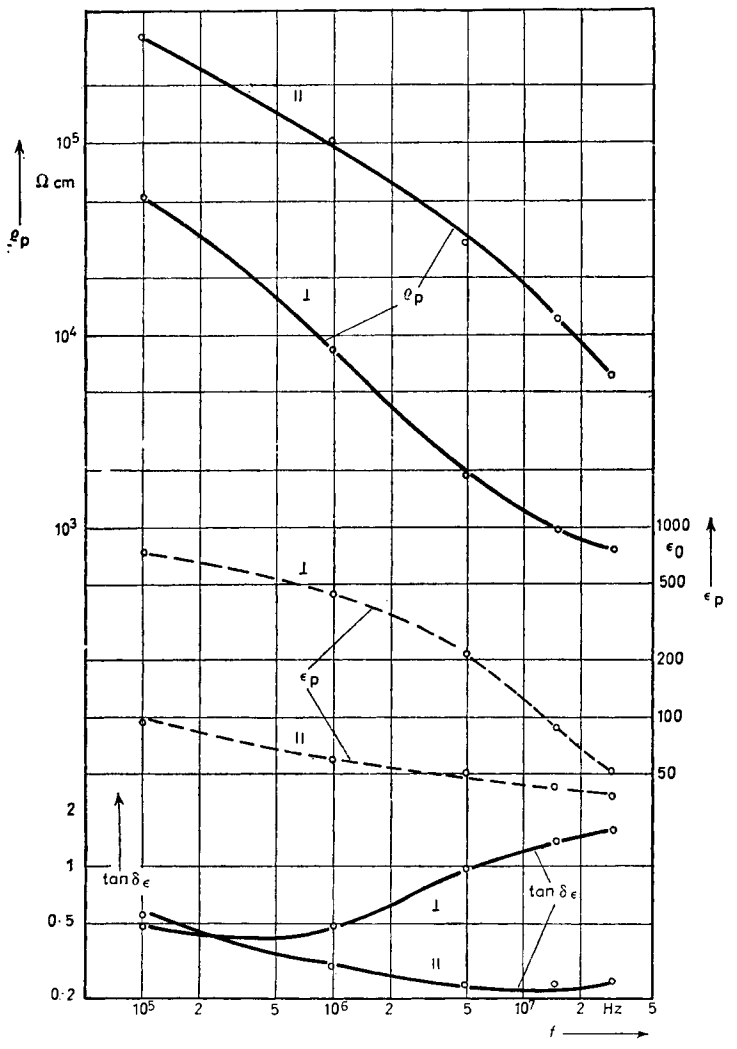



*Figure 8.15. Aligned barium ferrite* $BaO \cdot 6Fe_2O_3$ *measured parallel to ( ∥ ) and perpendicular to ( ⊥ ) the preferred direction of magnetisation: effect of frequency on electrical resistance* $\varrho_D$ *dielectric constant* $\varepsilon_p$*, and dielectric loss factor tan* $\delta_\varepsilon$[26]

**Table 8.4** ELECTRICAL PROPERTIES OF $Ni_{0\cdot4}Zn_{0\cdot6}Fe_2O_4$ ANNEALED IN AIR AT 1280°C AND SLOWLY COOLED IN AIR (MEASUREMENTS MADE AT ROOM TEMPERATURE)[19]

| $f$ (kHz) | $\varrho_p$ (kΩ cm) | $\varepsilon_p$ ($\varepsilon_0$) | tan $\delta_\varepsilon$ |
|---|---|---|---|
| 0·16 | 1 870 | 1 980 | 3·05 |
| 0·25 | 1 750 | 1 870 | 2·20 |
| 0·50 | 1 430 | 1 520 | 1·66 |
| 1 | 1 050 | 1 090 | 1·59 |
| 2 | 740 | 610 | 2·00 |
| 4 | 580 | 256 | 3·03 |
| 8 | 520 | 93 | 4·70 |
| 16 | 500 | 37 | 6·10 |
| 32 | 490 | 22 | 5·20 |
| 64 | 480 | 17 | 3·40 |
| 100 | 470 | 16 | 2·40 |

**Table 8.5** ELECTRICAL PROPERTIES OF ORIENTED BARIUM AND LEAD FERRITES ($\varrho_p$ AND $\varepsilon_p$ MEASURED AT 30 MHz; $\varrho$ MEASURED WITH DIRECT CURRENT AND AT ROOM TEMPERATURE)[26]

| *Ferrite* | *Preferred direction of magnetisation* | $\varrho_p$ (Ω cm) | $\varrho$ (MΩ cm) | $\varepsilon_p$ ($\varepsilon_0$) | $d$ (g/cm³) |
|---|---|---|---|---|---|
| $BaO{\cdot}6Fe_2O_3$ | ⊥ | 740 | 5 | 56 | 5·0 |
| | ∥ | 5 700 | 5 | 37 | 5·0 |
| $PbO{\cdot}4Fe_2O_3$ | ⊥ | 410 | 30 | 73 | 5·1 |
| | ∥ | 680 | 30 | 62 | 5·1 |

the smaller anisotropy of this sample—the anisotropy in question was purely that produced by pressing, i.e. without the help of an orienting direct field.

Derry and Wills[11] carried out measurements on nickel ferrite at various reduced values of the stoichiometry (atomic proportions). Figure 8.16 shows their results: it will be seen that n-type conduction occurs with an excess of $Fe_2O_3$ and a sintering temperature above 1165°C and that the conductivity increases with the sintering temperature. This is in agreement with the observations of Van Uitert[30] (see Figure 8.13). An excess of NiO causes the conductivity to pass over into the p-type and, again, to increase with the sintering temperature.

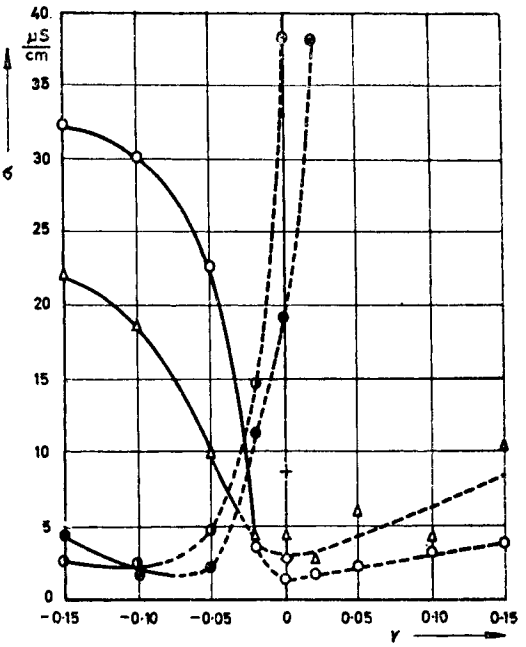



*Figure 8.16. Apparent conductivity at 10* MHz *of nickel ferrite* $NiO(Fe_2O_3)_{1+\gamma}$*; solid lines, p-conductivity; broken lines, n-conductivity*[11]

## 8.2 DIELECTRIC CONSTANT AND LOSS ANGLE

### 8.2.1 Heterogeneous bodies (dust cores)

The apparent dielectric constant of moulded metallic cores of well-dried Mo-Permalloy dust having an effective permeability of $\mu_e = 14$–$26\mu_0$ is roughly $\varepsilon = 100$[23]. Absorption of moisture causes $\varepsilon$ to rise 10–15 fold.

The dielectric loss factor of a carefully dried dust core having $\mu_e = 14\mu_0$ can be some $8\times10^{-3}$ at 100 kHz. If the core is allowed to remain for a few weeks at more than 50% humidity, then tan $\delta_\varepsilon$ will rise to about $80\times10^{-3}$.

### 8.2.2 Ferrites

It has been known since the investigations of Blechschmidt[4] in 1938 that ferrites have a high dielectric constant and that this depends strongly on frequency. The loss factor tan $\delta_\varepsilon$ is generally very high at low frequency, falling by several orders of magnitude as the frequency rises.

Koops[19] found that the dielectric constant of Ni–Zn ferrite $Ni_{0.4}Zn_{0.6}Fe_2O_4$ followed much the same course with changing frequency as the electrical resistance, i.e. it fell with rising frequency down to a very small value. Actual

measured values are shown in Figure 8.17 up to $10^5$ Hz, together with a theoretical curve plotted on the assumption that a ceramic core can be treated like a dust core. The basis of the calculation will be briefly indicated.

Figure 8.18 shows, on the left, two equivalent electrical circuits. In the left-hand diagram, $R_1$, $R_2$, $C_1$, and $C_2$ are constants; in the middle diagram,

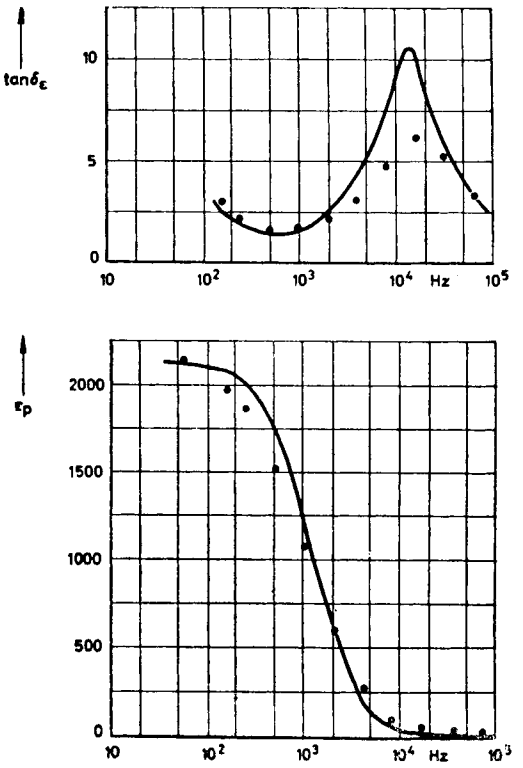



*Figure 8.17. Dependence on frequency of loss factor tan $\delta_\varepsilon$ and dielectric constant $\varepsilon_p$ for* $Ni_{0.4}Zn_{0.6}Fe_2O_4$[19]

the magnitudes $C_p$ and $R_p$ obey a dispersion law. A heterogeneous body is shown, schematically, at the right in the same figure. Particles of the material (2) are separated by partition layers (1). Let $\varrho_1$ and $\varepsilon_1$ be the specific electrical resistance and the dielectric constant of the poorly conducting partition layers, and $\varrho_2$ and $\varepsilon_2$ the corresponding values for the more conductive granules; further, let $x$ be the thickness ratio of partition layer to granule: then for the electrical resistance (in parallel connection),

$$\varrho_p = \varrho_p^\infty + \frac{\varrho_p^0 - \varrho_p^\infty}{1+\tau_\varrho^2\omega^2}$$

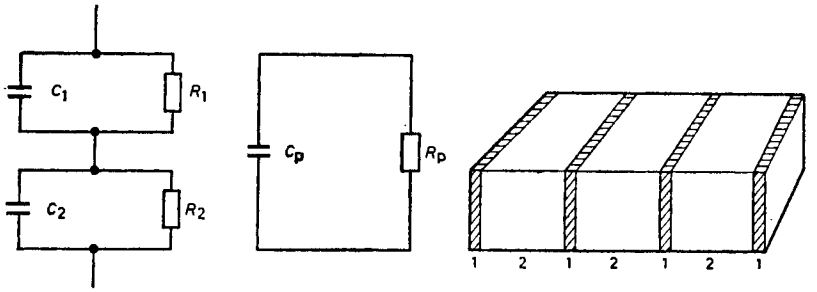



*Figure 8.18. Equivalent circuit and model for heterogeneous bodies (dust cores, ferrites)*

In this expression

$$\varrho_p^\infty = \frac{\varrho_1\varrho_2(\varepsilon_1+x\varepsilon_2)^2}{\varrho_1\varepsilon_1^2+x\varrho_2\varepsilon_2^2} = \text{high-frequency value of } \varrho_p$$

$$\varrho_p^0 = x\varrho_1+\varrho_2 = \varrho_p \text{ at very low frequencies}$$

and

$$\tau_\varrho = \varepsilon_0\sqrt{\left[\frac{\varrho_1\varrho_2(\varrho_1\varepsilon_1^2+x\varrho_2\varepsilon_2^2)}{x\varrho_1+\varrho_2}\right]} = \text{relaxation constant for } \varrho_p$$

The formula for the dielectric constant is built on a very similar plan:

$$\varepsilon_p = \varepsilon_p^\infty + \frac{\varepsilon_p^0-\varepsilon_p^\infty}{1+\tau_\varepsilon^2\omega^2}$$

where

$$\varepsilon_p^\infty = \frac{\varepsilon_1\varepsilon_2}{\varepsilon_1+x\varepsilon_2} = \text{high-frequency value of } \varepsilon_p$$

$$\varepsilon_p^0 = \frac{x\varrho_1^2\varepsilon_1+\varrho_2^2\varepsilon_2}{(x\varrho_1+\varrho_2)^2} = \varepsilon_p \text{ at very low frequencies}$$

and

$$\tau_\varepsilon = \varepsilon_0\frac{\varrho_1\varrho_2(\varepsilon_1+x\varepsilon_2)}{x\varrho_1+\varrho_2} = \text{relaxation constant for } \varepsilon_p$$

The curves of Figures 8.14 and 8.17 are drawn on the particular assumptions that

$$\varrho_1 = 3{\cdot}3\times10^8\,\Omega\text{ cm} \qquad \varepsilon_1 = 17$$
$$\varrho_2 = 5{\cdot}0\times10^5\,\Omega\text{ cm} \qquad \varepsilon_2 = 17$$
$$x = 0{\cdot}4\%.$$

A comparison of the curves with the plotted measured points shows that there is excellent agreement with the hypothesis. Koops was also able to show that the same dispersion law held for very differently annealed ferrites with greater or less FeO content.

The measured values quoted by Koops[19] for $\varrho_p$, $\varepsilon_p$, and tan $\delta_\varepsilon$ are shown in Table 8.4. As may be seen from Figure 8.17, both the measured and the calculated maximum for tan $\delta_\varepsilon$ occur at a higher frequency than the corresponding turning point of the $\varepsilon$ curve.

Table 8.6 gives the electrical properties of a few ferrites at 172·5 MHz, following measurements by Wagenknecht[39]. Okamura, Fujimura, and Date[22] carried out measurements at a wavelength of 6·6 cm. Table 8.7, based on

**Table 8.6** ELECTRICAL AND MAGNETIC PROPERTIES OF A FEW FERRITES AT 172·5 MHz[39]

| *Ferrite* | $\varepsilon$ | tan $\delta_\varepsilon$ | $\mu$ | tan $\delta_\mu$ | $\varrho$ (kΩ cm) |
|---|---|---|---|---|---|
| $MgO \cdot Fe_2O_3$ | 14·0 | 0·63 | 7·3 | 0·53 | — |
| $MnO \cdot Fe_2O_3$ | 57·2 | 0·42 | 17·2 | 0·38 | 0·42 |
| $NiO \cdot Fe_2O_3$ | 12·4 | 0·46 | 6·1 | 0·34 | 1·4 |
| $CuO \cdot Fe_2O_3$ | 11·1 | 0·21 | 3·9 | <0·14 | 0·44 |

**Table 8.7** DIELECTRIC CONSTANTS, PERMEABILITY, AND tan $\delta$ OF SOME FERRITES AT A WAVELENGTH OF 6·6 cm (SAMPLE THICKNESS 1·5 mm)[22]

| *Ferrite* | *Cooling* | $\varepsilon$ | $\varepsilon'$ | tan $\delta_\varepsilon$ | $\mu$ | $\mu'$ | tan $\delta_\mu$ |
|---|---|---|---|---|---|---|---|
| $MgO \cdot Fe_2O_3$ | Quenched from 1200°C | 9·66 | 0·174 | 0·018 | 1·20 | 0·974 | 0·128 |
| | Slowly cooled | 8·53 | 0·132 | 0·016 | 2·84 | 0·341 | 0·120 |
| $CuO \cdot Fe_2O_3$ | Quenched from 1000°C | 9·29 | 0·520 | 0·056 | 1·94 | 1·240 | 0·639 |
| | Slowly cooled | 8·65 | 0·089 | 0·010 | 1·38 | 0·740 | 0·543 |
| $CoO \cdot Fe_2O_3$ | Quenched from 1200°C | 9·49 | 0·045 | 0·047 | 1·57 | 0·211 | 0·138 |
| | Slowly cooled | 9·00 | — | — | 1·90 | 0·116 | 0·061 |
| $NiO \cdot Fe_2O_3$ | Quenched from 1200°C | 13·40 | 3·520 | 0·260 | 1·74 | 0·460 | 0·264 |
| | Slowly cooled | 8·88 | 0·155 | 0·017 | 1·47 | 2·377 | 1·620 |
| $MnO \cdot Fe_2O_3$ | Quenched from 1200°C | 9·30 | 0·475 | 0·051 | 2·31 | 2·040 | 0·883 |

samples either quenched or slowly cooled from 1200°C, gives the values of $\varepsilon$ and tan $\delta$, from which one may deduce that quenched nickel ferrite has the highest dielectric constant and that tan $\delta_\varepsilon$ is lowest for slowly cooled copper ferrite.

It can be concluded from measurements by Möltgen[21] on copper ferrites that the frequency at which the end-value of $\varepsilon$ is reached depends on the

composition and on the conductivity of the ferrite. While the dielectric constant of Koops' Ni–Zn ferrite fell most steeply around 1 kHz and had attained its limiting value at 100 kHz, it was found that for barium ferrite of composition $BaO \cdot 6Fe_2O_3$ the $\varepsilon$ value began to drop steeply only at a frequency of several megahertz.

The dielectric constant and loss factor of a magnetically anisotropic barium ferrite showed anisotropic results just as did the specific electrical resistance. The maximum point of the tan $\delta_\varepsilon$ curve is not reached even at 30 MHz (see Figure 8.15)[26]. The dielectric constant, $\varepsilon$, of ferrites measured at low frequencies is of the general order of $10^5$; the loss factor is high, and above 150 Hz it usually exceeds unity (Table 8.4). Barium ferrite $BaO \cdot 6Fe_2O_3$ and also those ferrites set out in Table 8.6 give, however, somewhat lower values.

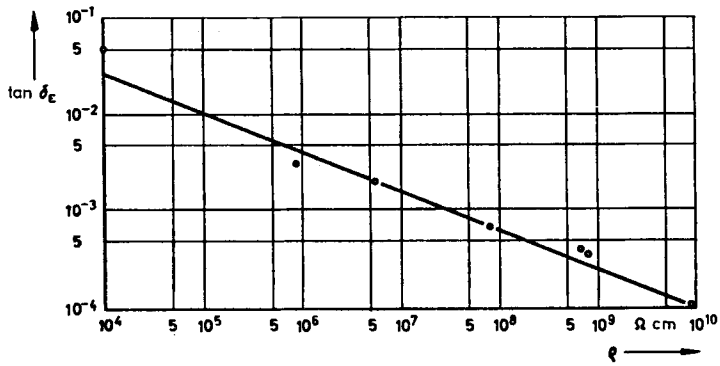



*Figure 8.19. Dependence of dielectric loss factor at 9·4 GHz on d.c. resistance for a nickel ferrite*[25]

It can be quite another matter at very high frequencies: thus Rowen and Kankowski[25] were able to show that at 9.4 GHz the tan $\delta_\varepsilon$ of a pure nickel ferrite enriched with manganese fell very sharply with increasing specific electrical resistance. Tan $\delta_\varepsilon$ drops to $5 \times 10^{-4}$ or less for a d.c. resistance of $10^4$ MΩ cm (Figure 8.19).

Fairweather and Frost[13] investigated the temperature dependence of the dielectric constants of magnesium ferrite and Mg–Al ferrites. They found in all cases that both the dielectric constant and the conductivity rose with temperature at high and low frequencies. The maximum of the tan $\delta$ curve shifted toward higher frequencies with rising temperature. The measurements given in Figure 8.20 for a sample of $MgAl_{0.4}Fe_{1.6}O_4$ are taken from this work. In this figure, $\sigma_{HF}$ stands for conductivity and $f_m$ for the frequency at which the maximum tan $\delta_{max}$ was measured. The slopes of the three straight lines are practically the same, as are, the activation energies. Kamiyoshi[17] was able to establish that for nickel and cobalt ferrites, also, the two activation energies are equal, and it may be concluded from this that the underlying mechanism is the same.

The high dielectric constant of the ferrites gives rise to a resonance effect whose cause was first suggested by Brockman, Dowling, and Steneck[9].

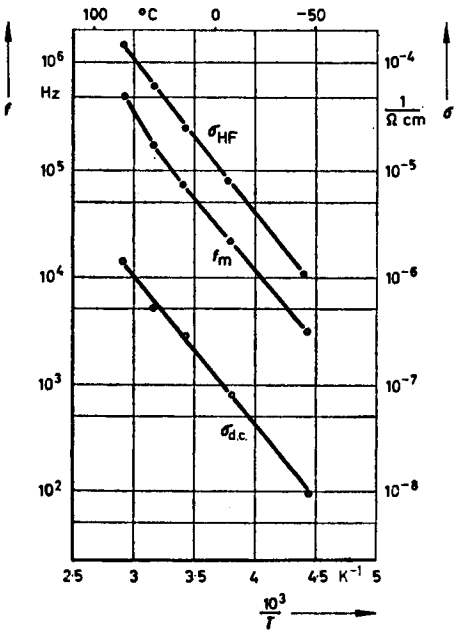



*Figure 8.20. High-frequency conductivity $\sigma_{HF}$, d.c. conductivity $\sigma_{d.c.}$ and frequency $f_m$ as functions of temperature for the ferrite* $MgAl_{0.4}Fe_{1.6}O_4$[13]

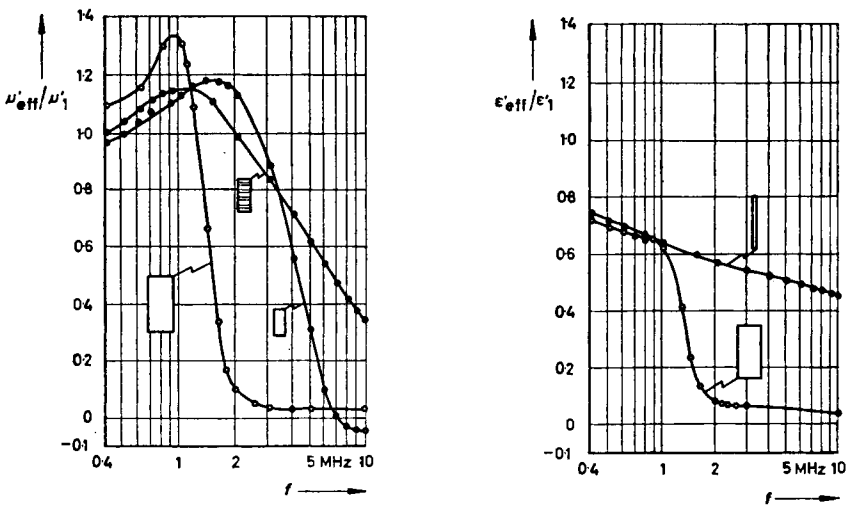



*Figure 8.21. Effect of the volume of a specimen on the shape of the frequency characteristics of permeability and dielectric constant for* Mn–Zn *ferrite*[9]

They investigated a core of Mn–Zn ferrite having a relatively large cross-section and discovered that the permeability dropped sharply at frequencies over 1 MHz. The same phenomenon was observed for the frequency curve of the dielectric constant. The relative measured values at 1 kHz are shown in Figure 8.21. The greatest cross-section used amounted to 25 mm$\times$12·5 mm. When the cross-section was reduced, or the sample laminated, the drop in $\mu$ was shifted towards the higher frequencies and the whole laminated core gave the same results as for an individual lamina. The drop in $\varepsilon$ between 1 MHz and 2 MHz could be made to vanish completely by reducing the cross-section.

It can be concluded from the effect of sectional changes that the measured falling off of $\mu$ is in no sense a property of the material but is, rather, a dimensional effect. In fact, it is a question of the appearance of a resonance brought about by the fact that the permeability and the dielectric constant are both high simultaneously. If the smallest core dimension in which an electromagnetic wave is propagated is equal to half the wavelength, then resonance occurs. If $\lambda_m$ is the wavelength in the medium and $\lambda_0$ the wavelength in vacuo, then the following equation holds

$$\lambda_m = \frac{\lambda_0}{\sqrt{(\mu\varepsilon)}}$$

In our example, $\mu = 10^3$, $\varepsilon = 10^5$, and $\lambda_m = 1$ cm, giving an approximate value for $\lambda_0 = c/f$ of $10^4$ cm, or $f \doteq 10^6$ Hz.

The high dielectric constants of the ferrites at room temperature and at low frequencies, discussed above, suggests that they would make excellent

**Table 8.8** DIELECTRIC CONSTANT AND LOSS FACTOR TAN $\delta_\varepsilon$ FOR Fe–Sn FERRITES MANUFACTURED BY A 4 h SINTER OF THE OXIDE AT 1225°C IN NITROGEN HAVING 5% O CONTENT (50 Hz, 20°C, 2 V)[24]

| *Composition* | $\varepsilon$ | tan $\delta_\varepsilon$ |
|---|---|---|
| 99% $Fe_2O_3$, 1% $SnO_2$ | 2 000 000 | ~2 |
| 98·5% $Fe_2O_3$, 1·5% $SnO_2$ | 5 000 000 | ~4 |
| 89·5% $Fe_2O_3$, 10·5% $SnO_2$ | 7 000 000 | ~5 |

dielectrics for capacitors. There has thus been no lack of attempts to develop ferrites characterised by especially high dielectric constants. Whereas Cu–Zn ferrites, Mn–Zn ferrites, Cu–Cd ferrites, and Ni–Zn ferrites have a maximum $\varepsilon$ of $10^4$–$10^5$, Pierrot, Lescroël and Bernard[24] found for Fe–Sn ferrites the values quoted in Table 8.8. However, up to the present, ferrites have not apparently been used in the construction of capacitors because tan $\delta_\varepsilon$ is too high.

## REFERENCES


1. ARMCO STEEL CORP., MIDDLETOWN: Magnetic ingot iron (1959).
2. ARNOLD ENGNG. CO., MARENGO: Bulletin TC 101 A (1960).
3. V. AUWERS, O.: Magnetisch weiche und harte Werkstoffe der Mess- und Nachrichtentechnik (ETZ **63** (1942) 341–348).
4. BLECHSCHMIDT, E.: Dielektrische Eigenschaften von Manganferriten (Phys. Z. **39** (1938) 212–216).
5. BOCHIROL, L.: Resistivité des ferrites de zinc, de nickel, de cobalt, de magnesium et de cuivre en fonction de la température (C. R. **233** (1951) 736–738).
6. BOOTHBY, O. L. and BOZORTH, R. M.: A new magnetic material of high permeability (J. Appl. Phys. **18** (Feb. 1947) 173–176).
7. BRADBURN, T. E. and RIGBY, G. R.: The electrical conductivity of spinels (Trans. Brit. Cer. Soc. **52** (1953) 417–435).
8. BRAILSFORD, F.: Magnetic Materials. Methuen & Co. Ltd., London/John Wiley & Sons Inc., New York (1951).
9. BROCKMAN, F. G., DOWLING, P. H. and STENECK, W. G.: Dimensional effects resulting from a high dielectric constant found in a ferromagnetic ferrite (Phys. Rev. 77 (2) (Jan. 1950) 85–93).

9a BUCKLEY, S. E.: Permalloys (Steels in Mod. Ind. (1951) 379–395).

10. CHEVENARD, P.: Les alliages á hautes teneurs en nickel et en chrome (Rev. metallurg. **25** (1928) 14–34).

10a CLEAVES, H. E. and HIEGEL, J. M.: Properties of high purity iron (J. Res. Nat. Bur. Stds. **28** (1942) 643–667).

11. DERRY, R. and WILLS, M. S.: Microwave Faraday effect and conductivity in nickel ferrites and ferrite-aluminates (Proc. IEE **104 B** (1957) 324–330).
12. ELMEN, G. W.: Magnetic alloys of iron, nickel and cobalt (El. Engng. **54** (12) (Dec. 1935) 1292–1299; (1936) 887–889).
13. FAIRWEATHER, A. and FROST, E. J.: Dielectric behaviour of granular semiconducting aggregates, with special reference to some magnesium ferrites (Proc. IEE (IIa) **100** (1953) 15–22).

13a FRASER, R. W., EVANS, D. J. I. and MACKIW, V. N.: Herstellung und Eigenschaften von duktilem Kobalt-Band (Kobalt **23** (June 1964) 62–69).

14. GUILLAUD, C. and BERTRAND, R.: Etude expérimentale de la résistance de quelques ferrites semi-conducteurs (J. Rech. **11** (1950) 73–82).
15. GUMLICH, E.: Magnetische Messungen. Friedr. Vieweg & Sohn, Braunschweig (1918).
16. HARVEY, R. L., HEGYI, I. J. and LEVERENZ H. W.: Ferromagnetic spinels for radio frequencies (RCA Rev. **11** (Sept. 1950) 321–363).
17. KAMIYOSHI, K.: Low frequency dispersion in Ni- and Co-ferrites (Sci. Rep. Res. Inst. Tohoku Univ. (A) **3** (1951) 716).
18. KOMAR, A. P. and KLJUSCHIN, W. W.: Temperaturabhängigkeit des elektrischen Widerstandes von Ferriten (Isv. Akad. Nauk., SSSR, Phys. Ser. **18** (1954) 400–402; Chem. Zentr. Bl. **28** (1955) 6457).
19. KOOPS, C. G.: On the dispersion of resistivity and dielectric constant of some semiconductors at audiofrequencies (Phys. Rev. **83** (2) (1951) 121–124).
20. MASUMOTO, H. and SAITO, H.: On the effect of heat treatment on the magnetic properties of iron–aluminium alloys, III. The change of electric resistance and magnetostriction due to water quenching (Sci. Rep. Res. Inst. Tohoku Univ. (A) **4** (1952) 338–346).
21. MÖLTGEN, G.: Dielektrische Untersuchungen an Ferriten (Z. ang. Phys. **4** (6) (1952) 216–224).
22. OKAMURA, T., FUJIMURA, T. and DATE, M.: Dielectric constant and permeability of various ferrites in the microwave region (Phys. Rev. **85** (2) (1952) 1041–1042).
23. OWENS, C. D.: Stability characteristics of molybdenum permalloy powder cores (El. Engng. **75** (Mar. 1956) 252–256).

24. PIERROT, A., LESCROEL, Y. and BERNARD, N.: Verfahren zur Herstellung von dielektrischem Material. DBP 1 125 340 (applic. 6. 4. 60).
25. ROWEN, J. H. and KANKOWSKI, E. F.: see Van Uitert (ref. 34).
26. RUPPRECHT, J. and HECK, C.: Anisotropie der dielektrischen Eigenschaften von gerichtetem Barium- und Blei-Ferrit (Ber. Arbg. Ferrom. (1958) Riederer (1959) 98–100).
27. SHACKELTON, W. J. and BARBER, I. G.: Compressed powdered permalloy (Trans. AIEE **47** (1928) 429–437).
28. STANDARD TELEPHONES & CABLES LTD. (ITT): Permalloy (1968).
28a TELCON METALS LTD, CRAWLEY: H. C. R. Alloy, 3rd edn (1962).
28b TELCON METALS LTD, CRAWLEY: Properties and Applications of Telcon Metals, 5th edn.
29. TOHOKU METAL IND. LTD, SENDAI (JAPAN): Sendust Data Sheet.
30. VAN UITERT, L. G.: D.C. resistivity in the nickel zinc ferrite system (J. Chem. Phys. **23** (10) (Oct. 1955) 1883–1887).
31. VAN UITERT, L. G.: Low magnetic saturation ferrites for microwave applications (J. A. P. **26** (Nov. 1955) 1289–1290).
32. VAN UITERT, L. G.: Nickel copper ferrites for microwave applications (J. A. P. **27** (1956) 723–727).
33. VAN UITERT, L. G.: High resistivity nickel-ferrites. The effect of minor additions of manganese or cobalt (Proc. Conf. Magnetism Magn. Mat. AIEE (1955) 299–304).
34. VAN UITERT, L. G.: Dielectric properties of and conductivity in ferrites (Proc. IRE **44** (10) (Oct. 1956) 1294–1303).
35. VAN UITERT, L. G.: Magnesium–copper–manganese–aluminium ferrites for microwave application (J. A. P. **28** (3) (Mar. 1957) 320–322).
36. VACUUMSCHMELZE GMBH: Permenorm 5000 Z. Data Sheet M 014 (Apr. 1961).
37. VACUUMSCHMELZE GMBH: Magnetoflex. Data Sheet M 016 (Sept. 1969).
38. VACUUMSCHMELZE GMBH: Vacodur 16. Data Sheet. M 009 (Mar. 1962).
38a VACUUMSCHMELZE GMBH: Handbuch Weichmagnetische Werkstoffe.
39. WAGENKNECHT, F.: Über die dielektrischen und magnetischen Eigenschaften einiger Ferrite bei Hochfrequenz (Frequenz **5** (5) (June 1951) 145–155).
40. WENT, J. J., RATHENAU, G. W., GORTER, E. W. and VAN OOSTERHOUT, G. W.: Ferroxdure, un groupe de nouveaux matériaux pour aimants permanents (Rev. Techn. Phil. **13** (1952) 361–376).
41. WESTINGHOUSE ELECTRIC CO.: Spec. techn. data 52–163 (1962).
42. WESTINGHOUSE ELECTRIC CO.: Spec. techn. data 52–167 (1962).
43. WESTINGHOUSE ELECTRIC CO.: Spec. techn. data 52–165 (1966).
44. YENSEN, T. D.: The magnetic properties of the ternary alloys Fe–Si–C (Trans. AIEE **43** (1924) 145–175).

# 9

# Permanent-magnet Materials

## 9.1 ROLE OF THE PERMANENT MAGNET

Permanent-magnet materials are differentiated from the softer substances more particularly by their high coercivity. This is mostly above 2 kA/m, so the material is not magnetically altered by weak field intensities, i.e. its magnetic condition is quasi-permanent. In contrast to the soft materials, the tendency is to try to develop the greatest possible coercivity and a large hysteresis loop. Permanent magnets are mostly used under static conditions.

In technology the role of a permanent magnet is to maintain a magnetic field within a prescribed region. This region is often the space between the poles of an appropriately shaped magnet. Frequently, special pole-pieces of soft iron are attached to the ends of the magnet in order to conduct the magnetic field into a suitable path and allow the magnet itself to assume a readily manufacturable form. Magnets of cylindrical and rectangular sections are generally the most popular.

A permanent magnet is not a store of energy to be made available as required. If this were so, the energy content would fall every time the magnet was used and would finally become exhausted. There could then be no sense in speaking of a permanent magnet! The energy of a permanent magnet is only so much potential energy and resembles, therefore, the earth's gravitational field. A magnet does work each time it attracts a piece of iron. An equal amount of work must then be performed to pull the iron away from the magnet.

## 9.2 DESCRIPTIVE CHARACTERISTICS OF PERMANENT-MAGNET MATERIALS

The magnetic properties of magnet material can be expressed in terms of the following quantities:

Demagnetisation curve $B = f(H)$ or $J = f(H)$
Remanence $B_r$ or $J_r$
Coercivity ${}_BH_c$ or ${}_JH_c$
Working field strength $H_w$

Working flux density $B_w$
Maximum product $(BH)_{max}$
Fulness factor, $\eta$
Permanent permeability $\mu_p$

The difference between the $J(H)$ and the $B(H)$ curves has already been explained (page 81). In technology it is usual to give preference to the induction or flux density $B$ rather than the polarisation $J$, and this will be a guideline throughout the following pages.

The working range of an electromagnet always lies in the first quadrant of the $B$–$H$ plane, and that of a permanent magnet, on the other hand, in the second quadrant. The theoretical working point for a permanent magnet lies on the outermost demagnetisation curve between $+B_r$ and $-{}_BH_c$. Measurement of this major demagnetisation curve requires high measuring intensities, as may be seen from the example of a Co–Ni–Cu magnet in Figure 9.1.

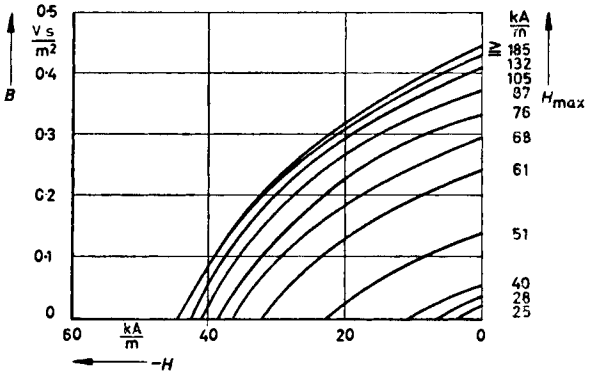



*Figure 9.1. Demagnetisation curves for the alloy 37% Co–23% Ni–40% Cu at various magnetic field strengths* $H_{max}$[25]

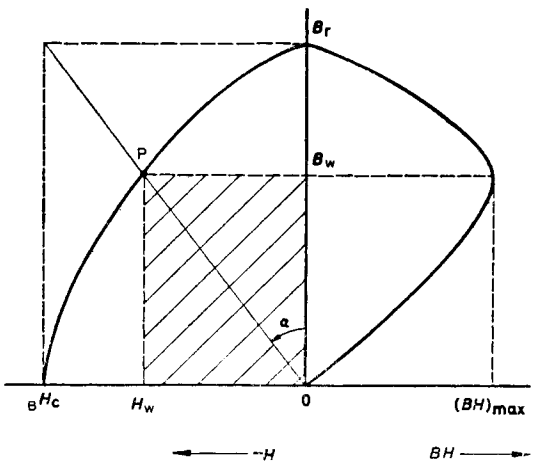



*Figure 9.2. Demagnetising curve of a permanent magnet and the corresponding energy-product curve (diagrammatic)*

In Figure 9.2 the working point ($B_wH_w$) has been so determined that the product of flux density and field strength shows a maximum; this is designated by the familiar symbol $(BH)_{max}$. It is generally advantageous to work in the neighbourhood of this point, which corresponds to maximum energy density, so that magnets can be made as small as possible. Nevertheless, it is not always the case that the $(BH)_{max}$ point is the most desirable; in many applications and for many materials—for example, when stability considerations are dominant—it is sometimes better to choose another working point.

At each point on the demagnetisation curve, the energy density is approximately equal to half the product of the coordinates of this point.

## 9.3 THE OPTIMUM WORKING POINT

Permanent magnets are never used in a completely closed magnetic circuit. For a zero air-gap, the remanence point would be the working point; for an 'infinite' gap (i.e. an open magnetic circuit), the working point shifts (with increasing gap) towards the coercive-force point. When a magnetic circuit is being designed, the air-gap is so dimensioned that $(BH)$ is as great as possible. There are three ways of finding this point on the characteristic:

1. The product of corresponding coordinates for all values of $B$ and $H$ is formed. A curve like that at the right of Figure 9.2 results. It is easy

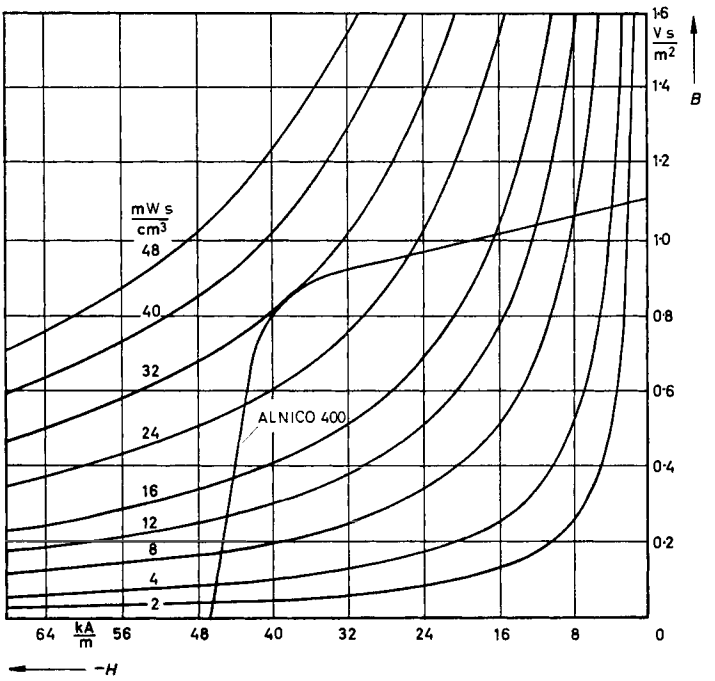



*Figure 9.3. Family of hyperbolae BH = const. for the determination of* $(BH)_{max}$

to pick out the maximum and to read off the $B_w$ point. Going across from $B_w$ to the characteristic, the desired working point P is found. If a straight line is drawn through O and P, the 'shear line' and the 'shear angle' are found.

2. More simply, the $(BH)_{max}$ point is found by plotting the demagnetising curve in a family of hyperbolae $BH$ = const. The contact point gives the $(BH)_{max}$ value. An example is plotted in Figure 9.3 for the magnet material Alnico 400. The particular hyperbola $BH = 32$ mW s/cm$^3$ just touches the demagnetising curve, so $(BH)_{max}$ for this material can be taken as 32 mW s/cm$^3$.
3. An approximate method of estimating $(BH)_{max}$ is often sufficiently close; such a method is indicated in Figure 9.2. The rectangle $B_rH_c$ is constructed and the diagonal drawn; this cuts the demagnetising curve in point P. The product of $B$ and $H$ at this intersection can be taken as a fair approximation to the required maximum.

## 9.4 DIMENSIONING A PERMANENT MAGNET (AND THE CORRESPONDING MAGNETIC CIRCUIT)

A knowledge of the maximum energy density is very important for the designer because it determines the volume of his magnet. If $V_m$ is the required volume of the magnet, $B_m$ the flux density, and $H_m$ the field strength in the material, and if the corresponding values in the air-gap are $V_a$, $B_a$ and $H_a$, then

$$V_m = C \frac{V_a B_a H_a}{B_m H_m} \tag{9.1}$$

where $C$ is a constant which depends on the ratio of the dimensions and on the stray field. It can be calculated approximately but is usually found more accurately by empirical means. It can be deduced from the equation that $V_m$ is a minimum for $B_m H_m$ a maximum.

However, the formula gives no indication of the ratio of length to cross-section, so in this respect it is ambiguous. This means that the same $BH$ hyperbola may be tangential either to a demagnetising curve having high $B_r$ and low $H_c$ or to one with low $B_r$ and high $H_c$— an ambiguity of which Figure 9.4 furnishes an example: the different shear angles $\alpha_1$ and $\alpha_2$ correspond to different ratios $H_w/B_w$, whereas the products $H_1B_1$ and $H_2B_2$ are identical.

To calculate the cross-sectional area $A_m$, of the magnet, the assumption is made that the air-gap flux and the magnet flux are proportional and, apart from errors due to stray lines, must be equal. Then, according to equation 3.3,

$$A_m = c_1 \frac{B_a A_a}{B_m} \tag{9.2}$$

Further, if there is no stray flux, $H_a l_a = H_m l_m$ and so, taking $l_m$ as the length of the magnet,

$$l_m = c_2 \frac{H_a l_a}{H_m} \tag{9.3}$$

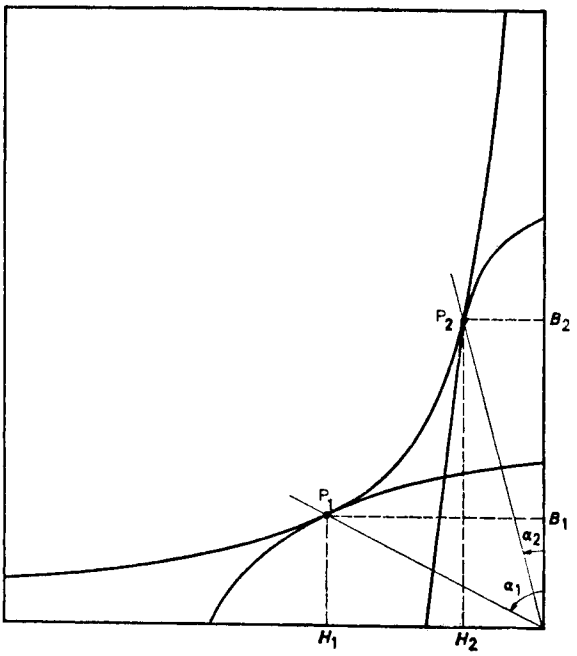



*Figure 9.4. Different demagnetising characteristics for the same $(BH)_{max}$ value*

The symbols $c_1$ and $c_2$ stand for constants for which the relation $c_1c_2 = C$ holds; they are often determined empirically.

The cross-section of a magnet must therefore be made greater the smaller the values of $B_m$ and $B_r$; and the length can be made smaller the larger the values of $H_m$ and the coercivity. The smallest possible dimensions for a material occur when $B_m$ and $H_m$ correspond to the $(BH)_{max}$ point.

In working out a magnetic circuit which, in addition to the magnet itself and the working air-gap, may have soft-iron pole-pieces, one may always fall back on the basic fact that there is a closed flux circuit for which $\Phi = BA$. This circuit can be formally treated like an electrical circuit. Corresponding to Ohm's law ($I = V/R$) is the relation

$$\Phi = \frac{F}{W}$$

where $F$ is the magnetomotive force which drives the flux and is given by the flow relation

$$F = Hl$$

The $W$ of the equation is the magnetic 'resistance', which for a circuit of $n$ elements, length $l$, cross-section $A$, and permeability $\mu$ obeys the relation

$$W = \sum_n \frac{l_n}{\mu_n A_n} = \frac{l_1}{\mu_1 A_1} + \frac{l_2}{\mu_2 A_2} + \ldots$$

Therefore

$$\Phi = \frac{Hl}{\sum_n (l_n/\mu_n A_n)} \tag{9.4}$$

The expression $l/\mu A$ is often called *reluctance* and $l/\mu$ the *reluctivity;* the reciprocal of the reluctance ($\mu A/l$) is the *permeance*. Equations 9.4 and 3.25 can easily be converted, one into the other, since $\Phi = \mu HA$.

Equation 3.85 holds for the dimensional ratio of length $l_m$ to diameter $d_m$; this states that $l_m/d_m$ is proportional to the ratio $B/H$. In practice, the following empirical formula may be used to determine the ratio $B/H$[133]

$$\frac{B}{H} = (1{\cdot}89 - \zeta)\left(\frac{l}{d} + \zeta\right)^{1{\cdot}82} \tag{9.5}$$

where $\zeta$ is a constant of the material derived from the fulness factor $\eta$, thus:

$$\zeta = 2\sqrt{\left(\frac{1}{\eta}\right) - \frac{1}{\eta}} \tag{9.6}$$

For the magnetic materials of technology, $\zeta$ lies between 0 and 1. Some examples are set out in Table 9.1.

**Table 9.1** THE CONSTANT $\zeta$ OF EQUATION 9.6 FOR SOME TECHNICALLY IMPORTANT MAGNETIC MATERIALS (SEE TEXT)[133]

| *Alloy* | $\zeta$ | *Alloy* | $\zeta$ |
|---|---|---|---|
| Carbon steel (1% C) | 0·735 | Alnico VB | 0·949 |
| Tungsten steel (5% W) | 0·758 | Alnico VC | 0·968 |
| Chrome steel (1% Cr) | 0·783 | Alnico XII | 0·149 |
| Chrome steel (6% Cr) | 0·718 | Cunico I | 0·530 |
| Cobalt steel (17% Co) | 0·715 | Cunife I | 0·879 |
| Cobalt steel (36% Co) | 0·715 | Cunife II | 0·686 |
| Alnico IA | 0·645 | Vicalloy I | 0·586 |
| Alnico IB | 0·739 | Vicalloy II | 0·950 |
| Alnico IC | 0·776 | Pt–Co (76·7% Pt, 23·3% Co) | 0·269 |
| Alnico VA | 0·901 | New KS | 0·561 |

Various suggestions for designing permanent-magnet systems are given, with worked numerical examples, by (among others) Fischer [38], Henning[49], Underhill[133], and Zumbusch[141]. The stray flux factors, i.e. $C_1 = \Phi_m/\Phi_a$, can be calculated making certain assumptions, based on an analogy with the distribution of electric field in a plate capacitor[59, 76, 121]. Müller[92] succeeded in developing a method of calculation even for quite complicated magnet shapes such as are used in various microwave devices (isolators, travelling-wave tubes, etc.) which gave good agreement between calculation and measurement[91].

## 9.5 FULNESS FACTOR

To obtain an expression for the shape of the demagnetising curve, the relation

$$\eta = \frac{(BH)_{max}}{B_{r\,B}H_c} \tag{9.7}$$

is introduced and is called the fulness factor.

If values taken from Figure 9.3 are substituted in equation 9.7, for example, then

$$\eta = \frac{32\times10^{-3}\ \text{W s/cm}^3}{(1{\cdot}1\ \text{V s/m}^2)(47\times10^3\ \text{A/m})} = 0{\cdot}62$$

$\eta$ is a dimensionless number which approaches the value unity with increasing rectangularity of the hysteresis loop.

## 9.6 STABILISING

In so far as the properties of a material can be described by its demagnetising curve, it can be characterised by $B_w$, $H_w$, $\eta$, and $(BH)_{max}$. However, those magnets which work on the extreme demagnetising curve are to be counted as exceptions.

The original working point is liable to shift owing to resistance changes in the magnetic circuit, temperature variations, external fields, and mechanical vibration. It does not, however, drift reversibly up and down the extreme demagnetising curve. It may, indeed, under the influence of an external field in the $-H$ direction, remain on the demagnetising curve, but cannot return in the reverse direction to the remanence point. A further fall in remanence will occur owing to disaccommodation. Thus magnets after they have been magnetised are necessarily more or less unstable. Accordingly, they are artificially brought into a 'permanent stable condition', which means that they are brought onto an inner demagnetising curve.

The stable condition can be reached if, for example, starting at a point $x$ on the extreme demagnetising curve, a stabilising field $\Delta H$ is switched on and off several times so that the working point P moves to Y along the route indicated by arrows in Figure 9.5. If the magnet is short-circuited, the working point shifts to $B_p$, which is said to be the point of permanence. The slope of the stabilisation loop is called the permanent permeability (see page 26). The permanent permeability is a measure of the material's resistance to change due to disturbing fields: this increases with the value of $\mu_p$. A disturbing field $\Delta H$ brings about a change in flux density ($\Delta B = \mu_p \Delta H$) inside the magnet. Comparisons between different magnet materials should not, therefore, neglect the quantity $\mu_p$.

Neumann[102] has proposed to make this matter visually clear by a system which has been used in preparing Figure 9.6. The $(BH)_{max}$ points of various materials, labelled 1–17, are plotted in the family of hyperbolae and the relevant $\mu_p$ values indicated by short lines of slope proportional to $\mu_p$. The data of the relevant materials are set forth in Table 9.2.

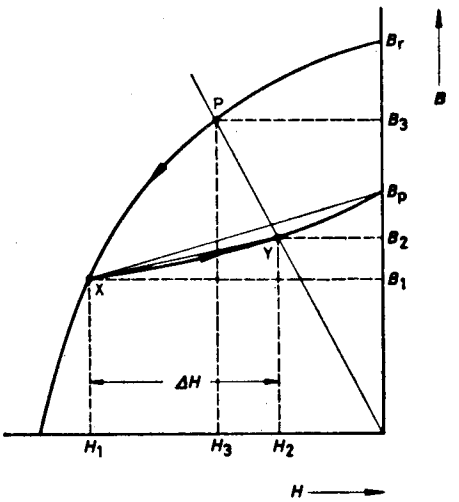



*Figure 9.5. Establishment of the condition of permanent stability*

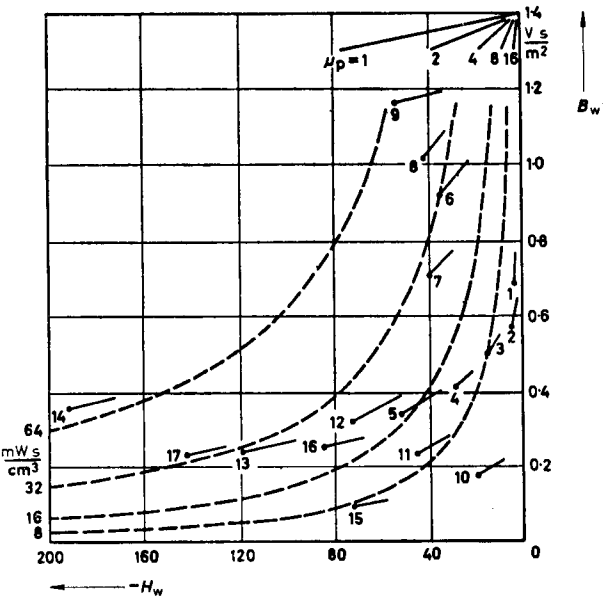



*Figure 9.6. Position of the working points of the permanent-magnet materials set out in Table 9.2 together with their $\mu_p$ lines*[102]

**Table 9.2** PARAMETERS OF THE MATERIALS DEALT WITH IN FIGURE 9.6

| *No.* | *Material* | $(BH)_{max}$ (mW s/cm³) | $B_w$ (V s/m²) | $H_w$ (kA/m) | $\mu_p$ ($\mu_0$) |
|---|---|---|---|---|---|
| 1 | Co 040 | 2·9 | 0·69 | 4·24 | 25 |
| 2 | Co 050 | 3·8 | 0·59 | 6·4 | 15 |
| 3 | Alni 090 | 8·0 | 0·51 | 16·0 | 8 |
| 4 | Alnico 160 | 12·7 | 0·42 | 29·6 | 5·5 |
| 5 | Alnico 250 | 17·5 | 0·35 | 49·6 | 3·5 |
| 6 | Alnico 400 | 34 | 0·93 | 36·8 | 5·7 |
| 7 | Alnico 400 | 29 | 0·71 | 41·6 | 5·2 |
| 8 | Alnico 550 | 44 | 1·03 | 42·4 | 5·5 |
| 9 | Alnico 800 | 63 | 1·17 | 53·6 | 1·1 |
| 10 | Cu–Ni–Fe | 3·6 | 0·18 | 20·0 | 3·1 |
| 11 | Tromalite 1000 | 10·4 | 0·24 | 43·2 | 3 |
| 12 | Pt–Fe | 25 | 0·33 | 74·4 | 2·6 |
| 13 | Pt–Co | 30 | 0·25 | 120 | 1·1 |
| 14 | Pt–Co | 72 | 0·37 | 194 | 1·02 |
| 15 | Barium ferrite (isotropic) | 7·2 | 0·10 | 72 | 1·3 |
| 16 | Barium ferrite (anisotropic) | 21 | 0·26 | 84 | 1·3 |
| 17 | Mn–Bi | 34 | 0·24 | 145 | 1·01 |

Reading from Figure 9.6 one can see that, in general, materials of low coercivity have higher permeability than those of higher coercivity and that they are also less stable. This was also brought out by the investigations of Fahlenbrach[31] who exposed various permanent-magnet materials to alternating fields and observed the changes in the demagnetising curves with differing amplitudes of the fields. As Figure 9.7 shows, the coercivity of a Koerzit 90 magnet has already fallen to a fraction of the original value for an alternating amplitude of 16 kA/m. The point P on the demagnetising curve moves on the shear line from $B = 0{\cdot}55$ V s/m² to $B = 0{\cdot}2$ V s/m².

The demagnetising characteristic of a barium ferrite designed for high coercivity (Koerox 300K) was scarcely affected by an alternating field strength of 20 kA/m. The $H_c$ point, in whose neighbourhood the changes are first noticeable, was lowered by 7·5%. In order to reduce $H_c$ to half its value, the alternating field must exceed 100 kA/m. The $(BH)_{max}$ point was hardly affected (see Figure 9.8).

According to Zumbusch[141] stabilisation can also be effected by taking the magnet some 20–30 times through a temperature interval from −70°C to +150°C. According to the investigations of Kronenberg and Bohlmann[65] excursions between room temperature and −65°C have proved more effective than cycling from room temperature to 100°C and back. Investigations by the same authors[65] have suggested that exposure of a magnet to an alternating field so adjusted as to bring down the remanence by 10% is the most effective stabilising treatment.

Prolonged experiments by Webb[135] with stabilised and unstabilised magnets have demonstrated that, in both cases, anisotropic magnets are more

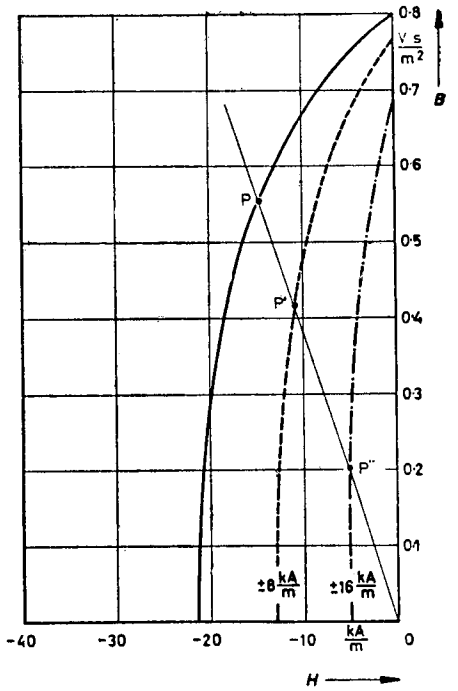



*Figure 9.7. Effect of alternating fields on the flux density of Koerzit 90*[31]

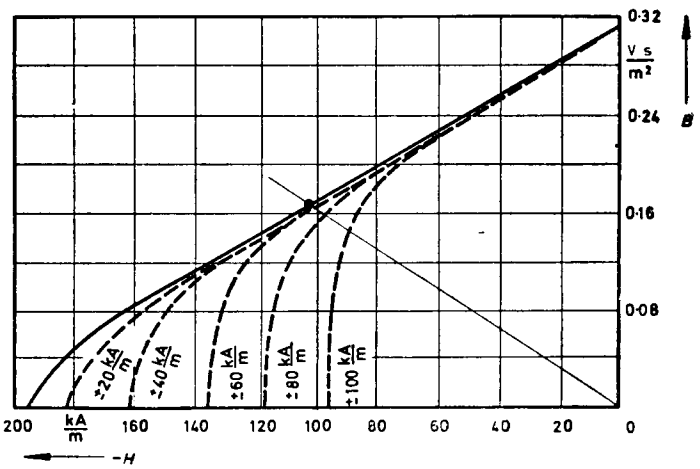



*Figure 9.8. Effect of alternating fields on the flux density of Koerox 300K*[31]

stable than isotropic magnets. The achievement of the least possible magnetic changes in high-grade materials makes high demands on accuracy of measurement. Using an improved magnetic balance, accuracies of the order of $10^{-4}$ are possible[140].

Greater artificial stabilisation is needed for isotropic alloys than for anisotropic ones; nevertheless, isotropic magnets drift more, especially under the influence of elevated temperatures[135]. Dietrich[28b] has measured many magnetic materials and established their minor loops and, indeed, whole families of hysteresis loops.

## 9.7 INFLUENCE OF TEMPERATURE

Two types of temperature effect are to be distinguished: those in the region of ordinary room temperature, which bring about changes in magnetic properties that are, in principle, reversible; and those which are effective at substantially higher or lower temperatures and which in certain cases lead to irreversible changes—sometimes referred to as ageing.

Around room temperature the 'strength' of a magnet falls off with increasing temperature and rises with decreasing temperature. It these changes are to be reversible, it must be assumed that the magnet has been stabilised. Even for stabilised magnets, however, there is usually no simple linear relation between flux density and temperature, so two coefficients need to be defined to describe the temperature relation. They are defined in accordance with the equation

$$B_t = B_0(1+\alpha t+\beta t^2) \tag{9.8}$$

where $B_t$ is the flux density at $t$°C and $B_0$ that at 0°C. The coefficients $\alpha$ and $\beta$ are usually negative. By reason of the non-linearity of the function $B = f(H)$ the temperature dependence is different for each individual value of flux density. Temperature relations are of greatest interest at the actual working point, but tables often give values merely at the remanence and coercivity points.

The remanence coefficient $\alpha$ is of the same general order of magnitude for all alloy magnets and lies between 200 ppm/K and 500 ppm/K. If a more exact value of the temperature coefficient is desired, it must be recalled that this depends on three factors: the composition of the alloy; the precise routine of heat treatment followed; and the dimension ratio or the working point of the magnet[44]. It is an aim of current research so to choose the material, its method of preparation, and its dimensions that the temperature coefficient may be vanishingly small over some limited temperature range. Gould[44] achieved this for Alcomax III (7·5% Al, 13·5% Ni, 24% Co, 3% Cu, 7% Nb) and for Alnico VI (7·5% Al, 15% Ni, 24% Co, 3% Cu, 1% Ti).

In somewhat more detail may be noted the measurements carried out on cobalt steel by Whiffin[137]. In the alloy range 3–35% Co, the temperature coefficient fell (absolutely) with increasing cobalt content from $-215$ ppm/°C to $-180$ ppm/K.

For an Fe–Al–Ni alloy having 13·6% Al, 23·5% Ni, and 4% Cu the temperature coefficient amounted to $-304$ ppm/K (at 20°C), and for an

Fe–Al–Ni–Co alloy having 10% Al, 18% Ni, 6% Cu, and 12% Co it was found to be −246 ppm/°C. The temperature coefficients were lower at higher temperatures. Table 9.3 gives a few temperature coefficients for Fe–Al–Ni and Fe–Al–Ni–Co alloys according to measurements by Zumbusch[141]. In this case all the quoted examples show that $\alpha$ rose with temperature.

**Table 9.3** TEMPERATURE COEFFICIENTS OF Fe–Al–Ni AND Fe–Al–Ni–Co ALLOYS[141]

| *Material (remainder iron)* | | | | | *Temperature range* (°C) | $\alpha$ (ppm/K) |
|---|---|---|---|---|---|---|
| Ni | Al | Co | Cu | Ti | | |
| 28 | 13 | — | — | — | −70 to + 20 | 208 |
| | | | | | +20 to +100 | 253 |
| 18 | 7 | 19 | 4 | 3 | −70 to + 20 | 160 |
| | | | | | +20 to +100 | 195 |
| 15 | 8 | 23 | 4 | — | −70 to + 20 | 383 |
| | | | | | +20 to +100 | 396 |

The second coefficient $\beta$ lay between 0·3 ppm/K and 0·8 ppm/K for the magnet materials investigated by Whiffin.

As far as is known at present, barium ferrite is exceptional among all magnet materials in having a very high temperature coefficient, namely (at the remanence point) $\alpha = -2000$ ppm/K. At the optimum working point, this becomes 1700–1800 ppm/K. However, Tenzer[131] was able to prove that the duration of the dust-grinding process had a striking effect: in a particular investigation a barium ferrite powder, after a 60 h pulverising time, showed a coercivity which was practically independent of temperature; longer or shorter milling made the temperature coefficient negative or positive. If barium ferrite or strontium ferrite was prepared by deposition, the temperature coefficient at the coercive point was substantially lower than for sintered ferrite[80].

At temperatures appreciably above 200°C, irreversible processes occur in many magnets to an extent which depends on the material and on the magnet dimensions[23, 79]. If Alnico magnets are heated above 550°C then, although there are no very significant metallurgical changes, the magnetisation falls irreversibly, nor is this fall prevented by previous stabilisation. The magnet must be remagnetised if its former usefulness is to be restored.

According to the investigations of Roberts and Mitchell[114], Fe–Al–Ni–Co–Ti alloys (Alnico V and Alnico VI) can be used successfully not only throughout the range from −196°C to +500°C but even, for a short time (i.e. a few hours), above this temperature. Although these magnets cannot be used for very long above, say, 550°C because of the considerable precipitation of constituents that takes place, McCaig[79b] showed that Alnico magnets can withstand temperatures in excess of 550°C. He investigated the effect of temporarily elevated temperatures on the working line and found that magnets

so dimensioned that the operating point lay very near to the $(BH)_{max}$ point lost more of their magnetism than did more elongated magnets operated nearer the remanence point.

Changes of structure, which in turn bring about other changes of magnetic properties, may occur in steels that have been quenched but not subsequently tempered or in metal-dust magnets whose particles have been insufficiently protected against oxidation[45].

The temperature coefficient and decline of remanence of a few types of British and American magnet materials are given for 300°C and 500°C in

**Table 9.4** TEMPERATURE EFFECTS FOR ALNI AND ALNICO ALLOYS FOLLOWING INVESTIGATIONS BY VON TENZER, CLEGG, AND MCCAIG, AND BY ROBERTS AND MITCHELL

| *Material** | $\left(\frac{B}{H}\right)$ | *Total drop* | | *Irreversible drop* | | *Temperature coefficient* | |
|---|---|---|---|---|---|---|---|
| | | 300°C | 500°C | 300°C | 500°C | α (ppm/°C) | *Range* (°C) |
| Alni (13% Al, 2% Cu, | 37·4 | 14·1 | 27·2 | 5·9 | 11·5 | 240 | |
| 26% Ni) (British) | 21·6 | 16·2 | 32·0 | 8·3 | 15·6 | 220 | 0–200 |
| | 9·5 | 17·3 | 37·0 | 11·1 | 24·1 | 140 | |
| Alnico III (12% Al, | 44·5 | — | — | 3·3 | — | — | |
| 26% Ni) (USA) | 16·0 | — | — | 8·0 | — | 220 | 0–80 |
| | 5·0 | — | — | 11·6 | — | — | |
| Alnico (10% Al, 13% | 37·4 | 9·2 | 18·2 | 3·2 | 5·6 | 190 | |
| Co, 6% Cu, 17·5% | 21·6 | 11·0 | 21·5 | 4·6 | 8·3 | 140 | 0–200 |
| Ni) (British) | 9·5 | 10·7 | 20·8 | 5·4 | 9·7 | 160 | |
| Alcomax III (8% Al, | 37·4 | 6·5 | 12·6 | 0·6 | 1·0 | 220 | |
| 24% Co, 3% Cu, | 21·6 | 6·3 | 11·3 | 1·0 | 2·0 | 130 | 0–200 |
| 0·8% Nb, 13% Ni) (British) | 9·5 | 5·4 | 11·5 | 1·1 | 1·9 | 130 | |
| Alnico V (8% Al, 24% | 44·5 | — | — | — | — | 220 | |
| Co, 3% Cu, 14% Ni) | 19·0 | — | — | 1·1 | — | 160 | 0–80 |
| (USA) | 11·5 | — | — | 2·1 | — | 160 | |
| Alnico V (8% Al, 24% | 135 | — | — | 1·8† | 1·5† | 100 | |
| Co, 3% Cu, 14% Ni) | 47 | — | — | 6·8† | 6·5† | 120 | 0–20 |
| (USA) | 2·4 | — | — | 10·5† | 13·0† | 125 | |
| Alnico VI (8% Al, 24% | 44·5 | — | — | 0·5 | — | 320 | |
| Co, 3% Cu, 15% Ni, | 16·0 | — | — | 1·6 | — | 200 | 0–80 |
| 1·25% Ti) (USA) | 5·0 | — | — | 2·9 | — | 0 | |
| Alnico VI (8% Al, 24% | 135 | — | — | 1·2† | 1·8† | 78 | |
| Co, 3% Cu, 15% Ni, | 47 | — | — | 2·7† | 3·5† | 78 | 0–200 |
| 1·25% Ti) (USA) | 2·4 | — | — | 6·7† | 10·5† | 52 | |

* Alcomax III, Alnico V, and Alnico VI are anisotropic; the others isotropic.
† Remanence drop after some cycles between −70°C and the quoted temperature.

Table 9.4 taken from a collection by McCaig[79]. As can be deduced from Table 9.4, the effect of temperature on permanent magnets also depends on the ratio $B/H$, i.e. on whether the working point chosen lies above or below $(BH)_{max}$. Fahlenbrach[31] was able to show that for oriented and also non-oriented barium ferrite the changes in remanence induced by temperature are reversible as long as the working point lies above the $(BH)_{max}$ point. The $(BH)_{max}$ point itself, however, suffers irreversible changes, during the cooling down of anisotropic material; this is clearly seen in Figure 9.9.

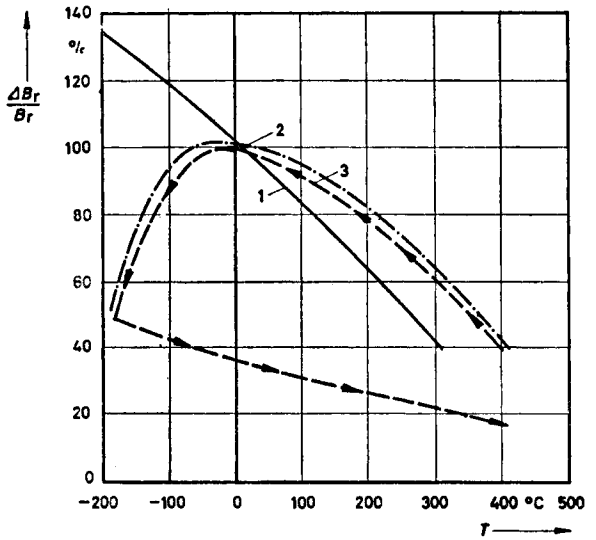



*Figure 9.9. Remanence of barium ferrite magnets as a function of temperature: 1, Koerox 100 and Koerox 300 above the $(BH)_{max}$ point, 2, Koerox 300 at the $(BH)_{max}$ point magnetised in each case at the temperature quoted; 3, Koerox 300 at the $(BH)_{max}$ point magnetised at 400°C*[31]

Schwabe[118] has developed a procedure for the calculation of temperature curves for magnets of anisotropic barium ferrite. Dietrich[28a] summarises the various methods of determining the temperature dependence of the demagnetising curve.

## 9.8 RESIDUAL EFFECT AND AGEING

A process that is hardly perceptible at room temperature, but clearly visible at elevated temperatures, is the falling off of the flux density of a magnet with time: the process is usually reversible at low temperatures, i.e. it can be inverted by remagnetising and will then fall off in the same way as before. This reversible change of flux density is called 'residual effect' or magnetic viscosity[126, 127]. Kronenberg and Bohlmann[67] see in this phenomenon a process of remanence adaptation. They have demonstrated that the time-fall of remanence for barium ferrite or Alnico magnets can be 2% a year or less. Figure 9.10 is based on their researches.

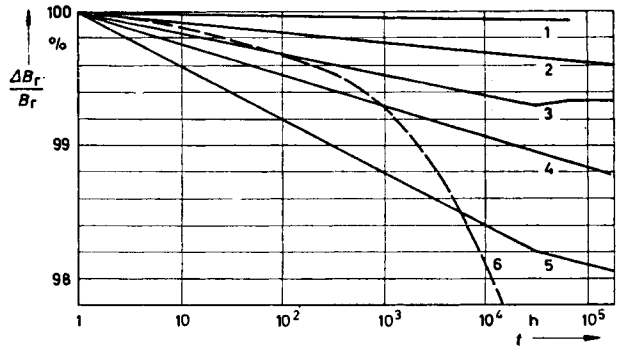



*Figure 9.10. Fall of remanence with time for various permanent-magnet materials with the following dimensional ratios l/d: 1, Alnico V (l/d = 8·0); 2, Indox V (l/d = 0·8); 3, Alnico VII (l/d = 3·5); 4, Alnico V (l/d = 3·5); 5, Alnico III (l/d = 3·5);* Cr–Co *steel (l/d = 5·9)*[67]

Whereas the steel magnet used for comparison showed ageing effects, there were no more than local adaptations in the ceramic and Alnico materials. The term 'ageing' is applied if the process is irreversible. (Note that stabilisation is often referred to as ageing but this is to be deprecated.)

Krainer and Raidl[64] were able to observe quite clearly the effect on the secular drop in $(BH)_{max}$ of adding various alloying elements to chrome steel. The influence of temperature on ageing for a new material, a Pt–Co alloy, is clearly shown in Table 9.5. Platinax II, a Pt–Co alloy having a $(BH)_{max}$ value

**Table 9.5** PERCENTAGE DROP IN FLUX DENSITY FOR PLATINAX II AT ELEVATED TEMPERATURES[86]

| *Temperature* °C | *Time* | | |
|---|---|---|---|
| | 5 min | 2 h | 1000 h |
| 120 | 3 | 5·5 | 7·5 |
| 200 | 16 | 18·5 | 22·5 |
| 250 | 21·5 | 26 | 29 |
| 350 | 43·5 | 50·5 | 51 |

of 73·5 mW s/cm³, shows a greater percentage loss of flux density with time the more the material is heated. After 1000 h the drops has more or less flattened out[86]. If the temperature had been only a little above room temperature, the magnets could have been restored to full efficiency by remagnetising them, but, if the temperature rises above 250°C, the original values cannot be recovered by any magnetising process. For example, after a sample has been heated to 350°C and then remagnetised at room temperature, the $(BH)_{max}$ value is 8·7% below the original figure.

Magnets which are hardened by precipitation are usually cooled from 1300°C in air or in water and subsequently heated (tempered) for 2–4 h at

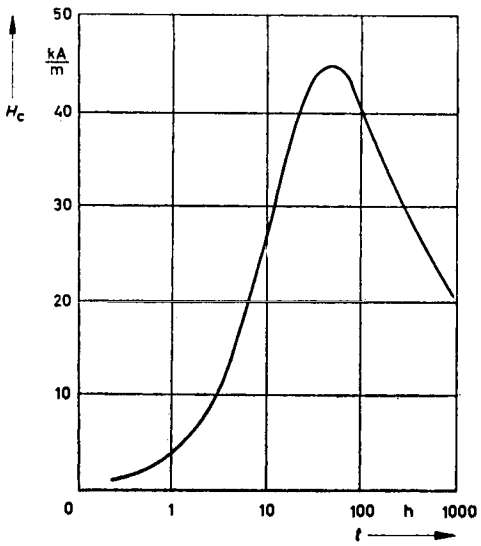



*Figure 9.11. Dependence of coercivity $H_c$ on duration of tempering time at 600°C for a* Cu–Ni–Fe *alloy*[17]

650°C. This may give rise to two phases, both stable. If the precipitated particles are small, the coercive force is high. The particles grow in size with further tempering and larger islands and inclusions are formed: the coercivity now falls again (see, for example, Figure 9.11)[17].

These processes can be influenced over a wide range—and so can be matched to particular design considerations (such as magnet volume)—by a suitable adjustment of the quenching and retempering conditions. Different heat treatments, however, have a pronounced effect on the residual effect.

The drop in flux density $\Delta B$ in permanent magnets follows a logarithmic law of the form

$$\Delta B = S \ln t + \text{const.}$$

where $S$ is a measurable parameter and $t$ is the time which has elapsed since

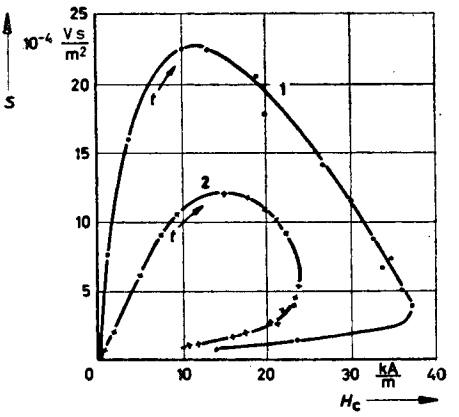



*Figure 9.12. Curves of constant S as a function of coercivity for variously heat-treated Alnico magnets (see text)*[128]

a sudden change in the magnetic force acting on the sample. Street, Woolley, and Smith[128] have determined $S$, together with the coercivity, of an Alnico material for two different heat treatments. The results are shown in Figure 9.12: curve 1 shows the effect of cooling time when the material is cooled from 1300°C, starting with a quenching in water and ending with slow cooling achieved by simply switching off the furnace. In case 2 a quenching in cold water was followed by a 700°C tempering (annealing). The actual baking time varied from 5 min to 140 h. It can be seen from the measured results that, up to 12 kA/m, the residual effect is greater the higher the coercivity but that, over 12 kA/m, the residual effect falls with increasing coercivity.

## 9.9 THE WORKING LINE

The straight line drawn from the origin of coordinates to the working point on the demagnetising curve gives the 'working line' or the 'shear line', characterised by the relation $\tan \alpha = H_w/B_w$ (see Figure 9.2). If $H_w$ and $B_w$ are the coordinates of the $(BH)_{max}$ point, the corresponding line is the best working line.

A family of radiating working lines may be drawn for the various dimensional ratios $l/d$ of a magnet. The optimum ratio corresponds to the line through the $(BH)_{max}$ point. Many magnet manufacturers include this line among the listed characteristics of their product. Figure 9.13 shows an example.

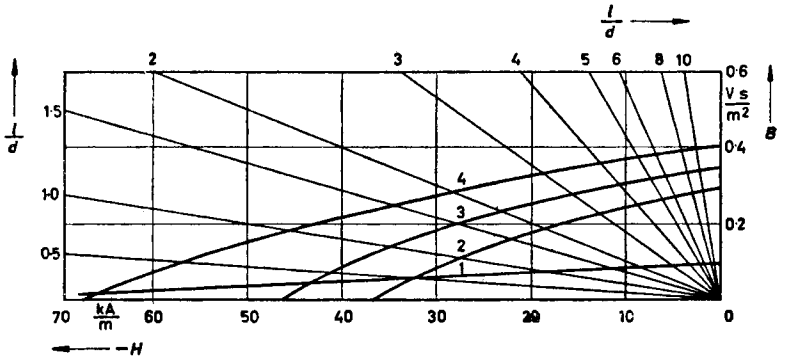



*Figure 9.13. Demagnetisation curves of moulded magnets: 1, Sprox; 2, Prac 120; 3, Prac 160; 4, Prac 250*[75]

ple. If the demagnetising factor $N$ is plotted in place of $l/d$, this will increase in the reverse direction, i.e. $N$ is zero in the direction of the $B$ axis (closed circuit) and increases with increasing $\alpha$ (see Figure 9.14). Practical work with plotted characteristics of permanent-magnet materials is facilitated if graphs are provided of the following four basic characteristics:

1. The magnetising curve of the major loop.
2. A few of the minor demagnetising curves.
3. The $BH$ = const. curves.
4. The family of working lines.

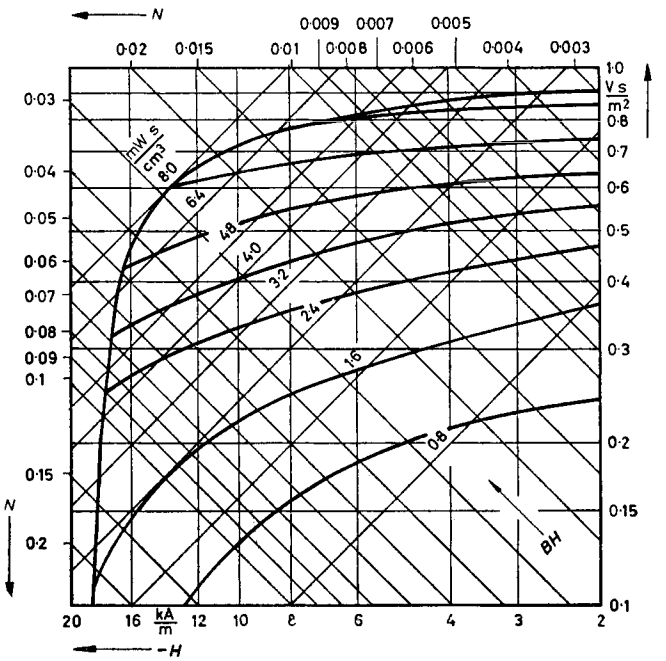



*Figure 9.14. Demagnetisation of cobalt steel with 34% Co: the curves are plotted on logarithmic scales whereby HB = const., and also the curves of the demagnetisation factor N become two series of parallels*[84]

The example of Figure 9.14 is drawn for a cobalt steel having 34% Co. Double-logarithmic paper is used for the curves, following the suggestion of Meyer[84], so that the curve of $BH = \text{const.}$ and the family of curves of $N$ form a set of parallel lines—which for many purposes simplifies the design procedure.

## 9.10 THE FUNDAMENTAL TYPES OF PERMANENT-MAGNET MATERIALS

According to the above exposition a good material for permanent-magnet construction will have high remanence and coercivity, a large fulness factor, low permanent permability, and low sensitivity to external influences (shock, temperature fluctuations, stray fields).

High remanence is principally a matter of composition: materials which are to show high saturation values demand optimum constituent ratios. The remanence value can be significantly increased if magnetic anisotropy can be produced. This anisotropy often leads to an increased fulness factor.

Constancy of values in a permanent magnet is achieved by proper choice of working point and also by suitable pretreatment and dimensioning. The coercivity is a structure-dependent magnitude and can, therefore, be altered within wide limits by appropriate manipulation of structure. Magnets can thus be regarded from the viewpoint of the means available for manipulating

the structure to increase the coercivity. Increasing the coercivity means taking pains to reduce self-demagnetising processes. Here, two possibilities present themselves: to hinder the mobility of the Bloch walls and to keep it as low as possible; and to avoid Bloch walls altogether so that only rotational processes, demanding higher field strengths, can take place. Wall mobility can be discouraged in various ways: one way is to introduce stress variations induced by irregularities in the crystal lattice and by magnetostriction; another is by means of non-magnetic inclusions or foreign bodies. Sometimes both means may co-operate. The existence of Bloch walls may be prevented if the effective magnetic particles are too small for them to form[125], i.e. are of dimensions comparable with those of the Bloch walls themselves.

The critical particle size for Bloch-wall formation can be evaluated from the two energy relations (equations 4.1 and 4.2): if $l$ is the length of the edge of an elementary domain, taken to be cubic, whose demagnetising factor is taken to be the same as that of a sphere ($N = \frac{1}{3}$), then

$$E_m = \tfrac{1}{2} N l^3 J_s^2 = \tfrac{1}{6} l^3 J_s^2 \tag{9.9}$$

For the critical size of particle this static energy must equal the Bloch-wall energy ($E_w = e_w A$, where $e_w$ is the energy of a surface element and $A$ the surface area of the Bloch wall). In the case of closed internal flux loops, with

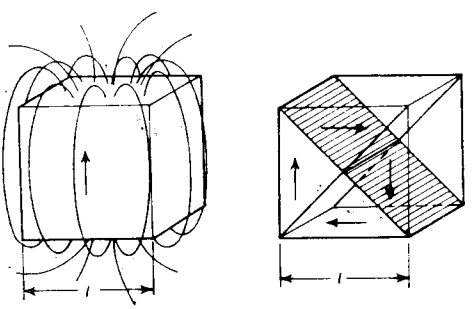



*Figure 9.15. Diagrammatic representation of a die-shaped body with flux lines closed externally and internally*

no external stray field at all (see the sketches of Figure 9.15), we may set $A = 2^{3/2} l^2$. This leads to the following relation

$$\tfrac{1}{6} J_s^2 l^3 = 2^{3/2} e_w l^2 \tag{9.10}$$

If $e_w$ is put at about 1 erg/cm$^2$, then for iron $l = 10$ nm. A more exact calculation made by Néel[96] gives 32 nm for the critical particle size. If this order of size is not exceeded, one can fairly reckon on a single-domain structure. Investigations of iron dust yielded values very near to these results[22]. The critical particle size for $BaO{\cdot}6Fe_2O_3$ amounted to about 1 μm. The demagnetising energy of the single domain can be increased if stress anisotropy, crystal anisotropy, shape anisotropy, or exchange anisotropy occurs. Quite generally, the various forms of anisotropy are conducive to high coercive force.

**Table 9.6** GROUP CLASSIFICATION OF PERMANENT-MAGNET MATERIALS

| | | |
|---|---|---|
| 1. | Steels | Iron–carbon<br>Iron–chrome–carbon<br>Iron–cobalt–carbon<br>Iron–tungsten–carbon<br>Iron–aluminium–carbon |
| 2. | Precipitation alloys | Iron–cobalt–tungsten<br>Iron–cobalt–molybdenum<br>Iron–aluminium–nickel<br>Iron–aluminium–nickel–cobalt-(copper)–(titanium)-(niobium)<br>Iron–nickel–copper<br>Cobalt–nickel–copper<br>Cobalt–iron–titanium<br>Cobalt–nickel–titanium<br>Iron–nickel–titanium<br>Iron–cobalt–vanadium |
| 3. | Alloys hardened by cold deformation | Iron–cobalt–vanadium–(chrome)<br>Silver–nickel–chrome<br>Silver–manganese–aluminium |
| 4. | Superstructure alloys | Platinum–iron<br>Platinum–nickel<br>Platinum–cobalt |
| 5. | Dust magnets | Manganese–bismuth<br>Manganese–aluminium<br>Cobalt–rare-earth metals<br>Iron dust; iron-alloy dust |
| 6. | Ceramic magnets | Barium (strontium, lead) ferrites |
| 7. | Materials exhibiting exchange anisotropy | Cobalt–cobaltoxide<br>Iron–cobalt–(Fe–Co ferrite) |

Hence, in the classification of the various permanent magnet materials, the dominant type of anisotropy, together with the technical means whereby it may be achieved, will serve as guidelines. Seven broad groups of materials may be differentiated and these are set out with the principal alloys concerned in Table 9.6. They will now be considered individually:

1. *Martensitic steels.* High coercivity is produced by means of internal stresses and inhomogeneities connected with a change of phase ($_BH_c$ up to 4 kA/m).
2. *Precipitation alloys.* In these, a high $H_c$ is achieved by induction of a precipitation phase through suitable tempering routines (shape anisotropy) and is in many cases increased by additional crystal anisotropy ($_BH_c \leqq 65$ kA/m).

3. *Alloys hardened by deformation.* Mechanical hardness and high coercivity produced by rolling are associated with a directional precipitation.
4. *Superstructural magnetic materials.* Magnetic hardness is linked with an ordering process.
5. *Dust magnets.* The type and shape of the magnetically effective particles generally determine the magnetic properties of these materials. The magnetic values can be further increased if the particles are marked by high crystal anisotropy. Values of ${}_BH_c$ of more than 2000 kA/m are attainable.
6. *Ceramic magnets.* These form a special subgroup of powder magnets differing mainly in the details of the sintering process applied after pressing. By reason of their special engineering importance they will be separately treated. Note that ${}_BH_c$ values range up to 90 kA/m.
7. *Materials which exhibit exchange anisotropy.*

### 9.10.1 Martensitic steels

Among steels, i.e. alloys of iron and carbon, Martensite is to be understood as an unstable phase having a tetrahedral lattice obtained by quenching from the Austenite range (crystal mixture called $\gamma$-iron). Martensite exhibits a partly dissociated solid solution of iron carbide in iron and is harder than Austenite. Stresses appear in the crystal lattice, which is why rapid quenching of steel is also spoken of as 'hardening'. In this hardening process a steel containing some 0·8% Co is heated to about 800°C and then quenched. Cobalt steels with some 35% Co must be heated to around 950°C before quenching since the reaction temperature is higher.

Because of magnetostriction an increase in coercivity takes place in parallel with the purely mechanical hardening. This can amount to 4 kA/m for pure carbon steels with 1% C, and may reach 18 kA/m for cobalt steels.

Magnets made before 1910 were of carbon steel. By reason of the low $H_c$ and relatively high $B_r$, as judged by modern standards, magnets had to be long in relation to their cross-section (see equations 9.2 and 9.3). In order to reduce strays, magnets were bent into the form of a horseshoe, which became the accepted symbol for a magnet. It was not possible to obtain higher $(BH)_{max}$ values than 1·6 mW s/cm$^3$ with such material. However, as far back as 1880 it was known, through the study of tungsten steel, that $(BH)_{max}$ might be increased by means of additional alloying elements. During World War I, chrome steel having about 1% C and up to 6% Cr came into general use. This chrome steel enabled a $(BH)_{max}$ of, say, 2·5 mW s/cm$^3$ to be obtained.

In 1917 Honda discovered cobalt steel in which a part of the iron was replaced by cobalt (KS steel)[52]. Cobalt contents up to 36% were known. With these steels $(BH)_{max}$ values as high as 8 mW s/cm$^3$ together with an $H_c$ of 20 kA/m were achieved. Even today a certain quantity of cobalt steel is manufactured and used. It is to be remembered that strong magnetic fields are not required in every case. Very often the emphasis is on attaining good mechanical properties for steel magnets since these permit both very thin and also very complicated magnets to be satisfactorily made, using techniques

commercially available in iron-works. Figure 9.16 shows the demagnetising curves of certain chrome, tungsten, and cobalt steels.

The magnetic and electrical properties of martensitic steel at room temperature remain constant over long intervals of time. But even at the moderate temperatures of 70°–100°C the coercivity falls sharply in a short time. Jellinghaus[53] has investigated tempering routines for martensitic steel in detail.

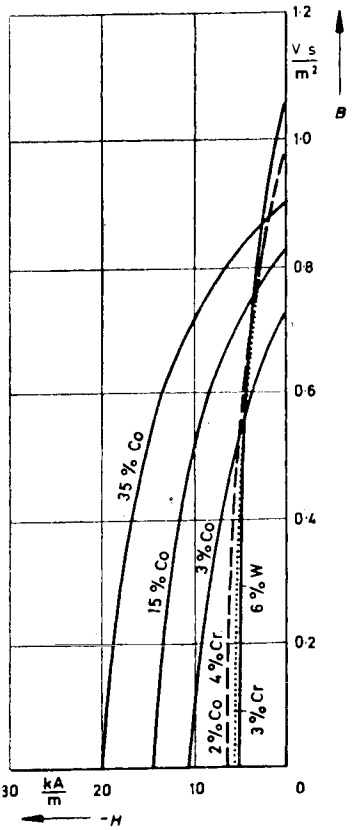



*Figure 9.16. Demagnetising curves of chrome steel, tungsten steel, and cobalt steels*[3]

The German Standard for permanent magnets (Table 9.7) no longer lists magnet steels even though they are still manufactured. A few data are collected in Table 19.4. Besides the quoted cobalt content, steels contain some 0·7–1·0% C.

During the last war a magnet steel (MT magnet) was developed in Japan which was free of the conventional alloy additives, nickel and cobalt[88]. By a composition involving 8±0·2% Al and 2±0·1% C (remainder iron), the values $B_r = 0{\cdot}5$ V s/m², $H_c \geqslant 16$ kA/m, and $(BH)_{max} = 3{\cdot}6$ mW s/cm³ were achieved. The aluminium cannot be replaced by silicon since this, in proportions of more than 0·2%, has an unfavourable effect on the magnetic

properties; a cobalt additive, on the other hand, can be useful as it raises the remanence without greatly changing the coercivity[77, 88a].

To what extent precipitated iron carbide or the shape of its particles influences the inner stresses in martensitic steel is a subject not yet fully investigated.

### 9.10.2 Precipitation alloys

The most important class of magnets is, today, free from carbon and owes its mechanical and magnetic hardness to precipitation processes.

The development of these materials began in 1931 with the discovery of Fe–Co–W and Fe–Co–Mo alloys by Köster[63] and also with Mishima's discovery[87, 88] of the Fe–Ni–Al alloys, which were called MK steels (M and K are the initials of the inventor's family names—natural and adoptive). A little after this came the Fe–Al–Ni–Co–Ti alloys of Honda[51] which had improved properties. The Köster alloys never came to the fore, technically, as they were so soon overtaken by the Fe–Al–Ni alloys which were, moreover, easier and cheaper to make.

The following physical process forms the basis of precipitation hardening. In particular alloys, complete mutual solution of the constituents is achieved only by baking at a high temperature. The solution is not stable at room temperature: the non-soluble components separate out. To keep them in solution at low temperatures, however, the alloy must be cooled quickly from the dissolving temperature. The resulting solution is in a 'supersaturated' state. Using a moderate 'tempering' heat (500°–700°C), a controlled precipitation of the insoluble particles results. The tempering, as this heat treatment is called, can be so carried out as to precipitate a dispersion of fine particles or to produce particles of a size which promotes optimum coercivity.

An observation of Kronenberg[66] is noteworthy in this connection: he found that in all his investigations Fe–Al–Ni–Co alloys of various compositions and quite different magnetic properties led always, in the precipitation phase, to the same lattice constant. One may suspect, therefore, that for these alloys the precipitation has always the same chemical composition and that the varying magnetic values arise chiefly from the size, shape, and orientation of the particles formed during heat treatment. Nowadays it is assumed that in many 'precipitation-hardened' alloys (for example, Fe–Al–Ni–Co and Sm–Co–Cu alloys) precipitation need not occur or may be accompanied by other processes. The hardening should, in fact, be treated as a spinodal demixing process[50a].

#### 9.10.2.1 The Fe–Al–Ni and Fe–Al–Ni–Co alloys

Originally, the Japanese still called their Fe–Al–Ni alloys 'steel', but according to modern usage steel is an iron alloy which contains carbon. There is no carbon, however, in the Fe–Al–Ni alloys. It is, indeed, an unwanted constituent of such alloys as it spoils all those properties most important for a permanent magnet, namely $B_r$, $H_c$, and $(BH)_{max}$, as Betteridge[15] was able to show (Figure 9.17).

**Table 9.7** PERMANENT-MAGNET MATERIALS TO DIN 17 410[29]

| *Abbreviated name* | *Material* | *Chemical composition (remainder iron)* (wt %) | | | | | *Densitiy* (g/cm³) | $(BH)_{max}$ (mWs/cm³) | $B_r$ (V s/m²) | ${}_BH_c$ (kA/m) | $B_w$ (V s/m²) | $H_w$ (kA/m) | $\mu_p$ ($\mu_0$) |
|---|---|---|---|---|---|---|---|---|---|---|---|---|---|
| | | Al | Co | Cu | Ni | Ti | | | | | | | |
| AlNi 120 | 1.3728 | 12–13 | 0–4 | 2–4 | 25–28 | 0–1 | 6·8 | 9 | 0·58 | 50·5 | 0·34 | 30·5 | 4·5–5·5 |
| AlNiCo 160 | 1.3743 | 9–13 | 12–17 | 2–6 | 18–24 | 0–1 | 7·1 | 12 | 0·66 | 56 | 0·39 | 33·5 | 4–5 |
| AlNiCo 190 | 1.3745 | 9–12 | 12–17 | 2–4 | 19–24 | 0–1 | 7·1 | 14·5 | 0·75 | 61 | 0·45 | 35·2 | 4–5 |
| AlNiCo 229 | 1.3756 | 6–8 | 24–30 | 3–6 | 13–19 | 5–9 | 7·2 | 16 | 0·62 | 80 | 0·36 | 45·6 | 3–4 |
| AlNiCo 350 | 1.3758 | 6·5–7·5 | 30–34 | 4–5 | 14–16 | 5–6 | 7·2 | 26 | 0·84 | 92 | 0·52 | 56 | 3–4 |
| AlNiCo 400 | 1.3760 | 8–9 | 23–25 | 3–4 | 14–15 | 0–1 | 7·3 | 30 | 1·12 | 49 | 0·90 | 37·6 | 4–5 |
| AlNiCo 500 | 1.3761 | 8–9 | 23–25 | 3–4 | 14–16 | — | 7·3 | 35·5 | 1·20 | 50·5 | 0·95 | 40 | 4·5–6 |
| Barium ferrite 100 | 1.3641 | $BaO \cdot 6Fe_2O_3$ | | | | | 4·9 | 6·5 | 0·21 | 132 | 0·10 | 68 | 1·1–1·2 |
| Barium ferrite 300 | 1.3643 | | | | | | 5·0 | 20 | 0·35 | 152 | 0·20 | 112 | 1·1–1·2 |

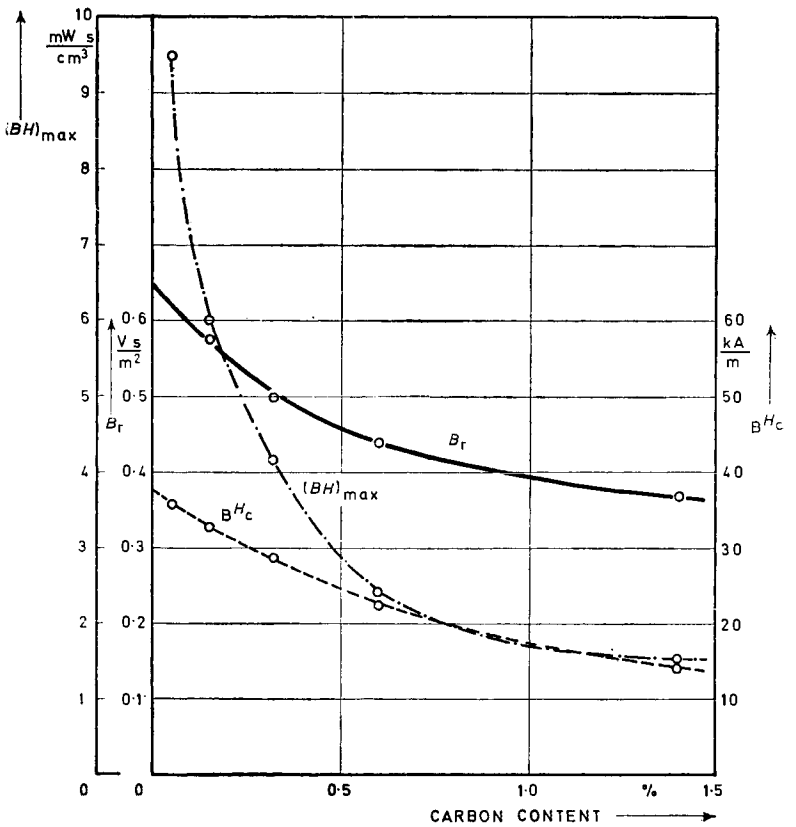



*Figure 9.17. Effect of carbon on the magnetic properties of* Fe–Al–Ni *alloys*[15]

Originally it was thought that for Fe–Ni and Fe–Al-Ni–Co alloys, as for steel, a lattice reaction was accompanied by stress changes, these being the cause of the observed high coercivity. It can be taken as certain, however —at least for Fe–Al–Ni alloys having 12·5% Al, 29% Ni, and 58·5% Fe— that magnetostriction cannot be held responsible for the high coercivity since this, according to investigations by Nesbitt[99], is sensibly zero for these alloys.

Later investigations carried out with the help of the electron microscope have shown that small rod-shaped particles are precipitated by the tempering process; according to Heidenreich and Nesbitt[48], these particles have dimensions of, roughly, 40 nm×8 nm×8nm and are so embedded in the matrix that their long axes lie parallel to the [100] direction of the matrix crystals. The separation between the layers of rods amounts to about 20 nm. If a magnetic field (see below) is applied during the cooling stage, it is possible, for certain compositions of the alloy, to align these rod-like particles.

It emerges from the investigations that, for Alnico 5 at least, it is shape anisotropy that is the determining factor for coercivity; crystal anisotropy plays a comparatively subordinate role. The dimensional ratio of these

precipitated particles is important in practice for attaining satisfactory coercivity[100].

De Jong, Smeets, and Haanstra[56], using an electron microscope, examined formations of high-coercivity Alnico alloys from 20 nm to 40 nm in width and 100–150 nm long but left it open whether these displayed an actual second phase or whether it was a question of periodic variations in composition.

According to Vallier, Bronner, and Pfeffer[134a], two conversion processes are involved.

1. The stable high-temperature phase passes over into the two phases $\alpha_1$ and $\alpha_2$. All three phases crystallise in cubic space-centred lattices. The $\alpha$-phase is ferromagnetic and is characterised by high iron and cobalt content; $\alpha_2$ is only weakly magnetic and forms a matrix throughout which $\alpha_1$ is finely disseminated. The magnetic properties are determined by the composition, orientation, and distribution of the $\alpha_1$-phase.
2. At high temperatures a further phase, the magnetically undesirable $\gamma$-phase, is precipitated from the $\alpha$-phase. This is cubic face-centred and, on cooling, a conversion into the $\alpha_2$ cubic body-centred phase takes place. The suppression or delay of the $\alpha$–$\gamma$ conversion would seem to offer the possibility of improving the hardening qualities of the Fe–Al–Ni–Co alloys. Titanium additives should act in a similar way.

By the choice of a suitable heat treatment, the precipitated particles can be brought to such a size that Bloch walls scarcely exist so that cyclic magnetisation involves rotational processes almost entirely. According to Wohlfahrt[138] it is the shape anisotropy of the particles which is responsible for the high coercivity.

Many modifications by the addition of further components have been tried and innumerable investigations devoted to this type of alloy (especially to the Fe–Al–Ni–Co alloys) since their discovery. Development is not complete even now. Figure 9.18 gives a few typical demagnetisation curves for isotropic and anisotropic Fe–Al–Ni–Co alloys with the compositions given in Table 9.8.

*Influence of composition*

The relation between magnetic properties and composition for three-component alloys can be made very clear, as Betteridge[15] has demonstrated for Fe–Al–Ni, by the use of triangular coordinates. It is his work which formed the basis for Figures 9.19–9.24.

These displays serve to show why, in practice, one is concerned with so great a variety of alloys. Thus it is seen from Figure 9.19 that the coercivity of Fe–Al–Ni alloys increases with the aluminium and with the nickel content, reaching a maximum of 44 kA/m for 13% Al, 58% Fe, and 29% Ni, but this maximum does not coincide with the maximum for $B_r$ which occurs, as Figure 9.20 shows, at a composition of 15% Al, 61% Fe, and 24% Ni (0·725 V s/m$^2$). At the same time, the $(BH)_{max}$ value is highest for a composition intermediate between the $H_c$ and $B_r$ optima, i.e. for some 13% Al,

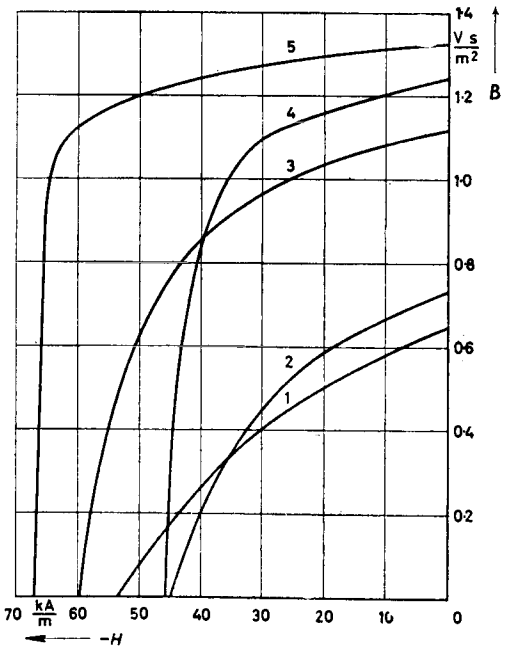



*Figure 9.18. Demagnetising curves of* Fe–Al–Ni–Co *alloys*[3]

**Table 9.8** COMPOSITION OF Fe–Al–Ni–Co ALLOYS ILLUSTRATED IN FIGURE 9.18

| *Number* | *Composition (remainder iron)* | | | | | *Remarks* |
|---|---|---|---|---|---|---|
| | Al | Ni | Co | Cu | Nb | |
| 1 | 11 | 24 | 9·5 | 3·5 | — | |
| 2 | 10 | 19 | 12 | 6 | — | |
| 3 | 8 | 13·5 | 24 | 3 | 2 | Magnetic treatment |
| 4 | 8 | 11·5 | 21 | 4 | — | Magnetic treatment |
| 5 | 8 | 13·5 | 24 | 3 | 0·5 | Columnar crystals |

60% Fe, and 27% Ni. It can be seen from Figure 9.21 that for this combination the $(BH)_{max}$ value amounts to 10·8 mW s/cm³.

However, the $(BH)_{max}$ peak is not always the optimum solution of a magnetic-circuit design problem. Sometimes a higher coercivity is desirable and in other constructions the designer would do better with a higher remanence value. The manufacturer can, in general, bias his Fe–Al–Ni magnets towards higher coercivity or higher remanence, as may be required, without any very great changes in composition.

If further constituents are added to the three-component Fe–Al–Ni, the

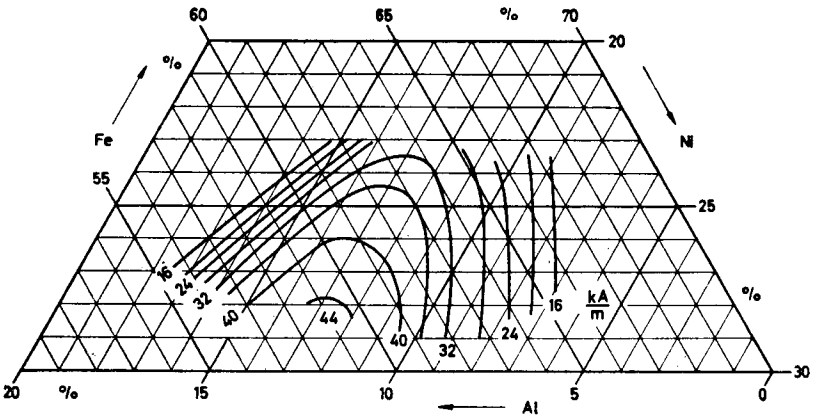



*Figure 9.19. Coercivity ${}_{B}H_{c}$ in the* Fe–Al–Ni *system*[15]

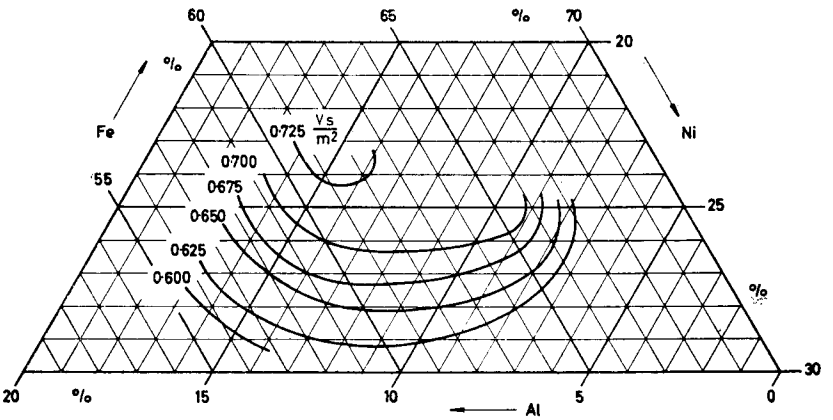



*Figure 9.20. Remanence values $B_r$ in the* Fe–Al–Ni *system*[15]

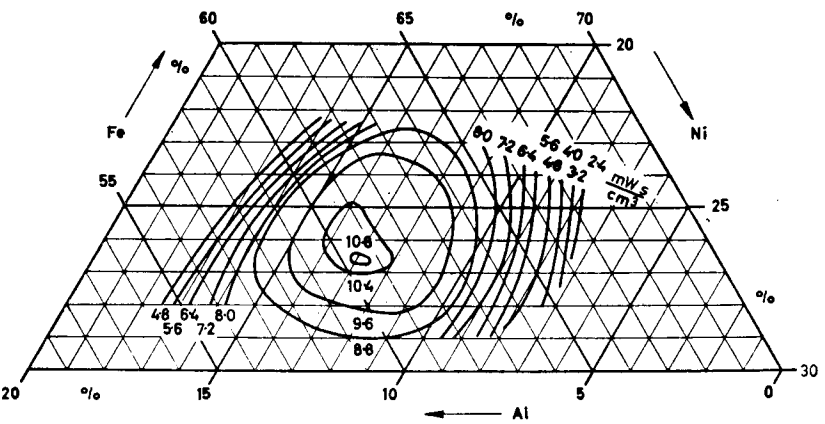



*Figure 9.21. $(BH)_{max}$ values in the* Fe–Al–Ni *system*[15]

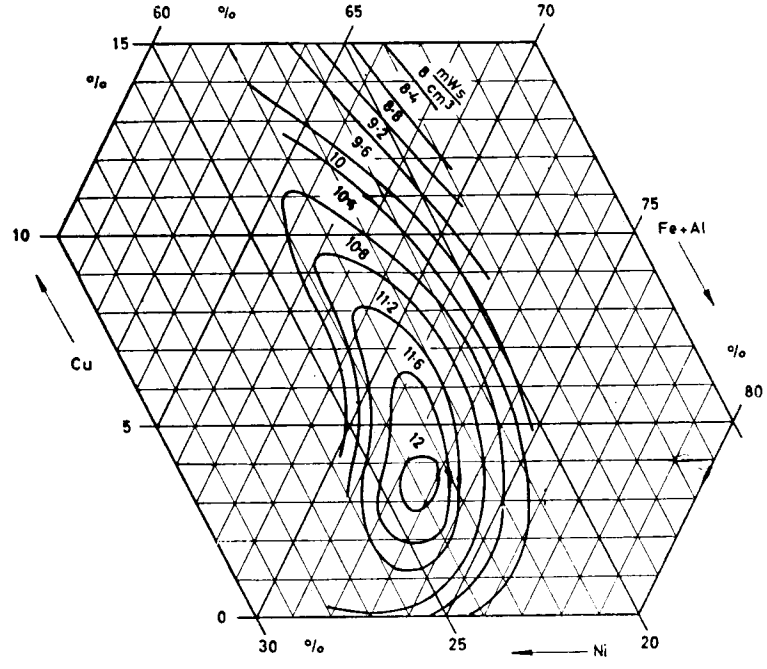



*Figure 9.22. Effect of copper on the* $(BH)_{max}$ *values of* Fe–Al–Ni *alloys with 13%* Al[15]

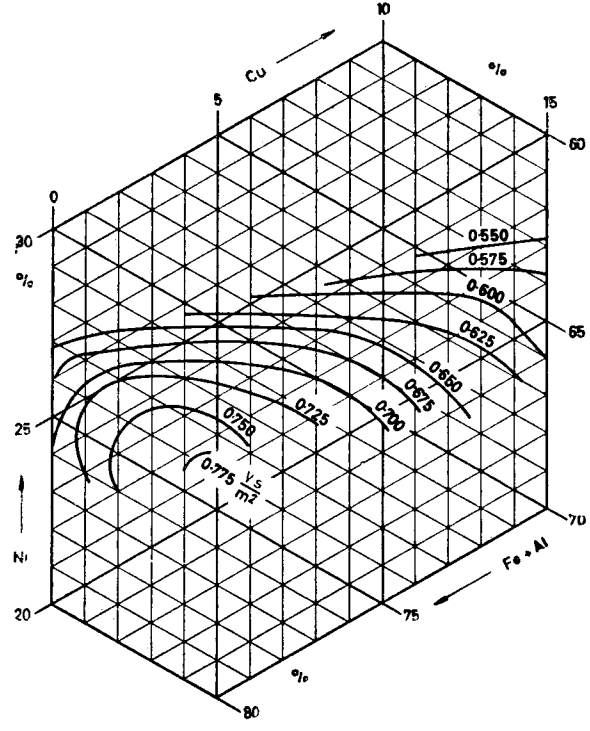



*Figure 9.23. Effect of copper on the remanence values of* Fe–Al–Ni *alloys with 13%* Al[15]

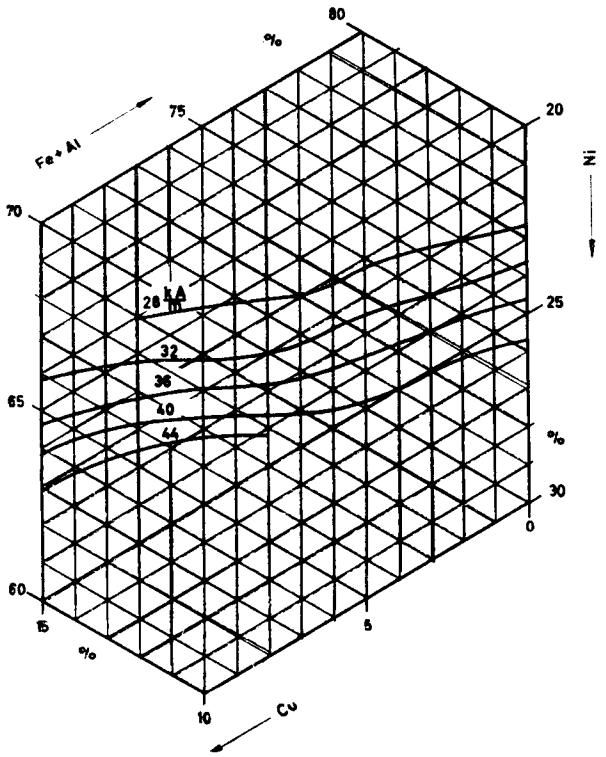



*Figure 9.24. Effect of copper on the coercivity of* Fe–Al–Ni *alloys with 13%* Al[15]

whole picture changes. Small additions of copper are often employed. For an alloy having 13% Al to which an increasing quantity of copper is added, Betteridge[15] reports that an optimum $(BH)_{max}$ of 12 mW s/cm$^3$ is reached with 59·5% Fe, 24% Ni, and 3·5% Cu (Figure 9.22). This improvement, however, involves a smaller rise in remanence and coercivity (Figures 9.23 and 9.24). Furthermore, copper accelerates the precipitation process, which means more rapid quenching—a result not always easy to achieve for larger magnets.

Cobalt has the opposite effect to copper, i.e. it delays precipitation and thereby facilitates the manufacture of larger magnets. By the simultaneous use of copper and cobalt in suitable balance, the manufacturer possesses the means of adjusting the rate of precipitation.

Two further useful properties of cobalt are that it increases saturation levels and shifts the Curie temperature in the high-temperature direction. The remanence also increases as the saturation flux density increases. It is a very fortunate fact that the coercivity increases at the same time. The improvement achieved by adding cobalt to Fe–Al–Ni alloys is particularly noticeable for a proportion of 6% Co or more. This will be shown by two examples provided by Zumbusch[141].

For an alloy series having 11–12% Al, 22–24% Ni, and 3–5% Cu, the addition of 14% Co brings about a $(BH)_{max}$ of 14·4 mW s/cm$^3$ (Figure 9.25).

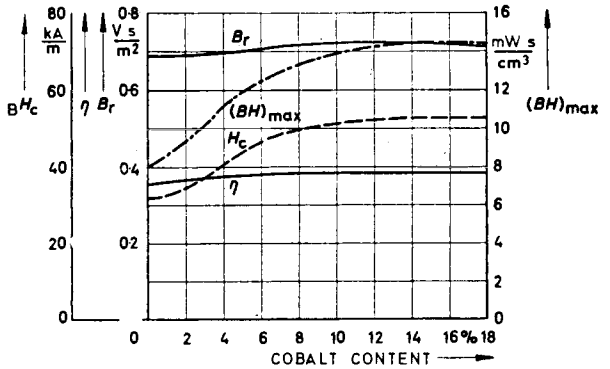



*Figure 9.25. Magnetic properties of alloys having 22–24% Ni, 11–12% Al, and 3–5% Cu (remainder iron) as functions of cobalt content*[140]

No further advantage follows from increasing cobalt content beyond 14%.

For another series having 8–10% Al, 14–16% Ni, and 2–5% Cu, the same $(BH)_{max}$ value was achieved, namely 14·4 mW s/cm³, with 17% Co and this rose to 15·2 mW s/cm³ with 25% Co (Figure 9.26). It is worthy of note that the fulness factor $\eta$ is greater in these alloys than in the nickel-rich series previously discussed.

For the Fe–Al–Ni alloys investigated by Zumbusch, titanium shows no fundamentally favourable effect. The simultaneous use of copper and titanium, in fact, produced a deterioration. On the other hand, in Fe–Al–Ni–Co alloys, the addition of 5–8% Ti brought about a noteworthy improvement. Thus Vallier, Bronner, and Pfeffer[134a] were able to show that the remanence was reduced if 2–8% Ti was added to an alloy of 34% Co, 7% Al, and 15% Ni (remainder iron), but the coercivity rose in such a way that at 7% Ti a maximum $(BH)_{max} = 35$ mW s/cm³ was achieved.

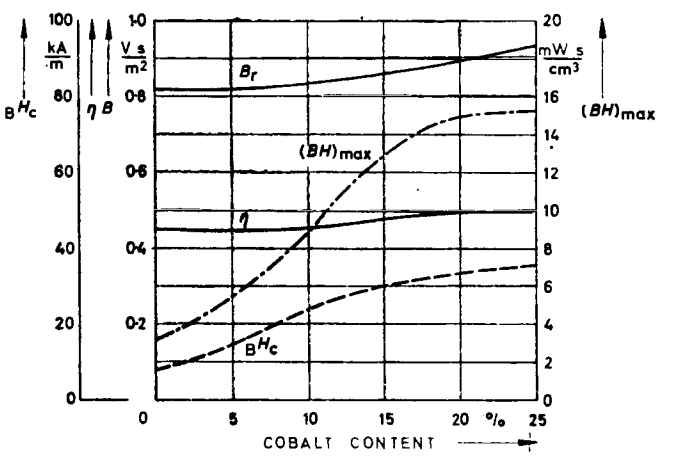



*Figure 9.26. Magnetic properties of alloys having 14–16% Ni, 8–10% Al, and 2–5% Cu (remainder iron) as functions of cobalt content*[140]

*Effect of magnetic processing*

It is possible to bring about a still further improvement in the magnetic properties of many Fe–Al–Ni alloys by applying a magnetic field of some 350 kA/m. The field is applied while the material to be magnetically processed passes slowly from a higher temperature (1200°C) through its Curie point. In this way Nesbitt and Williams[100] achieved an ordered precipitation with a corresponding magnetic anisotropy. The remanence ratio $B_r/B_s$ was improved from 0·67 to 0·72.

Investigations first successfully carried through by Oliver and Shedden[106], in 1938, on a Mishima alloy (18% Ni, 10% Al, 54% Fe, 12% Co, and 6% Cu) were quickly extended to numerous Fe–Ni–Al–Co alloys and led to many technically useful results. According to Zumbusch[141], materials which lend themselves particularly well to thermomagnetic treatment are those with a total content of nickel and cobalt of 30–36% in which the cobalt content is some 1·6 times the nickel content and is associated with an aluminium content of 7·5–9·5% and with a copper content of 2–5%.

Jellinghaus[55] found that magnetic treatment had the best effect when the aluminium amounted to about 8·7%. As Figure 9.27 demonstrates, an addition of 8·7% Al to an alloy of 23% Co, 15% Ni, and 3% Cu raised the $(BH)_{max}$ value by a factor of almost 3.

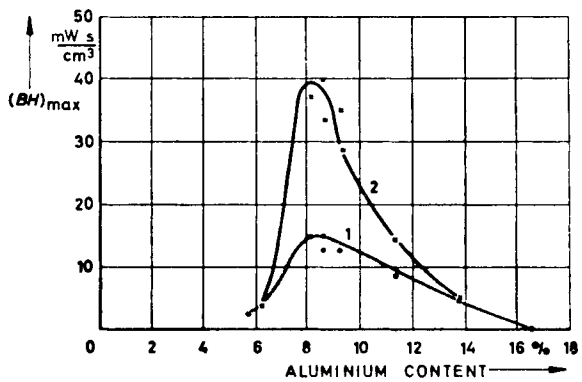



*Figure 9.27. Effect of aluminium content on the $(BH)_{max}$ values of iron alloys having 23% Co, 15% Ni, and 3% Cu: 1, without magnetic treatment; 2, with magnetic treatment*[55]

The typical effect of magnetic treatment is seen in the example of an Alnico 5 magnet having a composition of 24% Co, 13·5% Ni, 8% Al, 3% Cu, and 51·5% Fe (Figure 9.28). The middle curve of the three displays the demagnetising curve of a material cooled without the application of a field: $(BH)_{max}$ comes to 17·6 mW s/cm³. If the same material is heated to 1300°C and cooled to room temperature in a magnetic field of 80–240 kA/m and finally tempered for a few hours at 625°C, then, in a direction parallel to the applied field, the upper of the three curves is relevant (41·6 mW s/cm³). Normal to this direction, low remanence and low coercivity are found while

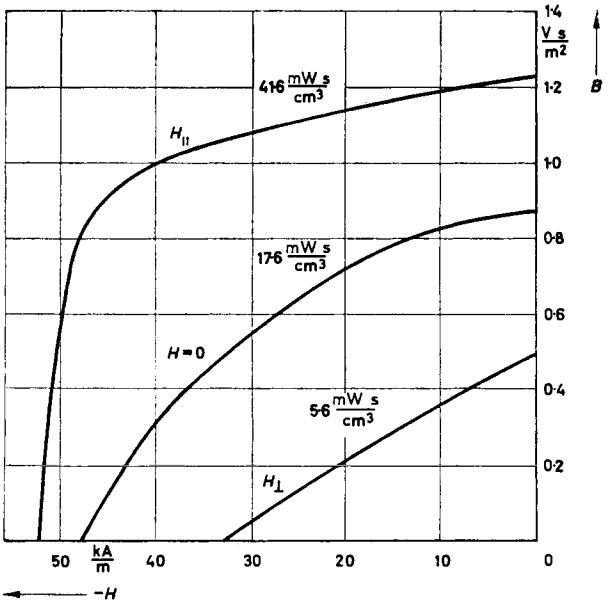



*Figure 9.28. Demagnetisation characteristics of an* Fe–Al–Ni–Co *permanent-magnet alloy (Alnico 5) without magnetic treatment ($H = 0$), together with curves for a magnetic field applied during cooling and measured parallel to this field ($H_\parallel$) and perpendicular to it ($H_\perp$)*[13]

$(BH)_{max}$ attains a value of only 5·6 mW s/cm³. Thermomagnetic treatment not only improves the $B_r$ and $H_c$ values but also increases the fulness factor $\eta$ from 0·42 to 0·65[18].

## *Effect of crystal orientation*

It has already been pointed out that the precipitated particles of the Alnico alloys, if formed in the absence of a magnetic field, are directed along the cube-edges of the matrix crystallites. An improvement in the magnetic properties was therefore to be expected if it should prove possible to direct these crystallites to lie parallel to the edges, i.e. to achieve directional crystallisation after the cooling of the melt, and in addition—through thermomagnetic processing—to produce precipitations parallel to the principal direction. In fact this endeavour has been successful: it proved feasible, by various special means, to achieve 'columnar' crystallisation[109].

By a combination of crystal orientation and directional precipitation of nearly optimally dimensioned particles in a magnetic field, $(BH)_{max}$ values could be improved (on a laboratory basis) to 96 mW s/cm³ [50b, 61]. The corresponding values of $B_r$ and ${}_BH_c$ are 1·185 V s/m² and 106 kA/m respectively. A material consisting of an alloy of 34% Co, 15% Ni, 7% Al, 4% Cu, 5% Ti, and 35% Fe yielded a fulness factor $\eta$ of 0·76. Using a similar alloy of 24% Co, 13·5% Ni, 8% Al, 3% Cu, 0·5% Nb, and remainder iron, whose demagnetisation curve is labelled 5 in Figure 9.18, it was even possible to

raise the fulness factor to 0·78. In this case $(BH)_{max}$ was 69 mW s/cm$^3$, $B_r$ was 1·32 V s/m$^2$, and ${}_BH_c$ was 67 kA/m.

It is with Alnico magnets prepared in this fashion that the best value of $(BH)_{max}$ known to date has been achieved for parts manufactured in quantity; the absolute maximum of $(BH)_{max}$ is held by Co–Sm magnets (Section 9.10.5.2). The reproduction of the above-mentioned values, however, is still difficult and therefore costly. In Japan special casting moulds have been developed in which columnar crystals can grow, and cylindrical or square-section magnets have been commercially produced[88]. By a 'columnar crystallisation' that is only partial, high-grade magnet materials can be made at little expense and these are a significant improvement on non-ordered materials[45a].

*Sintered magnet materials*

Alnico magnets produced by casting usually have a relatively rough surface which in many cases necessitates further machine operations. However, Fe–Al–Ni and Fe–Al–Ni–Co alloys have the considerable disadvantage that, being very hard and brittle, post-machining and grinding operations are expensive. It is therefore often better to go over to sintered Alni and Alnico magnets. This process brings in its train a whole series of added advantages. Thus sintered magnets have a finer structure than cast magnets, leading to an increase in rigidity from 200–500 N/mm$^2$ up to 1000–1500 N/mm$^2$; they are homogeneous and this leads to a more uniform partition of flux; by reason of the smoother surface and consequent smaller manufacturing tolerances the production cost and the material wastage are diminished; pole-pieces of soft iron can be sintered-on during the manufacturing process; also, tiny magnets weighing less than a gramme can be made by sintering. The methods of powder metallurgy are more economical than casting for magnets weighing under 15 g.

So Fahlenbrach[30] refers to magnets made by sintering methods with thicknesses of 0·4 mm, or to those having dimensions of 1 mm×1 mm×0·25 mm. By means of sintering techniques it is possible to make not only very small magnets but also complicated magnet shapes having depressions, slots, threads, or inserts without special manufacturing difficulties—but with the restriction that the slots and depressions must lie in the moulding direction.

Various technologies sometimes require some modification of composition. For example, while in cast Alnico 5 an addition of 0·5–2% Nb improves the magnetic properties, in sintered material the niobium must not exceed 0·7%. Higher amounts of the additive give rise to a porous skin, a rapid growth of grain size, and a loss of rigidity[130]. Similar effects may be the cause of the fact that, for sintered magnets, the magnetic constants are often at the lower limit of what can be achieved by cast magnets.

The differences in the properties of cast and sintered Alnico magnets may be reduced if the powder used is a mixture of the ordinary metallic powder and an Alnico powder produced in a ball mill from a cast Alnico alloy.

Planchard and Bronner[109a], using this method, obtained an Alnico 5 composition whose $(BH)_{max}$ was 39 mW s/cm³ compared with only 36 mW s/cm³ when plain sintering was used.

The investment costs of sintered magnets are very high. The heavy tool costs can only be justified by a long manufacturing run[13].

Table 9.9 collects together the magnetic properties for some common Alnico alloys, permitting a comparison between sintered and cast materials[16]. The table is supplemented by the presentation of the demagnetising curves of certain sintered Alnico materials (Figure 9.29). The upper curve of Figure

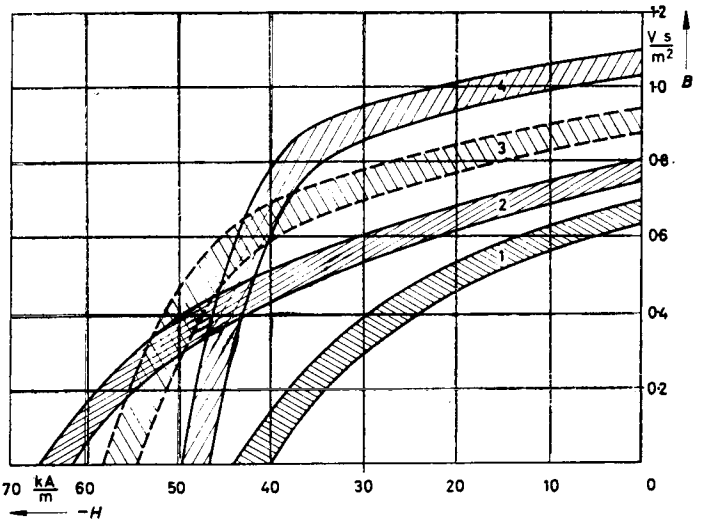



*Figure 9.29. Sintered Alnico materials: 1, Alnico; 2, Hycomax; 3, Alcomax IV; 4, Alcomax III*[93]

9.29 holds for 'ideal measuring conditions', i.e. completely smooth bar magnets of rectangular section, and the lower for the guaranteed minimum values[93]. Chemical composition and physical properties of the individual materials may be taken from Table 19.5.

### *Moulded magnets*

As the Fe–Al–Ni–Co alloys are very brittle, it is easily possible to fragment them and reduce them to dust. This fact is made use of in the manufacture of moulded magnets. The dust is mixed with an insulating material such as Duroplast or Thermoplast and pressed up into shape. The first magnets produced in this way were called Tromalit by their inventor, M. Baermann[9]. Moulded magnets using a bonding substance are to be distinguished from sintered magnets which may also be moulded.

Specially small magnets can be commercially produced in large quantities by these means. Even scrap magnets can be turned to account in this way. The magnetic properties achieved compare well with those of sintered

unoriented barium ferrite. The following data refer to type T1100: ${}_{B}H_{c}=81{\cdot}6$ kA/m, $B_r = 0{\cdot}45$ V s/m², and $(BH)_{max} = 10{\cdot}8$ mW s/cm³.

The filling or bonding material naturally reduces the magnetic characteristics. According to Dehler[27], the reduction in magnetic values can amount to some 20% compared with cast magnets. The appropriate physical properties, according to the same author, are set out in Table 9.10. Figure 9.13 shows a

**Table 9.9** MAGNETIC PROPERTIES OF CAST AND SINTERED ALNICO PERMANENT-MAGNET MATERIALS[16]

| *Alloy (remainder iron)* | | | | *Designation* | $B_r$ (V s/m²) | ${}_{B}H_{c}$ (kA/m) | $(BH)_{max}$ (mW s/cm³) |
|---|---|---|---|---|---|---|---|
| Al | Ni | Co | Cu | | | | |
| 10 | 19 | 12 | 6 | Alnico, standard | | | |
| | | | | Cast | 0·71–0·79 | 46–38 | 11·1–14·2 |
| | | | | Sintered | 0·64–0·77 | 44–36 | 11·1–13·2 |
| 10 | 21 | 12 | 6 | Alnico, $H_c$-biased | | | |
| | | | | Cast | 0·63–0·73 | 53–44 | 11·1–14·2 |
| | | | | Sintered | 0·58–0·64 | 51–47 | 11·1–13·2 |
| 10 | 17 | 12 | 5·5 | Alnico, $B_r$-biased | | | |
| | | | | Cast | 0·80–0·88 | 34–26 | 10·4–13·6 |
| | | | | Sintered | 0·73–0·80 | 36–28 | 10 –11·6 |
| 8 | 11·5 | 21 | 4 | Alcomax II | | | |
| | | | | Cast | 1·27 | 46 | 34 |
| | | | | Sintered | 1·12 | 45 | 26 |
| 9 | 21 | 20 | 2 | Hycomax | | | |
| | | | | Cast | 0·85 | 63 | 21·6 |
| | | | | Sintered | 0·76–0·82 | 65–61 | 19·2–22·3 |

few demagnetisation curves for moulded magnets based on barium ferrite Ox 100, AlNi 120, AlNiCo 160, and AlNiCo 250[75].

The temperature stability of pressed and bonded magnets is determined by the properties of the bonding substance and is mostly less than that of the solid material. Dietrich[28c] investigated the ageing of moulded magnets in relation to material composition and found it to be between twice and ten times as great as for solid magnets under comparable conditions. He attributed the observed behaviour to the increased degree of internal gapping in the moulded product[28d].

Moulded magnets are used in tachometers, vibration counters, electricity meters, and countless other applications.

**Table 9.10** MOULDED MAGNETS OF ALNICO ALLOYS[27]

| | |
|---|---|
| Bending modulus | 1200 N/cm$^2$ |
| Compression modulus | 1200 N/cm$^2$ |
| Density | 5·5–6·2 g/cm$^3$ |
| Shock resistance | 125$g$ at $f$ = 10 Hz ($g$ = 9·81 m/s$^2$) |
| Centrifugal safety | 35 m/s |
| Temperature stability | Up to 160°C |
| Linear coefficient of expansion | 15 ppm/K |

### 9.10.2.2 Cu–Ni–Co and Cu–Ni–Fe alloys

Besides the Fe–Al–Ni and Fe–Al–Ni–Co alloys there exists another series of permanent-magnet alloys hardened by precipitation. Both alloys of nickel, cobalt, and copper, and alloys of nickel, copper, and iron belong to this group. They do not attain the high peak values of Alnico magnets but neither do they share their poor mechanical properties; their manufacture involves fewer technical difficulties and they are to some extent capable of being worked even after hardening.

Heat treatment mostly proceeds according to the following routine: after a homogenisation baking at a high temperature (for example 1100°C), a rapid cooling and then a tempering at 600°C take place. The effect of heat treatment for a composition of 65% Cu, 20% Ni, and 15% Fe is shown in Figure 9.11 after Biedermann and Kneller[17].

Cu–Ni–Co alloys have been closely investigated, particularly by Dannöhl and Neumann[25]. They achieved a highest $(BH)_{max}$ value of 8 mW s/cm$^3$ using a composition of 35% Cu, 24% Ni, and 41% Co. The coercivity obtainable with this alloy is 36 kA/m. It can be raised to 44 kA/m by choosing a composition of 50% Cu, 21% Ni, and 29% Co. However, the $(BH)_{max}$ value drops to 5·3 mW s/cm$^3$. The fulness factor of this alloy comes to 42%; the permanent permeability $\mu_p$ is 4·4$\mu_0$.

The most commonly used Cu–Ni–Co alloy has the approximate composition 35% Cu, 24% Ni, and 41% Co. It is isotropic and is chiefly used in the form of wire or strip, though it can also be cast. Steinitz[124] obtained a $(BH)_{max}$ of 5·6 mW s/cm$^3$ with a sintered alloy of 30% Co, 45% Cu, and 25% Ni.

With the Cu–Ni–Fe alloys $(BH)_{max}$ values of 8–11 mW s/cm$^3$ are attainable[101, 103]. The best known compositions are: 60% Cu, 20% Ni, and 20% Fe; and 50% Cu, 20% Ni, 27·5% Fe, and 2·5% Co (these are $D_1$ and $D_2$ in Figure 13.26).

The alloys are anisotropic and are easily workable even after heat treatment. Wire of less than 5 mm diameter yields the best magnetic properties. The demagnetising characteristics of a Cu–Ni–Fe and a Cu–Ni–Co alloy are displayed in Figure 9.30[4]. However, for economic reasons, these alloys do not have a significant role in technology.

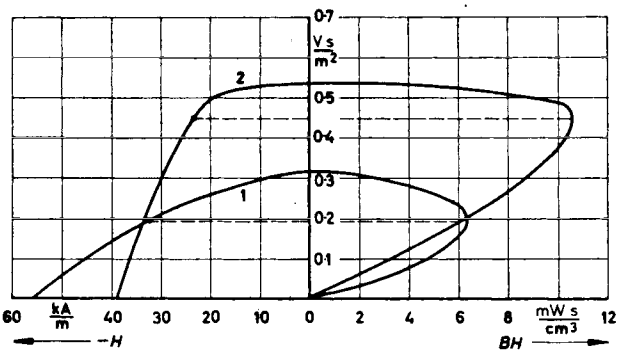



*Figure 9.30. Demagnetising curves: 1, alloy comprising 29% Co, 21% Ni, and 50% Cu; 2, alloy comprising 60% Cu, 20% Ni and 20% Fe*[4]

### 9.10.2.3 Co–Mo–Fe alloys

Co–Mo–Fe alloys may be cold worked after a homogenisation annealing. After tempering (1 h at 680°C), whereby the optimum magnetic properties are brought out, the alloy is mechanically hard and behaves mechanically like an Alnico alloy, i.e. it can only be worked by grinding.

A frequently used composition is 12% Co, 17% Mo, and 71% Fe. The demagnetising curve of this material is shown in Figure 9.31. The density is 8·1–8·2 g/cm³, the specific electrical resistance $\varrho$ is 45 $\mu\Omega$ cm, the remanence $B_r$ is 1 V s/m², the coercivity ${}_BH_c$ is 18–20 kA/m. A value of 8–9 mW s/cm³ is usually quoted for $(BH)_{max}$[105].

The properties resemble, therefore, those of a cobalt steel with 36% Co, but the material is cheaper to produce and more stable. The alloy is suitable for either casting or sintering[94] and is workable in the cast and the rolled condition.

### 9.10.2.4 Fe–Co–V alloys (see also Section 9.10.3.1)

Just as workable, but magnetically superior to the Cu–Ni–Co, Cu–Ni–Fe, and Co–Mo–Fe alloys are certain Fe–Co–V alloys having about 50% Co and 10% V. These alloys can be heat treated like normal precipitation alloys, i.e. by heating to a high temperature (800°–1200°C) followed by quenching and then tempering at a moderate heat (600°C). A $(BH)_{max}$ of around 8 mW s/cm³ can then be reached. If the alloy is first hot worked and then cold drawn or profiled, the value can be raised considerably (see next section).

This precipitation hardened Fe–Co–V alloy is known in the literature under the title Vicalloy I (V = vanadium, i = iron, c = cobalt), and like the alloy Vicalloy II, which is hardened by deformation (see below), it goes back to the investigations of Nesbitt[98].

Nesbitt stated that the best composition for Vicalloy I was 38% Fe, 52% Co, and 10% V. The best heat treatment proved to be: 20 min at 1200°C,

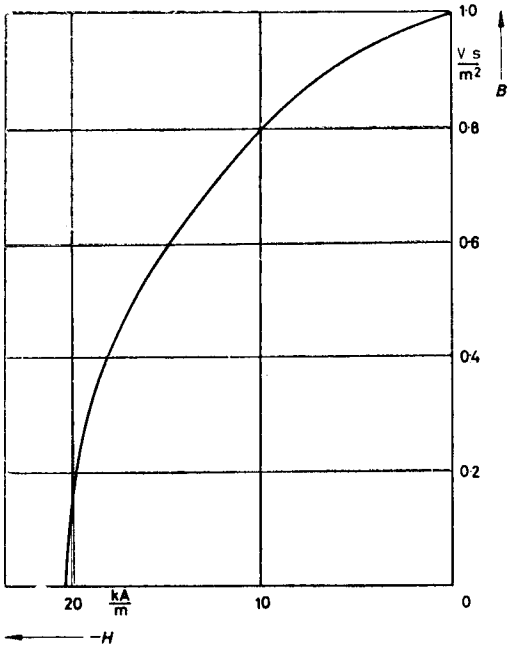



*Figure 9.31. Demagnetisation curve of an* Fe–Co–Mo *magnet (Comalloy)*[105]

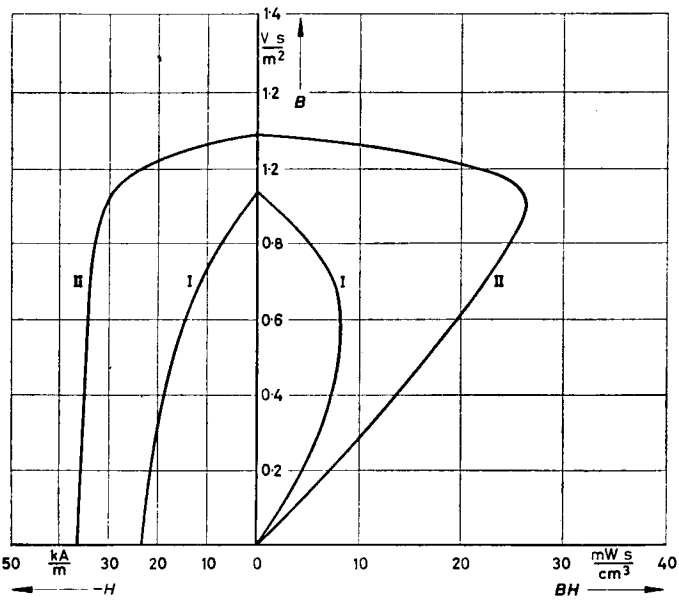



*Figure 9.32.* Fe–Co–V *alloys: I, Vicalloy I (52%* Co, *38·5%* Fe, *9·5%* V*); II, 0·15* mm *wire of Vicalloy II (52%* Co, *35%* Fe, *13%* V*)*[98]

oil quenching, and 8 h tempering at 600°C. This yielded a material with $B_r = 0{\cdot}9$ V s/m$^2$, ${}_BH_c = 24$ kA/m and $(BH)_{max} = 8$ mW s/cm$^3$. The demagnetising characteristic is designated curve I in Figure 9.32. This alloy is not magnetically affected by cold working. An important property for the practical manufacture of this alloy is that the acceptable range of quenching temperature is unusually wide and the rate of cooling uncritical. The alloy is isotropic and may be used with advantage in the form of wire or strip for magnetic recording, for induction motors, and for compass needles.

### 9.10.2.5 (Fe–), (Co–), (Ni–) Ti alloys

Japanese metallurgists have given much attention to alloys of titanium and the ferromagnetic elements, namely to the series Co–Ni–Ti, Co–Fe–Ti and Fe–Ni–Ti. These studies yielded, as a practical end-product, the materials known as 'Honda alloy' or 'New KS steel'—which, indeed, contain all three of the basic ferromagnetic metals. This is an alloy having the composition 27% Co, 18% Ni, 7% Ti, 4% Al, remainder iron, a combination which is very close to certain titanium-enriched Alnicos. A $(BH)_{max}$ of 16 mW s/cm$^3$ can be achieved[3] with $B_r = 0{\cdot}65$ V s/m$^2$ and ${}_BH_c = 72$ kA/m.

## 9.10.3 Cold-deformed permanent magnets

In Section 9.10.2.4 it was stated that certain precipitation alloys can be mechanically formed after a homogenisation annealing and that cold working can lead to significant improvement in magnetic quality. This holds not only for certain Fe–Co–V alloys but also for Fe–Ni–Cr alloys having about 18% Cr and 8% Ni and, again, for three-component alloys based on Fe–Mn with some 13% Mn and additions of chromium, aluminium, or titanium. Cold deformation brings about a conversion of non-ferromagnetic Austenite into ferromagnetic Martensite. Tempering induces an increase of coercivity whereby part of the Martensite is reconverted to Austenite.

### 9.10.3.1 Fe–Co–V alloys

Nesbitt[98] had observed that, for an alloy of 52% Co, 38% Fe, and 10% V, higher values of $(BH)_{max}$ could be obtained if it was rolled or drawn into wire. Profile rolling gave better values than surface rolling. An alloy having 14% V was almost non-magnetic before cold working (austinitic structure). Following a reduction in cross-section of about 95% and a tempering at 600°C, a $(BH)_{max}$ of 22·4 mW s/cm$^3$ was measured for a wire 1 mm thick. Alloys improved by deformation were known by the name Vicalloy II.

Nesbitt considers that the optimum composition for Vicalloy II is an alloy of 34% Fe, 52% Co, and 14% V, cold worked to a 98% deformation and tempered at 600°C. This gives ${}_BH_c = 41$ kA/m, $B_r = 1$ V s/m$^2$, $(BH)_{max} = 28$ mW s/cm$^3$. Magnetic wire made in this way had a diameter of 0·15 mm. The demagnetising curve (curve II) of a similar alloy appears in Figure 9.32.

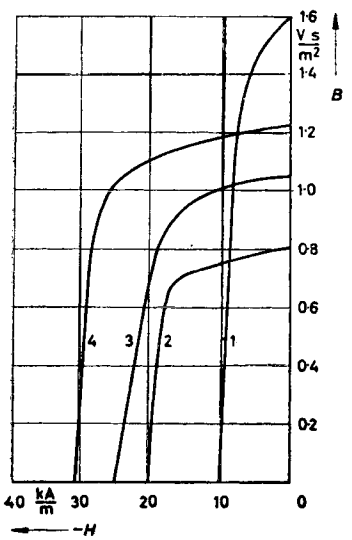



*Figure 9.33.* Fe–Co–V *alloys: 1, Koerflex 200 strip; 2, Gaussite 180; 3, Koerflex 300 strip; 4, Koerflex 300 wire*[32,75]

The remanence of these three-component alloys can be raised—though at the expense of coercivity (4 kA/m)—to 1·8 V s/m$^2$, the highest remanence value known for a permanent-magnet material. Further development of these Fe–Co–V alloys led to an improved composition having 52% Co, 36% Fe, 8% V, and 4% Cr, which became known under the names Koerflex 300 and Koerflex 200[11, 32]. Mishima[88] reports on a similar Japanese alloy (51·3% Co, 6·7% V, and 4·5% Cr, remainder iron).

The optimum tempering heat lies at about 550°C. The value of $H_c$ rises to 16 kA/m and $B_r$ to 1·3 V s/m$^2$. Cold deformation of 85%, following the tempering process, raises the coercivity to 62 kA/m while $B_r$ remains almost unchanged[88].

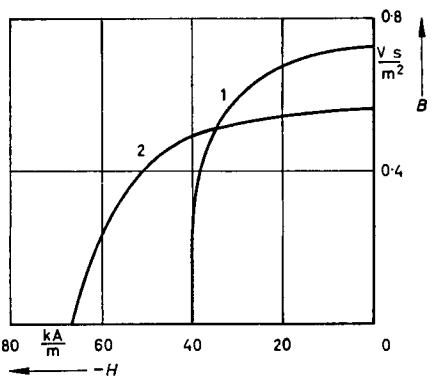
Just as for Vicalloy, wire proves superior to strip for these new alloys (Figure 9.33). The material is used for the manufacture of compass needles and measuring magnets, and also for miniature magnets down to 0·02 g weight. The linear extension should, in the most favourable case, be 7–12 times the transverse extension. A special feature of the alloy worth bringing out is its high stability up to temperatures of some 350°C. For wire diameters over 3 mm and strip thicknesses more than 0·6 mm it is not possible with present methods of production to achieve figures as good as these.

Other Fe–Co–V permanent-magnet materials developed in Germany are known by the name Magnetoflex[134], and in particular Magnetoflex 35 (52% Co, 13% V, 35% Fe), which is anisotropic, and Magnetoflex 40 (52% Co, 8% V, 40% Fe), which may be produced in either an isotropic or an anisotropic version.

### 9.10.3.2 Fe–Ni–Cr alloys

Steel with about 18% Cr and 8% Ni, known for its anticorrosion properties, generally possesses the structure of paramagnetic $\gamma$-iron (cubic face-centred lattice). A ferromagnetic $\alpha$-phase (cubic body-centred lattice) can be pre-

*Figure 9.34.* Fe–Ni–Cr *alloys (see text)*[112]




cipitated by means of rolling; by reason of fineness of division within the basic substance, this phase can show coercivities up to 32 kA/m and thus possesses the qualities of a permanent-magnet material.

By continuing the investigations of Mathieu[78], Rassmann and Henkel[112] were able to achieve further improvements: by repeated cold rolling and annealing of an alloy with 12% Cr, 15·2% Ni, and 0·28% C, remainder iron, the coercivity could be raised to 64 kA/m. Figure 9.34 shows demagnetisation curves for 0·05 mm wire made of this alloy. The wire was produced in the following way. It was homogenised at a diameter of 1·35 mm and then cold drawn to bring it to a diameter of 0·7 mm. After that, it was tempered at 525°C for 15 min and again cold drawn to 0·1 mm. After a further tempering treatment of 15 min at 525°C, the sample was finally drawn to a diameter of 0·05 mm. A $(BH)_{max}$ of 18·5 mW s/cm³ was reached (curve 1). In another case (curve 2), the first cold drawing took the wire to a diameter of 0·154 mm and the second to 0·069 mm. The first heat treatment lasted 15 min at 500°C and the second 15 min at 525°C. The value of $(BH)_{max}$ was brought up to 20·4 mW s/cm³ and, at the same time, $H_c$ was increased at the expense of $B_r$.

The considerable 'spread' of the characteristics indicates an anisotropy of the material, which Rassmann and Henkel[111] attribute to shape anisotropy.

### 9.10.3.3 Ag–Mn–Al alloys

A permanent-magnet material of interest in certain practical applications is a silver alloy called Silmanal, comprising 8·8% Mn and 4·5% Al with 86·7% Ag[110]. This material is to be classified as easily workable and is characterised by high coercivity and low remanence: $B_r = 0{\cdot}055$ V s/m², ${}_JH_c = 480$ kA/m, ${}_BH_c = 43$ kA/m, and $(BH)_{max} = 0{\cdot}64$ mW s/cm³. Ease of working permits the production of thin foils which, because of the high coercivity, can be magnetised normally to the surface. Such surface magnets are used in, for example, flux-measuring instruments[115] where the high price of the material is of less account than it would be in instruments for everyday use.

### 9.10.4 Superstructure alloys

High coercivities are attainable with the two-component alloys Pt–Fe, Pt–Ni, and Pt–Co. These alloys are hardened by a similar precipitation mechanism to that of other hardened alloys but with the difference that the precipitated (tetrahedral phase) is ordered (superstructure transformation), while the underlying matrix is unordered.

Jellinghaus[54] recognised this first in alloys of platinum and iron. Kussmann and v. Rittberg[68] found optimal permanent-magnet properties in an alloy comprising 70% Pt and 30% Fe, giving a ${}_{B}H_c$ of 130 kA/m, a $B_r$ of 0·6 V s/m² and a $(BH)_{max}$ of 26·5 mW s/cm³. At the same time they established that the magnetostriction was low, which led to the supposition that internal stresses could not be considered responsible for the high coercivity. According to recent investigations[8] exchange anistropy seems to be involved.

Even higher coercivities can be achieved with Pt–Co alloys than with Pt–Fe alloys. An alloy known as Platinax II comprises 76·7% Pt and 23·3% Co[86]. It attained the highest coercivity that was measured before the discovery of the cobalt–rare earth intermetallic compositions. The $(BH)_{max}$ value is exceeded by only the best Alnico magnets with columnar crystals and by the above-mentioned intermetallic combinations. Its properties are: $B_r$ = 0·64 V s/m², ${}_{B}H_c$ = 385 kA/m, $B_w$ = 0·34 V s/m², $H_w$ = 215 kA/m, and $(BH)_{max}$ = 74 mW s/cm³. To realise these high values, the material must be quenched in oil from 1250°C and tempered at 650°C. The density is very high on account of the high proportion of platinum, amounting to $d$ = 15·5 g/cm³. The permanent permeability $\mu_p$ is 1·13–1·16$\mu_0$. It is true that the working flux density falls off at temperatures at or above 250°C (20% at 250°C), but it still remains very high.

As may be seen from Figure 9.35 there is not much 'bulging' of the demagnetising curve ($\eta$ = 0·30), indicating that the material is isotropic. A corresponding alloy of almost identical performance has come into commercial

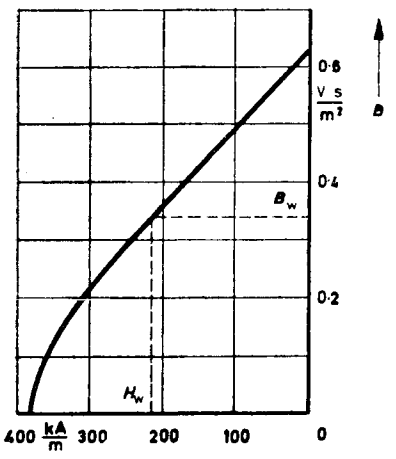



*Figure 9.35.* Co–Pt *alloy (Platinax II)*[86]

use under the name Oerstite 900[28]. It finds practical application in electric-clock motors, miniature microphones, and hearing aids. Further, it facilitates the manufacture of complicated components because the material can be readily formed prior to heat treatment; it may be manufactured by a smelting process or by sintering techniques.

The ordered phase of the Fe–Pd alloys is characterised by an unusually high crystal energy ($K_1 = 26 \times 10^6$ erg/cm$^3$). Saturation is thus not reached before a field strength of 3200 kA/m[68a].

### 9.10.5 Materials for dust magnets

The development of powdered magnetic materials, or magnetic dust, is of recent date. Yet it seems that as far back as 1779 Gavin Knight constructed magnets from powdered magnetite[70].

Not until 150 years later (1931) did Kato and Takei[57] produce the magnetite–cobalt oxide magnets called OP magnets, and it was another 10 years before Guillard[46] achieved coercivities of more than 300 kA/m with a 'Heusler' alloy of manganese and bismuth. A further 10 years were to pass before hexagonal barium ferrite reached a point of development where the manufacture of the isotropic material was feasible on a practical scale[35, 136]. Barium ferrite with a preferred magnetic direction appeared soon after[129].

The development of iron dust magnets followed a parallel course. It was founded on the long-known fact that coercivity increased with diminishing particle size[5, 6, 43, 116]. It was radically advanced, however, by the fundamental work of Kittel[58] and Néel[96, 97] on the critical size and shape of magnetic particles. However, $H_c$ does not increase indefinitely with diminishing particle size but reaches a maximum (at about 32 nm for iron) and then falls off again. According to investigations by Carman[22], a maximum was reached for iron at a particle size of 25 nm, to which corresponded an ${}_JH_c$ value of 80 kA/m (Figure 9.36).

The development of dust magnets entered its latest stage, one not yet necessarily closed, with the discovery of the ESD (elongated single domain)

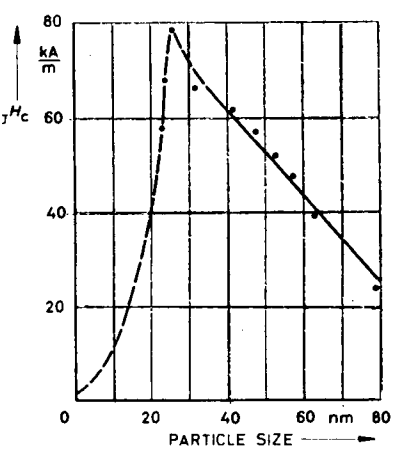



*Figure 9.36. Coercivity as a function of particle size for iron dust*[22]

**Table 9.11** MAGNETIC VALUES FOR DUST-MAGNET MATERIALS

| *Material* | | $B_r$ (V s/m²) | ${}_BH_c$ (kA/m) | $(BH)_{max}$ (mW s/cm³) | *Reference* |
|---|---|---|---|---|---|
| MnBi | Best lab. values | 0·48 | 290 | 43 | 2 |
| | Theoretical limits | 0·78 | 620 | 120 | |
| $BaO \cdot 6Fe_2O_3$ | Practical values | 0·375 | 155 | 25 | 119 |
| | Best lab. values | 0·40 | 153 | 29 | |
| | Theoretical limits | 0·475 | 380 | 45 | |
| Co ferrite | Practical values | 0·16 | 72 | 4 | 70 |
| | Best lab. values | 0·40 | 160 | 13 | 47 |
| | Theoretical limits | 0·53 | 420 | 56 | 70 |
| Fe | Practical values | 0·60 | 38 | 8 | 70 |
| Fe–Co | Practical values | 0·86 | 33 | 13 | 70 |
| Mn–Al | Best lab. values | 0·43 | 220 | 28 | 60 |
| | Theoretical limits | 0·62 | 500 | 76 | 60 |
| ESD iron | Practical values | 0·79 | 45 | 18 | |
| | Best lab. values | 0·915 | 61 | 34 | 74 |
| | Theoretical limits | 1·43 | 290 | 300 | |
| ESD Fe–Co | Practical values | 0·9 | 88 | 29 | |
| | Best lab. values | 1·08 | 78 | 52 | 70 |
| | Theoretical limits | 1·63 | 330 | 400 | |
| $SmCo_5$ | Best lab. values | 0·9 | 720 | 160 | 128b |
| | Practical values | 1·0 | 800 | 187 | |

materials. Table 9.11, which is drawn from a summary by Luborsky[70], offers a comparison between various dust materials. Theoretical expectations are compared and contrasted with those obtaining in current technology.

### 9.10.5.1 Mn–Bi and Mn–Al alloys

The alloys discovered in 1901 by Heusler and later named after him differ from other magnetic materials by the fact that they contain none of the elements iron, cobalt, and nickel. They do, however, contain manganese, the

element which precedes them in the periodic table. Manganese is not itself ferromagnetic but can assume ferromagnetic properties in many of its compounds, in particular if the relation between lattice spacing and ionic radius attains a critical magnitude (see page 103).

Mn–Bi compounds were investigated extensively by Guillaud[46]. He observed the very high crystal anisotropy of $11{\cdot}6 \times 10^6$ erg/cm$^3$, and this may be considered the reason for the high coercivity. Adams[1] in 1952 achieved the following values: ${}_BH_c = 272$ kA/m, $B_r = 0{\cdot}43$ V s/m$^2$, and $(BH)_{max} = 34{\cdot}4$ mW s/cm$^3$. The best achieved to date, using an alloy of 80% Bi and 20% Mn, is the following set: $B_r = 0{\cdot}43$ V s/m$^2$, ${}_BH_c = 280$ kA/m, and $(BH)_{max} = 37$ mW s/cm$^3$. The highest known[2] value of $(BH)_{max}$ is 43 mW s/cm$^3$.

Moulding conditions affect the coercivity obtainable. Low density of a pressing hinders the fusion of the dust particles during sintering so that a high coercivity is possible[2]. During the moulding process a pulsating field of about 1600 kA/m is applied in order to align the particles. A moulding temperature of 300°C and the presence of liquid bismuth facilitates the orientation. A urea-based resin (fluid at 80°C) may be used as a binder in place of liquid bismuth and will evaporate at about 200°C[77a].

Japanese scientists have established that the magnetic phase is $Mn_3Bi_2$ and not, as was once thought, MnBi[77]. Makino and Suzuki[77a] suggested 260°C as the most favourable sintering temperature. They succeeded in making Mn–Bi magnets having the following properties: $B_r = 0{\cdot}25$–$0{\cdot}38$ V s/m$^2$, ${}_BH_c = 96$–$116$ kA/m, and $(BH)_{max} = 12$–$28$ mW s/cm$^3$.

For this result the powder was mixed with 6% resin and moulded under a magnetic field of 800 kA/m at 100°C and at a pressure of 250 N/mm$^2$. In spite of the excellent values attainable, Mn–Bi combinations have scarcely found any practical application. The high cost of the raw materials is against them as is, also, the complex manufacturing process. To these difficulties must be added a poor corrosion resistance and a high temperature coefficient[60, 77a].

A value for $(BH)_{max}$ of 28 mW s/cm$^3$ was achieved in Japan[77] for the ferromagnetic phase of a Heusler alloy of manganese and aluminium[62], a value also reached by Koch and his colleagues[60]. Crystal anisotropy amounts to some $10^7$ erg/cm$^3$ and saturation magnetisation to $0{\cdot}62$ V s/m$^2$. Various indications suggest that exchange anisotropy plays an important part in the Mn–Al alloys[60]. Makino and his co-workers[77b] produced an alloy with 68–70% by weight of manganese by smelting in a crucible of aluminium dioxide in an atmosphere of argon. The material was quenched at 1100°–1150°C and tempered at 500°C. They achieved a $B_r$ of $0{\cdot}27$ V s/m$^2$ and a ${}_JH_c$ of 80 kA/m.

### 9.10.5.2 Cobalt–rare earths

More promising, even, than intermetallic combinations of manganese and aluminium are intermetallic compounds of rare earths and the transition metals, iron, nickel, and cobalt. The atoms of the rare earths exhibit incomplete 4f electron shells, which induce ferromagnetism much as do the uncompleted 3d shells of iron, nickel, and cobalt (see page 101).

It has long been known that gadolinium, which occupies mid-place in the rare-earth series, is ferromagnetic (see page 18). It was further understood

that the metals of the rare-earth series tend to form intermetallic compounds, for example $R_2Co_{17}$, $RCo_5$, and $R_2Co_7$ (R standing for one of the rare earths). To probe more carefully the extensive range of possible compounds seemed therefore an attrative field of study.

Extensive investigations began around 1960. The work of Hubbard, Adams, and Gilfrich[52a], as well as that of Strnat, Hoffer, and Ray[128a], is particularly worthy of mention. Surprisingly high and not previously attainable coercivities were found—in the combination $GdCo_5$, for example. Existing measuring devices frequently proved inadequate to determine the precise values[26a, 52a]. These preliminary successes led workers to concentrate particularly on the intermetallic compounds of cobalt since their hexagonal crystal structure led to the expectation of particularly high crystal anisotropy[52a, 100a].

The investigations, to be sure, were not without their disappointments: the Curie temperatures of many of the combinations investigated turned out to be very low—too low to lead to commercial products suitable for normal environmental conditions. Compounds of the rare earths with iron were rejected at the outset since the Curie temperatures were confined to the range from $-180°C$ to $+187°C$[128a]. On the other hand, compounds of the type $RCo_5$ showed themselves particularly suitable. Buschow and Velge[21b] found among them high Curie temperatures and anisotropic field strengths up to 23 000 kA/m. Not only high coercivity but also—by reason of the high cobalt content—high values of magnetic saturation were measured, so high $(BH)_{max}$ figures were obtained: ${}_BH_c = 400$ kA/m and $(BH)_{max} = 65$ mW s/cm$^3$. Calculation of the optimum theoretical values to be expected became possible after the results of basic investigations into the corresponding physical data had been published, i.e. saturation polarisation and anisotropic field strengths. Laboratory investigations led, in a relatively short time—particularly as regards the compound $SmCo_5$—to extremely satisfactory results which soon came very near theoretical expectations.

Table 9.12 gives values for the most important $RCo_5$ compounds taken from a comprehensive summary by Strnat[128b]. Besides the Curie temperatures, coercivities, and saturation values, the table sets out the $(BH)_{max}$ values; in fact the theoretical values are comparable with the practical values achieved up to the present. It is truly astonishing that $SmCo_5$ yielded, after so brief a development period, 80% of the expected optimum of 187 mW s/cm$^3$. In this respect $SmCo_5$ is exceptional among the members of the series, so one must

**Table 9.12** SOME MEASURED RESULTS FOR MAGNETS OF COBALT–RARE EARTH MATERIAL[128b]

| | $SmCo_5$ | $YCo_5$ | $LaCo_5$ | $CeCo_5$ | $PrCo_5$ |
|---|---|---|---|---|---|
| Curie temperature (°C) | 724 | 648 | 567 | 374 | 612 |
| Saturation polarisation (V s/m$^2$) | 0·965 | 1·06 | 0·909 | 0·77 | 1·20 |
| Coercivity, ${}_BH_c$ (kA/m) | 720 | 128 | 268 | 120 | 214 |
| $(BH)_{max}$ (mW s/cm$^3$) | | | | | |
| Theoretical | 187 | 225 | 165 | 118 | 288 |
| Measured | 160 | 12 | 46·5 | — | 34·4 |

suppose that various favourable conditions of preparation converged. $PrCo_5$, from which the best values of the series are to be expected, cannot yet be made with anything like the same excellent results.

In order to illuminate the practical problems met with in magnet manufacture, a short account will be sketched of the evolution of a $SmCo_5$ magnet. To begin with the production of the alloy, the components are melted together in the correct proportions. The rare earths are very active at high temperatures so, especially for small specimens, an electric arc must be used or, alternatively, a crucible of high-purity aluminium oxide with a protective atmosphere of argon (or a vacuum). The resulting alloy is very brittle and so may be readily pulverised, particularly at reduced temperatures. As the grain-size falls, the coercivity rises, falling off again after passing a maximum. This $H_c$ maximum lies around 160–500 kA/m for most $RCo_5$ compounds. A falling off of coercivity is observed after moulding which is attributable to a light superficial oxidation of the particles. Only $SmCo_5$ yields significantly superior results.

The dust must be very heavily compressed if the highest results are to be achieved; the theoretical values presuppose 100% compression. Various moulding processes are in use. According to Buschow, Naastepad, and Westendorp[21a], the $SmCo_5$ dust should undergo a chemical treatment, after grinding, whereby the coercivity may be raised from 880 kA/m to a value of 1760 kA/m.

The compression of the dust is carried out in two stages. First, the specimen is preformed in a press producing only a low pressure and under the influence of a magnetic field of 2400 kA/m and is then subjected to a pressure of 20 kbar in a hydraulic press. This procedure gives the pressing a density of 82%. In the second stage of moulding, the pressing is subjected to the same hydraulic pressure but is wrapped in lead foil moistened with mercury. An easily deformable lead amalgam is formed which clings closely to the surface of the pressing. An additional 15–20% plastic deformation takes place during this pressing operation so that a final density of 97% is achieved.

Another method of achieving high densities is by a sintering process. According to Das[26a], in this process the particles of dust are first tinned. During pressing the particles are again subjected to the aligning action of a magnetic field, and the pressings are then sintered for 1 h at a temperature of 1000°C.

Both processes have so far yielded values up to 160 mW s/cm$^3$, i.e. almost five times that of the best commercial Alnico magnets and almost twice the value achievable in the laboratory. To achieve the highest energy densities the particle size must not exceed 10 nm; all particles must lie in the required preferred direction; and the density must approach 100% as nearly as possible. Densities reached so far are quoted up to 8·5 g/cm$^3$. Up to the present the best combinations of properties rest with the Ce–Pr–Sm alloys. The following values for magnets sintered in the fluid state were measured by Martin and Benz[77c]: $B_r = 0{\cdot}996$ V s/m$^2$, ${}_BH_c = 544$ kA/m, and $(BH)_{max} = 184$ mW s/cm$^3$. Magnets made from $SmCo_5$ have a specific electrical resistance of 50 Ω cm.

There are various processes for producing Co–Sm magnets apart from the different ways of making the dust. Dense Sm–Co and Ce–Co alloys in which

part of the cobalt has been replaced by copper can exhibit good permanent-magnet properties. Tempering the quenched alloy induces two phases through spinodal decomposition, namely a modified $SmCo_5$ phase and a copper-rich non-magnetic matrix. Coercivities of 1600 kA/m and energy densities of 64 mW s/cm$^3$ have been measured[50a]. High coercivity depends not only on the composition but also on the rate of cooling, the alignment of the $SmCo_5$-rich phase, and the heat treatment.

Table 9.12 makes it clear that, for a series of $RCo_5$ compounds, the Curie temperatures, saturation polarisations, and coercivities meet the necessary requirements for technical magnet materials.

Little is so far generally known about the reproducibility of the magnetic values. No really substantial production is yet under way, so no wide-ranging experience has been accumulated which might permit an authoritative statement. Further, not much has so far been published as to investigations into stability. Investigation of copper-containing $SmCo_5$ magnets, however, have shown that these are completely stable at room temperature but that they age above 100°C, though this scarcely affects the $(BH)_{max}$ value at high coercivities. Copper-free Co–Sm magnets are also said to show a tendency to age at room temperature[128b]. However, before any pronouncement can be made the results of further research must be awaited.

The general introduction of Co–Sm magnets must founder—at any rate for the time being—on the question of cost. Not only is cobalt an expensive metal, but samarium is even more so. Nevertheless, there are good grounds for hoping that the price of samarium may come down drastically in future[128b]. Cerium mixture metal, comprising 55% Ce and 45% of a mixture of other rare earths, costs today about the same as cobalt. Thus magnets made of cobalt and cerium mixture metal should shortly cost about 1–1$\frac{1}{2}$ times as much as do the best Alnico magnets now. The prospects are therefore good, seeing that McCaig[79a] has already succeeded in reaching $(BH)_{max}$ values of 80 mW s/cm$^3$ with $(MM)Co_5$ magnets. Magnets of pure $SmCo_5$ will presumably be four to five times dearer than Alnico magnets. Other experiments are in progress with a view to replacing part of the cobalt by other metals such as copper or iron[50a, 100b], which would seem to offer the possibility of further price reduction.

Quite apart from the price factor, however, there are many places where Co–Sm magnets could find an application. Their use is particularly indicated where the small size of the magnet is an important consideration, as in the already mentioned wrist-watch motors and certain special miniature d.c. motors or, again, for hearing aids and for special magnets in travelling-wave tubes[26a] and other microwave vacuum tubes. By reason of the extraordinarily high values of its magnetic properties, Co–Sm could replace Pt–Co and even undercut it in price since Pt–Co having 75% Pt is the most expensive of all magnet materials. To what extent technical difficulties in the working of cobalt–rare earth magnets may arise is not yet clear.

The superiority of Co–Sm magnets will be clear from the demagnetising curves displaced in Figure 9.37. The characteristic curves of even the best Alnico and strontium ferrite magnets lie well below those of $SmCo_5$. The demagnetising curve of $SmCo_5$ is also shown (broken line) translated into the form $H = f(J)$.

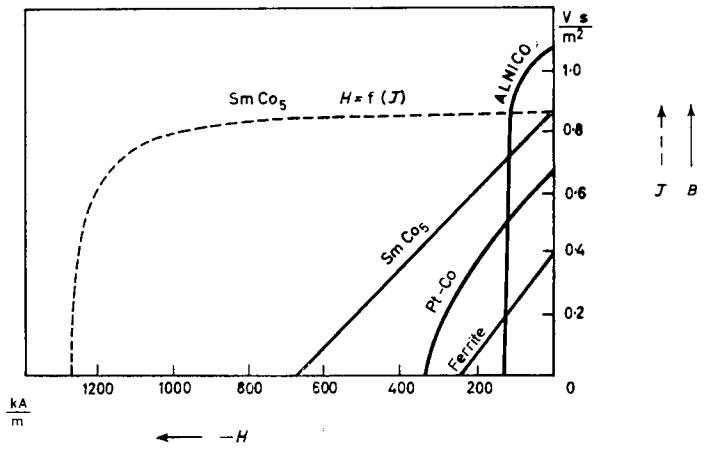



*Figure 9.37. Demagnetisation curves for* $SmCo_5$ *magnets: for comparison, curves are plotted for the best Alnico, ferrite, and* Pt–Co *magnets*

### 9.10.5.3 Iron-dust and alloy-dust materials

Dust magnets of iron and of alloys were developed in France[104].

In Figure 9.36 it is shown that with fine iron dust of a mean grain diameter of 25 nm coercivities of ${}_JH_c = 80$ kA/m can be obtained. Luborsky and Paine[73] found an $H_c$ maximum for iron particles of some 13 nm. The maximum shifts towards smaller particle size for cobalt: about 106 kA/m was reached for the coercivity at a particle size of 3 nm. The same authors found a ${}_JH_c$ of 110 kA/m at a moderate particle size of 24 nm for an alloy consisting of 44% Fe and 56% Co (Figure 9.38a). A further reduction in particle dimensions may introduce super-paramagnetism and $H_c$ will vanish; this occurs at a particle size which is characteristic of each material. The critical size is 5 nm for iron, less than 2·5 nm for cobalt, and around 4 nm for the Fe–Co alloys. The onset of super-paramagnetic processes below the $H_c$ peak is due to powerful temperature effects on the minute particles (Figure 9.38b).

Extremely fine iron dust can be made by the reduction of iron oxide in pure hydrogen at some 300°C, or by electrolytic deposition at a mercury cathode. By reason of the relatively large surface of the particles, they must not be exposed to air or they will react strongly with its oxygen component, oxidising rapidly with considerable generation of heat (they are pyrophoric). Magnets made from fine dust must therefore be protected against atmospheric oxygen by the application of an organic coating (paraffin wax or other waxes). Particle size is measured by the broadening of lines of an x-ray spectrum. With commercially manufactured magnets using nearly spherical iron dust, the following values were achieved: $B_r = 0{\cdot}4$–$0{\cdot}7$ V s/m², ${}_BH_c = 26$–$40$ kA/m, and $(BH)_{max} = 4{\cdot}8$–$8{\cdot}8$ mW s/cm³.

Iron powder made up with a plastic binder yields smaller densities (around 4 g/cm³) and lower remanence, though the coercivity is higher. At high densities around 5 g/cm³, attainable by eliminating binding or insulating

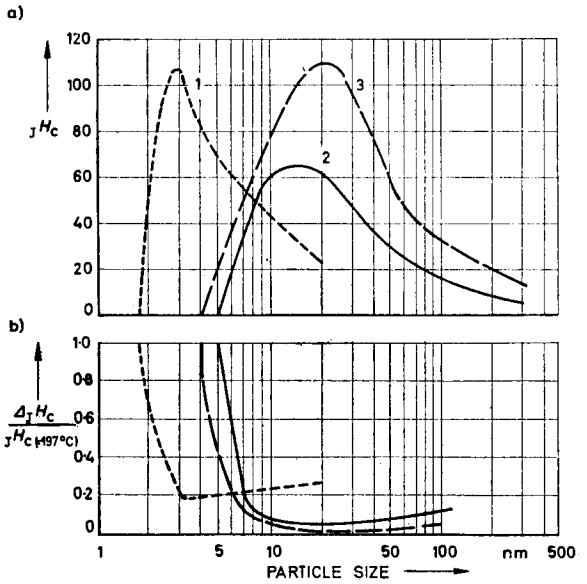



*Figure 9.38. (a) Dependence of the coercivity $_JH_c$ on mean particle diameter (at −197°C); (b) dependence of temperature coefficient on $_JH_c$ between −197°C and −66°C. 1, cobalt; 2, iron; 3, 56% Co–44% Fe*[73]

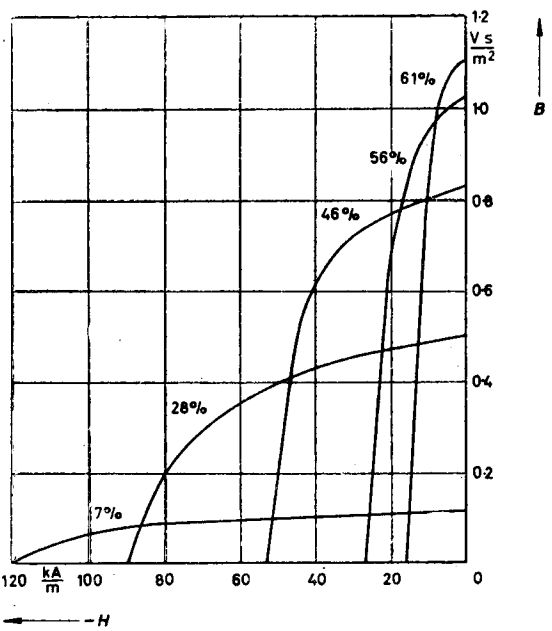



*Figure 9.39. Demagnetisation curves for iron-dust magnets of various packing densities (% iron)*[83]

substances, higher remanences but lower coercivities are obtained. These magnet materials are like the Fe–Al–Ni–Co alloys and the ferrites in that varieties slanted towards better coercivity or better remanence can be made.

As Figure 9.39 makes clear, it is possible to pass from one type to the other. The drawing shows demagnetising curves for various volume proportions of iron and, in consequence, for different packing densities[83]. The value of $H_c$ falls and that of $B_r$ rises with increasing iron content. There is thus a $(BH)_{max}$ optimum which occurs at 40–50% Fe (Figure 9.40).

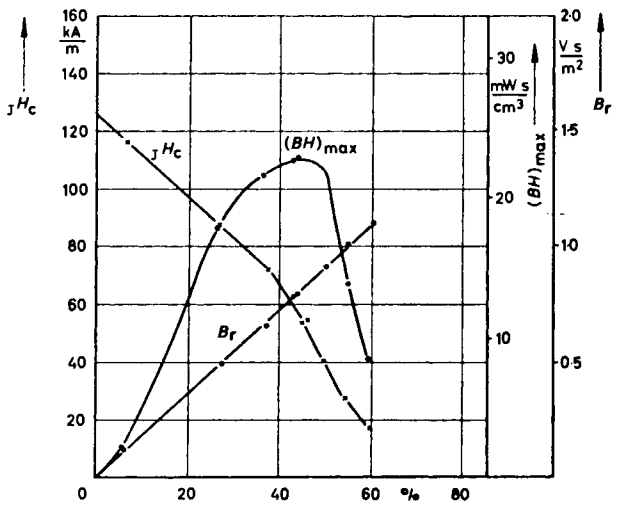



*Figure 9.40. Effect of packing density of iron dust on $_JH_c$, $B_r$, and $(BH)_{max}$*[83]

As against pure iron, the use of alloy powders of iron and cobalt brings about an improvement in the values[3], as follows: $B_r$ = 0·6–0·9 V s/m², $_BH_c$ = 28–50 kA/m, and $(BH)_{max}$ = 8·8–13·2 mW s/cm³. Similar values are obtained with Ni–Co dust (87·5% Co and 12·5% Ni). Falk and Hooper[37] gave a value of $(BH)_{max}$ = 10 mW s/cm³ for a more or less spherical dust.

These values may be exceeded by using elongated, shape-anisotropic particles of iron or of Fe–Co alloys[71]. This can be made clear by considering a series of experiments by Paine, Mendelsohn, and Luborsky[107]. If the length–diameter ratio of iron particles of about 15 nm average diameter is increased from 1·3 to 4·6, then the coercivity rises from 87 kA/m to 148 kA/m (Table 9.13). Since, at the same time, the remanence is high (0·6–0·9 V s/m²), the corresponding value of $(BH)_{max}$ rises to 28 mW s/cm³.

It has been calculated that, with iron particles of the critical size, a $(BH)_{max}$ of 312 mW s/cm³ should be attainable. Of course this assumes that all the particles are in parallel alignment and that magnetisation involves coherent rotation of the magnetisation vectors. As experience shows, these conditions are very difficult to realise (see Section 4.6). In high-density materials the particles can touch each other and the single domain character is then lost: Bloch walls may form. With increasing packing density the parallel align-

**Table 9.13** MEASURED PROPERTIES OF SINGLE-DOMAIN IRON PARTICLES HAVING VARIOUS DIMENSIONAL RATIOS[107]

| *Sample* | *Mean diameter* (nm) | *Length–diameter ratio* | ${}_{J}H_{c}$ (kA/m) |
|---|---|---|---|
| A | 14·5 | 1·3 | 87 |
| B | 15·0 | 2·7 | 108 |
| C | 14·0 | 3·0 | 128 |
| D | 10·4 | 4·0 | 128 |
| E | 17·5 | 4·6 | 148 |

**Table 9.14** PROPERTIES OF IRON DUST MAGNETS[3, 70]

| | $B_r$ (V s/m²) | ${}_{B}H_{c}$ (kA/m) | $(BH)_{max}$ (mW s/cm³) |
|---|---|---|---|
| Iron (spherical) | 0·4–0·7 | 26–40 | 4·8–8·8 |
| Fe–Co (spherical) | 0·6–0·9 | 28–50 | 8·8–13·2 |
| ESD iron | 0·79–0·92 | 49–60 | 17–34 |
| ESD Fe–Co | 0·9–1·08 | 68–79 | 29–52 |

ment of the particles becomes more and more difficult. Investigations by Luborsky, Paine, and Mendelsohn[74] have suggested that, even at high dilution (5% Fe in mercury), aligning fields of the order of 300 kA/m are required. With elongated particles of Fe–Co a figure for $(BH)_{max}$ of 52 mW s/cm³ has so far been achieved, with a corresponding ${}_{B}H_{c}$ of 80 kA/m, while a theoretically expected value would be 400 mW s/cm³ (again under the assumption of coherent rotational processes) (Table 9.14)[70].

If it should seem improbable that the theoretically expected values can be attained, it must, nevertheless, be borne in mind that great strides have been made towards the goal. Magnets made from soft metallic dust have considerable advantages: they can be moulded into any desired shape and can be worked, as required, without difficulty. It is also a considerable convenience, in tailoring the dimensions of a magnet (note the gapping factor) to suit the imposed requirements, that recourse may be had to the influence of the packing density on the magnetic values (Figure 9.39). By a suitable choice of matrix material, there is the possibility of making light 'plastic magnets', which may be of great importance in, for example, mobile magnets[69].

Again, solderable magnets can be made quite readily. A further advantage lies in the simple practicability of the manufacturing routines: the material can be checked at each stage and the end-result thereby made predictable and adjustable. Further, the temperature coefficient of shape-anisotropic materials is better than that of crystal-anisotropic substances[72, 73].

Experience in recent years has shown that technological difficulties in manufacture are more severe than had been expected[107a]. Nevertheless, ESD magnets have proved successful, especially in the smaller sizes. They appear on the market under the names Lodex and Lodox (see page 704).

### 9.10.6 Ceramic magnet materials (ferrites)

The high $(BH)_{max}$ values attainable with the above-mentioned intermetallic compounds are not possible with magnetic materials based on the iron oxide $Fe_2O_3$; nevertheless, these materials—particularly the barium ferrites $BaO \cdot 6Fe_2O_3$—have great commercial value. Indeed, half the German magnet production consists of barium ferrite (see Table 9.15).

Barium ferrite is usually made as follows: powder mixtures with a stoichiometric composition of $BaO \cdot 6Fe_2O_3$, comprising iron oxide ($Fe_2O_3$) and barium carbonate ($BaCO_3$) are pre-sintered (calcined) at 1000°–1100°C, ground, pressed into shape, and finally sintered at 1200°–1400°C. The sintering atmosphere is air[113b].

Sintering causes a solid-state chemical reaction to take place which leads to the formation of $BaO \cdot 6Fe_2O_3$. This hexagonal ferrite, like the cubic ferrites, is brittle and can be ground or worked only with 'ultrasonic drills'. Barium ferrite has the following advantages, among others, compared with the already mentioned metallic magnet materials: it has a high specific electrical resistance ($\varrho$ = 10–100 MΩ cm), so alternating fields have little harmful effect; it has high stability and low ageing; above all, however, the coercivity is so high that very short magnets can be used (the best length–diameter ratio being about unity). The density $d$ is 4·8–5 g/cm³.

On the other hand there is the disadvantage of the relatively high temperature coefficient of barium ferrite: it amounts to −2000 ppm/K for the remanence and +3000 ppm/K for the coercivity. The high stability of the material is manifested in its low permanent permeability, namely 1·0–1·2$\mu_0$. The linear coefficient of expansion is about 9 ppm/K and is thus little more than half the value for metallic magnet materials.

While the original magnetite-containing magnet materials of Kato and Takei[57] used cobalt oxide additives, today's cobalt-containing hexagonal

**Table 9.15** MAGNET PRODUCTION AND PROPORTIONS OF INDIVIDUAL MATERIALS IN THE MOST IMPORTANT PRODUCING COUNTRIES[89]

| *Country* | *Production* (metric tons) | | *Proportion* (%) | | | |
|---|---|---|---|---|---|---|
| | *Monthly* | *Yearly* | *Cast magnets* | *Sintered magnets* | *Ferrites* | *Various* |
| Germany | 200–250 | 2 500 | 20 | 20 | 55 | 5 |
| France | 110–120 | 1 200 | 60 | 5 | 30 | 5 |
| England | 200–220 | 2 400 | 80 | 4 | 6 | 10 |
| Japan | 300–350 | 4 000 | 82 | 0 | 12 | 6 |
| USA | 400–480 | 5 000 | 75 | 5 | 12 | 8 |

**Table 9.16** PROPERTIES OF FERRITE MAGNETS ($BaO \cdot 6Fe_2O_3$)

| | *Isotropic* | *Anisotropic* | *Theoretical maximum* |
|---|---|---|---|
| $B_r$(V s/m²) | 0·20–0·22 | 0·38–0·40 | 0·465 |
| ${}_BH_c$ (kA/m) | 120–155 | 120–240 | 380 |
| ${}_JH_c$ (kA/m) | 190 | 320 | 1 250 |
| $(BH)_{max}$ (mW s/cm³) | 7–8 | 23–30 | 45 |
| $\mu_p$ ($\mu_0$) | 1·1 | 1·1 | — |
| $T_c$ (°C) | 450 | 450 | — |
| $\alpha_{B_r}$ (ppm/K) | −2 000 | −2 000 | — |
| $\alpha_{H_c}$ (ppm/K) | +3 000 | +3 000 | — |

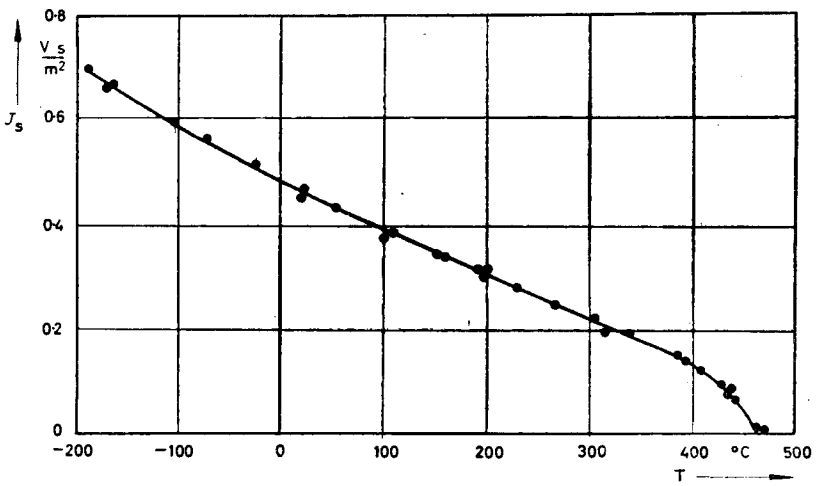



*Figure 9.41. Relation between saturation polarisation and temperature for dense* $BaO \cdot 6Fe_2O_3$[113]

ferrites are less used than the cobalt-free materials. Magnets made in 1933 by Kato and Takei comprised something like half each of cobalt ferrite ($CoO \cdot Fe_2O_3$) and magnetite ($FeO \cdot Fe_2O_3$). The mixed powders were moulded, sintered at 1000°C, and cooled from 300°C to room temperature in a magnetic field. The best magnetic values arrived at by this routine were $B_r = 0{\cdot}4$ V s/m², ${}_BH_c = 50$ kA/m, and $(BH)_{max} = 8$ mW s/cm³. In 1950 Guillaud[47], using pure cobalt ferrite, reached a $(BH)_{max}$ of 12 mW s/cm³. With Co–Fe ferrites in which part of the magnetite was replaced by $Fe_2O_3$, coercivities of 144 kA/m and $(BH)_{max}$ values of 8 mW s/cm³ were reached, according to Buffet[21].

Barium ferrite has the advantage over cobalt compounds that it is cheaper to produce. Barium oxide is available in large quantities at a low price. The most important magnetic constants are collected together in Table 9.16. Figure 9.41 shows, following Rathenau[113], the dependence of saturation

polarisation on temperature. The almost linear shape of the curve is unusual, though understandable in view of the crystal structure. If the ferrite powder is subjected to a directing magnetic field during the pressing operation then, after pre-sintering (or calcining) at temperatures between 1200°C and 1300°C, an anisotropic material is obtained whose remanence is almost doubled. The coercivity is much the same as for the isotropic material. The heat treatment, however, can be so managed that the coercivity is raised at the expense of the remanence. Thus barium ferrites can be classified into remanence-biased or coercivity-biased anisotropic products. Demagnetising curves for isotropic and for both sorts of anisotropic barium ferrite are shown in Figure 9.42, following Fahlenbrach[33]. The actual shape of the characteristic can be changed within wide limits by varying the production routines[41].

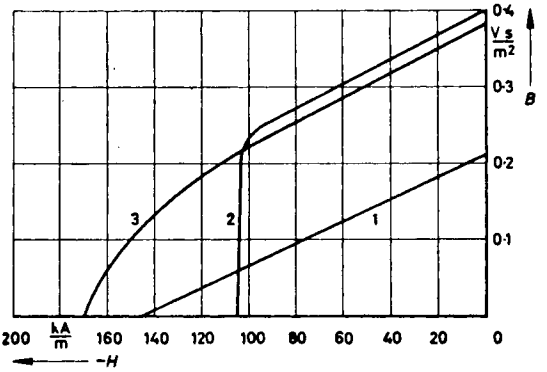



*Figure 9.42. Demagnetisation curves for barium ferrite: 1, isotropic; 2, anisotropic remanence-biased; 3, anisotropic, coercivity-biased*[33]

According to investigations by Sixtus, Kronenberg, and Tenzer[120], the course of the magnetising process for barium ferrite depends on the size of the particles and, if they are plate-like in shape, on their thickness. If the thickness is less than 5 μm the sample is magnetically 'conditioned' by rotational processes, whereas, over 10 μm, wall-shift dominates. As the critical grain size falls at lower temperatures, the size and shape of the particles determine the temperature coefficient[119]. A consideration of all conditions leading to an increase in remanence and coercivity suggests that a $(BH)_{max}$ double the figure obtained so far should be theoretically possible[90, 132]. Table 9.16 compares the theoretical values with those obtained in practice.

Improvements in the values can be brought about by (among other ways) 'doping' the normal mixtures, for example by an admixture of silicon dioxide[20], bismuth oxide ($Bi_2O_3$), or sodium bismuthide ($NaBiO_3$)[88]. The addition of 2% barium phosphate can raise the $(BH)_{max}$ of cobalt ferrite to 14·4 mW s/cm³. According to Nakamura, Kawai, and Yoshida[95], a $(BH)_{max}$ of 15·6 mW s/cm³ can be reached, under improved conditions, by a cobalt ferrite.

Dust magnets of barium ferrite using elastic or plastic binders are of great practical interest. Such flexible magnets—sometimes called rubber magnets—are easily workable and can be cut into any desired shape. They are used as, for example, sealing strips on refrigerator doors. The sealing force

depends on the concentration of the dust particles in the plastic matrix as well as on the arrangement and mutual reactions with other substances[117].

Lead ferrite ($PbO \cdot 6Fe_2O$) is crystallographically related to barium ferrite ($BaO \cdot 6Fe_2O_3$). Combinations of PbO and $Fe_2O_3$ were thoroughly investigated, in particular by Pawlek and his co-workers[14, 108]. They found that additions of $SiO_2$ had a favourable effect and demonstrated the superiority of the constitution $PbO \cdot 4Fe_2O_3$ over the 'normal' composition $PbO \cdot 6Fe_2O_3$. The best values achieved for anisotropic material were: $B_r = 0{\cdot}3$ V s/m$^2$, ${}_BH_c = 150$ kA/m, and $(BH)_{max} = 15$ mW s/cm$^3$.

Cochardt[24] gives the following values for hexagonal strontium ferrite: $B_r = 0{\cdot}41$ V s/m$^2$, ${}_JH_c = 240$ kA/m, and $(BH)_{max} = 32$ mW s/cm$^3$. He considered that values up to 40 mW s/m$^2$ for $(BH)_{max}$ should be attainable.

A good deal of recent development effort has been devoted to raising the anisotropic performance. This has been made possible, in part, by improved technical processing and also by the use of mixtures such as barium, lead, and strontium ferrite so that, nowadays, $(BH)_{max}$ values up to 30 mW s/cm$^3$ and more, with ${}_BH_c$ values over 200 kA/m can be achieved in the preferred direction.

Ferrite magnets having a preferred direction can be made from powders susceptible of orientation in a magnetic field. Two such processes have undergone parallel development and are in current use, namely dry pressing and wet pressing[113b]. By means of extrusion forming and the action of certain antifriction substances, a partial orientation of the particles can be achieved. This is the so-called anisotropic pressure effect. The preferred direction of the pressings is normal to the surface and also perpendicular to the direction of extrusion. The process is not, of course, as widely applicable as moulding in a magnetic field but has proved acceptable for flat bars or pot-type magnets[113b].

To obtain these easily oriented powders, dense pre-sintered stock should be used, yielding particle sizes between 0·5 μm and 1·3 μm by either wet or dry grinding. The dust particles should be, as far as possible, fault-free single crystals which can be made to follow the directing magnetic forces—aided by tapping and by the addition of fluxing materials to promote easy flow.

### 9.10.7 Materials having exchange anisotropy

Exchange anisotropy and its effect on coercivity have been known since 1956[82]. Exchange anisotropy is a mutual reaction between a basic ferromagnetic substance, for example iron or cobalt, and a ferrimagnetic or antiferromagnetic layer induced on its surface. Meiklejohn had found an asymmetrical hysteresis loop, having a coercivity of 300 kA/m (see Figure 3.65), in a cobalt dust whose particles were covered with a coating of cobalt oxide. The asymmetry of the hysteresis loop is brought out if the material is cooled in a strong magnetic field to the temperature of liquid air.

Such shifts were also established for oxidised cobalt iron particles and certain other compositions[26]. An exchange anisotropy was also noted in

superstructured Pt–Fe alloys[8] and in Pd–Cr alloys[113a]. It is unfortunate, from an engineering standpoint, that the anisotropic action brings about its effect on magnetic values at a relatively low temperature. Meiklejohn[81] measured $(BH)_{max}$ values of 32 mW s/cm$^3$ at the temperature of liquid nitrogen. It seems profitable to look for a marked exchange-anisotropic effect at higher temperatures also.

Falk and Hooper[36] produced single-domain particles of Fe–Co by electrolytic deposition and added a surface coating of ferrite, of determinate thickness, by a controlled oxidation process. The elongated (ESD) particles were aligned by moulding in a magnetic field and anisotropic magnets thus constructed. An asymmetrical shift in the hysteresis loop was not observed in this case but certainly a high coercivity was achieved.

The most favourable composition was found to be 57% Fe, 31% Co, and 12% O. Values of ${}_BH_c$ up to 560 kA/m were measured for particles at −196°C. The following values hold for moulded magnets of the given composition at 25°C: $B_r = 0{\cdot}62$ V s/m$^2$, ${}_BH_c = 124$ kA/m, and $(BH)_{max} = 32$ mW s/cm$^3$.

The density of these magnets came to 3·7 g/cm$^3$, and their stability was maintained up to 100°C. Between −196°C and +50°C the remanence fell (reversibly) by less than 1%. Luborsky and Roth[74a], using a mixture of barium, lead, or strontium ferrite with potassium ferrite ($KFe_{11}O_{17}$) that had been heated to between 900°C and 1400°C and cooled in a magnetic field of 800 kA/m, observed an exchange anisotropy which held at room temperature.

## 9.11 VARIETIES OF PERMANENT-MAGNET MATERIALS AVAILABLE FROM INDUSTRY

It is not possible to introduce into industry all the permanent-magnet materials developed in the laboratory. The types most commonly met with in practice are listed in Tables 19.1–19.11. In Germany, DIN 17 410[29] recommends an Fe–Al–Ni alloy together with six different Fe–Al–Ni–Co combinations and two types of barium ferrite (see Tables 9.7 and 19.1). It is possible to meet most engineering and technical requirements with these materials. Actually 70–80% of all magnet problems involving alloys are solved by the use of AlNiCo 400 or AlNiCo 500. Something like half the magnets manufactured in Germany are made of barium ferrite (Table 9.15)[89]. In England, on the other hand, cast magnets, and to a certain extent even steel magnets, predominate—or did until recently.

Many manufacturers are ready to produce special materials to meet special requirements (see Tables 19.1 and 19.2). A collection of the trade names given in the tables will be found on pages 733–741.

## 9.12 APPLICATIONS OF PERMANENT MAGNETS

According to a recently published study by Brinkmann[19], the greater part of all permanent magnets made are used in measuring technology and in the communication industry (altogether about 65%). Heavy machine in-

dustry accounts for about 20%, which are used for brake, coupling, or sealing devices, while some 15% are used for dynamos and motors.

It is of interest to note the parallel and reciprocal influence in the communications industry of apparatus and magnetic material development. It is seldom clearly pointed out how even the external shape of, say, a desk telephone reflects the current state of magnet development. An old tungsten-steel magnet is shown in the foreground of Figure 9.43 (see plate section) and behind it the telephone instrument in which it was used. Alongside the steel magnet, the tiny modern Alnico magnet which replaces it in a modern

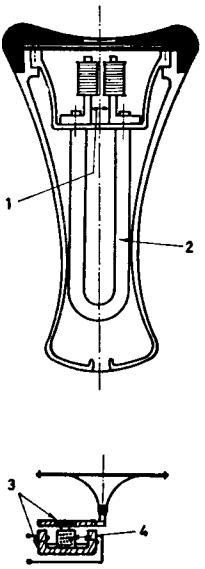



*Figure 9.44. Sectional drawing of the receiver capsules of Figure 9.43: 1, iron pole-piece; 2, tungsten-steel magnet, 3,* Ni–Fe; *4, Alnico*[42]

receiver capsule may be seen. The different constructions of the two earpieces is clearly shown in the line-diagrams of Figure 9.44[42]. In telephone installations permanent magnets are found not only in the earpiece (receiver) but also in the ringer, in many microphones and in polarised relays.

The telephone industry, however, employs only a small part of the permanent magnets of the total communication complex. The greater part find their way into the factories of the radio and television industry. In the communications industry 70% of all permanent magnets are loudspeaker magnets. It is mostly a question of 'dynamic' loudspeakers with moving coils vibrating in an annular air-gap. The most-used magnet material is barium ferrite or, if the speaker must be small, Alnico alloys. The efficiency of loudspeaker magnets depends not only on the material employed but, to a high degree, on correct dimensioning[122].

Besides loudspeakers, a host of smaller magnets are used in television devices: the cathode beam can be brought to the middle of the screen by radially magnetised ring magnets—the so-called centring magnets. To avoid 'cushion distortion' small rod-magnets or little plastic magnets are used.

The corner distortion still present can be eliminated by using 'correction magnets'.

Permanent magnets are used extensively in microwave techniques: one example is the magnetron, where magnets are used to direct the electrons into their spiral path, and another is the focusing of the electron beam in travelling-wave tubes or in isolators, phase-shifters, and circulators for the pre-magnetisation of the ferrites. In travelling-wave tubes with periodic focusing a low $l/d$ ratio is advantageous.

What is chiefly required in a measuring device is high stability and insensitivity to vibration, temperature changes, and external fields. The old horseshoe magnets did not meet these requirements to the same extent as do high-grade Fe–Al–Ni–Co alloys. The newer materials allow a more compact construction and lead to a simplification in the manufacturing process in so far as magnet and pole-piece can be sintered together or joined by inductive soldering[122]. One may include among the measuring devices petrol-pump meters and speedometers in motor cars, where rotating magnets and multipole ring magnets in Vicalloy find useful application. Again, brake-magnets in a.c. electricity meters play an important part[123].

For magnetic gramophone pick-ups, magnets are manufactured from AlNiCo 400 or from Pt–Co or barium ferrite, for example. Price of material plays a quite secondary role in these often very tiny magnets (for example, 1 mm×1 mm×3 mm). D.C. generators (dynamos) use magnets to create the excitation field[85]. Also, various types of a.c. generators such as lighting sets, ignition generators, telephone ringers, and hysteresis motors[40] contain permanent magnets. A relatively new range of application for permanent magnets is represented by small synchronous or d.c. motors for watches[86, 128b] and by frictionless bearings[7, 128b].

The holding force of permanent magnets acting on magnetisable material is often utilised in various sorts of holding magnets[7, 10, 33, 34, 117], whether to seal cabinet doors, to hold work-pieces on a bed-plate, or to cause items to adhere to a surface while being, at the same time, easily removable. In this group may be included the iron catchers and scrap sorters used in various manufacturing processes as well as the grips, grabs, and lifters used in handling sheet-iron.

For magnetic drive couplers, barium ferrite magnets, especially, find multiple applications. According to the principles employed they may be classified as synchronous couplers, hysteresis couplers, or eddy-current couplers[12, 39, 139].

## REFERENCES

1. ADAMS, E.: A new permanent magnet from powdered manganese bismuthide (Rev. Mod. Phys. **25** (Jan. 1953) 306–309).
2. ADAMS, E., HUBBARD, W. M. and SYELES, A. M.: A new permanent magnet from powdered manganese bismuthide (J. A. P. **23** (11) (Nov. 1952) 1207–1211).
3. ANSELIN, F.: Permanent magnet materials (Cobalt (June/Sept. 1959) 3–24).
4. ARNOLD ENGNG. CO., MARENGO: Magnetic Materials, Bulletin GC 106 C (Oct. 1961).

5. V. AUWERS, O.: Über den Einfluss der Korngrösse auf die magnetischen Eigenschaften (Z. techn. Phys. **9** (1928) 475–478).
6. V. AUWERS, O.: Über den Einfluss der Korngrösse auf die magnetischen Eigenschaften des Eisens (Wiss. Ver. Siemens-Konz. **7** (II) (1929) 197).
7. BACKERS, F. TH.: Ein magnetisches Lager (Phil. T. Rdsch. **22** (7) (1960/61) 252–259).
8. BACON, G. E. and CRANGLE, I.: Chemical and magnetic order in platinum-rich Pt–Fe alloys (Proc. Roy. Soc. (A) **272** (Mar. 1963) 387–405).
9. BAERMANN, M.: Permanenter Magnet und Verfahren zu seiner Herstellung. DRP 656 966 (12. 7. 34).
10. BARAN, W.: Berechnung von Anziehungs- und Haftkräften für magnetisierte Körper mit quaderförmiger Gestalt (T. Mitt. Krupp **19** (1961) 223–228; **20** (1962) 50–55).
11. BARAN, W., BREUER, W., FAHLENBRACH, H. and JANSSEN, K.: Über Eisen-Kobalt-Dauermagnetlegierungen mit Zusätzen von Vanadium und Chrom. A. Grundlagen-Untersuchungen (T. Mitt. Krupp **18** (1960) 81–90).
12. BARAN, W. and HELLBARDT, G.: Zur Berechnung von Dauermagnetkupplungen (T. Mitt. Krupp **20** (1962) 18–28).
13. BARTELS, H. J.: Wirtschaftliche Gesichtspunkte bei der Herstellung von Dauermagneten und Dauermagnetsystemen (DEW-T. Ber. **3** (1963) 19–22).
14. BERGER, W. and PAWLEK, F.: Kristallographische und magnetische Untersuchungen im System Bleioxyd (PbO)-Eisenoxyd ($Fe_2O_3$) (Arch. Eisenhüttenw. **28** (1957) 101–108).
15. BETTERIDGE, W.: Nickel–iron–aluminium permanent magnet alloys (J. Iron Steel Inst. **139,** 187p–208p).
16. DE BIE, E. and DOYEN, P.: Production and utilization of cobalt powders (Cobalt **10** (Mar. 1961) 22–32).
17. BIEDERMANN, E. and KNELLER, E.: Gefüge und magnetische Eigenschaften von Dauermagnetlegierungen während der isothermen Ausscheidungshärtung (Z. Metallkde. **47** (1956) 760–774).
18. BOZORTH, R. M.: Ferromagnetism. Van Nostrand Co. Inc., Toronto/New York/London (1951).
19. BRINKMANN, K.: Allgemeiner Bericht über die Anwendung von Dauermagneten (DEW-T. Ber **3** (1) (1963) 23–32).
20. LIGNES TÉLÉGRAPHIQUES ET TÉLÉPHONIQUES, PARIS: A Process for the manufacture of non-metallic or ceramic permanent magnets. Brit. Pat. 879 794 (10. 12. 57) and 883 047 (27. 1. 59).
20a BRONNER, C., HABERER, J.-P., PLANCHARD, E. and SAUZE, J.: Über den Einfluss von Niob auf die magnetischen Eigenschaften von Alnico-Legierungen mit 4.5 bis 6.5% Titan (Kobalt (46) (Mar. 1970) 13–19).
21. BUFFET, P.: Verfahren zur Herstellung eines Dauermagneten (DBP 1 029 950; applic. 6. 7. 54).
21a BUSCHOW, K. H. J., NAASTEPAD, P. A. and WESTENDORP, F. F.: Preparation of $SmCo_5$ permanent magnets (J. A. P. **40** (1969) 4029–4032).
21b BUSCHOW, K. H. J. and VELGE, W. A. J. J.: Permanent magnet materials of rare earth cobalt compounds (Z. ang. Phys. **26** (1969) 157–160).
22. CARMAN, E. H.: The coercive force of fine iron powders (Powder Met. (4) (1959) 1–14).
23. CLEGG, A. G. and MCCAIG, M.: The high temperature stability of permanent magnets of the iron–nickel–aluminium system (Brit. J. A. P. **9** (May 1958) 194–199; Nickelber. **16** (1958) 245).
24. COCHARDT, A.: Modified strontium ferrite, a new permanent magnet material (J. A. P. **34** (4) (Apr. 1963) 1273–1274).
25. DANNÖHL, W. and NEUMANN, H.: Über Dauermagnetlegierungen aus Kobalt, Kupfer und Nickel (Z. Metallkde. **30** (7) (July 1938) 217–231).

26. DARNELL, F. J.: Exchange anisotropy in oxidized iron–cobalt particles (J. A. P. **32** (3) (Mar. 1961) 186S–187S).
26a DAS, D. K.: Twenty million energy product samarium-cobalt magnet (IEEE Trans. **Mag-5** (1969) 214–216).
27. DEHLER, H.: Pressmagnete mit Kunststoffbindemittel (Stahl u. Eisen **47** (1942) 983–986).
28. DEUTSCHE EDELSTAHLWERKE AG, MAGNETFABRIK, DORTMUND: Druckschrift Dauer magnetwerkstoffe Oerstit 900.
28a DIETRICH, H.: Verfahren zur Bestimmung der Temperaturabhängigkeit der Entmagnetisierungskurve von Dauermagnetwerkstoffen (DEW-T. Ber. **7** (1) (1967) 29–38).
28b DIETRICH, H.: Die inneren Magnetisierungsschleifen von Dauermagnetwerkstoffen (Feinwerkstechnik **73** (4) (1969) 171–180; (5) (1969) 199–208).
28c DIETRICH, H.: Alterungsverhalten von kunststoffgebundenen AlNiCo-Dauermagneten, (ETZ-A **90** (22) (1969) 569–572).
28d DIETRICH, H.: Einfluss verschiedener Stabilisierungsbehandlungen auf die natürliche Alterung von Dauermagnetsystemen (Feinwerkstechnik **72** (1968) 313–322, 425–433).
29. DIN 17 410: Permanent magnet materials. Technical conditions of delivery.
30. FAHLENBRACH, H.: Beitrag zu den magnetischen Eigenschaften und der Verwendbarkeit pulvermetallurgisch hergestellter Dauermagnete (Arch. Eisenhüttenw. **20** (1949) 301–304).
31. FAHLENBRACH, H.: Fortschritte auf dem Gebiet der Dauermagnetwerkstoffe (T. Mitt. Krupp **14** (1) (1956) 2–11).
32. FAHLENBRACH, H.: Grundlagenuntersuchung an Vicalloy-Legierungen (Kobalt (49) (Dec. 1970) 174–182).
33. FAHLENBRACH, H.: Haftmagnetsysteme unter Verwendung von Oxydmagneten (Werkst. u. Betr. **90** (1957) 735–743).
34. FAHLENBRACH, H.: Haftdauermagnete ohne Eisenleitstücke und ihre Anwendung in der Praxis (Werkst. u. Betr. **51** (1961) 29–33).
35. FAHLENBRACH, H. and HEISTER, W.: Oxydische Dauermagnete aus Bariumoxyd und Eisen-III-Oxyd (Arch. Eisenhüttenw. **24** (1953) 523–528).
36. FALK, R. B. and HOOPER, G. D.: Elongated iron–cobalt–ferrite, a new lightweight, permanent magnet material (J. A. P. **32** (3) (1961) 190S–191S).
37. FALK, R. B. and HOOPER, G. D.: Properties of single-domain particles of cobalt nickel (J. A. P. **32** (Dec. 1961) 2536–2538).
38. FISCHER, J.: Abriss der Dauermagnetkunde. Springer, Berlin/Göttingen/Heidelberg (1951).
39. GERNHARDT, P.: Dauermagnetische Kupplungen (DEW-T. Ber. **2** (1962) 153–159).
40. GÖDDECKE, H.: Der Hysteresemotor (T. Mitt. Krupp **20** (1962) 83–87).
41. GORDON, I.: Preparation and properties of a ceramic permanent magnet (Am. Cer. Soc. Bull. **35** (5) (1956) 173–175).
42. GORDON SMITH, C.: Magnetic materials (Electr. Rev. **167** (1960) 253–259).
43. GOTTSCHALK, V. H.: The coercive force of magnetite powders (Phys. **6** (Apr. 1935) 127–132).
44. GOULD, J. E.: The reversible temperature coefficient of anisotropic Al–Ni–Co–Fe permanent magnets (Vortrag auf d. Tagg. d. Arbeitsgemeinsch. Ferromagnet., Karlsruhe 1962).
45. GOULD, J. E.: Permanent magnet stability (Instr. Practice **12** (Oct. 1958) 1083–1091).
45a GOULD, J. E.: Magnete mit säulenförmiger Kristallisation (Kobalt (23) (June 1964) 69–73).
46. GUILLAUD, C.: Ferromagnétisme des alliages binaires de manganèse. Thesis, Strassburg (1943).
47. GUILLAUD, C.: Les nouveaux matériaux ferromagnétiques à haute coercivité, à haute perméabilité, à faibles pertes (Mem. Soc. Ing. Civ., France **104** (1951) 538–576).

48. HEIDENREICH, R. D. and NESBITT, E. A.: Physical structure and magnetic anisotropy of Alnico 5 (J. A. P. **23** (Mar. 1952) 352–365).
49. HENNIG, G.: Dauermagnet-Technik. Francis-Verlag, München (1952).
50. HEUSLER, F.: Über magnetische Manganlegierungen (Verh. D. Phys. Ges. **5** (1903) 219).
50a HOFER, F.: Physical metallurgy and magnetic measurements of $SmCo_5$–$SmCu_5$ alloys (IEEE Trans. **Mag-6** (1970) 221–224).
50b HOFFMAN, A. and STÄBLEIN, H.: Investigation of high-coercivity Alnico alloys. (IEEE Trans. **Mag-6** (1970) 225–230).
51. HONDA, K., MASUMUTO, H. and SHIRAKAWA, Y.: New K. S. magnet steel (Sci. Rep. Tohoku Imp. Univ. **23** (Aug. 1934) 365–373).
52. HONDA, K. and SAITO, S.: On KS magnet steel (Sci. Rep. Tohoku Imp. Univ. **9** (1920) 417–422).
52a HUBBARD, W. M., ADAMS, E. and GILFRICH, J. V.: Magnetic moments of alloys of gadolinium with some of the transition elements (J. A. P. **31** (1960) 368S–369S).
53. JELLINGHAUS, W.: Anlassvorgänge in Martensit (Arch. Eisenhüttenw. **27** (July 1956) 433–438).
54. JELLINGHAUS, W.: Neue Legierungen mit hoher Koerzitivkraft (Z. techn. Phys. **17** (1936) 33–36).
55. JELLINGHAUS, W.: Eisen-Nickel-Aluminium-Kobalt-Kupfer-Legierungen mit magnetischer Vorzugsrichtung (Arch. Eisenhüttenw. **16** (June 1943) 247–252).
56. DE JONG, J. J., SMEETS, J. M. G. and HAANSTRA, H. B.: Some results of an electron microscopical study of the metallographic structure of two alloys for permanent magnets (Ticonal G and Ticonal X) (J. A. P. **29** (1958) 297–298).
57. KATO, Y. and TAKEI, T.: Permanent oxide magnet and its characteristics (J. Inst. El. Engrs., Japan **53** (1933) 408–412; Jap. Pat. 98 844).
58. KITTEL, C.: Theory of the structure of ferromagnetic domains in films and small particles (Phys. Rev. **70** (1946) 965–971).
59. KOPF, J.: Berechnung von Dauermagneten unter besonderer Berücksichtigung des Streufaktors (VALVO-Ber. **7** (1961) 131–158).
60. KOCH, A. J., J., HOKKELING, P., VAN D. STEEG, M. G. and DE VOS, K. J.: New material for permanent magnets on base of Mn and Al (J. A. P. **31** (1960) 75S–77S).
61. KOCH, A. J. J., VAN D. STEEG, M. G. and DE VOS, K. J.: Dauermagnete mit hoher Koerzitivkraft auf der Basis von Fe–Co–Ni–Al-Legierungen (Ber. Arb. Ferrom. (1959) 130–139). A contribution to the study of permanent magnet alloys of the Fe–Co–Ni–Al type (Conf. Magnetism Magnet. Mat., Boston (1956) 173–183).
62. KONO, H.: On the ferromagnetic phase in manganese–aluminium system (J. Phys. Soc. Japan **13** (Dec. 1958) 1444–1451).
63. KÖSTER, W.: Mechanische und magnetische Ausscheidungshärtung der Eisen-Kobalt-Wolfram- und Eisen-Kobalt-Molybdän-Legierungen (Arch. Eisenhüttenw. **6** (1) (1932) 17–23).
64. KRAINER, H. and RAIDL, F.: Einfluss verschiedener Legierungszusätze auf die Eigenschaften chromhaltiger Dauermagnetstähle (Arch. Eisenhüttenw. **16** (Jan. 1943) 253–260).
65. KRONENBERG, K. J. and BOHLMANN, M. A.: Long term magnetic stability of Alnico V and other permanent magnet materials (Wright Air Devel. Center Techn. Rep. 58–535 (Dec. 1958); Nickelber. **18** (1960) 57).
66. KRONENBERG, K. J.: Crystal lattice investigation of the permanent magnet precipitate in various Alnico materials (J. A. P. **32** (1961) 196S–198S).
67. KRONENBERG, K. J. and BOHLMANN, M. A.: Long term magnetic stability of Alnico and barium ferrite magnets (J. A. P. **31** (May 1960) 82S–84S).
68. KUSSMANN, A. and V. RITTBERG, G.: Über magnetische Eigenschaften von Platin-Eisen-Legierungen (Ann. Phys. (6) **7** (1950) 173–181).
68a KUSSMANN, A. and MÜLLER, K.: Magnetische Eigenschaften der geordneten Phase FePd im homogenen und heterogenen Bereich (Z. ang. Phys. **17** (7) (1964) 509–511).

69. LEVER, R. C., YAMARTINO, E. J. and FALK, R. B.: Physical and magnetic properties of elongated single domain iron and iron–cobalt permanent magnets (J. A. P. **29** (3) (1958) 304–305).
70. LUBORSKY, F. E.: Development of elongated particle magnets (J. A. P. **32** (3) (Mar. 1961) 171S–183S).
71. LUBORSKY, F. E.: The formation of elongated iron and iron-cobalt particles by electrodeposition into mercury (J. Electrochem. Soc. **108** (12) (Dec. 1961) 1138–1146).
72. LUBORSKY, F. E., MENDELSOHN, L. I. and PAINE, T. O.: Reproducing the properties of Alnico permanent magnet alloys with elongated single-domain cobalt–iron particles (J. A. P. **28** (11) (Mar. 1957) 344–351).
73. LUBORSKY, F. E. and PAINE, T. O.: Coercive force and remanence of 25 Å to 2000 Å diameter cobalt, iron and iron–cobalt alloy (J. A. P. **31** (5) (May 1960) 68S–70S).
74. LUBORSKY, F. E., PAINE, T. O. and MENDELSOHN, L. I.: Permanent magnets from elongated single domain particles (Powder Met. (4) (1959) 57–78).
74a LUBORSKY, F. E. and ROTH, W. L.: Magnetic exchange anisotropy in mixtures of barium, strontium or lead ferrite with potassium ferrite (J. A. P. **35** (Mar. 1964) 966–967).
75. MAGNETFABRIK, BONN: Dauermagnete (Apr. 1970).
76. MAHNER, H.: Berechnung von Magnetsystemen mit starren Magneten (ETZ-A **83** (1962) 780–786).
77. MAKINO, N.: Die Entwicklung von Dauermagneten in Japan (Kobalt (17) (Dec. 1962) 3–9).
77a MAKNO, N. and SUZUKI, M.: A study of Mn–Bi and Mn–Al alloys as permanent magnet materials (Trans. Jap. Inst. Met. **2** (4) (Oct. 1961) 228–233).
77b MAKINO, N., KIMURA, Y. and SUZUKI, M.: On heat treatment and magnetic properties of MnAl alloy (J. Jap. Inst. Met. **27** (1963) 216–221).
78. MATHIEU, K.: Einfluss von Legierungsgehalt und Versuchsbedingungen auf die $\gamma$-$\alpha$-Umwandlung bei der Kaltverformung austenitischer Stähle (Arch. Eisenhüttenw. **6** (1942) 215–218).
79. MCCAIG, M.: Permanent magnets at high temperatures (Kobalt (5) (Dec. 1959) 3–5).
79a MCCAIG, M.: Experiments on $RCo_5$ and related compounds with permanent magnet properties (IEEE Trans. **Mag-6** (1970) 198–201).
79b MCCAIG, M.: Leistungsfähigkeit von Dauermagneten bei Temperaturen oberhalb 550°C (Kobalt (41) (Dec. 1968) 174–176).
79c MARTIN, D. L. and BENZ, M. G.: Dauermagnetlegierungen des Kobalts mit Seltenen Erdmetallen (Kobalt (50) (Mar. 1971) 10–14).
80. MEE, C. D. and JESCHKE, J. C.: Single domain properties in hexagonal ferrites (J. A. P. **34** (4) (Apr. 1963) 1271–1272).
81. MEIKLEJOHN, W. H.: Eine neue Art von magnetischen Werkstoffen (Phys. Bl. **14** (1958) 311–313).
82. MEIKLEJOHN, W. H. and BEAN, C. P.: New magnetic anisotropy (Phys. Rev. **102** (1956) 1413–1414; **105** (1957) 904–913).
83. MENDELSOHN, L. I., LUBORSKY, F. E. and PAINE, T. O.: Permanent magnet properties of elongated single-domain iron particles (J. A. P. **26** (10) (Oct. 1955) 1274–1280).
84. MEYER, E.: Zur Auswertung der Kennlinien von Dauermagnetwerkstoffen (Arch. Elektrot. **40** (1952) 363–366).
85. MIMMEL, H. and TENDELOO, K.: Eigenschaftsuntersuchungen von Dauermagneten für kleine Gleichstrommaschinen (ETZ-A **83** (1962) 776–780).
86. MINTERN, R. A.: Platinum alloy permanent magnets (Plat. Met. Rev. **5** (3) (July 1961) 82–88).
87. MISHIMA, T.: New high magnetic M. K. Steel (Ohm **19** (July 1932) 353; Jap. Pat. 96 371.
88. MISHIMA, T.: Recenti sviluppi nella fabbricazzione dei magneti permanenti in Giappone (Metallurg. Ital. **54** (Oct. 1962) 447–456).

88a MISHIMA, T. and MAKINO, N.: Studies of industrialization of MT permanent magnet (J. Iron Steel Inst. Jap. **43** (1957) 556–560, 647–652, 726–732).
89. MOREAU, L.: L'industrie des aimants permanents (L'usine Nouvelle (Spring 1963) 1–26).
90. MÜLLER, H. G.: Zur Theorie der Koerzitivkraft des Bariumferritdauermagneten Maniperm (Wiss. Z. Hochsch. Verkehrsw. Dresden **3** (1) (1955) 7–12).
91. MÜLLER, M.: Die Randstreuung des Kondensators aus endlich dicken Platten mit Anwendung auf Magnetberechnungen (Frequenz **15** (9) (1961) 286–293).
92. MÜLLER, M.: Dimensionierung und Ausführung eines unsymmetrisch geschirmten Permanentmagneten für Wanderfeldröhren (Ber. Arb. Ferrom. (1959); Stahleisen (1960) 247–255).
93. MUREX LTD, RAINHAIM: Sintered permanent magnets P. U. 52.
94. MUREX LTD, RAINHAIM: Sintered Comalloy magnets.
95. NAKAMURA, H., KAWAI, N. and YOSHIDA, H.: (Powder Met. **6** (1959) 155).
96. NÉEL, L.: Propriétés d'un ferromagnétique cubique en grains fins (C. R. **225** (1947) 1488–1490).
97. NÉEL, L.: Le champ coercitif d'une poudre ferromagnétique cubique à grains anisotropes (C. R. **225** (1947) 1550–1551).
98. NESBITT, E. A.: Vicalloy-A workable alloy for permanent magnets (Metals Techn. **13** (Feb. 1946) 1–11).
99. NESBITT, E. A.: The magnetostriction of permanent magnet alloys (J. A. P. **21** (Sept. 1950) 879–888).
100. NESBITT, E. A. and WILLIAMS, H. J.: Shape and crystal anisotropy of Alnico 5 (J. A. P. **26** (10) (Oct. 1955) 1217–1221).
100a NESBITT, E. A., WILLIAMS, H. J., WERNICK, J. H. and SHERWOOD, R. C.: Magnetic moments of compounds of cobalt with rare-earth elements having a $Cu_5Ca$ structure (J. A. P. **32** (1961) 342S–343S).
100b NESBITT, E. A., WILLENS, R. H., SHERWOOD, R. C., BUEHLER, E. and WERNICK, J. H.: New permanent magnet materials (Appl. Phys. Letters **12** (1968) 361–362).
101. NEUMANN, H.: Über magnetisch harte Eisen-Nickel-Kupfer-Legierungen (Metallwirtschaft **14** (1935) 778–779).
102. NEUMANN, H.: Der magnetische Arbeitspunkt von Dauermagneten als Werkstoffkennzeichen und Abnahmewert (Arch. Eisenhüttenw. **27** (8) (Aug. 1956) 539–546).
103. NEUMANN, H., BÜCHNER, H. and REINBOTH, H.: Mechanisch weiche Eisen-Nickel-Kupfer-Dauermagnetlegierungen (Z. Metallkde. **29** (1937) 163–185).
104. NOT KNOWN: Micropowder magnets (Met. Ind. **83** (1953) 27–29).
105. OLIVER, D. A. and HADFIELD, D.: Permanent magnet materials (J. I. E. E. **95** (I) (96) (Dec. 1948) 531–538).
106. OLIVER, D. A. and SHEDDEN, J. W.: Cooling of permanent magnet alloys in a constant magnetic field (Nature **142** (1938) 209).
107. PAINE, T. O., MENDELSOHN, L. I. and LUBORSKY, F. E.: Effect of shape anisotropy on the coercive force of elongated single magnetic domain iron particles (Proc. Conf. Magnetism Magnet. Mat. (1955) 158–164).
107a PARKER, R. J.: Fine-particle iron–cobalt magnet achievements in the permanent-magnet industry (IEEE Trans. **Mag-6** (June 1970) 249–251.
108. PAWLEK, F. and REICHEL, K.: Herstellung von anisotropen Bleiferrit-Dauermagneten ohne Anwendung eines Magnetfeldes beim Pressvorgang (Naturw. **44** (1957) 390–391).
109. PHILIPS N. V. GLOEILAMPENFABRIEKEN. Brit. Pat. 557 749 (1941).
109a PLANCHARD, E. and BRONNER, C.: Improvement to the preparation of sintered Al–Ni–Co alloys (IEEE Trans. **Mag-6** (1970) 304).
110. POTTER, H. H.: Some magnetic alloys and their properties (Phil. Mag. (7) **12** (1931) 255–264).
111. RASSMANN, G. and HENKEL, O.: Über die Ursache der magnetischen Härte von kaltverformten Fe-Ni-Cr-Legierungen (Phys. Stat. Sol. **1** (5) (1961) 517–522).

112. RASSMANN, G. and HENKEL, O.: Weiterentwicklung verformbarer Eisen-Nickel-Chrom-Dauermagnetlegierungen (Ber. Arb. Ferrom. (1958). Rieder (1959) 120–126).
113. RATHENAU, G. W.: Saturation and magnetization of hexagonal iron oxide compounds (Rev. Mod. Phys. **25** (Jan. 1953) 297–301).
113a RAULT, J. and BURGER, J. P.: Exchange anisotropy in Pd–Cr alloys (IEEE Trans. **Mag-5** (1969) 220–221).
113b RICHTER, H. G. and VÖLLER, H.: Über die Herstellung von hartferritischen Dauermagneten unter Berücksichtigung spezieller Formgebungsverfahren. (DEW-T. Ber. **8** (4) (1968) 214–221).
114. ROBERTS, W. H. and MITCHELL, D. L.: Effects of high temperature on performance of Alnico V and Alnico VI permanent magnets (US. At. Energy Comm. APEX. 384 (Feb. 1957); Nickelber. **17** (1959) 200–201).
115. RUDER, W. E.: Permanent magnet steels (Iron Age **157** (1946) 65–69).
116. SAPPA, O.: Proprietà di sostanze ferromagnetiche in polvere (Ric. Sci. Progr. Tecn. Econ. Naz. (II) **8** (1937) 413–421).
117. SCHÜLER, K.: Untersuchung der Haftkraft an kunststoffgebundenen oxydischen Dauermagneten (DEW-T. Ber. **2** (1962) 72–78).
118. SCHWABE, E.: Über die Temperaturabhängigkeit der magnetischen Eigenschaften von Bariumferrit (Z. ang. Phys. **9** (4) (1957) 183–187).
119. SIXTUS, K. J.: Recent advances in the field of permanent magnets (Conf. Magnetism Magnet Mat., AIEE (Oct. 1955) 142–149).
120. SIXTUS, K. J., KRONENBERG, K. J. and TENZER, R. K.: Investigations on barium ferrite magnets (J. A. P. **27** (1956) 1051–1057).
121. SIXTUS, K. J. and ZEHLER, V.: Die Streuung in Dauermagnetkreisen (AEG-Mitt. **52** (1962) 205–210).
122. STEINGROEVER, E.: Maximaler magnetischer Wirkungsgrad von Ringspalt-Dauermagneten (Arb. Ferrom. (1959). Düsseldorf (1960) 264–266).
123. STEINGROEVER, E.: Brems- und Dämpfungsmagnete in der Messtechnik (Vort. Arbgem. Ferrom. Karlsruhe (1962). D. Ges. Metallkde. (1962).
124. STEINITZ, R.: Permet, a nonferrous permanent magnet made from powders (Powder Met. Bull. **1** (1946) 45–47)
125. STONER, E. C. and WOHLFARTH, E. P.: A mechanism of magnetic hysteresis in heterogeneous alloys (Phil. Trans. Roy. Soc. **240** (1948) 599–642).
126. STREET, R. and WOOLLEY, J. C.: A note on magnetic viscosity (Proc. Phys. Soc. (B) **62** (1949) 141–142).
127. STREET, R. and WOOLLEY, J. C.: Time decrease of magnetic permeability in Alnico (Proc. Phys. Soc. (B) **63** (1950) 509–519).
128. STREET, R., WOOLLEY, J. C. and SMITH, P. B.: The influence of heat treatment on magnetic viscosity in permanent magnet alloys (Proc. Phys. Soc. (B) **65** (1952) 461–462).
128a STRNAT, K., HOFFER, G. and RAY, A. E.: Magnetic properties of rare earth–iron intermetallic compounds (IEEE Trans. **Mag-2** (1966) 489–493).
128b STRNAT, K. H.: The recent development of permanent magnet materials containing rare earth metals (IEEE Trans. **Mag-6** (1970) 182–190).
129. STUIJTS, A. L., RATHENAU, G. W. and WEBER, G. H.: Ferroxdure II und III, anisotrope dauermagnetische Werkstoffe (Phil. T. Rdsch. **16** (1955) 221–228).
130. SUGIYAMA, M. and SHIDA, K.: The effect of the addition of niobium on sintered Alnico magnet properties (Trans. Jap. Inst. Met. **3** (Apr. 1962) 76–78; Nickelber. **21** (7) (July 1963) 213).
131. TENZER, R. K.: Influence of particle size on the coercive force of barium ferrite powders (J. A. P. **34** (4) (Apr. 1963) 1267–1268).
132. TOMHOLT, F.: Technologie von Bariumferritmagneten (Vort. Arb. Ferrom. (1962).
133. UNDERHILL, E. M.: Permanent magnet design. Crucible Steel Co. of America.
134. VACUUMSCHMELZE GMBH: Magnetoflex, Data sheet M 016 (Apr. 1962).

134a VALLIER, G., BRONNER, C. and PFEFFER, R.: Über den Einfluss von Titan auf Al–Ni–Co-Legierungen mit 34% Kobalt (Kobalt (34) (1967) 9–15).
135. WEBB, C. E.: The stability of permanent magnets (Proc. IEE **108 C** (14) (1961) 317–324).
136. WENT, J. J., RATHENAU, G. W., GORTER, E. W. and VAN OOSTERHOUT, G. W.: Ferroxdure, eine Gruppe neuer Werkstoffe für Dauermagnete (Phil. T. Rdsch. **13** (1952) 361–376).
137. WHIFFIN, A. C.: The effect of change of temperature on the strength of permanent magnets, with special reference to modern magnet steels (J. IEE **81** (Dec. 1937) 727–740).
138. WOHLFARTH, E. P.: Hard magnetic materials (Adv. Phys. **8** (30) (Apr. 1959) 87–224).
139. WULLKOPF, H.: Berechnung und Anwendung magnetischer Synchronkupplungen (Vort. Arb. Ferrom. Karlsruhe (1962). D. Ges. Metallkde. (1962)).
140. ZINGERY, W. L., WENINGER, R. M. and ROMBERG, E. B.: Long-term magnetic stability (Proc. Intermag (1963) 1–5).
141. ZUMBUSCH, W.: Neuere Entwicklung der Dauermagnete aus Eisen-Nickel-Aluminium-Legierungen mit und ohne Zusatz von Kupfer, Kobalt und Titan, deren Formgebung und Anwendung (Elektrotechn. Maschinenbau **60** (51/52) (1942) 533–547).

# 10

# Magnetic materials in heavy-current engineering

## 10.1 REQUIREMENTS FOR LAMINATED MATERIALS

By heavy-current engineering is to be understood that field of technology involving relatively high currents at constant voltage in the frequency range 0–100 Hz [usually d.c. ($f = 0$) or a.c. at 50–60 Hz]. This field, broadly speaking, embraces electromagnets, motors, generators, power transformers, and level converters. Transductors, which belong to the same classification, will be handled separately in the next section. Material for lamination—electrosheet—is, in the main, used in that range of electrotechnology concerned with energy partition or energy conversion. On the other hand, it is the function of light-current engineering or information technology to transform, process, or store information.

In both fields, magnetic materials are used which are not fundamentally different but which have to satisfy different requirements. The magnetic problems of communication technology will therefore be separately treated.

Magnetic materials for electric-machine construction are of few kinds but used in massive quantities. The iron content of electrosheet is usually as much as 94% and over. In comparison, nickel and cobalt, setting aside certain special applications (see page 348), fade, with their alloys, into the background. The great commercial importance of electric-machine construction is evident from the fact that, for example, in 1960 electric motors, generators, and power transformers to the value of £250 million were manufactured by the West German republic. A large part of this value appeared as production of magnetic sheet material for use in these devices.

The aim and tasks of heavy-current engineering demand a magnetic material showing a high saturation density, available in large quantities, and relatively cheap. All these requirements are well met by iron: among the three ferromagnetic elements, iron, nickel, and cobalt, it has the highest saturation flux density (see Table 3.3); it is the most abundant in Nature; and, finally, it is not difficult to obtain or to work.

Iron is therefore by far the most used magnetic material in electrotechnology. Over a long period of development it was found possible to improve appreciably the iron alloys, to adapt their properties to current working conditions, and to manufacture them more and more economically.

### 10.1.1 Requirements for transformer sheet

In a transformer, that inductive action is used whereby electromagnetic energy is transferred from a primary to a secondary conductive circuit. In order to link tightly the two current-carrying circuits, both circuits comprise coils mounted on a common ferromagnetic core. This core should be closed on itself, as far as possible, since any air-gap normal to the flux direction will increase the loss of flux by strays. It is required of any transformer core material that flux density should rise steeply with the excitation field. The knee of the hysteresis loops should be reached at low field strengths; the coercivity should also be low. The area of the hysteresis loop, and hence the energy of cyclic magnetisation or 'lost' energy, should be as low as possible.

That part of the hysteresis loop lying above the knee is of little practical importance for transformer cores since, from this point up, any increase in flux density involves a disproportionate increase in magnetising current and this leads to greater expenditure on copper in the windings. It follows from this that the $W_{1.5}$ value is sometimes more useful than the $W_1$ value as a criterion for the type of transformer sheet to be used. Energy losses, however, occur not only in the core of the transformer but in its windings. The correct partitioning of these losses is an important aim of the designer[85].

### 10.1.2 Requirements for dynamo sheet and electrosheet

In dynamo sheet, that part of the hysteresis loop which lies above the knee is also of importance. Apart from the magnitude of the cyclic losses, the saturation density is a determining factor for assessing the usefulness of dynamo sheet. Since the saturation density in iron falls when alloyed with silicon, an Fe–Si alloy of low silicon content is chosen for the production of dynamo sheet. It is usually less than 3%.

Electrosheet is hot rolled as a rule, and sheets used for motors are mostly cold rolled but with no preferred direction. Sheet of 0·35 mm thickness is hot rolled, as is 0·5 mm sheet where the silicon content is rather high: some 0·5 mm sheet of low silicon content is cold rolled. In general, no advantage is to be gained by the use of anisotropic sheet material.

Higher flux densities than are obtainable in iron can be achieved by the use of alloys of the Fe–Co type. In cases where the high cost of cobalt is not a major consideration, the manufacturer may have recourse to such alloys.

### 10.1.3 Requirements for materials for level-convertor cores*

In order to facilitate the measurement of high currents, voltages, and powers, it is necessary to introduce measuring 'converters' to transform currents of

* Level converters are transformers whose main purpose is not the transfer of power but the production of stepped up or stepped down voltages and currents. Current transformers are a particular case.

high intensity and high tension into low-current low-voltage form. If there is no external load and no stray field, the ratio of the currents $I_1$ and $I_2$ after transformation is only inversely proportional to the turns ratio, i.e.

$$I_1 n_1 = I_2 n_2.$$

Stray fields can be largely avoided by using a toroidal core.

The condition for no external load may be expressed in the form

$$\omega L_i \gg \omega L_o + R_i + R_o$$

where $\omega = 2\pi f$ is the circular frequency, $L_i$ the internal inductance of the short-circuited device, $L_o$ the external inductance of the load, and $R_i$ and $R_o$ represent the corresponding resistances of the device and the load. The permeability of the core material must be high and its loss resistance low in order to give a high internal inductive reactance $\omega L_i$. The performance of a level converter is thus determined by the permeability and losses of the core material[66].

In order that converters should introduce no appreciable errors due to small changes in operating conditions, the permeability should rise uniformly up to the saturation knee of the hysteresis loop[56]. The constancy of the permeability can be improved by gapping the core or by impressing on it a d.c. premagnetisation. The effect of the air-gap and the direct field, however, are dependent on the amplitude of the alternating field. The condition can be eased by a suitable choice of material. The losses should be low in level transformers as well as in power transformers. However, in level transformers there is the added requirement of high permeability, so the same material is not necessarily suitable for both applications.

In level converters for light-current engineering, lower flux densities are usual than for those in heavy-current technology, so a different type of material must be used. Only core materials designed for high flux density will be considered in this section, but the light current equivalent will be dealt with in Chapter 13 together with voice-frequency transformers.

The following four groups of materials are relevant to heavy-current applications: unalloyed iron, Fe–Si alloys, Fe–Al alloys, and Fe–Co alloys; choice is determined not only by the magnetic properties but by considerations of cost and workability. Workability determines whether sheets can be rolled out very thin to minimise eddy-current loss or whether laminations or strips can be punched out from the sheet without excessive tool wear.

## 10.2 UNALLOYED IRON

Iron without the addition of alloying elements is only usable as magnetisable material for d.c. magnets, relays, or pole-shoes on account of its high specific electrical conductance. Iron, however, has been very thoroughly investigated and as a basic substance in the electrical industry it plays a major role, so as far as possible all its properties should be known. On the basis of knowledge of unalloyed material the effect of additives and procedures for improving workability have developed, and from the results of

these studies the possibilities and the limitations of new compositions and production routines have emerged.

Iron which is derived from the usual commercial processes always contains a series of other elements which are present either in solution or as finely divided compounds distributed throughout the mass. As long as metallurgy has been concerned with iron, there has been no lack of attempts to create 'pure iron' in order to study its physical properties. But really pure iron does not exist. It is not so long ago, in fact, that it was realised that even as little as 0·001% of carbon, oxygen, or hydrogen could radically affect the properties of the metal, so these slight impurities could by no means be left out of account. According to Yensen and Ziegler[105], the maximum permeability of a sample of iron having 0·001% C and 0·002% $O_2$ was $\mu_m = 220\,000\mu_0$. Without the presence of the oxygen it should have been $\mu_m = 500\,000\mu_0$. With 0·01% C a $\mu_m$ of $20\,000\mu_0$ only was measured.

With increasing refinements in production methods and techniques of analysis, iron of a high degree of purity has recently been produced. But one should not really speak of 'pure' iron unless one means the simple element, iron, with no additions whatsoever. Iron to which no other elements have been deliberately added will be referred to here as 'unalloyed iron'. If the carbon content of the iron exceeds 0·04% but is less than 1·7%, then one speaks of 'steel'[105].

There are various ways of producing iron with a high degree of purity. One of these was earlier discussed on page 163: the annealing of the material in hydrogen at a high temperature. Iron obtained by Cleaves and Hiegel[22], using chemical procedures, contains very few impurities, and its purity has not yet been improved on. In its production, iron nitrate was recrystallised, converted into iron oxide, reduced to spongy iron, and this smelted in hydrogen or in vacuo. The samples, for the most part, contained less than a total of 0·0083% foreign substance. A few physical values published as a result of many determinations are given in Table 10.1.

**Table 10.1** PHYSICAL PROPERTIES OF HIGH-PURITY UNALLOYED IRON

| *Property* | *Symbol* | *Value* |
|---|---|---|
| Density at 20°C (g/cm³) | $d$ | $7{\cdot}874 \pm 0{\cdot}001$ |
| Melting point (°C) | $T_M$ | $1539 \pm 1$ |
| $\alpha$–$\gamma$ transformation (°C) | $T_A$ | 910–910·5 |
| $\gamma$–$\alpha$ transformation (°C) | | Some 8°C lower than $T_A$ |
| Specific electrical resistance at 20°C ($\mu\Omega$ cm) | $\varrho$ | $9{\cdot}71 \pm 0{\cdot}01$ |
| Temperature coefficient of $\varrho$ | $\frac{R_{100}-R_0}{100R_0}$ | $0{\cdot}006\,51 \pm 0{\cdot}000\,01$ |
| Magnetic saturation (V s/m²) | $J_s$ | $2{\cdot}158 \pm 0{\cdot}001$ |
| Maximum permeability ($\mu_0$) | $\mu_m$ | 88 400 |
| Least coercivity at $B_m = 1{\cdot}508$ V s/m² (A/m) | $H_c$ | 3·24 |
| Linear thermal coefficient of expansion at 20°C (ppm/K) | $\alpha$ | $11{\cdot}7 \pm 0{\cdot}2$ |
| Elastic modulus (Young's modulus) (N/m²) | $E$ | $(2{\cdot}05 \pm 0{\cdot}03) \times 10^{11}$ |

The maximum permeability and coercivity achieved by Cleaves and Hiegel do not reach the excellent values which Yensen and Ziegler[105] obtained from vacuum-melted material or Cioffi[20] found by his famous vacuum-annealing procedure (see Table 10.2). Cioffi, Williams, and Bozorth[21], using unalloyed iron, obtained for a single crystal a $\mu_m$ value of $680\,000\mu_0$, a value which it was later found possible to increase to $1\,400\,000\mu_0$[12]. It is worth noting that Gumlich[49], using a method of extrapolation, succeeded in determining material constants which approximated to those given by Cleaves and Hiegel:

| | |
|---|---|
| Density | $d = 7{\cdot}876$ g/cm$^3$ |
| Specific electrical resistance | $\varrho = 9{\cdot}56$ μΩ cm |
| Saturation polarisation | $J_s = 2{\cdot}162$ V s/m$^2$ |

This procedure is not suitable for finding such structure-sensitive magnitudes as coercivity and permeability.

The practical value of unalloyed iron is limited to static applications: high permeability and high saturation are desired qualities in the cores of d.c. magnets or relays; the low electrical resistance does not matter. Apart

**Table 10.2** MAGNETIC PROPERTIES OF UNALLOYED IRON

| *Material* | $\mu_i$ ($\mu_0$) | $\mu_m$ ($\mu_0$) | $H_c$ (A/m) | $B_s$ (V s/m$^2$) | $W_h$ (erg/cm$^3$ c) | *Reference* |
|---|---|---|---|---|---|---|
| Laboratory results | | | | | | |
| Electrolytic iron | 1 000 | 26 000 | 7·2 | 2·15 | — | 76 |
| Carbonyl iron | 3 000 | 20 000 | 6·4 | 2·2 | — | 31a |
| Smelted in vacuo | — | 207 500 | 2·2 | — | 70 | 105 |
| Annealed in vacuo | 14 000 | 280 000 | — | — | 190 | 20 |
| Vacuum smelted and hydrogen annealed | — | 88 400 | 3·2 | 2·16 | — | 22 |
| Single crystal | — | 680 000 | — | — | — | 21 |
| Single crystal after magnetic treatment | — | 1 430 000 | 12 | — | — | 12 |
| Types of Commercial iron | | | | | | |
| AME | | 6 000 | <80 | 2·15 | — | 91a |
| Armco | 200–300 | 3 500–8 000 | 100–50 | — | — | 5 |
| CDW magnetic soft iron | — | 5 000–6 000 | <80 | — | — | 19a |
| Hyperm O | 300 | 8 000 | 40 | 2·15 | — | 38 |
| *Magnetreineisen S | 1 500† | 30 000 | 12 | 2·15 | — | 93a |
| *Magnetreineisen S2 | 1 500† | 30 000 | 12 | 2·15 | — | 93a |
| *Magnetreineisen S1 | 2 000† | 40 000 | 6 | 2·15 | — | 93a |

* Magnetreineisen is a registered trade name such as Armco or CDW.
† Measured at 4 mA/cm.

from switching on or off, eddy currents cannot arise. On the basis of laboratory experience, manufacturers can now produce commercial iron with a relatively high degree of purity. Such a commercial iron will normally contain 99·9% Fe. The principal impurities are approximately:

0·020% C
0·035% Mn
0·025% S
0·015% P
0·002% Si

This material has a specific electrical resistance of around 10·7 μΩ cm and a density of 7·86 g/cm³. The coercivity amounts to 80 A/m, the remanence to 1·0 V s/m². All these figures apply at room temperature. A few further physical data are collected together in Table 10.3[5]. The temperature dependence of the specific electrical resistance is given in Table 8.2.

**Table 10.3** PROPERTIES OF COMMERCIALLY PURE IRON AT 20°C[5]

| | |
|---|---|
| Specific heat (cal/g K) | 0·1075 |
| Thermal conductivity (cal/K cm s) | 0·175 |
| Linear coefficient of expansion (ppm/K) | 12 |
| Young's modulus (N/m²) | $2{\cdot}139\times10^{11}$ |
| Breaking point (N/mm²) | 294 |
| Elastic limit (N/mm²) | 190 |
| 'Rockwell' hardness | B 40–45 |
| Melting point (°C) | 1 532 |
| Specific electrical resistance (μΩ cm) | 10·7 |
| Saturation flux density (V s/m²) | 2·155 |
| Initial permeability ($\mu_0$) | 200–500 |
| Maximum permeability ($\mu_0$) | 3 500–20 000 |
| Coercivity at $B_m$ = 1 V s/m² (A/m) | 20–100 |
| Hysteresis loss at $B_m$ = 1 V s/m² (erg/cm³) | 700–4 000 |

The hysteresis loop of a commercial iron with an $H_c$ of 80 A/m is shown in Figure 10.1: at flux densities over 1 kA/m the flux density rises only slowly, and attains a value of 2 V s/m² only above 20 kA/m[38].

To reach saturation level in the iron, field intensities of more than 40 kA/m must be applied. In practical applications the question often arises: what field strength must be brought to bear to produce a flux density of 1·0 V s/m² or 1·5 V s/m², for example? Figure 10.2 gives the hysteresis loops of an annealed toroidal core for these two characteristic densities[5]; in Figure 13.10 the loops are shown for an amplitude excursion of 0·5 V s/m². It can be seen from the figures that a field strength of 65 A/m produces a flux density of 0·5 V s/m², and a field of 200 A/m a flux density of 1 V s/m², but that almost 700 A/m would be needed to reach a figure of 1·5 V s/m².

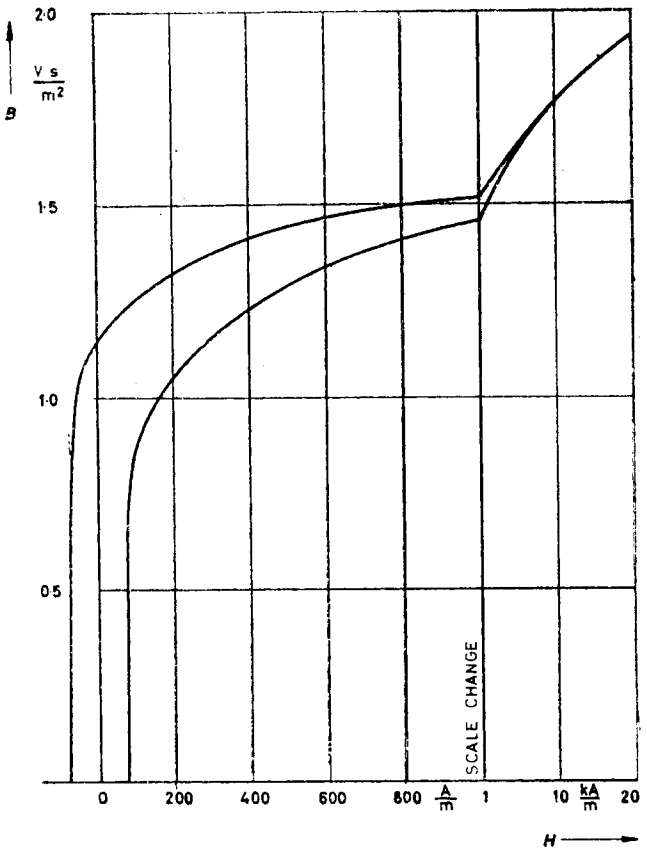



*Figure 10.1. Hysteresis loop of a commercially pure iron*

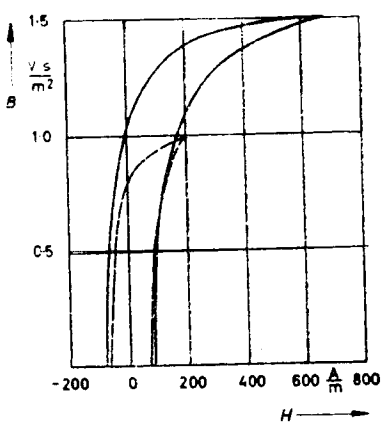



*Figure 10.2. Unalloyed iron taken up to 1·0* V s/m² *and 1·5* V s/m² [5]

Any type of mechanical working—cropping, stamping, respooling—must be followed as a rule by a 'softening' annealing operation in order to remove internal stresses. Normally this consists of packing the material to be treated in a pot and putting it in the annealing oven where it is subjected to a predetermined heat routine. The annealing pot must be well sealed to avoid oxidation of the sheet or strip and, for the same reason, should be filled as completely as possible by the material to be treated. Today, this pot annealing is mostly replaced by annealing in a standardised protective atmosphere of hydrogen.

The annealing temperature usually lies between 725°C and 1000°C and must be adapted to the sizes of the workpieces and to the flux density to be expected in use. The cooling should proceed slowly so that it does not introduce further stresses.

This simple annealing does not suffice for cases where a particularly high permeability is required or where it is desired to achieve high flux densities with the smallest possible field intensity. The heat treatment must then be so designed as not only to remove internal stress but to eliminate carbon and sulphur from the material. This necessitates a high-temperature vacuum annealing.

Figure 10.3 shows the result of such special annealing in comparison with the ordinary routine: by reduction of the coercivity and steepening of the hysteresis loop, the flux density peak value of 1 V s/m$^2$ is reached at 50 A/m instead of 200 A/m. In order to be able to use unalloyed iron in alternating fields of higher frequency, eddy currents must be kept low by a thorough breakdown of the solid material. An illustration of this is provided by 'flake' iron. Thin flakes of about 15–20 μm thickness are rolled-out from electrolytically deposited or sponge iron. This material was used in line-transformer cores for television sets[19, 79] but has now largely been replaced by ferrites. The maximum permeability attainable with flake iron is still significantly lower than that of sintered iron[27] since, in spite of the elongated shape of the particles, a considerable amount of gapping exists (Figure 10.4).

## 10.3 Fe-Si ALLOYS

In a.c. machines, in motors and generators as well as in power and level transformers, unalloyed iron can only conditionally be used because, on account of the low electrical resistance, large eddy currents flow. By rolling the sheet very thin, eddy currents can, in principle, be reduced as effectively as by increasing the resistance. According to equation 3.64, losses increase in proportion to the square of the thickness whereas the specific electrical conductance is directly proportional to only the thickness. In small asynchronic motors, therefore, it is possible to use sheet of unalloyed iron with advantage[78a].

Nevertheless, rolling operations are costly; besides, the use of thin laminae leads to a poor volume space-factor and, if the laminations are thinner than 0·1 mm, the magnetic properties suffer as well. Thus increasing the resistance of the sheet offers the more suitable solution. The possibility still remains, of course, of rolling down the alloy sheets as far as may prove commercially reasonable.

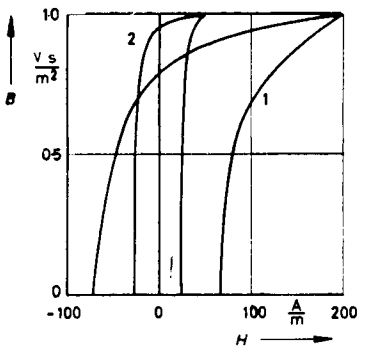



*Figure 10.3. Loops for unalloyed iron: 1, after an ordinary annealing; 2, after special vacuum annealing*[5]

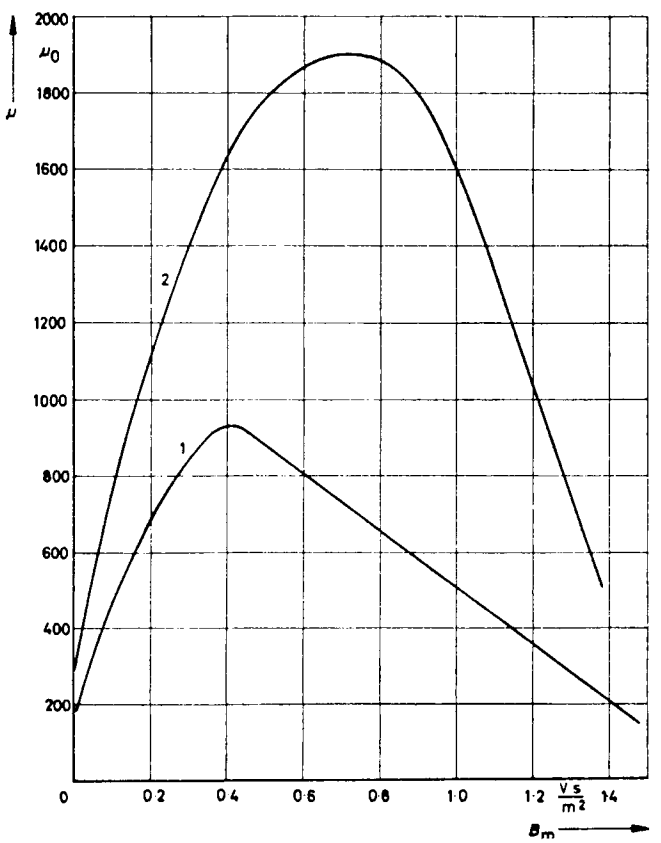



*Figure 10.4. Permeability as a function of flux density: 1, for flake iron; 2, for sintered iron*[27]

The fundamental investigation of Fe–Si alloys began before the turn of the century and is associated with the name of Hadfield. A detailed publication of the work by Barret, Brown, and Hadfield[11] appeared in 1902. The Fe–Si steels produced at that time, however, were not yet technically satisfactory[50]. At about the same time a vigorous programme of research was set up under Gumlich at the Physikalisch-Technische Reichanstalt in Germany. In co-operation with the steel industry, efforts were made to solve the technical problems associated with the manufacture of the largely unrollable Fe–Si alloys[47]. At the outset, the melting and casting of silicon steel presented no less difficulty than the rolling and flattening of this tough material[95]. Success crowned these efforts and in Germany it became commercially feasible to manufacture Fe–Si alloys in 1903[16].

In Germany, at the end of 1904, steels having 0·08% C and 3·45% Si were smelted in the Siemens-Martin furnaces and subsequently worked into fine sheet[99]. In the stage reached by 1905, figures of $W_1 = 1{\cdot}5$–$1{\cdot}8$ W/kg were usual. Electrosheet first came onto the market in large quantities in 1905 in the USA and in 1906 in England.

By the end of the World War I, Germany was in a position to roll alloy sheet, for use in light-current engineering, down to a thickness of 0·05 mm[48]. The following values of the characteristics had become realisable in practice for 0·35 mm transformer sheet:

$$H_c = 38 \text{ A/m}$$
$$B_r = 0{\cdot}78 \text{ V s/m}^2$$
$$\mu_m = 7500\ \mu_0$$
$$W_1 = 1{\cdot}27 \text{ W/kg}$$
$$W_{1{\cdot}5} = 3{\cdot}39 \text{ W/kg}$$

Yensen[103], working in the laboratory, vacuum-melted pure electrolytic iron together with 0·15% and 3·4% Si, forging the result under the hammer and following this by an annealing in vacuo at 900°C and 1100°C. In this way he succeeded in achieving remanence values of 1·2–1·4 V s/m². In addition, the following constants were measured:

$$\mu_m = 66\,500\ \mu_0$$
$$W_1 = 0{\cdot}2 \text{ W/kg}$$
$$W_{1{\cdot}5} = 0{\cdot}7 \text{ W/kg}$$

(Note that the $W_1$ and $W_{1{\cdot}5}$ figures are d.c. results not comparable with the usual a.c. losses.) These laboratory results were important in pointing the way to further practical developments.

New momentum came in 1934 through the development of cold-rolling techniques and the production and utilisation of grain-oriented material having a preferred magnetic direction along the direction of rolling* (Goss

* Cold-rolled sheet is measured in the rolling direction—which is also the preferred direction; hot-rolled sheets are cut and then assembled half in the rolling and half in the transverse direction.

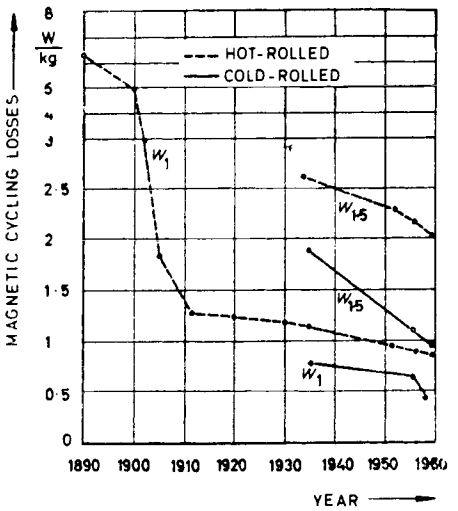



*Figure 10.5. Reduction of magnetic cycling losses $W_1$ and $W_{1\cdot5}$ in transformer sheet since 1890*

texture). Then, in 1957, the centre of interest passed to materials with cubic-grain structure. The reduction of energy loss $W_1$ achieved since 1890 is set out in Figure 10.5 from an exposition by Pawlek[77].

### 10.3.1 Effect of silicon content

The rise of specific electrical resistance with silicon content is shown in Figure 8.1. According to some measurements carried out at 60 Hz by Ruder[82], the total loss falls with increasing silicon content; this reaches a minimum at 6·5% Si and then rises again (Figure 10.6). Daeves[26], using statical methods, found a loss minimum at around 4·3% Si. Magnetic saturation falls with rising silicon content: with each percent of silicon it falls, proportionally,

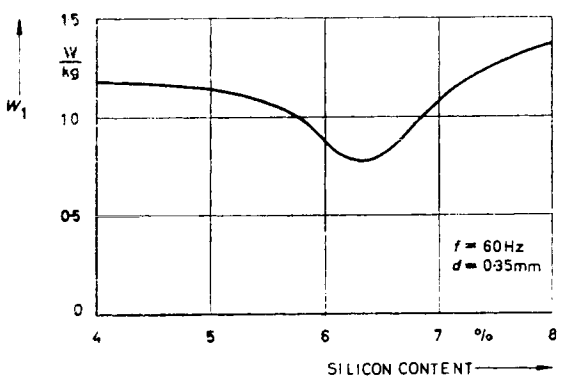



*Figure 10.6. Total a.c. losses at 60 Hz for 0·35 mm iron-alloy sheet as a function of silicon content*[82]

by about 0·05 V s/m². According to Gumlich, the following formula holds:

$$B_s = (2{\cdot}160 - 0{\cdot}048p) \text{ V s/m}^2 \qquad (10.1)$$

However, the fall in saturation is only effective at flux densities above 1·2 V s/m². Figure 10.7 displays the curves for $B - \mu_0 H$ against $H$ for various strongly alloyed, hot-rolled commercial sheets, supplemented by an alloy having 6% Si which can no longer be considered commercially extant.

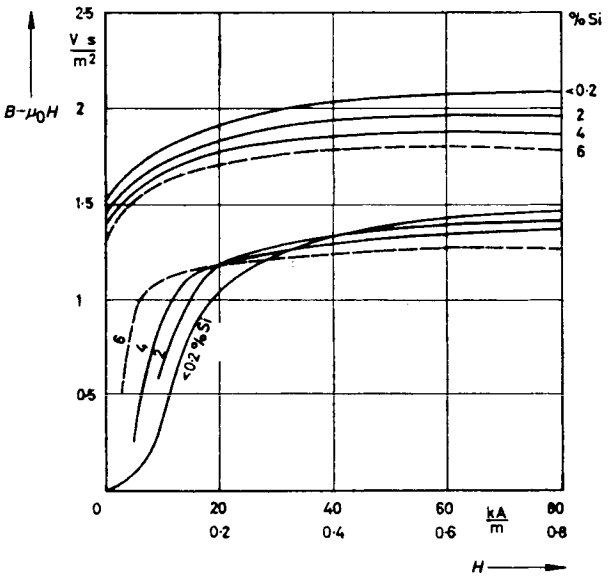



*Figure 10.7. Typical magnetising curves for sheets of high-quality* Fe–Si *steel*[13]

In appears from the graphs that the permeability at low intensities rises with increasing silicon content. The curve for the sometimes more highly alloyed sheet materials lies above that for lower silicon content. Above some 1·2 V s/m² the rank order of the types reverses[13].

The Curie temperature behaves as does the saturation value: it falls with rising silicon content. Up to 4% Si it drops from 780°C to 740°C. Both phenomena—drop in saturation density and drop in Curie temperature—are understandable since a proportion of the iron atoms are replaced by those of the non-magnetic substance, silicon. As is clear from Figure 10.8, the density $d$, the anisotropic constant $K_1$, and the Steinmetz coefficient $\eta$ fall according to Brailsford's investigations[13] with increasing silicon content.

Gumlich[48] has proposed the following formula for the drop in density with silicon content:

$$d = (7{\cdot}874 - 0{\cdot}0622p) \text{ g/cm}^3 \qquad (10.2)$$

This shows a linear relation between the density $d$ and the percentage of silicon $p$. Figure 10.8 shows, however, that the linear relationship holds only for low values of silicon content.

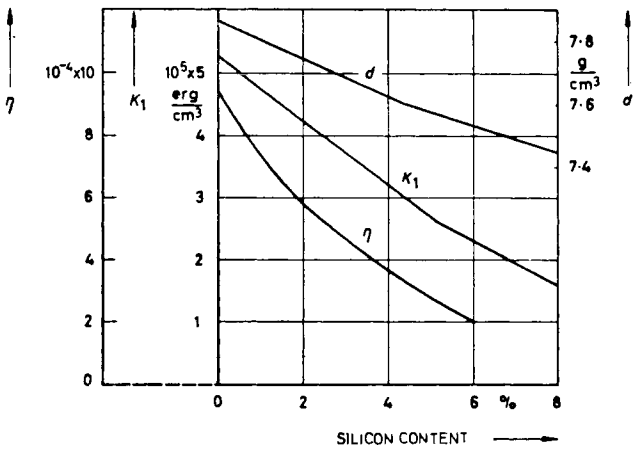



*Figure 10.8. Relation between silicon content and density d, anisotropic constant $K_1$, and the Steinmetz coefficient $\eta$ for silicon iron*[13]

Table 10.4 gives the specific electrical resistance and density of a few Fe–Si alloys according to the latest measurements[73]. As a result of this relation between density and electrical resistance it becomes possible, by means of a resistance measurement, to find the density and silicon content

**Table 10.4** SPECIFIC ELECTRICAL RESISTANCE AND DENSITY OF Fe–Si ALLOYS[73]

| *Silicon content* (%) | $\varrho$ ($\mu\Omega$ cm) | $d$ (g/cm³) |
|---|---|---|
| 0·25 | 16 | 7·85 |
| 1·05 | 25 | 7·80 |
| 1·75 | 33 | 7·75 |
| 2·55 | 42 | 7·70 |
| 3·35 | 51 | 7·65 |
| 4·15 | 60 | 7·60 |
| 4·85 | 68 | 7·55 |

$p$, at least approximately, of an Fe–Si alloy. If $\varrho$ is in $\mu\Omega$ cm and $p$ in %, then

$$p = \frac{\varrho - 13{\cdot}25}{11{\cdot}3} \tag{10.3}$$

and

$$d = 7{\cdot}865 - 0{\cdot}065\left(\frac{\varrho - 13{\cdot}25}{11{\cdot}3}\right) \text{ g/cm}^3 \tag{10.4}$$

The measurement must be carried out on surface-cleaned strip under care-

fully specified conditions. According to the German Standard DIN 50 463[31], the density of an electrosheet of Fe–Si alloy (Epstein test) can be obtained in terms of the product of density $d$ with specific electrical resistance $\varrho$, according to the formula

$$d\varrho = \frac{Rm}{l_\varrho l} \tag{10.5}$$

where $R$ is the electrical resistance, $m$ the mass, $l$ the length of the sample, and $l_\varrho$ the separation of the potential take-off points. The graphical form of

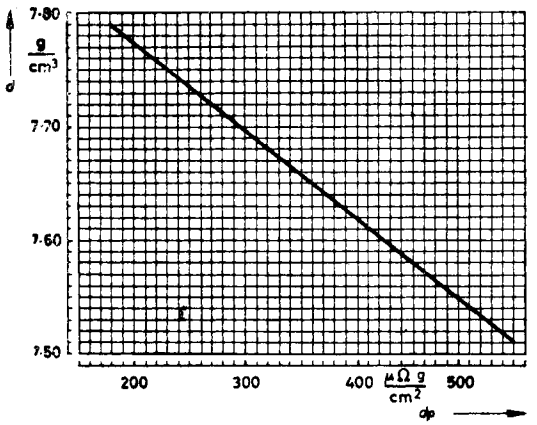



*Figure 10.9. Density of* Fe–Si *sheet in relation to the product* $d\varrho$[31]

this formula is to be seen in Figure 10.9. The actual basic formula from which the curve was drawn is

$$d = 7{\cdot}928\ \text{g/cm}^3 - \left(\frac{0{\cdot}773\times10^{-3}}{\mu\,\Omega\,\text{cm}}\right)\frac{Rm}{l_\varrho l}$$

It holds for silicon content between 1% and 5%, an aluminium content of 0·4% at most, and total content of other alloyed elements of less than 0·4%,

The improvement, with increasing silicon content, of permeability (Figure 10.7), losses, and coercivity suggests that it would be desirable to choose the highest possible silicon content. Difficulties in working the material, however, set limits to this idea. Figure 10.10 shows the rise in brittleness with the degree of alloying, according to Pilling[78]. The criterion he used was the amount of flexure possible with a specified sample strip. The curve yields the information that for more than 3·5% Si the given material breaks, when bent, at room temperature. This, however, is not the case for the same alloy at 100°C or 200°C, so this alloy may be worked at high temperatures.

This knowledge is also the basis of the fact that high-silicon transformer sheet is prepared by hot rolling. At the present time the highest proportion of silicon used in industry is about 4·5%, and for cold-rolled sheet it stands at 3% or less.

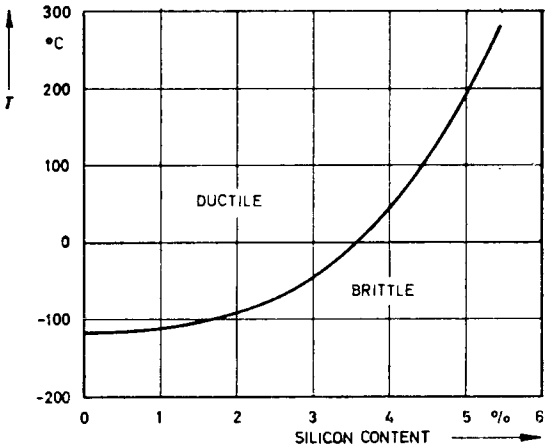



*Figure 10.10. Effect of silicon content on the brittleness of* Fe–Si *alloys*[78]

### 10.3.2 Effect of impurities

As in unalloyed iron, the presence of carbon in Fe–Si alloys is harmful. Long ago, Gumlich recognised 'that the favourable effect of silicon in iron mainly depends on the successful removal of the harmful effect of carbon impurities since, during annealing, silicon obviously causes, or favours, the precipitation of part of the carbon originally in the form of combined carbon into a harmless graphitic mass'.

According to the investigations of Yensen and Ziegler[106], even very small quantities of carbon strongly reduce the maximum permeability (Figure 10.11) and at the same time increase the coercivity (Figure 10.12). Daeves[26] established the fact that the $W_1$ value rises more or less linearly when the carbon increases from 0·04% to 0·11%. The carbon content of commercial

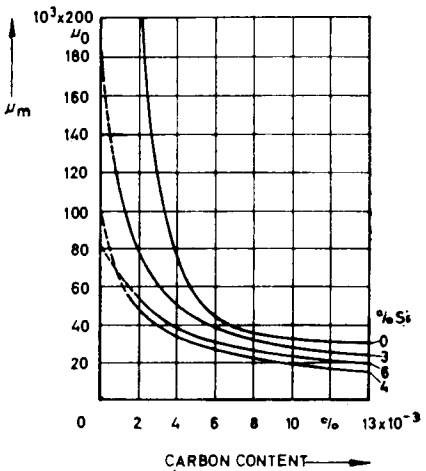



*Figure 10.11. Effect of carbon and silicon content on the maximum permeability of iron*[106]

dynamo and transformer sheet usually lies between 0·07% and 0·08%, or in many cases even lower.

According to Yensen's investigations[104], sulphur and manganese increase the hysteresis losses—more, in fact in unalloyed steel than in silicon steel. Phosphorus in unalloyed steel, up to 0·14% P, has little effect on the hysteresis losses, which are practically independent of the concentration in this range, and its presence in silicon steel may even reduce the losses.

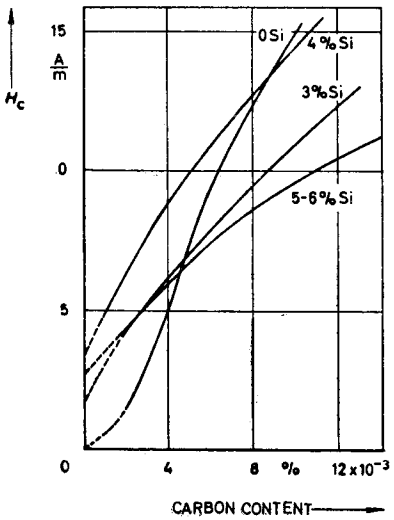



*Figure 10.12. Effect of carbon and silicon content on the coercivity of iron at $B = 1$ V s/m² [106]*

According to Daeves[26], the very flat loss curve has a maximum at 0·018% P, while a manganese content of 0·05–0·3% is without any marked influence.

Small quantities of oxygen for 3% Si or more have little effect on the magnetic values, since oxygen combines with silicon to form $SiO_2$ which is mostly precipitated in large particles during the melt. However, as a rule, it is to be expected that oxygen, next to carbon, has the greatest influence on the quality of Fe–Si sheet[70]. Its effect is harmful not only in that it can be built into the iron mixture-crystal but also because it hinders the formation of a uniform crystal texture.

Kussmann, Scharnow and Messkin[57] investigated the effect of copper on the magnetic properties of Fe–Si alloys having 1·5% and 4% Si. Up to 0·7% Cu there was practically no change in the magnetisability, coercivity, and maximum permeability compared with copper-free steel. Above 0·7% Cu the addition was found to be harmful. However, a small addition of copper may be useful as a means of enchancing corrosion resistance.

The presence of a certain quantity of impurities is obviously important for the formation of crystal orientation[62]. The quantity and distribution of the material is here more effective than its kind (nitride, sulphide, oxide). Also, the temperature range over which the texturing occurs may be influenced by the kind and quantity of impurity[65].

### 10.3.3 Effect of grain size

A typical property of Fe–Si alloys is their sometimes coarse-grained crystal structure. In particular, sheet of good magnetic quality often shows coarse-grained crystallites. There has, therefore, been no lack of attempts to relate this coarse-grained structure to the magnetic properties. To follow the abundant literature relating to the 'problem of grain size' is to receive an ambiguous picture, as the results of different workers often contradict each other[9, 10, 25, 49, 81, 102, 104].

Gerlach[42] put the matter on a firmer footing when he established that it was not the chemical purity or the crystal dimensions which was the decisive factors but rather 'magnetic purity', i.e. it was the quality of the crystal formation that determined the magnetic properties. This was also confirmed by Moos, Oertel, and Scherer[70].

However, the fact that it is just in the more highly alloyed Fe–Si sheets that the formation of coarse grains is so marked is, according to Daeves[26], connected with the observation that, for a silicon content above 1·3%, the $\gamma$-configuration no longer appears whatever the temperature. As already mentioned on page 200, the cubic body-centred $\alpha$-lattice of unalloyed iron goes over, around 900°C, into the cubic face-centred $\gamma$-lattice. The missing $\gamma$-range in highly alloyed Fe–Si inhibits the grain size reduction associated with the $\alpha$–$\gamma$ transformation.

### 10.3.4 Temperature dependence of losses

The connection between the various losses and the ambient temperature has been frequently studied for various types of sheet material—with wide-ranging results. Brown and Brennand[17] have carried out a new investigation into a common commercial Fe–Si alloy with 4·3% Si, using a toroidal core of square laminations 0·35 mm thick, over a temperature range from −253°C to 0°C. The total losses are shown in Figure 10.13 for a frequency range 20–200 Hz. It can be appreciated from the graphs that the frequency function shows the same form for all measured temperatures and flux densities: the losses rise with falling temperature.

Harms[52] found that, at high temperatures also, the core losses dropped as the temperature was increased. He established this using a grain-oriented Fe–Si alloy with 3% Si. Between 30°C and 550°C the drop amounted to 60%. At flux densities up to 1 V s/m² the exciting field fell off with rising temperature, and above this figure it rose again.

### 10.3.5 Properties of hot-rolled electrosheet

Dynamo and transformer sheet is usually made in thicknesses of 0·35 mm and 0·5 mm. Rolling the sheet at a fairly high temperature facilitates shaping operations. To avoid a too rapid cooling after the rolling operation, it is usual to stack several strips together. Thus the final rolling of 0·35 mm transformer sheet involves an eightfold stack 2·8 mm high.

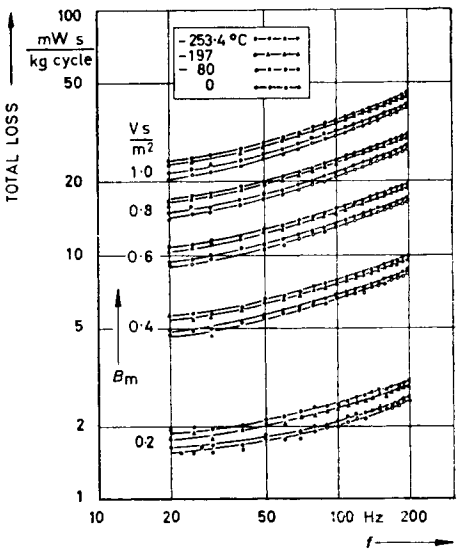



*Figure 10.13. Total core loss as a function of frequency*[17]

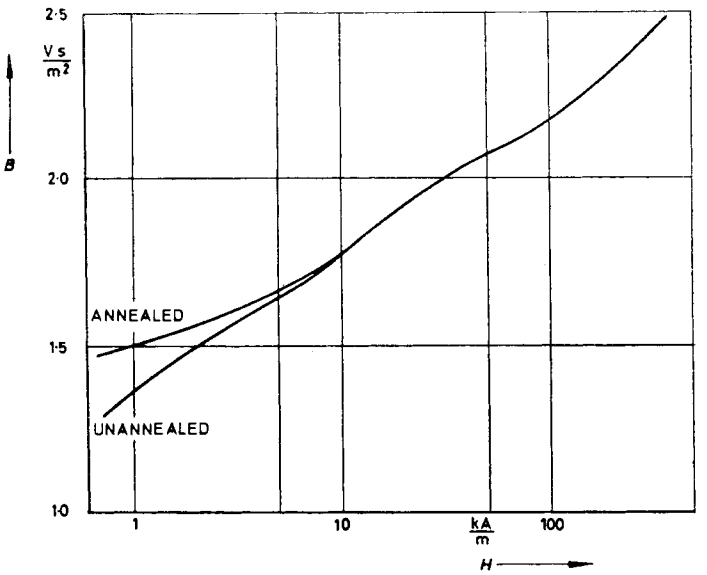



*Figure 10.14. Magnetising curves of strips of hot-rolled dynamo sheet before and after annealing at 850°C*[24]

This hot-rolled sheet does not possess completely isotropic properties. The prescibed measuring techniques (using the Epstein test) attempt to take care of this in that measuring samples are cut from the stock half in the rolling direction and half transversely in order to obtain a representative mean value (for information on the determination of the magnetic properties of electrosheet by the Epstein test, see DIN 50 461 and 50 462[29, 30]). It has been shown, however, that for the slightly anisotropic hot-rolled sheet, the easiest direction of magnetisation coincides with the rolling direction; on the other hand, the hardest direction does not always fall along the transverse direction but may sometimes make an angle of 60°–75° with the direction of rolling[37]. The results of the Epstein test, therefore, do not give a true mean in this case. The observed anisotropy is more marked at low intensities than at high.

The relation between flux density and field strength is given in Figure 10.14, following Czerlinsky[24], for measuring-samples taken from 0·35 mm dynamo sheet having 1·56% Si. The lower curve shows the function $B = f(H)$ directly after the sample has been stamped out, while the upper curve is taken after an annealing at 850°C. It appears from this that the effect of deformation is only perceptible at low measuring intensities.

Annealing after stamping also reduces the hysteresis losses of the laminations. Losses introduced by stamping are greater for narrow than for broad

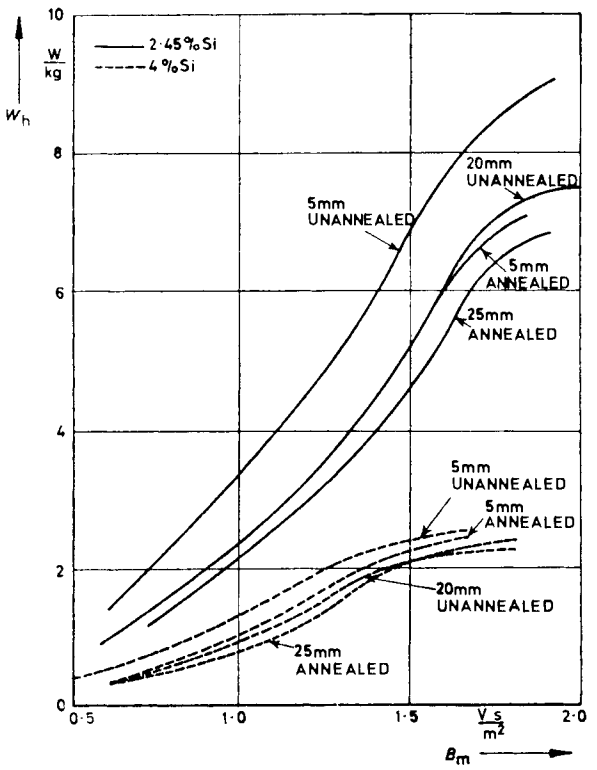



*Figure 10.15. Hysteresis loss of toroidal cores of various widths made from hot-rolled dynamo sheet before and after annealing at 850°C*[24]

rings. Figure 10.15 shows this effect[24] for sheet having 2·45% and 4% Si in rings of various widths both before and after annealing. The more highly alloyed material is here seen to be less sensitive than the less alloyed.

Appreciable losses, additional to those of normal magnetic material, are often to be reckoned with owing to the working of the sheets or stacks of sheets (stamping, flattening, machining)[87]. However, they can be reduced or completely removed by suitable heat treatment. Sometimes, in this connection, the choice of a particular alloy can be important. Additional losses, such as those due to uneven flux partition in the teeth of armatures or those induced in d.c. machines between pole-faces and armature teeth, cannot be removed in this simple way[59].

The texture and magnetic anisotropy produced by hot rolling can be utilised under certain circumstances, i.e. if the laminations are not randomly directed, as given by the Epstein test, but are so arranged that they are magnetised along the direction of easiest magnetisability; the $W_1$ value of 1·0 W/kg can be significantly reduced. According to composition and manufacturing routine, $W_1$ values in commercial practice lie between 0·75 W/kg and 0·95 W/kg, and $W_{1.5}$ values between 1·88 W/kg and 2·37 W/kg[97]. Today, hot-rolled transformer sheet is available whose $W_1$ values can be chosen anywhere in the range 0·75–3·6 W/kg with $W_{1.5}$ values lying between 1·88 W/kg and 8·6 W/kg.

For certain English types of sheet, which are shown in Table 10.5, Brailsford and his co-workers give the following additives: 0·03% C, 0·02% S, 0·02% P, and 0·15% Mn.

**Table 10.5** LOSS VALUES FOR ENGLISH HOT-ROLLED Fe–Si SHEET[15]

| *Approximate silicon content* (%) | *Sheet thickness* (mm) | *Total loss at* 50 Hz (W/kg) | |
|---|---|---|---|
| | | $B_m$ = 1 V s/m² | $B_m$ = 1·3 V s/m² |
| 0·4 | 0·41 | 2·96 | 4·83 |
| 1·5 | 0·41 | 2·20 | 3·60 |
| 3·0 | 0·41 | 1·71 | 2·93 |
| 4·0 | 0·36 | 1·30 | 2·20 |
| 4·3 | 0·36 | 1·08 | 1·89 |

The field strength at which a given flux density is reached serves as a further characteristic figure for heavy-engineering sheet. The German Standard DIN 46 400 therefore introduces the magnitudes $B_{25}$, $B_{50}$, $B_{100}$, and $B_{300}$, which specify the flux densities corresponding to 25 A/cm, 50 A/cm, 100 A/cm, and 300 A/cm. Magnetic parameters for hot-rolled electrosheet and tape to DIN 46 400[28] are given in Table 10.6. In addition, the loss anisotropy is quoted, derived from the formula $(W_n - W_p)/(W_n + W_p)$, $W_n$ being the cyclic loss normal to the rolling direction and $W_p$ the cyclic loss parallel thereto.

**Table 10.6** MAGNETIC PROPERTIES AND DENSITIES OF HOT-ROLLED ELECTROSHEET AND STRIP TO DIN 46 400[28]

| *Material designation* | *Sheet thickness* (mm) | $W_1$ (W/kg) | $W_{1\cdot5}$ (W/kg) | $B_{25}$ $\left(\frac{\text{V s}}{\text{m}^2}\right)$ | $B_{50}$ $\left(\frac{\text{V s}}{\text{m}^2}\right)$ | $B_{100}$ $\left(\frac{\text{V s}}{\text{m}^2}\right)$ | $B_{300}$ $\left(\frac{\text{V s}}{\text{m}^2}\right)$ | *Loss anisotropy* (%) | *Density* (g/cm³) |
|---|---|---|---|---|---|---|---|---|---|
| V 90-35 B | 0·35 | 0·9 | 2·3 | 1·47 | 1·59 | 1·70 | 1·88 | ±8 | 7·55 |
| V 100-35 B | 0·35 | 1·0 | 2·5 | 1·47 | 1·59 | 1·70 | 1·88 | ±8 | 7·55 |
| V 110-35 B | 0·35 | 1·1 | 2·7 | 1·47 | 1·59 | 1·70 | 1·88 | ±8 | 7·55 |
| V 130-35 B | 0·35 | 1·3 | 3·3 | 1·47 | 1·59 | 1·70 | 1·88 | ±8 | 7·6 |
| V 110-50 B | 0·5 | 1·1 | 2·7 | 1·47 | 1·59 | 1·70 | 1·88 | ±8 | 7·55 |
| V 125-50 B | 0·5 | 1·25 | 3·1 | 1·47 | 1·59 | 1·70 | 1·88 | ±8 | 7·55 |
| V 135-50 B | 0·5 | 1·35 | 3·3 | 1·47 | 1·59 | 1·70 | 1·88 | ±8 | 7·6 |
| V 150-50 B | 0·5 | 1·5 | 3·6 | 1·47 | 1·59 | 1·70 | 1·88 | ±8 | 7·6 |
| V 170-50 B | 0·5 | 1·7 | 4·1 | 1·48 | 1·60 | 1·71 | 1·89 | ±8 | 7·6 |
| V 200-50 B | 0·5 | 2·0 | 4·8 | 1·49 | 1·61 | 1·72 | 1·93 | ±6 | 7·65 |
| V 230-50 B | 0·5 | 2·3 | 5·4 | 1·51 | 1·63 | 1·74 | 1·96 | ±6 | 7·65 |
| V 260-50 B | 0·5 | 2·6 | 6·1 | 1·53 | 1·64 | 1·75 | 1·97 | ±6 | 7·7 |
| V 300-50 B | 0·5 | 3·0 | 6·9 | 1·54 | 1·65 | 1·76 | 1·99 | ±6 | 7·75 |
| V 360-50 B | 0·5 | 3·6 | 8·2 | 1·56 | 1·67 | 1·77 | 2·0 | ±6 | 7·8 |

### 10.3.6 Cold-rolled Fe–Si sheet

Before 1935, almost all electrosheet was hot-rolled. Since then more and more sheet material has been, and continues to be, cold rolled, particularly sheet without preferred direction for applications in motors and with a well-marked preferred direction for transformers. This has happened mainly because of the superior magnetic quality of cold-rolled sheet but also because of its greater uniformity and conformity to specification. The smoother surface also allows a denser packing in the core. As cold-worked sheet and strip are more lightly alloyed, there is less wear on the cropping and stamping tools than with highly alloyed and more brittle materials. However, it still holds for cold-rolled Fe–Si alloys that the losses are less the higher the proportion of silicon in the alloy. Schlüter and Stäblein[86] carried out investigations of this sort into dynamo strip.

The cyclic magnetisation losses $W_1$ and $W_{1\cdot5}$ of cold-rolled electrosheet and tape to DIN 46 400[28] are set out in Table 10.7. The loss anisotropy is something like twice as great as for hot-rolled electrosheet and tape (see Table 10.6). The values are standard mean values; they are better in the preferred direction, coinciding with the strip direction, and worse transversely. Advantage can sometimes be taken of this anisotropy. Further, the flux density of 'electrostrip' measured at the same field strength lies some 0·01–0·05 V s/m² higher than for hot-rolled sheet. The initial permeability in the strip direction is around $350\mu_0$ and in the cross-direction about $300\mu_0$, the corresponding maximum permeabilities being $12\,000\mu_0$ and $6000\mu_0$.

It is possible, also, taking hot-rolled material of a particular thickness, to cold-roll it further without intermediate annealing, so producing a texture.

**Table 10.7** MAGNETIC PROPERTIES AND DENSITIES OF COLD-ROLLED ELECTROSHEET AND TAPE TO DIN 46 400[28]

| *Material designation* | *Sheet thickness* (mm) | $W_1$ (W/kg) | $W_{1\cdot5}$ (W/kg) | $B_{25}$ $\left(\frac{V\ s}{m^2}\right)$ | $B_{50}$ $\left(\frac{V\ s}{m^2}\right)$ | $B_{100}$ $\left(\frac{V\ s}{m^2}\right)$ | $B_{300}$ $\left(\frac{V\ s}{m^2}\right)$ | *Loss anisotropy* (%) | *Density* (g/cm³) |
|---|---|---|---|---|---|---|---|---|---|
| V 110-35 A | 0·35 | 1·1 | 2·7 | 1·49 | 1·60 | 1·71 | 1·89 | ±14 | 7·6 |
| V 130-35 A | 0·35 | 1·3 | 3·3 | 1·49 | 1·60 | 1·71 | 1·89 | ±14 | 7·65 |
| V 135-50 A | 0·5 | 1·35 | 3·3 | 1·49 | 1·60 | 1·71 | 1·89 | ±14 | 7·6 |
| V 150-50 A | 0·5 | 1·5 | 3·5 | 1·50 | 1·60 | 1·71 | 1·89 | ±14 | 7·65 |
| V 170-50 A | 0·5 | 1·7 | 4·0 | 1·51 | 1·61 | 1·72 | 1·90 | ±14 | 7·65 |
| V 200-50 A | 0·5 | 2·0 | 4·7 | 1·52 | 1·62 | 1·73 | 1·94 | ±12 | 7·7 |
| V 230-50 A | 0·5 | 2·3 | 5·3 | 1·54 | 1·64 | 1·75 | 1·97 | ±12 | 7·7 |
| V 260-50 A | 0·5 | 2·6 | 6·0 | 1·55 | 1·65 | 1·76 | 1·98 | ±12 | 7·75 |
| V 300-50 A | 0·5 | 3·0 | 6·8 | 1·56 | 1·66 | 1·77 | 2·0 | ±12 | 7·8 |
| V 360-50 A | 0·5 | 3·6 | 8·1 | 1·58 | 1·68 | 1·78 | 2·01 | ±12 | 7·8 |

This, however, is not particularly well marked. By a refining heat treatment the $W_{1\cdot5}$ losses can be reduced to 1·35 W/kg. Whether it will be possible to reduce this value in the future appears doubtful[77].

A really well-marked grain orientation, with good magnetic properties, can be achieved only by a particular routine of cold-working operations and recrystallisation annealing. Cold-rolled Fe–Si alloys have usually a smaller silicon content than hot-rolled sheet, namely 2·5–3·5% Si against 4–4·5% Si. A sacrifice of part of the high specific electrical resistance has to be accepted and exchanged (in the cold-worked material) for improved workability, smaller hysteresis loss, and higher flux density.

Finally, it must not be forgotten that cold-rolled sheet has higher losses in the transverse direction than the almost isotropic hot-rolled sheet. Also losses will be higher in cold-rolled sheet if the direction of magnetisation changes from lengthwise to crosswise. An example taken from an investigation by Ruess[83] will make this clear. In Figure 10.16 the losses in hot-rolled electrosheet IV (solid curves) and in cold-rolled stress-free annealed electrosheet (broken curves) are plotted in the same graph. Loss curves for cross-magnetisation are labelled 1; curves labelled 2 are for lengthwise magnetisation; and curves 3 for both directions. In this case the lamination stacks were butted; overlapping gives somewhat lower losses but the general run of the curves is the same.

### 10.3.6.1 Sheets with Goss texture

Transformer sheet of the highest quality met with on the market today is grain oriented. By rolling and annealing treatment the crystallites are, to a large extent, so directed that the preferred direction of magnetisation [100] lies along the direction of rolling. In this direction the hysteresis losses are lowest and the permeability highest.

The relation between the permeability $\mu$ and the flux density $B$ is shown in Figure 10.17, taken from Bozorth[12], for a grain-oriented cold-rolled Fe–Si

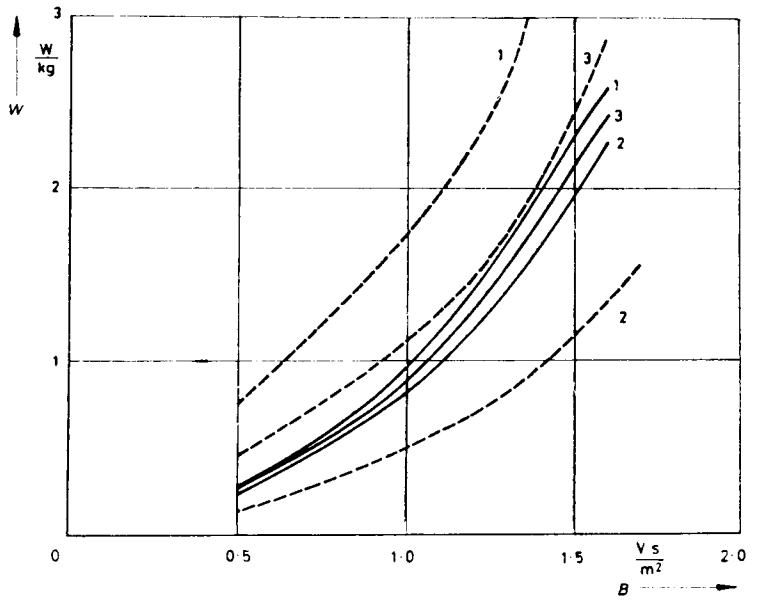



*Figure 10.16. Cyclic magnetic loss for electrosheet IV with butt-jointed stacks of strips 500* mm×*30* mm[83]

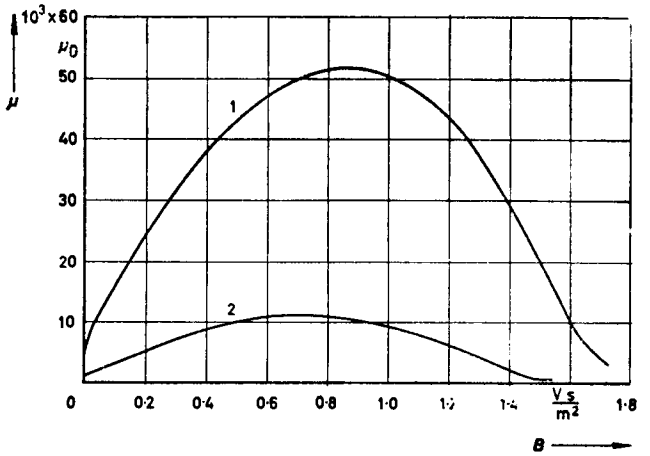



*Figure 10.17. Permeability curves: 1, grain-oriented* Fe–Si *with 3% Si; 2, hot-rolled* Fe–Si *with 4% Si, measured in the direction of rolling*[12]

alloy with 3% Si (curve 1) and for an almost isotropic hot-rolled alloy with 4% Si (curve 2). The maximum permeability for the grain-oriented material, measured in the preferred direction, is about five times as high as for the hot-rolled sheet.

The search for an improved (hot-rolled) transformer sheet goes back, mainly, to Goss, who took out a US patent in 1934 for the process since named after him[45]. This Goss process is characterised by the following steps: The 2·4 mm hot-rolled sheet is annealed at 800°–950°C; the surface is descaled by pickling or sand blasting, and the sheet is then cold rolled to about 0·75 mm; after a brief annealing at 875°–1025°C the material is rolled down to the final thickness of 0·35 mm. The mill settings for the two cold rollings are 6–10 and 4–8[91].

The final annealing whereby, in conjunction with a recrystallisation, the crystal orientation is produced takes place at 1000°–1200°C in pure dry hydrogen. This treatment, incidentally, reduces the carbon content: at the end of the process it is generally not higher than 0·005%. The presence of slight impurities is important for the achievement of Goss texture. Markuszewicz[62] was able to prove from samples of Fe–Si, made by the techniques of powder metallurgy, that it is not possible to produce Goss texture from an absolutely pure material.

Further, Fast[35] in his investigation of cold-rolled Fe–Si with 3% Si observed that a (110) [001] texture could not be produced if extremely pure base material was used. On the other hand, there is no difficulty in achieving anisotropy, by the same rolling and heating routines, in commercial alloys.

A large degree of impurity leads to a fine-grain sheet characterised by high coercivity and low anisotropy. Good orientation is obtainable in sheet materials that have not too great a degree of impurity yet are not by any means free of them. At the same time relatively large grains and medium coercivity are obtained.

Figure 10.18, following measurements made by Stäblein and Meyer[91], shows the directionality of the magnetic properties of textured sheet in comparison with hot-rolled sheet: in the transverse direction the power loss of cold-rolled sheet is some three times as great as in the preferred direction. The permeability difference is even greater, the ratio being around 1 : 6. Hot-rolled sheet, on the other hand, shows an almost isotropic relation. Cole[23] has shown that the anisotropy of permeability for Goss sheet at 1·5 V s/m$^2$ is significantly more marked than, for example, at 800 A/m (Figure 10.19).

The individual steps in the cold-rolling routine also produce texturing —the so-called rolling texture[69]. This is not identical to recrystallisation texture and will not be further pursued since we are, in principle, concerned only with the properties of the end-product.

In recrystallisation texture the preferred magnetic direction lies along the direction of rolling and is thus parallel to the [100] direction of the crystallites. The [110] direction lies perpendicular to the rolling direction, and the [111] direction forms an angle of 54·7° with it (see Figures 5.1 and 10.21).

The exact location of the crystal directions is found by x-ray crystallography using the Laue technique[32] or by counter devices[18]. Sommerkorn[90] describes a summation device for the determination of texturing in large-crystal samples which enables a 30 cm strip to be x-ray tested.

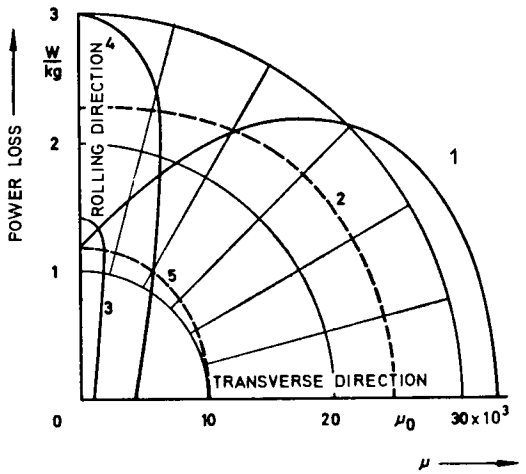



*Figure 10.18. Permeability $\mu$ and power loss for textured sheet in relation to measuring direction: 1, $W_{1\cdot5}$ for grain-oriented strip; 2, $W_{1\cdot5}$ for hot-rolled sheet with 4% Si; 3, $\mu$ of cold-rolled strip at 1·5 V s/m²; 4, same but at 1·0 V s/m²; 5, $\mu$ of hot-rolled sheet at 1 V s/m²* [91]

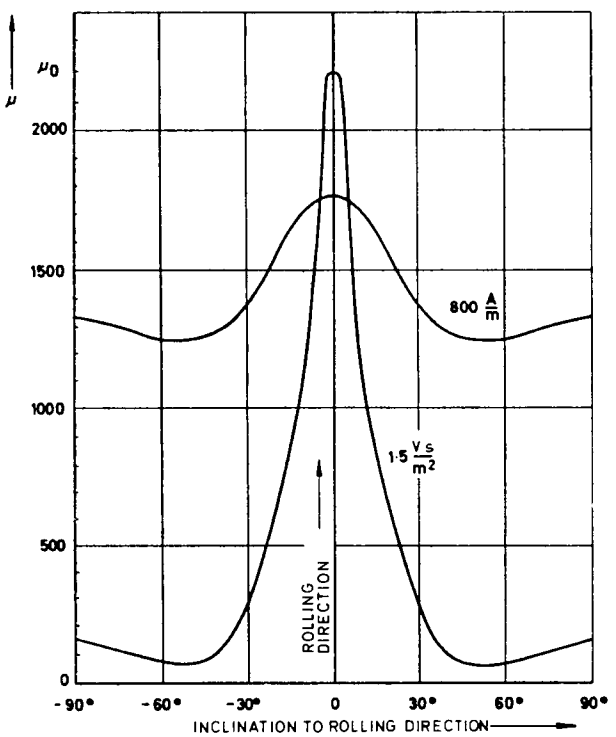



*Figure 10.19. Permeability at 1·5 V s/m² and at $H$ = 800 A/m at various inclinations to the rolling direction (material: oriented Fe–Si alloy Al-S1-M7-TRAN-COR 3x-0)* [23]

The preferred magnetic direction can be quite simply determined by measuring the turning moment of a circular disc cut from the sheet to be measured and placed in a magnetic field, i. e. by applying the method which is also used to determine the anisotropic constant (see page 89). According to Goss[45], the measurement of turning moment can also be used to determine the required annealing temperature by measuring the moment of a sample taken after the last cold rolling and before the annealing. The apparatus used for this is described in the patent.

Figure 10.20 gives an example of a turning-moment curve for a cold-rolled transformer steel with 3·25% Si. The solid line shows the measured results. The turning-moment curve calculated for a single crystal in the (110) plane is shown dashed for comparison[15].

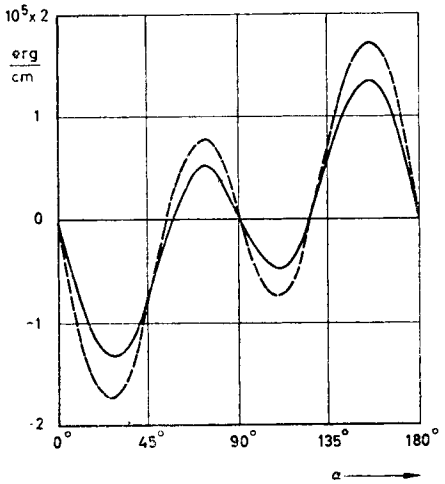



*Figure 10.20. Turning-moment curves; solid line, measured curve for a cold-rolled transformer steel with 3·25% Si; broken curve, calculated curve for a single crystal of iron with 3·25% Si in the (110) plane*[15]

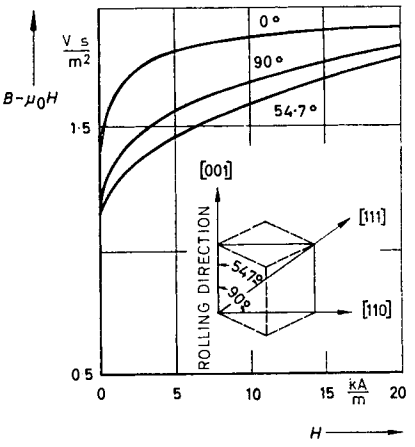



*Figure 10.21. Magnetising curves of cold-rolled* Fe–Si *steel with 3% Si at various inclinations to the rolling direction (for which α = 0)*[15]

Figure 10.21 gives the $B - \mu_0 H$ characteristic plotted against the field strength H (compare Figure 5.4). As already mentioned above, the hysteresis losses are functions of the direction. Figure 10.22 shows the hysteresis loss against polarisation for Fe–Si sheet having 3% Si. Figure 6.7 demonstrates the reduction in cyclic loss produced by cold rolling as against hot rolling. It can be seen from the turning-moment curve of Figure 10.20, which was taken for a commercial cold-rolled transformer steel, that the degree of orientation is represented by 80%. The chemical impurities in this material were roughly 0·004% C, 0·01% S, 0·004% P, 0·01% Al, and 0·06% Mn.

According to Ruess[84], the best value of $W_{1{\cdot}5}$ is around 1·1 W/kg for a transformer sheet manufactured by the Goss process. A numerical comparison, taken from actual practice, may serve to show how this loss reduction in core material works out in transformer design. In a large 30 MVA transformer, the substitution of cold-worked grain-oriented sheet for the once-

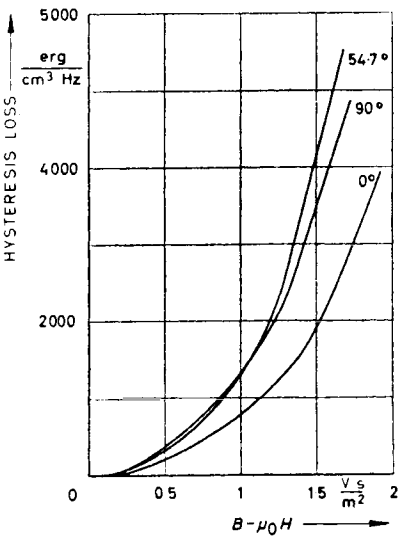



*Figure 10.22. Relation between hysteresis loss and rolling direction for cold-rolled* Fe–Si *steel with 3% Si*[15]

usual hot-rolled material brought down the open-circuit loss by 40%, the magnetising (no-load) current by 60%, and the loudness level on load by 10% (in decibels). At the same time, the overall weight was reduced by 15%. The higher cost of the grain-oriented sheet was, in this way, partially offset[55]. In smaller transformers, also, the substitution of oriented core material is advantageous because of the considerable reduction in the size of the core and of the windings for a given power[7].

### 10.3.6.2 Effect on magnetic properties of the shape of core and lamination

The advantages of the preferred direction in Goss sheet can be fully realised, technically, only if the sheet is cut up into strips, parallel to the rolling direction, and these are rolled into cores. The disadvantage of the closed-ring core, namely that it is difficult to fit the coil windings onto it, can be met by using a divided core. Such cores are known as split cores or C cores[1, 6, 27a, 53b].

Of course, the division of the core shifts the hysteresis loop in shear, but by accurate grinding of the butting surfaces the effective air-gap of the assembled core can be reduced to about 5 μm so that, especially in the larger type of core, the loss of efficiency does not weigh very heavily[7]. Figure 10.23 (see plate section) shows a few commercially used core shapes for power transformers[1].

In the manufacture of laminated cores care must be taken that the longitudinal direction of the sheet coincides with the rolling direction and with the direction of magnetisation. Unavoidable transition zones at the corners of the stacks of laminations introduce additional losses. Even under the most favourable conditions, i. e. by using laminations that have been annealed after stamping, the actual $W_{1{\cdot}5}$ core-losses are always higher than would

be found in a measuring strip[33]. The highest value of cyclic loss occurs at an angle of about 70° to the direction of rolling (see Figure 10.18); the $W_{1\cdot5}$ losses are some three times those appropriate to the rolling direction.

The effect of butt joints in laminated or stacked cores cannot be avoided altogether. Even the use of alternate stampings with air-gaps out of register involves a reduced effective cross-section[2]. Figure 10.24 gives, in schematic

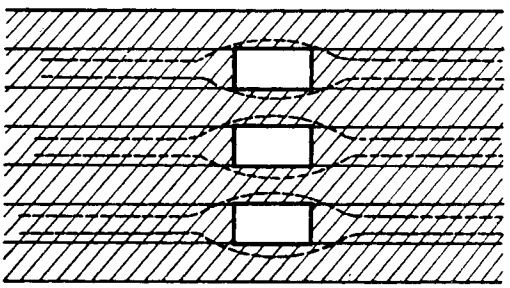


*Figure 10.24. Magnetic effect of butt joints*

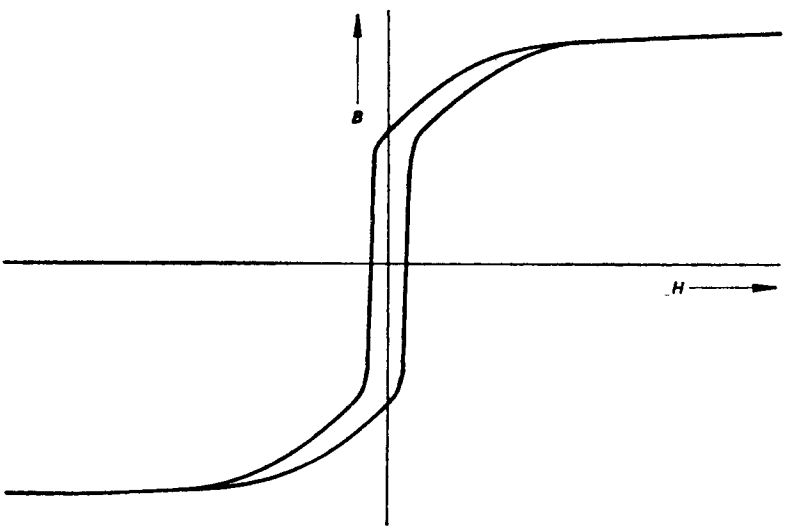



*Figure 10.25. Hysteresis loop showing effect of butt joints*[80]

form, an example of an M core which was laminated in the usual way. The drawing shows a section through the longitudinal dimension of the tongue and gives the flow of the magnetic lines at the joints. Since the flux seeks to pass round the air-gap, it increases twofold the flux in the contiguous material. In consequence, saturation occurs at half the normal saturation field. The hysteresis loop then takes the form sketched in Figure 10.25[80]. A further worsening of magnetic properties occurs in cores of textured material by reason of the fact that the flux at the corners of the core must turn, temporarily, into less favourable directions[14]. Direction-transitions and butt joints

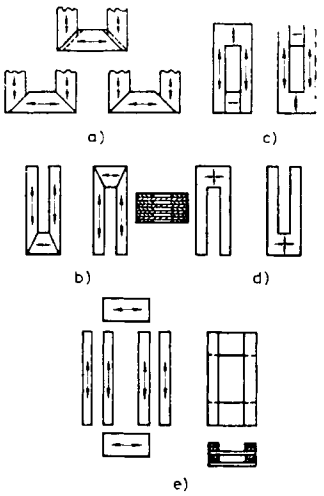



*Figure 10.26. Build-up of laminated cores from anisotropic stampings; in each case two consecutive stampings are shown; the preferred direction is indicated by arrows; a, b, c, and e are of Goss-texture sheet, and d is of cubic-texture sheet*

are thus to be avoided as far as practicable. However, it has proved possible to develop lamination shapes for stacked cores which go a long way to meet the requirements for texture quality while being but little inferior to strip cores. Figure 10.26 shows a few examples well-known in the literature[60, 80, 88].

### 10.3.6.3 Fe–Si sheet of cubic texture

The longitudinal and transverse directions of sheet and strip are magnetically equivalent only if they have been given 'cubic texture' by rolling and recrystallisation. For this texture, often referred to as [100] (100) texture, a cube edge-direction lies, as for Goss texture, in the direction of rolling, but in addition a cube face must lie in the rolling plane (see Figure 5.1). There also exists an intermediate position in which the cube face lies in the rolling plane and the cube edges are randomly oriented. This structure can be used with advantage in certain cases[93b]. The [100](100) texture can be achieved to a good degree of approximation by following out the processes recommended by Assmus, Detert, and Ibe[8] and by Möbius and Pawlek[68] (see page 141). Commercial products of this kind exist, for example Cubex[75a].

To achieve a well-formed texture, a series of effects must be taken into account: silicon content; additional alloy substances such as nickel, copper, and manganese; degree of purity of the raw material; degree of deformation (first and second); mill setting; sense in which the sheet is rolled; and surface treatment before the final annealing. No cubic texture can be achieved, according to Möbius and Pawlek[68], with less than 1·8% Si since at this silicon content the extreme limit of the $\alpha+\gamma$ domain lies at 1120°C. But again, according to the same authors, it is harder to obtain the desired texture for more than 2·2% Si.

The improvement in magnetic properties achieved by this cubic texture compared with Goss texture can be understood from a parallel comparison by Walter and his co-workers[96]. They constructed UI transformer cores

from Fe+3% Si sheet having cubic texture and also from sheets having Goss texture, and they determined the losses as a function of flux density. The measured results referred to 50 Hz are given in Figure 10.27. Curve 2 for cubic texture shows better figures than that for Goss-texture sheet (curve 1), particularly in the high-flux range. At 1·7 V s/m² the core losses of the cubic-texture material amounted to about 68% of those of the Goss sheet. The current needed to produce this flux density (1·7 V s/m²) is only half that needed in the core of Goss material.

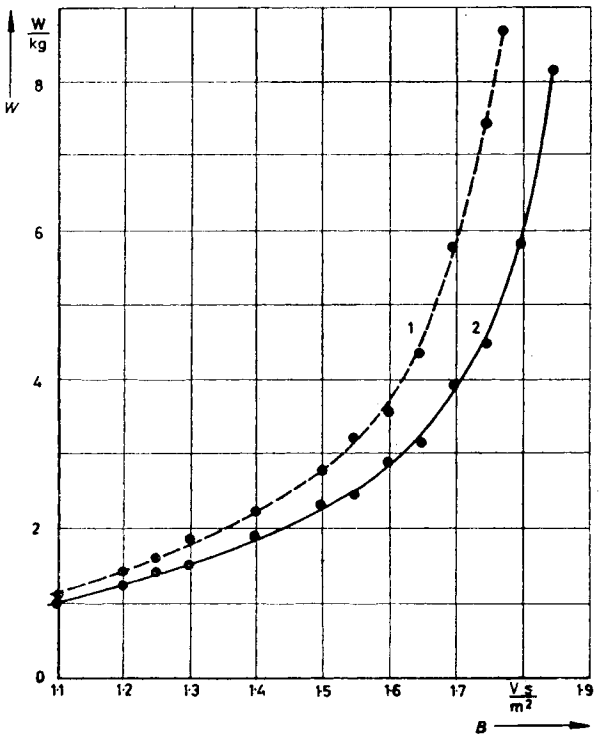



*Figure 10.27. Energy loss in relation to flux density for* Fe–Si*: 1, Goss texture; 2, cubic texture*[96]

Certain other characteristics, measured with direct current for the same comparison materials, are collected together in Table 10.8. From this it is seen that the sheet with cubic texture not only is superior in the transverse direction—which is to be expected—but also gives rather better results in the rolling direction.

A comparison of the curve of turning moment for the cubic-texture sheet with that for a single crystal shows that, in textured sheet, more than 90% of the turning moment of the single crystal can sometimes be achieved. Wiener, Albert, and Trapp[100] were able to align up to 99% of the volume of all crystallites without thereby achieving any significant further improvement in the values.

**Table 10.8** EFFECT OF TEXTURE ON MAGNETIC VALUES FOR Fe–Si SHEET HAVING 3% Si[96]

| | *Goss texture* | | *Cubic texture* | |
|---|---|---|---|---|
| | *Rolling direction* | *Transverse direction* | *Rolling direction* | *Transverse direction* |
| Maximum permeability ($\mu_0$) | 55 000 | 8 000 | 116 000 | 65 000 |
| Coercivity (A/m) | 6·4 | 21·6 | 5·6 | 6·4 |
| Remanence, $B_r$ (V s/m$^2$) | 0·95 | 0·175 | 1·22 | 1·15 |
| $B_m$ at 160 A/m (V s/m$^2$) | 1·63 | 1·10 | 1·66 | 1·60 |
| $W_{1·5}$ (W/kg) | 0·88 | 2·24 | 0·85 | 1·0 |

According, to the measurements of Ganz[39], the flux density of small-crystal strip-wound cores with Goss texture lies below the values for large-crystal material with cubic texture, within the measuring range shown in Figure 10.28. The coercivity of the cores having cubic texture is only about half that for cores of Goss material (Figure 10.29). In both cases it increases as the sheet thickness decreases.

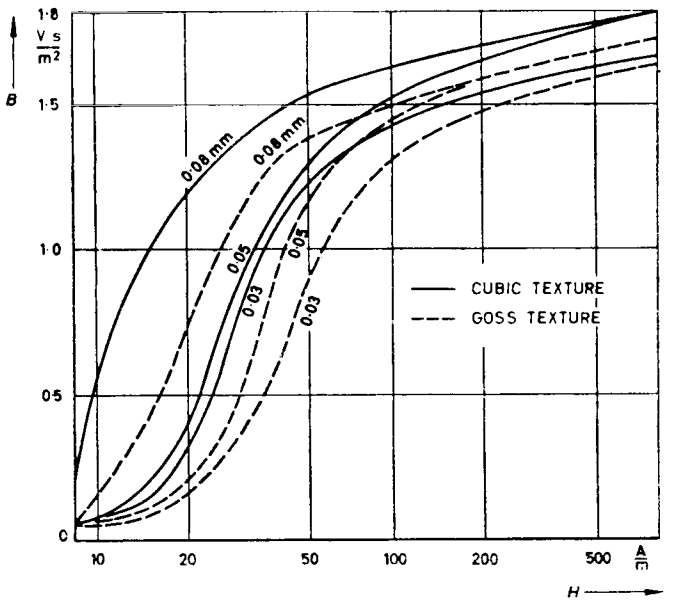



*Figure 10.28. Static magnetising curves for* Fe–Si *toroidal strip-wound cores of various structures and textures and different strip thicknesses*[39]

If the total loss is measured at $B = 1·0$ V s/m$^2$, then the frequency dependence shown in Figure 10.30 is obtained, according to Ganz[39]. From this set of curves it can be seen that the losses in the low-frequency range are higher the further the sheet is rolled down. Ganz[40] explained this effect by the higher coercivity of the thin sheet and the fact that the surface layer is

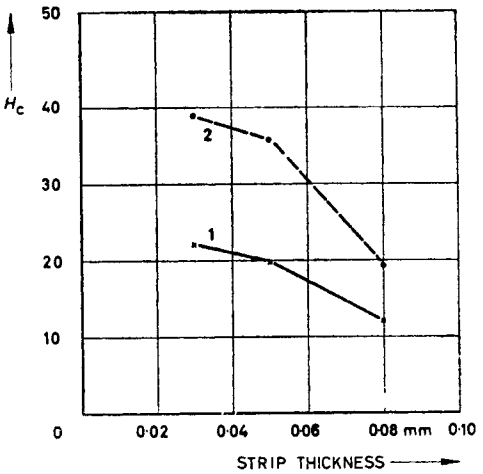



*Figure 10.29. Coercivity in relation to sheet thickness for* Fe–Si *toroidal strip-wound cores of various textures: 1, cubic texture (coarse-grain); 2, Goss texture (fine-grain)*[39]

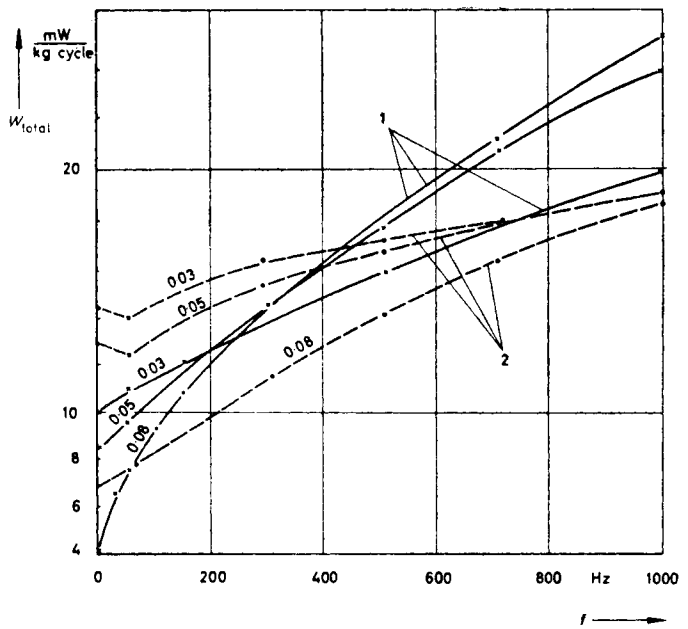



*Figure 10.30. Total loss per cycle for* Fe–Si *toroidal strip-wound cores in relation to frequency: 1, cubic texture; 2, Goss texture*[39]

the more disturbed; with falling thickness this occupies a greater proportion of the whole. Figure 10.30 further shows that the losses in fine-grained Goss-texture sheet are higher than in coarse-grained cubic-texture sheet at low frequency but that the relation is reversed at higher frequencies.

The total losses $W_1$ and $W_{1\cdot5}$ are plotted as a function of direction in Figure 10.31, following Möbius[67]. The comparison with material produced by Goss routines shows that only in the rolling direction, and within an angle of not more than 10° to it, has the Goss sheet somewhat lower losses than the cubic-texture sheet. Later measurements by Ganz[41] confirm this relation. This is not a matter of the different silicon content of the measuring

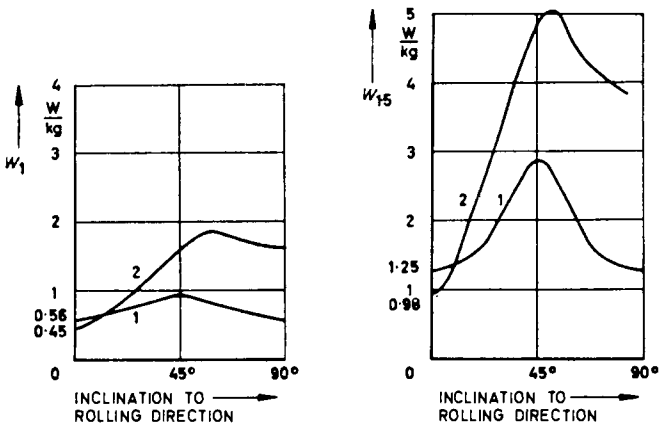



*Figure 10.31. Directionality of overall loss $W_1$ and $W_{1\cdot5}$ (50 Hz) for sheets with Goss texture (0.33 mm thick, 3·1% Si content) and with cubic texture (0·35 mm thick, 2·05% Si content): 1, cubic texture; 2, Goss texture*[67]

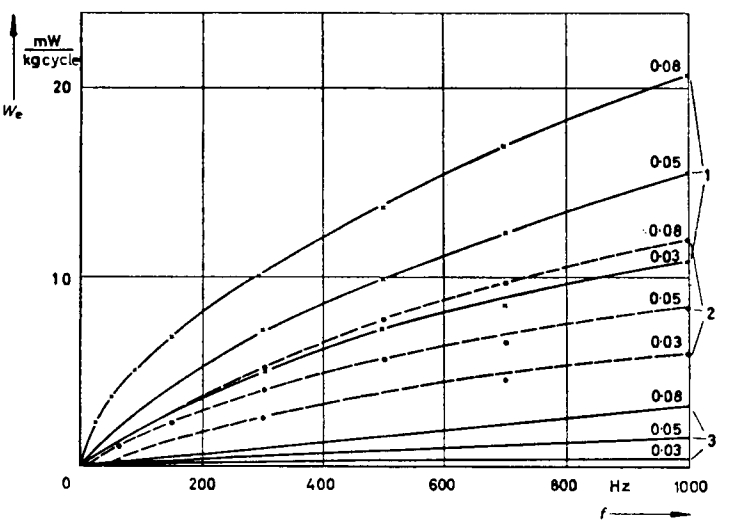



*Figure 10.32. Proportion of eddy-current loss $W_e$ for Fe–Si textured sheet as a function of frequency: 1, cubic texture; 2, Goss texture; 3, calculated*[39]

samples but is a consequence of anomalous eddy-current loss, which appea rs also in the variation with frequency of Figure 10.30.

The rise in loss with frequency is steeper in these materials than one would expect from 'classical' theory. This anomalously large eddy-current component, which has also been observed in other cases, is larger with coarsely crystalline sheet having cubic texture than with finely crystalline Goss sheet. This will be clear from Figure 10.32[39] in which the eddy-current loss, calculated from the formula

$$W_e = \frac{W}{f} = \frac{\pi^2 B^2 D^2 f}{6\varrho}$$

has been plotted against frequency. The same figure shows the eddy-current loss component as the difference between total loss and hysteresis loss. The measured values exceed the values calculated from the hitherto accepted theory by an order of magnitude (see also page 52).

### 10.3.6.4 Further possibilities of improvement in Fe–Si electrosheet

The best figures for the $W_1$ and $W_{1\cdot5}$ loss values hitherto achieved with grain-oriented Fe–Si sheet are about 0·40 W/kg and 0·90 W/kg. Whether in the future further significant improvements are attainable depends on whether it proves possible to improve the alignment of the crystallites and to reduce the anomalous eddy-current loss by producing fine-grain materials. However, fineness of grain, high purity, and well-marked texturing seem, according to present-day knowledge, not to be mutually consistent.

An improvement in magnetic properties would be possible, in principle, by increasing the silicon content, but this would at the same time increase the difficulty of working the material. A further possibility for improving magnetic materials lies in magnetic treatment. In an alloy with 6·5% Si, magnetic treatment leads to a squared hysteresis loop coupled with a maximum permeability of $3\,800\,000\mu_0$, the highest permeability value so far measured[44]. For comparison: for single iron crystals having 3·85% Si, Williams[101] achieved only $\mu_m = 1\,380\,000\mu_0$ in the preferred direction; and Cioffi, Williams, and Bozorth[21] have measured a $\mu_m$ of $1\,330\,000\mu_0$ in single crystals of an Fe–Ni alloy with 66% Ni after magnetic treatment. After a process of magnetic treatment the $W_1$ losses could indeed be brought down to 0·20 W/kg and the $W_{1\cdot5}$ losses down to 0·45 W/kg, according to an estimate by Pawlek[77], but many difficulties stand in the way of commercial realisation.

Basically, Fe–Si alloys can be made in powder form. Reasonable manufacturing techniques seem possible in this way, as against casting methods, especially for highly alloyed materials. The manufacturing costs, however, appear to be rather high[76].

Another method of manufacture, mentioned by Sixtus[89], deserves attention. Silicon, heat treated in an atmosphere of silicon chloride, is precipitated onto a lightly alloyed textured sheet and then, at 1200°C, caused to diffuse homogeneously throughout the body of the material. Experimentally, silicon contents up to 9% were tried. The grain-size of the material is hardly altered

by this procedure, and the texture also remains unchanged. Further development of the process might well lead to interesting theoretical and practical results.

### 10.4 Fe–Al ALLOYS

Aluminium steels were first investigated by Hadfield[58]. Guillet[43], in his book published in 1906, described them perceptively, realising also their potential importance for the design of electrical machines. These and other investigators established the fact that aluminium, as an alloying element with iron, increased the specific electrical resistance in much the same manner as silicon (see Figure 8.1).

The magnetic properties of the Fe–Al alloys, for low aluminium contents, do not greatly differ from those of the Fe–Si alloys: coercivity, hysteresis loss, and saturation flux density fall with increasing aluminium content. Gumlich[48] gives the following relation for saturation density:

$$B_s = (2{\cdot}164 - 0{\cdot}057p)\ \text{V s/m}^2 \tag{10.6}$$

The density $d$ follows a similar formulation up to 5·4% Al (see Figure 7.10):

$$d = (7{\cdot}865 - 0{\cdot}117p)\ \text{g/cm}^3 \tag{10.7}$$

Gumlich obtained higher values of hysteresis loss than for good Fe–Si alloys, using the samples investigated by the Physikalisch-Technische Reichsanstalt. As in the case of silicon, he perceived that an increased aluminium content leads only indirectly to improved quality in that it induces the transformation of pearlitic carbon into a magnetically less harmful form.

In a report in 1925 Gumlich[51] mentioned an Fe–Al steel having 10·85% Al which, despite the high degree of alloying, could yet be rolled and was characterised by a high value of specific electrical resistance $\varrho = 120\ \mu\Omega\,\text{cm}$. In 1940 an iron alloy having 3·5% Al was produced in the Bell Telephone Laboratories by cold rolling and cold drawing and was found to have anisotropic properties[12].

In the rolling direction—the preferred direction of magnetisation—a maximum permeability of 25 000 $\mu_0$ and an $H_c$ of 6·4 A/m were attained. The best value of $\mu_m$ attainable by hot rolling was 13 000$\mu_0$. Cold-drawn rods annealed at 1330°C showed hysteresis losses only one-third to one-quarter of those of cold-rolled sheet measured at 1 V s/m² (see Table 10.9). Following an annealing of the cold-rolled material at 1200°C the orientation of the crystals proved to be optimum: at higher annealing temperatures it became worse again.

Fe–Al alloys up to 17% Al were investigated in Japan, during World War II, by Masumoto and Saito[64]. Above this composition the alloy became paramagnetic. At 16% Al an alloy was produced called Alperm (formed from *al*uminium and *perm*eability) which after quenching from 600°C yielded the following values:

$$\left.\begin{aligned} \mu_m &= 55\,000\mu_0 \\ \mu_i &= 3\,100\mu_0 \\ H_c &= 3{\cdot}2\ \text{A/m} \\ W_h &= 41\ \text{erg/cm}^3 \\ \varrho &= 140\text{–}150\ \mu\Omega\,\text{cm} \end{aligned}\right\} \text{at} \quad B_m = 0{\cdot}3\ \text{V s/m}^2$$

**Table 10.9** CHARACTERISTIC PROPERTIES OF SOME HOT-ROLLED AND COLD-ROLLED Fe–Al ALLOYS (HYSTERESIS LOSS AT $B_m = 1$ V s/m²)[12]

| *Treatment* | $\mu_m$ ($\mu_0$) | $\mu$ *at* 1·4 V s/m² ($\mu_0$) | $H_c$ (A/m) | $W_h$ (erg/cm³) |
|---|---|---|---|---|
| Hot-rolled sheet annealed at 1000°C | 13 000 | 1 600 | 32 | — |
| Cold-rolled sheet annealed at 1000°C | 14 000 | 5 000 | 32 | 1 200 |
| Cold-drawn bar annealed at 1000°C | 16 000 | 7 000 | 32 | 800 |
| Cold-drawn bar annealed at 1330°C | 20 000 | 600 | 8 | 350 |

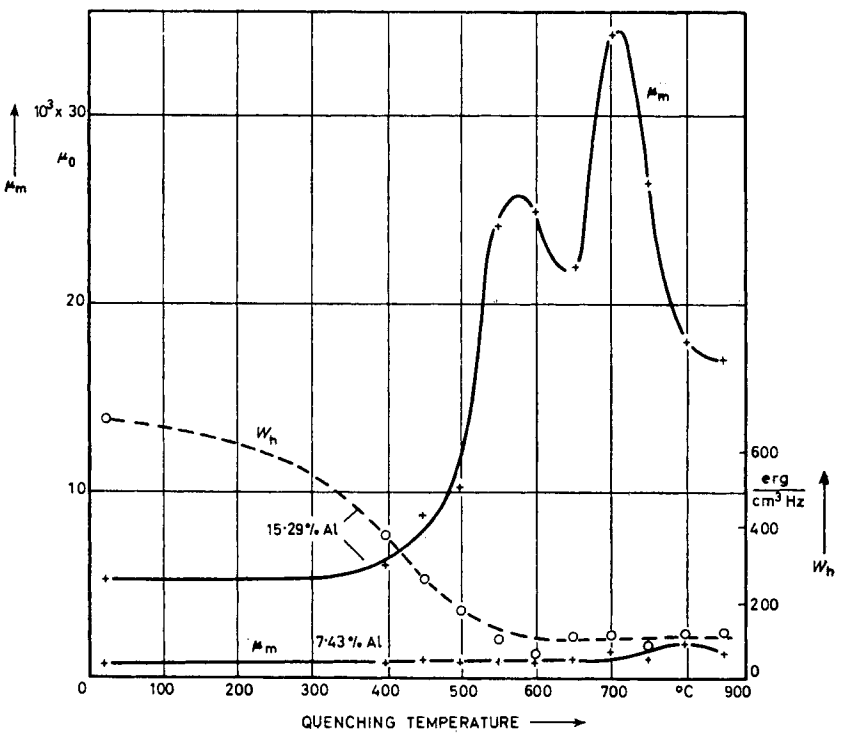



*Figure 10.33. Relation between hysteresis loss $W_h$ at $B_m = 0{\cdot}5$ V s/m² and the quenching temperature for an* Fe–Al *alloy with 15·29%* Al *and also the effect of quenching temperature on maximum permeability $\mu_m$ for* Fe–Al *alloys with 7·43% and 15·29%* Al[64]

For these superstructure alloys, the effect of quenching on the hysteresis loss, coercivity, and remanence is opposite to the effect on permeability (Figure 10.33). The lowest coercivity was obtained with an alloy having 14·87% Al quenched in water from 750°C: the value was 1·6 A/m.

Attempts to develop this material still further were made in the USA after World War II. Nachman and Buehler[71] succeeded in making films 8 μm thick. The material was known by the name Alfenol. To make the test samples, electrolytic iron and 99·99% pure aluminium were used. The alloy was melted in pure hydrogen and the bar material was hot rolled at 1000°C. As the material is very heat-resistant, it could be rolled at even higher temperatures. This, however, would encourage large-grain formation, making further working difficult. A temperature of 575°C proved to be the optimum cold-rolling temperature.

**Table 10.10** COMPARISON OF MAGNETIC PROPERTIES FOR Fe–Si STRIP AND Fe–Al SHEET AT VARIOUS FREQUENCIES FOR $B = 0{\cdot}5$ V s/m²

| *Core type* | *Thickness* | *Core loss* (W/kg) | | |
|---|---|---|---|---|
| | | 60 Hz | 400 Hz | 1000 Hz |
| Oriented Fe–Si strip | 0·025 | — | 2·6 | 7·1 |
| Fe–Al sheet with 16% Al | 0·175 | 0·11 | 1·5 | 6·0 |

Because of the relatively high specific electrical resistance of 153 μΩ cm for an iron alloy, the total losses remain fairly low even at high frequencies. Table 10.10 compares the core losses for cold-rolled Fe–Si strip of 0·025 mm thickness with those of a 0·175 mm sheet, made from Fe–Al with 16% Al, at 0·5 V s/m². In spite of the greater sheet thickness, the Fe–Al material shows less loss at 1 kHz than the Fe–Si alloy[71]. The increase of loss with flux density is plotted for various frequencies in Figure 10.34.

The following further properties of this alloy are worthy of note: it shows no crystallographic texture; it shows less magnetic anisotropy in the turning-moment test than hot-rolled Fe–Si sheet; the hysteresis loop is nevertheless rectangular, as is obvious from Figure 10.35 after Nachman and Buehler[71]. The following data were quoted by Lufcy and Heath[61] for Alfenol:

$$\mu_i = 3450\mu_0 \ (B = 0{\cdot}002 \text{ V s/m}^2)$$
$$\mu_m = 116\,000\mu_0$$
$$H_c = 2 \text{ A/m}$$
$$B_s = 0{\cdot}78 \text{ V s/m}^2$$
$$B_r = 0{\cdot}38 \text{ V s/m}^2$$

Initial permeabilities of $5000–7000\mu_0$ and $B_s$ values of 0·9 V s/m² are quoted for the commercially available Fe–Al alloy with 16% Al, called Vacodur 16; $\varrho = 145$ μΩ cm[94].

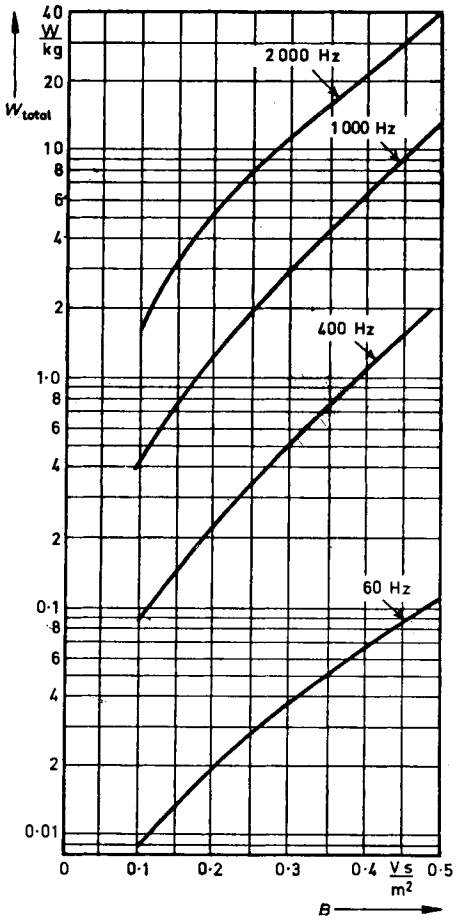



*Figure 10.34. Overall loss for laminated cores of 0·35* mm *sheet of* Fe–Al *with 16%* Al[71]

Thermenol, comprising 16% Al, 3·3% Mo, and remainder iron, is a still later development of these Fe–Al alloys with 16% Al[72]. The characteristic properties of a water-quenched sample are:

$$\varrho = 162\ \mu\Omega\ \text{cm}$$
$$d = 6{\cdot}5\text{–}6{\cdot}6\ \text{g/cm}^3$$
$$\mu_{20} = 7750\mu_0$$
$$\mu_m = 130\,000\mu_0$$
$$H_c = 1\text{–}1{\cdot}5\ \text{A/m}$$
$$B_r = 0{\cdot}25\ \text{V s/m}^2$$
$$B_m = 0{\cdot}6\text{–}0{\cdot}7\ \text{V s/m}^2\ (H_m = 2{\cdot}4\ \text{kA/m})$$

The figures depend on the rate of cooling: the material in this range of

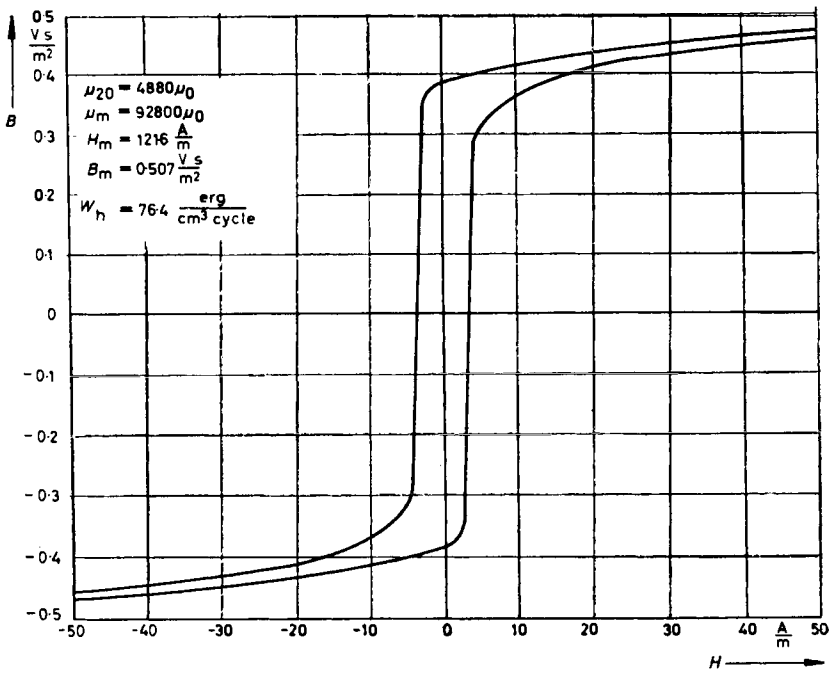



*Figure 10.35. Hysteresis for an* Fe–Al *alloy with 16%* Al[71]

composition is structure-sensitive on account of the directive processes brought into play by slow cooling. Slowly cooled (and therefore well-aligned) samples have low permeability and high coercivity while, conversely, quenched specimens show high permeability and low coercivity[75].

Adams[3] compared Fe–Al alloys and Fe–Si alloys with less than 10% of alloying elements. He found no great difference between the two groups for isotropic alloys subjected to a standard annealing operation at 1000°C in hydrogen. For smaller degrees of alloying, the aluminium alloys were somewhat superior to the silicon alloys; for richer alloys it is the other way round. The figures are given in Table 10.11.

The loss values, originally quoted in W/lb at 60 Hz, were here converted to W/kg at 50 Hz by multiplying by a factor of 1·74. The $B_m$ values hold for $H_m = 2{\cdot}4$ kA/m. The two last values in the table were measured for specimens which had been annealed in a magnetic field of 135 A/m. The Fe–Al alloys with an aluminium content less than 12% are, like the Fe–Si alloys, affected by annealing in a magnetic field. Figure 10.36 shows results obtained by Helms[53]: in the range 8–10% Al, the maximum obtainable permeability involves an annealing in a magnetic field of 135 A/m. The quoted value of $50\,000\mu_0$ can, indeed, be reached by alloys having more than 12% Al without this magnetic treatment, but the deformability of the less-rich alloy is better.

A cubic texture can be produced in Fe–Al alloys with 3% Al[96]. Foster and Pavlovic[36] achieved a 70% alignment in 0·6 mm sheet. At 800 A/m the flux

**Table 10.11** COMPARISON OF MAGNETIC PROPERTIES OF Fe–Si AND Fe–Al ALLOYS[3]

| *Aluminium or silicon content** (%) | $f = 0$ | | | | | $f = 50$ Hz |
|---|---|---|---|---|---|---|
| | $\mu_{20}$ ($\mu_0$) | $\mu_m$ ($\mu_0$) | $H_c$ (A/m) | $B_r$ (V s/m²) | $B_m$† (V s/m²) | $W_1$ (W/kg) |
| 1·0 Al | 2 041 | 20 214 | 26·32 | 1·4101 | 1·6348 | 1·22 |
| 0·94 Si | 860 | 14 780 | 35·36 | 1·4140 | 1·6400 | 1·20 |
| 3·0 Al | 1 923 | 12 815 | 36·00 | 1·3741 | 1·6278 | 1·22 |
| 2·81 Si | 1 720 | 17 440 | 15·36 | | 1·5340 | 0·99 |
| 5·0 Al | 2 381 | 12 625 | 26·32 | 1·0153 | 1·5446 | 1·12 |
| 4·8 Si | 1 410 | 17 160 | 16·08 | 0·7410 | 1·5230 | 0·75 |
| 8·0 Al | 513 | 3 461 | 44·00 | 0·3242 | 1·3392 | 1·86 |
| 6·4 Si | 1 720 | 28 860 | 11·76 | 1·1310 | 1·4050 | 0·70 |
| 8·0 Al‡ | 1 140 | 50 900 | 21·42 | 1·0900 | 1·2800 | 0·78 |
| 6·4 Si‡ | 1 390 | 66 940 | 15·76 | 1·2100 | 1·4600 | 0·64 |

* Annealed at 1 000°C in hydrogen.
† $H_m$ = 2·4 kA/m.
‡ Annealed in a magnetic field of 135 A/m.

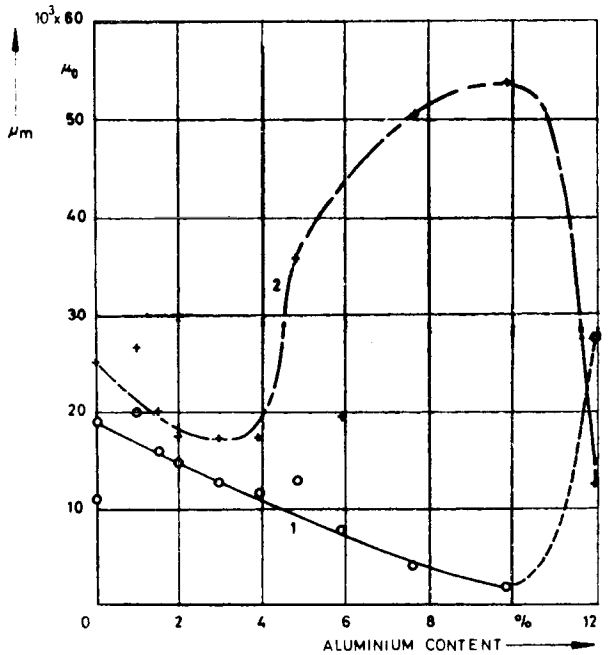



*Figure 10.36. Susceptibility of* Fe–Al *alloys to annealing in a magnetic field of 135* A/m: *1, annealed without field; 2, annealed with field*[53]

density was 1·6 V s/m² parallel to the rolling direction and 1·53 V s/m² in the perpendicular direction, while at 45° only 1·39 V s/m² was obtained. The texture was less well developed in thinner sheets. The coercivity $H_c$ was 20 A/m in the rolling direction and 23·2 A/m transversely. The corresponding loss figures at 60 Hz and 1·5 V s/m² were 4·39 W/kg and 5·10 W/kg.

That the useful properties of Fe–Al alloys have so far made little impact on the manufacture of electrosheet may be because Fe–Si alloys are more easily melted and because, at one time at least, it was harder to get the aluminium into solution. By the use of modern induction furnaces, however, it should now be possible largely to overcome these difficulties[3].

## 10.5 Fe-Si-Al ALLOYS

Aside from a few pioneering efforts, such as the patent[74] granted in 1918 for an Fe–Si–Al alloy with carbon below 0·25% and Al+Si up to 7%, the first thorough investigations of the ternary alloys of iron, silicon, and aluminium were undertaken by the Kaiser Wilhelm Institute for Iron Studies. Wever and Hindrichs[99] found that, at some 4% Si and 0·5% Al, $W_1$ values of 1·1 W/kg could be obtained for sheet 0·35 mm thick, with corresponding $W_{1·5}$ values of about 3 W/kg. With less silicon content they observed higher power losses. Table 10.12 gives the measured results.

Round about the same time (1932), Masumoto[63] found that for an iron alloy with 9·6% Si and 5·4% Al an initial permeability of 35 100$\mu_0$ was obtainable. The magnetic and electrical properties of this range of alloys are given in Table 10.13, based on tests made by him on 150 samples, and it will be seen that the value quoted above appears therein as a maximum. The symbol $B_{\mu m}$ in the table indicates the flux density at which maximum permeability is found. The hysteresis loss $W_h$, the remanence $B_r$, and the coercivity $H_c$ were measured at 1 V s/m² for the first three entries in the table and at 0·5 V s/m² for the remainder. The measuring field strength for the magnetisation amounted to 96 kA/m. The temperature coefficient $\alpha$ of the specific electrical resistance is given for the range 0°–40°C.

All magnetic values were determined ballistically using cast toroidal cores. It is evident from the results that an optimum occurs for about 9·62% Si, 5·38% Al, remainder iron, at which a maximum permeability of 117 500$\mu_0$ and a coercivity of 1·8 A/m are registered. The hysteresis loss came to 28 erg/cm³ per cycle. Moreover, the specific electrical resistance is high, so eddy currents are low.The material could nevertheless not be introduced for transformer cores as it is difficult to work by reason of its brittleness. However, it can be readily powdered and is therefore mainly used in the dust cores of light-current engineering (see Sendust, page 53).

Only with the development of the processes of powder metallurgy, such as the sintering of dust pressings, did the way seem open in recent times for the use of the ternary Fe–Si–Al alloys in heavy-current engineering[3]. By casting a slurry of the powder followed by sintering, a power loss of 0·37 W/kg was attained for sheets of 0·55 mm[4]. Using loosely sintered (therefore unpressed) powder, it was possible to achieve a density of 6·3 g/cm³, an initial permeability of 11 500$\mu_0$, and a coercivity of 6·4 A/m.

**Table 10.12** POWER LOSS AND SPECIFIC ELECTRICAL RESISTANCE OF Fe–Al–Si SHEET[99]

| *Silicon content* (%) | *Aluminium content* (%) | *D* (mm) | $W_1$ (W/kg) | | $\varrho$ (μΩ cm) |
|---|---|---|---|---|---|
| | | | $D$ = 0·35 mm | $D$ = 0·5 mm | |
| 4·33 | 0·25 | 0·55 | 1·12 | 1·27 | 76·8 |
| 4·03 | 0·38 | 0·41 | 1·03 | 1·20 | — |
| 3·95 | 0·59 | 0·36 | 1·08 | 1·22 | — |
| 3·91 | 0·62 | 0·36 | 1·05 | 1·20 | — |
| 3·29 | 0·28 | 0·66 | 1·20 | 1·35 | 60·5 |
| 3·06 | 1·39 | 0·59 | 1·12 | 1·27 | 69·9 |
| 2·65 | 1·16 | 0·61 | 1·14 | 1·29 | 65·7 |
| 2·41 | 3·37 | 0·44 | 1·19 | 1·34 | — |
| 2·40 | 2·98 | 0·38 | 1·21 | 1·36 | — |
| 2·35 | 1·81 | 0·46 | 1·12 | 1·27 | — |
| 2·34 | 0·28 | 0·62 | 1·43 | 1·58 | 46·8 |
| 2·31 | 1·64 | 0·58 | 1·21 | 1·36 | 64·8 |
| 2·28 | 0·98 | 0·38 | 1·27 | 1·42 | — |
| 2·10 | 0·25 | 0·37 | 1·38 | 1·53 | — |
| 2·02 | 0·24 | 0·37 | 1·37 | 1·52 | — |
| 1·90 | 0·74 | 0·35 | 1·52 | 1·68 | — |
| 1·81 | 0·63 | 0·65 | 1·69 | 1·84 | 44·1 |
| 1·63 | 0·27 | 0·58 | 1·71 | 1·86 | 38·7 |
| 1·51 | 1·74 | 0·55 | 1·37 | 1·52 | 57·4 |
| 1·47 | 0·52 | 0·61 | 1·55 | 1·70 | 41·6 |
| 1·44 | 0·35 | 0·59 | 1·77 | 1·92 | 138·2 |
| 1·13 | 1·53 | 0·57 | 1·59 | 1·74 | 50·6 |
| 1·13 | 1·41 | 0·53 | 1·49 | 1·64 | 50·3 |
| 0·95 | 0·99 | 0·34 | 1·66 | 1·82 | — |
| 0·94 | 1·12 | 0·53 | 1·74 | 1·89 | 41·9 |
| 0·90 | 0·68 | 0·51 | 1·76 | 1·91 | 32·6 |
| 0·90 | 0·29 | 0·48 | 2·08 | 2·20 | 29·7 |
| 0·80 | 0·04 | 0·49 | 2·06 | 2·19 | 25·5 |
| 0·61 | 0 .7 | 0·53 | 1·96 | 2·14 | 33·5 |
| 2·12 | 1·51 | 0·37 | 1·68 | 1·83 | — |

Another possible process for working Sendust is the following[53a]: a Sendust powder is made with about 25% Fe missing from its composition, and the iron is mixed in as powder; the powdered mixture is then rolled out to a strip of 0·8 mm; after heat treatment and a further rolling to 0·3–0·48 mm, the sheets are stamped out and are sintered at 1300°C in an atmosphere of argon. In this way values of $\mu_{20} = 12\,000\mu_0$, $\mu_m = 28\,600\mu_0$, and $H_c = 8{\cdot}6$ A/m are obtained.

Seeger[87] mentions an unfavourable property of the Fe–Si–Al alloys with high aluminium content: in one type of sheet having 2·99% Si and 0·12% Al, the additional loss $\Delta W$ due to machining the stack of sheets is 0·31 W/kg measured at 1 V s/m². In another type of sheet, however, with 2·40% Si and 0·43% Al, the value $\Delta W$ was 1·22 W/kg. The aluminium content favours ridge formation in the sheet and this increases the eddy currents. He therefore specified that, having regard to deformation losses, the aluminium content should not exceed 10% of the silicon content.

**Table 10.13** MAGNETIC AND ELECTRICAL PROPERTIES OF Fe–Al–Si ALLOYS[63]

| *Silicon content* (%) | *Aluminium content* (%) | $\mu_i$ ($\mu_0$) | $\mu_m$ ($\mu_0$) | $B_{\mu m}$ (V s/m$^2$) | $W_h$ (erg/cm$^3$) | $B_r$ (V s/m$^2$) | $H_c$ (A/m) | $J$ (V s/m$^2$) | $\varrho$ ($\mu\Omega$ cm) | $\alpha$ (ppm/K) |
|---|---|---|---|---|---|---|---|---|---|---|
| 8·57 | 5·61 | 6 500 | 20 500 | 0·287 | 522 | 0·390 | 16 | — | 74·7 | 3 260 |
| 8·78 | 5·59 | 14 000 | 78 600 | 0·330 | 113 | 0·440 | 4 | — | — | — |
| 9·37 | 5·59 | 28·400 | 85 300 | 0·460 | 87 | 0·490 | 3 | — | 83·5 | 2 010 |
| 9·62 | 5·38 | 35 100 | 117 500 | 0·390 | 28 | 0·335 | 1·8 | 1·1 | 81·2 | 2 810 |
| 10·00 | 5·57 | 14 300 | 88 200 | 0·388 | 106 | 0·450 | 3·4 | — | 95·8 | 2 260 |
| 10·38 | 5·58 | 16 000 | 19 500 | 0·021 | 16 | 0·030 | 1·2 | — | — | — |
| 10·69 | 5·39 | 5 200 | 25 600 | 0·333 | 108 | 0·380 | 7·3 | — | — | — |
| 11·63 | 5·35 | 1 300 | 4 590 | 0·184 | 293 | 0·195 | 20 | — | 98·5 | 500 |

## 10.6 Fe-Co ALLOYS

Motor manufacturers desire a dynamo sheet whose magnetic saturation is as high as possible. It has been known since the investigations of Weiss and Forrer[98] in 1928 that only Fe–Co alloys with a cobalt content up to 75% yield higher saturation values than pure iron (Figure 10.37). Maximum saturation of these Fe–Co alloys occurs at 35% Co. Even here, however, the improvement of some 10% must be dearly paid for since cobalt is a costly metal which is not so frequently found in the upper part of the earth's crust as, for example, iron. It is even 15 times rarer than nickel with which it is often found.

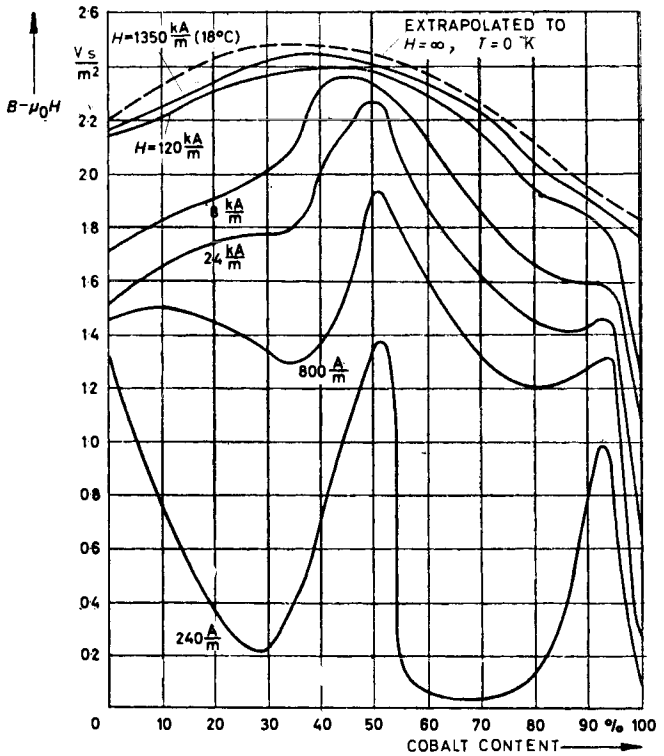



*Figure 10.37. Polarisation of* Fe–Co *alloys at various field strengths*[12, 98]

The use of Fe–Co alloys in the design of electric machinery is limited, therefore, to the rare cases where the high price seems justified (generators and servomotors in aircraft).

Two alloy types have become familiar: 50% Fe with 50% Co to which 1·7% V has been added to make rolling easier; and 64% Fe, 35% Co, and 1% V or 1% Cr. Both alloys are of low carbon content: it is well below 0·1%, as it should be for all electrosheet. In practice they contain less than 0·005% C.

Figure 10.38, following Brailsford and co-workers[15], shows the superiority of these two alloys as against an ordinary dynamo sheet. The total iron loss at 1·4 V s/m² seems to correspond to that of dynamo sheet with 1% Si at the usual frequencies of heavy-current engineering. At high densities the losses in Fe–Co sheet appear to be more favourable. Gould and Wenny[46]

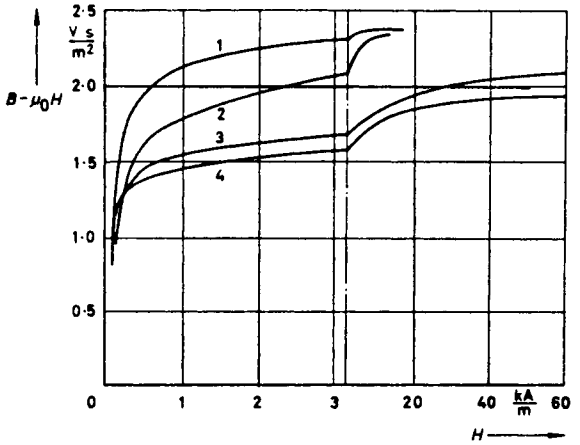



*Figure 10.38. Magnetising characteristics: 1, 50% Co, 50% Fe; 2, 35% Co, 64·5% Fe, 0·5% Cr; 3, ordinary dynamo sheet (about 99·6% Fe); 4, transformer sheet (96% Fe, 4% Si)*[15]

obtained, even at the lower densities, lower losses using an Fe–Co–V alloy called Supermendur than for grain-oriented steel sheet. For 0·1 mm strip at 400 Hz they quote losses, at 1·5 V s/m², of 19·5 W/kg for Fe–Si and 12·1 W/kg for magnetically pretreated Supermendur strip of the same thickness (see page 368). For Vacoflex 48, which also has about 50% Co, losses of 25 W/kg are quoted at 400 Hz and 2 V s/m² for 0·1 mm strip[93c].

## 10.7 FERRITE CORES FOR POWER TRANSFORMERS

Losses in transformer cores rise more or less quadratically with increasing frequency; it is especially the eddy-current losses which are responsible for the rise. The use of thin laminae with high specific electrical resistance is one means of minimising the loss. The specific electrical resistance of alloy sheet can, however, even in the most favourable case, be raised to only a little over 0·1 mΩ cm.

The ferrites have, in principle, a much higher resistance; for high-permeability Mn–Zn ferrite it is higher by a factor of $10^6$. By using cores of this material, power transformers can be built which introduce no eddy currents to speak of, even up to 20 kHz. Such transformers are used, in television apparatus, for example[93]. As line output transformers, they are driven at 10–15 kHz for the forward sweep and at 60 kHz for fly-back.

According to measurements made by Fälker and Hücking[34], a hysteresis loss of 36–48 mW/cm³ and a total loss of about 43–58 mW/cm³ are obtained

in U-cores at $f = 15$ kHz and $B_m = 0{\cdot}1$ V s/m$^2$. The ratio of total loss to hysteresis loss lies between 1·1 and 1·2.

The alternating-field permeability of ferrite transformer cores depends to a large degree on the kind and quality of the material and on the flux excursion. The flux densities used are generally from 0·1 V s/m$^2$ to 0·2 V s/m$^2$. Even materials having more or less the same initial permeability can differ widely in permeability at higher flux densities. Figure 10.39 shows this for two similar cores of different manufacture[34]. For comparison, the function $\mu = f(B)$ for flake iron, taken from Figure 10.4, is plotted (broken line); this is the material used in the cores of television transformers in the early days.

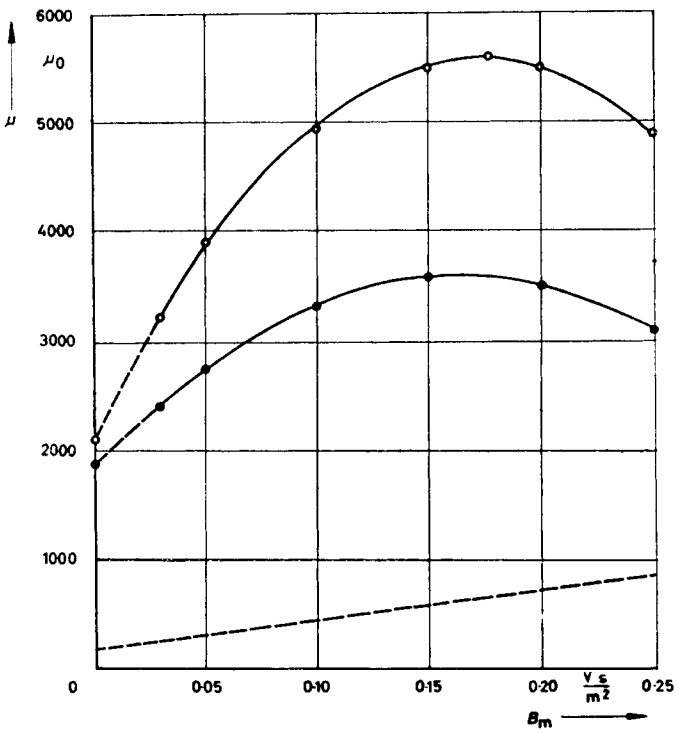



*Figure 10.39. Alternating-field permeability in relation to peak flux density $B_m$ for two transformer cores of different origin (broken line indicates flake iron, see Figure 10.4)*[34]

No systematic connection between permeability and loss has been observed for ferrite cores. Joksch[54] found that the power loss per unit volume of core could be represented by the following empirical formula:

$$W = Af^{K_1}B_m^{K_2}$$

Constants $K_1$ and $K_2$ lie within the following limits for various materials:

$$1 < K_1 < 1{\cdot}3$$

$$1{\cdot}85 < K_2 < 2{\cdot}1$$

The factor $A$ is a material constant which, for U-cores, takes values between 150 A m/V s and 350 A m/V s. Deviations from the value 1 for $K_1$ can be explained as an eddy-current effect; $K_2$ corresponds to the Steinmetz coefficient (see page 130). As an example, the losses will be calculated for a transformer core where $A = 200$ A m/V s, $K_1 = 1$, and $K_2 = 2$ for $f = 15$ kHz, while $B = 0{\cdot}2$ V s/m$^2$. Then

$$W = 200 \times 0{\cdot}04 \times 15 \times 10^{-3} \frac{\text{A m}}{\text{V s}} \left(\frac{\text{V s}}{\text{m}^2}\right)^2 \frac{1}{\text{s}}$$

$$= 120 \text{ mW/cm}^3$$

$$= 25 \text{ W/kg}$$

if $d$ is taken as 4·8 g/cm$^3$. Meyer[66a] investigated the relation between core loss and overall loss. In general, the losses mount with rising temperature.

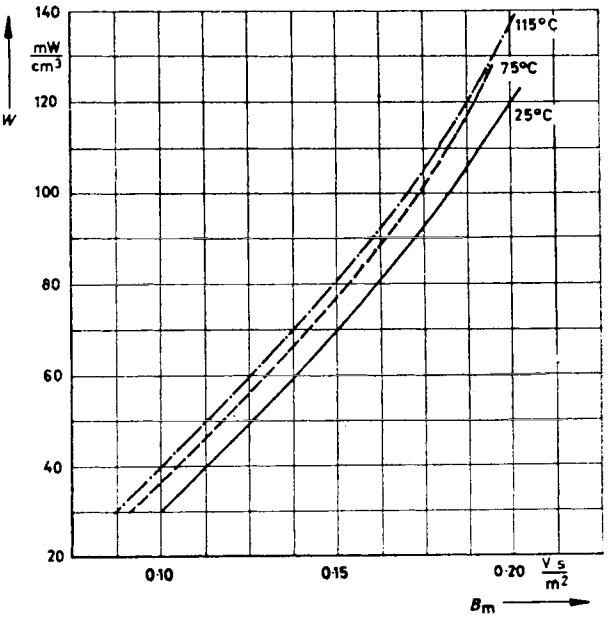



*Figure 10.40. Losses in a ferrite core (Keraperm 20 505); flux density sinusoidal at $f = 15$ kHz*[92]

Figure 10.40 illustrates this[92]. Materials have been developed, however, having almost constant loss over a wide temperature range[92]. If falling losses with rising temperature can be achieved, additional heating of the core is avoided. Ferrite cores having this property are currently available[94a].

## REFERENCES


1. ACKERMANN, F. W.: Über die Herstellung und die magnetischen Eigenschaften der C-Kerne (T. Mitt. Krupp **13** (1955) 98–103).
2. ACKERMANN, F. W.: Trennfugen in weichmagnetischen Kreisen geringer Induktionsbelastung (T. Mitt. Krupp **14** (1956) 18–23).
3. ADAMS, E.: Recent developments in soft magnetic alloys (J. A. P. **33** (4) (1962) 1214–1220).
4. ADAMS, E. and HUBBARD, W. M.: Sintered magnetic alloy and methods of production. US Pat. 2 988 806 (20. 6. 61).
5. ARMCO STEEL CORP., MIDDLETOWN: Magnetic ingot iron for dc applications (1959).
6. ASSMUS, F. and BOLL, R.: Schnittbandkerne als neue Form weichmagnetischer Werkstoffe (ETZ-A **75** (1954) 221–225, 292).
7. ASSMUS, F. and BOLL, R.: Kleinere Transformatoren durch Schnittbandkerne (Elektronik **4** (1955) 220–223).
8. ASSMUS, F., DETERT, K. and IBE, G.: Über Eisen-Silizium mit Würfeltexturen. Ausbildung der Textur (Z. Metallkde. **48** (6) (1954) 344–349).
9. V. AUWERS, O.: Über den Einfluss der Korngrösse auf die magnetischen Eigenschaften silizierter Bleche (Z. techn. Phys. **6** (1925) 578–582).
10. V. AUWERS, O.: Über den Einfluss der Korngrösse auf die magnetischen Eigenschaften II. (Z. techn. Phys. **9** (1928) 475–478).
11. BARRETT, W. F., BROWN, W. and HADFIELD, R. A.: Researches on the electrical conductivity and magnetic properties of upwards of one hundred alloys of iron (J. IEE **31** (1902) 574–729).
12. BOZORTH, R. M.: Ferromagnetism. Van Nostrand Co. Inc., Toronto/New York/London (1951).
13. BRAILSFORD, F.: Magnetic Materials. Methuen & Co. Ltd, London/John Wiley & Sons Inc., New York (1951).
14. BRAILSFORD, F. and MAZZA, V. R.: Transformer flux distribution (Electr. Rev. **171** (25) (1962) 979–980; Proc. IEE **109 A** (1962) 173).
15. BRAILSFORD, F., OLIVER, D. A., HADFIELD, D. and POLGREEN, G. R.: Magnetic Materials (J. IEE (I) **95** (96) (Dec. 1948) 522–543).
16 Brit. Pat. 2273 AD 1904 (12. 6. 03).
17. BROWN, E. H. and BRENNAND, J. R.: Magnetic losses at low temperatures (J. A. P. **30** (1) (Jan. 1959) 112–114).
18. BUNK, W., LÜCKE, K. and MASING, G.: Zur Anwendung des Zählrohres für die Texturbestimmung (Z. Metallkde. **45** (1954) 269–275, 311).
19. CAMPBELL, G. and WOOD, F. J.: A laminated flake-iron powder for use at audio and ultrasonic frequencies; in Soft magnetic materials for telecommunications (ed. Richards and Lynch) (1953) 268–277).

19a C. D. WÄLZHOLZ, HOHENLIMBURG: Magnetweicheisen.

20. CIOFFI, P. P.: New high permeabilities in hydrogen treated iron (Phys. Rev. **45** (1934) 742).
21. CIOFFI, P. P., WILLIAMS, H. J. and BOZORTH, R. M.: Single crystals with exceptionally high magnetic permeabilities (Phys. Rev. **51** (1937) 1009).
22. CLEAVES, H. E. and HIEGEL, J. M.: Properties of high purity iron (J. Res. Nat. Bur. Stds. **28** (1942) 643–667, R. P. 1472).
23. COLE, G. H.: Grain-oriented iron–silicon alloys (El. Engng. **72** (1953) 411–416).
24. CZERLINSKY, E.: Die Eigenschaften handelsüblicher warmgewalzter Dynamobleche (Arch. Eisenhüttenw. **27** (1956) 35–40).
25. DAEVES, K.: Der Einfluss der Korngrösse auf die Verlustziffern von Dynamo- und Transformatorenblechen (Stahl u. Eisen **44** (1924) 1283–1286).

26. DAEVES, K.: Der Einfluss des Siliziums auf die magnetischen Eigenschaften der Stähle (Z. Elektrochem. **32** (1926) 479–481).
27. DIETRICH, H.: Magnetische Eigenschaften von Sintereisen (Z. Metallkde. **52** (1961) 232–235).
27a DIN 41 309, Schnittbandkerne (Oct. 1967).
28. DIN 46 400, Kalt- und warmgewalztes nichtkornorientiertes Elektroblech und -band. (1971).
29. DIN 50 461, Testing of steel. Determination of the magnetic properties of electrical steel sheet in the 50 cm Epstein frame.
30. DIN 50 462, Testing of steel. Determination of the magnetic properties of electrical steel sheet in the 25 cm Epstein frame.
31. DIN 50 463: Bestimmung der Dichte von Elektroblech aus Eisen-Silizium-Legierungen (Dec. 1965).
31a DUFTSCHMID, F., SCHLECHT, L. and SCHUBARDT, W.: Die technische Verarbeitung von pulverförmigem Carbonyleisen nach dem Sinterverfahren (Stahl u. Eisen **52** (1932) 845–849).
32. DUNN, C. G.: On the determination of preferred orientations (J. A. P. **30** (6) (June 1959) 850–857).
33. ELSNER, R.: Grenzleistungen von Transformatoren (ETZ-A **76** (1955) 867–868).
34. FÄLKER, R. and HÜCKING, E. E.: Magnetische Messungen an Ferrit-U-Kernen für Horizontal-Ausgangsübertrager (Elektron. Rdsch. (8) (1958) 270–274).
35. FAST, J. D.: The influence of the recrystallization texture of cold-rolled 3% silicon iron (Phil. Res. Rep. **11** (1956) 490–491).
36. FOSTER, K. and PAVLOVIC, D.: Magnetic properties of oriented 3% aluminium iron sheets (J. A. P. **34** (Apr. 1963) 1325–1326).
37. FRANCK, S. and RUDOLPHI, A.: Über die Abhängigkeit der Induktion von der Walzrichtung bei Dynamoblechen (ETZ **60** (17) (1939) 503–505).
38. FRIEDR. KRUPP, WIDIA-FABRIK, ESSEN: D. 546 Hyperm, Magnetisch weiche Sonderwerkstoffe.
39. GANZ, D.: Textur und Verlustprobleme bei Si Fe (Ber. Arb. Ferrom. (1959) Stahleisen (1960) 59–65).
40. GANZ, D.: Private communication.
41. GANZ, D.: Über die Richtungsabhängigkeit magnetischer Eigenschaften von 3% Silizium-Eisen-Blechen mit Goss- und Würfeltextur (Z. ang. Phys. **14** (5) (1962) 313–322).
42. GERLACH, W.: Eiseneinkristalle (Z. Phys. **38** (1926) 828–840).
43. GUILLET, L.: Etude industrielle des alliages metalliques. Dunod, Paris (1906) 367, 930).
44. GOERTZ, M.: Iron–silicon alloys heat treated in a magnetic field (J. A. P. **22** (1951) 964–965).
45. GOSS, N. P.: Electrical sheet and method and apparatus for its manufacture and test. US Pat. 1965 559; Verfahren zur Verbesserung der Eigenschaften von Transformatoren- und Dynamoblechen aus warmgewalztem Siliziumstahl. DRP 763 989.
46. GOULD, H. L. B. and WENNY, D. H.: Supermendur (El. Engng. **76** (Mar. 1957) 208–211).
47. GUMLICH, E.: Über das Verhältnis der magnetischen Eigenschaften zum elektrischen Leitvermögen magnetischer Materialien (ETZ **23** (1902) 101–102).
48. GUMLICH, E.: Magnetische Messungen. Friedr. Vieweg & Sohn, Braunschweig (1918).
49. GUMLICH, E.: Über die Abhängigkeit der magnetischen Eigenschaften, des spezifischen Widerstandes und der Dichte der Eisenlegierungen von der chemischen Zusammensetzung und der thermischen Behandlung (Wiss. Abh. P. T. R. **4** (3) (1918) 267–420).
50. GUMLICH, E.: Diskussionsbemerkung. (Trans. AIEE **43** (1924) 173).
51. GUMLICH, E.: Neuere Fortschritte in der Herstellung ferromagnetischer Stoffe (Z. techn. Phys. **6** (1925) 670–682).

52. HARMS, H. B.: Magnetic materials in ultra high temperature electronic transformers (El. Engng. **77** (1958) 408–412; ETZ-B (1959) 18).
53. HELMS, H. H.: see Ref. 3.
53a HELMS, H. H. and ADAMS, E.: Sendust sheet processing techniques and magnetic properties (J. A. P. **35** (3) (1964) 871–872).
53b IEC Publication 329 (1971): Strip wound cut cores of grain oriented silicon–iron alloy used for electronic and telecommunication equipment.
54. JOKSCH, CH.: Ferritkerne in Horizontal-Ausgangs-Transformatoren (Radiomentor 26 (1960) 102–107).
55. JURASEK, L.: Wandertransformator mit kaltgewalzten Kernblechen (CEG-Berichte 2 (2) (1956) 74–75).
56. KETTLER, H.: Entwicklungstendenzen im Messwandlerbau (Siemens-Z. 31 (1957) 427–434).
57. KUSSMANN, A., SCHARNOW, B. and MESSKIN, W. S.: Gekupferter Stahl für Dynamo- und Transformatorenbleche (Stahl u. Eisen **50** (1930) 1194–1197).
58. HADFIELD, R. A.: Aluminium-Steel (J. Iron Steel Inst. (II) (1890) 161–230).
59. LAMME, B. G.: Eisenverluste an Gleichstrommaschinen (Proc. AIEE (Mar. 1916); E. u. M. **34** (1916) 422–423).
60. LANG, A.: Magnetische Verstärker für die Steuerungs- und Regelungstechnik (ETZ-B **8** (4) (1956) 120–123).
61. LUFCY, C. W. and HEATH, W. T.: Alloy improves magnetic recording (Electronics (June 1955) 137–139).
62. MARKUSZEWICZ, M. J.: Effect of some impurities on grain growth and magnetic anisotropy of 3·25% silicon-iron strips (J. Iron Steel Inst. **200** (3) (1962) 223–228).
63. MASUMOTO, H.: On a new alloy 'Sendust' and its magnetic and electric properties (Sci. Rep. Tohoku Imp. Univ. **25** (1936) 388–402).
64. MASUMOTO, H. and SAITO, H.: On the effect of heat treatment on the magnetic properties of iron–aluminium alloys, II. The change of permeabilities, intensity of magnetization and magnetic hysteresis loss due to quenching and a new alloy 'Alperm' (Sci. Rep. Res. Tohoku Imp. Univ. (A) **4** (1952) 321–337).
65. MAY, J. E. and TURNBULL, D.: Effect of impurities on the temperature dependence of the (110) [001] texture in silicon iron (J. A. P. **30** (4) (Apr. 1959) 210S–212S).
66. MEYER, H. H. and FAHLENBRACH, H.: Magnetische Werkstoffe für Wandler, insbesondere Messwandler (T. Mitt. Krupp **7** (1939) 123–132).
66a MEYER, M.: U-Kern-Eigenschaften und ihre Bedeutung für die Horizontalablenkung (Valvo-Ber. VI (4) (1960) 107–120).
67. MÖBIUS, H. E.: Die Richtungsabhängigkeit der magnetischen Eigenschaften bei Silizium-Eisen-Legierungen mit Würfellage (Ber. Arb. Ferrom. (1959). Stahleisen (1960) 175–180).
68. MÖBIUS, H. E. and PAWLEK, F.: Die Würfellage als Rekristallisationstextur bei Eisen-Silizium-Legierungen (Arch. Eisenhüttenw. **29** (7) (July 1958) 423–432).
69. MÖLLER, H. and STÄBLEIN, H.: Walztexturen von Transformatorenstahl (Arch. Eisenhüttenw. **29** (6) (June 1958) 377–390).
70. V. MOOS, M., OERTEL, W. and SCHERER, R.: Glühversuche zur Verbesserung von Transformatorenblechen (Stahl u. Eisen **48** (1928) 477–485).
71. NACHMANN, J. F. and BUEHLER, W.: 16 percent aluminium-iron alloy cold rolled in the order-disorder temperature range (J. A. P. **25** (3) (Mar. 1954) 307–313).
72. NACHMANN, J. F. and BUEHLER, W. J.: Thermenol—a new 'soft' magnetic alloy (El. Manuf. (Nov. 1956) 140–145, 354).
73. N. N.: Leitsätze für Prüfungen und Lieferbedingungen für Magnetbleche (Bull. Ass. Suisse electr. **44** (1953) 121–124).
74. OBERSCHLESISCHE EISENINDUSTRIE AG F. BERGBAU U. HÜTTENBETRIEB IN GLEIWITZ: Widerstandsmaterial. DRP 359 610 (1. 11. 18).
75. PAVLOVIC, D. and FOSTER, K.: Effect of atomic ordering on magnetic properties of 10

to 17 weight percent aluminium iron alloys (Proc. Conf. Magn. Mat., Boston (1956) 251–257).

75a PAVLOVIC, D. M. and CLARK, J.J.: High temperature tape-wound cores for space power applications (Proc. Electronic Components Conf. IEEE, New York (May 1968) 180–190).

76. PAWLEK, F.: Magnetische Werkstoffe. Springer, Berlin/Göttingen/Heidelberg (1952).

77. PAWLEK, F.: Zukunftsaussichten für die Entwicklung magnetischer Werkstoffe (ETZ-A **80** (17) (Sept. 1959) 561–565).

78. PILLING, N. B.: Low temperature brittleness in silicon steels (Trans. AIMME **69** (1923) 780–790).

78a REICHE, H.: Der Einsatz von siliziumfreien Elektroblechen in kleinen Asynchronmotoren (Elektrie (7) (1965) 288–290).

79. REINBOTH, H.: Ein neuer Kernwerkstoff für Wechselfeld-Magnetisierung (Nachrichtentechn. **6** (1956) 196–198).

80. ROLF, E. and DIETZ, H.: Neuzeitliche Kernwerkstoffe und Kernbauformen für magnetische Verstärker (Siemens-Z. **30** (1956) 73–80).

81. RUDER, W. E.: Grain growth in silicon steel (Trans. Am. Inst. Min. Eng. **47** (1914) 569–586).

82. RUDER, W. E.: New magnetic materials (Proc. IRE (1942) 437–440).

83. RUESS, L.: Zur Bestimmung der Ummagnetisierungsverluste hochwertiger Elektrobleche (ETZ-B **8** (1956) 229–232).

84. RUESS, L.: Über die Richtungsabhängigkeit magnetischer Eigenschaften von Elektroblechen und ihre Messung (ETZ-A **80** (1959) 588–593).

85. SCHÄFER, W.: Transformatoren. de Gruyter & Co., Berlin (1949).

86. SCHLÜTER, H. and STÄBLEIN, F.: Kaltgewalzte Dynamobänder (ETZ-A **80** (1959) 576–582).

87. SEEGER, D.: Erhöhung der Eisenverluste von Dynamoblechen durch verschiedene Bearbeitungsvorgänge beim Bau elektrischer Maschinen (ETZ-A **84** (1963) 622–627).

88. SIXTUS, K.: Neue magnetische Werkstoffe und ihre Bedeutung für die technische Entwicklung (ETZ-A **77** (1956) 790–799).

89. SIXTUS, K.: Magnetfeldglühung von Eisen-Silizium-Blechen mit 3 bis 9% Silizium (Z. ang. Phys. **14** (1962) 241–243).

90. SOMMERKORN, G.: Vorrichtung zur röntgenographischen Texturüberprüfung grobkristalliner dünner Metallbänder (T. Mitt. Krupp **14** (1956) 16–17).

91. STÄBLEIN, F. and MEYER, H. H.: Kaltgewalztes Transformatorenblech (ETZ-B **7** (10) (1955) 368–373).

91a STAHLWERKE RÖCHLING-BUDERUS AG: Prospekt Sonderweicheisen AME (1962).

92. STEATIT MAGNESIA AG, DRALOWID-WERK PORZ: Weiche Ferrite Keraperm (Catalogue 8D 63).

93. TORSCH, C. E.: A universal ceramic iron core sweep transformer (Tele-Tech. (Dec. 1949) 23–25, 49; (Jan. 1950) 34–35).

93a VACUUMSCHMELZE GMBH, HANAU: Data Sheet MO 28 (Aug. 1970).

93b VACUUMSCHMELZE GMBH, HANAU: Data Sheet M 20 (Apr. 1964).

93c VACUUMSCHMELZE GMBH, HANAU: Data Sheet M 39 (Mar. 1970).

94. VACUUMSCHMELZE GMBH, HANAU: Vacodur 16. Data Sheet M 009 (Mar. 1962).

94a VALVO GMBH: Handbuch Ferroxcube, Sorte Fxc 3C6 (1970).

95. WALLMANN, C.: Herstellung und Eigenschaften von Siliziumstahl (Stahl u. Eisen **48** (1928) 817–822).

96. WALTER, J. L., HIBBARD, W. R., FIEDLER, H. C., GRENOBLE, H. E., PRY, R. H. and FRISCHMANN, P. G.: Magnetic properties of cube textured silicon-iron magnetic sheet (J. A. P. **29** (1958) 363–365).

97. WALZWEK NEVIGES. EBG Katalog Elektrobleche (Jan. 1972).

98. WEISS, P. and FORRER, R.: La saturation absolue des ferromagnétiques et les lois d'approche en fonction du champ et de la température (Ann. Phys. **12** (1929) 279–372).

99. WEVER, F. and HINDRICHS, S.: Über die Herstellung von Silizium-Aluminium-Stählen für Dynamo-und Transformatorenbleche im Hochfrequenzinduktionsofen (Mitt. K. W. I. Eisenforschg. **13** (194) (1931) 273–289).
100. WIENER, G., ALBERT, P. A. and TRAPP, R. H.: Cube texture in body centered magnetic alloys (J. A. P. **29** (3) (Mar. 1958) 366–367).
101. WILLIAMS, H. J.: Magnetic properties of single crystals of silicon iron (Phys. Rev. **52** (1937) 747–751).
102. WOLFF, C.: Metallurgische Untersuchungen über die Möglichkeit weiterer Verminderung der Wattverluste in hochsiliziertem Transformatoren- und Dynamomaterial. Dissertation, Breslau (1920).
103. YENSEN, T. D.: Magnetic and other properties of iron-silicon-alloys melted in vacuo (Trans. AIEE **34** (1915) 2601–2641).
104. YENSEN, T. D.: The magnetic properties of the ternary alloys Fe–Si–C (Trans. AIEE **43** (1924) 145–175).
105. YENSEN, T. D. and ZIEGLER, N. A.: Magnetic properties of iron as affected by carbon, oxygen and grain-size (Trans. Am. Soc. Met. **23** (1935) 556–576).
106. YENSEN, T. D. and ZIEGLER, N. A.: Effect of carbon, oxygen and grain size on the magnetic properties of iron silicon alloys (Trans. Am. Soc. Met. **24** (1936) 337–358).

# 11

# Materials for transductor cores

The development of transductors (magnetic amplifiers and regulators) goes back to the start of the century. Burgess and Frankenfeld[3] were granted an American patent in 1903 for 'Means for the regulation of electric currents.' Work in Germany followed some ten years later with thoroughgoing studies of transductor circuits and connections[19, 30]. Important strides were made there during World War II. Transductors with Mumetal cores were used in the V1 rocket[27]. After the war, activity in the field of transductors increased greatly in other countries. In 1950 alone there were some 100 papers and communications on this subject[26].

The majority of these publications were concerned with questions of measurement and similar applications, and only a small fraction with the materials employed. For this reason, the improvements which have followed the development of new magnetic materials since then have proved a stimulus to the wider application of transductors. In particular, the appearance on the market of textured sheet led to great progress and a broadening in transductor technology. Anisotropic Fe–Si sheet made possible the building of larger units with power ratings up to 3000 kW.

## 11.1 PRINCIPLES AND PROPERTIES OF A TRANSDUCTOR

A transductor comprises an arrangement of coils with ferromagnetic or ferrimagnetic cores in which the non-linear magnetic properties of the core material are used for the control and regulation of currents and voltages in an a.c. circuit. A magnetic amplifier is a special case of a transductor whose inductive reactance can be changed within wide limits by means of a relatively low control current[6, 22]. Transductors can be classified into various types. According as the transductor in question is a current regulator or a voltage regulator, the hysteresis loop is, by the use of different circuit arrangements, differently traversed. Thus the initial point A of Figure 11.1 may lie on the flank of the loop or in the region of saturation.

The transductor carries control windings and operational windings, and looks, externally, like an ordinary transformer. The initial point A of the magnetic cycle is determined by means of the control windings. As can be seen from Figure 11.1, the periodically traversed portion of the hysteresis

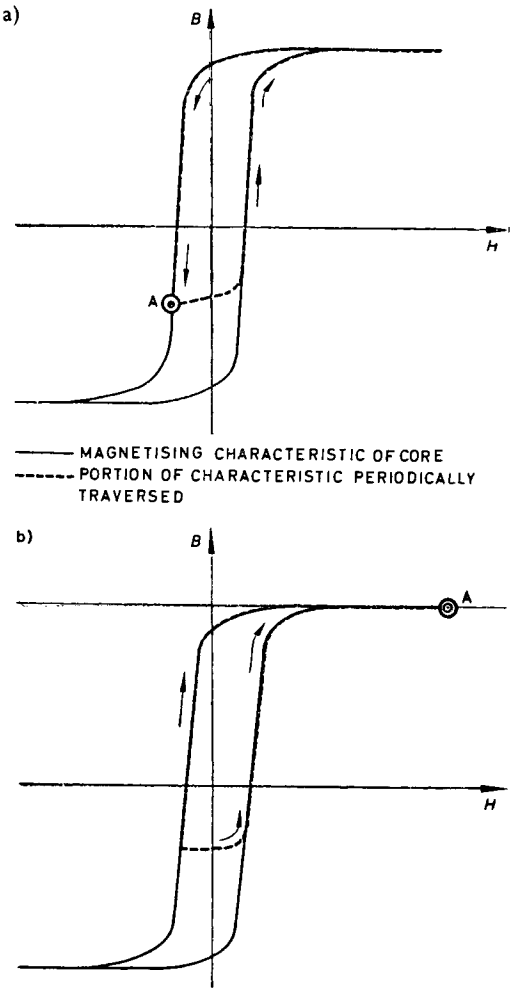



*Figure 11.1. Diagrammatic example of the utilisation of the magnetising characteristic of a transductor core*[6]

loop, shown by a broken line, is disposed asymmetrically with respect to the midpoint of the loop. The two half-waves are therefore differently affected. Positive and negative half-waves are of different magnitudes and distinct shapes. To compensate for the difference, it is usual to employ two equal coils working in opposition. Series- or parallel-connected coils can be used.

A few basic circuit arrangements are shown in Figure 11.2, following Glenk and Zott[12]. In the schematic diagram $I_c$ is the control current, $V_L$ the load voltage, and $R_L$ the ohmic resistance of the circuit.

The properties of these connections and their effect on the operational behaviour of the transductor are given in detail in many places in the specialist literature[2, 4, 8–11, 15, 16a, 16c, 17, 20, 21, 24, 28, 31–34, 37]. Explanations are

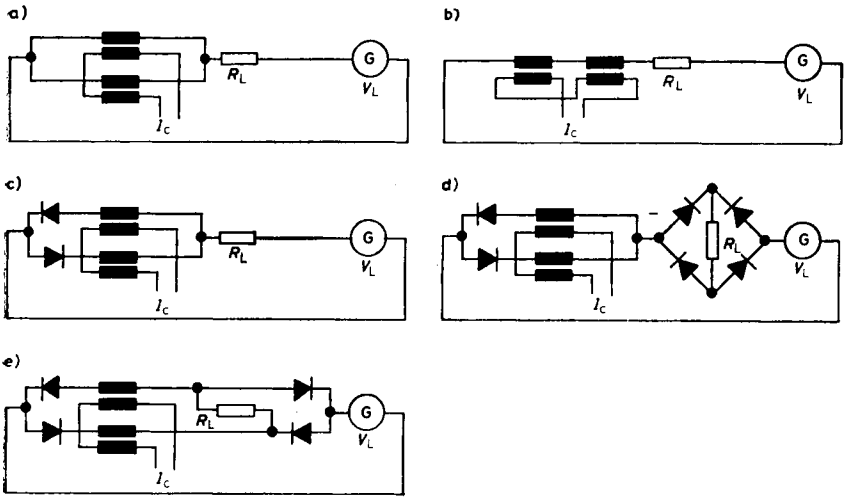



*Figure 11.2. Basic schematics of magnetic amplifiers*[12]

therefore left to these references. The technical terms appropriate to transductor technology are here briefly explained.

An important characteristic of a transductor is the rated control characteristic. Such a working control curve is shown schematically in Figure 11.3 from DIN 42 630[6]. The figure shows the relation between the output current $I_o$ and the control current $I_c$ or, alternatively, between the output voltage $V_o$ and the control voltage $V_c$. The amplitude range lying between the lowest driving point U and the working point W is called the working amplitude range $a_w$. The most important part of the characteristic is the linear amplitude range $a_l$ between the points $L_1$ and $L_2$: the corresponding control currents can be read off from Figure 11.3.

A comparison between the performance of transductors at various frequencies leads to the definition of a figure of merit $F$, namely the quotient of the amplification $A_T$ (with reference to time) and the input frequency $f_i$:

$$F = \frac{A_T}{f_i} \tag{11.1}$$

In this formula, $A_T$ is the quotient of the power amplification $A_P$ and the time constant $T$, both measured in the linear range of the working control curve. Therefore

$$F = \frac{A_P}{Tf_i} \tag{11.2}$$

The figure of merit is a dimensionless number since the dimensions of the time constant and of the frequency cancel. For the slope $S$ the following relation holds:

$$S = \frac{\text{Change of output magnitude}}{\text{Change of control magnitude}}$$

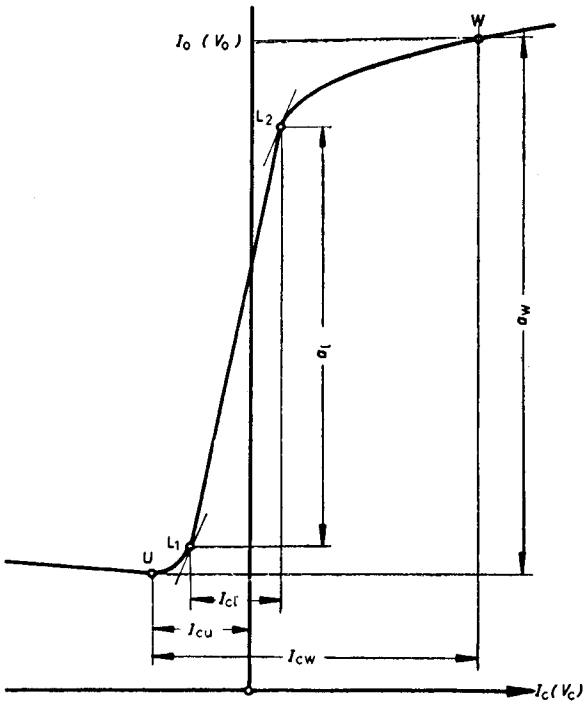



*Figure 11.3. Rated control characteristic of a transductor with $I_o(V_o)$ as output magnitudes and $I_c$ ($V_c$) as control magnitudes*

For current amplification, therefore,

$$S = A_I = \frac{\Delta I_o}{\Delta I_c} \tag{11.3}$$

while the corresponding expression for voltage is

$$A_V = \frac{\Delta V_o}{\Delta V_c} \tag{11.4}$$

and, again, for power amplification

$$A_P = A_I A_V = \frac{(\Delta I_o)^2}{(\Delta I_c)^2} \frac{R_o}{R_c} \tag{11.5}$$

Compared with valve amplification, for example, transductors have the disadvantage that they do not operate without delay. It is therefore necessary to define a *response time*. Thus, for example, $T_{63}$ or $T_{95}$ is the time interval between an instantaneous change in control current (or voltage) and the instant at which the corresponding output magnitude attains 63% or 95% of its final value. The time elapsing before the start of a significant change in

the output magnitude is called the dead time $T_d$. The *time constant* $T$ of a transductor can be arrived at if the 'time transfer', i.e. the temporal relation between an output function and the corresponding sudden change of control, can be represented, with sufficient accuracy, by an exponential curve. Then $T = T_{63}$. This follows from the known properties of an exponential function (Figure 11.4).

Since equation 11.2 holds for the response time, it is seen that the response time may be reduced if the frequency is raised or if a lower amplification

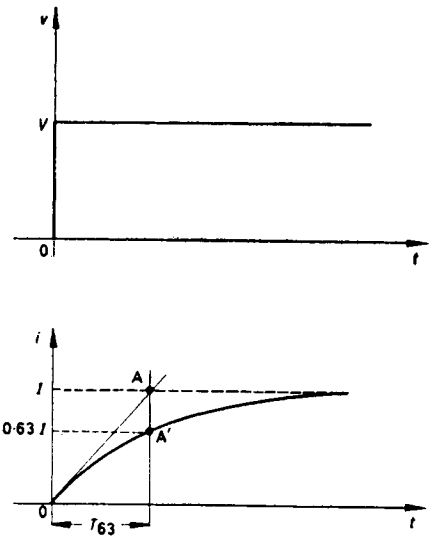



*Figure 11.4. Derivation and significance of the time constant $T = T_{63}$: assuming an exponential current rise after switching on the voltage, the initial tangent cuts the horizontal line through the end-value I at point A; the corresponding point A' on the curve has reached 63% of the end-value*

can be tolerated. Short response times associated with high amplification can be achieved only by connecting several low-amplification stages in cascade[38].

That transductor amplifiers are saddled with a delay time is of no consequence in many applications, so the merits of these devices can be fully used: namely good amplifying characteristics, robustness in use, absence of moving parts, immediacy of application, no warming-up time, and almost indefinite life.

## 11.2 TRANSDUCTOR APPLICATIONS

Transductors find a place in many fields of technology: in control and regulation techniques as voltage regulators, current regulators, frequency regulators, and speed regulators. They are to be found in battery-charging equipment and as auxiliaries to welding transformers and also as built in devices for regulating machine drives in rolling mills, forging plants, or printing works[39]. In machine-drive control the response speed is usually a secondary consideration, so transductors can be used with profit particularly within the power range of 10–300 kW. The high efficiencies attained, amount-

ing to as much as 97% in the higher power ratings[29], constitute a most useful feature of transductors.

The transductor can also be used as a magnetic switch[25], as a power amplifier[21], as a suppressor of voltage or current variations, as a temperature regulator[2, 39], and in many other ways. A comprehensive review of the literature on transductors and saturable reactors will be found in Lang[23], for example.

Transductors having various figures of merit are required for various applications. Optimal solutions normally entail consideration of the purpose in view and must be seen from a practical and commercial standpoint involving a study of core material, core shape, and type of winding.

## 11.3 REQUIREMENTS FOR CORE MATERIAL

Requirements for transductor core material are partly similar to those for transformer cores:

1. The hysteresis loop should be as narrow as possible, i.e. $H_c \to 0$.
2. The flanks of the loop should be straight lines so that the control characteristic will have an extended linear range.

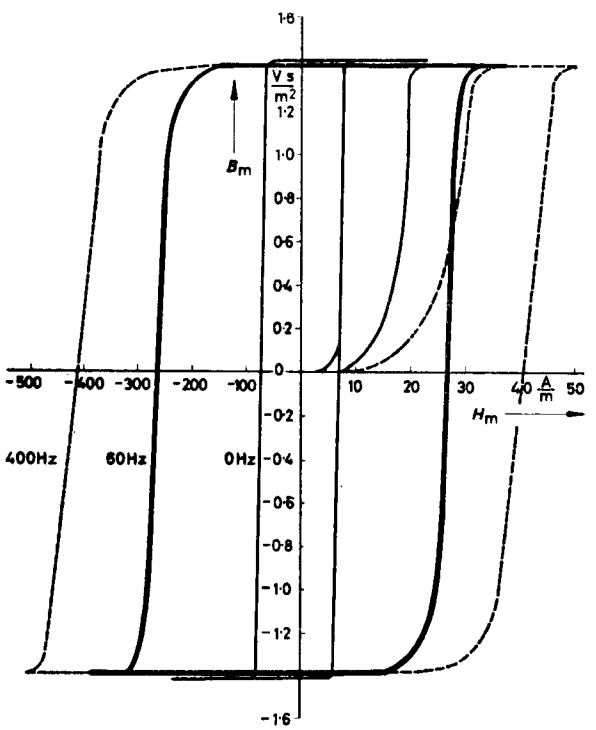



*Figure 11.5. Static hysteresis loop and dynamic loops at 60* Hz *and 400* Hz *for a grain-oriented* Fe–Ni *alloy (Deltamax)*[1]

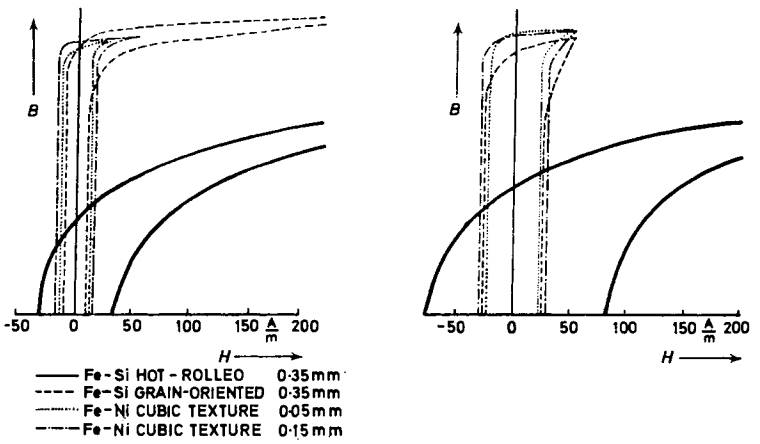



*Figure 11.6. Static loops (left) and dynamic loops (right) for toroidal cores of typical core material taken at 50* Hz[34]

3. The knee of the curve should be well marked and lie as close as possible to the saturation range, i.e. above the knee the loop should be as flat as possible and the reversible permeability should approach unity[16].
4. The response time of the transductor should be as short as possible.
5. The dependence on frequency should be as small as possible.
6. The core losses should be low.
7. The magnetic properties should be stable and influenced as little as possible by temperature changes or by mechanical shock and vibration.

A steeply rising hysteresis loop, i.e. a high permeability and a high saturation value, are ideal requirements for transductor core material, especially if the transductor is to be used as a magnetic amplifier. High flux density is particularly necessary for output amplifiers but is useful in all cases since it leads to a lower cross-section of core and the size of the windings may be reduced, resulting in reduced stray fields.

Compared with the statically measured hysteresis loop the dynamically traversed loop is not only broader but less steep (Figures 11.5 and 11.6). Reduced steepness of the flanks makes greater control excitation necessary.

The requirement of low frequency dependence agrees, in general, with the need for reduced eddy-current loss. The reduction of eddy currents demands a high specific electrical resistance and a thoroughgoing lamination of the core. In this connection it must be remembered (see page 181) that the magnetic properties of the various materials cannot always be realised for all thicknesses of sheet and strip.

## 11.4 MISCELLANEOUS MATERIALS

Unalloyed iron finds almost no application in transductors on account of its low electrical resistance. The principal role is played by the Fe–Ni and the Fe–Si alloys. Which of the two is used in a given case is often decided on

cost. Jentsch and Lehn[16] have shown that, relative to weight and to volume, grain-oriented Fe–Si sheet is the more economical. In the graphical presentation of Figure 11.7 taken from their work, it must be noted, in fact, that the price of electrosheet is in terms of a strip thickness of 0·35 mm. It is not possible to cover nickel-free materials in, for example, thicknesses of 0·05 mm. The core for which the relative prices were worked out had dimensions of

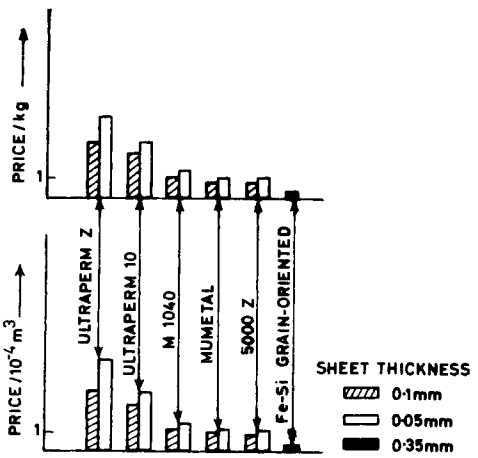



*Figure 11.7. Comparative prices of various core materials for transductors*[16]

100 mm×80 mm×20 mm and consisted of strip material 0·05 mm and 0·1 mm thick.

It is therefore on the ground of cost, in the first place, that grain-oriented Fe–Si is generally used for transductors of high output power (0·1–50 kW, while Fe–Ni alloys are used for smaller units. On the other hand, Walter[41] was able to show that Fe–Si alloys of good texture and high chemical purity in no way fall behind the Fe–Ni alloys and may even prove superior. This is demonstrated by comparing Tables 11.2 and 11.3. Further, in Fe–Si strip of high purity, the temperature relations are very favourable: at 500°C the properties of very pure Fe–Si are as good as those of Deltamax at room temperature[41].

### 11.4.1 Hot-rolled Fe–Si sheet

Curves 4 and 5 of Figure 11.8 show the alternating-field magnetising characteristics for hot-rolled Fe–Si sheet[22]. As can be seen, the requirements for a linear rise and a sharp knee are met only roughly. Although high-performance transductors cannot be constructed with this material, nevertheless its properties are good enough in many cases where the favourable price of this kind of sheet is decisive. A comparison of curves 4 and 5 demonstrates that strip-wound cores show appreciably better properties than sheet cores with EI laminations.

### 11.4.2 Grain-oriented Fe–Si sheet

It can be deduced from the material requirements outlined above that anisotropic materials having approximately rectangular hysteresis loops in the preferred direction fit the conditions better than do isotropic materials.

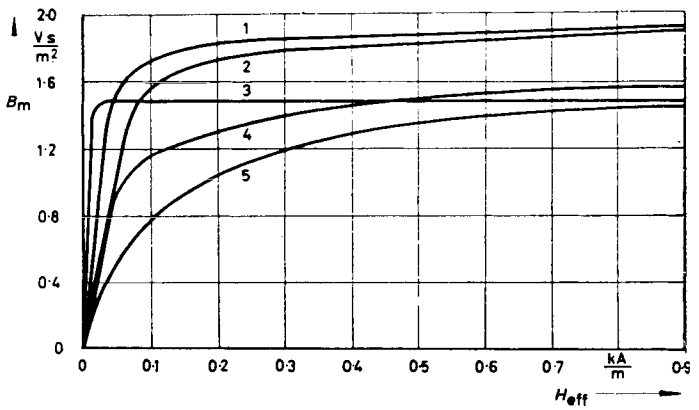



*Figure 11.8. Alternating-field magnetising characteristics: 1, toroidal strip-wound core or core of UI laminations from cold-rolled material; 2, cold-rolled sheet, U laminations; 3, Permenorm 5000Z or Hyperm 50T (strip-wound toroids or U laminations); 4, hot-rolled sheet (strip-wound toroids or U laminations); 5, hot-rolled sheet (EI laminations)*[22]

This is clearly brought out in Figure 11.8, where various materials are displayed against each other: the magnetising characteristic (curve 1) of a strip-wound core of cold-rolled Fe–Si rises steeply to a flux density of some 1·4 V s/m² and then opens in a relatively narrow arc into the straight saturation curve. Grain-oriented Fe–Si sheet with 3–3·5% Si is frequently used as core material, particularly for power amplifiers.

The magnetic properties of Fe–Si sheets with 3% Si are shown in Table 10.8 for materials of cubic texture and Goss texture. Which of these two materials the designer chooses depends both on technical considerations (size and shape of the transductor, electrical requirements, operating frequency) and on what is economically acceptable. Sheet having cubic texture is still the more expensive and cannot yet be manufactured to all dimensions that might be required. It is clear from Figure 10.28 that the effect of sheet thickness on the magnetic properties cannot be overlooked. Those grain-oriented Fe–Si sheet materials with 3–3·5% Si to be found on the market are roughly categorised by the characteristics set out in Table 11.1.

The hysteresis loops, taken at 160 and 800 A/m peak and various frequencies, of an Fe–Si alloy with 3·1% Si which had been rolled out to 0·025 mm in thickness and had assumed, in the final annealing, a pronounced orientation in the (110) [100] direction yielded the characteristic values of Table 11.2[41].

**Table 11.1** PROPERTIES OF SOME COMMERCIALLY AVAILABLE MATERIALS FOR TRANSDUCTORS

| *Material* | *Composition (remainder iron)* | $B_s$ (V s/m²) | $H_c$ *at 0* Hz (A/m) | $W_{0.5}(W_{1.0})$ $[W_{1.5}]$ *at 50* Hz (W/kg) | $T_c$ (°C) | $\varrho$ (μΩ cm) | $10^{-3}\mu_m$ ($\mu_0$) | *Reference* |
|---|---|---|---|---|---|---|---|---|
| Grain-oriented Fe–Si | 3–3·5% Si | 1·8–2·0 | 8 | — | 735 | 45–50 | 18–55 | |
| Trafoperm N2 | 3% Si | 2·03 | 8 | (0·45) | 750 | 40 | 35 | 40 |
| Permenorm 5000Z | 65% Ni | 1·55 | 12 | [0·8] | 470 | 45 | 50 | 40 |
| Permalloy F | 50% Ni | 1·40 | 4 | — | 470 | 26 | 200–400 | 36 |
| Deltamax | 50% Ni | 1·35–1·55 | 3·2–12 | — | — | 45 | 70–250 | 1 |
| Mumetal | 77% Ni, 5% Cu, 2% Cr | 0·65–0·8 | 1·2 | 0·025 | 410 | 55 | 120 | 40 |
| M 1040 | 72% Ni, 14% Cu, 3% Mo | 0·58 | 0·64 | 0·015 | 270 | 60 | 150 | 40 |
| Supermalloy | 79% Ni, 5% Mo | 0·68–0·8 | 0·2–0·7 | — | 400 | 65 | 300–900 | 1 |
| Ultraperm Z | 70–80% Ni, Cu, Mo | 0·8 | 0·8 | 0·015 | 410 | 55 | 250 | 40 |
| Hyperm 900T | 75% Ni, Mo, Cr | 0·8 | — | — | 400 | 55 | 40 | 10a |
| H. C. R. Alloy | 50% Ni | 1·56–1·60 | 10·4 | — | — | — | 110 | 37a |
| Permax Z | 65% Ni | 1·25 | 2 | (0·07) | 520 | 60 | 35 | 40 |
| Vacoflux Z | 49% Co, 1·8% V | 2·35 | 20 | (0·8) | 950 | 35 | 40 | 40 |
| Hyperm Co 50T | 50% Co, V | 2·40 | 20 | (0·7) | 950 | 35 | 70 | 10a |

**Table 11.2** CONSTANTS DEDUCED FROM THE STATIC AND DYNAMIC HYSTERESIS LOOPS OF A STRIP-WOUND CORE MADE FROM 25 μm STRIP OF Fe–Si ALLOY HAVING 3·1% Si AND A GOSS TEXTURE (110) [001][41]

| $f$ (Hz) | $H_m$ (A/m) | $H_c$ (A/m) | $B_r$ (V s/m²) | $B_m$ (V s/m²) | $B_r/B_m$ | $\mu_m$ ($\mu_0$) | $B_{\mu_m}$ (V s/m²) |
|---|---|---|---|---|---|---|---|
| 0 | 160 | 6·8 | 1·55 | 1·79 | 0·87 | 122 000 | 1·33 |
| | 800 | 8·0 | 1·63 | 1·85 | 0·88 | 100 000 | 1·30 |
| 60 | 160 | 22·4 | 1·67 | 1·85 | 0·91 | 28 100 | 1·22 |
| | 800 | 20·0 | 1·73 | 1·93 | 0·90 | 39 200 | 1·30 |
| 400 | 160 | 36·0 | 1·78 | 1·85 | 0·96 | 20 250 | 1·34 |
| | 800 | 36·0 | 1·83 | 1·94 | 0·94 | 20 250 | 1·34 |
| 1 000 | 160 | 56·8 | 1·83 | 1·88 | 0·97 | 14 200 | 1·46 |
| | 800 | 58·4 | 1·85 | 1·95 | 0·95 | 12 750 | 1·35 |

### 11.4.3 Fe–Ni alloys

The Fe–Ni alloys used for transductors contain either 45–50% or 65–80% Ni. Sheet is used with either isotropic or anisotropic magnetic properties. Preference, however, is often given to 50% Fe–Ni sheet with cubic texture. It is known commercially as Permalloy F, Permenorm 5000Z, Hyperm 50T, Deltamax, H. C. R. alloy, Hipernik V, Orthonol, Orthonik, Permeron, Rectimphy, etc. The properties of this material vary somewhat, within the limits quoted in Table 11.1. Static and dynamic hysteresis loops are shown in Figures 11.5 and 11.6. Fe–Ni alloys with 65% Ni are dealt with in Section 13.4. Table 11.3 sets out the static and dynamic values of a Deltamax alloy, in the form of 25 μm strip, at various frequencies and field strengths[41].

**Table 11.3** MAGNETIC PROPERTIES TAKEN FROM THE STATIC AND DYNAMIC HYSTERESIS LOOPS OF A 25 μm DELTAMAX STRIP-WOUND CORE (50% Fe, 50% Ni)[41]

| $f$ (Hz) | $H_m$ (A/m) | $H_c$ (A/m) | $B_r$ (V s/m²) | $B_m$ (V s/m²) | $B_r/B_m$ | $\mu_m$ ($\mu_0$) | $B_{\mu_m}$ (V s/m²) |
|---|---|---|---|---|---|---|---|
| 0 | 160 | 12·0 | 1·36 | 1·41 | 0·96 | 66 000 | 1·21 |
| | 800 | 13·6 | 1·38 | 1·45 | 0·95 | 65 800 | 1·24 |
| 60 | 160 | 16·8 | 1·42 | 1·475 | 0·98 | 49 100 | 1·26 |
| | 800 | 17·6 | 1·40 | 1·480 | 0·95 | 50 900 | 1·29 |
| 400 | 160 | 20·8 | 1·475 | 1·505 | 0·98 | 38 300 | 1·26 |
| | 800 | 21·6 | 1·455 | 1·510 | 0·96 | 33 700 | 1·18 |
| 1 000 | 160 | 26·4 | 1·49 | 1·505 | 0·99 | 25 300 | 1·30 |
| | 800 | 27·2 | 1·49 | 1·545 | 0·96 | 25 250 | 1·25 |

The excellent characteristic curve of Fe–Ni with cubic texture (see Figure 11.8, curve 3) makes this material especially suitable for transductors. Nevertheless, it is usually found only in small or medium-size units since the material price is relatively high and, moreover, the high saturation values of Fe–Si are not obtained. Its permeability is high and the coercivity is very low, so this type of material is especially suited to magnetic amplifiers, which require low control power. Power amplification at 50 Hz can amount to[23] around 1000.

Texture is less pronounced for the 48% alloys; but here, too, for a given composition, the better oriented materials show themselves superior, particularly in remanence ratio. On the other hand, a hysteresis loop with sharp corners seems to require a higher starting intensity for the cyclic magnetisation process than a loop with a somewhat rounded knee[42]—a fact also observed in storage devices constructed from ferrite.

For a given coercivity and orientation, materials of low thickness are best. This holds even in cases where eddy currents are not of primary importance[42]. A few of the best-known highly alloyed Fe–Si types gathered from various publications[16, 35] are listed, with some additions, in Table 11.1.

### 11.4.4 Fe–Co alloys

If core materials for transductors are required with high flux-density values, some Fe–Co alloys could serve very well. High saturation values allow a size reduction for a given power. If the amplification ratio can be increased, it may be possible in many cases to reduce the amplifier stages from two to one.

Good magnetic properties can be achieved by, for example, the use of an alloy of very pure Co–V–Fe which has become known as Supermendur[13]. The alloy consists of about 49% Fe, 49% Co, and 2% V. It contains less than 0·01% carbon and sulphur. The material is readily workable and permits a 99·6% deformation, i.e. it can, for example, be rolled down from 2·25 mm to 0·008 mm without intermediate annealing. The magnetic properties are broadly as follows:

| | |
|---|---|
| Maximum permeability | $\mu_m = 93\,000\mu_0$ |
| Saturation flux density | $B_s = 2{\cdot}4$ V s/m$^2$ |
| Remanence | $B_r = 2{\cdot}2$ V s/m$^2$ |
| Coercivity | $H_c = 16$ A/m |
| Curie temperature | $T_c = 980$°C |
| Specific electrical resistance | $\varrho = 26\ \mu\Omega$ cm |
| Hysteresis loss | $W_h = 2000$ erg/cm$^3$ per cycle |

The considerable steepness of the hysteresis loop for this alloy, compared with the Fe–Si and Fe–Ni alloys, can be seen from Figure 11.9[13]. It is produced by giving the material a uniaxial anisotropy by annealing in a magnetic field. The temperature of 850°C must not be exceeded in this process lest a phase conversion occur which would spoil the magnetic properties.

In the cooling process, too high a rate and too low a rate are to be avoided.

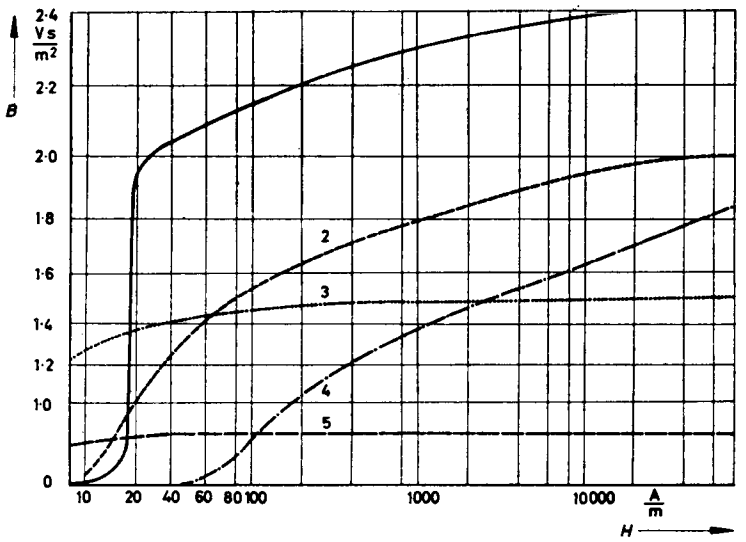



*Figure 11.9. Magnetising curves of some important magnetic materials: 1, 49% Fe–49% Co–2% V (Supermendur); 2, 97% Fe–3% Si (oriented); 3, 50% Ni–50% Fe (Deltamax); 4, 96% Fe–4% Si (electrosheet); 5, 79% Ni–16% Fe–5%Mo (Supermalloy)*[13]

Something like 1 K/min is considered a suitable rate of cooling. The field applied during the cooling should amount to 80 A/m or more. In spite of high deformation at low temperatures, the material shows no grain orientation, the relatively large grains of the annealed material being randomly oriented. We are here concerned, therefore, with uniaxial anisotropy associated with directional superstructure (see page 91). Keller and Hillmann[16a] used specially purified raw materials for making these alloys and were then able to reach a maximum permeability of 154 000$\mu_0$ and a coercivity of 10 A/m.

This material finds applications not only for transductors but for transformer cores, switching and storage cores, and diaphragms in telephone handsets.

### 11.4.5 Ferrites

Transductors lend themselves best to high-frequency operation, in view of the response time, and ceramics are well suited to this purpose[43]. Dodson and Morgan[7] investigated the behaviour of ferrite transductors up to $f = 1$ MHz. They found that the amplification at 500 kHz is 100 times greater than, that of the best transductors using ordinary sheet materials, at 60 Hz; the response time was the same.

Investigations by Glenk and Zott[12] using toroidal cores of the ferrite material called Keraperm 09405 yielded particularly good time ratios—and hence a higher performance—than did laminated cores. Figure 11.10 gives

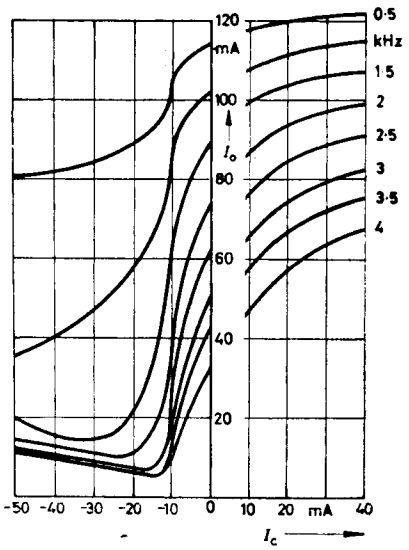



*Figure 11.10. Characteristics of a transductor with ferrite core, connected as in Figure 11.2e*

the characteristic curves for 0·5–4 kHz; they were taken using the circuit arrangements of Figure 11.2e. The control winding had 100 and the load winding 400 turns; the load resistance $R_L$ was 100 Ω and the output voltage 24 V.

## 11.5 EFFECT OF CORE CONSTRUCTION

The core of a transductor must, as far as possible, be constructed without an air-gap to avoid loop-shift. The following example shows how important this is. Using a material whose maximum permeability was 100 000 $\mu_0$, the presence of a 25 μm air-gap, giving an average ratio of gap length to magnetic path length of 0·2%, led to a drop in working permeability to 4700 $\mu_0$ (see Figure 3.12). With a gap half this width, the effective permeability was 9000 $\mu_0$. It may be deduced from this that air-gaps are not only harmful in themselves but, by reason of possi le variations in their width, may so greatly change the effective magnetic characteristics as to make reliable production very difficult.

The air-gap can be made particularly low by using strip-wound cores: for very thin material the strip-wound core is, indeed, the only possible solution. The flux needs only to jump the distance between the individual turns of the spiral, and this can generally be kept very small in relation to the whole circuit by tight winding of the core and the use of the thinnest possible insulation layer. A few detailed examples are sketched in Figure 11.11. In order to protect the lightly annealed core against possible deformation, it is sometimes desirable to enclose it in a protective cradle of metal or plastic (nylon, for example) to which the windings may be applied by a toroidal winding machine[40a].

Winding of toroidal cores is not as great a problem as in earlier times by reason of improvements in toroidal winding machines. Nevertheless, for

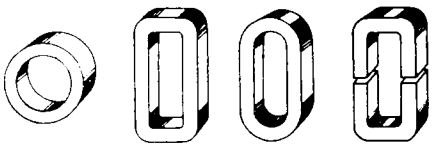


*Figure 11.11. Various shapes of strip-wound core*

manufacturing reasons it is often better to wind the coils on empty formers and then to slip them over the cores. This is facilitated by the use of split cores, but even so, air-gaps cannot be wholly avoided. In the most favourable case 2–3 μm gaps occur at the butt joint. According to DIN 41 309[5], the separation is to be 30 μm unless otherwise agreed[15a]. Split cores are nowadays usually made with rectangular winding windows and can be fitted with coils in a variety of ways. Figure 11.12 shows a few of the possibilities.

According to DIN 41 309[5], split cores are so dimensioned that bobbins of the M series can be used (DIN 41 303). For large transductors the advantage generally lies with cores of stacked laminations as these are more easily handled. Laminated cores of U-shaped laminations (see Figure 10.26) can be used in alternating positions so that the air-gaps are not in register. In spite of overlapping, there remains an effective air-gap. Certain improvements can be achieved by special means. In laminations having Goss texture, the transverse portion of the yoke is doubled relative to the shank; this leads to reduced magnetic reluctance, a quantity which causes an increase in stray field. Cubic-textured laminations used in this way give results scarcely inferior to toroids. For non-oriented dynamo sheet and for sheet with cubic structure, U-laminations as in Figure 10.26d, lead to quite small strays when used in the construction of transductors: the broad yoke greatly reduces the effective air-gap.

Complete splitting of this sort cannot be used with sheet having only a single preferred direction because the yoke resistance is increased. An arrangement such as that shown in Figure 10.26c is employed in which a crosspiece is fitted between the two shanks in such a way as to preserve the preferred direction; or the arrangement of Figure 10.26b may be used in which yoke and shank are obliquely butted.

A version of this type of section, having improved properties, is shown in Figure 10.26a. The larger number of elements used certainly increases the number of joints, but the overlapping and the broadening of the yoke section lead to strays which are not substantially higher. Figure 10.26e shows a strip core with increased yoke width; it is more easily stacked than a core with oblique joints and is also easier to wind. The stray fields are of the

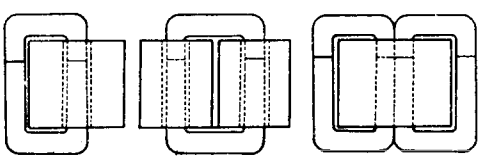


*Figure 11.12. Various arrangements of split cores with coils*

same order as for cores built with U laminations. The poor space-factor of the yoke is, of course, unfavourable.

Krabbe and Giesenhagen[18] proposed a butt-free laminated core, for sheet having Goss texture, which is similar to the form used in the Epstein tester except that double-width yokes are used to avoid the poor iron space-factor of the shanks. The strays of the operational windings of a transductor may be reduced if the cross-section of the shank carrying the operational winding is made smaller than that of the yoke and of the shank which carries the control winding[18].

Fairly close relations hold between core material, core shape, rated flux density, rated field strength, and amplitude ratio for control and regulation transductors (see Table 11.4)[22]. Thus for hot-rolled Fe–Si sheet, used as M or EI laminations, an amplitude ratio $I_o/I_{o(min)}$ of only 5–10 is attainable. Also, the magnetising power of the magnetic circuit is eight times as great as for a core with grain-oriented sheet. In spite of the greater expense, however, the performance is typically only 80% of that of the oriented core material.

For many control jobs of limited range the excellence of the core is not an outstanding consideration, so the lower cost of hot-rolled sheet favours its use. Further, with M and E sections a single core often suffices (the middle shank carries the control winding and the two outer shanks carry the operational winding), whereas the use of U cores generally necessitates two cores.

Figure 11.13 shows the performance of transductors as a function of output power for various core shapes[34]. Sheet with Goss texture was used in all cases. The figure of merit $F$ was determined in a single-phase bridge-connection with d.c. output: the strip core of Figure 10.26e proved itself the best in this case (double core type, $d_1$). The single core type ($d_2$) is only slightly better than the toroidal core. The U core with oblique butt joints

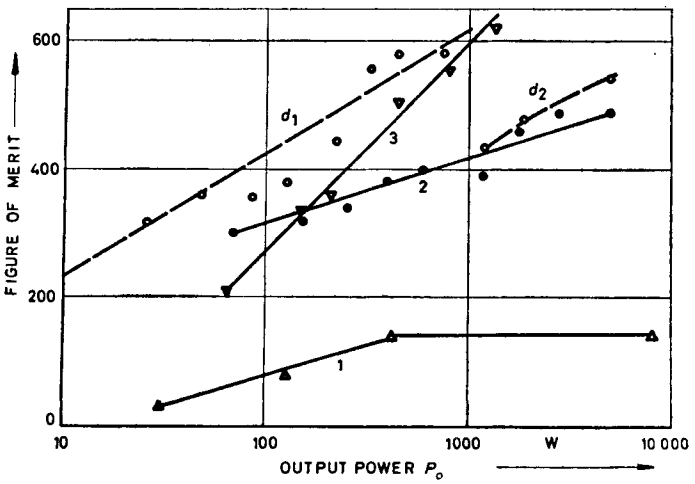



*Figure 11.13. Comparison of figures of merit for transductors of various core shapes made from cold-rolled* Fe–Si *sheet measured in bridge-connection: 1, U core; 2, toroidal core; 3, U core with oblique butt joint; $d_1$ and $d_2$, strip cores with overlap*[34]

**Table 11.4** TYPE OF CORE AND MAGNETIC PROPERTIES OF MAGNETIC AMPLIFIERS FOR CONTROL AND REGULATION PURPOSES[22]

| *Core* | *Material* | *Rated flux density* (V s/m²) | *Rated field strength* (A/m) | *Amplitude ratio* $I_o/I_{o(min)}$ | *Application* |
|---|---|---|---|---|---|
| Strip-wound toroidal core | 50% Fe, 50% Ni (5000 Z, Hyperm 50T) | 1·4 | 13 | 100–300 | Preamplifier; control amplifier |
| | Fe–Si, grain-oriented | 1·5 | 35 | 50–150 | Control amplifier; power amplifier for large range |
| EI stampings | Fe–Si, hot-rolled | 1·2 | 320 | 5–10 | Premagnetised current transformers; low-range adjusting chokes |
| U stampings | Fe–Si, hot-rolled | 1·2 | 130 | 10–20 | Power amplifiers |
| | Fe–Si, hot-rolled | 1·3 | 60 | 30–50 | Power amplifiers |
| UI stampings | Fe–Si, cold-rolled | 1·5 | 40 | 40–120 | Power amplifiers |

offers no significant advantage at small powers, but its superiority is seen at high power ratings.

If one considers the power–weight ratio, the poor iron space-factor of the shank of a strip core makes itself obvious. In this respect the U core with oblique butt joints is superior. The U core with a complete split is, for sheet with only one preferred direction, much inferior.

In Figure 11.13 a merit figure of 300, for example, is given for an output power of 70 W. This means that for $f = 50$ Hz and $T = 0{\cdot}1$ s, the power

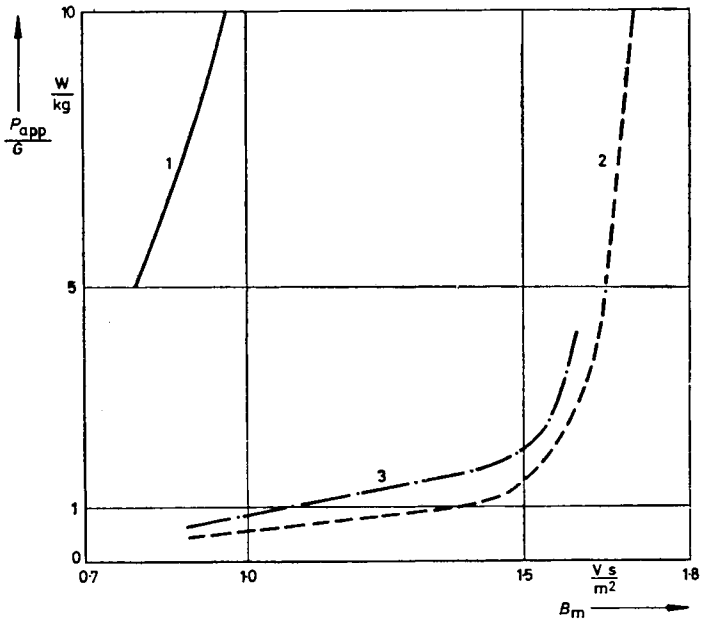



*Figure 11.14. Specific apparent excitation power for toroidal cores: 1, hot-rolled 0·35* mm Fe–Si *sheet; 2, cold-rolled 0·35* mm Fe–Si *sheet; 3, 0·15* mm Fe–Ni *sheet*[34]

amplification comes to $A_P = 1500$ and this requires a control power $P_c$ of $70/1500 = 0{\cdot}048$ W.

The specific apparent excitation power $P_{app}$ can be used to assess the virtue of a given core shape in terms of a toroidal core. Figure 11.14 gives measurements (in watts) for toroidal cores of three typical materials, namely Fe–Ni sheet with cubic texture, cold-rolled Fe–Si sheet, and hot-rolled Fe–Si sheet. The curve for the Fe–Ni sheet stops at 1·55 V s/m² since saturation is reached at this point; the curve for the Goss sheet rises very steeply before reaching saturation. The characteristics look much the same if the effective excitation field, instead of the apparent power, is plotted against flux density (Figure 11.15). The apparent power $P_{app}$ over the core weight $G$, and the effective excitation field $H_{eff}$ can be related by the following formula:

$$\frac{P_{app}}{G} = \frac{H_{eff}}{z} l_m \times 4{\cdot}44 f z B_m A_m \left(\frac{1}{d l_m A_m}\right) = H_{eff}\left(\frac{4{\cdot}44 f B_m}{d}\right) \quad (11.6)$$

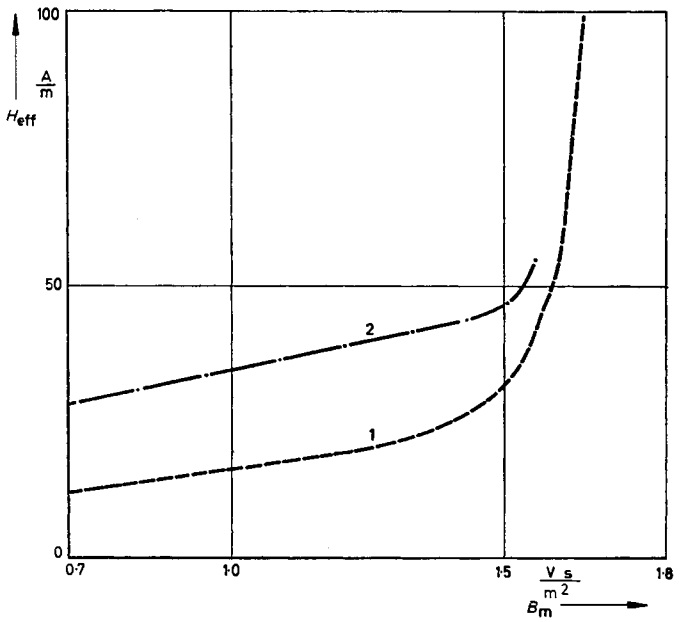



*Figure 11.15. Effective field strength of toroidal strip-wound cores for 50* Hz *sinusoidal voltages: 1, cold-rolled* Fe–Si *sheet 0·35* mm *thick; 2,* Fe–Ni *strip 0·15* mm *thick*[34]

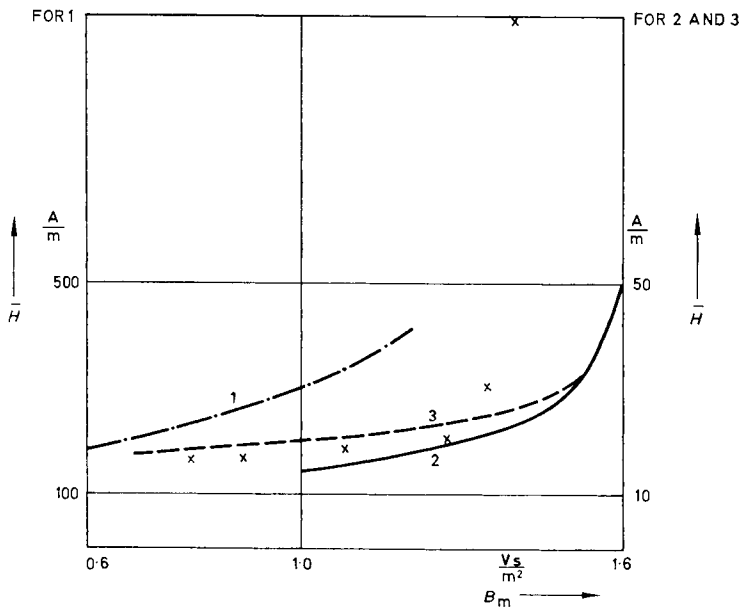



*Figure 11.16. Excitation by rectified sinusoidal voltages at 50* Hz*: 1, toroid of 0·35* mm *hot-rolled stampings* Fe–Si *sheet; 2, cold-rolled 0·35* mm Fe–Si *strip; 3, strip-wound core of 0·1* mm Fe–Si *strip*[34]

where $l_m$ is the magnetic path length, $A_m$ the magnetic cross-section, $z$ the number of turns, and $d$ the density. These characteristics—they are shown in Figure 11.15—are also known as effective-value characteristics. In this example they were obtained by current–voltage measurements on strip-wound toroids of 0·15 mm thick Fe–Ni sheet and 0·35 mm thick cold-rolled Fe–Si sheet[34].

Figure 11.16 shows characteristics acceptable for transductors in which the mean value of excitation $\overline{H}$ is plotted against flux density $B_m$. It is easy to

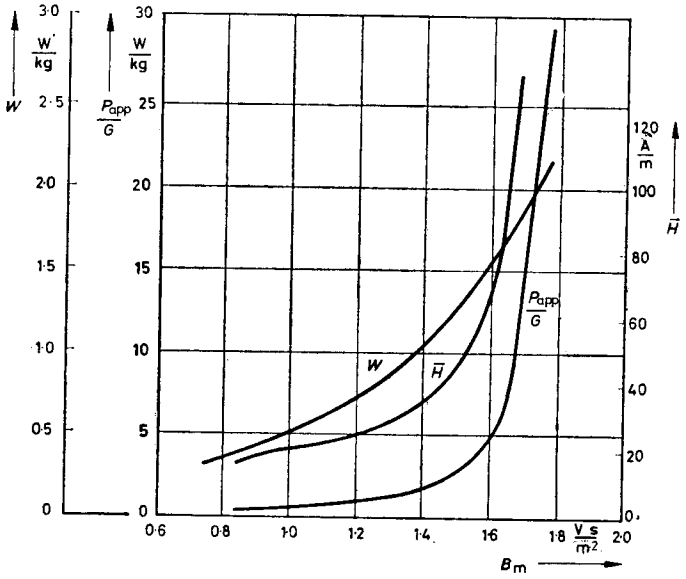



*Figure 11.17. Magnetic characteristics of an annealed cold-rolled* Fe–Si *sheet specimen measured in the Epstein test rig*[34]

see that these characteristics are comparable with those of Figure 11.14 and 11.15, so any of the three methods can be chosen for comparing the performance of transductor cores.

Figure 11.17 collects together the three characteristic curves which are important for transductor cores for an annealed 'Epstein' sample (strip dimensions 28 cm×3 cm) of cold-rolled Fe–Si sheet[34]: the power loss $W$, the specific apparent power of excitation $P_{app}$, and the mean value of excitation $\overline{H}$ of the rectified magnetising current. For unannealed specimens the measured values are rather higher.

## REFERENCES

1. ARNOLD ENGNG CO., MARENGÓ: Properties of Deltamax. Technical Bulletin TC-101A (1960).
2. BAEHR, H.: Regeln und Steuern durch magnetische Verstärker, Vieweg & Sohn, Braunschweig (1960).

3. BURGESS, C. F. and FRANKENFIELD, B.: Regulation of electric circuits. US Pat. 720 884 (17. 2. 03).
4. CROW, L. R.: Saturating Core Devices. Scient. Book Publ. Co., Vincennes Ind. (1949).
5. DIN 41 309, Schnittbandkerne (Oct. 1967).
6. DIN 42 630, Transduktoren. Begriffe und Benennungen (Dec. 1961).
7. DODSON, G. C. and MORGAN, R. E. See Wilson (ref. 43).
8. ETTINGER, G. M.: Magnetic Amplifiers. Methuen, London, J. Wiley & Sons Inc., New York (1953).
9. FINZI, L. A.: Introducing young engineers to the appreciation of magnetic amplifier problems (Trans. AIEE **77** (I) (Mar. 1958) 119–126).
10. FINZI, L. A. and CRITSCHLOW, D. L.: Dynamic core behaviour and magnetic amplifier performance (Trans. AIEE **77** (I) (May 1957) 229–240).
10a FRIEDRICH KRUPP, WIDIA-FABRIK, ESSEN: D 546 Hyperm, Magnetisch weiche Sonderwerkstoffe.
11. GEYGER, W. A.: Magnetic Amplifier Circuits, 2nd edn. McGraw-Hill Book Co., New York/Toronto/London (1957).
12. GLENK, H. and ZOTT, H.: Untersuchungen an Magnetverstärkern mit Ferritkernen (Stemag-Nachr. **34** (Apr. 1962) 929–933).
13. GOULD, H. L. B. and WENNY, D. H.: Supermendur (El. Engng. **76** (Mar. 1957) 208–211).
14. HOWE, G. H.: Dynamax, a new crystal and domain oriented magnetic core material (Proc. Conf. Magnetism Magn. Mat. (1955) 264–272; Trans. AIEE **75** (1956) 548–551).
15. HUBBARD, R. M. and BISHOP, M. M.: A comprehensive study of magnetic-amplifier design (Trans. AIEE **77** (I) (Nov. 1958) 562–583).
15a IEC Publication 329 (1971): Strip wound cut cores of grain oriented silicon-iron alloy used for electronic and telecommunication equipment.
16. JENTSCH, W. and LEHN, W.: Weichmagnetische Werkstoffe für Transduktoren (AEG-Mitt. **49** (1959) 387–392).
16a KAFKA, W.: Der Transduktor—ein Baustein der Automatisierung. Dr. A. Hüthig Verlag, Heidelberg.
16b KELLER, H. and HILLMANN, H.: Eisen-Kobalt-Legierungen mit niedrigen Koerzitivfeldstärken (Z. ang. Phys. **14** (4) (1962) 243–245).
16c KIELGAS, H.: Transduktor—Aufbau, Wirkungsweise—Anwendung. Dr. A. Hüthig Verlag, Heidelberg.
17. KRABBE, U. H.: The Transductor Amplifier. Lindhska Boktryckeriet, Orebo, Sweden (1947).
18. KRABBE, U. and GIESENHAGEN, G. H.: Eine neue Bauweise für hochwertige Transduktorkerne (ETZ-A **78** (1957) 712–716).
19. KÜHN, L.: Über ein neues radiotelephonisches System (ETZ **35** (1914) 816–819).
20. LAMM, A. U.: The Transductor, 2nd edn. Esselte Aktiebolag, Stockholm, Sweden (1948).
21. LANG, A.: Magnetische Leistungsverstärker für Steuer- und Regelzwecke (ETZ-A **75** (1954) 753–760).
22. LANG, A.: Magnetische Verstärker für die Steuerungs- und Regelungstechnik (ETZ-B **8** (1956) 120–123).
23. LANG, A.: State of the art of transductor application in Germany (Proc. Intermag Conf. (1963) 8-1; Regelungstechn. **12** (1964) 97–104).
24. LEHTONEN, E. W. and CRONAUER, E. A.: A–c controlled magnetic amplifiers (Trans. AIEE **77** (I) (Sept. 1958) 476–480).
25. LONSDORF, H. and RIEMER, W.: Der Transduktorschalter, ein neuer Magnetschalter für den Bergbau (SEL-Nachr. **6** (1958) 143–145).
26. MILES, J. G.: Bibliography of magnetic amplifier devices and the saturable reactor art (Trans. AIEE **70** (II) (1951) 2104–2123).
27. MILNES, A. G.: Magnetic amplifiers (Proc. IEE **96** (II) (1949) 329–338).

28. MILNES, A. G.: Transductors and Magnetic Amplifiers. Macmillan & Co. Ltd., London (1957).
29. OFFER, U., WATZINGER, H. and ZABEL, R.: Transduktor-Gleichstrom-Antriebe mit Transidyn-Regelung (Siemens-Z. **34** (1960) 648–652).
30. PUNGS, L.: Die Steuerung von Hochfrequenzströmen durch Eisendrosseln mit überlagerter Magnetisierung (ETZ **44** (1923) 78–81).
31. REYNER, J. H.: The magnetic amplifier. Stuart and Richards, London (1950).
32. SAY, M. G. (ed.): Magnetic Amplifiers and Saturable Reactors. George Newnes, London (1954).
33. SCHILLING, W.: Grundlagen einer Theorie des magnetischen Verstärkers (ETZ-A **71** (1950) 7–13).
34. SCHILLING, W.: Der Transduktor. R. Oldenbourg, Munich (1958).
35. SIDERIS, G.: Soft magnets for amplifiers (Electronics (Feb. 1959) 55).
36. STANDARD TELEPHONES & CABLES LTD.: Permalloy F. Technical Data Sheet MM 104.
37. STROM, H. F.: Magnetic amplifiers. J. Wiley & Sons Inc., New York (1955)
37a TECLON METALS LTD., CRAWLEY: H. C. R. Alloy, 3rd edn (1962).
38. TSCHERMAK, M. and KAFKA, W.: Magnetverstärker-Regelung in Anlagen der Starkstromtechnik. Der Magnetverstärker als Regler (Siemens-Z. **29** (1955) 350–356).
39. TSCHERMAK, M. and KAFKA, W.: Anwendungen der Magnetverstärker-Regelung in Anlagen der Starkstromtechnik (Siemens-Z. **29** (1955) 386–395).
40. VACUUMSCHMELZE GMBH, HANAU: Weichmagnetische Werkstoffe. Data Sheet (1967).
40a VACUUMSCHMELZE GMBH, HANAU: Data Sheet MO32 (Apr. 1967).
41. WALTER, J. L.: Thin tapes of high purity silicon–iron for magnetic amplifiers (Proc. Nonlinear Magnetics (1961) 43–64).
42. WARD, C. E. and LITTMANN, M. F.: Relation of d–c magnetic properties of oriented 48% nickel-iron to magnetic amplifier performance (Proc. Conf. Magnetism Magn. Mater. (1955) 228–235).
43. WILSON, V. C.: Applications of ferrites (Proc. Conf. Magnetism Magn. Mater. (1955) 278–285).

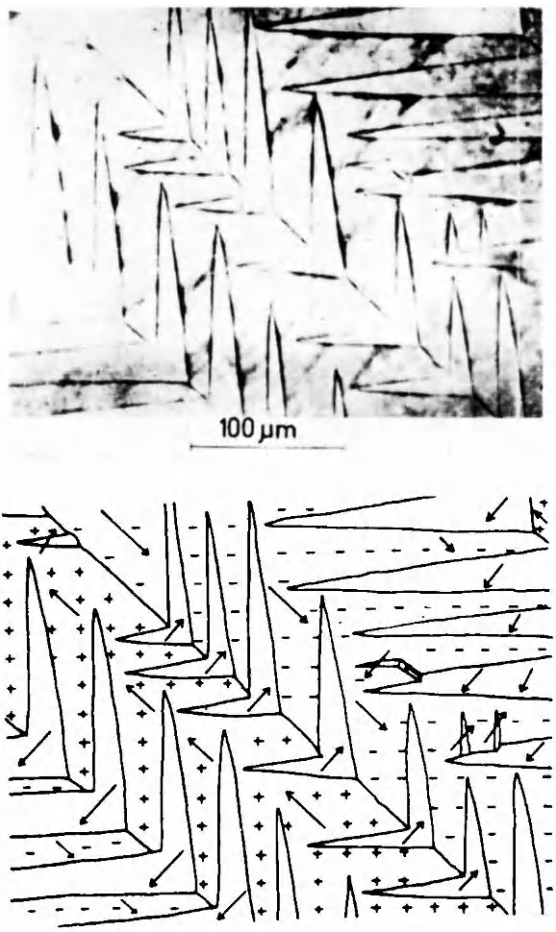
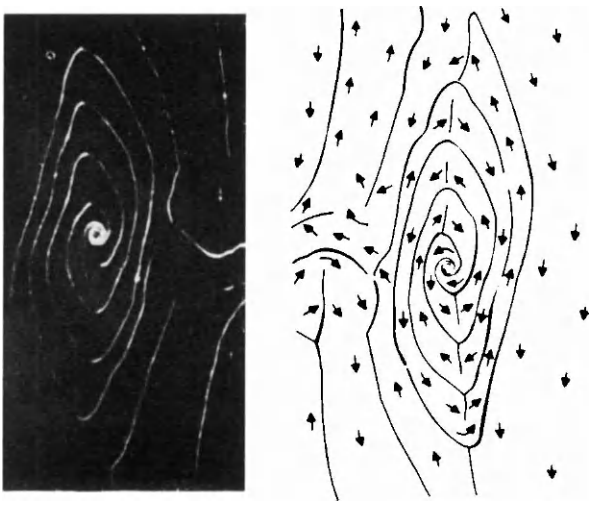



*Figure 4.5. Closure domains in iron with 4% Si*[13]



*Fignre 4.7. Spiral domains in very thin Permalloy foil*[12]

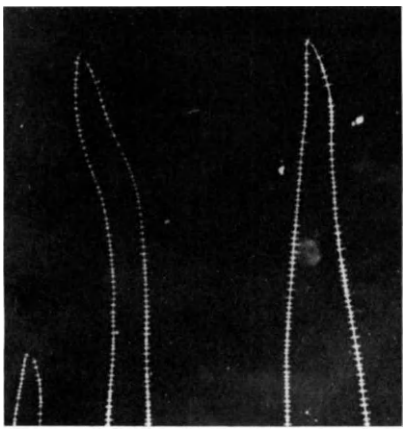


*Figure 4.32. Barbed-wire configuration in an 80* nm *film of* Ni–Fe[26]



*Figure 7.11. Transfluxor core stamped out from a sheet of ferrite*

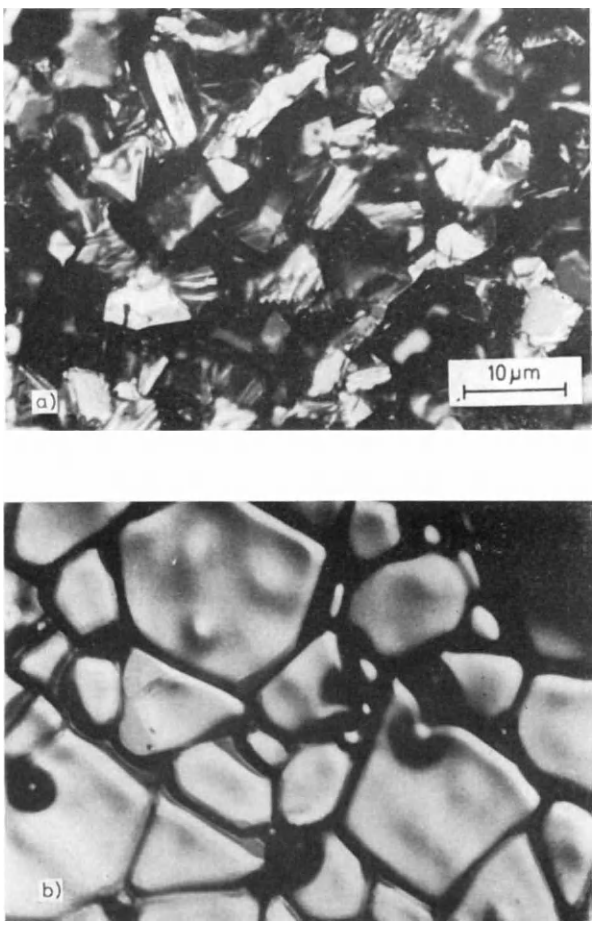



*Figure 7.12. Surface configuration of* Mg–Mn *ferrite having 38%* MnO*: (a) cooled from 1400°C in air; (b) cooled in an inactive gas*[14]



*Figure 9.43. Old and new desk telephones with their magnets*[12]



*Figure 10.23. Practical versions of split cores and C-cores*[1]

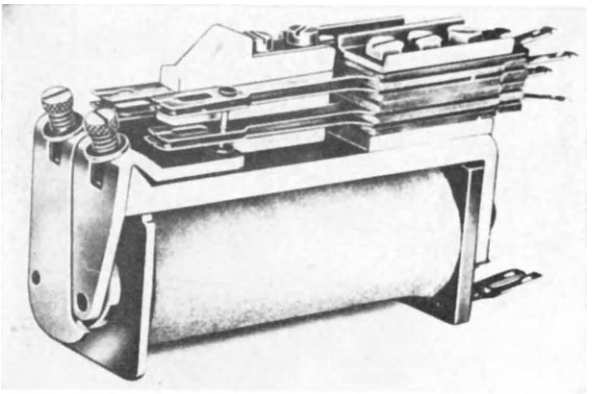


*Figure 12.1. GEC step relay with two-part armature*[10]

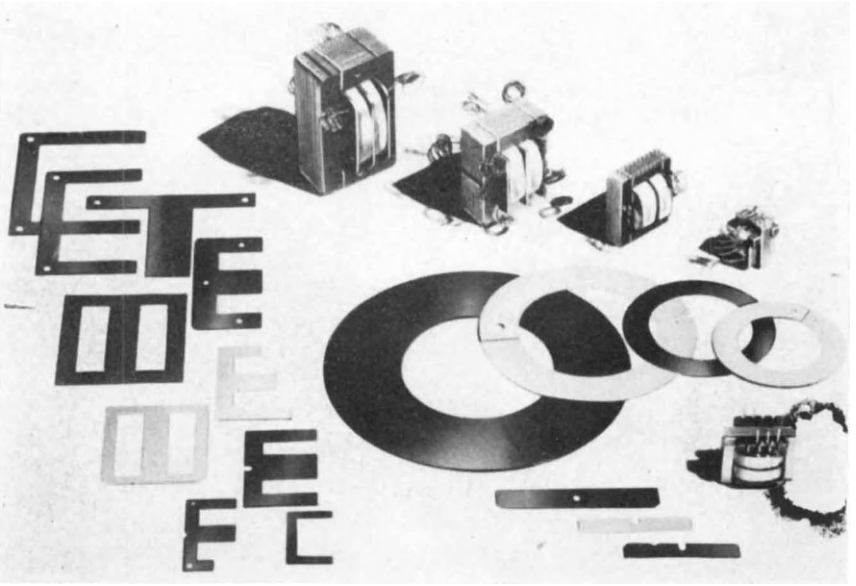


*Figure 13.1. Some core stampings and voice-frequency transformers*[131]

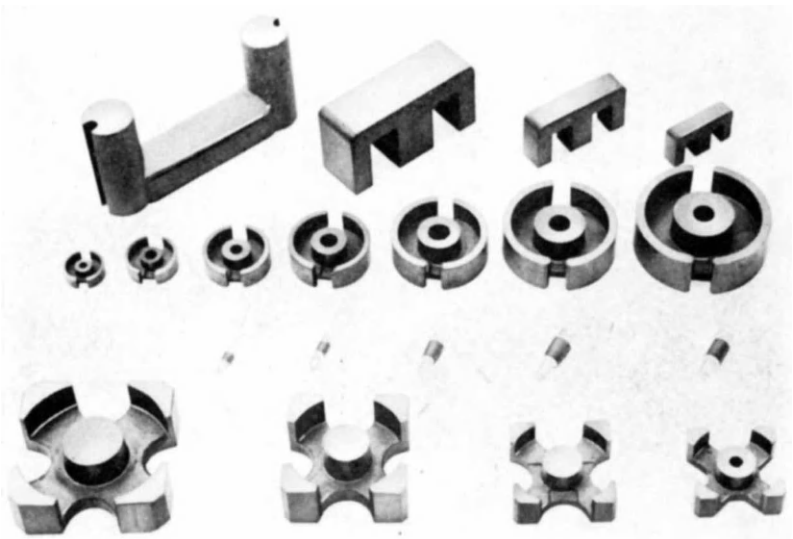


*Figure 13.63. A few of the commonly used ferrite cores in present-day communications. Top row: cores for line transformers, and E cores; middle row, standard series of pot cores with their adjusting elements; bottom row, various X cores*

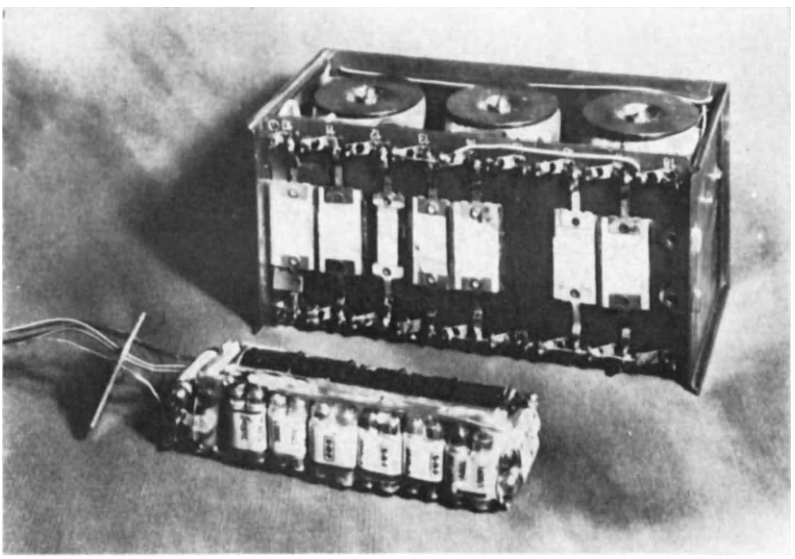


*Figure 13.64. Channel filter with dust cores (background) and with ferrite cores (foreground)*[56]

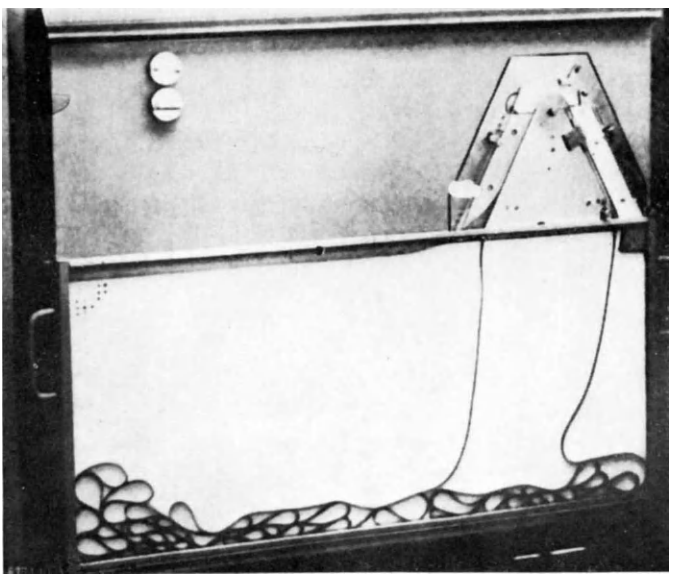


*Figure 15.4. Tape-loop recorder of Bell Telephone Manufacturing Co. Ltd*[176]

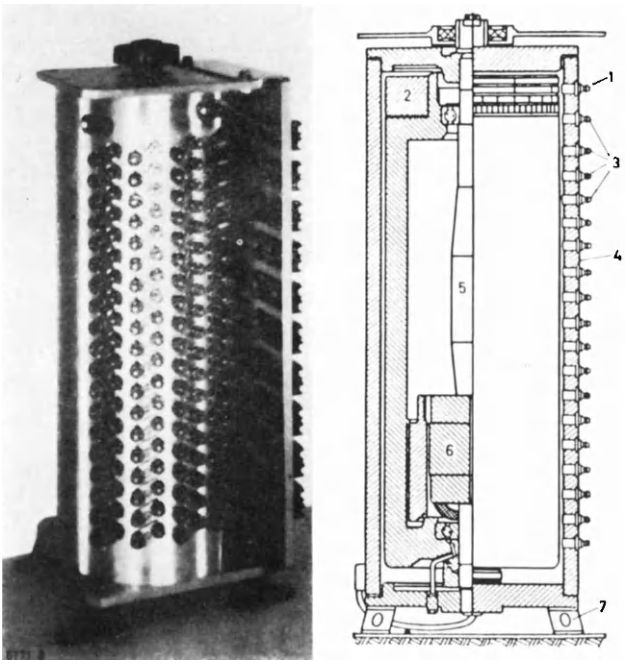



*Figure 15.8. Section and general view of drum store by Standard Electric Lorenz AG: 1, track head; 2, track ring; 3, signal heads; 4, case; 5, fixed axis; 6, external drive motor; 7, vibration absorber made of metal and rubber*[176]

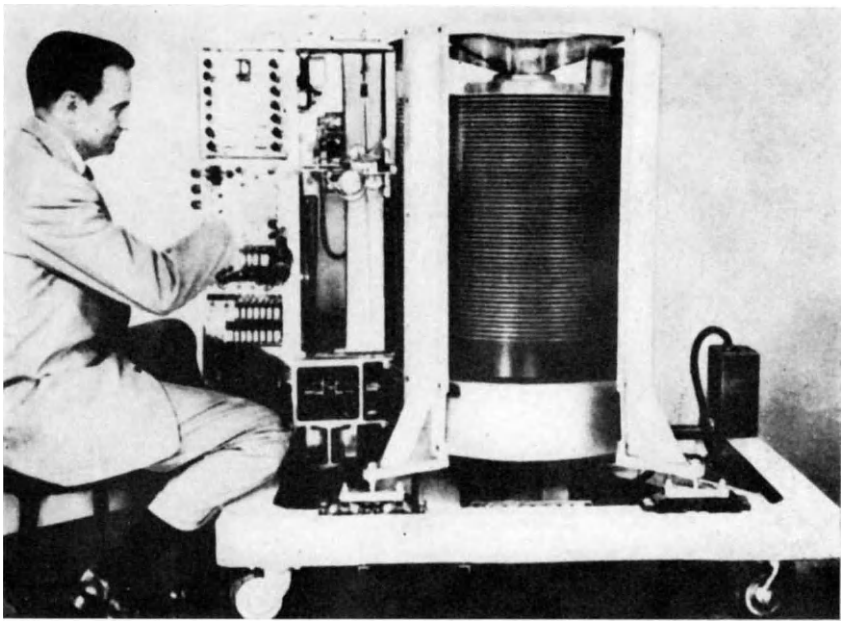


*Figure 15.10. The IBM 305 magnetic disc store*[176]

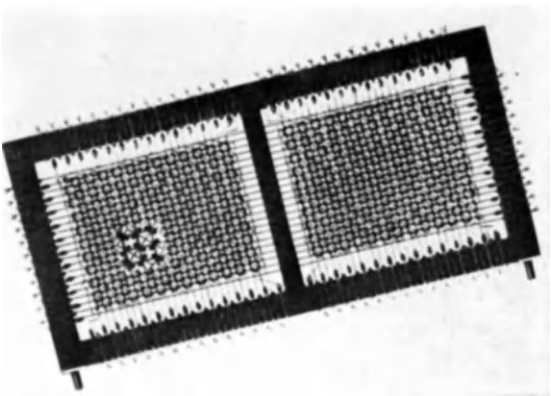


*Figure 15.11. Memory matrix of a working store (left-hand half shows a section magnified)*[126]

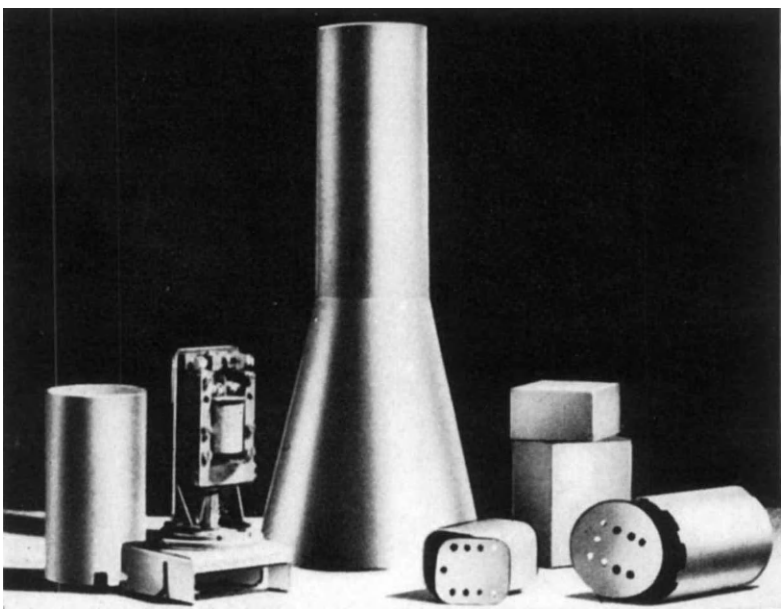


*Figure 17.3. Screens of Permalloy B and Permalloy C*[10]

# 12

# Magnetic materials for relays

## 12.1 USES AND PROPERTIES OF THE ELECTROMAGNETIC RELAY

An electromagnetic relay is an electromagnet which, by means of flux changes in its core, opens or closes one or more electrical circuits. Besides electromagnetic relays there exist, also, electrodynamic, electrostatic, and thermoelectric relays. In principle, magnetostrictive and piezo-electric relays are possible: they are rarely used, however. In the following exposition, 'relay' is always to be understood as meaning 'electromagnetic relay'.

A relay is, then, especially useful when a relatively weak current is required to control a stronger current. This case occurs very often in communications technology. Hence the relay is one of the earliest components in the field of communications. It was invented in 1835 by Joseph Henry and further developed between 1837 and 1838 by Cook and Wheatstone and also by Morse. Even today it plays an overriding role in communications engineering compared with all other components. Not without reason did one expert declare that telephone exchanges are built around relays[30]. The German Post Office, for example, had about 60 million relays in service in 1960.

The great advantage of the relay over other control and amplifying devices, even in modern electrotechnology, is that the exciting circuit and the operating circuit are electrically separated from each other. The relay, moreover, is insensitive to temperature rises and so operating temperatures up to 120°C are quite often found[4]. It can be heavily overloaded, electrically, without being put out of action, but, above all, it lends itself to a great variety of circuit connections.

The external form of the relay has been altered many times during its 125-year history. Because it is required in vast numbers, it has always paid to seek to improve it. In the course of time, following the development of new magnetic materials, the relay has not only become smaller and more sensitive[4], but its reliability and its life have been improved. The original open contacts (Figure 12.1—see plate section), which were affected by atmospheric constituents (oxygen, moisture, dust), are today hermetically sealed[4] and often work in gaseous atmospheres of chosen composition (Figure 12.2)[24].

The excited part of a relay, like that of any other electromagnet, comprises a coil and a magnetisable core. To this is to be added a yoke to conduct

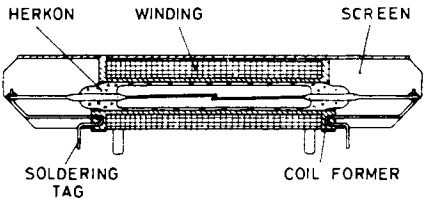



*Figure 12.2. Section through a sealed Herkon relay HR 80/1 (Herkon is a trade name signifying hermetically sealed contacts)*[24]

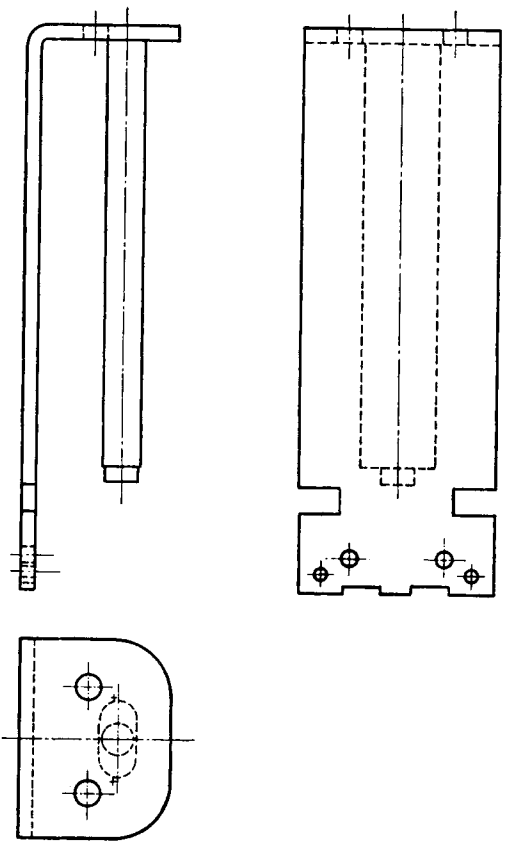


*Figure 12.3. Core–yoke subassembly of a telephone relay*

back the magnetic flux, and a movable part called the armature or the tongue (according to the field of construction) which must also be magnetised. Figure 12.3 is a drawing of these parts—core and yoke—for a telephone relay.

Relays may be operated by a direct or by an alternating current. In order that the force of attraction of an a.c. relay shall remain constant and so that there shall be no mechanical chatter, it is sometimes arranged that, for example, the exciting flux shall be split into two parts mutually out of phase by 90°. The resonance relay offers another solution.

Two kinds of relays are distinguished according to construction and principle of operation, namely the polarised and the unpolarised relay[17]. Schematic diagrams of these relays are shown in Figure 12.4. In the unpolar-

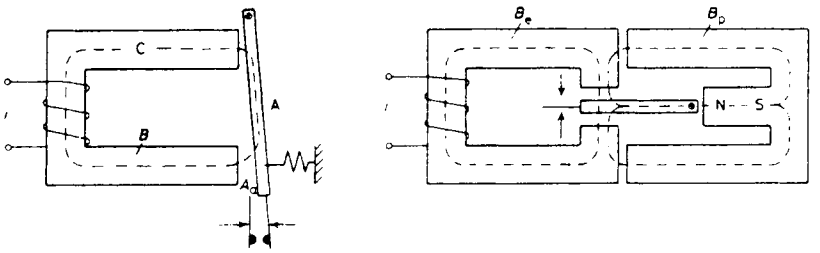



*Figure 12.4. Electromagnetic relays: left, unpolarised relay; right, polarised relay (diagrammatic)*[17]

ised relay the armature A is attracted by the core C with a force which is proportional to the air-gap cross-section $A_a$ and to the square of the flux density $B$ produced by the current $i$ flowing in the coil:

$$P = C_1 A_a B^2$$

In the polarised relay the armature, as well as the exciting flux, is traversed by a permanent flux produced by a magnet (labelled N–S in Figure 12.4). The force of attraction acting on the armature depends equally on the permanent flux density $B_p$ and on the flux density $B_e$ of the exciting flux. Any change, therefore, in the exciting flux causes a change $\Delta P$ in the attractive force. Thus

$$\Delta P = C_2 B_p \Delta B_e$$

It follows from a consideration of the pull of a polarised relay that $P$ is proportional to the reversible permeability[14].

The sensitivity of the polarised relay is superior to that of the unpolarised relay. It follows, also, that in consideration of the directions of permanent or exciting fluxes and the choice of operating and rest positions, the polarised relay offers a greater variety of possible circuit connections. The constants $C_1$ and $C_2$ are determined by questions of material and manufacture.

It is not necessary to discuss here the various detailed forms a relay may take, nor requirements of power, operational speed, and contact arrangements, since these matters have no direct relevance to the materials chosen for core or armature. Further discussion of these matters can be found in the specialised literature[10, 11, 16, 17, 19–22, 25, 26].

## 12.2 MATERIAL REQUIREMENTS FOR CORE AND YOKE

The same considerations apply to the core material of relays as were set out for electromagnets on page 309: a high flux density and a narrow hysteresis loop are the prime considerations. Also, the values should remain constant with time and the material should be as cheap as possible, should be readily workable, and should be insensitive to external influences. The desired corrosion resistance is usually secured by plating with nickel, cadmium, etc. Thus, although the material need not be corrosion-resistant in itself, it must, at least, be such that a protective coating will adhere to it well.

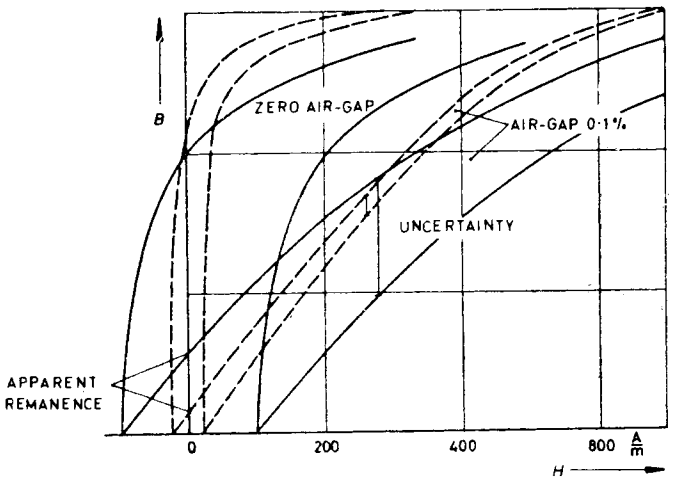



*Figure 12.5. Effect of coercivity on the range of uncertainty*[15]

Loss values should be low and permeability high. As already pointed out, reversible permeability is also of importance for polarised relays. Where eddy currents are to be expected, by reason of rapid flux changes, the material must show a high specific electrical resistance. This is required in relays which are to have a short release time, for example.

The magnetic requirements are related to the functioning of the relay in the following way: a weak magnetic field strength, i.e. a low exciting current, should produce a high flux density in the air-gap so that, without much elaboration, a high attractive force acts on the armature. The coercivity must thus be low and the permeability high. Moreover, a low coercivity is required on other grounds: it ensures that the relay releases easily when the exciting current is interrupted. No special requirements are imposed on the actual remanence of the material since, in order to avoid failure of release, the magnetic circuit is kept open even when the contacts are closed. For this purpose a small distance-piece, the so-called antifreeze disc, made of non-magnetic or weakly magnetic material, is interposed.

The coercivity determines the sensitivity and the range of uncertainty of a relay. To elucidate this, Figure 12.5 shows the hysteresis loops of two

magnetic materials having almost the same true remanence. In the same figure the hysteresis loops are drawn for the magnetic circuit having an air-gap of 0·1%[15]: The broken curves demonstrate that the difference in apparent remanence has become greater. The material with lower coercivity shows the smaller apparent remanence. At the same time the distance between the upward and downward branches of the curve is smaller. This difference is called the 'uncertainty'. Sometimes one finds the term 'uncertainty' applied in the literature to the width of the loop ($2\,H_c$).

Relay cores of low uncertainty are particularly important for those relays where the armature is required to pull up at a clearly defined field strength and to drop off at the same field strength, as nearly as possible. This necessitates, in general, a wide air-gap. However, materials of low coercivity need less gapping than highly coercive materials. In this way the excitation can be made smaller, which leads to lower size and a saving in copper in the windings. Miniaturisation of relays necessitates, among other things, a reduction of coercivity in the core material.

## 12.3 MAGNETIC AGEING

The requirement of constancy in the properties of the core material introduces the concept of ageing. This means the irreversible changes of magnetic properties during storage or as a result of relatively small temperature rises. Hysteresis losses and coercivity both rise as a result of ageing; remanence and maximum permeability fall.

Fifty years ago an ageing coefficient[9] was introduced for electrosheet and defined as the percentage change of the loss figure $W_1$ following an initial heating for 600 h at 100°C. This coefficient was often found insufficiently informative, however. An assessment of the ageing process involved not only the loss figure but also the numerical values of the changing coercivity, remanence, and maximum permeability. Gumlich[9] limited himself, in describing ageing, to the increase of coercivity. He found ageing figures between 1·1 and 2·8 for steel. Today, according to the German Standard DIN 17 405[5], an ageing factor is used as a measure of ageing. It gives the percentage change of coercivity when the specimen is heated for 100 h at 100°C.

Köster[13] was able to show that, particularly at low temperatures, a very slight solubility of nitrogen in iron caused ageing. In electrosteel, however, there may well be 0·008–0·16% N. During storage at only slightly elevated temperatures, the insoluble part of the nitrogen is precipitated as iron nitride. The rise in coercivity associated with the precipitation of fine particles is shown in Figure 12.6, and the solubility curve for nitrogen in iron is plotted in Figure 12.7. These relations shift somewhat if carbon is present in the alloy at the same time.

The tendency to age falls off with increasing content of carbon, silicon, and aluminium. However, under particular manufacturing conditions, a distinct ageing effect is to be observed even for Fe–Si alloys with 2–3% Si and low carbon content. Pfeiffer and Mager[23] were able to show that, according to the annealing temperature, either an $\varepsilon$-carbide phase precipitated out, which in particular greatly increased the coercivity, or, alternatively, a combined

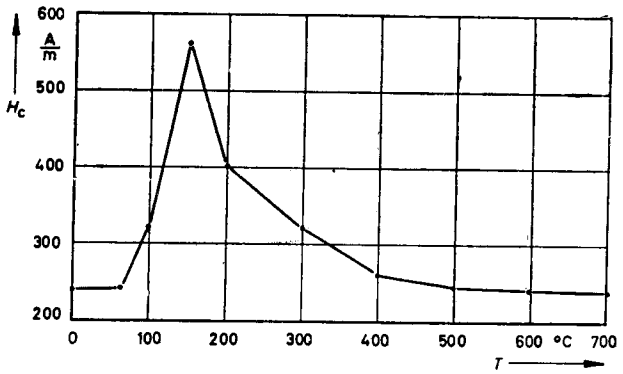



*Figure 12.6. Effect of tempering on the coercivity of nitrogen-containing iron (tempering duration, 1 h)*[13]

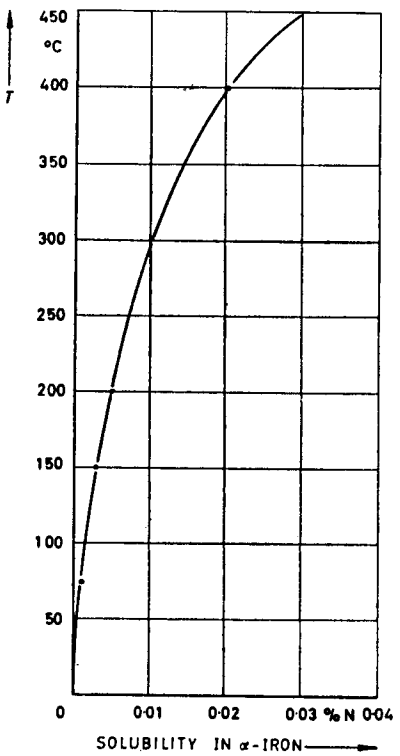



*Figure 12.7. Curve of solubility of nitrogen in α-iron*[13]

Fe–Si carbide which is less effective magnetically. This observed ageing effect can be eliminated by a short annealing at 600°–700°C.

A high nitrogen content can quite significantly increase the coercivity of a material. Köster[13] found that $H_c$ rose by 256 A/m for various steels if 0·01% N was separated out at 100°C. The specific electrical resistance fell under the same circumstances by 13 $\mu\Omega$ cm.

Ageing can have serious effects on the functioning of a relay. For example, certain delayed-release relays showed a change of release current after a time and often the armature failed to fall-off altogether[28]. A check then showed that the coercivity had risen to the point where the fall-off effect of the springs was exceeded. It was found that difficulty could be overcome by subjecting the armature to an annealing in hydrogen. Where the fall-off force, following the usual hermetic annealing, rose by 1·2 N after 1000 h it

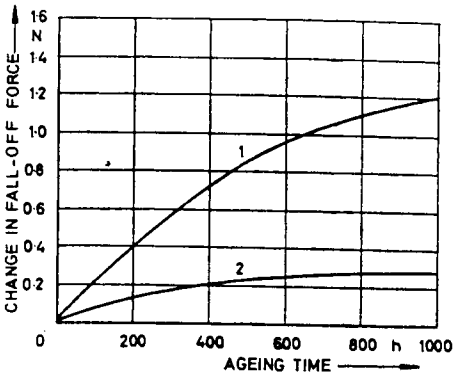



*Figure 12.8. Effect of annealing conditions on ageing of relay iron: 1, normal annealing (hermetically sealed); 2, annealing in hydrogen*[28]

now only rose by 0·28 N after the same interval (Figure 12.8). This annealing had another desirable result at the same time: the permeability of the material was significantly increased and so the attractive force of the armature was increased by approximately 50%.

Since the use of cracked gas is not unusual as an annealing atmosphere, nitrogen which is present can become occluded in the iron, resulting in cores which are susceptible to ageing. The best results are obtained by annealing in a furnace lined with aluminium oxide and by the use of wet hydrogen for the annealing atmosphere. The base material should be as free from additives as possible. As Slausen[28] makes clear, relay iron whose properties have drifted owing to occlusion of nitrogen can be regenerated by a hydrogen annealing.

Fairweather and his co-workers[6], using 'pure' iron whose total impurities in no case exceeded 0·002%, obtained maximum permeabilities of 49 000$\mu_0$ for $H_c$ = 8 A/m. Also, if hydrogen annealing in an oven containing an auxiliary tube of aluminium oxide was carried out, these values did not change after artificial ageing by storing at 100°C. These values could not be achieved if the tube was of silicon oxide. Following annealing in commercial nitrogen, the authors[6] obtained $\mu_m$ = 23 200$\mu_0$ and $H_c$ = 21·6 A/m.

**Table 12.1** EFFECT OF HEAT TREATMENT ON THE COERCIVITY OF UNALLOYED IRON (SEE TEXT)[6]

| *Temperature* (°C) | *First annealing* | | *Aged* $H_c$ (A/m) | *Second annealing* | | *Aged* $H_c$ (A/m) |
|---|---|---|---|---|---|---|
| | *Gas* | $H_c$ (A/m) | | *Gas* | $H_c$ (A/m) | |
| 1 000 | Nitrogen | 69·6 | 101·6 | Hydrogen | 52·0 | 76·8 |
| 1 200 | | 98·4 | 217·6 | | 35·2 | 53·6 |
| 1 000 | Cracked gas | 80·8 | 173·6 | Hydrogen | 64·2 | 94·4 |
| 1 200 | | 60·0 | 206·6 | | 40·8 | 44·8 |

After artificial ageing these values deteriorated to $\mu_m = 13\,600\mu_0$ and $H_c = 40$ A/m.

The summary of Table 12.1 makes the effect of annealing clear[6]. The annealing was carried out on ring specimens within a tube of aluminium oxide. The particular iron investigated contained approximately the following:

| | |
|---|---|
| 0·020% C | <0·005% Cr |
| 0·034% Mn | <0·005% Al |
| 0·030% S | 0·011% Si |
| 0·008% P | 0·116% Cu |
| 0·089% Ni | |

The effectiveness of annealing depends on its duration, the composition of the specimen, the annealing temperature, and the dimensions of the sample. In the examples referred to annealing lasted 3 h.

Pawlek[18] gives another possible method of avoiding ageing in unalloyed iron: the addition of aluminium to the melt causes the formation of aluminium nitride, which passes into the slag. According to Fairweather and coworkers[6], the aluminium component should be about 0·1%.

## 12.4 CLASSIFICATION OF MAGNETICALLY SOFT MATERIALS FOR RELAYS

From a metallurgical standpoint the core and yoke materials used in relays are similar to dynamo sheet. However, they are not employed in the same way in relays, so the guaranteed performance must be determined by other properties. This has led to the specification of a Standard[5] laying down the most important guaranteed values for various materials.

The German Standard classifies the materials into three groups: unalloyed steels, silicon steels, and nickel alloys. Relay materials can be represented by abbreviated names or material numbers. The abbreviation consists of the letter R for relay, the symbol Fe, Si, or Ni to indicate the alloy classification, and a number giving the coercivity in A/m. The standardised materials with their classification codes are given in Table 12.2. They hold for materials

**Table 12.2** CORE MATERIALS FOR RELAYS TO DIN 17 405[5]

| *Type of material* | | $H_c$ (A/m) | *Ageing number* | *Least value of flux density for specified field strength* (V s/m²) | | | | | | | | |
|---|---|---|---|---|---|---|---|---|---|---|---|---|
| *Abbreviated name* | *Material reference number* | | | 20 (A/m) | 50 (A/m) | 100 (A/m) | 200 (A/m) | 300 (A/m) | 500 (A/m) | 1 000 (A/m) | 4 000 (A/m) | 0 (A/m) |
| | | | | *Unalloyed steels* | | | | | | | | |
| RFe 140 | 1.1011 | <140 | | — | — | — | — | 1·15 | 1·30 | — | 1·60 | — |
| RFe 120 | 1.1012 | <120 | | — | — | — | — | 1·15 | 1·30 | 1·45 | 1·60 | — |
| RFe 100 | 1.1013 | 40–100 | | — | — | — | 1·00 | 1·20 | 1·30 | 1·45 | 1·60 | 1·00 |
| RFe 80 | 1.1014 | 40– 80 | <10 | — | — | — | 1·10 | 1·20 | 1·30 | 1·45 | 1·60 | 1·10 |
| RFe 60 | 1.1015 | <60 | | — | — | — | 1·15 | 1·25 | 1·35 | 1·45 | 1·60 | 1·20 |
| RFe 40 | 1.1016 | <40 | | — | — | — | 1·15 | 1·25 | 1·35 | 1·45 | 1·65 | 1·20 |
| RFe 20 | 1.1017 | <20 | | — | — | — | 1·15 | 1·25 | 1·35 | 1·45 | 1·65 | 1·20 |
| RFe 12 | 1.1018 | <12 | | — | — | — | 1·15 | 1·25 | 1·35 | 1·45 | 1·65 | 1·20 |
| | | | | *Silicon steels* | | | | | | | | |
| RSi 48 | 1.3840 | <48 | | — | — | 0·60 | — | 1·10 | 1·20 | — | 1·50 | 0·50 |
| RSi 25 | 1.3842 | <24 | <5 | — | — | 0·60 | — | 1·10 | 1·20 | — | 1·50 | 0·70 |
| RSi 24 | 1.3843 | <24 | | — | — | 1·20 | — | 1·30 | 1·35 | — | 1·50 | 1·00 |
| RSi 12 | 1.3845 | <12 | | — | — | 1·20 | — | 1·30 | 1·35 | — | 1·50 | 1·00 |
| | | | | *Nickel steels and nickel alloys* | | | | | | | | |
| RNi 24 | 1.3911 | <24 | | 0·20 | 0·45 | 0·70 | — | 0·90 | 1·00 | — | 1·18 | 0·45 |
| RNi 12 | 1.3926 | <12 | | 0·50 | 0·90 | 1·10 | — | 1·25 | 1·35 | — | 1·45 | 0·60 |
| RNi 8 | 1.3927 | < 8 | <5 | 0·50 | 0·90 | 1·10 | — | 1·25 | 1·35 | — | 1·45 | 0·60 |
| RNi 5 | 2.4596 | < 5 | | 0·50 | 0·65 | 0·70 | — | — | — | — | 0·75 | 0·30 |
| RNi 2 | 2.4595 | < 2·5 | | 0·50 | 0·53 | 0·55 | — | — | — | — | 0·58 | 0·20 |

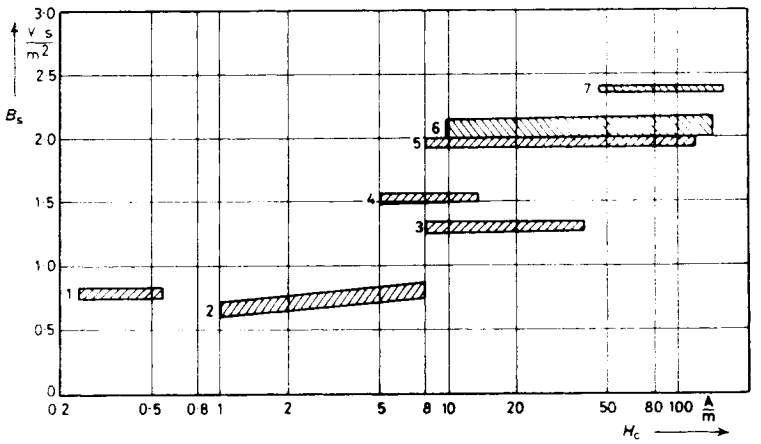



*Figure 12.9. Saturation flux density and coercivity of soft magnetic materials: 1, Supermalloy; 2, Permalloy-type alloys; 3, iron with 36% Ni; 4, iron with 50% Ni; 5, iron with 3–4% Si; 6, unalloyed iron; 7, iron with 50% Co*[3]

after the final annealing. The designations of the chemical composition together with certain physical properties are given in Table 12.3. Figure 12.9 is a schematic representation of the two chief requirements, high saturation flux density and low coercivity, set against each other for the most important materials. It can be seen from this diagram that materials of high saturation density usually show high coercivity and those which have low coercivity have also low saturation flux density[3].

## 12.5 UNALLOYED IRON

High flux densities are most easily and economically achieved with unalloyed iron. The characteristic values obtained in the laboratory for the most significant properties are set out in Table 10.2. The hysteresis loop of commercially pure iron is given in Table 10.3. Unalloyed iron dominates the field of relay cores today as it did decades ago.

Industry manufactures materials of different grades which differ mainly in the guaranteed value of coercivity. In general, the $H_c$ values lie between $<12$ A/m and $<140$ A/m. The saturation value amounts to around 2·15 V s/m². Table 12.4 gives a few d.c. values of flux density at various intensities for a common commercial material known as Hyperm 0[8]. Other trade names for similar unalloyed iron are, for example, Armco pure iron[2], Swedish charcoal-iron, AME[5a] and Minimum[9a].

High-grade materials having an $H_c$ value below 20 A/m are necessary in light-current work (telephone relays), but in the heavy-current field the requirements are usually less severe. The lowest coercivities can be obtained only by using rolled strip. Auto-machining iron gives higher coercivities. In choosing between different grades of iron, the deciding factor may well be workability or material cost.

**Table 12.3** CHEMICAL COMPOSITION AND SOME PHYSICAL PROPERTIES OF RELAY-CORE MATERIALS TO DIN 17 405[5]

| *Type of material* | *Chemical composition (remainder iron)* | *Density* (g/cm³) | *Hardness* (HV) | *Specific electrical resistance* (μΩ cm) |
|---|---|---|---|---|
| | *Unalloyed steels* | | | |
| RFe 140 | 0·10% C | 7·8 | 80–135 | 15 |
| RFe 120 | 0·10% C | 7·8 | 80–135 | 15 |
| RFe 100 | 0·10% C | 7·8 | 80–135 | 15 |
| RFe 80 | 0·05% C, 0·15% Si | 7·8 | 80–135 | 15 |
| RFe 60 | 0·05% C | 7·8 | 80–135 | 12 |
| RFe 40 | 0·05% C | 7·8 | 60–135 | 12 |
| RFe 20 | 0·05% C | 7·8 | 60–135 | 10 |
| RFe 12 | 0·05% C | 7·8 | 60–135 | 10 |
| | *Silicon steels* | | | |
| RSi 48<br>RSi 25<br>RSi 24<br>RSi 12 | ≤0·08% C, 2·5–4% Si | 7·7–7·55 | 130–200 | 42–60 |
| | *Nickel steels and nickel alloys* | | | |
| RNi 24 | ~36% Ni | 8·2 | 130–180 | 75 |
| RNi 12 | ~50% Ni | 8·3 | 130–180 | 45 |
| RNi 8 | ~50% Ni | 8·3 | 130–180 | 45 |
| RNi 5 | 70–80% Ni + small quantity Cu, Cr, Mo | 8·6 | 120–170 | 50 |
| RNi 2 | | 8·6 | 120–170 | 55 |

The bending index in the flexible pre-annealed condition should be over 2 for all types of material. The drawing depth of pre-annealed deep-drawing sheet, 1 mm thick, amounts for RFe to between 9 and 11 and for RNi to over 8; RSi materials cannot be deep-drawn.

**Table 12.4** D.C. VALUES OF FLUX DENSITY IN RELATION TO FIELD STRENGTH FOR RELAY IRON (HYPERM 0)[8]

| *H* (kA/m) | *B* (V s/m²) |
|---|---|
| 0·5 | 1·38 |
| 1 | 1·50 |
| 2·5 | 1·64 |
| 5·0 | 1·72 |
| 10 | 1·86 |
| 20 | 1·98 |
| 30 | 2·05 |

With a view to improving the mechanical workability of iron, it is often enriched with small quantities of lead or phosphorus. These additives help the ductility of auto-machining iron[1], but at the same time they worsen the magnetic properties (material RFe 140).

Time constancy of irons available today is generally sufficient: for a hundred hours heating at 100°C, a rise in coercivity of less than 10% may be reckoned. Naturally, every user would prefer not to have to reckon with any change at all in magnetic properties with time.

Mechanical processing by cropping, stamping, bending, etc., should generally be followed by an annealing operation which removes internal stress and brings out the optimum magnetic qualities. Each material calls for an individual treatment, but a few general rules have already been given on page 312. The guaranteed values for RFe 60 to RFe 120 listed in Table 12.2 refer to a material which received a final annealing for 4 h at 820°C in electrolytic hydrogen and was then cooled from 550°C, in the oven, at a rate not exceeding 30K/h. In special cases the softening annealing is combined with a refining annealing in a hydrogen atmosphere or in vacuo. After a slow cooling down to between 100°C and 200°C, the annealed parts can be brought into contact with the normal atmosphere.

Further magnetic and electrical properties of unalloyed iron are given at the beginning of Table 12.5. The differences between minimum and maximum values are due to variations of types and manufacturers. In the individual classes the suppliers will usually guarantee closer tolerances.

The carbon content of unalloyed steel amounts as a rule to 0·05–0·1% while the silicon content remains below 0·15%.

There are cases where the properties of iron, open or vacuum smelted, do not meet the requirements. The use of carbonyl iron can then bring improvements in relay manufacture. Carbonyl iron is practically free from metallic

**Table 12.5** MAGNETIC AND ELECTRICAL PROPERTIES OF RELAY MATERIALS

| *Material* | $B_{\mu_m}$ (V s/m²) | $B_r$ (V s/m²) | $B_s$ (V s/m²) | $\mu_m$ ($\mu_0$) | $H_c$ (A/m) | $\varrho$ (μΩ cm) |
|---|---|---|---|---|---|---|
| Auto-machining iron | — | 0·8 | 2·05 | 4 300–8 000 | 60–140 | 12–15 |
| Open-smelted iron | 0·8 | 0·9 | 2·15 | 2 200–7 500 | 24–120 | 15 |
| Vacuum-smelted iron | — | — | 2·15 | — | 16– 40 | 12 |
| Carbonyl iron | — | 0·8 | 2·15 | 30 000 | 8–24 | 10 |
| Carbonyl iron critically stretched | — | 0·8 | 2·15 | 40 000 | 6–10 | 10 |
| Fe–Si | | | | | | |
| 1% Si | 0·7 | 0·9–1·45 | 2·1 | 4 000–15 000 | 30–120 | 20–25 |
| 2·5% Si | 0·8 | 0·8–1·2 | 2·0 | 4 000–12 000 | 12–120 | 40–50 |
| 4·0% Si | 0·7 | 0·8–1·2 | 2·0 | 5 000–20 000 | 5– 90 | 45–55 |
| Fe–Ni | | | | | | |
| 36% Ni | 0·5 | 0·8 | 1·3 | 6 000– 14 000 | 8–24 | 70–75 |
| 50% Ni | 0·6 | 0·8–1·2 | 1·55 | 15 000– 60 000 | 5–14 | 40–45 |
| 78% Ni | 0·3 | 0·5–0·75 | 0·6–0·8 | 5 000–300 000 | 1– 8 | 50–53 |

by-products (see page 436). It is procured in powder form, can be sintered, and can also be worked into sheet or strip. Coercivities between 8 A/m and 25 A/m are attainable. The value of 8 A/m can be further reduced if strip material is stretched to a critical degree and subjected to recrystallising annealing[29]. The cost of carbonyl iron treated in this way is relatively high, so it is only worth using in special cases[15].

## 12.6 Fe–Si ALLOYS

If silicon is alloyed with iron, the coercivity is reduced. It varies, according to production methods and to silicon content, between 5 A/m and 120 A/m. For the materials listed in Table 12.2 (to DIN 17 405), the carbon content is

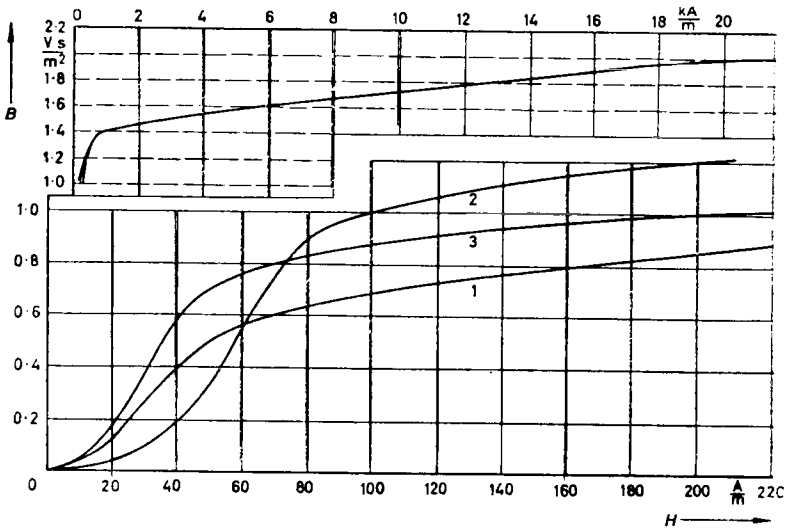



*Figure 12.10. Magnetising characteristics of* Fe–Si *alloys with 2·5–4% Si: 1, Hyperm 1; 2, Hyperm 2; 3, Hyperm 4*[8]

less than 0·08% and the silicon content lies between 2·5% and 4%; $H_c$ varies here between 12 A/m and 48 A/m.

Fe–Si sheet is generally more economical than high-grade unalloyed iron. It also has a better time-stability. On the other hand, the flux density for a given field strength is lower and the workability is not so good. By reason of its brittleness, Fe–Si sheet is not suitable for deep drawing, for example, and, if highly alloyed, must be heated to 100°–200°C even to bend it. Finally, Fe–Si is difficult to nickel-plate uniformly.

The magnetisation curves for three commercial qualities, having 2·5–4% Si, are shown in Figure 12.10[8]. The guaranteed coercivity for the type Hyperm 4, for example, is less than 24 A/m. The values actually achieved are significantly lower. The designer must, however, always reckon with the spread of tolerances and can rarely count on peak values. Reduction of the

range of tolerances is therefore more important for relay design than an improvement in the peak values—a principle which holds for all high-grade mass-produced articles.

Material for relays is produced in bars, or in sheets of corresponding thickness, having isotropic properties. The cores, yokes, and armatures are stamped out, drilled, and formed, and are finally annealed. Usually they are annealed in a protective atmosphere at 800°–850°C and then slowly cooled while still in the oven.

## 12.7 Fe–Ni ALLOYS

A glance at Tables 12.2 and 12.5 shows that with Fe–Ni alloys it is possible to achieve particularly low coercivities, down to 1–2 A/m. If a relay is to have a short release time, then Fe–Ni alloys of 30–50% Ni are used for the

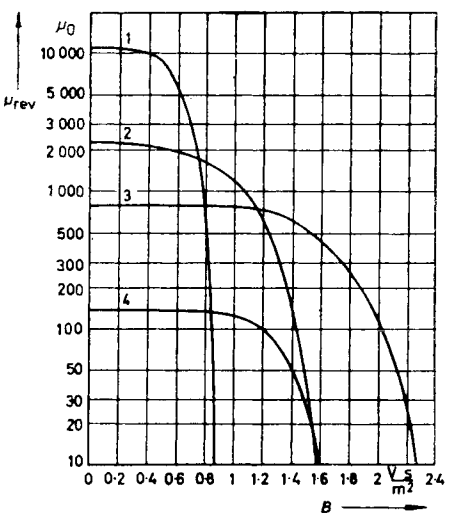



*Figure 12.11. Reversible permeability of a few alloys: 1, 4 Mo-Permalloy; 2, 45 Permalloy; 3, 2 V-Permendur; 4, iron*[14]

core, or alternatively Mumetal, an Fe–Ni alloy with a copper additive. The greater sensitivity justifies the higher price of material.

Table 12.5 makes it clear that the saturation density of richly alloyed materials is not even half that of iron or of Fe–Si. They are not, therefore, very widely used for relay cores. On the other hand, corrosion resistance and ageing stability are very valuable properties of the Fe–Ni alloys.

The magnetisation characteristics for the three principal groups of Fe–Ni alloys are given in Figure 13.24. The 50% alloy has the highest saturation density, the alloy with 76% Ni the greatest initial permeability and smallest coercivity, while the alloy with 36% Ni offers economic advantages by reason of the reduced nickel content. The reversible permeability for a few Permalloy-type alloys is plotted in Figure 12.11[14].

## 12.8 Fe–Co ALLOYS

Fe–Co alloys having 50% Co are distinguished by their very high flux densities (see Figures 12.9 and 13.24). Since the attractive force on a relay armature is proportional to $B^2$, Fe–Co alloys such as Permendur or V-Permendur (see page 428) would seem to be particularly suitable. The high reversible permeability of these materials is also very favourable (see Figure 12.11). However, their high price is against them for most relay applications. The use of Remendur is discussed on the next page.

## 12.9 FERRITES

Since the saturation density of ferrites is even lower than that of richly alloyed Fe–Ni their use for relays is hardly a practical proposition. In this connection, however, a special case should be mentioned in which a particular type of ferrite performs a special function. In a switching device called a Ferreed—the name is compounded of 'ferrite' and 'reed'—a ferrite material is used for the yoke which is more like a permanent-magnet material in its

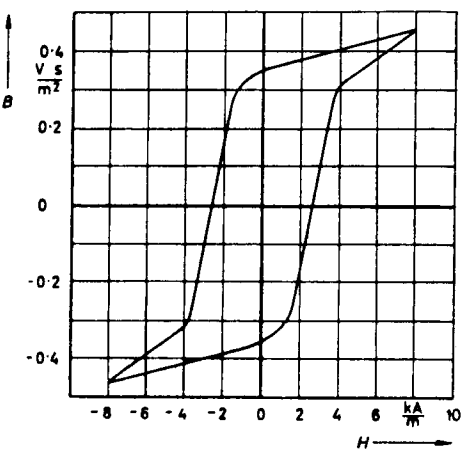



*Figure 12.12. Hysteresis loop of a cobalt ferrite used in a Ferreed relay*[7]

characteristics than the ordinary type of relay material[7]. The relay has to have a high operating speed (operating time around 1 ms). The operating conditions demand, also, as rectangular a hysteresis loop as possible. A cobalt ferrite with a ${}_{B}H_c$ of 2400 A/m (Figure 12.12) fits the imposed conditions well. We are here concerned with a material which was not designed for the highest possible coercivity, like permanent magnets, nor yet for the lowest coercivity like ordinary relay iron: rather must a predetermined $H_c$ value be attained in a definitely specified hysteresis loop.

Besides cobalt ferrite and Co–Zn ferrite[7], it is also possible, according to Schüler[27] and Kikuchi[12], to arrive at the desired properties by using barium ferrite.

A material called Remendur (49% Co, 2·5% V, remainder iron), having a remanence ratio of 0·95 a coercivity of 1·6–4·8 kA/m, and $B_r$ = 1·6–2·15 V s/m$^2$, is admirably adapted to the imposed conditions[7a].

## REFERENCES


1. ACKERMANN, F.: Weichmagnetische Werkstoffe für den Relaisbau (ATM Z 911–10 (263) (Dec. 1957) 279–282).
2. ARMCO STEEL CORP., MIDDLETOWN: Magnetic ingot iron for dc applications (1959).
3. BOLL, R.: Metallische Magnetwerkstoffe und Kernformen in der Nachrichtentechnik (ETZ-A **80** (1959) 582–588).
4. DARR, C.: Miniaturrelais (VDE-Fachber. **19** (1956) II/173–II/176).
5. DIN 17 405, Soft magnetic materials for d.c. relays. Technical conditions for delivery (Apr. 1970).

5a EDELSTAHLWERKE BUDERUS AG, WETZLAR: Data Sheet, Sonderweicheisen AME.

6. FAIRWEATHER, A., HANDS, A. L., LAZENBY, F. and MARR, D.: Specification, treatment and properties of soft irons for electromagnetic relays (Proc. IEE **109 B** (1962) Suppl. 21, 219–228).
7. FEINER, A., LOVELL, C. A., LOWRY, T. N. and RIDINGER, P. G.: The ferreed. A new switching device (Bell Syst. Tech. J. **39** (Jan. 1960) 1–30).

7a FEINER, A.: The ferreed (Bell Syst. Tech. J. **43** (Jan. 1964) 1–14).

8. FRIEDR. KRUPP, WIDIAFABRIK, ESSEN: Hyperm. Data Sheet 546.
9. GUMLICH, E.: Über die Abhängigkeit der magnetischen Eigenschaften, des spezif. Widerstandes und der Dichte der Eisenlegierungen von der chemischen Zusammensetzung und der thermischen Behandlung (Wiss. Abh. P. T. R. **4** (3) (1918) 267–420).

9a GUSSSTAHLWERK BOCHUMER VEREIN AG, BOCHUM: Data Sheet.

10. HEBEL, M. and VOLLMEYER, W.: Das Fernmelderelais. Oldenbourg, München (1961).
11. JAHN, S.: Das Relais in der Praxis. Philler, Minden/Westf.
12. KIKUCHI, H.: Reed relays using barium ferrite magnet (NEC Res. Devel. (4/5) (Apr. 1963) 25–36).
13. KÖSTER, W.: Zur Frage des Stickstoffs im technischen Eisen: (Arch. Eisenhüttenw. **3** (Apr. 1930) 637–658; Stahl u. Eisen **50** (1930) 629–631; Arch. Eisenhüttenw. **4** (1930) 145–150; Stahl u. Eisen **50** (Oct. 1930) 1401–1402).
14. LEGG, V. E.: Survey of magnetic materials and application in the telephone system (Bell Syst. Tech. J. **18** (1939) 438–464).
15. MEYER, H. H. and FAHLENBRACH, H.: Magnetische Werkstoffe für Relaiskerne u. ähnliche Verwendungen (T. Mitt. Krupp **8** (1940) 29–32).
16. MEYERS, M.: The electromagnetic relay (Electron. Techn. (1962) 127–130).
17. MURMANN, D.: Aufbau und Eigenschaften von Relais für die Telephon- und Signaltechnik (Fernmeldepraxis **38** (1961) 625–637).
18. PAWLEK, F.: Magnetische Werkstoffe. Springer, Berlin/Göttingen/Heidelberg (1952).
19. PEEK, R. L.: Analysis of measured magnetization and pull characteristics (Bell Syst. Tech. J. **33** (1954) 79–108).
20. PEEK, R. L.: Estimation and control of the operate time of relays (Bell Syst. Tech. J. **33** (1954) 109–186).
21. PEEK, R. L.: Principle of slow release relay design (Bell Syst. Tech. J. **33** (1954) 187–217).
22. PEEK, R. L. and WAGAR, H. N.: Magnetic design of relays (Bell Syst. Tech. J. 33 (1954) 23–78).

23. PFEIFFER, I. and MAGER, A.: Über Carbidausscheidungen in Siliziumeisen (Phys. Verh. **3** (1962) 372).
24. SCHEIDIG, R.: Herkon Relais 80. Eine Relais-Reihe mit hermetisch abgeschlossenen Kontakten für gedruckte Schaltungen (SEL-Nachr. **7** (1959) 6–8).
25. SCHINDLER, G.: Das Telegraphenrelais als Feingerät und Baustein (Feinwerktechnik **62** (1958) 382–388).
26. SCHLÖGL: Zum Problem der Lebensdauer von Relais und Kontakten in der Fernsprechvermittlungstechnik (Z. Post & Fernmeldew. **13** (1961) 581–584).
27. SCHÜLER, K.: Dauermagnetwerkstoffe für Reed- und Ferreedkontakte (DEW-Techn. Ber. **2** (1962) 148–152).
28. SLAUSEN, W. C.: Improved U, UA and Y type relays (Bell Lab. Rec. **29** (Oct. 1951) 466–470).
29. STÄBLEIN, F.: Technische Werkstoffe grosser magnetischer Weichheit (Z. techn. Phys. **13** (1932) 532).
30. WAGAR, H. N.: Economics of telephony relay applications (Bell Syst. Tech. J. **33** (1954) 218–256).

# 13

# Core materials for inductance coils and transformers

## 13.1 MAGNETIC MATERIALS IN COMMUNICATIONS TECHNOLOGY

The number of types of magnetic material used in heavy-current engineering is only small, but each kind is produced and used in great bulk. It is very different in light-current or communications engineering: the requirements for the cores of coils, transformers, or transducers, or for shielding materials or for switching and storage devices are so numerous, and so widely different, that a great number of types of material is necessary. The quantity of any given material used is often small, but the magnetic properties adapted to particular cases can be of decisive importance for the proper functioning of a device in a communications system[43].

A further point of difference between heavy-current engineering and communications engineering is the low flux densities which appear in the cores of coils and transformers in the latter field. In heavy-current work, the field strengths involved are relatively high, whereas, in weak-current technology, moderate and also extremely low values have to be catered for. In communications-type coils, magnetic fields are generally used which come within the Rayleigh range of the core material.

The frequency range in heavy-current work lies between 0 Hz and $10^2$ Hz, but it extends from $10^2$ Hz to $10^{10}$ Hz in communications work (see Table 13.1). The range of powers lies between $10^2$ W and $10^7$ W in heavy-current technology, whereas in the field of communications small powers from $10^2$ W down to $10^{-10}$ W are used.

From the many-sidedness of communications technology spring the multiple requirements for the magnetic materials it uses.

## 13.2 INDUCTIVELY LOADED CONDUCTORS

Before going into the requirements for coils and transformers in communications, something must be said about inductive loading.

According to Heaviside[53], the inductive reactance of long lines (particularly cables) is too low in relation to their capacitance, i.e. the conductors are too

**Table 13.1** FREQUENCY SPECTRUM AND WAVELENGTH RANGES[22a]

| *Range* | *Frequency* | *Wavelength* | *Usual abbreviation* | |
|---|---|---|---|---|
| | | | *German* | *International* |
| 10 000 metre waves | 3– 30 kHz | 100 km – 10 km | — | v.l.f. |
| Kilometre waves | 30– 300 kHz | 10 km – 1 km | LW | l.f. |
| 100 metre waves | 300–3000 kHz | 1000 m –100 m | MW | m.f. |
| 10 metre waves | 3– 30 MHz | 100 m – 10 m | KW | h.f. |
| Metre waves | 30– 300 MHz | 10 m – 1 m | UKW | v.h.f. |
| Decimetre waves | 300–3000 MHz | 10 dm – 1 dm | — | u.h.f. |
| Centimetre waves | 3– 30 GHz | 10 cm – 1 cm | — | s.h.f. |
| Millimetre waves | 30– 300 GHz | 10 mm – 1 mm | — | e.h.f. |
| Decimillimetre waves | 300–3000 GHz | 1 mm– 0·1 mm | — | — |

'light' and need to be 'loaded' to increase their effectiveness. He proposed the rule for distortionless conductors: the product of resistance $R$ and capacitance $C$ should equal the product of inductance $L$ and leakance $G$, i.e.

$$RC = LG$$

Since this condition is not met by an unloaded line, the current flowing in it is so strongly attenuated that, in the case of a long line, only a weak current arrives at the output end.

Two methods of loading a line are available: continuous loading and discontinuous (or lumped) loading. In continuous loading, sometimes named after Krarup[87], the conductors are wound with a wire or strip of magnetic material. In contrast, Pupin[115] proposed to load the line discretely by means of cores whose inductance and mutual spacing can be calculated.

One speaks of heavy or light Pupin loading according as to whether the inductance used is high (for example, 177 mH) or low (for example, 88·5 mH). Heavy loading reduces attenuation more than light, but the high-frequency cut-off is lowered. In the course of time, therefore, with an ever-increasing emphasis on wide-band transmission, loading became progressively lighter. This was possible without increasing the attenuation because, in the meantime, it had been found that attenuation could be combated by installing amplifiers or 'repeaters'. Fewer coils were then needed in the actual conductors, and they appeared therefore, in different form, in the terminal apparatus, i.e. at the input or the output of the line.

Continuous loading is particularly convenient for telegraph cables which have to be laid in rivers, lakes, and oceans. In telephone cables this type of loading is used only in special cases, as in lead-in or junction cables[54, 100], where the designer is not limited to lengths which have to be integral multiples of the loading interval as in lump-loaded lines. It was, in fact, the desire to find a better Krarup (continuous-loading) material that gave impetus to the research into Fe–Ni alloys and into the multiple-component alloys to which they in turn led. As a result, the transatlantic telephone cable actually laid after the World War II was not a Krarup cable, as had originally been

expected, but a lightly and discontinuously loaded cable with built-in repeaters.

However, the development of high-permeability materials, capable of being rolled down to thin strips, was of more importance to the communications industry as a whole. The materials developed for continuous loading could be used equally well for lumped loading, and they were also suitable for coils used in filter circuits either in compact form as strip-wound cores or as dust cores. Even today, loading coils are made and used—if not in the same quantity as 25 years ago. The core material is almost always ferrite.

The historical development of inductive loading from 1899 to 1940 was described in detail, particularly from the American viewpoint, by Shaw[125]. Dolezalek and Ebeling[32] give an account of the first successful investigations of cables and open-wire lines.

## 13.3 SPECIFIED REQUIREMENTS FOR INDUCTANCE COILS AND TRANSFORMER CORES

High permeability and low power loss head the requirements laid down for a good core material in the communications field. High permeability implies fewer turns on a coil for a given inductance. Hysteresis should be low, especially for coils to be used in filter circuits. These stringent requirements apply to transformers only when they are to be 'distortionless', i.e. free from harmonics of the applied frequencies.

In coil design, particularly for cable loading, two further requirements have played an important part in development, namely constancy of permeability at low field strengths over as wide an intensity range as possible, and independence of the a.c. permeability from the effects of superposed direct fields —i.e. high stability. As a rule, however, high constancy and good stability can be achieved only by a partial surrender of high permeability. Until now, high constancy in respect of time and temperature has been attainable only by introducing air-gaps into the magnetic circuit. Stability and constancy are improved by increased gapping of the core (see page 59). Gapping also reduces the loss resistance due to eddy currents and the residual loss. It is to be noted that, to meet the requirements of a loading-coil specification, the effective resistance of the coil must be small in relation to the resistance of the section of unloaded line.

For coil applications in filter work, a further requirement must be imposed: the temperature coefficient of permeability must be of such magnitude and sign that, in conjunction with the other circuit elements, such as capacitors, the maximum independence of temperature is secured for the working properties.

During the last 50 years the frequencies that have to be transmitted have consistently risen. In the last years of the previous century and the first 15 of this, it was sufficient if voice frequencies could be transmitted, but, following the introduction of carrier telephony and the invention of the vacuum-tube amplifier, much higher frequencies were involved, culminating in the extension to microwave frequencies. Each extension of the frequency range brought with it new magnetic-material problems. At the highest frequencies

other physical laws than those which apply in the audio range are, as it were, brought into play. This fact transforms the requirements to be imposed on magnetic materials for the microwave range, and so their discussion will be deferred to a later chapter. Within the frequency range up to 600 MHz, on the other hand, the language so far used in magnetism is valid.

The dependence of magnetic properties on frequency determines the range of application of the various materials and the form they take. Laminated cores of sheet material in various thicknesses can normally be used in the audio range; the frequency range can be extended upwards if the strip and sheet are sufficiently thin. Cores of solid material, i.e. wire, strip, or sheet, are seldom used, however, above 20 kHz, although the foil cores of storage technique are an exception. For frequencies above 20 kHz, core material must be more finely divided or else materials of greater specific electrical resistance must be used. Compacted or dust cores made of very finely divided iron or of fine particles of iron alloy offer one way to solve the problem and ferrites offer another.

The use of cores in high-frequency coils rests on a compromise: originally, coils without cores were used—the so-called air-cored coils—which were naturally free from core losses. For a given inductance, however, an air-cored coil must have more turns than one having a ferromagnetic core and so the copper resistance is higher. On the other hand, the use of a ferromagnetic core leads to a smaller coil by reason of the smaller amount of copper. Further, by reducing the number of turns, the winding capacity is made smaller. Air-cored coils often need specially shielding whereas, with iron-cored coils, the shielding can be made an integral part of the core (pot cores and shell cores). The inductance of an air-cored coil is not adjustable, but a cored coil is easily adjusted. A whole series of advantages can thus be set against the unwanted core loss, so air-cored coils are now used only in special cases. Moreover, through a wide possible choice of core material, a designer has freedom of manoeuvre in seeking optimum solutions for his circuit problems.

## 13.4 SOLID METAL AND ALLOY CORE MATERIALS

### 13.4.1 Core shapes

#### 13.4.1.1 Toroidal cores

The first cores for coils and transformers were toroidal cores of sheet, wire, or strip. Toroidal cores made from stacks of stamped laminations made sense only for isotropic materials (see Figure 5.2a). Wire cores are made of drawn wire, and strip-wound cores out of rolled strip wound into spirals of the kind sketched in Figure 5.2b.

Wire cores are rarely made today. Formerly, hard-drawn steel wire having a thickness of 0·1 mm and a permeability of about $115\mu_0$ was used[125]. It is true that higher permeabilities are to be obtained with lightly annealed wire,

but hard wire possesses two advantages: because of its higher coercivity the initial permeability remains constant over a wider range of field intensity, and the hysteresis losses in the Rayleigh range are less[130]. This kind of wire was also used for continuous loading.

Strip-wound cores were used for converters, transformers, and transductors where the strays had to be kept low. The use of strip-wound cores is particularly advantageous if the material has a preferred magnetic direction along the strip. If optimum results are to be secured, attention must be paid to the effect of the manufacturing procedure and to the correct dimensioning. Besides the toroidal shape, strip-wound cores may be oval or rectangular[98]. Figure 11.11 shows a few examples. Because of ease of production, the closed shape of the split core is often preferred (see Figure 11.12)[31].

In order to keep eddy currents as low as possible, the strip is often rolled down to the minimum thickness which is commercially acceptable. Strip thicknesses generally used in communications are 40–100 μm. The use of modern multiple-rolling techniques makes the production of 10–30 μm strip feasible[8, 9]; still further reduction in thickness can be achieved by etching, but the expense is justified only in special cases.

Individual turns are insulated from each other to avoid metallic contact. Sometimes an oxide insulator is used which, for materials that have to have a final annealing, performs the added function of preventing the layers sticking to each other. Thus it is possible using a suspension of magnesia in carbon tetrachloride, for example, to deposit a film 1 μm thick which is proof against the effects of heat treatment[10]. In many cases, especially where there is to be no final annealing, a superficial oxidation of the surface or a light lacquer spray is sufficient.

Strip-wound cores are relatively loosely wound in order to avoid unnecessary stresses. They must then be given some rigidity before the copper windings are applied. This is achieved by a suitable dipping or by imbedding the sensitive core in a protective casing of Perlon or some similar material. It must be remembered that eddy currents are greater for broad than for narrow strips and heat treatment is made more difficult. In many cases it pays to use several cores of short axial length rather than one large one.

### 13.4.1.2 Laminated cores

As a rule, cores made from definite-shaped laminations are easier to wind than toroidal cores. DIN 41 302[30] classifies laminations into M, EI, L, and UI shapes. They are so named by reason of their similarity to the corresponding letters. The M-type is electromagnetically superior to the other types for isotropic materials but has the disadvantage that threading these laminations into a coil is time consuming and may sometimes have an effect on the magnetic properties (see page 185).

Figures are used as well as the usual letters to designate core shapes and are related to the external dimensions: an M42 core, for example, has an edge dimension of 42 mm; a UI39 core consists of I laminations 39 mm long with U laminations having a 39 mm shank. Since the sizes of coil formers are

**Table 13.2** LAMINATIONS FOR TRANSFORMERS TO DIN 41 302[30]

| *Core sheet* | *Sheet thickness* (mm) | *Air-gap* (mm) | *Area* (cm²) | *Magnetic path length* (cm) |
|---|---|---|---|---|
| M 20 | 0·05 0·1 0·15 | 0·3 | 2·86 | 4·70 |
| M 30 | 0·05 0·1 0·15 | 0·3 | 6·27 | 7·15 |
| M 42 | 0·05 0·1 0·15 0·35 0·5 | 0 0·3 0·5 1 | 11·93 | 10·2 |
| M 55 | 0·1 0·15 0·35 0·5 | 0 0·3 0·5 1 | 21·72 | 13·1 |
| M 65 | 0·1 0·15 0·35 0·5 | 0 0·5 1 | 30·19 | 15·5 |
| M 74 | 0·15 0·35 0·5 | 0 0·5 1 | 39·95 | 17·6 |
| M 85 | 0·35 0·5 | 0 0·5 1 2 | 56·14 | 19·7 |
| M 102 | 0·35 0·5 | 0 0·5 1 2 | 79·59 | 23·8 |
| EI 42 | 0·35 0·5 | | 11·38 | 8·4 |
| EI 48 | 0·35 0·5 | | 14·98 | 9·6 |
| EI 54 | 0·35 0·5 | | 19·06 | 10·8 |
| EI 60 | 0·35 0·5 | | 23·62 | 12·0 |
| EI 66 | 0·35 0·5 | | 28·40 | 13·2 |
| EI 78 | 0·35 0·5 | | 39·92 | 15·6 |
| EI 84 | 0·35 0·5 | | 46·40 | 16·8 |
| EI 96 | 0·35 0·5 | | | |
| EI 108 | 0·35 0·5 | | | |
| EI 120 | 0·35 0·5 | | | |
| EI 150N | 0·35 0·5 | | | |
| EI 170 | 0·35 0·5 | | | |
| EI 195 | 0·35 0·5 | | 240·1 | 44·5 |
| UI 30 | 0·1 0·15 0·35 0·5 | | 11·62 | 12·0 |
| UI 39 | 0·35 0·5 | | 19·90 | 15·6 |
| UI 48 | 0·35 0·5 | | 30·08 | 19·2 |
| UI 60 | 0·35 0·5 | | 47·36 | 24·0 |
| UI 75 | 0·35 0·5 | | 74·05 | 30·0 |
| UI 90 | 0·35 0·5 | | 106·1 | 36·0 |
| UI 114 | 0·35 0·5 | | 169·5 | 45·6 |
| UI 132 | 0·35 0·5 | | 228·5 | 52·8 |
| UI 150 | 0·35 0·5 | | 296·2 | 60·0 |
| UI 168 | 0·35 0·5 | | 372·5 | 67·2 |
| UI 180 | 0·35 0·5 | | 428·2 | 72·0 |
| UI 210 | 0·35 0·5 | | 580·9 | 84·0 |
| UI 240 | 0·35 0·5 | | — | — |

also standardised (DIN 41 303) the height of the stack is effectively standardised. Table 13.2 sets out the standard M, EI, and UI laminations, their thickness, and the air-gap length (for M stampings). DIN 41 302 also deals with EE, E, and ED stampings, which are not listed in Table 13.2. Besides these, there is a great number of non-standard sizes in use[139] which were developed to meet special conditions or for historical reasons (see, for example, Figure 13.1 in plate section)[131].

The growing demands of technology necessitate new core shapes. The cores listed in Table 13.2 do not include the recent 'miniature' cores (EE8 to EE25 and U13/5·2 to U35/14)[140]. To avoid the difficulty involved in 'coring' a coil, manufacturers often supply their stampings in suitable prestuck packets which can be used if the air-gaps do not have to overlap[141].

### 13.4.2 Types of materials for the cores of communications transformers

Since the number of materials used as sheet or strip for the cores of audio and other light-current transformers is large, it has proved useful to divide them into groups or classes. DIN 41 301[29] distinguishes five classes labelled A, C, D, E, and F. Classes A and C are of nickel-free steel (Fe–Si alloys); D, E, and F are Fe–Ni alloys. Classes A, C, and D are further divided into subclasses designated by adding the figures 1, 2, or 3. The materials in the subclasses differ in the magnitude of their permeabilities and also the change $\delta$ of permeability with field strength. The Standard recognises sheet thicknesses of 0·05 mm, 0·10 mm, 0·15 mm, 0·20 mm, 0·35 mm, and 0·5 mm though they are not all required for every type of material. Table 13.3 lists these materials.

### 13.4.3 Fe–Si alloys

In Chapter 10 the Fe–Si alloys were considered, in the first place, with reference to their use in heavy-current practice, i.e. where the question is one of high flux densities and low frequencies. Statements made there as to density, workability, specific electrical resistance, and anisotropy are valid also for sheet used at low intensities. Preferred magnetic directions, of course, can be used only for cores made of strip or of certain special section-shapes (see Section 11.5).

Here we shall deal only with those properties not hitherto discussed which are important in the low-intensity range—in particular, initial permeability and loss coefficients, together with their dependence on temperature and frequency.

In 1920 the initial permeability reached by the usual commercial Fe–Si sheet materials, such as Stalloy, was around $250\mu_0$[20]. The values were still lower for wire annealed at 800°C in hydrogen. The maximum permeability achieved at $H = 100$ A/m was $4000\mu_0$. Some 20 years later, values of $\mu_i = 800\mu_0$ were reached with commercial alloys containing 3–4% Si. Improvements were due to the use of purer raw materials and, even more, to the development of more suitable heat treatments. Pure hydrogen proved its value as an efficient annealing atmosphere. The degree of purity of the

hydrogen is of critical importance for the success of the annealing. Pawlek[104] was able to show that the presence, in the hydrogen, of quite small nitrogen contamination lowered the initial permeability (see Figure 13.2). In a similar way, carbon was found to lower the permeability. In the experiments, carbon was introduced into the hydrogen in the form of naphthaline. The presence of $1{\cdot}9\times10^{-5}$ vol. % naphthaline, for example, reduced the permeability at $H = 2$ A/m from $2600\mu_0$ to $2200\mu_0$; $1{\cdot}2\times10^{-3}$ vol. % reduced it to $1600\mu_0$ and $3{\cdot}8\times10^{-3}$ vol. % $600\mu_0$. The influence of nitrogen in the hydrogen was hardly perceptible at field strengths over 8 A/m and, in fact, the effect of the naphthaline became progressively less as the intensity increased.

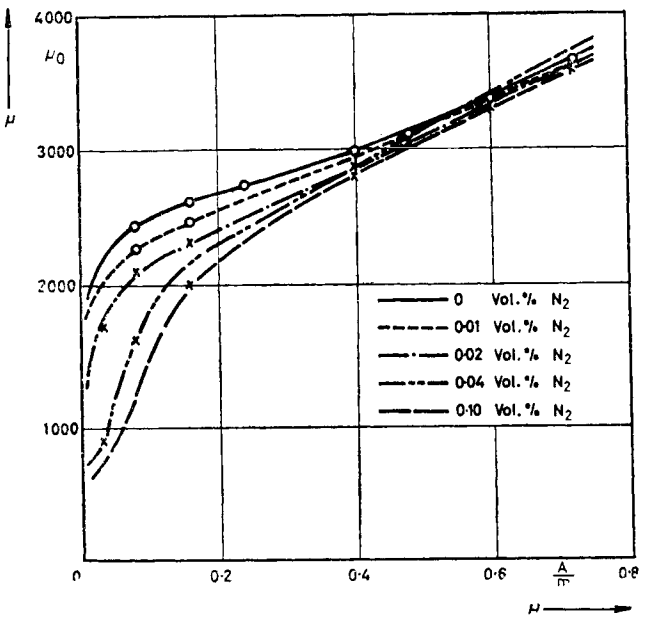



*Figure 13.2. Effect of nitrogen in the hydrogen annealing atmosphere on the permeability of an* Fe–Si *alloy with 3% Si*[104]

High annealing temperatures (1200°–1400°C) were found to be effective. Pawlek[104] obtained initial permeabilities of $1600$–$1700\mu_0$ in an atmosphere of pure hydrogen (see Figure 13.3). Even a figure of $\mu_i = 2000\mu_0$ was reached after vacuum annealing. The values quoted were obtained from measurements made with M42 cores. The presence of some magnetic anisotropy could therefore scarcely have much effect. The permeabilities of single crystals of high-purity iron alloyed with 3·85% Si are given in Figure 4.23. A permeability $\mu_i = 6000\mu_0$ was here obtained in the direction of easiest magnetisation, [100], and in the hardest direction, i.e. the cube diagonal [111], the permeability $\mu_i$ was at least $2000\mu_0$. Thus a $\mu_i$ of $4000\mu_0$ ought to be attainable in polycrystalline material.

Fahlenbrach and Houdremont[39], in their researches, found that an improvement in initial permeability is possible for Fe–Si alloys by low-temperature tempering (400°–800°C) if there is some oxygen in the annealing atmosphere.

**Table 13.3** MATERIALS AND CHARACTERISTIC VALUES FOR TRANSFORMER COILS TO DIN 41 301[29]

| *Abbreviated name* | *Chemical composition* | *Density* (g/cm³) | $\varrho$ (μΩ cm) | $H_c$ (A/m) | $B_s$ (V s/m²) | $T_c$ (°C) | *Sheet thickness* (±10%) (mm) | $\mu_{20}$ ($\mu_5$) | $\delta_5$ $\left(\frac{10^4\ m^2}{V\ s}\right)$ | $\delta_{100}$ $\left(\frac{10^4\ m^2}{V\ s}\right)$ | $\alpha_{\mu_{20}}$ (ppm/K) |
|---|---|---|---|---|---|---|---|---|---|---|---|
| A0 | Steel with ~2·5–4·5% Si | 7·7 | 40 | 100 | 2·03 | 750 | 0·50<br>0·35 | ⩾400 | — | — | +1 000 |
| A2 | | 7·63 | 55 | 60 | 2·0 | | 0·35 | ⩾800 | — | ⩽12·5 | |
| A3 | | 7·57 | 68 | 35 | 1·92 | | 0·35 | >800 | — | — | |
| | | | | | | | 0·20 | >750 | | | |
| C2 | Steel with 3·5–4·5% Si | 7·55 | 50 | 30 | 2·0 | 750 | 0·35 | ⩾1 300 | — | ⩽12·5 | |
| C5* | | 7·65 | 45 | 15 | | | | >800 | | | |
| D1† | Steel with ~36–40% Ni | 8·15 | 75 | 60 | 1·3 | 250 | 0·35<br>0·20<br>0·10 | 2 100±200 | ⩽3·75 | ⩽2·5 | |
| | | | | | | | 0·05 | 2 050±200 | | | |
| D1a | | | | 50 | | | 0·35<br>0·20<br>0·10 | 2 400±300 | | | |

| | | | | | | | | | | | |
|---|---|---|---|---|---|---|---|---|---|---|---|
| | | | | | | | 0·05 | 2 300 ± 300 | | | |
| D3 | | | | 15 | | | 0·35<br>0·20<br>0·10 | ≥2 900 | — | — | +2 000 |
| | | | | | | | 0·05 | ≥2 500 | | | |
| E3 | | 8·6 | 50 | 2 | 0·7–0·8 | 400 | 0·35<br>0·20 | (≥20 000) | | | |
| | | | | | | | 0·10 | (≥18 000) | | | |
| | Ni–Fe alloy with ~75% Ni +additive | | | | | | 0·05 | (≥16 000) | — | — | |
| E4 | | | | | | | 0·35 | (≥35 000) | | | |
| | | 8·7 | 55 | 1 | 0·6–0·8 | 270–400 | 0·20 | (≥40 000) | | | |
| | | | | | | | 0·10 | (≥35 000) | | | |
| | | | | | | | 0·05 | (≥30 000) | | | |
| F3 | Ni–Fe alloy with ~50% Ni | 8·25 | 45 | 10 | 1·5 | 470 | 0·35<br>0·20<br>0·10<br>0·05 | (≥4 000) | — | — | Still to be fixed |

* Grain-oriented material: values hold only for the rolling direction.
† Type D1 should not be used for the development of new transformers.

As Figure 13.4 shows, values of $2300\mu_0$ were obtained. However, the improvement occurred only in those specimens which showed a 'Richter' residual effect. This form of residual effect, which was first noted by Richter[121] in carbonyl iron, is characterised by a strong dependence on temperature. It also occurs in Fe–Si alloys if these are annealed in hydrogen at an elevated temperature, for example at 1100°C. The rise in initial permeability brought about by subsequent tempering of the specimen in an oxygenated atmosphere goes hand in hand with a reduction of the residual effect. At the maximum permeability this thermal residual effect has practically no influence.

If the residual effect of the Fe–Si alloy is reduced by a vanadium additive, higher permeability values are found than without the vanadium. Tempering the vanadium-enriched Fe–Si alloys brings about no further improvement in initial permeability[39].

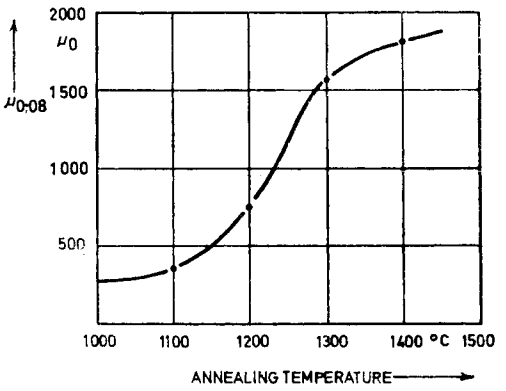



*Figure 13.3.* Fe–Si *sheet with 3% Si; permeability at H = 0·08* A/m *as a function of annealing temperature (4* h *in electrolytic hydrogen)*[104]

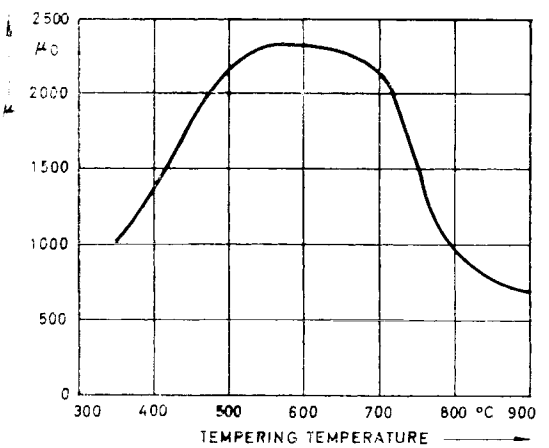



*Figure 13.4. Permeability at B = 0·5* mV s/m² *as a function of tempering heat for a toroid of* Fe–Si *with 3% Si after optimum duration of tempering*[39]

### 13.4.4 Fe–Al alloys

The Fe–Al alloys behave in many respects like the Fe–Si alloys (see Chapter 10). Both alloys are therefore often treated together in the literature. Thus in Fe–Al alloys with 3–5% Al the improvement in initial permeability described in Section 13.4.3 due to tempering at 500°–600°C is also found[39]. In practice, however, the Fe–Al alloys play a role subordinate to the Fe–Si alloys. Of considerable importance are certain richly alloyed Fe–Al alloys known under the trade names Alperm ($\mu_i = 3100\mu_0$), Alfenol ($\mu_i = 3450\mu_0$), and Thermenol ($\mu_i = 7750\mu_0$). The composition and production procedures of these alloys were discussed in Section 10.4. Table 10.11 gives, for comparison, the initial permeabilities relative to $\mu_{20}$ and the other magnetic properties of the Fe–Si and Fe–Al alloys.

### 13.4.5 Fe–Si–Al alloys

In the three-component system comprising iron, silicon, and aluminium there exists a range of composition around 10% Si, 5% Al, remainder iron, having a very high initial permeability. Peak values of $\mu_i = 35\,000\mu_0$ and $\mu_m = 120\,000\mu_0$ are met. The material, however, is very brittle and so cannot be made in sheet or strip form. On the other hand, it can be readily granulated and made into dust cores. Its properties will therefore be dealt with later (Section 13.5.4.4).

### 13.4.6 Fe–Ni alloys

In the second decade of this century, as workers sought a magnetic material whose permeability would exceed that of iron, Elmen and co-workers[3, 37] and also Yensen[149] found Fe–Ni alloys having valuable magnetic properties. These alloys, it is true, had already turned up in the investigations of Hopkinson (1890)[67], of Barret, Brown, and Hadfield (1900), and of Panebianco (1910)[116], but were now really developed for the first time. It was discovered that these materials have a higher specific electrical resistance than iron and that they can be readily worked, so thin strip can be made from them. In the years which followed, Fe–Ni alloys not only gave excellent service at low field strengths but have found a wide range of usefulness at medium and high intensities.

As the graph of Figure 7.4 shows[51], the Curie temperatures are only single-valued for more than 30% Ni, i.e. on heating or cooling the spontaneous magnetism disappears and re-appears always at the same temperature. One speaks, therefore, of 'reversible' alloys. Like nickel, they show a face-centred cubic crystal lattice[96]. In the iron-rich 'irreversible' alloys, heating and cooling bring about a lattice transformation which expresses itself as a break in the curve of Curie temperature. Alloys having less than 30% Ni play only a minor role among magnetic materials, except in special cases, because of this irreversible effect.

The specific electrical resistance of the Fe–Ni alloys is at its highest at 30% Ni and then falls with increasing nickel content (Figure 13.5)[37]. Among the reversible Fe–Ni alloys, those with a composition having some 50% Ni have the highest values of saturation at room temperature (Figure 13.6)[59]. The highest value of initial permeability, as can be seen from Figure 13.7[37], occurs at about 78% Ni. A comparison of the curves of Figures 13.5–13.7 demonstrates that the composition that yields the highest permeability shows a relatively low specific electrical resistance and low values of saturation polarisation. Conversely, an alloy which is characterised by high resistance shows low permeability. As a consequence of this, three groups of alloys are commonly met in practice: those containing roughly 80% Ni, 50% Ni, or between 30% and 40% Ni. According to DIN 41 301 (Table 13.3) these are the groups which correspond to the designations E, F, and D. Each of these groups has its own range of usefulness. Those alloys having around 78% Ni were termed Permalloy by Arnold and Elmen[3] (*Permalloy* = *perm*eability + *alloy*). Later it was sometimes accepted practice to call the whole series of reversible Fe–Ni alloys 'Permalloys' and to indicate the nickel content by a prefixed number, so true Permalloy becomes 78-Permalloy. More usually, nickel content is indicated by a suffixed letter.

The following shows a typical composition for a Permalloy, according to Arnold and Elmen[3].

| | |
|---|---|
| 78·23% Ni | 0·22% Mn |
| 21·35% Fe | 0·37% Co |
| 0·04% C | 0·10% Cu |
| 0·03% Si | Traces of P |
| 0·035% S | |

The basic materials are the purest commercially obtainable iron and nickel, which are melted together in an induction furnace; alternatively powders, as free from impurities as possible, may be sintered. The use of sintered materials is particularly favourable for very thin strips, which show no change in their properties when rolled down to 25 μm thick, though cast material shows a definite fall in permeability and a rise in coercivity[120, 146].

To obtain optimum permeability values from Permalloy it must undergo a special heat treatment after it has been rolled to the final thickness required. This involves two separate annealing operations. First, the material, in the shape of a strip-wound core, is annealed for an hour at 900°–950 K with air excluded and cooled in the oven at a rate of 100 K/h. The measured $\mu_i$ values after this operation lie on curve 1 of Figure 13.7 for the reversible Fe–Ni alloys. In order to achieve the significantly higher value of curve 2, the material must be reheated to 600°C and cooled quickly, for example by removing it from the furnace and laying it on a copper plate kept at room temperature. It is said that a rate of 1500°C/min is the best cooling rate. Initial permeabilities of 13 000$\mu_0$ can thus be obtained[3]. The same procedure is suitable for producing a high maximum permeability: Elmen[37] achieved over 100 000$\mu_0$. The heat treatment that gives the highest permeability is also the condition for getting the lowest $H_c$ value.

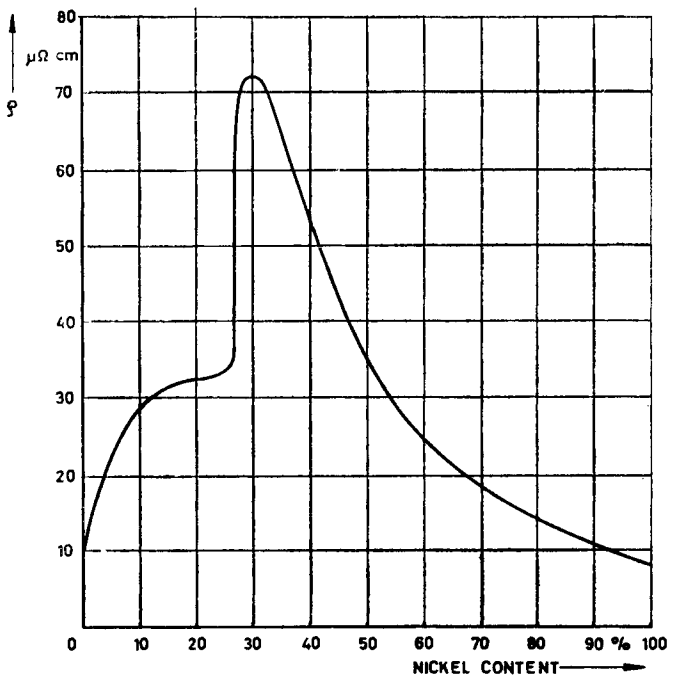



*Figure 13.5. Specific electrical resistance of* Fe–Ni *alloys*[37]

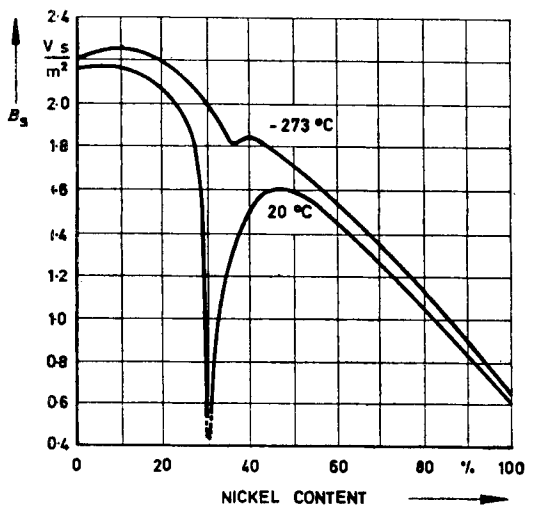



*Figure 13.6. Saturation flux density of* Fe–Ni *alloys*[59]

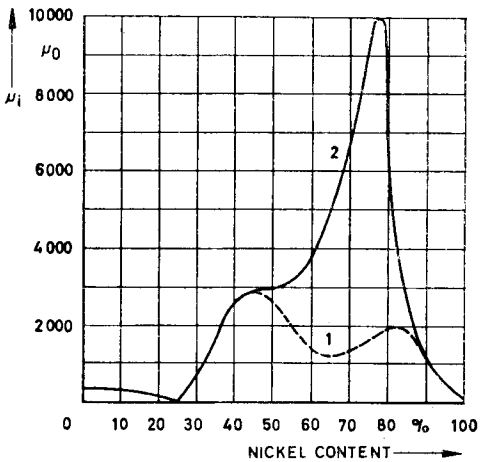



*Figure 13.7. Initial permeability of* Fe–Ni *alloys in relation to heat treatment: 1, slowly cooled; 2, normal Permalloy treatment*[37]

The question of why, precisely, the particular ratio of 78·5% Ni and 21·5% Fe yields such extreme magnetic properties has often been debated. For its elucidation it is important to consider the connection between composition and magnetostriction. This is indicated in Figure 13.8[13], from which it is seen that the magnetostriction along the cubic diagonal [111], the preferred direction for this alloy, passes through zero at 80% Ni. Vanishing magnetostriction means the disappearance of stress—hence the high permeability. That the $\mu$-maxima lie at a point corresponding to rather less than 80% Ni depends, according to Bozorth[12], on the fact that crystal anisotropy also has an effect on the permeability. Crystal anisotropy $K$, however, as is clear from Figures 4.26 and 13.8, passes a null point at around 75% Ni.

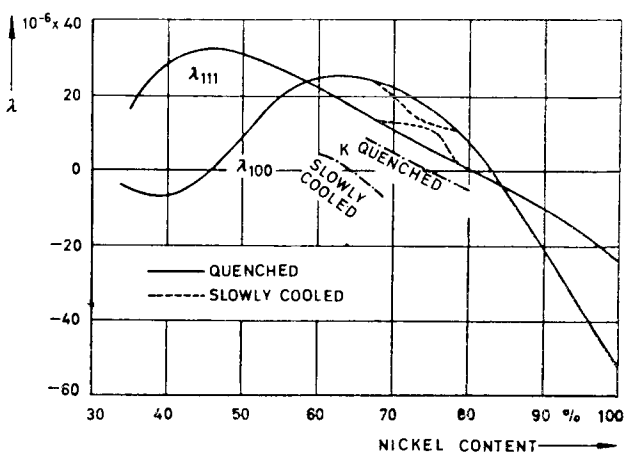



*Figure 13.8. Magnetostriction* $\lambda$ *of quenched and of slowly cooled (aligned)* Fe–Ni *alloys; crystal anistropy K at which magnetostriction passes through zero*[13]

Because of the considerable influence of cooling rate on magnetic performance, a relation arises between the values measured for a particular sample and its dimensions. If the superficial area is small compared with the cubic content, there is no way of realising the expected peak values with such a specimen. This effect of sample size on measured performance creates a difficulty in material production.

It is thus seen to be a matter of importance to reduce the sensitivity of the material to cooling rate by suitable changes in production techniques. To this end it becomes necessary to apply a magnetic field during the long cooling period of the specimen. Thus Kelsall[72], working with an alloy having 78·5% Ni, was able to obtain a $\mu_m$ of 140 000$\mu_0$ for a strip-wound core by employing the following routine: heating to 600°C; cooling to 550°C in an alternating field of 600 A/m; maintenance of this temperature for 5 h; then cooling to 300°C or less before switching off the field. The maximum permeability so achieved is closely related to an initial permeability which is lower than that obtainable by the double annealing and rapid final cooling process: it amounts to around 1750$\mu_0$.

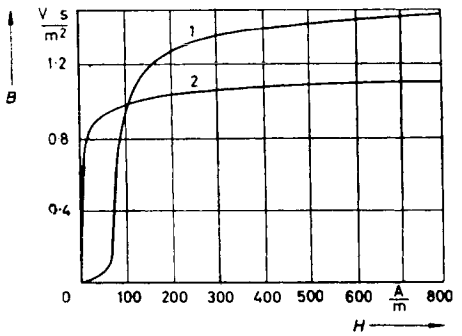



*Figure 13.9. Magnetising curves of unalloyed iron and Permalloy: 1, Armco iron; 2, Permalloy*

Figures 13.9–13.11 give some of the properties of 78·5% Permalloy compared with those of a high-grade unalloyed iron: the flux density of the Permalloy has almost reached saturation before that of the iron has reached the point where flux density rises steeply with applied field intensity. At a flux amplitude up to $B = 0{\cdot}5$ V s/m², the ratio of the loop area of the iron to that of the Permalloy is 16 : 1. Further, it is seen from the plot of $\mu$ against $B$ that the maximum permeability $\mu_m$ of the Permalloy occurs at about half the flux density for which the iron shows a maximum, and that the Permalloy maximum exceeds that of the iron by an order of magnitude.

High-permeability Permalloy strip of 3·1 mm×0·15 mm was first applied to the submarine cable laid in 1924 between New York and the Azores[125]. The telegraphic speed was some 1900 signals per minute[125]. The Krarup strip had a permeability of 2300$\mu_0$, which was 20 times as high as that of the wire that had been used for loading three years previously on the Key-West–Havana cable[17].

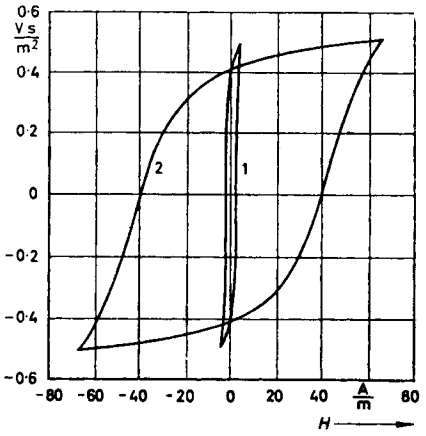



*Figure 13.10. Hysteresis loops for a flux excursion up to 0·5 V s/m²: 1, Permalloy; 2, Armco iron*

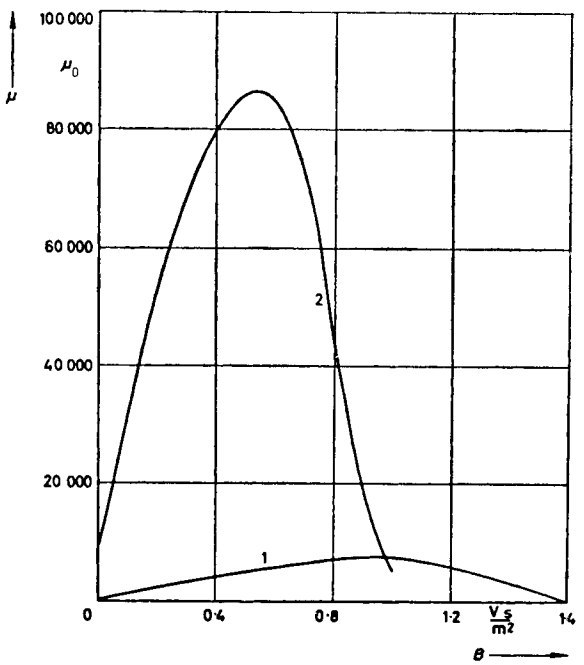



*Figure 13.11. Curves of permeability: 1, Armco iron; 2, Permalloy*

The high nickel content is reflected in the high cost of Permalloy. Moreover, the relatively low saturation density is unsuited to many applications. In applications where high permeability is not so necessary and where costs must be kept down, less richly alloyed materials are used. The most suitable, on economic grounds, are sheets and strips having 30–40% Ni; higher densities are obtained with the 50% alloys.

As far back as 1924, Yensen[149], working with a magnetically isotropic alloy called Hypernik, found that in the range 40–60% Ni it was also feasible, by suitable production procedures, to obtain permeabilities of more than $100\,000\mu_0$, allied to low hysteresis loss, for thin sheet or strip of 0·1–0·35 mm thickness. The material is annealed in hydrogen at high temperatures, which effects a certain purification. Values of $\mu_i$ up to $50\,000\mu_0$ are obtainable in commercial alloys having about 50% Ni[141a]. The alloy known as Permax is further characterised by low coercivity ($H_c = 1{\cdot}2$ A/m) and low loss ($W_1 = 0{\cdot}09$ W/kg for 0·1 mm strip), so this material is especially suitable for the cores of level convertors.

A most valuable property can be obtained with 50% Fe–Ni alloys, namely a well-marked rectangularity of the hysteresis loop (see Figures 5.3 and 11.5). This is brought about by means of a cubic texturing obtained by special treatment procedures (see page 138). Near-rectangular hysteresis loops can also be produced in alloys having 60–65% Ni. Thus remanence ratios ($B_r/B_m$) greater than 0·9 are obtained for Permax Z. The preferred magnetic directions along and transverse to the rolling direction can be commercially utilised in strip-wound cores or by the use of specially shaped stampings. A particularly important field of application has grown up round transductor design (see Chapter 11).

### 13.4.7 Fe–Ni–Mo alloys

It was natural to attempt a reduction of the relatively high conductivity of Permalloy by alloying other constituents with it. Manganese, molybdenum, chrome, tungsten, and copper have proved the most efficacious. Commercially, Mo-Permalloy (Permalloy C), Cr-Permalloy and Mumetal (Mo–Cu-Permalloy) play an important role. Figure 13.12 shows that, in an alloy having 78·5% Ni, the addition of 4% Mo can almost triple the electrical resistance. A similar increase in resistance occurs with those Fe–Ni alloys which are poor in nickel[12].

It was then essential that increases in electrical resistance were not secured at the expense of magnetic quality, but rather that the magnetic properties should show some measure of improvement. It is true that the saturation value fell, as expected, with increased molybdenum content; with 4% Mo it dropped from 1·1 V s/m$^2$ to 0·8 V s/m$^2$ and fell to zero with a 15% Mo content[11], but the initial permeability was materially increased and its sensitivity to changes in cooling rate reduced. If, for example, the material was cooled at a rate of 20–70 K/min, a $\mu_i$ of $25\,000\mu_0$ was obtained[11]. The optimum rate of cooling alters somewhat with the composition of the alloy. Figure 4.19 shows the family of hysteresis loops for 4-79 Permalloy[1].

The Mo-Permalloy known as Supermalloy[10] offers still further improve-

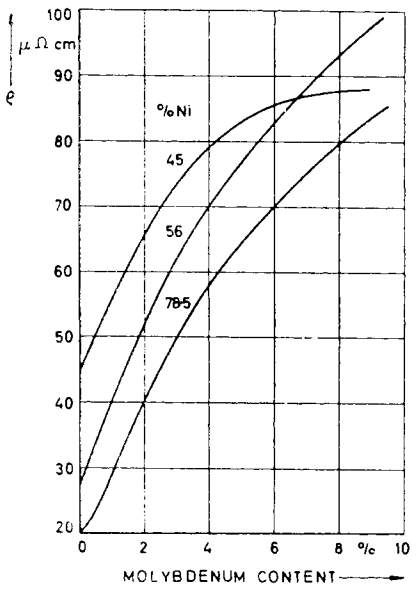



*Figure 13.12. Specific electrical resistance of* Ni–Fe–Mo *alloys as a function of the molybdenum content*[12]

ments. The approximate composition is 79% Ni, 5% Mo, 15% Fe, and 0·5% Mn. Harmful impurities, such as silicon, carbon, and sulphur, are particularly low in this alloy. Thin strips can be made from the material by the usual hot-rolling or cold-rolling operations. Strip-wound cores made from it are usually annealed at 1300°C in pure dry hydrogen and cooled at a critical rate, depending on the actual composition, through the temperature range from 600°C to 300°C.

The most important magnetic properties of Supermalloy are displayed in Figures 13.13–13.15[10]. Figure 13.13 shows the hysteresis loops for Permalloy and Supermalloy measured in a 0·35 mm sheet at an amplitude excursion up to 0·5 V s/m². The ratio of the energies of cyclic magnetisation is 50 : 5.

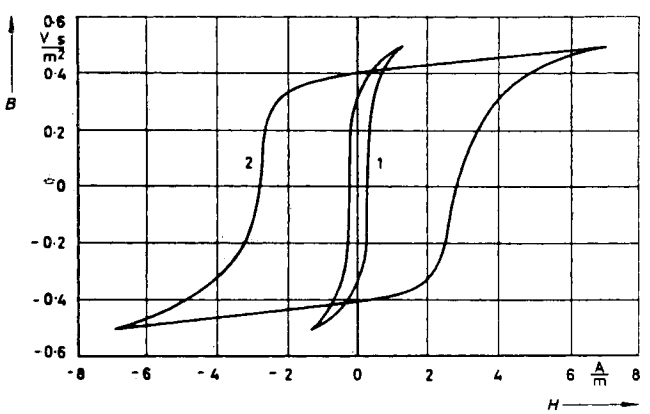



*Figure 13.13. Hysteresis loops: 1, Supermalloy; 2, Mo-Permalloy*[10]

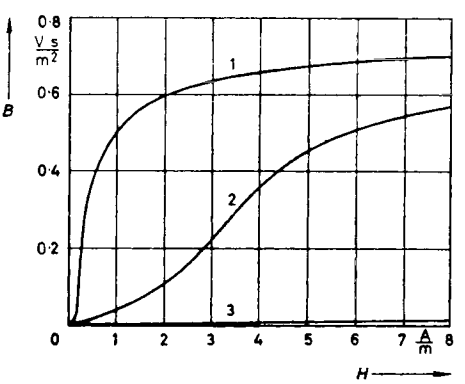



*Figure 13.14. Magnetising curves of Supermalloy, Mo-Permalloy, and iron at low field intensities: 1, Supermalloy; 2, Mo-Permalloy; 3, iron*[10]

There is therefore a similar relation between the two alloys as between iron and Permalloy (Figure 13.10). The hysteresis family of Supermalloy, taken with a 60 Hz sinusoidal current, is shown in Figure 13.16[1]. The rise in flux density with field strength in the lower intensity range is displayed in Figure 13.14. At around $B = 0{\cdot}3$ V s/m² a $\mu_m$ of 900 000 is reached (Figure 13.15); at higher $B$ values, for example 0·7 V s/m², $\mu$ is less than for Mo-Permalloy or iron. The saturation flux density of Supermalloy is somewhat lower than that of Mo-Permalloy, amounting to about $B_s = 0{\cdot}79$ V s/m².

The maximum permeability which can be obtained with Supermalloy depends on the strip thickness: for an insulated 100 μm strip it is twice as high as for a 25 μm strip. In production, the mean value of $\mu_m$ for 25 μm strips is 250 000$\mu_0$ and $H_c$ is 1·2 A/m[10]. For strips 350 μm thick the following values may be taken:

| | |
|---|---|
| Initial permeability | $\mu_i = 50\,000$–$150\,000\mu_0$ |
| Maximum permeability | $\mu_m = 600\,000$–$1\,200\,000\mu_0$ |
| Coercivity | $H_c = 0{\cdot}16$–$0{\cdot}40$ A/m |
| Hysteresis loss ($B_m = 0{\cdot}5$ V s/m²) | $W_h = 5$ erg/cm³ per cycle |
| Curie point | $T_c = 400$ °C |
| Specific electrical resistance | $\varrho = 65$ μΩ cm |

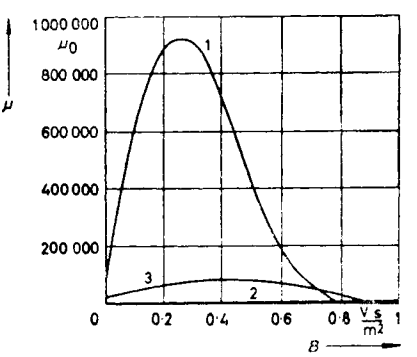



*Figure 13.15. Permeability as a function of flux density for 0·35* mm *Supermalloy strip; for comparison, iron and Mo-Permalloy are also plotted: 1, Supermalloy; 2, iron; 3, Mo-Permalloy*[10]

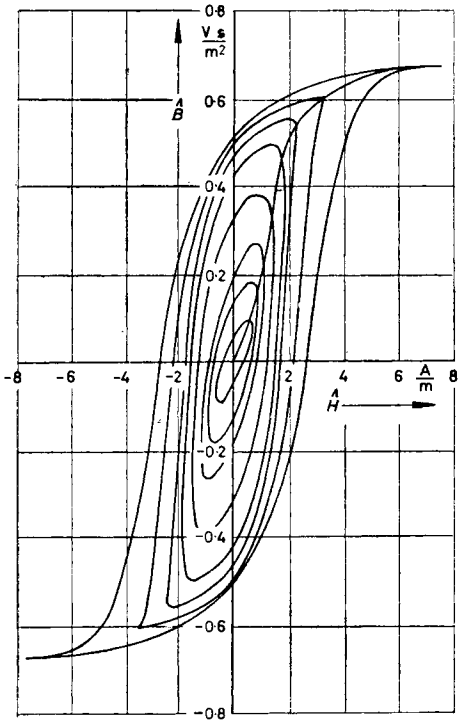



*Figure 13.16. Family of hysteresis loops for Supermalloy at 60* Hz *and with sinusoidal current*[1]

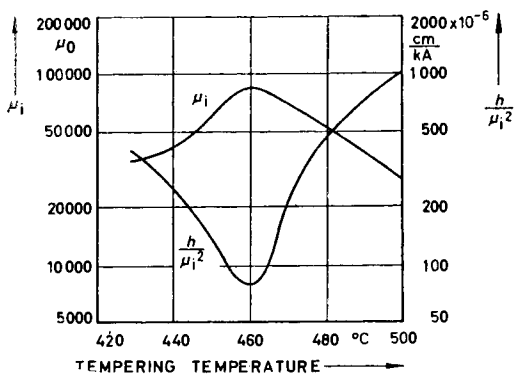



*Figure 13.17. Variation of $\mu_i$ and $h/\mu_i^2$ for a strip-wound core of 0·05* mm *Mo-Permalloy in relation to the tempering heat following annealing at 1200*°C[108, 109]

Pfeifer[108, 109] found a tempering effect for the Permalloys which is specially effective for the initial permeability and the hysteresis factor: if a tempering at 400°–600°C follows the high-temperature annealing at 1000°–1200°C, then the hysteresis factor $h$ is reduced. Figure 13.17 shows an example of this in which the annealing temperature was 1200°C and the tempering heat varied. At about 460°C there occurs a minimum of the referred hysteresis factor $h/\mu_i^2$ together with a maximum initial permeability. It was the final treatment, rather than the temperature of the main annealing, that was decisive for the improvement obtained. This is clearly deducible from Figure 13.18 in that the $h/\mu_i^2$ value lies in a narrow range of variation for the various annealing temperatures employed, while the initial permeability rises with temperature. Rather higher values of $h/\mu_i^2$ are obtained for laminated cores than for strip-wound cores. Experiments with decreasing strip thicknesses show that $h/\mu_i^2$ remains practically constant, i.e. independent of thickness, whereas $\mu_i$ falls. For example, if the thickness is reduced from 50 μm to 10 μm, then $\mu_i$ falls from 80 000$\mu_0$ to 40 000$\mu_0$.

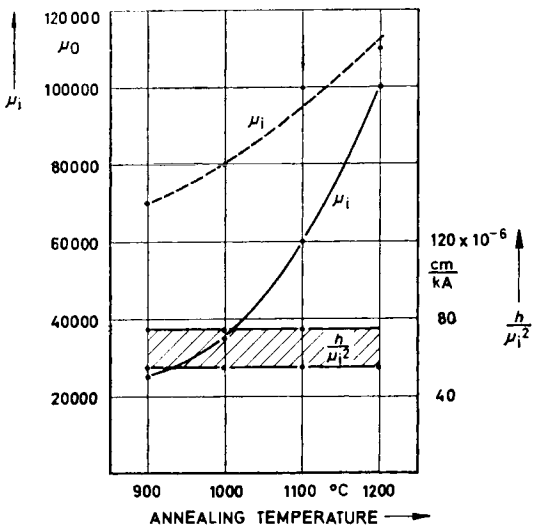



*Figure 13.18. Variation of $\mu_i$ and $h/\mu_i^2$ for a strip-wound core 35* mm×*25* mm×*10* mm *of 0·05* mm *Mo-Permalloy in relation to annealing temperature with optimum tempering; the broken curve applies to an alloy containing copper*[108]

The hysteresis loops of Permalloy and Mo-Permalloy are normal (Figures 4.19 and 13.16). By means of a tempering routine in the critical range 400°–600°C, which lies above the Curie temperature, a rectangular hysteresis loop can be obtained without the use of a magnetic field[109]. It is thus a matter of spontaneous 'squaring'; the material remains isotropic. By varying the tempering heat within a relatively narrow range, one alloy can yield either a high permeability or a high remanence ratio. A maximum remanence ratio $B_r/B_m > 0{\cdot}9$ occurs at some definite amplitude of intensity, for example at $H_m = 7H_c$[109].

The addition of molybdenum also increases the resistance of alloys having a lower nickel content than Permalloy (Figure 13.12). According to Hart[49a] each 1% by weight of molybdenum in an alloy of 65% Ni effects, on the one hand, a 4% reduction in remanence and a 20°C drop in Curie temperature and, on the other hand, a rise of specific electrical resistance of 11 μΩ cm. On this basis, a 65% Ni alloy known as Dynamax was developed[68]. The name is intended to suggest that the dynamic hysteresis loop is especially good and does not broaden much with rising frequency. The coercivity of Dynamax may be as high at 400 Hz as that of molybdenum-free alloy at 60 Hz.

Dynamax contains, besides its 65% Ni and 33% Fe, some 2% Mo and, to improve workability, 0·3% Mn. High permeabilities were achieved in strip-wound cores after a 4 h annealing in pure dry hydrogen and a slow cooling (for example, 150 K/h) from 650°C downwards, in a magnetic field of 800–950 A/m. It was found that the values achieved for maximum permeability, namely about 1 000 000–1 600 000$\mu_0$, can be improved upon if a second recrystallisation annealing is introduced at 1200°C. Howe[68] gives the following values:

$$B_m = 1{\cdot}26 \text{ V s/m}^2$$
$$B_r = 1{\cdot}19 \text{ V s/m}^2$$
$$H_c = 0{\cdot}44 \text{ A/m}$$
$$W_h = 250 \text{ μW s/kg per cycle}$$
$$\varrho = 48 \text{ μΩ cm}$$
$$T_c = 560 \text{ °C}$$

The good magnetic properties of the alloy result from the co-operation of two processes: crystal orientation and magnetic treatment. The texture is characterised by the fact that one of the [100] directions of the elementary cube lies in the rolling direction while the (102) plane lies parallel to the rolling plane.

### 13.4.8 Fe–Ni–Cr alloys

If 4% Cr is alloyed with a 78% Permalloy, the specific electrical resistance is raised from about 20 μΩ cm to 65 μΩ cm—a desirable result; the saturation density is lowered from about 1·1 V s/m² to 0·75 V s/m². The sensitivity of initial permeability to rate of cooling is reduced for Cr-Permalloy as for Mo-Permalloy. By 'furnace cooling' of an alloy containing 3·8% Cr, best values of initial permeability up to 12 500$\mu_0$ can be obtained, while chrome-free alloy treated according to **a** Permalloy routine yields values around 9000$\mu_0$. If the chrome content is 2·1% and if a Permalloy treatment is applied[11], this material can yield $\mu_i = 16\,000\mu_0$. The maximum permeability of commercial alloys with 3·8% Cr lies around $\mu_m = 35\,000\mu_0$. Values of $\mu_m = 65\,000\mu_0$ were achieved in the laboratory[11]. Figure 13.19 gives the reversible permeability of commercially available Cr-Permalloy, and Figure 13.20 sets out the relation between permeability and flux density[37].

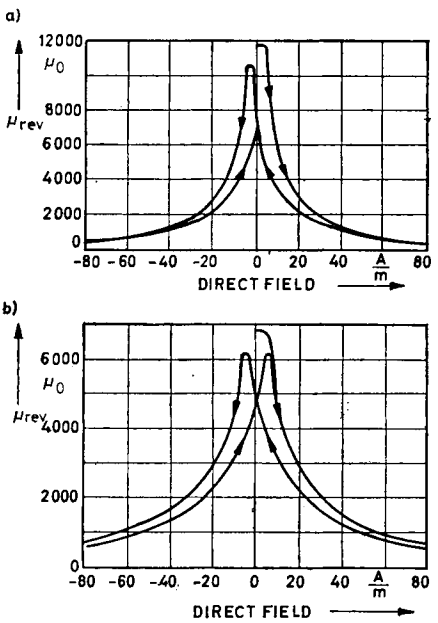



*Figure 13,19. Reversible permeability: (a) Mo-Permalloy; (b) Cr-Permalloy*[37]

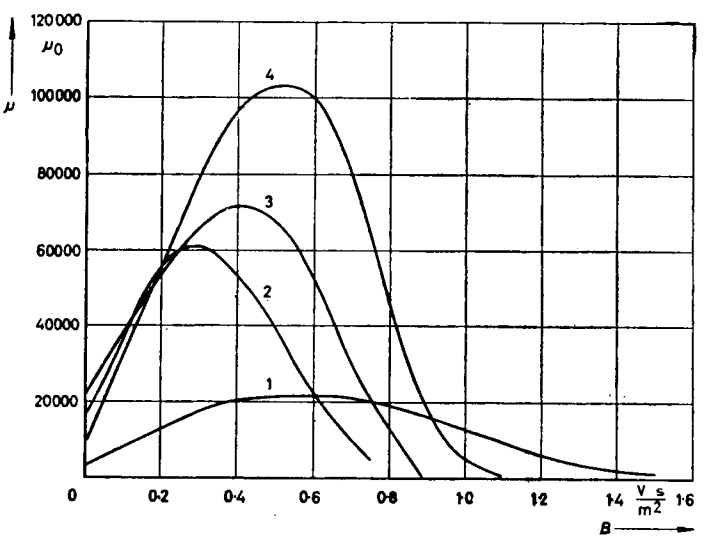



*Figure 13.20. Permeability curves of some* Fe–Ni *alloys: 1, 45% Ni; 2, 3·8 Cr-Permalloy; 3, 3·8 Mo-Pemalloy: 4, 78·5 Permalloy*[37]

A four-component alloy based on Cr-Permalloy is that which has become known as Mumetal ($\mu$-metal)[116]. It contains 75% Ni, 18% Fe, 5% Cu, and 2% Cr. The name Mumetal is also used by some suppliers to indicate an alloy which is identical to 4-79 Mo-Permalloy[11] or which contains molybdenum in place of chromium; for definitions and names of Fe–Ni alloys, see also DIN 17 745[22b].

It is possible with Mumetal to overcome the already mentioned production difficulties of Permalloy and, at the same time, to improve the specific electrical resistance to about 45–55 $\mu\Omega$ cm. The material can be worked into thin strips without special difficulty. The hysteresis family of Mumetal is given in Figure 13.21. At a peak density $B_m$ of 0·8 V s/m², the coercivity $H_c$ is about

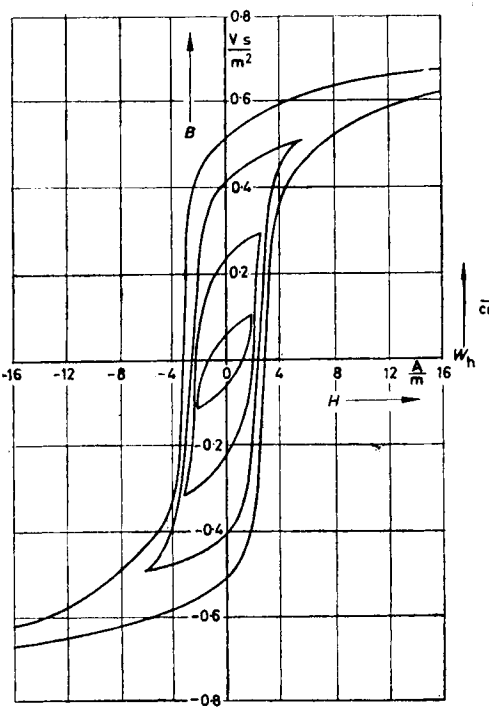



*Figure 13.21. Hysteresis family of Mumetal*[116]

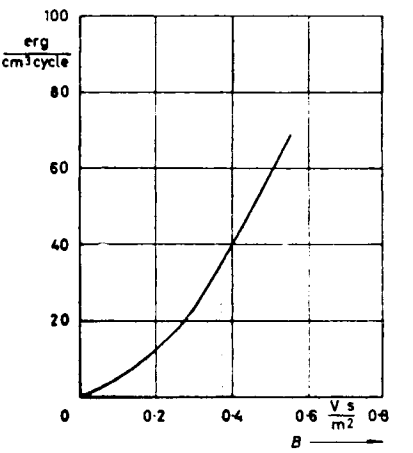



*Figure 13.22. Dependence of hysteresis loss on flux density for Mumetal*[116]

2·4 A/m. The initial permeability or, more accurately, the permeability measured at 0·08 A/m, amounts to 30 000–130 000 $\mu_0$. The hysteresis losses for one magnetic cycle are plotted against peak flux density in Figure 13.22. Table 13.4, after Randall[116], gives a few values of total loss at a peak density of 0·5 V s/m² as a function of sheet thickness and frequency. The loss at 50 Hz is only a quarter that of ordinary Fe–Si sheet.

The effect of post-annealing treatment on highly annealed materials, already mentioned in connection with Mo-Permalloy, i.e. the need for a tempering operation at 400°–600°C, is equally effective with Cr-Permalloy.

**Table 13.4** TOTAL LOSSES FOR MUMETAL ($B_m$ = 0·5 V s/m²)[116]

| *Sheet thickness* (mm) | *Frequency* (Hz) | $W_{0.5}$ (mW/kg) |
|---|---|---|
| 0·37 | 50 | 150 |
| | 600 | 9 000 |
| 0·2 | 5 000 | 18 |
| 0·1 | 5 000 | 5·5 |

Investigations by Pfeifer[108, 109], for example, brought out clearly the influence of tempering sheet on the shape of the hysteresis loop, on the coercivity, and on the remanence ratio. Mumetal 40, Supermumetal 50, and Supermumetal 100 offer further illustrations of this class of materials (see Table 19.14).

### 13.4.9 Fe–Ni–Co alloys

It was a natural consequence of the search for alloys having better magnetic properties than the binary Fe–Ni series that a triple series Fe–Ni–Co, comprising only ferromagnetic elements, should be investigated. In this way the Perminvar alloys, whose composition is set out in Figure 5.12, were discovered. The typical relevance of these alloys to the occurrence of constricted loops was brought out on page 145 and amplified in Figures 5.9, 5.10 and 5.14.

At low field strengths the permeability stays nearly constant over a considerable intensity range and the hysteresis loss remains low. These are properties which are well suited to the inductive loading of cables. It was proposed, therefore, in the 1920s, to use a Perminvar alloy for a telephone cable to be laid between Iceland and Newfoundland[125]. Experimental lengths laid in the Bay of Biscay had, indeed, confirmed the possibility[18], but the project came to nothing because of the economic depression of 1930. Later, the project proceeded on other lines.

The Perminvar treatment consists of a 24 h tempering at 400°–500°C followed by slow cooling. Fe–Ni alloys which have been slowly cooled after a tempering operation, and which show, in consequence, low permeability values (Figure 13.7, curve 1), behave very like Perminvar.

Among the Fe–Ni–Co alloys, that having 45% Ni and 25% Co (point 5 in Figure 5.12) has been intensively investigated. Perminvar-type behaviour is very strongly marked in these alloys (Figure 5.10). Again, in the collective display of Figure 13.23, the typical Perminvar behaviour, in contrast to that of the Permalloy-type alloys, is very clear: the permeability of Perminvar is practically constant even at high intensities where the permeability of the Permalloys is beginning to enter the region of saturation (see also Figure 13.24 and Table 13.5).

The relatively low specific electrical resistance $\varrho = 18\ \mu\Omega$ cm is a point against the Perminvar alloy with 45% Ni and 25% Co. The resistance can be

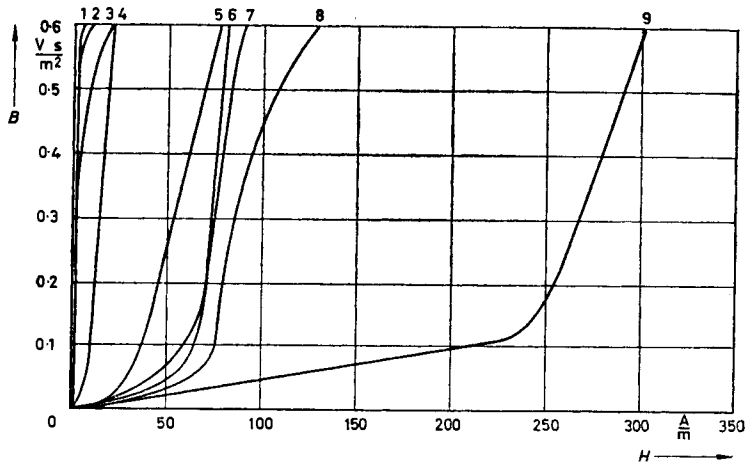



*Figure 13.23. Magnetising curves of Permalloy-type alloys and of Permendur at medium flux densities*[37]

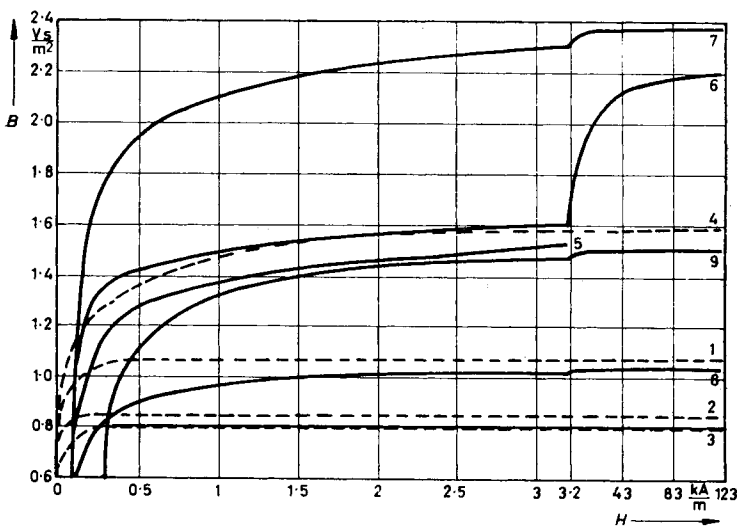



*Figure 13.24. Magnetising curves of Permalloy-type alloys and of Permendur at high densities*[37]

**Table 13.5** PROPERTIES OF THOSE MATERIALS WHOSE CHARACTERISTICS ARE SHOWN IN FIGURES 13.23 AND 13.24[37]

| *Curve* | *Material* | Ni (%) | Fe (%) | Mo (%) | Cr (%) | Co (%) | $\mu_i$ ($\mu_0$) | $\mu_m$ ($\mu_0$) | $B_s$ (V s/m²) |
|---|---|---|---|---|---|---|---|---|---|
| 1 | Permalloy | 78·5 | 21·5 | — | — | — | 10 000 | 105 000 | 1·07 |
| 2 | Mo-Permalloy | 78·5 | 17·7 | 3·8 | — | — | 20 000 | 75 000 | 0·85 |
| 3 | Cr-Permalloy | 78·5 | 17·7 | — | 3·8 | — | 12 000 | 62 000 | 0·80 |
| 4 | Ni–Fe | 45 | 55 | — | — | — | 2 700 | 23 000 | 1·60 |
| 5 | Fe–Si (4% Si) | — | 96 | — | — | — | 600 | 6 000 | 2·0 |
| 6 | Armco iron | — | 99 | — | — | — | 250 | 7 000 | 2·2 |
| 7 | Permendur | — | 50 | — | — | 50 | 700 | 7 900 | 2·4 |
| 8 | Mo-Perminvar | 45 | 23 | 7 | — | 25 | 550 | 3 700 | 1·03 |
| 9 | 45 Perminvar | 45 | 30 | — | — | 25 | 400 | 2 000 | 1·55 |

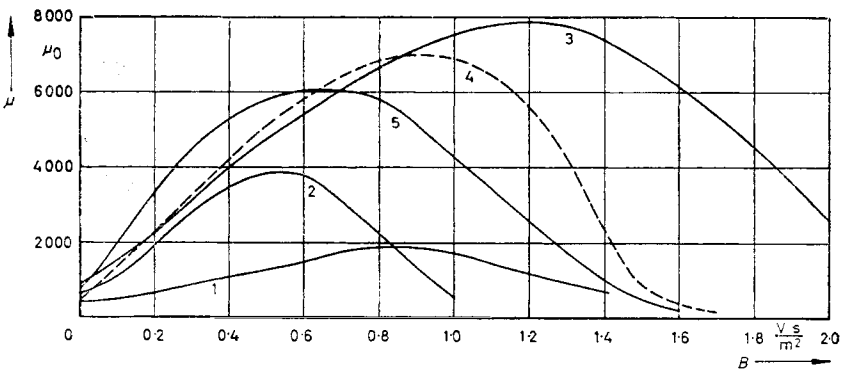



*Figure 13.25. Permability curves of Perminvar and Permendur compared with Armco iron and silicon steel: 1, Perminvar with 45% Ni, 25% Co; 2, Mo-Perminvar with 7% Mo, 45% Ni, 25% Co; 3, Permendur; 4, Armco iron; 5,* Fe–Si

increased by alloying molybdenum without appreciably spoiling the favourable hysteresis properties. Thus alloy having 7% Mo produces $\varrho = 80\,\mu\Omega$ cm; the permeability of the alloy does not, however, remain constant over so wide an intensity range though the maximum permeability is higher than for molybdenum-free alloys (Figure 13.25)[37].

### 13.4.10 Fe–Ni–Cu alloys

The three-component Fe–Ni–Cu system yields both magnetically hard and magnetically soft combinations, the relevant ranges of alloys being indicated in Figure 13.26. The permanent-magnet members of the Cu–Ni–Fe series were dealt with in Section 9.10.2.2. Among the magnetically soft members, Mumetal (which may also be regarded as a four-component material obtained by modifying the Fe–Ni–Cu series) was dealt with in Section 13.4.8.

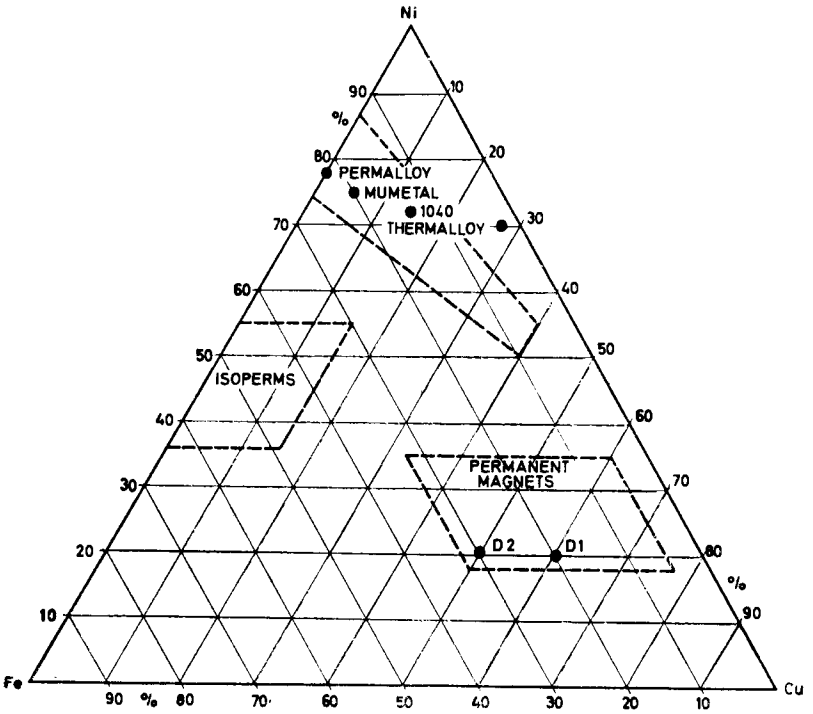



*Figure 13.26.* Fe–Ni–Cu *alloys*

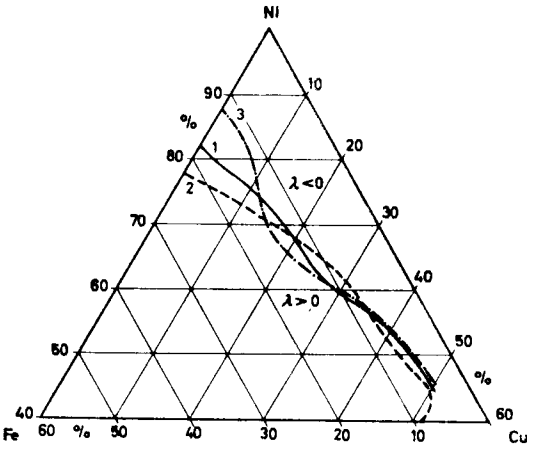



*Figure 13.27. Polycrystalline* Fe–Ni–Cu *alloys: 1, curve for magnetostriction* $\lambda = 0$*; 2, curve for maximum initial permeability assuming Permalloy treatment; 3, curve for maximum initial permeability after 2* h *annealing at 1100°C and slow oven cooling*[6]

The high-permeability Fe–Ni–Cu alloys lie in a region which stretches from Permalloy towards the corner of the triangle labelled 'copper', reaching as much as 50% Cu. According to measurements by v. Auwers and Neumann[5], permeabilities $\mu_i$ of up to 12 000$\mu_0$ can be obtained with these three-component alloys. The highest values of initial permeability follow, more or less, the course of the curve relating composition to the magnetostriction null point ($\lambda = 0$) (Figure 13.27). Later, and somewhat deviant measurements of the curve of $\lambda = 0$ can be found in Bradley[14].

The effect of cooling conditions makes itself felt for alloys having low copper content, just as it does for Permalloy (compare curves 2 and 3 of Figure 13.27). Alloys of greater copper content are less sensitive to variations in heat treatment, but they show a general falling off in saturation density with increasing copper. According to v. Auwers and Neumann[5], the curve relating composition to minimum coercivity follows a similar course to the curve of maximum permeability. Minimum values down to $H_c = 2$ A/m can be reached (for $H_m = 800$ A/m).

A group of alloys known as the Isoperms have a composition of about 0–15% Cu, 36–55% Ni, and are characterised by constancy of low-intensity permeability (see page 155). To obtain the Isoperm effect, a high cold-deformation is required. Figure 13.28 shows an example taken from Kersten[73]: an Fe–Ni alloy having 45% Ni has a normal type of hysteresis loop in the annealed state (curve 3), but the loop is broadened by cold rolling (curve 1). If 9% Cu is added to the alloy and the result annealed for 2 h at 900°C and then cold-worked to 97% deformation, a lancet-shaped hysteresis loop is obtained having very low remanence; this is generally called an Isoperm

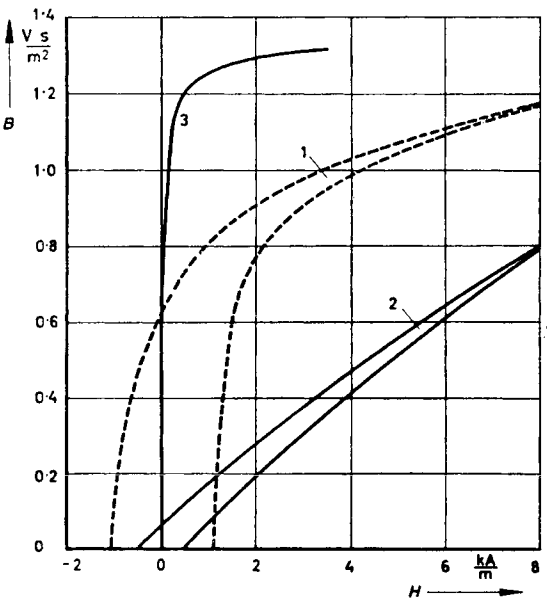



*Figure 13.28. Hysteresis loops of a cold-rolled* Fe–Ni *alloy having 45% Ni, with and without an addition of 9% Cu: 1,* Fe–Ni *rolled; 2,* Fe–Ni–Cu *rolled; 3,* Fe–Ni *and* Fe–Ni–Cu *annealed*

**Table 13.6** LOSS COEFFICIENTS FOR VARIOUS TYPES OF DUST CORES

| *Material* | *Binding material* (Vol. %) | (Wt %) | *Moulding pressure* ($N/m^2$) | $\mu_i$ ($\mu_0$) | $e$ ($\mu s$) | $r$ (‰) | $h$ (cm/kA) | *References* |
|---|---|---|---|---|---|---|---|---|
| Reduced iron | 30 | | 300 | 19 | 0·06 | 14 | 34 | 19 |
| Annealed electrolytic iron | 1 | | 800 | 90 | 8 | 30 | 1250 | 19 |
| | 5 | | 800 | 90 | 10 | 40 | 500 | 19 |
| | 30 | | 300 | 16 | 0·3 | 20 | 110 | 19 |
| Iron dust | | | | | | | | |
| A 1 | | | | 6±0·5 | 0·01 | 1 | 2 | 23 |
| A 2 | | | | 9±1 | 0·015 | 1·5 | 3 | 23 |
| B 1 | | | | 13±1 | 0·015 | 1·5 | 2 | 23 |
| B 2 | | | | 15±1 | 0·02 | 2 | 5 | 23 |
| C 1 | | | | 35±1·5 | 0·05 | 6 | 40 | 23 |
| C 2 | | | | 50±2 | 0·1 | 8 | 50 | 23 |
| C 3 | | | | 65±5 | 5 | 18 | 80 | 23 |
| Neosid E 2 | | | | 25 | 0·023 | 2·3 | 8 | 98a |
| Neosid E 10 | | | | 11 | 0·003 | 1 | 1 | 98a |
| Neosid E 10a | | | | 12 | 0·003 | 1 | 1 | 98a |
| Neosid E 20 | | | | 10 | 0·001 | 1 | 0·4 | 98a |
| Neosid E 100 | | | | 9·5 | 0·0004 | 1 | 0·2 | 98a |
| Neosid E 100a | | | | 5 | 0·0003 | 0·7 | 0·1 | 98a |
| Sirufer 1 | | | | 20 | 0·03 | | | 101 |
| Sirufer 2 | | | | 7 | 0·01 | | | 101 |

| | | | | | | | | |
|---|---|---|---|---|---|---|---|---|
| Sendust | | | | 60 | 0·02 | 11 | 36 | 118 |
| | | | | 100 | | | 80 | 137 |
| Sendust flakes | | | 1 600 | 230 | 0·8 | 22 | 600 | 68a |
| Carbonyl iron | | | | | | | | |
| C | | 4 | 300 | 16 | 0·04 | 12 | 45 | 19, 118 |
| E | | 4 | 300 | 10·5 | 0·005 | 4 | 1·9 | 19, 118 |
| H | | 4 | 300 | 10 | 0·002 | 2 | 1·25 | 19, 118 |
| SF | | 4 | 300 | 9 | <0·002 | 1 | 0·3 | 19, 118 |
| L | | 4 | 300 | 25 | 0·15 | 12 | 134 | 19, 118 |
| MC | 30 | | 300 | 14·5 | | 14 | 13·5 | 19, 118 |
| ME | 30 | | 300 | 11 | | 2 | 1 | 19, 118 |
| MF | 30 | | 300 | 9 | | 1 | <0·3 | 19, 118 |
| 81 Permalloy | | | | 26 | 0·7 | 3 | 11 | 88 |
| | | | | 75 | 3·8 | 3 | 44 | 88 |
| 80% Ni, 20% Fe | 35 | | 1 600 | 12 | 1·0 | 1·5 | 3·5 | 118 |
| | 17 | | 1 600 | 50 | 2·0 | 4 | 19 | 118 |
| | 5 | | 1 600 | 120 | — | 7 | 60 | 118 |
| 2Mo-Permalloy (81% Ni, 17% Fe) | | 1 | 1 500 | 125 | 2·4 | 4 | 34 | 118 |
| | | 3 | 1 500 | 26 | 0·2 | 2 | 8·3 | 118 |
| | | 3 | 1 500 | 26 | 0·13 | 6 | 7·4 | 118 |
| | | 12 | 1 500 | 14 | 0·10 | 1·5 | 3·5 | 118 |
| | | 12 | 1 500 | 14 | 0·05 | 3·3 | 3·0 | 118 |
| Ternary Ni–Fe alloy with 80% Ni | 35 | | 1 600 | 12 | 1 | 1·5 | 3 | 19 |
| | 17 | | 1 600 | 50 | 2 | 4 | 14·5 | 19 |
| | 5 | | 1 600 | 140 | — | 8 | 40 | 19 |

loop (curve 2). The hysteresis losses of an alloy containing copper are lower than for a copper-free material. The Isoperm property is lost if the material receives a final annealing.

An initial permeability $\mu_i = 60\mu_0$ is reached by strip-wound cores of Isoperm having 53% Fe, 36% Ni, and 11% Cu, together with the following Jordan loss coefficients: $h = 30$ cm/kA, $e = 2{\cdot}3$ μs, $r = 4{\cdot}3$ ‰. Isoperm is superior in respect of hysteresis factors to iron dust cores of similar permeability (see Table 13.6)[71]. Moreover, the instability is very low: it amounts to +0·2% as against as much as 0·5% for carbonyl-iron dust cores B1. However, Isoperms are difficult to produce, and so they play little part today in coil design.

A four-component alloy based on 72% Ni, 14% Cu, 3% Mo, remainder iron is the commercially important material M1040. It is similar to Mumetal and is characterised by a $\mu_i$ of around $30\,000\mu_0$ and a $\mu_m$ of $100\,000\mu_0$[99]. These values can be substantially improved by using the purest possible base materials and under optimum conditions of production. Thus Assmüss and Pfeifer[4] obtained initial permeabilities of $100\,000\mu_0$ and maximum permeabilities of up to $680\,000\mu_0$ in laboratory specimens. The composition of this alloy is quoted under E5 in Table 13.7 which also gives a few further alloys of note with their magnetic properties—properties maximised in general by a tempering routine. A composition K3 which comes nearest to the above-mentioned M1040 yields a coercivity of 0·28 A/m.

**Table 13.7** MAGNETIC PROPERTIES OF SOME Fe–Ni–Cu–Mo ALLOYS[4]

| *Alloy designation* | *Analysis* | | | *Quenched* | | | *Tempered* | | |
|---|---|---|---|---|---|---|---|---|---|
| | Ni (%) | Cu (%) | Mo (%) | $\mu_i$ ($\mu_0$) | $\mu_m$ ($\mu_0$) | $H_c$ (A/m) | $\mu_i$ ($\mu_0$) | $\mu_m$ ($\mu_0$) | $H_c$ (A/m) |
| B 5 | 79·25 | — | 4·8 | 12 000 | 80 000 | 1·2 | 91 000 | 475 000 | 0·40 |
| D 5 | 78·5 | 2·0 | 5·1 | 30 000 | 150 000 | 0·96 | 90 000 | 730 000 | 0·32 |
| E 3 | 76·3 | 5·0 | 3·15 | 20 700 | 123 000 | 1·52 | 92 000 | 680 000 | 0·32 |
| E 5 | 76·55 | 5·0 | 5·5 | 22 000 | 115 000 | 0·88 | 110 000 | 620 000 | 0·26 |
| H 3 | 73·65 | 10·2 | 3·2 | 37 000 | 120 000 | 0·96 | 105 000 | 350 000 | 0·40 |
| K 3 | 71·0 | 14·0 | 3·2 | 33 000 | 190 000 | 0·48 | 92 000 | 370 000 | 0·28 |

The temperature coefficient of initial permeability in the region of room temperature is negative for the copper-free Fe–Ni–Mo alloys. Pfeifer[108] discovered that, by adding copper and by using a special final heat treatment, the temperature coefficient of these alloys could be varied over a wide range. As an example, Figure 13.29 shows a plot of permeability against temperature for a 50 μm strip of an alloy made up of 76% Ni, 5% Cu, and 4% Mo. The parameter of the curves is the cooling rate.

### 13.4.11 Fe–Co alloys

An alloy known as Permendur[37], comprising roughly equal parts of iron and cobalt, was produced for use in the communications field. As the comparison

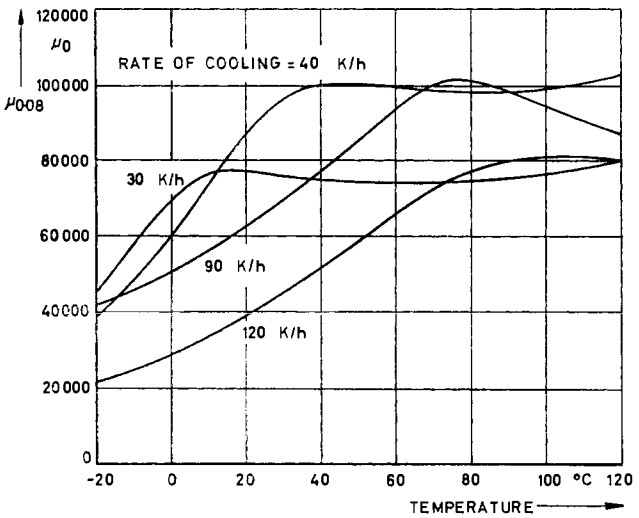



*Figure 13.29. Permeability at 0·08* A/m *as a function of temperature for cores of 50* μm *strip cooled at various rates; alloy comprises 76%* Ni, *5%* Cu, *4%* Mo, *remainder iron*[108]

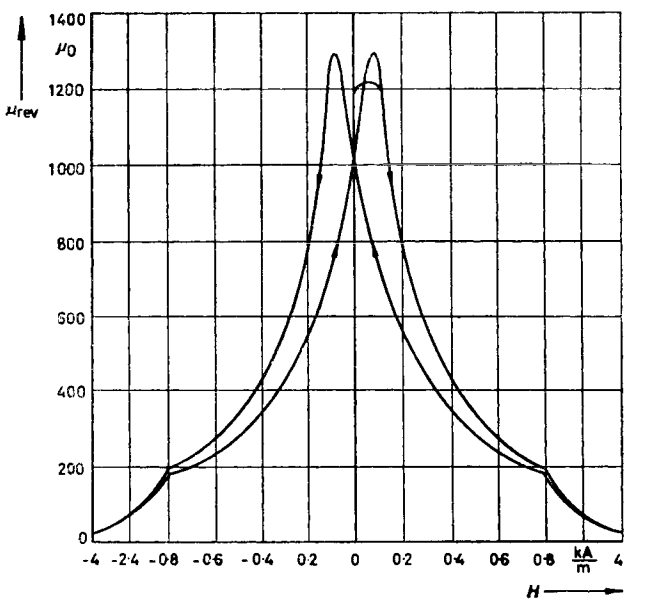



*Figure 13.30. Permendur (50%* Fe, *50%* Co*); reversible permeability as a function of field strength (alternating field: f = 200* Hz, *H = 0·34* A/m*)*[37]

curves of Figure 13.24 and 13.25 show, it is characterised by high permeability at high flux density. The name is intended to indicate that the *perm*eability *endur*es up to high flux densities relative to other similar materials. The initial permeability comes to about $1000\mu_0$ and the maximum permeability

to some $8000\mu_0$. The so-called 'butterfly curve' of reversible permeability is relatively flat (see Figure 13.30) and is distinguished by high $\mu$ values at high field strengths. By superposing a direct field of 800 A/m, the alternating-field permeability obtained for Armco iron is $40\mu_0$ and that for Permendur, amounts to $200\mu_0$.

There are two disadvantages to be set against the favourable properties of Permendur: the specific electrical resistance amounts to only 6 $\mu\Omega$ cm, and rolling out into thin sheets is very difficult because of the brittleness of the material. Both defects can be avoided by the addition of vanadium. For 1·7V-Permendur (i.e. Permendur with 1·7% V) the production of the thinnest strip offers no difficulty, while the specific electrical resistance is raised four-fold ($\varrho$ = 26 $\mu\Omega$ cm). The other properties of the material are as follows:

| | | |
|---|---|---|
| Density | | $d$ = 8·2 g/cm³ |
| Initial permeability | | $\mu_i$ = 700–1000$\mu_0$ |
| Maximum permeability | | $\mu_m$ = 3000–6000$\mu_0$ |
| | | ($H_{\mu_m}$ = 160–480 A/m) |
| Saturation density | | $B_s$ = 2·4 V s/m² |
| Coercivity | (at 2·0 V s/m²) | $H_c$ = 186 A/m |
| Remanence | (at 2·0 V s/m²) | $B_r$ = 1·6 V s/m² |
| Hysteresis loss | (at 2·0 V s/m²) | $W_h$ = 125 000 erg/cm³ per cycle |
| Total loss | | $W_{0.5}$ = 9·2 W/kg |

By reason of the high price of cobalt, V-Permendur is used only in special cases for the cores of transformers. Its main use is in the field of diaphragms for high-grade telephone instruments or for the pole-pieces of servomotors in the aircraft industry; in sum, where high flux density is needed and where price is not the major consideration. In its application to diaphragms for earpieces the high value of reversible permeability at high densities, as well as the high saturation density, is of importance (see Figure 12.11).

A later development of V-Permendur is called Supermendur[45]. This material, also, is readily workable and can be rolled down to strip thicknesses of 8 $\mu$m. A uniaxial anisotropy can be produced by annealing in a magnetic field (see Figure 11.9). Further details are given on page 368. Other Fe–Co alloys have become known, for example under the names Hyperm Co 35, Hyperm Co 50, Vacoflux 50, Vacoflux Z, and Hiperco (see Table 19.12).

## 13.5 DUST CORES

The idea of a dust core, or a core of compacted powder, is old and can be traced back to Heaviside (1887)[52]. As early as 1901 finely divided iron or iron-oxide cores were proposed for cable loading-coils and were made experimentally. However, the wire cores developed at the same time were both better and cheaper. At that time permeabilities of dust cores reached, at most, $10\mu_0$ whereas $\mu$ values of 30–60$\mu_0$ were desired. Cores having these

properties could be manufactured only after the introduction of high moulding pressures[130]. The permeability of a moulded dust core is not determined so much by the permeability of the basic material as by the relative proportion, by volume, of ferromagnetic material in the core. It rises, therefore, with moulding pressure, and this is especially true if the magnetic powder is soft and readily deformable, as in Mo-Permalloy.

Dust cores were first made in large quantities in the USA during World War I for loading coils. As the delivery of steel wire from Germany[74] and of diamond dies from Holland[125] fell off, it became essential to use powdered cores as a substitute. This, however, was only the final impetus to an already moving development. The advancing communications industry demanded stable coils which could then be obtained only by introducing an air-gap normal to the path of the magnetic flux[130].

Dust cores were introduced into high-frequency technology for the first time in Germany, some 30 years ago, under the name Ferrocart[19]. These were made by depositing insulated powder onto paper, which was then rolled up into a small tube or was built in layers into a block which could then be further processed. Dust cores as used today have been known since about 1935.

### 13.5.1 Core shapes

In the development of dust cores, as elsewhere, toroidal cores take precedence in time. In order to get dense, heavily compacted cores, circular discs were first pressed and several of these built into a stack. As moulding techniques improved it became possible to press the rings in one piece and to give them a cross-section suitable for accepting the necessary windings.

In the course of time, shaped cores of many different types evolved, adapted to the needs of high-frequency work. Thus there were H cores, cylindrical cores, threaded cores[101], shell cores, and pot cores—among which the pot core has proved outstandingly useful[25]. Advances in the techniques of pressing and injection facilitated the production of many different and complicated shapes. New plastics such as polystyrene became available as insulators for the powders and made possible the introduction of thermoplastic moulding processes.

Shaped cores triumphed finally over toroidal cores with the coming of core-adjustable inductances. Toroidal cores in an oscillatory circuit were tuned capacitatively by using so-called trimmer capacitors. Pot and shell cores, having an air-gap, needed only the introduction into the gap of a rod or screwed core to adjust the inductance. This method of adjustment is common even today, not only for dust cores but also for ferrite cores.

Pot cores with high-permeability material are especially used in coils for oscillatory and signal circuits, where stray fields must be kept low to reduce coupling with neighbouring coils or to make screening cans unnecessary (since these may introduce additional loss). In the mathematical and experimental researches of Kornetzki[79], the expectation was voiced that, with increasing 'toroidal' permeability of a pot-core material, the measured external stray field would first increase proportionally but finally approach a

fixed end-value, so the ratio of flux in the central boss to the stray flux would become more acceptable as the permeability of the material was raised.

### 13.5.2 Comparison of dust cores and laminated cores

The subdivision of a ferromagnetic core must definitely lead to a substantial fall in permeability and to an increase in the electrical resistance of the coil. Against this may be set the following advantages: lowering of losses, constancy of inductance with intensity, and a reduction of the dependence of permeability on temperature. Constancy with time is also improved by the implicit gapping.

The coil resistance $R_c$ is inversely proportional to the core permeability $\mu$ and the square of the linear dimension $l$:

$$R_c \triangleq \frac{1}{\mu l^2} \tag{13.1}$$

The external dimensions are usually fixed so that the designer has to choose the permeability of the core material.

In a dust core the effective permeability depends on the actual permeability $\mu$ of the ferromagnetic powder, on a packing factor $\alpha$, giving the proportion of ferromagnetic material in the total volume of the core, and on the relative proportion $\theta$ of insulator present. If $\mu$, $\alpha$, and $\theta$ are given, then according to Doebke[33]

$$\mu_{tor} = \frac{1+2\alpha-2\alpha\theta(\mu-1)/\mu}{1+2\alpha-\theta(\mu-1)} \tag{13.2}$$

Ollendorff[102] arrived at a similar formula, although his deductions followed a different route. He took a mean demagnetising factor $g$ for the dust particles, and the formula for $\mu_{tor}$ then took the form

$$\mu_{tor} = \frac{1+(\mu-1)(g\theta+1-\theta)}{1+(\mu-1)g\theta} \tag{13.3}$$

If we take the purely formal relation

$$\frac{1}{g} = 2\alpha+1 \tag{13.4}$$

the Doebke formula can be deduced from the Ollendorff formula.

A quantitative check of the formula is very difficult for various reasons. The permeability $\mu$ of the compressed particles is not measurable and certainly differs from that of the bulk material. Again, the estimation of the proportion $\theta$ of insulating material is very inexact since the manufacture of the core will introduce minute gas bubbles which affect the measured density $d_c$. All the same, some estimate of $\theta$ can be made, taking into account the core density $d_c$, the density of the pressed dust $d_m$, and the density $d_i$ of the insulation:

$$\theta = \frac{d_m-d_c}{d_m-d_i} \tag{13.5}$$

In this formula, $d_i$ can be neglected in comparison with $d_m$. Thus, for example, if $d_m$ be taken as 7·8 g/cm³ (iron) and $d_c = 7{\cdot}3$ g/cm³, then $\theta = 0{\cdot}06$. If $d_i$ is taken as unity, then $\theta$ comes to 0·07. The volume proportion of the insulation should thus be taken to lie between 0·06 and 0·1[22].

As the theoretically deduced formulae fail in many cases, Legg and Given[88] proposed the empirical formula

$$\mu_{tor} = \mu^{\alpha}$$

or

$$\log \mu_{tor} = \alpha \log \mu \tag{13.6}$$

Figure 13.31 shows that the estimation agrees well with the measured values.

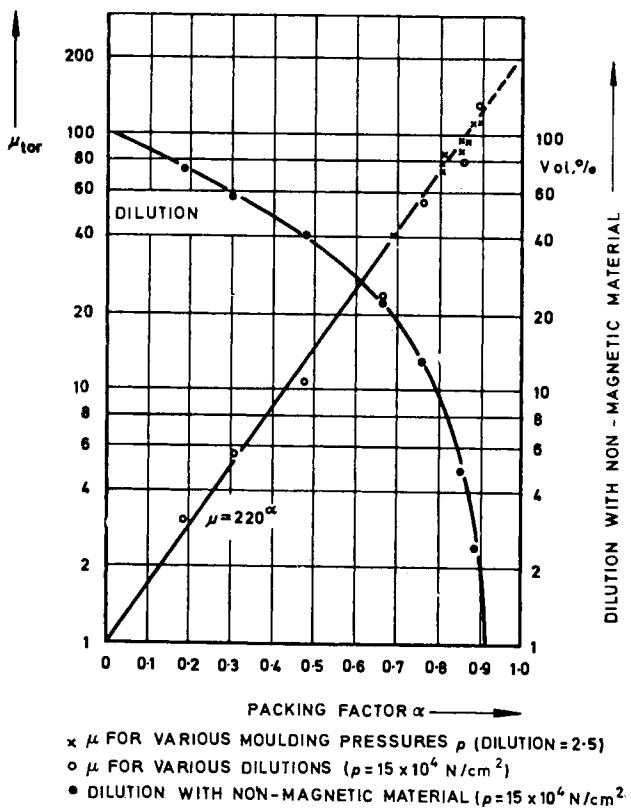
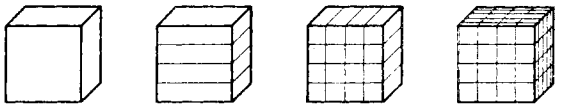



*Figure 13.31. Relation between metal packing factor, permeability, and percentage dilution of the magnetic material*[88]

The toroidal permeability (initial permeability) attainable in an iron dust core amounts to about $50\mu_0$. An example, following Deutschmann[22] is worked out in Figure 13.32, showing how the Rayleigh constant $\nu$ and the Jordan



| | SOLID CORE | LAMINATED CORE | WIRE CORE | DUST CORE | |
|---|---|---|---|---|---|
| $\mu_i$ | 500 | 475 | 450 | 50 | $\mu_0$ |
| $\nu$ | 220 | 220 | 220 | 0.3 | |
| $e$ | 1000 | 48 | 18 | 2 | μs |
| $r$ | 54 | 54 | 54 | 6 | ‰ |
| $h$ | 3200 | 3200 | 3200 | 40 | $\frac{cm}{kA}$ |

*Figure 13.32. Properties of cores with various amounts of subdivision*[22]

loss coefficients, $e$, $r$, and $h$ change if an iron die is cut up in stages, by suitable planes, into sheets, wires, and dust.

The difference between solid, laminated, and dust cores is brought out even more clearly if the effective resistance of a coil, considered as the sum of the ohmic and the loss resistance, is calculated for the four cases as a function of frequency and of current. Even for vanishing current intensity

**Table 13.8** LOSS RESISTANCE AS A FUNCTION OF FREQUENCY AND CURRENT INTENSITY FOR VARIOUS DEGREES OF SUBDIVISION[22]

| $f$ (kHz) | *Loss resistance* | $i = 0$ | | | | $i = 10$ mA | | | |
|---|---|---|---|---|---|---|---|---|---|
| | | *Solid* | *Sheet* | *Wire* | *Dust* | *Solid* | *Sheet* | *Wire* | *Dust* |
| 0·8 | $R_0$ | 0·1 | 0·1 | 0·1 | 1·00 | 0·1 | 0·1 | 0·1 | 1·00 |
| | $R_e$ | 60·0 | 2·9 | 1·1 | 0·12 | 60·0 | 2·9 | 1·1 | 0·12 |
| | $R_r$ | 3·3 | 3·3 | 3·3 | 0·36 | 3·3 | 3·3 | 3·3 | 0·36 |
| | $R_h$ | — | — | — | — | 27·0 | 27·0 | 27·0 | 1·00 |
| | $R_l$ | 63·4 | 6·3 | 4·5 | 1·48 | 90·4 | 33·3 | 31·5 | 2·48 |
| 1·6 | $R_0$ | 0·1 | 0·1 | 0·1 | 1·00 | 0·1 | 0·1 | 0·1 | 1·00 |
| | $R_e$ | 240·0 | 11·6 | 4·4 | 0·48 | 240·0 | 11·6 | 4·4 | 0·48 |
| | $R_r$ | 6·6 | 6·6 | 6·6 | 0·72 | 6·6 | 6·6 | 6·6 | 0·72 |
| | $R_h$ | — | — | — | — | 54·0 | 54·0 | 54·0 | 2·00 |
| | $R_l$ | 246·7 | 18·3 | 11·1 | 2·20 | 300·7 | 72·3 | 65·1 | 4·20 |
| 3·2 | $R_0$ | 0·1 | 0·1 | 0·1 | 1·00 | 0·1 | 0·1 | 0·1 | 1·00 |
| | $R_e$ | 960·1 | 46·4 | 17·6 | 1·92 | 960·0 | 46·4 | 17·6 | 1·92 |
| | $R_r$ | 13·2 | 13·2 | 13·2 | 1·44 | 13·2 | 13·2 | 13·2 | 1·44 |
| | $R_h$ | — | — | — | — | 108·0 | 108·0 | 108·0 | 4·00 |
| | $R_l$ | 973·3 | 59·7 | 30·9 | 4·36 | 1081·3 | 167·7 | 138·9 | 8·36 |

the dust core is superior to the other types. The difference, however, becomes more strongly marked if account is taken of the hysteresis coefficient at high current values: at 3·2 kHz and 10 mA, the effective loss resistance $R_l$ for the laminated core is 20 times as great as for the dust core (see Table 13.8). Against this must be set the permeability of the dust core which is less by a factor of 10. The constancy of permeability with current value is brought out by measured values obtained by Deutschmann[22] using a 22 mH coil. These

**Table 13.9** INDUCTANCE OF A DUST CORE AS A FUNCTION OF FIELD STRENGTH[22]

| $H$ (A/m) | $L_{meas}$ (mH) | $L_{calc}$ (mH) |
|---|---|---|
| 0·304 | 21·977 | 21·976 |
| 0·912 | 21·979 | 21·978 |
| 1·504 | 21·980 | 21·980 |
| 3·08 | 21·985 | 21·985 |
| 6·00 | 21·995 | 21·996 |
| 9·12 | 22·007 | 22·007 |

results are given in Table 13.9. The variation of inductance with field strength can be expressed by the linear equation

$$L = 21{\cdot}975\ (1+0{\cdot}000\ 165\ H)\ \text{mH}$$

The values calculated from this formula are given in the table against the measured values. The small linear rise of inductance extends to relatively high field strengths (2000 A/m) since for dust cores the hysteresis loop is not only very skew but very broad.

### 13.5.3 Production of dust cores

The production stages leading to a moulded core as end-product are: making the dust; insulating the particles; pressing or injection-moulding the core; final treatment. In what follows, only the most important processes will be briefly reviewed.

#### 13.5.3.1 Production of dust

One of the earliest methods for obtaining iron dust was by *reduction* of iron oxide in hydrogen. This procedure, however, has the disadvantage that it is relatively expensive. Iron dust obtained in this way is very soft, both mechanically and magnetically, and cannot, moreover, be pressed to the solidity of the wire in the cores previously used.

Another procedure for producing iron dust is the *electrolytic* process. Layers of metal 3–6 mm thick are deposited on a polished steel cathode

from an electrolyte, for example from an iron sulphate–iron chloride–ammonium sulphate solution. These are washed, peeled off the cathode, roughly pulverised, and finally ground in a ball mill. In this way a powder can be obtained that is up to 50% finer than 75 nm[130]. The conditions of deposition can be so regulated that a brittle material which is easy to granulate results. It is also possible to modify the process so that the powder itself falls away from the cathode[76].

By employing the *carbonyl process* it is possible to obtain the desired metallic dust directly without an intervening milling operation. To obtain the dust, carbon monoxide is passed over reduced iron in a pressure vessel, the purity of the iron at this stage not being tightly controlled. At 150°–200°C, iron pentacarbonyl, $Fe(CO)_5$, forms. From this a very fine spherical dust is obtained by evaporation and by breaking down of the material in a chamber heated by radiation.

By controlling the conditions of evaporation, a variety of grain sizes can be obtained. The particles are built in layers—rather like an onion—and have a diameter of 2–10 μm. Since the iron carbonyl contains carbon it will also be present in the dust. In the raw condition this amounts to some 0·8% C, and to this must be added about the same quantity of nitrogen. Individual particles have steel-like properties and are very hard. The crystallites from which the grains are formed have an average diameter of about 20 nm[135]. If ammonia is sublimed with iron pentacarbonyl, the carbon content of the resulting iron dust can be held to a very low value[97]. A further part of the carbon can be removed from the dust by a suitable heat treatment in a reducing atmosphere so that, finally, a dust of very high purity results in which only the following impurities remain:

| | |
|---|---|
| 0·005% N | 0·007% S |
| 0·005% C | 0·02% Mn |
| 0·01% P | 0·02% Si |

At the same time this heat treatment brings about a greater uniformity of texture in the individual grains.

Manufacturers generally offer many varieties of carbonyl iron dust in order to meet the requirements in the various frequency ranges where iron dust is used. Table 13.10 lists some of the varieties to be found on the market. The table also gives particle diameters, iron content, and the amount of adulteration by carbon, oxygen, and nitrogen[7, 41].

The attainable permeability values (toroidal permeabilities) are indicated schematically in Figure 13.33. The values depend not only on the properties of the dust but also on the density of packing and the proportion of insulating material in the core—as will be shown below. The preferred range of application for individual kinds of dust is indicated in Table 13.11; this can be deduced from the curves of Figure 13.34 which gives the quality factor $Q = 1/\tan \delta$, plotted against frequency. The factor $Q$ is arbitrarily referred to the dust variety called E, taken to have a $Q$ of 100%. For example, E and TH can profitably be employed at low frequencies, W and J at the highest frequencies.

**Table 13.10** TYPES OF CARBONYL IRON DUST

| *Designation* | *Mean particle diameter* (μm) | *Particle density* (g/cm³) | *Apparent density of dust* (g/cm³) | *Composition* (%) | | | | *Remarks* |
|---|---|---|---|---|---|---|---|---|
| | | | | Fe (min.) | C (max.) | O (max.) | N (max.) | |
| E | 8 | 7·8 | 2·5–3·5 | 98·0 | 0·8 | 0·3 | 0·8 | Raw dust, mechanically hard |
| TH | 5 | 7·8 | 2·5–3·5 | 98·0 | 0·8 | 0·3 | 0·8 | |
| SF | 3 | 7·8 | 2·5–3·5 | 98·0 | 0·8 | 0·3 | 0·8 | |
| J | 10 | 7·3 | 2·5–3·5 | 90·0 | 0·8 | 1·1 | 8·0 | Alloys, hard for high *Q* |
| W | 5 | 7·3 | 2·5–3·5 | 90·0 | 0·8 | 1·1 | 8·0 | |
| L | 20 | 7·8 | 1·8–3·0 | 99·5 | 0·05 | 0·3 | 0·05 | Reduced dust, mechanically soft |
| MR | 20 | 7·8 | 2·0–3·0 | 99·5 | 0·05 | 0·3 | 0·05 | |
| C | 10 | 7·8 | 2·5–3·0 | 99·5 | 0·2 | 0·3 | 0·1 | |
| HP | 10 | 7·8 | 2·5–3·0 | 99·5 | 0·05 | 0·3 | 0·05 | |
| GQ4 | 8 | 7·8 | 2·5–3·0 | 98·0 | 0·05 | 0·3 | 0·05 | Insulated reduced dust, soft for high *Q* |
| GS6 | 5 | 7·8 | 1·5–2·0 | 98·0 | 0·05 | 0·03 | 0·05 | |
| E | 4·5–5·2 | | 4·4 | 98·3 | 0·8 | 0·1 | 0·8 | Mechanically hard |
| EN8 | 3·6–4·5 | | 4·4 | 98·3 | 0·8 | 0·1 | 0·8 | |
| HF2 | 3·5 | | 4·4 | 98·3 | 0·6 | 0·1 | 0·8 | |
| HF1 | 3·0 | | 4·3 | 98·3 | 0·6 | 0·1 | 0·8 | |
| HF3 | 2·3–3·0 | | 4·3 | 98·3 | 0·6 | 0·3 | 0·8 | |
| HFF | 1·7–2·5 | | 4·3 | 98·3 | 0·6 | 0·3 | 0·8 | |
| CP* | 4–6 | | 4·3 | 99·6 | 0·03 | 0·16 | 0·01 | Decarbonised mechanically soft |
| CNst | 6·5–7 | | 4·3 | 99·5 | 0·10 | 0·20 | 0·01 | |
| CNS* | 5–6 | | 4·2 | 99·6 | 0·04 | 0·18 | 0·01 | |
| CNN | 6–7 | | 4·3 | 99·6 | 0·06 | 0·20 | 0·01 | |
| CCS* | 5–6 | | 4·2 | 99·6 | 0·05 | 0·20 | 0·01 | |
| SN | 6–7 | | 4·4 | 99·0 | 0·05 | 0·20 | 0·01 | |

* Less appropriate for dust cores.

**Table 13.11** APPLICATION RANGE AND DESIGNATION OF CARBONYL IRON DUSTS

| *Type of dust* | *German* | *American* | *British* |
|---|---|---|---|
| Very fine, for highest frequencies | HFF, HF3 | SF | MF |
| Fine, for highest frequencies | HF1, HF2 | TH | ME |
| Normal, for high frequencies | E, EN8 | E | ME |
| Soft, for carrier frequencies | CNN, CNst | C | MC |
| Special, for low frequencies | SN | L | MP |

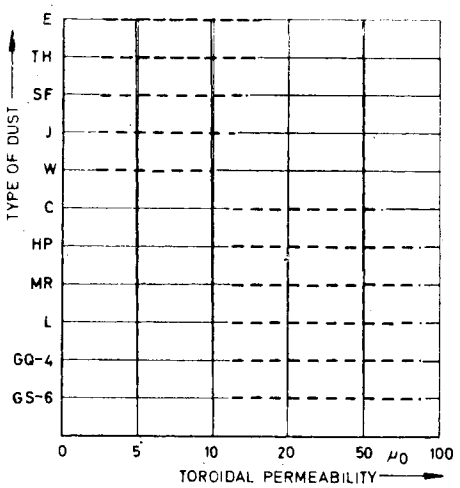



*Figure 13.33. Permeabilities attainable by various types of carbonyl iron according to packing density*[41]

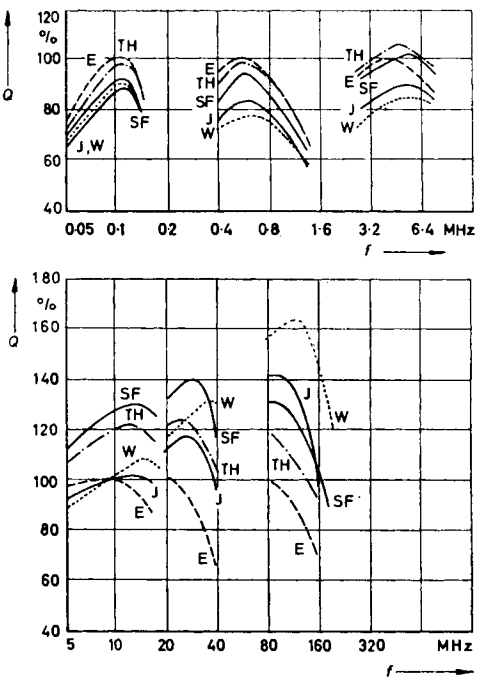



*Figure 13.34. Quality factor Q of various carbonyl iron dusts referred to a Q value of 100% for type E dust*[41]

Like iron dust, nickel dust can also be prepared by the carbonyl process. If this process is applied to iron and nickel at the same time, the breakdown stage leads to an Fe–Ni mixture which can be converted to an alloy by means of a homogenising annealing (20 h at 500°C)[119].

In many cases of alloy-dust manufacture the procedures described cannot be used. The manufacturer must then resort to one of the numerous methods of coarse or fine pulverisation. Two of the most important will be dealt with. In one method, the very fluid melt is thrown onto a rapidly rotating drum by means of a whirling stream of water; small spherules of metal are formed and are quenched by the water, and the oxide skin which forms on the metallic surface can be chemically reduced by suitable heat treatment[118]. A versatile atomising procedure is the vortex process or 'Hametag process'[76, 112]. To make iron dust in this way, iron wire is cut into short lengths and further broken in a Hametag mill, where particles are made to collide by means of a powerful gas jet. The process can be made continuous, the powder being sieved as it forms, or winnowed in an air stream. The Hametag process has made it possible to pulverise either soft or tough alloys which cannot be powdered in other kinds of mill. Such difficulties arise, for example, in the manufacture of Permalloy[3] or Mo-Permalloy dusts. However, it is possible to make these substances pulverisable by first making them brittle by means of suitable additives[124]. Cast ingots are first hot-rolled and, after granulating, are further milled. Of course, the brittle dust must undergo a softening heat treatment to render it fit again for moulding.

The above-mentioned difficulties of pulverisation do not apply to the Fe–Al–Si alloys known as Sendust. On the contrary, this material is so brittle by reason of its high silicon content that it is practically unusable except in the form of dust[95].

### 13.5.3.2 Insulating the dust

A great number of processes for insulating the dust particles have been developed, but they have only partly found their way into production. The difficulty lies in the need to cover the particles with a layer which is as thin as possible while completely enveloping the particles, and which remains intact during subsequent high-pressure operations so as to avoid metallic contact between grains. Thus there must always exist a compromise between two extremes: complete insulation by the extensive addition of insulant, which has to be paid for by accepting low core permeability; and, on the other hand, high permeability obtained by a sparing use of insulant with a consequent danger of high eddy-current loss.

All conceivable chemical compositions from asphalt to sugar have been tried as insulants. Shellac and waterglass have frequently been used for high-permeability moulded cores. A superficial oxidation of the dust has also sometimes proved advantageous[130], or insulating salts, to which binding materials, such as resin, adhere easily, can be built up on the grain surface, by mild pickling[114]. According to another procedure[148], the iron dust is left for some hours in contact with zinc flakes, which build up a tough thin insulating skin on the particles capable of withstanding moulding pressures and giving the core a high insulation resistance.

For cores which are to be subjected to heat treatment after moulding (see below), inorganic grain-insulators have proved valuable[35]. Many silicone lacquers offer a high-grade resistant insulant which gives considerable insulation even at 200°C. A certain difficulty arises in production because the raw pressings have only a small cohesion and must be stiffened up in the mould[113]. Almost all processes of moulded-core production involve the application, before pressing, of a matrix whose function is to give mobility to the particles during the pressing operation and to facilitate the mutual adherence of the grains. A greater proportion of binding matrix is needed for low-permeability high-frequency cores produced by injection moulding than for pressed-up cores. Low-loss plastics, such as polystyrene, Teflon, and Makrolon, are used.

### 13.5.3.3 Shaping dust cores

For the last-mentioned low-permeability high-frequency cores, i.e. for shell cores or threaded cores, fine-grained iron dust impregnated with a thermoplastic binder is hot-moulded in an injection-moulding machine or pressed-up cold with the aid of a suitable moulding matrix. A specific pressure of about 200 N/mm² is needed for this. Rod and tube cores can be produced continuously in an extrusion press.

Appreciably higher pressures are needed to mould insulated powders into high-permeability cores. In iron dust cores, permeabilities of 50–60$\mu_0$ (or 125$\mu_0$ for Mo-Permalloy cores) can be achieved only by using pressures of some 2000 N/mm². Figure 13.35, after Legg and Given[88], shows the increase in density with pressure for Mo-Permalloy cores for a 2·5% 'dilution'. It is seen that the maximum density attainable is 7·8 g/cm³ (the solid material has a density $d = 8{\cdot}7$ g/cm³). Pressures greater than 1500 N/mm² bring about no

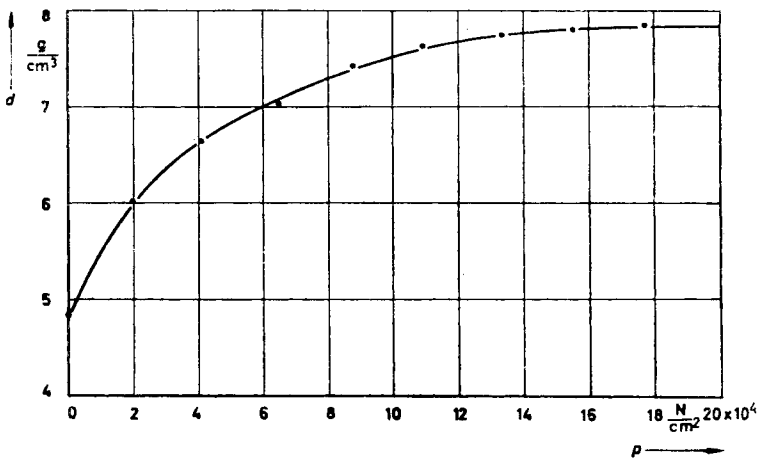



*Figure 13.35. Effect of moulding pressure on the density of a dust core (Mo-permalloy, 2·5% dilution)*[88]

further increase in density. Simultaneously with the rise in density with mounting pressure, the tensile strength of a moulded core also rises. It decreases, however, as the dilution increases.

Lightly annealed dust grains become plastically deformed under high pressure and form a dense structure[36]. At high compression the specific electrical resistance of the core falls and, in fact, the softer the dust used,

**Table 13.12** PROPERTIES OF CORES MADE FROM ANNEALED UNINSULATED IRON DUST[130]

| *Moulding pressure* (N/mm²) | *Density* (g/cm³) | $\varrho$ (mΩ cm) | $\mu$ ($\mu_0$) | $H_c$ (A/m) | $H$ (A/m) |
|---|---|---|---|---|---|
| 2 600 | 7·4 | 0·7 | 150 | 7·2 | 56 |
| 1 400 | 7·3 | 1·0 | 120 | 6·4 | 65 |
| 1 060 | 7·1 | 1·2 | 105 | 6·4 | 75 |
| 710 | 7·0 | 1·9 | 90 | 5·5 | 88 |
| 350 | 6·1 | 7·8 | 70 | 4·8 | 56 |

the more the resistance falls off[130]. This shows itself most impressively for non-insulated dust, as can be seen from Table 13.12, following investigations by Speed and Elmen[130]. With increased compression there is an increase in the permeability, coercivity, and electrical conductivity of the pressing. The percentage rise in $\mu$ also increases with pressure for insulated dust mixed

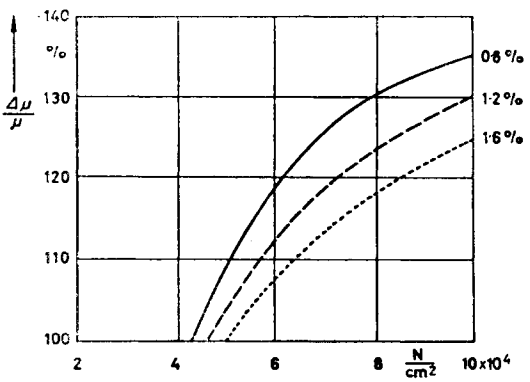



*Figure 13.36. Percentage increase of permeability as a function of moulding pressure: dust with 2% insulating material, three different amounts of binder*[41]

with a binding matrix. Figure 13.36 shows three curves for HP iron dust after it had been provided with 2% insulant and 0·8–1·6% binding matrix[41]. Figure 13.37 shows further examples for other carbonyl iron dusts[7]. For each dust designation the proportion of insulant is given in brackets. Note that for HF1, for example, $\mu$ is higher the greater the applied pressure and the smaller the proportion of insulant.

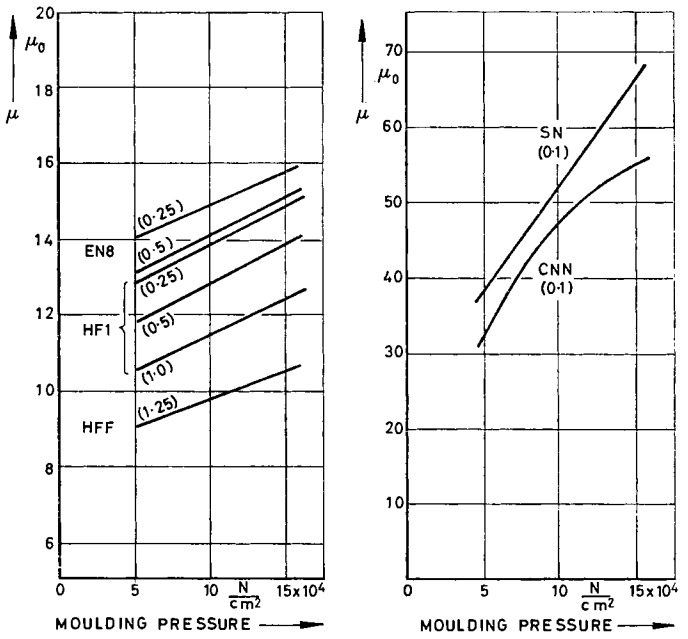



*Figure 13.37. Toroidal permeability of some carbonyl iron dust cores as a function of moulding pressure and of the proportion of insulation (quoted in brackets)*[7]

### 13.5.3.4 Final treatment

In order to increase the rigidity of the pressings and to protect them from atmospheric attack (by oxygen or moisture), they are generally subjected to an impregnation procedure using a suitable artificial resin or lacquer; this has sometimes to be cured at a rather high temperature (say 150°C).

Some cores, such as those made of Permalloy dust, must be given a post-forming heat treatment (at about 700°C) to arrive at the required values of permeability and stability[19]. It is found that ceramic insulants can withstand the temperature if oxygen is excluded during annealing[88]. Injection cores require no such final treatment.

## 13.5.4 Properties of dust cores

### 13.5.4.1 Iron dust cores

According to equations 13.2 and 13.3, the measured permeability of a moulded toroidal core depends on the permeability of the magnetic material used and the proportion of insulant. Figure 13.38 shows the relation between toroidal permeability $\mu_{tor}$ and the grain permeability $\mu$ for various proportions of insulant, according to measurements by Kersten[74]. It can be seen that

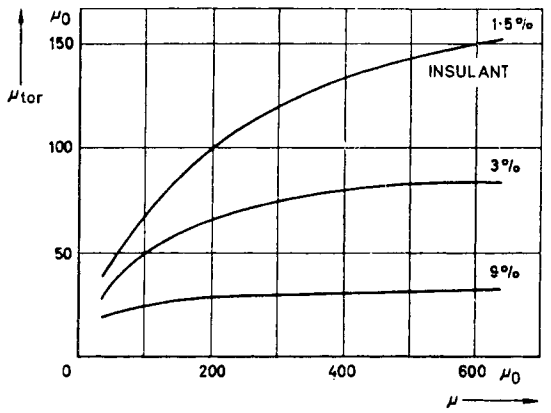



*Figure 13.38. Toroidal permeability of a dust core as a function of the true material permeability $\mu$ and the percentage by volume of insulant*[74]

the amount of insulant sets an upper limit to the permeability of the core. Since in practice the least proportion of insulating material is about 2%, it follows that, even with the highest possible grain permeability, the toroidal permeability of the dust core can reach $150\mu_0$ at most. Speed and Elmen[130], using iron dust cores at low intensities, obtained permeability figures, according to the kind of dust employed, of $26\mu_0$, $30\mu_0$, and $55\mu_0$. The values for the types of carbonyl iron used today are very similar. For the shell cores used in high-frequency work an even lower permeability is usually chosen, for example $\mu_{tor} = 6\mu_0$. The inductance can be adjusted with the help of a plunger or screw core whose position in the central hole of the coil can be altered (see page 466). Adjustable cores made by the injection moulding process have an effective permeability of about $2\mu_0$.

The temperature coefficient of initial permeability for iron dust cores depends on the type of dust, the proportion of insulant, and the temperature. For low-permeability materials, such as types E, TH, and SF, Polydoroff[113] found temperature factors of 10–50 ppm/K. Cores of higher permeability may have temperature factors of more than 100 ppm/K. The temperature factor of metallic dust cores rises with increasing temperature. Notterbrock and Weis[101] quoted negative temperature coefficients: both for toroidal cores having a $\mu_{tor}$ of $20\mu_0$ and for others where $\mu_{tor}$ was $7\mu_0$, they gave a temperature factor of $-50$ ppm/K.

While the permeability increases with rising temperature, the quality factor $Q$ becomes smaller. As is shown schematically in Figure 13.39, the increments lie between $-0{\cdot}01\%$ and $-0{\cdot}09\%$ according to the type of dust[41]. The varying effect of temperature comes from the fact that the loss coefficients show various temperature relations. The residual loss resistance increases and the eddy-current loss falls with rising temperature. In this way one finds that at low frequencies, where the residual loss predominates, the temperature coefficient of loss is positive, for example at 200 kHz it is $70\times10^{-4}$ for hard carbonyl iron dust and $10\times10^{-4}$ for lightly annealed dust. At around 2 MHz the temperature coefficient falls to zero and at

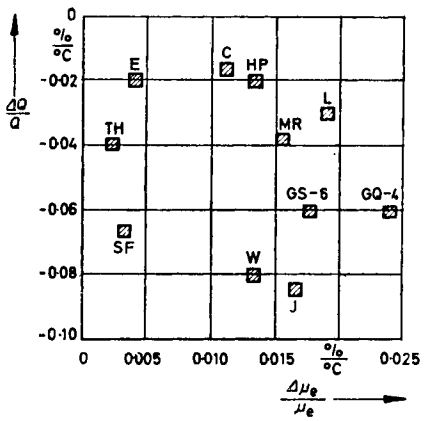



*Figure 13.39. Quality factor Q and effective permeability $\mu_e$ as functions of temperature for various carbonyl iron dusts*[41]

10 MHz, where eddy-current losses predominate, the coefficient has become negative. It may have values between $-7\times10^{-4}$ and $-30\times10^{-4}$ according to the particular specimen measured[113].

It is not only with temperature but also with time that magnetic values should change as little as possible. If foreign substances get into the cores during the manufacturing process, causing chemical changes, secular changes in magnetic values may result.

The permeability of moulded dust cores, in the neighbourhood of the initial permeability, changes in the presence of a direct magnetic field by an amount depending on the field-strength amplitude, in the manner shown in Figure 13.40: according to Sixtus[126], a dust core for which $\mu_{tor} = \mu_i = 55$ was traversed by a direct field, cycling between $\pm 2{\cdot}8$ kA/m, and the permeability increment $\Delta\mu/\mu_i$ was plotted against $H$.

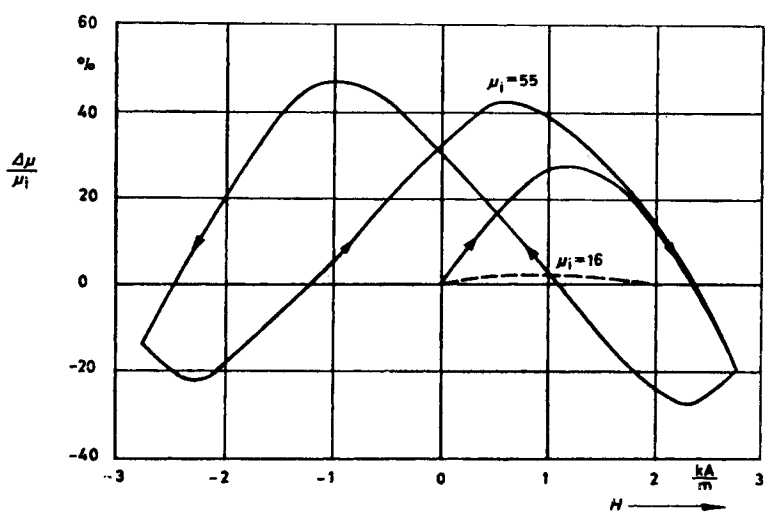



*Figure 13.40. Change of reversible permeability as a direct field is cyclically traversed*[126]

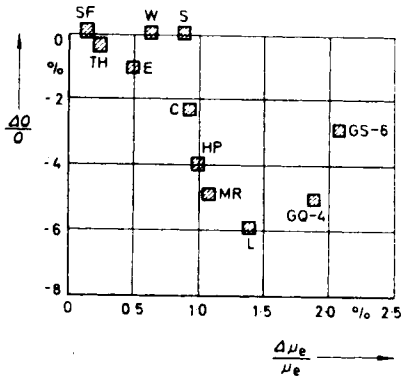



*Figure 13.41. Effect of magnetic shock on quality factor Q and effective permeability* $\mu_e$[41]

Cores should also remain unaffected by the sudden application of external fields. Such effects may occur owing to a short-circuit or to a lightening flash. This kind of stability can be checked in the following way, for example. The core is immersed in an alternating field of 8 kA/m and the changes in $\mu$ and $Q$ are measured. Figure 13.41 shows the measured changes at $f = 3$ MHz three minutes after the application of a magnetic shock[41]. The test methods recommended by the CCIT (Comité Consultatif International Téléphonique) are used to check loading coils. In this test the coil inductance should not change by more than $\pm 2\%$ after a d.c. pulse load between zero and 2 A and lasting about 5 s is applied to the winding. The measurements should be made 5 min after switching off the current[21]. Kiessling and Ludl[77] were able to show that the stability depends on the moulding pressure used in forming the core and, in fact, that after a d.c. pulse load of 6 kA/m the measured stability was higher the greater the forming pressure.

Two facts are of decisive importance in the design of dust cores: first, reduced particle size means reduced eddy-current and hysteresis values; and, second, an increased proportion of insulant in the core means that the residual-loss coefficient $r$ and the eddy-loss coefficient $e$ will fall proportionally, while $h$ will even decrease quadratically[75]. For example, in an iron dust core having a toroidal permeability $\mu_{tor} = 13\mu_0$, the following values are obtainable:

$$h < 1{\cdot}6 \text{ cm/kA}$$
$$e = 0{\cdot}012 \text{ } \mu\text{s}$$
$$r = 0{\cdot}8‰$$

The $Q$ factor corresponding to these figures is 740. The instability of a coil ($L = 1{\cdot}3$ mH) fitted with a core of such a material is very small, amounting to only $0{\cdot}06\%$ for a disturbing current of 1 A. Further measured results for dust cores of various kinds[19, 101, 118] are collected in Table 13.6.

The eddy-current coefficient $e$ of a dust core can be roughly calculated according to Kornetzki and Weis[86]. If in equation 3.49 the particle diameter $d$ is taken as 5 $\mu$m, the specific electrical resistance as 10 $\mu\Omega$ cm, and the toroidal permeability $\mu_{tor}$ as $13\mu_0$, then the very satisfactory eddy-current

coefficient of $e = 0{\cdot}004$ μs is obtained. In the application of equation 3.49 to practical cases, the particle diameter cannot always be fixed. There is, in addition, the role played by particle structure to consider, as Richards[117] has shown in comparative measurements carried out on carbonyl iron dust and electrolytic iron dust. Since even minute alloy contaminants raise the specific electrical resistance and since their distribution is not always uniform, there is also some uncertainty in the determination of $\varrho$.

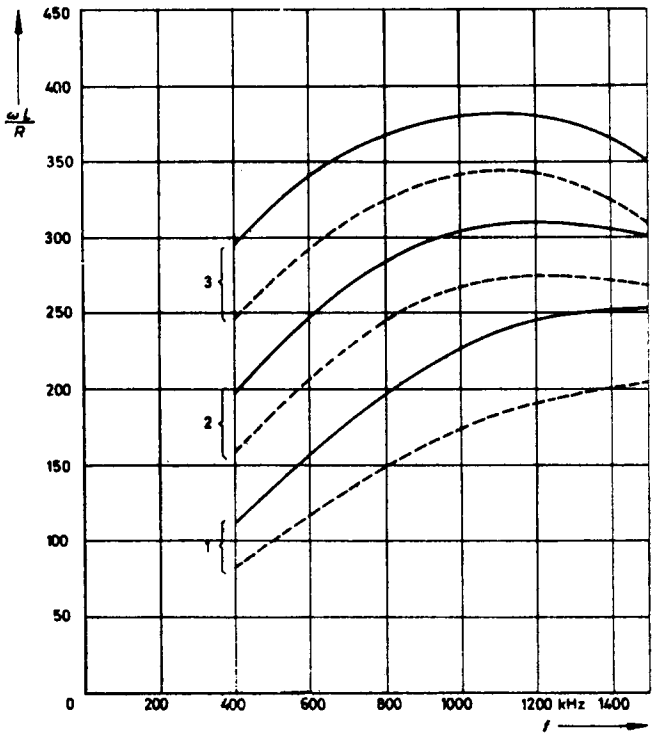



*Figure 13.42. Quality factor $\omega L/R$ of a coil as a function of frequency: 1, air-cored coil; 2, air-cored coil with cylindrical core inserted; 3, solenoidal coil as in Figure 13.43b; broken curves, same coils in aluminium can*[101]

The critical frequency $f_{cr}$ can be estimated from the eddy-current coefficient $e$ since the limiting frequency for a dust core is inversely proportional thereto[147]. In the above example, therefore,

$$f_{cr} = \frac{\varrho}{\pi^2 d^2 \mu_{tor}} = \frac{4{\cdot}1}{e}\ \text{MHz}$$

or

$$f_{cr} = \frac{14}{\mu_{tor}}\ \text{GHz} \approx 1\ \text{GHz}$$

There is no corresponding formula for estimating the hysteresis coefficient $h$ as there is for $e$. The coefficient $h$ depends on a series of factors: flux

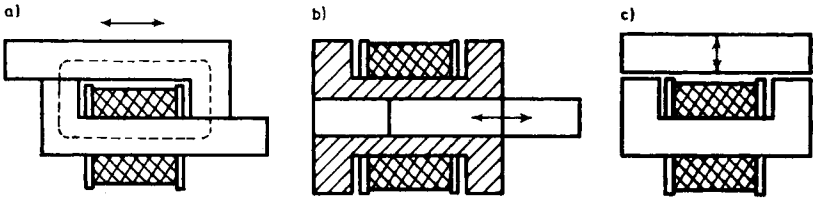



*Figure 13.43. Change of coil inductance: (a) with change in magnetic path length; (b) with change in magnetic cross-section; (c) with change in air-gap*

density, the previous magnetic history of the material, the annealing conditions, the grain size, the way the grains are insulated, and the internal structure of the particles[6].

Figure 13.42 plots the quality factor $\omega L/R = 1/\tan\delta$ against frequency for a high-frequency coil having an inductance $L = 200$ μH and made according to various types of construction[101]. Curve 1 is for a good air-cored coil (i.e. no magnetic core) wound with 20×0·05 mm litz wire. Curve 2 is a similar air-cored coil after a cylindrical core of 13 mm diameter has been inserted. Curve 3 is for a solenoidal core. If the coils are mounted in an aluminium shielding can, $Q$ is reduced by about 15–20%.

To cater for the case where a maximum quality factor is desired, which sometimes occurs in practice, the toroidal permeability $\mu_{tor}$ is so chosen that the sum of iron loss and copper loss is a minimum (see Figure 3.17). There is an optimum $\mu_{tor}$ for every type of coil at every frequency. The higher the frequency at which a coil is to be used, the lower the $\mu_{tor}$ value has to be. Pot cores, therefore, are not used in the short-wave or ultra-short-wave ranges: it is much better to use open-type coils with cylindrical-core inserts having an effective permeability of 3–5$\mu_0$. The loss factor will be about $10^{-3}$. For a discussion of adjustable coils (Figure 13.43) see Section 13.6.3.

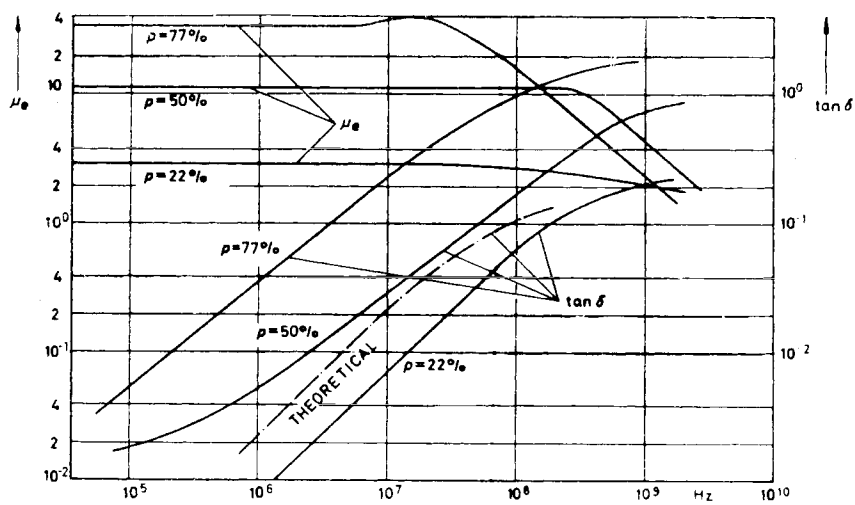



*Figure 13.44. Dust core of carbonyl iron CNN of grain size 5 μm; permeability $\mu_e$ and loss factor tan δ are plotted as functions of frequency for various space-factors*[60]

Heister[60] investigated the frequency curve of the loss factor tan $\delta$ for dust cores up to a frequency of 4 GHz. Figure 13.44, taken from this investigation, gives the results for a dust core of carbonyl iron CNN having a grain size of 5 μm. The permeability $\mu_e$ and tan $\delta$ are shown for three space-factors $p$ of 77%, 50%, and 22%. In addition, the tan $\delta$ curve to be expected on theoretical grounds is plotted for $p = 50\%$. The following facts appear: at low frequencies the loss factor tan $\delta$ rises proportionally to $f$; in the region of

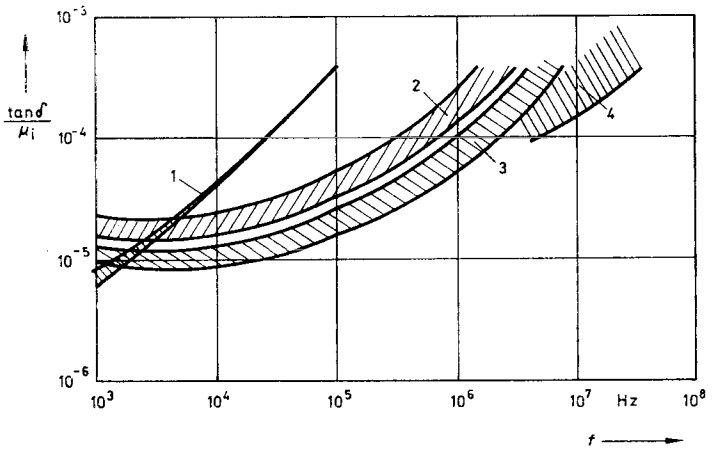



*Figure 13.45. Referred loss factor as a function of frequency for various dust cores (measured values are extrapolated to zero field strength): 1, Sendust ($\mu_i = 80\mu_0$), Mo-Permalloy ($\mu_i = 125\mu_0$); 2, carbonyl iron C ($\mu_i = 50\mu_0$); 3, carbonyl iron HF ($\mu_i = 14\mu_0$); 4, carbonyl iron HFF ($\mu_i = 5$–$10\mu_0$)*[81]

the limiting frequency it rises as $\sqrt{f}$; and it falls at very high frequency according to $f^{-(1-p)/2}$. For the purpose of comparing materials it is more convenient to plot the referred loss factor $(\tan\delta)/\mu_i$ (instead of tan $\delta$) against frequency. This is done in Figure 13.45 for dust materials of various initial permeabilities[81].

It will be seen that at high frequencies $(\tan\delta)/\mu_i$ is smaller the lower the initial permeability of the core—in good agreement with equation 3.43. On the other hand $Q$ increases as the proportion of insulant increases. If a quality factor of 100% is arbitrarily assigned to types HF1 or HHF with 0·25% insulant, then $Q$ alters with frequency and percentage insulant in the manner indicated in Figure 13.46 for the types of dust quoted in Table 13.10[7]. Coils intended for high or for low frequencies are, in this case, somewhat differently constructed.

### 13.5.4.2 Permalloy dust cores

Densities of 7.8–8.3 g/cm³ are obtainable with cores of Permalloy dust, according to Shackleton and Barber[124]. The density of the solid alloy is

about 8·6 g/cm³. The specific electrical resistance of a Permalloy core amounts to between 1 Ω cm and 20 Ω cm if the insulating process is carefully carried out. Practically constant values of permeability $\mu_{tor} = 80\ \mu_0$ can be attained in the range 0–0·01 V s/m², a value higher than that of iron dust cores. The hysteresis losses are small and appreciably lower than those of ordinary iron, as is shown by the contrasted figures of Table 13.13[124].

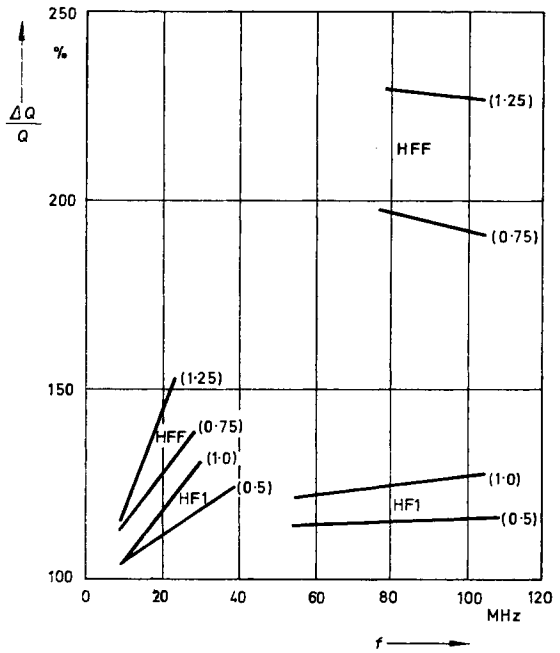



*Figure 13.46. Effect of proportion of insulant on the quality factor Q of two kinds of carbonyl iron dust cores; reference Q = 100% for HF1 (0·25% insulant)*[7]

Very fine carbonyl iron dust, however, is scarcely inferior in its hysteresis properties to the Fe–Ni alloys[118] (see Table 13.6). The composition and the treatment of the dust is of outstanding importance, as is the way the core is produced. For Fe–Ni dusts, the hysteresis loss, for example, increases with oxygen content, and both the permeability and the hysteresis loss—assuming constant moulding pressure—change with partial decarbonising of the carbonyl powder in the reverse sense to the residual carbon content[118]. Relevant comparisons can be drawn—with suitable caution—from Table 13.6.

Sizes of Permalloy coils can be reduced by taking account of the different values given in Table 13.13. The higher cost of raw materials is thus less unfavourable than it would otherwise be without this possibility of size reduction.

**Table 13.13** HYSTERESIS LOSS FOR IRON AND PERMALLOY DUST CORES[124]

| $B$ (mV s/m²) | $10^4 W_h$ erg/cm³ per cycle | |
|---|---|---|
| | *Iron* | *Permalloy* |
| 0·1 | 0·64 | 0·17 |
| 1·0 | 238 | 37 |
| 2·0 | 1 720 | 235 |

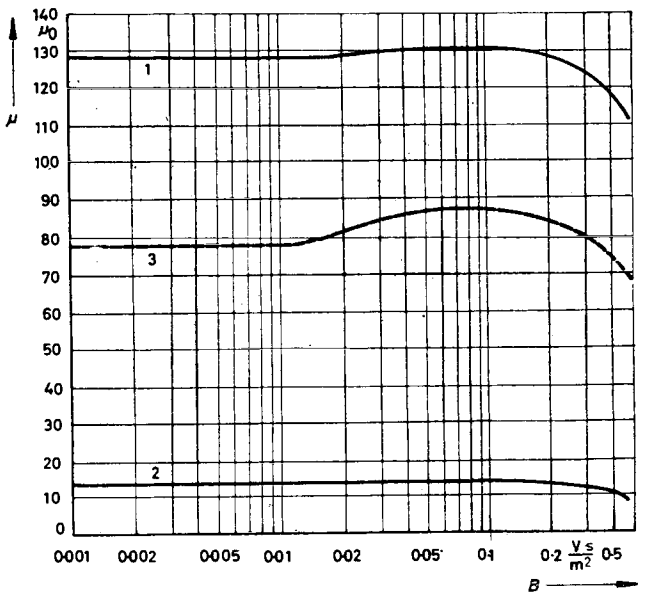



*Figure 13.47. Permeability as a function of flux density for dust cores: 1, Mo-Permalloy; 2, Mo-Permalloy; 3, Permalloy*[88]

### 13.5.4.3. Mo-Permalloy dust cores

An increase in permeability and an overall quality improvement can be obtained by using Permalloy alloys with 80–82% Ni to which is added 2% Mo. Such an alloy was proposed as long ago as 1928 by Shackleton and Barber[124]. The alloying of molybdenum acts, in the first instance, by raising the specific electrical resistance and thereby reducing the eddy-current loss coefficient. Besides this, there is also an increase in toroidal permeability $\mu_{tor}$ to 125 $\mu_0$. This value remains almost constant with rising flux density. It only rises by 2% up to $B = 0{\cdot}1$ V s/m² and then falls off steeply for higher densities, as is obvious from Figure 13.47[88]. It is noteworthy that the graph shows that the maximum permeability of dust cores is not very marked and

behaves at lower densities like that of solid cores (see, for example, Figure 13.20). This is related to the uneven partition of flux in the individual particles[103].

The high permeability of Mo-Permalloy cores is utilised only in low-frequency coils and in loading coils (see Figure 13.45). In channel filters (for carrier telephony), cores are generally chosen, up to a frequency of 108 kHz, with a $\mu_{tor}$ of $26\mu_0$ or $14\mu_0$[88]. Mo-Permalloy cores may be taken as very stable: after a direct-field premagnetisation up to saturation, a high-permeability core ($\mu_{tor}=125\mu_0$) changed by only 0·1% and a core with $\mu_{tor}=14\mu_0$ by 0·02%. Both remained stable with time following the changes (see Figure 13.48)[103]. Figure 13.49 sets out the fall in permeability, as a function of direct-field magnetisation, for four types of core[103].

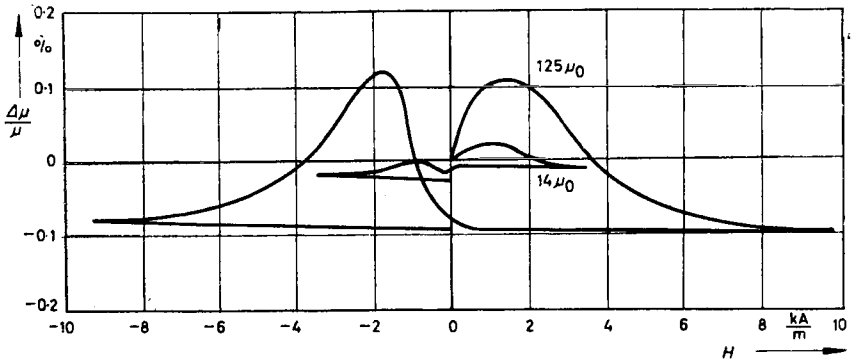



*Figure 13.48. Instability values for dust cores of Mo-Permalloy*[103]

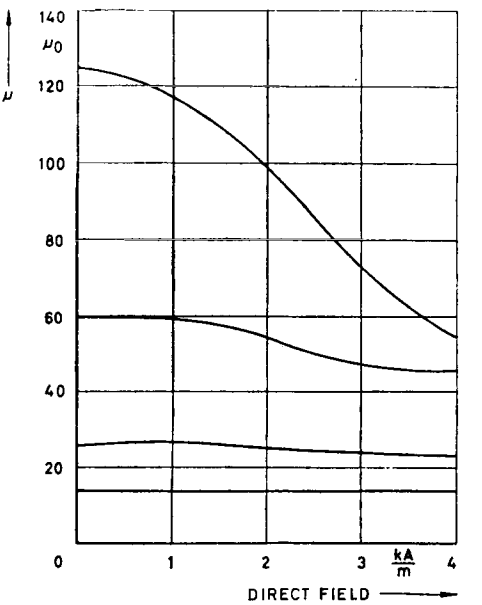



*Figure 13.49. Permeability as a function of superposed direct field for Mo-Permalloy dust cores of different permeabilities*[103]

Measured values of the Jordan loss coefficients $e$, $r$, and $h$, according to various authors[19, 88, 118], are reproduced in Table 13.6. The coefficient $e$ falls somewhat with rising temperature because the specific electrical resistance rises. No effect of temperature on $r$ and $h$, on the other hand, could be observed[103]. Figure 13.50 shows a comparison between Mo-Permalloy, Permalloy dust, and iron dust cores, on the basis of the $Q$ values, for three types of cores[88].

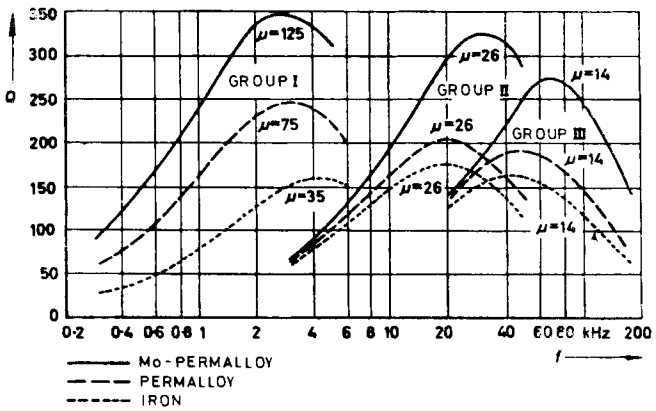



*Figure 13.50. Comparative Q-curves for filter coils using different core materials. For all coils, inductance L = 20* mH *and current i = 1* mA[88]. *Core dimensions are: group I,* $d_o$ = 7·8 cm, $d_i$ = 4·9 cm, $h$ = 2·1 cm; *group II,* $d_o$ = 6·1 cm, $d_i$ = 3·8 cm, $h$ = 1·5 cm; *group III,* $d_o$ = 4·7 cm, $d_i$ = 2·9 cm, $h$ = 1·5 cm

A very low temperature coefficient of initial permeability is essential for dust cores used in wide-band crystal filters in transmission devices. This can best be realised by adding to the Mo-Permalloy a small quantity of a particular 12% Mo-Permalloy alloy[88, 103]. This 12% Mo-Permalloy alloy has a Curie temperature in the neighbourhood of room temperature, and somewhat below this Curie temperature it possesses a strongly negative temperature coefficient whereas that of the 2-81 Mo-Permalloy is slightly positive. By a suitable choice of composition the designer can confine the change in permeability between, say, 0°C and 60°C to ±0·1% (Figure 13.51)[103].

To achieve a high permeability the core must be formed under a high pressure, for example 1500–1600 N/mm². It must then be finally annealed in hydrogen at 650°C in order to release the stresses set up during moulding. Calculations by Owens[103] have shown that, to achieve a $\mu_{tor}$ of 125 $\mu_0$, an individual grain which has a mean diameter of 40 μm must have an insulating layer some 0·32 μm thick. This layer must be very tough to withstand the pressure and the heat treatment without damage.

It is advisable to eliminate the action of moisture on the finished core as this leads to a drop in $\mu$. If wax-impregnated cores having, for example, $\mu_{tor}$ values of $125\mu_0$ and $10\mu_0$ is subjected to a relative humidity of about 40%, the permeability drops in 2 years by about 0·8% and 0·4% respectively[103]. Before the experiment the specimens were vacuum dried and were

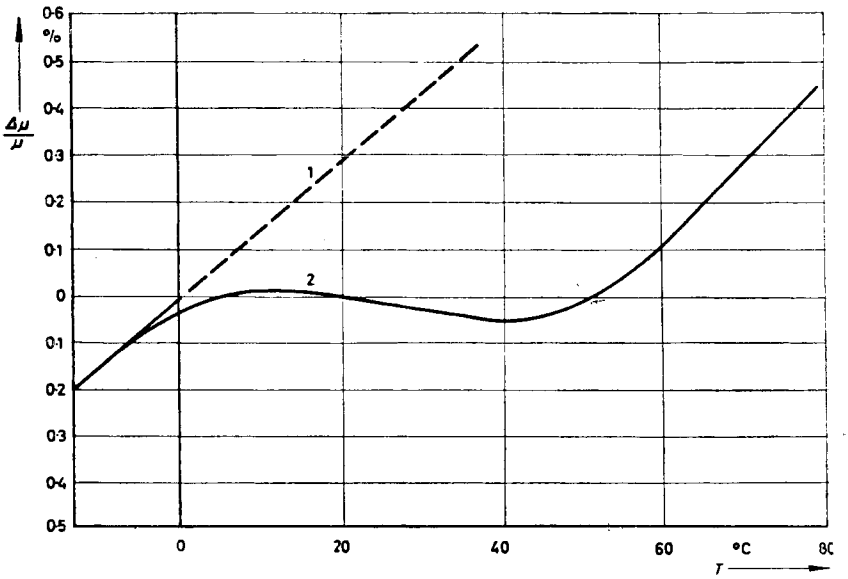



*Figure 13.51. Permeability as a function of temperature: 1, unstabilised Mo-Permalloy dust cores; 2, stabilised Mo-Permalloy dust cores*[103]

then impregnated. The original values could be recovered by a further vacuum drying. Moisture acts on the dielectric properties of a core more strongly than on its permeability. The dielectric-loss factor tan $\delta_\varepsilon$ and dielectric constant $\varepsilon$ can rise to 10 times their normal values. In cases where the highest constancy is essential, a protective layer of lacquer or enamel is not enough to arrest the effects of moisture. It is then necessary to achieve a vacuum-tight seal in a metallic case.

### 13.5.4.4 Fe–Al–Si dust cores

Ternary alloys with 7–13% Si and 4–7% Al, remainder iron, are characterised by high initial permeability and low hysteresis loss. The material is brittle and can thus easily be reduced to dust. Since these alloys were developed in Sendai (Japan), their inventor, Masumoto[95], named them Sendust.

The initial permeability of electrolytic iron amounts to some $140\mu_0$. By adding about 8% Si it can be raised to nearly $1200\mu_0$. With the three-component alloy having 9·62% Si and 5·38% Al, a $\mu_i$ of $35\,000\mu_0$ and a $\mu_m$ of $162\,000\ \mu_0$ were reached[95]. These peak values apply only to a narrow range of composition, as the three-dimensional diagrams of Figures 13.52 and 13.53 clearly show. The physical hypotheses on which the occurrence of these extreme values are based are, according to the researches of Saimowsky and Selissky[105, 122], similar to those applying to quenched Permalloy: crystal anisotropy and saturation magnetostriction become nearly zero at the particular composition of Sendust.

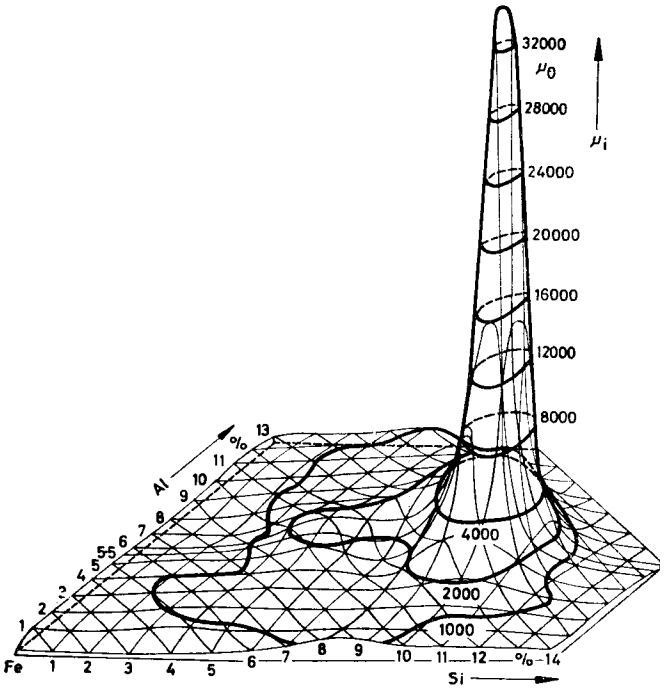



*Figure 13.52. Initial permeability of* Fe–Si–Al *alloys*[95]

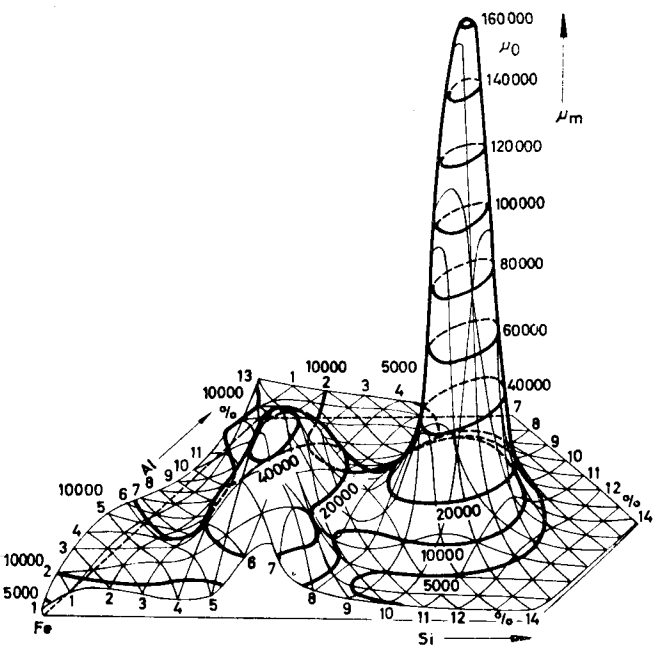



*Figure 13.53. Maximum permeability of* Fe–Si–Al *alloys*

Figure 13.54 shows the magnetising curve of Sendust, whose shape is reminiscent of Permalloy[95]. The flux density at which maximum permeability is measured occurs somewhat below that of Permalloy (Figure 13.55). The hysteresis loss for Sendust comes to 28 erg/cm³/cycle and to 73 erg/cm³/cycle for Permalloy. The coercivity of Sendust is also lower than that of Permalloy (1·76 A/m as against 4 A/m)[95]. The specific electrical resistance amounts to 81·2 $\mu\Omega$ cm and can be further increased by adding manganese, chromium,

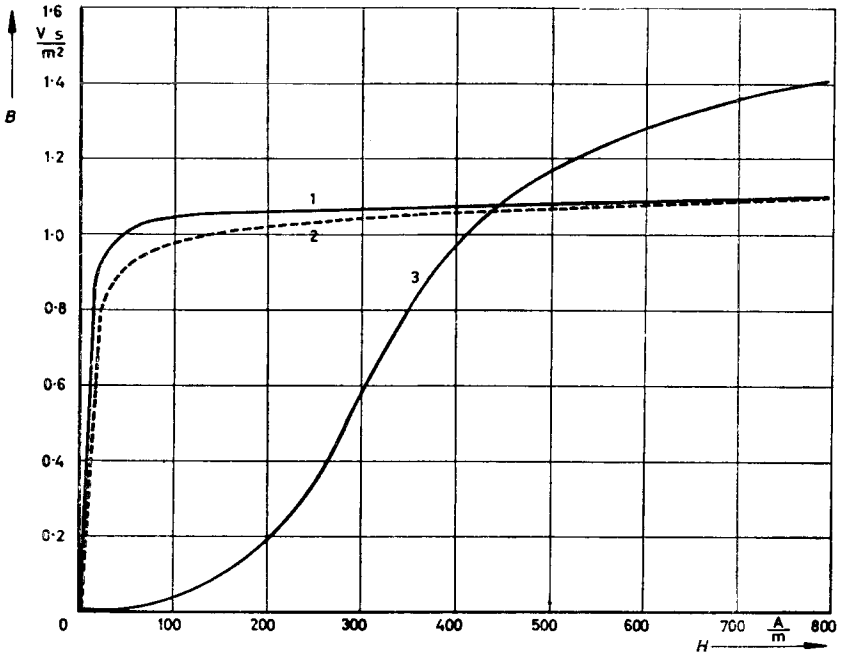



*Figure 13.54. Magnetising curves: 1, Sendust (9·62% Si, 5·38% Al, remainder iron); 2, Permalloy; 3, electrolytic iron*[95]

or molybdendum without appreciably affecting the magnetic properties. Commercially available solid cores yield the following values:

$$\mu_i = 10\,000\text{–}30\,000\mu_0$$
$$\mu_m = 80\,000\text{–}160\,000\mu_0$$
$$W_h = 20\text{–}100 \text{ erg/cm}^3 \text{ per cycle at } 0{\cdot}5 \text{ V s/m}^2$$

Dust cores can be produced with a $\mu_{tor}$ of 10–80$\mu_0$[137]. Measured values of the loss coefficients are set out in Table 13.6.

Kiessling and Ludl[77] demonstrated by measurements on moulded Sendust cores with $\mu_i = 100\,000\mu_0$ that the hysteresis coefficient depends significantly on field strength. In spite of the high permeability of the basic material, an effective permeability of only about $80\mu_0$ is reached for dust cores since the mechanically hard nature of the powder prevents higher density

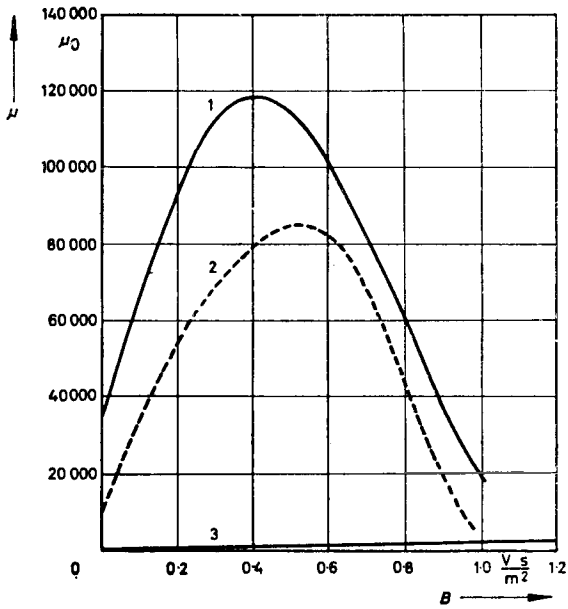



*Figure 13.55. Permeability curves: 1, Sendust; 2, Permalloy; 3, electrolytic iron*[95]

being achieved by compression. Moulding difficulties constitute a major obstacle to the wider use of Sendust[136]. These difficulties, however, can largely be mastered by the use of Sendust flakes, which are produced by heating Sendust to 400–500°C and then rolling it at 80°C. The resulting flakes are about 25 $\mu$m thick and have a diameter of approximately 100 $\mu$m. Cores made of such flakes can be pressed to a permeability of $230\mu_0$ with relatively low losses (see Table 13.6)[68a]. By reason of the high specific electrical resistance of the alloy, cores made from this material can be used at higher frequencies than, say, Mo-Permalloy cores.

#### 13.5.4.5 Ferrite dust cores

For ultra high frequency (u.h.f.), pulverised ferrites are sometimes used. The effective permeability lies around $3–5\,\mu_0$[2].

## 13.6 FERRITES

### 13.6.1 Comparison between dust cores and ferrite cores

In Table 3.5 it was shown what improvements could be obtained by using ferrite rather than dust cores. Ferrites have not only a higher material permeability but also lower loss factors. It follows that higher permeabilities are obtainable even with gapped ferrite cores, i. e. the same inductance is obtained with fewer turns if ferrite is used. Reduced copper, however, means

either a smaller size of coil or a higher $Q$. To match the inductance of a ferrite-cored coil to that of one using dust, the ferrite coil can be more heavily gapped. This is welcome in manufacture since a large external gap can be manufactured to tighter tolerances than a smaller one. Moreover, a desirable reduction of loss is achieved at the same time.

A very significant advantage of ferrite cores is that, by reason of the high permeability of the basic material, the designer has greater latitude in dimensioning a coil to secure optimum results than if he used dust. With dust cores, in order to obtain a $\mu_{tor}$ of 60–125$\mu_0$, it is often necessary to put up with heavy losses or to forego optimum dimensioning. One cannot, however,

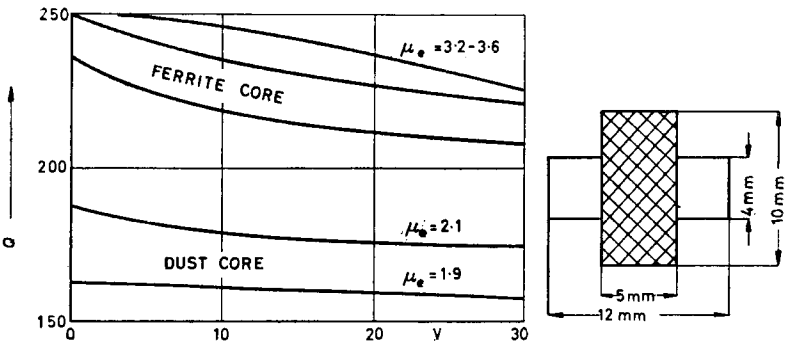



*Figure 13.56. Quality factors Q of coils with iron dust cores and ferrite cores (having the same dimensions) as functions of voltage across the coils (frequency, 500* kHz*)*[80]

simply replace the dust core in a coil by a ferrite one and expect improved quality. The other properties of the material usually make a change of coil-inductance necessary. In a band filter working at 468 kHz, a quality factor of 300–400, for example, is obtained with a pot core of iron dust. If this dust core is exchanged for a similar type of high-permeability core in ferrite, the $Q$ will drop to 10; the air-gap of the ferrite core is too small. Only a properly gapped ferrite core brings a significant gain in $Q$ over a dust core. This is brought out by curves obtained by Kornetzki[80] and shown in Figure 13.56: at 500 kHz using a 12 mm×4 mm dust core in a cross-type coil wound with 10×0·04 mm high-frequency wire, a $Q$ value of 160–180 is obtained, whereas, using ferrite, a figure of over 200 was achieved.

The $Q$ values fall for coils subjected to high voltage because of increased hysteresis loss. The fall is linear if $h$ is independent of the measuring intensity. It can be seen from Figure 13.56 that this is roughly true for dust cores but that various departures from linearity can occur in ferrite cores. An increase in the inductance is bound up with the drop in $Q$ and this shows itself as an amplitude-dependent detuning of the signal circuit. Taking an average value of $Q = 200$, a 10% drop corresponds to a detuning of about 0·1%[80].

In the change from dust to ferrite, the higher permeability shows up as increased leakage field. This may lead to increased stray-field loss, so ferrite-cored coils must be screened. The pot core is well adapted to this circum-

stance. If a coil provided with a pot core is given, in addition, a metal screen, $Q$ drops very little; whereas for a dust core, having, for example, $\mu_{tor} = 40\mu_0$, in an aluminium can a drop of $Q$—lower in any case—of 30% is to be expected[81].

The higher permeability of the ferrite core produces a greater steepness of the 'adjustment curve' (see below). The greater permeability of the basic material allows a longer air-gap for the same effective permeability and this permits a tighter tolerance for $A_L$ assuming the same degree of production accuracy. A pot core of high basic permeability shows a looser coupling with neighbouring coils than one with a lower basic permeability.

The permeability of a ferrite core drops more with the superposition of a direct field than does that of a dust core. This effect can be put to use in the tuning of a high-frequency circuit[80, 145]. A 'magnet variometer', as such a tuning device is called, using a dust core, gives an inductance ratio in the medium-wave band of 1:13 at most, whereas much higher ratios can be obtained with ferrite cores[80].

Ferrites offer the considerable facility of meeting design requirements by enabling the temperature coefficient of initial permeability to be changed over a wide range and the disaccommodation to be lowered to the point where the coils can be considered as staying substantially constant under operating conditions. Where a ferrite fails to satisfy these requirements sufficiently closely, the gapping factor must be increased. Such time and temperature variations do not generally interfere with the performance of audio transformers, so high-permeability ungapped coils can be used.

Special kinds of ferrite with low permeability have been developed for the u.h.f. range. With these, a $Q$ value of 150–200 can be achieved at 100 MHz, for example, a value some two or three times that obtainable with dust cores[83]. The temperature coefficient of ferrite-cored coils of this kind may be about +200 ppm/K.

The simultaneous reduction of loss and increase of permeability makes ferrite very suitable for use in loading coils. Loading coils provided with ferrite cores are smaller and more stable than the corresponding dust-cored coils[110]. Again, inductive balance is better for these than for the older toroidal coils[66].

Table 13.14, after Pierrot[111], gives a comparison, for practical purposes, of the old techniques and the new. The mechanical and electrical properties of a set of coils for a long-distance circuit are compared: in 1948 coils with toroidal iron dust cores were provided; in 1955 ferrite cores were used, for example of a Mn–Zn ferrite called Fermalite 2002, while in 1957 cores were of an improved version of the same basic ferrite. In 1955 the two types were of similar volumes but the ferrite cores were lighter than the dust cores. The ferrite cores of 1957, however, occupied only half the space. The volume and weight of the three-coil set (two side circuits and one phantom) are seven times greater with dust cores than with ferrite cores. Further, with ferrite-cored coils, the loss-resistance, hysteresis factor, and instability are all smaller. Reduction in loading-coil size means smaller and lighter coil-pots. Thus, for example, the weight of a coil-pot for a long-distance cable having 127 quads was reduced in 1955 from 782 kg to 222 kg[110]. In 1957 a coil-pot containing 112 sets of coils weighed only 99 kg[111].

**Table 13.14** COMPARISON BETWEEN THE PROPERTIES OF COIL ASSEMBLIES WITH DUST CORES (1948) AND FERRITE CORES (1955 AND 1957) USED IN A LONG-DISTANCE COMMUNICATIONS SYSTEM: L = 88 mH (PHANTOM) AND 36 mH (SIDE CIRCUIT)[111]

| *Properties* | | *Circuit* | *Loading-coil core* | | |
|---|---|---|---|---|---|
| | | | *Dust core* (1948) | *Ferrite pot core* (1955) | *Ferrite pot core* (1957) |
| Core | Dimensions (mm) | — | 50×30×20 | 36×23 | 26×19 |
| | Volume ($cm^3$) | — | 22·4 | 23·7 | 9·7 |
| | Weight (g) | — | 161 | 75 | 23 |
| Set of three coils | Dimensions (mm) | — | 106×67×67 | 79·5×39·5 | 65×27·5 |
| | Volume ($cm^3$) | — | 394 | 98 | 40 |
| | Volume of the circumscribed parallelepiped ($cm^3$) | — | 475 | 125 | 50 |
| | Weight (g) | — | 1 300 | 435 | 180 |
| D.C. resistance (Ω) | | Side | 8·0 | 8·8 | 9·8 |
| | | Phantom | 4·0 | 4·4 | 4·9 |
| Loss resistance at 3400 Hz, 1 mA (Ω) | | Side | 4·5 | 2·2 | 3·0 |
| | | Phantom | 1·6 | 0·4 | 0·5 |
| Effective resistance at 3400 Hz, 1 mA (Ω) | | Side | 12·5 | 11·0 | 12·8 |
| | | Phantom | 5·6 | 4·8 | 5·4 |
| Hysteresis factor at 800 Hz, 1 mA | | — | 9 | 5 | 7 |
| Capacity (pF) | | Side | 1 300 | 3 100 | 3 000 |
| | | Phantom | 560 | 230 | 260 |
| Instability (%) | | — | ±1·0 | ±0·2 | ±0·2 |

Pot-core designs have almost wholly replaced those based on toroids for loading coils. Pot cores made of ferrite can be produced with such small variations of permeability that adjustment of the inductances is often unnecessary[66], or at least the adjustment can be carried out simply, without the introduction of additional regulating devices[111].

### 13.6.2 Core shapes

The form taken by early ferrite cores differed little from that of the laminated or dust cores they replaced. E cores mirrored the M and EI cores. In this way it was possible to pass smoothly from one core material to another: the size of core and bobbin remained the same, however. The German Standard DIN 41 295[27] provides for five types of E core corresponding to the M series of laminations, namely E20, E30, E42, E55, and E65 (Figure 13.57 and Table 13.15).

Ferrite pot cores[26] (see Figure 13.58 and Table 13.16) took the place of the old pot cores and shell cores of iron dust. The dimensions of the DIN series

**Table 13.15** FERRITE E CORES TO DIN 41 295[27]

| Type | *a* | | *t* | | *b* | | *c* | | *e* | |
|---|---|---|---|---|---|---|---|---|---|---|
| | *Value* | *Tolerance* | *Value* | *Tolerance* | *Value* | *Tolerance* | *Value* | *Tolerance* | *Value* | *Tolerance* |
| E20 | 20 | $+0{\cdot}7$ $-0{\cdot}4$ | — | — | 10·2 | −0·4 | 5·3 | −0·4 | 6·3 | +0·4 |
| E30 | 30 | $+0{\cdot}8$ $-0{\cdot}6$ | 0·1 | ±0·02 | 15·2 | −0·4 | 7·3 | −0·5 | 9·7 | +0·5 |
| E42 | 42 | $+1{\cdot}0$ $-0{\cdot}7$ | 0·15 | ±0·02 | 21·2 | −0·4 | 15·2 | −0·5 | 14·8 | +0·6 |
| E55 | 55 | $+1{\cdot}2$ $-0{\cdot}9$ | 0·4 | ±0·03 | 27·8 | −0·6 | 21·0 | −0·6 | 18·5 | +0·6 |
| E65 | 65 | $+1{\cdot}5$ $-1{\cdot}2$ | — | — | 32·8 | −0·6 | 13·7 | −0·6 | 22·2 | +0·7 |

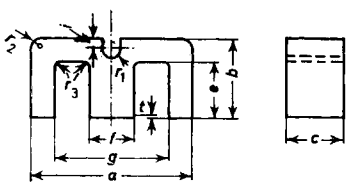



*Figure 13.57. Ferrite E cores to DIN 41 295[27] (see also Table 13.15)*

have been accepted by the IEC[69, 69a]. As against the E type of core, the pot type has the advantage that, aside from the reduced leakage, it favours the trend towards miniaturisation: on purely geometrical grounds the inductance per unit volume is smaller for E cores than for the pot-core series[56].

In a closed magnetic circuit the inductance $L$ is of course approximately determined by the cross-section $A_m$ and the mean length $l_m$ of the magnetic circuit according to equation 3.21:

$$L = z^2 \mu \frac{A_m}{l_m}$$

The relation giving the d.c. resistance $R_{d.c.}$ of the winding is

$$R_{d.c.} = z^2 \varrho \frac{l_w}{k A_w}$$

where $l_w$ is the mean length of turn, $A_w$ the winding cross-section, and $k$ the winding factor. The symbol $\varrho$ stands for the specific electrical resistance of the metallic conductor with which the coil is wound ($\varrho = 1{\cdot}7$ μΩ cm for copper). Eliminating the number of turns $z$ leads to

$$L = R_{d.c.} \frac{\mu}{\varrho} k \frac{A_w A_m}{l_w l_m}$$

(ALL MEASUREMENTS ARE IN MILLIMETRES)

| $f$ | | $g$ | | $i$ | $r_1$ | | $r_2$ | $r_3$ (max.) |
|---|---|---|---|---|---|---|---|---|
| Value | Tolerance | Value | Tolerance | Value | Value | Tolerance | | |
| 5·2 | −0·4 | 12·8 | +0·6 | 0 | 1·5 | +0·3 | 1 | 0·5 |
| 7·2 | −0·5 | 19·5 | +0·8 | 0 | 1·6 | +0·4 | 1 | 0·5 |
| 12·2 | −0·5 | 29·5 | +1·2 | 3 | 2·0 | +0·5 | 2 | 0·6 |
| 17·2 | −0·5 | 37·5 | +1·2 | — | — | — | 3 | 0·6 |
| 20·0 | −0·7 | 44·2 | +1·5 | — | — | — | 3 | 1·0 |

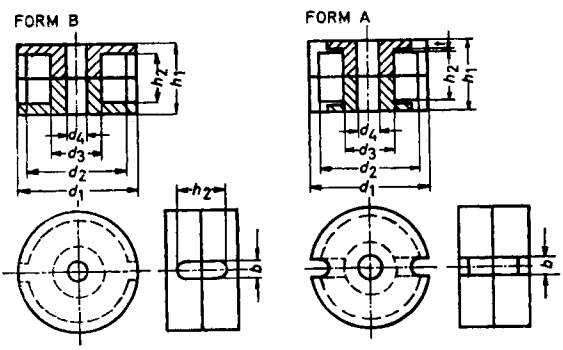



*Figure 13.58. Ferrite pot cores to DIN 41 293[26] (see also Table 13.16)*

The relation between coil volume and the four geometrical magnitudes $A_w$, $A_m$, $l_w$, and $l_m$ is plotted in Figure 13.59 for a few EE cores and pot cores, assuming the same permeability in each case. To go over from an EE30 core to a 23 mm×27 mm pot core means almost halving the coil volume, while passing to the 28 mm×27 mm pot core, which is of similar volume, means a significant increase in the coil inductance. Toroidal cores are hardly used any more for inductors and transformers. Pot cores have mostly taken their place, as they are easier to wind and can be readily adjusted when necessary.

Parallelepiped ferrite cores have been developed recently to improve space-utilisation in communications circuits. The transformer cores set out in DIN 41 299[28] under the title of X cores belong to this group (see Figure 13.60 and Table 13.17)[69b]. X cores are, in general, used for transformers; the smallest type is the X 22. For adjustable inductors and transformers having

**Table 13.16** FERRITE POT CORES TO DIN 41 203[26] (ALL MEASUREMENTS ARE IN MILLIMETRES)

| *Type* | $d_1$ | | $h_1$ | | $b$ *(min.)* | $d_2$ | | $d_3$ | | $d_4$ | | $h_2$ | | $t$ *(min.)* |
|---|---|---|---|---|---|---|---|---|---|---|---|---|---|---|
| | *Value* | *Tolerance* | *Value* | *Tolerance* | | *Value* | *Tolerance* | *Value* | *Tolerance* | *Value* | *Tolerance* | *Value* | *Tolerance* | |
| 9 | 9·3 | −0·3 | 5·4 | −0·2 | 1·8 | 7·5 | +0·25 | 3·9 | −0·2 | 2·0 | +0·1 | 3·6 | +0·3 | — |
| 11 | 11·3 | −0·4 | 6·6 | −0·2 | 1·9 | 9·0 | +0·4 | 4·7 | −0·2 | 2·0 | +0·1 | 4·4 | +0·3 | — |
| 14 | 14·2 | −0·4 | 8·5 | −0·3 | 2·5 | 11·6 | +0·4 | 6·0 | −0·2 | 3·0 | +0·2 | 5·6 | +0·4 | 0·25 |
| 18 | 18·2 | −0·6 | 10·7 | −0·3 | 2·8 | 14·9 | +0·5 | 7·6 | −0·3 | 3·0 | +0·2 | 7·2 | +0·4 | 0·3 |
| 22 | 22·0 | −0·8 | 13·6 | −0·4 | 3·2 | 17·9 | +0·6 | 9·4 | −0·3 | 4·4 | +0·2 | 9·2 | +0·4 | 0·4 |
| 26 | 26·0 | −1·0 | 16·3 | −0·4 | 3·2 | 21·2 | +0·8 | 11·5 | −0·4 | 5·4 | +0·3 | 11·0 | +0·4 | 0·5 |
| 30 | 30·5 | −1·0 | 19·0 | −0·4 | 3·7 | 25·0 | +0·8 | 13·5 | −0·4 | 5·4 | +0·3 | 13·0 | +0·4 | 0·6 |
| 36 | 36·2 | −1·2 | 22·0 | −0·6 | 4 | 29·9 | +1·0 | 16·2 | −0·6 | 5·4 | +0·3 | 14·6 | +0·4 | 0·6 |

dimensions smaller than those of X22, RM cores to DIN 41 980[31a] are introduced. The dimensions of the five types commonly used in Germany are indicated in Figure 13.61 and Table 13.18. Whenever reasonably possible, the letters denoting size are retained to facilitate comparison between RM cores and corresponding pot cores. The relevant IEC Publication further introduces size RM7, and type 5a is dropped.

The basic idea behind the RM core series is that of a coil which can be considered as an integral unit having a core so designed that, in conjunction

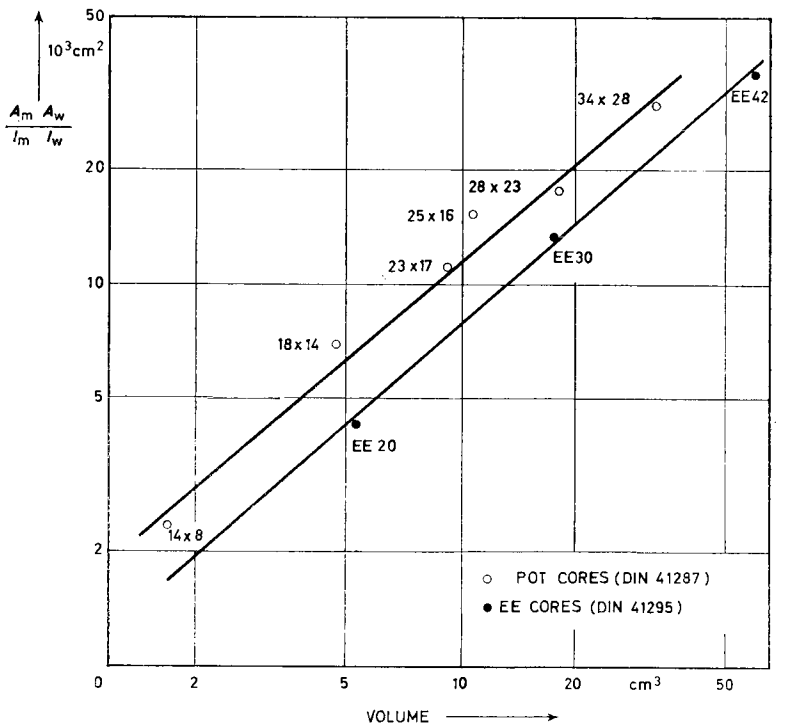



*Figure 13.59. Volume comparison of EE and pot cores of ferrite*[56]

with bobbin, winding, and mounting details, it forms a spatially economic element, fitting neatly into printed-circuit technique. The external dimensions of the connecting pins are built around the international grid pattern (see IEC Publication 97, 1970)[69c], in which a module (M) of 2·54 mm is recommended. Thus, for example, RM5 (rectangular module) occupies a mounting area of some 5M×5M, due allowance being made for necessary clearance.

The coils lend themselves to reasonable winding and finalising procedures. The two halves of the core are held together by sprung clamps, with corresponding recesses along the edges of the core to prevent slipping. Alternatively special gluing procedure may be used to secure the two halves. Compared with pot cores, the relevant RM series yields coils having an improved $Q$ value; alternatively, the volume is reduced if $Q$ remains unchanged[65a].

**Table 13.17** FERRITE X CORES TO DIN 41 299[28] (ALL DIMENSIONS ARE IN MILLIMETRES)

| *Type* | *a* | | *b* | *e* | $d_1$ | | $d_2$ | | $h_1$ | | $h_2$ | | $r_1$ | $r_2$ | $r_3$ | *e* |
|---|---|---|---|---|---|---|---|---|---|---|---|---|---|---|---|---|
| | *Value* | *Tolerance* | *(max.)* | *(min.)* | *Value* | *Tolerance* | *Value* | *Tolerance* | *Value* | *Tolerance* | *Value* | *Tolerance* | | | | |
| X22 | 21·3 | −0·8 | 12·6 | 8·9 | 20·5 | +0·8 | 9·6 | −0·4 | 14·4 | −0·4 | 9·2 | +0·4 | <1·0 | <0·35 | — | 1·5 |
| X25 | 24·5 | −0·9 | 13·7 | 10·0 | 23·6 | +0·9 | 9·8 | −0·4 | 15·6 | −0·4 | 9·6 | +0·4 | — | <0·35 | 5 | 1·5 |
| X30 | 29·6 | −1·2 | 16·4 | 11·8 | 28·4 | +1·2 | 11·4 | −0·4 | 23·6 | −0·6 | 15·0 | +0·6 | — | <0·35 | 6 | 2·0 |
| X35 | 34·6 | −1·4 | 20·3 | 14·8 | 32·2 | +1·4 | 14·3 | −0·5 | 28·0 | −0·6 | 18·4 | +0·6 | — | <0·35 | 8 | 3·0 |

**Table 13.18** RM CORES TO DIN 41 980[21a] (ALL DIMENSIONS ARE IN MILLIMETRES)

| *Type* | *a* | *b* | *c* | $d_2$ | | $d_3$ | | $d_4$ | | *e* | $h_1$ | | $h_2$ | | $r_1$ |
|---|---|---|---|---|---|---|---|---|---|---|---|---|---|---|---|
| | *(max.)* | *(max.)* | *(max.)* | *Value* | *Tolerance* | *Value* | *Tolerance* | *Value* | *Tolerance* | *(min.)* | *Value* | *Tolerance* | *Value* | *Tolerance* | *(max.)* |
| RM4 | 9·8 | 11·8 | 4·6 | 7·95 | +0·4 | 3·9 | −0·2 | 2 | +0·1 | 5·8 | 10·5 | −0·2 | 7 | +0·4 | 0·25 |
| RM5 | 12·3 | 14·9 | 6·8 | 10·2 | +0·4 | 4·9 | −0·2 | 2·04 | +0·06 | 6 | 10·5 | −0·2 | 6·3 | +0·4 | 0·25 |
| RM5b | 12·3 | 14·9 | 6·8 | 10·2 | +0·4 | 6 | −0·2 | 3 | +0·1 | 6 | 12·5 | −0·2 | 8·8 | +0·4 | 0·25 |
| RM6 | 14·7 | 18·3 | 8·2 | 12·4 | +0·5 | 6·4 | −0·2 | 3 | +0·1 | 8·4 | 12·5 | −0·2 | 8 | +0·4 | 0·25 |
| RM8 | 19·7 | 23·2 | 11 | 17 | +0·6 | 8·55 | −0·3 | 4·4 | +0·2 | 9·8 | 16·5 | −0·2 | 10·8 | +0·4 | 0·35 |

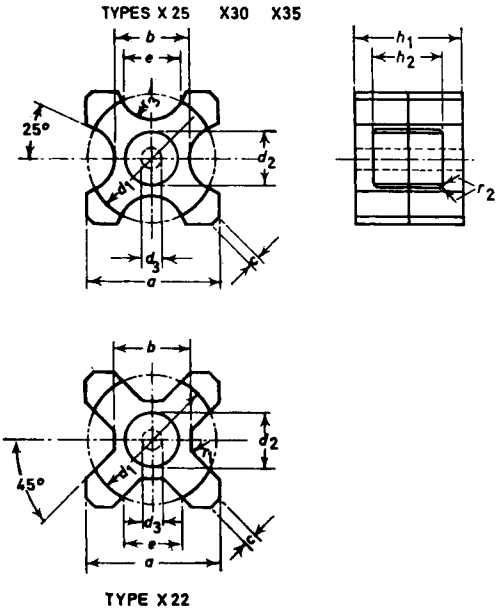



*Figure 13.60. Ferrite X cores to DIN 41 299[28] (see also Table 13.17)*

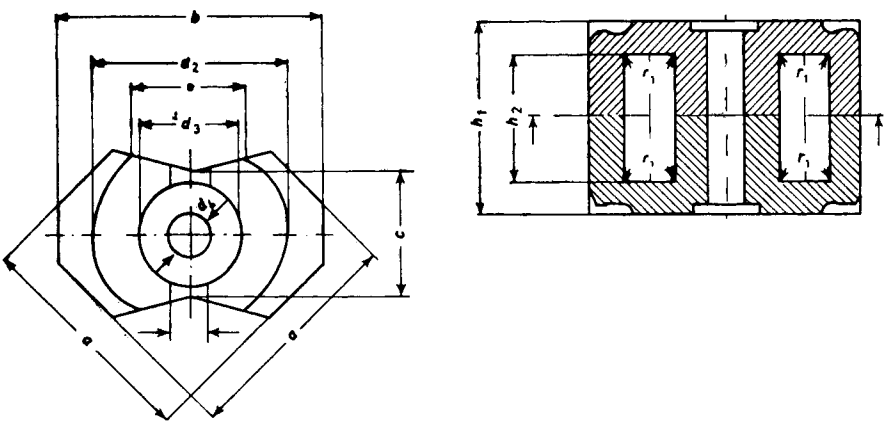



*Figure 13.61. RM cores to DIN 41 980[31a] (see also Table 13.18)*

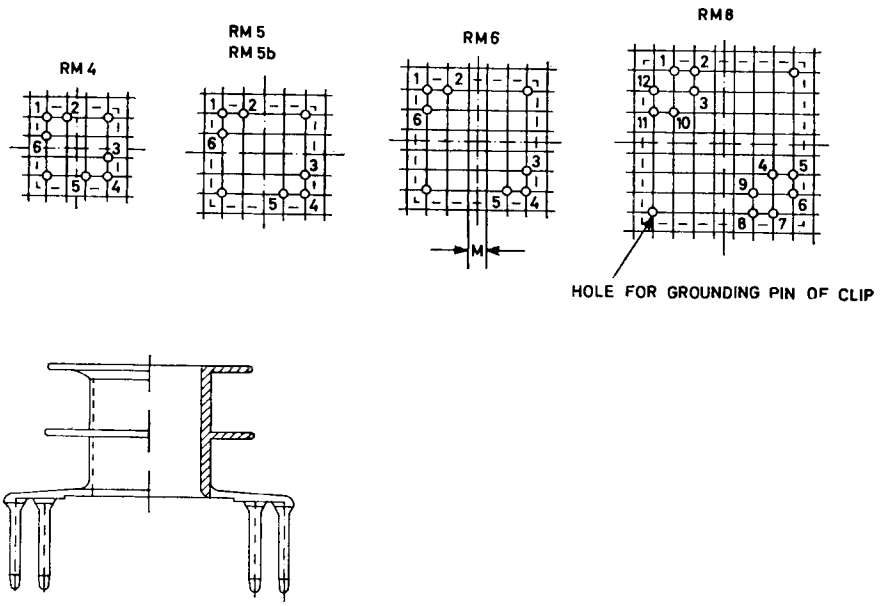



*Figure 13.62. Grid pattern for RM cores and coil former*

The grid module appropriate to the connections is specified in DIN 41 981[31b] and this is reproduced in Figure 13.62. In the IEC recommendations this spacing is indicated as essential, whereas small variations of actual core dimensions are permissible.

Cores in the shape of cylindrical beads are used in u.h.f. work, the coil winding being threaded through the central hole[78].

Rod, tube, or screw cores are used for the permeability adjustment of coils[24]. Screw cores are designated by the diameter and the pitch of the thread. A screw core 6×0·75 B×13, for example, has a nominal thread diameter of 6 mm, a pitch of 0·75 mm, and a core length of 13 mm. The letter B refers to production techniques. Cores labelled A are made by an anti-splinter process. The various production procedures lead to different tolerances for the external diameter. Nowadays the B process (not immune from splinter production) is used exclusively. A few ferrite core-shapes commonly used today in the field of communications are reproduced in Figure 13.63 (see plate section).

### 13.6.3 Adjustable cores

Very precise values of inductance are necessary in oscillatory circuits. As it is not possible to manufacture coils without a range of inductance and dimensional tolerance, special means are needed to tune the various coils to resonance.

For toroidal cores of carbonyl iron dust the accepted method was to fit small capacitors (trimmers) whose capacitance could be varied. Thus Figure

13.64 (see plate section) shows a channel filter built round the use of toroids having $\mu_{tor} = 50\mu_0$. The small trimmer capacitors which served for adjustment can be seen at the front of the unit[56]. These capacitors can be eliminated if the coils themselves are adjustable. To this end the following possibilities present themselves: (a) Change of magnetic path length; (b) change of the effective magnetic cross-section; (c) gapping, i.e. change of air-gap. Figure 13.43 shows the three basic forms[101]. Type (a) is hardly ever used; the commonest are (b) and (c), either individually or in combination.

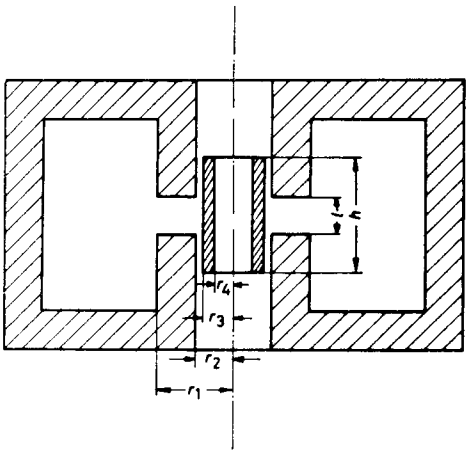



*Figure 13.65. Diagrammatic representation of pot core with adjusting element*

Pot cores incorporate—between the central bosses, for example—an air-gap. In the opening which passes axially through the stem a magnetic material is introduced forming a magnetic shunt across the air-gap. The inductance is altered by shifting this adjusting piece. The arrangement is illustrated schematically in Figure 13.65.

The design and production of an effective and reliable adjusting device presents a difficult problem. Among the numerous requirements which have to be met, only the following will be considered here:

1. The range of adjustment must have a specified magnitude.
2. The change of inductance should be as linear as possible and its curve have a specific gradient.
3. The curve should be smooth and without steps.
4. The inductance change should be free of hysteresis, i.e. as the device is screwed in and out the same inductance value should always be reached at the same position.
5. Adjustment of inductance should not affect any other properties of the coil, for example the temperature coefficient.
6. The inductance once fixed, the device must not go out of tune, i.e. the adjusting element must stay put and not shift with shock, vibration, or temperature change.
7. In many cases the adjusting element has to be confined within certain limits—it must not, perhaps, protrude from the coil.

These numerous requirements lead to tight mechanical limits and to high demands on constancy for the material used for the adjusting element.

The adjusting device generally comprises two parts: an adjusting plunger of plastic, brass, or non-magnetic steel, carrying the adjuster proper, and a female element threaded to receive the plunger. This is usually of plastic. The adjusting plungers belonging to the various pot cores pictured in Figure 13.63 are to be seen below the second row. The nut, or female part, is fixed inside the hole in the core.

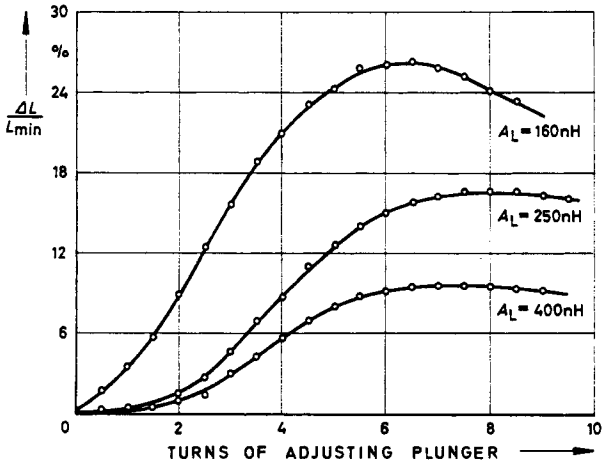



*Figure 13.66. Adjustment curves for an 18* mm×*11* mm *pot core using an auxiliary tube of diameters 2·6* mm *and 1·5* mm *and of length 3·5* mm[65]

The range of adjustment through which the inductance of the coil may be taken depends on the following dimensions: the air-gap $l$; the radii $r_1$ and $r_2$ of the pot core; and the dimensions $h$, $r_3$, and $r_4$ of the tuning core. The meaning of these symbols can be seen from Figure 13.65. Heister[65] has derived the following formula giving the maximum–minimum inductance ratio of an adjustable pot core:

$$\frac{L_{max}}{L_{min}} = 1 + \frac{1}{(r_1^2 - r_2^2)} \left[ \frac{1}{\frac{2}{h-l} \ln \frac{r_2}{r_3} + \frac{h}{\mu(r_3^2 - r_4^2)}} \right]$$

Measured adjustment curves for the case of a pot core 18 mm×11 mm to DIN 41 293 are reproduced in Figure 13.66[65]. The tubular core used had a permeability of $500\mu_0$ and the dimensions were, $d_o = 2r_3 = 2{\cdot}6$ mm, $d_i = 2r_4 = 1{\cdot}5$ mm, and $h = 3{\cdot}5$ mm. For a given regulating device the range of adjustment is greater the bigger the air-gap. The gradient of the adjustment curve also rises with the adjustment range. The calculated value of the range agrees well with the measured value. The calculation gave:

| | |
|---|---|
| $A_L = 400$ nH | $\Delta L/L_{min} = 9{\cdot}1\%$ |
| $A_L = 250$ nH | $\Delta L/L_{min} = 14{\cdot}7\%$ |
| $A_L = 160$ nH | $\Delta L/L_{min} = 25{\cdot}6\%$ |

It is to be noted from the curve that the first one or two turns of the adjusting plunger cannot be used since the first few threads serve only to hold the plunger.

Apart from tuning by the movement of an adjuster, another method has frequently been suggested: the central boss of the core is ground-off obliquely. By turning the two halves of the pot in opposite directions, the length of the air-gap is altered and, with it, the effective permeability and the inductance of the coil[111]. Such a coil is shown diagramatically in Figure 13.67.

In a variant of this arrangement the boss is not sloped; instead, the two surfaces remain parallel but have a small depression eccentric to the boss. The arrangement has proved a useful way of adjusting loading coils[111]. The

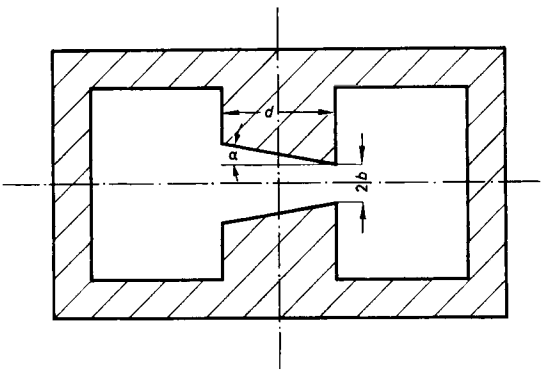



*Figure 13.67. Diagrammatic representation of a pot core with oblique air-gap*

oblique air-gap offers a greater range of variation than the other arrangement. Let $d$ be the boss diameter, $2b$ the width of the gap at its narrowed part, and $\alpha$ the slope of the oblique surface of the gap; then, according to Heister[65], the maximum–minimum inductance ratio, under the assumption of uniform flux partition, is

$$\frac{L_{max}}{L_{min}} = 2(1+\varrho)\{(1+\varrho)-\sqrt{[\varrho(2+\varrho)]}\}$$

where

$$\varrho = \frac{2b}{d\tan\alpha}$$

It can be deduced from the equation that at one limit ($\varrho \to 0$) the value $L_{max}/L_{min} \to 2$; at the other limit ($\varrho \to \infty$), $L_{max}/L_{min} \to 1$, i.e. a change of 100% should be theoretically possible.

By a suitable choice of $b$ and $\alpha$ the designer can predetermine the range of adjustment and its gradient. The magnitude of $\varrho$ is conveniently chosen to lie between 0·2 and 1·0. The relative inductance change

$$\frac{\Delta L}{L_m} = \frac{1-(L_m/L_{max})}{1+(L_m/L_{max})}$$

is plotted in Figure 13.68 as a function of the angle $\alpha$ for various gap widths $2b$; the symbol $L_m = \frac{1}{2}(L_{max}+L_{min})$.

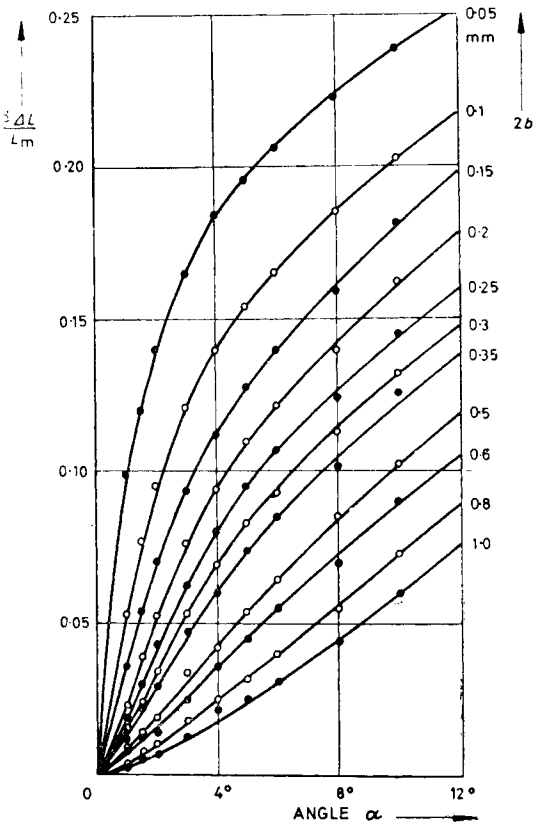



*Figure 13.68. Change of relative inductance as a function of the angle $\alpha$ for various gap widths $2b$*[65]

Figure 13.69 shows adjustment curves as a function of the angle of rotation $\beta$ measured on a 26 mm×16 mm pot core with three typical air-gaps $l_m = 2b+d \tan \alpha$ given in Table 13.19. If one compares the two tuning arrangements—shifting an element parallel to the gap, and opposite rotations of two half-pots—it can be seen that each method has its own advantages and disadvantages.

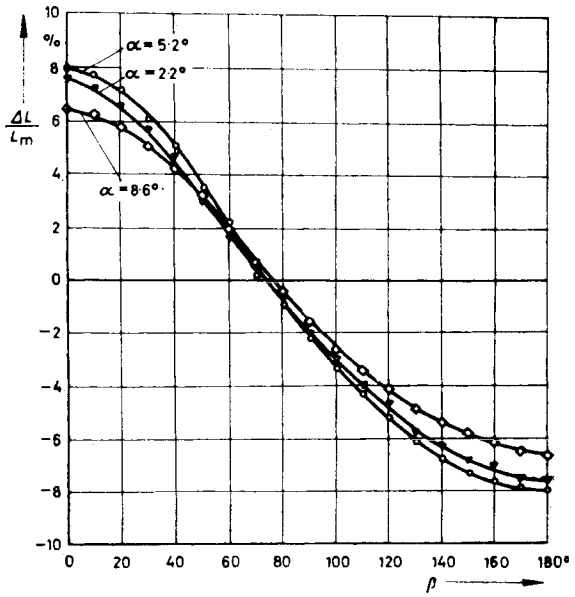



*Figure 13.69. Measured adjustment curves for 26* mm×*16* mm *pot cores with various airgaps*[65]

**Table 13.19** DIMENSIONS OF AIR-GAPS OF CORES ILLUSTRATED IN FIGURE 13.69

| $l_m$ (mm) | α (degrees) | $2b$ (mm) | $2b/d$ tan α |
|---|---|---|---|
| 0·48 | 2·2 | 0·14 | 0·41 |
| 1·00 | 5·2 | 0·22 | 0·25 |
| 1·87 | 8·6 | 0·55 | 0·42 |

The setting accuracy is greater with the plunger device than with the oblique air-gap, the set holds better, and the inductance may be adjusted without the need for any special tools. On the other hand, the use of the oblique air-gap is preferred, for small cores at least, since the adjusting elements cannot be reduced in size indefinitely and the necessary central hole involves a larger coil for a given winding space. The tuning element, moreover, increases the manufacturing cost of the coil and also introduces some uncertainty because, apart from the magnetic adjuster, other materials are involved, serving to guide and hold the device, and these might be affected by heat and humidity.

### 13.6.4 Properties of the more usual ferrites

Since the general formula for a ferrite ($MO \cdot Fe_2O_3$) offers innumerable possible combinations, one might expect to find a vast number of ferrites appearing on the market. However, this is not so. Certainly the multiplicity of available combinations presents the possibility of adapting materials to the solution of the many problems posed by technology. Nevertheless, in the rapid development which set in at the end of World War II it became increasingly clear that a relatively few basic types could be laid down to serve the whole communications industry. For coils and transformers used up to about 1MHz Mn–Zn ferrites were mainly employed; between 1 MHz and 100 MHz Ni–Zn ferrites were dominant; from 100 MHz to 1000 MHz nickel ferrites, supplemented by some special ferrites such as Ferroxplana, were used. Innumerable other systems were investigated in the early years of ferrite development, among which only the Cu–Zn and the Mg–Zn ferrites[129] need here be mentioned and without going further into their properties.

The Mn–Zn and Ni–Zn ferrites offer, according to detailed composition and manufacturing process, a great variety of possibilities adaptable, in their magnetic properties, to the various requirements (frequency range, temperature relations, and stability). The commonest types are standardised[23a]. Their most important properties, measured on toroidal cores of about 30 mm external and 20 mm internal diameter, with a height of some 10 mm, are set out in Table 6.11. Departures from these values are sometimes found for cores of other shapes.

#### 13.6.4.1 Mn–Zn ferrites

Great difficulties were experienced in the early development period in producing Mn–Zn ferrites of high permeability and low loss. Thus Snoek[129], one of the pioneers in the field, stated that he could obtain specimens of high permeability on one occasion while in another experiment they turned out to be almost non-magnetic. He also discovered the explanation of this: the properties of the product depend on the amount of oxygen which the specimens take up from the surrounding atmosphere during cooling.

The manufacture of commercial ferrites whose properties could be reliably reproduced became possible only when it was discovered how to control reliably the oxygen content in the sintering furnace. Further, it was also necessary that the chemical industry should make available raw materials of high purity and uniformity, at acceptable prices.

##### *Saturation polarisation*

Manganese ferrite is distinguished among all other pure ferrites in having the highest magnetic moment. Since all ferrites tend to have low saturation polarisation, because of the antiferromagnetic nature of their crystal struc-

**Table 13.20** MAGNETIC MOMENTS AND SATURATION POLARISATION OF A FEW SIMPLE FERRITES AT 0 K

| *Ferrite* | *Magnetic moment of a molecule of* $MO \cdot Fe_2O_3$ ($\mu_B$) | | $J_s$ (V s/m²) |
|---|---|---|---|
| | *Theoretical* | *Measured* | |
| $MnO \cdot Fe_2O_3$ | 5 | 4·6 | 0·70 |
| $FeO \cdot Fe_2O_3$ | 4 | 4·1 | 0·64 |
| $CoO \cdot Fe_2O_3$ | 3 | 3·7 | 0·60 |
| $NiO \cdot Fe_2O_3$ | 2 | 2·3 | 0·38 |
| $CuO \cdot Fe_2O_3$ | 1 | 1·3 | 0·20 |
| $MgO \cdot Fe_2O_3$ | 0 | 1·1 | 0·18 |

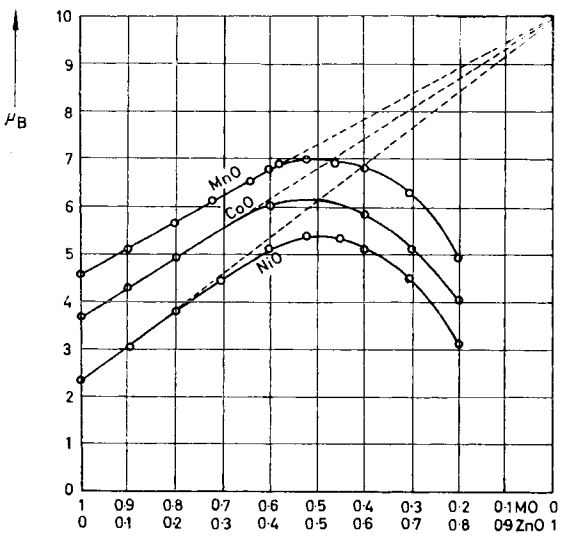



*Figure 13.70. Magnetic moments of some mixed ferrites containing zinc ferrite*[46]

ture, only those materials are of practical significance which stand out by reason of specially high saturation values. The magnetic moment, measured in Bohr magnetons $\mu_B$, alters with the particular metal ions to be found in the interstices of the octahedra. In Table 13.20 the theoretically expected magnetic moments are set against actually measured mean values[44, 46, 106, 107].

Where it is a question of high saturation values, pure ferrites are rarely used. It has in fact been shown that, for mixed ferrites composed of normal and of inverse spinel lattices, the saturation flux density can be raised. Thus, for example, the magneton number of manganese ferrite increases from $4{\cdot}6\mu_B$ to $7\mu_B$ by substituting zinc ions for half the quantity of manganese ions (see Figure 13.70)[46]. The given curves are extrapolated to infinite field

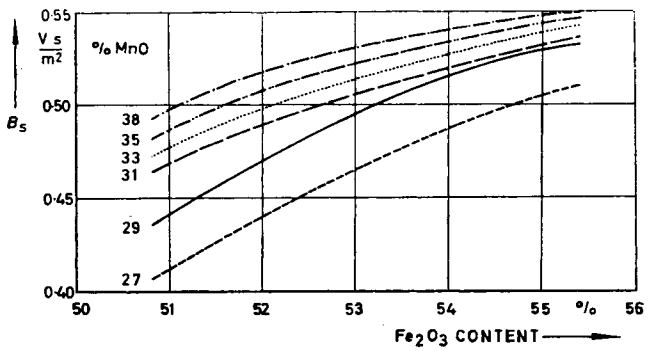



*Figure 13.71. Saturation flux density as a function of composition for a few* Mn–Zn *ferrites*[47]

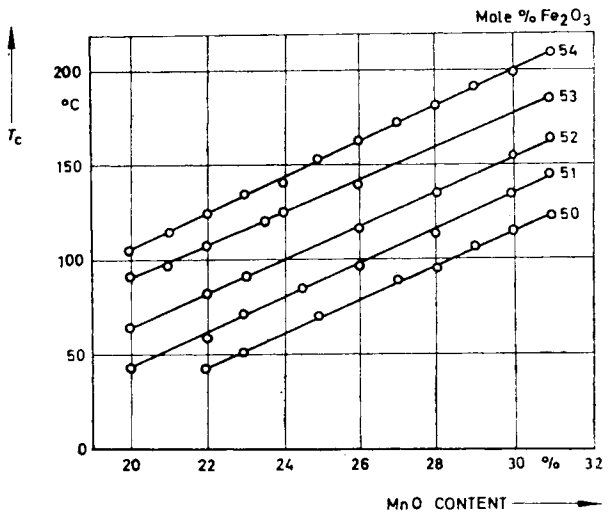



*Figure 13.72. Curie temperature as a function of composition for a few* Mn–Zn *ferrites*[58]

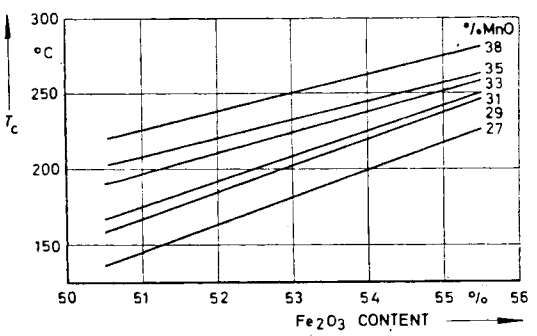



*Figure 13.73. Curie temperature as a function of* MnO *and* $Fe_2O_3$ *content for a few* Mn–Zn *ferrites*[47]

strength and to the absolute zero point. The measured values at room temperature are lower. Figure 13.71 gives some examples of ferrites of various MnO and $Fe_2O_3$ content[47].

*Curie temperature*

It follows from Figure 13.71 that the saturation magnetisation of manganese ferrites is higher the greater the proportion of iron and manganese oxides in the given range of composition. The Curie temperatures are shifted upwards at the same time. As is clear from Figure 13.72[58] and Figure 13.73[47], a more or less linear relation holds. One finds different authors quoting somewhat different Curie temperatures for the same compositions. This is related to the fact that, for identical proportions of the basic substances, different production procedures may lead to different end-products. In addition, measured values have to be corrected for structural differences which can occur, for example, for different degrees of porosity. Within the two series of experiments whose measurements are set out in Figures 13.72 and 13.73 the specimens were actually prepared in the same way.

*Permeability*

*Initial permeability*. Snoek[129] and also Scholts and Piskarew[123] working in the laboratory with Mn–Zn ferrites achieved initial permeabilities of 1500–2000$\mu_0$. No searching probe of manufacturing procedures was made. The

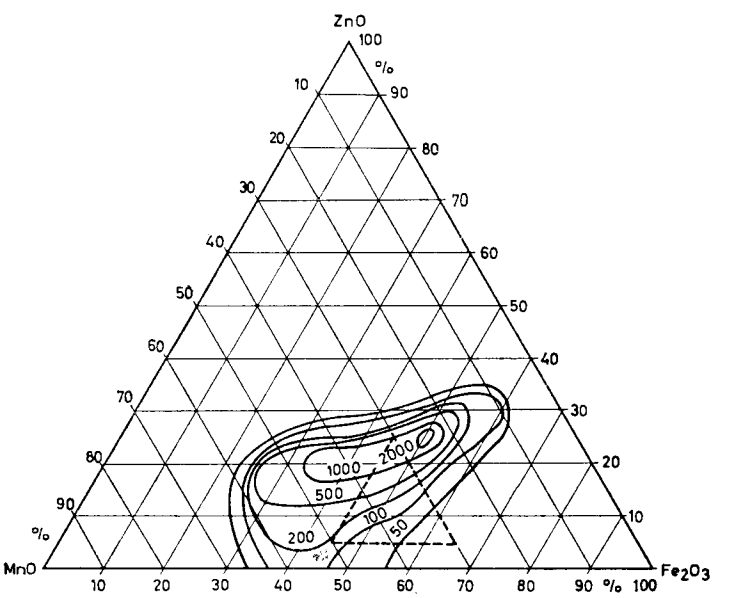



*Figure 13.74. Curves of equal initial permeability for* Mn–Zn *ferrites; the region within the dotted triangle was investigated by Lescroël and Pierrot (see Figure 13.75)*[123]

compositions investigated by Scholts and Piskarew can be read from Figure 13.74, in which curves of equal initial permeability are plotted. The maximum figure of $\mu_i = 2000\mu_0$ is obtained for a composition of $25ZnO \cdot 25MnO \cdot 50Fe_2O_3$.

Toropow and co-workers[138], in their investigations, started from analytically pure base materials which they sintered in nitrogen after a preliminary reaction, within the mixture, at 1250°C. The nitrogen was purified and then had an oxygen content of 0·1–0·01%. They noted a maximum value of initial permeability for a composition around $30ZnO \cdot 20MnO \cdot 50Fe_2O_3$. In spite of their carefully conducted research, they only achieved a $\mu_i$ of about $1000\mu_0$; the production procedures were evidently not optimal. Economos[34] gave more exact data of the partial pressure of oxygen which must be maintained if predictable properties are to be achieved, and, besides nitrogen,

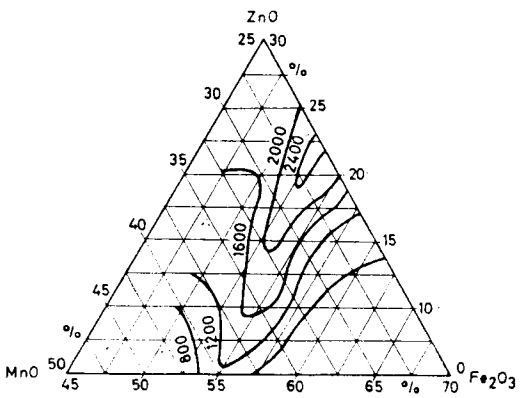



*Figure 13.75. Curves of equal initial permeability for* Mn–Zn *ferrites*[91]

tried the effect of an atmosphere of carbon dioxide or the inert gases; however, he was still unable to achieve the peak values of initial permeability known today.

By fixing the conditions of equilibrium very accurately it became possible to achieve an initial permeability of $4500\mu_0$ for a composition of $24MnO \cdot 24ZnO$[55]—one not far from the optimum given by Scholts and Piskarew. The factors which proved critical for the improvement obtained were: use of pure raw materials, carefully specified annealing atmosphere, and relatively high annealing temperature. The best value of initial permeability was obtained with a 4 h annealing at 1380°C[58]. Heister[63], using a somewhat different composition, and again at a high annealing temperature, achieved enhanced permeability figures (about 4000 $\mu_0$ after annealing at 1365°C).

Departures from the production conditions change the properties given in Figure 13.74; the equal-permeability curves are shifted. This is evident from Figure 13.75, taken from a study by Lescroël and Pierrot[91]. The permeability figures displayed were measured on specimens which had been annealed at 1240°C for 4 h in nitrogen containing 1% $O_2$. According to the same authors, the initial permeability can be raised to $5000\mu_0$ by raising the

annealing temperature. The composition range displayed in Figure 13.75 is that framed by dotted lines in Figure 13.74. It can be deduced from this that the attainable maximum of initial permeability obviously lies in the region of lower manganese content.

The oxygen present in the annealing atmosphere plays a significant role in the properties obtainable with Mn–Zn ferrites. The high-permeability Mn–Zn ferrites are mixtures containing a third ferrite component, namely 'ferro-ferrite' or magnetite $FeO \cdot Fe_2O_3$. The proportion of FeO, formed during the sintering process, for given basic compositions depends on numerous circumstances such as purity and fineness of the initial dust, the density of the pressing, and the already mentioned annealing or sintering conditions. By the use of extremely pure base materials, reduction in vacuo (at 1250°C),

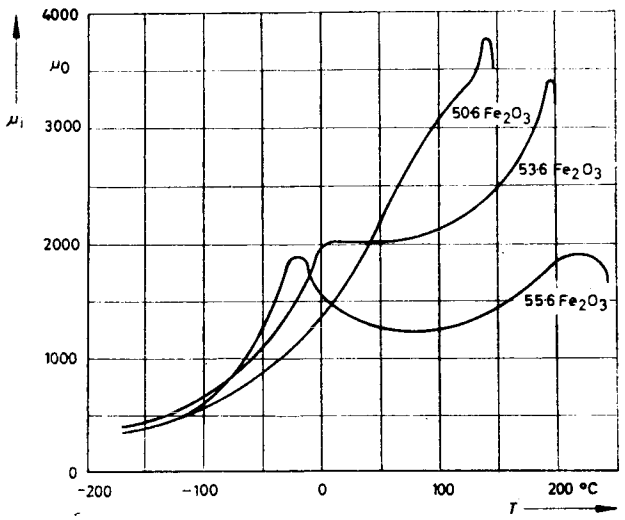



*Figure 13.76. Initial permeability as a function of temperature and composition for* Mn–Zn *ferrites having 31%* MnO[47]

introducig a specified proportion of oxygen (at 1330°C), and vacuum cooling, $\mu_i$ values of over 22 000 $\mu_0$ and $\mu_m$ values of 40 000$\mu_0$ were achieved[125a] in the laboratory for the ferrite $51Fe_2O_3 \cdot 24MnO \cdot 25ZnO$.

Röss, Hanke, and Moser[121a] achieved a $\mu_i$ of 21 000 $\mu_0$ using the ferrite $52{\cdot}5Fe_2O_3 \cdot 25{\cdot}5MnO \cdot 22ZnO$. According to Ohta[101a], the crystal anisotropy of this composition passes through zero—recognisable by the occurrence of a permeability peak—while, at the same time, the magnetostriction becomes very low. Internal stresses and intrinsic demagnetisation were kept low; the Curie temperature was around 130°C.

A further feature of interest is the observation that grain size grew (almost proportionally) with permeability increase, and the specific gravity approached the x-ray density. Shichijo, Asano, and Takama[125a] published a similar finding, namely that ferrites having the highest permeabilities showed remarkably high densities. The effect of FeO content on the permeability of a Mn–Zn ferrite becomes particularly clear if the initial permeability is not

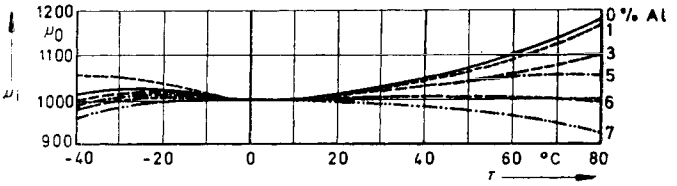



*Figure 13.77. Effect of* $Al_2O_3$ *content on the temperature dependence of initial permeability for a ferrite having 26%* MnO *and 53·5%* $(Fe_2O_3+Al_2O_3)$[47]

looked at simply at room temperature but followed throughout a wide temperature range.

Guillaud[47] was the first to be able to show that, for a fixed manganese content and increasing iron oxide, the slope of the curve of permeability against temperature became less steep; also that the curve sometimes showed a kink at low temperatures, after which (i.e. at higher temperatures) the temperature coefficient became negative (see Figure 13.76). This observation is of great practical value since it provides the possibility of obtaining, within certain limits, any desired temperature coefficient of initial permeability: for example—as can be seen from Figure 13.76—to make the temperature coefficient $\Delta\mu/\Delta T$ about zero between 10°C and 70°C. It is not necessary here to deal with the difficulty of meeting these conditions, with narrow tolerances, in actual practice. In any case the latest developments have shown that it is in fact possible.

The temperature coefficient of initial permeability can also be controlled by other methods: Guillaud[47] found that adding aluminium oxide brought about a change in the temperature dependence of initial permeability. He achieved a temperature coefficient which departed little from zero over the range −40°C to +80°C by adding 6% $Al_2O_3$ to a Mn–Zn ferrite with 26%

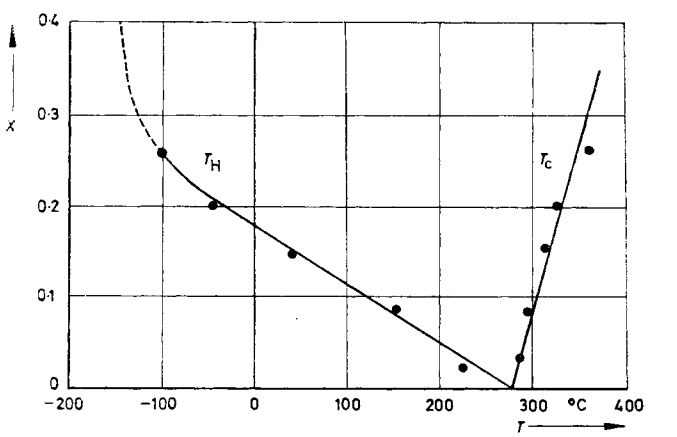



*Figure 13.78. Curie temperature* $T_c$ *and temperature* $T_H$ *at which the permeability curve shows a kink, for* Mn–Fe *ferrites to the formula* $xFeO\cdot(1-x)MnO\cdot Fe_2O_3$, *plotted as a function of* $x$[89]

MnO (Figure 13.77). The same quantity, namely 6%, of $Cr_2O_3$ acted similarly on a ferrite with 24% MnO. It is true that these non-magnetic additives lowered the permeability, saturation flux, and Curie temperature, but the relative loss factor $(\tan \delta)/\mu_i$ remained unaltered[47].

A Mn–Zn ferrite with 31% MnO was investigated under various annealing conditions by Heister[64]. It was found that the hump of the permeability–temperature curve could be shifted by varying the sintering temperature and the proportion of iron oxide. The investigations of Lescroël[89] bring out the decisive role played here by the proportion of FeO in a ferrite represented by $x\text{FeO}\cdot(1-x)\text{MnO}\cdot\text{Fe}_2\text{O}_3$: if, in a manganese ferrite, an increasing proportion of MnO is replaced by FeO, then the Curie temperature $T_c$ is

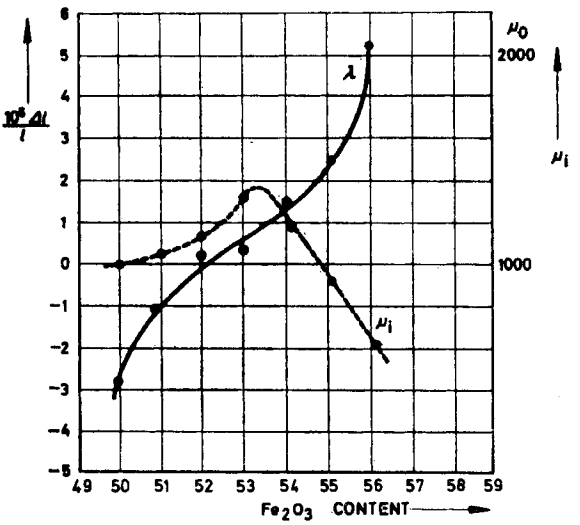



*Figure 13.79. Relation between magnetostriction $\lambda$, initial permeability, and iron oxide content for* Mn–Zn *ferrites with 32–39%* MnO[143]

shifted towards higher temperatures while the permeability 'hump' $T_H$ moves towards lower temperatures. The relevant data are reproduced in Figure 13.78[89]. Measured at room temperature, a maximum $\mu_i$ value occurs at $x = 0{\cdot}15$. It is worthy of note that it is only at this maximum that the hysteresis shows a 'normal' loop; at a smaller magnetite content it is rectangular, and at higher proportions it assumes a Perminvar character[89].

To explain the cause of the high permeability values, one may refer, in the case of Permalloy or Sendust (see page 453), to the passage of the magnetostriction through zero. This does not work in the same way for Mn–Zn ferrite, according to Vautier[143]. It is known in fact that magnetite $\text{FeO}\cdot\text{Fe}_2\text{O}_3$ has a positive and Mn–Zn ferrite a negative magnetostriction, but it appears that $30\text{MnO}\cdot17\text{ZnO}\cdot53\text{Fe}_2\text{O}_3$, for example, shows a permeability minimum at $\lambda = 0$ (i.e. zero magnetostriction), while the initial permeability of a Mn–Zn ferrite having 32–39% MnO passes through a maximum at $\lambda$ somewhat above zero ($0{\cdot}4$–$0{\cdot}7\times10^{-6}$ in fact) (Figure 13.79).

Enz[38] found that in the ferrite $28{\cdot}5MnO{\cdot}18ZnO{\cdot}53{\cdot}5Fe_2O_3$ the signs of $\lambda_{100}$ and $\lambda_{111}$ in the temperature range from $-200°C$ up to the Curie temperature are opposite, $\lambda_{111}$ being greater, and $\lambda_{100}$ less, than zero. Crystal anisotropy vanishes at 10°C. According to Ohta's investigations[101a] into single-crystal performance, the second permeability maximum (turning point) occurs at that temperature at which crystal anisotropy passes through zero.

*Maximum permeability.* Figure 3.4 shows the dependence of permeability on field strength for a high-permeability Mn–Zn ferrite, having the approximate constitution $53Fe_2O_3{\cdot}24MnO{\cdot}23ZnO$, at various temperatures. With increasing temperature the $\mu$-maximum shifts towards the lower intensities, i.e. the coercivity falls. For most high-permeability Mn–Zn ferrites, $H_c$ lies around 5–10 A/m.

*Reversible permeability.* As an example of the 'run' of the curve of reversible permeability for Mn–Zn ferrites, Figure 13.80 reproduces the 'butterfly' curve, known also for certain metals; it is given here for a ferrite of approximate composition $51Fe_2O_3{\cdot}26MnO{\cdot}23ZnO$.

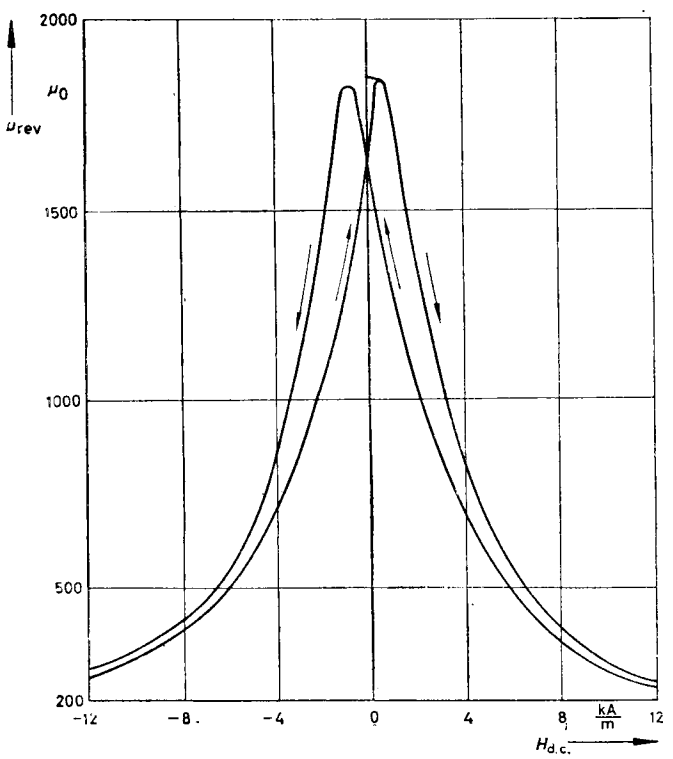



*Figure 13.80. Reversible permeability of a* Mn–Zn *ferrite* $26MnO{\cdot}23ZnO{\cdot}51Fe_2O_3$

*Loss coefficients*

Table 3.5 gave the loss coefficients of dust cores set against those of Mn–Zn ferrites and it was noted that the referred loss coefficients of the ferrite cores are better than those of the metallic cores by some orders of magnitude. It was further stated that the loss coefficients of the Mn–Zn ferrites were temperature dependent and, to some extent, depended also on the intensity; this makes for certain difficulties of assessment. The relevant measuring conditions must always be stated, therefore, when loss coefficients are quoted. We shall therefore look more closely at some of the results reflected in the literature.

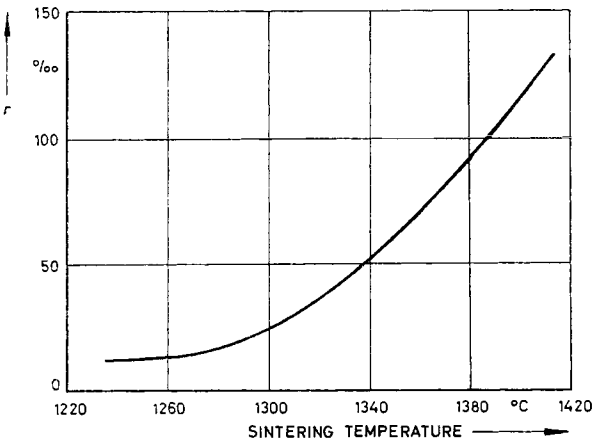



*Figure 13.81. Residual-loss coefficient r as a function of sintering temperature for a* Mn–Zn *ferrite 53*FeO•*28*MnO•*19*ZnO[63]

*Residual-loss coefficient.* Among all ferrites the Mn–Zn series shows the lowest residual loss, so they are especially suitable for use at low frequencies. The magnitude of the residual-loss coefficient $r$ may be affected by the sintering temperature and, in fact, $r$ is greater the higher the sintering temperature of the sample. Thus, for example, Heister[63] obtained the relation between sintering temperature and residual loss shown in Figure 13.81 for a ferrite of composition $53Fe_2O_3$•28MnO•19ZnO; the loss measurements were made at room temperature. At low sintering temperatures $r = 10‰$ but at 1400°C it is 120‰. As, at low sintering temperatures, $\mu$ is still less than $1000\mu_0$, the referred residual-loss factor is higher than, for example, after an annealing at around 1300°C.

Besides the dependence of $r$ on sintering temperature, there is also a dependence on measuring temperature. This has already been demonstrated in Figure 3.35 taken from measurements by Lescroël[90]. It is seen that $r$ rises both above and below room temperature.

Heister[62] obtained a residual-loss coefficient $r$ of 24‰ for the Mn–Zn ferrite Hyperox D1S measured at room temperature. Under the assumptions

that the eddy-current losses are negligible and that the loss which increased with frequency was attributable to a frequency-dependent residual effect, Heister obtained an increase in the $r$ value, between 5 kHz and 100 kHz, from 26‰ to 85‰ (see Table 13.21).

*Eddy-current coefficient.* The observed frequency dependence of the loss resistance for Mn–Zn ferrites can be traced, at least formally, to an eddy-current constant $e$, using the method of assessment given by Jordan (see Figure 3.18). This can be based on the concept of the ferrite as a non-uniform substance comprising electrically conducting particles covered by an insulating film (see Figure 8.18). Based on this assumption, it would seem possible to reduce the coefficient $e$ by improving the insulating properties of this film. In fact, Guillaud, Paulus, and Vautier[48] succeeded in reducing

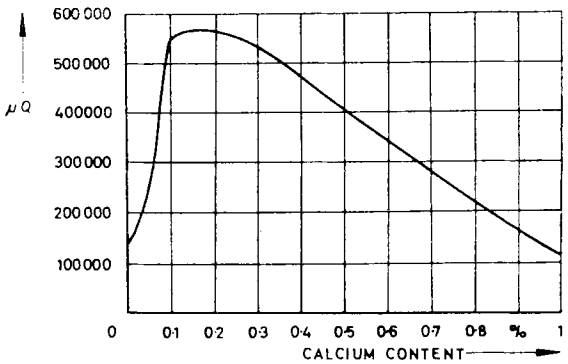



*Figure 13.82. Relation between the quality product $\mu Q$ of a* Mn–Zn *ferrite and the calcium content; composition 53*FeO•*28*MnO•*19*ZnO *($f$ = 40*kHz)*[48]

the eddy-current coefficient of a ferrite ($53Fe_2O_3 \cdot 28MnO \cdot 19ZnO$) by an order of magnitude by adding calcium. This calcium was added to the basic material in the form of $CaCO_3$. The improvement was secured without at the same time worsening the permeability, hysteresis, and residual effects. *In toto*, the quality product $\mu Q = \mu/\tan\delta$, could therefore be materially improved. At a calcium content of about 0·2%, the quality product $\mu Q$ measured at 40 kHz attained a maximum of 550 000, corresponding to a minimum value of $(\tan\delta)/\mu$ of $1{\cdot}8 \times 10^{-6}$ (see Figure 13.82).

Based on the assumptions that the initial permeability of a Mn–Zn ferrite increases with temperature according to the relation

$$\mu_i = \mu_{i_0}(1+\alpha T)$$

and that the electrical resistance of the ferrite falls with rising temperature according to the relation

$$\varrho = \varrho_0 \exp(-\beta T)$$

Lescroël[90] derived the following formula for the Jordan eddy-current coefficient $e$:

$$e = e_0(1+\alpha T)\exp(\beta T)$$

A straight line can be plotted over the temperature range 0°–100°C if a logarithmic scale is chosen for $e$. Figure 13.83 gives the curves for two materials whose eddy-current coefficients at 20°C are 0·28 μs and 0·67 μs.

Lescroël[90] also gives an approximate formula for the relation between eddy-current coefficient and measuring intensity at low field strengths. Starting from the Rayleigh relation

$$\mu = \mu_i(1 + aH)$$

and also

$$\varrho = \varrho_i(1 + bH)$$

he obtains

$$e = e_0(1 + a'H)$$

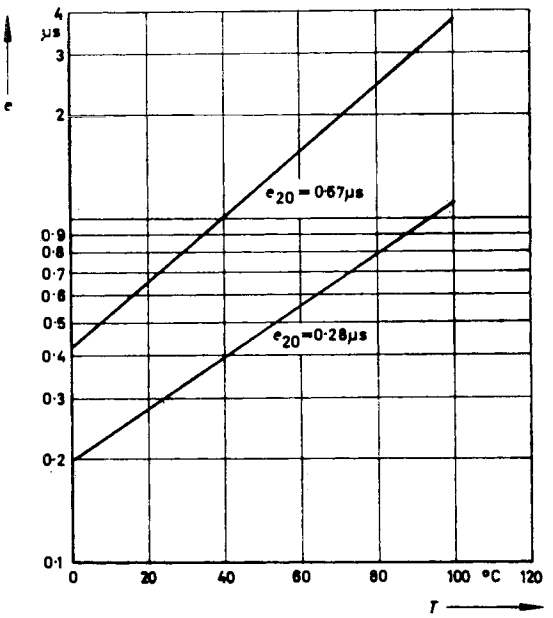



*Figure 13.83. Eddy-current coefficient e as a function of measuring temperature*[90]

This formula is in agreement with the example given in Figure 3.18 and with measurements made by Heister[62]. In a detailed example given by Lescroël, $e = 0{\cdot}29$ μs.

The coefficient $e$ can vary widely between samples since it depends, like all the loss coefficients, on the production history of the specimen. This is shown by an example of an already quoted experiment by Heister[63], set out in Figure 13.84, which demonstrates the dependence of $e$ on the sintering temperature. The values of $e$ for intensities up to 200 A/m are given, as well as $e_0$.

*Hysteresis coefficient.* Like the residual and the eddy-current coefficients, the hysteresis coefficient depends not only on the constitution of the ferrite

but also on the conditions prevailing during manufacture. To obtain low hysteresis coefficients, the impurities in the material must be kept low and the departure from stoichiometric proportions must be small. Further, the grains must have a predetermined size. According to Guillaud[47], the mean value of the grain size should not exceed 20 μm. If the crystallites are larger, internal pores appear and these lower the permeability and increase the hysteresis. Thus it may be found that the hysteresis losses increase the higher the final sintering temperature.

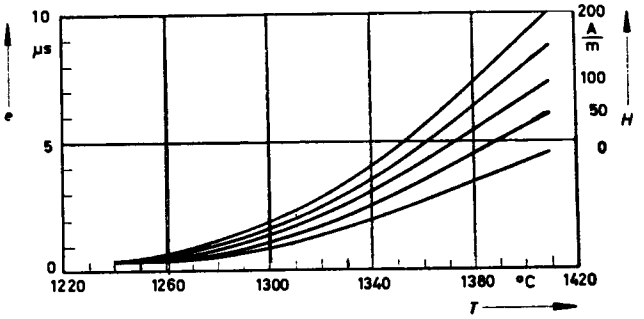



*Figure 13.84. Eddy-current coefficient e as a function of the final sintering temperature for various values of measuring field strength at room temperature*[63]

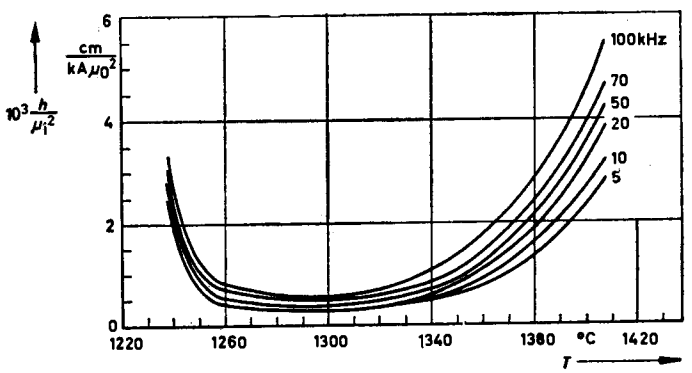



*Figure 13.85. Referred hysteresis coefficient $h/\mu_i^2$ as a function of the final sintering temperature and the measuring frequency*[63]

Heister[63] found a similar rise with sintering temperature for $h$ as for $e$ (Figure 13.84). Since the initial permeability for low annealing temperatures is still very low, a high referred hysteresis factor is found in this range, with a minimum at moderate annealing temperatures. Figure 13.85 for example, shows this for a ferrite having the composition $28MnO \cdot 19ZnO \cdot 53Fe_2O_3$[63]. A minimum $h/\mu_i^2$ of $300 \times 10^{-6}$ cm/kA $\mu_0^2$ is obtained at a sintering temperature of 1290°C. For a fixed sintering temperature a minimum value of $h/\mu_i^2$ is obtainable, depending on sintering time[91].

Figure 13.86, after Guillaud, shows the effect of composition on the hysteresis coefficient. As can be seen, all ferrites investigated have $h/\mu_i^2$ values which, when plotted against their $Fe_2O_3$ content, pass through a minimum. This minimum shifts towards higher $Fe_2O_3$ values with increasing MnO content but reaches, for example, lower $h/\mu_i^2$ values for low MnO content than for high.

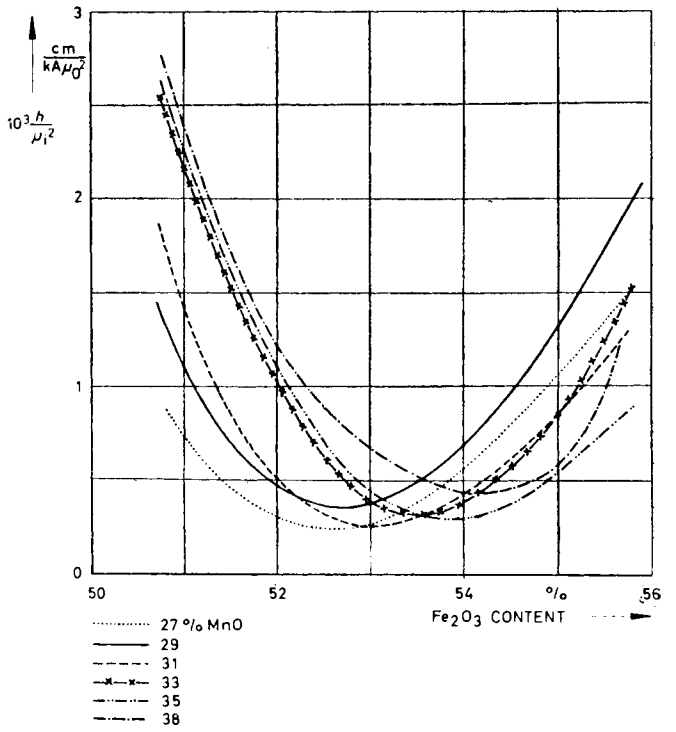



*Figure 13.86. Effect of composition on referred hysteresis coefficient*[47]

The values of $h/\mu_i^2$ plotted in Figure 13.85 clearly show a dependence on frequency. Values of $h/\mu_i^2$ as low as $130\times10^{-6}$ can be achieved by the use of very pure base materials[111].

A few numerical values are given in Table 13.21 for a similar ferrite core[62]. In another column the values of $h/\sqrt{\mu_i}$ are also set out and, to enable a comparison to be made with high-permeability Fe–Ni alloys, values for two kinds of Hyperm are also shown[61]. The expression $h/\sqrt{\mu_i}$ is useful for comparing coils in oscillatory and signal circuits on the basis of equal inductance and equal operating voltage. Against this, $h/\mu_i^2$ plays a role in relatively harmonic-free transformers, i.e. those provided with air-gaps. The highest frequency $f_h$ of a wide-band audio transformer is constant, being fixed by the geometry of the coil. At a low frequency the non-linear distortion factor is predetermined, but, in operation, the non-linear distortion factors are related to $h/\mu_i^2$.

**Table 13.21** LOSS COEFFICIENTS AS FUNCTIONS OF FREQUENCY FOR A Mn–Zn FERRITE; ALSO THE $h$ COEFFICIENT MEASURED AT 50 Hz FOR Fe–Ni ALLOYS IN 0·1 mm STRIP[62]

| | $f$ (kHz) | $h$ (cm/kA) | $r$ ($^0/_{00}$) | $10^6 h/\mu_i^2$ (cm/kA $\mu_0^2$) | $10^3 r/\mu_i$ ($^0/_{00}/\mu_0$) | $h/\sqrt{\mu_i}$ (cm/kA $\sqrt{\mu_0}$) |
|---|---|---|---|---|---|---|
| Ferrite | 5 | 1 900 | 26 | 430 | 12·4 | 41·5 |
| | 10 | 2 100 | 30 | 475 | 14·3 | 45·8 |
| | 20 | 2 300 | 36 | 520 | 17·1 | 50·2 |
| | 50 | 2 700 | 54 | 544 | 25·7 | 52·4 |
| | 70 | 3 600 | 68 | 708 | 32·4 | 76·0 |
| | 100 | 4 100 | 85 | 805 | 40·5 | 86·5 |
| Hyperm 36 | 0·05 | 13 000 | — | 1 850 | — | 252 |
| Hyperm 766 | 0·05 | 230 000 | — | 745 | — | 1 740 |

While in applications involving $h/\mu_i^2$ it is possible to compensate for a high $h$ by designing for a correspondingly high $\mu_i$, this compensation is substantially harder to achieve for $h/\sqrt{\mu_i}$. Thus for loading coils and coils in signal circuits every improvement in $h$ is valuable, even if it means somewhat lower permeability. Values of $h/\sqrt{\mu_i}$ of 15·3 cm/kA $\sqrt{\mu_0}$ were achieved for ungapped toroids[110]. This value, which in itself is rather low, can be further improved by gapping. Thus it can be reduced to 0·6 cm/kA $\sqrt{\mu_0}$ by inserting an air-gap 0·2 mm long.

It is found that, as the hysteresis coefficient falls, the rise in permeability with intensity also becomes less. This is also confirmed by the above example from Heister[62], in which $\delta_5 = 0{\cdot}69 \times 10^4$ m$^2$/V s and $\delta_{100} = 0{\cdot}45 \times 10^4$ m$^2$/V s were obtained. If $\delta$ is plotted against the temperature of final sintering, an increase with sintering temperature is obtained similar to that for the hysteresis coefficient, so it is not necessary to repeat the curve here. It may be mentioned that, up to a sintering temperature of 1300°C, the $\delta$ values of Heister's example fall, in general, within the limits of class D1 of DIN 41 302.

### *Loss factor and referred loss factor*

It can be discovered from numerous publications that the referred loss factor $(\tan\delta)/\mu$ of Mn–Zn ferrites passes through a minimum whether it is plotted against sintering time[91] sintering temperature[58, 63], or oxygen content[58, 91]. It would take us too far afield to explore, here, the production conditions necessary to achieve optimum results. Since $(\tan\delta)/\mu$ is given by a summation of the referred loss coefficients, the basic rules already given for the separate losses will apply.

The supplier has the difficult task of taking into account, in minute detail, all factors which contribute to an optimum overall reduction of loss factor, balancing them against each other, and admitting into practice only those which lend themselves to consistent reproduction. Curves for the various

features can only be meaningful where the treatment procedures are the same. Thus in Figure 13.87[91], which relates to the three-component system MnO–ZnO–$Fe_2O_3$, curves are plotted for $\mu Q$ values of 100 000, 150 000, and 200 000, all the ferrites investigated having been sintered at 1220°C in an atmosphere containing 5% $O_2$. The measuring frequency was 300 kHz. For this treatment and at this measuring frequency the lowest (tan $\delta$)/$\mu$ value was obtained for about 55% $Fe_2O_3$ and 8–16% ZnO.

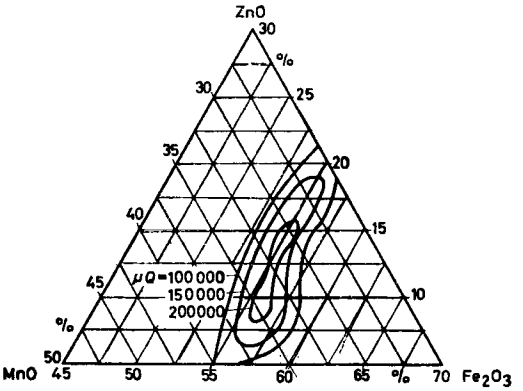



*Figure 13.87. Curves of equal $\mu Q$ product for* Mn–Zn *ferrites which have been sintered at 1220°C in an atmosphere containing 5% $O_2$; measured at 300* kHz[91]

Usually, (tan $\delta$)/$\mu$ is quoted in logarithmic units when plotted against frequency. At least four or five different grades of ferrites are needed to cover, optimally, a frequency range of from 1 kHz to 100 MHz. Suppliers usually offer a wider range of grades in order to meet more successfully the requirements of individual frequency ranges. It is therefore not possible to obtain optimal loss values over the whole frequency range with one kind of ferrite. For example, for ferrites showing a low (tan $\delta$)/$\mu$ at 10 kHz, the loss factor increases very steeply above 200 kHz. Conversely, another ferrite whose loss curve is flat between 200 kHz and 500 kHz and which, in consequence, is superior in this range to the first one cannot be used below 100 kHz since here (tan $\delta$)/$\mu$ scarcely drops with falling frequency but remains almost constant and is substantially worse at 1 kHz than the first.

The steepness of the tan $\delta$ curve is connected with the phenomenon of gyromagnetic resonance. In consequence of equation 3.73, the (tan $\delta$)/$\mu$ curve passes into the region of steep slope at frequencies which are lower the higher the value of permeability. A ferrite, therefore, which is to be worked at high frequency must have a low permeability. Considered over a wide frequency range, a family of curves is obtained like that shown, for example, in Figure 13.88[142]. Other families of curves relating to other suppliers are shown in Figures 19.2 and 19.3.

It is sometimes possible to find many ferrites with different variabilities of (tan $\delta$)/$\mu$ in particular frequency ranges; this is connected with the fact that, apart from the need for a low tan $\delta$, other factors play their part, such as

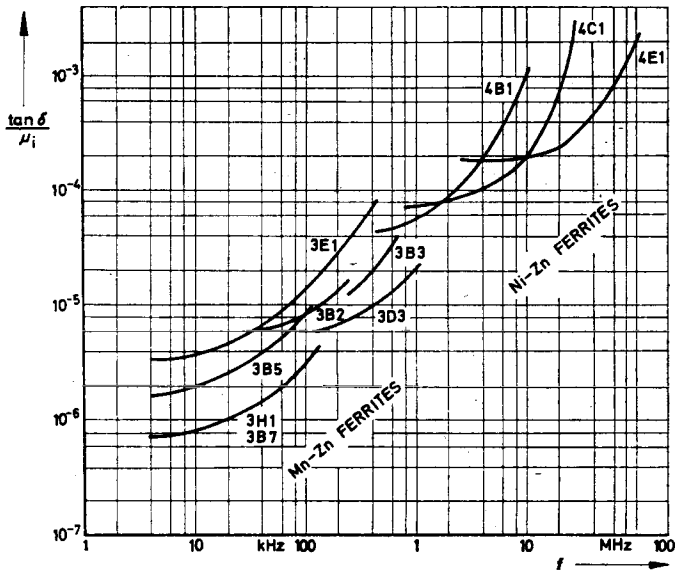



*Figure 13.88. Loss factor (tan δ)/$\mu_i$ as a function of frequency f for various types of ferrite (Ferroxcube)*[142]

temperature coefficient, and stability, which cannot be optimised at the same time as the loss factors but which may be of greater importance in some applications.

### *Disaccommodation*

Numerous investigations have been devoted to disaccommodation. Mn–Zn ferrite shows the effect to various extents according to composition. As already expounded in Section 3.2.8, disaccommodation is particularly sensitive to intensity and temperature changes. Lescroël and Pierrot[91] were able

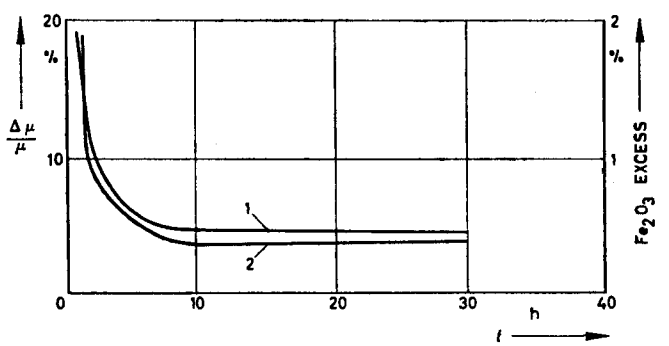



*Figure 13.89. Effect of duration of annealing on the drop of permeability with time and on the excess of* $Fe_2O_3$ *above 50%: 1,* $Fe_2O_3$ *excess; 2,* $\Delta\mu/\mu$[91]

to prove that disaccommodation was connected with excess iron oxide. Figure 13.89, taken from their studies, clearly shows the parallel course of the percentage fall-off in permeability (see below) and the excess of $Fe_2O_3$. This experiment brings out the fact that disaccommodation is very small for stoichiometric compositions and that it increases if the FeO content rises. The authors were also able to demonstrate the effect of MnO content.

**Table 13.22** EFFECT OF IRON OXIDE CONTENT ON FALL OF PERMEABILITY WITH TIME FOR A Mn–Zn FERRITE HAVING 26·3% MnO[91]

| *Specimen* | *Annealing* | FeO (%) | $Fe_2O_3$ (%) | $\Delta\mu/\mu$ (%) |
|---|---|---|---|---|
| 1 | 4 h, | 3·6 | 50·16 | 1·3 |
| 2 | 1240°C, | 4·7 | 50·34 | 2·6 |
| 3 | | 5·4 | 50·48 | 3·8 |
| 4 | $N_2$+1% $O_2$ | 6·0 | 50·32 | 4·4 |
| 5 | | 6·6 | 50·16 | 6·3 |
| 6 | | 7·1 | 50·50 | 7·0 |
| 7 | | 8·2 | 50·70 | 9·0 |
| 1′ | 4 h, | 3·5 | 51·10 | 4·1 |
| 2′ | 1240°C, | 4·1 | 51·30 | 5·0 |
| 3′ | | 4·6 | 51·66 | 6·0 |
| 4′ | $N_2$+5% $O_2$ | 5·2 | 51·50 | 7·4 |
| 5′ | | 5·6 | 51·76 | 9·2 |
| 6′ | | 6·0 | 52·26 | 9·1 |
| 7′ | | 7·4 | 52·00 | 13·1 |

Changes of permeability for ferrites having 26·3% MnO and various proportions of FeO and $Fe_2O_3$ are set out in Table 13.22 and plotted in Figure 13.90. These show the results of two annealing routines[91]: one involving sintering in nitrogen with a 1% $O_2$ content and the other in nitrogen with 5% $O_2$. The straight line showing the fall in permeability is shifted, almost parallel to itself, towards higher disaccommodation as the oxygen content of the sintering atmosphere is increased. The drops in permeability shown in Table 13.22 and Figure 13.90 were taken on specimens which were measured 1 min and 24 h after a conditioning at 50 Hz and at a field strength of 1·2 kA/m.

Braginski, Marais, and Merceron[15] have investigated, over a temperature range of from −200°C up to the Curie temperature, Mn–Zn ferrites differing in the molecular ratio $k$ of their initial mixture ($k = Fe_2O_3/MO$). The symbol MO here signifies MnO+ZnO with MnO at 30%. The ratio $k$ lay between 1·00 and 1·27. Disaccommodation was defined as the percentage fall in permeability 30 min after magnetic conditioning[93]. The results given in Figure 13.91 show disaccommodation maxima which are more pronounced the higher the value of $k$. The first maximum lies below the tempera-

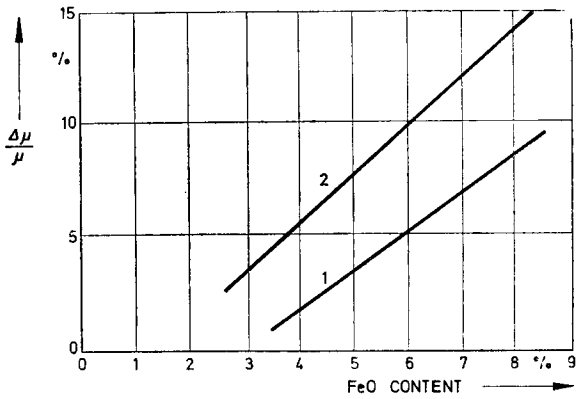



*Figure 13.90. Disaccommodation as a function of* FeO *content: 1, annealed in 1% $O_2$; 2, annealed in 5% $O_2$ (see Table 13.22)*[91]

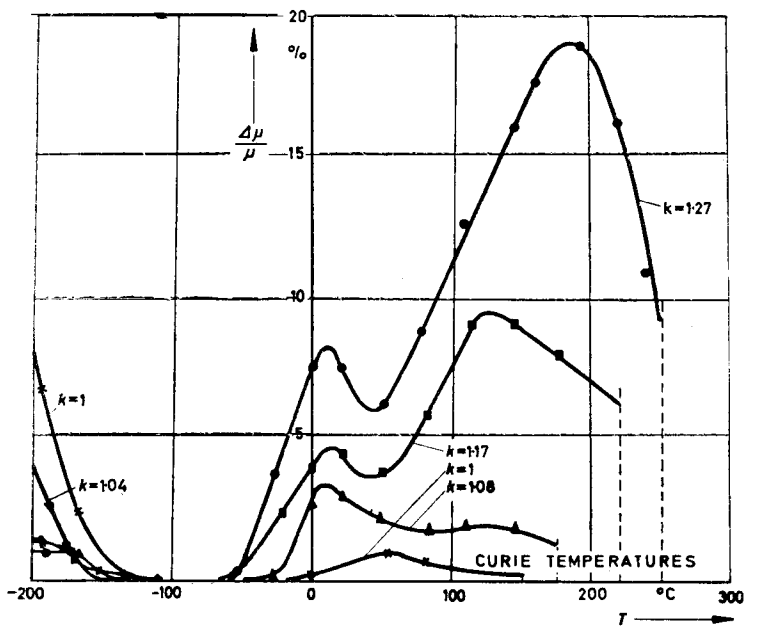



*Figure 13.91. Drop in permeability of a* Mn–Zn *ferrite with various mixture ratios k as a function of temperature*[15]

ture of liquid air and presumably is lower the higher the value of $k$. This shift can be attributed to electron exchange, which is linked, for $k = 1$, with an activation energy of 0·2 eV. The room-temperature maximum, on the other hand, does not shift in position with the $k$ value, but its value is higher for higher values of $k$. No relaxation for tan $\delta$ was found. The third maximum, between 100°C and 200°C is likewise higher for higher $k$ values and also shifts its position, with $k$, towards higher temperatures. To study this effect a specimen for which $k = 1{\cdot}27$ was subjected to a reduction and oxidising annealing. The reduction, at 1500°C, in pure nitrogen caused the maxima almost completely to disappear and the disaccommodation became very small (Figure 13.92). After annealing in an atmosphere of higher oxygen content, the maxima reappeared strongly. It can be deduced from these investigations that various relaxation mechanisms are operative in the Mn–Zn ferrites.

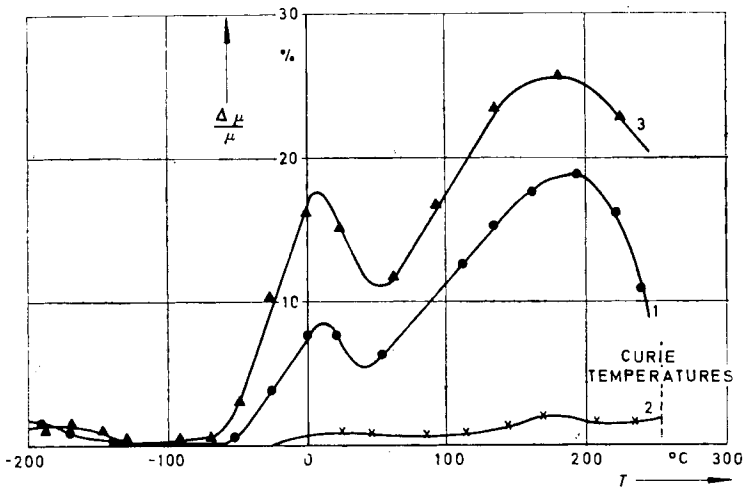



*Figure 13.92. Effect of oxygen in the annealing atmosphere for an annealing temperature of 1250°C: 1, 0·5% $O_2$; 2, pure $N_2$; 3, 5% $O_2$*[15]

A result similar to that of the experiments described can also be observed in the Mn–Zn ferrites used in practice. By way of illustration, certain measured results are given which we obtained with commercially used Mn–Zn ferrites. If the disaccommodation is measured over a longer interval and if the disaccommodation factors $D$ (see page 65) are calculated for time intervals (decades) of 1–10 min, 10–100 min, and 100–1000 min after magnetic conditioning, then the following facts can be stated. In the first interval the $D$ values are relatively low and vary little with temperature: a maximum appears at 10°C and also at 90°C, as Figure 13.93 shows. In the second and third intervals the maxima are more marked and the disaccommodation at a given temperature is thus greater. The minimum, which occurs in the third interval between the two maxima, dips further than the $D$ values of the first two intervals. At 20°C $D$ is almost identical in all three intervals. In this case

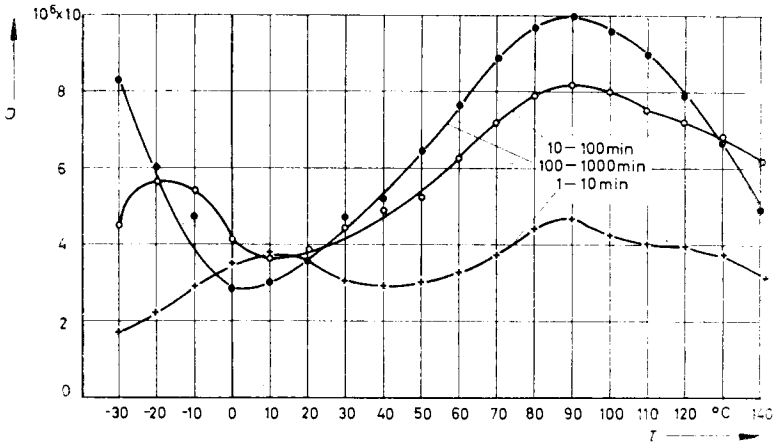



*Figure 13.93. Disaccommodation measured for a commercially available* Mn–Zn *ferrite*

the permeability falls off according to a law resembling that shown in Figure 3.36 (for another ferrite).

Two remarkable facts appear: the high-temperature maxima occur at the same temperature in all three intervals, namely 90°C; and the low-temperature maximum shifts between the first and third intervals from +10°C to −20°C and further to less than −30°C. In conformity with the researches of Braginski, Marais, and Merceron[15], it can be stated that the two residual-effect mechanisms are dependent not only on temperature but also on time.

In order to reduce disaccommodation, experiments have been made with additives of titanium, chromium, and calcium, and finally it has been found that the best results are obtainable with Mn–Zn ferrites if they are sintered in the correct atmospheres[144]. On the other hand, Marais and Merceron[94a] showed that the addition of lithium to Mn–Zn ferrites can appreciably reduce disaccommodation at room temperature.

### 13.6.4.2 Ni–Zn ferrites

Ni–Zn ferrites introduce fewer manufacturing difficulties than the Mn–Zn ferrites because of the smaller effect of the sintering atmosphere. Annealing can be carried out in air without any special precautions. It was thus possible to offer high-permeability Ni–Zn ferrites earlier than high-permeability Mn–Zn ferrites. Pioneer work on these Ni–Zn ceramics was done by Forestier and Vetter[40], Smolenski[128], Snoek[129], and Takai[134].

#### *Saturation polarisation*

Figure 13.70 demonstrates that, fundamentally, the high flux densities of the Mn–Zn ferrites are not achieved by the Ni–Zn ferrites.

Figure 13.94, following investigations by Guillaud[49], shows the saturation values at 20°C as a function of NiO content for various proportions of $Fe_2O_3$. Below 35% NiO the saturation polarisation rises with increasing content of iron oxide and reaches a maximum value which shifts somewhat towards lower NiO levels for higher proportions of $Fe_2O_3$.

*Curie temperature*

The Curie temperature of nickel ferrite is around 580°C[50]. By adding zinc ferrite it can be made nearly linear with respect to the additive down to the region of room temperature, as is clearly shown in Figure 13.95[57]. At about 12% NiO the Curie temperature and the room temperature coincide. However, only those mixed ferrites whose Curie temperature lies above at least 100°C are important for coils and transformers. Curves of equal Curie temperature for the three-component $Fe_2O_3$–NiO–ZnO system are given in Figure 13.96, after Harvey, Hegyi, and Leverenz[50] who were the first to publish a thorough investigation of the Ni–Zn ferrites. The specimens on which this research was based were sintered in air at 1400°C.

If the NiO proportion is held constant, the Curie temperature rises with increasing $Fe_2O_3$ content. This can be deduced from Figure 13.97, after Guillaud and co-workers[49], or may be extracted (in good agreement with the above) from the three-component diagram of Figure 13.96.

*Initial permeability*

The lowering of the Curie temperature by the addition of zinc ferrite is associated with a desirable increase in initial permeability (Figure 13.95)[57]. In 1951 Smolenski[128] achieved a maximum value of $\mu_i = 1200\mu_0$ (Figure 13.98). Snoek[129] had already reached a $\mu_i$ of $3800\mu_0$ in 1949. The highest values of initial permeability, which may exceed $5000\mu_0$[49], occur at 15% NiO (Figure 13.99) and are associated with a rather low Curie temperature.

The permeability maximum, occurring for stoichiometric compositions, is very marked for the Ni–Zn ferrites. This conclusion may be drawn from the investigations of Guillaud and co-workers[49]. Measurements of magnetostriction carried out by the same authors show that it increases with increasing NiO content and reaches a value $\lambda$ of approximately $-12\times10^{-6}$ for 35% NiO, while for 15% NiO it lies between $-1\times10^{-6}$ and $-2\times10^{-6}$ according to sintering temperature (Figure 3.51); thus with increase in magnetostriction goes a drop in initial permeability, as one might expect. The magnetostriction null-line, however, does not run parallel to the stoichiometric composition line but forms an angle with it. According to Harvey, Hegyi, and Leverenz[50], the negative maximum magnetostriction tends towards the pure nickel ferrite (ZnO content zero); the positive maximum occurs for a Zn–Fe ferrite (NiO content zero). Curves of equal magnetostriction are reproduced in Figure 3.52[50] (the absolute values of the measurements are missing, as they were in the original work).

The initial permability of Ni–Zn ferrites can be severely prejudiced by

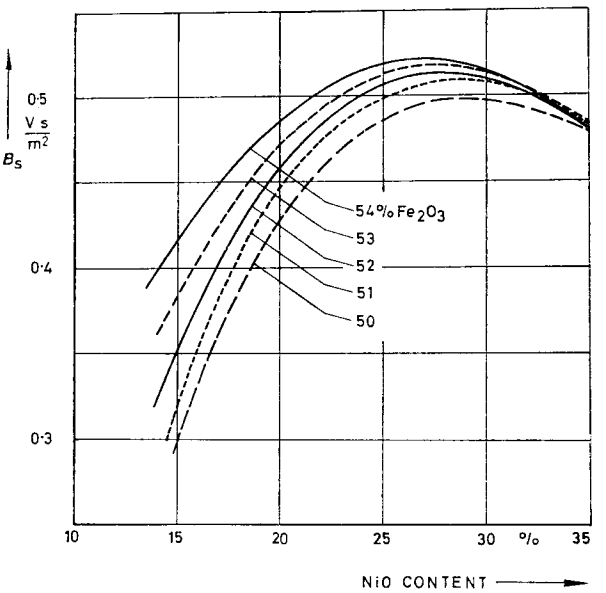



*Figure 13.94. Saturation flux density for a* Ni–Zn *ferrite as a function of* NiO *content*[49]

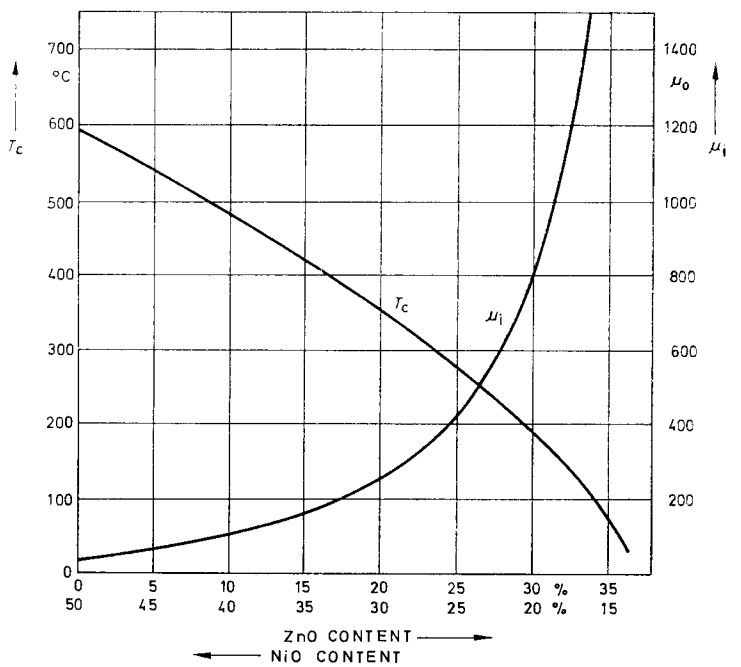



*Figure 13.95. Curie temperature $T_c$ and initial permeability $\mu_i$ for ferrites having 50%* $Fe_2O_3$ *as functions of* NiO *and* ZnO *content*[57]

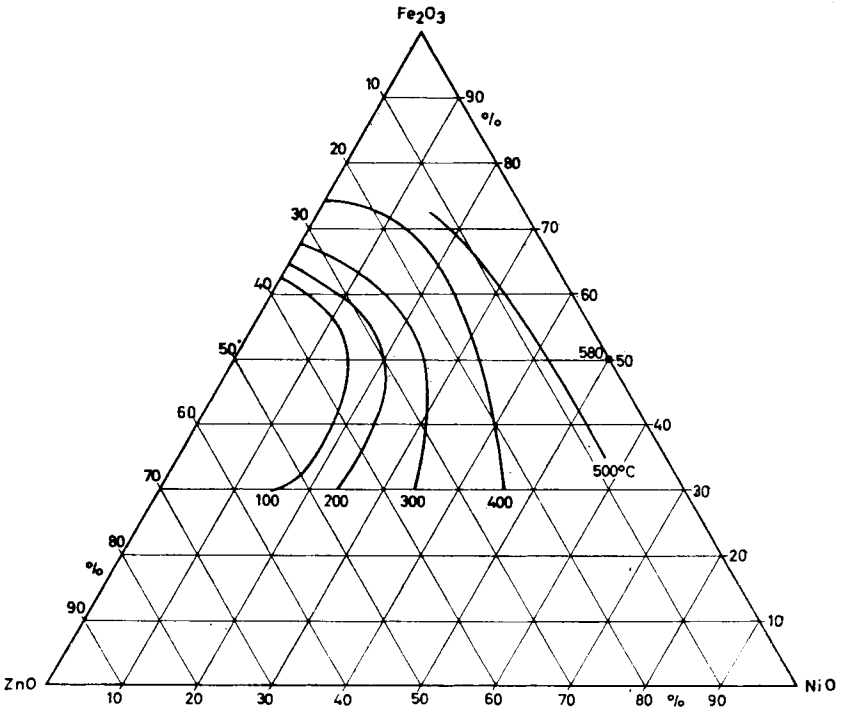



*Figure 13.96. Curie temperature of* Ni–Zn *ferrites which have been sintered at 1400°C in air*[50]

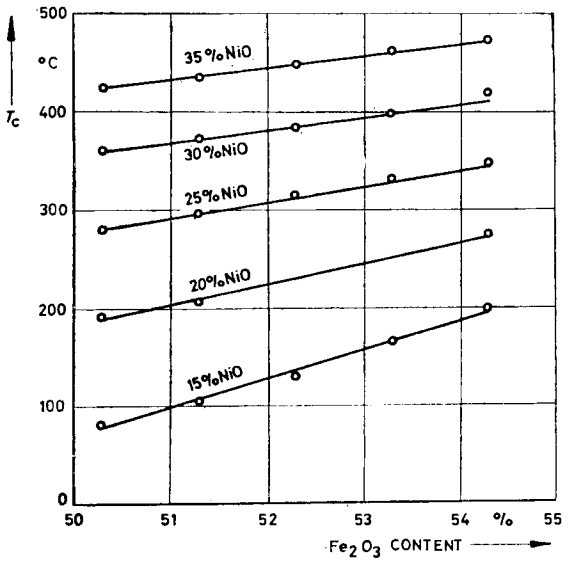



*Figure 13.97. Curie temperature of* Ni–Zn *ferrites as a function of* $Fe_2O_3$ *and* NiO *content*[49]

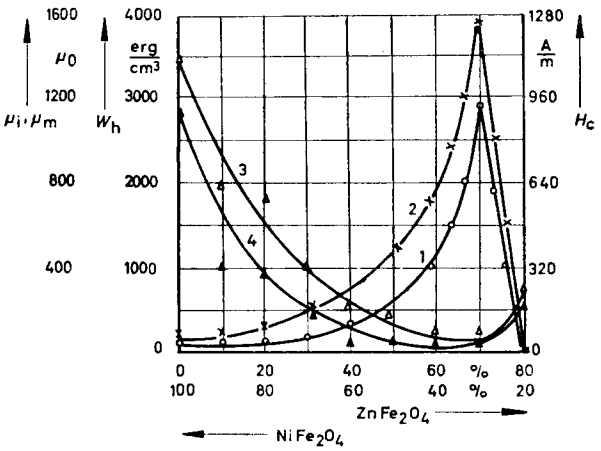



*Figure 13.98. Properties of* Ni–Zn *ferrites*[128]*: 1, initial permeability; 2, maximum permeability; 3, coercivity; 4, hysteresis loss per cycle at 0·1* V s/m²

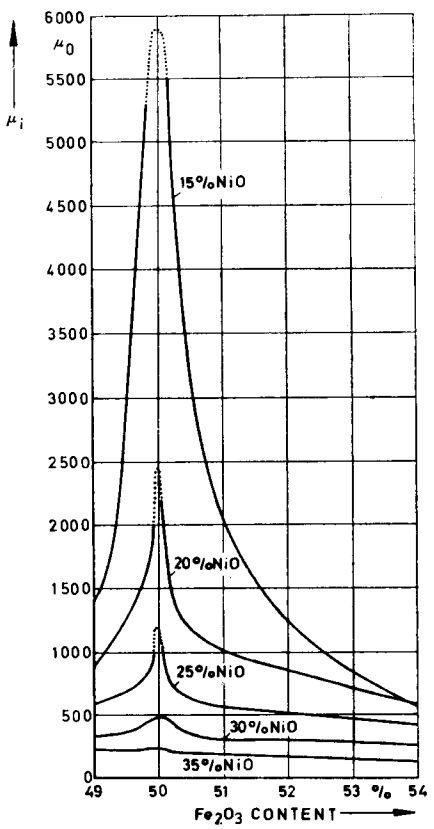



*Figure 13.99. Initial permeability of some* Ni–Zn *ferrites as a function of* $Fe_2O_3$ *content*[49]

impurities, particularly when it is a question of small amounts of the alkaline earths—of additives, in fact, having a relatively large ionic radius (see Figure 6.3)[49]. On the other hand, lithium added to stoichiometric Ni–Zn ferrites can lead to a rise in initial permeability. Thus an addition of 0·3% $Li_2O$ to the ferrite $15NiO \cdot 35ZnO \cdot 50Fe_2O_3$ effects an improvement in $\mu_i$ from, say, $3700\mu_0$ to $5700\mu_0$. More lithium additives and a higher NiO content than 25% are less effective[49].

The initial permeability is further affected by the duration and temperature of the annealing process and the associated grain size. According to Guillaud and co-workers[49], the maximum $\mu_i$ value of the composition $15NiO \cdot 35ZnO \cdot 50 Fe_2O_3$, already mentioned, can reach the value $5000\mu_0$ only if the mean particle size of the ferrite is optimum, i.e. about 10 μm. For half or for double this particle size, the permeability is only about half as high. The most favourable conditions consist of an approximately 20 h annealing at 1200°C–1250°C. A briefer annealing at a higher temperature has not the same effect as a longer baking at a lower heat. This can be seen, for example,

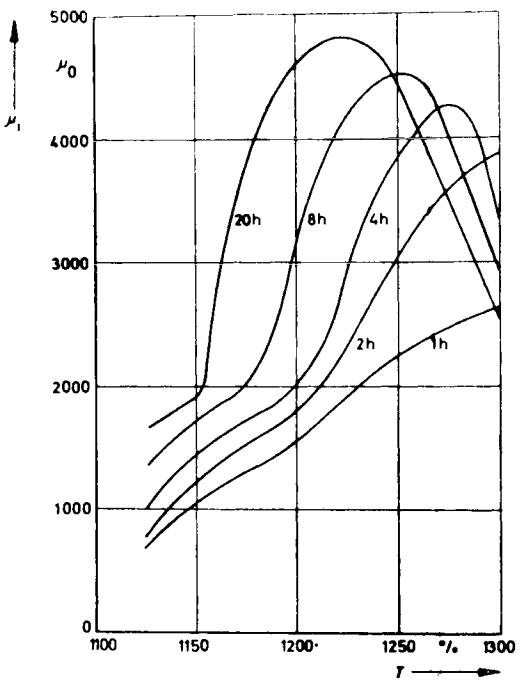



*Figure 13.100. Initial permeability of the* Ni–Zn *ferrite* $15NiO \cdot 35ZnO \cdot 50Fe_2O_3$ *as a function of sintering temperature for various sintering times*[49]

from the curves of Figure 13.100, in which the relation is shown between permeability and the temperature and duration of sintering (again for the ferrite $15NiO \cdot 35ZnO \cdot 50Fe_2O_3$).

Curves of equal initial permeability for the three-component system NiO–ZnO–$Fe_2O_3$ are plotted in Figure 13.101[50]. It is seen that the best value of

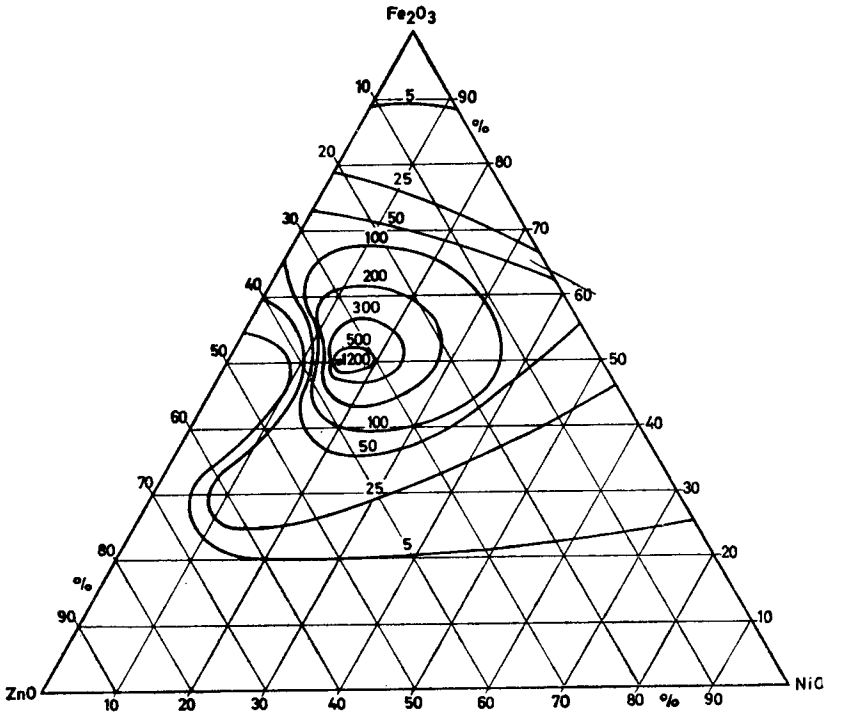



*Figure 13.101. Loci of equal initial permeability displayed in a three-component diagram for* NiO–ZnO–$Fe_2O_3$[50]

initial permeability occurs for stoichiometric compositions (50% $Fe_2O_3$) having 15% NiO.

Plotted against frequency, the initial permeability of the Ni–Zn ferrites, like that of the Mn–Zn ferrites, shows a nearly constant range, at the end of which there is a falling-off due to resonance phenomena. The fall occurs at a higher frequency the lower the initial permeability (see Figure 3.42).

A definite and generally low temperature coefficient of initial permeability is desirable for the cores of coils. This is generally positive and fairly large for stoichiometric Ni–Zn ferrites. It usually becomes smaller with decreasing $Fe_2O_3$ content and approaches zero for 42% $Fe_2O_3$. Figure 13.102 shows an example of this behaviour for a ferrite with 15% NiO and 35% ZnO, sintered at 1150°C. The coefficient $\alpha$ is plotted in percent for the temperature range $-40$°C to $+90$°C, within which the slope of the permeability–temperature curve may be taken as substantially linear[49]. In a similar way the relation between $\alpha$ and $Fe_2O_3$ content holds for all NiO proportions between 15% and 35%. However, as Figures 13.99 and 13.101 show, the initial permeability at 42% $Fe_2O_3$ is particularly low, so the use of ferrite of this composition is very restricted.

Guillaud and co-workers[49] were able to show that quite another means of lowering the temperature coefficient of stoichiometric Ni–Zn ferrite is

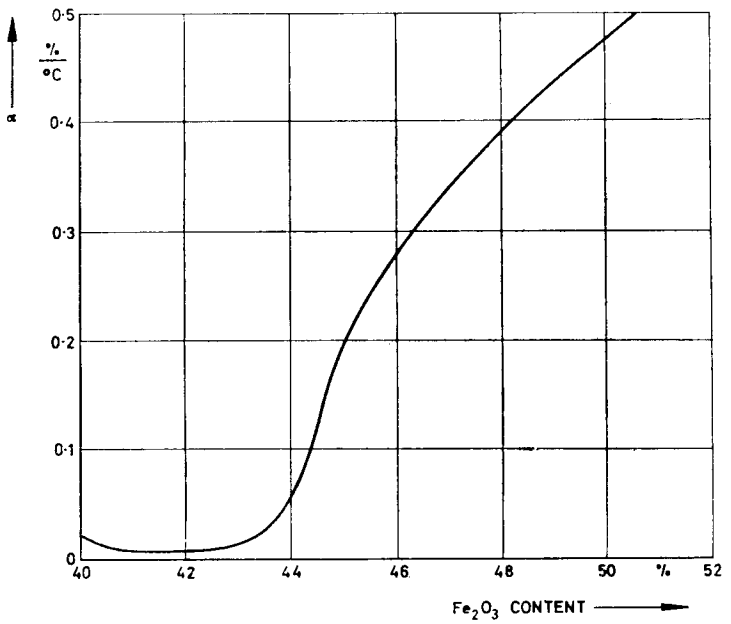



*Figure 13.102. Temperature coefficient α of initial permeability for the ferrite 15*NiO•*35*ZnO *as a function of* $Fe_2O_3$ *content*[49]

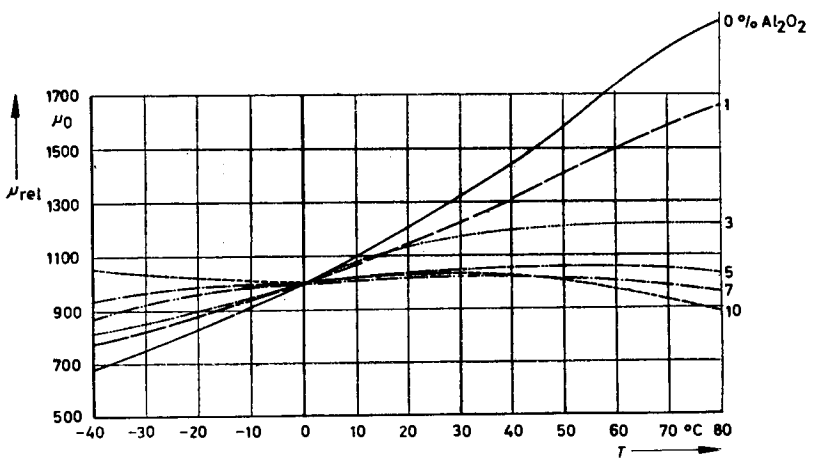



*Figure 13.103. Effect of* $Al_2O_3$ *on the temperature coefficient of a* Ni–Zn *ferrite 18*NiO•*32*ZnO•*50* $(Fe_2O_3+Al_2O_3)$[49]

available whereby a part of the $Fe_2O_3$ is replaced by $Al_2O_3$. It is true that the substitution of an aluminium ion for one of iron lowers saturation density, Curie temperature, and initial permeability to an undesirable extent and also increases tan $\delta$; but the advantage of the low temperature coefficient outweighs these defects in certain applications. The permeability of a Ni–Zn ferrite $18NiO \cdot 32ZnO \cdot 50(Fe_2O_3 + Al_2O_3)$, having 0–10% $Al_2O_3$, is plotted between $-40°C$ and $+80°C$ in Figure 13.103. To clarify the changes effected, a reference point is taken at $\mu_i = 1000\mu_0$ and $T = 0°C$ (see also Figure 6.5). For other proportions of $Fe_2O_3$ in the basic mixture, the amount of $Al_2O_3$ has other effects, and heat treatment is also relevant. The usual $Al_2O_3$ content is about 5%.

Like aluminium oxide, chromium oxide produces a change of temperature coefficient, so the designer has the opportunity of obtaining either a positive or a negative temperature coefficient within some given range of temperatures.

Some of the Ni–Zn ferrites have a constricted hysteresis loop, a so-called 'Perminvar' loop (see Section 5.3.2). This kind of hysteresis loop occurs more especially in those ferrites that have an excess of $Fe_2O_3$ or contain a certain quantity of added cobalt oxide. This kind of material is technically useful because the permeability alters only slightly with increasing intensity and frequency and because the losses in this range are unusually low (see below). Among the Ni–Zn ferrites, Perminvars are now known with initial permeabilities between about $5\mu_0$ and $200\mu_0$[82].

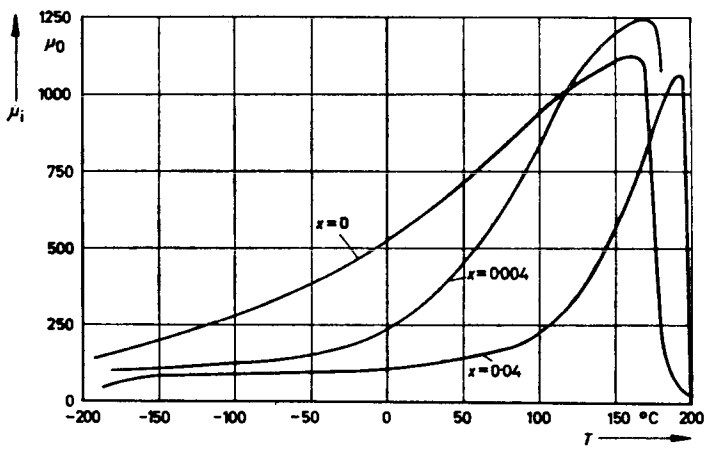



*Figure 13.104. Initial permeability as a function of temperature at 1* kHz *for* Ni–Zn *ferrites of the composition* $(Ni_{0\cdot4}Zn_{0\cdot6})_{1-x}\,Co_x\,Fe_{1\cdot92}O_4$ *with* $x = 0, 0\cdot004,$ *and* $0\cdot4$[127]

Figure 13.104 demonstrates how, for Ni–Zn ferrites with a cobalt additive, the positive slope of the temperature–permeability curve falls appreciably with increasing cobalt content. The curves, taken from an investigation by Sixtus[127], apply to a ferrite of composition $(Ni_{0\cdot4}Zn_{0\cdot6})_{1-x}Co_xFe_{1\cdot92}O_4$ where $x$ is given the values 0, 0·004, and 0·04.

*Coercivity*

The coercivity of the Ni–Zn ferrites falls with increasing ZnO content and reaches a minimum at about 35% ZnO, 15% NiO, i.e. for a composition where the permeability is highest. As can be seen from Figure 13.98, taken from measurements by Smolenski[128], $H_c$ falls from 1120 A/m to 80 A/m.

*Hysteresis loss*

The curve of hysteresis loss (with respect to ZnO content) for Ni–Zn ferrites is of much the same form as that of coercivity. It reaches a minimum for the ferrite $15NiO \cdot 35ZnO \cdot 50Fe_2O_3$ (see Figure 13.98).

*Loss coefficients*

*Residual-loss coefficient.* The residual-loss coefficient of the Ni–Zn ferrites is usually higher than that of the corresponding Mn–Zn ferrites of similar initial permeability, and as a rule it also rises more steeply with increasing temperature. The residual-loss coefficients for ferrites having various initial permeabilities (measured at 20°C) are plotted in Figure 13.105 over the range 0°–160°C[61].

*Eddy-current coefficient.* The eddy-current coefficient of the Ni–Zn ferrites depends on the manufacturing conditions; it rises with increasing temperature and time of sintering. Figure 13.106[49] shows an example for the ferrite $15NiO \cdot 35ZnO \cdot 50Fe_2O_3$. The run of the curves is similar for other stoichiometric Ni–Zn ferrites. Thus, to keep the losses low, a ferrite core must be sintered at the lowest possible temperature — just sufficient to enable the components to react and to form a ferrite. This means, however, that only low-permeability Ni–Zn ferrites can have low eddy-current losses.

Guillaud and co-workers[49] were further able to show that the specific electrical resistance of the ferrite falls with increasing sintering temperature and time. They attributed this to the fact that the resistance of the surface of the grains is appreciably greater than their internal resistance; with rising sintering temperature, however, the surface of the grain boundaries becomes relatively smaller.

*Hysteresis coefficient.* The Jordan hysteresis coefficient $h$ depends on the constitution of the ferrite, on the manufacturing conditions, and on the core dimensions. The hysteresis losses, like the eddy-current losses, rise with increasing temperature and time of the sintering operation. The hysteresis coefficients as a function of sintering temperature are given in Figure 13.107[49] for the ferrite $15NiO \cdot 35ZnO \cdot 50Fe_2O_3$. Comparison with Figure 13.106 makes it obvious that the curves illustrate very similar tendencies. To obtain low hysteresis loss, the ferrite must be sintered for a brief period at a low temperature. The properties of the crystallites formed depend on the sintering

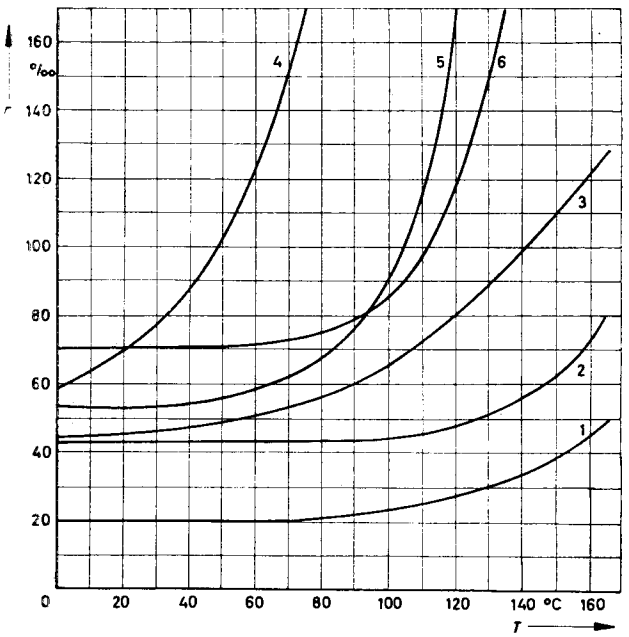



*Figure 13.105. Residual coefficient as a function of temperature for various ferrites: 1,* Mn–Zn *ferrite* ($\mu_i = 800\mu_0$, $T_c = 195°C$); *2,* Mn–Zn *ferrite* ($\mu_i = 750\mu_0$, $T_c = 195°C$); *3,* Mn–Zn *ferrite* ($\mu_i = 1000\mu_0$, $T_c = 195°C$); *4,* Ni–Zn *ferrite* ($\mu_i = 900\mu_0$, $T_c = 95°C$); *5,* Ni–Zn *ferrite* ($\mu_i = 800\mu_0$, $T_c = 150°C$); *6,* Ni–Zn *ferrite* ($\mu_i = 1000\mu_0$, $T_c = 160°C$)[61]

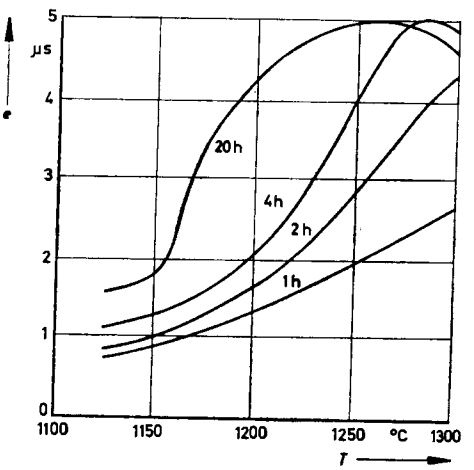



*Figure 13.106. Effect of sintering temperature and time on the eddy-current coefficient of the* Ni–Zn *ferrite* $15NiO \cdot 35ZnO \cdot 50Fe_2O_3$[49]

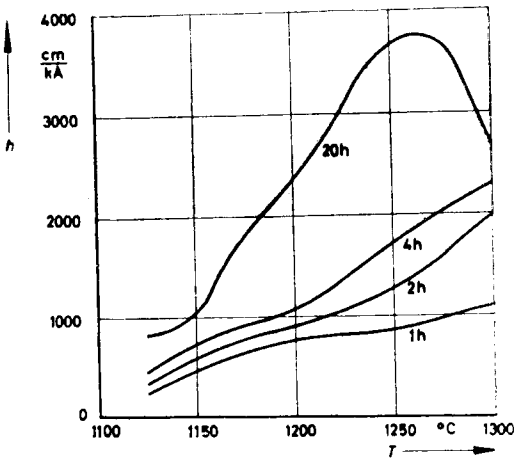



*Figure 13.107. Effect of sintering temperature and time on the hysteresis coefficient of the* Ni–Zn *ferrite* $15NiO \cdot 35ZnO \cdot 50Fe_2O_3$[49]

conditions, and it is the size and shape of these crystallites which influence the hysteresis coefficient. Holes formed within the crystallites at high temperatures also increase the hysteresis loss.

The course of the curves giving the hysteresis coefficient in terms of temperature is quite different for Ni–Zn ferrites and for Mn–Zn ferrites: whereas, for Mn–Zn ferrite, $h$ rises with increasing temperature, it falls for Ni–Zn ferrite. Figure 13.108[61] provides a few examples of this, the ferrites dealt with being those of Figure 13.105.

It can be seen from the contrasted figures of Table 13.23[84] that the referred hysteresis coefficient $h/\mu_i^2$ is greater the lower the permeability. This is also made clear in Figure 3.46.

One possibility of reducing the hysteresis coefficient is to add some cobalt oxide and so to give the hysteresis loop a Perminvar character. For example, the addition of some 0·2–0·3% $Co_2O_3$ to a ferrite having 18% NiO and 50% $Fe_2O_3$ reduces $h$ to one-tenth of its former values[49].

**Table 13.23** REFERRED HYSTERESIS COEFFICIENT OF A FEW FERRITES[84]

| | $\mu_i$ ($\mu_0$) | $10^3 h/\mu_i^2$ (cm/kA $\mu_0^2$) |
|---|---|---|
| Ni–Zn ferrites | 1 500 | 3–6 |
| | 450 | 15 |
| | 80 | 70 |
| | 30 | 100 |
| Mn–Zn ferrites | 1 300 | 1–2 |
| | 700 | 2–4 |

*Loss factor*

The loss factor, like the individual loss coefficients, is determined by the composition and the production conditions of the ferrite and by the dimensions of the core. The effect of production conditions is illustrated in Figure 13.109 for a ferrite with 24% NiO[49]: this shows that the quality factor represented by $\mu_i Q = \mu_i/\tan\delta$ depends on stoichiometry. The maximum value

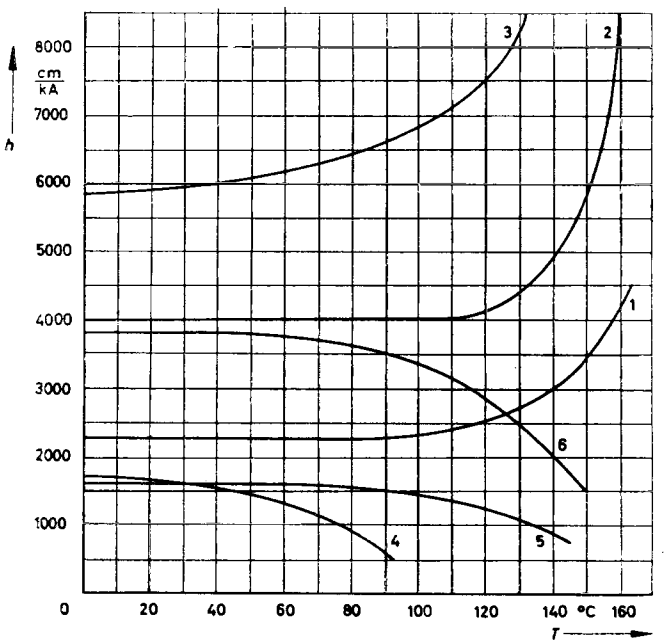



*Figure 13.108. Hysteresis coefficient as a function of temperature for the ferrites dealt with in Figure 13.105*[61]

lies around 50% $Fe_2O_3$. The figure also brings out the effect of the measuring frequency. The quality product falls with rising frequency; its optimum moves along the line of stoichiometric composition towards lower values. Ferrite having 24% NiO can be used at higher frequencies than that with 18% NiO. It can be taken as a guiding rule that the operating frequency shifts with the NiO content and in the same sense (see also Figure 13.110).

In order to be able to compare various ferrites, the loss factor with respect to the initial permeability, i.e. $(\tan\delta)/\mu_i$, is generally plotted, for the individual ferrites, against frequency using a logarithmic scale; alternatively, one may use the corresponding reciprocal, the quality product $\mu_i Q$. The resulting picture is as shown in Figure 13.111[84], for example, for Ni–Zn ferrites having initial permeabilities of $30\mu_0$, $80\mu_0$, $450\mu_0$ and $1500\mu_0$. As the drawing demonstrates, the optimum values can be joined by drawing the approximate

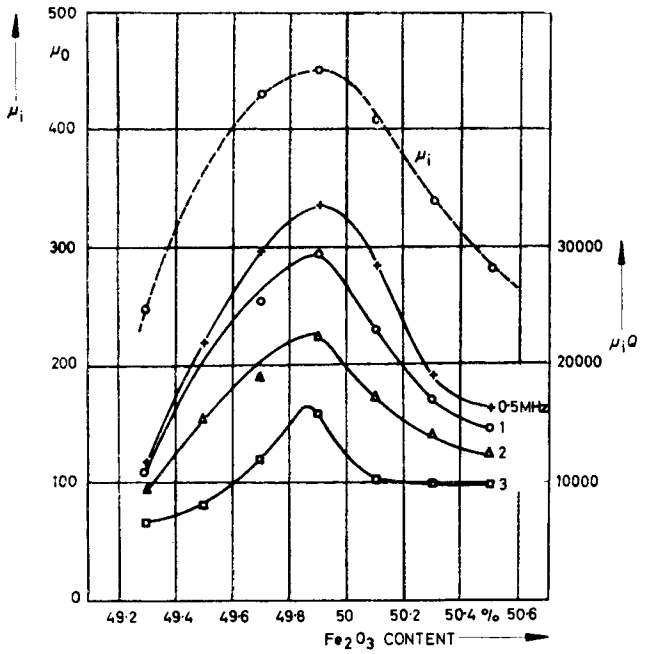



*Figure 13.109. Permeability $\mu_i$ and quality product $\mu_i Q$ of a ferrite having 24% NiO as a function of $Fe_2O_3$ content*[49]

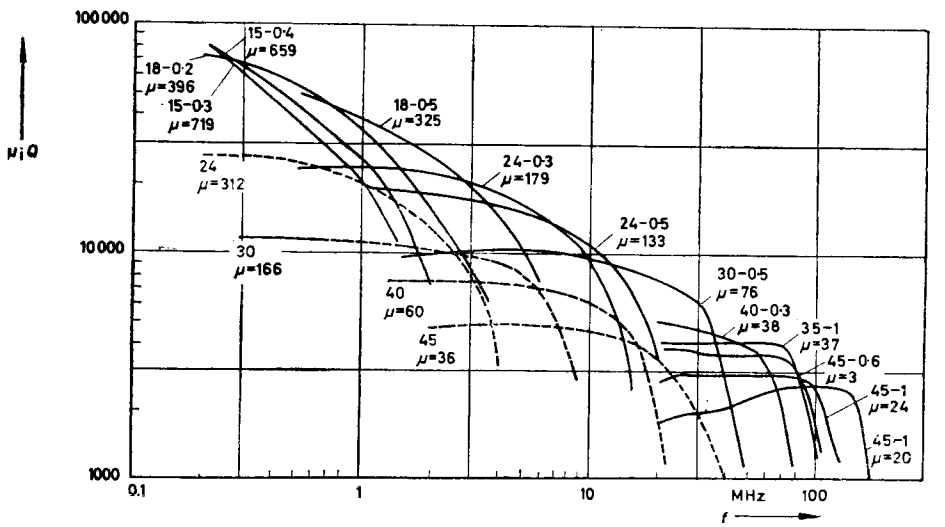



*Figure 13.110. Graphs of the quality product for Ni–Zn ferrites with (solid) and without (broken) $Co_2O_3$ additive*[49]

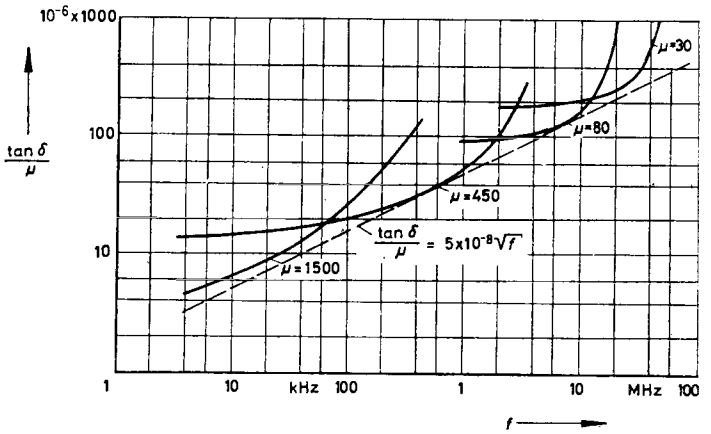



*Figure 13.111. Graphs of (tan δ)/μ for some* Ni–Zn *ferrites*[84]

common tangent, for which the following relation holds:

$$\frac{\tan \delta}{\mu_i} = p\sqrt{f}$$

Kornetzki and co-workers[84] have found that, for the Ni–Zn ferrites $p = 5 \times 10^{-8}\ s^{1/2}$.

Curves of loss factor for a few further ferrites are plotted in Figures 3.45, 13.88, 19.2, and 19.3, all of which display the same typical shape.

The loss factor of the Ni–Zn ferrites, like their hysteresis coefficient, can be improved by the addition of cobalt[49]. The optimum quantity of additive depends on the type of ferrite and frequency range within which it is to be used. If the proportion of NiO is kept constant, the product $\mu_i Q$ has an optimum at any given frequency for a particular $Co_2O_3$ content. Figure 13.112[49] shows this at four different measuring frequencies for the ferrite $18NiO \cdot 50Fe_2O_3$: at 0·5 MHz the maximum of the quality product comes at about 0·2% by weight $Co_2O_3$, and at about 0·4% for 5 MHz. The measured curves of Figure 13.113 are drawn as functions of the $Fe_2O_3$ content, at constant NiO and 0·5% by weight of $Co_2O_3$, for a ferrite containing 18% NiO: $\mu_i$ passes through a maximum at about 50·5% $Fe_2O_3$, whereas the product $\mu_i Q$ falls steeply for a similar composition. The form taken by the curve of $\mu_i Q$ is reminiscent of Figures 8.12 and 8.13, which also underline the importance of stoichiometry.

At each frequency an optimal Ni–Zn ferrite can be found with the most favourable $Co_2O_3$ content. As against cobalt-free ferrites, the principal virtue of these materials lies in the higher quality product to be obtained over the whole frequency range considered—up to more than 100 MHz. Figure 13.110 makes this obvious. The $\mu_i Q$ curves for the cobalt-free Ni–Zn ferrite are shown dashed. Numbers indicating the NiO content are attached to each of these curves and followed by the $\mu_i$ value. The solid lines are for Ni–Zn ferrites with cobalt additives, and the double numbers attached to

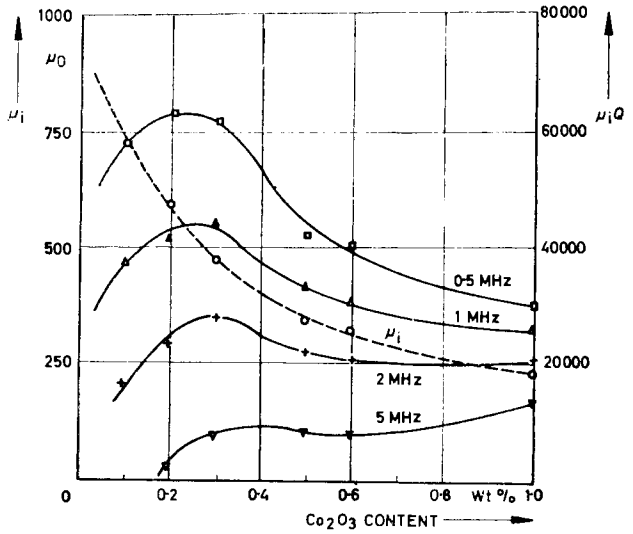



*Figure 13.112. Permeability $\mu_i$ and quality product $\mu_i Q$ of the* Ni–Zn *ferrite with 18%* Ni *and 50%* $Fe_2O_3$ *as functions of the* $Co_2O_3$ *additive*[49]

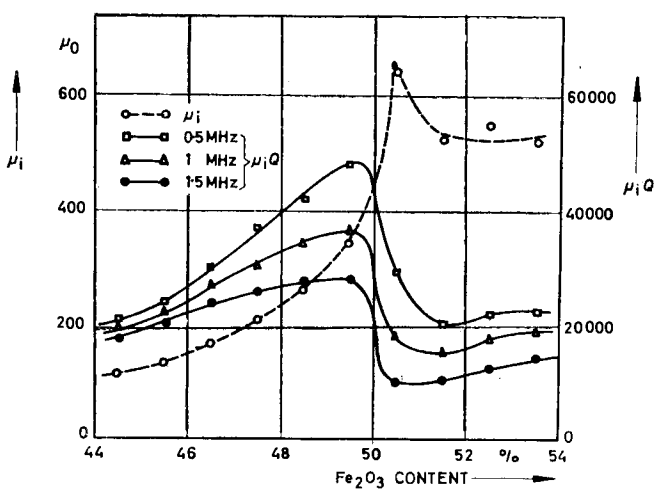



*Figure 13.113. Permeability $\mu_i$ and quality product $\mu_i Q$ as a function of $Fe_2O_3$ content for a constant proportion of 18%* NiO *and a fixed $Co_2O_3$ additive of 0·5% by weight*[49]

them represent the NiO content (first number) and the percentage by weight of $Co_2O_3$ (second number). It can be seen from the figure that the common tangent, supposed drawn through the different optima, is shifted towards higher values of quality product by the addition of cobalt. The curves of Ni–Zn ferrites with 50% $Fe_2O_3$ are basic to the series[49].

Experiments have now shown that further improvement of the quality product is possible in ferrites having an excess of iron oxide[91]: in these combinations we are concerned with Perminvar-type ferrites, for which tan $\delta$ is some 30% lower than for the ordinary Ni–Zn varieties. In Figure 13.114 the envelopes of the optimum $\mu_i Q$ curves are drawn: the upper curve holds for Ni–Zn ferrites with 58% $Fe_2O_3$ and the lower for those with 49% $Fe_2O_3$. In both cases the optimum additive of cobalt oxide was used.

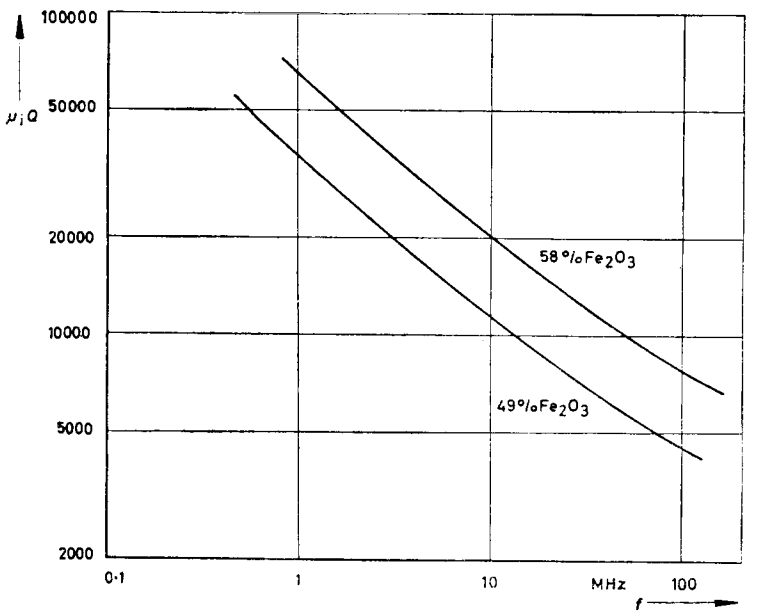



*Figure 13.114. Envelopes of the $\mu_i Q$ curves against frequency for* Ni–Zn *ferrites having 49% and 58%* $Fe_2O_3$ *and in each case optimum* CoO[91]

However, even without a cobalt additive, a significant reduction of (tan $\delta$)/$\mu_i$ is obtained for the Perminvar ferrites. Further, the steep rise of the loss factor (referred to $\mu_i$) only ensues—for the same permeability as that of an ordinary Ni–Zn ferrite—at higher frequencies. An example is shown in Figure 13.115 for two cores having $\mu_i = 40\mu_0$. The broken curve applies to an ordinary Ni–Zn ferrite and the solid curve to a Perminvar type. The curves are supplemented by two further examples of Perminvar ferrites based on Ni–Zn combinations[85].

In applications of Perminvar ferrites (and of other combinations) it has to be remembered that the low loss values are only found below a certain critical field strength, the so-called threshold intensity. As a rule, the threshold

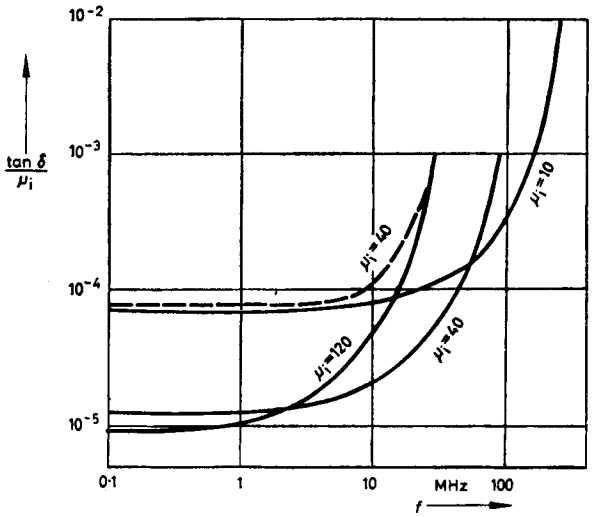



*Figure 13.115. Referred loss factor (tan δ)/$\mu_i$ for three Perminvar ferrites (nickel and* Ni–Zn *ferrites) as a function of frequency: broken curve applies to an ordinary* Ni–Zn *ferrite*[85]

intensity is lower the higher the initial permeability. For example, for Ni–Zn ferrites whose $\mu_i$ is $120\mu_0$, $40\mu_0$, or $10\mu_0$ the threshold intensity amounts to 200 A/m, 520 A/m, or 1360 A/m respectively[85]. If this critical intensity is exceeded, the losses become greater and do not return to their values after the field is switched off. The action of the higher field strength is to deform the hysteresis loop, which is more or less shifted towards a rectangular shape (see Figure 5.16). Rectangular loops, however, have higher losses, as is made obvious by the comparison curves of Figure 13.116. A Perminvar ferrite which has been spoilt by applying too high a field can only be brought back to its former state by renewed annealing and slow cooling.

Perminvar ferrites can be used ungapped by reason of their low losses. Thus, for example, small tubes of ferrite (i.e. beads) can be strung on a wire. For a 'coil' of this kind, an inductance $L$ of 0·3 μH per bead and, at 30 MHz, a $Q$ value of 500 can be obtained. Using a toroid of 40 mm outer diameter ($\mu_i = 40\mu_0$), a quality factor $Q$ of more than 1000 can be achieved in the range 0·4–1·5 MHz[85].

### *Disaccommodation*

The disaccommodation of Ni–Zn ferrites is less pronounced than that of the Mn–Zn ferrites. The following approximate picture emerges from recent investigations: the extent of the disaccommodation in Ni–Zn ferrites depends mainly on manufacturing conditions and, in particular, on the oxygen content of the annealing atmosphere; and the disaccommodation, measured on various specimens, is a function of the measuring temperature. Two or three maxima are to be distinguished. Marais and Merceron[94] have made and investigated a series of Ni–Zn ferrites, the basic mixtures for which have

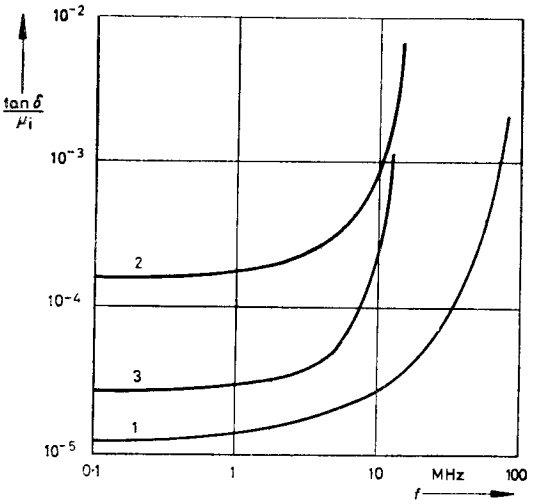



*Figure 13.116. Referred loss factor as a function of frequency for three different conditions of a Perminvar ferrite following slow cooling: 1, with no magnetic field (Perminvar, $\mu_i = 60\mu_0$); 2, in a longitudinal field (rectangular loop, $\mu_i = 20\mu_0$); 3, in a transverse field (Isoperm-type loop, $\mu_i = 120\mu_0$)*[85]

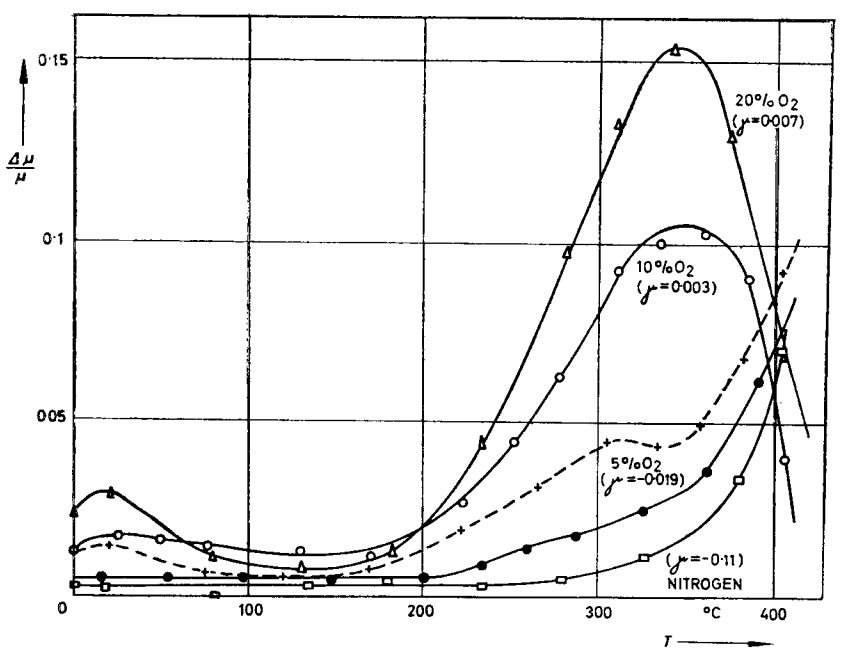



*Figure 13.117. Change in permeability as a function of the oxygen content of the sintering atmosphere for the ferrite* $Fe_{2\cdot104}Ni_{0\cdot584}Zn_{0\cdot312}O_{4+\gamma}$[94]

different molecular ratios $k$. Here $k$ stands for $Fe_2O_3/MO$ where M = Ni+Zn the nickel content being held constant at 1·17, 1·27, and 1·32. Figure 13.117, taken from their published work, shows the following interesting results: after annealing, the ferrite had the common formula $Fe_{2\cdot104}Ni_{0\cdot584}Zn_{0\cdot312}O_{4+\gamma}$. Toroidal cores were annealed at 1150°C with various partial pressures of oxygen and $\gamma$ was then calculated. It appeared that the character of the curve of disaccommodation altered suddenly as $\gamma$ became negative: the maximum in the region of room temperature diappeared and that observed at 350°C, when $\gamma$ was positive, shifted towards higher temperatures. It could not in fact be determined as it passed beyond the Curie temperature.

The broken line relates to an annealing with an oxygen content between 5% and 10%. Further annealing at various temperatures and in pure oxygen as well as in varying atmospheres led to the following conclusion: the Ni–Zn ferrites exhibit two kinds of relaxation mechanisms, according as empty sites, brought about by the non-uniformity of the specimen, are or are not effective. To give a relaxation effect at room temperature, both FeO and empty sites must be present. The presence of a small quantity of cobalt causes trivalent cobalt ions to enter the vacant sites. With increasing cobalt content the vacant sites are reduced in number and the activation energy increases[92].

### 13.6.4.3 Hexagonal ferrites

Cubic ferrites can be used for inductor cores up to frequencies of about 100 MHz. Above this frequency the permeability falls and the losses rise. This fact is understandable having regard to equation 3.73 which indicates that, at the highest frequencies, $\mu$ must ultimately fall to unity. The materials which come under the heading Ferroxplana are an exception to this restrictive rule in that they have a fairly high permeability even up to 1 GHz.

These materials are oxide mixtures which owe their existence to a combination of hexagonal barium ferrite ($BaO \cdot 6\,Fe_2O_3$) having a magnetoplumbite structure[132] (which we shall designate M), and cubic ferrites with a spinel-type structure (which we shall indicate by S). Jonker, Wijn, and Braun[70], the inventors of these special substances, have designated those combinations of most practical interest by the letters W, Y, and Z. The positions of these and other combinations are marked on the three-component diagram of Figure 13.118. Thus:

| | |
|---|---|
| $S = MeO \cdot Fe_2O_3$ | Where Me stands for the bivalent ion of cubic ferrites such as Mn, Fe, Co, Ni, Zn, Mg, or mixtures of these ions. |
| $B = BaO \cdot Fe_2O_3$ | Which otherwise has no value as a magnetic material. |
| $M = BaO \cdot 6Fe_2O_3$ | |
| $W = BaO \cdot 2FeO \cdot 8Fe_2O_3$ | |
| $X = Ba_2Fe_2^{II}\,Fe_{28}^{III}O_{46}$ | |
| $Y = Ba_2Me_2Fe_{12}O_{22}$ | |
| $Z = Ba_3Me_2Fe_{24}O_{41}$ | |

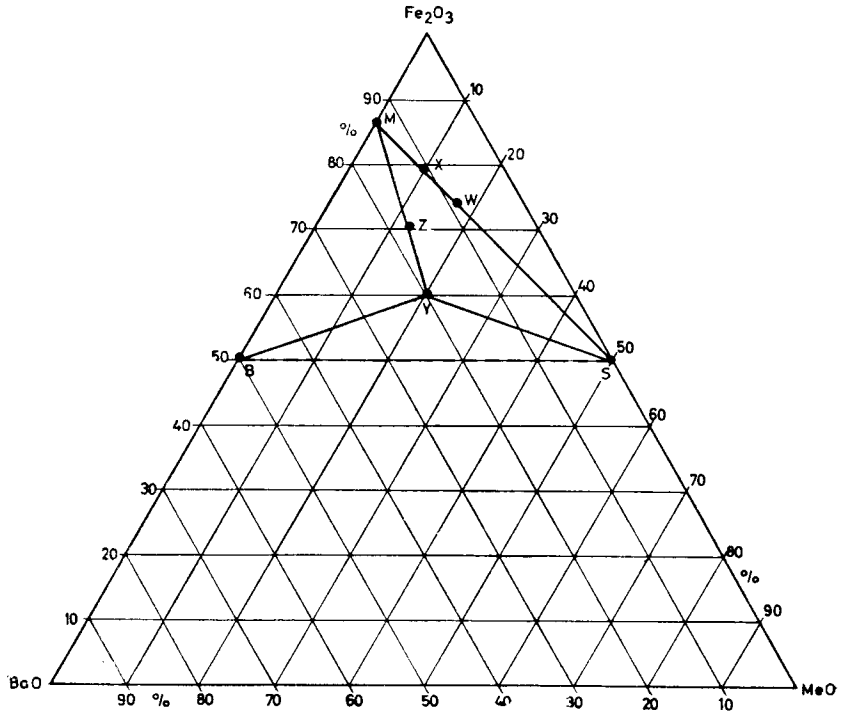



*Figure 13.118. Locus of Feroxplana compositions*[70]

The combinations X, Y, and Z have hexagonal crystal constructions which are related to those of M and W. The lattice constants were determined by Braun[16], and are listed in Table 7.1.

The crystallites of the Y composition orient themselves differently, in a magnetic field, from those of the Z composition: in the preparation Y, the hexagonal *c*-axis sets itself perpendicular to the field, but in the Z preparation it is parallel thereto, i.e. for the Z composition the *c*-axis is the preferred direction of magnetisation while for the Y arrangement the preferred direction lies in the *a* direction and is thus in the plane perpendicular to the principal hexagonal axis. Consequently, for the Y compositions, one may speak of a preferred plane. Preferred planes can also occur in the Z and W groups if cobalt is wholly or partly substituted for Me. It is the existence of this preferred magnetic plane that is the novel and important feature of *Ferroxplana* (ferrox = iron oxide, plana = plane).

The magnetic vector can be rotated very easily in the preferred plane, whereas large amounts of energy must be expended to turn the vector out of the plane. Ferroxplana materials are classified as magnetically soft but differ from the spinels both in their crystal lattice and by the fact that ferrimagnetic resonance occurs only at frequencies appreciably higher than for the spinels.

*Types of Ferroxplana without crystal orientation*

The saturation polarisations and Curie temperatures of a few types of Ferroxplana are set out in Table 13.24[70].

**Table 13.24** SATURATION POLARISATION $J_s$ AT 20°C, AND CURIE TEMPERATURES $T_c$ FOR SOME VARIETIES OF FERROXPLANA. VALUES OF FERROXCUBE 4E ARE ALSO GIVEN FOR COMPARISON. FIGURES CORRECTED FOR POROSITY[70]

| *Material* | $J_s$ (V s/m²) | $T_c$ (°C) |
|---|---|---|
| $Mn_2W$ | 0·40 | 410 |
| CoFeW | 0·45 | 430 |
| ZnFeW | 0·48 | 422 |
| $Ni_{0·5}Zn_{0·5}FeW$ | 0·46 | 425 |
| CoY | 0·29 | 340 |
| $Mg_2Y$ | 0·14 | 300 |
| $Co_2Z$ | 0·35 | 400 |
| Ferroxcube 4E | 0·326 | 595 |

The permeability for the polycrystalline material $Co_2Z$ is shown in Figure 13.119 as a function of frequency and, for comparison, the same diagram shows the corresponding curves for the nickel ferrite Ferroxcube 4E. If the limiting frequency is defined as that frequency for which $(\tan \delta)/\mu = \mu''/\mu' = 0{\cdot}1$, then it can be stated that the limiting frequencies of the two materials are 90 MHz and 400 MHz respectively. Even at 1000 MHz the permeability of $Co_2Z$ has hardly fallen below its low-frequency value[42].

In Figure 13.120 the corresponding comparison is drawn between the same nickel ferrite and another member of the Ferroxplana group, $Mg_2Y$. The permeability of $Mg_2Y$ is somewhat higher than that of $Co_2Z$ and has thus a rather lower limiting frequency[70].

*Crystal-oriented types of Ferroxplana*

The quoted magnetic values of the above-mentioned types of Ferroxplana can be measured in any direction within the specimen. These materials are therefore isotropic. The permeability of Ferroxplana materials can, however, be raised by alignment of the individual crystallites in a preferred direction without appreciably lowering the limiting frequency. Two textures can be produced, known as fan texture and leaf texture. Leaf texture is the more effective in this field[133]. One can so arrange matters that, by the use of a

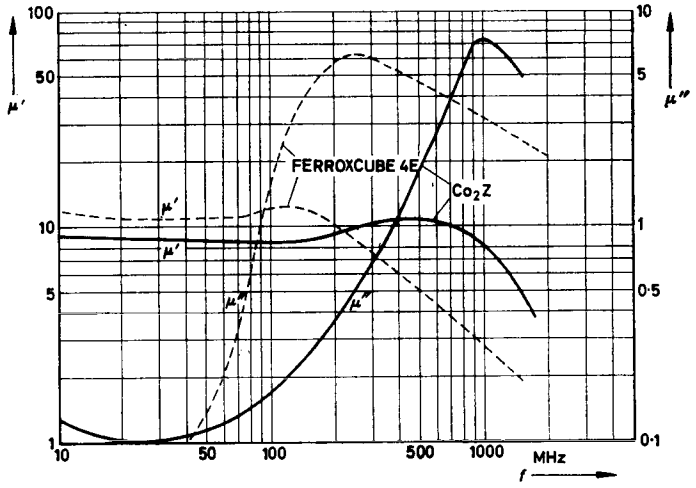



*Figure 13.119. Real and imaginary parts ($\mu'$ and $\mu''$) of initial permeability for the nickel ferrites Ferroxcube 4E and Ferroxplana* $Co_2Z$[42]

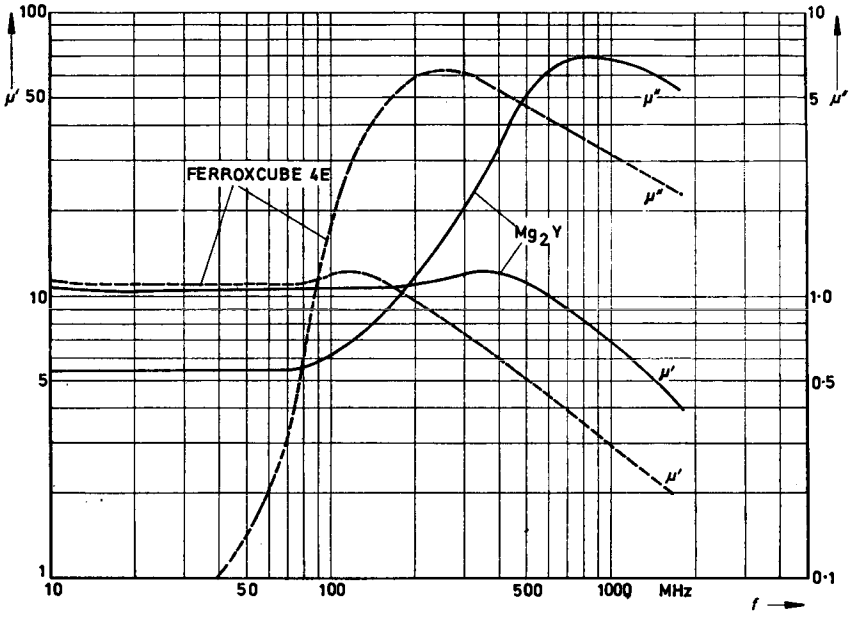



*Figure 13.120. Real and imaginary parts ($\mu'$ and $\mu''$) of initial permeability for the nickel ferrites Ferroxcube 4E and Ferroxplana* $Mg_2Y$[70]

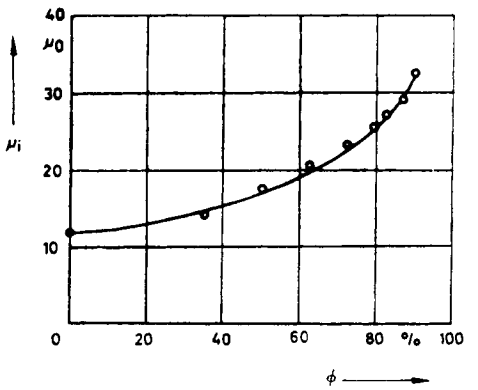



*Figure 13.121. Initial permeability $\mu_i$ of Ferroxplana $Co_2Z$ for various degrees of alignment $\phi$*[133]

magnetic field, the plate-shaped crystallites which show the preferred plane all lie parallel to one another. The magnetic field must rotate around an axis normal to the preferred axis since only in this way can a completely parallel alignment of the individual planes be achieved[42]. After the alignment of the particles the body is subjected to pressure. In order that the particles themselves can be kept mobile the powder is emulsified. The degree of orientation can be affected by changing the field strength of the rotating field. Figure 13.121, taking $Co_2Z$ as an example, shows how the permeability of the prepparation grows with increase in the degree of orientation $\phi$. The permeability of $Co_{0.8}Zn_{1.2}Z$ was increased from $22\mu_0$ to $55\mu_0$. The permeability is very

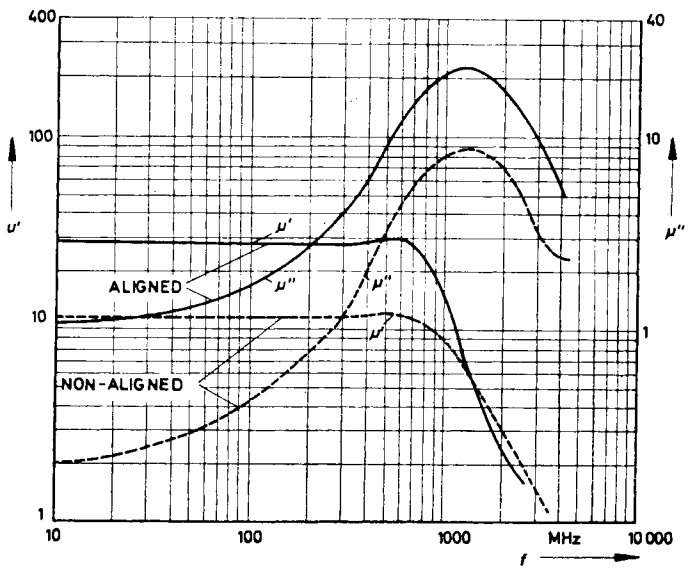



*Figure 13.122. Variation of $\mu'$ and $\mu''$ with frequency for aligned and non-aligned $Co_2Z$*[133]

low in a direction perpendicular to the preferred direction. For $Co_2Z$ with $\phi = 0{\cdot}91$ it amounts, for example, to only $2{\cdot}5\mu_0$.

It has been found that even if the orientation factor $\phi$ is relatively low in the pressing itself, by the use of a high sintering temperature the orientation can be improved through the growth of such crystallites as are favourably oriented. The effect of sintering temperature on orientation and initial permeability is made clear in Table 13.25[133];

**Table 13.25** EFFECT OF SINTERING TEMPERATURE $T$ ON THE DEGREE OF ORIENTATION $\phi$ AND THE INITIAL PERMEABILITY $\mu_i$ OF $Co_2Z$ PREPARATIONS[133]

| $T$ (°C) | $\phi$ (%) | $\mu_i$ ($\mu_0$) |
|---|---|---|
| 1 180 | 65 | 10·5 |
| 1 200 | 65 | 11·3 |
| 1 220 | 72 | 12·4 |
| 1 240 | 77 | 18·5 |
| 1 260 | 89 | 32·0 |

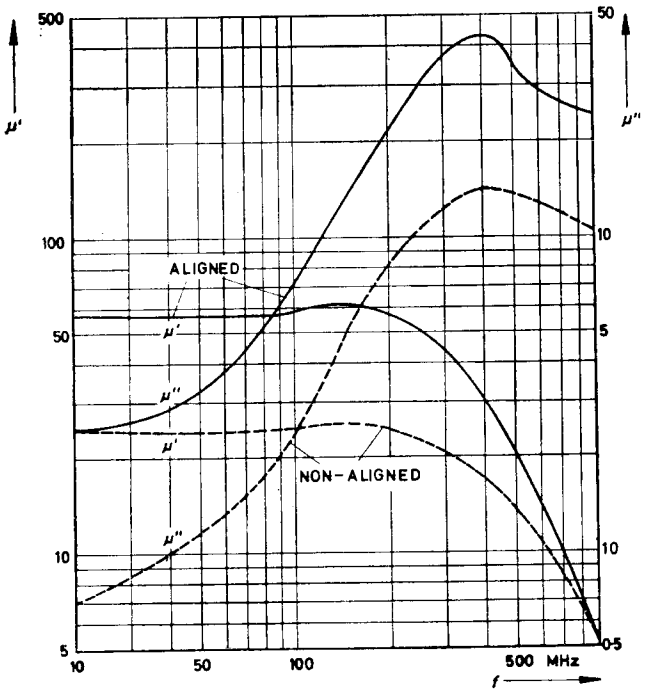



*Figure 13.123. Frequency characteristics of $\mu'$ and $\mu''$ for aligned and non-aligned* $Co_{0.8}Zn_{1.2}Z$[133]

By measuring the complex permeability of aligned and non-aligned Ferroxplanas it has been established that the value of the loss maximum and that of $\mu''$ occur at almost the same frequency in both cases: in spite of the rise in permeability, as a result of crystal orientation, the limiting frequency falls only slightly. The factor relating to frequency fall is, in any case, less than that for the rise in permeability. This is shown by two examples: $Co_2Z$ (Figure 13.122) and $Co_{0.8}Zn_{1.2}Z$ (Figure 13.123).

## REFERENCES


1. ARNOLD ENGINEERING CO.: Properties Deltamax, 4-79-Mo-Permalloy, Supermalloy. Bulletin TC-101 A (1960).
2. ARNOLD ENGINEERING CO.: Iron powder cores. Bulletin PC-109 A (Oct. 1961).
3. ARNOLD, H. D. and ELMEN, G. W.: Permalloy, an alloy of remarkable magnetic properties (J. Franklin Inst. **195** (1923) 621–632).
4. ASSMUS, F. and PFEIFER, F.: Höchstpermeable Legierungen im System NiFeCuMo (Metall **7** (1953) 189–191).
5. V. AUWERS, O. and NEUMANN, H.: Über Eisen-Nickel-Kupfer-Legierungen hoher Anfangspermeabilität (Wiss. Ver. Siemens Werke **14** (1935) 93–108).
6. BARDELL, P. R.: Factors influencing the measured value of hysteresis loss of powder cores; in Soft Magnetic Materials for Telecommunications (ed. Richards and Lynch), London (1953) 253–258.
7. BASF: Carbonyleisenpulver (Nov. 1971).
8. BOLL, R.: Metallische Magnetwerkstoffe und Kernformen in der Nachrichtentechnik (ETZ-A **80** (1959) 582–588).
9. BOLL, R.: Dünne Bänder aus weichmagnetischen Werkstoffen und ihre Anwendungsformen (Elektronik **10** (1961) 293–298).
10. BOOTHBY, O. L. and BOZORTH, R. M.: A new magnetic material of high permeability (J. A. P. **18** (Feb. 1947) 173–176).
11. BOZORTH, R. M.: Ferromagnetism. Van Nostrand Co. Inc., Toronto/New York/London (1951).
12. BOZORTH, R. M.: The Permalloy problem (Rev. Mod. Phys. **25** (Jan. 1953) 42–48).
13. BOZORTH, R. M. and WALKER, J. G.: Magnetostriction of single crystals of cobalt and nickel ferrites (Phys. Rev. (2) **88** (5) (Dec. 1952) 1209).
14. BRADLEY, E. M.: Properties of magnetic films for memory systems (J. A. P. **33** (3) (Mar. 1962) 1051–1057).
15. BRAGINSKI, A., MARAIS, A. and MERCERON, T.: Quelques résultats expérimentaux sur les phénomènes de relaxation des ferrites de Mn–Zn (C. R. **253** (1961) 239–241).
16. BRAUN, P. B.: The crystal structures of a new group of ferromagnetic compounds (Phil. Res. Rep. **12** (1957) 491–548).
17. BUCKLEY, O. E.: High speed ocean cable telegraphy (Bell Syst. Tech. J. **7** (1928) 225–267).
18. BUCKLEY, O. E.: The future of transoceanic telephony (J. IEE **89** (1) (1942) 454–461).
19. CHAMPION, D. F. W. and WILKINS, E. G.: Magnetic powder cores (Wireless World (1953) 83–86).
20. CAMPBELL, A.: On the magnetic properties of silicon iron (Stalloy) in alternating magnetic fields of low value (Proc. Phys. Soc. **32** (1920) 232–243).
21. CCIF-Weissbuch, Fernsprechübertragung Ausgabe Siemens & Halske AG (1940) 194).
22. DEUTSCHMANN, W.: Über Massekerne (El.: Nach. T. **9** (1932) 421–433).

22a DIN 40 015, Frequenz- und Wellenbereiche (Aug. 1963).

22b DIN 17 745, Nickel wrought alloys with iron (June 1963).

23. DIN 41 281, Magnetische Massekerne (Dec. 1945).

23a DIN 41 280, Weichmagnetische Ferritkerne (Mar. 1965).

24. DIN 41 286 Weichmagnetische Ferrit- und Pulver-Gewindekerne (Sept. 1967).

25. DIN 41 287, Schalen- und Topfkerne für Spulen (Nov. 1953).
26. DIN 41 293, Weichmagnetische Ferritkerne und Schalenkerne (Aug. 1971).
27. DIN 41 295, Weichmagnetische Ferrit-E-Kerne (Aug. 1962).
28. DIN 41 299, Weichmagnetische Ferritkerne (X-Kerne) (Mar. 1967).
29. DIN 41 301, Magnetische Werkstoffe für Übertrager (July 1967).
30. DIN 41 302, Kleintransformatoren, Übertrager und Drosseln, Kernbleche (Feb. 1970).
31. DIN 41 309, Schnittbandkerne (Oct. 1967).
31a DIN 41 980, Weichmagnetische Ferritkerne. RM-Kerne (draft. Feb. 1971).
31b DIN 41 981, Spulenkörper für weich magnetische Ferritkerne RM-Kerne (draft Feb. 1971).
32. DOLEZALEK, F. and EBELING, A.: Untersuchungen über telephonische Fernleitungen Pupin'schen Systems (ETZ **23** (1902) 1059–1063).
33. DOEBKE, W.: Ferromagnetische Mischkörper (Z. techn. Phys. **11** (1930) 12).
34. ECONOMOS, G.: A study on magnetic ceramics. OTS Technical Report **78** PB 111 625 (May 1954).
35. EHLERS, W.: Pupinspulen mit Massekernen (El. Nach. T. **2** (1925) 121–132).
36. EHLERS, W. and FALKENBERG, F.: Über die Wirkung des Pressdruckes auf die Eigenschaften von Massekernen für Pupinspulen (El. Nach. T. **3** (1926) 281–284).
37. ELMEN, G. W.: Magnetic alloys of iron, nickel and cobalt (El. Engng. **54** (12) (Dec. 1935) 1292–1299; (1936) 887–889).
38. ENZ, U.: Permeability, crystalline anisotropy and magnetostriction of polycrystalline manganese-zinc-ferrous ferrite (Proc. IEE **109 B** (1962) Suppl. 21, 246–247).
39. FAHLENBRACH, H. and HOUDREMONT, E.: Erhöhung der Anfangspermeabilität von niedriglegierten Eisen-Silizium- u. Eisen-Aluminium-Legierungen durch oxydierendes Glühen bei niedrigen Temperaturen (Arch. Eisenhüttenw. **25** (1954) 377–381).
40. FORESTIER, H. and VETTER, M.: Etude des systèmes $Fe_2O_3$•NiO–$Fe_2O_3$•MgO; $Fe_2O_3$• •NiO–$Fe_2O_3$•CuO; $Fe_2O_3$•NiO–$Fe_2O_3$•ZnO (C. R. **209** (1939) 164).
41. GENERAL ANILINE & FILM CORPORATION, NEW YORK : GAF Carbonyl iron powders. 5 M–5–60 M Exp.
42. GORDON, I., HARVEY, R. L. and BRADEN, R. A.: Preparation and magnetic properties of some hexagonal magnetic oxides (J. Am. Cer. Soc. **45** (6) (1962) 297-301).
43. GORDON SMITH, C.: Magnetic materials (Electr. Rev. **167** (1960) 253–259).
44. GORTER, E. W.: Saturation magnetization of ferrites with spinel structure (Nature **165** (1950) 798–800).
45. GOULD, H. L. B. and WENNY, D. H.: Supermendur (El. Engng. **76** (Mar. 1957) 208–211).
46. GUILLAUD, C.: Propriétés magnétiques des ferrites (J. Phys. Rad. **12** (1951) 239–248).
47. GUILLAUD, C.: The properties of manganese–zinc ferrites and the physical processes governing them (Proc. IEE **104 B** (1957) 165–178).
48. GUILLAUD, C., PAULUS, M. and VAUTIER, R.: La diminnation des pertes par courant de Foucault dans les ferrites de manganèse–zinc par addition de calcium (C. R. **242** (June 1956) 2712–2715).
49. GUILLAUD, C., VILLERS, G., MARAIS, A. and PAULUS, M.: Propriétés des ferrites mixtes de nickel–zinc; in Solid State Physics, Vol. 3 (ed. Désirant and Michiels), Academic Press, New York (1960) 71–90.
49a HART, A.: High resistivity nickel–iron alloys with rectangular hysteresis loops (Brit. J. Appl. Phys. **11** (2) (Feb. 1960) 58–60).
50. HARVEY, R. L., HEGYI, I. J. and LEVERENZ, H. W.: Ferromagnetic spinels for radio frequencies (RCA Rev. **11** (Sept. 1950) 321–363).
51. HANSEN, M.: Der Aufbau der Zweistofflegierungen. Berlin (1936).
52. HEAVISIDE, O.: The Electrician (1887) 302.
53. HEAVISIDE, O.: Electromagnetic Theory **1** (1893) 441.
54. HECK, C.: Über Messungen an Krarupleitern (Europ. Fernspr. D. **60** (1942) 23–29).
55. HECK, C.: SAF-ferrite. (SEG-Nachr. **3** (1) (1955) 43–44).

56. HECK, C.: Beiträge der Ferrite zur Miniaturisierung (VDE-Fachber. **19** (1956) II/157–II/161; SEG-Nachr. **5** (1957) 147–151).
57. HECK, C.: Ferrite (Radio Mentor **9** (1959) 707).
58. HECK, C. and WEBER, J.: Einfluss der Glühgase auf die magnetischen Eigenschaften der Ferrite (Arch. Eisenhüttenw. **29** (8) (Aug. 1958) 495–504).
59. HEGG, F.: Thermomagnetic study of iron–nickel alloys (Arch. sci. phys. nat. (4) **29** (1910) 592–617; **30** (1911) 15–45).
60. HEISTER, W.: Untersuchung der Frequenzabhängigkeit der Stoffwerte ferromagnetischer Mischkörper bis zu sehr hohen Frequenzen (Arch. Elektrot. **41** (1953) 142–160).
61. HEISTER, W.: Magnetische Werkstoffe für die Nachrichten- und Hochfrequenztechnik (T. Mitt. Krupp **12** (1954) 161–174).
62. HEISTER, W.: Mangan–Zink–Ferrite mit hoher Permeabilität und geringen Verlusten (T. Mitt. Krupp **15** (1957) 130–144).
63. HEISTER, W.: Einfluss der Sintertemperatur auf die magnetischen Eigenschaften und das Kristallgefüge von Mn–Zn–Ferriten (Ber. D. Ker. Ges. **35** (1958) 249–258).
64. HEISTER, W.: Temperaturgang und Desakkommodation der Anfangspermeabilität im System MnO–ZnO–$Fe_2O_3$ (T. Mitt. Krupp **17** (2) (1959) 82–89).
65. HEISTER, W.: Die Änderung der Induktivität von Schalenkernen ohne und mit Abgleichelement (T. Mitt. Krupp Forsch. Ber. **20** (3) (1962) 1–10).
65a HEISTER, W.: Entwicklung magnetischer Werkstoffe und neuer Formen für die Miniaturisierung von Übertragern und Filtern der Nachrichtentechnik (T. Mitt. Krupp, Forsch. Ber. **27** (2) (1969) 53–66).
66. HERING, H. and LEICHSENRING, F.: Neuzeitliche Pupinspulen mit Siferrit-Schalenkernen (Siemens-Z. **53** (1953) 124–129).
67. HOPKINSON, J.: Magnetic properties of alloys of nickel and iron (Proc. Roy. Soc. **48** (1890) 1–13).
68. HOWE, G. H.: Dynamax, a new crystal and domain oriented magnetic core material (Proc. Conf. Magnetism Magn. Mat. (1955) 264–272; Trans. AIEE **75** (1956) 548–551).
68a HUBBARD, W. M., ADAMS, E. and HABEN, J. F.: Sendust flake, a new magnetic material for low frequency application (Proc. Conf. Magnetism Magn. Mat., Boston (1956) 445–452).
69. I. E. C. Publication 133 (1971). Dimensions for pot cores made of ferromagnetic oxides.
69a I. E. C. Publication 218 (1966). Guide for the drafting of performance specifications for cores of tuned transformers and inductors of ferromagnetic oxides for telecommunication.
69b I. E. C. Publication 226 (1967). Dimensions of cross cores (X-cores) made of ferromagnetic oxides and associated parts.
69c I. E. C. Publication 97 (1970). Grid system for printed circuits.
69d I. E. C. Publication 329 (1971). Strip wound cut cores of grain oriented silicon–iron alloy used for electronic and telekommunication equipment.
70. JONKER, G. H., WIJN, H. P. J. and BRAUN, P. B.: Ferroxplana, hexagonale ferromagnetische Eisenoxydverbindungen für sehr hohe Frequenzen (Phil. T. Rdsch. **18** (9) (1957) 249–258).
71. JORDAN, H., VOLK, T. and GOLDSCHMIDT, R.: Pupinspulen mit Kernen aus Isoperm-Blech oder -Band (E. F. D. (36) (Jan. 1933) 8–14).
72. KELSALL, G. A.: Permeability changes in ferromagnetic materials heat treated in magnetic fields (Physics **5** (1934) 169–172).
73. KERSTEN, M.: Über anomale Eigenschaften neuer magnetischer Werkstoffe (Wiss. Ver. Siemens Konz. **13** (3) (1934) 1–9).
74. KERSTEN, M.: Spulen mit Masserkernen (ETZ **58** (1937) 1335–1338, 1364–1367).
75. KERSTEN, M. and HESSE, H.: Hysteresearme Massekernspulen für das Trägerfrequenz-Fernsprechen (El. Nach. T. **14** (1937) 66–74).
76. KIEFFER, R. and HOTOP, W.: Sintereisen und Sinterstahl (Vienna, 1948).

77. KIESSLING, G. and LUDL, O.: Neuere Erkenntnisse aus der Massekerntechnik (ETZ **63** (1942) 413–416).
78. KORNETZKI, M.: Streufeldfreie Hochfrequenzspule (DBP 975 749).
79. KORNETZKI, M.: Die magnetischen Kennwerte von Spulen mit Topfkernen aus Masseeisen (Frequenz **4** (1950) 105–113).
80. KORNETZKI, M.: Ferritkerne für Hochfrequenzspulen (Siemens-Z. **2** (1951) 94–100).
81. KORNETZKI, M.: Ferrit-Kerne für die Nachrichtentechnik (Siemens-Z. **27** (1953) 212–218).
82. KORNETZKI, M.: Perminvarferrite (ETZ-A **80** (1959) 605–609).
83. KORNETZKI, M. and BRACKMANN, J.: Kerne für UKW-Variometer (Frequenz **4** (1950) 318–320).
84. KORNETZKI, M., BRACKMANN, J., FREY, J. and GIESEKE, W.: Messergebnisse an hochpermeablen Ferritkernen (Z. ang. Phys. **4** (1952) 371–374).
85. KORNETZKI, M., BRACKMANN, J. and FREY, J.: Magnetische Werte von Ferritkernen mit Perminvarschleife (Siemens-Z. **32** (1958) 412–418).
86. KORNETZKI, M. and WEIS, A.: Die Wirbelstromverluste im Massekern (Wiss. Ver. Siemens-Werke **15** (1936) 95–111).
87. KRARUP, C. E.: Unterseeische Fernsprechkabel mit erhöhter Selbstinduktion (ETZ **23** (1902) 344–346).
88. LEGG, V. E. and GIVEN, F. J.: Compressed powdered molybdenum permalloy for high quality inductance coils (Bell Syst. Tech. J. **19** (1940) 385–406).
89. LESCROËL, Y.: Variation de la perméabilité avec la température dans certains ferrites; in Solid State Physics, Vol. 3 (ed. Desirant and Michiels). Academic Press, New York (1960) 142–148.
90. LESCROËL, Y.: Ferrites ferromagnétiques (Cables & Transm. **7** (4) (1953) 273–292).
91. LESCROËL, Y. and PIERROT, A.: Ferrites à faibles pertes utilisés dans les techniques de l'électronique et des télécommunications (Cables & Transm. **14** (3) (1960) 220–244).
92. MARAIS, A. and MERCERON, T.: Désaccommodation de la perméabilité de ferrites de nickel-zinc (C. R. **248** (17) (1959) 2976–2978).
93. MARAIS, A. and MERCERON, T.: Trainage de diffusion dans les ferrites de nickel-zinc riches en fer (C. R. **249** (Nov. 1959) 2511–2513).
94. MARAIS, A. and MERCERON, T.: Quelques résultats expérimentaux dans les phénomènes de relaxation des ferrites de Ni–Zn (C. R. **252** (1961) 3553–3555).
94a MARAIS, A. and MERCERON, T.: Effet d'addition de lithium sur la désaccommodation de ferrites de Mn–Zn (C. R. **256** (1963) 2560–2562).
95. MASUMOTO, H.: On a new alloy 'Sendust' and its magnetic and electric properties (Sci. Rep. Tohoku Imp. Univ. **25** (1936) 388–402).
96. MCKEEHAN, L. W.: The crystal structure of iron–nickel alloys (Phys. Rev. **21** (1923) 402–407).
97. MITTASCH, A.: Über Eisencarbonyl und Carbonyleisen (Z. anorg. Chem. **41** (30) (July 1928) 827–833).
98. MORRIS, A. L.: Tape wound magnetic cores (El. Engng. (Sept. 1952) 416–417).
98a NEOSID PEMETZRIEDER GMBH, HALVER I. W., Catalogue.
99. NEUMANN, H.: Die neue Legierung 1040 mit hoher Anfangspermeabilität. ATM **4** Z 913–5 T 168 (1934).
100. NOLL, F.: Krarupkabel für Trägerfrequenzübertragung (Europ. Fernspr. D. **61** (1942) 100–114).
101. NOTTEBROCK, H. and WEIS, A.: Einiges über das Hochfrequenzeisen Sirufer und seine Weiterentwicklung (HF-Technik. Elektroak **47** (1936) 100–103).
101a OHTA, K.: Magnetocrystalline anisotropy and magnetic permeability of Mn–Zn–Fe–Ferrites (J. Phys. Soc. Japan **18** (May 1963) 685–690).
102. OLLENDORF, F.: Magnetostatik der Massekerne (Arch. f. El. **25** (1931) 436–447).
103. OWENS, C. D.: Stability characteristics of molybdenum permalloy powder cores (El. Engng. **75** (Mar. 1956) 252–256).

104. PAWLEK, F.: Eisen-Silizium-Legierung hoher Anfangspermeabilität durch metallurgische Sonderbehandlung (Arch. Eisenhüttenw. **16** (1943) 363–366).
105. PAWLEK, F.: Magnetische Werkstoffe. Springer, Berlin/Göttingen/Heidelberg (1952).
106. PAUTHENET, R.: Variation thermique de l'aimantation spontanée des ferrites de nickel, cobalt, fer et manganèse (C. R. **230** (1950) 1842–1843).
107. PAUTHENET, R.: Aimantation spontanée des ferrites (Ann. Phys. **7** (1952) 710–747).
108. PFEIFER, F.: Möglichkeiten zur Beeinflussung der magnetischen Eigenschaften von Permalloylegierungen (ETZ-A **81** (1960) 945–949).
109. PFEIFER, F.: Permalloylegierungen mit Rechteckschleife (Z. ang. Phys. **13** (1961) 177–180).
110. PIERROT, A.: Bobines Pupin à noyaux de ferrite (Cables & Transm. **10** (1956) 215–244).
111. PIERROT, A.: Bobines Pupin à noyaux de ferrite d'encombrement très réduit (Cables & Transm. **12** (1958) 127–184).
112. PODSZUS, E.: DRP 395 075 (1922); 479 337 (1925).
113. POLYDOROFF, W. J.: Powdered magnetic cores (Tele-Tech. (1953) 69–71, 112, 114, 116, 118, 120, 128, 131, 132).
114. PONEMON, R. D.: High frequency cores. An important use for powdered iron (Prec. Met. Molding **11** (1953) 30–32, 74–80).
115. PUPIN, M. I.: Wave transmission over non-uniform cables and long-distance air lines (Trans. AIEE **17** (1900) 445–512).
116. RANDALL, W. F.: Nickel–iron alloys of high permeability, with special reference to mumetal (J. IEE **80** (1937) 647–667).
117. RICHARDS, C. E.: Some chemical and physical properties of iron powders and their effects on the magnetic properties; in Soft Magnetic Materials for Telecommunications (ed. Richards and Lynch), London (1953) 233–246.
118. RICHARDS, C. E., BARDELL, P. R., BUCKLEY, S. E. and LYNCH, A. C.: Some properties and tests of magnetic powders and powder cores (El. Comm. **28** (1951) 55–69; Proc. IEE **97** (56) (1950) 236–245).
119. RICHARDS, C. E. and SHOTTON, D. C.: 50/50 Carbonyl nickel–iron powders; in Soft Magnetic Materials for Telecommunications (ed. Richards and Lynch), London (1953) 247–252.
120. RICHARDS, C. E., WALKER, E. V. and LYNCH, A. C.: An experimental study of high-permeability nickel-iron alloys (Proc. IEE **104 B** (1957) 343–358).
121. RICHTER, G.: Über magnetische und mechanische Nachwirkung; in Probleme der technischen Magnetisierungskurve (Becker). Berlin (1938) 93–113.
121a RÖSS, E., HANKE, I. and MOSER, E.: Mangan-Zink-Ferrite mit Anfangspermeabilitäten bis über 20 000 und ihre Gefüge (Z. ang. Phys. **17** (7) (1964) 504–508).
122. SAIMOWSKI, A. S. and SELISSKY, I. P.: J. Phys. (USSR) **4** (1941) 563–565.
123. SCHOLTS, N. B. and PISKAREW, K. A.: Vergleich der electromagnetischen Eigenschaften ferromagnetischer Oxyde und anderer typischer magnetischer Stoffe (Is. Akad. Nauk. USSR Phys. **16** 739–747).
124. SHACKELTON, W. J. and BARBER, I. G.: Compressed powdered permalloy (Trans. AIEE **47** (1928) 429–437).
125. SHAW, T.: The evolution of inductive loading for Bell System Telephone facilities (Bell Syst. Tech. J. **30** (1951) 149–202, 447–472, 721–764, 1221–1243).
125a SHICHIJO, Y., ASANO, G. and TAKAMA, E.: High-permeability manganese–zinc–ferrite reduced in vacuum (J. A. P. **35** (5) (May 1964) 1646–1647).
126. SIXTUS, K.: Physik und Technik der Massekerne (AEG-Mitt. **41** (1951) 135–142).
127. SIXTUS, K.: Magnetische Eigenschaften und Nachwirkung bei Nickelzinkferrit mit Kobaltzusatz (Solid-State Physics in Electronics & Telecommunications **3** (1960) 91–103).
128. SMOLENSKI, G. A.: Ferrite zweiwertiger Metalle (Dokl. Akad. Nauk, SSSR **78** (5) (1951) 921–924).

129. SNOEK, J. L.: New Developments in Ferromagnetic Materials. Elsevier Publ. Co. Inc., New York/London/Amsterdam/Brussels (1949).
130. SPEED, B. and ELMEN, G. W.: Magnetic properties of compressed powder cores (J. AIEE **40** (1921) 596–609).
131. STANDARD TELEPHONES & CABLES LTD.: 'Permalloy and Permendur'. Technical Data Sheet MM 105 Ed 1/1 (1960).
132. STUIJTS, A. L., RATHENAU, G. W. and WEBER, G. H.: Ferroxdure II und III, anisotrope dauermagnetische Werkstoffe (Phil. T. Rdsch. **16** (1955) 221–228).
133. STUIJTS, A. L. and WIJN, H. P. J.: Crystal oriented Ferroxplana (Phil. T. Rev. **19** (7/8) (1958) 209–217).
134. TAKEI, T.: (J. Electrochem. Ass. Jap. **5** (11) (1937) 411–419).
135. TAYLOR, A.: The structure of carbonyl iron; in Soft Magnetic Materials for Telecommunications (ed. Richards and Lynch), London (1953) 202–217.
136. THURLBY, E. G.: High permeability 'Sendust' powder ring cores (Met. Progr. **60** (4) (Oct. 1951) 83–87).
137. TOHOKU METAL INDUSTRIES LTD, SENDAI (Japan): Sendust. Data Sheet.
138. TOROPOW, N. A., RABKIN, L. T., FREIDENFELD, E. S. and EPSTEIN, B. S.: Phasenzusammensetzung und einige ferromagnetische Eigenschaften von Mangan-Zink-Ferriten (J. prikl. Chim. **26** (1953) 982–990).
139. VACUUMSCHMELZE GMBH, HANAU: Handbuch weichmagnetische Werkstoffe (1967).
140. VACUUMSCHMELZE GMBH, HANAU: Data Sheet M 001.
141. VACUUMSCHMELZE GMBH, HANAU: Data Sheet M 012.
141a VACUUMSCHMELZE GMBH, HANAU: Data Sheet M 018 (Feb. 1964).
142. VALVO GMBH, HAMBURG: Ferroxcube. Data Sheet (Dec. 1961).
143. VAUTIER, R.: Influence de la magnétostriction sur la perméabilité initiale dans les ferrites de manganèse-zinc (C. R. **242** (1956) 2814–2827).
144. VERSCHOOR, J.: Discussion on 'Inductors, magnetic materials and transformers' (Proc. IEE **109 B** (1962) Suppl. 21, 249).
145. WEIS, A.: Das Magnetvariometer (Funk u. Ton **4** (1950) 508–518, 559–568).
146. WIGGIN: Die Nilomag-Legierungen (Nickel Rundschau (35) 12–14).
147. WOLMAN, W.: Der Frequenzgang des Wirbelstromeinflusses bei Übertragerblechen (Z. techn. Phys. **10** (1929) 595–598).
148. WOODRUFF, J. C.: US Pat. 1 292 206 (1919).
149. YENSEN, T. D.: Hipernik and other magnetic alloys (Met. Progr. **21** (1932) 28–34).

# 14

# Magnetic materials for the microwave region

## 14.1 ELECTROMAGNETIC WAVES IN WAVEGUIDES

At frequencies from 1 GHz to 300 GHz (s.h.f. and e.h.f.), waveguides are used to conduct electrical energy. Whereas at low frequencies two conductors are required (usually in the form of wires), in the microwave range the same purpose is served by a single tubular cylinder, of circular or rectangular section, down which flow electromagnetic waves. For a rectangular waveguide whose longer side is of length $d$, the following relation holds between the dimensions of the guide and the wavelength $\lambda$ of the transmitted signal:

$$d < \lambda < 2d$$

The oscillatory signal is propagated in such a form that the electric vector is parallel to the smaller side of the rectangular guide. This mode of propagation is called the $TE_{10}$ mode (see Figure 14.1a). In circular waveguides a mode named $TE_{11}$ (among others) is found, which can be turned at will about the axis by reason of the rotational symmetry of the guide. This is shown schematically in Figure 14.1b[4]. It is not possible here to go into the numerous other propagation modes which can occur.

The magnetic lines of force are closed curves perpendicular to the electrical lines. Figure 14.2 gives a schematic representation which will be further discussed below.

The propagation characteristics of wave transmission in a guide can be modified by the introduction of various materials. Thus dielectrics such as polystyrene, or glass plates thinly plated with metal, have long been used to influence the attenuation or the phase of the transmitted waves. Magnetic materials could not be used before the introduction (around 1950) of ferrites because the skin effect prevented the penetration of the waves into the interior of ferromagnetic materials. Microwaves were, however, able to penetrate into high-resistance ferrites and can thus be influenced by their passage through the material. This means that a mutual reaction between waves and electron spin—a determining factor for the magnetic properties of materials —can take place. The introduction of ferrites into microwave technique has led to a multitude of quite novel components.

Radical studies of the properties of ferrites in the microwave range date from about 1950[34, 71]. At the outset investigators were limited to those ferrites

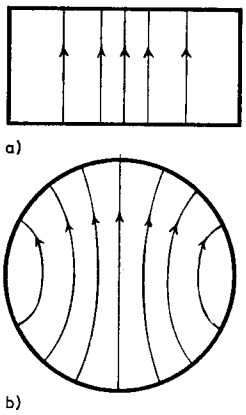



*Figure 14.1. (a) Waveguide of rectangular section, transmission mode $TE_{10}$ or $H_{10}$; (b) waveguide of circular section, transmission mode $TE_{11}$ or $H_{11}$; the electrical lines of force are drawn diagrammatically in both cases*[4]

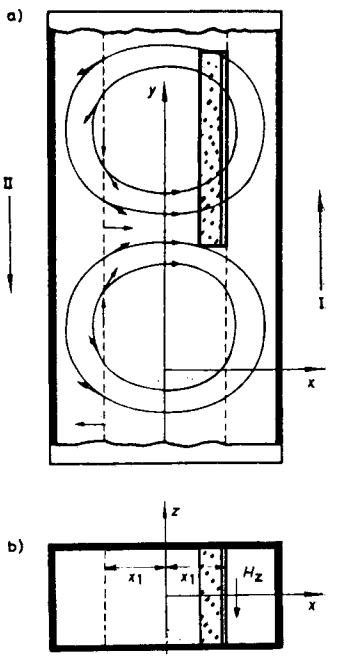



*Figure 14.2. Longitudinal and transverse sections of a rectangular waveguide; disposition of magnetic lines for the $TE_{10}$ mode. At a particular distance x from the centre-line the magnitude of the vector remains almost constant as it rotates uniformly; in a magnetised ferrite strip mounted at a distance x and parallel to $H_z$ gyromagnetic resonance occurs and this introduces attenuation in waves travelling in the reverse or II direction*[4]

available at the time, such as nickel ferrite[63], magnesium ferrite[71], or barium ferrite[4]. As knowledge deepened concerning the relation between the properties of the materials and the behaviour of the microwaves, a period of intensive and purposeful materials development set in which ultimately led to a comprehensive range of practical ferrites. In most cases it was the high-resistance mixture-ferrites that were involved.

It is true that, for a variety of reasons, standardised materials do not yet exist for this field: the bulk requirements for microwave ferrites are relatively small; more especially, the properties of the materials, the shape, dimensions, and arrangement of ferrite elements in the guide, and the frequency and

amplitude of the waves, as well as the details of the actual waveguides used, are so intimately associated that most solutions of microwave problems must rely on a compromise.

Today the development has reached a certain stage of completion, so many hundreds of publications—among them summaries and reviews in book form—are devoted to microwave ferrites, their manufacture, their properties and, above all, their applications[15, 45, 46].

## 14.2 THE RECIPROCITY PRINCIPLE

Ferrites are used in microwave fields mainly because they make possible the production of those non-reciprocal passive components which have become known as gyrators, isolators, non-reciprocal phase-shifters, circulators, etc.

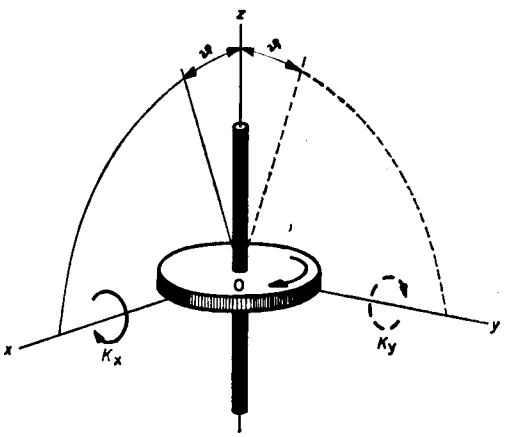



*Figure 14.3. Spinning top as an example of failure of the reciprocity principle*[4]

In constrast to the previously known circuit elements, namely resistors, transformers, capacitors, and inductances, all of which show reciprocal relations, the newer elements named above are non-reciprocal. This is to be interpreted as follows. If, in a branch A of a network having reciprocal components, a voltage $V$ is introduced, and if, in another branch B, the current $I$ is measured, then the same result is obtained if the voltage $V$ is applied in branch B and the current measured in branch A. In a.c. work this equality applies to phase as well as to magnitude. In this sense transformers are reciprocal four-poles and coils reciprocal two-poles (four-terminal and two-terminal devices).

The reciprocity principle applies not only in electrical theory but also in optics and mechanics (theory of elastic deformation). However, there are cases where the principle fails—especially, those physical processes which involve gyroscopic action. This can be made clear by taking the example of a mechanical top. The top shown in Figure 14.3[4] rotates about its axis, which coincides with the $z$-axis of coordinates, in the sense indicated by the

arrow[4]. A turning moment applied to the $x$-axis or the $y$-axis for a time $t$ causes a displacement of the top's axis through an angle $\vartheta$. For a positive turning moment $K_x$ around the $x$-axis, the displacement-angle $\vartheta$ is described in the $xz$ plane and $\vartheta = tK_x$. Seen from the $y$ direction the axis veers to the left. If an equal turning moment $K_x = K_y$ is applied around the $y$ axis, this will cause a deflection by an angle $\vartheta$ in the $yz$ plane, i.e. a deflection, seen from the $x$ direction, to the right. In both cases the magnitudes are of course the same, but the signs are different.

A further example of the failure of reciprocity is the Faraday effect (see page 6). The plane of polarisation of a plane-polarised light beam is independent of the direction of propagation in the medium, being always turned in a direction determined by that of the superimposed direct field. Seen,

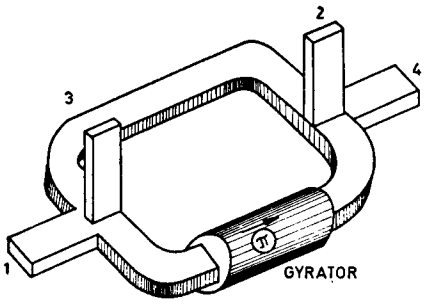



*Figure 14.4. Principle of the circulator first described by Hogan as the 'hybrid-T circulator' (the numbers are elucidated in Figure 14.48)*[34]

therefore, from the particular direction of arrival of the light-beam, the directions of rotation are in opposite senses for a forward or a backward propagation, the direction of the direct field being fixed. The same law holds for the microwave Faraday effect, which was first treated by Roberts[71] and by Hogan[34]. In place of the polarised light beam are electromagnetic oscillations whose frequency lies in the range 1–100 GHz. The deflecting device is a ferrimagnetic element in a waveguide. The ferrite—or, alternatively, a garnet—may be magnetised either along the direction of propagation or transversely.

A variety of non-reciprocal components can be built in this way. If the Faraday rotational effect is exploited, then the phase of the reflected wave is altered relatively to the forward wave. Directional phase-shifters can be constructed on this principle. A special case of directional phase-changing devices is the gyrator: according to Tellegen[23, 95], the term refers to a transmitting element which shows no phase-shift in one direction but produces a shift of 180° in the opposite direction (see Figure 14.4). If the returning wave is absorbed by some suitable means (see below) a different non-reciprocal element results, namely an isolator[30]. The various means of constructing such one-way devices and other derived components are discussed below.

The concept and practical importance of passive non-reciprocal components was already known before they could be made effective through the development of ferrites[5, 95].

## 14.3 ELECTRICAL PROPERTIES OF FERRITES AT SUPER-HIGH FREQUENCIES

If microwaves are to penetrate into the body of the ferrite, the specific electrical resistance must be as high as possible and should, in fact, be at least $10^6\,\Omega\,\text{cm}$[79]. To keep down the loss, the magnetic and dielectric losses ($\tan\delta_\mu$ and $\tan\delta_\varepsilon$) should both be low. Only in the case of the field-displacement isolator (see page 537) are medium or high dielectric losses acceptable.

Table 4.1, following a review by Van Uitert[99], lists a few ferrites whose 'parallel' dielectric constants $\varepsilon_p$ are shown in Figure 14.5 as a function of frequency. The low-frequency resistance, designated $\varrho_l$ in the table, was measured at 1 kHz, whereas the high-frequency resistance $\varrho_h$ of the specimen was measured at the frequency $f$ standing opposite to it in the next column.

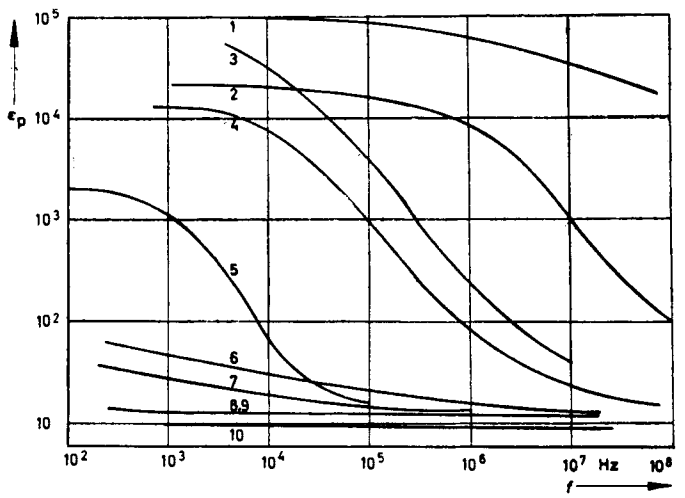



*Figure 14.5. 'Parallel' dielectric constant $\varepsilon_p$ as a function of frequency for the ferrites tabulated in Table 14.1*[4]

**Table 14.1** ELECTRICAL PROPERTIES OF THE FERRITES SHOWN IN FIGURE 14.5[99]

| *Curve number* | *Ferrite* | $\varrho_l$ ($\Omega$ cm) | $\varrho_h$ ($\Omega$ cm) | $f$ (MHz) |
|---|---|---|---|---|
| 1 | Mn–Zn | 130 | 10 | 100 |
| 2 | Ferramic B | $2\times10^5$ | 80 | 100 |
| 3 | Cu–Zn | $1\times10^3$ | 400 | 10 |
| 4 | Ferramic I | $5\times10^5$ | $3\times10^3$ | 10 |
| 5 | Ni–Zn | $2\times10^6$ | $5\times10^5$* | 0·1 |
| 6 | NM 1350 | $8\times10^5$ | $1\times10^5$ | 10 |
| 7 | N 1250 | $6\times10^6$ | $4\times10^5$ | 10 |
| 8 | NM 1250 | $2\times10^9$ | $1\times10^7$ | 10 |
| 9 | Crowloy BX 113 | $6\times10^8$ | $3\times10^6$ | 10 |
| 10 | Ferramic A | $2\times10^9$ | $1\times10^7$ | 10 |

* At 10 MHz about $5\times10^4$.

It can be deduced from curves 1–10 of Figure 14.5 that the dielectric constant of ferrites approaches a limiting value of 10–15 $\varepsilon_0$ at very high frequencies and that this value is reached, in general, at a frequency which is lower the higher the specific electrical resistance of the specimen. Values of $\varepsilon$ and tan $\delta_\varepsilon$ are listed for a few ferrites and garnets in Table 14.2.

The linewidth $\Delta H$ (also quoted in the table) is returned to on page 546. As for the magnitude $g_{\text{eff}}$, the following is worth noting: The Landé factor $g$ is given by the expression

$$g = 2 \times \frac{\text{total magnetic moment}}{\text{magnetic spin moment}}$$

If there is an orbital moment but no spin moment then $g = 1$, and when there is only a spin moment $g = 2$. In the ferrimagnetic spinels the magnetic moments of the ions of the tetrahedral and octahedral configurations are anti-parallel. Depending upon the moments of the individual constituents

**Table 14.2** PROPERTIES OF SOME FERRITES AND GARNETS[8,15]

| *Material* | $B_s$ (V s/m²) | $T_c$ (°C) | $\varepsilon$ ($\varepsilon_0$) | tan $\delta_\varepsilon$ | $\Delta H$ (kA/m) | $g_{eff}$ | $f$ (MHz) |
|---|---|---|---|---|---|---|---|
| $NiFe_2O_4$ | 0·35 | 565 | 12·7 | 0·0037 | 73·6 | 2·4 | |
| Mg–Mn Ferrite (Ferramic R 1) | 0·23 | 300 | 13·6 | 0·001 | 39·2 | 2·06 | |
| Mg–Mn Ferrite (Sperry) | 0·205 | 350 | — | — | 9·6 | — | |
| Mg–Mn Ferrite (Airtron 161) | 0·23 | 300 | — | — | 39·2 | — | |
| Mg–Mn–Al Ferrite (Trans-tech 414) | 0·06 | 100 | — | — | 9·6 | — | 3 000 ($\Delta H$) |
| Mg–Mn–Al Ferrite (Airtron 115) | 0·185 | 243 | 10·34 | 0·002 | 40·0 | 2·2 | |
| Mg–Mn–Al Ferrite (Siferrit GY 4) | — | — | — | — | 16·0 | 2·05 | 9 650 |
| Ni–Co Ferrite ($Ni_{1-\alpha}Co_\alpha Mn_{0·02} Fe_{1·9}O_4$) | 0·323 ($\alpha = 0$) | — | — | — | 14 ($\alpha = 0·027$)<br>72 ($\alpha = 0·1$) | 2·34<br>2·24 | |
| Y–Fe garnet ($5Fe_2O_3 \cdot 3Y_2O_3$) | 0·174 | — | — | 0·003 | 4 | — | 20 (tan $\delta_\varepsilon$) |
| Sm–Fe garnet ($5Fe_2O_3 \cdot 3Sm_2O_3$) | 0·170 | — | — | 0·002 | 200 | — | 20 (tan $\delta_\varepsilon$) |
| Yb–Fe garnet ($5Fe_2O_3 \cdot 3Yb_2O_3$) | 0·164 | — | — | 0·0025 | — | — | 20 (tan $\delta_\varepsilon$) |
| Er–Fe garnet ($5Fe_2O_3 \cdot 3ErO_3$) | 0·131 | — | — | 0·004 | — | — | 20 (tan $\delta_\varepsilon$) |

**Table 14.3** PHYSICAL PROPERTIES OF SOME MICROWAVE FERRITES[69]

| *Ferrite* | $J_s$ (V s/m²) | $\Delta H$ (kA/m) | $T_c$ (°C) | $\varrho$ (Ω cm) |
|---|---|---|---|---|
| $NiFe_2O_4$ | 0·33 | 44·8 | 580 | $4\times10^3$ |
| $NiAl_{0·12}Fe_{1·88}O_4$ | 0·27 | 33·6 | 540 | $4\times10^4$ |
| $NiAl_{0·35}Fe_{1·65}O_4$ | 0·12 | 67·2 | 430 | $4\times10^8$ |
| $NiAlFeO_4$ | 0·053 | 31·6 | 186 | $1\times10^9$ |
| $Mg_{0·9}Mn_{0·1}Fe_{1·6}O_{3·4}$ | 0·25 | 56·0 | 290 | $8\times10^8$ |

and on the structure of the ferrite, values departing more or less from $g = 2$ are found and are labelled $g_{eff}$ values.

To achieve a high specific electrical resistance the simultaneous presence in the ferrite of ions of the same element but of differing valency is to be avoided—in particular the ions $Fe^{2+}$ and $Fe^{3+}$. Ferrites are therefore used which have a defect of iron; or the $Fe^{3+}$ ions may be partly replaced by $Al^{3+}$, whereby electron exchange processes are largely obstructed. Table 14.3 shows this for Ni–Al ferrites. The resistance increases from $4\times10^3$ Ω cm to $10^9$ Ω cm if, in the combination $NiAl_xFe_{2-x}O_4$, the part represented by $x$ is increased from 0 to 1[69].

If ferrites of lower resistance are employed, it must be remembered that for a temperature rise of, say, 100°C the specific electrical resistance falls, in general, by an order of magnitude. Further details about ferrites of high specific electrical resistance are given in Chapter 8 and can be found, in particular, in Figures 8.11, 8.12, and 8.13.

## 14.4 MAGNETIC PROPERTIES OF FERRITES IN A MICROWAVE FIELD

### 14.4.1 Permeability

In microwave applications the permeability of a magnetic material cannot be taken as a scalar, as it often can at low frequencies, but must be regarded as a tensor. In a waveguide the ferrite element is subjected, simultaneously, to a direct field and to a high-frequency alternating field. The permeability tensor is thus of the second order. If the direct field saturates the ferrite, regarded as loss-free and of infinite extent, in the $z$ direction, the permeability tensor $\mu_T$ is given by

$$\mu_T = \mu_0 \begin{vmatrix} \mu & -j\varkappa & 0 \\ +j\varkappa & \mu & 0 \\ 0 & 0 & 1 \end{vmatrix} \tag{14.1}$$

The direct field may lie parallel to the direction of propagation (Faraday effect), but may also lie perpendicular to the propagation direction and to the magnetic field-structure of the microwaves.

The components $\mu$ and $\varkappa$ of equation 14.1 are given, according to Polder[68] by

$$\mu = \mu_0 - \gamma J \frac{\omega_p}{\omega_p^2 - \omega^2} \tag{14.2a}$$

and

$$\varkappa = \gamma J \frac{\omega}{\omega_p^2 - \omega^2} \tag{14.2b}$$

Here, $\mu_0$ is the absolute permeability, $\omega$ the (circular) measuring frequency, $\omega_T$ the precession frequency of an electron round the direction of the direct field (Larmor frequency), $J$ the magnetic polarisation, and $\gamma$ the gyromagnetic ratio for which approximately

$$-\gamma = 0{\cdot}22 \frac{\text{MHz}}{\text{A/m}} \tag{14.3}$$

The quantity $\gamma$ carries the negative sign because the magnetic moment is oppositely directed relative to the mechanical moment. The high-frequency permeability degenerates into a scalar for circularly polarised fields. For the positive circularly polarised wave,

$$\mu_+ = \mu_0 - \frac{\gamma}{\omega_p - \omega} J \tag{14.4}$$

and, for the negative circularly polarised wave,

$$\mu_- = \mu_0 - \frac{\gamma}{\omega_p + \omega} J \tag{14.5}$$

According to equations (14.2) the values of $\mu$ and $\varkappa$ would become indefinitely large at $\omega = \omega_p$ if no attenuation occurred. In fact, however, there is always attenuation and so the permeability is always finite.

If a plane wave progresses in a magnetic material, carrying a saturating field in the direction of propagation, it may be divided into two circularly polarised components, one positive and one negative. Equations 14.4 and 14.5 show that the permeabilities differ for the two components. In consequence, there are different velocities of propagation, and this causes a rotation of the plane of polarisation of the waves, whose components recombine to form a plane wave after passage through the material. The rotation is greater the longer the path through the ferrite and the higher the permeability and the effective dielectric constant. The angular displacement $\Phi$ per centimetre of path length is given by

$$\Phi = \frac{\omega}{2} \left( \frac{1}{v_-} - \frac{1}{v_+} \right) \tag{14.6}$$

where $v_-$ and $v_+$ are the velocities of the negative and positive circularly polarised waves. If $c$ is the velocity of light and $v = c/\sqrt{(\varepsilon \mu_0)}$, equation 14.6 can be rewritten as

$$\Phi = \frac{\omega}{2c} \sqrt{\varepsilon} \, (\sqrt{\mu_-} - \sqrt{\mu_+}) \tag{14.7}$$

In weak fields, where $\gamma H_z \ll \omega$, and if the saturation magnetisation $M$ is low (so that $\gamma M \ll \omega$), equation 14.7 can be put in the form

$$\Phi = \frac{M\gamma}{2}\sqrt{(\mu_0\varepsilon)} \quad \text{degrees/cm} \tag{14.8}$$

This shows that the angle of rotation increases if the $\varepsilon$ and $M$ of a ferrite increase, but that it does not depend on frequency. This relation ceases to hold if $\omega$ and $\omega_p$ do not differ much[34]. Hence, as magnetic materials are always 'lossy' the permeability components are complex.

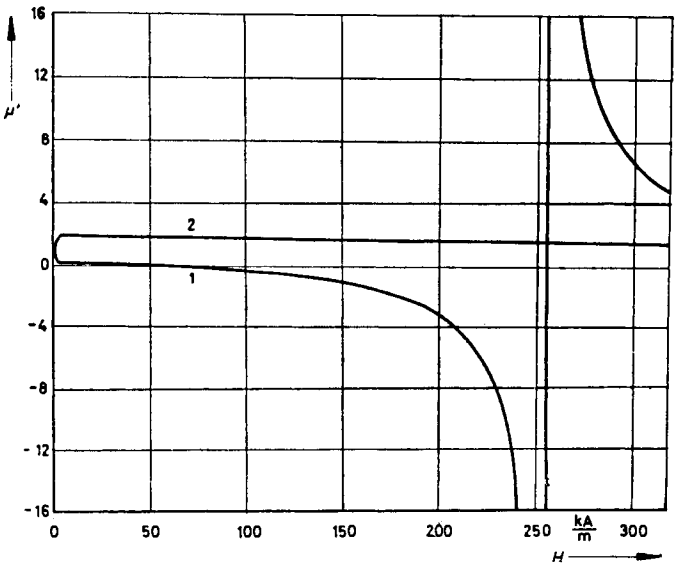



*Figure 14.6. Real part of the permeability of a ferrimagnetic substance magnetised parallel to the direction of propagation of an infinite plane wave ($f = 9$ GHz, $J_s = 0{\cdot}3$ V s/m$^2$, $\mu_i = 100\mu_0$): 1, positive circularly polarised component; 2, negative circularly polarised component*[35]

The relation between permeability and field strength is different for the positive and negative circularly polarised waves, in both the real component and the imaginary component. The permeability components can take either positive or negative values. Figures 14.6 and 14.7 show examples which are typical of the ferrites: the permeability components were calculated for a material having $J_s = 0{\cdot}3$ V s/m$^2$ and $\mu_i = 100\mu_0$ at a frequency of 9 GHz. It is seen that the negative circularly polarised parts of $\mu'$ and $\mu''$ are both very low and depend little on field strength. At the intensity for which the ferrimagnetic material shows an absorption line, the permeability $\mu''$ of the positive circularly polarised wave passes through a resonance.

The actual values measured for ferrites may depart from the theoretical values to be expected from the above formulae because the samples measured do not comply with the theoretical assumptions—in particular the wavelength may not be small compared with the size of the specimen. By means

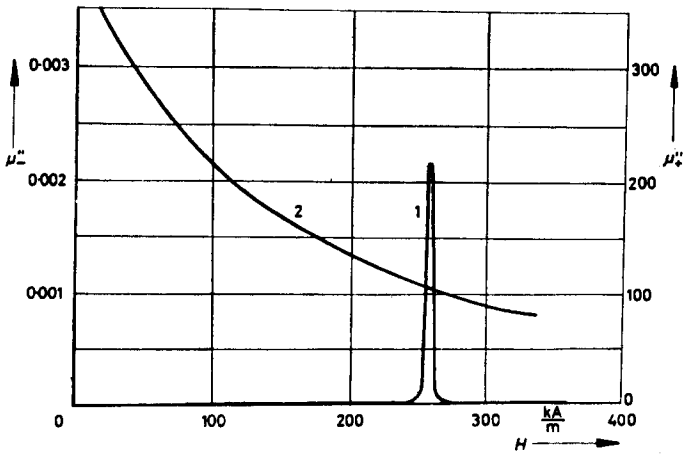



*Figure 14.7. Imaginary part of the permeability of a ferrimagnetic substance magnetised parallel to the direction of propagation of an infinite plane wave; the relaxation frequency was arbitrarily chosen as 19* MHz*: 1, positive circularly polarised component; 2, negative circularly polarised component*[35]

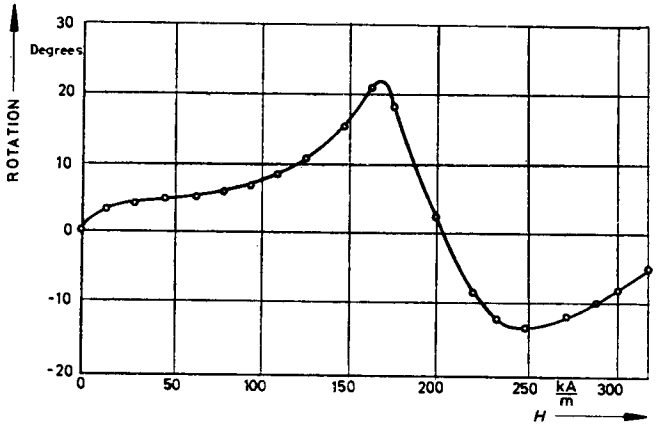



*Figure 14.8. Faraday rotation measured at 8·95* GHz *in a short rod of* Mg–Mn *ferrite*[36]

of an experimental set-up like that shown in Figure 2.3 ($TE_{11}$ mode), the Faraday rotation given by Figure 14.8[36] was measured at 8·95 GHz for a cylindrical ferrite rod 50 mm long and 3·2 mm in diameter having the composition $Mg_{1.5}Mn_{0.17}Fe_2O_{5.2}$. The results correspond to the theoretically expected curve given Figure 14.6.

Figure 14.9 shows the attenuation of a circularly polarised $TE_{11}$ wave measured in a circular-section waveguide for a Ni–Zn ferrite[36]. The measured curve agrees well with that expected on theoretical grounds. The individual portions of the permeability curves have different applications in technology. As Figure 14.10 makes clear schematically, the Faraday effect is important in the region of low field strength; at high field strength, resonance effects appear, and, at intermediate intensities, field displacement can be used.

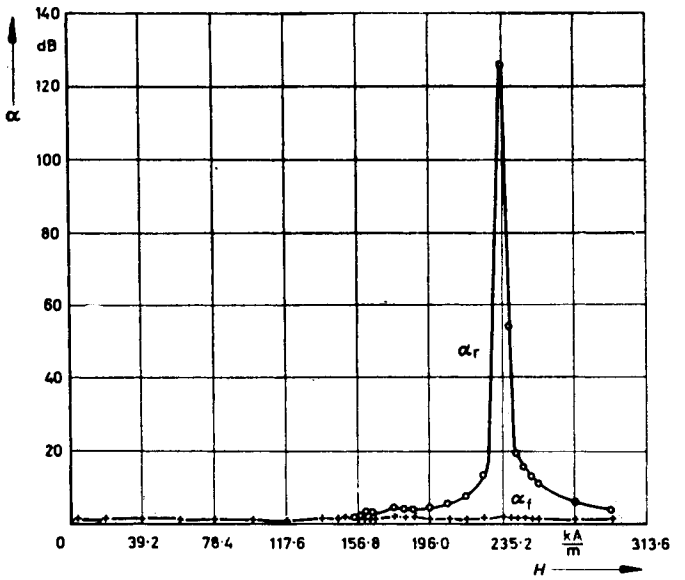



*Figure 14.9. Measured absorption of* Ni–Zn *ferrite in a circular waveguide (f=9·455* GHz*)*[36]

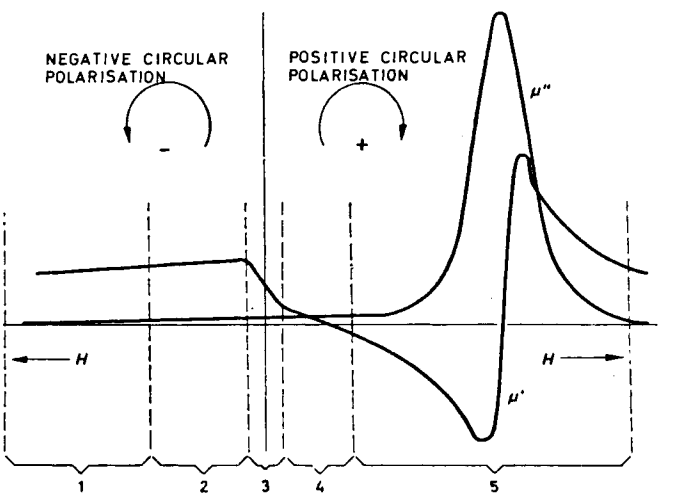



*Figure 14.10. Relation of μ′ and μ″ to field strength H for circularly polarised waves: 1, resonance; 2, field displacement; 3, Faraday rotation; 4, field displacement; 5, resonance*[57]

### 14.4.2 The Faraday effect

The schematic of a Faraday isolator, in which Faraday rotation is used to achieve the required directional effect, is shown in Figure 14.11. The rectangular section of the waveguide is interrupted by the insertion of a length of cylindrical guide, reflection being avoided by arranging a smooth transition. A cylindrical rod of ferrite is introduced into the cylindrical waveguide along its axis, the ends being tapered to a point—again to suppress reflection. If the whole cross-section of the waveguide were filled with ferrite, a whole series of unwanted modes might be excited along with the desired mode.

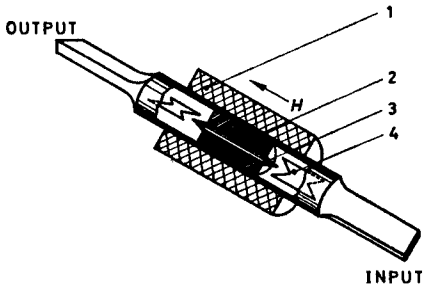



*Figure 14.11. Diagram of a Faraday isolator: 1, magnetising coil; 2, mounting (PVC foam); 3, ferrite rod; 4, absorption strip*

The ferrite rod is magnetised along its length by means of windings applied externally to the waveguide. A permanent magnet can be employed in place of the solenoid. The type of ferrite and the dimensions of the element can be so chosen that the waves leaving the isolator are turned, for example, through 45° relative to the input waves. A returning wave will be further turned in the same sense as the forward wave since the direction of the direct field is maintained. Seen from the input, the reflected wave makes an angle of 90° with the forward wave. However, a mode in which the electrical vector lies parallel to the longer side of the rectangular guide cannot form.

By using an absorbing strip, parallel to the electrical lines of force, made from a weakly absorbent material, the reflected wave can be suppressed. Carbon or graphite are suitable substances which can, for example, be applied to PVC film and stuck onto a mica substrate. By giving such a strip a suitable shape, reflections can be largely avoided[38]. Electromagnetic energy can therefore flow from A to B but cannot pass from B to A. Direction-sensitive guides based on the Faraday effect are called Faraday isolators or rotators.

Phase-shift induced by the Faraday effect is often applied directly; the component is then spoken of as a gyrator (*gyros* = top)[95]. In an ideal gyrator the phase-shift between the two directions of propagation should be 180°. Figure 14.12 shows, schematically, the corresponding device[4]: Figure 14.12a represents the piece of waveguide, Figure 14.12b indicates the form of the wave propagated from 1 to 2, and Figure 14.12c shows the form of the reflected wave. A few numerical examples may serve to extend the schematic presentation. Figure 14.13, following investigations by Hogan[34], shows the angle of rotation as a function of field intensity for a Mn–Zn ferrite. The rotation rises more or less linearly with increasing intensity and remains

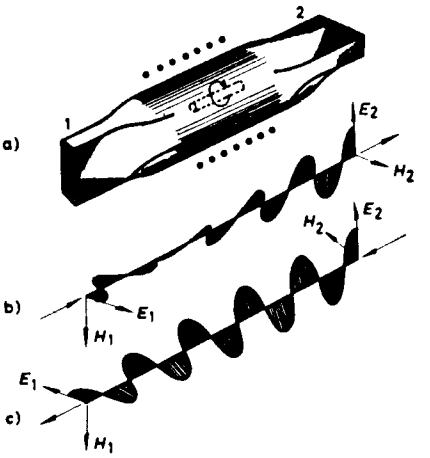



*Figure 14.12. Rotation of plane of polarisation of a microwave in a Faraday rotator: (a) section of guide with ferrite rod; (b) forward wave; (c) reflected wave*[4]

constant when magnetic saturation is reached. Other ferrites yield rotations of much the same order, namely between 100° and 200° per centimetre[2, 34].

Figure 14.14 shows the attentuation curves in the 'pass' and 'stop' directions for a Faraday isolator excited at 23·6–24·4 GHz. A barium ferrite ($BaO{\cdot}6Fe_2O_3$) was used as the ferrimagnetic element at $H = 5$ kA/m. It can be seen from the graph that in the pass direction (I) the attenuation amounts to about 1 dB, remaining almost unchanged over the whole band. The attentuation in the stop direction (II) is never less than 20 dB and reaches a maximum of 44 dB at a frequency of 24·0 GHz [4].

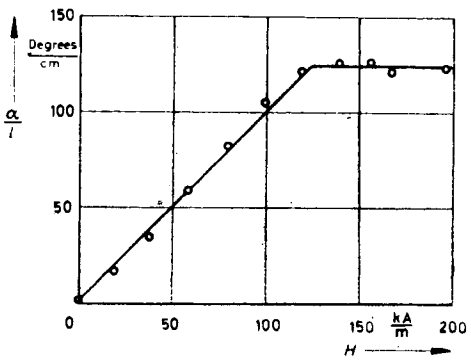



*Figure 14.13. Faraday rotation of a thin disc of* Mn–Zn *ferrite as a function of applied field strength*[34]

### 14.4.3 Resonance absorption

Ferromagnetic resonance was discussed theoretically in 1921 by Gans and Loyarte, 25 years before Griffiths was able to demonstrate the effect experimentally[42].

In their fundamental work in 1935 Landau and Lifshitz[43] predicted the occurrence of resonance in nickel within the microwave range. The theoretically expected behaviour of magnetic materials at extremely high frequencies

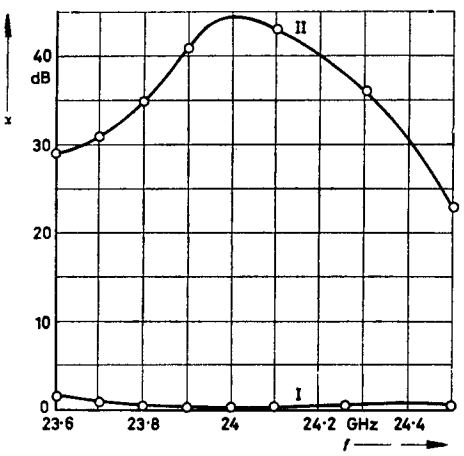



*Figure 14.14. Attenuation α in a Faraday directional isolator as a function of frequency f: I, forward direction; II, reverse direction*[4]

could be properly investigated only after the appearance of suitable ferrites. A good agreement was found, in general, between theory and measurement, nor was any fundamental difference between ferromagnetic and ferrimagnetic resonance observed. The contribution of a 3d electron in an atom of iron (see page 101) to the magnetisation of a ferromagnetic substance is related to its spin. If, now, a directional magnetic field $H$ acts on such a spinning electron, the electron behaves like a top. It executes a damped movement of precession about the field direction, the precession frequency $\omega_p$ being proportional to the effective field strength, $H_{eff}$:

$$\omega_p = \gamma H_{eff} \tag{14.9}$$

where $\gamma$ is the gyromagnetic ratio defined in equation 14.3. Conversely, one can determine from this equation what effective intensity must be applied to achieve resonance. A few examples are worked out in Table 14.4.

Suppose that, in a ferrite element, a high-frequency field $h$ of circular frequency $\omega = 2\pi f$ acts perpendicular to the d.c. magnetisation vector $H$. Let this magnetisation $h$ be circularly polarised with respect to $H$ and suppose it to be propagated as a wave transversely to $H$. The positive circularly polarised part of the field $h_+$ is associated with waves which proceed in the positive direction, and the negative part $h_-$ with waves which progress in the negative direction. Such an alternating field can establish itself at a particular distance $x$ from the central axis of a rectangular guide (see Figure 14.2).

If the circular frequency $\omega$ is of the same order as $\omega_p$, then resonance can occur, i.e. the precession of the electrons does not fade out but maintains itself at a definite amplitude. Thus the external alternating field transfers energy to the precessing electrons or, one may say, the 3d electrons of the ferrite element absorb energy from the electromagnetic wave traversing the waveguide. The energy is transferred to the crystal lattice; lattice vibrations manifest themselves as heat.

No coupling from the $h_-$ part of the field to the 'Larmor' precession can occur and hence there can be no attenuation. The $h_-$ component can thus

**Table 14.4** RESONANCE FIELD STRENGTHS $H_{eff}$ AT VARIOUS FREQUENCIES $f$

| $f$ (GHz) | $\lambda$ (cm) | $H_{eff}$ (kA/m) |
|---|---|---|
| 0·5 | 60 | 14·3 |
| 1 | 30 | 28·6 |
| 2 | 15 | 57·2 |
| 4 | 7·5 | 114·5 |
| 6 | 5 | 171·6 |
| 8 | 3·8 | 230 |
| 10 | 3·0 | 286 |
| 20 | 1·5 | 572 |
| 50 | 0·6 | 1 430 |
| 100 | 0·3 | 2 860 |

traverse the ferrite in the direction without (or almost without) opposition, whereas the returning wave is strongly attenuated. That there is a finite, if small, forward attenuation of the $h_-$ wave as it traverses the ferrite (as Figure 14.9 shows) is connected with the fact that the assumed resonance conditions apply only in a medium of infinite extent and for a particular internal field. For finite ferrite elements, anisotropies must be allowed for, i.e. the effective field strengths must be determined more exactly (see below).

### 14.4.4 Field displacement

In the non-reciprocal field-displacement isolator the 'distortion' of the field within a waveguide caused by the introduction of ferrite is made use of technically[23]. The principle will be understood by referring to Figure 14.15[83]. In a rectangular waveguide containing no ferrite, the electric field intensity is symmetrically distributed, being maximum along the axis of the guide and zero at the walls. If, now, a ferrite strip is laid along one of the internal walls,

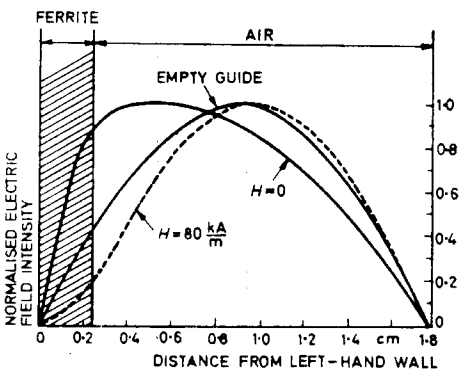



*Figure 14.15. Distribution of normalised electric field intensity as a function of distance from inner face in a rectangular guide with and without ferrite*[83]

the maximum of the field is shifted towards the ferrite. The field strength is greater within the ferrite than it was before at the same location. The distribution of intensity also changes with the field strength. The broken curve shows the case where the ferrite is magnetised with a field of 80 kA/m (ferrite properties: $J_s = 0{\cdot}18$ V s/m$^2$; $\varepsilon = 12\varepsilon_0$; thickness of strip 2·26 mm; waveguide, 17·5 mm$\times$10 mm). Premagnetising the ferrite seems therefore to reduce the width of the guide. The effect can be put to use for microwave switches[13, 83].

An isolator constructed on the field-displacement principle was described by Weisbaum and Seidel[107]. The ferrite strip is mounted at a small distance from the wall and its thickness is 10% of the width of the waveguide. It is

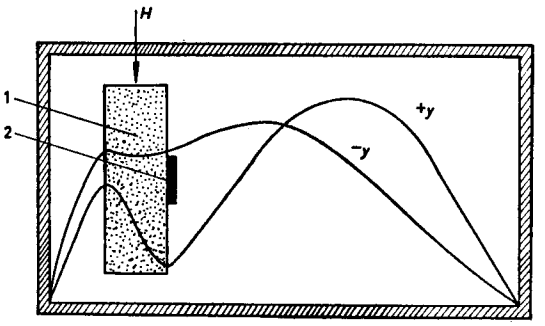



*Figure 14.16. Diagram of a field-displacement isolator: 1, ferrite; 2, resistive absorber*[107]

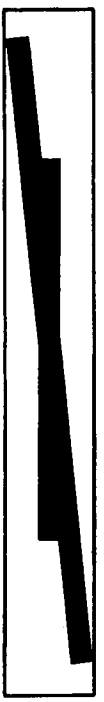


*Figure 14.17. Absorption resistance*[107]

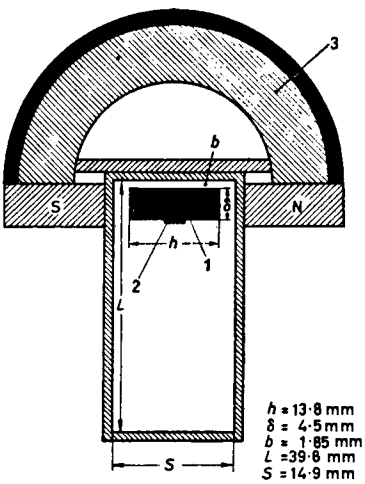



*Figure 14.18. Field-displacement isolator: 1, ferrite; 2, resistive absorber; 3, permanent magnet*[107]

so mounted in the waveguide that on the inner face of the ferrite—as shown in the schematic of Figure 14.16—the field of the forward wave ($_+y$) is almost zero, whereas that of the reflected wave ($_-y$) is very high. If, then, an absorbing material is applied to the face of the ferrite, the reflected wave ($_-y$) can be attenuated as required. Figure 14.17 shows the shape of such a resistive strip, and Figure 14.18 indicates the construction of a field-displacement isolator. Using such an arrangement, attenuation ratios of 30 : 0·2 can be achieved at 6 GHz[107] and 70 : 1 at 11 GHz[105].

The field-displacement isolator cannot be as widely applied as the Faraday isolator or the resonance-absorption isolator because optimum design conditions are not easily achieved.

### 14.4.5 Effect of specimen shape

It was mentioned above that Faraday rotation is proportional to the distance travelled in the ferrite by the waves. This does not hold universally, however, as, for example, in short lengths, for which the rotation per unit length is less than anticipated. Moreover, the amount of rotation depends on the cross-section of the ferrite. Optimally dimensioned ferrite elements have usually a specific rotation of 100°–200°/cm. However, 280°/cm is attainable at 11 GHz with Ni–Zn ferrite[23]. Non-reciprocal phase-shift in rectangular waveguides largely depends on the thickness of the asymmetrically mounted ferrite strip (Figure 14.19).

The value of $H_{\text{eff}}$ in equation 14.9 is different in a finite specimen from its value in an infinitely extended medium. Kittel[41] has established the formula for an ellipsoidal specimen. Let the demagnetising factors be $N_x$, $N_y$, and $N_z$ for the axial directions and suppose that the static field coincides with the $z$ direction; the Kittel equation then takes the form

$$H_{\text{eff}}^2 = [H_z+(N_y-N_z)M_z][H_z+(N_x-N_z)M_z] \qquad (14.10)$$

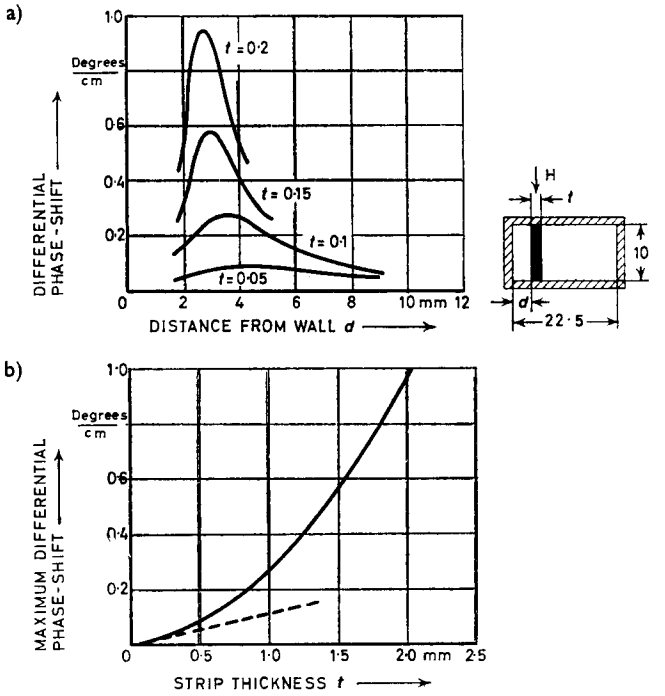



*Figure 14.19. Phase-shift using asymmetrically disposed strips of* Ni–Zn *ferrite (M = 240* kA/m*; $\varepsilon = 10\varepsilon_0$; $f = 9$* GHz*; $H_0 = 16$* kA/m*: (a) phase-shift of strips of various thickness as a function of spacing from guide-wall; (b) maximum phase-shift as a function of strip thickness (approximate value for thin strip shown as broken line)*[47]

The formula can be considerably simplified if the specimen takes certain special shapes. Thus, parallel to the surface of a disc-shaped specimen, $N_x = N_z = 0$ and $N_y = 1$ and so

$$H_{\text{eff}}^2 = H_z(H_z + M_z) \doteq \frac{H_z B_z}{\mu_0} \tag{14.11}$$

For a sphere with $N_x = N_y = N_z = \frac{1}{3}$,

$$H_{\text{eff}} = H_z \tag{14.12}$$

The flux density is thus not involved in spherical specimens. For measuring $\gamma$, therefore, ground and polished spheres are used for preference.

For a plane specimen in which the static magnetic field is perpendicular to the flat surface, $N_x = N_y = 0$ and $N_z = 1$, and therefore

$$H_{\text{eff}} = H_z - M_z \tag{14.13}$$

If the ferrite takes the form of a long cylinder with $N_z = 0$ and

$N_x = N_y = \frac{1}{2}$ then

$$H_{eff} = H_z + \tfrac{1}{2}M_z \tag{14.14}$$

According, therefore, to the form of the measuring sample, various effective field strengths, and thus various Faraday rotations, are obtained[75]; also, by equation 14.9, various resonance frequencies. Hlawiczka and Mortis[33] have worked out graphical solutions of Kittel's equation for various dimensional ratios and orientations of the ferrite element.

A numerical example may serve to show how markedly the resonance frequency can shift with changing shape: under the assumption that the microwaves penetrate into the iron, it can be calculated, theoretically, for $M = 1700$ kA/m that[41]:

| | At $H = 0$ | At $H = 80$ kA/m |
|---|---|---|
| Sphere | 0 | 2·8 GHz |
| Plane | 0 | 13·3 GHz |
| Round cylinder | 30 GHz | 32·8 GHz |

Sensiper[79] published the measured resonance curves for a number of commercially available ferrites (Ferramic and Ferroxcube) between 6 GHz and 10 GHz. It appears from the investigations that it is not only the dimensional ratio (as expressed through the demagnetising factor $N$) that is effective, but that the results can also be influenced by the absolute values of strip-thickness or rod-length. The losses are not proportional to the volume of ferrite but rise more steeply than this would suggest for increasing thickness, for example.

The optimal dimensioning of a ferrite rod or strip must thus frequently be sought either experimentally or by calculation. At the same time account must be taken of the temperature dependence of the isolator (see page 553).

### 14.4.6 Microwave losses

As can be seen from Kittel's equation (equation 14.10) the losses of a ferrite through which microwaves are propagated can generally be split into two components, each depending on field strength: losses in the unmagnetised (or only weakly magnetised) ferrite—initial or zero-field losses—and the resonance losses of ferrites at magnetic saturation. To the magnetic losses must be added the dielectric losses which extend throughout the intensity range and exceed the magnetic losses at very high frequencies[51]. The field-intensity dependence of total loss is shown schematically in Figure 14.20[36].

The working frequency of a Faraday isolator, which in general should have a low attenuation, is chosen near the minimum of the loss curve, assuming this is, in fact, clearly marked. At low frequencies relatively high losses may sometimes occur, even at the minimum, so in this case it is better to choose the working frequency above resonance.

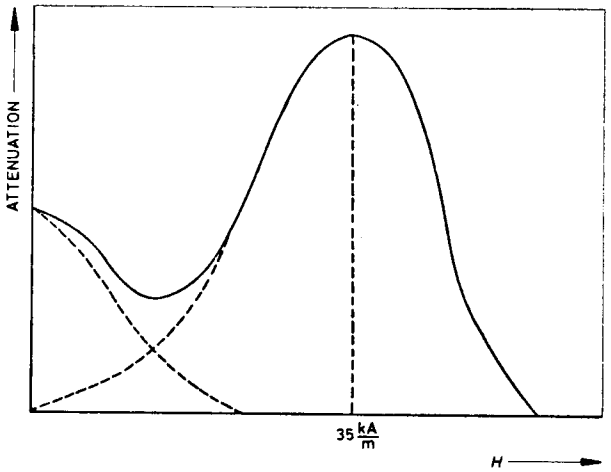



*Figure 14.20. Measured attenuation of a cylindrical ferrite rod used at 4* GHz *in a Faraday rotator*[36]

### 14.4.6.1 Initial losses

Without premagnetisation, all ferrites exhibit an increase in the loss factor $\tan \delta_\mu$ or in the imaginary part $\mu''$ of the permeability as the frequency is increased. After passing a maximum $\mu''$ falls off again, as is shown in Figures 13.119, 13.120, 14.21, and 14.22[104]. Snoek[81, 82], as far back as 1947, indicated that this was an effect of gyromagnetic resonance.

The losses occurring with a non-orienting direct field are distinguished from those which occur through resonance in saturated ferrite by the facts that, in general, they show a broad maximum and they are, moreover, reciprocal. They therefore act in the same way on forward and on reflected

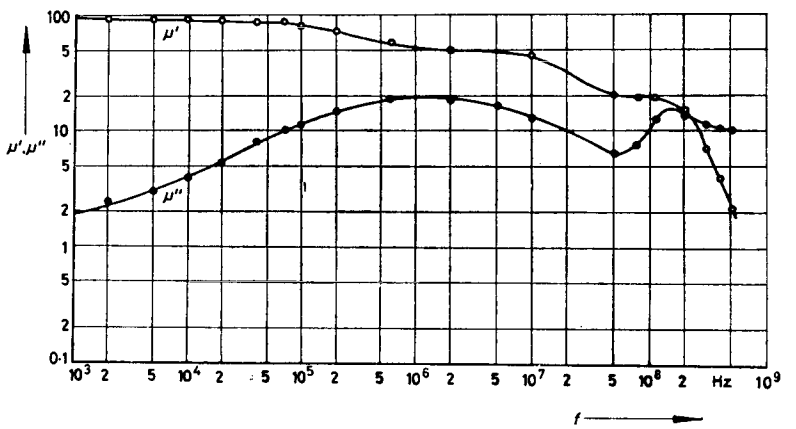



*Figure 14.21. Yttrium–iron garnet* $Y_3Fe_5O_{12}$*; frequency curves of real and imaginary parts,* $\mu'$ *and* $\mu''$*, of the permeability*[104]

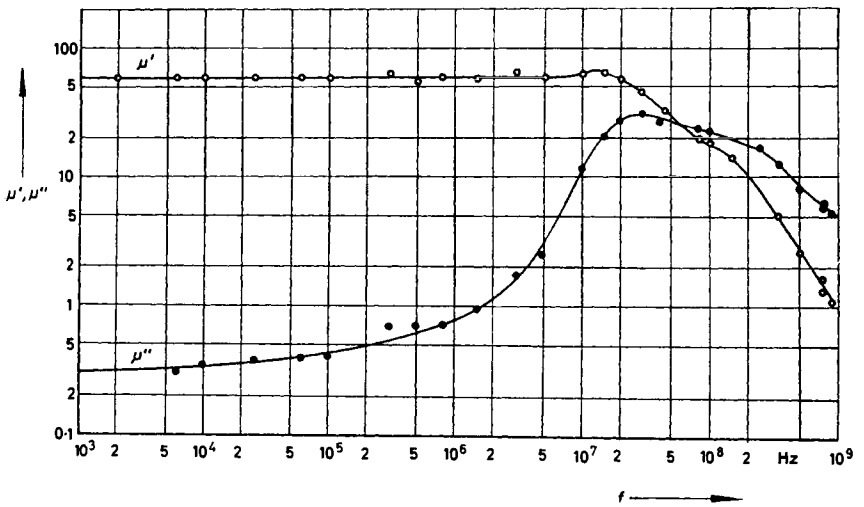



*Figure 14.22. Substitution yttrium–iron garnet* $Y_{2\cdot998}Ca_{0\cdot002}Fe_5O_{12}$*: frequency curves o* $\mu'$ *and* $\mu''$[104]

waves. Accordingly, zero-field losses make it difficult to use isolators at low frequencies.

The suspected origin of initial loss lies in the simultaneous presence of bivalent and trivalent ions of the same element. The initial loss falls off with rising field strength (see Figure 14.20). This fact seems obviously to be related to the gradual disappearance of Bloch-wall movements, although these do not explain the anisotropy actually observed[23]. At magnetic saturation the initial losses disappear.

The loss curve found at resonance field strength is also narrower with respect to frequency than the curve observed at low field strengths. This is obvious in Figure 14.23[3], where $\mu''$ is plotted against frequency for a nickel ferrite (Ferroxcube 4A). Curve 1 is for the case where no static field was applied, and curve 2 for a direct field of 4 kA/m. The point of maximum loss shifts from 5 MHz to 5 GHz.

The initial losses can be reduced by lowering the saturation flux density of the ferrite. This can be achieved by, for example, replacing part of the iron ions by aluminium ions[102]. Figure 14.24[36] shows, for a magnesium ferrite having some added manganese, how rotation and loss alter in respect to field strength with falling saturation density. The drop in initial loss is striking —but of course it does not disappear entirely. This is connected with the fact that, in individual ferrite grains, microscopic saturation-moments may still exist which are sometimes 10–20% greater than the macroscopic moments. This can be traced back to the fact that the ferrites are not usually sintered to maximum density. Kittel's equation takes only macroscopic saturation into account. By means of aluminium substitution, it was found that the Faraday rotation in relation to attenuation could, for example, be improved from 10°–20°/dB up to 500°/dB[102].

The lowest working frequency of an isolator is determined, apart from

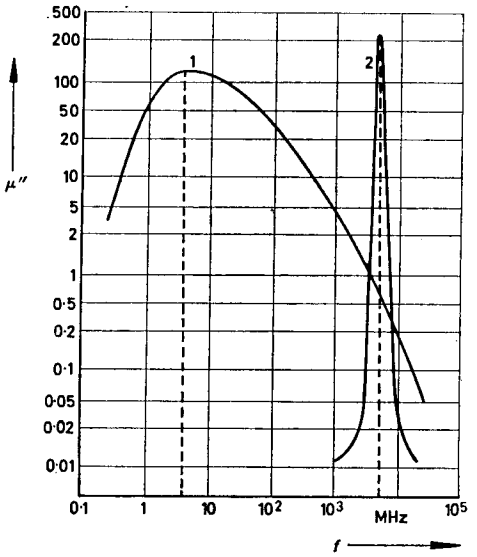



*Figure 14.23. Resonance curves of the ferrite Ferroxcube 4A plotted against frequency: 1, external magnetic field $H = 0$; 2, $H = 4$ kA/m³*

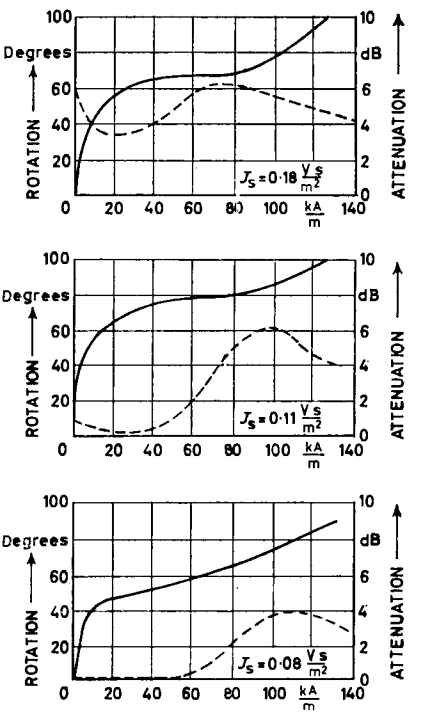



*Figure 14.24. Rotation and attenuation of longitudinally magnetised ferrite cylinders with different values of saturation $J_s$ measured at 4 GHz in a circular waveguide; rotation is shown by the solid line and losses by the broken line*[36]

saturation magnetisation, by the anisotropic field strength $H_a$ of the ferrimagnetic material. Anisotropy can be kept low by choice of a suitable composition. This can be achieved, for example, in manganese or nickel ferrite by an admixture of cobalt ferrite since the crystal anisotropy of the cobalt ferrite is positive and that of the other ferrites negative. By mixing the two kinds, ferrite mixtures can be produced with the desired degree of crystal anisotropy.

The problem of initial loss will be illuminated by an example due to Hogan[36]. For a ferrite having an anisotropic field strength $H_a = 32$ kA/m and for which $J_s = 0{\cdot}2$ V s/m$^2$ and $M_s = 160$ kA/m, high losses occur, when there is no direct field, in the frequency range between $\gamma H_a$ and $\gamma(H_a + M_s)$, i.e. between 1120 MHz and 6720 MHz.

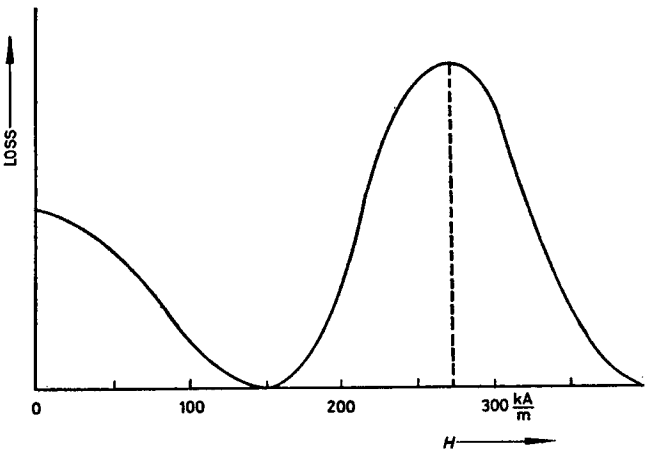



*Figure 14.25. Measured attenuation as a function of field strength for the ferrite of Figure 14.20; here however the ferrite is used in the form of a disc mounted coaxially in a circular guide or as a strip in a rectangular guide arranged as in Figure 14.27b*[36]

In a magnetised ferrite cylinder, resonance occurs at 4 GHz for $H = 35$ kA/m (see Figure 14.20), which is only slightly above the anisotropic field strength $H_a$. If $J_s$ is lowered, for example to 0·072 V s/m$^2$, then ferrimagnetic resonance occurs in a long ferrite cylinder, as soon as it is magnetised, at 1 GHz. If, however, instead of the ferrite cylinder a disc of the same material is used, to which the above values apply ($H_a = 32$ kA/m, $J_s = 0{\cdot}2$ V s/m$^2$), and if it is magnetised in the axial direction, then the formula which holds for the resonance (equation 14.13) may be written in the following form:

$$H_z = \frac{\omega}{\gamma} + M_s \tag{14.15}$$

The resonance field strength at 4 GHz comes to:

$$H_z = (115 + 160)\ \text{kA/m} = 275\ \text{kA/m}$$

Since the material is saturated at 160 kA/m the initial losses have completely disappeared before resonance appears. The total attenuation thus exhibits the type of curve shown in Figure 14.25.

The same ferrite can be used with advantage in a waveguide in the form of a thick disc but is unsuitable as a long magnetised cylinder.

According to equation 14.8 the rotation of the plane of polarisation is greater the higher the saturation magnetisation of the ferrite. If this saturation magnetisation is greatly reduced, then, in order to achieve the same rotation, the ferrite element must be so enlarged that it may cease to be acceptable practically.

### 14.4.6.2 Linewidth

Low loss in the pass range and high loss in the stop range are requirements imposed on ferrites which are to be used as resonance-absorption isolators. Experience shows that the pass (or forward) loss is low if the width of the resonance curve, the so-called half-width or linewidth $\Delta H$ is small. Values between 1 kA/m and 200 kA/m for linewidths are quoted in the literature. They depend on ferrite composition, ferrite structure (porosity), manufacturing procedure, and, for single crystals, on crystal direction. Values for polycrystalline spheres measured at room temperature are given in Table 14.5[111].

The linewidth for a polycrystalline ferrite is mostly of the same order of magnitude as the effective crystal-anisotropy field. This is about 40 kA/m for nickel ferrite, for example. A very low linewidth was found for a lithium ferrite single crystal, namely $\Delta H = 70{\cdot}7$ A/m at 5·4 GHz and 139°C. At the same frequency, $\Delta H$ was 134·4 A/m at room temperature[70a]. Materials with low crystal anisotropy are particularly suitable, as are single crystals,

**Table 14.5** LINEWIDTH OF POLYCRYSTALLINE FERRITES MEASURED AT 24·164 GHz AND AT ROOM TEMPERATURE[111]

| *Ferrite* | *Linewidth* $\Delta H$ (kA/m) | $g_{ett}$ |
|---|---|---|
| $MgFe_2O_4$ | 82·4 | 2·01 |
| $MgFe_2O_4$ | 69·6 | 2·04 |
| $NiFe_2O_4$ | 41·6 | 2·18 |
| $CoFe_2O_4$ | Very broad | — |
| $Mn_{0·2}Zn_{0·8}Fe_2O_4$ | 41·6 | 2·005 |
| $Mn_{0·3}Zn_{0·7}Fe_2O_4$ | 36·4 | 2·005 |
| $Mn_{0·4}Zn_{0·6}Fe_2O_4$ | 37·2 | 2·01 |
| $Mn_{0·46}Zn_{0·54}Fe_2O_4$ | 54·8 | 2·02 |
| $Mn_{0·52}Zn_{0·48}Fe_2O_4$ | 44·0 | 2·01 |
| $Mn_{0·8}Zn_{0·2}Fe_2O_4$ | 134·0 | 2·07 |
| $Mn_{0·9}Zn_{0·1}Fe_2O_4$ | 101·0 | 2·07 |
| $MnFe_2O_4$ | 49·4 | 2·02 |

for use at low frequencies. Materials distinguished by especially low crystal anisotropy are the garnets (see page 569). At room temperature a linewidth of 4 kA/m[16] for an yttrium–iron garnet was measured at 3 GHz, and less than 80 A/m [84] at 9·3 GHz. If a forward attenuation of 0·5 dB is acceptable then, for a halfwidth of 8 kA/m, 2 GHz can be taken as the lowest usable frequency for a Faraday isolator[44].

The linewidth is temperature and frequency sensitive. Figure 14.35 shows, for example, the temperature variation of $\Delta H$ for single crystals and for polycrystalline Mn–Zn ferrite; Figure 14.46 shows the same thing for single crystals of Ni–Fe ferrite, and Figure 14.47 shows it for an yttrium–iron garnet. In general, the linewidth increases with rising frequency. This increase is itself dependent on temperature, as is shown by the example of a manganese ferrite dealt with in Figure 14.45.

The linewidth can be influenced by suitable additives: the resonance line of a manganese ferrite was broadened by the addition of cobalt[94], while a cobalt substitution brought about a reduction of linewidth in a Ni–Al ferrite[57]. The different action of additives can frequently be attributed to structural changes in the ferrite. The presence of pores, for example, broadens the lines even of densely sintered ferrites[78].

### 14.4.6.3 Effect of power loss

In choosing the most suitable composition for a ferrite which is to operate in a given range, an important point must be borne in mind: a ferrite which is particularly suitable for a power of, say, 50 mW may sometimes be almost unusable at higher powers. Figure 14.26 offers a typical example[76]. It shows the attenuation of the positive circularly polarised wave for peak input powers of 10 kW and 100 kW as a function of the direct field. The resonance

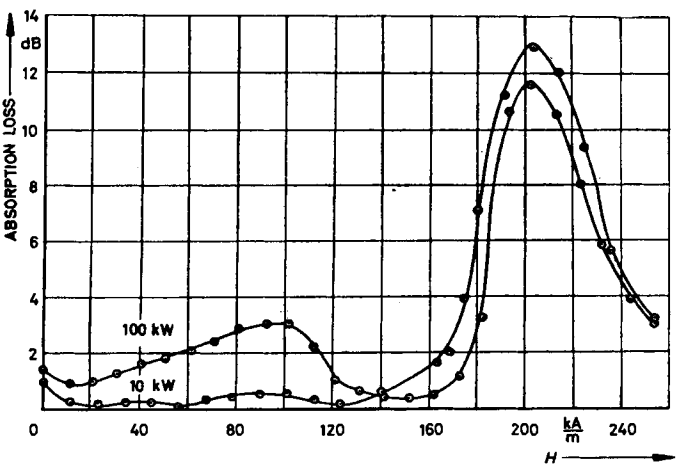



*Figure 14.26. Absorption loss for positive circularly polarised waves in a circular guide as a function of field strength; measurements at 9·4* GHz *using a ferrite cylinder 25* mm *long and 5·6* mm *in diameter*[76]

peaks are lower at the higher power, and at half the resonance field strength an auxiliary peak is formed.

By systematic investigation of Mn–Mg ferrites of various compositions, Sakiotis, Chait, and Kales[76] were able to develop ferrites which behaved particularly well at, say, a peak power of 100 kW. Such ferrites contained 5% MnO and 50–80% MgO.

According to Pringle and Hepburn[69], ferrites having broader resonances are to be preferred at higher powers, particularly at higher temperatures, because of the heating up of the ferrite—which in any case narrows the linewidth. The ferrite $NiAl_{0.12}Fe_{1.88}O_4$ is characterised by a high Curie temperature and a broad resonance line, so it is suitable for high-power operation (see Table 14.3). A ferrite having the composition $Mg_{0.9}Mn_{0.1}Fe_{1.6}O_{3.4}$ is recommended for low powers and a broad-band transmission while, if the frequency band is narrow, the ferrites $Mg_{0.55}Mn_{0.45}Fe_{1.33}O_3$ and $Ni_{0.975}Co_{0.025}Fe_2O_4$ have the advantage.

Thourel[97] established that the shape of the attenuation curve for the positive circularly polarised wave depends on the type of ferrite used. Linewidth and height of resonance can vary within wide limits for individual ferrites.

### 14.4.7 Isolators working on Faraday-absorption and resonance-absorption principles

The principal features of the two most important types of isolator may be restated thus: isolators based on resonance absorption have ferrite elements in strip form magnetised at right angles to the direction of propagation of the microwaves (see Figure 14.2); in contrast, the Faraday isolator carries cylindrical ferrite rods magnetised along their length and parallel to the direction of propagation. In rectangular guides it is necessary to insert a length of circular section.

There should be only a small absorption in the Faraday isolator; in the absorption isolator the absorption should be as low as possible only in the forward direction while in the reverse direction the waves should be as completely absorbed as possible. Where the Faraday effect is utilised, the precession frequency $\omega_p$ must not approach $\omega$ too closely, while in resonance absorption $\omega_p$ should not differ greatly from $\omega$. The Faraday effect is suitable for use in low-intensity fields since the rotation is relatively large for weak fields and losses are low. On the other hand, this implies a greater sensitivity to disturbance by nearby stray fields. Further, the Faraday arrangement is better suited to high than to low frequencies.

In resonance-absorption isolators the reflected wave must be absorbed by the ferrite. Where large powers are involved considerable heat is developed. It is thus important to ensure that the heat is conducted away by a good contact between strip and waveguide: under some circumstances artificial ventilation must be introduced to carry away the heat. A difficulty with absorption resonators at high frequencies is that the necessary high direct field can no longer be produced by permanent magnets. Thus in an arrangement like that of Figure 14.27a, having a ferrite element for which $J_s = 0{\cdot}3$ V s/m$^2$, a field strength of 1480 kA/m is needed for a frequency of 56 GHz[36].

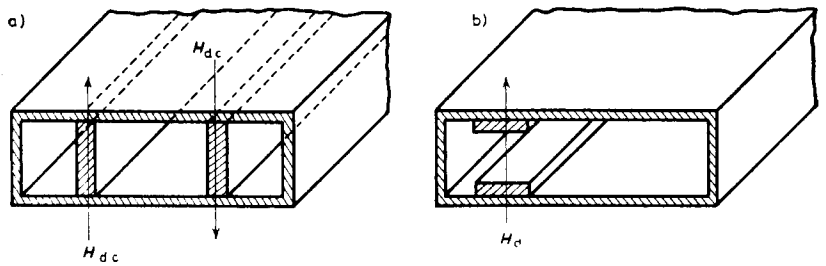



*Figure 14.27. Ways of arranging ferrite elements in rectangular waveguides*[36]

### 14.4.8 Arrangement of ferrite elements in the waveguide

In circular-section guides the ferrites are, in general, cylindrical rods lying in the axis of the guide. As shown above, it is sometimes preferable to mount a ferrite disc coaxially in the waveguide instead of as a cylinder. In either case the elements are given dumb-bell shaped ends of dielectric material (or else the cylinder is pointed) in order to keep reflection low. PVC foam, for example, may be used for fixing.

In a rectangular waveguide, ferrite strips can be mounted directly in a piece of tube of the same profile, as sketched in Figure 14.2, for example: the small ferrite plate is mounted at a distance $x_1$ from the axis in such a way that the broadest face is parallel to the direction of propagation. The direction of the magnetisation $H_z$ is perpendicular to the direction in which the waves are propagated and to the broader side of the guide. The distance $x_1$ must be so chosen that the magnitude of the alternating fielddoes not change periodically, owing to the passage of the waves, but changes only its direction, i.e. so that the magnetic vector rotates. The lines of magnetic force are drawn in Figure 14.2a. On the left is shown how the field vector rotates through 360° as it sweeps past at a distance $x_1$. At the right of the same diagram and at the same distance $x_1$, where the field vectors have the opposite sense of rotation, a ferrite strip is indicated. The direct field must therefore be applied in this case in the opposite direction (see Figure 14.27a). It is possible to mount ferrite strips at both locations having left–right symmetry with respect to the central axis of the guide and in this case, if the direct fields are oppositely directed, the attenuating action will be doubled. It is not necessary that the strips occupy the full height of the guide as shown in Figure 14.27a; it is even preferable, on various grounds, that they be shorter. For example, having regard to the need to remove heat, the arrangement of Figure 14.27b is to be preferred, especially when high powers are involved and high energy losses are to be conducted away.

The phase rotation also depends on the separation $x$. Figure 14.28 shows measured values of phase-shift between forward and reflected waves in a waveguide 22·5 mm×10 mm designed for 9·5 GHz. It is clear from this figure that the phase rotation is greatest at a wall-separation of about 13% of guide-width. For thinner strips the best location lies nearer the middle of the guide[23]. The relation between strip thickness and phase-shift is shown in Figure 14.19, following Lax, Button, and Roth[47]. If the ferrite strip is

mounted in the middle of the guide, it sometimes produces higher losses than if mounted along the narrow face. The phase-shift, however, is scarcely affected. Sakiotis and Chait[75] traced this lowering of loss near the wall of the waveguide to reduced dielectric losses in the region of low field strength.

Steinhart[88] stated that the best arrangement of ferrite in a rectangular waveguide was when the face of the strip and the broad face of the guide were parallel. The large area of the strip should thus lie in the *H* plane; however, the ferrite should not lie against the wall but should be disposed equidistantly from the large face of the tube, i.e. it should be symmetrically mounted. In the arrangement of Figure 14.2 the forward attenuation $\alpha_f$ is minimum. Experience shows, however, that the maximum reverse absorp-

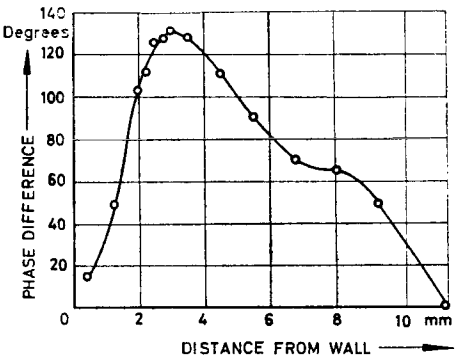



*Figure 14.28. Measured non-reciprocal phase-shift in a rectangular waveguide; f = 9·5* GHz*; H = 72* kA/m*; section of guide 22·5* mm×*10* mm*; ferrite strips of Ferramic 1331, 10* mm *high and 0·9* mm *thick*[23]

tion $\alpha_r$ does not coincide with the position of minimum forward attenuation (see Figure 14.29).

In Figure 14.27a the ferrite strips have the same height as the waveguide. This, however, brings about increased forward losses and the field can never be fully circularly polarised, so the attenuation ratio, $\alpha_f/\alpha_r$ is not satisfactory. The height of the strips is therefore reduced in many arrangements[11, 75, 88]. In these cases it becomes desirable to narrow the waveguide so that the strips can be magnetised by means of permanent magnets having air-gaps as small as possible[59].

As an actual example of a resonance-absorption isolator, the forward and reverse attenuations are plotted in Figure 14.29 as a function of the displacement of the ferrite from the guide-wall for a waveguide 7 mm×58·2 mm[11]. The measurements of the strips were 70 mm×4 mm×1·5 mm, and they were made of a Mg–Mn–Al ferrite. The measuring frequency was 4 GHz. The attenuation curve of an individual strip is shown by the solid line, and the broken lines give the attenuation values for the case in which, alongside the ferrite strip, a ceramic strip of similar size was mounted. By this means the reverse attenuation can be increased by 60–70% while the forward attenuation is scarcely affected. A further increase in attenuation ratio can be achieved if a second ferrite–ceramic strip is mounted in a similar position relative to the opposite wall of the waveguide. The return attenuation is increased 3·5 fold compared with the original single-strip case.

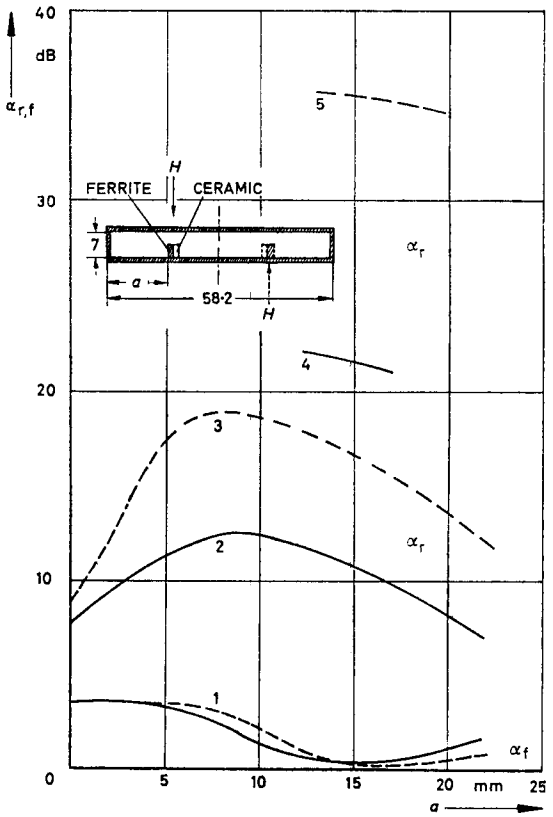



*Figure 14.29. Dependence of attenuations $\alpha_f$ and $\alpha_r$ on the arrangement of the ferrite strip in a waveguide ($f = 4$ GHz): 1, individual strips without ceramic (solid line) and two symmetrical strips with ceramic (broken line); 2, individual strips without ceramic; 3, individual strips with ceramic; 4, two symmetrical strips without ceramic; 5, two symmetrical strips with ceramic*[11]

Attenuation curves, all for the same ferrite and for optimum positioning but for different mounting arrangements, are plotted in Figure 14.30 as functions of the external magnetic field. The example refers to a ferrite for which $T_c = 225°C$, $B_s = 0{\cdot}15$ V s/m$^2$, $\varepsilon = 12\varepsilon_0$, $\mu_i = 26\mu_0$, $\varrho = 10^9\ \Omega$ cm and linewidth = 10 kA/m[11].

### 14.4.9 Bandwidth of an isolator

Optimal positioning of a ferrite strip in a rectangular waveguide involves a compromise—not only because the best position differs for forward and reverse transmission (Figure 14.29), but also in the matter of frequency. The transmitted frequency band can be determined by the interplay of various factors: geometry of the tube, dimensions of the ferrite, arrangement of the ferrite in the guide, and the properties of the ferrite itself.

According to Rowen[74], a Faraday rotator can be made broad-band if the ferrite is surrounded by a dielectric. An improvement in the angle of rotation can also be achieved in this way. According to Loss[52], an improved bandwidth can be achieved in a Faraday isolator by mounting two cylindrical ferrite rods, one behind the other, and magnetising them in opposite directions. In addition, the rods should have different diameters or else should be

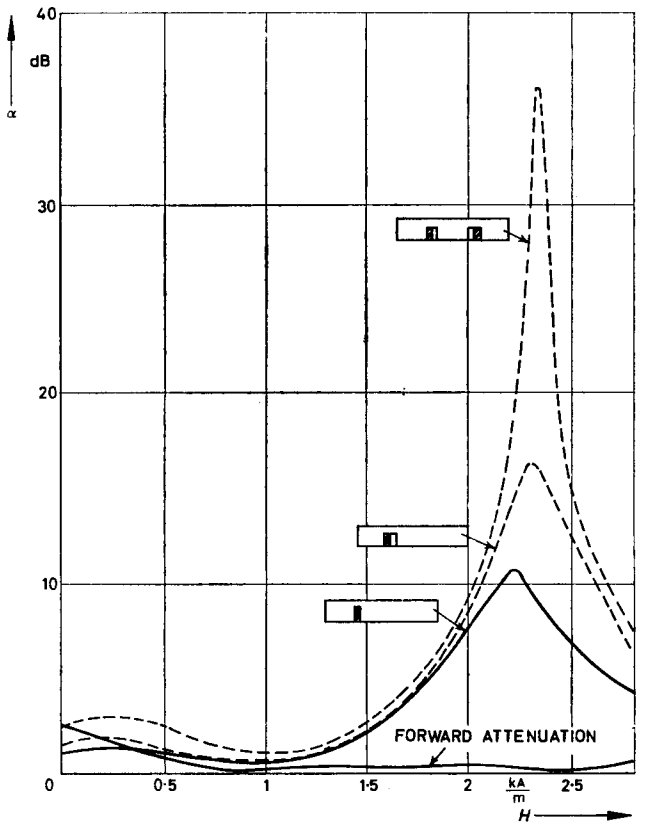



*Figure 14.30. Attenuation of optimally disposed ferrite–ceramic strips in a rectangular guide as a function of field strength ($f$ = 4 GHz)*[11]

made from different types of ferrite. Arrangements comprising two ferrite discs and one rod have also been recommended[44].

Steinhart[88] found that, where ferrite strips have their broad face parallel to the broad face of the guide (and therefore to the magnetic field), the absorption was relatively broad-band compared with the case where the strip is along the narrower face. Kales[39] proposed another arrangement: the circular guide is provided with two pairs of mutually perpendicular ribs, a device which greatly reduces the dependence of rotation on frequency (see Figure 14.31).

It goes without saying that the bandwidth of the isolator is also related to

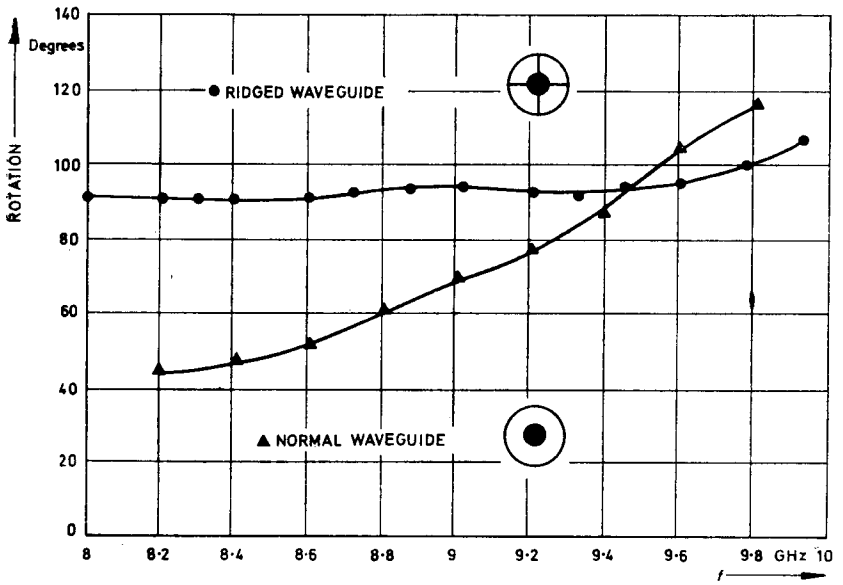



*Figure 14.31. Faraday rotation for a normal circular waveguide and for an arrangement proposed by Kales (ribbed guide) as a function of frequency*[39]

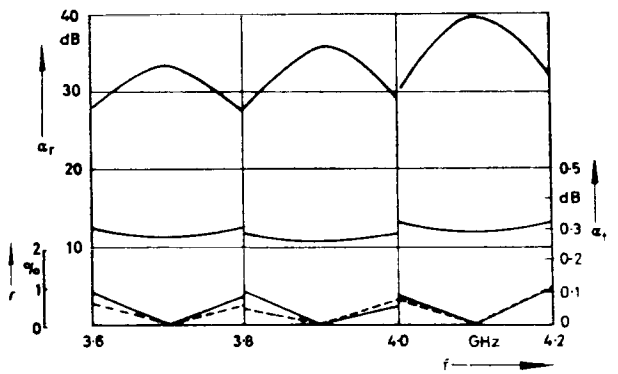



*Figure 14.32. Frequency characteristics of attenuations $\alpha_r$ and $\alpha_t$ together with reflection factors r for isolators; plotted in each case over a 200* MHz *bandwidth*[11]

that of the ferrite itself. Suppliers have therefore tried to develop particularly broad-band ferrites[88].

Figure 14.32 shows the measured frequency curve of attenuation for a 4 GHz isolator arranged in accordance with Figure 14.30[11].

### 14.4.10 Effect of temperature

Saturation polarisation falls with rising temperature. In order to retain an acceptable reverse loss at high temperatures, the premagnetisation field strength must be raised (equation 14.10). Change of saturation flux density

is greater in the vicinity of the Curie temperature than at appreciably lower temperatures, so ferrites with high Curie temperatures are less sensitive to temperature effects. This is made clear by the examples of Figures 14.33 and 14.34[79], which show measurements at 8·9 GHz on two different ferrites in a rectangular waveguide whose internal dimensions are 22·5 mm×10 mm. Specimens 0·25 mm and 0·27 mm thick were mounted at a distance of 6 mm from the narrow face of the guide.

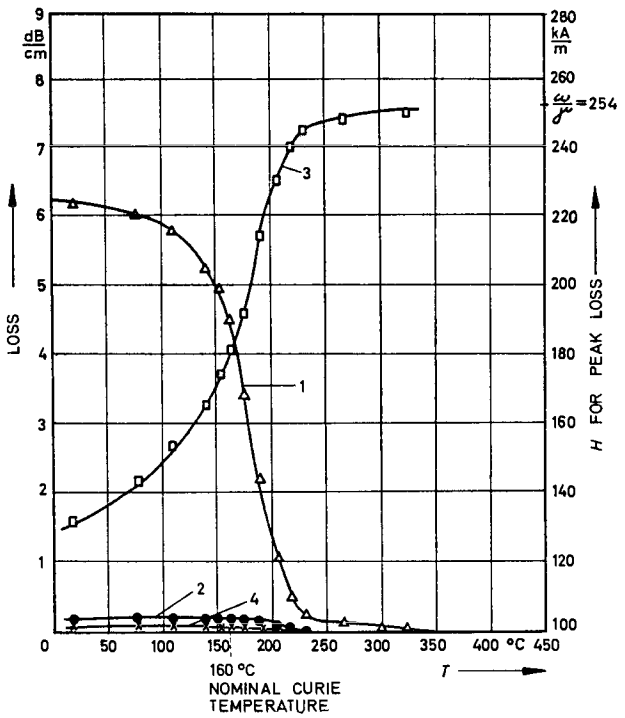



*Figure 14.33. Peak values of forward and reverse attenuation (together with direct field corresponding to peak value) and dielectric loss, as functions of temperature for 0·25* mm *strips of Ferramic G in a rectangular guide 22·5* mm×*10* mm *(ferrite-to-wall spacing 6* mm*; f = 8·9* GHz*): 1, peak reverse magnetic loss; 2, peak forward magnetic loss; 3, necessary field for optimum reverse loss; 4, dielectric loss (0·04* dB *or less)*[79]

The reverse attenuation for a material (Ferramic G) having a nominal Curie temperature $T_c$ of 160°C is plotted in Figure 14.33: $\alpha_r$ is very high but falls quickly above room temperature—and at an increasing rate—to a low value. The reverse attenuation of the basic material of Figure 14.34 (Ferroxcube 104), which has a Curie temperature of 385°C, is relatively low at room temperature. However, it continues to rise with increasing temperature and does not fall off again before 300°C. The isolator becomes better at higher temperatures since forward loss and dielectric loss show no temperature effects to speak of.

At the Curie temperature, $M_z$ of equation 14.11 becomes zero, so $H_{eff} = H_z$.

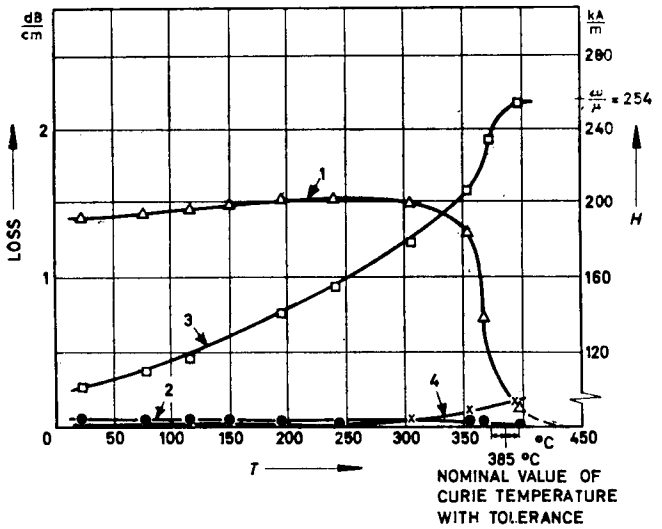



*Figure 14.34. Peak value of forward and reverse attenuation (together with direct field corresponding to peak value) and dielectric loss, as functions of temperature for 0·27* mm *strips of Ferroxcube 104 (position of specimen and measuring conditions as for Figure 14.33): 1, peak reverse magnetic loss; 2, peak forward magnetic loss; 3, necessary field for optimum reverse loss; 4, dielectric loss*[79]

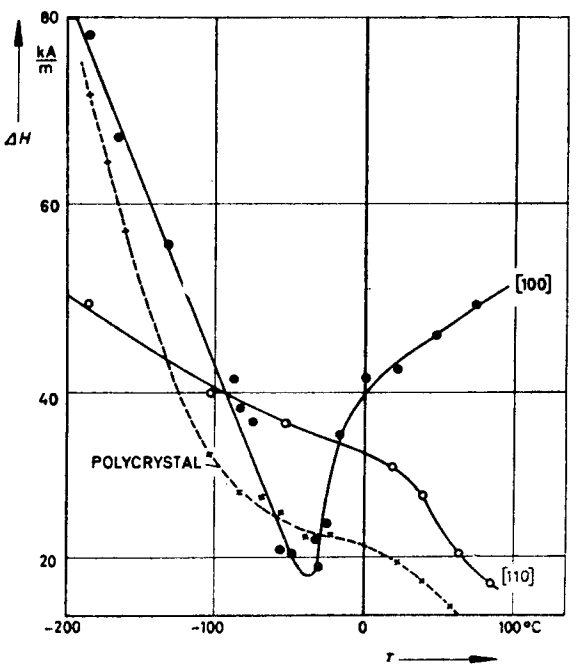



*Figure 14.35. Linewidth of* $MnO \cdot ZnO \cdot 2Fe_2O_3$ *as a function of temperature: broken line, polycrystalline specimen; solid line, single crystal in the [110] and [100] directions*[62]

Therefore at $f = 8{\cdot}9$ GHz, according to equation 14.9, $H_z = 254$ kA/m. This figure agrees well with the end-value reached by the curves $H = f(T)$ in Figures 14.33 and 14.34. (That the end-value is reached at a somewhat higher temperature than the Curie temperature given may be a matter of the way the Curie temperature is defined: at the true Curie temperature ferrimagnetic resonance disappears in any case.)

The initial loss also falls with rising temperature. For the types of ferrite which form the basis of Figures 14.33 and 14.34 it disappears at 100°C or between 145°C and 248°C[79].

It is clear from Figure 14.35 that the linewidth $\Delta H$ of a polycrystalline material falls with rising temperature. For many ferrites, however, $\Delta H$ rises again above a certain temperature[22, 93]. A decrease in phase-shift and Faraday rotation was observed at 9 GHz for the ferrite Ferramic R1 used in a circular-section guide[22].

The temperature sensitivity of an isolator can be much reduced, and even brought to vanishing point, by suitable dimensioning of the ferrite[9, 28]. According to Boronski[9], ferrite rods of triangular section gave good constancy of $H_{\text{eff}}$ between 20°C and 300°C. In order to compensate for the effect of temperature on the permanent-magnet system of an isolator, a temperature-sensitive magnetic shunt can be used, as proposed, for example, by Deutsch and Haken[18] for a 4 GHz isolator.

## 14.5 MATERIALS

Two types of magnetisable material are used for the non-reciprocal components of microwave technology: a permanent-magnet material to set up the powerful direct magnetic fields required, and high-frequency ferrites to act on the electromagnetic waves. What is mostly demanded from permanent magnets is a high energy-product so that the component can be kept small, and high constancy in respect of time and temperature. Müller[60] and Steinhart[89] carried out fundamental investigations into the problem of optimal dimensioning. However, this is not the place to discuss the properties of magnets since they have been dealt with in Chapter 9.

The properties of ferrites measured at low frequencies are often—as previous sections have emphasised—in many ways quite different from those which apply at very high frequencies. The following are the most important requirements laid down for microwave ferrites:

1. The ferrites should be of high density (ferrite strips moulded from dust with the help of a binding matrix generally show very high losses[23]).
2. The saturation magnetisation must satisfy the resonance conditions $M < \omega/\gamma$.
3. The specific electrical resistance should be as high as possible and, in general, should not lie below $10^6\ \Omega$ cm.
4. The Curie temperature should be as high as possible and, in general, should not be less than 150°C.

To these requirements must be added the usual engineering and commercial considerations: good reproducibility and easy working.

### 14.5.1 Mg–Mn ferrites

Ferrites containing magnesium lend themselves particularly well to microwave applications by reason of the very high specific electrical resistance ($10^8$–$10^{10}$ Ω cm) of magnesium ferrite. Because of this high resistance, electromagnetic waves of very high frequency can penetrate into the body of the material. Albers-Schoenberg[1] was able to show that good microwave prop-

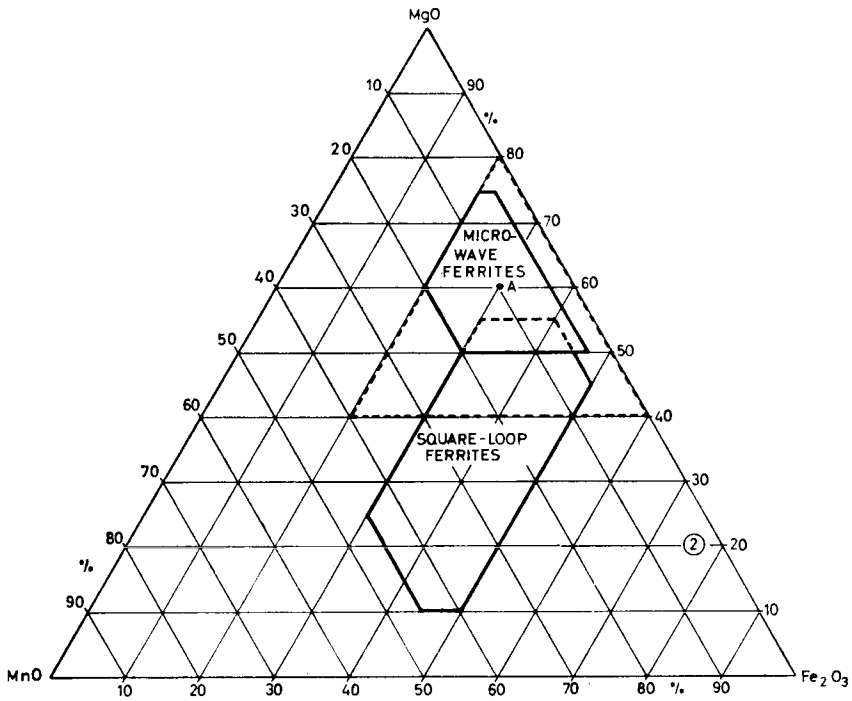



*Figure 14.36. Three-component diagram of* MgO–MnO–$Fe_2O_3$ *system with the most important ranges of application*[1]

erties were to be found particularly in the three-component system MnO–$Fe_2O_3$–MgO. The best-adapted compositions are defined in Figure 14.36. Those ferrites lying within the limit-lines have been made by many methods and in many variations and have been well investigated. One may consider the work of Fresh[24], Ljung[50], Roberts[71], Sakiotis and Chait[75], Standley and Peters[86], and Van Uitert, Schafer, and Hogan[102]—to name but a few.

Ljung[50] investigated a ferrite series within a range of composition enclosed by the broken line of Figure 14.36. A few important results of this work will be given. Measurements were carried out at 9·525 GHz in a round-section waveguide of 22 mm inner diameter. The ferrite specimens used were of cylindrical form, 33 mm long with a diameter of 6·6 mm. The direct magnetic field amounted to about 30 kA/m. Curves of equal Faraday rotation are set

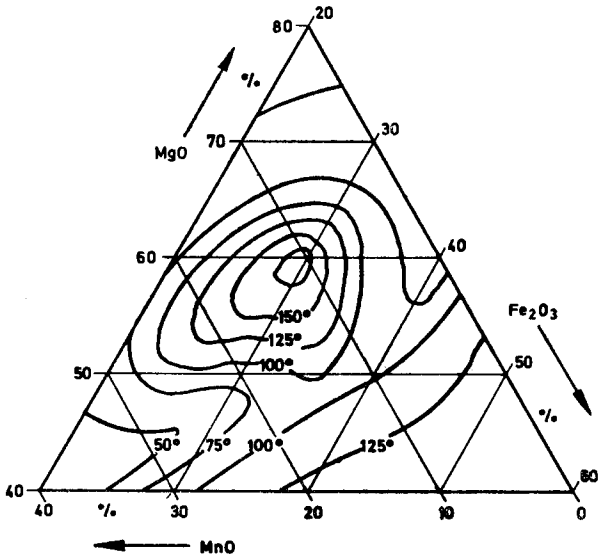



*Figure 14.37. Faraday rotation as a function of composition in the* $MgO–MnO–Fe_2O_3$ *system; measuring frequency 9·525* GHz[50]

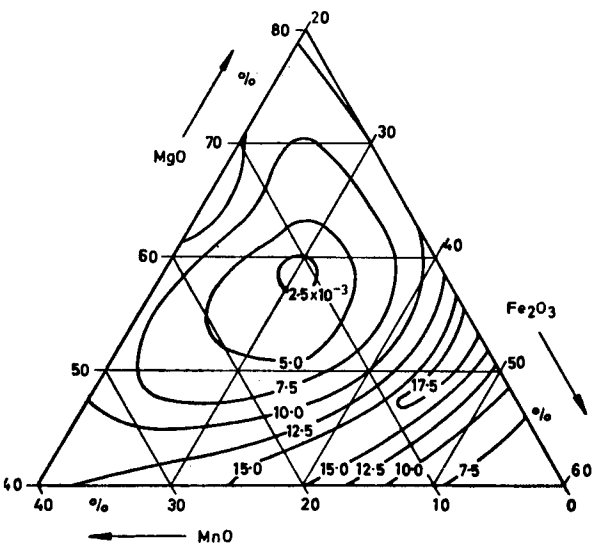



*Figure 14.38. Referred attenuation, measured in* dB/*degree, as a function of composition in the* $MgO–MnO–Fe_2O_3$ *system; measuring frequency 9·525* GHz[50]

out in Figure 14.37. The region of greatest angular shift lies around 60 MgO•10MnO•30$Fe_2O_3$. This composition is labelled A in Figure 4.36. If, for comparison, one looks at the curves of equal referred attenuation, set out in the same way in Figure 14.38, it can be stated that this referred attenuation shows a minimum for almost the same composition, namely a minimum of $2{\cdot}5\times10^{-3}$ dB/degree.

Fresh[24] investigated the Faraday rotation at 9·4 GHz for ferrites having a higher MnO content. With samples sintered at 1350°C, Faraday rotations of 100°/cm were found for 30% MnO and 40–50% $Fe_2O_3$ (see Figure 14.39).

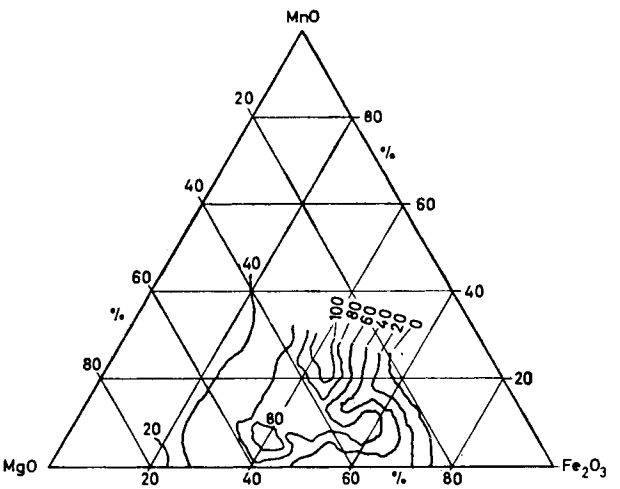



*Figure 14.39. Faraday rotation in degrees/*cm, *for* Mg–Mn *ferrites: sintering temperature 1350°*C*; measuring frequency 9·4* GHz[24]

Standley and Peters[86] investigated at 24 GHz and 35 GHz a ferrite which was polycrystalline but below stoichiometric proportions and contained 45% MgO and 5% MnO. They looked particularly at the effect of sintering temperature on the sharpness of resonance and were able to state that the linewidth fell from 80 kA/m to 40 kA/m if the sintering temperature was raised from 1250°C to 1350°C. Higher-temperature sintering generally brings about reduced porosity and an improvement in homogeneity.

Robinson[73] also found a clearly marked effect of heat treatment on the two Mg–Mn ferrites 61·6MgO•4·2MnO•34·2$Fe_2O_3$ and 49·9MgO•5·5MnO•44·5$Fe_2O_3$. In order to guard against a build-up of $Fe_3O_4$ it was found desirable to cool the material slowly after sintering.

In magnesium and Mg–Mn ferrites, saturation itself is largely dependent on the cooling rate and on the temperature from which the material is cooled: after a slow cooling, the ferrite $MgO_{0.9}Mn_{0.1}Fe_{1.6}O_{3.4}$ showed a $B_s$ of 0·25 V s/m$^2$; after quenching from 1300°C, however, $B_s$ was 0·29 V s/m$^2$ [69]. The saturation of quenched ferrites can sometimes, therefore, change markedly after being raised in temperature within the waveguide.

### 14.5.2 Mg–Mn–Al ferrites and Mg–Fe aluminates

The above-mentioned Mg–Mn ferrite, $60MgO \cdot 10MnO \cdot 30Fe_2O_3$, can be still further improved if some 2% $Fe_2O_3$ is replaced by the same quantity of $Al_2O_3$. Altering the composition slightly, Ljung[50] produced the ferrite $58MgO \cdot 11MnO \cdot 2Al_2O_3 \cdot 29Fe_2O_3$ and obtained a saturation polarisation $J_s$ of 0·16 V s/m² and a Curie temperature $T_c$ of 280°C. The referred attenuation came to $2{\cdot}1 \times 10^{-3}$ dB/degree. This material can be used with advantage in resonance-absorption isolators working at 9·5 GHz[38].

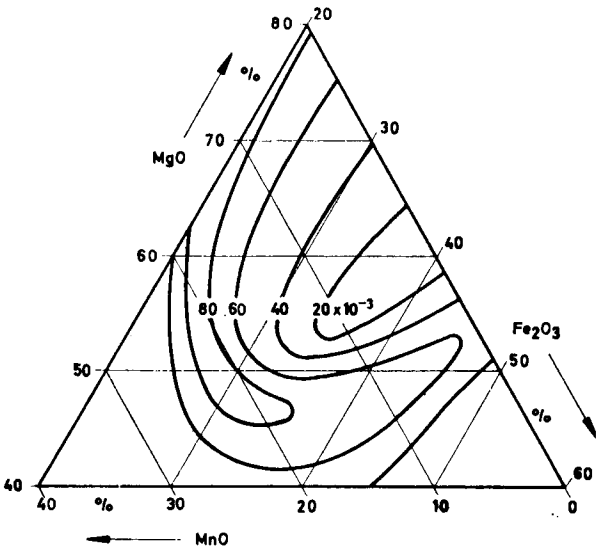



*Figure 14.40. Referred attenuation as a function of composition in the* MgO–MnO–$Fe_2O$ *system; measuring frequency 4·7* GHz[50]

If pure Mg–Mn ferrite is measured at 4·7 GHz in a round waveguide of inner diameter 47 mm (sample 62 mm long and 8·4 mm in diameter), high initial losses are registered and so a substitution of $Al_2O_3$ is to be recommended. This can be seen from the following two examples[50]. With the compositions which yielded the best values at 9·525 GHz (see Figure 14.38), the referred attenuation at 4·7 GHz, in the most favourable case, was $20 \times 10^{-3}$ dB/degree (Figure 14.40); but, on the basis of the aluminate shortly to be discussed (Figure 14.41), a referred attenuation of $5 \times 10^{-3}$ dB/degree is reached, at a direct field of about 20 kA/m, by the composition $50MgO \cdot 1{\cdot}8MnO \cdot 6{\cdot}5Al_2O_3 \cdot 41{\cdot}7Fe_2O_3$. The attenuation of a 45° rotator of this material comes, therefore, to 0·23 dB, a value considered satisfactory for many applications. The saturation polarisation of this ferrite is 0·08 V s/m² and its Curie temperature is 350°C[38].

It is to be expected that the substitution of a larger part of the $Fe_2O_3$ by $Al_2O_3$ should bring about a lowering of the saturation and of the Curie temperature, and this will be illustrated by a few further numerical examples.

**Table 14.6** PROPERTIES OF SOME Mg–Mn–Al FERRITES WITH ROUGHLY CONSTANT PROPORTIONS OF MANGANESE AND MAGNESIUM[32]

| *Composition* | | | | *Final sintering* | $\mu_i$ | $H_c$ | $T_c$ | $J_s$ | $10^3 \tan \delta_\varepsilon$ | $\Delta H$ *at* |
|---|---|---|---|---|---|---|---|---|---|---|
| Mg | Mn | Al | Fe | | ($\mu_0$) | (A/m) | (°C) | (V s/m²) | *at 2004* MHz | *2004* MHz (kA/m) |
| 1·47 | 0·165 | 0 | 2 | 2 h 1300°C, | 41 | 160 | 295 | 0·213 | 0·2 | ~48 |
| 1·47 | 0·165 | 0·25 | 1·75 | slowly cooled | 35 | 176 | 200 | 0·156 | 0·6 | 33·6 |
| 1·47 | 0·165 | 0·325 | 1·675 | 2 h 1350°C, quickly cooled | 38 | 88 | 169 | 0·135 | 0·3 | 14·4 |
| 1·47 | 0·165 | 0·375 | 1·625 | 2 h 1300°C, | 37 | 128 | 142 | 0·131 | 13 | 24·8 |
| 1·47 | 0·165 | 0·5 | 1·5 | slowly cooled | 51 | 64 | 101 | 0·086 | 1·1 | 20 |
| 1·47 | 0·165 | 0·5 | 1·5 | 2 h 1300°C, quickly cooled | 28 | 152 | 83 | 0·075 | 1·1 | 21·6 |
| 1·47 | 0·165 | 0·5 | 1·5 | 2 h 1350°C | 41 | 88 | 94 | 0·087 | 0·5 | 22·4 |

**Table 14.7** COMPOSITION AND PROPERTIES OF SOME Mg–Al–Mn FERRITES[98]

| *Specimen number* | *Composition* | | | | $J_s$ | $T_c$ | $H_c$ | $\mu_i$ | $d$ |
|---|---|---|---|---|---|---|---|---|---|
| | Mg | Al | Fe | Mn | (V s/m²) | (°C) | (A/m) | ($\mu_0$) | (g/cm³) |
| 1 | 1·143 | 0·229 | 1·771 | 0·114 | 0·166 | 215 | 104 | 48 | 4·36 |
| 2 | 1·143 | 0·400 | 1·600 | 0·114 | 0·128 | 145 | 72 | 54 | 4·30 |
| 3 | 1·180 | 0·572 | 1·428 | 0·118 | 0·073 | 70 | 32 | 100 | 4·20 |
| 4 | 1·098 | 0·583 | 1·417 | 0·121 | 0·070 | 64 | 16 | 190 | 4·20 |
| 5 | 1·075 | 0·624 | 1·376 | 0·118 | 0·054 | 51 | 4·8 | 250 | 4·16 |
| 6 | 1·042 | 0·676 | 1·324 | 0·120 | 0·027 | 30 | 0·16 | 302 | 4·14 |

Hickin, Werner, and Sidwell[32] took a ferrite having a nominal metal content of $Mg_{1·47}Mn_{0·167}Fe_2$ and, step by step, substituted aluminium for part of the iron. The values obtained after sintering at 1300°C and at 1350°C are given in Table 14.6: the initial permeability was affected only little, but the Curie temperature, saturation density, and linewidth were greatly reduced by the substitution.

A corresponding series of experiments performed by Van Uitert[98] with a ferrite having a lower magnesium content (and correspondingly lower saturation) is set out in Table 14.7: in the combination $Mg_{1·0}Al_xFe_{2-x}O_4$ the manganese content was held almost constant. The density of these ferrites is relatively high, since the sintering temperature amounted to 1400°C; this high density could not be achieved at a sintering temperature of, say, 1350°C. The initial permeability is also very low ($\mu_i = 40\mu_0$) at a sintering temperature

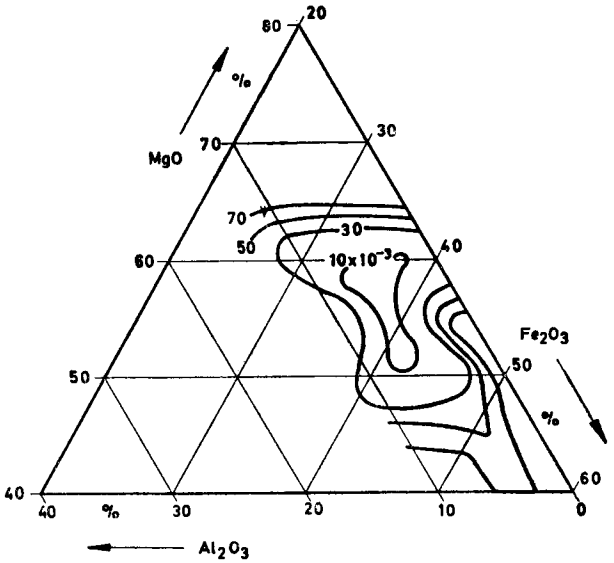



*Figure 14.41. Referred attenuation in the three-component system* $MgO–Fe_2O_3–Al_2O_3$*; measuring frequency 4·7* GHz[50]

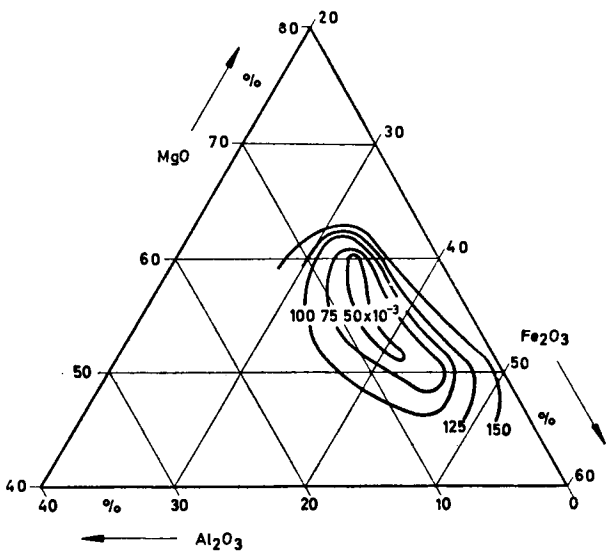



*Figure 14.42. Referred attenuation in the three-component system* $MgO–Fe_2O_3–Al_2O_3$*; measuring frequency 3·0* GHz[50]

of 1350°C, but it rises as the sintering temperature rises and can reach a peak of $600\mu_0$, measured at 100 kHz. The specific electrical resistance of all the samples lay around $10^{10}$ Ω cm.

The low coercivity found in the range of high-permeability compositions points to low crystal anisotropy. Resonances between 160 MHz and 1900 MHz were found for ferrites with the lowest saturation polarisation[91].

It can be seen from Figure 14.41 that the three-component system MgO–$Al_2O_3$–$Fe_2O_3$ with about 4–8% $Al_2O_3$ yields a series of compositions having low referred attenuation. Measured at 4·7 GHz in a round waveguide, values less than $10\times10^{-3}$ dB/degree were found. If 1·8% MgO is replaced by MnO, the attenuation can be halved[50]. Measured at 3 GHz in a waveguide of 69 mm inner diameter (specimen 51 mm in length and 17·5 mm in diameter), the same materials from the three-component system MgO–$Al_2O_3$–$Fe_2O_3$ yielded the referred attenuations shown in Figure 14.42. The lowest value, namely $50\times10^{-3}$ dB/degree, is still so high as to be unsuitable for practical applications. Pure Mg–Al cannot therefore be used in the microwave transmission range of 3–10 GHz.

### 14.5.3 Magnesium ferrite–chromite

Figure 14.43 shows the referred attenuation and Figure 14.44 the Faraday rotation, measured at 3·0 GHz in a waveguide of 69 mm clear width[50], for the three-component system MgO–$Fe_2O_3$–$Cr_2O_3$. With increasing chrome content the Faraday rotation falls and reaches zero at about 25% $Fe_2O_3$. At around 50% MgO and with 15–20% $Cr_2O_3$ there is a region where the referred attenuation is less than $5\times10^{-3}$ dB/degree. A referred attenuation of $2{\cdot}9\times10^{-3}$ dB/degree can be reached for a composition $50MgO{\cdot}35Fe_2O_3{\cdot}15Cr_2O_3$, so a 45° rotator can be made having an attenuation of 0·13 dB. The measurement is based on a direct field of 17 kA/m. The material has its Curie temperature at 170°C and the saturation polarisation is 0·07 V s/m$^2$. It has proved useful not only for Faraday rotators but also for resonance-absorption isolators at 3 GHz and 4·7 GHz[38].

A magnesium ferrite–chromite of composition $50MgO{\cdot}47Fe_2O_3{\cdot}3Cr_2O_3$ with a Curie temperature at 360°C has proved suitable for a field-displacement isolator[38].

### 14.5.4 Manganese ferrites and Mn–Zn ferrites

Tannenwald[93] compared the magnetic performance of low-resistance ($\varrho$ = 10 Ω cm) and high-resistance ($\varrho = 10^4$ Ω cm) manganese ferrites as a function of temperature and measuring frequency. For the low-resistance ferrite measured at 9·15 GHz, he found a small increase in linewidth with temperature and no effect from changing the dimensions of the specimen: on the other hand, the change in linewidth with temperature was more marked at 23 GHz. The effect of the size of the sample (spherical diameter) was also more obvious. The linewidth at room temperature lay between 16 kA/m and 60 kA/m for various specimens. A different behaviour was observed for

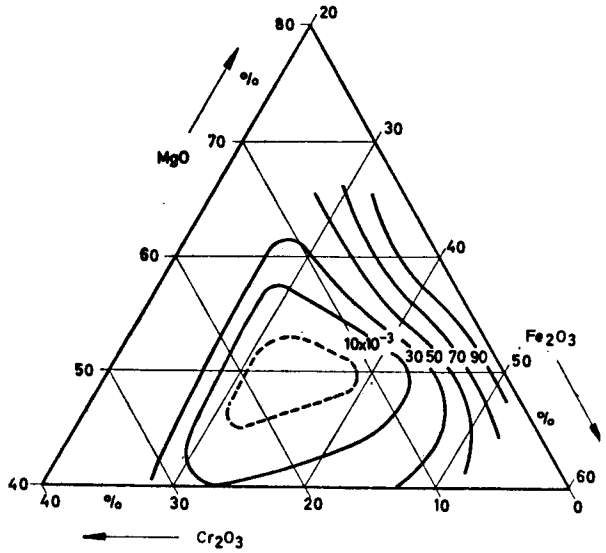



*Figure 14.43. Referred attenuation in the three-component system* $MgO–Fe_2O_3–Cr_2O_3$*: measuring frequency 3·0* GHz[50]

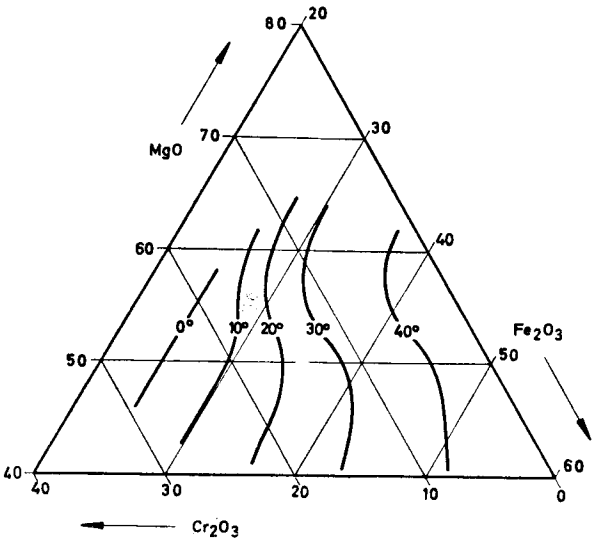



*Figure 14.44. Faraday rotation as a function of composition in the three-component system* $MgO–Fe_2O_3–Cr_2O_3$*; measuring frequency 3·0* GHz[50]

high-resistance Mn–Zn ferrites: if the temperature rose from 0K to 300K, the linewidth dropped from 32 kA/m to between 5 kA/m and 8 kA/m and was smaller at a measuring frequency of 5·6 GHz than at 9·15 GHz and 23 GHz.

According to Tannenwald[93], the linewidth of a manganese ferrite depends on crystal direction, being least in the [100] direction; further, linewidth is frequency sensitive, as is shown in Figure 14.45 for three different temperatures: usually the linewidth rises with increasing frequency, but a minimum could very well also appear between 5 GHz and 6 GHz.

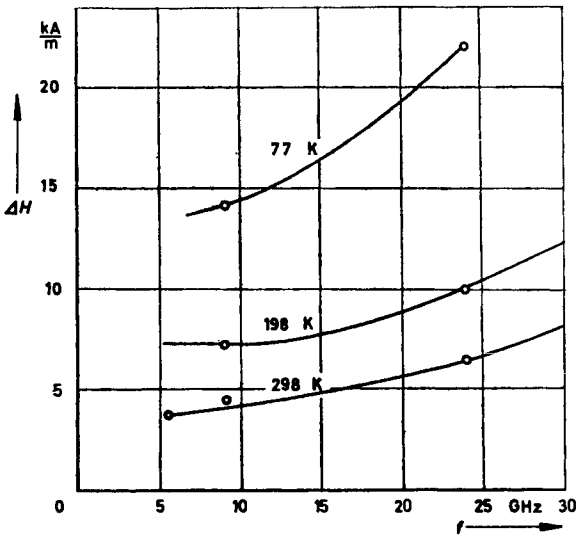



*Figure 14.45. Linewidth of a manganese ferrite as a function of frequency at three different temperatures*[93]

Okamura, Kojima, and Torizuka[62] also established that differences in linewidth occur depending on the crystallographic direction: the linewidths were measured in a single ferrite crystal of composition $MnO \cdot ZnO \cdot 2Fe_2O_3$ in the [100] and [110] directions at a wavelength of 3·22 cm. In the [100] direction $\Delta H$ decreases between $-185°C$ and $-40°C$ and then rises again at higher temperatures; $\Delta H$ falls continuously in the [110] direction, vanishing at the Curie temperature. A polycrystalline disc-shaped sample, 4·5 mm in diameter and 0·22 mm thick, showed a continuous drop in $\Delta H$ with temperature and this was especially steep below $-115°C$ (see Figure 14.35). The absolute values of linewidth were fairly high. The authors trace this to the shape and imperfection of the crystals.

If some of the $Fe_2O_3$ molecules in a pure manganese ferrite are replaced by $Al_2O_3$, then, according to Schulkes, Gorter, and Beljers[77], it is possible to obtain a ferrite of composition $50MnO \cdot 19Al_2O_3 \cdot 31Fe_2O_3$, for example, having a specific electrical resistance of $2 \times 10^6\ \Omega$ cm, a Curie temperature of about 185°C, and a saturation magnetisation $M$ of 92 kA/m. With a thin

plate (60 mm×22 mm×1 mm) of this material, a pass-attenuation of 0·6 dB and a stop-attenuation of 26 dB, i.e. an attenuation ratio of 43, was measured at 4 GHz in a rectangular waveguide.

Teale[94] investigated the influence of a cobalt additive in a manganese ferrite. If, in the combination $Co_xMn_{1-x}Fe_2O_4$, $x$ was given the values 0, 0·02, 0·04, 0·08, 0·10, then a large increase in linewidth was observed in small single crystals. At 20°C and 16·9 GHz the rise in $\Delta H$ per cobalt ion could be 320 kA/m in the [100] direction and 240 kA/m in the [111] direction; $\Delta H$ alters little with temperature, but rises somewhat at temperatures below 150K and shows clear anisotropy.

### 14.5.5 Nickel ferrite and nickel aluminate

The measured results which have been given for nickel ferrite show a clear dependence on measuring conditions, on the shape of the specimen, and on manufacturing procedures. Derry and Wills[17] investigated the connection between sintering temperature, electrical conductivity, and microwave losses for nickel ferrites. For stoichiometric compositions they obtained a Faraday rotation of 45° with a loss of less than 0·2 dB ($f = 9{\cdot}38$ GHz). Lack of oxygen in the ferrite caused a reduction of conductivity and of microwave losses. The lowest losses were observed with a nickel ferrite from which about 0·05% oxygen was removed by sintering at 1330°C.

Yager and co-workers[112] found no marked dependence of linewidth on crystal direction in a single crystal of pure nickel ferrite $NiO \cdot Fe_2O_3$ measured at 24 GHz. Measured values of $\Delta H$ lay between 5·6 kA/m and 6·2 kA/m if the direct field lay in the (110) plane and along the [100] and [111] directions respectively. Later, Yager, Galt, and Merritt[110] found a clear indication of a relation between linewidth and direction for single crystals of the nickel ferrite $(NiO)_{0{\cdot}75}(FeO)_{0{\cdot}25}Fe_2O_3$. Measured at 160K and 24 GHz in the [111] direction, a maximum linewidth was noted that was traced to electron jumps

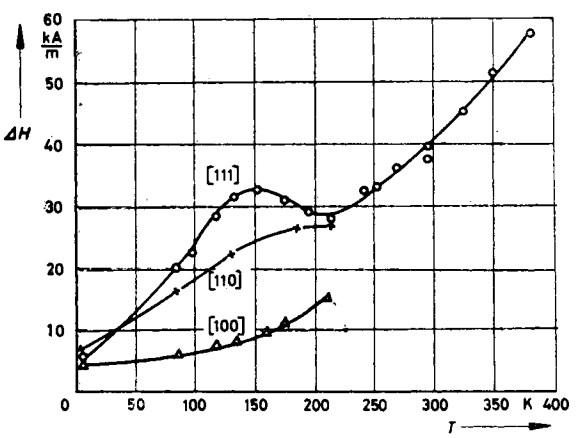



*Figure 14.46. Linewidth, in three crystal directions, of the* Ni–Fe *ferrite* $(NiO)_{0{\cdot}75}(FeO)_{0{\cdot}25}Fe_2O_3$[25]

between bivalent and trivalent iron ions[25]. The curves reproduced in Figure 14.46 were measured on a sphere of 0·23 mm diameter. At 150 K the line in the [111] direction is some four times as broad as in the [100] direction. The increase in linewidth above 200 K is attributed to an increase in conductivity. The specific electrical resistance of the sample amounted to only 1 Ω cm at room temperature. The observed linewidth and linewidth anisotropy were less for a ferrite with a higher nickel content. This 'comparison ferrite' had the composition $(NiO)_{0·95}(FeO)_{0·05}Fe_2O_3$.

Okamura and Torizuka[63] found a drop in linewidth with temperature for a nickel ferrite $NiO \cdot Fe_2O_3$ measured at 9·3 GHz in a polycrystalline sample having the form of a small disc of 4 mm diameter and 0·4 mm thick, or of a spherule 2 mm in diameter. A temperature rise from −175°C to +10°C corresponded to a drop in halfwidth from 54 kA/m to 31·2 kA/m.

Okamura, Torizuka, and Kojima[64] investigated, at 4 GHz and 9·3 GHz, nickel ferrites which had been sintered for 3 h at 1200°C in air. The disc-shaped or spherical specimens were cut from a larger block. At 4 GHz the absorption maxima for discs and for powder stood at about 38 kA/m, and for spheres of 10 mm diameter $H$ was 115 kA/m; at 9·3 GHz the resonance maxima of the discs were to be found around 145 kA/m and for the spheres (2·2 mm in diameter) at about 235 kA/m.

For nickel ferrite, as for manganese ferrite, the magnetic performance can be radically altered by substituting aluminium ions, in part, for those of

**Table 14.8** PROPERTIES OF SOME Ni–Zn–Al FERRITES[32]

| *Composition* | | | | *Final sintering* | $\mu_i$ ($\mu_0$) | $H_c$ (A/m) | $T_c$ (°C) | $J_s$ $\left(\frac{V\ s}{m^2}\right)$ | $10^3 \tan \delta_\varepsilon$ *at 2004* MHz | $\Delta H$ *at 2004* MHz (kA/m) |
|---|---|---|---|---|---|---|---|---|---|---|
| Ni | Zn | Fe | Al | | | | | | | |
| 0·5 | 0·5 | 1·2 | 0·8 | 2 h, 1300°C, slowly cooled | 58 | 104 | 140 | 0·140 | 64 | 20·8 |
| 0·5 | 0·5 | 1·2 | 0·8 | 2 h, 1325°C, quickly cooled | 52 | 160 | 129 | 0·134 | 19 | 17·6 |
| 0·5 | 0·5 | 1·2 | 0·8 | 2 h, 1350°C, quickly cooled | 58 | 160 | 128 | 0·144 | 19 | 16·8 |
| 0·5 | 0·5 | 1·15 | 0·75 | 2 h, 1350°C, quickly cooled | 48 | 112 | 92 | 0·124 | 0·9 | 18·4 |
| 0·5 | 0·5 | 1·1 | 0·8 | 2 h, 1300°C, slowly cooled | 42 | 184 | 83 | 0·125 | 0·8 | 16·0 |
| 0·5 | 0·5 | 1·1 | 0·8 | 2 h, 1325°C, quickly cooled | 46 | 160 | 87 | 0·126 | 0·5 | 12·8 |
| 0·5 | 0·5 | 1·1 | 0·8 | 2 h, 1350°C, quickly cooled | 59 | 72 | 85 | 0·122 | 0·6 | 13·6 |

**Table 14.9** DETAILED EXAMPLES OF ISOLATORS

| *Frequency* (GHz) | $\alpha_f$ (dB) | $\alpha_r$ (dB) | $\alpha_r/\alpha_f$ | *Ferrite* | *Reference* |
|---|---|---|---|---|---|
| | | | Resonance absorption isolator | | |
| 0·35–0·40 | 0·8 | 5·7–7·8 | 7–10 | — | 80 |
| 0·9 –1·6 | 0·4 | 20 | 50 | — | 80 |
| 1·25–1·35 | 0·6 | 20 | 33 | — | 80 |
| 1·7 –2·3 | 1·0 | 20 | 20 | Mg–Mn–Al | 54 |
| 1·75–2·05 | 0·8 | 23 | 29 | 182-2/5 | 109 |
| 1·8 –2·2 | 0·25 | 10·6 | 42 | Mg–Mn–Al | 32 |
| 1·8 –2·2 | 0·2 | 10·3 | 51 | Ni–Zn–Al | 32 |
| 3·6 –4·2 | 0·4 | 40 | 100 | G 40/1 | 11 |
| 3·8 –4·2 | 0·7 | 22 | 32 | ER 003 | 109 |
| 3·8 –4·2 | 0·25 | 26 | 104 | Gy–Siferrit | 19 |
| 5·9 –6·4 | 0·2 | 30 | 150 | Gy–Siferrit | 19 |
| 7·1 –8 | 0·3 | 50 | 165 | Gy–Siferrit | 19 |
| 9·37 | 1·0 | 48 | 48 | FXC 5B1 | 27 |
| | | | Faraday isolator | | |
| 3·65–4·18 | 1·5 | 20 | 13 | — | 40 |
| 4·7 | 0·5 | 20 | 40 | Mg–Mn–Al | 50, 51 |
| 23·6–24·5 | 1·0 | 44 | 44 | $BaO{\cdot}6Fe_2O_3$ | 4 |
| 35 | 0·5 | 30 | 60 | SER 1009 | 29 |
| | | | Field-displacement isolator | | |
| 6 | 0·2 | 30 | 150 | $B_s$ = 0·17 V s/m$^2$ | 107 |
| 11 | 1 | 70 | 70 | $B_s$ = 0·385 V s/m$^2$ | 105 |

iron. If aluminium is added, step by step, to the combination $NiFe_{2-x}Al_xO_4$, an almost linear drop in lattice constant, Curie temperature, and saturation intensity are obtained up to $x = 0{\cdot}5$[55]. Derry and Wills[17] altered $x$ in the formula $NiFe_{2-x}Al_xO_4$ from 0 to 0·22 and thereby obtained a nearly linear fall in saturation magnetisation from 0·32 V s/m$^2$ to 0·19 V s/m$^2$. Hickin, Werner, and Sidwell[32] investigated certain Ni–Zn–Al ferrites which showed good properties in absorption isolators within the frequency range 1·8–2 GHz. Table 14.8 gives a list of the materials and their production conditions. Attenuation ratios are shown in Table 14.9. The linewidth shows no significant connection with aluminium content[69].

On the other hand, McLean and Aitken[57], investigating the ferrite $NiAl_{0\cdot825x}Fe_{1-0\cdot175x}Al_{0\cdot175x}$ and increasing $x$ from 0 to 1, found not only a reduction of saturation flux density from 0·33 V s/m$^2$ to 0·056 V s/m$^2$ but also a reduction

of linewidth $\Delta H$ from 44·8 kA/m to 26·4 kA/m. The Curie temperature fell at the same time from 580°C to 186°C, and the dielectric loss factor tan $\delta_\varepsilon$ from 0·21 to 0·003. The linewidth of this material can be reduced if a small part of the nickel is replaced by cobalt. The nickel ferrite $NiAl_{0\cdot12}Fe_{1\cdot88}O_4$ is specially suitable for high-power transmission[69]. If some of the iron ions are replaced by indium or gallium, the saturation first rises (up to $x = 0\cdot7$) and falls below the saturation value of pure ferrite only for $x$ greater than 1·0[56]. The addition of copper causes the saturation magnetisation of nickel ferrite to fall in the manner expected[100], though only if a correction factor is applied to take care of porosity occurring during the sintering operation; otherwise, a maximum is obtained at 0·1% Cu since this is where the highest relative density (about 99%) is reached.

### 14.5.6 Cobalt ferrite

It is known that the linewidth is very large for cobalt ferrite. Okamura, Torizuka, and Kojima[65], to avoid this difficulty with their measurements, used the fact that linewidth usually falls with rising temperature. They investigated polycrystalline discs 3 mm in diameter and 0·22 mm thick at 9·3 GHz and at high temperatures. They found a half-width of 200 kA/m at 100°C but only about half this at 450°C. Since crystal anisotropy also falls with temperature, the resonance field strength will fall with it. However, it rises again as the Curie temperature is approached because the saturation intensity falls drastically in this region.

### 14.5.7 Hexagonal barium ferrites

Barium ferrite is suitable as a gyrator material, especially at high frequencies, since its anisotropic field strength $H_a$ is very high. When $H_a$ is measured in the direction of the hexagonal axis, it amounts to about 1360 kA/m[80]. According to equation 14.9, this field strength in isolation—without the presence of an external field—corresponds to a resonance frequency of 48 GHz[108].

The frequency range can be extended by a partial substitution of aluminium ions for iron ions: the saturation magnetisation falls and the resonance frequency rises[101]. The circular frequency $\omega_p$ can be raised to 90 GHz by altering the proportion of aluminium[80]. Alternatively, the usable range of the ferrite can be displaced towards lower frequencies by means of additives, such as titanium, zinc, or cobalt, which reduce crystal anisotropy[53].

### 14.5.8 Garnets

Garnets are silicates whose basic formula is $A_3B_2Si_3O_{12}$, one example being $Ca_3Fe_2Si_3O_{12}$. The elementary cell is cubic and comprises eight molecules[6]. The iron ions are found in the octahedral sites and the silicon ions in the tetrahedral sites; calcium is found in positions surrounded by eight oxygen neighbours. In those garnets which are of interest here, $Fe^{3+}$ ions occur in

place of $Ca^{2+}$ and $Si^{4+}$; the sites of the A atoms are occupied by ions of the rare earths. The combinations thus have the formula $3A_2O_3 \cdot 5Fe_2O_3$[26]. The garnets are chemically simpler than the ferrites because all the magnetically effective ions are trivalent. The magnetic properties of these compositions were discovered by Bertaut and Pauthenet[7].

Among the garnets, yttrium–iron garnet ($Y_3Fe_5O_{12}$), abbreviated in what follows to YIG, has so far achieved the greatest technical usefulness. It can be successfully used at low frequencies for resonance-absorption isolators because its extraordinarily small linewidth leads to low forward attenuation. In particular, single crystals, which can be drawn out from the melt, for example[16, 61], show favourable resonance properties[20].

Figure 14.21 shows the real and imaginary components of the initial permeability of YIG as a function of frequency[104]. Between 1 kHz and 500 MHz, $\mu'$ falls from about 90 to 2 while $\mu''$ rises from 2 to 10 passing through two maxima. The permeability can be held nearly constant over a wide band by small additions of silicon and calcium. Figure 14.22 shows curves of $\mu'$ and $\mu''$ for $Y_{2.998}Ca_{0.002}Fe_5O_{12}$[104]. The initial permeability of polycrystalline YIG can be raised to $500\mu_0$ (up to $f = 1$ MHz) if 14% of the yttrium is replaced by indium[1a]. The narrowest linewidth can be achieved only if the YIG crystals are very dense. To obtain high density, high sintering temperatures of 1425°–1500°C must be used or the crystals must be drawn out from the melt. Whereas at low sintering temperatures densities of at most 4·9 g/cm$^3$ are reached, densities of 5·14–5·17 g/cm$^3$ can be achieved at the above-mentioned higher temperatures[103].

A small linewidth of only 1·6 kA/m was found for an YIG in which there was a slight deficiency of iron oxide and which had been sintered for 5 h at 1475°C in oxygen. Higher iron content with longer sintering times led to oxygen loss and to lower density. The specific electrical resistance of YIG is about $10^4$–$10^6$ Ω cm and can be raised by the addition of manganese, cobalt, or nickel without appreciably changing the linewidth at the same time[103].

The linewidth of YIG and of those iron garnets in which part of the yttrium has been replaced by ions of the rare earths is temperature sensitive. Dillon[21] found anisotropy, as shown in Figure 14.47, and this is representative of the results for other samples: the maximum linewidth lies at between about 30K and 150K, while its magnitude depends on crystal direction and on the

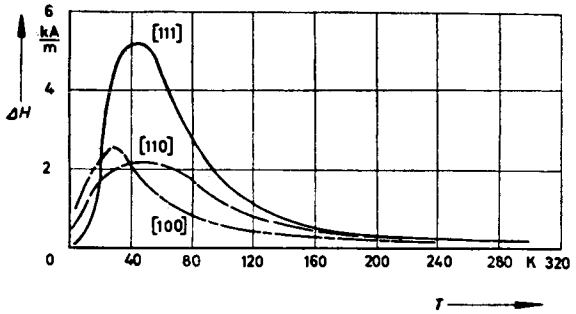



*Figure 14.47. Linewidth of a single crystal of YIG with 0·15% Nd as a function of temperature in three crystal directions ($f = 9{\cdot}25$ GHz)*[21]

measuring frequency. Dillon[20] found a $\Delta H$ of 1·04 kA/m at 9 GHz and 2·48 kA/m at 23 GHz measured at 295K for pure YIG parallel to the [100] direction. The smallest linewidth always occurred in the [100] direction: at 540K, for example, $\Delta$H was 640 A/m. By means of very careful preparation in the laboratory, a value of $\Delta H = 560$ A/m was achieved for polycrystalline YIG and 24 A/m for single crystals[85].

Other valuable properties of YIG are its low anisotropic field strength[16] and the possibility of obtaining saturation polarisations of 0·017–0·17 V s/m$^2$, without the Curie temperature falling below 280°C, by mixing various types of garnet. As a result, the garnets are the accepted materials for the lower frequencies in the microwave range, but even at higher frequencies they can often be used with advantage especially if prepared with a small iron deficiency. The linewidth of 1·6 kA/m, referred to above, was measured at a frequency of 16 GHz[103].

Table 14.2 lists a few types of ferrite and garnet which are used in practice and details their most important properties[15].

## 14.6 MICROWAVE COMPONENTS USING FERRITE

A whole series of non-reciprocal components has been developed on the physical basis of microwave resonance absorption, Faraday rotation, and the field-displacement effect; a short account will be given of a few of them.

The use of Faraday rotation for gyrators and for Faraday rotators or isolators has already been mentioned. Another important application of the Faraday effect is in the *Faraday circulator*. Its principle can be understood from Figure 14.48, which is taken from work by Fox, Miller, and Weiss[23] and is largely self-explanatory (see page 525). Circulators can also be used in

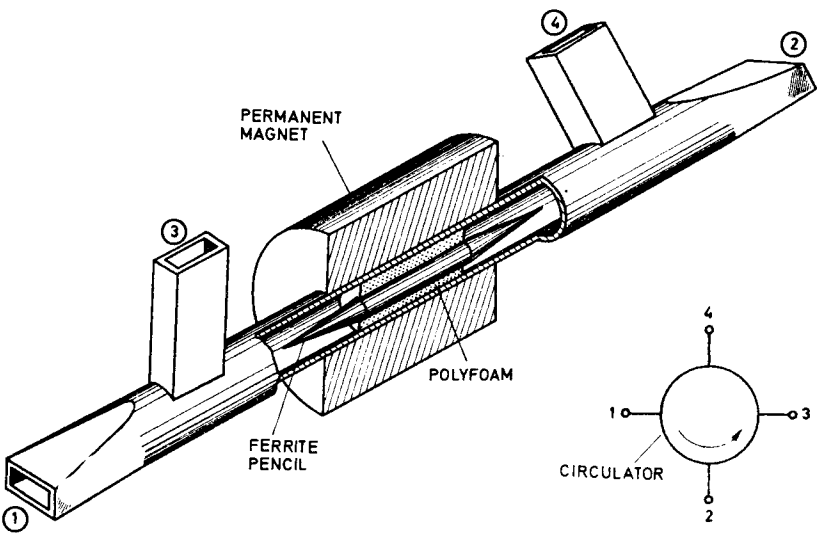



*Figure 14.48. Faraday circulator and the symbol for a four-arm circulator: arrow indicates direction of transmission between neighbouring arms*[23]

rectangular waveguides in the manner indicated in Figure 14.49. At the node-point of two crossed waveguides is placed a ferrite cylinder. This particular form, with four branches, is called an X circulator[113]. Three branches corre-

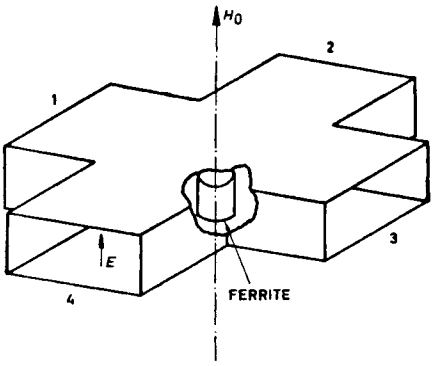



*Figure 14.49. Diagram of an X circulator*[113]

spond to the T or Y circulator[14]. The Y circulators, in particular, have many applications as they can be made smaller and lighter than other types[10]. Figure 14.4 shows a hybrid-T circulator.

Stripline circulators[9a] have found frequent application. Frank, Michael, and Schmid[23a] have shown that better attenuation ratios (for example, 0·06 : 30) can be obtained with circulators than with isolators. It thus becomes obviously advantageous to block one outlet of a Y circulator by means of an absorber and to substitute this arrangement for the normal isolator. Heller, Thaxter, and Stickler[31] described a Y circulator for 2 mm waves. The main difficulty at these extremely high frequencies lies in the satisfactory manufacture of the necessarily tiny components and in the maintenance of close tolerances.

Three-arm and four-arm circulators can also be made on the field-displacement principle[23] and can be built into combinations comprising a non-reciprocal phase-shifter and a so-called 3 dB coupler or 'magic T'[57, 67]. A circulator whose direction of rotation can be altered periodically is an electronically controlled *microwave switch*[12]. Operation times of 20 ns can be achieved. This time is of the same order of magnitude as the relaxation time of the ferrite material. Microwave switches have been designed round the Faraday effect and have high operating speeds and large bandwidths; others are suitable only for narrower bands but have a greater usable temperature range and are thus especially suitable for high-power transmission[10, 49, 92]. Microwave switches built on the field-displacement principle are described by Soohoo[83] and Caswell[13].

*Phase-shifters* can be applied to round or rectangular guides and they may be either reciprocal or non-reciprocal. The phase-shift depends on the difference in permeability shown by the ferrite for the two oppositely (circularly) polarised waves. Phase-shifters are mostly used in rectangular guides. A phase-shifter may consist, for example, of a ferrite rod magnetised lengthwise and mounted in the axis of the rectangular guide (reciprocal phase-

shifter)[70]. Phase-shift occurs as soon as the ferrite rod exceeds a critical diameter. At frequencies around 10 GHz it is possible to obtain approximately 100°/cm[10]. As normally applied, it is not the usual Faraday rotation of the plane of polarisation that is used but rather a concentration of alternating-field energy in the ferrite combined with a relatively low field intensity in the rest of the guide cross-section. The phase-shift depends on frequency and on temperature. Both temperature sensitivity and frequency dependence become less if the ferrite lies along the wall of the guide. The phase-shift is also thereby reduced, so longer elements and higher fields are needed. The details of shape and size for some non-reciprocal phase-shifters are to be found in Cacheris and Sakiotis[10].

A phase-shift can also be produced by ferrite strips magnetised in the transverse direction. By using two 13 cm ferrite strips, Weisbaum and Boyet[106] were able to design a broad-band phase-shifter for 5925–6425 MHz within a tolerance of $\pm 2\%$. Pivit and Stösser[67] used a similar non-reciprocal phase-shifter to build a circulator for the frequency ranges 5·4–5·8 GHz, 7·425–7·725 GHz, and 8·5–9·6 GHz.

The construction of a *Faraday isolator* was shown diagrammatically and explained in Figure 14.11. These isolators yield good attenuation ratios, particularly in the higher frequency range, as a few examples in Table 14.9 make clear. At lower frequencies, i.e. at 0·5–12 GHz, *resonance-absorption isolators* are mostly used (two illustrative examples are given in Figure 14.27); otherwise, the above-mentioned stripline Y circulator is preferable. Resonance isolators are also known for use in coaxial-cable transmissions. Figure 14.50 shows an arrangement suitable for 2 GHz[54]. One half of the space between the conductors is filled with a dielectric (polystyrene with barium titanate) whose dielectric constant $\varepsilon$ is $13{\cdot}8\varepsilon_0$. The dielectric is anchored by

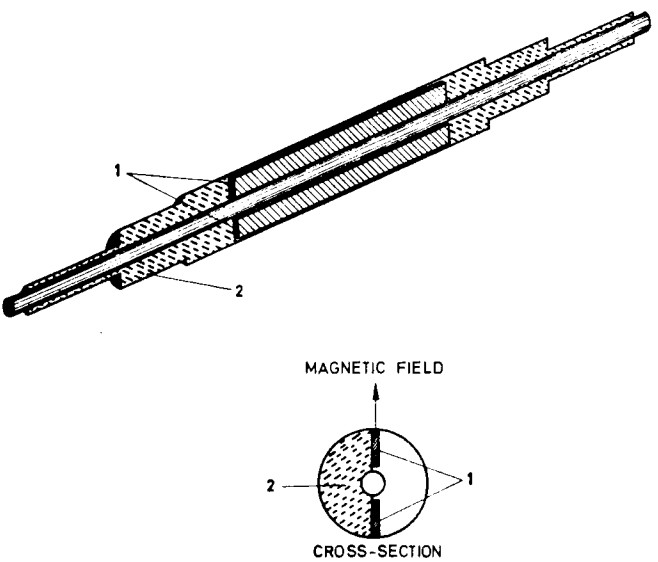



*Figure 14.50. Coaxial broad-band resonance isolator (diagrammatic): 1, ferrite; 2, dielectric*[54]

two ferrite slabs 75 mm×7 mm×2 mm. At a bandwidth of 250 MHz a reverse attenuation of 20 dB and a forward attenuation of 1 dB were obtained. The standing-wave ratio was 1·06.

Details of a few isolators, namely frequency range, forward and reverse attenuation, and attenuation ratio are given in Table 14.9. However, it must here be remembered that attenuation ratio is not the sole criterion of excellence in an isolator and that the values quoted do not only reflect the properties of the ferrites used: they depend also on careful design, on the arrangement of the ferrite in the waveguide, and on the accompanying use of suitable dielectric materials. Very often requirements must be met which cannot be read from tables, such as bandwidth, constancy, reflection factor, and power demands. Thus, most practical arrangements are the result of compromises between many conflicting requirements.

The differing shapes of the two curves 1 and 2 of Figure 14.23, which can pass into each other by the switching on or off of a direct field of 4 kA/m, offer the possibility of an *amplitude modulation*[3]. The working range falls on the descending branch of curve 2. Changes of field can give rise to eddy currents, and this fact must be reckoned with in the design of a modulator. Moreover, as small a switching power as possible is desired for a given modulation power. Le Craw[48] described a Faraday-rotation modulator. A further possibility involves the use of a ferrite rod in either a round or a rectangular resonator[72, 96].

The non-linear relationship between the magnetic properties of ferrites at high frequencies and the amplitude of the applied field can be used to achieve *frequency doubling*. A cross-magnetised ferrite element is mounted in the axis or along the side of a rectangular waveguide at a position of maximum alternating-field intensity[58]. The same basic procedure can be used for frequency mixing[66].

A subsequent development of this idea led to the invention of the *microwave amplifier* through the use of a suitable type of feedback. This is expounded in the work of Suhl[90] and has been studied theoretically by Hogan, Jepsen, and Vartanian[37]. Finally, tunable *microwave filters* must be considered as important microwave elements. These may be realised by the use of highly polished spheres of YIG. Quality factors of 12 000 are attainable in this way[74a]. In a filter described by Venator[104a] the sphere is placed in the middle of two crossed wire-loops, i.e. loops lying in mutually orthogonal planes. The direct magnetic field is parallel to the intersection of the loop planes. In the absence of a field, the coupling between the loops is zero—or nearly so—but increases, as the sphere is magnetised, in a manner depending on the applied direct field and the working frequency. The attenuation is low at the precise resonance frequency but high at all other frequencies. Venator[104a] should be consulted for further details.

The ever-increasing trend in recent years towards microminiaturisation has been felt also in the microwave domain. In 'microstrip technique' it has been found feasible to sinter together a variety of ferrite materials each with its own characteristic Curie temperature so that, with a non-magnetic ferrite or garnet serving as substrate, a suitable microwave ferrite takes over the function of active element (circulator, phase-shifter, etc.). 'Non-magnetic' in this special context is taken to mean that the Curie temperature lies below

zero. Thus, by this compound sintering, an integrated chip is obtained whereby the necessary strip lines can be achieved without the need of separate connections, a consideration that leads to improved reliability[97a].

## REFERENCES


1. ALBERS-SCHOENBERG, E.: Ferrites for microwave circuits and digital computers (J. A. P. **25** (1954) 152–154).

1a ANDERSON, E. E. and CUNNINGHAM, J. R.: High permeability garnets (J. A. P. **31** (9) (Sept. 1960) 1687–1688).

2. BELJERS, H. G.: Faraday-effect in magnetic materials with travelling and standing waves (Phil. Res. Rep. **9** (1954) 131–139).

3. BELJERS, H. G.: Amplitudenmodulation von Zentimeterwellen mit Hilfe von Ferroxcube (Phil. T. Rdsch. **18** (1956/1957) 15–20).

4. BELJERS, H. G.: Verwendung von Ferroxcube in nichtreziproken Wellenleitern (Phil. T. Rdsch. **18** (1956/57) 118–127).

5. BELJERS, H. G. and SNOEK, J. L.: Gyromagnetische Erscheinungen bei Ferriten (Phil. T. Rdsch. **11** (May 1950) 317–326).

6. BERTAUT, F. and FORRAT, F.: Structure des ferrites ferrimagnétiques des terres rares (C. R. **242** (1956) 382–384).

7. BERTAUT, F. and PAUTHENET, R.: Crystalline structure and magnetic properties of ferrites having the general formula $5Fe_2O_3 \cdot 3M_2O_3$ (Proc. IEE **104** B (1957) 261–264).

8. BITTEL, H. and HEMPEL, K. A.: Untersuchungen zur ferrimagnetischen Resonanz an Ferriten bei 10 und 24 GHz (Forsch. Ber. Nordrhein-Westfalen (1144) (1963).

9. BORONSKI, S.: Some properties and applications of ferrites at 3 cm wavelength (Proc. IEE **104 B** (1957) 331–337).

9a BOSMA, H.: On Stripline Y-circulation at UHF (IEE Trans., Microwave Theory **MTT-12** (1) (1964) 61–72).

10. CACHERIS, J. C. and SAKIOTIS, N. G.: Ferrite components for UHF and microwave systems (Electronics **34** (Sept. 1961) 37–42).

11. CARL, H., CRONE, W., HECK, C. and MÜLLER, M.: Hohlleiter-Bauelemente der Mikrowellentechnik im 4 GHz-Bereich (SEL-Nachr. **7** (3) (1959) 140–150).

12. CASWELL, D.: Ferrite applications at microwave frequencies (Electronics (Oct. 1953) 246–252).

13. CASWELL, D.: Microwave switches using cutoff phenomena in ferrite loaded waveguide; in Solid State Physics, Vol. 3 (ed. Désirant and Michiels). Academic Press, London (1960) 270–274.

14. CHAIT, H. N. and CURRY, T. R.: New microwave circulators (Electronics **32** (Dec. 1959) 81–83).

15. CLARRICOATS, P. J. B.: Microwave Ferrites. Chapman & Hall, London (1961).

16. CZERLINSKY, E. R. and FIELD, W. G.: Magnetic properties of ferromagnetic garnet single crystals; in Solid State Physics (ed. Désirant and Michiels) Academic Press, London (1960) 488–499.

17. DERRY, R. and WILLS, M. S.: Microwave Faraday effect and conductivity in nickel ferrites and ferrite-aluminates (Proc. IEE **104 B** (1957) 324–330).

18. DEUTSCH, J. and HAKEN, W.: Ein nichtreziprokes Dämpfungsglied (Richtungsleitung) für 4 GHz (Frequenz **11** (7) (1957) 217–220).

19. DEUTSCH, J., HAKEN, W. and V. HAZA-RADLITZ, C.: Neue Richtungsleitungen für Richtfunksysteme (NTZ (7) (1959) 367–370).

20. DILLON, J. F.: Ferrimagnetic resonance in yttrium–iron garnet (Phys. Rev. **105** (1957) 759–760).

21. DILLON, J. F.: Ferrimagnetic resonance in rare-earth-doped yttrium–iron garnet, III. Linewidth (Phys. Rev. **127** (Sept. 1962) 1495–1501).

22. DUNCAN, B. J. and SWERN, L.: Temperature behaviour of ferrimagnetic resonance in ferrites located in wave guides (J. A. P. **27** (Mar. 1956) 209–215).
23. FOX, A. G., MILLER, S. E. and WEISS, M. T.: Behaviour and application of ferrites in the microwave region (Bell Syst. Tech. J. **34** (1955) 5–103).
23a FRANK, A., MICHAEL, G. and SCHMID, G.: Mikrowellenbauteile (SEL-Nachr. **14** (2) (1966) 65–69).
24. FRESH, D. L.: Methods of preparation and crystal chemistry of ferrites (Proc. IRE **44** (1956) 1303–1311).
25. GALT, J. K. and SPENCER, E. G.: Loss mechanism in spinel ferrites (Phys. Rev. **127** (Sept. 1962) 1572–1576).
26. GELLER, S.: Magnetic interactions and distributions of ions in the garnets (J. A. P. **31** (5) (May 1960) 30S–37S).
27. GODFREY, R. M., HUMPHREYS, B. L., ALLIN, P. E. V. and MOTT, G.: Applications of ferrites at 3 cm wavelength (Proc. IEE **104 B** (1957) 355–361).
28. HAKEN, W. and V. HAZA-RADLITZ, C.: Ferritkörper mit temperaturunabhängigen gyromagnetischen Eigenschaften (A. E. Ü. **13** (4) (1959) 157–160).
29. HARVEY, A. F.: Ferrite structures for millimeter wavelengths (Proc. IEE **104 B** (1957) 346–354).
30. HELLER, G. S.: L-band isolator utilizing new materials (WESCON Conv., San Francisco (20. 8. 57).
31. HELLER, G. S., THAXTER, J. B. and STICKLER, J. J.: Ferrite and antiferromagnetic millimetre- and submillimetre-wavelength devices (Proc. IEE **109 B** (1962) 134–136).
32. HICKIN, E., M., WERNER, J. F. and SIDWELL, J. M.: Ferrites for resonance isolators in the frequency range 1700–2300 Mc/s (L'onde Electr. Suppl. **38** (1958) 621–628).
33. HLAWICZKA, P. and MORTIS, A. R.: Gyromagnetic resonance graphical design data (Proc. IEE **110** (4) (Apr. 1963) 665–670).
34. HOGAN, C. L.: The ferromagnetic Faraday-effect at microwave frequencies and its applications. The microwave gyrator (Bell Syst. Tech. J. **31** (1952) 1–31).
35. HOGAN, C. L.: The ferromagnetic Faraday-effect at microwave frequencies and its application (Rev. Mod. Phys. **25** (Jan. 1953) 253–263).
36. HOGAN, C. L.: The elements of non-reciprocal microwave devices (Proc. IRE **44** (1956) 1345–1368).
37. HOGAN, C. L., JEPSEN, R. L. and VARTANIAN, P. H.: New type of ferromagnetic amplifier (J. A. P. **29** (1958) 422–423).
38. JOSEPHSON, B. and LJUNG, P. E.: Microwave ferrites (Ericsson technics (1) (1958) 39–70).
39. KALES, M. L.: Propagation of fields through ferrite-loaded guides (Proc. Symp. Mod. Advances in Microwave Techniques. Polytechn. Inst., Brooklyn (1955) 215–228).
40. KAWAZU, S., MATZUMARU, K. and ISHII, H.: Wideband isolator at 4 kMc (Rep. ECL, NTT **5** (3) (Mar. 1957) 15–17).
41. KITTEL, C.: On the theory of ferromagnetic resonance absorption (Phys. Rev. **73** (1948) 155–161).
42. KITTEL, C.: Ferromagnetic resonance (J. Phys. Rad. **12** (1951) 291–302).
43. LANDAU, L. and LIFSHITZ, E.: On the theory of the dispersion of magnetic permeability in ferromagnetic bodies (Phys. Z. Sowjetunion **8** (1935) 153–169).
44. LAX, B.: Frequency and loss characteristic of microwave ferrite devices (Proc. IRE **44** (1956) 1368–1386).
45. LAX, B.: The status of microwave applications of ferrites and semiconductors (IRE Trans. **MTT-6** (1958) 5–18).
46. LAX, B. and BUTTON, K. J.: Microwave ferrites and ferritmagnetics. McGraw-Hill Book Co. Inc., New York/San Francisco/Toronto/London (1962).
47. LAX, B., BUTTON, K. J. and ROTH, L. M.: Ferrite phase shifters in rectangular waveguide (J. A. P. **25** (1954) 1413).
48. LECRAW, R. C.: High speed magnetic pulsing of ferrites (J. A. P. **25** (1954) 678).

49. LECRAW, R. C. and BRUNS, H. B.: Time delay in high-speed ferrite microwave switches (J. A. P. **26** (1955) 124).
50. LJUNG, P. E.: Ferrites for Faraday rotation at wavelengths of 3, 6 and 10 cm (Proc. IEE **104 B** (1957) 154–158).
51. LJUNG, P. E.: Development of a rotation isolator for 6 cm wavelength (Proc. IEE **104 B** (1957) 362–363).
52. LOSS, M. B.: Broadband characteristics of ferrites (IRE-Convention Rec. (8) (1955) 109–112).
53. LOTGERING, F. K.: Topotaktisch gerichtete Ferromagnetika (Phil. T. Rdsch. **21** (1959) 11–14).
54. MARRIAGE, A. J. and WERNER, J. F.: Some non-reciprocal coaxial devices at 2 Gc/s (Proc. IEE **109 B** (1962) 147–153).
55. MAXWELL, L. R. and PICKART, S. J.: Magnetization in nickel–ferrite–aluminates and nickel–ferrite–gallates (Phys. Rev. **92** (Dec. 1953) 1120–1126).
56. MAXWELL, L. R. and PICKART, S. J.: Magnetic and crystalline behaviour of certain oxide systems with spinel and perowskite structures (Phys. Rev. **96** (Dec. 1954) 1501–1505).
57. MCLEAN, R. and AITKEN, F. M.: Ferrites at microwaves (Electron Techn. (Jan. 1962) 2–9; (Feb. 1962) 70–76).
58. MELCHOR, J. L., AYRES, W. P. and VARTANIAN, P. H.: Microwave frequency-doubling from 9 to 18 kmc in ferrites (Proc. IRE **45** (1957) 643–646).
59. MÜLLER, M.: Vorteile von Schmalprofil-Hohlleitern für die Gestaltung von Breitband-Richtfunkgeräten (VDE-Fachber. **19** (1956) II 112–II 116).
60. MÜLLER, M.: Die Randstreuung des Kondensators aus endlich dicken Platten mit Anwendung auf Magnetberechnungen (Frequenz **15** (9) (1961) 286–293).
61. NIELSEN, J. W.: Improved method for the growth of yttrium–iron and yttrium–gallium garnets (J. A. P. **31** (5) (May 1960) 51S–52S).
62. OKAMURA, T., KOJIMA, Y. and TORIZUKA, Y.: Temperature dependence of the line half-width of ferromagnetic resonance in single crystals of zinc–manganese ferrite (Phys. Rev. **85** (2) (1952) 693–694).
63. OKAMURA, T. and TORIZUKA, Y.: Ferromagnetic resonance absorption in $NiOFe_2O_3$ and a new magnetic transition at low temperature (Sci. Rep. Res. Inst. Tohoku Univ. **A 3** (1951) 219–222).
64. OKAMURA, T., TORIZUKA, Y. and KOJIMA, Y.: Microwave resonance absorption in ferromagnetic semi-conductor, I. Nickel ferrite (Sci. Rep. Res. Inst. Tohoku Univ. **A 2** (1950) 663–672).
65. OKAMURA, T., TORIZUKA, Y. and KOJIMA, Y.: Ferromagnetic resonance in cobalt ferrite at high temperature (Phys. Rev. **84** (2) (1951) 372).
66. PIPPIN, J. E.: Frequency doubling and mixing ferrites (Proc. IRE **44** (1956) 1054–1055).
67. PIVIT, E. and STÖSSER, W.: Der Mikrowellenzirkulator (Frequenz **14** (Mar. 1960). 77–84).
68. POLDER, D.: On the theory of ferromagnetic resonance (Phil. Mag. **7** (300) (Jan. 1949) 99–115).
69. PRINGLE, D. H. and HEPBURN, W. D.: Some problems in the preparation of ferrites for various microwave devices; in Solid State Physics Vol. 3; (ed. Désirant and Michiels). Academic Press, London (1960) 252–269.
70. REGGIA, F. and SPENCER, E. G.: A new technique in ferrite phase shifting for beam scanning in microwave antennas (Proc. IRE **45** (Nov. 1957) 1510–1517).
70a REMEIKA, J. P. and COMSTOCK, R. L.: Properties of single-crystal lithium ferrite grown in the ordered state (J. A. P. **35** (11) (Nov. 1964) 3320–3321).
71. ROBERTS, F. F.: A note on the ferromagnetic Faraday effect at centimetre wavelengths (J. Phys. Rad. **12** (1951) 305–307).
72. ROBIEUX, M. and TREVOUX, P.: Modulation rapide sur guides à l'aide de ferrites; in Solid State Physics, Vol. 3 (ed. Désirant and Michiels). Academic Press, London (1960) 376–383.

73. ROBINSON, A. E.: The preparation of magnesium-manganese-ferrite for microwave application (Proc. IEE **104 B** (1957) 159–164).
74. ROWEN, J. H.: Ferrites in microwave application (Bell Syst. Tech. J. **32** (Nov. 1953) 1333–1369).
74a RÜPKE, H.-D.: Magnetisch abstimmbare Mikrowellenfilter mit hoher Güte (Z. ang. Phys. **26** (1) (1969) 32–35).
75. SAKIOTIS, N. G. and CHAIT, H. N.: Ferrites at microwaves (Proc. IRE **41** (Jan. 1953) 87–93).
76. SAKIOTIS, N. G., CHAIT, H. N. and KALES, M. L.: Behaviour of ferrite-loaded waveguides at high power levels; in Solid State Physics Vol. 3 (ed. Désirant and Michiels). Academic Press, London (1960) 337–346.
77. SCHULKES, J. A., GORTER, E. W. and BELJERS, H. G.: Verfahren zur Herstellung eines ferromagnetischen Materials zur Anwendung bei Mikrowellenfrequenzen (N. V. Philips Eindhoven). DBP 1 014 915.
78. SEIDEN, P. E. and GRUNBERG, J. G.: Ferrimagnetic resonance linewidth in dense polycrystalline ferrites (J. A. P. **34** (6) (June 1963) 1696–1698).
79. SENSIPER, S.: Resonance loss properties of ferrites in 9 kmc region (Proc. IRE **44** (1956) 1323–1342).
80. SEVERIN, H.: Neuere Mikrowellenferrite und ihre Anwendungen (Nachrichtent. Fachber. **23** (1961) 24–27).
81. SNOEK, J. L.: Gyromagnetic resonance in ferrites (Nature **160** (1947) 90).
82. SNOEK, J. L.: Dispersion and absorption in magnetic ferrites at frequencies above one Mc/s (Physica **14** (4) (1948) 207–217).
83. SOOHOO, R. F.: Cutoff phenomena in transversely-magnetized ferrites; in Solid State Physics, Vol. 3 (ed. Désirant and Michiels). Academic Press, London (1960) 149–161.
84. SPENCER, E. G., LE CRAW, R. C. and PORTER, G. S.: Microwave properties of yttrium–iron garnet; in Solid State Physics, Vol. 3 (ed. Désirant and Michiels). Academic Press, London (1960) 464–474.
85. SPENCER, E. G. and LE CRAW, R. C.: Ferromagnetic relaxation in yttrium–iron garnet and the relation to application (Proc. IEE **109 B** (1962) 66–70).
86. STANDLEY, K. J. and PETERS, J.: Ferrimagnetic resonance in a magnesium–manganese ferrite (Proc. IEE 104 **B** (1957) 206–208).
88. STEINHART, R.: Experimentelle Untersuchungen an Ferrit-Resonanz-Richtungsleitungen (NTZ **13** (1960) 183–191).
89. STEINHART, R.: Magnetsysteme für Ferrit-Richtungsleitungen. Arbeitsgem. Ferromagnetismus. Tagung Dauermagnete (1962). D. Ges. Metallkde. (Suppl.).
90. SUHL, H.: Proposal for a microwave amplifier in the microwave range (Phys. Rev. **106** (1957) 384).
91. SUHL, H., VAN UITERT, L. G. and DAVIS, J. L.: Ferromagnetic resonance in magnesium–manganese–aluminium ferrite between 160 and 1900 Mc. (J. A. P. **26** (Sept. 1955) 1180–1182).
92. SULLIVAN, R. F. and LE CRAW, R. C.: New type ferrite microwave switch (J. A. P. **26** (1955) 1282–1283).
93. TANNENWALD, P. E.: Ferromagnetic resonance in manganese–ferrite single crystals (Phys. Rev. **100** (Dec. 1955) 1713–1719).
94. TEALE, R. W.: Microwave resonance linewidth in single crystals of cobalt-substitued manganese ferrite (J. A. P. **33** (3) (1962) 1295–1297).
95. TELLEGEN, B. D. H.: Der Gyrator, ein elektrisches Netzwerkelement (Phil. T. Rdsch. **18** (1956) 88–93).
96. THOMPSON, G. H. B.: Microwave modulation using a ferrite rod in an $H_{11_0}$ cylindrical resonator (Proc. IEE **109 B** (1962) 154–162).
97. THOUREL, L.: Utilisation des ferrites dans les circuits U. H. F. de grande puissance; in Solid State Physics, Vol. 3 (ed. Désirant and Michiels). Academic Press, London (1960) 347–364.

97a TOLKSDORF, W. and HOLST, P.: Gemeinsames Sintern von Ferriten mit unterschiedlicher Sättigungsmagnetisierung und Curie-Temperatur für integrierte Mikrowellensysteme (Ber. D. Ker. Ges. **47** (10) (1970) 670–673).

98. VAN UITERT, L. G.: Low magnetic saturation ferrites for microwave applications (J. A. P. **26** (Nov. 1955) 1289–1290).

99. VAN UITERT, L. G. Dielectric properties of and conductivity in ferrites (Proc. IEE **44** (10) (Oct. 1956) 1294–1303).

100. VAN UITERT, L. G.: Nickel–copper ferrites for microwave applications (J. A. P. **27** (1956) 723–727).

101. VAN UITERT, L. G.: Magnetic induction and coercive force data on members of the series $BaAl_xFe_{12-x}O_{19}$ and related oxides (J. A. P. **28** (Mar. 1957) 317–318).

102. VAN UITERT, L. G., SCHAFER, J. P. and HOGAN, C. L.: Low-loss ferrites for applications at 4000 megacycles per second (J. A. P. **25** (1954) 925–926).

103. VAN UITERT, L. G., SWANEKAMP, F. W. and HASZKO, S. E.: Line widths in polycrystalline yttrium–iron garnet (J. A. P. **30** (1959) 363–365).

104. VERWEEL, J. and ROOVERS, B. J. M.: Magnetic properties and conduction phenomena in pure and substitued yttrium–iron garnets; in Solid State Physics, Vol. 3 (ed. Désirant and Michiels). Academic Press, London (1960) 475–487.

104a VENATOR, W.: Charting a simpler course to the design of YIG filters (Electronics **42** (5) (Mar. 1969) 118–126).

105. WEISBAUM, S. and BOYET, H.: A double-slab ferrite field displacement isolator at 11kmc (Proc. IRE **44** (1956) 554–555).

106. WEISBAUM, S. and BOYET, H.: Broad-band nonreciprocal phase shifts. Analysis of two ferrite slabs in rectangular guide (J. A. P. **27** (1956) 519–524).

107. WEISBAUM, S. and SEIDEL, H.: The field displacement isolator (Bell Syst. Tech. J. **35** (1956) 877–898).

108. WEISS, M. T.: The behaviour of Ferroxdure at microwave frequencies (IRE Conv. Rec. Pt. 8, Comm. Microw. (1955) 95–99).

109. WILLWACHER, E.: Die Anwendung von Ferriten bei Mikrowellen (VDE Fachber. **19** (1956) II 103–II 112).

110. YAGER, W. A., GALT, J. K. and MERRITT, F. R.: Ferromagnetic resonance in two nickel–iron ferrites (Phys. Rev. **99** (Aug. 1955) 1203–1210).

111. YAGER, W. A., MERRITT, F. R. and GUILLAUD, C.: Ferromagnetic resonance in various ferrites (Phys. Rev. **81** (Feb. 1951) 477–478).

112. YAGER, W. A., GALT, J. K., MERRITT, F. R. and WOOD, E. A.: Ferromagnetic resonance in nickel ferrite (Phys. Rev. **80** (4) (Nov. 1950) 744–748).

113. YOSHIDA, S.: X-Circulator (Proc. IRE **47** (1959) 1150).

# 15

# Magnetic materials for information storage

In modern technology the need frequently arises to store information and data for long periods. Without storage no automatic system, no electronic exchange technique, no computer apparatus is conceivable. Of the numerous possible methods of storage, mechanical, chemical, optical, or electrical[51], the magnetic method has steadily advanced in favour during recent years. It stands today in the first rank for the processing of information. Magnetic stores work quickly and reliably, they need no continuous energy feed, and can be cleared and re-used as often as required. The quality of reproduction of magnetic recorders is often superior to that of any other device[186].

Magnetic materials have two roles to play in electronic calculating machines: the first is in the construction of storage devices or 'magnetic memories', and the second is as switching elements in logical manipulation. Both kinds of application are of about the same age[57, 114, 175].

In everyday life, too, the possibilities and applications of magnetic storage are increasing rapidly. Tape recorders are not only used in radio and television studios to give permanence to sound or picture but find an increasing place in the home. In the USA, as long ago as 1953, some 200 million dollars were devoted to domestic tape recorders[17]. In West Germany about 678 000 tape recorders and 132 000 dictation devices were manufactured and sold during 1960[89]. Meanwhile, the commercial turnover and the general interest in these machines are increasing rapidly throughout the whole world.

## 15.1 TYPES OF MAGNETIC STORE

Storage on tape has served particularly well for private use. In communications technology a wider range of magnetic storage devices is available. The most important of these are magnetic drums, ferrite toroids, and thin-film stores. All these can exist side by side since every type has a range of application to which it is specially suited, overlapping with others only in the fringes. Besides the named types there are other magnetic storage devices which can render good service in special cases.

In the field of technology, storage systems are available for a wide variety of purposes. First of all come the massive stores which can hold millions of

the information elements called 'bits' (*bi*nary digi*ts*). To store a decade of numbers (or a word) often needs many bits. In a computer some 20–50 bits, according to size, are allocated to each word. The bigger the storage capacity, however, the longer the time required to recover a particular item of information, i.e. the 'access time' increases. Thus there have to be small and intermediate stores with short, or very short, access times (the so called short-term stores) to form, for example, the working memories of a computer.

Three time concepts are to be distinguished and have special functions to fulfil in computers:

1. The switching time. This is the time needed for a change in sign of the remanence. A more precise definition will be given later.
2. The access time. This is the interval elapsing between the arrival of an interrogation order and the response at the outlet of the store. Besides the switching time, the access time also includes the delay times of the various circuits.
3. The cycling time. This is the time which must elapse before the completion of an information cycle—switch, read, rewrite. The cycling time is thus longer than the access time, and this again is longer than the switching time.

For example, in a toroidal ferrite store having a switching time of 0·4 μs, the cycling time may comprise 0·4 μs (reading) +0·4 μs (rewriting) +0·6 μs (transfer to next unit)+0·2 μs (rise time and fall time for the pulse)=1·6 μs[193]. In the present connection the chief point of interest is the switching time of the magnetic material. The other time intervals mainly depend on size and geometry or on the connections and mode of operation of the store. The

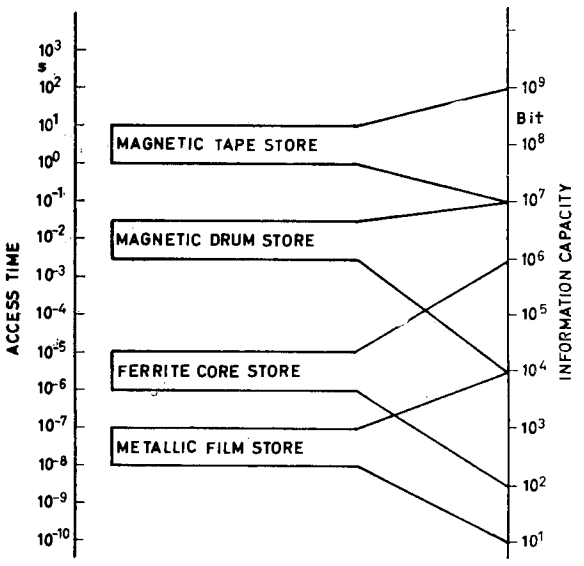



*Figure 15.1. Access time and information capacity of various kinds of storage devices*

designer of a magnetic store and the technologist developing the magnetic materials have the same kind of problem: to make all these intervals as short as possible. Rajchman[145] has published some observations on the limits of the possibilities.

An example of a 'slow' store with huge receptivity is the tape store. Its access time varies, according to size, from several seconds up to some minutes. Information can be retrieved more quickly from a drum store and more quickly still from a toroidal-core store or a thin-film store. Representative mean values of access times and information capacities of these storage devices are given, schematically, in Figure 15.1. Peak values of cycling time now lie around 100 ns for a store holding 40 000 bits[137, 162].

## 15.2 HISTORICAL

The first known publication on magnetic sound-recording appeared in the *Electrical World* in 1888. Among other matters, the author, Oberlin Smith[173] discussed a process whereby, using a microphone and a magnetising coil, speech could be impressed magnetically on an iron wire and later reclaimed with the aid of a telephone earpiece. A remarkable fact was the hint that the sound carrier need not be limited to an iron wire; a 'composition' wire could be used in which magnetic particles could be held in a brass or lead substrate or worked into a thread of cotton or silk. Here was born the idea of a plastic ribbon impregnated with iron dust[88].

It is not known whether Smith's invention was ever realised in practice. In any case, more stir was created in 1900, at the World Exhibition in Paris, by a device called a 'telegraphone' which was introduced by its inventor, Poulsen[135], and is referred to in the literature in more than 20 publications. Its purpose was magnetically to record telegraph signals on a steel wire which could be played back as often as required (at various speeds to keep pace with hand recording). The version of such a device made by Mix & Genest used a steel wire wound on a drum[89].

The original steel wire showed many defects which were gradually overcome. In 1917, Poulsen announced an improved telegraphone which, in this year, was used for the first time as a wire recorder in connection with a ciné-film. It may be noted that magnetic recording is older than the optical sound-track now used on ciné-films[16]. After further improvements in the means of reproduction and, more particularly, in amplifier technique, apparatus working on this principle was soon produced capable of meeting the stringent requirements of today[191].

The development of plastic sound-recording tape began in Germany in the 1920s. Its inventor was Pfleumer[133], who embedded carbonyl iron dust in paper or plastic foil. The result of this development was the 'Magnetophone' shown for the first time at the German Radio Exhibition in 1935[76]. Plastic magnetic tapes were developed, in particular, by I.G.-Farbenindustrie AG, which was also the source of the carbonyl iron. It was soon obvious that $\gamma$-oxide of iron is superior to metallic dust[150]. It is used today almost exclusively as magnetic coating for recording tape. On account of its low manufacturing cost, its superior flexibility, and other technical advantages,

magnetic tape has largely displaced magnetic wire except for special applications.

The fundamental improvements in tape-recording technique which have led to its present commercial success were introduced during World War II, especially in Germany[82]. The development of drum and disc storage devices is of more recent date and began about 15 years ago[18, 51, 158]. Storage by means of individual toroidal cores has been known since about 1945[51, 132, 181]. Some 10 years after this, the development of magnetic thin-film memories began and other devices followed; these will be explained later. Today, magnetic storage devices are by no means limited to registering sound waves at audiofrequencies (50–15 000 Hz) but are used, also, for recording the short impulses which are a feature of much modern information technology. Even pictures can be recorded magnetically[10, 159, 185], and for this purpose bandwidths up to 8 MHz are required.

## 15.3 TAPE RECORDERS

To store signals on wire or ribbon by magnetic means, electrical waves and pulses are converted into magnetic variations in the form of spacially distributed waves or impulses, and retranslated, at will, back into electrical form. For the various terms employed see DIN 66 010[48].

### 15.3.1 Operating principles

The general working of a tape recorder is shown schematically in Figure 15.2[103]. The tape passes first of all over the gap of the erase head E, where the previous recording is removed by the application of a high-frequency

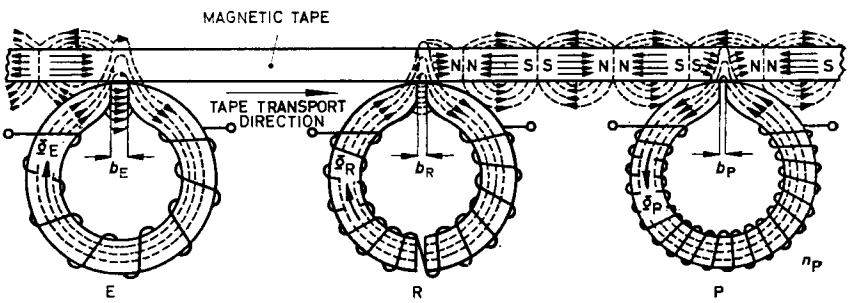



*Figure 15.2. Principle of magnetic recording (arrow indicates direction of tape movement, and path of lines of force are indicated by broken lines): E, erase head; R, recording head; P, reproducing head; $b_E$, $b_R$, $b_P$ are the air-gaps of E, R, P*[103]

field. Enregistering of information is taken care of by the recording head (or writing head) R[125]. The working point is determined by means of a superposed high-frequency magnetisation whose frequency lies well beyond the hearing range (for example, 100 kHz)[4, 32]. This procedure ensures a linear

transduction characteristic over the relevant band[9, 119, 186]. The alternating current in the coils of the heads produces corresponding magnetic fields in the gap, and these fields magnetise the passing elements of the tape in alternating directions[71]. The reproducing head (or playback head) P is similarly constructed to the recording head. The lines of force emanating from the tape induce electrical voltages $V$ in the coil, and these are proportional to the number of turns $n_P$ and the momentary change in flux $d\Phi_P$:

$$V = n_P \frac{d\Phi_P}{dt} \tag{15.1}$$

At very high signal frequencies the stationary magnetic head and fast-moving tape can sometimes be replaced with advantage by a more slowly moving tape and a rapidly moving head[10].

### 15.3.2 Magnetic tape

The magnetic tape consists of a mechanically strong, but thin and very flexible plastic foil in which the ferromagnetic or ferrimagnetic material is dispersed (impregnated tape) or on whose surface a film of magnetic material has been deposited (sputtered tape). The width of the tape is 12·7 mm or a multiple of this figure. Composition tapes are rarely used today as the concentration of particles attainable in this way is insufficient[150]. Cellulose acetate (CA), polyvinyl chloride (PVC), or polyester (PE) is used for the substrate or 'carrier'. Polyester tapes are coming more to the fore because of their excellent qualities. They have a high physical stability between $-60°C$ and $+95°C$ and absorb hardly any moisture.

The ferrimagnetic material ($\gamma$-$Fe_2O_3$) of the magnetisable layer is the cubic modification of iron oxide and is magnetic (in contrast to the $\alpha$ form, which is not). Indeed, $\gamma$-$Fe_2O_3$ is ferrimagnetically and structurally related to magnetite, $FeO \cdot Fe_2O_3$.

Since the powder is used in a heavily gapped magnetic circuit, permanent-magnet characteristics (i.e. high remanence and coercivity) are appropriate to it. By suitable choice of manufacturing procedures it becomes possible to determine the size and shape of the particles and so to influence the coercivity. At a critical particle size of 100–500 nm an $H_c$ of about 40 kA/m can be obtained. By enrichment with cobalt, values up to 120 kA/m can be achieved[91]. In most ordinary tapes, $H_c$ is 24 kA/m and $B_r$ is 0·08 V s/m$^2$. The use of particles of higher coercivity would only be worthwhile if $B_r$ could be raised at the same time. This could be done by using a higher proportion of $Fe_2O_3$ in the magnetic layer, but a filling factor of more than 55% by volume makes the tape brittle and less stable.

By depositing the particles from a liquid solution the process can be so controlled that needle-like particles of hydrated iron oxide are formed[151]. Using a suitable heat treatment at 250°–300°C, this can be converted into $\gamma$-$Fe_2O_3$ without changing the external shape of the particles. As a rule the particles have a mean length of 1 $\mu$m and a mean breadth of 0·1 $\mu$m [91].

If a magnetic field is applied when the powder is added to the carrier, a

**Table 15.1** MECHANICAL AND MAGNETIC PROPERTIES OF MAGNETIC TAPES[91]

| | *Standard-playing tape* | | | *Long-playing tape* | | | *Double-playing tape* | | |
|---|---|---|---|---|---|---|---|---|---|
| | *Min.* | *Mean* | *Max.* | *Min.* | *Mean* | *Max.* | *Min.* | *Mean* | *Max.* |
| | | | | Mechanical properties | | | | | |
| Carrier (μm) | 27 | 37 | 44 | 22 | 24 | 25 | 12 | 14·5 | 18 |
| Magnetic layer (μm) | 11 | 15·1 | 21·5 | 8·5 | 11·9 | 17 | 9 | 11·6 | 16 |
| Total thickness (μm) | 42 | 53 | 60 | 34 | 36·8 | 40 | 24·5 | 26·5 | 28·5 |
| Elastic stretch (%) | 0·8 | 1·04 | 1·35 | 1·16 | 1·55 | 2·25 | 1 | 1·75 | 2·9 |
| Plastic stretch (%) | 0·01 | 0·053 | 0·13 | 0·01 | 0·055 | 1·2 | 0·03 | 0·045 | 0·06 |
| Young's modulus ($N/mm^2$) | 2 640 | 3 380 | 3 700 | 1 990 | 2 890 | 3 780 | 2 120 | 3 120 | 5 700 |
| Breaking load (N) | 20 | 30 | 46 | 15 | 24·3 | 30 | 10 | 21·2 | 32 |
| Breaking stretch (%) | 20 | 51 | 202 | 20 | 79 | 146 | 25 | 71 | 128 |
| | | | | Magnetic properties | | | | | |
| Weight of oxide ($g/m^2$) | 13·6 | 21·3 | 37 | 9·4 | 16·6 | 21·2 | 11·1 | 16·9 | 25·7 |
| Volume space factor (%) | 22 | 29·7 | 37·5 | 23·5 | 29·5 | 33·5 | 25·5 | 29·2 | 35·8 |
| Remanence flux ($10^{-7}$ V s) | 0·049 | 0·0744 | 0·155 | 0·038 | 0·06 | 0·086 | 0·055 | 0·0597 | 0·09 |
| Coercivity (kA/m) | 16·8 | 20·8 | 24·4 | 16·4 | 19·2 | 24·0 | 16·4 | 20·1 | 24·0 |
| Specific remanence (V s $g/m^2$) | 0·049 | 0·0582 | 0·0665 | 0·051 | 0·066 | 0·0665 | 0·054 | 0·062 | 0·068 |
| Relative remanence | 0·66 | 0·73 | 0·83 | 0·64 | 0·73 | 0·83 | 0·68 | 0·77 | 0·85 |
| Relative initial permeability | 1·4 | 1·72 | 3·6 | 1·43 | 1·8 | 2·07 | 1·35 | 1·5 | 1·79 |
| Preferred directionality* | 1 | 1·5 | 1·9 | 1 | 1·6 | 2 | 1 | 1·67 | 2 |
| Characteristic wavelength (μm) | 42 | 53·5 | 65 | 45 | 51 | 62·5 | 39·5 | 49·0 | 57 |

* Preferred directionality = remanence in the longitudinal direction over that in the transverse direction.

parallel alignment of the particles can be achieved whereby the remanent flux of the tape is suitably increased. The iron oxide dust is intimately mixed with a special lacquer and applied to the plastic tape to form a layer between 15 μm and 40 μm thick. After it is dry, the magnetic layer adheres firmly to the substrate and shows considerable resistance to abrasion—a property which is clearly necessary to prevent the magnetic material being rubbed off as the tape passes over the magnetic heads.

Sometimes $Fe_3O_4$ (magnetite) is used as ferrimagnetic material in place of $\gamma$-$Fe_2O_3$. Also, chromic oxide ($CrO_2$) to which a few percent of cobalt has been added provides a highly coercive ferrimagnetic substance ($_JH_c$ = 48 kA/m) which can be used in the production of magnetic tape[62]. Considering the latest experience gained in the study of thin-film techniques (see below) and also present knowledge as to the production of single-domain particles (ESD, see page 281) the future use of materials of even higher coercivity cannot be ruled out[59, 106]. Table 15.1, taken from Krones[91], gives the mechanical and magnetic properties of various tapes, together with their ranges of tolerance.

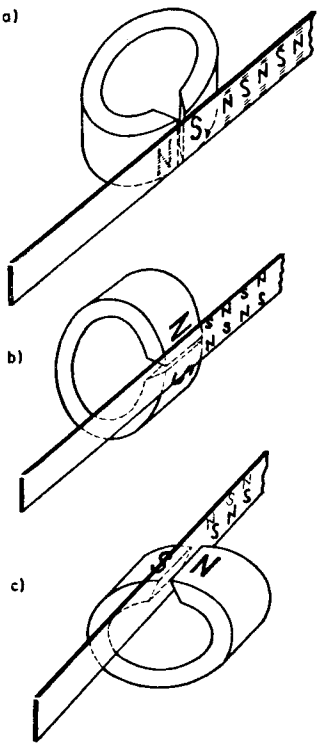



*Figure 15.3. Types of magnetisation: (a) longitudinal; (b) transverse; (c) cross*[155]

There are three fundamental choices for the direction of magnetisation in the tapes: longitudinal, transverse, and cross, and these are shown schematically in Figure 15.3[155]. Longitudinal magnetisation is almost universal today and is basic to most standardisation[155].

An actual example of a tape store is shown in Figure 15.4 (see plate section). The endless band is some hundred metres long and carries a number of parallel tracks. It runs at a speed of 1–6 m/s if data are to be recorded or retrieved. The information density amounts to 10–20 bits/mm. For other types see Hickman[82]; Maier[103] describes numerous other versions of magnetic-tape store.

### 15.3.3 Magnetic heads

#### 15.3.3.1 Construction

Figure 15.5 shows the basic construction of a magnetic head[17]: this consists of a coil having a magnetic core in whose circuit is a small gap. In order that the flux in the core should be proportional to the voice current, and to avoid

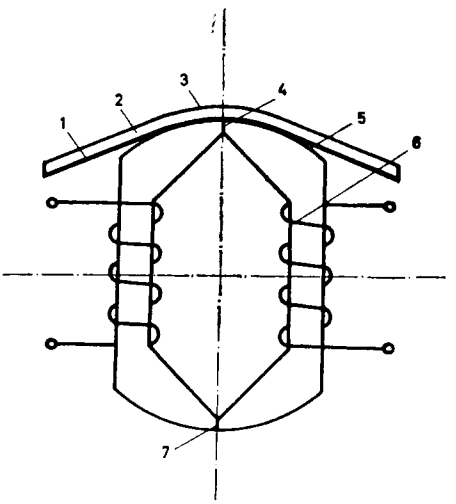



*Figure 15.5. Basic construction of a magnetic head: 1, magnetic coating of tape; 2, carrier tape; 3, magnetic tape; 4, gap; 5, pole-piece; 6, winding; 7, gap*[17]

the magnetic effects of switching, the speech head is provided with a second air-gap opposite the working gap. The field emanating from the working gap produces a magnetisation of the magnetic layer, as the tape passes over it, which is proportional to the current in the coil. There is a close relation between the gap-field, the gap-width, the thickness of the active layer, and the tape speed, which determines the quality of the performance in recording and reproduction. The gap-width varies according to the function of the head: it is about 5 μm for the recording head, 12 μm for the reproducing head, and something over 100 μm for the erase head (see Figure 15.2). The gap-width of the reproducing head must be less than the smallest wavelength to be read. A lower limit is set by the grain size and degree of porosity of the pole-piece material used and also by manufacturing possibilities[17]. The lower limit of technical possibility at present would be, say, 1 μm[177].

The magnetic head of a tape recorder or storage device is usually curved so that the passing tape makes a certain area of contact with it (Figure 15.5). The gap is filled with a non-magnetic substance such as copper or silver. The use of metals reduces the amount of power used in recording: the eddy currents produced in the metallic spacer by the build-up of the field force the magnetic lines out of the gap. Further, the inductance of the head is reduced in this way, and this is of great importance at high frequencies[129]. A special kind of glass is used as a gap spacer, instead of the metal, if the gap is very small[49].

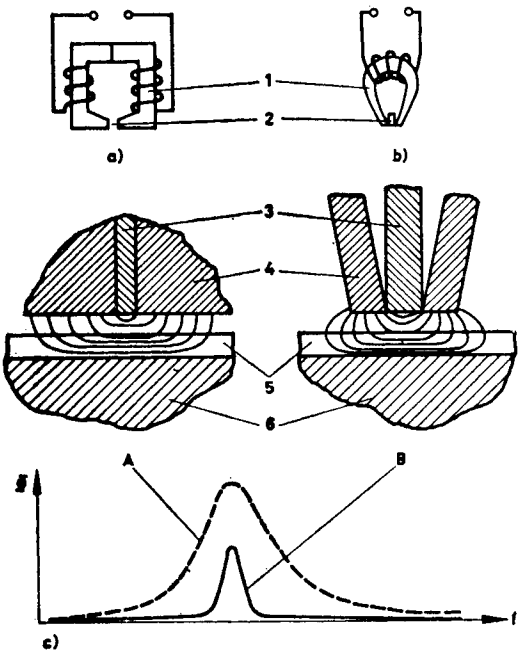



*Figure 15.6. (a) and (b) show magnetic heads and the field configurations in the gaps, with flat and pointed poles compared (1, core; 2, gap; 3, gap filler; 4, core; 5, coating; 6, drum); (c) curve A shows the magnetic read-out flux in flat pole-pieces; curve B shows the flux in pointed pole-pieces*[19]

The core of a magnetic head may be triangular[73] or toroidal (see Figures 15.2, 15.3, and 15.6b), but considerations of easy winding have usually suggested a more or less rectangular form (see Figure 15.5 and 15.6a). In order to give some idea of the magnitudes involved, core shapes in accordance with DIN 41 298 are sketched, with their essential dimensions, in Figure 15.7[47]. Pointed shapes have a smaller rubbing surface, so there is less friction between tape and head than for broader shapes. Wear is further reduced if a small slip of agate is inserted sideways into the pole-piece at the gap[103].

In storage devices where many data are to be recorded simultaneously, multiple heads are employed[36, 119], and the same principle is used in stereophonic sound recording[74]. Multiple heads exist for 14 or more tracks[103]. For very great recording speeds, magnetic heads having several channels are used[8].

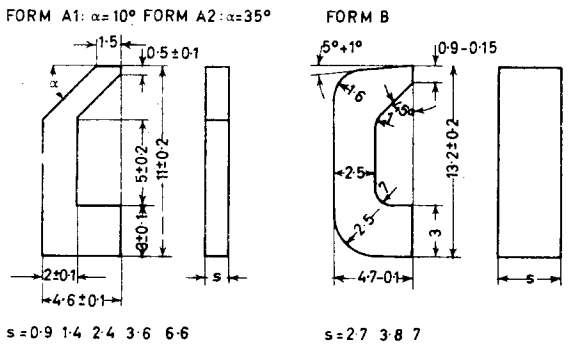



*Figure 15.7. Core shapes to DIN 41 298*[47]

Lazzari and Melnick[95a] have suggested magnetic heads in which the coil is integral with the core. The head is built only of thin foils produced under vacuum. Many heads can be made together in a single vacuum operation. The magnetic foils consist of an alloy having 81% Ni, 17% Fe, and 2% Cr, and are 3 μm thick. The coil comprises five turns of copper. Such heads may be used for both reading and writing.

### 15.3.3.2 Core materials

Laminae of metallic alloys are used for the cores of magnetic heads, as also is ferrite (see Table 15.2).

Mumetal from 10 μm to 100 μm thick is in the forefront of laminated core materials. The initial permeability can be as much as $30\,000\mu_0$—higher permeabilities would be better still but for laminated cores, which must be pressed up and then mechanically worked, they cannot be reproduced with high consistency. To avoid eddy currents, the thin sheets need to be insulated from each other. Mumetal has a specific electrical resistance $\varrho$ of 62 μΩ cm. Eddy currents in the core can be reduced if, instead of Mumetal, heavily alloyed Fe–Al sheets of Alfenol[102] or Vacodur (see page 341) are used. For these materials $\varrho = 145$ μΩ cm and $\mu_i = 6000\mu_0$. The same electrical quality is obtained with a 0·2 mm sheet of Fe–Al as with 0·1 mm Mumetal. Alloys with 16% Al content are of course brittle, but they may nevertheless be hot-rolled down to a thickness of 50 μm. A specially useful property of this material is its durability under abrasion which is five or 10 times greater than that of Mumetal[179a].

Alloys of the Sendust type, which are capable of being sintered, have also proved themselves of value for the core materials of magnetic heads[2]: they are hard, are of small grain-size, have high specific electrical resistance, and have adequate permeability.

Ferrites would seem to be the most suitable materials for magnetic heads because of their high specific electrical resistance and their hardness. Their brittleness and to some extent their porosity, which lead to roughness and irregularities, are sometimes much against use of ferrites, particularly for

**Table 15.2** CORE MATERIALS FOR MAGNETIC HEADS[2, 179a]

| *Material* | $\mu_i$ ($\mu_0$) | $\mu_m$ ($\mu_0$) | $H_c$ (A/m) | $B_s$ (V s/m²) | $\varrho$ ($\mu\Omega$ cm) | *Hardness* (Rockwell) |
|---|---|---|---|---|---|---|
| Mumetal | 30 000 | 100 000 | 4 | 0·7 | 62 | 35 RB |
| Permalloy | 25 000 | 100 000 | 2·4 | 0·9 | 55 | 35 RB |
| Sinimax | 5 000 | 40 000 | 8 | 1·1 | 55 | 76 RB |
| 16 Alfenol | 5 000 | 80 000 | 3·2 | 0·8 | 140 | 29 RC |
| Vacodur | 6 000 | 40 000 | 3·2 | 0·75 | 145 | 250 Vickers $HV_5$ |
| Si–Al–Fe | 6 500 | 25 000 | 8 | 0·9 | ~200 | 48 RC |
| Ferrite | 2 000 | 4 000 | 80 | 0·4 | $>10^8$ | 54 RC |

recording heads with their very narrow gaps. Nevertheless, it has proved possible to reduce the porosity of ferrite material (Ni–Zn ferrite in this case) to below 0·5%, so that it is possible not only to cope reliably with extremely narrow gaps but also to reduce greatly the susceptibility to abrasion[177]. Table 15.3 shows the relevant values for two densely sintered ferrites made for use in magnetic heads.

**Table 15.3** PROPERTIES OF DENSELY SINTERED FERRITES FOR MAGNETIC HEADS[177]

| *Designation* | $\mu_i$ ($\mu_0$) | *Porosity* (%) | $B_s$ (V s/m²) | $\varrho$ (MΩ cm) | $T_c$ (°C) |
|---|---|---|---|---|---|
| 8 C 1 | ~1 500 | <0·5 (usually 0·3) | 0·39 | >1 | ~130 |
| 8 D 1 | ~ 400 | <0·5 | 0·46 | >1 | ~300 |

These ferrite heads are of particular importance for picture storage (videotape machines). At the high bandwidths called for in this application, namely 7–8 MHz, they are used both for writing-in and reading-out. The same head is used for both functions, being switched, for reproduction, to the input of the playback amplifier[159].

It has long been possible to use ferrite cores for erase heads[156] since, by reason of the relatively wide gap, the grain-size and porosity are less harmful, and because, also, ferrite cores are especially well suited to high-frequency operation[43]. A high erase-frequency makes for clean erasure and reduces noise. An improved version of erase head has two gaps of different widths.

## 15.4 DRUM STORES

### 15.4.1 Operation and construction

The magnetic drum, like the magnetic tape, is a film (or surface) store in which information is stored by the action of a recording head on a magnetisable layer. The magnetic layer of a drum can be thicker than on a magnetic

tape and this makes for better efficiency[180]. However, thinner layers are more suitable for greater capacities or 'bit-densities'. An average drum store has an access time of about 10 ms and this is adequate in many cases. In operation, the drum is both cheap and reliable. It was developed during the war in Germany by Billing[18, 19] and in the USA by Eckert[51]; it is principally used for computer work.

The peripheral speed of a drum store is usually 20–80 m/s and corresponds to a multiple of the usual tape speed, so that, because of the greater danger of wear, the magnetic heads do not as a rule bear on the magnetised surface. This leads to a low information density. A rule of thumb states that the separation between the head and the magnetic surface should be, at most, 10% of the bit-length[104]. In a special case, by using a rubber coating in which the magnetic particles were embedded and using the rather low speed of 4·5 m/s, it was possible to allow contact between the coating and the head without damage to the surface[17].

In essence, a drum store consists of a carefully centred metal drum to whose outer surface the magnetic coating is applied. The angular speed depends on the diameter of the drum. A number of fixed magnetic heads which, in general, serve as writing and reading elements are mounted just above the surface. Figure 15.8 (see plate section) shows a view, together with a diagrammatic representation, of a drum store made by Standard Elektrik Lorenz AG[175]. Devices by other manufacturers are of similar construction[128].

### 15.4.2 The magnetisable coating

The magnetic coating of a drum store can be either metallic or an oxide. Alloys of Ni–Fe, Ni–Co, or Cu–Ni–Fe as well as direct nickel coatings can be galvanically or electrolytically deposited or wound as a helical strip around the drum, while oxide coatings can be applied as lacquers carrying a suspension of magnetite or $\gamma$-$Fe_2O_3$ as for magnetic tapes. In all cases the thickness of the coating, its uniformity, and its smoothness must be carefully controlled.

Since the magnetic surface is not disturbed by the heads, but lies at a distance of a few micrometres from them, the drum can be allowed to rotate continuously without the wear which makes frequent changes of head necessary on tape machines.

The factors which principally govern the type and thickness of the surface material are the bit-density and the required amplitude of the read-out signal. If high bit-density is required, i.e. if, for example, 5–10 units of information, or even more, are to be carried by a trace 1 mm long, then the coercivity of the drum coating must be high. Oxide coats, especially suspensions of $\gamma$-$Fe_2O_3$, achieve coercivities of about 20–25 kA/m and are therefore very often used for such drum stores. Bit-densities up to 12 bits/mm can be obtained in this way. Coatings containing iron oxide are easy to produce, have uniform characteristics, and may be easily renewed if necessary. It has also proved possible, however, to deposit alloys of nickel and cobalt having an $H_c$ of 25 kA/m and more[104]. Experiments with Cunife wire (Cu–Ni–Fe

alloy) whose coercivity amounts to 44 kA/m have shown that this material is capable of a bit-density of 40 bits/mm[11].

High writing currents are needed to saturate a high-coercivity layer. Where these high signal currents are not available, however, surface materials of lower coercivity are of interest. Materials with a coercivity of some 8 kA/m are adequate for bit-densities below 5 bits/mm. Low-coercivity oxides and also nickel-plating are capable of meeting these requirements. The mechanical and magnetic properties of galvanically or electrolytically deposited layers are very largely determined by the type of manufacturing procedure (composition of the plating bath, its temperature, and the rate of deposition). Information densities up to 14 bits/mm can be obtained with improved nickel-plating techniques.

The amplitude of the output signal depends on the remanence of the surfacing material. Metallic materials usually have a higher remanence than the oxides. Moreover, iron oxide particles embedded in a plastic matrix are highly 'gapped', whereas this is less true of compact ferromagnetic coatings.

There is an optimum thickness for each magnetic coating of a drum which may be determined experimentally. Thus Ball and co-workers[11] found that 5–7·5 μm was the best thickness for nickel-plating. If a thicker layer was used, the rectangularity of the hysteresis loop suffered and the field did not penetrate sufficiently into the material to saturate the whole layer. Thinner coverings are often insufficiently strong mechanically. May and co-workers[104], by using Ni–Co as the plating material, succeeded in producing layers of 2·5 μm or less without blemish. This thickness proved the best for a rapidly rotating drum with a bit-density of 14 bits/mm. The coercivity of the coating amounted to 25·6 kA/m.

### 15.4.3 Magnetic heads

In principle, similar specifications apply to the recording and reproducing heads of a drum recorder as for a tape machine, but the pole-pieces just above the surface must be designed to meet the conditions of the rotating drum. Since, with certain exceptions, the head is not in contact with the magnetic coating, the field crossing the gap must be as densely concentrated as possible. This is achieved more easily with a pointed than with a flat pole-piece. Figure 15.6 makes possible a comparison, following Leilich[96]: it is seen that, with a sharper pole-piece, the read-out flux is indeed lower but it gives a significantly sharper pulse. This is in spite of the further difficulty that, in the example given, the head with the pointed pole-piece had a wider gap than that with a flat pole-piece (60 μm against 30 μm). The greater flux concentration enables three times as great an information density to be obtained with the pointed type as with the flat type.

According to the investigations of Shew[167], the information density can be still further improved if not only the bit-length but also the bit-width (and with it, the width of the trace) is optimally chosen to give the maximum number of tracks on the external surface of the drum. As many as 1600 bits can be registered on a square millimeter with a contact-free recording head.

Consideration must be given to Ni–Fe alloys (Mumetal) or Mn–Zn

ferrites for the core material of the magnetic heads—remembering that drum recorders generally use the same head for the writing and for the reading function. The higher saturation density of Mumetal, which is important for the writing process, and its higher initial permeability, important for read-out, seem to make this alloy superior to the ferrites. However, aside from the manufacturing difficulties mentioned in connection with tape-recorder heads, the eddy-current effect tells against the use of a high-conductivity metal. Ferrites can be used without lamination: they have a high specific electrical resistance, which means lower losses at high frequencies. Moreover, they are cheaper to produce.

### 15.4.4 Detailed examples of drum stores

Magnetic drums are made in various sizes and in various forms, according to the proposed use. A few examples are here briefly mentioned.

The smallest drum store known up to the present measures 2·5 cm × 2·5 cm × 2·5 cm and can hold 4 096 twelve-bit words on a chemically applied coating of Ni–Co[123]. The access time is 7·8 ms and the capacity 40 bits/mm. Some 300 000 bits can be stored at a density of 14 bits/mm on a somewhat larger drum measuring 9·25 cm × 9·25 cm × 18·5 cm overall. The drum rotates at 12 000 rev/min. Also, this drum uses a plating of Co–Ni as its magnetic layer[104].

The device designed in the Technical University at Munich, which is called PERM (an acronym for *P*rogrammgesteuerte *E*lectronische *R*echen-anlage *M*ünchens, or programme-controlled electronic computer device) uses a drum 10 cm in diameter. It is 22 cm long and rotates at 15 000 rev/min. Its circumference carries 217 tracks, each bearing 6·5 units of information per millimetre. The 0·5 μs write-pulses have a peak current value of 500 mA. The drum can store *in toto* 409 600 bits[96].

The Siemens digital computer 2002 uses a magnetic drum[128] with a diameter of 40 cm and a height of 28 cm. This turns at 2610 rev/min and has a magnetic surface layer 20 μm thick. In the eight banks are 24 heads, whose cores are made of 'Siferrit' having a $\mu_i$ of $2000\mu_0$, a $B_s$ of 0·35 V s/m$^2$ and an $A_L$ value of 29 nH/turn$^2$. The heads are mounted at a distance of 40 μm from the magnetic surface. The writing density amounts to 3·6–4·2 bits/mm and the storage capacity can reach $10^6$ bits.

The magnetic drum memory of the (Philips) electronic computer called PASCAL turns at 6000 rev/min and can store 16 384 words of 44 bits each[121]. It works in conjunction with a tape memory store carrying $10^6$ words (each of 44 bits) and a magnetic toroid store which can hold 2 016 words of the same length.

## 15.5 MAGNETIC DISC STORES

The disc store has a capacity which is intermediate between that of a tape and a drum. The access time is about 0·5 s for a storage capacity of about $5 \times 10^6$ decimal figures. The disc memory store was developed in the USA

around 1955 and shown in Germany for the first time in 1957[158]. Experimental memories having a capacity of $50 \times 10^6$ units and a mean access time of 0·25 s have been made in Japan.

One version of the disc store consists of 50 aluminium discs 60 cm in diameter and 2·5 mm thick mounted on a common axle at a mutual spacing of 7·5 cm. The discs are provided on each face with a magnetic coating made of $\gamma$-$Fe_2O_3$ dust on which information is recorded by a movable writing head. The principle is shown in the sketch of Figure 15.9[19], while another version is pictured in Figure 15.10 (see plate section).

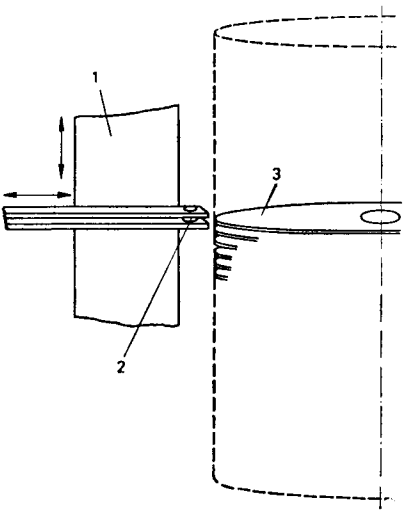



*Figure 15.9. Magnetic disc store by IBM (diagrammatic): 1, guide plate; 2, magnetic heads; 3, disc*[19]

Two read–write heads are mounted on a movable bracket and so arranged that one faces the upper side and one the under side of the disc. The arrangement slides up or down a guide pillar to the selected disc and then advances between the discs to the chosen track. There are 100 concentric tracks, spaced at 1·3 mm, on each face of each disc[152]. On average it takes 0·5 s to find the required track. The magnetic head does not touch the surface either in writing or in reading. A constant separation of 7·5 μm is maintained by a pneumatic device. There are four information units per millimetre on the innermost track, and 2·7 units per millimetre on the outermost track. Each of the two magnetic heads has two separate magnetic circuits for writing and erasure, the erasing track being always somewhat wider than the writing track.

A storage device which is similar in many respects to the disc store is the foil store[27, 94]. The rotating aluminium discs are replaced by eight polyester foils 50 μm thick coated on one side with a magnetic material. The magnetic heads are arranged on a mounting detail so designed that optimum separation can be maintained between the heads and the surface.

## 15.6 TOROIDAL CORE STORES

As compared with drum, tape, or disc storage devices, the memory store using individual cores has the great advantage that there are no moving parts. The toroidal store is an electronic store: it dispenses with all abrasion, the reliability is correspondingly greater, and the access time appreciably shorter—this amounts to between 1 μs and 5 μs where ferrite cores are used. In computer installations, magnetic tapes or drums serve well as input stores or as devices into which results can be fed, but it is the quick-operating electronic memory that is used as the computer's working store. The costs of a core memory are increased by the use of expensive reading devices.

The individual cores were originally strip-wound cores made of grain-oriented Ni–Fe (Permenorm 5000Z or Deltamax)[86]. Today they are principally ferrite toroids though strip-wound cores of the later-developed alloys can also be used for storage cores.

### 15.6.1 Principle of operation

The magnetic storage of data in individual cores often relies on the coincidence principle[132]: the cores are arranged in the form of a 'matrix', a practical version of which is shown in Figure 15.11 (see plate section)[126]. The wiring of the toroids can be seen in the enlarged portion in the left-hand half. The same thing can be seen in a different form in Figure 15.12, where it is set out schematically as an aid to understanding the principle[78].

The magnetic material employed has a rectangular hysteresis loop as shown in Figure 5.7[78]. The loop is driven to the maximum intensity $\pm H_m$,

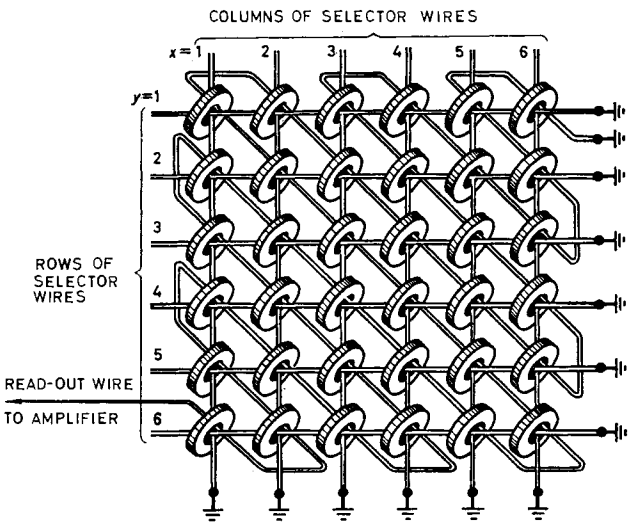



*Figure 15.12. Matrix for coincident current memory*

to which correspond ordinates of $\pm B_m$. With the field switched off, one of the two stable positions $+B_r$ or $-B_r$ is taken up. These are designated 1 and 0 in computer work[181]. Electronic (and other) computers are built on the binary system which, as the name implies, uses only two digits by means of which all numbers can be expressed. Numbers, in fact, can be expressed by means of successive powers of 2. Thus, for example, the number 13 can be written $1\times2^3+1\times2^2+0\times2^1+1\times2^0$. Similarly, 14 is written 1110 and 15 is written 1111, etc. Four bits are needed to register any of the above numbers.

In a rectangular loop the point $B_d$ is important as well as $B_m$ and $B_r$. As can be seen from Figure 5.7, this is defined as the flux density corresponding to $-H_m/2$. In what follows two designations will recur, namely

$$\text{Remanence ratio} \qquad R_v = B_r/B_m \tag{15.2}$$

and

$$\text{Rectangularity ratio} \qquad R_s = B_d/B_m \tag{15.3}$$

Either concept can occur in two ways: as a ratio either relating to a material or relating to a core. The assumption underlying the material value is that the wall thickness of the toroid is vanishingly small since only in this case will the field strength be uniformly distributed over the cross-section. In practice, however, the wall is of finite thickness. Thus, for example, a common ferrite ring may have dimensions 2 mm$\times$1·3 mm$\times$0·6 mm, so the ratio of diameters is 0·65 and this is well removed from unity. The magnetic force falls from the inner face to the outer face in the same ratio (see page 31). But the greater the intensity difference the greater the departure of the loop

$$\Phi = \int V \, dt = f(I)$$

from the rectangular shape[90]. Therefore, both the core remanence ratio $r_v = \Phi_r/\Phi_m$ and the core rectangularity ratio $r_s = \Phi_d/\Phi_m$ differ from the corresponding values for the material, as expressed by equations 15.2 and 15.3.

The core denoted in Figure 15.12 by the coordinates $x = 3$, $y = 4$ can be brought to state 1, according to the coincidence principle, in the following way: a half-pulse ($I/2$) is sent through the column wire 3 and the row wire 4. Only core (3, 4) is acted on by the two half-pulses simultaneously. They produce a magnetic intensity $H_m$ and so, after the passage of the pulse, the digit 1 will have been written in. All other cores of the matrix threaded by the $x$-wire 3 and the $y$-wire 4 receive only half-pulses. If some of these cores are in state 1, then this state remains essentially unchanged after a reversible change of intensity; if some find themselves in state 0, the magnetic intensity is insufficient to carry the material over the knee of the hysteresis loop. Ideally, then, only a reversible magnetic change occurs which cannot shift the core from the $-B_r$ position.

Memory-core materials must therefore have a hysteresis loop such that half-pulses cannot bring about an irreversible change of magnetic state. A high remanence ratio $R_v$ is thus not sufficient by itself: rather must the

rectangularity ratio $R_s$, defined by equation 15.3, have a value near unity. Rectangularity is not so strictly necessary for cores which are to be used only for switching.

A high rectangularity ratio $R_s$ is found in any given material only over a particular range of field intensity, as can be seen from Figure 4.18 and which is made even clearer by the example of a 'rectangular' ferrite shown in Figure 5.8[78]. Here, the remanence ratio $R_v$ remains constant from $H = 30$ A/m up to the highest intensity measured. On the other hand $R_s$ rises for low amplitudes, reaches the value $R_s \geqslant 0{\cdot}9$ at about 40 A/m, remains at this value to about 70 A/m, and then falls off steeply. In the plotted intensity range, $B_m$ and the apparent coercivity $H_1$ rise together. The ratio $H_m/H_1$ lies between 1 and 2.

If the magnetic state is 'interrogated' or 'read', then, keeping to the same example, a negative half-pulse is passed down wires $x = 3$ and $y = 4$. A full impulse then acts on the core at the intersection, and only on this core and, since it is now supposed to have been put into state 1, demagnetises it. This induces a signal voltage $V_R$ in the read-out wire. The interrogation process erases the information stored as '1' and, if it is still to remain stored, it must be written in again—which is feasible without too much difficulty.

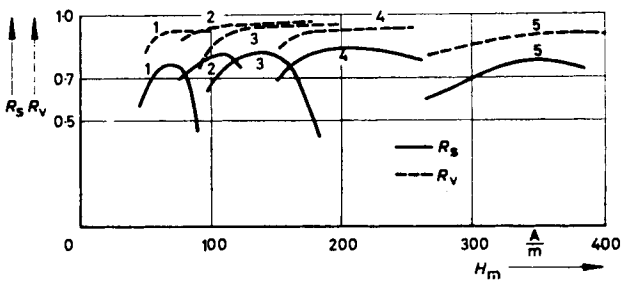



*Figure 15.13. Rectangularity ratio $R_s$ and remanence ratio $R_v$ of the ferrites labelled 1–5 in Table 15.8 as functions of peak field intensity $H_m$*[187]

According to the material employed, the range of rectangularity may be shifted towards higher or lower field intensities (see, for example, Figure 15.13). This is of importance in so far as the magnetic reversal time involved in the coincidence process depends on coercivity. In quick-operating memories the time taken for the remanence to change sign is of critical importance. The flux reversal is completed in a shorter time the higher the impressed field intensity. Figure 15.14 gives a family of curves which show the time dependence of induced signal voltage for various driving intensities[77]. It will be seen that, for increasing field intensity, the peak voltage of the read-out signal rises and the duration falls.

From the voltage curves one may define the switching time $t_s$ as the time needed for a signal pulse to rise from 10% of its peak value to maximum and then to fall back to 10% (see Figure 15.15). According to another definition, the switching time is measured from a reference time $t_1$. Here, $t_1$ is the time in which the interrogation pulse attains 10% of its peak value. The time required to reach peak voltage is called the peak time $t_p$. If the peak voltages

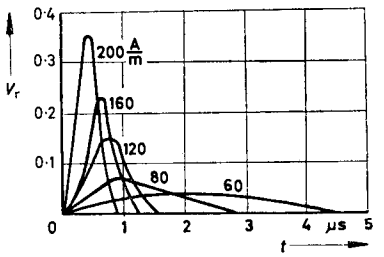



*Figure 15.14. Time dependence of signal voltage for a ferrite memory core 2* mm × *1·3* mm × *0·6* mm *(at a driving intensity of 200* A/m, *pulse rise-time* $t_r$ = *200* ns*)*[77]

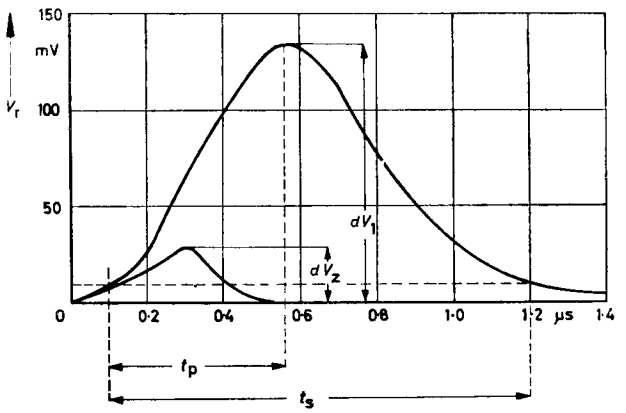



*Figure 15.15. Signal characteristics*

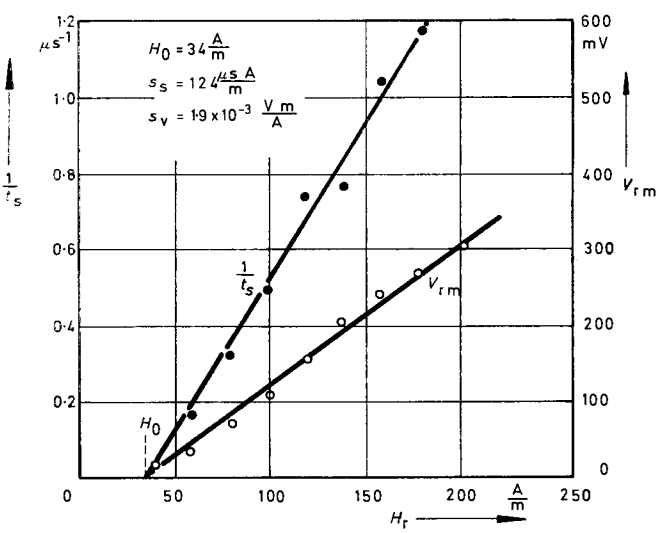



*Figure 15.16. Reciprocal switching time and maximum signal voltage* $V_{rm}$ *of a ferrite memory core as a function of read-out field strength* $H_r$[77]

taken from Figure 15.14 and the reciprocals of the switching times are plotted against the read-out field strength $H_r$, the result is nearly a straight line in both cases (see Figure 15.16). These straight lines do not pass through the origin but cut the abscissa at the critical field strength (or threshold field strength) $H_0$[77]. At field strengths below $H_0$, the core is not taken through the magnetic cycle. In general, $H_0$ is not very different from the apparent coercivity $H_1$. Figure 15.16 shows that $H_0 = 34$ A/m for this special core.

The voltage rises according to the linear equation

$$V = s_v (H - H_0) \tag{15.4}$$

where $s_v$ is called the *voltage constant*. For cores of a given volume it depends on core dimensions and on core material. For the 2 mm×1·3 mm×0·6 mm core already referred to, for example, $s_v = 1{\cdot}9 \times 10^{-3}$ V m/A. The *switching constant* $s_s$ can similarly be taken from Figure 15.16. The equation runs:

$$s_s = t_s (H - H_0) \tag{15.5}$$

In the example quoted, $s_v = 124$ μs A/m.

If, in a memory core, the half-pulse lies in the neighbourhood of the threshold field strength $H_0$, then the full pulse $H_m$ must be $2H_0$. Equation 15.5 then simplifies to

$$s_s = t_s H_0 \tag{15.6}$$

Since, however, $H_0 \doteq H_1$ and is therefore proportional to the coercivity $H_c$, it follows from equation 15.6 that, for materials having the same $s_s$, the time $t_s$ is shorter the greater the $H_c$ of the magnetic material. Experimental examples are given in Table 15.4 for two different types of core.

The switching constant is a function of the material and is susceptible to changes in its composition. Thus it is known that adding $Fe_2O_3$ to reduce the resistance also increases the switching time[67], whereas the addition of substances like MgO, which increase the resistance, lower the switching time[77]. As it is not yet possible to reduce the switching constant in this way by, say, an order of magnitude, the only way to obtain substantially shorter switching times is by raising the coercivity or by reducing the size of the core. A significant disadvantage associated with raising $H_c$ is the rising current drain. In practice, the reading current is limited to about 500 mA. The current can be less than this if the cores are of smaller section. Continual reduction in size, however, sets practical limits because of the increased difficulty of

**Table 15.4** CONSTANTS OF DIFFERENT TYPES OF FERRITE CORE[77]

| *Type* | $H_0$ (A/m) | $s_s$ (μs A/m) | $t_s$ (μs) |
|---|---|---|---|
| A. Low coercivity | 34 | 124 | 3·7 |
| B. High coercivity | 100 | 96 | 1·0 |

threading wires through tiny cores. It has nevertheless proved possible to mass-produce very tiny cores having an outer diameter of 0·3 mm and an inner diameter of 0·2 mm and to perform all necessary operations on them. Miniature cores with an inner diameter of 75 μm and an outer diameter of 225 μm can be made by electronic drilling[161]. It is expected that inner diameters of 50 μm and outer diameters of 80 μm will be achieved. Such sizes will permit the use of ferrite memory cores in integrated circuits.

In order to identify the magnetic state of a core, two interrogation wires are needed in the bit-organised system (as explained) in which positive or negative read–write half-pulses can be passed, together with a signal conductor, or retrieval wire, in which an output signal is induced and passed to an amplifier.

Another system which leads to quicker response and to reduced strays is that of a word-organised memory, in which a complete word is written in a single column of the matrix. The read-pulse is passed down the relevant column and the response appears in the corresponding rows. In this arrangement, the reading amplitude can be greater than in the coincidence system and gives shorter times and higher voltages. In the writing operation, a half-pulse is given to all column-conductors and a second half-pulse to all those row-conductors which pass through a core in which a 1 has to be inscribed.

Still another system, giving an improved signal-to-noise ratio, works with two cores per bit and takes the cores only partially round the magnetic cycle when interrogated[138]; a number is stored as the flux difference between these two cores. In order to achieve this partial cycling, the current pulses are kept very short. They must also have a short rise-time to give sufficiently large signals. Access times of less than 1 μs have been achieved.

### 15.6.2 The cyclic magnetising or flux-reversal process

If the field intensity is taken beyond the range shown in Figure 15.16 and if the switching time of a ferrite core is measured, the linearity indicated by the graph does not hold; instead, a stepped curve of reciprocal switching time is obtained. Shevel[165] was able to show that there are, in general, three distinct steps.

In Figure 15.17a the reciprocal switching time for a Mg–Mn ferrite is plotted at a reading field strength up to 1·6 kA/m. The switching constants deduced for the various intensity ranges of this curve are plotted in Figure 15.17b (curve 1). For a Mg–Mn ferrite, as can be seen, the measured low-intensity value of the switching constant ($s_s$ = 47 μs A/m) is maintained only up to about 300 A/m, after which it falls steeply to around 25 μs A/m. Above 1 kA/m the value of $s_s$ is lower still, amounting to only 10 μs A/m. The curves of switching constant against intensity are of the same general form for Mn–Cu, Mn–Mg–Zn, and Mn–Cd ferrites (curves 2, 3, and 4) but are shifted towards the lower intensity range. Rising temperature gives smaller values of switching current and a further shift towards lower intensities[165].

The three regions of the $s_s$ curve can be traced to three distinct flux-reversal mechanisms. At low intensities, flux is reversed by wall-shift

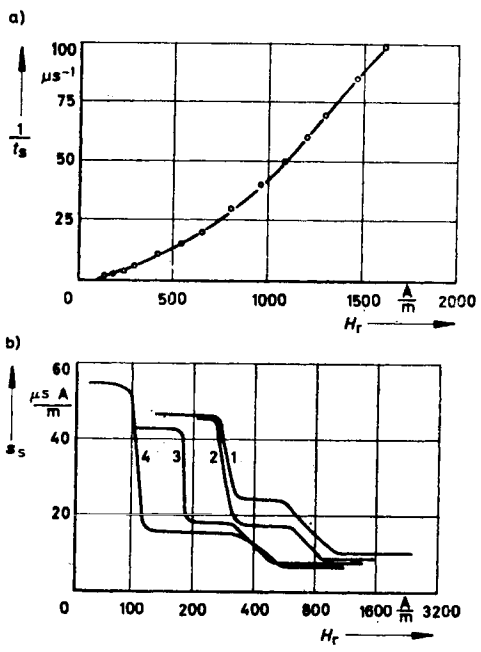



*Figure 15.17. (a) Reciprocal switching time as a function of field strength for* Mg–Mn *ferrite; (b) switching constants as a function of field strength: 1,* Mg–Mn *ferrite; 2,* Mn–Cu *ferrite; 3,* Mn–Mg–Zn *ferrite; 4,* Mn–Cd *ferrite*[165]

processes[112]. The process begins, for a field strength equal to the threshold intensity, at the inner surface of the toroid, where nuclei with opposing magnetic directions—of which there will always be a supply—begin to grow[14]. At the same time new nuclei appear, within the core, which can grow before the flux in the inner region is fully reversed. In this way the whole flux-reversal process in the core is significantly accelerated. The mechanism of flux reversal sketched here can be visually demonstrated[41] in thin ferromagnetic films by making the domains visible. Hesterman[81] considered in detail various models of flux reversal by wall movement.

The drop in switching constant at 2–5 times the threshold intensity means that another magnetising process has set in; in fact, flux reversal occurs because of incoherent (non-related) rotational processes. The domains change their direction of magnetisation, independently of each other, by reason of 180° rotations of the spin vectors[72]. This process takes place more quickly than wall shift, so the switching constant falls, according to the type of ferrite, to between 9 μs A/m and 33 μs A/m. At still higher intensities the switching constant falls to a value between 3 μs A/m and 16 μs A/m. In this process the direction of magnetisation changes over by coherent rotation of the spin vector.

Shevel[164] suggested a model which could show how flux reversal by coherent rotation occurs in toroidal cores; this is reproduced in Figure 15.18. In the original condition the lines of magnetic force run more or less parallel to the axis of the ring (Figure 15.18a), but at higher opposing field strengths the lines become helical (Figure 15.18b). The pitch of the helix falls at higher intensity values and becomes zero at a critical intensity, i.e. the lines fall into closed loops (Figure 15.18c). The magnetisation finally tips over and the

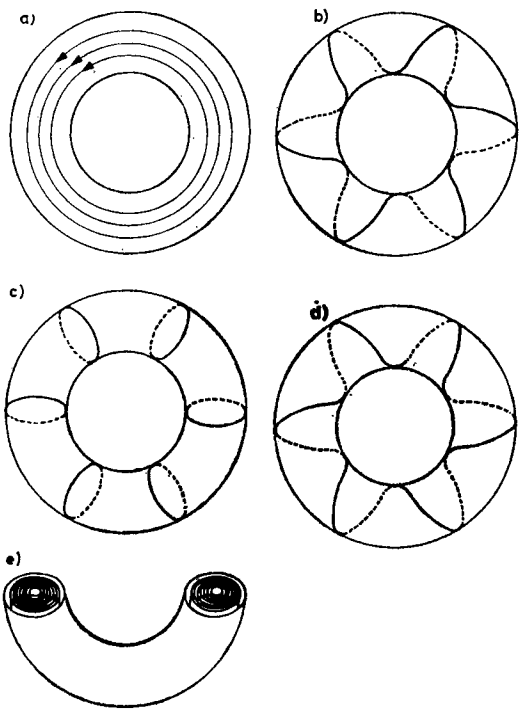



*Figure 15.18. Mechanism of flux reversal by coherent rotation in a solid toroidal core*[164]

lines of force again become helical but in the opposite sense (Figure 15.18d). The flux remains within the toroid at each stage. The model also prescribes that the magnetism of the core should consist of concentric shells of small wall-thickness (Figure 15.18e). The sign and pitch of the flux spirals are independent of each other in any given shell.

### 15.6.3 Requirements for core materials

The following requirements are laid down for toroidal memory-cores:

1. The core should experience no irreversible change of magnetisation on receipt of a half-pulse but should be fully changed over by a whole pulse: the core material should therefore have a rectangular-shaped hysteresis loop with a high rectangularity ratio.
2. Changes of magnetisation should occur quickly and the operating signal should therefore be short: the material should have a low switching constant $s_s$.
3. The useful (response) signal should have a high maximum, and stray (disturbing) signals should have as low a maximum as possible: the remanence of the material must therefore be high and the reversible permeability at the remanence point low.

4. The applied interrogation current should be low: this is achieved by using a material whose apparent coercivity $H_1$ is low.
5. The signal voltage should lie within close tolerances independently of the previous history of the core: the core material should therefore be very uniform and readily reproducible.

To these particular requirements must be added some general ones, such as constancy of properties with time and with temperature; adequate mechanical robustness to facilitate handling; finally, it should be possible to manufacture the cores economically.

Cores having rectangular hysteresis loops are used for switching circuits in communications engineering as well as for storage devices[56, 192]. In electronically controlled telephone circuits, in which they are used in conjunction with transistors, switching cores have proved to be indispensable components. They are used in shift registers, counting circuits, pulse generators, and code translators[168]. Where cores serve only to produce switching pulses, as high a degree of rectangularity as for storage cores is not required. Indeed, a high remanence ratio is often desirable but even more important, as a rule, are high flux density and low coercivity. Experience has shown that cores whose hysteresis loops are somewhat rounded at the corners switch more rapidly than those with sharp corners.

### 15.6.4 Characteristic curves of a memory core

It is true that the quoted requirements for storage and switching cores are intimately bound up with the properties of the hysteresis loop; nevertheless, the loop itself gives no more than a rough picture of what goes on in a core during magnetic reversal. The hysteresis loop is not a sufficient basis for judging the practical value of a memory-core material; rather must the core be tested under conditions which represent actual operating ratios of a core matrix. For this purpose it is normal practice to employ current pulses of defined shape and duration, which can be applied in a specified sequence to the test piece, and to observe the induced voltages occurring under various operating conditions and assumptions. Figure 15.19 gives a diagram of such a pulse-train[79]; the positive writing pulse is indicated by $I_w$ and the negative reading pulse by $I_r$.

After a 1 has been written in by means of a whole positive pulse, a full negative pulse $I_r$ is applied. This induces in the retrieval wire a read-out signal whose voltage is as high as possible. Since no 'disturbing pulse' precedes the read-out pulse, the undisturbed signal $V_1$ (labelled $uV_1$, indicating undisturbed) appears at the output. This is shown schematically at the bottom of Figure 15.19. A number of positive half-pulses (generally six to eight) now follow—these are the disturbing pulses referred to above—before another full reading pulse $I_r$ occurs; these should produce no significant change in the reading signal. Actually, a small disturbance signal appears and this has been labelled $dV_z$ (meaning disturbed zero).

In a similar manner, by acting on the state 1 with negative half-pulses and finally reading-out by the application of a full pulse, the signal designated

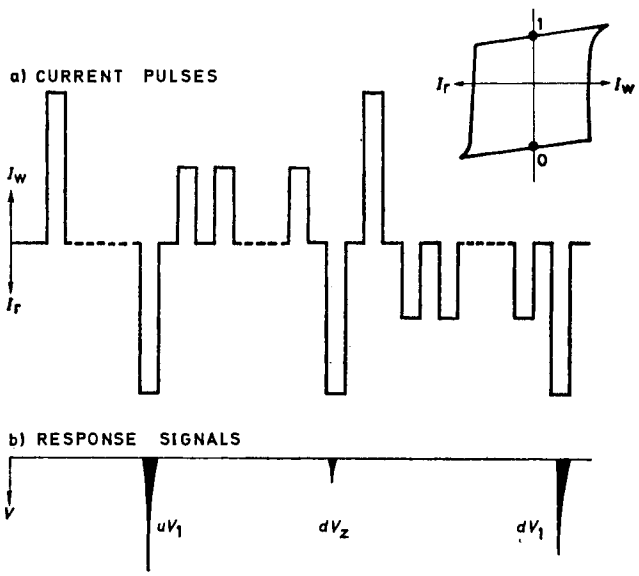



*Figure 15.19. Diagram of pulse sequence*[79]

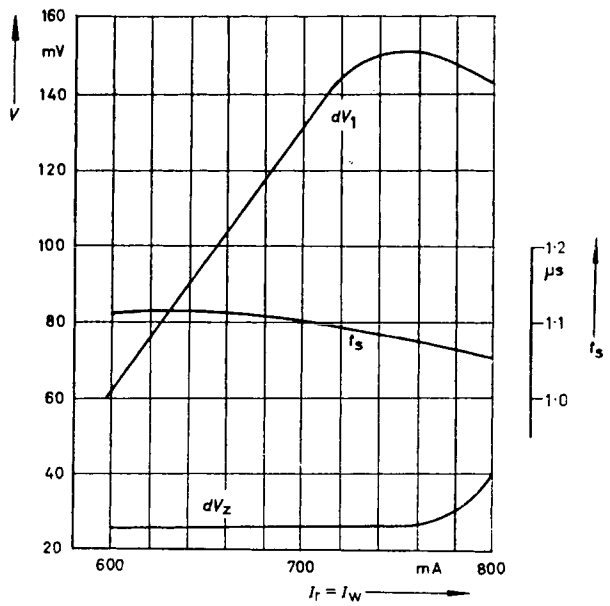



*Figure 15.20. Dependence of retrieval signal and switching time on current values for a ferrite memory core*[79]

$dV_1$ is obtained (see Figure 15.15). The voltage $dV_1$ is always less than $uV_1$ but the difference is very small in a good core.

Theoretically, it should be enough to give to the half-pulses the true half value of the full pulse—which is what the name suggests—the 'disturbance ratio' thus being 50%. In practice, the test employs somewhat sharper pulses to allow for the effect of tolerance limits. In core testing, the negative tolerance of the full pulses is taken and the positive tolerance of the half-pulses; in general, this amounts to about 10%. Thus instead of testing with, say, 740 mA and 370 mA, it is normal practice to use 670 mA and 410 mA, i.e. a disturbance ratio of 61%.

If this measuring method is used and if $I_r$ and $I_w$ are varied continuously, and if, further, the corresponding values $dV_1$ and $dV_z$ are measured, then the characteristic of a memory core can be plotted. As an example, Figure 15.20

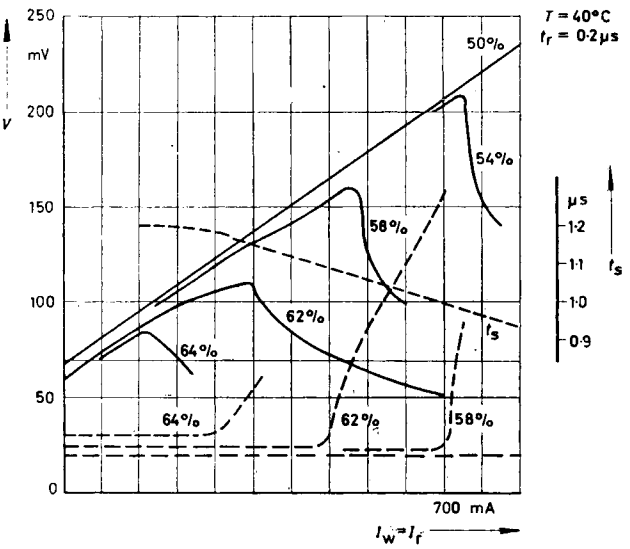



*Figure 15.21. Effect of the disturbance ratio on maximum output voltage*[79]

shows the characteristic of a ferrite core of 2 mm outer diameter[79]. The rise-time $t_r$ of the reading pulse was 0·2 µs, the disturbance ratio 61%, and the measuring temperature 40°C. As the reading amplitude increases, the signal voltage $dV_1$ reaches a maximum at 750 mA and then falls again; $dV_z$ remains nearly constant to about 750 mV and then rises with increasing steepness. The voltages were referred—as is common practice for memory cores—to a single turn. For individual materials, the rise of $dV_z$ and the fall of $dV_1$ occur at higher values of the amplitude $I_r$, the higher the coercivity. In the example referred to, the signal-to-noise ratio at 740 mA was 150 : 25.

The switching time as a function of the amplitude of the reading pulse is also plotted in Figure 15.20 and, as Figure 15.15 makes clear, this can be determined together with $dV_1$. The time $t_s$ falls slowly and has an average value of 1·1 µs.

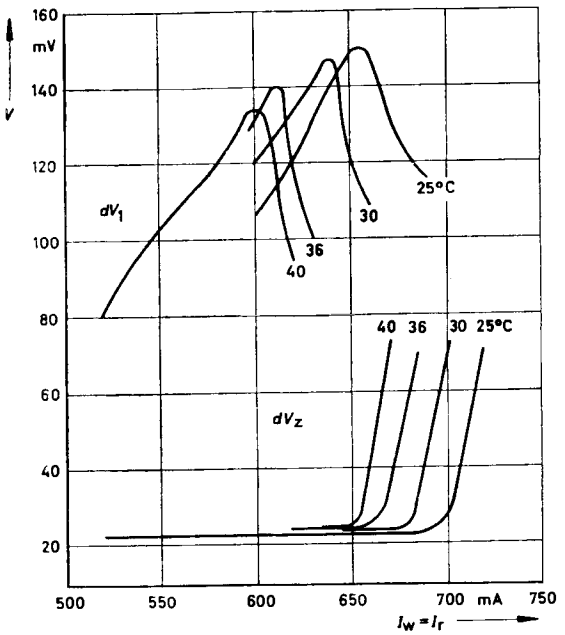



*Figure 15.22. Temperature variations of $dV_1$ and $dV_z$ for a ferrite memory core ($t_r$ = 0·2 μs, disturbance ratio = 61%)*[79]

If tests are conducted with square pulses of different rise-times $t_r$, it is found that the signal voltage and the switching time are affected: the steeper the front of the pulse, the higher is the maximum output or 'answering' pulse and the shorter the switching time. Again, the smaller the disturbance ratio used in the test, the higher the peak of the signal curve and the higher the $I$ value at which the peak occurs.

In Figure 15.21 characteristics are plotted for 40°C, and for the same pulse sequence, but for different disturbance ratios of 54%, 58%, 62%, and 64%. With increasing disturbance ratio, $dV_z$ increases and so the optimum signal ratio $dV_1/dV_z$ falls off continuously. The greater the disturbing pulse relative to the complete pulse, the more irreversible processes are involved. The optimum signal ratio falls off with the disturbance ratio more or less linearly. The slope of this fall is a function of the material of which the core is made.

It is the usual practice to test memory cores at 40°C. Experiment shows that at lower temperatures $dV_1$ is higher and $dV_z$ lower, i.e. the core becomes better. Figure 15.22 shows the shift of the optimum signal with temperature ($t_r$ = 0·2 μs and the disturbance ratio is 61%). The straight-line switching characteristic, $1/t_s = f(H)$, at temperatures between −115°C, and +250°C is plotted in Figure 15.23[80] for a toroid of $Cu_{0·25}Mn_{0·75}Fe_2O_4$: as the temperature rises $H_0$ and $s_s$ become smaller.

The test procedure described, largely—though not entirely—corresponds to core operating conditions but must be supplemented by various other tests. The pulse-train shown in Figure 15.19 consists of both positive and

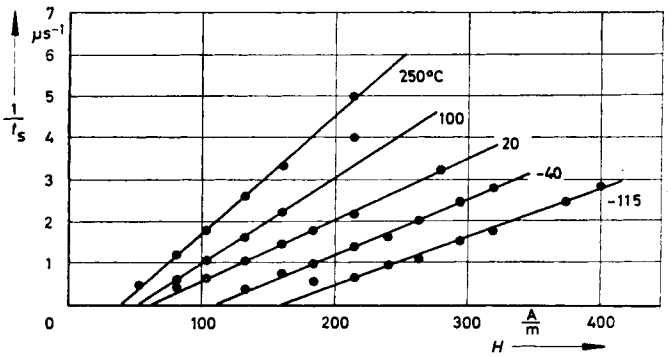



*Figure 15.23. Linear switching time characteristics $1/t_s = f(H)$ for the ferrite* $Cu_{0.25}Mn_{0.75}Fe_2O_4$[80]

negative pulses, generally eight in number and of equal amplitude. In actual operation, however, less-unidirectional pulses sometimes occur and so symmetry is no longer maintained. The magnetic disturbances during individual half-pulses are the cause of the so-called 'delta signal'[130].

The delta signal is defined as the difference between the half-voltages produced in a core which is in state 1 or state 0. This can be conceived as the difference in effective permeability, measured with a positive current pulse, of a core which is at either the positive point of apparent remanence or the negative. The maximum value of the delta signal lies, for all ferrites, somewhere around 10% of the maximum disturbance signal.

### 15.6.5 Core materials

When measurements were first performed on memory cores, in 1949, only alloy materials with rectangular loops were available[181]. Not until the discovery of 'square ferrites'[5] did core memories receive their first impetus. Meanwhile, noteworthy advances were made in the field of miniature or 'dwarf' cores made from metal foil[179] although the importance of ferrite cores was scarcerly diminished by them. Now, as before, ferrite memory cores with rectangular hysteresis loops play the major role.

#### 15.6.5.1 Ferrites

It was in 1949 that Snyder, Albers-Schoenberg, and Goldsmith[174] first referred to a square-loop ferrite. This was a Mg–Mn ferrite called 'Ferramic 34A' which also showed excellent microwave properties. In the three-component system $MgO–MnO–Fe_2O_3$ of Figure 14.36 its composition lies near the limiting region both for microwave value and for square-loop quality. The high specific electrical resistance demanded by microwave technique is also a requirement for storage cores which are to be switched rapidly. The introduction of ferrite cores enabled the switching time to be decreased by a factor of 40 : 1 compared with metal cores[64].

**Table 15.5** PROPERTIES OF A FEW Mg–Mn FERRITES WITH RECTANGULAR LOOPS[5]

| *Property* | 34 A | MF 1326B | MF 1374 |
|---|---|---|---|
| $\mu_i$ at 1 MHz ($\mu_0$) | 15 | 40 | 48 |
| $\mu_m$ at 0 Hz ($\mu_0$) | 100 | 515 | 1 600 |
| $B_s$ (V s/m$^2$) | 0·0850 | 0·178 | 0·195 |
| $B_r$ (V s/m$^2$) | 0·0615 | 0·159 | 0·187 |
| $H_c$ (A/m) | 280 | 120 | 56 |
| $t_s$ ($\mu$s) | 0·5 | 1–2 | 4–7 |
| $R_s$ | — | 0·89 | 0·96 |

The ferrite types MF 1326B and MF 1374, whose properties are listed in Table 15.5, represent an advance in loop squareness over the earlier types like Ferramic 34A[5]. The table confirms equation 15.3 which states that, to a first approximation, the switching time is inversely proportional to the coercivity of the core material.

The permeabilities of the Mg–Mn ferrites are usually rather low ($\mu_i < 100\mu_0$), the saturation value of the flux density being predominantly determined by the manganese content. Short switching times and low saturation are characteristic of Mg–Mn ferrites of high magnesium content.

In storage applications, one is always confined to the range of composition which shows high rectangularity of the hysteresis loop. According to Albers-Schoenberg[6], the 'rectangular ferrites' are below stoichiometric balance and contain 40–45% $Fe_2O_3$. The MgO component should not be under 8% and the MnO content should not be less than 4–5% (see Figure 5.6).

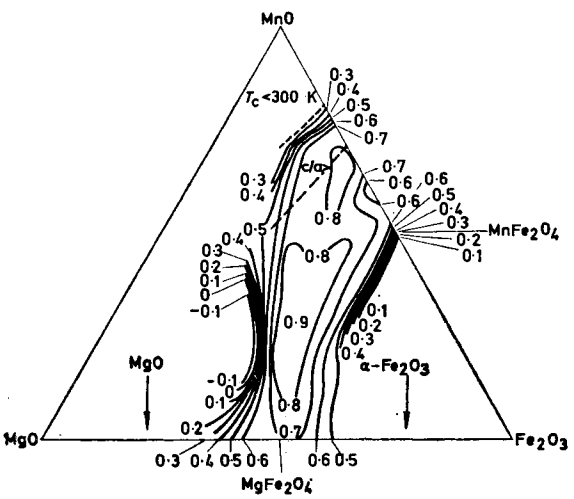



*Figure 15.24. The* MgO–MnO–$Fe_2O_3$ *system: curves of equal maximum rectangularity ratio at room temperature (arrows indicate precipitation of* MgO *at the grain boundaries and of* $\alpha$-$Fe_2O_3$ *in lamellae)*[66]

Economos[52] found the highest rectangularity ratio for a ferrite to the formula $Mg_{0.77}Mn_{0.58}Fe_{1.65}O_4$. Goodenough[66] established the fact that in the $MgO–MnO–Fe_2O_3$ system, precipitations of MgO and $\alpha$-$Fe_2O_3$ are to be avoided if square-type loops are sought. For mixture oxides sintered in air at 1200°–1450°C and finally annealed for 1 h at 1100°C in nitrogen, only a

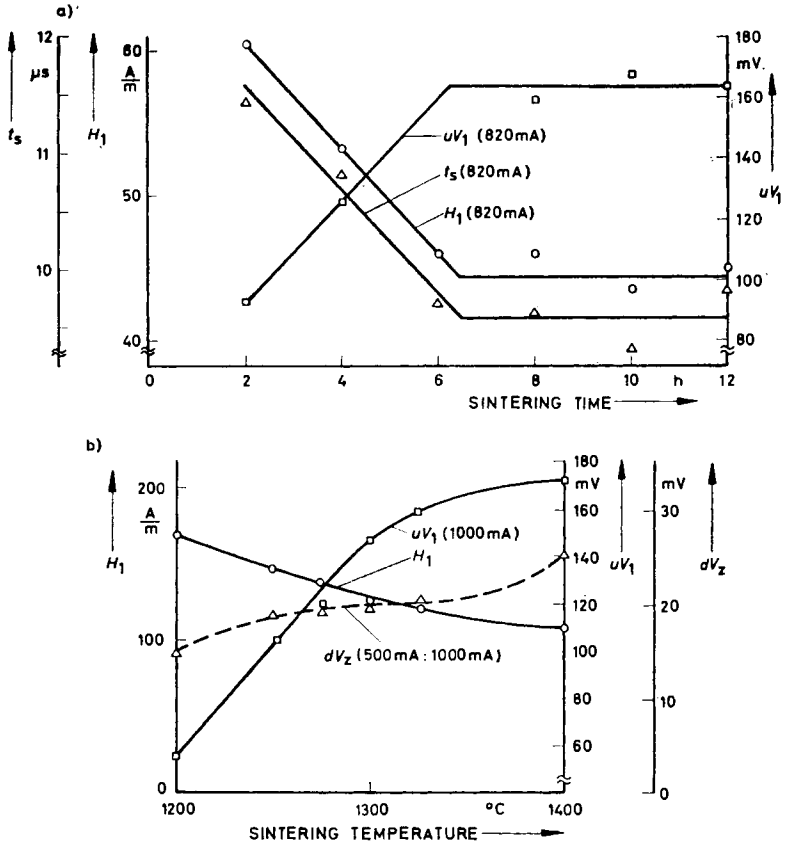



*Figure 15.25. Switching time $t_s$, apparent coercivity $H_1$, and voltages $dV_2$ and $uV_1$ as functions of sintering time and temperature for a memory core: (a) sintering temperature 1350°C; (b) duration of sinter 10* h[66]

narrow range of compositions exhibits very high rectangularity ratios $R_s$, beyond which they fall steeply by reason of the said precipitation (see Figure 15.24). Goodenough was further able to show how coercivity falls, with a corresponding increase in $uV_1$, with increasing duration and temperature of sintering (Figure 15.25).

Palmer, Johnston, and Schultz[131] substituted zinc for magnesium, step by step up to 90%, in a ferrite of composition $38Fe_2O_3 \cdot 27MnO \cdot 35MgO$. They established the following facts as a consequence of this zinc substitution: the Curie temperature falls steadily with increasing proportion of ZnO;

the flux density $B_{800}$, i.e. the density measured at 800 A/m, rises up to the point where about half the magnesium oxide has been replaced by zinc oxide and falls off steeply thereafter; the coercivity falls steadily with increasing ZnO content until it has reached about one-quarter the value appropriate to zinc-free ferrite (about 25 A/m) and then seems to rise again (Figure 15.26). The threshold field strength $H_0$ falls correspondingly from 40 A/m to about 10 A/m and the switching constant from around 80 μs A/m

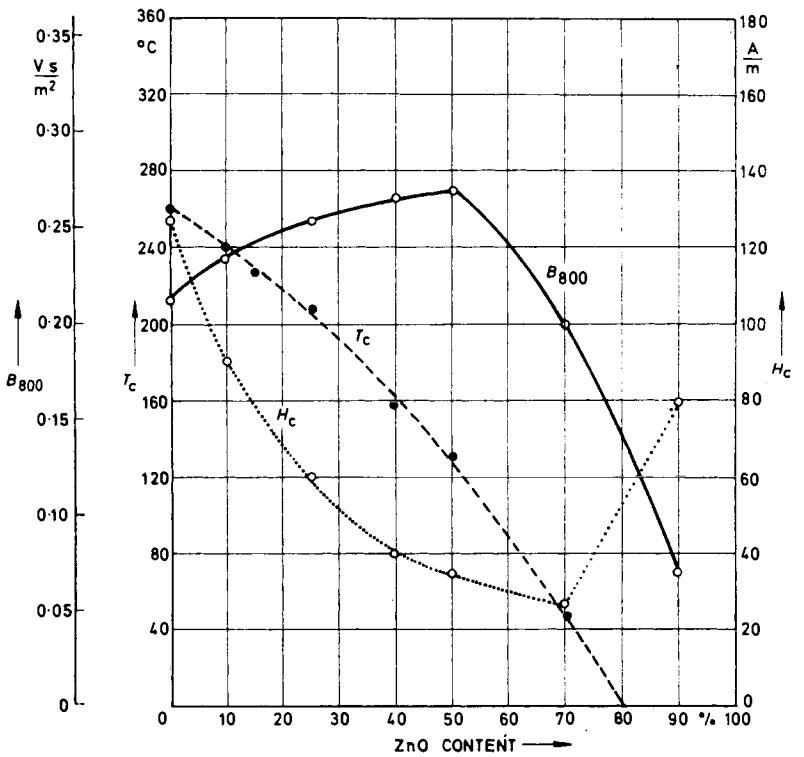



*Figure 15.26. Flux density at 800* A/m, *Curie temperature, and coercivity as functions of the* ZnO *component of the ferrite* $38Fe_2O_3 \cdot 27MnO \cdot xZnO \cdot (35-x)MgO$[131]

to 25 μs A/m. Moreover, the initial permeability $\mu_i$ rises with increasing proportion of ZnO: it rises almost linearly from about $10\mu_0$ to $1100\mu_0$ (at 70% Zn).

Goodenough[66] investigated the ferrite series $(Mn_3O_4)_{0\cdot15}(MgFe_2O_4)_{0\cdot85-x}(ZnFe_2O_4)_x$ and he found that the Curie temperature and the coercivity fell with increasing ZnO content whereas the saturation density and the maximum remanence ratio rose at first and fell off again after reaching a maximum (Figure 15.27).

The rectangularity ratio of Mg–Mn ferrites can be improved by small additions of calcium oxide and, in fact, brought almost to unity[6]. The improvement, however, involves a fall in coercivity and so the switching

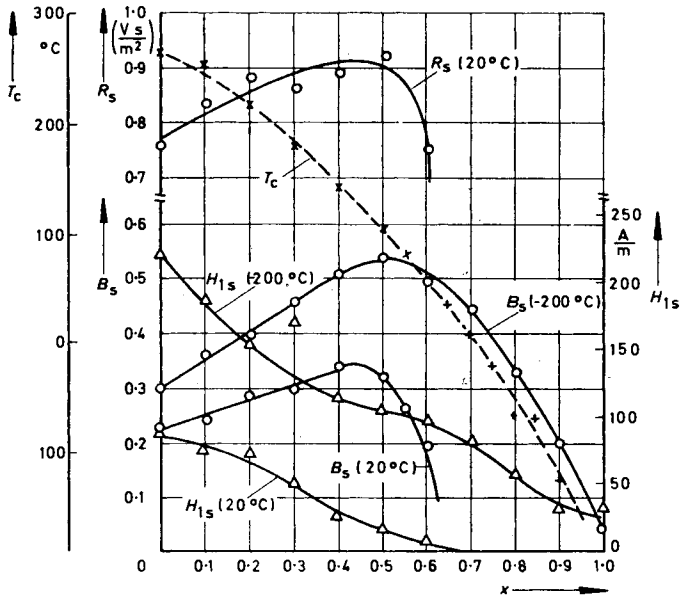



*Figure 15.27. Ferrite series* $(Mn_3O_4)_{0\cdot15}(MgFe_2O_4)_{0\cdot85-x}(ZnFe_2O_4)_x$*: Curie temperature* $T_c$*, maximum rectangularity ratio* $R_s$*, saturation flux density* $B_s$ *at* $H_s$ = 2·4 kA/m*, and apparent coercivity* $H_{1s}$*, all as functions of* $x$[66]

time is correspondingly lengthened. The action of CaO additives in raising the permeability is effective, for the Mg–Mn ferrites, only at maximum permeability. The properties of certain other ferrites not specifically designated by the author[6] are shown in Table 15.6.

According to equation 15.3, shorter switching times can only be achieved either by increasing the coercivity or by reducing the switching constant. Thus Eichbaum[55] was able to shorten the switching time of a Mg–Mn ferrite from 1·5 μs to 0·5 μs by raising the $H_c$ from 96 A/m to 280 A/m (see Table 15.7). This meant that the current rose about threefold. Table 15.7 also demonstrates that the use of steeper pulses improves the switching constant and the current demand of any particular core. If at the same time the core

**Table 15.6** PROPERTIES OF Mg–Mn FERRITES WITH CaO ADDITIVES[6]

| | | |
|---|---|---|
| $\mu_i(\mu_0)$ | 45 | 36 |
| $\mu_m(\mu_0)$ | 1 800 (at 0·14 V s/m²) | 2 700 (at 0·16 V s/m²) |
| $B_s$ (V s/m²) | 0·2 | 0·22 |
| $B_r$ (V s/m²) | 0·192 | 0·215 |
| $B_r/B_s$ | 0·96 | >0·97 |
| $H_c$ (A/m) | 48 | 16–32 |
| $t_s$(μs) | 4·7 | 4–7 |

**Table 15.7** PROPERTIES OF FERRITE CORES MEASURED IN THE COINCIDENCE ROUTINE AT 40°C[55]

| *Composition* | | | | | *Core properties* | | | | | | |
|---|---|---|---|---|---|---|---|---|---|---|---|
| MgO | MnO | $Fe_2O_3$ | CaO | $Cr_2O_3$ | *Inner diameter* (mm) | *Outer diameter* (mm) | $H_c$ *at 60* Hz (A/m) | $t_r$ (μs) | $I_r$ (mA) | $t_s$ (μs) | $s_s$ (μs A/m) |
| 37·5 | 22·5 | 40 | — | — | 1·25 | 2·0 | 96 | 0·2 | 670/410 | 1·5 | 76 |
| 37·5 | 22·5 | 40 | — | — | 1·25 | 2·0 | 280 | 0·2 | 1900/1160 | 0·5 | 76 |
| 37·5 | 22·5 | 40 | — | — | 1·25 | 2·0 | 280 | 0·1 | 1800/1100 | 0·46 | 66 |
| 37·5 | 22·5 | 40 | — | — | 0·75 | 1·25 | 280 | 0·1 | 1050/640 | 0·4 | 48 |
| 32·5 | 22·5 | 35 | 5 | 5 | 0·75 | 1·25 | 224 | 0·1 | 735/445 | 0·42 | 40 |

dimensions are reduced, the switching time can be shortened to 0·4 μs with a corresponding current reduction of 1050/640 mA. The current demand may be further reduced if, by enriching with CaO and $Cr_2O_3$, the ferrite can be so altered that, in spite of a drop in coercivity, the switching current can be brought down to 40 μs A/m (see the last column of Table 15.7).

Wijn and co-workers[187] gave a maximum rectangularity ratio of 0·81 (see Table 15.8) for a Mg–Mn ferrite of composition $(MgO)_{0.5}(MnO_{1+\delta})_{0.875}Fe_2O_3$; here, $\delta$ is intended to signify that the oxygen content of the MnO does not correspond exactly to the bivalent form of manganese. According to the same authors[187], $R_s$ lies around 0·83 for a nickel-containing ferrite $Mg_{0.4}Mn_{0.1}Ni_{0.5}Fe_2O_4$ (see Figure 15.13).

## Mg–Cu *ferrites*

To investigate mixed ferrites composed of magnesium ferrite and copper ferrite is technologically very attractive since both are characterised by extreme sintering temperatures: magnesium ferrite sinters at some 1200°C and copper ferrite at about 800°C.

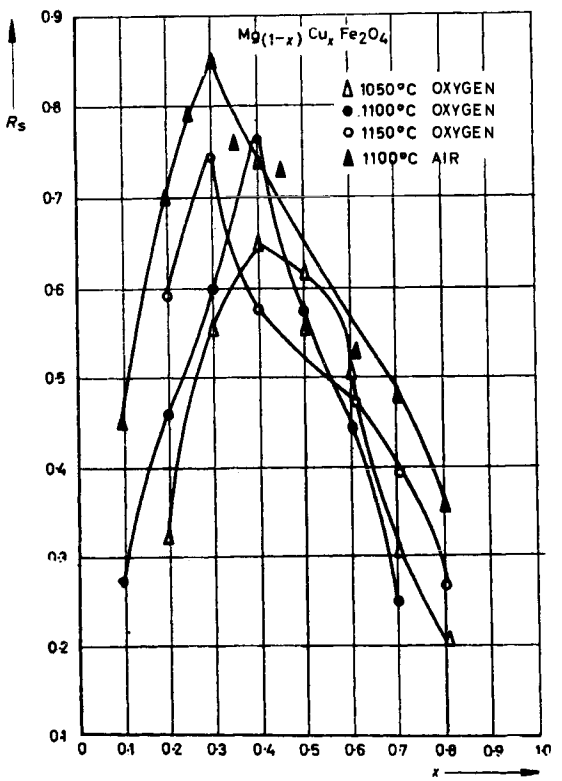



*Figure 15.28. Rectangularity ratio $R_s$ as a function of composition for* Mg–Cu *ferrites*[70]

One can see from Figure 15.28 how square loops occur in mixture ferrites[70]. The height and location of the peak value of $R_s$ depend on the sintering conditions. A best value is obtained for $x = 0{\cdot}3$ if the specimen is annealed at 1100°C in air. Individual values up to $R_s = 0{\cdot}94$ were observed. Quenching or annealing at low temperatures brings about a drop in rectangularity ratio and coercivity but an increase in saturation flux density.

The switching constant $s_s$ for these materials is 240 μs A/m and the switching time amounts to a few hundred microseconds.

## Mn–Cu *ferrites*

Wijn and co-workers[187] discovered ferrites having spontaneous square loops in the MnO–CuO–$Fe_2O_3$ system. A maximum rectangularity ratio $R_s$ greater than 0·6 was obtained, with a corresponding value of coercivity $H_c$

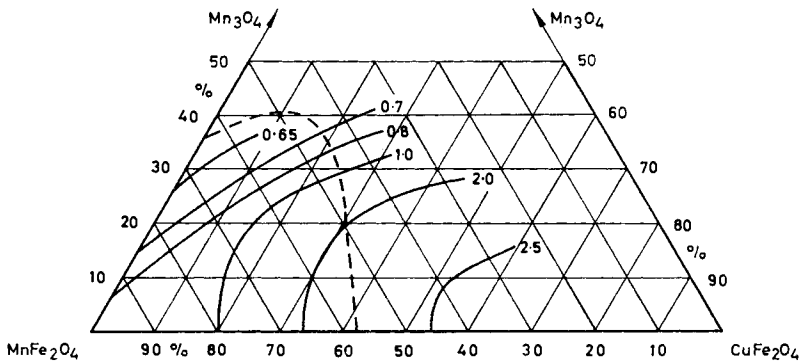



*Figure 51.29. Switching constant $s_s$ (solid line) and rectangularity ratio $R_s = 0{\cdot}75$ (broken line) for the system* $CuFe_2O_4$–$MnFe_2O_4$–$Mn_3O_4$[183]

below 320 A/m, for a ferrite to the formula $Cu_xMn_{1-x+y}Fe_2O_4$ if $x$ was in the region 0·05–0·2 and $y$ was less than 0·7[35]. For example, a rectangularity ratio of 0·75 and a coercivity of 80 A/m were obtained for the combination $Cu_{0.1}Mn_{1.1}Fe_2O_4$.

Weisz and Brown[183] carried out a detailed investigation of the system $MnFe_2O_4$–$CuFe_2O_4$–$Mn_3O_4$. Only at the manganese ferrite corner was a rectangularity ratio exceeding 0·75 obtained, namely with $MnFe_2O_4$ above 60% and $Mn_3O_4$ below 40% (see Figure 15.29). Obviously both bivalent copper and trivalent manganese, alone or in combination, contribute to rectangularity. The switching constant $s_s$ falls off with a higher manganese content. In a particular range of composition, in which the rectangularity ratio was very high, an $s_s$ of 48 μs A/m was found. The following values were measured in a toroidal core 2 mm in diameter made of Cu–Mn ferrite with a full pulse of 650 mA: $uV_1 = 80$ mV, $dV_z = 20$ mV, $t_p = 0{\cdot}75$ μs, and $t_s = 1{\cdot}42$ μs with a pulse rise-time $t_r$ of 0·2 μs[183].

**Table 15.8** PROPERTIES OF FERRITES WITH SPONTANEOUS RECTANGULAR HYSTERESIS LOOPS[80,187]

| *Ferrite* | $\mu_1$ ($\mu_0$) | $R_v$ | $R_s$ | $H_m$ *for* $R_s$ (A/m) | $s_s$ ($\mu$s A/m) | $H_0$ (A/m) | $t_s$ ($\mu$s) |
|---|---|---|---|---|---|---|---|
| 1. $(CuO)_{0\cdot1}(MnO_{1+\delta})_{1\cdot1}Fe_2O_3$ | 86 | 0·93 | 0·76 | 68 | — | — | — |
| $Cu_{0\cdot25}Mn_{0\cdot75}Fe_2O_4$ | — | — | — | — | 64 | 68 | 2·2 |
| 2. $(MgO)_{0\cdot5}(MnO_{1+\delta})_{0\cdot875}Fe_2O_3$ | 55 | 0·88 | 0·81 | 120 | 72 | 112 | 1·3 |
| 3. $Mn_{0\cdot1}Ni_{0\cdot5}Mg_{0\cdot4}Fe_2O_4$ | 138 | 0·95 | 0·83 | 136 | — | — | — |
| 4. $Mg_{0\cdot4}Ni_{0\cdot6}Fe_2O_4$ | 28 | 0·94 | 0·84 | 208 | — | — | — |
| $Mg_{0\cdot6}Ni_{0\cdot4}Fe_2O_4$ | — | 0·9 | 0·8 | 176 | 176 | 288 | 2·5 |
| 5. $Li_{0\cdot46}Ni_{0\cdot08}Fe_{2\cdot4}O_4$ | 40 | — | 0·78 | 344 | — | — | — |
| $Li_{0\cdot25}Cu_{0\cdot5}Fe_{2\cdot25}O_4$ | — | — | 0·75 | — | — | — | — |
| $Li_{0\cdot47}Ni_{0\cdot06}Fe_{2\cdot47}O_4$ | — | 0·93 | 0·85 | — | ~80 | 176 | 0·6 |
| $Co_{0\cdot1}Fe_{0\cdot9}Fe_2O_4$ | — | 0·97 | 0·95 | — | 8400 | 640 | 10 |
| Ferroxcube 6 A | — | 0·92 | 0·8 | 120 | 72 | 72 | 2·5 |
| $MnFe_2O_4$ | — | 0·9 | 0·8 | 40 | 256 | 40 | 11 |

### *Nickel ferrites*

A toroid cut from a single crystal of nickel ferrite, with the plane of the ring parallel to the (111) plane, yielded an almost square hysteresis loop. According to Miller and Barker[113], the coercivity was around 8 A/m and the switching constant 1520 μs A/m. The switching times, also, of the ternary nickel ferrites are generally longer than those of the Mg–Mn ferrites[54]. The properties of some Ni–Mg and Ni–Mg–Mn ferrites are quoted in Table 15.8[187]. The ferrite $Mg_{0.4}Ni_{0.6}Fe_2O_4$ is specially distinguished in that $R_s$ is only slightly dependent on temperature.

### Mn–Cd *ferrites*

Eichbaum[54] investigated Mn–Cd ferrites and found certain combinations which were characterised by low coercivity (about 12 A/m) and low switching constants $s_s$ (of around 16 μs A/m). The remanence ratio of these ferrites lies between 0·8 and 0·9. The apparent coercivity falls with increasing cadmium content from 44 A/m to 12 A/m (measuring field strength 200 A/m). As Table 15.9, taken from this investigation, makes clear, high $uV_1$ values are obtained at short switching times, for example $uV_1 = 1050$ mV at $t_s = 160$ ns. The ratio $uV_1/uV_2$ is between 5 : 1 and 10 : 1. In these measurements the rise-time of the pulses amounted to 50 ns. These quick-switching ferrites are not very suitable for the ordinary coincidence-switched memory. Table 15.9 offers a comparison of the switching properties of these ferrites with those of an ordinary Mg–Mn ferrite and a strip-wound core of Mo-Permalloy.

Braginski and co-workers[31] also investigated the properties of Mn–Cd ferrites. They found, however, no extensive squaring of the hysteresis loop. On the other hand, they were able to improve the rectangularity by means

**Table 15.9** COMPARISON OF MAGNETIC PROPERTIES OF Mg–Mn FERRITE WITH Cd–Mn FERRITES AND WITH MO-PERMALLOY STRIP-WOUND CORES (STRIP THICKNESS 4 μm, INNER DIAMETER 1·25 mm, OUTER DIAMETER 2·0 mm)[70]

| *Composition (%)* | | | $uV_1$ | $uV_2$ | $t_s$ | $H_c$ | $T_c$ | $s_s$ | $B_s$ |
|---|---|---|---|---|---|---|---|---|---|
| CdO | MnO | $Fe_2O_3$ | (mV) | (mV) | (ns) | (A/m) | (°C) | (μs A/m) | (V s/m²) |
| 20 | 40 | 40 | 1 000 | 200 | 90 | 12 | 90 | 17·6 | 0·15 |
| 20 | 35 | 45 | 1 000 | 200 | 90 | 18 | 95 | 16 | — |
| 16 | 47 | 37 | 1 100 | 120 | 110 | 24 | 130 | 20 | — |
| 15 | 50 | 35 | 1 200 | 120 | 120 | 32 | 135 | 20·8 | 0·18 |
| 10 | 50 | 40 | 1 050 | 130 | 160 | 52 | 160 | 24 | — |
| Mg–Mn Ferrite | | | 320 | 34 | 520 | 104 | 280 | 51·2 | 0·195 |
| Mo-Permalloy | | | 450 | 30 | 105 | 14 | 430 | 19·2 | 0·87 |

**Table 15.10** MAGNETIC PROPERTIES OF Mn–Mg–Zn AND Mn–Mg–Cd FERRITES WITH RECTANGULAR LOOPS[31]

| *Ferrite* | $B_m$ *at* 800 A/m (V s/m²) | $B_r$ (V s/m²) | $H_c$ (A/m) | $B_r/B_m$ | $T_c$ (°C) | $\mu_l$ ($\mu_0$) | $\mu_m$ ($\mu_0$) |
|---|---|---|---|---|---|---|---|
| Mn–Mg–Zn | 0·25 | 0·205 | 24 | 0·95 (at 44 A/m) | 160 | 260 | 4 500 |
| Mn–Mg–Cd | 0·24 | 0·200 | 16 | 0·92 (at 28 A/m) | 150 | 200 | 4 700 |

of magnesium additives. Compared with Mn–Zn ferrite, Mn–Cd ferrite has a lower coercivity and a higher remanence ratio. The Curie temperature of the cadmium-containing ferrites is about 5% lower than that of the zinc-containing specimens. Table 15.10 compares a commercially common Mn–Mg–Zn ferrite with a Mn–Mg–Cd ferrite of corresponding molar composition[31]. For generally similar magnetic properties, the coercivity is particularly low for Mn–Mg–Cd ferrite. Cadmium-containing ferrites are harder to reproduce than those containing zinc since cadmium evaporates more easily during heat treatment.

### *Lithium ferrites*

Wijn and co-workers[187] examined lithium ferrites of approximate composition $Li_{0.5}Fe_{0.5}Fe_2O_4$ and established the fact that positive or negative magnetostriction can be induced according to heat treatment. If this process is so adjusted that the magnetostriction scarcely departs from zero, then a material emerges having a rectangular hysteresis loop. The squareness and the mechanical properties of ferrites produced in this way are inadequate for engineering requirements; only with the addition of nickel ferrite is a worthwhile material obtained. As shown in Figure 15.13 and also in Table 15.8, a maximum value of $R_s = 0{\cdot}78$ is obtainable in this way. Practical Li–Ni ferrite cores of 0·8 mm outer diameter, tested under the usual conditions at 650/398 mA and with a pulse rise-time $t_r$ of 150 ns, have shown a switching time, in the temperature range 10°–70°C, of less than 550 ns, a $dV_z$ not greater than 7 mV and a $dV_1$ not below 28 mV[184]. Their temperature dependence is quite small.

Schwabe and Campbell[160] were able to show that, even in nickel-free lithium ferrites having some excess of lithium, very good rectangularity can be achieved if annealing is so carried out that no oxygen shortage can arise in the end-product. Experiments with specimens of the same composition but of differing grain size led to the result that, as the grain size falls, the threshold field grows and thus the switching time shortens, following equation 15.6. At a mean grain size of 2·3 μm, switching times of 120 ns were achieved in toroidal cores 1·25 mm×0·75 mm×0·75 mm ($t_r$ = 20 ns, $H_0$ = 520 A/m).

Fortin and Lessoff[60] developed two types of lithium ferrite having Curie temperatures above 600°C and differing in their coercivities; both, however,

could be used as storage cores over a temperature excursion of 100°C between −55°C and +300°C without temperature compensation.

Since lithium ferrite has a high Curie temperature of 632°C (see Table 3.3) and also a high coercivity (around 400 A/m)[160], the temperature coefficient (i.e. the percentage change of threshold field) is low in the neighbourhood of room temperature: it changes by only 1500 ppm/K. Mn–Mg ferrites with appreciably smaller threshold fields and lower Curie temperatures have temperature coefficients two or three times as large[77].

*Manganese ferrites*

In the ferrite series $Mn_{1+x}Fe_{2-x}O_4$, Matcovich and Kriessman[115] found a decrease in switching constant with increasing manganese content. Table 15.11 brings this out.

**Table 15.11** MAGNETIC PROPERTIES OF $Mn_{1+x}Fe_{2-x}O_4$[115]

| $x$ | $J_s$ (V s/m²) | $T_c$ (°C) | $K$ ($10^4$ erg/cm³) | $s_a$ (μs A/m) |
|---|---|---|---|---|
| 0 | 0·4896 | 567 | 4·28 | 44·0 |
| 0·43 | 0·3083 | 488 | 2·47 | 36·8 |
| 0·84 | 0·1721 | 416 | 1·54 | 28·8 |

*Garnets*

For very rapidly cycled magnetic materials, Shevel and Chang[166] lowered the flux density in an yttrium–gadolinium garnet series by adding $Al_2O_3$ with a view to reducing the inductive reactance. For compositions to the formula $Y_{3-y}Gd_yFe_{5-x}Al_xO_{12}$ the value of $J_s$ was between 0·01 V s/m² and 0·05 V s/m². In spite of the very low flux density, the signals were of considerable magnitude by reason of the rapid flux reversal. The switching time in certain memories, worked out in practice, was around 0·1 μs. In spite of the high frequency employed (2 MHz), the rise in effective core temperature was only 10°C.

*Ferrites having induced square loops*

A well-marked rectangularity of the hysteresis loop can be produced in many ferrites by thermomagnetic treatment. Experience, however, has shown that the switching time becomes longer the more the loop is squared[80]. The ferrite $Co_{0.1}Fe_{0.9}Fe_2O_4$ quoted in Table 15.8 has, for example, the highest rectangularity ratio and almost the longest switching time. Many ferrites having hysteresis loops of induced rectangularity show a smaller dependence on temperature and a higher permissible disturbance ratio than

**Table 15.12** TEMPERATURE DEPENDENCE OF THE SIGNAL PROPERTIES OF A THERMOMAGNETICALLY TREATED STORAGE CORE 1·25 mm×0·75 mm×0·4 mm (PULSE-WIDTH 2μs, PULSE RISE-TIME 0·2 μs)[182]

| $T$ (°C) | $uV_1$ (mV) | $dV_z$ (mV) | $t_p$ (μs) | $t_s$ (μs) |
|---|---|---|---|---|
| − 55 | 58 | 22 | 0·65 | 1·15 |
| + 25 | 76 | 22 | 0·58 | 1·10 |
| +100 | 100 | 24 | 0·52 | 1·03 |

do the spontaneously rectangular ferrites. Weisz[182], working with Mn–Fe and Ni–Fe ferrites which had been tempered at 200°–300°C in a field kept below saturation level, found the properties set out in Table 15.12 ($I_r$ = 1000/700 mA, $t_r$ = 0·2 μs). In the temperature range quoted, $dV_z$ and $t_s$ alter very little with temperature.

Using Ni–Zn Perminvar ferrites, Rabl[140] succeeded in manipulating the tempering operation so as to obtain switching times and switching constants which were by no means inferior to those of ferrites with spontaneous rectangularity. Further, cores of this material showed high thermal stability of switching time and of signal voltages $uV_1$ and $dV_z$.

Gorter and Esveldt[68] investigated the rectangularity ratio of cobalt-containing Mn–Fe, Ni–Fe, and Mg–Fe ferrites. They did not obtain satisfactory squaring of the loop with compositions containing less than 50% $Fe_3O_4$. Best values of maximum rectangularity ratio occurred in those mixtures showing a permeability peak in the curve $\mu = f(t)$ lying around room temperature (see Figure 5.19). A few compositions with high rectangularity ratios are shown in Table 15.13, taken from the extensive investigations of these authors.

**Table 15.13** PROPERTIES OF FERRITES WITH INDUCED RECTANGULAR HYSTERESIS LOOPS[68]

| *Ferrite* | $R_s$ | $H_m$ (A/m) | $Fe_2O_3$ (%) | *Annealing* |
|---|---|---|---|---|
| $Co_{0·1}Mn_{0·4}Fe_{0·5}Fe_2O_4$ | 0·8 | 480 | 15 | 2 h 1400°C |
| $Co_{0·2}Mn_{0·3}Fe_{0·5}Fe_2O_4$ | 0·85 | 800 | 12·5 | 2 h 1350°C |
| $Co_{0·3}Mn_{0·2}Fe_{0·5}Fe_2O_4$ | 0·85 | 1 680 | 11·4 | |
| $Co_{0·4}Mn_{0·1}Fe_{0·5}Fe_2O_4$ | 0·85 | 2 240 | 12 | |
| $Co_{0·02}Mn_{0·18}Fe_{0·8}Fe_2O_4$ | 0·9 | 240 | 23·4 | 2 h 1400°C |
| $Co_{0·1}Mn_{0·1}Fe_{0·8}Fe_2O_4$ | 0·9 | 720 | 21·2 | |
| $Co_{0·1}Ni_{0·5}Fe_{0·4}Fe_2O_4$ | 0·9–0·95 | 960 | 12·8 | 2 h 1350°C |
| $Co_{0·2}Mg_{0·3}Fe_{0·5}Fe_2O_4$ | 0·8 | 2 160 | 12·6 | |
| $Co_{0·3}Mg_{0·2}Fe_{0·5}Fe_2O_4$ | 0·8 | 3 280 | 12·7 | 2 h 1350°C |
| $(Mg_{0·6}Ni_{0·4})_{0·98}Co_{0·02}Fe_2O_4$ | 0·95 | 240 | ~1 | 2 h 1420°C |

Working within the ferrite series $(NiO)_{0\cdot4875-x}(CdO)_x(Fe_2O_3)_{0\cdot4875}(Co_2O_3)_{0\cdot01}(MoO_3)_{0\cdot005}$, Lessoff and Greifer[98] varied $x$ between 0 and 0·30. All these compositions gave ferrites with constricted loops which could be converted into squared loops by means of a suitable heat treatment. Rising cadmium content causes the Curie temperature $T_c$ and the coercivity $H_c$ to fall, whereas the maximum rectangularity ratio rises.

An increase in $R_s$ and a decrease in $H_c$ is observed with rising temperatures. $R_s$ could be brought very near to unity by a carefully controlled sintering routine (see Figure 15.30). If cadmium is wholly or partially replaced by

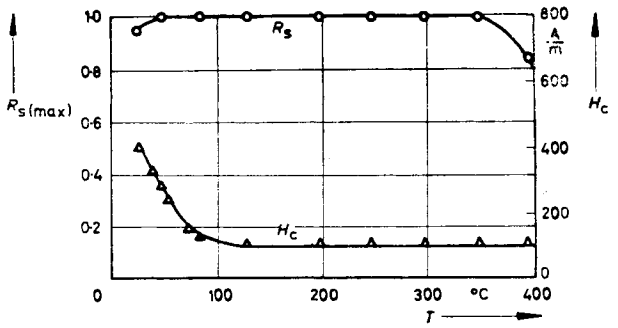



*Figure 15.30. Coercivity $H_c$ and maximum rectangularity ratio $R_s$ for a nickel ferrite having 10% CdO; annealing, 1 h at 1300°C*[98]

zinc, the properties of the material change completely. Without a proportion of molybdenum even the Perminvar characteristics are lost.

The magnetic values for the ferrite $Co_{0\cdot1}Fe_{0\cdot9}Fe_2O_4$ are set out in Table 15.8[80].

### 15.6.5.2 Alloy cores

According to investigations by Menyuk[111], the switching constant of toroidal cores wound from thin Mo-Permalloy strip is largely determined by the thickness of the ribbon. The switching constant is therefore given as the sum of two constants, namely $s_s = s_{se} + s_{sr}$, of which one ($s_{se}$) depends on the magnitude of the eddy currents, which is related to the square of the strip thickness, and the other ($s_{sr}$) is traceable to spin-relaxation effects. In strips more than 25 μm thick the eddy currents are the decisive factor for switching speed; at a thickness of 10 μm the effects of eddy currents and of spin relaxation are about equally pronounced; at 4 μm the eddy-current effect can be neglected at frequencies up to a few megahertz. If, then, tiny toroids are constructed from strip 3–5 μm thick, and measured in a similar way to ferrite cores, similar signal curves are obtained for magnetic reversal.

The switching constant of the 4 μm Mo-Permalloy strip at −196°C comes to about 32 μs A/m. It falls steadily with increasing temperature but at 270°C still has a value of 25·6 μs A/m and shows no irregularities throughout

**Table 15.14** PROPERTIES OF A FEW METALLIC CORE MATERIALS MADE FROM THIN STRIP[179]

| *Property* | *Ultraperm Z* | | *Ultraperm ZE* | | *Permenorm 5000ZE* | |
|---|---|---|---|---|---|---|
| | 6μm | 3μm | 6μm | 3μm | 10μm | 6μm |
| $H_c$ (static) (A/m) | 3·2 | 5·6 | 5·6 | 9·6 | 20 | 24 |
| $B_s$ (V s/m²) | 0·80 | 0·80 | 0·86 | 0·86 | 1·60 | 1·60 |
| $R_v$ | 0·92 | 0·94 | 0·94 | 0·95 | 0·95 | 0·95 |
| $s_s$ (μs A/m) | 32 | 28 | 36 | 32 | 172 | 108 |
| $H_0$ (A/m) | 14·4 | 13·6 | 28 | 28 | 40 | 44 |
| $\varrho$ (μΩ m) | 60 | 60 | 55 | 55 | 45 | 45 |
| $T_c$ (°C) | 410 | 410 | 430 | 430 | 470 | 470 |
| $d$ (g/cm³) | 8·75 | 8·75 | 8·6 | 8·6 | 8·25 | 8·25 |

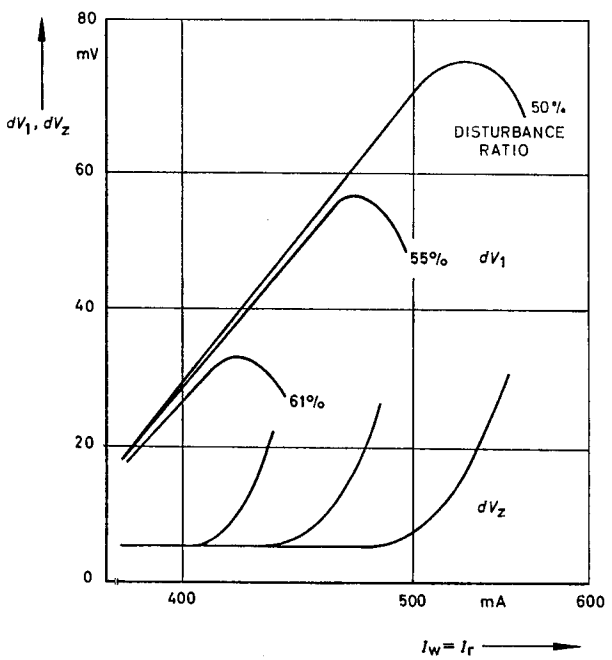



*Figure 15.31. Characteristics for memory cores of Ultraperm ZE (core type Z KK 2/1–0·003×25; $t_r$ = 0·5 μs)*[179]

this range. For the thicknesses investigated, it was found that the threshold field and the coercivity fell more or less to half their value when taken through the same temperature range. Thus, for example, the $H_0$ of 4 μm strip falls from 18 A/m to 10 A/m if the temperature rises from −196°C to 270°C[111]. Boll[28] quoted an $H_c$ of 5·6 A/m for 3 μm Permalloy strips. The static remanence ratio $R_v$ is 0·94 and the switching time, when a magnetising intensity of 80 A/m is applied, is given as 0·4–0·5 μs.

Ni–Fe strip with 50% Ni has found application, as well as Permalloy; the $H_c$ is greater and the specific electrical resistance smaller, so corresponding strips must be made thinner if they are to introduce the same eddy-current loss (see also Table 6.7).

For miniature or 'dwarf' cores, alloy strips having inner diameters down to 1·5 mm are produced[179]. The strip is wound on a thin-walled ceramic former to give the necessary rigidity. Also, memory cores can be built up from stamped elements of thin foil[28]. This is particularly advantageous when complicated core shapes are needed (see Section 15.11, on transfluxors).

The magnetic properties of core materials for subminiature strip-wound cores are set out in Table 15.14[179]. Figure 15.31 gives the characteristic curves of $dV_1$ and $dV_z$ for disturbance ratios of 50%, 55%, and 61%, the material being a 3 μm strip of Ultraperm ZE. Reading from the curves, it can be seen that for $I_r = 400$ mA and a disturbance ratio of 61% the signal-to-noise ratio is about 6 : 1.

## 15.7 FERRITE STORAGE PLATES

Besides the individual cores discussed there exist sheets or plates of ferrite in which holes have been drilled. The material immediately surrounding a hole corresponds to an individual core[110, 149]. Since the holes can be kept very narrow, only low interrogation currents are needed and very many elementary cells can be accommodated. The volume of ferrite bordering the portion actually switched—and thus rather further from the hole—raises the disturbance signal, however. Furthermore, tight requirements as to uniformity of the magnetic material, both within a single plate and from one plate to another, are not easy to meet and so the process leaves much to be desired, commercially. It is in fact possible to obtain some improvement if one is prepared to compensate for lack of homogeneity in the ferrite plate by, say, using two holes for one bit of information[120].

On the other hand, the plate technique offers the possibility of overcoming the difficulty of threading extremely small individual cores: conductors can, to some extent, be printed[143]. Thus 16×16 holes of diameter 0·6 mm have been accommodated on a plate of ferrite 2·5 cm×2·5 cm. Up to 64 such plates can then be assembled into a stack; a quantity of such stacks constitutes a memory store. Both bit-organised and word-organised memories are possible.

The micro-aperture memory is a further development of this principle[162]. In small (2 mm×2 mm×0·25 mm) ferrite platelets, 25 μm holes are drilled by means of an electron beam. They have a mutual separation of 50 μm. By the use of a suitable technique the holes are lined with a layer of silver

and the connections are provided by copper tracks laid down by a photo-etching process. These tiny plates are built up, as mosaics, into large units. The switching time of an individual platelet is 30 ns. The total cycling time in a 1000-word memory of this kind was 150 ns.

Laminated ferrite stores may also be considered as examples of plate memories[163]. A storage unit comprises three laminae of ferrite bonded together. Between each outer sheet and the middle sheet of the sandwich is inserted one of the mutually crossed conductor planes, which are therefore insulated from each other by the middle sheet which keeps them at a definite spacing of 125 μm. Such a stack is sintered together in a suitable manner but only after the sandwich is complete.

The cyclic time of an experimental store having 128 bits (16 eight-bit words) was 100 ns and the reading current 350 mA. Large memories holding 10–100 million bits seem likely to emerge. They are expected to be fairly economical in hardware and electric power and so promise to be commercially viable.

## 15.8 THIN-FILM STORES

It is known[87] that in sufficiently thin films of magnetic material (say 100–300 nm) energy considerations are unfavourable to the formation of domain boundaries with the result that magnetic reversal relies, in principle, on rotational processes; these are free of hysteresis and proceed more quickly than any other magnetic process. Switching times less than 1 μs are therefore to be expected by utilising this fact. Further, it is anticipated that employing evaporation techniques to make these microfilms will lead to a cheaper way of building a matrix than the ordinary use of individual cores.

In 1955 Blois[22] found these expectations largely substantiated. Numerous older experiments—in particular the then recently published investigations of Crittenden and Hoffman[42]—served as a basis for the production methods used to make thin metal film. Blois was the first to look into the possibility of building a memory store of thin-film elements. Employing seven Permalloy films, precipitated one onto the other and mutually insulated, he obtained a switching time of 0·5 μs for a retrieval field strength of 112 A/m ($H_1$ = 56 A/m). Coercivities down to 8 A/m and less were obtainable. Values of $H_c$ up to 3200 A/m were obtained with cobalt films.

In the following decade, scientific and technical research into the problems of thin-film memories was vigorously pursued. In comparison with ferrite-core memories, a better understanding of the underlying physics led to an appreciable shortening of the switching time while a considerable saving in manufacturing costs was also achieved[45, 96a, 184a]. Far-reaching theoretical studies promoted important insights into the physical basis of operation, particularly in micromagnetics. Up to 1967 more than 2000 articles have appeared devoted to thin magnetic films and this work is reflected in the filing of over 200 patents[35b]. At first, investigations focused on plane magnetic films, but at the end of the 1960s cylindrical layers (i.e. in the form of plated wires) took the stage. As far as can be estimated at the present time, these cylindrical forms are likely to supersede plane films. The reason for this will emerge in subsequent discussion.

### 15.8.1 Manufacture of thin films

Thin films of the pure metals iron, nickel, and cobalt, as well as alloys such as Permalloy or Mo-Permalloy, may be produced by various methods: galvanically, electrolytically[190], by thermal decomposition[92], by cathode sputtering[61, 85], or by vacuum evaporation[22, 116, 169, 170]. Sublimation techniques appear to be the most usual nowadays, although, for plated wires, electrolysis is preferred. The other processes have advantages in many respects but it is not necessary to go into them here.

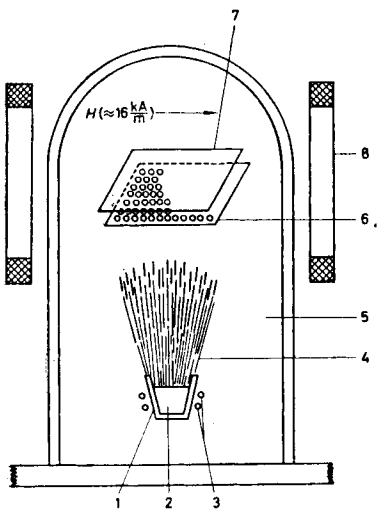



*Figure 15.32. Diagram of apparatus for deposition by evaporation: 1, crucible of aluminium oxide; 2, Permalloy melt; 3, HT induction heating; 4, metal vapour; 5, vacuum (around $10^{-5}$ torr); 6, metal mask; 7, heated glass substrate (50 mm × 50 mm × 0·0125 mm); 8, field coil providing orienting magnetic field*[169]

An evaporation device is shown schematically in Figure 15.32[169]. The melt (2) is placed in an inductively heated crucible (1). In place of the crucible, tungsten wires are sometimes used from which the alloy material is evaporated. The metallic vapour (4) passes through a mask (6) and is deposited on the heated substrate (7). Glass, mica, quartz, carbon, or collodion[3] can be used as substrate material, but metals such as silver or aluminium are also in use. Metals conduct away the heat very well and their surface is more easily worked than ceramic or other special non-metallic substances. The substrate temperature lies, as a rule, around 300°C. It influences the properties of the sublimed film, particularly its stress condition and the crystal size, so it is important to fix the optimum value.

The two coils (8) serve to ensure that the magnetic film, as it is produced, comes under the influence of a directive field amounting to about 2–20 kA/m. Permanent magnets can be used in place of the coils. The direction of the applied field $H$ is also the direction of easiest magnetisability of the memory element. The hardest direction forms an angle of 90° with this. It is only in the preferred direction that a squared loop appears (induced uniaxial anisotropy); in the transverse direction, measurements indicate an almost hysteresis-free magnetising curve (Figure 15.33).

In order to produce a matrix-like arrangement of storage cells, circular or square spots are formed on the underside of the substrate (7) having a linear dimension of 0·3–2·5 mm. Generally, shields or interposed masks are used to delimit the area of metal or alloy precipitation, but it is also possible to achieve definite areas of deposition by using an etching technique to form small islands of material. Certain disadvantages, which show up as edge effects in the individual elements, can be eliminated if, by the use of a suitable wiring arrangement, mechanical subdivision can be avoided[30, 117].

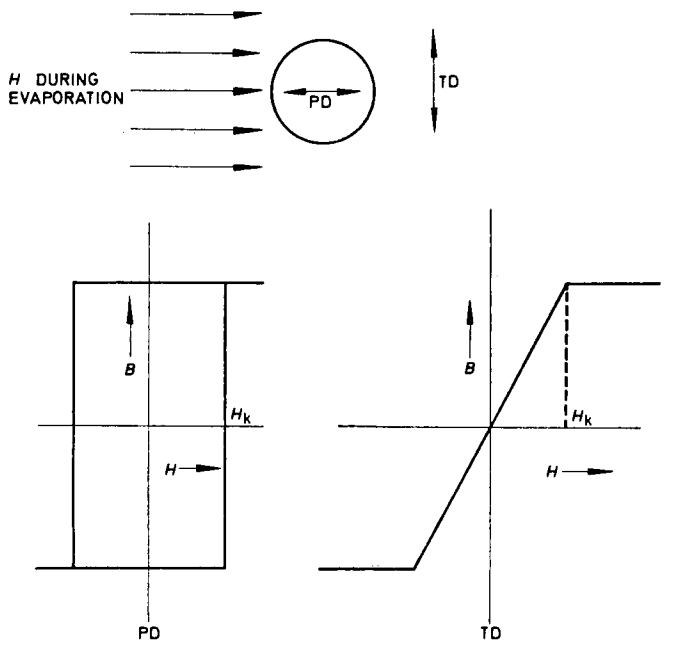



*Figure 15.33. Hysteresis loops of a Permalloy storage element in the preferred direction (PD) and the transverse direction (TD)*

The build-up rate is 1–80 nm/s. A Permalloy film of the usual thickness (80 nm) can thus be produced in around 1–60 s. The vacuum in the evaporation chamber amounts to $10^{-5}$–$10^{-7}$ torr. Vacua down to $2\times10^{-10}$ torr have already been produced experimentally[69]. Nickel films, in the best obtainable vacuum, yield uniaxial anisotropies of from $10^3$ erg/cm$^3$ to $3\times10^3$ erg/cm$^3$. Thus the effect of residual gas hardly seems to be significant.

Ferrite films can also be produced by vacuum deposition. The metallic alloys corresponding to the desired composition are evaporated, in the correct proportions, onto a suitable substrate and finally undergo an oxidising heat treatment at 600°–1000°C to induce ferrite formation[12]. A reactive sputtering technique has been suggested by Brook and Kingery[35a]. An Fe–Ni alloy is used as cathode and an oxygen–argon mixture as the reactive gas. Films deposited on substrates at temperatures below 0°C are of non-crystalline $NiFe_2O_4$, whereas films deposited at higher temperatures are

polycrystalline. Another process for producing ferrite film starts from a suspension which is deposited on the substrate by suitable means[97]. Isotropic films are produced having a high remanence ratio $R_v$ greater than 0·95.

### 15.8.2 Materials used for magnetic films

Apart from the Permalloy with 80% Ni and 20% Fe used by Blois[22], Fe–Ni–Mo[50] and the pure metals (iron, cobalt[97], and nickel[118]), as well as ferrites[12, 97], have been used as film materials, at least experimentally. Permalloy would seem to be the material most studied in this connection. The following facts point to Permalloy as a suitable memory material: Permalloy has the highest initial permeability and maximum permeability of all the Fe–Ni alloys (see page 410). These high values are connected with the fact that, in the neighbourhood of 80% Ni–20% Fe, magnetostriction and crystal anisotropy fall to zero (see Figure 13.8). Storage elements of this material, therefore, suffer no elongation during magnetic reversal and are thus not subject to stress variations.

The correct composition of the alloy can thus be found easily by observing the hysteresis loop under test conditions and making sure that it does not change shape when the film is bent. The magnetostriction curve of an Fe–Ni alloy with 2% Ni also passes through zero. In consequence, this material has also often proved attractive in experiments on the suitability of materials for memory stores.

### 15.8.3 The magnetic spot

These storage elements, or magnetic spots, have the following approximate dimensions: the diameter of round spots lies between 0·75 mm and 2·5 mm; rectangular elements have also been used[137] with side dimensions of 0·3 mm×0·65 mm and a mutual separation of about 0·3–0·4 mm. For rapid stores, which must operate with low powers, the elements need to be very small. Experiments on spots of 125 μm diameter show that production is technically feasible[93]. The thickness of the magnetic film is generally less than 100 nm and for Permalloy is about 80 nm. The least thickness is some 10 nm. Films whose thickness exceeds 100 nm often exhibit low rectangularity of hysteresis loop or, sometimes, the loop is constricted. If films are too thin, the magnetic properties can no longer be accurately reproduced; moreover, the volume of material cycled is so small that it becomes difficult to detect the answering signal.

The phenomenon of uniaxial anisotropy is not yet fully explained. Obviously various mechanisms are brought into play: internal stress, filamentary structure, pair formation of atoms, conditions of the surface of the substrate, and the geometry of the evaporation device can all play decisive roles[38, 170]. Heating of a Permalloy film can induce superstructure[3].

In constrast with the toroidal core, the magnetic spot possesses an open magnetic circuit, i.e. the flux lines are closed in space. In spite of this, the demagnetisation factor can be largely neglected because the lengthwise

spread of the film is so much greater than the thickness. The ratio, for example, for a 100 nm spot of 1 mm diameter is 10 000 : 1. The ratio can be made better still by producing a second spot on the rear face of the 'setting' conductor so that the stray flux can be closed through this auxiliary spot[142]. This does not eliminate the stray flux altogether, however, but it can be done by wire-plating[100] or by specially prepared wiring systems[153]. Theoretically, a thin magnetic spot behaves as a single domain and this was frequently noted experimentally[42]. Nevertheless, grain boundaries have often

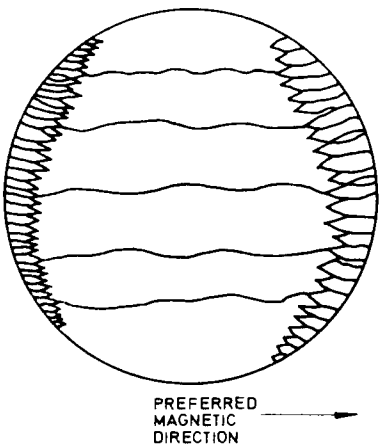



*Figure 15.34. Schematic drawing of domain pattern as observed in composite Bitter photographs of a round* Ni–Fe *spot*[15]

been observed inside the film[83, 188]. In particular, nuclei of opposite magnetisation have often been found around the edges of the spot and have been traced to incompleteness in the manufacturing processes (Shadow effect) (Figure 15.34)[15]. The formation of Bloch walls is always harmful since this lengthens the magnetic reversal process.

### 15.8.4 The storage element and its functioning

In order to build a store out of magnetic spots a number of them are assembled into a matrix of, say, 5 cm×5 cm. On a substrate of this size, 64×36 = 2304 elements can be accommodated[137]. For setting, writing, and reading, three conductors are needed, which are laid flat over the spots. Setting and information (writing) conductors run parallel to each other and at right angles to the sensing (reading) conductor. A more uniform field is obtained with broad conductors than with narrow ones but an increased eddy-current loss has to be reckoned with. The thickness of the ribbon conductor is about 1 μm and the width up to 1 mm. There is a separation of about 10 μm between conductors[53]. Writing and reading can be achieved in various ways which will not be examined here. The reader can refer to a review by Kayser[85a].

A single element is sufficient to store one bit[142]. In another scheme two elements per bit are used[20]: the operation of a thin-film storage element will be briefly discussed on the basis of this example. Figure 15.35 shows the

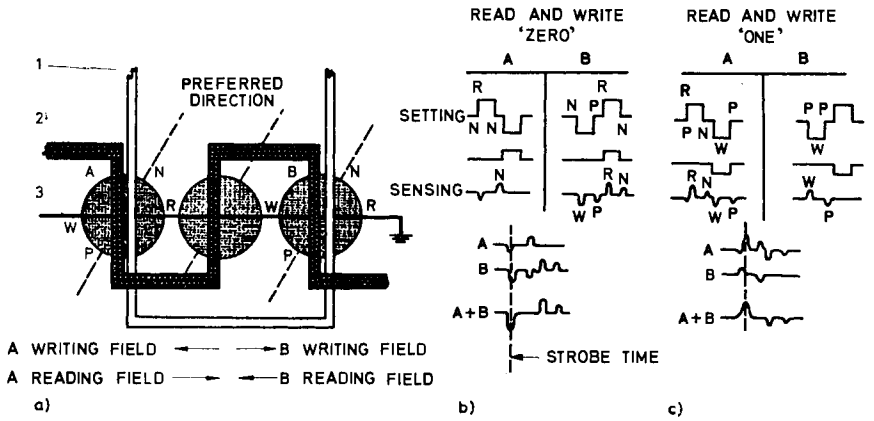



*Figure 15.35. Two alternately sited spots as used to store one information unit: 1, setting conductor; 2, information conductor; 3, sensing conductor*[20]

arrangement of conductors[20]. The preferred direction of the film spot shown makes an angle of 45° with the conductors. Each spot can be regarded as a tiny compass needle which can take up two stable positions, here designated N and P. The P condition may correspond to the storage of a 1 and the N condiction to the storage of a 0. To store an information unit two next-but-one neighbours are used, designated A and B in Figure 15.35a. If both elements are in the N condition a 0 is stored, while if both are in the P condition a 1 is registered.

When a 0 is read out, the following sequence takes place. Both films find themselves in the N condition. If, now, a reading pulse is passed along the setting conductor, the direction of magnetisation in A turns from N to R and in B from N to W. The rotation from N to R induces a negative signal in the reading wire and the rotation from N to W gives, one after the other, a small positive and then a negative signal. As a result, a negative signal appears in the reading wire (see Figure 15.35b). After the completion of the writing pulse the magnetisation in A turns back once more to N but in B it turns to P. In order to write in a 0 again, a setting pulse of two-thirds the amplitude of a complete switching pulse is sent through the setting wire, and at the same time a current of one-third the switching amplitude is sent through the information conductor. In spot A the fields are opposed, whereas they add together in spot B. Therefore A remains in the N condition while B returns through R to the N condition.

In order to read a stored 1 (and then to rewrite it) a reading pulse is again sent through the setting conductor. In film A the field vector turns from P to R inducing a small negative signal in the reading wire followed by a positive signal. In film B the rotation from P to W induces a positive signal. In the reading wire both signals are summed into a positive signal, which thus has a sign opposite to that of the reading signal for a stored 0 (see Figure 15.35c). After the reading process the N condition exists in spot A while B returns to the P condition. In order to re-inscribe a 1, a conditioning and

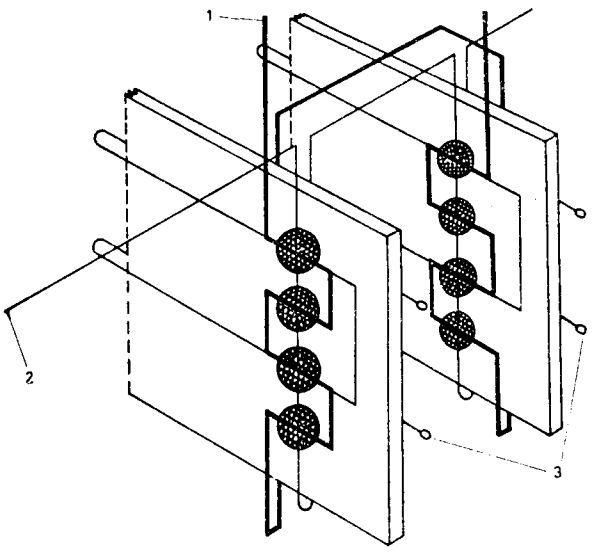



*Figure 15.36. Construction of a thin film store using planes arranged in pairs: 1, information conductor; 2, sensing conductor; 3, setting conductor*[20]

a writing pulse of opposite polarity are sent, as before, through the corresponding wire. Spot B remains in the P condition (amplitude differential) and A turns back again to the P condition (amplitude summation).

In order to achieve a satisfactory signal-to-noise ratio, it was suggested that planes having the arrangement just described should be used in pairs as shown, for example, in Figure 15.36[20]. Further, disturbance-free read-out on the coincidence principle has been used[124].

### 15.8.5 The switching process in film elements

The physical conditions appropriate to the reversal process of magnetisation in thin films were investigated by (among others) Smith[171], Conger[40], and Olson and Pohm[127]. According to these workers, three magnetic mechanisms are relevant, namely wall shift, incoherent rotational processes, and coherent rotational processes. Switching times of the order of 1 μs are associated with wall-shift mechanisms while coherent rotation of the spin vectors can cause flux reversals to occur in as little as 1 ns. Incoherent rotations occur at a rate between 10 ns and 100 ns.

Coherent rotation is the process sought after for the construction of fast memory stores. Which mechanism applies to the magnetisation of a thin-film spot in a given case depends on the type and structure of the storage element but, even more, on the field intensity used. The critical curve for the occurrence of coherent rotations is obtained by striking a balance between anisotropic energy $E_k = K \sin^2 \Phi$ and the field intensity in both the longitudinal

and the transverse directions[171]. The normalised anisotropic intensity $H_k = 2K/M$ in the preferred (longitudinal) direction can be denoted by $h_L$ and the intensity in the hardest (transverse) direction by $h_T$.

If, while $h_L = 0$, the direct field strength $h_T$ increases from 0 to 1, the hysteresis loop measured in the preferred direction passes over into the reversible S form. Figure 15.37 shows four loops for which $h_T$ is 0, 0·2, 0·6, and 1·0. Thus, with rising cross-field, the coercivity measured in the preferred direction falls to zero. This is easily understood since the cross-field helps to overcome the anisotropic field.

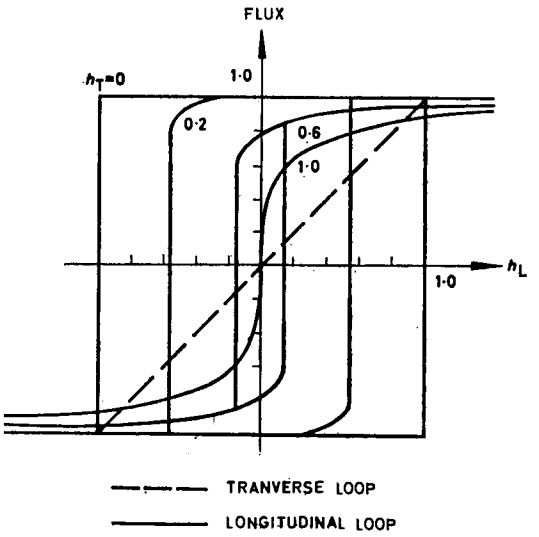



*Figure 15.37. Theoretical hysteresis loops for thin films*[171]

If $h_L$ is put equal to $h_c$—which is near enough correct—a parametric relation is established connecting $h_c$ and $h_T$ with the angle $\Phi$ between the preferred direction and the magnetising vector:

$$h_c = \cos^3 \Phi \qquad h_T = \sin^3 \Phi \tag{15.7}$$

Experimental comparison gives a good approximation to the theoretical curve (Figure 15.38)[171]. Eliminating $\Phi$ gives the equation

$$H_L^{2/3} + H_T^{2/3} = H_k^{2/3} \tag{15.8}$$

whose plot is an asteroid. In Figure 15.39, representing the asteroid of equation 15.8, an intensity vector $H$ is drawn having three different amplitudes. As long as the end-point of the intensity vector falls within the curve, i.e. tangents can be drawn to the two branches of the asteroid from the tip of the vector, there will be two stable positions of magnetisation; if the tip of the vector falls outside the asteroid, the direction of magnetisation can fall into only one stable position: in the first case it is a question of reversible and in the second case of non-reversible magnetic changes.

Actual observations of hysteresis loops and reading pulses have shown, however, that the simple scheme of Figure 15.39 does not really hold: wall shifts occur as well as the rotations, so the critical curve must be supplemented[127]. The asteroid then looks rather as in Figure 15.40[136]. This diagram is especially suitable for illustrating coincidence processes in film stores: two half-pulses must be so limited in magnitude that each of the magnetising vectors produced lies inside the blank region of the asteroid, while their sum reaches the range of coherent rotation. Above all, the shaded region within the asteroid, which is the region of wall shift, is to be avoided.

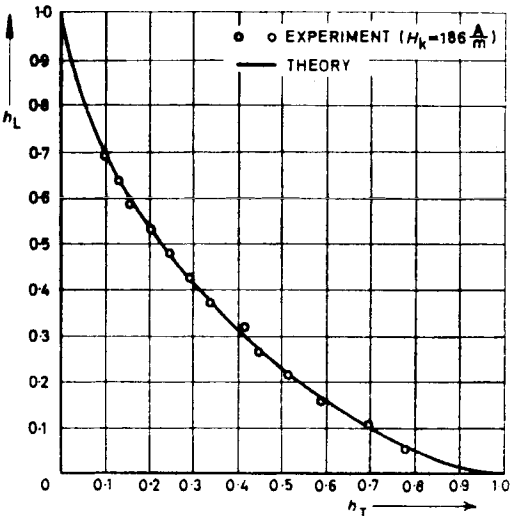



*Figure 15.38. Equilibrium positions of the magnetising vector for longitudinal and transverse fields*[171]

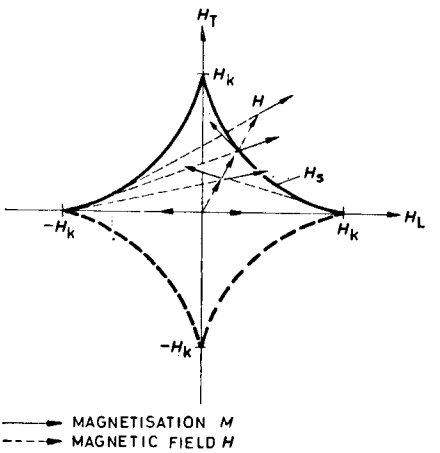



*Figure 15.39. Critical curve of cyclic magnetisation (asteroid)*[136]

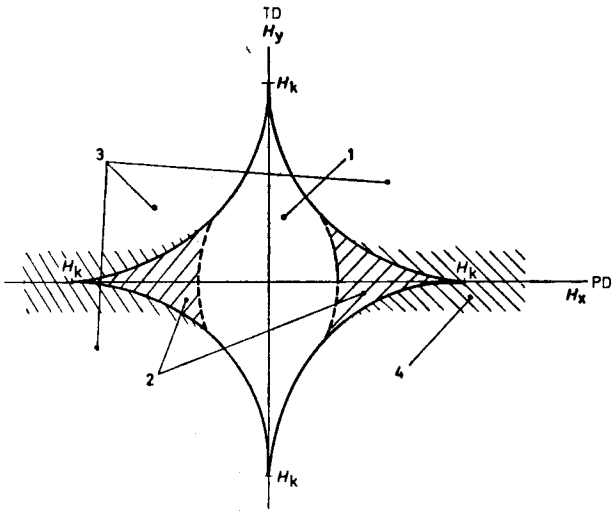



*Figure 15.40. Regions of flux change in film-store elements having uniaxial anisotropy: 1, no flux reversal; 2, wall movement; 3, coherent rotation; 4, incoherent rotation (PD = preferred direction, TD = transverse direction)*[136]

### 15.8.6 Advantages and disadvantages of plane film storage elements

The following properties are amongst the advantages offered by plane film spots used as storage elements:

1. High-speed cycling (switching time ≙ 1 ns, access time ≙ 10 ns, cycling time ≙ 100 ns).
2. Low temperature-dependence.
3. Low heat generation and good heat dissipation.
4. Relatively low production cost.

On the other hand, the following unfavourable properties may be noted:

1. Faulty elements cannot be found and eliminated till the matrix is complete.
2. The magnetic values sometimes vary from one element to another (anisotropic field strength and preferred direction[37]), so all elements of the sheet are not always usable.
3. Sometimes disturbing edge-effects appear and upset the switching times.
4. Because of the 'open' magnetic flux, unwanted coupling can occur with the result that the elements cannot be packed as closely as one would wish.

Film stores have been built since 1959 and found to work satisfactorily[21, 124, 141, 142]. It is generally reckoned that future film memories will be built to store up to one million bits[46, 134, 142].

## 15.9 CYLINDRICAL THIN-FILM STORAGE ELEMENTS

Avoidance of stray fields in plane film elements and their associated disadvantages is possible only if the magnetic flux remains within the element throughout its path. This can be achieved if, for instance, the magnetic film is deposited on a cylindrical wire. The switching properties of such films were investigated by Long[100], for example. The literature suggests a variety of technical solutions, one of which is the orthocore memory proposed by Sallo[153]. The wiring of a storage matrix is confined to single planes; one, for example, carries the 'word wires', another, at right angles to it, the 'bit wires', and so forth. Each wiring plane is printed on plastic foil, and foils are stacked and welded together. A ferromagnetic substance is chemically precipitated onto this mechanically solid matrix. The material consists of, for instance, about 65% Ni, 33% Co, and 2% P. The coercivity is about 40 A/m though it can be increased beyond this. In this development more emphasis is placed on versatility and reliability than on extremely fast switching. The switching constant amounts to some 160 μs A/m.

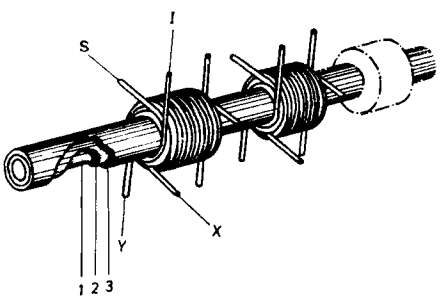



*Figure 15.41. Magnetic rod with bunched coils for coincident-current memory mode: I, inhibit (first winding); S, sense (second winding); Y, y-drive (third winding); X, x-drive (fourth winding); 1, glass rod; 2, conductor; 3, magnetic material*[108]

Another fast-operating storage element is known by the title of ROD[107, 108, 109]. As the name implies, the element takes the form of a rod, provided with a magnetic coating. What is, in fact, used, is a small glass rod of 0·33 mm diameter. A silver coating is deposited on its surface and acts as a conductor to whose surface the Fe–Ni film is applied (see Figure 15.41). In the original version the magnetic film comprised 98% Fe and 2% Ni and had a thickness of a few hundred nanometres—on average, say, 300 nm. It had an $H_c$ of 1·12 kA/m and a high rectangularity ratio ($R_s$ = 0·95). When it was used in a coincidence store, a signal-to-noise ratio of 5 : 1 and a switching time of 70 ns were achieved. In a later version there is a double layer of magnetic substance[109]. On a Be–Cu base an isotropic film of 97% Fe and 3% Ni is first electrolytically deposited and over this a uniaxially arranged film of 79% Ni and 21% Fe. The total thickness of the coating is 500–600 nm and it has an $H_c$ between 640 A/m and 720 A/m, and an $H_k$ of some 960 A/m. The switching constant being about 16 μs A/m, the film switches in about 25 ns if the excess field is about equal to $H_c$.

Windings for reading, writing, and blocking are wound on the rod independently of each other in single layers. With half pulses of 200 mA, signal pulses of 10–40 mV per turn are obtained, according to film thickness. Up

to four bits can be stored on 1 cm of rod. Special advantages ascribed to ROD are its temperature insensitivity and the excellent coupling between film and winding. Between $-100°C$ and $+200°C$ fault-free coincidence working was found possible.

The plated-wire memory seems to offer the best solution to the problem of the efficient use of cylindrical elements of magnetic film. This memory can compete with single-core ferrite memories and also with fast semiconductor memories. Cycling times are shorter than those of ferrite-core memories, namely 0·1–1 μs as against 1–10 μs. Further advantages are: non-destructive read-out (NDRO) is readily achieved; operating speed is increased; and the necessary electronics is both simple and cheap. Equally important in practice is good reproducibility combined with the possibility of applying automation to testing and packaging.

The technique for producing plated wires was first described by Long[100]. This was in 1960. Many modifications to the original scheme have, of course, been necessary during the subsequent decade in order to reach the state of the art as it exists today.

The basic non-magnetic substrate is a wire 75–200 μm in diameter (usually about 127 μm) made of a Be–Cu alloy containing 2% Be. The beryllium reduces the conductivity to a quarter but pure copper is unsuitable, being too soft. It was found possible, also, to use a phosphor-bronze alloy. Zr–Co alloy was considered but gave inferior results, and wires of gold and of platinum might have been acceptable had they not been too soft. The wire should be stiff, straight, and stable and should not age appreciably even after many years. The surface must be smooth enough to secure a well-defined surface yet sufficiently rough to adhere well to the electrodeposited film of Permalloy.

Frequently an intermediate layer of copper—or sometimes of a noble metal—is applied to the substrate before the deposition of the Permalloy[148a]. Electropolishing before deposition is sometimes specified. The Permalloy film is about 500–800 nm thick for memories of 250–750 ns. Requirements which the magnetic alloy must further meet are: zero magnetostriction; uniformity of thickness and composition; low anisotropic field $H_k$ and a low angle of skew for the preferred direction of magnetisation. It is possible to co-deposit nickel and iron in the correct proportions but the process is highly critical[43a].

Attempted methods for defining optimum manufacturing conditions leading to a useful and reproducible Permalloy film on wire have been well summarised by Mathias and Fedde[103a]. Tempering at about 350°C stabilises the properties of the wire, but recrystallisation is to be avoided[11a]. A life of at least 10 years at 50°C is believed to be realistic[103a, 105a]. The preferred direction of magnetisation lies circumferentially around the wire and is induced by passing a current through the wire during deposition of the magnetic film. The 1s and 0s are represented by one or other of the preferred directions.

The length of a storage element is about 1·27 mm. Its position is defined by the position of word-lines, which cross the plated wires perpendicularly and form solenoids around the wires. The construction is comparable with that of the twistor memories shown in Figure 15.48. The word-current

produces a magnetic field parallel to the axis of the plated wires and rotates the field vectors out of the circumferential rest position towards the axis of the wire. In this way a voltage is produced which can be sensed at the end of the plated wire. The magnetisation vector returns to the original position with the cessation of the current, thus achieving a non-destructive read-out. Writing information into the wire is achieved by coincidence of bit-current and word-current so that the magnetisation vector lies in one or other of the two directions.

According to Mathias and Fedde[103a], plated memories are likely, in the next few years, to attain a cycling time of some 100 ns together with a capacity of some 500 000 bits. They further believe that production costs will come down, so that a 100 ns memory will cost no more than does a 500 ns memory today. Semiconductor memories are more expensive in modules larger than 60 000 bits. It is confidently forecast that further plated wires will be constructed with a packing density of 2 bits/mm, with drive-currents of 200–300 mA, and having film properties optimised for high-speed operation. Many companies throughout the world are already in large-scale production of plated-wire memories[105b].

## 15.10 THE WAFFLE-IRON MEMORY STORE

The waffle-iron store is related to the film store and allows also non-destructive read-out[25, 172]. It results from an attempt to overcome production difficulties which mount rapidly as the size of individual toroid cores is reduced. It consists of a foil of Fe–Ni with a rectangular hysteresis loop, and an underlying ferrite plate in whose smooth polished surface have been cut grid-like grooves, giving it the appearance of a tiny tablet of chocolate or a miniature waffle-iron. Memory stores built on this plan are therefore known as waffle-iron stores.

The ferrite plate is made from a high-permeability material ($\mu$ greater than $1000\mu_0$) and serves as a magnetic termination, or closure, for the storage elements of alloy film. For example, Ni–Zn ferrite with a Curie temperature of 70°–100°C and a specific electrical resistance $\varrho$ of more than $10^4\ \Omega$ cm may be used. The electrical resistance has to be high to avoid short-circuits.

The grooves between the square or rectangular islands are about 125 $\mu$m wide and just deep enough to contain the writing and reading wires. The area of an island for a 'cubic' waffle-iron store measures 250 $\mu$m$\times$250 $\mu$m. A 7·5 $\mu$m foil of 4-75 Permalloy with an $H_c$ of 400 A/m serves, for example, as storage material. An alloy of 97% Fe and 3% Ni, electrolytically deposited on copper, has been found even better. Its Curie temperature is 770°C. For a layer 1·2 $\mu$m thick the coercivity is 720 A/m, the rectangularity ratio is 0·95, and the switching constant is 16 $\mu$s A/m.

The foil must make the best possible contact with the ferrite to keep the flux gap-free. In practice, separations of 500 nm have been measured.

The best results were achieved with a store which used four islands for one bit. With a reading current of 800 mA, signal voltages of 100 mV and switching times of 250 ns were measured ($t_r$ = 200 ns). In an improved experimental version, writing and reading times of about 50 ns were reached.

Information densities of 176 bits/cm$^2$ are possible. It follows that a waffle-iron store can be regarded as a quick-operating device. It is very flexible, offers a wide range of applications, has low temperature sensivitivity, and is free from difficulties in material production. It appears capable of still further improvement, so even greater information densities and shorter switching times are to be expected. If the anisotropic Permalloy film is replaced by a pair of coupled anisotropic films, output signals as large as 15 mV and as short as 20 ns are readily available[179b]. A certain difficulty always remains, however, with the air-gap and this can never be fully avoided.

## 15.11 TRANSFLUXORS

In 1955 a new kind of storage element appeared under the name of transfluxor. It was developed by Rajchman and Lo[146]. A ferrite with a spontaneously squared hysteresis loop served as the magnetic material. A transfluxor differs from an ordinary memory core in having several apertures to which can correspond several magnetic fluxes. This makes possible, among other things, the non-destructive recovery of stored information. The name of this component is intended to suggest that its working principle depends on the transfer of flux from one yoke to another (*trans*fer of *flux*). In American publications, transfluxors are sometimes known by the acronym MAD (*m*ulti-*a*perture *d*evices).

### 15.11.1 Working principles of a transfluxor

The principles will be discussed in terms of the simplest form, the two-aperture transfluxor. The three yokes are labelled 1, 2, and 3 in (Figure 15.42). Their cross-sections are so dimensioned that the sizes of yokes 1 and 2 are equal while that of yoke three is about equal to the sum of the other two. A winding is applied to each yoke, namely an input, an output, and a control winding[1].

Yoke 3 is magnetised to saturation by a heavy pulse of unidirectional current. The flux in the other two yokes takes a configuration such that the

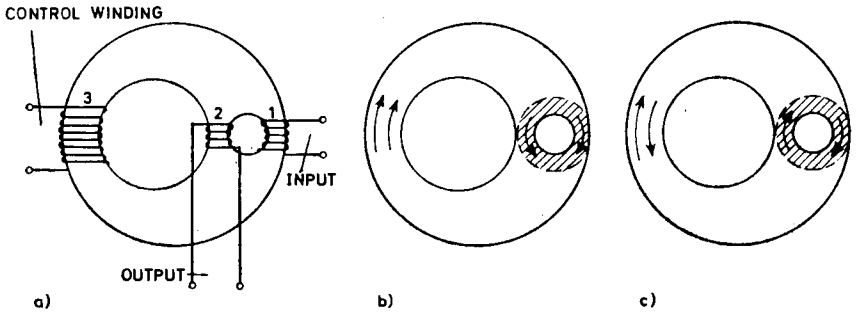



*Figure 15.42. Transfluxor: (a) wiring schematic; (b) blocked; (c) unblocked*[146]

flux lines of yoke 3 are closed. By way of example, we suppose the flux round the larger aperture runs clockwise. After the end of the saturating pulse, the condition remains substantially unchanged, especially if the ferrite material has a high remanence ratio. An alternating current in the input winding induces no voltage in the winding of yoke 2: the transfluxor is blocked.

If, now, the control winding receives a current pulse of opposite sign and of an amplitude half as great as is needed for blocking, then some of the magnetising vectors are turned in the opposite direction—those, in fact, lying in the region of greatest field intensity and thus at the edge of the large hole. In this way the direction of the flux in yoke 2 is turned round. A closed flux can now build up in a clockwise direction around the small hole: the transfluxor is 'set' (Figure 15.42c). An alternating current in winding 1 causes the flux around the small hole to change direction with the rhythm of the changing current. The flux is alternately transferred from yoke 1 to yoke 2 and vice versa. Thus, in the unblocked state, a signal can be transferred from winding 1 to winding 2.

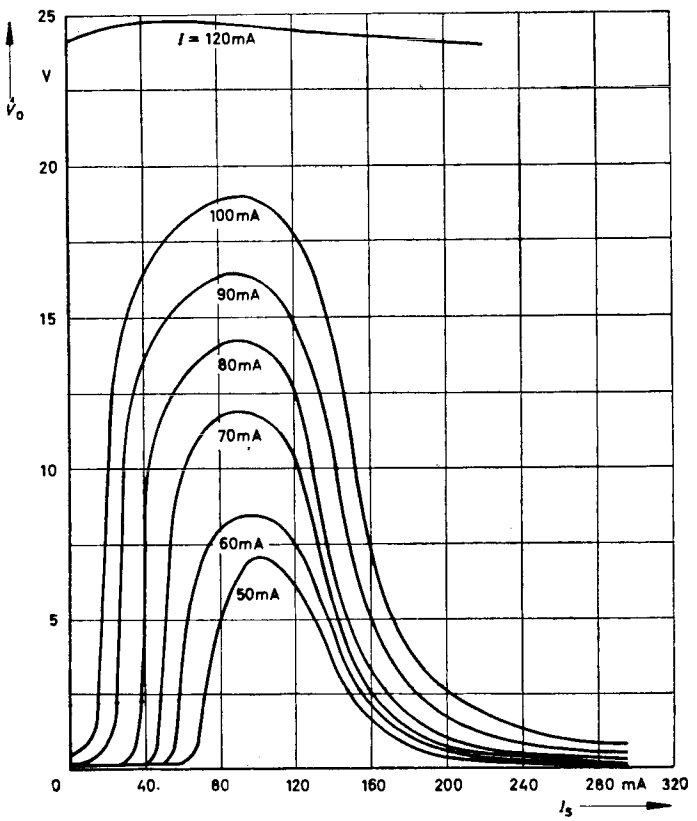



*Figure 15.43. Peak output voltage $\hat{V}_0$ of a transfluxor as a function of the setting current $I_s$ on open circuit, for various input currents I ($f$ = 50 kHz, $n_1 = n_2 = n_3$ = 20 turns); follows measurements by H. Reiner*

The setting of the transfluxor corresponds to the writing process and the changeover to the interrogation or reading routine of ordinary memory stores. Interrogation can take place as often as may be required without the need to reset.

What, in the example, has been called 'setting the transfluxor' is the 'optimum setting'. The setting current can, however, be continuously varied. A measured example of this, taken on a transfluxor of the form shown in Figure 7.11, is displayed in Figure 15.43. The rectangular ferrite used had the following properties: $B_s = 0{\cdot}196$ V s/m$^2$, $B_r = 0{\cdot}185$ V s/m$^2$, $H_c = 59{\cdot}2$ A/m. The yoke widths were 3 and 6 mm, the core thickness 5 mm and the diameter of the holes 3 and 12 mm. The figure shows the relation between peak output voltage $\hat{V}_o$ and various input currents measured at 50 kHz. As can be seen, the optimum setting occurs for a current of 95 mA.

### 15.11.2 Applications of transfluxors

The two-hole transfluxor can be used like a storage toroid in a memory matrix. The blocked state corresponds to the writing of a 0, the 'set' state to a 1. Figure 15.44 shows an arrangement for non-destructive readout by

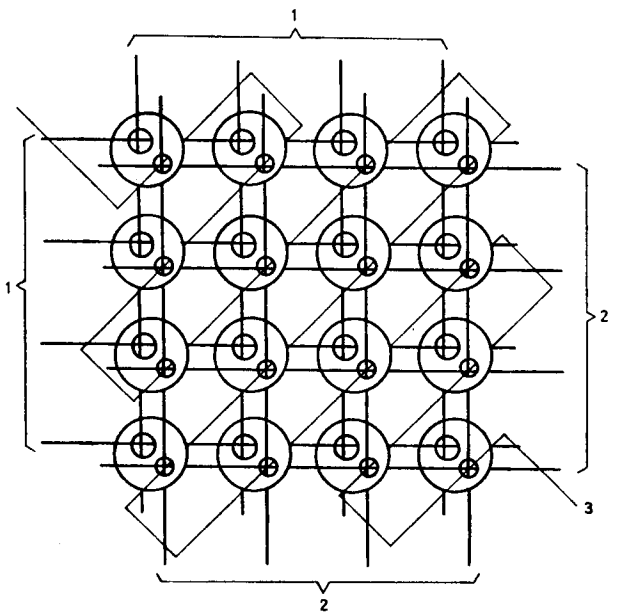



*Figure 15.44. Transfluxor matrix: 1, write-lines; 2, read-lines; 3, read-out winding*[144]

means of a transfluxor matrix using coincidence currents[144]. The writing pulse is applied in $x$ and $y$ wires which pass through the large hole so that yoke 3 can be magnetised. The sign of the writing pulse determines whether, in a particular core, the blocked or the unblocked state is set up. For read-

out, suitable pulses are passed along the chosen row and column. The corresponding wires pass through the small hole and can thus magnetise yoke 1. To obtain a signal, oppositely directed pulses are given to each of the selected wires passing through the particular core. If the transfluxor is blocked, there is no flux change around the small hole, but, if it is in the unblocked state, there is a double change of flux in yokes 1 and 2 and the original state is re-established. When there is a flux change, a voltage is induced in the reading conductor passing through the small hole. Since the interrogated core returns to its original state, rewriting becomes unnecessary. Further, it is possible to write at one site while reading at another.

The controlled, reversible inductance of a transfluxor can be used for analogue-type stores[75]. A transfluxor may be compared to a selector-relay and can perform the functions of an electromechanical cross-bar selector switch; it operates, however, more rapidly and more reliably since no contacts are involved. Transfluxors can also be adapted as current regulators by taking advantage of the differing inductive reactance in the blocked and unblocked states[144].

A whole series of other storage and switching operations of considerable complexity can be carried out with multiple-hole transfluxors, for example coincidence storage of the 'supercontrol' type[84, 95] whereby extremely short switching times become possible. Multi-aperture transfluxors can perform complicated logical operations[39, 63, 65, 99]: they can act as switches[1], amplifiers[157], and counters[148], and anti-valence switching can be carried out with their help in a practical fashion[148]. Frequently, there is a useful saving of diodes and transistors in circuits built round transfluxors. It is specially fortunate that transfluxors will work reliably over a relatively high temperature range; thus experimental transfluxors[148] showed signal ratios of 25 dB between the blocked and the unblocked state over a temperature range of 200°C. Rozenblat[152a] uses multi-aperture cores for the realisation of threshold functions of many variables. This list by no means exhausts all the possible applications of transfluxors of various kinds. The technique of magnetic circuitry analogous to electrical networks is still in its infancy and shows great development potential.

### 15.11.3 Transfluxor materials

The requirements for transfluxor material are scarcely to be distinguished from those which apply to magnetic material for memory cores. Basically, then, the same materials can be used in both cases. Very often it is the switching aspect of the transfluxor which is of primary concern, so in many cases a high remanence ratio is more important than a high rectangularity ratio.

Among the ferrites, Mg–Mn ferrite is particularly suitable for transfluxor production. Since thermomagnetically processed Perminvar ferrites show a particularly well-marked induced rectangularity, they would appear to be suitable, also, for transfluxors. However, the flux must always be considered with reference to the preferred direction for these materials, so the magnetic treatment must be designed to take this into account. If this is taken care of, the good rectangular properties of tempered Perminvar can be advantageous,

particularly in facilitating the blocking process: the characteristic falls more steeply than for the spontaneous rectangular ferrites[139].

The output voltage of transfluxors operating with square-wave pulses is higher than for those using sinusoidal currents. The rise-time $t_r$ of the pulse is highly significant[139].

Metallic materials are also suitable for the manufacture of transfluxors. Square hysteresis loops are associated, in particular, with the following alloys[44, 178]:

1. Fe–Ni alloys having 50% Ni and a cubic grain structure.
2. Mo-Permalloys with 4–5% Mo.
3. Fe–Ni alloys having 67% Ni and induced rectangularity.
4. Fe–Co alloys having 50% Co and induced rectangularity.

The materials having induced rectangularity are harder to produce than those with a recrystallisation structure and the added advantages obtained do not justify the extra expense involved. Therefore, in practice, only the materials quoted under 1 and 2 above are used for transfluxor cores[44].

Strip-wound cores from textured sheet are less suitable since the preferred direction can be utilised in only one of the circuits, not in the others.

Magnetic circuits built up from stampings or etched foil offer better transfluxor properties[28]. Frame-type cores made from U stampings are used or Mo-Permalloy foil in which the special transfluxor shape has been etched. Foils having 1152 transfluxor units have been made. They had switching constants of 11·2–136 μs A/m and a working temperature range of from −70°C to +150°C without any need for temperature compensation[33, 34].

## 15.12 THE TWISTOR

In 1957 Bobeck[23, 24] developed storage elements which became known as twistors; they rely, fundamentally, on two observations based on the Wiedemann effect (see page 8):

1. The twisting of a magnetised wire produces an electrical voltage between its ends (Figure 15.45a).
2. The voltage observed between the ends of a magnetised nickel wire under torsion is appreciably greater than the voltage $V_1$ measured in a search-coil on the wire (Figure 15.45b).

These observations lead to the conclusion that the magnetic flux in the wire takes a helical path. Direction and magnitude of the applied torsion determine the sign and amplitude of the measured voltage.

If a nickel wire is twisted in a clockwise sense, then tensional stresses appear in a right-handed helix and compressional stresses in the opposite sense (Figure 15.46). Since magnetostriction is negative for nickel, the magnetic flux follows the direction of the compressional stress. The use of nickel wire in torsion is somewhat inconvenient in practice. It is technically

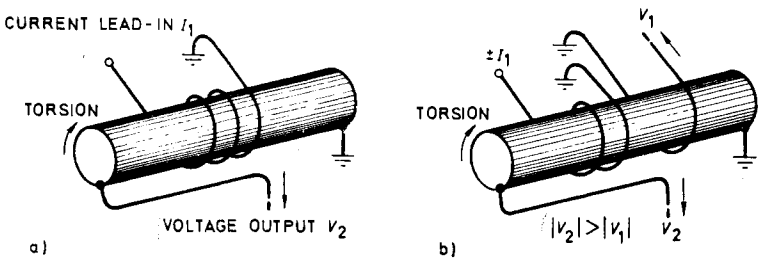



*Figure 15.45. Basic forms of twistor*[23]

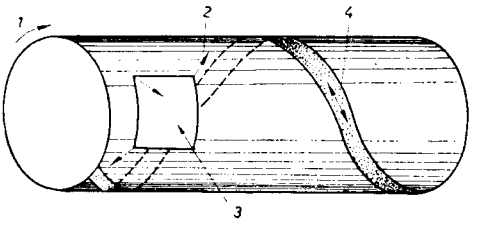



*Figure 15.46. Stress relations in a twisted nickel wire: 1, twist direction; 2, tension; 3, compression; 4, flux path*[23]

simpler to produce a twistor by winding a flat Permalloy tape spirally round an insulated copper conductor (Figure 15.47). Thus a spiral flux path is obtained without the use of torsional stress. In this case the name twistor is actually not appropriate.

The tape wound on the copper conductor has, for example, a pitch angle of 30° or 45° and a section of 8 μm×75 μm; the pitch spacing is 250 μm. The 30° angle has an advantage in as much as it allows larger current components in the coil. For reading out, it is true, a 60° angle would be preferable, but a high signal output can also be achieved by heavier winding of the conductor since the magnetically cycled volume is of first importance for the signal voltage. A Mo-Permalloy is used for making the magnetic tape as this is characterised by high specific electrical resistance, insensitivity to

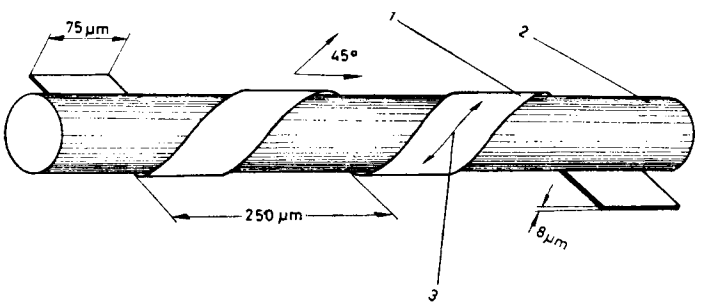



*Figure 15.47. Construction of a twistor: 1, flat Permalloy conductor; 2, 75* μm *copper wire; 3, directions of magnetisation*[24]

stress, low coercivity, low saturation flux density, and ease of working. Insensitivity to stress is secured by not annealing after rolling.

There are basically three possible ways to store information in a twistor. One may use two coils, wound round the wire, which magnetise a short length of the twistor when two half-pulses meet, following the coincidence principle. The current direction determines the direction of magnetisation. According to another method, a full impulse is passed through the twistor or through a coil wound over it. A third method is more used than either of the others just mentioned: one half-pulse is sent through the twistor wire (circumferential magnetisation) while the other half-pulse is passed through a coil mounted coaxially with it (longitudinal magnetisation) (Figure 15.48). The amplitudes of these pulses are so proportioned that the conjunction of the two half-pulses produces a magnetisation along the tape and a piece of the twistor about 2·5 mm long becomes magnetised. One sense corresponds to 0 and the opposite sense to 1.

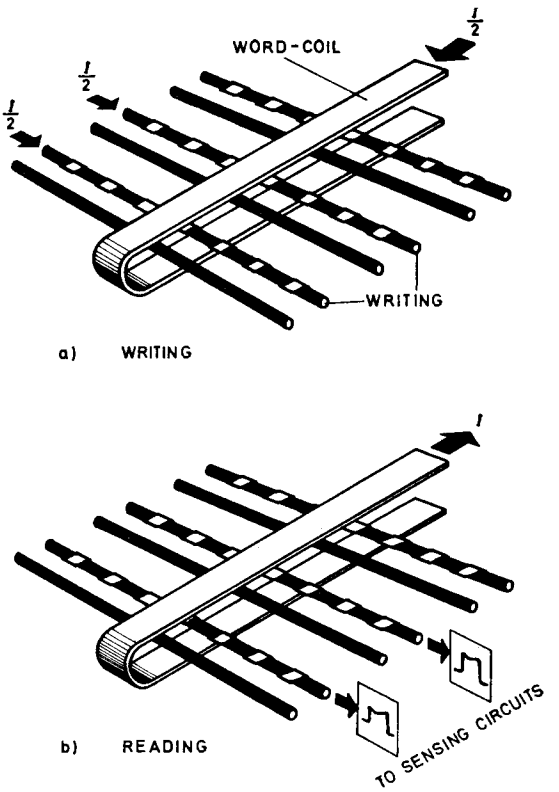



*Figure 15.48. Writing and reading process in a twistor device*

To read the twistor, a full pulse is sent through the coil in the reverse direction. This turns the magnetisation around, producing a signal in the twistor wire. Thus the conductor of the twistor has two functions: it is at

once the writing wire and the reading wire; in addition, it serves to carry the recording tape. The volume of cyclically magnetised material in a twistor amounts to about 1/1000 of that in an ordinary memory core. The signal is therefore low.

McCabe[105] gives as typical values for a twistor of 175 μm copper wire wound at 30° with a 375 μm wide tape:

| | |
|---|---|
| Writing current (in coil) | 120 mA |
| Twistor information current | 112 mA |
| Reading current (in coil) | 500 mA |
| $dV_1$ signal | 39 mV |
| $dV_z$ signal | 6 mV |
| Switching time | 400 ns |

The cycling time[24] of a small store may amount to some 3–4 μs and the information density to 30–60 bits/cm$^3$.

The main advantage claimed for the twistor is its ease of manufacture: automatic methods can be employed allowing continuous testing during production. It is, moreover, little subject to temperature effects since a metal tape is used whose flux falls off by only 1000 ppm/K with rising temperature[105].

The twistor can be seen as a competitor to the ferrite store, since its principal application is in the field of the larger memory with a capacity of more than $10^6$ bits. A twistor also offers advantages as a shift register. The information can be shifted along the twistor wire without the use of diodes[26]. A disadvantage lies in the relatively poor coupling between twistor and winding, which means that high currents are needed. Further, by reason of the open flux path of the twistor, stray fields, particularly if the information density is high, can affect neighbouring storage elements and so an optimum solution must be sought by appropriate bit-separation and storage-element length[13].

A practically useful version is the semipermanent twistor store[7, 101, 147]. The magnetic condition of those twistor elements which are not to be switched by the interrogation current, namely the 0s, is fixed by means of permanent magnets lying directly above them, whereas the condition of other elements can be changed, so giving out a 1 signal. To achieve this, a card carrying a pattern of permanent magnets is mounted above each twistor layer. The permanent magnet material is Vicalloy with an $H_c$ of 16 kA/m and a $B_s$ of 1 V s/m$^2$. A Vicalloy tape of 50 μm thickness is stuck onto a plastic card. Little rod-like magnets having an area of 0·5 mm×1·5 mm are etched out and magnetised—where this is required—in the direction of their length, running parallel to that of the twistor wire. The card, with its magnets, is pressed against the coil winding by means of springs so that it is separated from the reading conductor by only a few micrometres. The stray magnetic flux is low. A field strength of 1600 A/m is measured immediately underneath a magnet and only 80 A/m above the nearest neighbour.

The cards are changeable and are 'written' by a special device. The twistor, then, serves as a sensor for the magnetic condition of the elements on the card. This permits a non-destructive read-out. The cycling time of a store with 130 000 words, each of 44 bits, amounts to about 5·5 μs; the 1 to 0 ratio is 3 in the most unfavourable case; the read-out signal is 1 mV, and the information density about 10 bit/cm$^3$.

## 15.13 THE MAGNETOSTRICTIVE DELAY LINE

The information registered in a semipermanent store is rarely changed. On the other hand stores, are needed which hold their information for only a short time. Delay lines of magnetostrictive materials serve as short-term memories with a holding time of the order of a few milliseconds[57, 58, 154]. Short pulses are fed into one end of a magnetostrictive wire, pass down the wire as waves of magnetostriction, and can be taken off as electromagnetic pulses at the other end. By suitable means, a continuous flow of information pulses can be maintained.

**Table 15.15** EXPERIMENTAL VALUES OF TEMPERATURE COEFFICIENTS FOR THE TIME DELAY OF LONGITUDINAL WAVES (100 kHz) IN VARIOUS MATERIALS[154]

| *Material* | *Temperature coefficient of time delay* (ppm/K) |
|---|---|
| Hard nickel | +148 |
| Piano wire | +136 |
| Ni-Span C | + 44 |
| Steel R 31 | + 6·7 |
| Ni–Fe–Ti alloy | |
| as delivered | + 28·8 |
| after heat treatment | − 45 |

If a material is to be used in a delay line, the waves should traverse it, as far as possible, without loss, and neither delay nor waveform should be affected by temperature. Further, the electromechanical coupling factor (see next section) should be high to guarantee high transmission efficiency. Since no substance exists offering these different requirements in equal degree, the following device has proved useful for long delay lines. Two different materials are used, one having high electromagnetic coupling and the other having low loss and negligibly low temperature coefficient of delay[154]. A comparison of the various materials set out in Table 15.15 shows that it is possible to reduce the delay temperature coefficient of a Ni–Fe–Ti alloy to an almost arbitrary extent by suitable heat treatment. Annealed nickel, certain Fe–Ni and Ni–Co alloys, together with some ferrites, have high electromechanical coupling factors[29] (see also Table 16.3).

The delay in a line depends on its length and on the speed of wave propagation through it. The speed with which a pressure wave travels through a ferrite rod amounts to 5·5 km/s while a shear wave (torsion-excited) travels at 3·3 km/s[189]. The speed of propagation of a pressure wave is some 4·75 km/s in nickel and about 5·2 km/s in the alloy 49% Co–29% Fe–2% V[29].

An example of a magnetostriction delay line is given by Scarrott and Naylor[154]. A Ni–Fe–Ti wire 0·7 mm in diameter and 9 m long was formed into a spiral, the mean diameter of which was 40 cm. The delay obtained was 3·2 ms. At a repetition frequency of 500 kHz, therefore, 1600 digits could be stored. The temperature coefficient of the conductor was 4 ppm/K. Bradfield[29] describes a delay line built with the help of a ferrite. A nickel ferrite tube 100 mm long, having an inner clearance of 6 mm and an outer diameter of 12·5 mm, is magnetised circumferentially. Two 3 mm long coils of 50 turns each and an inner diameter of 13·75 mm are mounted on the tube and can be shifted along it as required. If a square-wave pulse of 60 mA amplitude and 1–2 μs in duration is injected into one coil, then a somewhat later signal of 14 mV appears in the other. By increasing the coil separation, the delay can be adjusted up to 30 μs. It may be mentioned also that delay lines can be constructed on other principles, for example using inductances and capacitors.

## 15.14 THE ORTHOFERRITE MEMORY

Apart from the various magnetic storage and transfer elements outlined in this chapter, a great many variants of the same principles are now known, such as Ferrod[10a], Flute[13a], Chain[96a], and BIAX[122a], and many others which cannot here be discussed in detail. However, for the sake of completeness, one special storage principle will be explained—at least in broad outline—namely the orthoferrite memory.

Orthoferrites have the general formula $RFeO_3$, where R stands for yttrium or one of the rare earths, and can be taken as antiferromagnetic with a weak superposed ferromagnetism. Saturation polarisation lies between 0·0062 V s/m² and 0·0143 V s/m². Néel temperatures of some 400°C are characteristic of all the orthoferrites. A specific property of these orthoferrites is the high field value at which crystal nuclei form (over 100 kA/m). Even in the saturated condition, thin plates having their principal axis normal to the surface are fully stable with no supplementary fields. On the other hand, domain walls can be set in motion by fields below 100 A/m. The stability and mobility of cylindrical domains form the basis for storage techniques which can be applied to shift registers and logic circuits[26a,26b].

Examples of orthoferrites often investigated are $TmFeO_3$, $TbFeO_3$, and $Sm_{0·55}Tb_{0·45}FeO_3$. Materials showing similar behaviour are magnetoplumbite, barium ferrite, and Mn–Bi. For the construction of memory stores, thin single-crystal platelets some 50 μm thick are used; they are cut from the orthorhombic crystal in such a way that the preferred magnetic axis is perpendicular to the surface of the platelet.

With the aid of a direct magnetic field the zig-zag strip domains usually available can be made to yield single-wall domains, having cross-sections of,

say, 20–100 μm, which can be aligned by the field. These domains can be rendered visible by means of the Faraday effect. Orthoferrites are transparent to red light. There is thus no difficulty in examining each individual platelet to determine its usability (homogeneity, porosity, etc.).

To enable the domain movement to be followed and its actual position located, Permalloy dots of 0·5 μm diameter are distributed in matrix formation over the surface of the platelet—this, at least, is one of several possible procedures. By applying strip loops—based on thin-film technique – magnetic fields can be created which can drive the domains through the platelet in any desired fashion. A domain can be driven, for example, across the thickness dimension in less than 100 ns, which corresponds to a data rate of $10^6$ bit/s[26b]. The coercivity of the materials is an important parameter for determining the speed of propagation. In very pure materials, $H_c$ values of 0·8 A/m are attainable, mostly they are something less than 40 A/m.

The ambient temperature also affects the magnitude and the drift-velocity of the 'bubbles', as the cylindrical domains are sometimes named. The wall energy of $YFeO_3$ is relatively insensitive to temperature changes[151a], remaining nearly constant between 100K and 350K.

## REFERENCES


1. ABBOT, H. W. and SURAN, J. J.: Multihole ferrite core configurations and applications (Proc. IRE **45** (1957) 1081–1093).
2. ADAMS, E.: Recent developments in soft magnetic alloys (J. A. P. **33** (4) (1962) 1214–1220).
3. ADAMSKY, R. F.: Preferred orientation and ordering in evaporated films of Fe, Ni and Fe–Ni (J. A. P. **31** (5) (May 1960) 289S–290S).
4. ALBACH, W.: Zur Wirkung der Hochfrequenzmagnetisierung beim Magnettonverfahren (Funk u. Ton 7 (1953) 628–630).
5. ALBERS-SCHOENBERG, E.: Ferrites for microwave circuits and digital computers (J. A. P. **25** (1954) 152–154).
6. ALBERS-SCHOENBERG, E.: Square hysteresis loop ferrites in the system MgO–MnO–$Fe_2O_3$ (Ceram. Bull. **35** (7) (1956) 276–279).
7. ALEXANDER, E. J., MCALEXANDER, J. C., YOUNG, L. H. and SALHANY, R. J.: A permanent magnet twistor memory element of improved characteristics (J. A. P. **33** (Mar. 1962) 1075–1076).
8. ANDERSON, M. E.: Magnetic head reads tape at zero speed (Electronics **32** (Mar. 1959) 58–60).
9. AXON, P. E.: An investigation into the mechanism of magnetic-tape recording (Proc. IEE **99** (III) (59) (May 1952) 109–126).
10. BACKERS, F. TH. and WESSELS, J. H.: Magnetische Fernsehaufzeichnung mit einer Ein-Kopf-Anlage (NTZ **15** (12) (Dec. 1962) 644–649).

10a BALDWIN, JR., J. A.: A magnetic device for high-speed sensing of small currents (AIEE Trans., Comm. Electr. (53) (Mar. 1961) 1–8).

11. BALL, A. G., WRIGHT, J. E., HOOD, D. L. and BUTCHER, J. A. W.: The design of recording heads for use on a magnetic storage drum, and the characteristics of various recording surfaces (Proc. IEE **109 B** (1962) 165–174).

11a BALTZ, A.: Annealing of cylindrical Ni–Fe films (IEEE Trans. **Mag-5** (Mar. 1969) 2–6).

12. BANKES, E., RIEDERMAN, N. H., SCHLENNING, H. W. and SILBER, L. M.: Preparation and properties of thin ferrite films (J. A. P. **32** (3) (1961) 44S–45S).

13. BARRETT, W. A.: Demagnetization of twistor bits (J. A. P. **32** (3) (Mar. 1961) 35S–36S).
13a BARTKUS, E. A., BROWNLOW, J. M., CRAPO, W. A., ELFANT, R. F., GREBE, K. R. and GUTWIN, O. A.: An approach towards batch fabricated ferrite memory planes (IBM Journ. (Apr. 1964) 170–176).
14. BATES, L. F. and MARTIN, D. H.: Domains of reversal magnetization (Proc. Phys. Soc. **66** (2) (1953) 162–166).
15. BECKERMANN, M. and BEHRNDT, K. H.: The influence of edge effects on domain structure and coercive force of circular nickel-iron films (IBM J. Res. Dev. **4** (Apr. 1960) 198–201).
16. BEGUN, S. J.: Recent developments in the field of magnetic recording (J. Soc. Mot. Pict. Engrs. **48** (1) (1947) 1–13).
17. BEGUN, S. J.: A survey of magnetic recording (El. Engng. **73** (Dec. 1954) 1115–1118).
18. BILLING, H.: Numerische Rechenmaschine mit Magnetophonspeicher (Z. ang. Math. Mech. **29** (1/2) (1949) 38–42).
19. BILLING, H.: Die Magnetspeicher bei elektronischen Rechenmaschinen; in Technik der Magnetspeicher (ed. Winkel), Springer (1960) 282–328.
20. BITTMANN, E. E.: Using thin films in high-speed memories (Electronics **32** (June 1959) 55–57).
21. BITTMANN, E. E.: Thin film memories: some problems, limitations and profits (Proc. Intermag Conf. (1963) 9-1).
22. BLOIS, M. S.: Preparation of thin magnetic films and their properties (J. A. P. **26** (8) (Aug. 1955) 975–980).
23. BOBECK, A. H.: A new storage element suitable for large-sized memory arrays, the twistor (Bell Syst. Tech. J. **36** (Nov. 1957) 1319–1340).
24. BOBECK, A. H.: The twistor: a new magnetic memory element (Bell. Lab. Rec. (Nov. 1959) 406–410).
25. BOBECK, A. H.: The cube waffle-iron memory (1963 Proc. Intermag Conf. (T-149) (1963) 3-2).
26. BOBECK, A. H. and FISCHER, R. F.: Reversible, diodeless, Twistor shift register (J. A. P. **30** (Apr. 1959) 43S–44S).
26a BOBECK, A. H.: Properties and device applications of magnetic domains in orthoferrites (Bell Syst. Tech. J. (Oct. 1967) 1901–1925).
26b BOBECK, A. H., FISCHER, R. F., PERNESKI, A. J., REMEIKA, J. P. and VAN UITERT, L. G.: Application of orthoferrites to domain wall devices (IEEE Trans. **Mag-5** (3) (Sept. 1969) 544–553).
27. BODENSTEIN, C. and OTTO, R.: Magnetische Aufzeichnung auf luftstabilisierter, rotierender Folie (Entwicklungsber. S & H **25** (Nov. 1962) 103–110).
28. BOLL, R.: Metallische Magnetwerkstoffe und Kernformen in der Nachrichtentechnik (ETZ-A **80** (1959) 582–588).
29. BRADFIELD, G.: Practical applications and measurements on ferrite electromechanical transducers (Proc. IEE **104 B** (1957) 558–561).
30. BRADLEY, E. M.: Properties of magnetic films for memory systems (J. A. P. **33** (3) (1962) 1051–1057).
31. BRAGINSKI, A., CIASTON, W., KULIKOWSKI, J. and MAKOLAGWA, S.: Square loop ferrites containing cadmium (Proc. IEE **109 B** (47) (Sept. 1962) 380–382).
32. V. BRAUNMÜHL, H. J. and WEBER, W.: Verfahren zur magnetischen Schallaufzeichnung. DRP 743 411 (1940).
33. BRIGGS, G. R. and TUSKA, J. W.: Permalloy-sheet transfluxor-array memory (J. A. P. **33** (3) (1962) 1065–1066).
34. BRIGGS, G. R. and TUSKA, J. W.: Design and operating characteristics of a high bit density permalloy sheet transfluxor memory stack (Proc. Intermag Conf. (1963) 3–4).
35. Brit. Pat. 759248: Improvements in or relating to methods of manufacturing non-metallic cores having a substantially rectangular hysteresis loop (22. 12. 54, Priority;

Netherlands 1953).
35a. BROOK, R. J. and KINGERY, W. D.: Nickel ferrite thin films. Microstructure and magnetic properties (J.A.P. **38** (Aug. 1967) 3589–3594).
35b. CHANG, H. and LIN, Y. S.: Bibliography of thin magnetic films (1963–1967) (IEEE Trans. **Mag-3** (1967) 653–700).
36. CHRISTIAN, E.: Einspur- und Mehrspur-Kombiköpfe (Funkschau **31** (9) (1959) 205–206).
37. CHU, W. W. L., WOLFE, J. E. and WAGNER, B. C.: Some observations on evaporated permalloy films (J. A. P. **30** (1959) 272S–273S).
38. COHEN, M. S., HUBER, E. E., WEISS, G. P. and SMITH, D. O.: Investigation into the origin of anisotropy in oblique-incidence films (J. A. P. **31** (5) (1960) 291S–292S).
39. COHLER, E. U. and BAKER, T. E.: Geometric factors in multiaperture ferrite devices (Proc. Nonlinear Magnetics Conf. (1961) 215–250).
40. CONGER, R. L.: Magnetization reversal in thin films (Phys. Rev. **98** (6) (June 1955) 1752–1754).
41. CONGER, R. L. and MOORE, G. H.: Direct observation of high-speed magnetization reversal in films (J. A. P. **34** (4) (1963) 1213–1214).
42. CRITTENDEN E. C. and HOFFMAN, R. W.: Thin films of ferromagnetic materials (Rev. Mod. Phys. **25** (1) (Jan. 1953) 310–315).
43. CRUEL, R.: Entwicklungsbericht über Ferritmagnettonköpfe (Techn. Hausm. NWDR **5** (1953) 60–65).
43a DAHMS, A. and CROLL, I.: The anomalous codeposition of iron-nickel alloys (J. Electrochem. Soc. **112** (1965) 771–775).
44. DELLER, R.: Metalltransfluxoren (Z. ang. Phys. **13** (4) (1961) 180–182).
45. DIETRICH, W. and PROEBSTER, W. E.: Millimicrosecond magnetization reversal in thin magnetic films (J. A. P. **31** (5) (May 1960) 281S–282S).
46. DIETRICH, W., PROEBSTER, W. E., DUNLOP, L. J. and LOUIS, H. P.: The design of a one-million bit 100 nanosecond magnetic film memory (Proc. Intermag Conf. (1963) 9-2).
47. DIN 41 298, Weichmagnetische Ferritkerne für Magnetköpfe (Magnetkopf-Kerne) (Aug. 1971).
48. DIN 66 010, Magnetbandtechnik für Informationsverarbeitung. (Feb. 1965).
49. DUINKER, S.: Durable high-resolution ferrite transducer heads employing bonding glass spacers (Phil. Res. Rep. **15** (1960) 342–367).
50. ECKARDT, J.: Untersuchungen an dünnen Nickel-Eisen-Molybdän-Schichten (Z. ang. Phys. **14** (4) (1962) 189–191).
51. ECKERT, J. P.: A survey of digital computer memory systems (Proc. IRE (1953) 1393–1406).
52. ECONOMOS, G.: Magnetic properties of square loop ferrites within the system MgO–MnO–$Fe_2O_3$ (J. Am. Cer. Soc. **38** (1955) 408–411).
53. EGGENBERGER, J. S.: Influence of nearby conductors of thin film switching (J. A. P. **31** (5) (May 1960) 287S–288S).
54. EICHBAUM, B. R.: Evaluation of new high-speed magnetic ferrite system for use in computer components (J. A. P. **30** (Apr. 1959) 49S–52S).
55. EICHBAUM, B. R.: Development of high-speed coincident current memory cores (J. A. P. **31** (5) (May 1960) 117S–118S).
56. ELDRIDGE, D. and DOREY, P. F.: A core-transistor logical element (Proc. IEE **104 B** (1957) 512–522).
57. FAGEN, M. D.: Bibliography of ultrasonic delay lines. Bell Telephone System Monograph 2317.
58. FAIRCLOUGH, J. W.: A sonic delay-line storage unit for a digital computer (Proc. IEE **103 B** (1956) 491–496, 535–536).
59. FISHER, R. D.: Hysteresis and saturation recording (NRZ) characteristics of chemically deposited cobalt (Proc. Intermag Conf. (1963) 4–5).

60. FORTIN, E. G. and LESSOFF, H.: Temperature-stable ferrites for memory applications (Proc. Intermag Conf. (1963) 1–3).
61. FRANCOMBE, M. H. and NOREIKA, A. J.: Some properties of uniaxial permalloy films prepared by cathodic sputtering (J. A. P. **32** (1961) 97S–98S).
62. FUJI SHASHIN FILM. DBP 1 116 134 (Magnetogrammträger (1960)).
63. GANZHORN, K.: Magnetische logische Grundschaltungen in Rechenanlagen (Elektron. Rdsch. **11** (1957) 299).
64. GELBARD, E.: Magnetic properties of ferrite materials (Tele-Tech. **11** (May 1952) 50–52, 82, 84).
65. GIANOLA, U. F. and CROWLEY, T. H.: The laddic, a magnetic device for performing logic (Bell Syst. Tech. J. **38** (1959) 45–72).
66. GOODENOUGH, J. B.: The influence of chemistry on B/H loop shape, coercivity and flux reversal time in ferrites (Proc. IEE **104 B** (1957) 400–411).
67. GOODENOUGH, J. B.: Discussion on square loop materials (Proc. IEE **104 B** (1957) 434).
68. GORTER, E. W. and ESVELDT, C. J.: Square loop ferrites obtained by magnetic annealing of new compositions (Proc. IEE **104 B** (1957) 418–421).
69. GRAHAM, C. D. and LOMMEL, J. M.: Effect of pressure during evaporation on the magnetic properties of nickel films (J. Phys. Soc. Japan **17 BI** (1962) 570–574).
70. GREIFER, A. P. and CROFT, W. J.: Some crystallographic and magnetic properties of square loop materials in ferrite systems containing copper (J. A. P. **30** (1959) 34S–36S).
71. GUCKENBURG, W.: Die Wechselbeziehung zwischen Magnettonband und Ringkopf bei der Wiedergabe (Funk u. Ton **4** (1950) 24–33).
72. GYORGY, E. M.: Rotational model of flux reversal in square loop soft ferromagnets (J. A. P. **29** (1958) 283).
73. HOAGLAND, A. S.: Magnetic recording head design (Proc. Western Joint Comp. Conf. (85) (1956) 26–31).
74. HAAR, H.: Mehrspur- und Stereoköpfe für Studio- und Heimgeräte (Funkschau **31** (9) (1959) 207–208).
75. HAASS, G. F.: Der Transfluxor als Analogspeicher (NTZ **14** (8) (1961) 410–415).
76. HANSEN, W. H.: Das Magnetophon (ETZ **56** (45) (1935) 1232).
77. HECK, C.: Zur Phänomenologie der Ummagnetisierung von Speicherferriten (ETZ-A **80** (1959) 161–168).
78. HECK, C. and REINER, H.: Rechteckferrite und die Prüfung ihrer Speichereigenschaften (NTZ **11** (1958) 360–369; SEL Nachr. **6** (1958) 199–208).
79. HECK, C. and WEBER, J.: Ferritkerne für Schnellspeicher und ihre Betriebseigenschaften (NTZ **14** (4) (1961) 196–202).
80. VAN DER HEIDE, H., BRUIJNING, H. G. and WIJN, H. P. J.: Schaltzeiten bei Ferriten mit rechteckiger Hystereseschleife (Phil. T. Rdsch. **18** (1957) 334–344).
81. HESTERMAN, V.: Evaluation of flux-switching models for magnetic devices (Proc. Non-linear Magnetics Conf. (1961) 265–292).
82. HICKMAN, R. E. B.: Magnetic Recording Handbook. George Newnes Ltd. London (1962).
83. HUBER, E. E., SMITH, D. O. and GOODENOUGH, J. B.: Domain wall structure in permalloy films (J. A. P. **29** (3) (1958) 294–295).
84. HUNTER, L. P. and BAUER, E. W.: High speed coincident-flux storage principles (J. A. P. **27** (1956) 1257–1261).
85. KAY, E.: Magnetic thin films prepared by sputtering (J. A. P. **32** (1961) 99S–101S).
85a KAYSER, W.: Übersicht über Speicherverfahren für Speicher mit dünnen magnetischen Schichten (Elektron Rechenanl. **4** (1962) 60–70).
86. KINCAID, M., ALDEN, J. M. and HANNA, R. B.: Static magnetic memory for low cost computers (Electronics **24** (Jan. 1951) 108–111).

87. KITTEL, C.: Physical theory of ferromagnetic domains (Rev. Mod. Phys. **21** (4) (Oct. 1949) 541–583).
88. KLINKMÜLLER, J.: Zur Geschichte der elektromagnetischen Schallaufzeichnung (ETZ-A **76** (1955) 48–50).
89. KLUTH, H.: Entwicklung und gegenwärtiger Stand der Magnettontechnik (ETZ-B **13** (1961) 463–468).
90. KORNETZKI, M. and BURGER, H.: Das Verhalten von Ferritkernen mit rechteckförmiger Hystereseschleife im inhomogenen Magnetfeld und bei Scherung (Frequenz **9** (1955) 306–309).
91. KRONES, F.: Herstellung und elektroakustische Eigenschaften von Magnetbandspeichern für die Schallaufzeichnung; in Technik der Magnetspeicher (ed. Winkel), Springer (1960) 474–540.
92. JABLONOWSKI, E. J.: Versuche über die Herstellung dünner Kobaltfilme durch thermische Zersetzung von Kobalt-Acetylacetonat (Kobalt (14) (Mar. 1962) 30–32).
93. KRIESSMAN, C. J. MATCOVICH, T. J. and FLANNERY, W. E.: Low power thin film memory (Proc. Intermag Conf. (1963) 3-3).
94. LABORATOIRE CENTRAL DE TÉLÉCOMMUNICATIONS S.A.: Méthodes et moyens de réalisation de pistes sans fin pour l'enregistrement d'informations, par example sur matériaux magnétiques. Fr. Pat. 1 119 186 (1954).
95. LAWRENCE, W. W.: Recent developments in very-high-speed magnetic storage techniques (Proc. Eastern Joint Comp. Conf. (Dec. 1956) 101–103).
95a LAZZARI, J.-P. and MELNICK, I.: Integrated magnetic recording heads (IEEE Trans. **Mag-7** (Mar. 1971) 146–150).
96. LEILICH, H. O.: Technische Probleme bei der Entwicklung von Magnettrommelspeichern (Elektron. Rdsch. **9** (10) (1955) 365–368).
96a LEILICH, H. O.: The chain: a new magnetic film memory device (J. A. P. **37** (3) (Mar. 1966) 1361–1362).
97. LEMAIRE, H. P. and CROFT, W. J.: Ferrite thin films (J. A. P. **32** (3) (1961) 46S–47S).
98. LESSOFF, H. and GREIFER, A. P.: Perminvar characteristics of nickel-cadmium ferrites with small additions of cobalt and molybdenum (J. A. P. **33** (3) (Mar. 1962) 1199–1200).
99. LOCKHART, N. F.: Logic by ordered flux changes in multipath ferrite cores (IRE Nat. Conv. Rec. (4) (1958) 268).
100. LONG, T. R.: Electrodeposited memory elements for a nondestructive memory (J. A. P. **31** (5) (1960) 123S–124S).
101. LOONEY, D. H.: A twistor matrix memory for semipermanent information (Proc. Western Joint Comp. Conf. (Mar. 1959) 36–41).
102. LUFCY, C. W. and HEATH, W. T.: Alloy improves magnetic recording (Electronics **28** (June 1955) 137–139).
103. MAIER, H.: Magnetband-Registrier- und Speichergeräte (Elektronik **4** (8) (Aug. 1955) 177–184; (9) (Sept. 1955) 223–228).
103a MATHIAS, J. S. and FEDDE, G. A.: Plated-wire technology: a critical review (IEEE Trans. **Mag-5** (Dec. 1969) 728–751).
104. MAY, M., MILLER, G. P., HOWARD, R. A. and SHIFRIN, G. A.: A high speed, small size magnetic drum memory unit for subminiature digital computers (Proc. Eastern Joint Comp. Conf. (1959) 190–199).
105. MCCABE, P. N.: Twistor memories (Instr. Contr. Syst. **34** (1961) 1242–1245).
105a MCCALLISTER, J. P. and STROBL, S. J.: Quantitative prediction of aging effects in plated wires (IEEE Trans. **Mag-5** (Sept. 1969) 495–500).
105b MCCALLISTER, J. P.: Plated-wire memories: How far can we go? (IEEE Trans. **Mag-6** (Sept. 1970) 525–528).
106. MEE, C. D.: Magnetic tape recording materials (Proc. Intermag Conf. (1963) 4–1).

107. MEIER, D. A.: Millimicrosecond magnetic gating and storage element (J. A. P. **30** (1) (1959) 122–123).
108. MEIER, D. A.: Millimicrosecond magnetic switching and storage element (J. A. P. **30** (4) (Apr. 1959) 45S–46S).
109. MEIER, D. A.: A five-megacycle DRO thin-film ROD memory (Proc. Intermag Conf. (1963) 9–4).
110. MEINKEN, R. H.: A memory array in a sheet of ferrite (Conf. Magnetism Magn. Mat., Boston (1956) 674).
111. MENYUK, N.: Magnetic materials for digital computer components—Magnetic characteristics of ultra-thin molybdenum-permalloy cores (J. A. P. **26** (June 1955) 692–697).
112. MENYUK, N. and GOODENOUGH, J. B.: Magnetic materials for digital computer components. A theory of flux reversal in polycrystalline ferromagnetics (J. A. P. **26** (1955) 8–18).
113. MILLER, J. C. and BARKER, R. C.: Switching properties of a single crystal specimen of nickel ferrite (J. A. P. **34** (4) (1963) 1129–1130).
114. MINNICK, R. C.: Magnetic switching circuits (J. A. P. **25** (Apr. 1954) 479–485).
115. MATCOVICH, T.J. and KRIESSMAN, C.J.: Remagnetization experiments in $Mn_{1+x}Fe_{2+x}O_4$ (J. A. P. **30** (4) (1959) 26S–27S).
116. MOORE, D. W.: The preparation of magnetic films by high vacuum evaporation (Proc. Nonlinear Magnetics & Magn. Ampl. 1958, 278–295).
117. MOORE, A. C. and YOUNG, A. S.: Some physical properties of thin magnetic films (J. A. P. **31** (5) (1960) 279S–280S).
118. NEUGEBAUER, C. A.: Structural aspects of the magnetization in ultrathin ferromagnetic films (Z. ang. Phys. **14** (4) (1962) 182–185).
119. NEUMANN, H.: Neue Bauformen von Magnetköpfen (Siemens-Z. **28** (1954) 405–408).
120. NEWHOUSE, V. L., KORNFIELD, N. R. and KAUFMAN, M. M.: End-fired memory uses ferrite plates (Electron. engl. iss. (Oct. 1958) 100–103).
121. NIJENHUIS, W.: 'PASCAL' eine sehr schnelle elektronische Ziffernrechenmaschine für das Philips-Rechenzentrum (Phil. T. Rdsch. **23** (1) (1961) 1–20).
122. NIPPON ELECTRIC CO. LTD., TOKYO: (NEC News **1** (2) (1963).
122a NISTLER, P. J.: Phenomenological model for the BIAX (IEEE Trans. **Mag-1** (Dec. 1965) 292–295).
123. NOT KNOWN: Tiny drum memory holds 4096 words on 1-inch rotor (Electr. Des. **10** (June 1962) 34–35).
124. OAKLAND, L. J. and ROSSING, T. D.: Coincident-current nondestructive readout from thin magnetic films (J. A. P. **30** (1959) 54S–55S).
125. OERDING, R.: Der Aufzeichnungsvorgang beim Magnetton-Verfahren (Funk u. Ton **5** (1951) 262–270, 287–299).
126. OHMANN, F.: Der Magnetkernspeicher als Arbeitsspeicher im Siemens-Digitalrechner 2002 (Entwicklungsber. S & H **22** (Oct. 1959) 63–73).
127. OLSON, C. D. and POHM, A. V.: Flux reversal in thin films of 82% Ni 18% Fe (J. A. P. **29** (Mar. 1958) 274–282).
128. OTTO, R.: Die Magnettrommel des Siemens-Digitalrechners 2002 (Entwicklungsber. S & H **22** (Oct. 1959) 85–92).
129. OTTO, R.: Der Einfluss metallischer Spaltfolien auf den Scheinwiderstand von Magnetköpfen (Hochfrequenz und Elektroak. **71** (1962) 181–186).
130. OVERN, W. M. and KORKOWSKI, V. J.: Study of the residual states of ferrite cores in computer memory operation (J. A. P. **30** (1959) 52S–53S).
131. PALMER, G. G., JOHNSTON, R. W. and SCHULTZ, R. E.: Magnetic properties and associated microstructure of zinc-bearing square-loop ferrites (J. Am. Cer. Soc. **40** (Aug. 1957) 256–262).

132. PAPIAN, W. N.: A coincident-current magnetic memory cell for the storage of digital information (Proc. IRE **40** (Apr. 1952) 475–478).
133. PFLEUMER, F.: Lautschriftträger. DRP 500 900 (31.1.28).
134. POHM, A. V., ZINGG, R. J., SMAY, T. A., WATSON, G. A. and STEWART, R. M.: Large, high speed, DRO film memories (Proc. Intermag Conf. (1963) 9-5).
135. POULSEN, V.: The telegraphone, a magnetic speech recorder (Electrician **46** (Nov. 1900) 208–210; Ann. Phys. **3** (1900) 754–760).
136. PROEBSTER, W. E.: Dünne magnetische Schichten als Speicher- und Schaltkreiselelemente (Elektron. Rechenanl. (**1**) (4) (1959) 164–171).
137. PROEBSTER, W. E.: The design of a high speed thin-magnetic-film memory (Proc. Int. Sol. State Circ. Conf. (1962) 38–39).
138. QUARTLY, C. J.: A high-speed ferrite storage system (Electron. Engng. (Dec. 1959) 756–758).
139. RABL, H.: Ferrit-Transfluxoren (Siemens-Z. **34** (1960) 385–390, 397–404).
140. RABL, H.: Ferrite mit rechteckförmiger Hystereseschleife für ein weites Betriebstemperaturgebiet (Siemens-Z. **35** (1) (Jan. 1962) 60–67).
141. RAFFEL, J. I.: Operating characteristics of a thin film memory (J. A. P. **30** (1959) 60S–61S).
142. RAFFEL, J. I., CROWTHER, T. S., ANDERSON, A. H. and HERNDON, T. O.: Magnetic film memory design (Proc. IRE **49** (1961) 155–164).
143. RAJCHMAN, J. A.: Ferrite apertured plate for random access memory (Proc. IRE **45** (1957) 325–334).
144. RAJCHMAN, J. A.: A survey of magnetic and other solid-state devices for the manipulation of information (Trans. Prof. Group Circuit Theor. (Sept. 1957) 210–225).
145. RAJCHMAN, J. A.: Magnetic memories—capabilities and limitations (J. A. P. **34** (4) (Apr. 1963) 1013–1018).
146. RAJCHMAN, J. A. and LO, A. W.: The transfluxor—a magnetic gate with stored variable setting (RCA-Rev. **16** (June 1955) 303–311).
147. REED, E. D.: 1963 Magnetic memory devices (Electron. Switch. Symp., Bell Tel. Labs Holmdel (1963) 5-1–5-11).
148. REINER, H.: Digitale Schaltungen mit Transfluxoren (NTF **21** (1960) 69–75).
148a RICHARDS, H. D., HUMPAGE, J. and HENDY, J.: Topography control of plated wire memory elements (IEEE Trans. **Mag-4** (1968) 351–355).
149. RIDLER, D. S.: The magnetic cell—a new circuit element (Proc. IEE **104 B** (1957) 445–456).
150. ROBL, R.: Die Geschichte der Herstellung des Magnetophonbandes (Die BASF **7** (4) (1957) 158–161).
151. ROBL, R.: Über ferromagnetische Eisenoxyde (Angew. Chem. **70** (12) (1958) 367–371).
151a ROSSOL, F. C.: Temperature dependence of rare earth orthoferrite properties relevant to propagating domain device applications (IEEE Trans. **Mag-5** (3) (1969) 562–565).
152. ROYSE, D.: The IBM 650 RAMAG system disk storage operation (Proc. Western Joint Comp. Conf. (1957) 43–49).
152a ROZENBLAT, M. A.: The use of multiaperture cores for the realization of threshold functions of many variables (IEEE Trans. **Mag-5** (Sept. 1969) 196–200).
153. SALLO, J. S.: 'Orthocore'—a new magnetic storage device (Proc. Intermag Conf. (1963) 3–6).
154. SCARROTT, G. G. and NAYLOR, R.: Wire type acoustic delay lines for digital storage (Proc. IEE **103 B** (1956) 497–508, 535–536).
155. SCHIESSER, H.: Die Normung in der Magnetspeichertechnik: in Technik der Magnetspeicher. (ed. Winkel), Springer (1960) 541–584.
156. SCHMIDBAUER, O.: Ferrite als Kernmaterial für Magnettonköpfe (Funk u. Ton (4) (1954) 169–173).
157. SCHREIBER, F.: Der Transfluxor als Verstärker (NTF **21** (1960) 76).

158. SCHRÖTER, O.: Der Magnetplattenspeicher (Elektron. Rdsch. **11** (1957) 109–118).
159. SCHUT, TH. G. and OOSTERKAMP, W. J.: Die Anwendung elektronischer Gedächtnisse in der Radiologie (Elektron. Rdsch. **14** (1960) 19–20).
160. SCHWABE, E. A. and CAMPBELL, D. A.: Influence of grain size on square-loop properties of lithium ferrites (J. A. P. **34** (4) (Apr. 1963) 1251–1253).
161. SHAHBENDER, R. A.: National Electron. Conf. (Oct. 1963), see Electronics (Nov. 1963) 72–74).
162. SHAHBENDER, R., NELSON, Z., LOCHINGER, R. and WALENTINE, J.: Microaperture high speed ferrite memory (RCA-Rev. **23** (4) (Dec. 1962) 539–566).
163. SHAHBENDER, R., WENTWORTH, C., LI, K., HOTCHKISS, S. and RAJCHMAN, J. A.: Laminated ferrite memory (AFIPS Conf. Proc. **24** (1963) 77–90).
164. SHEVEL, W. L.: Observations of rotational switching in ferrites (IBM J. Res. Dev. **3** (1) (Jan. 1959) 93–95).
165. SHEVEL, W. L.: Millimicrosecond switching properties of ferrite computer elements (J. A. P. **30** (4) (Apr. 1959) 47S–48S).
166. SHEVEL, W. L. and CHANG, H.: New approach to high speed storage—Low flux density materials (J. A. P. **31** (5) (May 1960) 125S–126S).
167. SHEW, L. F.: High density magnetic head design for noncontact recording (IRE Trans. El. Comp. **EC 11** (6) (Dec. 1962) 764–773).
168. SIX, W. and KOOLHOF, R. A.: Some applications of square loop ferrite cores in telecommunication switching circuits (Proc. IEE **104 B** (1957) 491–501).
169. SMITH, D. O.: Thin magnetic films for digital computer memories (Electronics **32** (June 1959) 44–45).
170. SMITH, D. O.: Anisotropy in nickel–iron films (J. A. P. **32** (3) (Mar. 1961) 70S–80S).
171. SMITH, D. O.: Static and dynamic behaviour of thin permalloy films (J. A. P. **29** (3) (Mar. 1958) 264–273).
172. SMITH, J. L.: Waffle iron—a new memory structure (J. A. P. **34** (4) (Apr. 1963) 1167–1168).
173. SMITH, O.: Some possible forms of phonographs (El. World **12** (Sept. 1888) 116–117).
174. SNYDER, C. L., ALBERS-SCHOENBERG, E. and GOLDSMITH, H. A.: Magnetic ferrites (El. Manuf. **44** (1949) 86–91).
175. STEINBUCH, K.: Elektronische Nachrichtenspeicher (EZT-A **73** (1952) 489–496).
176. STEINBUCH, K.: Elektrische Gedächtnisse für Ziffern (ETZ-A **77** (1956) 799–807, SEG-Nachr. **4** (1956) 165–173).
177. STUIJTS, A. L., VERWEEL, J. and PELOSCHEK, H. P.: Dense ferrites and their applications (Proc. Intermag Conf. (1963) 1–2).
178. VACUUMSCHMELZE GMBH, HANAU: Aus metallischen Werkstoffen aufgebauter Transfluxor. Applications review 1 830 500.
179. VACUUMSCHMELZE GMBH, HANAU: Data Sheet M 005 (1967).
179a VACUUMSCHMELZE GMBH, HANAU: Vacodur 16, Data Sheet M 009 (Mar. 1962).
179b VAN KHAI, T. and MEUNIER, P.: NDRO waffle-iron memory (IEEE Trans. **Mag-5** (Sept. 1969) 584–585).
180. WACKERHAGEN, F. H.: Manufacturing techniques for magnetic drums (Western El. Eng. **3** (1959) 36–39).
181. WANG, A. and WOO, W. D.: Static magnetic storage and delay line (J. A. P. **21** (Jan. 1950) 49–54).
182. WEISZ, R. S.: Square loop ferrites with temperature-independent properties and improved disturb ratio (J. A. P. **32** (6) (June 1961) 1152–1153).
183. WEISZ, R. S. and BROWN, D. L.: Square loop properties of copper–manganese ferrites (J. A. P. **31** (5) (1960) 269S–270S).
184. WEMPER, D.: Speicherkerne mit kleinem Temperaturkoeffizienten (Elektron. Rdsch. (6) (1963) 293–294).
184a WENIGER, K.: Memory systems comparison (Electron. Eng. **26** (5) (May 1967) 118–119).

185. WESSELS, J. H.: Magnetische Aufzeichnungen von Fernsehbildern auf einem Speicherrad (Phil. T. Rdsch. **22** (1960) 37–47).
186. WESTMIJZE, W. K.: Der Aufnahme- und Wiedergabevorgang bei Magnettongeräten (Phil. T. Rdsch. **14** (Apr. 1953) 299–302).
187. WIJN, H. P. J., GORTER, E. W., ESVELDT, C. J. and GELDERMANS, P.: Bedingungen für eine rechteckige Hystereseschleife bei Ferriten (Phil. T. Rdsch. **16** (Oct./Nov. 1954) 124–134).
188. WILLIAMS, J. H. and SHERWOOD, R. C.: Magnetic domain patterns on thin films (J. A. P. **28** (5) (1957) 548–555).
189. WILSON, V. C.: Applications of ferrites (Proc. Conf. Magnetism Magn. Mat. (1955) 278–285).
190. WOLF, I. W.: Electrodeposition of magnetic materials (J. A. P. **33** (3) (1962) 1152–1159).
191. WOLFF, F.: Das Drahttongerät, ein moderner Schallspeicher (SEG-Nachr. **1** (1) (1953) 27–29).
192. WRIGHT, E. P. G.: The application of square loop ferrite material in data-processing systems (Proc. IEE **104 B** (1957) 502–511).
193. ZSCHEKEL, H.: Schnellspeicher und Grosspeicher der Informationsverarbeitungstechnik (Feinwerkst. **67** (2) (1963) 46–54).

# 16

# Materials for magnetomechanical resonators

When a magnetic material is placed in an alternating field, a mechanical vibration occurs because of magnetostriction; this is what gives rise to the familiar humming noise in power transformers, for example. If the magnetic body is of suitable dimensions, then resonance can occur between the magnetic field and the mechanical vibration. The sharpness of such a resonance depends on the material properties of the oscillator and on the type of material surrounding it.

## 16.1 APPLICATIONS

As far back as 1929 Pierce[21] recognised the high quality factor of mechanical oscillators and showed that the resonance of metal rods could be used for the frequency control of vacuum tubes. The resonance of certain materials is so sharp that frequency stabilisers and filter circuits can be built around them which, in many cases, can be used in place of quartz-controlled cirtuits[12, 27]. In general, the oscillatory frequency lies below 100 kHz but can be as high as 500 kHz[2]. Mechanical oscillators are largely free of parasitic frequencies. Oscillatory circuits at radiofrequencies are small and relatively cheap.

Another technically important field of application of the magnetostriction phenomenon is the magnetomechanical transducer, which plays a significant role as a generator of sound (or of ultrasound) up to frequencies of 50 kHz. Ultrasonic waves have many uses: they serve to measure distance in water (echo sounders), to locate whales or shoals of fish, and to check for cracks, etc., in solid bodies; they can also be used to work brittle substances like ferrites or glass; and metal and ceramic piece-parts can be washed and cleaned by ultrasonic means[5, 18]. Ultrasonic waves have also been applied to metallurgical processing or for aluminium soldering[15]. In all these cases, electromagnetic oscillations have to be converted into mechanical movements.

The following properties of magnetic materials must be considered when magnetostriction oscillators are designed. First, at low field intensities the magnetostriction effect is only small and more or less follows the law

$$\frac{\Delta l}{l} = aB^2 \tag{16.1}$$

Secondly, both the positive and the negative half-wave of an exciting field produce changes of shape of the same sign in the material, so the magnetostriction field has twice the frequency of the excitation. Large excursions at the frequency of the exciting field can be produced if polarised fields are used or if the core is brought to the remanence condition by a d.c. pulse of the proper magnitude. Either a direct electric field or a permanent magnet may be used to produce polarised magnetic fields.

## 16.2 REQUIREMENTS SPECIFIED FOR THE MATERIAL

Stringent requirements must be imposed simultaneously on the magnetic, mechanical, and magnetomechanical properties of the material if the conversion of electromagnetic into mechanical vibrations and vice versa is to take place with high efficiency. These, in detail, are:

1. Magnetostriction should be large ($|\lambda_s| > 20\times10^{-6}$).
2. A high Curie temperature will permit operation at elevated temperatures (for example, in metallurgical applications).
3. The specific electrical resistance $\varrho$ should be reasonably high to keep down eddy currents as far as possible. Materials of high conductivity must be laminated.
4. The mechanical quality factor should be high.
5. The temperature coefficient of the modulus of elasticity should be low.
6. The material should not show variations with time.
7. The magnetomechanical coupling factor $k$ should be as large as possible.

The mechanical quality factor of an oscillating bar is defined as the ratio of the fundamental oscillator frequency to the difference of the two frequencies (above and below the frequency of the bar) for which the specimen changes its length by $\sqrt{2}$ of the maximum change[23].

The coupling factor $k$, which is a complex quantity, plays a most important role: it specifies a relation between the magnetic and mechanical properties of the material. According to Sussman and Ehrlich[30], the real part $k'$ of the magnetomechanical coupling factor is defined by

$$(k')^2 = \frac{4\pi\lambda_r^2\mu_{rev}}{E} \tag{16.2}$$

where $\lambda_r$ is the dynamic magnetostriction constant defined by

$$\lambda_r = \left(\frac{\partial P}{\partial B}\right)_S \tag{16.3}$$

$\mu_{rev}$ is the reversible permeability defined by

$$\mu_{rev} = \left(\frac{\partial B}{\partial H}\right)_S \tag{16.4}$$

and $E$ is the modulus of elasticity (Young's modulus) given by

$$E = \left(\frac{\partial P}{\partial S}\right)_B \tag{16.5}$$

In these relations, $P$ = pressure, $S$ = spread (i.e. extension), and the suffixes indicate the constant parameter.

The value of $\lambda_r$ rises with increasing flux density $B$ while $\mu_{rev}$ falls, especially near saturation. The product $\mu_{rev}\lambda_r$, and also $(k')^2$, pass through maxima at clearly determined field intensities. Apart from this maximum value, designated $k'_m$, the magnitude $k'_{rem}$ is often of interest; it is the coupling factor taken at the remanence point.

## 16.3 THE MAGNETOMECHANICAL COUPLING FACTOR

The magnetomechanical coupling factor can be determined from the difference of the natural frequencies of a radially vibrating toroidal core whose windings are first open-circuited and then short-circuited[9]. The magnitude of $k^2$ is a measure of the (partial) conversion of magnetic into mechanical or mechanical into magnetic energy under the assumption of no loss and no radiation; the relevant frequency is here below the resonant frequency of the oscillator[7, 27]. The value of $k'$ is zero in the virgin and in the saturated condition. At around $0{\cdot}7B_s$ $k'$ has an optimum, $k'_m$. The field intensity needed to reach $k'_m$ is about 650 A/m for most alloys, and for ferrites must be increased twofold or fourfold[8, 11].

The following relation connects $k'_m$ with the anisotropic energy of the material:

$$(k'_m)^2 = \frac{\lambda_s^2 E_s}{\Sigma A} \tag{16.6}$$

Here, $E_s$ is the modulus of elasticity of the magnetically saturated material and $\Sigma A$ stands for the sum of the anisotropic energies comprising crystal anisotropy $K$, internal stress anisotropy $\lambda_s\sigma_i$, and the shape anisotropy of pores and inclusions. Since stress anisotropy and shape anisotropy can be kept small by proper manufacturing routines, $\Sigma A$ in the formula consists chiefly of crystal anisotropy $K_1$. Crystal anisotropy depends on the composition of the material.

The real part of the magnetomechanical (or piezomagnetic) coupling factor taken with the mechanical quality factor $Q_v$ and the magnetic quality factor $Q_\mu$ determines the potential electro-acoustic efficiency $\eta_e$:

$$\eta_e \doteq 1 - \frac{2}{k'\sqrt{(Q_\mu Q_v)}} \tag{16.7}$$

The suffix v of the mechanical quality factor indicates that the oscillator is supposed to vibrate in vacuo.

Reference must be made, for further theoretical details, to the works of van der Burgt[4–8a], Schweitzerhof[26], Sixtus[27], and Struszynski[28].

## 16.4 FORMS OF MECHANICAL OSCILLATOR

By and large, three shapes are used for bodies which are to be excited to resonance: rings (toroids), rods, and tubes. Toroids mostly vibrate radially, though they can also exhibit torsional vibrations (Figure 16.1). Thin rods or bars are generally excited in longitudinal modes (Figure 16.2). Torsional modes can also be produced through the Wiedemann effect. Tubes are used almost exclusively as torsional vibrators.

'Frame' vibrators, made from bars joined at their ends by plates, are used especially as ultrasonic generators (Figure 16.3). Barium ferrite vibrators in

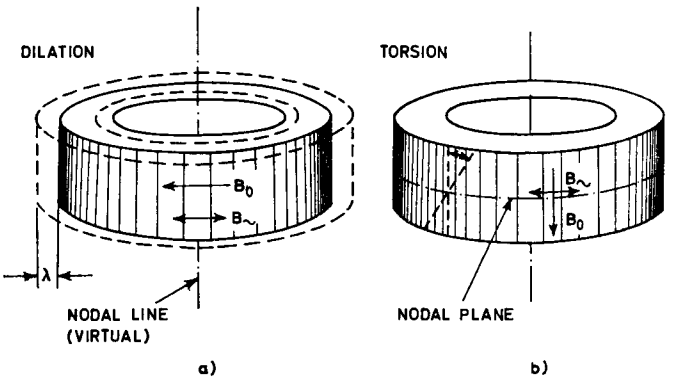



*Figure 16.1. Magnetostrictive toroidal vibrators: (a) radial vibrator; (b) torsional vibrator*[26]

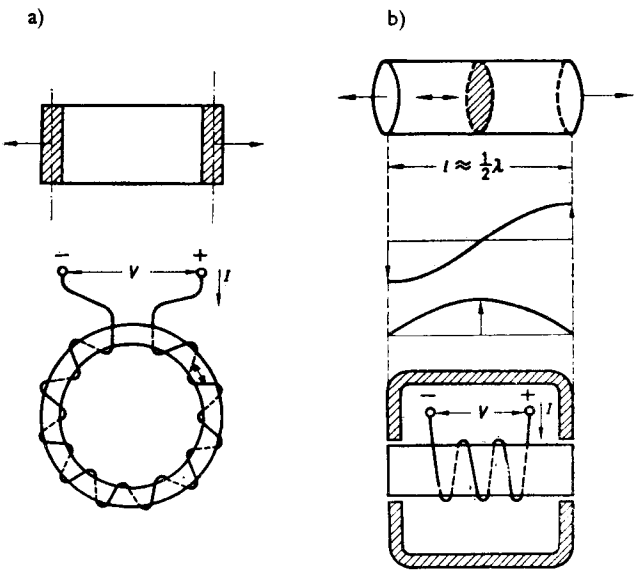



*Figure 16.2. Simple types of piezomagnetic transducers: (a) thin-walled ring or tube transducer; (b) thin $\lambda/2$ rod*[7]

platelets 1 mm or 2 mm thick, suitable for polarised arrangements, can be assembled from several dumbell-shaped elements closed by oscillating plates of ferrite. The arrangement shown in Figure 16.3 radiates to the right. In choosing the shape of a vibrator, the required frequency range is of first importance but there may be problems of mounting to consider. In general, air-gaps are to be avoided as far as possible in order to achieve a high coupling factor. In many cases, nevertheless, an air-gap is necessary if the effect of temperature variation is to be reduced.

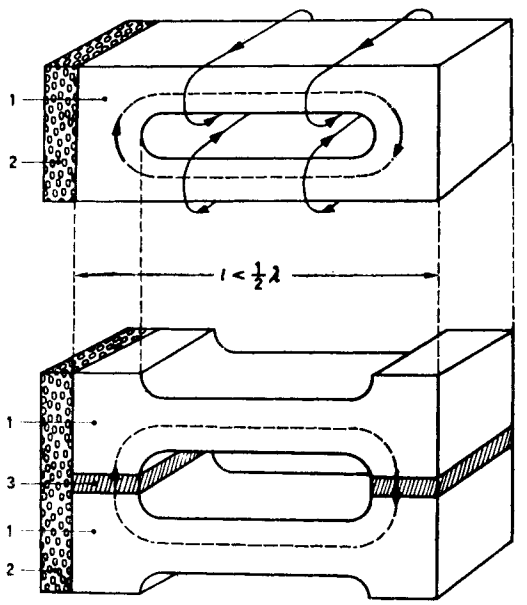



*Figure 16.3. Frame-type vibrator as magnetomechanical transducer: top, ferrite frame moulded in one piece (1); below, frame assembled from dumbell frames (1) with intermediate permanent magnet layer (3) (Ferroxdure 300); those faces of a submerged transducer required not to radiate are foam-damped (2)*[7]

The dimensions of a vibrator depend not only on the material and the frequency but also on the type of vibration desired. The length of a resonator is always equal to half the wavelength of the vibration. The product of wavelength and frequency is equal to the speed of propagation of the waves in the given material (speed of sound). This speed $v$ is greater for compressional than for shear waves. A longitudinal vibrator must therefore be longer than a torsional vibrator for a given frequency (some 60%) for most materials. These differences are significant, also, for the mechanical quality factor, reversible permeability, coupling factor, and magnetostriction constants. Table 16.1, after Popper[22], reproduces a comparison between the relevant constants for longitudinal and torsional modes of certain ferrites distinguished by their various initial permeabilities and saturation values. Table 16.2 gives some values of propagation velocity for longitudinal vibrators[24].

**Table 16.1** MAGNETIC AND MECHANICAL PROPERTIES OF SOME FERRITES AS LONGITUDINAL (l) AND TORSIONAL (t) VIBRATORS[22]

| *Property* | | *III B* | *IV A* | *IV B* | *IV C* | *IV D* | *IV E* |
|---|---|---|---|---|---|---|---|
| $Q_v$ | l | 3 300 | 4 000 | 3 300 | 2 860 | 2 660 | 1 575 |
| | t | 5 400 | 5 400 | 5 500 | 4 900 | 4 300 | 8 600 |
| $\mu_{rev}(\mu_0)$ | l | 1 180 | 430 | 170 | 70 | 35 | 11 |
| | t | 750 | 480 | 250 | 96 | 56 | 11·5 |
| $10^4 k_m$ | l | 15 | 550 | 490 | 670 | 490 | 490 |
| | t | 9·9 | 550 | 300 | 500 | 950 | 780 |
| $10^{-6}\ \lambda_r$ (N/V s) | l | 0·016 | 0·89 | 1·14 | 2·35 | 2·30 | 4·10 |
| | t | 0·072 | 0·52 | 0·35 | 0·57 | 2·20 | 4·10 |
| $\mu_i\ (\mu_0)$ | | 1 000 | 650 | 250 | 85 | 45 | 17 |
| $J_s$ (V s/m$^2$) | | 0·465 | 0·367 | 0·417 | 0·403 | 0·355 | 0·246 |

**Table 16.2** ESSENTIAL CONSTANTS OF A FEW MATERIALS USED IN MECHANICAL FILTERS[24]

| *Material* | $d$ (g/cm$^3$) | $v$ (km/s) | $Q_v$ |
|---|---|---|---|
| Armco iron | 7·76 | 5·13 | 850 |
| Ferrites | 4·46 | 5·58 | 1 250 |
| Nickel | 8·88 | 4·94 | 450 |
| Ni-Span C | 7·99 | 4·80 | 900 |
| Steel (rolled) | 7·71 | 5·04 | 1 100 |
| Aluminium | 2·73 | 5·11 | 4 000 |
| Brass (hard) | 8·54 | 3·64 | 2 500 |
| Brass (soft) | 8·50 | 3·52 | 2 000 |
| Invar | 8·62 | 4·01 | 5 000 |
| Monel K | 10·3 | 5·67 | 3 300 |
| Lead | 11·3 | 1·49 | 40 |
| Phosphor bronze | 8·9 | 3·52 | 2 000 |

No standardised shapes have been proposed for vibrating bodies up to the present. Certain shapes available from manufacturers have, however, emerged[33, 34], as can be gathered from the case of frame vibrators (Figure 16.3). Summaries of the various shapes of vibrating bodies and their different couplings and modes, as used in mechanical filters, are to be found in, for example, Aschmoneit[1], Enz[13a], and Roberts and Burns[24].

## 16.5 EXAMPLE OF A MAGNETOSTRICTIVE FILTER

A combination of vibrating parts and transducer elements is used to make up a filter. An intermediate-frequency filter for 455 kHz is shown schematically in Figure 16.4, for example[31]. Transducer coils (2) are seen at the input and output of the filter (1) and are in resonance at 455 kHz. A nickel rod (3)

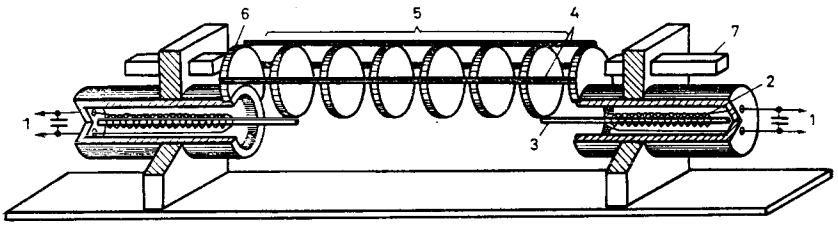



*Figure 16.4. Principle of a mechanical intermediate-frequency filter for 455* kHz *(explanation in text)*[31]

within the input coil vibrates at the same frequency and is mechanically coupled to a vibrating disc (5). The disc is built up into a resonant system in conjunction with five other discs joined together by a bridging piece. The final disc is coupled to the output vibrator (3) in the same way as at the input. The bridges (4) rest with their ends on the load discs (6). The two permanent magnets (7) serve to premagnetise the transducer rods. Each filter disc has a quality factor of about 2000.

## 16.6 MATERIALS

### 16.6.1 Metals and alloys

There are certain non-ferromagnetic (or only weakly ferromagnetic) metals and alloys, such as aluminium and invar, which exhibit the highest mechanical quality factors. These values are set out in Table 16.2 for longitudinally vibrating rods. In order to excite non-magnetic rods, they must be plated with a ferromagnetic substance such as nickel.

The quality factor of ferromagnetic metals and alloys is generally lower, and, indeed, the greater the magnetostriction, the lower $Q$, and vice versa[25]. The $Q_v$ values set out in Table 16.2 depart at many places from those quoted by other authors. Thus, according to Scarrott and Naylor[25], the $Q_v$ of hard nickel is 800, that of Ni-Span C is 2500, and that of piano wire is 4500. Different results are to be attributed to differences of material structure, composition, shapes of specimen, and conditions of measurement. The surface treatment of a vibrator and the disposition of the windings can lead to changes in the optimal properties. In this sense, all tabulated values should be taken rather as guides than as established constants.

### 16.6.1.1 Nickel and nickel alloys

Unalloyed nickel is distinguished by a high saturation value of magnetostriction ($\lambda_s = -34\times10^{-6}$). The relation between magnetostriction and polarisation is plotted in Figure 16.5; the magnetostriction coefficient $a$ from equation 16.1 is given in Table 16.6.

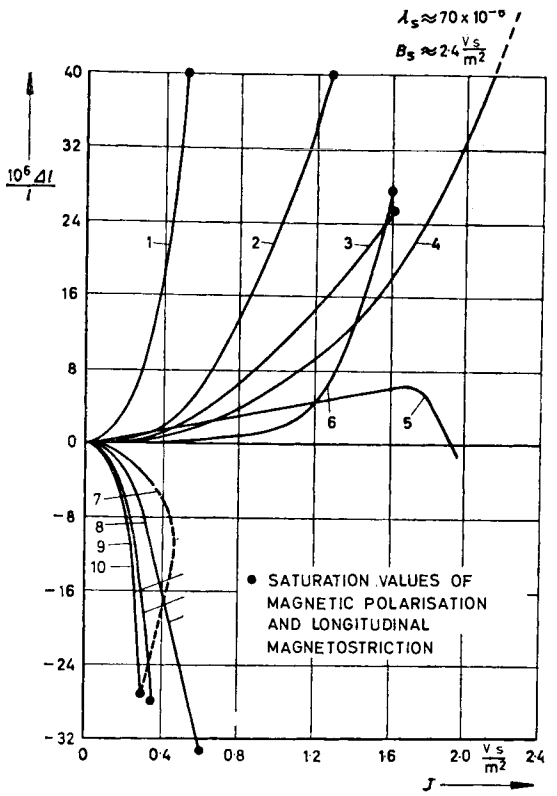



*Figure 16.5. Relative change of length (i.e. longitudinal strain $\lambda = \Delta l/l$) of piezomagnetic material ('virgin' curve): 1, magnetite; 2, 13 Alfer; 3, Permenorm 5000; 4, Vacoflux 50, 2V-Permendure; 5, iron; 6, 45 Permalloy; 7, Ferroxcube 4A; 8, nickel; 9, Ferroxcube 7A1, 7A2; 10, Ferroxcube 7B*[5]

The magnetomechanical coupling factor attains a value of 0·31. The core of a classical magnetostriction vibrator consists, therefore, of nickel sheet which is sometimes stamped out to shape and built into a stack corresponding to the schematic representation of Figure 16.3 (upper sketch). The high corrosion resistance of nickel is a particularly welcome feature of such magnetomechanical transducers since they may have to operate in 'corrosive' liquids like sea-water.

In many applications, it is true, the somewhat low Curie temperature is

**Table 16.3** PROPERTIES OF PIEZOMAGNETIC MATERIALS AT ROOM TEMPERATURE[8]

| *Material* | | $T_c$ (°C) | $\varrho$ ($\mu\Omega$ cm) | $10^6\lambda_s$ | $k_m$ | $H$ at $k_m$ (A/m) |
|---|---|---|---|---|---|---|
| Nickel | 99·9% Ni | 358 | 7 | −33 | 0·15–0·31 | 640–960 |
| Nickel–cobalt | 96% Ni, 4% Co | 410 | 10 | −31 | Up to 0·51 | — |
| Hipernik<br>Permenorm 5000 | 50% Ni, 50% Fe | 500 | 40 | +25 | 0·18–0·35 | — |
| 45 Permalloy | 45% Ni, 55% Fe | 440 | 45 | +27 | 0·18–0·35 | — |
| 2V-Permendur<br>Vacoflux 50 | 49% Co, 49% Fe, 2% V | 980 | ~30 | +70 | 0·20–0·37<br>0·25–0·32 | — |
| 13 Alfer | 87% Fe, 13% Al | ~500 | ~90 | +40 | — | — |
| Magnetite | $Fe_3O_4$ | 580 | $\sim 10^4$ | +40 | — | — |
| Cobalt ferrite | $CoFe_2O_4$ | 510 | $>10^{10}$ | ~−200 | <0·01 | — |
| Ferroxcube 4E | $Ni_{0.994}Co_{0.006}Fe_2O_4$ | 590 | $>10^{10}$ | −27 | 0·18–0·21 | — |
| Ferroxcube 7A1 | Ni–Cu–Co ferrite | 530 | $10^8$–$10^9$ | −28 | 0·25–0·32 | 960–1600 |
| Ferroxcube 7A2 | Ni–Cu–Co ferrite | 530 | $10^8$–$10^9$ | −28 | 0·20–0·26 | 720–1120 |
| Ferroxcube 7B | $Ni_{0.973}Co_{0.027}Fe_2O_4$ | 590 | $>10^{10}$ | −28 | 0·22–0·27 | 2000–4000 |
| Vibrox | Ni–Cu ferrite | — | $>4\times10^8$ | −30 | — | — |

troublesome (see Table 16.3). The pure metal has the further disadvantage that its specific electrical resistance is very low. Nickel sheet can therefore be used only at low frequencies. At higher frequencies the electromechanical conversion efficiency $\eta_e$ falls off rapidly with rising frequency (see Figure 16.6). The mechanical quality factor attained by nickel rods[23, 24] is generally below 500. The speed with which a compressional wave is propagated amounts to some 4·75 km/s (see also Table 16.2)[4].

Numerous nickel alloys possess a lower conductivity than nickel and many exhibit a better coupling factor. This holds for alloys with 50% and 55% Fe or with 4% Co and also for Ni–Cr–Co alloys[9, 20] (see Table 16.3).

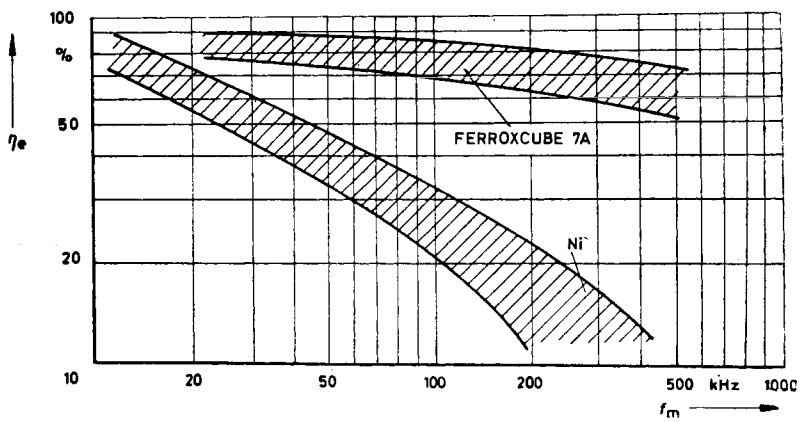



*Figure 16.6. Frequency curve of electro-acoustical efficiency for a laminated nickel transducer and a solid ferrite transducer*[8]

The Ni–Co alloy with 4·5% Co shows the highest magnetomechanical coupling factor, namely $k_m = 0{\cdot}59$. The alloy composition was so chosen that the crystal anisotropy approached zero (see equation 16.6). The Curie temperature of this material is, however, only slightly higher than for nickel. For the alloy containing 18·4% Co, $T_c$ can be raised to 570°C, but the optimum magnetomechanical coupling factor is still 0·46[9]. Further properties of these alloys are detailed in Table 16.4. The alloy showing the highest electro-acoustic efficiency contains 2·3% Cr and 1·4% Co. A possible $\eta_e$ of 0·82 was calculated[10] for a 0·15 mm sheet at a frequency of 30 kHz. The Curie temperature of this nickel alloy is 340°C and $k_m = 0{\cdot}37$.

**Table 16.4** MAGNETIC PROPERTIES OF PIEZOMAGNETIC MATERIALS[9]

| *Material* | *At remanence* | | | *Optimally polarised* | | |
|---|---|---|---|---|---|---|
| | $k'_{rem}$ | $10^{-6}\lambda_r$ (N/V s) | $\mu_{rev}$ | $k'_m$ | $10^{-6}\lambda_r$ (N/V s) | $\mu_{rev}$ |
| Nickel | 0·23 | 7·8 | 160 | 0·30 | 16·7 | 70 |
| Ni+4% Co | 0·34 | 8·3 | 250 | 0·59 | 32·3 | 130 |
| Ni+18% Co | 0·23 | 4·6 | 390 | 0·46 | 18·7 | 150 |
| 49·5% Fe, 1% W, remainder Co | 0·31 | 11·9 | 160 | 0·31 | 11·9 | 160 |
| 35% Co, 0·5% Cr, remainder Fe | 0·14 | 5·1 | 123 | 0·17 | 8·0 | 75 |

Emphasis should not be placed on independence of temperature changes for every resonator material, but for cases where a high degree of constancy of elasticity modulus is demanded several Ni–Fe alloys with around 40% Ni have been developed. Ni-Span C[13] contains, besides iron, 42·2% Ni, 5·3% Cr, 2·5% Ti, and 0·03% C. Sometimes it may also contain 0·4% Mn, Si, and Al. Saturation magnetostriction lies between $15\times10^{-6}$ and $25\times10^{-6}$. Between the temperatures −45°C and +65°C, the elastic modulus changes by only 0·1%.

An alloy called Vibralloy[14] has almost the same nickel content (43%). The broadening of the minimum of the temperature-dependence curve for the modulus of elasticity, which occurs near room temperature, is brought about by cold forming. The modulus of elasticity $E$ is relatively high: its value is 161 500 N/mm². The material is stabilised by annealing after cold deformation at 400°–500°C. In order to increase the elastic limit from 350 N/mm² to 750 N/mm² and to make the alloy less sensitive to changes in composition, it is given 9% Mo as an additive. Between −40°C and +80°C the permeability of the hard-worked alloy amounts to around 700–850$\mu_0$. The alloy called Thermelast 4009 offers a constancy of modulus of elasticity, around 177 000 N/mm², over the temperature range from −60°C to +140°C; this also is achieved by cold rolling. The material was, in fact, developed less with its resonant properties in mind than for the construction of springs[35].

### 16.6.1.2 Iron and iron alloys

Unalloyed iron has almost no application as a transducer or vibrator material. On the other hand, steel can be used in many cases in the form of a thin-walled tube, thus giving scope to its high mechanical quality factor (see Table 16.2). The magnetostriction of plain iron is too low, its conductivity too high, and its corrosion resistance insufficient. By means of certain alloying additives, the magnetostriction effect can be increased, the conductivity lowered, and a relatively high magnetomechanical coupling achieved.

Among iron alloys, those with 12–16% Al content have been particularly investigated. Technically useful alloys in this range of composition have been made under the titles Alfenol and Alfer[11, 16, 19]. As Tables 16.3 and 16.5 show, values of $k_m$ are comparable with those of nickel and Ni–Fe alloys. This holds, however, only for aligned alloys. Quenched (and unaligned) materials show a $k_m$ only half as great. The values of the modulus of elasticity $E$, the reversible permeability $\mu_{rev}$, and the magnetostriction con-

**Table 16.5** COMPARISON OF THE PROPERTIES OF VARIOUS MAGNETOSTRICTIVE MATERIALS[11]

| *Material* | $k_m$ | $10^{-11}E$ (N/m²) | $\mu_{rev}$ | $10^{-6}\lambda_r$ (N/V s) | $10^{-6}\lambda_r\mu_{rev}$ (N/V s) |
|---|---|---|---|---|---|
| Nickel | 0·312 | 2·1 | 22 | 27 | 590 |
| V-Permendur | 0·332 | 2·4 | 80 | 16·5 | 1 320 |
| 95% Ni, 4·5% Co, 0·5% Mn | 0·366 | 2·45 | 22 | 34·5 | 760 |
| 35% Ni, 65% Fe | 0·198 | 1·0 | 87·6 | 5·9 | 518 |
| 40% Ni, 60% Fe | 0·376 | 1·4 | 106·6 | 11·8 | 1 258 |
| 50% Ni, 50% Fe | 0·326 | 1·7 | 86 | 12·7 | 1 090 |
| 60% Ni, 40% Fe | 0·188 | 1·6 | 43·4 | 10·1 | 438 |
| Alfenol: | | | | | |
| 11·7% Al, 88·3% Fe (aligned) | 0·318 | 1·1 | 183 | 6·9 | 1 260 |
| 11·7% Al, 88·3% Fe (unaligned) | 0·071 | 1·26 | 68·9 | 2·7 | 183 |
| 12·5% Al, 87·5% Fe (aligned) | 0·304 | 1·7 | 104 | 10·3 | 1 070 |
| 12·5% Al, 87·5% Fe (unaligned) | 0·068 | 1·32 | 114 | 1·7 | 196 |
| $Ni_{0·973}Co_{0·027}Fe_2O_4$ | 0·221 | 1·8 | 23 | 17·4 | 390 |
| $Ni_{0·969}Co_{0·027}Fe_{0·04}Fe_2O_4$ | 0·338 | 1·7 | 24 | 25·4 | 600 |
| $Ni_{0·967}Co_{0·027}Fe_{0·06}Fe_2O_4$ | 0·378 | 1·8 | 19 | 33 | 630 |
| $Ni_{0·965}Co_{0·027}Fe_{0·08}Fe_2O_4$ | 0·258 | 1·8 | 20 | 21·8 | 430 |

stant $\lambda_r$ are taken from a larger series of experiments by Davis and Ferebee[11] and are displayed in Table 16.5 for two different alloy compositions. The high reversible permeability ($\mu_{rev} = 183$) is a noteworthy feature of the aligned alloy with 11·7% Al.

An iron alloy with some 35% Co and 0·5% Cr is that called Hiperco (see Table 16.4); it attains a maximum efficiency of 0·28 at 32 kHz. The specific electrical resistance of this alloy is 23 μΩ cm and the magnetostriction con-

stant $8{\cdot}0\times10^6$ N/V s. The optimum polarisation is around 1·5 V s/m$^2$, and the driving field is then 1·6 kA/m. The saturation flux density $B_s$ is 2·45 V s/m$^2$ and the Curie temperature 980°C[30]. Longitudinal vibrations are propagated at a speed $v$ of 5·1 km/s[4].

Higher $k_m$ values can be achieved using V-Permendur or Vacoflux 50 which contain, besides iron, 49% Co and 2% V. Like Hiperco, these alloys possess particularly high Curie temperatures and very high saturation magnetostriction (see Table 16.3). The relation between magnetostriction and polarisation is plotted for these and a few other alloys in Figure 16.5.

### 16.6.2 Ferrites

Ferrites can exhibit much the same magnetomechanical properties as the metallic alloys but without the need for lamination, since the high specific electrical resistance of the ferrites allows no eddy currents worth mentioning to flow. For this reason the efficiency, already high in its own right, is less dependent on frequency than for the metals (see Figure 16.6)[8]. Ferrites used for magnetomechanical transducers can be operated at 500°C, which is not, in general, possible with nickel and its alloys[10]. Ferrites, being ceramic bodies, are more liable to breakage than the metals, but, on the other hand, their manufacture is less costly. More than 20 years ago Mg–Zn and Co–Zn ferrites and, most of all, Ni–Zn ferrites were tested for their possible value as magnetostrictive resonators[2, 12, 27].

According to Diethelm[12], Mg–Zn and Co–Zn ferrites are unsuitable for resonators. Also, van der Burgt[4] found only small magnetomechanical coupling factors of 0·001–0·027 for Mg–Zn and Co–Zn ferrites as also for Fe–Li–Zn, Cu–Zn, and barium ferrites. On the other hand, Ni–Zn ferrites with a zinc content up to 40% proved acceptable as resonators. For pure nickel ferrite the saturation magnetostriction $\lambda_s$ is $-26\times10^{-6}$, while a $\lambda_s$ value of $-21\times10^{-6}$ is reached for the mixture ferrite $Ni_{0{\cdot}8}Zn_{0{\cdot}2}Fe_2O_4$. The values are thus not all that far off those of nickel and meet the requirements laid down on page 656 (see Table 16.6).

Sixtus[27] was able to achieve a circuit quality factor of 2000 in a toroidal core of Ni–Zn ferrite for which the temperature coefficient of resonance

**Table 16.6** MAGNETIC CONSTANTS OF NICKEL AND OF NICKEL FERRITES[12]

| | *Nickel* | *Nickel ferrite* | $Ni_{0{\cdot}8}Zn_{0{\cdot}2}Fe_2O_4$ |
|---|---|---|---|
| $\mu_i(\mu_0)$ | 110 | 12 | 32 |
| $\mu_m(\mu_0)$ | 600 | 55 | 165 |
| $J_s$ (V s/m$^2$) | 0·61 | 0·31 | 0·42 |
| $H_c$ (A/m) | 272 | 960 | 400 |
| $10^4\,a$ (m$^4$/N$^2$s$^2$) | −1 | −2·75 | −0·85 |
| $10^6\,\lambda_s$ | −32 | −26 | −21 |

**Table 16.7** STATIC AND DYNAMIC PROPERTIES OF SOME FERRITES IN RING FORM (MEAN DIAMETER ABOUT 12 mm, HEIGHT ABOUT 4 mm)[4]

| | *Composition* (%) | | | | | | | | |
|---|---|---|---|---|---|---|---|---|---|
| | | NiO | 15 | 17 | 17·5 | 18 | 25 | 32 | 40 | 50 |
| | | ZnO | 35 | 33 | 32·5 | 32 | 25 | 18 | 10 | 0 |
| | | $Fe_2O_3$ | 50 | 50 | 50 | 50 | 50 | 50 | 50 | 50 |
| | Apparent density, $d$ (g/cm³) | | 5·06 | 4·90 | 4·90 | 4·90 | 4·85 | 4·85 | 4·76 | 4·20 |
| | Conductivity, $\sigma$ (1/Ω cm) | | $<10^{-2}$ | $<10^{-2}$ | $<10^{-2}$ | $<10^{-3}$ | $<10^{-3}$ | $<10^{-3}$ | $<10^{-3}$ | $<10^{-3}$ |
| | Curie temperature, $T_c$ (°C) | | 85 | — | — | 200 | 290 | 410 | 490 | 595 |
| | Apparent saturation polarisation, $J_s$ (V s/m²) | | 0·26 | 0·33 | 0·35 | 0·37 | 0·44 | 0·47 | 0·42 | 0·26 |
| | Saturation magnetostriction, $10^6\lambda_s$ | | −2 | −4 | −4·5 | −5 | −11 | −16 | −21 | −26 |
| Radial oscillation at remanence ($f$ = 60–75 kHz) | Magnetomechanical coupling factor, $k_{rem}$ | | 0·034 | 0·067 | 0·066 | 0·073 | 0·082 | 0·093 | 0·112 | 0·08 |
| | Modulus of elasticity, $E$ ($10^{11}$ N/m²) | | 1·80 | 1·63 | 1·63 | 1·62 | 1·53 | 1·50 | 1·37 | 0·93 |
| | Mechanical quality factor in air, $Q_a$ | | 2 780 | 1 490 | 1 420 | 1 260 | 920 | 1 430 | 2 150 | 2 040 |
| | Relative reversible susceptibility, $\varkappa_r$ | | 1 210 | 735 | 600 | 491 | 139 | 85 | 35 | 18 |
| | Propagation velocity of wave, $v$ (km/s) | | 5·97 | 5·79 | 5·79 | 5·76 | 5·62 | 5·57 | 5·37 | 4·71 |
| Torsional oscillation, optimum polarisation ($f$ = 350–450 kHz, $J \simeq 0{\cdot}7J_s$) | Magnetomechanical coupling factor, $k_m$ | | 0·063 | 0·089 | 0·080 | 0·115 | 0·110 | 0·105 | 0·130 | 0·090 |
| | Shear stress constant, $G$ ($10^{11}$ N/m²) | | 0·68 | 0·63 | 0·62 | 0·62 | 0·59 | 0·58 | 0·54 | 0·36 |
| | Mechanical quality factor in air, $Q_a$ | | 1 740 | 2 000 | 1 640 | 2 450 | 3 150 | 4 250 | 5 650 | 4 450 |
| | Relative reversible susceptibility, $\varkappa_r$ | | 880 | — | 417 | 469 | 127 | 84 | 34 | 15 |
| | Propagation velocity of wave, $v$ (km/s) | | 3·67 | 3·59 | 3·57 | 3·55 | 3·49 | 3·45 | 3·37 | 2·93 |

frequency was below 20 ppm/K. Resonance frequency and the value of $Q$ can be altered by premagnetisation. The detailed change is characteristic of a given material and is bound up with the conditions of manufacture. Van der Burgt[4] gives the values of speed of propagation of compressional waves in Ni–Zn ferrites which are set out in Table 16.7. The figure mentioned in Table 16.2 thus corresponds to a mean value.

Roberts[23], who investigated various ferrites, found that the best magneto-mechanical results were obtained from a simple nickel ferrite which had been annealed at 1300°–1400°C for 1·5 h and then slowly cooled. For broad-band filters, Bache[2] used Ni–Zn ferrite to which impurities were deliberately introduced to damp the sharpness of mechanical resonance.

As Hoffmann[17] observed, the addition of magnesium ferrite to nickel ferrite brings about no improvement. With an increasing proportion of magnesium ferrite the coercivity rises, while remanence, reversible permeability, saturation magnetostriction, and electromechanical coupling factor all fall.

Van der Burgt[6] and Schweizerhof[26] found that small additions of cobalt lowered the temperature dependence of the elasticity modulus and also the magnetic losses of Ni–Zn ferrites. According to Schweizerhof[26], the temperature coefficient of resonance, between 20°C and 50°C, of a ferrite sintered in a particular way, amounted to some 6 ppm/K. Ageing of the ferrite was forestalled by temperature cycling. Quality factors up to 10000 were achieved. For the ferrite used by Bache[2] for broad-band filters in the frequency range 100–500 kHz, it seems that the temperature coefficient was below 6 ppm/K.

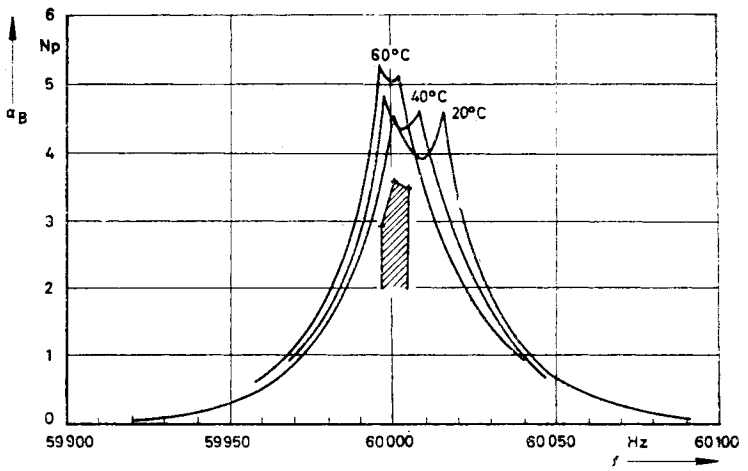



*Figure 16.7. Attenuation curve of a pilot suppressor having two ferrite vibrators*[26]

Attenuation curves for a cross-member having ferrite oscillators are given in Figure 16.7 for three temperatures; they are quoted from Schweizerhof[26]. This example was concerned with a pilot suppressor in a carrier-frequency system. Figure 16.8, after van der Burgt[6], sets out the temperature dependence

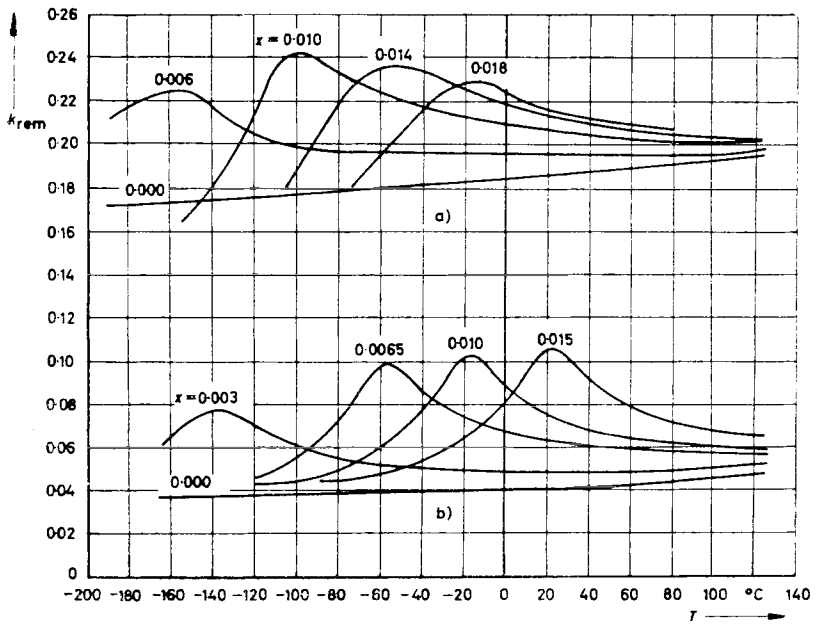



*Figure 16.8. Real part of the magnetomechanical coupling factor as a function of temperature: (a)* Ni–Co *ferrite; (b)* Li–Co *ferrite*[6]

of the magnetomechanical coupling factor at the remanence point for various nickel and lithium ferrites with cobalt additives. The two experimental series can be expressed by means of the formulae: $CoFe_2O_4[Ni_{1-x}Co_xFe_2O_4]$ and $CoFe_2O_4[(Li_{0\cdot5}Fe_{0\cdot5})_{1-x}Co_xFe_2O_4]$. The coupling factor was increased in both series by the cobalt additive. They did not, however, show a linear temperature variation but had a maximum which shifted towards higher temperatures with increasing proportions of cobalt. The lithium ferrites in no case reached the values for the nickel ferrites. The mechanical quality factor of the improved Ni–Zn–Co ferrites exceeds 2000. The temperature coefficient of the real part of the permeability is reduced by the cobalt substitution. Further, the imaginary part of the permeability also drops so that the magnetic quality factor rises.

The effect of cobalt additives on the temperature–resonance relation can be appreciated from Figure 16.9[32]. This temperature coefficient is at its lowest for a composition around $Ni_{0\cdot99}Co_{0\cdot01}Fe_2O_4$. Based on the results of this investigation, Thiele[32], using rods 38 mm long made of Ni–Zn ferrite with a cobalt additive, built a narrow-band filter. At the mean frequency of 41 770 Hz, the bandwidth was $7\pm0\cdot25$ Hz and the temperature coefficient $-$ 8 Hz/K. Coarse adjustment was achieved by grinding the ferrite core and fine adjustment by the movement of an adjustable iron dust core. The filter proved very stable with time.

It follows from the quoted investigations that the usual ferrites developed to have magnetic properties suited to the switching circuits of communications technology do not, at the same time, show optimal resonance character-

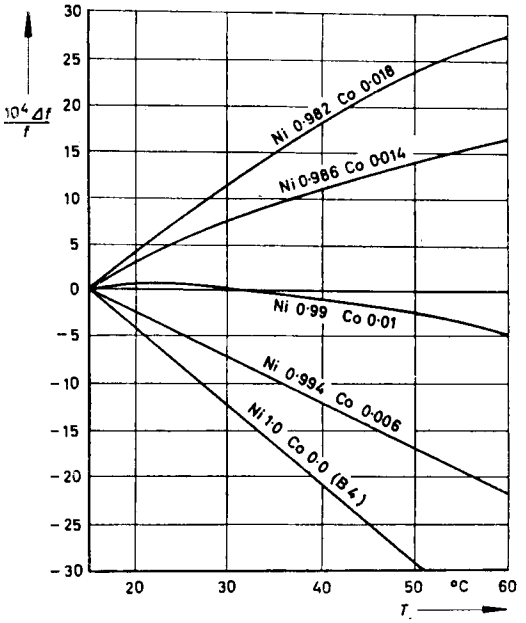



*Figure 16.9. Frequency shift of* Ni–Co *ferrites with temperature, for various compositions*[32]

istics. Thus the porosity of the ordinary Ni–Zn ferrites is so great that the saturation flux density attains only 75–92%, according to composition, of the tabulated value. Both coupling factor and acceptable mechanical loading are reduced by porosity, though this porosity can often be avoided by sintering at a higher temperature. Van der Burgt[6] was able to demonstrate that, by a small raising of the sintering temperature from 1240°C to 1270°C, the porosity of the ferrite he used was reduced to a half and this increased the coupling factor appreciably without any significant effect on the temperature coefficient.

Copper additives act as fluxes for ferrites and so a higher density, with a porosity reduction to 1–4%, can be achieved by suitable sintering[8]. Transducers made from such ferrites are characterised by a high electroacoustic efficiency $\eta_e$, which falls only slightly with frequency (see Figure 16.6).

Stuijts, Verweel, and Peloschek[29] were able to improve the density of ferrites over the hitherto known value. They reached an optimal coupling factor, $k'_m$, of 0·495 and 0·60 for linear and torsional oscillations respectively; the torsional value was 0·66 for the ferrite $Ni_{0·972}Co_{0·028}Fe_2O_4$ having a porosity below 6% and a density of 5·325 g/cm$^3$. The saturation magnetostriction $\lambda_s$ of this dense ferrite amounted to $-29\times10^{-6}$. It has already been mentioned that the temperature dependence of resonator properties of Ni–Zn ferrites can be improved by cobalt substitution, but the absolute value of $k$ can also be improved if the proportion of cobalt is somewhat increased. This is of importance in those cases where temperature changes do not weigh very heavily, for example for underwater radiators and receivers. Van der

Burgt[5], for Ni–Co ferrites in the remanence condition, achieved $k_{rem}$ values up to 0·25 and, for optimum polarisation, $k'_m$ values of 0·30.

Brockmann, Beck, and Steneck[3] achieved a coupling factor $k_m$ of 0·30, associated with a very low temperature dependence, by using a compound material of modified Ni–Zn–Co ferrites. Two layers of $(Ni_{0·90}Zn_{0·10})_{0·878}Co_{0·022}Cu_{0·1}Fe_2O_4$ were mounted on the two faces of the ferrite $(Ni_{0·90}Zn_{0·10})_{0·874}Co_{0·026}Cu_{0·1}Fe_2O_4$. The three layers of this sandwich were pressed into a single block and then annealed. Interdiffusion of the components took place only at the contact surfaces. One of the ferrites had, in itself, a maximum $k$ at 5°C and the other at 20°C (falling off steeply). The compounded material showed a $k$ which remained greater than 0·3 between 0°C and 20°C without any pronounced maximum. The individual ferrite with the 20°C maximum gave a $k_m$ value of 0·34.

The magnetic constants of a few Ni–Co ferrites are collected in Tables 16.3 and 16.5.

## REFERENCES


1. ASCHMONEIT, E.-K.: Mechanische Filter für elektrische Schwingungen (Nickel-Ber. **20** (7) (1962) 207–213).
2. BACHE, H.: A practical electromechanical filter (Marconi Rev. **22** (1959) 144–153).
3. BROCKMANN, F. G., BECK, P. W. and STENECK, W. G.: Magnetostrictive ferrites with small change in coupling coefficient from 0° to 20°C (J. Am. Cer. Soc. **46** (Apr. 1963) 167–170).
4. VAN DER BURGT, C. M.: Dynamical physical parameters of the magnetostrictive excitation of extensional and torsional vibrations in ferrites (Phil. Res. Rep. **8** (1953) 91–132).
5. VAN DER BURGT, C. M.: Ferroxcube-Werkstoffe für piezomagnetische Schwinger (Phil. T. Rdsch. **18** (1957) 277–290).
6. VAN DER BURGT, C. M.: Ferrites for magnetic and piezomagnetic filter elements with temperature-independent permeability and elasticity (Proc. IEE **104 B** (1957) 550–557).
7. VAN DER BURGT, C. M.: Ferroxcube 7A1 und 7A2, neue piezomagnetische Werkstoffe für Ultraschallschwinger höherer Leistung (VALVO-Ber. **5** (1) (Apr. 1959) 1–33).
8. VAN DER BURGT, C. M.: Piezomagnetic ferrites (Electron. Techn. **37** (Sept. 1960) 330–341).

8a VAN DER BURGT, C. M. and STUIJTS, A. L.: Developments in ferrite ceramics with strong piezomagnetic coupling (Ultrason. **1** (1963) 199–210).

9. CLARK, C. A.: The dynamic magnetostriction of nickel–cobalt-alloys (Brit. J. A. P. **7** (1956) 355–360).
10. CLARK, C. A.: Improved nickel-base alloys for magnetostrictive transducers (J. Acoust. Soc. Amer. **33** (1961) 930–933; Nickel-Ber. **20** (1962) 98–99).
11. DAVIS, C. M. and FEREBEE, S. F.: Effect of composition and processing on the activity of some magnetostrictive materials (J. A. P. **30** (4) (1959) 113S–115S).
12. DIETHELM, C. W.: Ferrite als magnetostriktive Resonatoren und deren Anwendung als Elemente elektrischer Filter (T. Mitt. PTT **29** (1951) 281–297).
13. ENGELHARD INDUSTRIES INC., UNION, N. J.: Data Sheet, Wilco Ni-Span C Constant Modulus alloy.

13a ENZ, U.: Die Erzeugung von Ultraschall mit Ferriten (T. Mitt. PTT **33** (1955) 209–212).

14. FINE, M. E.: Vibralloy—a new ferromagnetic alloy (Bell Lab. Rec. **30** (1952) 345–348).

15. HARVEY, R. F.: Abschrecken mit Ultraschall, ein neues Anwendungsgebiet für Kobaltlegierungen (Cobalt (15) (June 1962) 18–19).
16. HENKEL, O.: Eisen-Aluminium-Legierungen für magnetostriktive Wandler (Hochfrequenzt. u. Elektroak. **71** (1962) 161–166).
17. HOFFMANN, P. O.: Magnetic and magnetostrictive properties of magnesium–nickel ferrites (J. Am. Cer. Soc. **40** (7) (1957) 250–252).
18. INTERN. NICKEL COMPANY (MOND) LTD.: Nickel-containing magnetic Materials. Publ. 2144 (May 1962).
19. MASUMOTO, H.: Dynamical characteristics of magnetostriction alloy 'Alfer' (Sci. Rep. Res. Inst. Tohoku Univ. **2** (1950) 413–419).
20. NISHINA, T.: (Jap. Nickel Rev. **7** (1939) 45–62).
21. PIERCE, G. W.: Magnetostriction oscillators (Proc. IRE **17** (1929) 42–88).
22. POPPER, P.: The magnetostriction ferrites; in Soft Magnetic Materials for Telecommunications (ed. Richards and Lynch), London (1953) 322–332.
23. ROBERTS, W. VAN B.: Some applications of permanently magnetized ferrite magnetostrictive resonators (RCA-Rev. **14** (Mar. 1953) 3–16).
24. ROBERTS, W. VAN B. and BURNS, L. L.: Mechanical filters for radio frequencies (RCA-Rev. **10** (1) (Mar. 1949) 348–365).
25. SCARROTT, G. G. and NAYLOR, R.: Wire type acoustic delay lines for digital storage (Proc. IEE **103 B** (1956) 497–508, 535–536).
26. SCHWEIZERHOF, S.: Über Ferrite für magnetostriktive Schwinger in Filterkreisen (NTZ **11** (4) (1958) 179–185).
27. SIXTUS, K.: Über Ferritschwinger (Frequenz **5** (11/12) (1951) 335–339).
28. STRUSZYNSKI, W.: A theoretical analysis of torsional electro-mechanical filters (Marconi Rev. **22** (1959) 119–143).
29. STUIJTS, A. L., VERWEEL, J. and PELOSCHEK, H. P.: Dense ferrites and their applications (Proc. Intermag. Conf. (1963) 1–2).
30. SUSSMAN, H. and EHRLICH, S. L.: Evaluation of the magnetostrictive properties of Hiperco (J. Acoust. Soc. Am. **22** (1950) 499–506).
31. TETZNER, K.: Amateur-Bandempfänger Collins 75 A–4 (Funkschau **31** (1959) 66–67).
32. THIELE, A.: Narrow-band magnetostrictive filters (Electron. & Radio Eng. **35** (11) (Nov. 1958) 402–411).
33. VACUUMSCHMELZE GMBH, HANAU: Data Sheet M 013.
34. VALVO: Handbook, Einzelteile II (1964).
35. VACUUMSCHMELZE GMBH, HANAU: Data Sheet F 001 (June 1957).

# 17

# Materials for magnetic shielding

In the field of telecommunications, the designer is often faced with the need to protect circuits and components against the effect of nearby electrical and magnetic fields. The problem has two aspects: on the one hand it is sought to prevent strong field-radiators like transformers or permanent magnets from affecting their surroundings and, on the other hand, sensitive circuits such as telephone lines or filter coils must be protected against stray fields.

## 17.1 STRAY-FIELD EFFECTS

It is particularly in the case where apparatus consists of tightly packed components, or assemblies, that screening presents an important problem. Only a few examples will be given here.

The information stored on a magnetic tape can be ruined, or even completely destroyed, by the effect of a strong field. The tapes must therefore be stored in shielded containers[6]. *Relays* may fall off under an external field, or they may stick or their action be delayed.

If coils and transformers are mounted in the neighbourhood of powerful magnets, their performance may be affected, for example the frequency of a resonant circuit may be shifted. Vacuum tubes are very sensitive to the influence of stray fields, particularly when the electron path is long.

External fields have a defocusing effect on cathode-ray tubes. Asymmetries are produced in travelling-wave amplifiers, possibly leading to loss of power and to frequency shifts. Travelling-wave amplifier tubes with periodic arrangements of magnets are less susceptible.

The magnitude of the stray fields emitted by the magnets of microwave tubes depends on the shape of the magnets and the arrangement of the air-gaps. The designer must form as exact a picture as possible of the magnitude and distribution of the strays if he is to achieve effective shielding.

The conjunction of magnets and isolators is critical in waveguide systems. Frequently the interaction of two circuits can be reduced by their orientation so that a less far-reaching shielding is required. Again, the disposition of

loudspeaker magnets in radio or television apparatus can have a pronounced influence on the operation of the various valves, and particularly on the picture tube.

It goes without saying that measuring instruments and magnetic heads have to be protected against disturbing fields.

## 17.2 OPERATION OF A SHIELD

High-frequency alternating fields can easily be confined by the use of copper or aluminium screens. The eddy currents produced by the alternating field in the surface of a sheet are in such a sense that they create an opposing magnetic field and so prevent a deeper penetration into the lamina (skin effect).

The depth $d$ of penetration of an alternating field into a metallic lamina or a ferrite body is inversely proportional to the square root of the electrical conductance $\sigma$, the permeability $\mu$, and the frequency, $f$. Therefore

$$d \triangleq \frac{1}{\sqrt{(\sigma \mu f)}}$$

At low frequencies, therefore, the magnetic penetration can be considerable and so the sheets have to be correspondingly thicker for a given shielding effect. This means that the shielding cans become more and more massive and expensive. The use of magnetic shielding material becomes more effective the higher the permeability.

The shielding effect of a magnetic material depends not only on skin effect but to some extent on the induction of an opposing field in the magnetised material. Shielding against a static field ($f = 0$) is possible only on the basis of this second effect. The direct field penetrates into the interior of a magnetically shielded region. Magnetic lines of force produced in the shielding material are closed outside the body and directed oppositely to the impressed field. In this way a region is produced around the ferromagnetic substance which is empty of lines of force. Thus we get the well-known picture (see Figure 17.1) which seems to suggest that passing lines of force are sucked into the body.

There are always losses in a magnetic shield and these must be supplied by the exciting field; they are greatest in regions of high field intensity. Thus a shield which shows equal field intensities at all points is the best. A shielding can may therefore be brought nearer to those parts of the shielded component where the field intensity is low and must be more widely spaced where the stray field is stronger. The losses introduced into a coil by shielding are greater the greater the stray flux of the coil and the smaller the separation from the source of disturbance. The shielding case of a toroidal coil can be brought quite close to the winding without causing any significant loss. Moreover, a shielding can increases the self-capacitance of a coil, and the effect is more marked the nearer the wall of the can comes to the coil. The increase in capacity causes a drop in the quality factor and alters the resonance curve of the circuit.

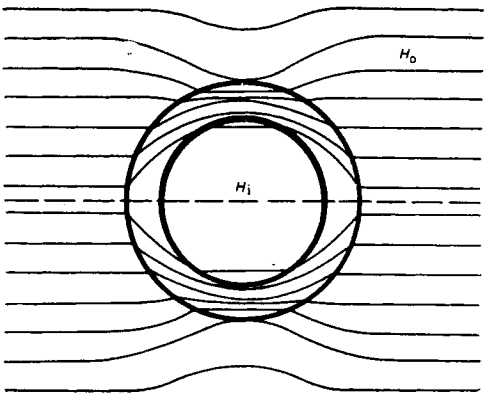



*Figure 17.1. Shielding action of a magnetic ring in a homogeneous magnetic field*[12]

At high frequencies it is fairly common practice to substitute for the closed shielding can a wire cage or an arrangement of parallel bars or wires. The manifold problems of shielding, from the point of view of physics, are treated by Kaden[5, 5a], Mager[6a, 13], Moeller[8], and others.

## 17.3 THE SHIELDING FACTOR

In order to have a rough numerical criterion whereby the effectiveness of a shielding arrangement may be judged, it is convenient to introduce a shielding factor $f_s$. It is defined as the ratio of the external field $H_o$ to the internal field $H_i$ of a magnetisable can of specified thickness and at a given frequency:

$$f_s = \frac{H_o}{H_i}$$

Figure 17.2 gives an example[12]. An M42 coil was mounted without a core in a shielding can 53 mm in diameter, 56 mm high, and having a wall-thickness of 1 mm. The can was made, successively, from four different materials. If $f_s$ be measured as a function of $H_o$ at 50 Hz, then a curve is obtained which rises at first and then passes through a maximum and falls again steeply. It is seen that the maxima of the materials Permenorm 5000 H2 and Trafoperm N3 occurred at higher intensities than for Mumetal and M1040: the highest ratio $H_o/H_i$ was found for M1040, then comes Mumetal, Permenorm 5000 H2, and lastly Trafoperm N3. The rank order remains unchanged if the test coil is fitted with a core of Mumetal laminations. The absolute value of $f_s$ falls to half or less, as shown by the broken lines in Figure 17.2.

The shielding factor for low intensities can be estimated. We have

$$f_s = \frac{4}{3}\left(\frac{d}{D}\right)\frac{\mu}{\mu_0}$$

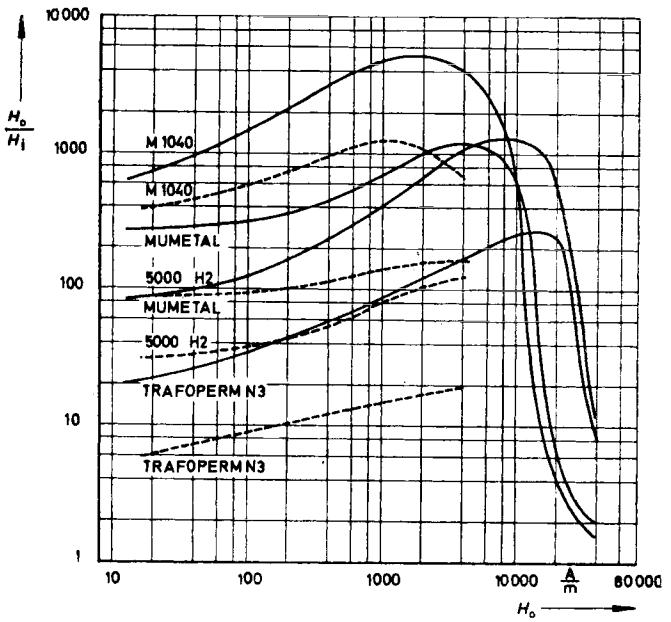



*Figure 17.2. Shielding factor $H_0/H_1$ as a function of external field strength $H_0$ ($f = 50$ Hz)*[12]

**Table 17.1** COMMERCIALLY COMMON SHIELDING MATERIALS

| *Material* | $\mu_5$ ($\mu_0$) | $f_s$ | *Reference* |
|---|---|---|---|
| M1040 | 30 000 | 720 | |
| Vacoperm 100 | 40 000 | 880 | |
| Mumetal | 25 000 | 500–630 | 12, 13, 14 |
| Permenorm 5000 H | 5 000 | 85 | |
| Permenorm 3601 K2 | 2 000 | 50 | |
| Hyperm 900 | 80 000 | | |
| Hyperm 800 | 65 000 | | 2 |
| Hyperm 766 | 35 000 | | |
| Hyperm 36 | 2 000 | | |
| Permalloy C | 25 000–50 000 | | |
| Permalloy B | 5 000 | | 10a |
| Cryoperm 10 | 70 000 | | 14 |

in which $d$ is the sheet thickness, $D$ the mean diameter of the can or housing in the field direction, and $\mu$ the permeability[13]. Representative values of $f_s$, applicable to the above-mentioned can, are given for a few materials in Table 17.1[12]. A magnetic shield acts on a coil to reduce its inductance $L_1$. The magnitude of the drop can be calculated if the coupling $k$ between coil and can is known. The resulting inductance $L$, according to Ulbricht[11], is

$$L = L_1(1-k^2)$$

The factor $k$ can be calculated roughly from the following can dimensions: $D_o$ = outer diameter, $D_i$ = inner diameter, $h$ = external height; and $R$ = radius to the middle of the upper end and $r$ = radius to the middle of the lower end of the coil in its can, both measured from one edge of the seating of the can. Then

$$k^2 \triangleq \frac{D_i^2(R-r)}{D_o^2 h}$$

For example, if $D_i = 25$ mm, $D_o = 40$ mm, $r = 25$ mm, $R = 60$ mm, and $h = 70$ mm, then $k \triangleq 0{\cdot}44$ and $L \triangleq 0{\cdot}8L_1$.

## 17.4 MAGNETIC-SHIELD MATERIALS

It is clear from the foregoing paragraph that a magnetic shield is more effective the higher the permeability at the appropriate field strength. Using a carefully constructed shielding can made of Mumetal, Randall[9] observed a field-intensity reduction in the ratio 1 : 1000 and a noise attenuation of 40–50 dB. Mumetal is some 10–20 times as effective as ordinary iron. For low and medium fields, high-permeability materials of classes E3 and E4 (to DIN 41 301) are used (see Table 13.3). High strays can be contained by 'low' alloys of Fe–Ni (classes F3 and D3). In many cases, cost has to be considered, and this is greatest for E4 types. It is therefore often possible to manage with less richly alloyed shielding materials such as Permenorm 5000 H, Hyperm 36, Hyperm 50, or Permalloy B. Some commercial shielding materials are set out in Table 17.1. Some common shapes used for coils and for cathode-ray tubes are shown in Figure 17.3 (see plate section)[10].

For use at low temperatures, for example at the temperature of liquid helium (4·4 K) or of vaporising nitrogen (77·5 K), shielding materials developed for ordinary ambient temperatures do not as a rule offer optimum solutions. Thus, if Ultraperm 10 is cooled from 20°C to −195·7°C, its initial permeability falls from 100 000$\mu_0$ to 10 000$\mu_0$, while over the same temperature interval the coercivity of Ultraperm Z increases from 1 A/m to 2 A/m. Special low-temperature materials have therefore been developed and sold commercially under the name Cryoperm[14]. Thus the initial permeability of Cryoperm 10 amounts to 70 000$\mu_0$ at 4·4–77·5 K and the maximum permeability in the same range is 250 000$\mu_0$.

Figure 17.4 gives an interesting example[3] of how shielding losses can be reduced with the aid of ferrites. If a 450 kHz transformer having an iron dust core is mounted in a shielding can, the quality factor falls by 25%. However,

if two small ferrite rods are placed near the coil, then the quality factor is reduced only 10% by the shielding can. The example demonstrates that many shielding problems can be eased by proper design precautions. This becomes particularly clear if one considers the emission of flux from low-frequency transformers. M and EI cores have the highest stray losses while UI and P cores (Philbert cores) give the better ratios[1]. The core joins should lie as far as possible within the coils and should be well overlapped.

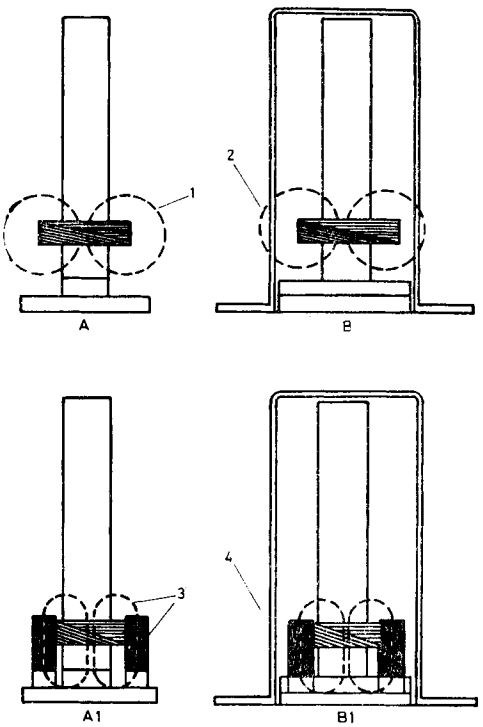



*Figure 17.4. Reduction of shielding loss by use of ferrites: 1, alternating magnetic field; 2, flux shown cutting the can material to produce eddy currents; 3, flux path through ferrite rods; 4, reduction of linked flux compared with B*[3]

Many shielding problems, for example those relating to vacuum tubes and cables, can be solved with advantage by wrapping them, lengthwise, with layers of different permeabilities[4]. Often a single layer of strip or sheet of high-permeability material will suffice, but sometimes several layers are more satisfactory.

Shielding foils are produced from various alloys in thicknesses from 50 μm to 150 μm. By the use of foils, shielding problems can often be solved conveniently by a purely empirical approach. The component to be protected is merely wrapped in as many layers as may be sufficient to secure the desired degree of shielding[7].

## REFERENCES


1. BERGTOLD, F.: Die Abschirmung niederfrequenter magnetischer Ausstreuungen (Funkschau (4) (1956) 135–137).
2. FRIEDR. KRUPP, WIDIA-FABRIK, ESSEN: D. 546 Hyperm, Magnetisch weiche Werkstoffe.
3. JONES, V. A. and CAMPBELL, G.: Some current and future applications for ferrite components in radio and television receivers (Proc. IEE **104 B** (1957) 526–533).
4. JORGENSON, C. M.: Using magnetic shielding materials (El. Des. News **8** (3) (1963) 136–137).
5. KADEN, H.: Die elektromagnetische Schirmung in der Fernmelde- und Hochfrequenztechnik. Springer-Verlag (1950).

5a KADEN, H.: Die Ausbreitung elektrischer und magnetischer Wechselfelder in offenen Abschirmrohren (Frequenz **24** (1970) 27–32).

6. LONGMIRE, D. E.: Magnetic shielding practice in electronic packaging (Electron. Tech. **71** (Jan. 1963) 63–66).

6a MAGER, A. J.: Magnetic shields (IEEE Trans. **Mag-6** (Mar. 1970) 67–75).

7. MAGNETIC SHIELD DIVISION: Netic and Co-Netic Magnetic Shielding Manual.
8. MOELLER, F.: Die elektromagnetische Abschirmung (Arch. El. Üb. **2** (1948) 328–333).
9. RANDALL, W. F.: Nickel–iron alloys of high permeability, with special reference to mumetal (J. IEE **80** (1937) 647–667).
10. STANDARD TELEPHONES & CABLES LTD., LONDON: Technical Data sheet MM 105 Ed 1/1.

10a STANDARD TELEPHONES & CABLES LTD. LONDON: (ITT), Permalloy (1968).

11. ULBRICHT, H.: Abschirmung von Spulen (Funk-Technik (18) (1949) 553–554).
12. VACUUMSCHMELZE GMBH, HANAU: Data Sheet M 007 (Nov. 1961).
13. VACUUMSCHMELZE GMBH, HANAU: Magnetische Abschirmungen. FS-M9 (1969).
14. VACUUMSCHMELZE GMBH, HANAU: Data Sheet MO 37 (Apr. 1969 and Aug. 1970).

# 18

# Materials for temperature compensation

## 18.1 PROBLEM AND PRINCIPLES

Among the means employed to reduce the temperature dependence of a magnetic circuit may be considered temperature-compensation methods. They are applied to measuring instruments, relays, and electricity meters, for example.

The principle is as follows. To the main flux of a permanent magnet is added a magnetic shunt whose flux falls more sharply than that of the main magnet as the temperature rises (see Figure 18.1). By suitably dimensioning

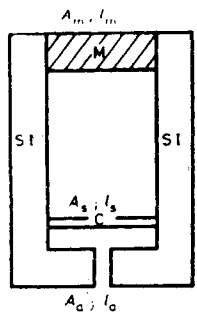



*Figure 18.1. Disposition of compensation material C in a barium ferrite device: M, barium ferrite magnet; SI, soft iron pole-shoe; $A_m$, $A_s$, and $A_a$ are the cross-sections of the magnet, the shunt, and the air-gap, whose corresponding lengths are $l_m$, $l_s$ and $l_a$[3].*

the shunt it is possible to achieve temperature independence for the main flux within certain limits. The correct proportioning of the shunt involves its cross-section and the temperature characteristic of the magnetic material used, i.e. $B = f(T)$.

One possible way of, for example, regulating temperature effects or performing switching operations by means of ferrites is as follows. An oscillatory circuit carries a coil connected between cathode and grid. If the inductance is high, the circuit does not oscillate, but, if the coil carries a ferrite core which becomes heated, the inductance falls until the coil begins to oscillate. By adding series inductance to the coil, a suitable working point may be established. By this method temperature variations of less than 0·01°C can be dealt with[10].

## 18.2 MATERIALS

Temperature compensation is usually confined to the range from −20°C to 100°C. Since magnetic changes are always more marked in the neighbourhood of the Curie temperature (see Figure 3.3), compensation materials are chosen with Curie temperatures lying between 40°C and 120°C. It is also required of the material that the temperature coefficient of flux density should be reasonably linear and, further, that the temperature-controlled changes in magnetisation are reversible.

### 18.2.1 Metallic compensation materials

The number of alloys with low Curie temperatures is very great[4], since even small additions of non-magnetic elements to iron or nickel lower the Curie temperature. In practice, however, importance attaches only to nickel alloys with iron or copper additives. Stäblein[7] first drew attention to Ni–Fe alloys with some 30% Ni (see Figure 7.4). By slight changes of composition, $\mu = f(T)$ curves can be obtained which run almost parallel to each other as can be seen in Figure 18.2[8]. On account of the rather flat shape of the curves near $B = 0$, the Curie temperatures are generally defined by a linear

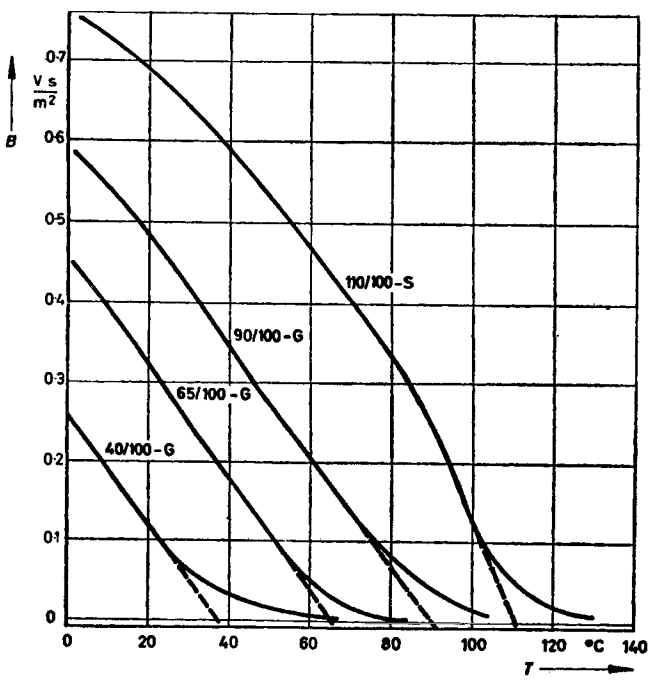



*Figure 18.2. Curves* $B = f(T)$ *for* Ni–Fe *alloys commonly used for temperature compensation*[8]

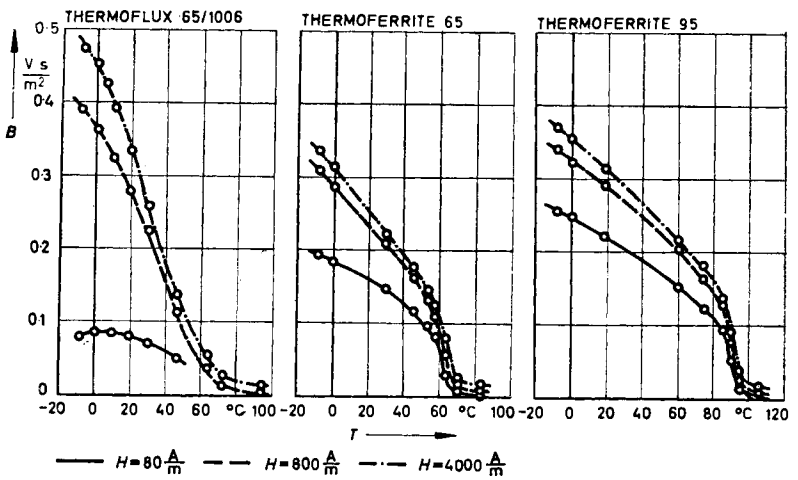



*Figure 18.3. Curves $B = f(T)$ for three compensation materials, with magnetic field strength as parameter*[3]

extrapolation (shown broken). The slope of the curves is affected by the composition but is also dependent on field strength (see Figure 18.3). The curves are less steep at low than at high intensities, but at higher field strengths the linearity is, in general, more extended than at low. The flux-density values increase with field strength at all temperatures[7].

The alloy with some 30% Ni is in general used under many trade names, such as Thermoflux, Thermoperm, Mutemp, Compensator Alloy, Variaperm, Shunt Steel, N.M.H.G., and R 2799 alloy[4, 7a]. Because the composition is near the limit of a two-phase range, its reversibility presents some difficulty. The composition has to be very accurately maintained. Even a change in nickel content of 0·25% can lead to a 10°C change in Curie temperature.

Other substances having similar properties are Fe–Ni–Mo, Fe–Ni–Cr, and Ni–Cu alloys (Figure 18.4). Chrome and molybdenum additives lower the

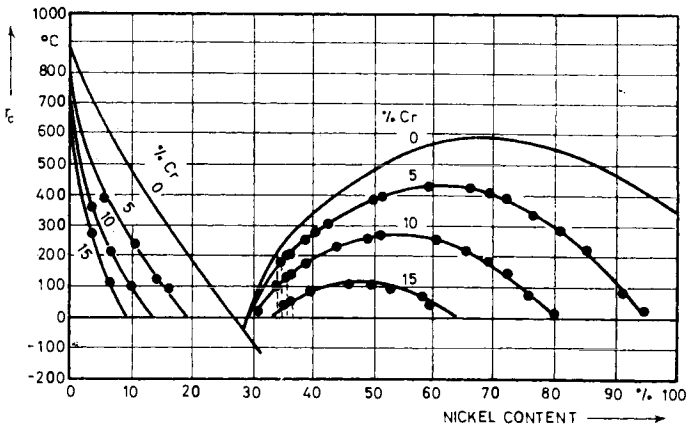



*Figure 18.4. Curie temperatures of* Ni–Fe *and* Ni–Fe–Cr *alloys*[1]

Curie temperature and, at the same time, reduce the sensitivity of the alloy to small variations in nickel content[1]. Among the Ni–Cu alloys, compositions of 88% Ni, 9·5% Cu, 2·2% Fe and 66·5% Ni, 30% Cu, 2·2% Fe have become known under the names Calmaloy and Thermalloy[5]. The Ni–Cu alloys exhibit a lower temperature sensitivity than the Ni–Fe alloys (Figure 18.5) but are fully reversible.

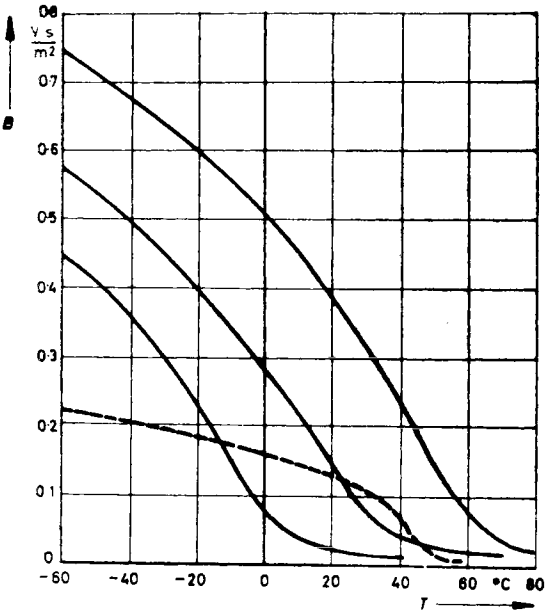



*Figure 18.5. Typical characteristics at 8* kA/m *for* Fe–Ni *alloys (solid line) and* Ni–Cu *alloys (broken line)*

Vial[9], among others, reported on the range of compensation attainable and on ways of checking temperature coefficients. According to Fahlenbrach[2, 6], the accuracy of compensation can be increased by the use of two compensation strips having different Curie temperatures or by deliberately heterogeneous sintering of a Ni–Fe alloy of low Curie temperature. The alloys are made and used in the form of thin strips 1–4 mm thick or as flat sections.

### 18.2.2 Ferrites

Haarmann[3] was able to show that with ferrites, just as with alloys, temperature compensation of permanent magnetic circuits is possible. As Figure 18.3 demonstrates, the temperature dependence of flux density for the material called Thermoferrite shows tendencies very similar to those of comparable alloys. The flux density–temperature curve is traversed reversibly, so that, even with frequent switching, the switching temperature does not change.

In order to compensate the changes of flux density with temperature in a magnet, using a ferrite shunt, the flux density of the compensation material

must fall linearly with rising temperature. If the characteristic of the compensation material is curved, the flux density in the air-gap of the magnet follows a more or less curved plot.

Haarmann[3] found that the $B = f(T)$ curves for magnet and compensator must run parallel to each other. The slope of the curve for the compensation material can be so adjusted, by changes in cross-section, that the curves are, in fact, made to run parallel. The flux density in the air-gap itself depends on the dimensioning of the shunt. A large density is found in the gap if the shunt is long and of small cross-section.

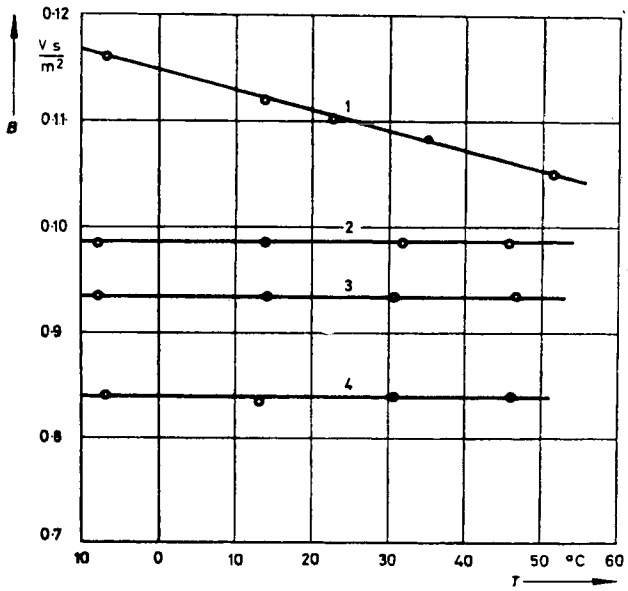



*Figure 18.6. Flux density as a function of temperature for the barium ferrite system of Figure 18.1 with and without compensation: 1, uncompensated; 2, Thermoflux 65/100G ($A_s = 18$); 3, Thermoferrite 65 ($A_s = 33{\cdot}7$); 4, Thermoferrite 95 ($A_s = 45$)*[3]

Figure 18.6 shows an example of compensation. A barium ferrite system as at C in Figure 18.1 was compensated by means of three materials, shown in Figure 18.3. Each of them gave constant values of flux density between $-10°C$ and $+50°C$ though at different heights. The cross-sections $A_s$ of the shunt are given in each case in brackets (see caption).

If $m = \Delta B/\Delta T$ and $m_s = (A_m/A_s)m$, where $A_m$ and $A_s$ represent the cross-sections of magnet and shunt respectively, then the optimum value of $A_s$ is given by

$$A_s = \frac{m}{m_s}\left(\frac{l_s}{l_a}\right)A_m$$

where $l_a$ is the length of air-gap and $l_s$ is the length of shunt. According to Haarmann[3], the flux density $B_a$ in the air-gap is then given by

$$B_a = B_m - \frac{A_s l_s}{A_a l_s} B_s$$

## REFERENCES


1. CHEVENARD, P.: Les alliages à hautes teneurs en nickel et en chrome (Rev. Metallurg. **25** (1928) 14–34).
2. FAHLENBRACH, H.: Diskussionsbemerkung (Ber. Arb. Ferrom. (1959). Düsseldorf (1960) 270).
3. HAARMANN, M.: Probleme der Temperaturkompensation von Dauermagnetsystemen (DEW-Techn. Ber. **2** (4) (1962) 159–166).
4. HEDDLE, T. A.: On the temperature sensitivity of special magnetic materials (Brit. J. A. P. **4** (6) (June 1953) 161–166).
5. KINNARD, I. F. and FAUS, H. T.: Self-compensating temperature indicator (Trans. AIEE **49** (1930) 949–951).
6. SCHRADER, H. and FAHLENBRACH, H.: Pulvermetallurgie (Z. VDI **91** (19) (1949) 485–492).
7. STÄBLEIN, F.: Thermoperm, ein Werkstoff mit temperaturveränderlicher Magnetisierbarkeit (T. Mitt. Krupp **2** (1934) 127–128).

7a TELCON METALS LTD., CRAWLEY: Data sheet, Properties and Applications of Telcon metals, 5th edn.

8. VACUUMSCHMELZE GMBH, HANAU: Thermoflux. Data Sheet M 015 (Mar. 1962).
9. VIAL, H.: Die Verwendung und Prüfung ferromagnetischer Legierungen mit niedrigem Curiepunkt zur Kompensation des Temperaturfehlers von Messinstrumenten (Ber. Arb. Ferrom. (1959). Düsseldorf (1960) 267–270).
10. WILSON, V. C.: Applications of ferrites (Proc. Conf. Magnetism Magn. Mat. (1955) 278–285).

# 19

# Tables

## 19.1 TABLES OF MATERIALS

Tables 19.1–19.8 should offer the reader a rough guide to the magnetic materials available today on the market. It is not here intended to offer a comparative assessment of the various products. This is not possible on three counts: first, the list is not exhaustive; secondly, the data quoted by the manufacturers are presented from various viewpoints and are quite often tailored to meet the special needs of their customers; and thirdly, not all the parameters which bear on the choice of a material are taken into account. Supplementary details should always be sought from the supplier.

For metallic materials the composition is always given in percentage by weight; oxide materials are more usually quoted in mole percentage.

### 19.1.1 Permanent-magnet materials

Standardised materials for permanent magnets, to DIN 17 410, are set out in Table 9.7. Manufacturers often use code markings, some of which are collected together in Table 19.1. The table also includes, at the end, some non-standardised AlNiCo and barium ferrite materials to make the list more complete. In the tables which follow, certain other non-standardised magnet materials are listed.

The following groups of materials are classified in accordance with Table 9.6:

1. *Martensitic steels.* These are largely obsolete in Germany, but are still in production in other countries (see Table 19.4).
2. *Precipitation alloys.* Among these alloys, varieties of AlNiCo take pride of place. Composition and properties frequently depart from the data of the DIN series. Different properties are to be found, according to individual supplier, even under a single code designation. Table 19.5 gives nominal values for French, British, Italian, and Japanese Fe–Al–Ni–(Co) alloys. For German examples see Tables 19.1 and 19.2 in conjunction with Table 9.7.

Particular types of material are often divided into subgroups. For example, among the columnar species of the Columax type, certain less well-oriented varieties are included under the designations Alcomax IISC, Alcomax IIISC, and Alcomax IVSD; these can be more economically produced than the fully aligned types[90]. Table 19.6 shows some of the permanent-magnet materials offered on the American market under the heading 'Columax'.

The distinguishing features of Alnico types as offered in the USA are broadly as follows:

*Alnico I* is a development of Alnico III in which some 5% Ni is replaced by cobalt. The magnetic properties vary only marginally from those of Alnico III. Alnico I responds better to heat treatment on account of its higher cobalt content and is mostly used for magnets of considerable size.

*Alnico II* contains more cobalt and, in addition, more copper, so the cost of magnets made from it is somewhat higher than for magnets of Alnico I, Alnico III, and Alnico IV. Alnico II has the highest $(BH)_{max}$ value of all isotropic Alnicos.

*Alnico III* is the original 'Alnico' alloy. However, it now contains no cobalt and is used chiefly for small cheap magnets. Alnico I and Alnico III have the lowest densities of the series.

*Alnico IV* differs from Alnico I in having 28% Ni content in place of 20%. It has a higher coercivity than types I–III, so it is particularly useful for short magnets.

*Alnico V* is anisotropic and offers the highest $(BH)_{max}$ value of all the Alnico alloys, namely up to 56 mW s/cm$^3$.

*Alnico VI* arose out of Alnico V in that 1% Ti was added to increase the coercivity. However, since the remanence is thereby reduced, the $(BH)_{max}$ value is less than for Alnico V.

*Alnico VII* has a still higher titanium content; the alloy achieves very high coercivities, exceeding 80 kA/m.

*Alnico VIII and Alnico XII* are also characterised by high coercivity. By reason of the high cobalt and titanium content, Alnico XII is very brittle and difficult to produce[30].

Besides the Alnicos, certain other precipitation alloys are in use: some of these are set out in Table 19.7.

3. *Cold-worked permanent magnets.* The best-known types of non-German manufacture are given in Table 19.8; the German types are contained in Table 19.2.
4. *Superstructure alloys.* These are to be found in Tables 19.2 and 19.9.
5. *Dust magnets.* Some important magnet materials now available on the market, mostly of American origin, are listed in Table 19.10.
6. *Ceramic magnets.* Ferrite magnets are listed in Tables 19.2 and 19.11.

**Table 19.1** SUPPLIERS' DESIGNATIONS FOR AlNi, AlNiCo, AND BARIUM FERRITE MAGNETS CORRESPONDING TO DIN 17 410 (SEE ALSO TABLE 9.7)

| *Abbreviated name according to DIN specifications* | *Bosch* | *Böhler* | *DEW* | *Krupp* | *Magnetfabrik Bonn* | *Vacuumschmelze (SAG)* | *Valvo* |
|---|---|---|---|---|---|---|---|
| AlNi 120 | Sl 12 | Permanit 120 | Oerstit 120 | Koerzit 120 | Alni 120 | AlNi 120 | Reco 120 |
| AlNiCo 160 | Sl 17 | Permanit 160 | Oerstit 160 | Koerzit 160 | Alnico 160 | AlNiCo 160 | Reco 160 |
| AlNiCo 190 | Sl 19 | Permanit 190 | Oerstit 190 | Koerzit 190 | Alnico 190 | AlNiCo 190 | |
| AlNiCo 220 | | Permanit 220 | Oerstit 260 | Koerzit 260 | Alnico 260 | AlNiCo 250 | |
| AlNiCo 350 | | Permanit 350 | | | Alnico 350 | AlNiCo 350 | Ticonal 360 |
| AlNiCo 400 | Sl 18 | Permanit 400 | Oerstit 450 | Koerzit 400 | Alnico 400 | AlNiCo 400 | |
| AlNiCo 500 | Sl 18 | Permanit 500 | Oerstit 500 | Koerzit 500 | Alnico 500 | AlNiCo 500 | Ticonal 500 |
| Ba-Ferrite 100 | Barium ferrit 100 | | Oxit 100 | Koerox 100 | Ox 100 | (DB 1) | FXD 100 |
| Ba-Ferrite 300 | | | Oxit 300 | Koerox 300 | Ox 300 | | FXD 300 |
| *Non-standard varieties (see also Table 19.2)* | | Permanit 600 | Oerstit 700<br>Oxit 150<br>Oxit 330<br>Oxit 360 | Koerzit 450<br>Koerzit 700<br>Koerox 330<br>Koerox 360 | Alni 90<br>Alnico 300<br>Alnico 580<br>Alnico 700<br>Ox 330<br>Ox 360<br>Ox 400 | AlNiCo 450<br>AlNiCo 600<br>AlNiCo 700<br>AlNiCo 800<br>(DS 1)<br>(DS 2) | Reco 140<br>Ticonal 450<br>Ticonal 750<br>FXD 280<br>FXD 330<br>FXD 360 |
| *Reference* | 99 | 37 | 23 | 33 | 66 | 101,123b | 133 |

**Table 19.2** GERMAN PERMANENT-MAGNET MATERIALS (OTHER THAN THOSE LISTED IN TABLE 19.1)

| *Material group* | *Abbreviated name* | *Composition (remainder iron)* (Me = Ba, Sr, Pb) | $d$ (g/cm³) | $(BH)_{max}$ (mW s/cm³) | $B_r$ (V s/m²) | ${}_BH_c$ (kA/m) | $\mu_p$ ($\mu_0$) | $T_c$ (°C) | *Reference* |
|---|---|---|---|---|---|---|---|---|---|
| Precipitation alloys | Alni 90 | 11% Al, 21% Ni | 6·8 | 7·2 | 0·75 | 20 | 7 | | 66 |
| | Alnico 300 | 10% Al, 18% Ni, 20% Co, 4% Cu | 7·1 | 21·6 | 0·88 | 56·8 | 4 | | 66 |
| | Alnico 580 | 8% Al, 15% Ni, 24% Co, 3% Cu | 7·2 | 41·6 | 1·20 | 54·4 | 5 | | 66 |
| | AlNiCo 450 | 8% Al, 14% Ni, 38% Co, 3% Cu, 6% Ti | 7·2 | 33·5 | 0·86–0·88 | 92 | 3·5 | 860 | 123b |
| | AlNiCo 600 | 8% Al, 14% Ni, 24% Co, 3% Cu | 7·4 | 47 | 1·26 | 53 | 3·0 | 850 | 123b |
| | AlNiCo 700 | 8% Al, 13% Ni, 25% Co, 3% Cu | 7·5 | 55 | 1·30 | 60–64 | 2·2–2·5 | 850 | 123b |
| | AlNiCo 800 | 8% Al, 13% Ni, 24% Co, 3% Cu | 7·6 | >59 | 1·30 | 68 | 1·1 | 850 | 123b |
| | Alnico 700 | 8% Al, 15% Ni, 24% Co, 3% Cu | 7·2 | 52 | 1·30 | 54·4 | 5 | | 66 |
| | Koerzit 50 | | 6·7 | 4 | 0·85 | 9–7 | — | | 33 |
| | Koerzit 260 | | 7·2 | 16–22·4 | 0·58–0·68 | 104–88 | 2·8–3·5 | | 33 |
| | Koerzit 450 | | 7·3 | 27·9–38·20 | 0·75–0·92 | 111–88 | 2·5–3·5 | | 33 |
| | Koerzit 700 | | 7·3 | >51·7 | >1·25 | > 56 | 4·5–5·5 | | 33 |
| | Oerstit 700 | 8% Al, 15% Ni, 24% Co, 3% Cu | 7·3 | >48·5 | >1·25 | >55 | 4·5–5·5 | | 23 |
| | Ticonal 450 | 7·5% Al, 14·5% Ni, 34% Co, 4·5% Cu, 5% Ti | 7·3 | 34 | 0·85 | 106·8 | 2·5–3 | | 133 |
| | Ticonal 600 | 8·5% Al, 14% Ni, 24% Co, 3% Cu | 7·3 | 46 | 1·31 | 51·6 | 3–4 | | 133 |

*Table 19.2 continued*

| *Material group* | *Abbreviated name* | *Composition (remainder iron)* (Me=Ba, Sr, Pb) | *d* (g/cm³) | $(BH)_{max}$ (mW s/cm³) | $B_r$ (V s/m²) | ${}_BH_c$ (kA/m) | $\mu_p$ ($\mu_0$) | $T_c$ (°C) | *Reference* |
|---|---|---|---|---|---|---|---|---|---|
| | Ticonal 750 | 8·5% Al, 14% Ni, 24% Co, 3% Cu | 7·3 | 60 | 1·34 | 60·8 | 3–4 | | 133 |
| | Permanit 600 | 8% Al, 14% Ni, 24% Co, 3% Cu | 7·3 | 52 | 1·25 | 56 | 3·9 | | 37 |
| Co–Fe–V alloys | Magnetoflex 35 | 52% Co, 13% V | 8·1 | 12·5–20 | 0·9–0·8 | 24–28 | 7 | 700 | 127 |
| | Magnetoflex 40 | 52% Co, 8% V | 8·1 | 6·5–9·5 | 1·2–0·8 | 10·5–18·5 | 9 | 700 | 127 |
| | Koerflex 30 | 30% Co, 15 %Cr | 7·85 | 3·2–4·8 | 1·7–1·8 | 3–1·5 | 25–40 | | 33 |
| | Koerflex 200 | 52% Co, 2% V, 7·5% Cr | 8·10 | 4–11·9 | 1·3–1·6 | 18–5 | 7–15 | | 33 |
| | Koerflex 300 Bd | 52% Co, 8% V, 4% Vr | 8·15 | 13·5–17·5 | 0·95–1·1 | 26–22 | 4–8 | | 33 |
| | Koerflex 300 Dt | 52% Co, 8% V, 4% Cr | 8·15 | 22·3–27·1 | 1·08–1·22 | 33–27 | 3–7 | | 33 |
| Superstructure alloys | Oersit 900 CP | 78% Pt, 22% Co | 15·5 | 56·8–74·4 | 0·6–0·55 | 332–382 | 1–1·5 | 500 | 23 |
| Ceramic materials | DS 1 | $SrO{\cdot}6Fe_2O_3$ (anisotropic) | 4·6 | 26·4–31·2 | 0·36–0·4 | 288–320 | ~1·2 | | 101 |
| | DS 2 | $SrO{\cdot}6Fe_2O_3$ (anisotropic) | 4·4 | 20·8–26·4 | 0·32–0·36 | 256–288 | ~1·2 | | 101 |
| | Ferroxdure 280 | $MeO{\cdot}6Fe_2O_3$ (anisotropic) | 4·6 | 23·2 | 0·355 | 238 | ~1 | ~450 | 133 |
| | Ferroxdure 330 | $MeO{\cdot}6Fe_2O_3$ (anisotropic) | 4·8 | 26·4 | 0·37 | 238 | ~1 | ~450 | 133 |
| | Ferroxdure 360 | $MeO{\cdot}6Fe_2O_3$ (anisotropic) | 4·9 | 28·8 | 0·39 | 175 | ~1 | ~450 | 133 |
| | Koerox 330 | $MeO{\cdot}6Fe_2O_3$ (anisotropic) | 4·8 | 24–27 | 0·34–0·38 | 255–207 | 1·1 | | 33 |
| | Koerox 360 | $MeO{\cdot}6Fe_2O_3$ (anisotropic) | 4·9 | 26·2–30·2 | 0·37–0·41 | 230–160 | 1·1 | | 33 |

| | | | | | | | | | |
|---|---|---|---|---|---|---|---|---|---|
| | Maniperm 830 | $MeO \cdot 6Fe_2O_3$ (anisotropic) | 4·5–5·1 | 8·8–12·8 | 0·22–0·26 | 141–191 | 1·1–1·3 | 450 | 134a |
| | Maniperm 850 | $MeO \cdot 6Fe_2O_3$ (anisotropic) | 4·5–5·1 | 20·0–25·6 | 0·32–0·37 | 123–200 | 1·1–1·3 | 450 | 134a |
| | Maniperm 860 | $MeO \cdot 6Fe_2O_3$ (anisotropic) | 4·5–5·1 | 25·6–32·0 | 0·37–0·41 | 160–240 | 1·1–1·3 | 450 | 134a |
| | Maniperm 860K | $MeO \cdot 6Fe_2O_3$ (anisotropic) | 4·5–5·1 | $\geqslant$22·3 | $\geqslant$0·34 | >215 | 1·1–1·3 | 450 | 134a |
| | Ox 400 | $MeO \cdot 6Fe_2O_3$ (anisotropic) | 4·7 | 28·8 | 0·38 | 224 | 1·1 | | 66 |
| | Oxit 150 | $MeO \cdot 6Fe_2O_3$ (anisotropic) | 4·9 | 10·5–12·5 | 0·27–0·24 | 160–184 | 1·1–1·15 | | 23, 98b |
| | Oxit 330 | $MeO \cdot 6Fe_2O_3$ (anisotropic) | 4·8 | 24·5–27·5 | 0·38–0·36 | 206–247 | 1·05–1·15 | | 23 |
| | Oxit 360 | $MeO \cdot 6Fe_2O_3$ (anisotropic) | 4·9 | 27·0–30·0 | 0·40–0·38 | 152–184 | 1·05–1·15 | | 23 |
| Moulded magnets | Prac 120 | Alni 120 with binder | 5·4 | 3·2 | 0·29 | 36·8 | 3 | | 66 |
| | Prac 160 | Alnico 160 with binder | 5·5 | 5·2 | 0·34 | 46·4 | 3 | | 66 |
| | Prac 260 | Alnico 260 with binder | 5·6 | 8·0 | 0·40 | 68 | 3 | | 66 |
| | T 500 | AlNiCo with binder | — | 4·5 | 0·37 | 41·8 | — | | 13a |
| | T 700 | AlNiCo with binder | — | 6·8 | 0·44 | 50·8 | — | | 13a |
| | T 1100 | AlNiCo with binder | — | 10·8 | 0·45 | 81·6 | — | | 13a |
| | FXD P30 | $MeO \cdot 6Fe_2O_3$ with Thermoplast | 3·1 | 2·8 | 0·125 | 88 | ~1·1 | | 133 |
| | FXD P40 | $MeO \cdot 6Fe_2O_3$ with Thermoplast | 3·6 | 3·6 | 0·145 | 92 | ~1·15 | | 133 |
| | FXD D55 | $MeO \cdot 6Fe_2O_3$ with Duroplast | 4·0 | 4·8 | 0·17 | 112 | ~1·15 | | 133 |
| | FXD Sp10 | $MeO \cdot 6Fe_2O_3$ with Thermoplast | 2·3 | 0·96 | 0·066 | 52 | ~1·05 | | 133 |
| | FXD Sp50 | $MeO \cdot 6Fe_2O_3$ with Thermoplast | 3·95 | 4·4 | 0·155 | 111 | ~1·15 | | 133 |
| | FXD Sp130 | $MeO \cdot 6Fe_2O_3$ with Thermoplast | 3·4 | 11·2 | 0·24 | 175 | ~1·05 | | 133 |
| | Koerox G | $MeO \cdot 6Fe_2O_3$ with binder | ~3·6 | 4–8 | 0·15–0·20 | 120–103 | 1·1 | | 33 |
| | Koerox P | $MeO \cdot 6Fe_2O_3$ with binder | ~3·6 | 3·2–4·8 | 0·14–0·16 | 103–88 | 1·1 | | 33 |

*Table 19.2 continued*

| *Material group* | *Abbreviated name* | *Composition (remainder iron)* (Me = Ba, Sr, Pb) | *d* (g/cm³) | $(BH)_{max}$ (mW s/cm³) | $B_r$ (V s/m²) | ${}_BH_c$ (kA/m) | $\mu_p$ ($\mu_0$) | $T_c$ (°C) | *Reference* |
|---|---|---|---|---|---|---|---|---|---|
| | Oxilit G | $MeO \cdot 6Fe_2O_3$ with rubber binder | 3·2 | 3·9–5 | 0·18–0·15 | 102–118 | 1·1–1·15 | | 23 |
| | Oxilit D | $MeO \cdot 6Fe_2O_3$ with Duroplast | 3·7 | 3·9–5 | 0·18–0·15 | 102–118 | 1·1–1·15 | | 23 |
| | Oxilit P | $MeO \cdot 6Fe_2O_3$ with Thermoplast | 3·7 | 3·9–5 | 0·18–0·15 | 102–118 | 1·1–1·15 | | 23 |
| | Oxilit Ga | $MeO \cdot 6Fe_2O_3$ with rubber binder | 3·7 | 7·4–8·6 | 0·21–0·19 | 95–105 | 1·1–1·15 | | 23 |
| | Oxilit Da | $MeO \cdot 6Fe_2O_3$ with Duroplast | 3·2 | 5·5–6·4 | 0·20–0·18 | 105–108 | 1·1–1·15 | | 23 |
| | Prox 200 | $BaO \cdot 6Fe_2O_3$ with binder | 3·8 | 14·4 | 0·28 | 168 | 1·1 | | 66 |
| | P 1500 a | $BaO \cdot 6Fe_2O_3$ with binder | — | 7·3 | 0·20 | 160 | — | | 13a |
| | Sprox 1 H | $BaO \cdot 6Fe_2O_3$ with binder | 2·4 | 1 | 0·08 | 52 | 1·1 | | 66 |
| | Sprox 2 H | $BaO \cdot 6Fe_2O_3$ with binder | 4·0 | 2 | 0·15 | 96 | 1·1 | | 66 |

**Table 19.3** HEAT TREATMENT OF PERMANENT-MAGNET MATERIALS (SEE TABLES 19.4–19.8)

| *Number* | *Annealing* (°C) | *Cooling* | *Hardening temperature* (°C) | *Cooled in* | *Tempering* | |
|---|---|---|---|---|---|---|
| | | | | | *Duration* (h) | *Temperature* (°C) |
| 1 | 690 | Slowly | 840 | Oil | | |
| 2 | 690 | Slowly | 850 | Oil | | |
| 3 | 700 | Slowly | 820 | Water | | |
| 4 | 650–750 | Slowly | 930–960 | Oil | | |
| 5 | 750 | Slowly | 1 150 | Air | | |
| | | | 750 | Air | | |
| | | | 1 000 | Air-stream | | |
| 6 | 770 | Slowly | 1 150 | Air | | |
| | | | 750 | Air | | |
| | | | 1 000 | Air-stream | | |
| 7 | 770 | Slowly | 1 150 | Air | | |
| | | | 750 | Air | | |
| | | | 950 | Oil | | |
| 8 | 900 | Slowly | 1 250 | Air | 2 | 560 |
| 9 | | | 1 200 | Oil | 8 | 600 |
| 10 | | | 1 200 | Oil | | 650 |
| 11 | | | 1 040 | Water | 3 | 650 |
| 12 | | | 1 150 | Air-stream | 2 | 560 |
| 13 | | | 1 200 | Air | | 700 |
| 14 | | | 1 250 | Air | 2 | 560 |
| 15 | 700 | | 1 100–1 250 | Air | 2 | |
| | | | 600–730 | Air | | |
| | | | 950–1 020 | Oil | | |
| 16 | *Thermomagnetic treatment:* In the range 1250°–1300°C or 900°–950°C, in a field of at least 120 kA/m, cool till below the Curie temperature (840°–860°C); then either temper for a long time at 590°–560°C or for a shorter time followed by very slow cooling from 650°C to 560°C. | | | | | |

**Table 19.4** MAGNET STEELS

| *Country* | *Abbreviated name* | *Chemical composition (remainder iron)* | $\varrho$ ($\mu\Omega$ cm) | $d$ (g/cm$^3$) | $(BH)_{max}$ $\left(\frac{mW\,s}{cm^3}\right)$ | $B_r$ (V s/m$^2$) | ${}_BH_c$ (kA/m) | $T_c$ (°C) | *Heat treatment** | *Reference* |
|---|---|---|---|---|---|---|---|---|---|---|
| Austria | Permanit 30 | 4% Cr | | 7·8 | >2·08 | 0·84 | 4·5 | | | 37 |
| | Permanit 35 | 4% Cr | | 7·8 | >2·32 | 0·84 | 5·0 | | | 37 |
| | Permanit 40 | 4% Cr, 2% Co | | 7·9 | >2·72 | 0·94 | 5·6 | | | 37 |
| | Permanit 50 | 8% Cr, 6% Co | | 7·9 | >3·68 | 0·92 | 9·6 | | | 37 |
| | Permanit 70 | 9% Cr, 16% Co | | 8·0 | >5·2 | 0·95 | 14·4 | | | 37 |
| France | Co 35 | 35% Co | 17 | 8·2 | 7·2 | 0·95 | 18 | 890 | | 41 |
| | Co 15 | 15% Co | 16 | 8·2 | 5·2 | 0·87 | 13·6 | 840 | | 41 |
| | Co 10 | 10% Co | 14 | 8·1 | 4·0 | 0·84 | 12 | 840 | | 41 |
| | Cr Co | 3% Co | 32 | 8 | 2·4 | 0·75 | 8 | 780 | | 41 |
| Great Britain | 35% Co steel | 35% Co, 6% Cr, 5% W, 0·9% C | 80 | 8·2 | 7·56 | 0·90 | 19·9 | 890 | 7 | 5, 94 |
| | 15% Co steel | 15% Co, 9% Cr, 1·5% Mo, 1% C | 70 | 7·9 | 4·93 | 0·82 | 14·3 | 840 | 6 | 5, 94 |
| | 9% Co steel | 9% Co, 9% Cr, 1·5% Mo, 1% C | 70 | 7·8 | 3·98 | 0·78 | 12·7 | 840 | 6 | 5, 94 |
| | 6% Co steel | 6% Co, 9% Cr, 1·5% Mo, 1% C | 70 | 7·75 | 3·50 | 0·75 | 11·5 | 830 | 5 | 5, 94 |
| | 3% Co steel | 3% Co, 9% Cr, 1·5% Mo, 1% C | 70 | 7·7 | 2·78 | 0·72 | 10·3 | 800 | 5 | 5, 94 |
| | 2% Co steel | 2% Co, 4% Cr, 0·6% W, 1% C | 50 | 7·85 | 2·54 | 0·98 | 6·4 | 775 | 3 | 5, 94 |

| | | | | | | | | | | |
|---|---|---|---|---|---|---|---|---|---|---|
| | 6% W steel | 6% W, 0·3% Cr, 0·7% C | 40 | 8·2 | 2·38 | 1·05 | 5·2 | 760 | 3 | 5, 94 |
| | Cr steel | 3% Cr, 0·3% Mn, 0·9% C | 40 | 7·85 | 2·27 | 0·98 | 5·6 | 760 | — | 5, 94 |
| USA | 3% Fe Co | | 28 | 7·7 | 4 | 1·0 | 5·2 | | 5 | 119 |
| | 17% Fe Co | 17% Co, 8% W, 2·5% Cr, 0·75% C | 30 | 8·3 | 6 | 1·04 | 14 | | | 119 |
| | 36% Fe Co | 35% Co, 6% Cr, 5% W, 0·9% C | 31 | 8·6 | 7·2 | 1·04 | 20·8 | | 7 | 119 |
| Japan | MT | | | 6·9 | 3·6 | 0·6 | 16 | | | 77 |
| | Cr steel | | | | 2·4–3·2 | 0·9–1 | 5·6–4·8 | | | 69 |
| | Co steel A | | | | 4·8–15·2 | 0·85–0·95 | 16–12 | | | 69 |
| | Co steel B | | | | 7·2–8·8 | 0·9–1·0 | 19·2–16 | | | 69 |

* See Table 19.3.

**Table 19.5** Fe–Al–Ni–(Co) ALLOYS OF FRANCE,

| *Country* | *Abbreviated name* | *Chemical composition (remainder iron)* |
|---|---|---|
| France | Nial B (isotropic) | 25% Ni, 12% Al |
| | Nialco K (isotropic) | 5% Co, 20% Ni, 10% Al, 3% Cu |
| | Nialco W (isotropic) | 12% Co, 20% Ni, 10% Al, 3% Cu |
| | Nialco Z (isotropic) | 27% Co, 15% Ni, 7% Al, 4% Cu, 7% Ti |
| | Sermalloy A1 | 7·5% Al, 14% Ni, 38% Co, 3% Cu, 8% Ti |
| | Sermalloy A4 | 7·5% Al, 15% Ni, 34% Co, 3% Cu, 4·3% Ti, 1·2% Nb |
| | Sermalloy A5 | 7·5% Al, 14% Ni, 34% Co, 3% Cu, 6% Ti, 1% Nb |
| | Ticonal G (anisotropic) | 24% Co, 14% Ni, 8% Al, 3% Cu |
| | Ticonal E (anisotropic) | 24% Co, 15% Ni, 8% Al, 3% Cu, 1·5% Ti |
| | Ticonal M (anisotropic) | 24% Co, 14% Ni, 8% Al, 3% Cu, 2% Nb |
| | Ticonal X (anisotropic) | 34% Co, 14·5% Ni, 7% Al, 4·5% Cu, 5% Ti |
| | Ticonal I (anisotropic) | 24% Co, 14% Ni, 8% Al, 3% Cu |
| | Ticonal GG (anisotropic) | 24% Co, 14% Ni, 8% Al, 3% Cu |
| | Ticonal 600 | |
| | Ticonal 700 | |
| | Ticonal 750 | |
| | Ticonal 800 | |
| | Ticonal 1 500 | |
| | Ugimax | 24% Co, 14% Ni, 8% Al, 3% Cu |
| | Nialco I | |
| | Nialco II | |
| | Nialco III | |
| | Nialco IV | |
| | Nialco IV A | |
| Great Britain | Columax | 8% Al, 24% Co, 3% Cu, 13·5% Ni, 0·5% Nb |
| | Alcomax II | 8% Al, 21% Co, 4% Cu, 11·5% Ni |
| | Alcomax III | 8% Al, 24% Co, 3% Cu, 13·5% Ni, 0·5% Nb |
| | Alcomax IV | 8% Al, 24% Co, 3% Cu, 13·5% Ni, 2% Nb |
| | Hycomax I | |
| | Hycomax II | 7% Al, 14% Ni, 29% Co, 3% Cu, 4% Ti, 2% Nb |
| | Hycomax III | 7% Al, 14% Ni, 34% Co, 4% Cu, 5% Ti |
| | Hycomax IV | 7% Al, 14% Ni, 40% Co, 3% Cu, 8% Ti |
| | Hynico II | |
| | Alnico (high remanence) | 10% Al, 12% Co, 5·5% Cu, 17% Ni |
| | Alnico (normal) | 10% Al, 12% Co, 6% Cu, 19% Ni |

| $\varrho$ ($\mu\Omega$ cm) | $d$ $\left(\frac{g}{cm^3}\right)$ | $(BH)_{max}$ (mW s/cm$^3$) | $B_r$ (V s/cm$^2$) | $_BH_c$ (kA/m) | $T_c$ (°C) | $\mu_p$ ($\mu_0$) | *Heat treatment** | *Reference* |
|---|---|---|---|---|---|---|---|---|
| 63 | 6·9 | 10·4 | 0·65 | 40·4 | 760 | 6 | | 41 |
| 75 | 6·9 | 12 | 0·70 | 46·4 | 740 | 5 | | 41 |
| 65 | 6·9 | 14 | 0·75 | 52·2 | 760 | 6 | | 41 |
| 62 | 7·2 | 18·4 | 0·67 | 76 | 800 | 4 | | 41 |
| | | 44·8 | 0·74 | 164 | | | | 16a |
| | | 44–48 | 0·9–0·92 | 120–124 | | | | 16a |
| | | 44–48 | 0·84 | 144 | | | | 16a |
| 47 | 7·3 | 41·6 | 1·27 | 46·4 | 860 | 4 | | 41 |
| 50 | 7·3 | 33·6 | 1·13 | 56·4 | 860 | 5 | | 41 |
| 50 | 7·3 | 39·2 | 1·17 | 63·2 | 860 | 5 | | 41 |
| 50 | 7·3 | 36 | 0·88 | 104 | 880 | 3 | | 41 |
| 47 | 7·3 | 49·6 | 1·33 | 57·6 | 860 | 4 | | 41 |
| 48 | 7·3 | 64 | 1·35 | 65·6 | 860 | 4 | | 41 |
| 47 | 7·3 | 42·2 | 1·26 | 50·1 | 860 | 3 | | 4 |
| 47 | 7·3 | 39·8 | 1·16 | 55·7 | 860 | 3 | | 4 |
| 50 | 7·3 | 35·0 | 1·10 | 59·7 | 860 | 3·5 | | 4 |
| 50 | 7·3 | 34·2 | 1·06 | 63·6 | 870 | 3 | | 4 |
| 50 | 7·35 | 39·8 | 0·85 | 115·4 | 880 | 2·5 | | 4 |
| 47 | 7·3 | 50·9 | 1·35 | 55·7 | 860 | 2·5 | | 4, 65 |
| 65 | 7 | 11·1 | 0·65 | 42·1 | 725 | 4 | | 4 |
| 65 | 7 | 11·9 | 0·63 | 51·7 | 750 | 4 | | 4 |
| 65 | 7·1 | 13·5 | 0·70 | 54·9 | 775 | 4·5 | | 4 |
| 62 | 7·1 | 15·1 | 0·57 | 79·6 | 775 | 2·8 | | 4 |
| — | 5·45 | 8·0 | 0·30 | 79·6 | — | 1·8 | | 4 |
| — | 7·35 | 60·0 | 1·35 | 59·2 | 860 | 1·8 | 16 | 94, 94a |
| 50 | 7·35 | 43·2 | 1·30 | 46·4 | 840 | 2·6 | 16 | 94, 94a |
| 55 | 7·35 | 43·2 | 1·26 | 52·0 | 860 | 3·1 | 16 | 94, 94a |
| 60 | 7·35 | 36·0 | 1·15 | 60 | 860 | 4·4 | 16 | 94, 94a |
| | 7·25 | 25·6 | 0·90 | 66 | | 4·0 | | 94, 94a |
| | | 73 | 1·13 | 109 | | | | 42a |
| | | 90·4 | 1·10 | 124 | | | | 42a |
| | | 79·2 | 0·83 | 152 | | | | 42a |
| | 7·3 | 14·4 | 0·6 | 72 | | 4·2 | | 94a |
| 65 | 7·3 | 13·5 | 0·8 | 39·8 | 800 | 7·0 | 8 | 94, 94a |
| 65 | 7·3 | 13·5 | 0·73 | 44·6 | 800 | 6·0 | 8 | 94, 94a |

| *Country* | *Abbreviated name* | *Chemical composition (remainder iron)* |
|---|---|---|
| Great Britain (*cont.*) | Alnico (high coercivity) | 10% Al, 12% Co, 6% Cu, 21% Ni |
| | Alni (high remanence) | 13% Al, 4% Cu, 24% Ni |
| | Alni (normal) | 13% Al, 4% Cu, 25% Ni |
| | Alni (high coercivity) | 13% Al, 4% Cu, 27% Ni |
| | Ticonal GX | 8% Al, 14% Ni, 24% Co, 3% Cu |
| | Ticonal G | 8% Al, 14% Ni, 24% Co, 3% Cu |
| | Ticonal C | 8% Al, 14% Ni, 24% Co, 3% Cu |
| | Ticonal F | 8% Al, 14% Ni, 24% Co, 3% Cu, 0·5% Ti |
| | Ticonal S | 8% Al, 14% Ni, 24% Co, 3% Cu |
| | Ticonal E | 8% Al, 14% Ni, 24% Co, 3% Cu, 1·5% Ti |
| | Ticonal D | 8% Al, 14% Ni, 24% Co, 3% Cu, 1% Ti |
| | Ticonal K | |
| | Reco 2A | 7% Al, 20% Ni, 20% Co, 6·5% Ti |
| | Reco 3A | Sintered |
| | Alnico | |
| | Alcomax II | |
| | Alcomax III | |
| | Alcomax IV | |
| | Hycomax | |
| Italy | Alni | 25% Ni, 12% Al, 4% Cu |
| | Coalni | 25·5% Ni, 11·5% Al, 4% Co, 4% Cu |
| | Alnico II | 20% Ni, 9·5% Al, 12% Co, 6% Cu |
| | Coercimax I | 15% Ni, 8% Al, 24% Co, 3% Cu, 0·5% Ti |
| | Coercimax II | 14·5% Ni, 7% Al, 35% Co, 5% Cu, 5% Ti |
| | Coalnimax | 14% Ni, 8% Al, 24% Co, 3% Cu |
| | Ansemax | 14% Ni, 8% Al, 24% Co, 3% Cu |
| Japan | YCM-1D | (Alnico-5DG) |
| | HI-MAG I | (Alnico-5-7) |
| | HI-MAG II | (Alnico-5-7) |
| | YCM-2B | (Alnico-6) |
| | YCM-4A | (Alnico-3) |
| | YCM-4B | (Alnico-4) |
| | YCM-8B | (Alnico-8) |
| | Mishima Metal | 13·5% Al, 28·5% Ni |
| | MK | 13% Al, 4% Cu, 25% Ni |
| | NKS3 | 8% Al, 24% Co, 3% Cu, 14% Ni |
| | New KS | 4% Al, 27% Co, 18% Ni, 7% Ti |
| | Honda Alloy | 8% Al, 27% Co, 18% Ni, 7% Ti |
| | Unicolumn | 8% Al, 24% Co, 3% Cu, 17·7% Ni |
| | TK8 | |
| | Alni | |
| | Alnico A (isotropic) | |
| | Alnico B (isotropic) | |
| | Alnico C (isotropic) | |
| | Alnico X (anisotropic) | |
| | Alnico Y (anisotropic) | |
| | Alnico Z (anisotropic) | |

* See Table 19.3.

*Table 19.5 cotinued*

| $\varrho$ ($\mu\Omega$ cm) | $d$ $\left(\frac{g}{cm^3}\right)$ | $(BH)_{max}$ (mW s/cm³) | $B_r$ (V s/cm²) | ${}_BH_c$ (kA/m) | $T_c$ (°C) | $\mu_p$ ($\mu_0$) | *Heat treatment** | *Reference* |
|---|---|---|---|---|---|---|---|---|
| 65 | 7·3 | 13·5 | 0·65 | 49·3 | 800 | 5·2 | 8 | 94, 94a |
| 65 | 6·9 | 10 | 0·62 | 38·2 | 760 | 5·5 | 12 | 94, 94a |
| 65 | 6·9 | 10 | 0·56 | 46·1 | 760 | 5·0 | 12 | 94, 94a |
| 67 | 6·9 | 10 | 0·50 | 54·1 | 760 | 4·0 | 12 | 94, 94a |
| 47 | 7·3 | 60 | 1·35 | 57·6 | | | | 79 |
| 47 | 7·3 | 45·6 | 1·35 | 46·6 | | | | 79 |
| 48 | 7·3 | 40 | 1·25 | 54·4 | | | | 79 |
| 48 | 7·3 | 38·4 | 1·24 | 48·0 | | | | 79 |
| 50 | 7·1 | 33·6 | 1·11 | 49·6 | | | | 79 |
| 50 | 7·3 | 32·8 | 1·11 | 59·2 | | | | 79 |
| 50 | 7·4 | 30·4 | 1·20 | 48·0 | | | | 79 |
| 58 | 7·2 | 28·8 | 0·85 | 92 | | | | 79 |
| 62 | 7·2 | 15·4 | 0·55 | 80 | | | | 79 |
| 65 | 7·1 | 13·6 | 0·72 | 51·6 | | | | 79 |
| 64 | 6·7 | 12 | 0·70 | 44 | | | | 83 |
| — | 7·0 | 28·8 | 1·10 | 44 | | | | 83 |
| 50 | 7·0 | 32·8 | 1·10 | 49·6 | | | | 83 |
| — | 6·65 | 28 | 0·95 | 58 | | | | 83 |
| — | 6·9 | 20·8 | 0·81 | 64·8 | | | | 83 |
| | | 11·2 | 0·65 | 43·2 | | 4·3 | | 19 |
| | | 11·2 | 0·58 | 52 | | 4·5 | | 19 |
| | | 13·6 | 0·73 | 48 | | 5·6 | | 19 |
| | | 36 | 1·15 | 57·6 | | 4·0 | | 19 |
| | | 32 | 0·8 | 112 | | 2·8 | | 19 |
| | | 46 | 1·28 | 52 | | 3·5 | | 19 |
| | | 60 | 1·3 | 57·6 | | 2·1 | | 19 |
| 47 | 7·3 | 44–50·4 | 1·28–1·35 | 52–57·6 | 890 | 4·0 | | 43a |
| 47 | 7·3 | 56–65·6 | 1·35–1·45 | 56–60 | 890 | 2·0 | | 43a |
| 47 | 7·3 | 54·4–64 | 1·3–1·4 | 54·4–62·4 | 890 | 2·0 | | 43a |
| 50 | 7·3 | 28–33·6 | 1·0–1·15 | 56–60 | 860 | 4·0 | | 43a |
| 75 | 6·9 | 10·4–12·8 | 0·5–0·65 | 40·8–48 | 800 | 3·5 | | 43a |
| 75 | 6·9 | 14·4–16·8 | 0·6–0·65 | 50·4–56 | 800 | 3·5 | | 43a |
| 50 | 7·3 | 38·4–44 | 0·88–0·96 | 110–120 | 845 | 3·0 | | 43a |
| | | 9·6 | 0·66 | 41 | | | | |
| | 6·9 | 10 | 0·60 | 45 | | | | 69 |
| | 7·3 | 40 | 1·25 | 54 | | | | |
| | 7·4 | 16 | 0·65 | 72 | | | | 5 |
| | 7·4 | 16 | 0·65 | 72 | | | | 5 |
| | | 64 | 1·4 | 59 | | | | 70 |
| | | 60 | 1·45 | — | | | | 70 |
| | | 8·8–9·6 | 0·58–0·65 | 48–36 | | | | 69 |
| | | 10·4–11·2 | 0·60–0·70 | 48–40 | | | | 69 |
| | | 12–12·8 | 0·70–0·80 | 48–40 | | | | 69 |
| | | 12–12·8 | 0·60–0·70 | 56–48 | | | | 69 |
| | | 28·8–31·2 | 1·05–1·15 | 54·4–62·4 | | | | 69 |
| | | 38·4–42·4 | 1·2–1·25 | 53–48 | | | | 69 |
| | | 44–48 | 1·25–1·35 | 54·4–48 | | | | 69 |

**Table 19.6** Fe–Al–Ni–(Co)

| *Abbreviated name* | *Chemical composition (remainder iron)* | $\varrho$ ($\mu\Omega$ cm) | $d$ (g/cm$^3$) |
|---|---|---|---|
| Alnico IB | 12% Al, 21% Ni, 5% Co, 3% Cu | 75 | 6·9 |
| Alnico I | 12% Al, 18% Ni, 5% Co | 75 | 6·9 |
| Alnico IIB | 10% Al, 19% Ni, 13% Co, 3% Cu | 65 | 7·1 |
| Alnico II | 10% Al, 17% Ni, 12·5% Co, 6% Cu | 65 | 7·1 |
| Alnico IIIA | 12% Al, 26% Ni, 3% Cu | 63 | 6·9 |
| Alnico IIIB | 12% Al, 25% Ni, 3% Cu | 63 | 6·9 |
| Alnico IIIC | 12% Al, 24% Ni, 3% Cu | 63 | 6·9 |
| Alnico 3 (III) | 12% Al, 25% Ni | 60 (62) | 6·9 |
| Alnico IVA | 12% Al, 28% Ni, 5% Co | 75 | 7·0 |
| Alnico IVB | 12% Al, 27% Ni, 5% Co | 75 | 7·0 |
| Alnico V-7 | 8% Al, 14% Ni, 24% Co, 3% Cu | 47 | 7·3 |
| Alnico V A | 8% Al, 15% Ni, 24% Co, 3% Cu | 47 | 7·3 |
| Alnico VAB | 8% Al, 14·5% Ni, 24% Co, 3% Cu | 47 | 7·3 |
| Alnico VABDG | 8% Al, 14·5% Ni, 24% Co, 3% Cu | 47 | 7·3 |
| Alnico VB (V) | 8% Al, 14% Ni, 24% Co, 3% Cu | 47 | 7·3 |
| Alnico VBDG | 8% Al, 14% Ni, 24% Co, 3% Cu | 47 | 7·3 |
| Alnico V C | 8% Al, 13% Ni, 24% Co, 3% Cu | 47 | 7·3 |
| Alnico V E | 8% Al, 14·5% Ni, 23% Co, 3% Cu, 0·5% Ti | 47 | 7·3 |
| Alnico VI A | 8% Al, 17% Ni, 23% Co, 3% Cu, 4% Ti | 50 | 7·4 |
| Alnico VI B | 8% Al, 16% Ni, 24% Co, 3% Cu, 1% Ti | 50 | 7·4 |
| Alnico VI C | 8% Al, 15% Ni, 24% Co, 3% Cu, 0·5% Ti | | 7·3 |
| Alnico 6, VI | 8% Al, 15% Ni, 24% Co, 3% Cu, 1·2% Ti | 50 | 7·3 |
| Alnico 7, VII | 8% Al, 18% Ni, 24% Co, 3% Cu, 5% Ti | — | 7·1 |
| Alnico 8 (VIII) | 7% Al, 15% Ni, 35% Co, 5% Ti, (4% Cu) | 50 | 7·3 |
| Alnico XII | 6% Al, 18% Ni, 35% Co, 8% Ti | 62 | 7·5 |
| Alnicus USM 75 | 8% Al, 14% Ni, 24% Co, 3% Cu | | 7·3 |
| Alnicus USM 65 | 8% Al, 14% Ni, 24% Co, 3% Cu | | 7·3 |
| Columax 5 | | 47 | |
| Columax 9 | | 54 | |

• See Table 19.3.

ALLOYS OF THE USA

| $(BH)_{max}$ (mW s/cm³) | $B_r$ (V s/m²) | $_BH_c$ (kA/m) | $T_c$ (°C) | *Heat treatment** | $\mu_p$ ($\mu_0$) | *Reference* |
|---|---|---|---|---|---|---|
| 11·2 | 0·71 | 36 | | 13 | | 22 |
| 11·2 | 0·71 | 36 | | | 6·8 | 9, 141 |
| 13·6 | 0·75 | 46 | 800 | 8 | | 22 |
| 12·8 | 0·73 | 46 | 800 | | 6·4 | 9, 141 |
| 10·8 | 0·64 | 45 | 760 | 12 | | 22 |
| 10·8 | 0·68 | 39 | | | | 22 |
| 10·8 | 0·75 | 32 | 760 | 12 | | 22 |
| 11·2 | 0·70 | 38 | | | 6·5 | 9, 40, 141 |
| 10·8 | 0·55 | 58 | | 10 | | 9 |
| 11·6 | 0·60 | 53 | | | | 22 |
| 56 | 1·28 | 62 | 860 | | 3·8 | 10, 49 |
| 40 | 1·20 | 58 | | 16 | | 9, 40 |
| 44 | 1·25 | 55 | | 16 | | 22 |
| 52 | 1·31 | 56 | | | | 22 |
| 44 | 1·27 | 52 | | 16 | | 22, 40, 141 |
| 52 | 1·33 | 55 | | 16 | | 22 |
| 44 | 1·32 | 46 | | 16 | | 22 |
| 36 | 1·10 | 56 | | 16 | | 22 |
| 22 | 0·75 | 78 | | 16 | | 22 |
| 29·2 | 1·05 | 61 | | | | 22, 141 |
| 32 | 1·10 | 56 | | | | 5 |
| 29·6 | 1·04 | 66 | | | 5·0 | 9, 40, 119 |
| 24 | 0·75 | 88 | | | 3·5 | 9, 40, 48, 119 |
| 36 | 0·87 | 116 | | | 3·0 | 8, 21, 40, 50, 119 |
| 14 | 0·65 | 74 | | | | 141 |
| 60 | 1·39 | 59 | | | | 122 |
| 52 | 1·35 | 55 | | | | 122 |
| 60 | 1·35 | 60 | | | 1·8 | 119 |
| 80 | 1·04 | 126 | | | 2·7 | 119 |

**Table 19.7** PRECIPITATION ALLOYS OTHER THAN Fe–Al–Ni–(Co) ALLOYS
(SEE ALSO TABLES 19.1 AND 19.2)

| *System* | *Abbreviated name* | *Chemical composition (remainder iron)* | $\varrho$ ($\mu\Omega$ cm) | $d$ $\left(\frac{\text{g}}{\text{cm}^3}\right)$ | $(BH)_{max}$ $\left(\frac{\text{mW s}}{\text{cm}^3}\right)$ | $B_r$ (V s/m$^2$) | $_BH_c$ (kA/m) | $T_c$ (°C) | $\alpha$ $\left(\frac{\text{ppm}}{\text{K}}\right)$ | *Heat treatment** | *Reference* |
|---|---|---|---|---|---|---|---|---|---|---|---|
| Fe–Co–Mo | Comol | 17% Mo, 12% Co | 41 | 8·2 | 8·8 | 1·05 | 18 | 900 | 200 | | 65 |
| | Comalloy | 17% Mo, 12% Co | 41 | 8·2 | 8·8 | 1·05 | 18 | 900 | 200 | | 84 |
| | Remalloy | 17% Mo, 12% Co | 45 | 8·1 | 8·8 | 1·05 | 18–20 | 900 | 200 | | 9 |
| | Indalloy | 17% Mo, 12% Co (sintered) | 48 | 7·4 | 7·2 | 0·9 | 18 | 900 | | | 30 |
| Fe–Cr–Mo | Mo I | 23% Mo, 2·5% Cr | | | 6·4 | 0·7 | 20 | | | | 5 |
| Fe–Co–W | | 15% Co, 18% W | | | 6·2 | 1·15 | 12 | | | | 5 |
| Cu–Ni–Fe | Cunife I | 60% Cu, 20% Ni | 18·5 | 7·8 | 10·4–12 | 0·54 | 40 | 450 | 400 | 11 | 9, 26, 47, 65 |
| | Cunife II | 50% Cu, 20% Ni, 2·5% Co | 18 | 8·6 | 6·2 | 0·73 | 20 | | | | 30 |
| Cu–Ni–Co | Cunico I | 50% Cu, 29% Co, 21% Ni | 24 | 8·3 | 6·8 | 0·34 | 57 | ~880 | 200 | | 9, 65 |
| | Cunico II | 35% Cu, 41% Co, 24% Ni | 26 | 8·3 | 8·0 | 0·53 | 36 | | | | 30 |
| Fe–Co–V | Vicalloy I | 52% Co, 11% V | 60 | 8·2 | 8·0 | 0·9 | 24 | ~860 | Small | 9 | 65 |
| | Vicalloy | 52% Co, 10% V | 60–67 | 8·2 | 7·2–11·2 | 0·8–0·95 | 17·6–21·2 | | | | 9, 26, 119, |
| Co–Ni–Ti | | 27% Co, 18% Ni, 7% Ti, 4% Al | | | 16 | 0·65 | 72 | | | | 140, 148 |

* See Table 19.3.

**Table 19.8** COLD-WORKED PERMANENT MAGNETS (SEE ALSO TABLE 19.2)

| *System* | *Abbreviated name* | *Chemical composition (remainder iron)* | $\varrho$ ($\mu\Omega$ cm) | $d$ (g/cm$^3$) | $(BH)_{max}$ $\left(\frac{\text{mW s}}{\text{cm}^3}\right)$ | $B_r$ (V s/m$^2$) | ${}_BH_c$ (kA/m) | $T_c$ (°C) | $\alpha$ | *Heat treatment** | *Reference* |
|---|---|---|---|---|---|---|---|---|---|---|---|
| Fe–Co–V | Vicalloy II | 52% Co, 14% V | 60 | 8·1 | 24 | 1·0 | 36 | ~860 | Small | 9 | 65 |
| Ag–Mn–Al | Simanol | 86% Ag, 9% Mn, 4% Al | | 9 | 0·64 | 0·055 | 44 | 360 | | | 65 |
| | Silmanal | 87% Ag, 9% Mn, 4·5% Al | | | 0·60 | 0·055 | 44 | | | | 93 |

* See Table 19.3.

**Table 19.9** SUPERSTRUCTURE MAGNETS (SEE ALSO TABLE 19.2)

| *System* | *Abbreviated name* | *Chemical composition (remainder iron)* | $d$ (g/cm$^3$) | $(BH)_{max}$ (mW s/cm$^3$) | $B_r$ (V s/m$^2$) | ${}_BH_c$ (kA/m) | $T_c$ (°C) | *Reference* |
|---|---|---|---|---|---|---|---|---|
| Co–Pt | Platinax | 77% Pt, 23% Co | 15·9 | 72 | 0·63 | 328 | 590 | 65 |
| | Platinax II | 76·7% Pt, 23·3% Co | 15·5 | 74 | 0·64 | 385 | | 74 |
| Fe–Pt | Platinum | 78% Pt | 15·5 | 24 | 0·58 | 125 | ~450 | 30 |
| Mn–Al | | 72% Mn, 28% Al | — | 28 | 0·43 | 220 | 380 | 65 |

**Table 19.10** DUST MAGNETS

| *Designation* | *Material composition (approx.)* | $d$ (g/cm³) | $(BH)_{max}$ (mW s/cm³) | $B_r$ (V s/m²) | ${}_BH_c$ (kA/m) | $T_c$ (°C) | $\alpha$ (ppm/K) | *Reference* |
|---|---|---|---|---|---|---|---|---|
| Bismanol | 79·2% Bi, 20·8% Mn | 6·9 | 42·4 | 0·48 | 290 | 360 | 300 | 65 |
| Raytheon Sm Co | $SmCo_5$ | 8 | 160 | 0·9 | 720 | 850 | — | 98a |
| GEC Sm Co | $SmCo_8$ | 7·6 | 112 | 0·75 | 536 | >700 | 500 | 39a |
| Gecalloy M | Fe powder with and without binder | 4–5 | 8 | 0·7 | 26·4 | 770 | 3 000 | 65 |
| Gecalloy H | Fe powder with and without binder | — | 12 | 0·9 | 27 | 980 | 300 | 65 |
| Lodex 31 | 7·5% Co, 11·5% Fe, 72% Pb, 9% Sb | 8·9 | 28 | 0·62 | 88 | 980 | 150 | 39, 93b |
| Lodex 32 | 10% Co, 15% Fe, 66% Pb, 9% Sb | 8·6 | 28 | 0·75 | 76 | 980 | 150 | 39, 93b |
| Lodex 41 | 7·5% Co, 11·5% Fe, 72% Pb, 9% Sb | 9·9 | 12 | 0·43 | 80 | 980 | 150 | 39, 93b |
| Lodex 42 | 10% Co, 15% Fe, 66% Pb | 9·6 | 12 | 0·53 | 68 | 980 | 150 | 39, 93b |
| Lodex 55 | 31% Co, 57% Fe, 12% $O_2$ | 3·6 | 32 | 0·62 | — | 500–980 | <100 | 39, 93b |

**Table 19.11** HEXAGONAL FERRITES (SEE ALSO TABLES 19.1 AND 19.2)

| *Designation* | *Material* (BF = $BaO \cdot 6Fe_2O_3$) | $(BH)_{max}$ ($mWs/cm^3$) | $B_r$ (V $s/m^2$) | ${}_BH_c$ (kA/m) | $d$ ($g/cm^3$) | $\varrho$ ($\Omega$ cm) | $T_c$ (°C) | $\mu_p$ ($\mu_0$) | *Reference* |
|---|---|---|---|---|---|---|---|---|---|
| Arnox III | BF | 3·2 | 0·20 | 88 | 4·8 | $10^6$ | | | 11 |
| Arnox Va | BF, anisotropic | 28 | 0·39 | 120 | 5·0 | $10^4$ | 450 | | 11 |
| Caslox III | BF, with resin | 3·6 | 0·15 | 88 | 3·4 | $10^{10}$ | — | 1·2 | 95a |
| Caslox IV | BF, with rubber | 8 | 0·23 | 128 | 4·0 | $10^{10}$ | — | 1·1 | 95a |
| Caslox VI | BF, isotropic | 7·6 | 0·21 | 136 | 4·8 | $10^5$ | 450 | 1·1 | 95a |
| Caslox XII | BF, isotropic | 8 | 0·22 | 144 | 4·8 | $10^5$ | 450 | 1·1 | 95a |
| Caslox VIIA | BF, semi-aligned | 16 | 0·30 | 208 | 4·8 | $10^5$ | 450 | 1·1 | 95a |
| Caslox VIII | BF, fully aligned | 20 | 0·33 | 248 | 4·8 | $10^5$ | 450 | 1·1 | 95a |
| Caslox IX | BF, anisotropic | 24 | 0·36 | 240 | 4·8 | $10^5$ | 450 | 1·1 | 95a |
| Caslox X | BF, anisotropic | 29 | 0·39 | 200 | 4·8 | $10^5$ | 450 | 1·1 | 95a |
| Ceramagnet | BF, isotropic | 8·1 | 0·22 | 136 | | | 450 | 1·23 | 106 |
| Ceramagnet | BF, anisotropic | 24 | 0·38 | 136 | 4·9 | | 450 | | 65 |
| Cromag | BF, isotropic | 6·4 | 0·20 | 124 | | $10^6$ | 385 | | 30 |
| F300 | BF, isotropic | 6·7 | 0·20 | 128 | | $10^6$ | 445 | | 30 |
| Ferbalite 5802 | BF, isotropic | 11·2 | 0·26 | 136 | | $10^6$ | | | 30 |
| Ferbalite 5803 | BF, isotropic | 4·8 | 0·18 | 120 | | $10^6$ | | | 30 |
| Ferbalite 5804 | BF, isotropic | 7·2 | 0·21 | 128 | | $10^6$ | | | 30 |
| Fercolite 5201 | Co ferrite, isotropic | 12 | 0·24 | 144 | | $10^2$ | | | 30 |
| Fercolite 5203 | Co ferrite, isotropic | 9·6 | 0·26 | 80 | | $10^2$ | | | 30 |

*Table 19.11 continued*

| *Designation* | *Material* (BF = $BaO{\cdot}6Fe_2O_3$) | $(BH)_{max}$ (mW s/cm³) | $B_r$ (V s/m²) | ${}_BH_c$ (kA/m) | $d$ (g/cm³) | $\varrho$ (Ω cm) | $T_c$ (°C) | $\mu_p$ ($\mu_0$) | *Reference* |
|---|---|---|---|---|---|---|---|---|---|
| Ferdurite | BF, isotropic | 7·2 | 0·21 | 128 | 4·7 | | 450 | 1·2 | 113 |
| Feroba I | BF, isotropic | 8 | 0·22 | 140 | 4·8 | | 450 | 1·1 | 65, 94a |
| Feroba II | BF, anisotropic | 25·4 | 0·39 | 140 | 5·0 | | | 1·05 | 94a |
| Feroba III | BF, anisotropic | 21·6 | 0·34 | 200 | 4·7 | | | | 94a |
| Ferrinet Q1 | BF, isotropic | 8–9·6 | 0·23–0·25 | 140–160 | 4·9–5·0 | $>10^6$ | | | 120 |
| Ferrinet Q6 | BF, anisotropic | 29–34 | 0·41–0·44 | 128–152 | 5·0–5·2 | $>10^4$ | | | 120 |
| Ferrimag I | BF, isotropic | 8·4 | 0·23 | 148 | 4·8 | $>10^6$ | | | 21 |
| Ferrimag II | BF, anisotropic | 28 | 0·40 | 160 | 5·0 | | | | 21 |
| Ferriflex I | BF, with binder | 5 | 0·16 | 92 | 3·8 | | | | 4 |
| Ferriflex II | BF, with binder | 3·5 | 0·13 | 88 | 3·5 | | | | 4 |
| Genox 1 | BF, isotropic | 8·8 | 0·23 | 156 | 4·7 | $10^6$ | | | 40 |
| Genox 5 | BF, anisotropic | 27·2 | 0·38 | 192 | 5·0 | $10^6$ | | | 40 |
| Genox 6 | BF, anisotropic | 21·6 | 0·33 | 224 | 5·0 | $10^6$ | | | 40 |
| Indox I | BF, isotropic | 8 | 0·22 | 146 | 4·8 | $10^6$ | 450 | 1·15 | 51 |
| Indox II | BF, semi-aligned | 13·2 | 0·27 | 180 | 4·5 | | 450 | 1·15 | 51 |
| Indox V | BF, anisotropic | 28 | 0·38 | 176 | 5·0 | | 450 | 1·05 | 51 |
| Indox VIa | BF, anisotropic | 20·8 | 0·33 | 240 | 4·5 | | 450 | 1·06 | 51 |
| Magnadur 1 | BF, isotropic | 7·6 | 0·20 | 140 | 4·8–5·0 | $10^8$ | 450 | 1·2 | 78 |
| Magnadur 2 | BF, anisotropic | 25·6 | 0·39 | 152 | 4·8–5·0 | $10^8$ | 450 | 1·0 | 78 |
| Magnadur 3 | BF, anisotropic | 20·8 | 0·34 | 208 | 4·8–5·0 | $10^8$ | 450 | 1·0 | 78 |

| | | | | | | | | | |
|---|---|---|---|---|---|---|---|---|---|
| Morrite 100 | BF, isotropic | 7·0 | 0·20 | 140 | 4·8 | $10^6$ | 450 | 1·2 | 77a |
| Morrite 300 | BF, anisotropic | 25 | 0·38 | 130 | 5·1 | $10^6$ | 450 | 1·1 | 77a |
| MO 1 | BF, isotropic | 8 | 0·22 | 144 | | $10^9$ | 450 | 1·2 | 3c |
| MO 6 C | BF, anisotropic | 20 | 0·33 | 224 | 4·9 | | 450 | 1·09 | 3b |
| Plastiform | BF, anisotropic with rubber | 8 | 0·21 | 104 | 3·7 | $10^{10}$ | — | 1·2 | 63 |
| Plastoferrite I | BF, with binder | 6 | 0·17 | 100 | 4·1 | | | | 4 |
| Plastoferrite II | BF, with binder | 5 | 0·16 | 96 | 3·9 | | | | 4 |
| Plastoferrite III | BF, with binder | 2·5 | 0·10 | 76 | 3·3 | | | | 4 |
| Sinterox I | BF, isotropic | 7·2 | 0·21 | 136 | 4·7 | $\sim 10^{12}$ | 450 | 1·2 | 19 |
| Sinterox II | BF, anisotropic | 18·4 | 0·32 | 192 | 4·7 | $\sim 10^{10}$ | 450 | 1·0 | 19 |
| Sinterox III | BF, anisotropic | 24 | 0·37 | 144 | 4·8 | $\sim 10^{10}$ | 450 | 1·0 | 19 |
| Spinal | BF, isotropic | 7·5 | 0·22 | 131 | 4·7–4·9 | | | | 4 |
| Spinalor 1S | | 24·7 | 0·37 | 165 | 4·6–4·8 | | | | 4 |
| Spinalor 1B | | 26·3 | 0·39 | 135 | 4·8–5 | | | | 4 |
| Spinalor 1H | Ba or Sr ferrite, anisotropic | 22 | 0·34 | 199 | — | | | | 4 |
| Spinalor 2S | | 26·3 | 0·37 | 239 | 4·6–4·8 | | | | 4 |
| Spinalor 3B | | 27 | 0·40 | 143 | 4·7–4·9 | | | | 4 |
| Spinalor 4B | | 28·3 | 0·41 | 175 | 4·6–4·8 | | | | 4 |
| Spinalor 4H | | 26·2 | 0·37 | 254 | 4·4–4·6 | | | | 4 |
| Vectolite | $22Co_2O_3 \cdot 30FeO_3 \cdot 44Fe_3O_4$ | 4·8 | 0·16 | 80 | — | | | | 93 |
| Westro $\alpha$ | Anisotropic | 29·3 | 0·40 | 176 | 4·8 | $10^8$ | 460 | 1·05 | 146a |
| Westro $\beta$ | Anisotropic | 24 | 0·36 | 252 | 4·5 | $10^8$ | 460 | 1·05 | 146a |

## 19.2 Sheet and strip

It will be seen by a comparison of the relevant Standardisation sheets that the classification of permanent-magnet materials on the basis of their differing $(BH)_{max}$ values (DIN 17 410, see Table 9.7) is appreciably simpler than the classification of materials for coils and transformers (DIN 41 301, see Table 13.3). For electrosheet used in heavy-current engineering (DIN 46 400, see Table 10.7) the proportions of alloying substances in iron and the corresponding changes in power loss can serve as distinguishing criteria. For sheet used in communications transformers, however, the problems are more manifold and the frequency spectrum broader. Correspondingly more alloy types are available to the user and these can be adapted to special conditions by a suitable choice of manufacturing procedure, after-treatment, and choice of sheet dimensions.

Unfortunately, manufacturers have not yet been able to agree on a uniform nomenclature as makers of permanent magnets usually have. Thus, for example, Oerstit 400 has much the same properties as Koerzit 400 or Alnico 400 and all conform to the limits set down in the Standard (see Table 19.1).

The names and numbers given to sheet and strip often refer to the composition. This is particularly true of the Ni–Fe alloys. Nevertheless, as already explained, materials of identical chemical composition can exhibit very different properties following various hot- or cold-working procedures. Thus an alloy containing 50% Fe and 50% Ni can be made, entirely on demand,

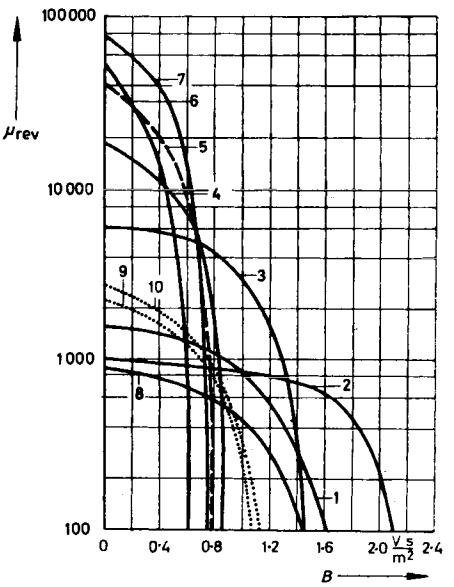



*Figure 19.1. Reversible permeability as a function of flux density: 1, Trafoperm N2/OR; 2, Vacoflux 50; 3, Permenorm 5000 H2; 4, Permalloy C; 5, Mumetal; 6, M1040; 7, Ultraperm 10; 8, Trafoperm N1; 9, Permenorm 3601 K1; 10, Permenorm 3601 K2*[123]

**Table 19.12** SHEET AND STRIP OF NICKEL-FREE ALLOYS (SEE ALSO TABLES 10.6 AND 10.7)

| *Alloys* | *Material designation* | *DIN 41 301* | $\mu_5$ ($\mu_0$) | $\mu_m$ ($\mu_0$) | $H_c$ (A/m) | $B_s$ (V s/m²) | $W_1$ (W/kg) | $T_c$ (°C) | *Strip thickness of strip wound cores* (mm) | *Reference* |
|---|---|---|---|---|---|---|---|---|---|---|
| Fe–Si | Trafoperm N2 | C5 | 3 000 | 35 000 | 8 | 2·03 | 0·45 | 750 | 0·3 | 123 |
| | Trafoperm N3 | | 1 000 | 30 000 | 16 | 2·03 | | 750 | Solid core | 123 |
| | Trafoperm W, WF | | 3 000 | 35 000 | 8 | 2·03 | 0·5 | 750 | 0·1 | 123 |
| | Hyperm 1 | A2, A3 | 1 000 | | 40 | 2·0 | 0·9 | 750 | 0·35 | 35 |
| | Hyperm 3 | C2 | 1 500 | | | 2·0 | 0·9 | 750 | 0·35 | 35 |
| | Hyperm 4 | | 800 | | | 2·0 | 0·8 | 750 | 0·35 | 35 |
| | Hyperm 4T | | 1 500 | 20 000 | 8 | 2·0 | 0·55 | 750 | 0·35 | 35 |
| | Hyperm 5T | | 2 500 | 35 000 | 8 | 2·0 | 0·45 | 750 | 0·35 | 35 |
| | Hyperm 7 | | | | 8 | 2·0 | | 750 | 0·35 | 35 |
| | Hyperm 7T | | 4 000 | 35 000 | 8 | 2·0 | 0·45 | 750 | 0·35 | 35 |
| | Imphysil | | | 30 000 | 12 | 1·9 | 1·8 ($W_{1·7}$) | 750 | 0·35 | 104 |
| Fe–Al | Vacodur 16 | | 8 000 | 40 000 | 4 | 0·9 | | 350 | 0·2 | 123, 126 |
| | Alfenol | | 4 000 | 100 000 | 1·9 | 0·76 | | | | 1, 85 |
| | Hypermal | | 4 000 | 30 000 | 8 | 1·4 | | | | 69, 72 |
| | Alperm | | 7 000 | 60 000 | 2·2 | 0·9 | | 350 | | 69, 72 |
| Fe–Co | AFK 1 | | | 2 500 | 160 | 2·4 | 8 ($W_{1·8}$) | | | 102 |
| | AFK 502 | | | 8 000 | 100 | 2·35 | 5 ($W_2$) | | | 102 |
| | Hyperm Co 35 | | | | 200 | 2·4 | | 950 | | 35 |
| | Hyperm Co 50 | | 1 000 | 11 000 | 80 | 2·4 | 1·2 | 950 | 0·2 | 35 |
| | Hyperm Co 50T | | 300 | 70 000 | 20 | 2·4 | 0·7 | 950 | 0·2 | 35, 41a |
| | Vacoflux 48 | | 1 200 | 20 000 | 40 | 2·35 | | 950 | 0·2 | 130 |
| | Vacoflux 50 | | 1 000 | 12 000 | 80 | 2·35 | 2·0 | 950 | 0·3 | 130 |
| | Vacoflux Z | | | 60 000 | 20 | 2·35 | 0·8 | 950 | 0·1 | 130 |
| | Vacoflux S, S2 | | | 10 000 | 80 | 2·35 | | 950 | Sintered solid parts | 130 |
| | V Permendur | | 700–1 000 | 3 000–6 000 | 185 | 2·4 | 8·8 ($W_{1·8}$) | | | 110 |
| | Hiperco | | 650 | 10 000 | 80 | 2·42 | | 970 | | 145 |
| | Supermendur | | | 93 000 | 16 | 2·4 | | 980 | | 41b |

**Table 19.13** SHEET AND STRIP OF Ni–Fe ALLOYS HAVING 36–50% Ni

| *Alloys* | *Material designation* | *DIN 41 301* | $10^{-3}\mu_5$ ($\mu_0$) | $10^{3}\mu_m$ ($\mu_0$) | $H_c$ (A/m) | $B_s$ (V s/m²) | $W_1(W_{0\cdot5})$ (W/kg) | $10^{-3}h/\mu_i^2$ (cm/kA) | $T_c$ (°C) | *Strip thickness of strip-wound cores* (mm) | *Reference* |
|---|---|---|---|---|---|---|---|---|---|---|---|
| 36–48% Ni | Anhyster B | | 2 | 7 | 56 | 1·3 | 1·1 | — | 230 | 0·3 | 103 |
| | Hyperm 36 | D1 | 2 | 8 | — | 1·3 | 1·1 | — | 250 | 0·35 | 35 |
| | Hyperm 36M | | 3 | 16 | 16 | 1·3 | 0·6 | — | 250 | 0·35 | 35 |
| | Magnifer 36W | | 2·5 | 12·5 | 16 | 1·2 | 0·6 | — | — | — | 135 |
| | Niromet 46 | | | 30 | 16 | 1·6 | — | — | 440 | — | 148 |
| | Permalloy B | | 2–5 | 15–40 | 12 | 1·6 | (0·24) | — | 440 | 0·38 | 58a, 69 |
| | Permalloy D | | 2–4 | 12–30 | 12 | 1·3 | (0·44) | — | 380 | 0·38 | 58a, 69 |
| | Permenorm 3601 K1 | D1, D1a | 2 | 8 | 40 | 1·3 | 1·1 | 1·2 | 250 | 0·3 | 123 |
| | Permenorm 3601 K2 | D3 | 3 | 20 | 16 | 1·3 | 0·55 | 3 | 250 | 0·3 | 123 |
| | Permenorm 3601 K3 | | 3 | 15 | 20 | 1·3 | — | — | 250 | Solid core | 123 |
| | Radiometal 36 | | 3 | 20 | 16 | 1·2 | — | — | 280 | — | 118b |
| | Supranhyster 36 | | 2·5 | 20 | 16 | 1·3 | 0·5 | — | 230 | 0·3 | 103 |
| 50% Ni | Anhyster D-DS | | 2·8 | 60 | 8 | 1·6 | 0·4 | | 450 | 0·3 | 103 |
| | Conpernik | | 1·5 | 2 | 40 | 1·6 | 0·7 | | — | | 145 |
| | Deltamax | | 0·4–1·7 | 70–250 | 3–13 | 1·35–1·55 | — | | — | | 9 |
| | H. C. R. alloy | | — | 100 | 10·4 | 1·56–1·60 | — | | — | | 118c |
| | Hipernik | | 4 | 100 | 4 | 1·6 | 0·06 | | 500 | | 145 |

| | | | | | | | | | | |
|---|---|---|---|---|---|---|---|---|---|---|
| Hyperm 50 | | 3 | 35 | 6 | 1·5 | — | | 470 | | 35 |
| Hyperm 51 | | 8 | 60 | — | 1·5 | 0·25 | | 470 | 0·1 | 35 |
| Hyperm 52 | | 12 | 80 | — | 1·5 | — | | 470 | | 35 |
| Hyperm 53 | | 50 | 120 | — | 1·5 | 0·12 | | 450 | 0·1 | 35 |
| Hyperm 50T | | 0·25 | — | — | 1·55 | — | | 470 | | 35 |
| Niron 52 | | — | 50 | 8 | 1·6 | — | | 500 | | 148 |
| Permalloy F | | 0·4–1 | 200–400 | 4 | 1·4 | $W_{1\cdot4}$=0·66 | | 550 | 0·1 | 58a |
| Permax M | | 50 | 125 | 1·2 | 1·5 | 0·09 | | — | 0·1 | 129a |
| Permenorm 5000 Z | | — | 50 | 12 | 1·55 | — | 40 | 470 | 0·1 | 123, 124 |
| Permenorm 5000 H2 | F3 | 6–12 | 60–80 | 4 | 1·55 | 0·1 | 50 | 470 | 0·2 | 123, 124 |
| Permenorm 5000 H3 | | 5 | 35 | 8 | 1·55 | 0·25 | 55 | 470 | Solid core | 123, 124 |
| Permenorm 5000 S | | 5 | 35 | 6·4 | 1·6 | — | | 470 | Solid core | 123, 124 |
| Radiometal 50 | | 3·5 | 30 | 12 | 1·6 | — | | 500–550 | | 118b |
| Rectimphy | | — | 100 | 8–16 | 1·6 | — | | 475 | | 102 |
| Sendelta | | — | — | 9·6 | 1·53 | — | | — | | 120a |
| Superradiometal 50 | | 10 | 100 | 3·2 | 1·6 | — | | 500–550 | | 118b |
| Supranhyster 50 | | 5 | 90 | 0·5 | 1·6 | 0·3 | | 450 | 0·3 | 103 |
| Textur-Isoperm | | 0·11 | 1·8 | 52 | 1·6 | 6·6 | | 470 | | 123, 124 |
| Viperm 5 B | | 5 | 38 | — | 1·3 | (0·085) | | — | | 137a |

**Table 19.14** SHEET AND STRIP OF Ni–Fe ALLOYS HAVING 60–80% Ni

| *Material designation* | *DIN 41 301* | $10^{-3}\mu_5$ ($\mu_0$) | $10^{-3}\mu_m$ ($\mu_0$) | $H_c$ (A/m) | $B_s$ (V s/m²) | $W_{0\cdot5}$ (W/kg) | $10^{-6}h/\mu_i^2$ (cm/kA) | $T_c$ (°C) | *Strip thickness of strip-wound cores* (mm) | *Reference* |
|---|---|---|---|---|---|---|---|---|---|---|
| Balco | | — | 250 | 2·4 | 1·25 | — | | 610 | | 148 |
| Hyperm 766 | E3 | 35 | 90 | 2·4 | 0·8 | 0·025 | | 400 | 0·1 | 35 |
| Hyperm 800 | E4 | 65 | 130 | — | 0·8 | — | | 400 | | 35 |
| Hyperm 900 | | 80 | 150 | 0·8 | 0·8 | — | | 400 | | 35 |
| Hyperm Max | | 125 | 280 | — | 0·8 | — | | 400 | 0·05 | 35 |
| M1040 | | 75 | 150 | 0·8 | 0·58 | 0·015 | | 270 | 0·1 | 123, 124 |
| M1040 | | 40 | 80 | 1·2 | 0·58 | — | 100 | 270 | Solid core | 123, 124 |
| Magnifer 75 | E3 | 20 | 70 | — | — | 0·1 | | 430 | | 136 |
| Mumetall | E3 | 45 | 120 | 1·2 | 0·8 | 0·025 | | 400 | 0·2 | 123, 124 |
| Mumetall | | 25 | 60 | 2·8 | 0·8 | — | 200 | 400 | Solid core | 123, 124 |
| Mumetal | | 35 | 100 | 1·6 | 0·85 | 0·45 | | — | 0·3 | 103 |
| Mumetal 40 | | 48 | 150 | 1·6 | 0·75 | — | | 390 | | 118a |
| Permalloy C | | 25–50 | 70–150 | 2·4 | 0·8 | 0·9 | | 380 | 0·1 | 58a, 69 |
| Permalloy Super C | | 50–80 | 200–300 | 0·64 | 0·8 | 0·018 | | 380 | 0·1 | 58a |
| Permax F | | — | — | 4–16 | 1·25 | — | | 520 | 0·05 | 129a |
| Permax Z | | — | 250 | 2 | 1·25 | 0·07 | | 520 | 0·05 | 123 |
| Permimphy 1 | | 50 | 160 | 1·2 | 0·85 | 0·025 | | 350 | 0·15 | 103 |
| Permimphy 2 | | 75 | 250 | 0·8 | 0·85 | 0·02 | | 350 | 0·15 | 103 |
| Permimphy 3 | | 110 | 300 | 0·56 | 0·85 | 0·015 | | 350 | 0·15 | 103 |

| | | | | | | | | | | |
|---|---|---|---|---|---|---|---|---|---|---|
| Supermalloy | | 55–120 | 300–900 | 0·24–0·75 | 0·65–0·78 | — | | 400 | | 9, 69 |
| Supermumetal 50 | | 50 | 200 | 0·8 | 0·8 | — | | 390 | | 118b |
| Supermumetal 100 | | 100 | 250 | 0·6 | 0·8 | — | | 390 | | 118b |
| Ultraperm 10 | | 130 | 300 | 0·5 | 0·8 | 0·01 | 70 | 400 | 0·05 | 123, 124 |
| Ultraperm F | | — | — | 0·8–4 | 0·8 | — | | 410 | 0·05 | 129a |
| Ultraperm Z | | — | 250 | 0·8 | 0·78 | 0·027 | | 410 | 0·05 | 123, 124 |
| Vacoperm 100 | E4 | 75 | 250 | 0·8 | 0·78 | 0·015 | | 400 | 0·1 | 123, 124 |
| Vacoperm 100 | | 40 | 100 | 1·2 | 0·8 | — | | — | Solid core | 123, 124 |
| Viperm 10 | | 16 | 70 | — | 1·1 | 0·047 | | 460 | | 137a |
| 4-79Mo-Permalloy | | 10–40 | 70–250 | 1·6–5·6 | 0·65–0·8 | — | | — | | 9, 148 |

to yield normal or squared hysteresis loops, leading to entirely different fields of application. Magnetically soft alloys are therefore very flexible and lend themselves to being tailored, to a considerable degree, to suit a variety of requirements; thus DIN values serve as no more than guidelines.

In Tables 19.12–19.14 certain materials are listed which can be related —partly according to the manufacturer—to the DIN classes. The values of $\mu_{rev}$ missing from these tables are shown in Figure 19.1, for certain types of sheet, as a function of flux density.

### 19.1.3 Ferrites for inductance coils and communications transformers

As for metallic alloys, the magnetic properties of ferrites used in coils and communications transformers are usually based on toroid measurements. This is also the way the values in the ferrite-manufacturers' tables are reached. There is a certain difficulty here, namely the translation of these values to make them relevant to bodies of other shapes. Departures from the toroidal values are sometimes observed in practice for pot cores and are traceable to the fact that in a toroid the material is more simply and compactly distributed than in a complex pot core with its slots and grooves. Again, the ratio of surface to volume, particularly for the smaller pot cores, is generally greater than for toroids, so the regulation of atmospheric conditions during sintering becomes more critical. Moreover, flux distribution is not so uniform in a pot core and this gives rise to higher hysteresis losses. To master all these difficulties demands much experience and knowledge on the part of the manufacturer of ferrite parts.

In classifying the various sorts of ferrite that can be used for inductance coils and weak-current transformers, the frequency range in which the ferrite will operate is a useful preliminary criterion. To characterise one of these ferrites it is usual to plot the loss factor, referred to the initial permeability, against frequency. Some examples of this dependence of $(\tan \delta)/\mu_i$ have already been shown in Figure 13.88. The various types of ferrites offered by individual suppliers can thus, in a general way, be grouped together. At low frequencies, up to a few megahertz, Mn–Zn ferrites are generally used, and, at higher frequencies, Ni–Zn ferrites.

It appears from Figure 13.88, as also from Figures 19.2 and 19.3 which give further practical examples, that the ranges of individual ferrite types often intersect and overlap and that in many frequency ranges several sorts are offered, differing among themselves in their quality factors; whereas it might be thought that, in a given case, it would be enough to quote that type which has the least $(\tan \delta)/\mu_i$. This is connected with the fact that $(\tan \delta)/\mu_i$ is not the only criterion for the usability of a ferrite core in a given coil. The hysteresis loss, the disaccommodation, the temperature coefficient, and, not least, the cost—determined both by the nature of the raw material and by the manufacturing process—can be decisive for the choice of a core material. Thus, convenient as a graphical plot of $(\tan \delta)/\mu_i$ may be for a preliminary selection, it must be supplemented by further data (see Table 6.11).

The properties of some commercially available ferrites are listed in Tables 19.15 and 19.16.

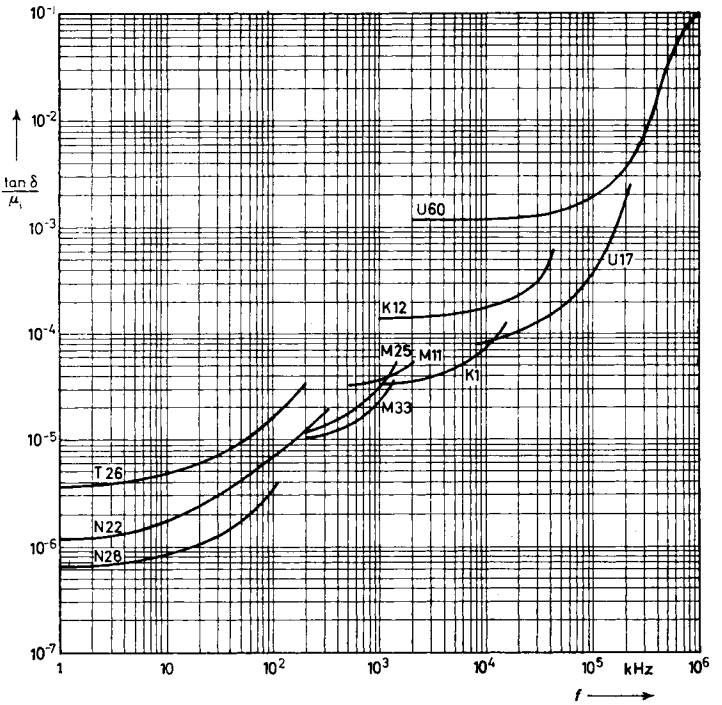



*Figure 19.2. Characteristics of some types of Siferrit*[101]

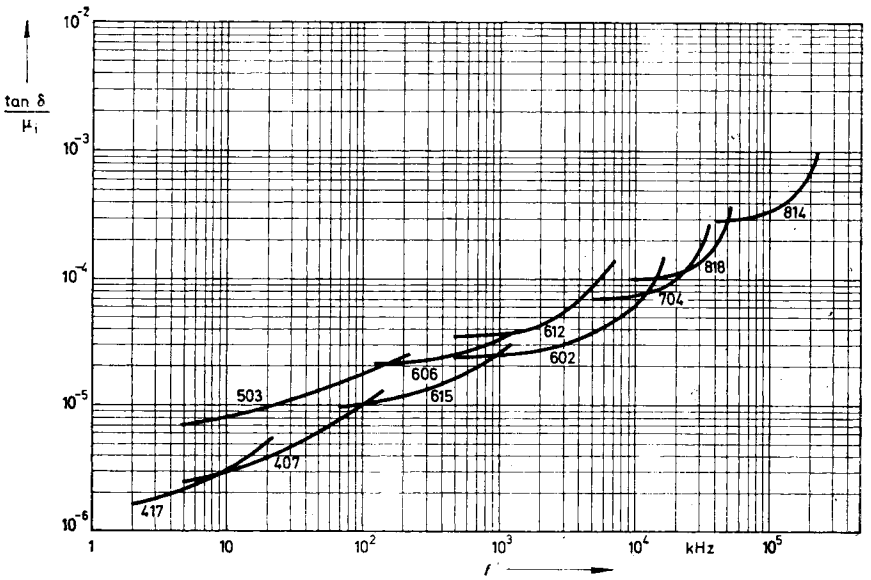



*Figure 19.3. Characteristics of some types of Keraperm*[114]

**Table 19.15** FERRITES FOR CORES OF INDUCTION COILS AND COMMUNICATIONS TRANSFORMERS,

| *Material* | $\mu_i$ ($\mu_0$) | $T_c$ (°C) | $d$ (g/cm³) | $\varrho$ (Ω cm) | $B_m$ $\left(\frac{Vs}{m^2}\right)$ ($H$) (A/m) | ($f$) (kHz) | $\frac{10^6 \tan \delta}{\mu_i}$ |
|---|---|---|---|---|---|---|---|
| Ferroxcube 3B | 900 | >150 | 4·7–4·9 | > 20 | 0·34 (800) | | |
| 3B3 | 900 | >150 | 4·7–4·9 | >100 | 0·34 (800) | (250) | <27 |
| 3B5 | 1 400 | >150 | 4·7–4·9 | > 20 | 0·34 (800) | (100) | <10 |
| 3B7 | 2 300 | >170 | 4·7–4·9 | >100 | 0·34 (800) | (100) | < 5 |
| 3C2 | 900 | >150 | 4·7–4·9 | > 10 | 0·35 (800) | | |
| 3C6 | 1 200 | >190 | 4·8–4·9 | >100 | 0·42 (800) | | |
| 3C8 | 1 200 | >190 | 4·8–4·9 | >100 | 0·45 (800) | | |
| 3D3 | 750 | >150 | 4·5–4·9 | >150 | 0·35 (800) | (100) | < 8 |
| 3E1 | 2 700 | >125 | 4·7–4·9 | > 30 | 0·35 (800) | (100) | <15 |
| 3E2 | > 5 000 | >130 | 4·7–4·9 | > 10 | 0·42 (800) | (100) | <15 |
| 3E3 | >10 000 | >130 | 4·8–4·95 | > 5 | 0·40 (800) | (100) | <50 |
| 3H1 | 2 300 | >130 | 4·7–4·9 | >100 | 0·34 (800) | (100) | < 5 |
| Hyperox D1S2 | 2 400 | 170 | | | | (100) | < 5 |
| D1S3 | 2 200 | 210 | | | | (100) | < 5 |
| D1S5 | 800 | 200 | | | | (100) | <25 |
| D1S1 | 3 500 | 175 | | | | (100) | <10 |
| D1S11 | 5 000 | 120 | | | | (100) | <20 |
| Keraperm 407 | 1 200 | >150 | | >100 | 0·38 (800) | (50) | 6·5 |
| 417 | 2 400 | >100 | | >100 | 0·43 (800) | (50) | 12 |
| 421 | 4 000 | >150 | | > 20 | 0·40 (800) | (50) | 13·5 |
| Siferrit N22 | 1 500 | >145 | 4·8 | 100 | 0·38 (3 000) | (200) | <20 |
| N27 | 2 000 | >200 | 4·8 | 100 | 0·43 (3 000) | | |
| T26 | 2 200 | >150 | 4·8 | 100 | 0·39 (3 000) | | |
| N28 | 2 200 | >150 | 4·7 | 100 | 0·39 (3 000) | (100) | < 5 |
| N29 | 2 400 | >150 | 4·7 | 100 | 0·39 (3 000) | (100) | < 5 |
| N30 | 3 500 | >130 | 4·8 | 50 | 0·39 (3 000) | | |
| T35 | 5 000 | >130 | 4·8 | 40 | 0·38 (3 000) | | |
| T38 | 10 000 | >130 | 4·9 | 20 | 0·38 (3 000) | | |
| Telefunken K5 | 6 000 | >100 | | 40 | 0·30 (1 000) | (20) | 3·5 |
| K4 | 4 000 | >120 | | 40 | 0·36 (1 000) | (20) | 3 |
| M3 | 2 400 | >150 | | 100 | 0·40 (1 000) | (100) | 4 |
| M10 | 2 500 | >180 | | 100 | 0·46 (1 000) | (100) | 4 |
| M4 | 850 | >200 | | 100 | 0·44 (1 000) | (1 000) | 15 |

I: HIGH-PERMEABILITY FERRITES FOR LOW FREQUENCIES (IN GENERAL, Mn–Zn FERRITES)

| $(f)$ (kHz) | $\frac{10^{-3}h}{\mu_i^2}$ (cm/kA) | $(\Delta T)$ (°C) | $\frac{\alpha}{\mu_i}$ (ppm/K) | $10^6 D$ | $H_c$ (A/m) | *Reference* |
|---|---|---|---|---|---|---|
| | | (20–50) | 0–3 | | | 132 |
| (4) | $<8{\cdot}2$ | (20–50) | 0–2 | $<11$ | | 132 |
| (4) | $<1{\cdot}7$ | (20–50) | 0·5–2·3 | $<7{\cdot}5$ | | 132 |
| (4) | $<1{\cdot}25$ | (20–70) | $-0{\cdot}6$–$0{\cdot}6$ | $<4{\cdot}3$ | | 132 |
| | | | | | | 132 |
| | | | | | | 132 |
| | | | | | | 132 |
| (100) | $<2{\cdot}1$ | (20–70) | 0–2 | $<12$ | | 132 |
| (4) | $<2{\cdot}75$ | (20–50) | 0–4 | $<6$ | | 132 |
| (4) | $<1{\cdot}25$ | | | $<1{\cdot}9$ | | 132 |
| (4) | $<1{\cdot}25$ | | | $<1{\cdot}9$ | | 132 |
| (4) | $<1{\cdot}25$ | (5–70) | 0·5–1·5 | $<4{\cdot}3$ | | 132 |
| (5) | $<1$ | (23–60) | 0·5–1·5 | $<4$ | | 36 |
| (5) | $<1$ | (23–60) | $\pm 0{\cdot}5$ | $<4$ | | 36 |
| (5) | $<1{\cdot}5$ | (23–60) | 2·0 | $<10$ | | 36 |
| (5) | $<1{\cdot}5$ | (23–60) | 1·5 | $<6$ | | 36 |
| (5) | $<1{\cdot}5$ | | | | | 36 |
| | | (20–70) | 2 | | 15 | 114 |
| | | (20–70) | 3 | | 16 | 114 |
| | | (20–70) | 2 | | 10 | 114 |
| (20) | $<1{\cdot}5$ | (20–55) | 0·8–1·8 | $<8$ | 30 | 101 |
| | | (20–55) | 5 | | 20 | 101 |
| (20) | $<2$ | (20–55) | 0–3 | | 20 | 101 |
| (20) | $<1$ | (20–55) | 0·5–1·5 | $<6$ | 20 | 101 |
| (20) | $<1$ | (20–55) | $\pm 0{\cdot}6$ | $<6$ | 20 | 101 |
| (20) | $<1{\cdot}5$ | (20–55) | 1 | | 15 | 101 |
| (20) | $<1{\cdot}5$ | | | | 10 | 101 |
| (20) | $<1$ | | | | 4 | 101 |
| (20) | 0·7 | (25–65) | 1·5 | 1 | | 2a |
| (20) | 0·5 | (25–65) | 1·5 | 1 | | 2a |
| (20) | 0·5 | (25–65) | 1 | 3 | | 2a |
| (20) | 0·8 | (−20 to +70) | $-0{\cdot}1$ | 4 | | 2a |
| (20) | 1 | (25–65) | 1·5 | 10 | | 2a |

| *Material* | $\mu_i$ ($\mu_0$) | $T_c$ (°C) | $d$ (g/cm³) | $\varrho$ (Ω cm) | $B_m$ $\left(\frac{Vs}{m^2}\right)$ ($H$) (A/m) | ($f$) (kHz) | $\frac{10^6 \tan \delta}{\mu_i}$ |
|---|---|---|---|---|---|---|---|
| Fermalite 1002 | 1 800 | >160 | 4·4 | 200 | 0·38 (800) | (250) | <11 |
| 1004 | 1 500 | >140 | 4·4 | 200 | 0·35 (800) | (100) | <10 |
| 1005 | 1 000 | >170 | 4·4 | 400 | 0·38 (800) | (500) | <14 |
| 2002 | 2 500 | >150 | 4·2 | 50 | 0·35 (800) | (100) | < 9 |
| 2003 | 4 000 | >150 | 4·6 | 25 | 0·35 (800) | | |
| 2005 | 2 500 | >150 | 4·2 | 50 | 0·35 (800) | (100) | < 9 |
| Ferrinox T4 | 6 000 | >130 | | | 0·35 (800) | (20) | < 6·5 |
| T5 | 4 000 | >140 | | | 0·35 (800) | (50) | < 4 |
| T6 | 3 500 | >160 | | | 0·41 (800) | (50) | < 6 |
| T10 | 2 200 | >160 | | | 0·41 (800) | (100) | < 5 |
| T14 | 2 200 | >160 | | | 0·41 (800) | (100) | < 5 |
| T22 | 1 500 | >160 | | | 0·38 (800) | (100) | <10 |
| T31 | 750 | >220 | | | 0·42 (1 600) | (100) | < 8 |
| Stanferite SA 500L | 2 000 | >150 | 4·7 | | 0·33 (800) | (100) | < 6·7 |
| SA 500T | 2 100 | >150 | 4·7 | | 0·39 (800) | (100) | < 8 |
| SA 502 | 2 250 | >150 | 4·7 | | 0·39 (800) | (100) | < 5 |
| SA 503 | 2 250 | >150 | 4·7 | | 0·39 (800) | (100) | < 5 |
| SA 601 | 3 500 | >150 | 4·7 | | 0·39 (800) | (100) | <10 |
| SA 611 | 5 000 | | | | | | |
| TDK H5A | 3 300 | >130 | 4·8 | | 0·41 (1 200) | (100) | <10 |
| H5B | 5 000 | >130 | 4·8 | | 0·42 (1 200) | (100) | <40 |
| H5C2 | 10 000 | >120 | 4·8 | | 0·38 (1 200) | (10) | < 7 |
| H6A | 2 000 | >130 | 4·6 | | 0·35 (1 200) | (100) | < 3·5 |
| H6B | 2 000 | >130 | 4·6 | | 0·35 (1 200) | (100) | < 2·5 |
| H7A | 4 500 | >200 | 4·8 | | 0·46 (1 200) | (100) | <20 |
| Tokin 801 F | 800 | >160 | 4·6 | 4 000 | 0·40 (800) | (500) | <20 |
| 1801 F | 1 800 | >145 | 4·8 | 200 | 0·39 (800) | (100) | < 4·5 |
| 2001 F | 2 000 | >150 | 4·7 | 700 | 0·40 (800) | (100) | < 2·3 |
| 2000 H | 2 000 | >120 | 4·9 | 2 000 | 0·10 (800) | (100) | <15 |
| 4000 H | 4 000 | >140 | 4·9 | 5 | 0·10 (800) | (100) | <35 |
| 5000 H | 5 000 | >125 | 4·9 | 20 | 0·095 (800) | (100) | <50 |
| 7000 H | 7 000 | >110 | 5·0 | 8 | 0·06 (800) | (100) | <45 |

*Table 19.15 continued*

| $(f)$ (kHz) | $\frac{10^{-3}h}{\mu_i^2}$ (cm/kA) | $(\Delta T)$ (°C) | $\frac{\alpha}{\mu_i}$ (ppm/K) | $10^6 D$ | $H_c$ (A/m) | *Reference* |
|---|---|---|---|---|---|---|
| | $<1$ | (10–60) | $-1{\cdot}2$ to $+1{\cdot}2$ | $<12$ | 8 | 64 |
| | $<1{\cdot}5$ | (10–60) | 0·4–1·4 | $<6$ | 8 | 64 |
| | $<1{\cdot}5$ | ($-40$ to $+100$) | 0·72 | | 16 | 64 |
| | $<1$ | (10–60) | $-0{\cdot}5$ to $+1{\cdot}5$ | $<6$ | 8 | 64 |
| | $<1$ | | | $<6$ | 8 | 64 |
| | $<1$ | (10–60) | $-0{\cdot}5$ to $+0{\cdot}5$ | $<6$ | 8 | 64 |
| (20) | $<0{\cdot}75$ | (20–60) | $-0{\cdot}5$ to $+1{\cdot}5$ | $<5$ | 6·4 | 20 |
| (20) | $<0{\cdot}75$ | (20–60) | 0·5–1·5 | $<5$ | 9·6 | 20 |
| (20) | $<0{\cdot}75$ | (20–60) | 0–2 | $<5$ | 12 | 20 |
| (20) | $<1$ | ( 0–60) | $\pm 0{\cdot}6$ | $<5$ | 24 | 20 |
| (20) | $<1$ | ( 0–60) | $1\pm 0{\cdot}5$ | $<5$ | 24 | 20 |
| (20) | $<2$ | (20–60) | 0·8–2 | $<8$ | 24 | 20 |
| (20) | $<2$ | ( 0–60) | 0–2·5 | $<15$ | 60 | 20 |
| (4) | $<1{\cdot}1$ | (23–55) | 0·5–1·5 | $<7$ | 32 | 111 |
| (4) | | (23–55) | $-1$ to $+3$ | | 32 | 111 |
| (4) | $<0{\cdot}75$ | (23–55) | $0\pm 0{\cdot}5$ | $<4$ | 32 | 111 |
| (4) | $<0{\cdot}75$ | (23–55) | 0·5–1·5 | $<4$ | 32 | 111 |
| (4) | $<0{\cdot}9$ | (23–55) | $-2$ to $+2$ | $<8$ | 32 | 111 |
| (4) | $<1{\cdot}24$ | (23–70) | $-1$ to $+2$ | | | |
| | | ($-30$ to $+70$) | $-0{\cdot}5$ to $+2{\cdot}0$ | $<3$ | 8 | 118d |
| | | ($-30$ to $+70$) | $-0{\cdot}5$ to $+2{\cdot}0$ | $<3$ | 8 | 118d |
| | | ($-30$ to $+70$) | 0–1·5 | $<2$ | 7·2 | 118d |
| | | ($-30$ to $+70$) | 0–2·5 | $<3$ | 24 | 118d |
| | | ($-30$ to $+70$) | 0·5–2·5 | $<3$ | 20 | 118d |
| | | ($+20$ to $+70$) | $-2{\cdot}5$ to 0 | $<3$ | 16 | |
| | | (0–60) | 0–5 | 60 | 40 | 120b |
| | | (0–60) | 0·5–2 | 3 | 30 | 120b |
| | | (0–60) | 0·5–1·5 | 5 | 25 | 120b |
| | | (0–60) | 0–3 | 10 | 12 | 120b |
| | | (0–60) | $-0{\cdot}5$ to $+2$ | 2 | 10·4 | 120b |
| | | (0–60) | 0–3 | 2 | 8 | 120b |
| | | (0–60) | 0–2 | 2 | 4·8 | 120b |

**Table 19.16** FERRITES FOR CORES OF INDUCTORS AND TRANSFORMERS, II: FERRITES WITH

| *Material* | | $\mu_i$ ($\mu_0$) | $T_c$ (°C) | $d$ (g/cm³) | $\varrho$ (Ω cm) | $B_m$ ($H$) ($\frac{Vs}{m^2}$)(kA/m) | ($f$) (MHz) | $10^6 \tan\delta / \mu_i$ |
|---|---|---|---|---|---|---|---|---|
| Ferroxcube | 4A3 | 450 | 125 | 4·7–5·1 | $>10^5$ | — | (2) | $<$ 70 |
| | 4A4 | 500 | 125 | 4·7–5·1 | $>10^5$ | 0·27 (0·8) | (2) | $<$ 70 |
| | 4B1 | 250 | 250 | 4·4–4·8 | $>10^5$ | 0·33 (1·6) | (1) | $<$ 90 |
| | 4C1 | 125 | 350 | 4·2–4·6 | $>10^5$ | 0·28 (2·4) | (3) | $<$160 |
| | 4C6 | 120 | 350 | 4–5 | $>10^5$ | 0·38 (2·4) | (10) | $<$100 |
| | 4D1 | 50 | 400 | 4–4·4 | $>10^5$ | 0·24 (3·2) | (10) | $<$300 |
| | 4E1 | 15 | 500 | 3·5–4 | $>10^5$ | 0·18 (4·8) | (20) | $<$300 |
| Hyperox | E4 | 400 | 350 | | $>10^5$ | 0·45 (1) | (0·2) | 20–30 |
| | E5 | 150 | 400 | | $>10^5$ | 0·43 (4) | (0·5) | 80–100 |
| | E7 | 30 | 600 | | $>10^5$ | 0·23 (1) | (10) | 400–600 |
| Keraperm | 606 | 300 | $>$130 | | $>10^6$ | 0·29 (4) | (1·5) | 42 |
| | 612 | 200 | $>$300 | | $>10^6$ | 0·30 (4) | (1·5) | 40 |
| | 602 | 125 | $>$350 | | $>10^7$ | 0·38 (4) | (5) | 35 |
| | 704 | 40 | $>$300 | | $>10^6$ | 0·25 (4) | (10) | 75 |
| | 818 | 25 | $>$300 | | $>10^6$ | 0·26 (4) | (20) | 110 |
| | 814 | 12 | $>$400 | | $>10^8$ | 0·22 (4) | (100) | 340 |
| Neosid | F03 | 1 000 | 150 | | $10^2$ | | (0·5) | ~20 |
| | F1 | 500 | 170 | | $10^3$ | | (1) | ~25 |
| | F2 | 250 | 300 | | $10^3$ | | (2) | ~40 |
| | F5is | 140 | 250 | | $10^9$ | | (5) | ~90 |
| | F10b | 100 | 300 | | $10^6$ | | (10) | ~90 |
| | F20 | 40 | 350 | | $10^5$ | | (20) | ~130 |
| | F40 | 25 | 400 | | $10^7$ | | (40) | ~300 |
| | F100 | 10 | 450 | | $10^8$ | | (100) | ~400 |
| Siferrit | M33 | 600 | $>$200 | 4·5 | $5\times10^2$ | 0·4 (3) | (1) | $<$ 30 |
| | M11 | 250 | $>$170 | 4·6 | $10^7$ | 0·34 (3) | (2) | $<$ 50 |
| | K1 | 80 | $>$350 | 4·4 | $10^7$ | 0·36 (3) | (12) | $<$ 100 |
| | K12 | 24 | $>$400 | 4·2 | $10^7$ | 0·15 (3) | (40) | $<$ 600 |
| | U17 | 10 | $>$500 | 4·1 | $10^7$ | — | (220) | $<$1 700 |
| | U60 | 9 | $>$250 | 4·8 | $10^7$ | 0·11 (3) | (350) | 9 500 |
| Telefunken | M7 | 100 | $>$400 | | $10^8$ | — | (10) | 50 |
| | M8 | 18 | $>$450 | | $10^8$ | — | (100) | 250 |
| | M9 | 80 | $>$350 | | $10^8$ | 0·3 (1) | (10) | 60 |
| | M11 | 24 | $>$450 | | $10^8$ | 0·25 (1) | (40) | 500 |
| | M12 | 13 | $>$450 | | $10^8$ | 0·2 (1) | (100) | 400 |
| Fernilite | 1102 | 200 | 280 | 4·6 | $>10^5$ | 0·42 | (5) | 67 |
| | 1103 | 100 | 380 | 4·4 | $>10^5$ | 0·39 | (10) | 90 |
| | 1104 | 30 | 480 | 4·2 | $>10^5$ | 0·35 | (30) | 140 |
| | 1105 | 15 | 580 | 3·7 | $>10^5$ | 0·25 | (100) | 280 |
| | 1112 | 150 | 340 | 4·6 | $>10^5$ | 0·35 | (5) | 38 |
| | 1113 | 75 | 400 | 4·4 | $>10^5$ | 0·30 | (10) | 83 |

LOWER PERMEABILITY FOR MEDIUM AND HIGH FREQUENCIES (IN GENERAL, Ni–Zn FERRITES)

| $(f)$ (kHz) | $\frac{10^{-3}h}{\mu_i^2}$ (cm/kA) | $(\Delta T)$ (°C) | $\frac{\alpha}{\mu_i}$ (ppm/K) | $10^6 D$ | $H_c$ (A/m) | *Reference* |
|---|---|---|---|---|---|---|
| (100) | < 2·1 | (20–70) | 5–15 | | | 132 |
| | | (20–50) | 0–8 | | | 132 |
| | | (20–50) | 0–12 | | | 132 |
| (100) | < 7 | (20–50) | 0–6 | | | 132 |
| | | (20–50) | 0–15 | | | 132 |
| | | (20–50) | 0–15 | | | 132 |
| (5) | < 15 | (20–70) | <12 | | 160 | 36 |
| (5) | < 40 | (20–70) | <15 | | 320 | 36 |
| (5) | <150 | (20–70) | <20 | | 800 | 36 |
| | | (20–70) | 8 | | 100 | 114 |
| | | (20–70) | 8 | | 150 | 114 |
| | | (20–70) | 25 | | 250 | 114 |
| | | (20–70) | 20 | | 400 | 114 |
| | | (20–70) | 20 | | 1 000 | 114 |
| | | (20–70) | 40 | | 1 700 | 114 |
| | | | | | | 86a |
| | | | | | | 86a |
| | | | | | | 86a |
| | | | | | | 86a |
| | | | | | | 86a |
| | | | | | | 86a |
| | | | | | | 86a |
| | | | | | | 86a |
| (20) | < 2 | (20–55) | 0·5–2·5 | <15 | 100 | 101 |
| (20) | < 4 | (20–55) | 14 | | 150 | 101 |
| (20) | < 40 | (20–55) | 1–6 | <35 | 500 | 101 |
| (20) | < 50 | (20–55) | 1–10 | <50 | 1 200 | 101 |
| (20) | < 10 | (20–55) | 20–90 | | 1 500 | 101 |
| | | (20–55) | 100–350 | | 1 000 | 101 |
| (20) | 10 | (20–65) | 3 | | | 2a |
| (20) | | (25–65) | 20 | | | 2a |
| (20) | 33 | (−20 to +70) | 55 | 27 | | 2a |
| (20) | 40 | (25–65) | 6 | 35 | | 2a |
| (20) | | (25–65) | 60 | | | 2a |
| | | (10–60) | 15 | | 100 | 64 |
| | | (10–60) | 20 | | 320 | 64 |
| | | (10–60) | 30 | | 480 | 64 |
| | | (10–60) | 40 | | 1 200 | 64 |
| | | (−40 to +100) | 17 | | 135 | 64 |
| | | (−40 to +100) | 29 | | 320 | 64 |

| *Material* | | $\mu_i$ ($\mu_0$) | $T_c$ (°C) | $d$ (g/cm³) | $\varrho$ (Ω cm) | $B_m$ $\left(\frac{Vs}{m^2}\right)$ ($H$) (kA/m) | ($f$) (MHz) | $10^6 \tan\delta / \mu_i$ |
|---|---|---|---|---|---|---|---|---|
| Ferramic | Q1 | 125 | 350 | | | 0·33 | (1) | 21 |
| | Q2 | 40 | 450 | | | 0·24 | (10) | 90 |
| | Q3 | 16 | 500 | | | 0·26 | (100) | 430 |
| | TC4 | 95 | 425 | | | 0·33 | (10) | 120 |
| Ferrinox | H20 | 250 | >320 | 4·4 | | 0·3 (1·6) | (2) | < 50 |
| | H30 | 100 | >400 | 4·4 | | 0·35 (4·8) | (10) | < 100 |
| | H32 | 80 | >400 | 4·2 | | 0·35 (4·8) | (10) | < 100 |
| | H50 | 40 | >450 | 4·3 | | 0·3 (4·8) | (20) | < 250 |
| | H52 | 25 | >450 | 4·1 | | 0·3 (4·8) | (40) | < 400 |
| | H60 | 15 | >550 | 4·2 | | 0·27 (16) | (40) | < 300 |
| TDK | K5 | 290 | >280 | 4·7 | | 0·33 (1·2) | (5) | < 105 |
| | K6a | 70 | >350 | 4·7 | | 0·30 (2·4) | (10) | < 60 |
| Tokin | 10L | 10 | >500 | 4·4 | $10^6$ | 0·2 (8) | (200) | < 1 000 |
| | 20L | 20 | >500 | 4·3 | $10^6$ | 0·22 (8) | (100) | < 190 |
| | 40L | 40 | >400 | 4·5 | $3\times10^5$ | 0·23 (4) | (10) | < 75 |
| | 80L | 80 | >400 | 4·5 | $10^5$ | 0·25 (0·8) | (10) | < 65 |
| | 100L | 100 | >350 | 4·5 | $5\times10^5$ | 0·25 (0·8) | (10) | < 100 |
| | 150L | 150 | >350 | 4·5 | $2\times10^5$ | 0·25 (0·8) | (5) | < 80 |
| | 250L | 250 | >320 | 4·4 | $2\times10^6$ | 0·32 (0·8) | (5) | < 90 |
| | 400L | 400 | >140 | 4·4 | $2\times10^6$ | 0·27 (0·8) | (1) | < 30 |
| | 2000L | 2 000 | >100 | 5·2 | $10^4$ | 0·25 (0·4) | (1) | < 360 |

*Table 19.16 continued*

| $(f)$ (kHz) | $\frac{10^{-3}h}{\mu_i^2}$ (cm/kA) | $(\Delta T)$ (°C) | $\frac{\alpha}{\mu_i}$ (ppm/°C) | $10^6 D$ | $H_c$ (A/m) | *Reference* |
|---|---|---|---|---|---|---|
| | | (25–80) | 0–8 | | 167 | 58 |
| | | (25–80) | 0–8 | | 374 | 58 |
| | | (25–200) | 0–24 | | 1 671 | 58 |
| | | (25–60) | 3·5–6·5 | | 254 | 58 |
| | | (20–60) | −5 to +5 | | 80 | 20 |
| | | (20–60) | 0–15 | | 160 | 20 |
| | | ( 0–60) | 1–6 | <35 | 160 | 20 |
| | | (20–60) | 0–40 | | 400 | 20 |
| | | ( 0–60) | 0–10 | | 400 | 20 |
| | | (20–60) | −50 to 0 | | 800 | 20 |
| | | (20–70) | 0–3 | <30 | 80 | 118d |
| | | (−30 to +70) | 2·5–7·5 | <15 | 480 | 118d |
| (50) | 44 | (0–60) | −150 to +150 | 50 | 800 | 120b |
| (50) | 44 | (0–60) | −150 to +150 | 50 | 800 | 120b |
| (50) | 66 | (0–60) | 3–18 | 30 | 640 | 120b |
| (50) | 44 | (0–60) | 0–15 | 6 | 640 | 120b |
| (50) | 33 | (0–60) | 0–6 | 10 | 240 | 120b |
| (50) | 44 | (0–60) | 2–8 | 10 | 240 | 120b |
| (50) | 22 | (0–60) | 0–5 | 20 | 160 | 120b |
| (50) | 9 | (0–60) | 2–8 | 5 | 160 | 120b |
| (50) | 6 | (0–60) | 3–15 | 3 | 16 | 120b |

**Table 19.17** FERRITES AND GARNETS

| *Material* | *Designation* | *Frequency range* (GHz) | *Typical application* |
|---|---|---|---|
| Mg–Mn ferrites | Ferramic R1 | >8·5 | Phase shifter |
| | Ferramic R4 | >7 | Phase shifter, resonance isolator |
| | Raytheon R151 | >3 | Resonance isolator |
| | TDK G 0 | | |
| | TDK G 03 | | |
| | TDK G 10 | | |
| | Trans. Tech. TT 390 | >8·5 | Phase shifter, circulator |
| Mg–Mn–Al ferrites | Airtron C8 | | |
| | Airtron C9c | | |
| | Airtron C43 | | |
| | Ferramic R5 | >2·5 | Phase shifter, isolator |
| | Ferramic R6 | >1 | Phase shifter, isolator |
| | TDK G 139 | | |
| | TDK G 201 | | |
| | Telefunken RF2 | >6 | Circulator, isolator |
| | RF3 | >5 | |
| | RF4 | >3 | |
| | RF6 | >4 | |
| | Tokin 1080 M | >0·5 | Phase shifter |
| | 1140 M | >2 | Phase shifter |
| | 1210 M | >5 | Field displacement |
| | 1230 M | >5 | Resonance isolator |
| | Trans. Tech. TT 1-103 | >2 | Phase shifter, isolator |
| | TT 414 | >2 | |
| | TT 1-109 | >2 | |
| | TT 1-105 | >0·5 | |
| Ni–Zn ferrites | Raytheon R 161 | | |
| | TDK G 40 | | |
| | TDK G 100 | | |
| | Tokin 1480 M | >5 | Faraday rotation |
| | Trans. Tech. TT 2-111 | >30 | Faraday rotation |
| Ni–Co ferrites | Raytheon R 191 | | |
| | Trans. Tech. TT 2-101 | >5 | Faraday rotation isolator |
| | TT 2-118 | >0·5 | Resonance isolator |
| Ni–Al ferrites | Trans. Tech. TT 2-113 | >1 | Phase shifter |

| $J_s$ (V s/m²) | $T_c$ (°C) | ($f$) (GHz) | $\Delta H$ (kA/m) | $\varepsilon'$ ($\varepsilon_0$) | $g_{eff}$ | $d$ (g/cm³) | $\gamma$ $\left(\frac{\text{MHz m}}{\text{A}}\right)$ | Reference |
|---|---|---|---|---|---|---|---|---|
| 0·176 | 290 | | 39 | | | >4·1 | 0·232 | 56 |
| 0·178 | 320 | | 30 | | | >4·15 | 0·227 | 56 |
| 0·22 | 300 | | 36·4 | 12 | | | 0·220 | 98 |
| 0·29 | 330 | | 20 | 14 | | 4·4 | | 118d |
| 0·24 | 300 | | 24 | 12 | | 4·4 | | 118d |
| 0·28 | 300 | | 24 | 12 | | 4·4 | | 118d |
| 0·215 | 320 | | 43·2 | 13 | 2·10 | | | 121 |
| 0·21 | 290 | (9·2) | 40 | 14 | 2·1 | | | 64a |
| 0·15 | 250 | (9·2) | 54 | 11·5 | 2·0 | | | 64a |
| 0·115 | 200 | (9·2) | 26 | 10 | 2·0 | | | 64a |
| 0·111 | 140 | | 17·6 | | | >3·95 | | 56 |
| 0·073 | 100 | | 9·6 | | | >3·90 | | 56 |
| 0·13 | 170 | | 16 | 11 | | 4·2 | | 118d |
| 0·13 | 170 | | 32 | 8 | | | | 118d |
| 0·235 | 290 | (9·3) | 20·8 | 13 | 2·0 | | | 2a |
| 0·175 | 210 | (9·3) | 13·6 | 12·5 | 2·0 | | | 2a |
| 0·123 | 145 | | 9·6 | 12 | 2·0 | | | 2a |
| 0·140 | 155 | | 10·4 | 12 | 2·0 | | | 2a |
| 0·085 | 95 | (1) | 7·2 | 13 | | 4 | | 120c |
| 0·135 | 250 | | 20 | 12 | | 4·3 | | 120c |
| 0·160 | 280 | | 22·4 | 12 | | 4·3 | | 120c |
| 0·210 | 300 | | 28 | 13 | | 4·3 | | 120c |
| 0·057 | 120 | | 6·4 | 11·2 | 2·0 | | | 121 |
| 0·068 | 100 | | 8·0 | 11·5 | 2·02 | | | 121 |
| 0·125 | 166 | | 12·4 | 11·5 | 2·0 | | | 121 |
| 0·170 | 225 | | 16 | 12 | 2·13 | | | 121 |
| 0·32 | 590 | | 38·4 | 13 | | | 0·25 | 98 |
| 0·42 | 300 | | 12 | 16 | | 4·9 | | 118d |
| 0·44 | 310 | | 12 | 13 | | 4·8 | | 118d |
| 0·48 | 330 | (9·5) | 14·4 | 13 | | 5·1 | | 120c |
| 0·50 | 375 | (9·3) | 9·6 | 12·5 | 2·08 | | | 121 |
| 0·30 | 590 | | 18 | 10·5 | | | 0·243 | 98 |
| 0·30 | 585 | (9·3) | 28 | 12·5 | 2·21 | | | 121 |
| 0·18 | 500 | | 72 | 9·5 | 2·55 | | | 121 |
| 0·05 | 160 | (3) | 12·4 | 9·0 | 1·54 | | | 121 |

| *Material* | *Designation* | *Frequency range* (GHz) | *Typical application* |
|---|---|---|---|
| Ni aluminate | Trans. Tech. TT 2-125 | >5 | Resonance isolator |
| | TT 2-115 | >5 | High-power circulator |
| | TT 2-130 | >0·5 | Resonance isolator |
| Y–Fe garnet | TDK Y1 | | |
| | TDK Y2 | | |
| | TDK Y5 | | |
| | TDK Y12 | | |
| | Trans. Tech. G 113 | >1 | |
| | G 300 | | |
| | G 500 | >1 | Y circulator, phase shifter |
| | G 800 | | Phase shifter |
| | G 1200 | | Wide-band circulator |
| | G 1600 | >1 | Phase shifter, isolator |
| Y–Fe–Al garnet | Airtron D 40 | | |
| | YAF 26 | | |
| | YAF 29 | | |
| | YAF 28 | | |
| | Telefunken RG 1 | >1·5 | Circulator |
| | RG 3 | >1·2 | |
| | RG 4 | >2·5 | |
| | RG 5 | >3·5 | |
| | RG 7 | 1·3 | Phase shifter, circulator |
| | RG 8 | | |
| | Tokin 2060 M | >0·5 | Stripline circulator, coaxial circulator |
| | 2070 M | >0·5 | |
| | 2120 M | >0·5 | |
| | 2150 M | >4 | Field displacement |
| | 2160 M | >4 | |
| | 2170 M | >4 | |
| Y–Fe–Gd garnet | Trans. Tech. G 1002 | | Temperature stabilised |
| Special garnets | Hermsdorf M 650 | | |
| | M 651 (T) | | |
| | M 655 | | |

*Table 19.17 continued*

| $J_s$ (V s/m²) | $T_c$ (°C) | ($f$) (GHz) | $\Delta H$ (kA/m) | $\varepsilon'$ ($\varepsilon_0$) | $g_{eff}$ | $d$ (g/cm³) | $\gamma$ $\left(\frac{\text{MHz m}}{\text{A}}\right)$ | *Reference* |
|---|---|---|---|---|---|---|---|---|
| 0·20 | 500 | (9·3) | 34 | 12·8 | 2·31 | | | 121 |
| 0·15 | 450 | (9·3) | 26·3 | 12·0 | 2·45 | | | 121 |
| 0·10 | 400 | | 24 | 12·0 | 2·70 | | | 121 |
| 0·120 | 240 | | 6·4 | 14 | | 4·9 | | 118d |
| 0·095 | 220 | | 6·4 | 14 | | 4·9 | | 118d |
| 0·060 | 180 | | 6·4 | 14 | | 4·9 | | 118d |
| 0·180 | 285 | | 6·4 | 14 | | 4·9 | | 118d |
| 0·178 | 280 | | $<3·6$ | 16 | 2·01 | | | 121 |
| 0·030 | 110 | | $<3·6$ | 14 | 2·00 | | | 121 |
| 0·055 | 160 | | $<5·2$ | 14 | 2·00 | | | 121 |
| 0·08 | 230 | | 4·4 | 14·5 | 1·98 | | | 121 |
| 0·12 | 260 | | $<4·4$ | 15·5 | 1·99 | | | 121 |
| 0·160 | 265 | | $<4$ | 16 | 2·00 | | | 121 |
| 0·038 | 130 | | 3·2 | 14·5 | 2·0 | | | 64a |
| 0·048 | 140 | | 3·2 | 14·5 | 2·0 | | | 64a |
| 0·058 | 160 | | 3·2 | 14·5 | 2·0 | | | 64a |
| 0·100 | 210 | | 3·6 | 15·0 | 2·0 | | | 64a |
| 0·061 | 145 | (9·3) | 2·0 | 14·5 | 2·0 | | | 2a |
| 0·046 | 120 | (9·3) | 3·2 | 14 | 2·0 | | | 2a |
| 0·100 | 150 | (9·3) | 2 | 14·5 | 2·0 | | | 2a |
| 0·133 | 175 | (9·3) | 2 | 15 | 2·0 | | | 2a |
| 0·048 | 130 | (9·3) | 24 | 14 | 1·8 | | | 2a |
| 0·109 | 210 | (9·3) | 4 | 14·5 | 2·0 | | | 2a |
| 0·063 | 175 | | 6·4 | 14 | | 5 | | 120c |
| 0·075 | 190 | | 6·4 | 14 | | 5 | | 120c |
| 0·120 | 240 | | 6·4 | 15 | | 5 | | 120c |
| 0·150 | 260 | | 7·2 | 15 | | 5 | | 120c |
| 0·160 | 270 | | 8 | 15 | | 5 | | 120c |
| 0·170 | 280 | | 8 | 15 | | 5 | | 120c |
| 0·100 | 280 | | 8 | 15 | 2·01 | | | 121 |
| 0·180 | 270 | (9·3) | 5·6 | 15 | | | | 134a |
| 0·068 | 200 | (9·3) | 9·6 | 18 | | | | 134a |
| 0·050 | 250 | (9·3) | 8·0 | 15 | | | | 134a |

### 19.1.4 Ferrites for microwave applications

The suppliers of microwave components (isolators, phase-shifters, circulators, etc.) are often, also, the manufacturers of the ferrites used in their construction but without offering them separately on the market. This practice stems from the fact that ferrite types are sometimes developed to meet a particular application problem and exhibit their optimum properties only when so used. In spite of this there exists a whole series of ferrite types with the help of which the most varied problems can be solved if care is taken to get the best out of them by a proper choice of material and dimensions. A few popular varieties of ferrite are listed in Table 19.17. They are available in the form of tubes, discs, or rods and with either a circular or a rectangular cross-section; very often, if the user does not wish to burden himself with the task, the supplier will make them available in suitable sizes and ready for use.

### 19.1.5 Core materials for storage and switching devices

The most important numerical properties of a few storage cores of various sizes are listed in Tables 19.18–19.20. In comparable types, differences in the properties of cores can, in part, be traced to small differences in the dimensional ratios of the cores, since the nominal values given at the head of the table vary somewhat with different suppliers. Sometimes, however, testing conditions also vary, as can be seen by looking at the columns headed 'd.r.' (disturbance ratio) and 'measuring temperature'. The figures shown in the tables are, in general, guaranteed values which will give the quoted slope when tested with square pulses.

The material properties to be inferred from the hysteresis loop are, in general, no longer quoted for storage cores. On the other hand, these are usually given for switching cores. In this case, it is to be noted that the remanence ratio $R_v = B_r/B_m$, the coercivity $H_c$, and the saturation density play an important part. Usually what is required is a large change of flux for

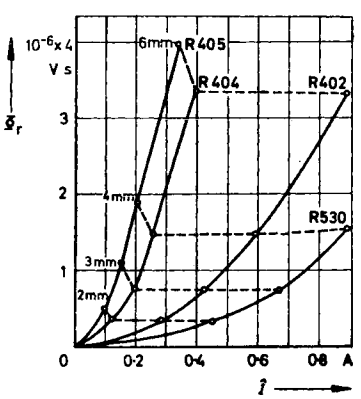



*Figure 19.4. Remanence flux $\Phi_r$ and switching current $\hat{I}$ of some switching toroids for an amplitude $\hat{I} = 1{\cdot}6\, I_c$*[73]

**Table 19.18** FERRITE STORAGE CORES HAVING THE DIMENSIONS 2 mm×1·3 mm×0·6 mm

| *Designation* | *Type* | $I_w$ (mA) | $I_{pw}$ (mA) | $uV_1$ (mV) | $dV_z$ (mV) | $t_s$ (μs) | $t_p$ (μs) | $t_r$ (μs) | *d.r.* (%) | *Measuring temperature* (°C) | *Reference* |
|---|---|---|---|---|---|---|---|---|---|---|---|
| Ferramic | MC 113 | 740 | 470 | ⩾100 | ⩽30 | ⩽1·3 | 0·56 | 0·2 | 63 | 24 | 57 |
| | MC 151 | 360 | 220 | ⩾ 35 | ⩽ 8 | ⩽4·0 | 1·8 | 0·5 | 61 | 24 | 57 |
| | MC 169 | 560 | 340 | ⩾120 | ⩽38 | ⩽1·15 | ⩽0·51 | 0·2 | 61 | 24 | 57 |
| Ferroxcube | 6B2 | 405 | 247 | ⩾ 72 | ⩽24 | ⩽2·1 | 0·75–1·0 | 0·3 | 61 | 40 | 134 |
| Siferrit | R 530 | 400 | 220 | 75 | 16 | 2·0 | 0·95 | 0·2 | 55 | 25, 40 | 101 |
| | R 450 | 700 | 450 | 110 | 12 | 2·1 | 0·9 | 0·25 | 55 | 25, 60 | 101 |

**Table 19.19** FERRITE STORAGE CORES HAVING THE APPROXIMATE DIMENSIONS 1·3 mm × 0·8 mm × 0·35 mm

| *Designation* | *Type* | $I_w$ (mA) | $I_{pw}$ (mA) | $uV_1$ (mV) | $dV_2$ (mV) | $t_s$ (μs) | $t_p$ (μs) | $t_r$ (μs) | *d.r.* (%) | *Measuring temperature* (°C) | *Reference* |
|---|---|---|---|---|---|---|---|---|---|---|---|
| Ferramic | MC 138 | 450 | 285 | ≥ 45 | < 9 | ≤1·25 | 0·56 | 0·2 | 63 | 24 | 57 |
| | MC 140 | 400 | 245 | ≥ 45 | <11 | ≤1·25 | 0·58 | 0·2 | 61 | 24 | 57 |
| | MC 147 | 260 | 158 | ≥ 20 | < 4 | ≤2·2 | 1·2 | 0·5 | 61 | 24 | 57 |
| | MC 161 | 630 | 385 | ≥100 | <18 | ≤0·65 | 0·35 | 0·2 | 61 | 24 | 57 |
| | MC 163 | 750 | 455 | ≥110 | <30 | ≤0·55 | 0·29 | 0·2 | 61 | 24 | 57 |
| | MC 165 | 380 | 220 | ≥ 70 | <12 | ≤1·25 | 0·70 | 0·5 | 58 | 24 | 57 |
| | MC 167 | 300 | 180 | ≥ 45 | <12 | ≤1·5 | 0·80 | 0·5 | 60 | 24 | 57 |
| | MC 171 | 320 | 195 | ≥ 40 | < 8 | ≤1·6 | 0·83 | 0·5 | 61 | 24 | 57 |
| | MC 175 | 380 | 220 | ≥ 40 | < 8 | ≤1·25 | 0·68 | 0·5 | 58 | 24 | 57 |
| | MC 176 | 470 | 280 | ≥ 72 | <21 | ≤0·75 | 0·35 | 0·2 | 60 | 24 | 57 |
| Ferroxcube | 6D5 | 330 | 200 | ≥ 42 | ≤14 | ≤1·60 | 0·55–0·70 | 0·2 | 61 | 40 | 134 |
| | 6C1 | 530 | 275 | 60 | ≤ 8 | 0·93 | 0·48 | 0·2 | 61 | 25 | 134 |
| | 6C2 | 755 | 415 | 65 | ≤ 7 | 0·95 | 0·50 | 0·25 | 61 | 25 | 134 |
| R C A | 0140 M5 | 450 | 225 | 48 | 6 | 1·48 | 0·78 | 0·4 | 50 | 25 | 96 |
| Siferrit | R 501 | 400 | 220 | > 40 | < 8 | 1·10 | 0·55 | 0·2 | 55 | 25, 40 | 101 |
| | R 452 | 550 | 305 | ≥ 50 | ≤ 9 | 0·9 | 0·5 | 0·2 | 55 | 25–60 | 101 |
| | R 454 | 750 | | 70 | 7 | 0·95 | 0·44 | 0·2 | 57 | 25 | 101 |

**Table 19.20** FERRITE STORAGE CORES HAVING THE APPROXIMATE DIMENSIONS 0·8 mm×0·4 mm×0·2 mm

| *Designation* | *Type* | $I_w$ (mA) | $I_{pw}$ m(A) | $uV_1$ (mV) | $dV_z$ (mV) | $t_s$ (μs) | $t_p$ (μs) | $t_r$ (μs) | *d.r.* (%) | *Measuring temperature* (°C) | *Reference* |
|---|---|---|---|---|---|---|---|---|---|---|---|
| Ferramic | MC 159 | 520 | 318 | ⩾35 | ⩽11 | ⩾0·48 | 0·24 | 0·1 | 61 | 24 | 57 |
| | MC 177 | 450 | 275 | ⩾32 | ⩽11 | ⩽0·45 | 0·24 | 0·1 | 61 | 24 | 57 |
| | MC 178 | 400 | 228 | ⩾40 | ⩽15 | ⩽0·4 | 0·17 | 0·1 | 57 | 24 | 57 |
| Ferroxcube | 6F3 | 820 | 450 | 58 | ⩽ 5 | 0·5–0·6 | 0·26–0·34 | 0·15 | 61 | 10 | 134 |
| | 6F8 | 710 | 360 | 53 | 5 | 0·4 | 0·22 | 0·1 | 61 | 25 | 134 |
| R C A | 0135 M5 | 380 | 190 | 28 | 2·5 | 1·2 | 0·7 | 0·4 | 50 | 25 | 96 |
| | 0138 M5 | 310 | 155 | 22 | 2·5 | 1·48 | 0·8 | 0·4 | 50 | 25 | 96 |
| | 263 M1 | 550 | 335 | 25 | 3 | 1·0 | 0·65 | 0·5 | 61 | 25 | 96 |
| Siferrit | R 491 | 640 | | 42 | 7 | 0·38 | 0·2 | | 55 | 25, 40 | 101 |

a small magnetising current. Materials, therefore, having a relatively low coercivity are more often used for switching cores than those having a higher coercivity. Tables 19.21 and 19.22 show a few practical examples. Since, moreover, high magnetic fluxes are easier to achieve with large than with small cores, switching cores are usually larger than storage cores. Core diameters lying between 3 mm and 30 mm are to be found in manufacturers' lists.

**Table 19.21** PROPERTIES OF SOME FERRITES FOR SWITCHING CORES (NOMINAL VALUES AT 40°C)[132]

| *Material* | $H_m$ (A/m) | $H_c$ (A/m) | $B_m$ (V s/m²) | $B_r/B_m$ | $t_s$ (μs) | $s_s$ (μs A/m) |
|---|---|---|---|---|---|---|
| Ferroxcube 6 E1 | 30 | — | 0·165 | 0·91 | 8 | 80 |
| | 39·5 | — | 0·198 | 0·93 | 5 | |
| | 64 | — | 0·232 | 0·94 | 2 | |
| Ferroxcube 6 D | 110 | 68 | 0·17 | >0·9 | <2 | 96 |
| | 220 | 91 | 0·21 | >0·9 | <1 | |

**Table 19.22** COERCIVITY AND REMANENCE OF SOME SWITCHING-CORE MATERIALS[73]

| *Material* | $H_c$ (A/m) | $B_r$ (V s/m²) |
|---|---|---|
| Siferrit H 460 | 120 | 0·28 |
| Siferrit R 530 | 57 | 0·19 |
| Siferrit R 402 | 32 | 0·19 |
| Siferrit R 404 | 18 | 0·19 |
| Siferrit R 405 | 13 | 0·23 |

Figure 19.4, for example, shows how the flux increases with core size for a given material, following Metzdorf and Rabl[73]. The relations between switching current, remanent flux, and core size, shown in the figure, were measured in toroidal cores, the materials being those of Table 19.22.

## 19.2 TRADE NAMES AND PRODUCERS OF MAGNETIC MATERIALS

The numbers in the third column of the following list denote the producers of the various materials in accordance with the code set out in Tables 19.23 and 19.24. Besides the materials to be found at present on the market, some are listed which have no practical standing today. As, however, the reader may come across them in the technical literature, it seemed worthwhile to give their composition and source. The fourth column gives the references.

| | | | |
|---|---|---|---|
| AFK 1 | 25% Co, 75% Fe | 3.9 | 102 |
| AFK 502 | 49% Co, 2% V, 49% Fe | 3.9 | 102 |
| Alcomax | 21% Co, 11·5% Ni, 8% Al, 4% Cu, remainder Fe | 2.7, 2.15 | 83 |
| Alcomax III | 24% Co, 13·5% Ni, 8% Al, 3% Cu, 0·8% Nb, remainder Fe | 2.7, 2.15 | 83 |
| Alcomax IV | 24% Co, 13·5% Ni, 8% Al, 3% Cu, 2·5% Nb, remainder Fe | 2.7, 2.15 | 83 |
| Alfenol | 16% Al, 84% Fe | 12.28 | 85 |
| Alfer | 13% Al, 87% Fe, high magnetostriction | 14.27 | 71a, 120a |
| Allegheny 4750 | Ni–Fe alloy sheet with 48% Ni, square loop | 12.1 | 16 |
| Alnico 1–8 | Fe–Al–Ni–(Co) alloys | 1.11, 2.7, 2.15, 4.1, 12.7, 12.13, 12.14, 12.25, 12.30 | 5, 19, 22, 30, 69, 119 |
| Alnico I–XII | (Tables 19.1–19.6) | | |
| Alnicus | Alnico V alloy with columnar crystals | 12.27 | 122 |
| Alperm | 83% Fe, 17% Al | — | 69, 72 |
| Alphasil | Fe with 3–3·5% Si, grain-oriented | 12.18 | 15 |
| AME | Unalloyed iron | 1.9, 1.15 | 109 |
| Anhyster M | Corresponds to Mumetal | 3.9 | 103 |
| Anhyster B | 36% Ni, 64% Fe | | |
| Anhyster D | 50% Ni, 50% Fe | | |
| Anko 2 | 9% Al, 20% Ni, 15% Co, 4% Cu, remainder Fe | USSR | — |
| Anko 3 | 10% Al, 19% Ni, 18% Co, 3% Cu, remainder Fe | | |
| Anko 4 | Corresponds to Alnico V | | |
| Ansemax | 24% Co, 14% Ni, 3% Cu, 8% Al, remainder Fe | 4.1 | 19 |
| Arnox | $BaO \cdot 6\ Fe_2O_3$ | 12.25 | 11 |
| Balco | 70% Ni, 30% Fe | 12.31 | 148 |
| Bismanol | $Mn_3Bi_2$ | — | 2 |
| Calmaloy | 88% Ni, 9·5% Cu, 2·2% Fe | 12.12, 12.30 | 62 |
| Carbonyleisen | Iron dusts made from iron carbonyl: C, E, J, L, HP, SF, TH, | 12.3 | 38 |
| | E, HF2, HF1, CNst, CNS, CNN, CCS, SN | 1.3 | 14 |
| Carpenter 49 | Ni–Fe alloy with 49% Ni, square loop | 12.5 | 16 |
| Caslam | Flake iron dust | 2.8 | 18 |

| | | | |
|---|---|---|---|
| Caslite | Iron dust cores | 2.8 | 95 |
| CDW | Magnetically soft iron (unalloyed Fe) | 1.5 | 18a |
| Ceramag | Magnetically soft ferrites | 12.24 | 107 |
| Ceramagnet | $BaO \cdot 6\ Fe_2O_3$ | 12.24 | 106 |
| Coalnimax | 24% Co, 14% Ni, 3% Cu, 8% Al, remainder Fe | 4.1 | 19 |
| Coercimax | Fe–Al–Ni–Co–Ti alloy | 4.1 | 19 |
| Columax | Fe–Al–Ni–Co alloy with columnar crystals | 2.7, 12.26 | 119 |
| Comalloy | 12% Co, 17% Mo, 71% Fe, isotropic | 2.15 | 84 |
| Comol | 12% Co, 17% Mo, remainder Fe | 2.15 | 30 |
| Compensator Alloy | — | 12.5, 12.23 | 43 |
| Co-Netic | Magnetic shielding material | 12.19 | 68 |
| Conpernik | 49% Ni, remainder Fe, constant permeability | 12.30 | 145 |
| Cromag | $BaO \cdot 6\ Fe_2O_3$ | — | 30 |
| Cryoperm 10, F, Z | High-permeability alloy for 4·2–77K | 1.18 | 125a |
| Cubex | Fe+3% Si, cubic textured | 12.30 | 93a |
| Cunico I | 50% Cu, 21% Ni, 29% Co | 2.15 | 30, 87, 117 |
| Cunico II | 35% Cu, 24% Ni, 41% Co | | |
| Cunife I | 60% Cu, 20% Ni, 20% Fe | 12.1, 12.4 | 9, 30, 87 |
| Cunife II | 50% Cu, 20% Ni, 2·5% Co, 27·5% Fe | | |
| Deltamax | 50% Fe, 50% Ni, square loop | 12.1, 12.25 | 12 |
| Di-Max M | Hot-rolled electrosheet | 12.4 | 6 |
| Dynamax | 65% Ni, 2% Mo, 33% Fe | 12.12 | 45 |
| Elinvar | Ni–Fe, alloy with constant Young's modulus from −100°C to +100°C | 3.9 | 105 |
| F 300 | $BaO \cdot 6\ Fe_2O_3$ | 12.8 | 30 |
| Feralex | Ferrite cores | 2.10 | — |
| Ferbalite | $BaO \cdot 6\ Fe_2O_3$ | 3.5 | 30 |
| Fercolite | Hexagonal cobalt ferrite | 3.5 | 30 |
| Ferdurite | $BaO \cdot 6\ Fe_2O_3$ | 9.2 | 113 |
| Fermalite | Mn–Zn ferrites | 3.5, 9.2 | 64, 113 |
| Fernilite | Ni–Zn ferrites | 3.5 | 64 |
| Feroba | $BaO \cdot 6\ Fe_2O_3$ | — | 5 |
| Ferramic | Ferrites for inductors, memory-stores, and microwaves | 12.14 | 56, 58 |
| Ferribrox | Mn–Zn and Ni–Zn ferrites | 14.27 | 120a |
| Ferriflex | Barium ferrite in rubber | 3.1 | 4 |

| | | | |
|---|---|---|---|
| Ferrimag 1 | $BaO \cdot 6Fe_2O_3$, isotropic | 12.7 | 21 |
| Ferrimag V | $BaO \cdot 6Fe_2O_3$, anisotropic | 12.7 | 21 |
| Ferrinet Q1 | $BaO \cdot 6Fe_2O_3$, isotropic | 14.27 | 120a |
| Ferrinet Q6–Q8 | $BaO \cdot 6Fe_2O_3$, anisotropic | 14.27 | 120a |
| Ferrinox | Cubic ferrites | 3.3 | 100 |
| Ferrocarit | Magnetically soft ferrite | 1.22 | 138 |
| Ferrocart | Dust-core material | 1.22 | 138 |
| Ferroxcube | Cubic ferrites | 1.19, 2.5, 12.10 | 80, 132 |
| Ferroxcube 3 | Mn–Zn ferrites (see Table 19.15) | 1.19, 2.5, 12.10 | 80, 132 |
| Ferroxcube 4 | Ni–Zn ferrites (see Table 19.16) | 1.19, 2.5, 12.10 | 80, 132 |
| Ferroxcube 5 | Microwave ferrites | 3.2 | — |
| Ferroxcube 6 | Square-loop ferrites (see Tables 19.18 and 19.19) | 1.19, 2.5, 12.10 | 80, 132 |
| Ferroxcube 7 | Magnetostrictive ferrites | 1.19, 2.5, 12.10 | 80, 132 |
| Ferroxdure | $BaO \cdot 6Fe_2O_3$ (see Table 19.2) | 1.19 | 133 |
| Ferroxplana | Hexagonal magnetically soft ferrites | 1.19 | 59 |
| Gecalloy | Iron dust magnets | 12.12 | 91 |
| Genox | $BaO \cdot 6Fe_2O_3$ | 12.13 | 40 |
| Gyralite | Microwave ferrites | 3.5 | — |
| H.C.R. alloy | 50% Fe, 50% Ni, square loop | 2.13 | 118c |
| Hiperco 27 | 27% Co, 0·5% Cr, remainder Fe | 12.30 | 142 |
| Hiperco 35 | 35% Co, 0·4% Cr, remainder Fe | 12.30 | 118 |
| Hiperco 50 | 50% Co, 50% Fe | 12.30 | 142 |
| Hipernik | Ni–Fe alloys with 50% Ni, isotropic | 12.30 | 145, 149 |
| Hipernik V | 50% Fe, 50% Ni, square loop | 12.30 | 144 |
| Hipernom | 78–81% Ni, 4–5% Mo, remainder Fe | 12.30 | 143 |
| Hipernom V | 78–81% Ni, 4–5% Mo, remainder Fe, square loop | 12.30 | 145 |
| Hipersil | Fe+3% Si alloy, oriented | 12.30 | 16 |
| Honda alloy | 27% Co, 18% Ni, 7% Ti, 4% Al | — | 5 |
| Hycomax | Fe–Al–Ni–Co–Ti alloys | 2.7 | 42a, 83 |
| Hy Mu 80 | 79% Ni, 4% Mo, remainder Fe | 12.18 | 15 |
| Hynical | 12% Al, 32% Ni, remainder Fe | — | 79 |

| | | | |
|---|---|---|---|
| Hynico | 21% Ni, 12% Co, 10% Al, 6% Cu | — | 5 |
| Hyperm 0 | Unalloyed iron (see Table 10.2) | 1.10 | 35 |
| Hyperm 1–7 | Fe–Si alloys (see Table 19.12) | 1.10 | 35 |
| Hyperm 36, 50, 766, 800, 900, Maximum | Fe–Ni alloys (see Tables 19.13 and 19.14) | 1.10 | 35 |
| Hyperm Co35, Co50 | Fe–Co alloys (see Table 19.12) | 1.10 | 35 |
| Hypermal | 12% Al, remainder Fe | — | 69 |
| Hyperox | Magnetically, soft mixture-ferrites (see Table 19.15) | 1.10 | 36 |
| Imphisil | Fe–Si alloy, grain-oriented | 3.9 | 104 |
| Indalloy | 12% Co, 17% Mo, remainder Fe, sintered | — | 30 |
| Indox | $BaO \cdot 6Fe_2O_3$ | 12.14 | 51 |
| Invar | 64% Fe, 36% Ni | 3.9 | 25, 61, 105 |
| Isoperm | Ni–Fe alloy, low remanence | 1.1 | 60 |
| Keraperm | Ferrites for inductors, transformers, and memory stores (see Table 19.15 and 19.16) | 1.6 | 114 |
| Koerflex | Fe–Co–V alloys (see Table 19.2) | 1.10 | 33 |
| Koerox | $MeO \cdot 6Fe_2O_3$ (see Tables 19.1 and 19.2) | 1.10 | 33 |
| Koerzit | Fe–Al–Ni–(Co) alloys (see Table 19.1) | 1.10 | 33 |
| KS-1 | 35% Co, 6% Cr, 5% W, 0·9% C | — | 5, 76 |
| KS-2 | 15% Co, 9% Cr, 1·5% Mo, 1% C | — | 5 |
| Lodex, Lodox | ESD permanent-magnet material | 12.12 | 65, 93b |
| M5 | Fe–Si, oriented | 12.30 | — |
| M1040 | 72% Ni, 14% Cu, 3% Mo (replaced by Vacoperm 100) | 1.18 | 88, 123 |
| Magloy 1 | 24% Co, 14% Ni, 8% Al, 3% Cu, remainder Fe | — | 46 |
| Magnadur 1–3 | $BaO \cdot 6Fe_2O_3$ | 2.5 | 30 |
| Magnesil | Fe with 3–3·5% Si, grain-oriented | 12.18 | 15 |
| Magnetoflex | Permanent–magnet alloys, rollable | 1.18 | 26, 127 |

| | | | | |
|---|---|---|---|---|
| Magnetoflex 35 | 52% Co, 13% V, 35% Fe (see Table 19.2) | 1.18 | | 127 |
| Magnetoflex 40 | 53% Co, 8% V, 40% Fe (see Table 19.2) | 1.18 | | 127 |
| Magnetreineisen | High-purity Fe 99.95% | 1.18 | | 123c |
| Magnifer 36W<br>Magnifer 36K | 36–38% Ni, remainder Fe | 1.21 | | 135 |
| Magnifer 75 | ~75% Ni, remainder Fe | 1.21 | | 136 |
| Manifer | Magnetically soft ferrite | 1.20 | | 134a |
| Maniperm | Permanent-magnet ferrite | 1.20 | | 134a |
| Megaperm | 65% Ni, 25% Fe, 10% Mn and 45% Ni, 45% Fe, 10% Mn | | — | 16, 42 |
| Minimum | Fe+0·04% C (max.) | 1.4 | | 15b |
| Mishima metal | ~25% Ni, 12% Al, 63% Fe | | — | 16 |
| MK magnet | 25% Ni, 13% Al, 62% Fe | | — | 75, 76 |
| Mo-Permalloy | 79% Ni, 4% Mo, remainder Fe | 12.25 | | 12 |
| MT Magnet | Fe–Al–C alloy | | — | 70 |
| Mumetal | 75% Ni, 5% Cu, 2% Cr and 75% Ni, 5% Cu, 4% Mo, remainder Fe | 1.18 | | 3a, 97, 123 |
| Mumetal 40 | 77% Ni, 5% Cu, 5% Mo, 14% Fe | 2.13 | | 118a |
| Mutemp | 30% Ni, 70% Fe, compensation alloy | 2.9 | | 43 |
| Neferrite | Mn–Zn ferrites | 14.27 | | 3, 89 |
| Neosid | Material for cores of inductors and transformers | 1.13 | | 86a |
| Netic | Magnetic screening material | 12.19 | | 68 |
| Nialco | Fe–Ni–Al alloys, isotropic | 3.1 | | 4 |
| Nicromet 46 | 45% Ni, 55% Fe | 12.31 | | 148 |
| Nilomag | Ni–Fe–Mo alloys | 2.14 | | 147 |
| Nipermag | 12% Al, 30% Ni, 0·4% Ti, remainder Fe | | — | 30 |
| Niron 52 | 50% Ni, 50% Fe | 12.31 | | 148 |
| Ni-Span C | Fe–Ni–Cr alloy with constant Young's modulus (41·0–43·0% Ni, 5·1–5·7% Cr, 2·2–2·6% Ti, remainder Fe) | 2.14, 12.9 | | 29, 147 |
| NMHG | Compensation alloys, $T_c = -10°C$ to $+200°C$ | 3.9 | | 43 |
| NKS | 3·7% Al, 17·7% Ni, 27·2% Co, 6·7% Ti, remainder Fe | | — | 16, 44 |
| Oerstit | Fe–Al–Ni (Co) and other permanent-magnet materials (see Table 19.1) | 1.7 | | 23 |

| | | | |
|---|---|---|---|
| OP-Magnet | Corresponds to Vectolite | — | 76, 93 |
| Oriented, T, T-S, M | Magnetically anisotropic electrosheet | 12.4 | 6 |
| Orsi | Grain-oriented electrosheet | — | 65a |
| Orthonik | See 48-Orthonik | 12.4 | 16 |
| Orthonol | 50% Fe, 50% Ni, square loop | 12.18, 12.28 | 15 |
| Ox | $BaO \cdot 6Fe_2O_3$ | 1.11 | 66 |
| Oxilit | Barium ferrite powder plus matrix | 1.7 | 23 |
| Oxit | $BaO \cdot 6\ Fe_2O_3$ | 1.7 | 23 |
| Permalloy A | 78% Ni, 22% Fe | 2.2 | 16 |
| Permalloy B | 55% Fe, 45% Ni, (1% Mn) | 2.2 | 110 |
| Permalloy C | 78% Ni, 4% Mo, 5% Cu, remainder Fe | 1.8, 2.2 | 110, 123 |
| Permalloy D | 36% Ni, remainder Fe | 2.2 | 110 |
| Permalloy F | 50% Ni, remainder Fe, magnetically anisotropic | 2.2 | 112 |
| Permalloy G | As Permalloy B but with square loop | 2.2 | 112 |
| Permanit | Fe–Al–Ni, Fe–Co, and Fe–Cr alloys (see Table 19.1) | 6.1 | 37 |
| Permax F | 60–65% Ni, 40–35% Fe, high pulse permeability | 1.18 | 129a |
| Permax M | ~50% Ni, 50% Fe, $\mu_5 = 50\,000\mu_0$ | 1.18 | 129a |
| Permax Z | 60–65Ni remainder Fe, $B_r/B_m > 0{\cdot}9$ | 1.18 | 123a |
| Permendur | 50% Co, 50% Fe | 2.2, 12.29 | 28 |
| Permenorm 3601 | 64% Fe, 36% Ni | 1.18 | 123 |
| Permenorm 5000G3 | 50% Fe, 50% Ni, sintered *solid alloy* | 1.18 | 123 |
| Permenorm 5000H2 | 50% Fe, 50% Ni, normal loop | 1.18 | 123 |
| Permenorm 5000H3 | 50% Fe, 50% Ni, fused *solid alloy* | 1.18 | 123 |
| Permenorm 5000Z | 50% Fe, 50% Ni, square loop | 1.18 | 123 |
| Permenorm 5000 ZE | 50% Fe, 50% Ni, sintered 5000Z | 1.18 | 128 |
| Permeron | 50% Fe, 50% Ni, square loop | — | — |
| Permet | Cu–Ni–Co alloy, sintered | — | 117 |
| Permimphy 77 | 77% Ni, 19% Fe, 4% Mo | 3.9 | 103 |
| Perminvar | Fe–Ni–(Co) alloys (34% Ni, 29% Co, 34% Fe, 3% Mo) | — | 27 |
| Plastiform | Barium ferrite in rubber | 12.16 | 63 |

| | | | |
|---|---|---|---|
| Plastoferrite | Barium ferrite with binder | 3.1 | 4 |
| Platinax II | 76·7% Pt, 23·3% Co | 12.15 | 74 |
| Platinum | 77·8% Pt, 22·2% Fe | — | 30, 93 |
| Polyiron | Dust core with Sendust | 14.27 | 120a |
| Prac | Fe–Al–Ni dust plus 6% binder | 1.11 | 66 |
| Prox | Barium ferrite dust plus 8% binder | 1.11 | 66 |
| Radiometal | 50% Fe, 50% Ni (45% Ni, 5% Cu, 50% Fe) | 2.13 | 16 |
| Radiometal 36 | 36% Ni, 64% Fe | 2.13 | 118b |
| Reco | Fe–Al–Ni alloys, isotropic | 1.19, 2.5 | 133 |
| Rectalite | Mg–Mn and Cu–Mn ferrites, square loop | 3.5 | — |
| Rectimphy | 50% Ni, 50% Fe alloy, anisotropic | 3.9 | 102 |
| Remalloy | 12% Co, 17% Mo, remainder Fe | 2.15 | 84, 30 |
| Remendur | 49% Co, 2·5% V, remainder Fe | 12.21 | 15a |
| Rhometal | 40–45% Ni, 5% Cr, 3% Si, remainder Fe | 2.13 | 16 |
| Semendur | Fe–Co | 14.27 | 120a |
| Sempermax | Fe–Ni, high-permeability | 14.27 | 120a |
| Sempersil | Fe+3% Si, oriented | 14.27 | 120a |
| Sendelta | 50% Fe, 50% Ni, square loop | 14.27 | 120a |
| Sendust | 7–13% Si, 4–7% Al, remainder Fe | 14.27 | 71, 120 |
| Sermalloy | Fe–Al–Ni–Co alloys | 3.8 | 16b, 16c |
| Shunt Steel | Compensation alloy | — | 43 |
| Siferrit | Cubic ferrite (see Tables 19.15 and 19.16) | 1.16 | 101 |
| Silectron | Fe+3% Si, grain-oriented | 12.1 | 13 |
| Silmanal | 86·7% Ag, 8·8% Mn, 4·5% Al | — | 93 |
| Sincomax | Sintered material, iron plus magnetite | — | 83 |
| Sinterox | $BaO \cdot 6Fe_2O_3$ isotropic and anisotropic | 4.1 | 19 |
| Sirufer | Iron dust cores | 1.16 | 92, 101 |
| Spinal | $BaO \cdot 6Fe_2O_3$, isotropic | 3.1 | 4 |
| Spinalor | $BaO \cdot 6Fe_2O_3$, anisotropic | 3.1 | 4 |
| Sprox | Barium ferrite powder plus 20% binder | 1.11 | 66 |
| 49 Squaremu | Ni–Fe alloy, corresponding to Deltamax | 12.17 | 139 |
| Stalloy | Fe–Si alloy | — | 17 |

| | | | |
|---|---|---|---|
| Stanferrite | Ferrites for inductors and transformers | 2.2 | 112 |
| Supermalloy | 79% Ni, 5% Mo, remainder Fe | 12.25 | 12 |
| Supermendur | 49% Co, 49% Fe, 2% V | 12.21, 12.30 | 146 |
| Supermimphy 77 | 77% Ni, 19% Fe, 4% Mo | 3.9 | 103 |
| Supermu 30 | Thermally stable sheet-core material | 12.17 | 67 |
| Supermumetal 100 | 77% Ni, 14% Fe, 4% Mo | 2.13 | 46a |
| Superradio-metal 50 | 50% Ni, 50% Fe | 2.13 | 118b |
| Supranhyster 36 | 36% Ni, 64% Fe | 3.9 | 103 |
| Supranhyster 50 | 50% Ni, 50% Fe | 3.9 | 103 |
| SWB electro-sheet | Cold-rolled electrosheet in strip form | 1.8 | — |
| Thermalloy | 66·5% Ni, 30% Cu, 2·2% Fe | 12.12, 12.30 | 62 |
| Thermelast | Ni–Fe alloy with constant Young's modulus | 1.18 | 125 |
| Thermenol | 16% Al, 3·3% Mo, 80·7% Fe | 12.28 | 86 |
| Thermoflux | Ni–Fe compensation alloy | 1.18 | 129 |
| Thermoperm | 30% Ni, 70% Fe compensation alloy | 1.10 | 108 |
| Ticonal | Fe–Ni–Al–Co–(Ti) alloys, anisotropic | 1.19, 3.1, 3.4, 6.1, 2.2 | 4, 41, 133 |
| TK 8 | Fe–Al–Ni–Co alloy with columnar crystals | — | 70 |
| TM Alloy | Permalloy, low-coercivity | 14.27 | 120a |
| Trafoperm | Fe with ~3% Si (see Table 19.12) | 1.18 | 123, 131a |
| Trancore | Hot-rolled electrosheet with 4–4·7% Si | 1.8 | |
| Tran-Cor A5, A6, M14 | Hot-rolled electrosheet | 12.4 | 7 |
| Tran-Cor T | High-permeability anisotropic electrosheet | 12.4 | 7 |
| Tran-Cor 3x | Fe+3% Si | 12.4 | 16 |
| Tromalit | Alni and Alnico moulded magnets | 1.12 | 5 |
| Ugimax | Fe–Ni–Al–Co alloy with columnar crystals | 3.1 | 4 |
| Ultraperm F | Fe with 70–80% Ni | 1.18 | 129a |
| Ultraperm Z and 10 | Fe with 70–80% Ni | 1.18 | 123, 131 |

| | | | |
|---|---|---|---|
| Uni 80 | Fe–Al–Ni–Co alloy with columnar crystals | — | 70 |
| Vacodur 16 | Fe + 16% Al | 1.18 | 126 |
| Vacoflux 48 | ~50% Fe, 50% Co, normal loop | 1.18 | 130 |
| Vacoflux 50 | 50% Fe, 50% Co, normal loop | 1.18 | 130 |
| Vacoflux S, S2 | 50% Fe, 50% Co, sintered, hot-rolled | 1.18 | 130 |
| Vacoflux Z | 50% Fe, 50% Co, square loop | 1.18 | 130 |
| Vacoperm 100 | Ni–Fe alloy with 70–80% Ni | 1.18 | 123 |
| Varioperm | Fe–Ni compensation alloy | 8.1 | 43, 137 |
| Vectolite | $26Co_2O_3 \cdot 30Fe_2O_3 \cdot 44Fe_3O_4$ | — | 93 |
| Vibralloy | 43% Ni, 9% Mo, remainder Fe, constant Young's modulus | — | 32 |
| Vibrox | Ni–Cu ferrite for magnetostriction oscillators | 14.27 | 120a |
| Vicalloy 1 | 52% Co, 38·5% Fe, 9·5% V | 12.1, 12.30 | 30, 119 |
| Vicalloy II | 52% Co, 35% Fe, 13% V | 12.26, 12.31 | 148 |
| Viperm 5A | 50% Fe, 50% Ni | 8.1 | 137a |
| Viperm 5B | 50% Fe, 50% Ni | 8.1 | 137 |
| Viperm 5C | 50% Fe, 50% Ni with constant $\mu$ | 8.1 | 137a |
| Viperm 10 | Ni–Fe alloy, high permeability | 8.1 | 137 |
| VS 30 | 30% Co, 15 Cr, remainder Fe | 1.10 | 31a |
| Westro | Oxide permanent-magnet material | 12.30 | 146a |
| 2V-Permendur | 49% Co, 2% V, remainder Fe | 12.29 | — |
| 36 KNM | 22% Ni, 36% Co, 3% Mo, remainder Fe | — | — |
| 4-79Ni | 79% Ni, 4% Mo, 17% Fe | 12.31 | 148 |
| 48 Alloy | Ni–Fe alloy with 48% Ni, anisotropic | 12.18 | 15 |
| 48 Orthonik | Ni–Fe alloy with 48% Ni, anisotropic | 12.4 | 6 |

**Table 19.23** PRODUCERS OF MAGNETIC MATERIALS, 1

| *Country* | *Manufacturer* | *Permanent magnets* | | Fe, Fe–Si *strip, sheet* | Ni–Fe *alloys* | *Dust cores* Ni–Fe, Fe (*dust*) | *Ferrite cores* |
|---|---|---|---|---|---|---|---|
| | | *Metal* | *Ceramic* | | | | |
| Germany | 1.1 AEG-Telefunken, D-715 Backnang | | | | | | + |
| | 1.2 August Thyssen-Hütte AG, D-41 Duisburg-H | | | + | | | |
| | 1.3 Badische Anilin & Soda-Fabrik, D-67 Ludwigshafen | | | | | (+) | (+) |
| | 1.4 Bochumer Verein f. Gussstahlfabr. AG, Bochum | | | + | | | |
| | 1.5 C. D. Wälzholz, D-585 Hohenlimburg | | | + | | | |
| | 1.6 CRL Electronic Bauelemente GmbH Dralowidwerk, D-505 Porz | | | | | | + |
| | 1.7 Deutsche Edelstahlwerke AG, D-46 Dortmund | + | + | | | | |
| | 1.8 Elektroblech-Gesellschaft mbH, D-463 Bochum | | | + | | | |
| | 1.9 Edelstahlwerke Buderus AG, D-633 Wetzlar | | | + | | | |
| | 1.10 Friedr. Krupp Widiafabrik, D-43 Essen | + | + | + | + | | + |
| | 1.11 Magnetfabrik Bonn, D-53 Bonn | + | + | | | | |
| | 1.12 Max Baermann, D-506 Bensberg | + | + | | | | |
| | 1.13 Neosid Pemetzrieder GmbH, D-5894 Halver/W | | | | | + | + |
| | 1.14 Robert Bosch GmbH, D-7 Stuttgart | + | + | | | | |
| | 1.15 Röchlingsche Eisen- und Stahlwerke GmbH, D-662 Völklingen | | | + | | | |
| | 1.16 Siemens AG, D-8 München | | + | | | + | + |
| | 1.17 Stahlwerke Südwestfahlen AG, D-5930 Hüttental-Geisweid | | | + | | | |
| | 1.18 Vacuumschmelze GmbH, D-645 Hanau | + | | + | + | | |
| | 1.19 Valvo GmbH, D-2 Hamburg | + | + | | | | + |
| | 1.20 VEB Keramische Werke, Hermsdorf/Thür. | | + | | | | + |

| | | | | | | | |
|---|---|---|---|---|---|---|---|
| | 1.21 Vereinigte Deutsche Metallwerke AG, D-599 Altena | | | | + | | |
| | 1.22 Vogt & Co KG, D-8391 Erlau | | | | | + | + |
| Great Britain | 2.1 Balfour Darwin Ltd, Capital Steel Works, Sheffield 3 | + | + | | | | |
| | 2.2 ITT CG-E Magnetic Materials Division, Harlow | | | | + | + | + |
| | 2.3 James Neill & Co., Napier Street, Sheffield | + | | | | | |
| | 2.4 Jessop Saville Ltd, Brightside Works, Sheffield 9 | + | | | | | |
| | 2.5 Mullard Ltd, Torrington Place, London WC1 | + | + | | | | + |
| | 2.6 Neosid Ltd, Howardsgate, Welwyn Garden City, Herts | | + | | | + | |
| | 2.7 Permanent Magnet Association, Sheffield | + | + | | | | |
| | 2.8 Plessey Co. Ltd, Wood Burcote, Towcester, Northants | + | + | | | | + |
| | 2.9 RTB Ltd, Stourport on Severn | | | + | | | |
| | 2.10 Salford Electrical Instruments Ltd, Eccles, Manchester | | | | | + | + |
| | 2.11 Steel Company of Wales, Newport, Mon. | | | + | | | |
| | 2.12 Swift Levick & Sons Ltd, Levison Street, Sheffield | + | + | | | | |
| | 2.13 Telegraph Construction and Maintenance Co. Ltd, Crawley | | | | + | | |
| | 2.14 Henry Wiggin & Co., Hereford | | | | + | | |
| | 2.15 Murex Ltd, Rainham, Essex | + | | | | | |
| France | 3.1 Allevard, Ugine, Grenoble | + | + | | | | |
| | 3.2 Cie de Produits Elémentaires p. Ind. Mod., Paris | | | | | | + |
| | 3.3 Compagnie des Ferrites Electronique, Montreuil | | | | | | + |
| | 3.4 Giffey-Prêtre, Paris | + | | | | | |
| | 3.5 Lignes Télégraphiques et Téléphoniques, Conflans-Ste Honorine | | + | | | + | + |
| | 3.6 R.T.C. La Radiotechnique Compelec, Coprim 27, Evreux (Eure) | | | | | | + |

*Table 19.23 continued*

| *Country* | *Manufacturer* | *Permanent magnets* | | Fe, Fe–Si *strip, sheet* | Ni–Fe *alloys* | *Dust cores* Ni–Fe, Fe (*dust*) | *Ferrite cores* |
|---|---|---|---|---|---|---|---|
| | | *Metal* | *Ceramic* | | | | |
| France (*cont.*) | 3.7 S.A. de Télécommunications, Paris 13e | | | | | | |
| | 3.8 Société d'Etudes et de Recherches Magnétiques, 38 St. Martin d'Héres | + | | | | | |
| | 3.9 Société Metallurgique d'Imphy, Paris | | | + | + | | |
| Italy | 4.1 Centro Magneti Permanenti, 20 123 Milan | + | + | | | | |
| | 4.2 I.O.S. Industria Ossidi Sinterizzati, 21 023 Malgesso/Varese | | + | | | | |
| | 4.3 SAMPAS, 20 123 Milano | | + | | | | |
| Yugoslavia | 5.1 Iskra, Nabavne Organizacije, Kranj | | + | | | | + |
| Austria | 6.1 Gebr. Böhler & Co. AG, Vienna | + | + | | | | |
| Poland | 7.1 Polfer Zaklad Materialow Magtycznych, Warsaw-47 | | | | | | + |
| Switzerland | 8.1 Vimetal S.A., Geneva | | | | + | | |
| Spain | 9.1 Piher, S. A. Ceramica, Poligono Ind. CIA, Tudela-Navarra | | + | | | | |
| | 9.2 Standard Electrica S. A., Madrid | | | | | | + |
| Czecho-slovakia | 10.1 Pramet, Unecowska, Sumperk | | + | | | | + |
| Hungary | 11.1 Kőbányai Porcelángyár, Budapest V | | + | | | | |

**Table 19.24** PRODUCERS OF MAGNETIC MATERIALS, II

| *Country* | *Manufacturer* | *Permanent Magnets* | | Fe, Fe–Si *strip, sheet* | Ni–Fe *alloys* | *Dust cores* Ni–Fe, Fe (*dust*) | *Ferrite cores* |
|---|---|---|---|---|---|---|---|
| | | *Metal* | *Ceramic* | | | | |
| USA | 12.1 Allegheny Ludlum Steel Corp., Pittsburgh, Pa. | | | | + | | |
| | 12.2 Allen Bradley Co., Milwaukee, Wis. | | + | | | | + |
| | 12.3 Antara Chemicals, New York, N. Y. | | | | | (+) | |
| | 12.4 Armco Steel Corp., Middletown, Ohio | | | + | + | | |
| | 12.5 Carpenter Steel Corp. | | | | + | | |
| | 12.6 Ceramic Magnetics Inc., Little Falls, N. J. | | | | | | + |
| | 12.7 Crucible Steel Co. of America, Pittsburgh, Pa. | + | + | | | | |
| | 12.8 D.M. Steward Mfg. Co., Chattanooga, Tenn. | | + | | | | |
| | 12.9 Engelhard Industries Inc., Union, N. J. | | | | | | + |
| | 12.10 Ferroxcube Corp. of America, Saugerties, N. Y. | | | | | | + |
| | 12.11 General Analine Film Corp., New York, N. Y. | | | | | (+) | |
| | 12.12 General Electric Co., Edmore, Mich. | + | + | | | | |
| | 12.13 General Magnetic Corp., Detroit, Mich. | | + | | | | |
| | 12.14 Indiana General Co., Valparaiso, Ind., Keasbey, N. J. | + | + | | | | + |
| | 12.15 Johnson Matthew Co. Ltd | + | | | | | |
| | 12.16 Leyman Corp. Magnetics Div., Cincinnati, Ohio | | + | | | | |
| | 12.17 Magnetic Metals Comp., Camden, N. J. | | | + | + | | |
| | 12.18 Magnetics Inc., Butler, Pa. | | | | + | | + |
| | 12.19 Magnetic Shield Division, Chicago, Ill. | | | + | + | | |
| | 12.20 National Moldite Comp., Hillside, N. J. | | + | | | + | + |
| | 12.21 Radio Corporation of America, Harrison, N. J. | | | | | | + |
| | 12.22 Raytheon Co., Waltham 54, Mass. | | | | | | + |
| | 12.23 Simonds Saw and Steel Comp. | + | | | + | | |
| | 12.24 Stackpole Carbon Comp., St. Marys, Pa. | + | | | | + | + |

*Table 19.24 continued*

| *Country* | *Manufacturer* | *Permanent Magnets* | | Fe, Fe–Si *strip, sheet* | Ni–Fe *alloys* | *Dust cores* Ni–Fe, Fe (*dust*) | *Ferrite cores* |
|---|---|---|---|---|---|---|---|
| | | *Metal* | *Ceramic* | | | | |
| USA (*cont.*) | 12.25 The Arnold Engineering Co., Marengo, Ill. | + | + | | + | + | + |
| | 12.26 Thomas Skinner Inc., Indianapolis, Ind. | + | | | + | | |
| | 12.27 US. Magnet Alloy Corp., Bloomfield, N. J. | + | | | | | |
| | 12.28 US Naval Ordinance Lab., White Oak, Silver Spring, Md. | | | | + | | |
| | 12.29 Western Electric Co., New York, N. Y. | | | + | + | | |
| | 12.30 Westinghouse Electric Corp., Blairsville, Pa. | | + | + | + | | |
| | 12.31 Wilbur B. Driver Comp., Newark, N. J. | + | | | + | | |
| India | 13.1 Morris Electronics (P) Ltd, Poona-26 | | + | | | | + |
| | 13.2 Permanent Magnets Ltd, Borivli (East) Bombay-92 | | + | | | | |
| | 13.3 Semiconductors Ltd, Poona-14 | | + | | | | + |
| | 13.4 ELPRO International Ltd, Chinchwad, Poona 19 | | + | | | | |
| Japan | 14.1 Akashi Gokin, Toshima, Kita-ku, Tokyo | | | | + | | |
| | 14.2 Chino Magnet Mfg., Himonya, Meguro-ku, Tokyo | + | | | + | | |
| | 14.3 Chiyoda, Nakazato-cho, Kita-ku, Tokyo | | | + | | | |
| | 14.4 Daiichi Gokin, Nagata-cho, Chiyoda-ku, Tokyo | | | | + | | |
| | 14.5 Denshi Jiki Kogyo, Ebisu Shibuya-ku, Tokyo | + | | | | | |
| | 14.6 Fujitsu, Marunouchi, Chiyoda-ku, Tokyo | | | + | | | |
| | 14.7 Fujidenki Kagaku, Shinbashi, Minato-ku, Tokyo | | | | | | + |
| | 14.8 Hitachi Metal, Marunouchi, Chiyoda-ku, Tokyo | + | | + | | | |
| | 14.9 Iriichi Tsushin, Sekiguchi-cho, Bunkyo-ku, Tokyo | | | + | | | |
| | 14.10 Kawakami Jishaku, Toshima, Kita-ku, Tokyo | + | + | | | | |

| | | | | | | |
|---|---|---|---|---|---|---|
| 14.11 Kogyosha Tsushin, Mita, Minato-ku, Tokyo | + | | | | | |
| 14.12 Matsushita, Kadoma-shi, Osaka | | + | | | | + |
| 14.13 Mitsubishi Denki, Marunouchi, Chiyoda-ku, Tokyo | | | | + | | |
| 14.14 Mitsubishi Kinzoku Kogyo, Otemachi, Chiyoda-ku, Tokyo | + | | | | | |
| 14.15 Mitsubishi Seiko, Otemachi, Chiyoda-ku, Tokyo | + | | | | | |
| 14.16 Murata Mfg., Nagaoka-machi, Otokuni-gun, Kyoto | | + | | | | |
| 14.17 Nakano Permalloy, Higashi-nakano, Nakano-ku, Tokyo | | | | + | | |
| 14.18 Nihon Kinsoku, Marunouchi, Chiyoda-ku, Tokyo | + | | + | | | |
| 14.19 Nippon Ferrite, Hyakunin-cho, Shinjuku-ku, Tokyo | | | | | | + |
| 14.20 Shinon Denki, Sumiyoshi-ku, Osaka | + | | | | | |
| 14.21 Sumitomo Special Metal, Kitahama, Higashi-ku, Osaka | + | + | | + | | + |
| 14.22 Sony, Kita-shinagawa, Shinagawa-ku, Tokyo | | | | | | + |
| 14.23 Taiyo Yuden, Soto-Kanda, Chiyoda-ku, Tokyo | | | | | | + |
| 14.24 Tamura Mfg., Higashi-Oizumi-machi, Nerima-ku, Tokyo | | | + | | | |
| 14.25 Tanaka Precious Metal, Nihonbashi, Kayaba-cho, Chuo-ku, Tokyo | + | | | | | |
| 14.26 TDK Electric, Uchi-Kanda-Chiyoda-ku, Tokyo | | | | | | + |
| 14.27 Tohoku Metal Ind., Ginza-higashi, Chuo-ku, Tokyo | | | + | + | | + |
| 14.28 Tokyo Shibaura Electric, Horikawa-machi, Kawasaki-shi, Kanagawa | | | | + | | |
| 14.29 Tokyo Ferrite Seizo, Tabato-shin-machi, Kita-ku, Tokyo | | + | | | | |
| 14.30 Tomita Denki, Gyoto-ku, Totori-shi, Totori | | | | | | + |

## REFERENCES


1. ADAMS, E.: Recent developments in soft magnetic alloys (J. A. P. **33** (4) (1962) 1214–1220).
2. ADAMS, E.: A new permanent magnet from powdered manganese bismuthide (Rev. Mod. Phys. **25** (Jan. 1953) 306–309).

2a AEG-Telefunken: Catalogue Telefunkenferrite AW WB 331c. (1971).

3. AKASHI, T.: Improvement of Mn–Zn-Ferrites: Neferrite (NEC-Research & Development (2) (Sept. 1961) 1–5).

3a Allegheny Ludlum Steel Corp., Pittsburgh: Mumetal EM 12, 8th edn.

3b Allen-Bradley Co., Milwaukee: Technical Bulletin 5506 (1966).

3c Allen-Bradley Co., Milwaukee: Technical Bulletin 5650 (1965).

4. Allevard-Ugine, Grenoble: Leaflet, Caracteristiques des nuances (1968).
5. ANSELIN, F.: Permanent magnet materials (Cobalt (June/Sept. 1959) 3–24).
6. Armco Steel Corp., Middletown, Ohio: Oriented electrical steels (1961).
7. Armco Steel Corp., Middletown, Ohio: Bulletin, Thin electric steels (1960).
8. Arnold Engineering Co., Marengo, Ill.: Bulletin PM 119 (1961).
9. Arnold Engineering Co., Marengo, Ill.: Magnetic Materials Bulletin GC 106C (Oct. 1961).
10. Arnold Engineering Co., Marengo, Ill.: Bulletin PM 123 (1963).
11. Arnold Engineering Co., Marengo, Ill.: Bulletin PM 117 (1959).
12. Arnold Engineering Co., Marengo, Ill.: Properties Deltamax, 4–79 Mo-Permalloy, Supermalloy. Bulletin TC-101A (1960).
13. Arnold Engineering Co., Fullerton, Cal.: Bulletin PDL-125.

13a Max Baermann, Bensberg, Data Sheet V 1859 (1971).

14. BASF, Ludwigshafen: Merkblätter über Carbonyleisenpulver.
15. BARKER, R. C.: Magnetization in tape wound cores (Proc. Nonlinear Magnetics (1958) 1–46).

15a Bell Lab. Rec. **42** (3) (Mar. 1964) 102; **43** (6) (June 1965) 260.

15b Bochumer Verein AG, Bochum: Leaflet E 187–1–654 Minimum.

16. BOZORTH, R. M.: Ferromagnetism. Van Nostrand Co. Inc., Toronto/New York/London (1951).

16a BRONNER, C., HABERER, J.-P., PLANCHARD, E. and SAUZE, J.: Beitrag zur Untersuchung von gesinterten Al-Ni-Co-Legierungen (Kobalt (49) (Dec. 1970) 167–170).

16b BRONNER, C., HABERER, J.-P., PLANCHARD, E. and SAUZE, J.: Über den Einfluss von Niob auf die magnetischen Eigenschaften von Alnico-Legierungen mit 4·5 bis 6·5% Titan (Kobalt (46) (Mar. 1970) 13–19).

16c BRONNER, C., PLANCHARD, E. and SAUZE, J.: Beitrag zur Untersuchung der physikalischen und magnetischen Eigenschaften einiger hochremanenter Alnico-Legierungen mit 24% Co: Sermalloy $A_2$, Sermalloy $A_2$ GD, Sermalloy $A_2$ GDH (Kobalt (37) (Dec. 1967) 163–169; (49) (Dec. 1970) 67).

17. CAMPBELL, A.: On the magnetic properties of silicon iron (Stalloy) in alternating magnetic fields of low value (Proc. Phys. Soc. **32** (1920) 232–243).
18. CAMPBELL, G. and WOOD, F. J.: A laminated flake-iron powder for use at audio and ultrasonic frequencies; in Soft Magnetic Materials for Telecommunications (ed. Richards and Lynch) (1953) 268–277.

18a C. D.Wälzholz, Hohenlimburg: Data Sheet, Magnetweicheisen.

19. Centro Magneti Permanenti, Milano: Data Sheet.
20. Cofelec, Montreuil: Catalogue Ferrinox (1969/70).
21. Crucible Steel Co. of America, Pittsburgh, Pa.: Leaflet, Ferrimag.
22. Crucible Steel Co. of America, Pittsburgh, Pa.: Standard and Stock Alnico Magnets (1962).
23. Deutsche Edelstahlwerke AG, Dortmund: Leaflet 1141/5 (Jan. 1971).

24. Deutsche Edelstahlwerke AG, Dortmund: Leaflet 1141/12 (Apr. 1962).
25. DIETRICH, H.: Tieftemperatureigenschaften von Invar (Nickel-Ber. **25** (3) (Mar. 1967) 37–45).
26. EASTWOOD, G. W.: Ductile permanent-magnet materials (Post Office el. Engrs. J. **53** (1961) 262–264; Nickel-Ber. **19** (1961) 167).
27. ELMEN, G. W.: Magnetic properties of perminvar (J. Franklin Inst. **206** (1928) 317–338).
28. ELMEN, G. W.: Magnetic alloys of iron nickel and cobalt (El. Engng. **54** (12) (Dec. 1935) 1292–1299; (1936) 887–889).
29. Engelhard Industries Inc., Union, N. J.: Data Sheet, Wilco Ni-Span C Constant Modulus alloy.
30. FABIAN, R. J.: Permanent magnet materials (Mat. Des. Engng. **50** (July 1959) 108–114).
31. FAHLENBRACH, H. and BARAN, W.: Weitere Untersuchungen an Legierungen auf Vicalloybasis, insbesondere an der Legierung VS 30 mit kleiner Koerzitivfeldstärke (T. Mitt. Krupp Forsch. Ber. **22** (1) (1964) 1–9).
32. FINE, M. E.: Vibralloy—a new ferromagnetic alloy (Bell. Lab. Rec. **30** (1952) 345–348).
33. Friedr. Krupp, Widia-Fabrik, Essen: Koerzit-Koerflex-Koerox. Leaflet W 220, 12.0 d 470 1. 0. 1 (1962).
34. Friedr. Krupp, Widia-Fabrik, Essen: Koerex VS 31, Drucksache 691 (1961).
35. Friedr. Krupp, Widia-Fabrik, Essen: Hyperm. Leaflet W 546, 3d: 467.
36. Friedr. Krupp, Widia-Fabrik, Essen: Hyperox. Leaflet 749–4.
37. Gebrüder Böhler & Co. AG: Leaflet, Permanit.
38. General Aniline & Film Corp., New York: GAF carbonyl iron powders. 5 M-5-60 M Exp.
39. General Electric Co., Edmore: Leaflet, Lodex (Feb. 1961).
39a General Electric Co., Edmore: Preliminary Data Sheet.
40. General Magnetic Corp., Detroit, Mich.: Characteristics table of permanent magnets.
41. Giffey-Prêtre, Paris. Data Sheet.
41a GÖDDECKE, H.: Weichmagnetische Eisen-Kobalt- und Eisen-Nickel-Legierungen (T. Mitt. Krupp **21** (4) (1963) 197–205).
41b GOULD, H. L. B. and WENNY, D. H.: Supermendur (El. Engng. **76** (Mar. 1957) 208–211).
42. GUMLICH, E., STEINHAUS, W., KUSSMANN, A. and SCHARNOW, B.: Über Materialien mit hoher Anfangspermeabilität (El. Nachr. T. **7** (1930) 231–235).
42a HARRISON, J. and WRIGHT, W.: Stengelkristallisation von kobalt- und titanreichen Dauermagnetlegierungen (Kobalt (35) (June 1967) 59–63).
43. HEDDLE, T. A.: On the temperature sensitivity of special magnetic materials (Brit. J. A. P. **4** (6) (June 1953) 161–166).
43a Hitachi Metals Ltd.: Permanent Magnets. Leaflet HE-B13-69.
44. HONDA, K., MASUMOTO, H. and SHIRAKAWA, Y.: New K. S. magnet steel (Sci. Rep. Tohoku Imp. Univ. **23** (Aug. 1934) 365–373).
45. HOWE, G. H.: Dynamax, a new crystal and domain oriented magnetic core material (Proc. Conf. Magnetism Magn. Mat. (1955) 264–272; Trans. AIEE **75** (1956) 548–551).
46. Inco Mond Nickel, (5) (July 1963) 10.
46a Inco Mond Nickel, (8) (June 1964) 8.
47. Indiana General Corp., Valparaiso, Ind.: Bulletin 303 (1968).
48. Indiana General Corp., Valparaiso, Ind.: Form 364 (1968).
49. Indiana General Corp., Valparaiso, Ind.: Form 350 (1969).
50. Indiana General Corp., Valparaiso, Ind.: Form 363 (1968).
51. Indiana General Corp., Valparaiso, Ind.: Form 397.
52. Indiana General Corp., Valparaiso, Ind.: Form 380 (1962).

53. Indiana General Corp., Valparaiso, Ind.: Form 381 (1962).
54. Indiana General Corp., Valparaiso, Ind.: Form 376 (1962).
55. Indiana General Corp., Valparaiso, Ind.: Form 373 (1961).
56. Indiana General Corp., Keasbey, N. J.: Bulletin 29.
57. Indiana General Corp., Keasbey, N. J.: Ferramic Memory Core Specifications.
58. Indiana General Corp., Keasbey, N. J.: Ferramic Components (1970).
58a ITT: Permalloy, Nickel–Iron Alloys. Leaflet 6532/256 E (Apr. 1968).
59. JONKER, G. H., WIJN, H. P. J. and BRAUN, P. B.: Ferroxplana, hexagonale ferromagnetisch Eisenoxydverbindungen für sehr hohe Frequenzen (Phil. T. Rdsch. **18** (9) (1957) 249–258).
60. JORDAN, H., VOLK, T. and GOLDSCHMIDT, R.: Pupinspulen mit Kernen aus Isoperm-Blech oder -Band (E. F. D. (36) (Jan. 1933) 8–14).
61. KATSUKI, A.: On the magnetic properties of Invar alloys (Brit. J. A. P. **18** (1967) 199–203).
62. KINNARD, I. F. and FAUS, H. T.: Self-compensating temperature indicator (Trans. AIEE **49** (1930) 949–951).
63. Leyman Corp., Cincinnati: Data Sheet, Plastiform Permanent Magnets (1961).
64. Lignes Télégraphiques et Téléphoniques, Paris: Catal. Ferrites.
64a Litton Precision Prod. Inc., Airtron Div., Morris Plains, N. J.: Technical Data.
65. LUBORSKY, F. E.: Permanent Magnets (El. Technol. (July–Sept. 1962).
65a Mannesmann AG, Düsseldorf: Leaflet 5716.
66. Magnetfabrik, Bonn: Dauermagnete (Apr. 1970).
67. Magnetic Metals Co., Camden, N. J.: Bulletin A 11 (1/15/61 R).
68. Magnetic Shield Division: Netic and Co-Netic Magnetic Shielding Manual.
69. Magnet Industries Association, Tokyo: Guide.
70. MAKINO, N.: Die Entwicklung von Dauermagneten in Japan (Kobalt (17) (Dec. 1962) 3–9).
71. MASUMOTO, H.: On a new alloy 'Sendust' and its magnetic and electric properties (Sci. Rep. Tohoku Imp. Univ. **25** (1936) 388–402).
71a MASUMOTO, H.: Dynamical characteristics of magnetostriction alloy 'Alfer' (Sci. Rep. Res. Inst. Tohuku Univ. **2** (1950) 413–419).
72. MASUMOTO, H. and SAITO, H.: On the effect of heat treatment on the magnetic properties of iron–aluminium alloys, II. The change of permeabilities, intensity of magnetization and magnetic hysteresis loss due to quenching and a new alloy 'Alperm' (Sci. Rep. Res. Tohuku Imp. Univ. (A) **4** (1952) 321–337).
73. METZDORF, W. and RABL, H.: Die wesentlichen Eigenschaften von Ferrit-Ringkernen mit rechteckförmiger Hystereseschleife und ihre Wechselbeziehungen (Elektron. Rechenanl. **5** (1963) 168–173, 216–220).
74. MINTERN, R. A.: Platinum alloy permanent magnets (Plat. Met. Rev. **5** (3) (July 1961) 82–88).
75. MISHIMA, T.: New high magnetic M. K. Steel (Ohm **19** (July 1932) 353; Jap. Pat. 96 371).
76. MISHIMA, T.: Recenti sviluppi nella fabbricazzione dei magneti permanenti in Giappone (Metallurg. Ital. **54** (Oct. 1962) 447–456).
77. MISHIMA, T. and MAKINO, N.: Studies of industrialization of MT permanent magnet (J. Iron Steel Inst. Jap. **43** (1957) 556–560, 647–652, 726–732).
77a Morris Electronics (P) Ltd., Poona (India): Data Handbook.
78. Mullard Ltd., London: Data Sheet, Magnadur Permanent Magnets.
79. Mullard Ltd., London: Data Sheet, Permanent Magnets.
80. Mullard Ltd., London: Data Sheet, Ferroxcube Issue 2.
81. Mullard Ltd., London: Data sheet, Ferroxcube Storage Cores.
82. Mullard Ltd, London: Data Sheet, Microwave Ferrites.
83. Murex Ltd, Rainham: Sintered permanent magnets P. U. 52.
84. Murex Ltd, Rainham: Sintered Comalloy magnets.

85. NACHMAN, J. F. and BUEHLER, W.: 16 percent aluminium–iron alloy cold rolled in the order-disorder temperature range (J. A. P. **25** (3) (Mar. 1954) 307–313).
86. NACHMAN, J. F. and BUEHLER, W.: Thermenol—a new 'soft' magnetic alloy (El. Manuf. (Nov. 1956) 140–145, 354).
86a Neosid Pemetzrieder GmbH, Halver: Catalogue (1969).
87. NEUMANN, H.: Über magnetisch harte Eisen-Nickel-Kupfer-Legierungen (Metallwirthschaft **14** (1935) 778–779.
88. NEUMANN, H.: Die neue Legierung 1040 mit hoher Anfangspermeabilität. ATM 4Z913–5T168 (1934).
89. Nippon Electric Co. Ltd, Tokyo: Data Sheet, Ne-Ferrite.
90. Not Known: Permanent Magnet Materials (Iron Steel **29** (June 1956) 323; Nickel-Ber. **14** (1956) 192).
91. Not Known: Micropowder magnets (Met. Ind. **83** (1953) 27–29).
92. NOTTEBROCK, H. and WEIS, A.: Einiges über das Hochfrequenzeisen Sirufer und seine Weiterentwicklung (HF-Techn. Elektroak. **47** (1936) 100–103).
93. PAINE, T. and MENDELSOHN, L. T.: High coercive force permanent magnet materials and their applications (El. Engng. **76** (1954) 891–895).
93a PAVLOVIC, D. M. and CLARK, J. J.: High temperature tape-wound cores for space power applications (Proc. Electronic Components Conf. IEEE, New York (May 1968) 180–190).
93b PARKER, R. J.: Fine-particle iron–cobalt magnet achievements in the permanent-magnet industry (IEEE Trans. **Mag-6** (June 1970) 249–251).
94. Permanent Magnet Association, Sheffield: Permanent Magnets.
94a Permanent Magnet Association, Sheffield: Technical Bulletin 1.
95. Plessey Co. Ltd, Ilford, Essex: Caslite iron dust cores (1969).
95a Plessey Co. Ltd, Towster: Caslox ferroceramic magnetic materials (1969).
96. Radio Corporation of America: Data Sheets (1963).
97. RANDALL, W. F.: Nickel–iron alloys of high permeability with special reference to mumetal (J. IEEE **80** (1937) 647–667).
98. Raytheon Co., Waltham, Mass.: Technical Data, Microwave Ferrites 10–900.
98a Raytheon Co., Lexington, Mass.: Information Package 2441-1-T.
98b RICHTER, H. G. and VÖLLER, H.: Über die Herstellung von hartferritischen Dauermagneten unter Berücksichtigung spezieller Formgebungsverfahren (DEW-Techn. Ber. **8** (4) (1968) 214–221).
99. Robert Bosch GmbH, Stuttgart: Leaflet, Alni-, Alnico- und Oxydmagnete.
100. SIBILLE, R.: Matériaux ferrites à très faible coefficient de température pour hautes fréquences (L'onde éléctr. **40** (Sept. 1960) 586–589).
101. Siemens AG, München: Data Book, Siferrit- und Sirufer-Material (1972/73).
102. Société Métallurgique d'Imphy, Paris: Leaflet, Überblick der Sorten (1971).
103. Société Métallurgique d'Imphy, Paris: Leaflet, Alliage Fe-Ni.
104. Société Métallurgique d'Imphy, Paris: Leaflet, Imphisil.
105. Société Métallurgique d'Imphy, Paris: Leaflet, Legierungen der Präzisionsmetallurgie.
106. Stackpole Carbon Co., St. Marys, Pa.: Bulletin RC-12 A.
107. Stackpole Carbon Co., St. Marys, Pa.: Bulletin, Ceramag and Ceramagnet.
108. STÄBLEIN, F.: Thermoperm, ein Werkstoff mit temperaturveränderlicher Magnetisierbarkeit (T. Mitt. Krupp. **2** (1934) 127–128).
109. Edelstahlwerke Buderus AG, Wetzlar: Data Sheet, Sonderweicheisen AME; Röchling'sche Eisen- und Stahlwerke, Völklingen: AME Steels.
110. Standard Telephones and Cables Ltd, London: Leaflet MM/105.
111. Standard Telephones and Cables Ltd (ITT): Ferrite Pot Cores. MM 240 (1968).
112. Standard Telephones and Cables Ltd (ITT), London: Permalloy (1968).
113. Standard Electrica S. A., Madrid: Leaflet, High quality ferrite cores.

114. CRL Electronic Bauelemente GmbH, Dralowid-Werk, Porz/Rhein: Ferrite catalogue (1971/72).
115. Steatit Magnesia AG, Dralowid-Werk, Porz: Data Sheet, Mikrowellenferrite.
116. Steatit Magnesia AG, Dralowid-Werk, Porz: Dralodur-Ferrit-Dauermagnete.
117. STEINITZ, R.: Permet, a nonferrous permanent magnet made from powders (Powder Met. Bull. **1** (1946) 45–47).
118. SUSSMAN, H. and EHRLICH, S. L.: Evaluation of the magnetostrictive properties of Hiperco (J. Acoust. Soc. Am. **22** (1950) 499–506).
118a Telcon Metals Ltd, Crawley: Data Sheet, Mumetal 40.
118b Telcon Metals Ltd, Crawley: Data Sheet, Properties and applications of Telcon Metals, 5th edn.
118c Telcon Metals Ltd, Crawley: Data Sheet, H. C. R. Alloy, 3rd edn (1962).
118d TDK-Electronics Co. Ltd: TDK-Ferrites Catalogue (1972).
119. Thomas & Skinner Inc., Indianapolis, Ind.: Bulletin M 304.
120. Tohoku Metal Industries Ltd, Sendai: Sendust Data Sheet.
120a Tohoku Metal Industries Ltd, Sendai: A guide to our products. Catalogue 651.
120b Tohoku Metal Industries Ltd: Technical Data, Ferrite cores. Catalogue FR-07E.
120c Tohoku Metal Industries Ltd: Ferrites for microwaves.
121. Trans-Tech. Inc., Gaithersburg, Md.: Microwave Ferrite Characteristics (Jan. 1963).
122. U. S. Magnet & Alloy Corp., Bloomfield, N. J.: Leaflet, Alnicus.
123. Vacuumschmelze GmbH, Hanau: Weichmagnetische Werkstoffe, Data Sheet (1967).
123a Vacuumschmelze GmbH, Hanau: Data Sheet M 026 (Apr. 1965).
123b Vacuumschmelze GmbH, Hanau: Dauermagnetwerkstoffe. Data Sheet FS-M8 (1969).
123c Vacuumschmelze GmbH, Hanau: Magnetreineisen. Data Sheet M 028 (Aug. 1970).
124. Vacuumschmelze GmbH, Hanau: Handbuch Weichmagnetische Werkstoffe (1967).
125. Vacuumschmelze GmbH, Hanau: Thermelast 4009. Data Sheet F 001 (June 1957).
125a Vacuumschmelze GmbH, Hanau: Data Sheet M 037 (Apr. 1969; Aug. 1970).
126. Vacuumschmelze GmbH, Hanau: Vacodur 16. Data Sheet M 009 (Mar. 1962).
127. Vacuumschmelze GmbH, Hanau: Magnetoflex. Data Sheet M 016 (Sept. 1969).
128. Vacuumschmelze GmbH, Hanau: Permenorm 5000 Z. Data Sheet M 014 (Apr. 1961).
129. Vacuumschmelze GmbH, Hanau: Thermoflux. Data Sheet M 015 (Mar. 1962).
129a Vacuumschmelze GmbH, Hanau: Data Sheet M 031 (Dec. 1969).
130. Vacuumschmelze GmbH, Hanau: Data Sheet M 39 (Mar. 1970).
131. Vacuumschmelze GmbH, Hanau: Data Sheet M 008 (Apr. 1960).
131a Vacuumschmelze GmbH, Hanau: Data Sheet M 20 (Apr. 1964).
132. Valvo GmbH, Hamburg: Valvo-Handbuch Ferroxcube (1970).
133. Valvo GmbH, Hamburg: Valvo-Handbuch Permanentmagnete (1970).
134. Valvo GmbH, Hamburg: Valvo-Handbuch Kernspeicher, Magnetköpfe (1971).
134a VEB Keramische Werke, Hermsdorf: Handbuch Ferrite (1970).
135. Vereinigte Deutsche Metallwerke AG, Altena/Westf.: Magnifer 36 W und 36 K (Nov. 1959).
136. Vereinigte Deutsche Metallwerke AG, Altena/Westf.: Magnifer 75 (Nov. 1959).
137. Vimétal S. A., Geneva: Varioperm (Microtecnic **5** (1) (1951) supplement).
137a Vimétal S. A., Geneva: Viperm (Microtecnic **5** (2) (1951) supplement).
138. Vogt & Co., Erlau and Passau: Leaflet, Magnetische Werkstoffe Ferrocart, Ferrocarit (1970).
139. WALTER, J. L.: Thin tapes of high purity silicon–iron for magnetic amplifiers (Proc. Nonlinear Magnetics (1961) 43–64).
140. Westinghouse Electric Co., Blairsville, Pa.: Spec. techn. data 52–167 (1962).
141. Westinghouse Electric Co., Blairsville, Pa.: Bulletin 52–152.
142. Westinghouse Electric Co., Blairsville, Pa.: Spec. techn. data 52–163 (1962).

143. Westinghouse Electric Co., Blairsville, Pa.: Hipernom alloy. Spec. techn. data 52–161 (1966).
144. Westinghouse Electric Co., Blairsville, Pa.: Spec. techn. data 52–165 (1966).
145. Westinghouse Electric Co., Blairsville, Pa.: Magnetic alloys. Bulletin 52–150 (1962).
146. Westinghouse Electric Co., Blairsville, Pa.: Bulletin 52–100.
146a Westinghouse Electric Co., Blairsville, Pa.: Bulletin 52–168 (1962).
147. Wiggin & Co. Ltd: Introduction to Wiggin alloys.
148. WILBUR, B.; Driver Co., Newark, N. J.: Ductile magnetic alloys. Bulletin MA-63.
149. YENSEN, T. D.: Hypernik and other magnetic alloys (Met. Progr. **21** (1932) 28–34).

# Index


Absorption resistance, 538
Absorption strip, 534
Access time, *see* Stores
Accommodation, 62
Activation energy, 152, 218, 233
Additional loss, 52, 53
Adjustment, of coils, 431, 447, 466, 467, 468, 469
Adjustment curves, 467, 468, 469, Plate 13.63
Adjustment devices, 467, 468, Plate 13.63
After-effect, *see* Residual effect
Ageing coefficient, 383
  definition of, 66
  of dust cores, 444
  of magnets, 252–254
  of relays, 383–385
  stability of, 391
Air-cored coils, 399, 446
Air-excluded annealing, *see* Hermetic annealing
Air-gap, 370, 457, 458, 467, 468, 659, 684
Air-gap ratio, 32, 33
Airtron, 528
Alcohol, 17
Alcomax, 248, 250, 272, 273, 687, 696–699, 733
Alfenol, 193, 341, 407, 590, 665, 709, 733
Alfer, 661, 662, 665, 733
Alignment
  degree of, 330
  percentage, 516
Alkaline-earth metals, 165, 497
Allegheny 4750, 733
48 Alloy, 741
Alni, 250, 688, 696–699
Alni magnets, 220, 246, 267, 688
Alnico and AlNiCo magnets, 87, 130, 192, 193, 245, 246, 250, 252, 261, 262, 273, 274, 295, 296, 321, 686, 688, 696, 703
  composition of, 264
  heat treatment of, 250, 254, 693
  stability of, 250
Alnicus, 700–701, 733
Alperm, 339, 407, 709, 733
Alphasil, 733
Aluminate, 560
Aluminium, 16, 222, 660
  substitution, 543, 565, 567, 568
Aluminium nitride, 385
Aluminium oxide, 167, 385, 478, 499, 500, 618
AME, 309, 388, 733
Amplifiers
  magnetic, 357, 359
  microwave, 285, 574
Amplitude modulation, 574
Anhyster, 733
Anisotropic constant, 79, 87, 122, 317
Anisotropic energy, 629, 657
Anisotropic field strength, 545, 569, 571, 622
Anisotropy
  crystal, 79
  exchange, 56, 93, 258, 280, 294
  magnetic, 79, 86
  shape, 91, 257, 279, 289
  stress, 91
  uniaxial, 91, 150, 626
Annealing, *see* Heat treatment
Annealing atmosphere, 175, 223, 283, 406, 476, Plate 7.12
Antiferromagnetic materials, 18
Antiferromagnetism, 18, 104
Argon, 17, 285, 290

Armature, 381
Armco iron, 163, 213, 309, 411–412, 421–423, 660
Armco pure iron, 358
Arnox, 705, 733
Asteroid 631, 632
Atomic separation, 103
Attenuation
  forward, 536, 546, 550, 553, 554, 555, 568
  in waveguides, 551, 563
  relation to Faraday rotation, 558, 559, 560, 562, 564
  reverse, 536, 546, 551, 554, 555, 568
Attenuation ratio, 566, 568, 573
Austenite, 258, 277

Balco, 712–713, 733
Band filters, 457
Bandwidth, *see* Isolators
Barbed-wire pattern, Plate 4.32
Barium, 16, 166
Barium ferrite, *see* Ferrites
Barium phosphate, 293
Barkhausen effect, 13
Barkhausen jumps, 53
Barnet effect, 10, 11
Bells, 296
Benzene, 17
Beryllium, 17
Biax, 645
Binding matrix, 273, 283, 287, 439–441
Bismanol, 704, 733
Bismuth, 17
Bismuth oxide, 293
Bit density, *see* Information density
Bitter process, 108
Bloch lines, 109, 126
Bloch wall, 109, 256
  energy, 111, 126, 256
  mobility, 256
  shift, 53, 110, 600
Bobbin cores, *see* Cores
Bohr magneton, 20
Boron, 17
Boron oxide, 179
Brass, 660
Brittleness, 319, 439
Bubble domain, 646
Buckling, 125
Butt joints, 331, 332
Button cores, *see* Cores
Buzzers, 296

C cores, *see* Cores
Cable loading, *see* Loading
Cadmium, 17
Cadmium oxide, 167
Calcium, 16, 166, 210, 482, 492, 570
Calcium carbonate, 17
Calcium oxide, 143, 611, 612
Calmalloy, 683, 733
Carbide, 383
Carbon, 162–165, 167, 216, 260, 308, 319, 320, 403, 436, 449
Carbon dioxide, 476
Carbonyl Fe–Ni alloys, 173, 439
Carbonyl iron, 72, 165, 173, 309, 390, 426, 427, 428, 436, 437, 442, 444, 446, 447, 450, 733
Carbonyl nickel, 173, 439
Carbonyl process, 436
Carpenter 49, 733
Caslam, 733
Caslite, 734
Cast magnets, 291
Cathode sputtering, 92, 126, *see also* Evaporation deposition
CDW magnetically soft iron, 309, 734
Centrifugal mill, 439
Centring magnets, 296
Ceramag, 734
Ceramagnet, 705, 734
Cerium, with rare earths, 286
Chain of spheres, 125
Channel filter, Plate 13.64
Characteristic curves
  of memory stores, 603
  of permanent magnets, 81
Charcoal iron, 388
Chromium, 16, 217, 492
  trivalent, 167
Chromium oxide, 16, 143, 479, 500, 563, 586, 612, 613
Circuit, magnetic, 241
Circulator, 526, 571
Closure domain, 105, 106, Plate 4.5
Coating, magnetic, 584
Cobalt, 13, 22, 74, 78, 87, 93, 101, 209, 213, 217, 247
  dust, 93, 287, 290
  substitution, 547, 566, 569, 584, 668, 669
Cobalt alloys
  Co–Pt, 241, 246, 252, 257, 280
  Co–Sm, 284–287
  with rare earths, 257, 280, 283
Cobalt ferrite, *see* Ferrites

Cobalt oxide, 16, 93, 281, 500, 505, 506, 507
Coercivity, 81, 87, 163, 164, 241, 255, 281, 308, 310, 320, 339, 430, 441, 455
  apparent, 115, 145
Coherent rotation, 125, 601, 629
Coils, inductance, 396, 673
Coincidence working, 595, 612, 629, 634, 638
Cold rolling, 138, 169, 277, 279, 425
  of Fe–Al sheet, 340
  of Fe–Si sheet, 56, 314, 325
Cold working, 54
Columnar crystals, 270
Columnax, 687, 696–699, 734
Comalloy, 276, 702, 734
Combination alloys, 56
Comol, 702, 734
Compensation materials, 681
Compensator alloy, 681, 682, 734
Compressional rigidity, 209, 274
Conduction mechanism, 224
Conductivity, *see* Resistance
Co-Netic, 733
Conpernik, 710–711, 734
Constancy, secular, 389, 663
Conversion efficiency
  electro-acoustic, 657
  temperature, 258
Copper, 17, 588
  in Fe–Si alloys, 164, 320
  in ferrites, 167, 569
Copper oxide, 16, 17
Cores
  bead, 466
  bobbin, 431
  button, 431
  C cores, 331, 371, Plate 10.23
  construction of, 370
  dwarf, 607, 622
  E cores, 183, 372, 401, 458, 460, 678, Plate 10.23
  H cores, 431
  laminated, 129, 139, 184, 364, 371, 400, 454, Plate 13.1
  M cores, 186, 187, 371, 401, 459, 678
  memory, 595–620
  P cores (Philbert), 678
  pot, 431, 457, 461, 467, Plate 13.63
  RM cores, 463
  rod, 466
  shapes, 182, 184, 331, 372, 399–402, 432, 440, 459–466, 599
  stacked, 184, 431
  toroids, 29, 32, 80, 139, 331, 365, 367, 370, 372, 374, 375, 399
  U cores, 186, 349, 371, 400, 678
  wire, 399, 434, 435
  X cores, 461, 465
  *see also* Dust cores, Ferrites
Correcting magnets, 297
Corrosion resistance, 382, 392
Cotton–Mouton effect, 6, 9
Coupling, magnetic, 297
Coupling factor, magnetomechanical, 644, 655, 656, 659, 661, 664, 666
Cracked gas, 255
Cromag, 705, 734
Cropped tape cores, *see* C cores
Crosstie walls, 127
Cr-Permalloy, 213, 414, 419, 420, 423
Cryoperm, 10, 676, 734
Crystals
  anisotropy, 79
  directions and planes, 89, 119, 199, 205
  energy, 86
  orientation, *see* Texture
  structure, 199, 203, 206, 270, Plate 7.12
Cubic texture, 138, 139, 140, 169, 333–336, 365, 414
  in Fe–Al, 343
  in Fe–Ni, 138, 140, 365, 414
  in Fe–Si, 139, 141, 315, 331–338
Cunico, 43, 239, 241, 274, 702, 734
Cunife, 43, 241, 246, 253, 275, 511, 702, 734
Curie law, 17
Curie temperature, 19, 23, 59
  of ferrites, 22, 61, 245, 247, 475, 480, 493, 528, 561, 567, 617, 618
  of metals and alloys, 20, 22, 103, 201, 316, 368, 407, 415, 661, 666, 682
Curling, 125
Current transformer, 306
Cyclic demagnetisation, 60, 62
Cycling energy loss, 51, 315, 329, 334, 342, 343, 346, 351, 421, 547
Cycling time, 581
Cylindrical coils, 82, 83
Cylindrical cores, 446, *see also* Cores

D318 696/7/8/9, 734
Deep drawing, 209, 389
Delta signal, 607
Deltamax, 140, 213–214, 362, 366, 367, 369, 595, 700–701, 734
Demagnetisation, 60, 62

Demagnetisation curve, 27, 81, 238, 239, 242, 244, 254, 255, 259, 264, 269, 273, 275, 276, 279, 280, 288
Demagnetisation factor, 85, 254, 255, 539, 626
Density, 205, 206, 207, 213–214, 274, 308, 316, 317, 318, 389, 430
Diamagnetism, 17, 20, 101
Diamond, 17
Diaphragms, telephone, 369, 430
Dielectric constant, 226–235, 453, 527, 528
Dielectric loss, 541
Diffusion, 64, 149, 164, 170, 338
Dimax, 734
Di-Max-M, 734
Dimensional ratio, 83, 182, 243, 254
Disaccommodation, 63, 64, 65
  of iron alloys, 63
  of Mn–Zn ferrites, 64–67, 489–492
  of Ni–Zn ferrites, 509
  of permanent magnets, 244
Disaccommodation factor, 64
Dispersion, 226
Distortion, non-linear, 44
Distortion factor, 47
Disturbance ratio, 605
Disturbing pulse, 491, 603
Domains
  closure, 105, 106, Plate 4.5
  elementary, 18, 105–111
  theory of, 105
Dot, magnetic, 626, 627, 646, *see also* Permalloy
Double refraction, 9
Draladur, 705, 734
Drum store, 581, 583, 590, 591, Plate 15.8
Dual system, 596
Ductility, 390
Dust, metallic, 345, *see also* Powder metallurgy
Dust cores, 36, 43, 44, 71, 193, 206, 229, 231, 426–427, 436–459
  production of, 435–442
Dust magnets, 257, 258, 290
Dwarf cores, 607, 622
Dynamax, 418, 734
Dynamo sheet, 50, 169, 187, 306, 322, 323, 349
Dysprosium, 22

E cores, *see* Cores
Eddy-current coefficient, 37, 42, 61
  as function of temperature, 61
  of dust cores, 443
  of Mn–Zn ferrites, 42, 62
  of Ni–Zn ferrites, 501, 502
Eddy-current loss, 49, 50, 337, 338
  anomalous, 52, 53
EI laminations, 72, 365, 372, 373, 400, 401
Einstein–de-Hass effect, 11, 63
Elastic limit, 239
Elastic modulus, 209, 234, 308, 657, 664, 667
Electric-clock motors, 281
Electric motors, 297
Electricity meters, *see* Meter magnets
Electrolytic iron, 165, 233, 314, 426, 427, 446
Electrolytic manganese, 165
Electrolytic nickel, 165
Electrolytic precipitation, 126, 435, 635
Electromagnets, 297
Electron microscopy, 262
Electron shells, 101, 102
Electron spin, 102
Electrosheet, 305, 314, 369
Electrostrip, 325
Elementary domains, 18, 105–111
Elinvar, 734
Ellipsoid, 85, 118
Elongated single domain, *see* ESD
Encapsulation, 189
Energy, 238
  magnetostatic, 106
Energy density, 240
Epstein test, 323
Erase head, 583, 590
Erbium, 22
ESD magnets, 290, 704
ESD particles, 281–295, 586
Evaporation deposition, 92, 126
  apparatus for, 624
Exchange force, 103
Expansion, thermal coefficient, 209, 274, 291, 308, 310
'Extra' loss, 52, 53

Fanning, 125, 126
Faraday circulator, 571
Faraday effect, 6, 534, 536
Faraday isolator, *see* Isolators
Faraday rotation, 17, 526, 532, 535, 553, 558, 563, 564
Faraday rotator, 535, 542, 560, 563
Ferbalite, 705, 734
Fercolite, 705, 734

Ferdurite, 705, 734
Fermalite, 458, 716–719, 734
Fernilite, 716–719, 734
Feroba, 705, 734
Ferramic, 527, 541, 550, 554, 607, 724, 729, 730, 731, 734
Ferreed, 393
Ferribrox, 734
Ferriflex, 705, 734
Ferrimag, 705, 735
Ferrimagnetic materials, 16, 18
Ferrimagnetism, 103, 104
Ferrinet, 635
Ferrinox, 716–719, 720–723, 734
Ferrite cores 456–471, 716–732
  dust cores, 455
  materitals for, 194
Ferrite stores, 595–620, 623
Ferrites
  Ba, 22, 87, 193, 205, 219, 226, 227, 228, 231, 233, 246, 249, 251, 256, 257, 261, 281–293, 394, 511, 524, 535, 568, 559, 658, 659, 666, 680, 684, 688, 705
  Co, 22, 75, 78, 87, 123, 218, 232, 282, 291, 293, 393, 473, 545, 546, 569
  Co–Fe, 75, 142, 149, 291, 292, 612, 615, 620
  Co–Mn, 78
  Co–Zn, 22, 61, 78, 394, 474, 666
  Cu, 22, 218, 232, 473
  Cu–Cd 235, 472, 527, 666
  Fe, *see* Magnetite
  Fe–Li–Zn, 666
  Fe–Sn, 235
  hexagonal, 205, 511–517
  K, 295
  Li, 22, 546, 617, 669
  Li–Co, 669
  Li–Cu, 615
  Li–Fe, 22
  Li–Ni, 615, 617
  Mg, 22, 176, 218, 221, 232, 473, 524, 546, 557, 668
  Mg–Al, 222, 233, 234, 561, 562
  Mg–Cr–Fe, 22, 563, 564
  Mg–Cu, 142, 222, 613
  Mg–Fe, 142, 149–154, 619
  Mg–Mn, 116, 142, 143, 532, 542, 548, 557–580, 601, 607–613, 615, 616, Plate 7.12
  Mg–Mn–Al, 550, 560, 561, 608, 615
  Mg–Mn–Al–Cu, 222
  Mg–Mn–Zn, 601, 609, 610, 611, 617
  Mg–Ni–Co, 153, 154
  Mg–Zn, 472, 666
  Mn, 22, 78, 87, 123, 177, 232, 473, 546, 565, 615
  Mn–Cd, 143, 601, 603, 616
  Mn–Cd–Mg, 617
  Mn–Co, 142
  Mn–Cu, 142, 600, 601, 607, 614, 615
  Mn–Fe, 618, 619
  Mn–Zn, 9, 10, 25, 42, 43, 60, 78, 87, 130, 157, 158, 166, 167, 175, 178, 179, 180, 233, 234, 235, 349, 472–489, 490, 491
  Ni, 22, 78, 89, 90, 193, 218–221, 225, 229, 233, 473, 509, 514, 524, 529, 546, 566, 569, 616, 666
  Ni–Al, 22, 528, 529, 566, 568
  Ni–Cd, 620
  Ni–Co, 548, 665, 669, 670
  Ni–Cr, 22
  Ni–Cu–Mn, 223
  Ni–Fe, 566, 619
  Ni–Mg, 615, 619, 668
  Ni–Mg–Mn, 143, 165
  Ni–Mn, 221, 222, 223
  Ni–Zn, 72, 76, 78, 87, 191, 204, 219, 223–228, 230, 472, 492–512, 527, 533, 534, 590, 619, 635, 666–669
  Ni–Zn–Al, 567
  Ni–Zn–Co, 142, 151
  Pb, 205, 226, 228, 257, 294
  production methods, 175, 263, 567, 568
  Sr, 205, 249, 257, 294, 295
  Zn, 218, 219
Ferrocart, 431, 735
Ferrod, 645
Ferromagnetic materials, 16, 18
Ferroxcube, 488, 513, 514, 541, 544, 554, 555, 615, 661, 662, 663, 716–719, 720–730, 735
Ferroxdure, 688, 689, 735
Ferroxplana, 511–517
Field constant, magnetic, 20
Field displacement, 537
Field strength
  critical, 599
  of magnets, 20
Figure of merit, *see* Transductors
Filling factor, 289, 448, 584
Film memory store, 594
Filter, magnetostrictive, 660
Filter magnet, 297
Final annealing, 390
Flake iron, 312, 313, 342, 426, 427, 456

Flux
  chemical, *see* Sintering
  magnetic, 21
Flux lines, 256
Flux reversal, 600, 602, 629, 632
Foil, *see* Film memory store
Foliate texture, 513
Form factor, 83
Forming, *see* Moulding
Forward attenuation, 536, 546, 551, 553, 554, 555, 568
Frequency doubling, 574

Gadolinium, 18, 221, 283
Gadolinium-cobalt, 284
Gallium, 569
Gapping, 58, 86, 398
Gapping angle, 241
Garnets, 18
Gauss (unit), 21
Gaussit, 278, 689, 735
Gecalloy, 704, 735
Generator, 297
Genox, 705, 735
German Standards
  DIN 1325 (magnetic field), 19
  DIN 1339 (units), 21
  DIN 17405 (relay materials), 383, 387, 389
  DIN 17410 (permanent magnets), 184, 245, 261, 686, 688, 708
  DIN 41280 (ferrite core materials), 194
  DIN 41281 (dust cores), 426, 427, 445
  DIN 41287 (shell and pot cores), 463
  DIN 41293 (ferrite pot cores), 461
  DIN 41295 (E cores), 460, 463
  DIN 41298 (magnetic heads), 588, 599
  DIN 41299 (X cores), 461, 465
  DIN 41301 (magnetic materials for transformers), 24, 402, 404, 405
  DIN 41302 (core stampings), 183, 185, 187, 400, 401
  DIN 41309 (C cores), 371
  DIN 42630 (transductors), 359, 360
  DIN 46400 (hot- and cold-rolled), 52, 524
  DIN 50461 (Epstein frames, 50 cm), 323
  DIN 50462 (Epstein frames, 25 cm), 323
  DIN 50463 (density of Fe–Si sheet), 318
  DIN 66010 (tape-recorder terminology), 583
Germanium, 17
Gold, 17
Gold–cobalt, 105
Goss process, 328
Goss texture, 139, 140, 326, 333–337, 367, 372, *see also* Texture
Graphite, 17
Gyralite, 735
Gyrator, 526, 534
Gyromagnetic effects, 12
Gyromagnetic ratio, 11, 12, 70, 530, 536

H cores, *see* Cores
Half-pulse, 596
Hametag process, 439
Hardening, 163, 258
Hardness, 163, 209, 389, 590
HCR alloy, 213, 214, 366, 367, 710, 711, 735
Hearing aids, 281, 286
Heat treatment
  in vacuo, 309, 313, 403
  of dust cores, 439
  of Fe–Ni, 171, 408, 410, 421
  of Fe–Si, 171, 321, 324, 329, 402
  of precipitation alloys, 71, 252, 260, 270, 274, 275, 368
  of unalloyed iron 70, 313, 385, 390
  *see also* Magnetic treatment, Tempering
Helium, 17
Hercon, *see* Relay
Hermetic annealing, 385
Heusler alloys, 13, 17, 103, 281, 283
Hexagonal ferrites, 205, 511–517
Hiperco, 213, 430, 665, 709, 735
Hipernik, 213, 214, 367, 413, 661, 710, 711, 735
Hipernom, 735
Hipersil, 735
Holding magnet, 293, 297
Honda alloy, 277, 696–699, 735
Hopkinson effect, 9
Hopkinson temperature, 59
Hot rolling, 169, 324, 340
Hughes effect, 14
Hybrid-T circulator, 526, 571
Hycomax, 273, 696–699, 735
Hydrogen, 17
Hydrogen annealing, 163, 164, 170, 305, 309, 383, 386, 390, 403
Hy-Mu-80, 735
Hynical, 735
Hynico, 696–699, 736
Hyperm Co, 366, 430, 709, 736

Hyperm Max, 71, 72, 712, 713, 736
Hyperm O, 309, 389, 736
Hyperm 1, 391, 709, 736
Hyperm 2, 215, 709, 736
Hyperm 3, 709, 736
Hyperm 4, 391, 709, 736
Hyperm 7, 709, 736
Hyperm 1T, 4T, 5T and 7T, 709
Hyperm 36 and 36M, 486, 709, 736
Hyperm 50 and 50A, 232, 367, 373, 702, 736
Hyperm 766, 71, 72, 486, 709, 736
Hyperm 800, 676, 712, 713, 736
Hyperm 900, 676, 712, 713, 736
Hypermal, 709, 736
Hyperox, 72, 481, 716–719, 720–723, 736
Hysteresis, 17
Hysteresis coefficient, 37, 43, 45, 47, 72, 129
  of iron dust cores, 426, 427, 445
  of Mn–Zn ferrite, 43, 61, 72, 483–486, 501
  of Ni–Fe, 72, 416, 417, 426, 427, 486
  of Ni–Zn ferrite, 72, 503, 504
Hysteresis constant, 46
Hysteresis factor, 46
Hysteresis family, 115
  Fe–Ni, 140, 146, 420
  Mg–Mn ferrite, 116
  Mg–Fe ferrite, 156
  Mumetal, 420
  4–79 Permalloy, 117
  steel wire, 116
  Supermalloy, 416
Hysteresis loop, 79, 80, 101, 332, 393
  differentiated, 114
  Isoperm, 155–159
  normal, 136, 159, 176, 311, 313, 363, 412, 414
  Perminvar, 145–154
  rectangular (square), 137–145, 158, 182, 343, 362, 363, 413, 592, 595, 615, 619, 636, 415
  *see also* Rayleigh loop, Rotational hysteresis
Hysteresis loss, 51, 54, 72, 131, 323, 331, 340, 347, 368, 420, 430, 455, 496, 501
  in Rayleigh loops, 129
  in rotational fields, 54–57
Hysteresis motor, 54

Ideal magnetisation, 115
Imphisil, 736
Impregnated tape, 584
Impulse train, *see* Pulse sequence
Incoherent rotation, 601
Indalloy, 702, 736
Indium, 569, 570
Indox, 252, 688, 705, 736
Inductance control, steepness of, 470
Induction, magnetic, 20
Induction constant, 20, *see also* Permeability
Inductivity factor, 34, 35
Information density, 587, 591, 592, 643
Information storage, 580, 581, *see also* Stores
Initial loss, 542, 556, *see also* Loss
Initial permeability, *see* Permeability
Instability, 428, 445, 451
Insulation for strip and dust cores, 287, 400, 431, 432, 433
Intermetallic compounds, 283, 284
Invar, 660, 661
Ionic diffusion, 92
Ionic radius, 56, 204
Iron alloys
  Fe–Al, 60, 193, 201, 207, 222, 339–345, 407, 665
  Fe–Al–Mo, 79
  Fe–Al–Ni, 155, 174, 246, 257, 260–274
  Fe–Al–Ni–Co, 92, 171, 210, 257, 260–274
  Fe–Al–Ni–Co–Nb, 271
  Fe–Al–Ni–Co–Ti, 260, 268
  Fe–Al–Ni–Cu, 266, 267–270
  Fe–Al–Si, 192, 213, 214, 345, 346, 406, 453–456
  Fe–Au, 65
  Fe–C, 258
  Fe–Co, 92, 174, 193, 202, 206, 213, 214, 257, 288, 348, 349, 368, 369, 393, 429, 640, 663
  Fe–Co–Cr, 664
  Fe–Co–Mo, 171, 257, 260, 275
  Fe–Co–Ni–Ti, 260, 277
  Fe–Co–Ti, 257, 277
  Fe–Co–V, 142, 193, 257, 275–278, 348, 349, 368, 666
  Fe–Co–W, 257, 260
  Fe–Cr, 8, 149, 257
  Fe–Cu, 164
  Fe–Mn, 165, 215, 277
  Fe–Ni, 26, 27, 60, 62, 79, 87, 92, 111, 121, 122, 138, 142, 148, 154, 155, 171, 182, 193, 201, 209, 216, 367, 386–392, 407–413, 421–425, 426,

Iron alloys — *cont.*
Fe–Ni — *cont.*
427, 591, 622, 633, 640, 644, 664, 665, 681, 683, Plate 4.32
Fe–Ni–Co, 79, 147, 362, 375, 421–423
Fe–Ni–Co–Mo, 423
Fe–Ni–Cr, 60, 156, 216, 257, 275, 278, 418, 420, 682
Fe–Ni–Cu, 155, 171, 174, 222, 274, 423, 591, 681, 683
Fe–Ni–Cu–Mo, 62, 171, 268, 428, 429
Fe–Ni–Mo, 79, 142, 165, 413–418, 423, 682
Fe–Ni–Ti, 257, 277, 644
Fe–Pd, 87, 105, 287
Fe–Pt, 246, 257, 280, 294
Fe–Si, 34, 53, 56, 60, 62, 63, 78, 79, 88, 89, 140–142, 148, 164, 169, 171, 174, 188, 191–193, 201, 209, 212–214, 253, 312–338, 341, 344, 349, 363–365, 369, 372–376, 388–392 402–407, 423, Plate 4.5
Fe–Si–V, 406
Fe–V, 60
Fe–W, 222
Iron carbide, 16, 22
Iron chloride, 18
Iron dust
cores, *see* Dust cores
magnetic properties, 173, 426, 427, 441, 448
magnets, 222, 288, 290, 704
particle size, 281, 288, 290
production methods, 287, 435
pyrophoric, 287
Iron nitride, 383
Iron oxide, 18, 64, 177, 257, 435, 479, 489, 570, 586, 599
$\gamma$-oxide, 582, 584, 591, 594
Iron pentacarbonyl, 436
Iron phosphide, 22
Iron wire, 411, 425
Irreversible Fe–Ni alloy, 201, 407
Isolators, 526
bandwidth of, 528, 546, 548, 556, 561, 565, 566, 567, 570
Faraday, 526, 534, 536, 548, 552, 568, 573
field constriction, 526, 537, 538, 563, 568
resonant absorption, 548, 568, 573
Isoperm, 155, 206, 424, 425, 428, 736
ferrites, 157, 158
loops, 155, 158, 425, 428

Joule effect, 4, 5

Keraperm, 351, 369, 715, 716–719, 729, 730, 736
Kerr effect, 9, 108
Kittel's equation, 539, 543
36 KNM, 741
Koerflex, 689, 736
Koerox, 247, 251, 688, 689, 705, 736
Koerzit, 247, 278, 279, 688, 689, 736
Krarup loading, 397
KS-1 and KS-2, 258, 736

Laminated cores, *see* Cores
Laminations, thickness of, 70, 181, 185, 186, 187, 335, 336, 365, 417
Landé factor, 12, 528
Lanthanum oxide, 167
Larmor frequency, 530, 536
Lattice constant, 200, 204, 205, 260
Lead, 17, 390, 660
Lead ferrite, *see* Ferrites
Limiting frequency, 67, 69
Limiting hysteresis loop, 114, 115
Line retrieval, in storage devices, 600
Line transformer, 312, 349
Linewidth, 528, 546, 547, 555, 556, 561, 563, 566, 571
Lithium,16, 166, 492
Lithium oxide, 497
Loading, inductive, 396, 421, 458, 459
continuous, 397
Krarup, 397
lumped, 398, 431, 451, 459, 469, 486
Lodex, 704, 736
Lodox, 736
Loschmidt number, 20
Loss
anomolous, 52, 53
cyclic, 51, 315, 329, 334, 342, 343, 346, 351, 421, 547
eddy-current, 49, 50, 337, 338
Loss angle, 38, 44
Loss coefficient
according to Jordan, 35, 434
according to Legg, 39
of dust cores, 44, 443, 452
of ferrite cores, 44, 62, 481–486, 501–504
of strip cores, 44, 486
Loss factor
dielectric
of dust cores, 229, 453

Loss factor — *cont.*
dielectric — *cont.*
of ferrites, 229–235, 527, 528, 561, 567, 569
magnetic, 38, 40, 447, 448
of dust cores, 71, 72
of Mn–Zn ferrites, 61, 71, 486, 487, 527, 714
of Ni–Zn ferrites, 71, 488, 504, 506, 509, 714
of Perminvar ferrites, 509
of strip cores, 71, 92
Loss partition, 41, 49
Loss resistance, 35, 434

M cores, *see* Cores
M5, 736
M583, 712, 713
M1040, 213, 214, 364, 366, 424, 428, 675, 676, 705, 712, 713, 736
MAD, *see* Transfluxors
Magloy, 736
Magnadur, 705, 736
Magnesil, 736
Magnesium, 16, 166, 599
Magnesium ferrite, *see* Ferrites
Magnet variometer, 29, 458
Magnetic amplifier, 357, 359
Magnetic disc, *see* Stores
Magnetic drum, *see* Stores
Magnetic head, 583, 587, 588, 590, 592, 594, 674
Magnetic tape, 584–587, 673
Magnetic tape recorder 581, 582–590, Plate 15.4
Magnetic treatment, 145, 147, 172, 264, 269, 270, 309, 338, 344, 368, 418
Magnetisation, 23
curve, 81, 117, 170, 316, 322, 330, 349, 369, 391, 411, 415
cycle, 115
energy, *see* Loss
extreme characteristic, 239, 244, 254
ideal characteristic, 115
inner characteristic, 244, 252
kinds of, 101, 104
process, 101, 110
spontaneous, 102
*see also* Hysteresis loop
Magnetite, 4, 13, 22, 78, 79, 87, 90, 123, 149, 218, 219, 220, 281, 292, 473, 477, 559, 584, 586, 591, 661, 662
Magnetocaloric effect, 14
Magnetoflex, 213, 214, 278, 736
Magnetomechanical coupling factor, 643, 656, 657, 660, 661, 664, 666, 667
Magnetomechanical effects, 13, *see also* Piezomagnetic materials
Magnetomotive force, 242
Magneton, 20
Magnetophone, 582, *see also* Magnetic tape recorder
Magnetoplumbite, 18, 206, 511
Magnetostriction, 4, 5, 7, 72–79, 121, 410, 424, 479, 493, 617, 655, 662
Magnetostriction constant, 77–79, 656, 659
Magnetothermal effect, 14
Magnetreineisen, 233, 309
Magnifer, 710–711, 712–713, 737
Manganese, 16, 281, 320
Manganese alloys
Mn–Ag–Al, 81, 171, 257, 279
Mn–Al, 17, 257, 282, 324
Mn–As, 19
Mn–Bi, 22, 87, 246, 257, 281, 282
Mn–Cu, 17
Mn–Fe–Si, 320
Manganese oxide, 18, 64, 177
Mangenese selenide, 18
Manifer, 737
Maniperm, 737
Manufacturers, 742–747
Marine cable, 411
Martensitic steel, 258, 259, 277
Matrix store, *see* Stores
Matteucci effect, 7, 8
Megaperm, 737
Memory, magnetic, 580–646
cores, 595–622
*see also* Stores
Mercury, 17, 285, 287
Metamagnetism, 19
Meter magnets, 297
Microferrite disc memory, 622, *see also* Stores
Micromagnetics, 124, 623
Microstrip technique, 574
Microwave amplifier, 285, 574
Microwave ferrites, 130, 556–570, 724–727
Microwave filters, 445
Microwave losses, 541, *see also* Forward attenuation, Reverse attenuation
Microwave switches, 572, *see also* Field displacement, Gyrator, Isolators, Waveguides
Microwaves, 523
Miller indices, 199

Mineralisation, 179
Miniature microphones, 281
Miniature motors, 286
Miniaturisation, 383, 458, 460, 574
Minimum, 388, 737
Mishima alloy, 269
Mishima metals, 698, 737
Mixture ferrites, 203, 257
MK-steel magnets, 260, 696–699, 737
Mo–Cu Permalloy, *see* Mumetal
Mohs hardness, 208, 209
Moisture, 442, 452
Mol, 702
Molecular viscosity, *see* Residual effect
Molybdenum, 217, 620
Molybdenum oxide, 167, 620
Moment, magnetic, 20, 473, 528
Monel-K, 660
Mo-Permalloy, 191, 206, 213, 214, 389, 419, 426, 427
4Mo-Permalloy, 389
Mo-Perminvar, 423
Moulding, 440
Multiple heads, 588
Mumetal, 14, 168, 181, 186, 188, 193, 213, 214, 217, 364, 366, 392, 413, 420, 421, 424, 589, 590, 593, 675, 676, 677, 705, 712, 713, 737
Mutemp, 682, 737

N 1250, 527
Natural frequency, 657
Néel spikes, 107
Néel temperature, 18
Néel wall, 126, 127, 627, 629
Neferrite, 737
Neosid, 426, 427, 737
Netic, 737
Neutron radiation, 191
New KS steel, 277, 696–699
4-79 Ni, 741
Nial, 696–699
Nialco, 696–699, 737
Nickel, 13, 22, 78, 87, 101, 102, 142, 209, 213, 214, 217, 591, 644, 660, 662–665
  dust, 439
  plating, 591
  single crystals, 73
  wire 138, 140
Nickel alloys
  Ni–Au, 171
  Ni–Co, 591, 593, 644, 663, 664, 665
  Ni–Co–Cr, 663
  Ni–Co–Cu, 171, 239, 257, 274
  Ni–Co–P, 633
  Ni–Co–Ti, 257, 277
  Ni–Cu, 682, 683
  Ni–Pt, 257, 280
Nickel ferrite, *see* Ferrites
Nickel oxide, 18
Nicromet, 737
Nilomag, 737
Nipermag, 737
Niromet, 710–711
Niron, 710–711, 737
Ni-span C, 644, 660, 737
Nitrogen, 17, 64, 162, 164, 179, 384, 386, 403, 476
NKS, 698, 737
NM 1250, 527
NMHG, 682

Oersted (unit), 21
Oerstit, 281, 688, 689, 737
OP magnet, 281, 738
Oriented superstructure, 92, 156
Oriented T, T-5 and M, 738
Orsi, 738
Orthocore, 633
Orthoferrite store, 645
Orthoferrites, 515, 645, 646
Orthonik, 367, 738
48 Orthonik, 741
Orthonol, 367, 738
Oscillatory modes in waveguides, 524
Ox, 373, 688, 689–692, 705, 738
Oxilit, 689–692, 738
Oxit, 688, 705, 738
Oxygen, 162, 164, 175, 180, 224, 320, 403, 442, 449, 476, 489, 490, 491, 510, 566, 613
Oxygen–argon mixture, 625

P core, *see* Cores
Packing density, 288, 289
Packing factor, 432, 433
Parametric materials, 16
Particle size, 285, 287, 289, 290
  critical, 256, 281, 288, 289, 293, 584
PASCAL, 593
Peak time, 597
PERM, 593
Permalloy, 13, 137, 181, 191, 306, 388, 408, 411, 412, 413, 422, 424, 425, 439, 455, 456, 479, 590, 635, Plate 4.7, Plate 17.3
  dots, 646

Permalloy — *cont.*
dust, 439, 440, 448
film, 625, 626
tape, 181, 411, 620, 641
treatment of, 171, 408, 424
Permalloy A, 213, 214, 738
Permalloy B, 213, 214, 676, 710, 711, 738, Plate 17.3
Permalloy C, 14, 185, 213, 214, 413, 676, 688, 712, 713, 738, Plate 17.3
Permalloy D, 213, 214, 710, 711, 738
Permalloy F, 213, 214, 366, 367, 710, 711, 738
Permalloy G, 738
45 Permalloy, 389, 662, 663
65 Permalloy, 366
78·5 Permalloy, 419
81 Permalloy, 426–427
4-75 Permalloy, 635
4-79 Permalloy, 193, 213–214, 713
Permanent magnets, 172, 238–297
dimensions of, 241
materials for, 255, 257
production rates, 291
temperature coefficient of, 248, 249
Permax Z, 366, 413
Permeability
absolute, 23, 29
amplitude, 25
apparent, 31
complex, 33, 34, 43, 531
differential, 29
effective, 31, 33, 35, 432
field-strength dependence of, 25, 58, 327, 412, 415, 419
frequency dependence of, 67, 68, 367
inductive, 33
initial, 24, 69, 310, 341, 347, 402, 407, 408, 410, 415, 416, 417, 418, 420, 428, 430, 454, 475–479, 493–501, 515, 561, 567, 590, 608, 615
locus of, 34
maximum, 25, 163, 308, 310, 319, 328, 338, 343, 344, 368, 406, 408, 411, 415, 418, 428, 430, 454, 455, 480, 496, 590
permanent, 27, 239, 244
relative, 24
resistive, 33
reversible, 27, 28, 382, 392, 419, 429, 444, 480, 656, 665, 688
superposed, 26–28
temperature dependence of, 57, 58, 444, 478, 497
tensor, 529
toroidal, 29, 438, 442
Permeability number, 24
Permeability rise factor, 44–47
Permeance, 343
Permendur, 213, 214, 393, 422, 423, 428, 738
Permenorm 3601, 71, 676, 710–711, 738
Permenorm 5000G, 710–711, 738
Permenorm 5000H, 675, 676, 677
Permenorm 5000Z, 213–214, 365, 366, 367, 373, 595, 621, 661, 662, 710–711, 738
Permeron, 367, 738
Permet, 738
Permimphy, 712–713, 738
Perminvar, 92, 145, 146, 421, 423, 479, 500, 738
ferrites, 92, 131, 500, 509, 510
loop, 145–154
treatment, 421
45 Perminvar, 423
45-25 Perminvar, 213–214, 421
7-45-25 Perminvar, 213–214
Phase shifter, 525, 540, 550, 572
Philbert core, 678
Phosphorus, 162, 164, 216, 320, 390
Piano wire, 116, 644
Picture-frame sections, 119
Picture storage, 583
Piezomagnetic materials, 661, 662, 664, 666–668
Plastic magnets, 289, 290, 293
Plastiform, 705–707, 738
Plastoferrite, 705–707, 739
Platinax, 252, 280, 703, 739
Platinum
element, 16
trade name, 703, 739
Polarisation, magnetic, 20, 23, 348, 473, 492
Pole-pieces, 238, 587
Pole-shoes, 307, 588, 592, 680
Polyiron, 739
Porosity, 179, 475, 546, 547, 559, 587, 589, 670
Potassium, 16, 165
Powder metallurgy, 172, 338, 345, 408
Power loss
cold working, 56
flux density dependence of, 53
frequency dependence of, 52, 322, 341
Si-content dependence of, 315, 346
temperature dependence of, 61, 321
*see also* Loss

Prac, 433, 689–692, 739
Precipitation, 269
Precipitation alloys, 67, 257, 260–275
Precipitation hardness, 260, 280
Precipitation Isoperm, 155
Pressure values, 433, 440, 441
Principal directions and planes, *see* Crystals
Production figures of permanent magnets, 291
Prox, 739
Pulse sequence, 604–606
Pupinisation, *see* Loading, lumped
Purification, *see* Refining
Pyrophoric iron, 287

Q factor
  dust cores, 438, 444, 445, 447, 452
  mechanical, 656, 660, 667
Quality product, 482, 486, 487, 505, 507, 508

R 2799 alloy, 682
Radiation, 62, 193
Radiometal, 213–214, 710, 711, 739
Rare-earth magnets, 105, 284, 285
Rayleigh constant, 128, 433, 434
Rayleigh loop, 128, 132
RCA ferrite, 729, 731
Read-out field strength, 598
Read-out head, *see* Reproducing head
Read-out process, 597
Read-out wire, 597
Reciprocity principle, 525
Reco, 688, 689–692, 696–699, 739
Recording head, 583
Recrystallisation, 170, 328, 391
Recrystallisation annealing, 138, 141, 326 418
Recrystallisation texture, *see* Texture
Rectalite, 739
Rectangular loops, 137–145, 417, 619
  in ferrites, 143, 152, 153, 607, 618
Rectangularity ratio, 144, 153, 597, 608, 611, 613, 614, 615, 617, 618, 619, 620, 639, 655
Rectimphy, 367, 710–711, 739
Refining, 163
Relaxation, 149
Relays, 130, 379, 381, 673, 680, Plate 12.1
  Herkon, 380
  materials for, 208, 382, 386–394
  polarised, 381
  sensitivity of, 381, 382
  unpolarised, 381
Reluctance, 243
Reluctivity, 34, 243
Remalloy, 209, 739
Remanence, 80, 115, 238, 255, 342, 368, 340
  apparent, 115, 382
Remanence ratio, 144, 155, 181, 368, 394, 597, 615, 617, 639
Remendur, 394, 739
Reoxidation, 177
Reproducing head, 583, 587, 594, *see also* Magnetic head
Residual coefficient, 37, 44, 62
  in dust cores, 44, 426–427, 445, 452
  in Mn–Zn ferrites, 62, 481, 486, 502
  in Ni–Zn ferrites, 501, 502
Residual effect, 36, 42, 406
  in Fe–Si, 406
  in permanent magnets, 251–254
Resin encapsulation, *see* Encapsulation
Resistance
  magnetic, 242
  specific electrical, 212, 656
    conduction mechanism of, 224
    frequency dependence of, 226
    of Co, 213–214, 217
    of dust cores, 216, 441
    of Fe, 213–214, 217, 308, 310
    of Fe–Al, 215, 339, 342, 590
    of Fe–Al–Si, 346, 366, 590
    of Fe–Co, 228
    of Fe–Co–V, 368
    of Fe–Cu, 214
    of Fe–Mn, 214, 215
    of Fe–Ni, 181, 214, 366, 389, 409, 661
    of Fe–Ni–Cr, 213–214, 232
    of Fe–Ni–Mo, 366, 414, 415, 452
    of Fe–Si, 212, 213–214, 228, 317, 389
    of ferrites, 218–228, 527, 529, 563, 590, 661
    of garnets, 570
    of Ni, 213–214, 217, 661
    of Ni–Co, 661
    temperature coefficient of, 215, 218, 219, 224, 308
Resistopermalloy, 213–214
Resonance
  ferrimagnetic, 536
  ferromagnetic, 536
  field strength, 537
  gyromagnetic, 70, 487, 536, 542
  losses, 541
Resonance absorption, 535, 548

Resonator, magnetomechanical, 655
Reverse attenuation, 536, 546, 550, 553, 554, 555, 568
Reversible Fe–Ni alloys, 201, 408
Rhometal, 213–214, 739
Ribbon cores, *see* Strip-wound cores
Rigidity, 208, 209, 274
Ring cores, *see* Toroids
Rise time of pulses, 606
ROD, 633, 634
Rod cores, *see* Cores
Rolling
  deformation, 138, 168, 321
  temperature, 169
  *see also* Cold rolling, Hot rolling
Rolling texture, *see* Texture
Rotational hysteresis, 54–57, 93, *see also* Hysteresis
Rotational processes, 53, 112, 256, 602, 628, *see also* Turning process
Rotator, *see* Faraday rotator
Rubber magnets, *see* Plastic magnets

Samarium–cobalt, 284–287
Saturation
  flux density, 22, 113, 114, 142, 181, 310, 315, 339, 366, 368, 389, 409, 430, 474, 494, 528, 559, 568, 590, 614, 662, 709, 710–711, 712–713
  magnetisation, *see* Magnetisation
  magnetostriction, *see* Magnetostriction
  polarisation, 20, 308, 310, 348, 473, 492, 513, 560, 561, 567, 571, 660, 662
Screening, *see* Shielding materials
Screw cores, *see* Cores
Selenium, 17
Semendur, 739
Semipermanent store, 643, *see also* Stores
Sempermax, 739
Sempersil, 739
Sendelta, 710–711, 739
Sendust, 213–214, 345, 426–427, 448, 453, 455, 456, 479, 589, 739
Shape
  effect of, 181, 182, 331, 411, 539–541
  of stampings and cores, 373, 400
Shape anisotropy, 91
Shearing angle, 241
Shearing line, 86
Shell cores, *see* Cores, pot
Shell model, atomic, 102
Shielding materials, 676, 677, 678
Shift, *see* Field displacement
Shock, resistance to, 274
Shrinking, 189, 210
Shunt, magnetic, 680
Shunt Steel, 682, 739, *see also* Compensator alloy
Siferrite, 528, 568, 593, 689–692, 729, 730, 731, 739
Signal voltage, 597–599
Silicon, 17, 569
Silicon dioxide, 179, 191, 293, 385
Silmanal, 279, 702, 739
Silver, 17, 588
Silver–aluminium–manganese alloys, 81, 279
Simanol, 702
Sincomax, 739
Single crystals, 118–123
  cobalt, 74, 75, 122, 123
  Fe–Ni, 79, 120
  Fe–Si, 79, 106, 120, 403, Plate 4.5
  ferrites, 75, 79, 123, 555, 566
  garnets, 570
  iron, 5, 73, 79, 107, 118, 309
  nickel, 73, 79, 120, 121
Single-domain particles, 281–295, 586
Sinimax, 590
Sintered ferrites, 175
Sintered iron, 313
Sintered materials, 171
Sintered metallic dusts, 172, 173, 174
Sintered permanent magnets, 174, 271, 273, 291
Sintering, 172
  compound, 575
  conditions, 484, 489, 497, 501, 503, 559, 609, 613
  process, 285
Sirufer, 426–427, 739
Skin effect, 674
SI 12, 17, 18 and 19, 688
Sodium, 16
Sodium bismuthide, 293
Softening by heat, 312, 323
Solderable magnets, 289
Solubility limits, 164
Space factor, 288, 289, 447, 584
Specific heat, 208, 209, 310
Specimen, *see* Sample
Speed of sound, 659, 660, 667
Spin, 101, 103, 104
Spin moment, 528
Spin relaxation, 70
Spinal, 707, 739

Spinalor, 707, 739
Spinel and inverse spinel, 17, 104, 202, 203, 205, 473, 511
Spiral domains, Plate 4.7
Split-ribbon cores, *see* Cores, C cores
Sponge iron, 172
Spontaneous magnetism, 103
Spot, magnetic, *see* Dot
Sprox, 254, 691, 739
Sputtering, 623–625, *see also* Cathode sputtering, Evaporation deposition
Squaremu, 739
49 Squaremu, 739
Stabilising
  of dust cores, 452, 453
  of permanent magnets, 244
  of resonators, 669
Stabilising field, 244
Stability, 192, 252, 391, 425, 432, 442, 445, 451
Stacked stampings, 186
Stalloy, 402, 739
Stamping process, 323
Stanferite, 718, 740
Starting field, 368, 599, 610, 615, 617, 621, 622
Steel, 63, 92, 257, 660
  carbon, 243, 257, 389, 660
  chrome, 193, 243, 259, 689, 694
  cobalt, 243, 246, 255, 257, 259, 689, 694
  Cr–Co, 252
  silicon, 314, 389, 404
  tungsten, 243, 259, 296, 695
  wire, 399, 431, 582
Steinmetz coefficient, 130, 317, 351
Steinmetz law, 130
Stoichiometry, 226, 454, 493, 504, 506, 566
Storage elements, 581, 625–633
Stores, 580–645
  bubble domain, 645
  capacity of, 581, 593
  cores for, 595–620, 729, 730, 731
  disc, 583, 593, 594, Plate 15.10
  foil, 594
  magnetic drum, 581, 583, 590, 591, Plate 15.8
  magnetic spot, *see* Dot
  magnetic tape, 582–590
  magnetised layer, 126, 584, 623–632
  matrix, 595, 638, Plate 15.11
  orthoferrite, 645
  plated wire, 634, 635
  semipermanent, 643
  twistor, 640–644
  waffle iron, 635
  *see also* Memory, magnetic
Stray field, 109, 431, 587, 627, 633, 643, 673
Stray flux factor, 243
Stress anisotropy, 91
Stressing, *see* Shrinking
Strip cores, 371, 372, 374
Strip-wound cores, 29, 139, 185, 365, 367, 370, 373, 399, 400, 401, 414, *see also* Cores
Strontium, 166
Strontium ferrite, *see* Ferrites
Structure effects, 162
Sublimation, *see* Evaporation deposition
Substrate, 624, 633
Sulphur, 17, 162, 164, 216, 320
Supermalloy, 13, 68, 193, 213, 366, 369, 388, 414, 415, 416, 712–713, 740
Supermendur, 193, 213–214, 349, 368, 369, 430, 709, 740
Supermimphy, 740
Supermu, 740
Supermumetal, 373, 712–713, 740
Super-paramagnetism, 287
Superradio metal, 711, 748
Superstructure, 25, 92, 280, 626
Superstructured alloys, 258, 280, 341
Supplementary loss, *see* Additional loss
Supranhyster, 711, 740
Surface grinding, *see* Workability
Surfacing, *see* Workability
Susceptibility, 16, 20, 28, 85
SWB sheet, 739
Switching
  core, 597, 728, 732
  element, 580
  process in storage devices, 600–602, 629–631
  time, 581, 597–600, 605, 608, 609, 611, 612, 616, 619
Switching characteristic, straight-line, 606
Switching constant, 597–600, 609–611, 614–618, 619, 633, 635, 640

Tantalum, 16
Tape recorder, 580, 581, 582–590, Plate 15.4
Tape stores, 581, 582–590, *see also* Stores
Telegraphic speed, 411
Telegraphone, 582
Telephone earpieces, 296, 430, Plate 9.43
Temperature coefficient, 57
  of dust cores, 443

Temperature coefficient — *cont.*
of Mn–Zn ferrites, 477, 478
of Ni–Zn ferrites, 498, 499, 668
of permanent magnets, 248, 249, 250, 293
of specific electrical resistance, 217, 218
of strip cores, 428
time delay, 644
Temperature compensation, 640, 680–684
Temperature stability, 274
Tempering, 171, 252, 253, 257, 260, 384, 406, 416, 428
for permanent magnets, 253
Tensor permeability, 23, 529
Tesla (unit), 21
Test pulse, 604
Texture, 138, 320, 325–331, 418, 513
determination of, 330
foliate and fan, 513
Isoperm, 92, 155, 710–711
recrystallisation, 138, 328
rolling, 329
sheet, 328–330
Thallium, 17
Thermal compensation, *see* Temperature compensation
Thermal conductivity, 209, 310
Thermalloy, 424, 683, 740
Thermelast, 664, 740
Thermenol, 193, 215, 342, 407, 740
Thermoferrite, 682, 684
Thermoflux, 682, 684, 740
Thermomagnetic treatment, 60, 92, 137, 152, 154, 156, 269, 344, 619
Thermoperm, 682, 740
Thin-film memory, 126, 584, 623–632
Ticonal, 688, 689, 696
Titanium, 268, 492, 569
TK, 696, 740
TM alloy, 740
Toroids, 29, 32, 80, 139, 331, 365, 367, 370, 372, 374, 375, 399
Trafoperm, 675, 709, 740
Tran-Cor, 329, 740
Trancore, 740
Trans Tech, 724, 726
Transducer, magnetomechanical, 658, 662, 663
Transductors, 357
characteristic of, 358, 360, 370
circuit arrangements, 358, 359
dead time of, 361
figure of merit, 359, 372
materials for, 363–370
response time of, 360
time constant of, 361
Transfluxors, 636–640
Transformers
communications, 396, 660, 673, Plate 13.1
power, 169, 306, 315, 321, 349, 350
Travelling-wave amplifier, *see* Microwave amplifier
Tromalit, 246, 740
TT alloys, 724–727
Tubular cores, 466, *see also* Cores
Tungsten, 16, 413, 624
Turning process, 53, 111, 112, 256, 602, 629
for measurement of moment, 89, 330
moment curve, 88, 330, 334
Twistor, 640–644

U cores, *see* Cores
U and UI laminations, 186, 349, 365, 371, 373, 400, 401
Ugimax, 696, 740
Ultraperm 10, 70, 364, 705, 713, 740
Ultraperm Z, 364, 366, 621, 713, 740
Ultrasound, 210, 655
Unalloyed iron, 13, 16, 22, 53, 78, 87, 101, 112, 137, 142, 170, 200, 209, 217, 307–312, 313
Uncertainty, of relays, 383
Uni 80, 741
Uranium, 16

Vacant sites, 64
Vacodur, 16
Vacoflux, 349, 366
Vacoperm, 712–713, 741
Vacuum annealing, *see* Heat treatment
Vacuum deposition, *see* Cathode sputtering
Vacuum melting, 163, 174, 309, 390
Vanadium, 406, *see also* Iron alloys
Varioperm, 682, 741
Vectolite, 707, 741
Verdet's constant, 6
Vibralloy, 664
Vibrators, 655, 657–659, 660
Vibrox, 663, 741
Vicalloy, 213–214, 243, 275–278
Villari effect, 8
Viperm, 711, 713, 741
Virgin curve, *see* Magnetisation curve
Viscosity, magnetic, *see* Residual effect
Volume resonance, 70, 234, 235

Vortex magnetisation, 124, 125
V-Permendur, 193, 213–214, 392, 393, 430, 663, 665, 666, 709
1·7V-Permendur, 430
2V-Permendur, 193, 389, 662, 663
VS 30, 741

Waffle iron store, *see* Stores
Wall, *see* Bloch wall, Crosstie walls, Néel wall
Water, 17
Waveguides, 523, 524, 537, 538, 540, 544
Wavelength range, 397
Weber (unit), 21
Weiss domains, *see* Elementary domains
Westro, 707, 741
Wiedemann effect, 8, 640, 658
Winding loss, 38
Wire cores, *see* Cores
Wires, plated, 634, 635
Workability, 210, 271, 274, 275–277, 279, 318, 389, 391
Working field strength, 238, 245
Working flux density, 239, 245
Working line characteristic, 254
Working point, optimum, 130, 240, 245
Working store, 595, Plate 15.1
Wrist-watch motors, 286
Writing head, *see* Magnetic head
Writing process, 596, 543, 547, 570

X cores, *see* Cores

YIG, *see* Yttrium–iron garnet
Yttrium–gadolinium garnet, 618, 726
Yttrium–iron garnet, 528, 543, 726

Zementit, *see* Iron carbide
Zinc, 17, 569, 609
Zinc oxide, 177, 610
Zone-melting process, 163